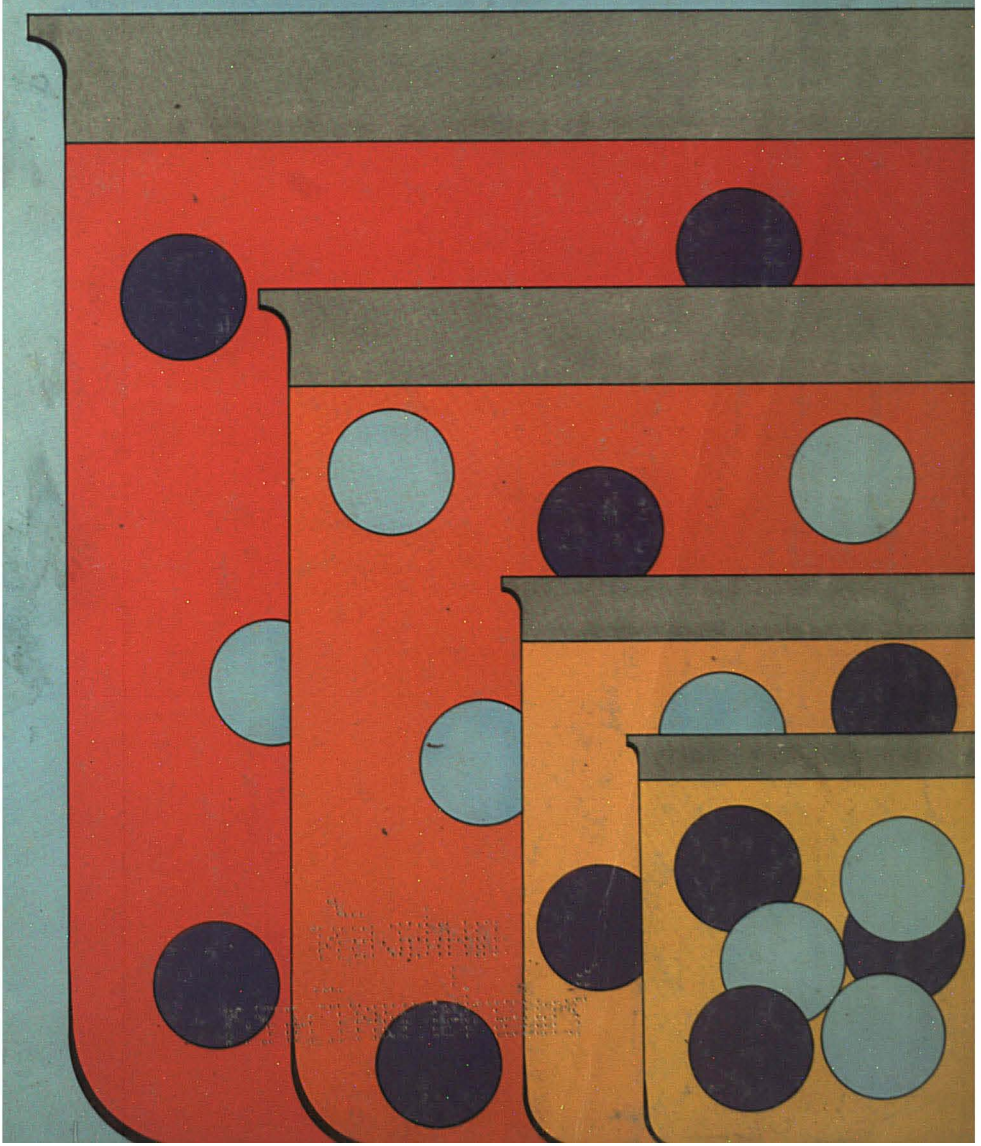
AUGUST 1981

analytical chemistry



When your applications change,



recorder changes with them

Plug in your choice of modules and the Omnigraphic® Model 2000 is tailored to your need

The Omnigraphic Model 2000 is the world's best known most versatile X-Y recorder. The basic building block is a rugged die cast metal mainframe. A choice of 27 modules enables the recorder to perform in virtually any application.

- 30 in./sec. speed (40 in./sec. available)
- ±0.2% accuracy
- Best common mode rejection
- Same servo response on both axes
- Modules can be changed in minutes
- Amplifiers interchangeable
- Priced from $1325* OEM discounts available.

® Registered Trademark of Houston Instrument

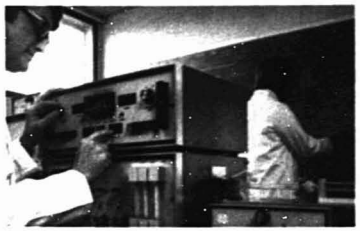
* U.S. Domestic Price Only

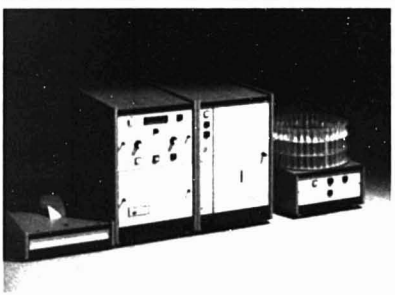
Circle 99 for Literature. Circle 100 to have a Representative Call

Even Better Ways of Doing What Dohrmann Does Best

Measuring traces of nitrogen, sulfur, and halides

Dohrmann analyzer systems are leaders in the field for *fast, accurate* and *sensitive* determinations of traces of N, S, and Cl in solids, liquids and gases at the ppm level. Dohrmann's ongoing development of sampling accessories and methodology make this technique a powerful analytical tool in any laboratory. For details, contact your local Dohrmann agent.





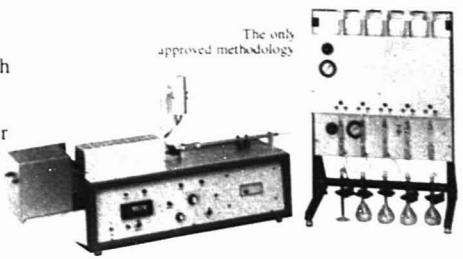
The most practical and versatile TOC Analyzer

Utilizing EPA approved methodology, the new Dohrmann DC-80 Total Organic Carbon Analyzer sets the standard for reliable, uncomplicated operation. Automatic sampling capability (optional) allows unattended operation. Full range capability, from drinking water to industrial waste water, with this superior low temperature UV-promoted system.

Dohrmann does it all in TOC.
For details, call your local Dohrmann agent.

The DX-20 Total Organic Halide Analyzer

The DX-20 is a must item for everyone concerned with waste management and safe drinking water standards. In fact, the DX-20 is the *only approved* methodology for determining total organic halides. Developed under EPA Contract No. 68-03-2833, the DX-20 has already proven itself in the U.S. and abroad. Customers include universities, public health organizations, and industrial users.



DOHRMANN
Division of XERTEX Corporation

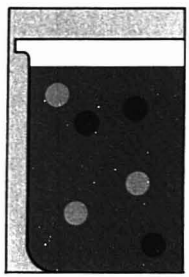
3240 Scott Boulevard
Santa Clara, California 95050
Telex 346 395

CALL TOLL FREE
(800) 538-7708
In Alaska, California, Hawaii, call collect (408) 727-6000

CIRCLE 50 ON READER SERVICE CARD

analytical chemistry

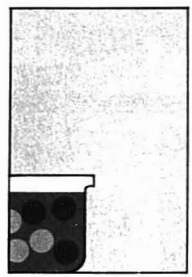
AUGUST 1981 COVER FEATURE



REPORT

Preconcentration for trace analysis of organic compounds. F. W. Karasek and co-workers discuss the enrichment methods that they have found workable and useful for analysis of trace organic constituents in environmental samples

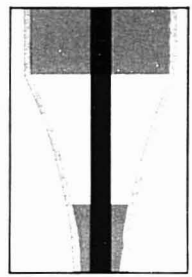
1050 A



REPORT

Preconcentration for trace element determination in aqueous samples is often necessary when analytical methods lack the requisite sensitivity, selectivity, or freedom from matrix interferences, according to Donald Leyden and Wolfhard Wegscheider

1059 A



INSTRUMENTATION

Microvoltammetic electrodes are 10 times smaller in diameter than a human hair. Because of their very small size, writes Mark Wightman of Indiana University, they exhibit very different voltammetric properties than do conventional-size electrodes

1125 A

FOCUS

Infrared analyzer developed for NASA. Foxboro Analytical has designed an instrument to test for the presence of leaking oxidant at space shuttle landings

1067 A

Volume 53, No. 9
August 1981
ANCHAM
53(9) 1023A–1140A
1313–1552 (1981)
ISSN 0003 2700

Copyright © 1981 by the American Chemical Society

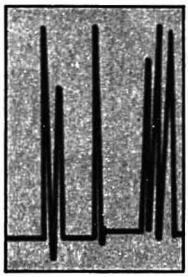
Published monthly with review issue added in April and Laboratory Guide in August by the American Chemical Society from 20th and Northampton Sts., Easton, Pa 18042. Executive and Editorial headquarters, American Chemical Society, 1155 16th St., N.W., Washington, D.C. 20036 (202) 872-4600. Second class postage paid at Washington, D.C., and at additional mailing offices.

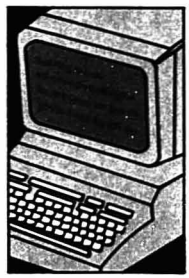
Claims for missing numbers will not be allowed if loss was due to failure of notice of change of address to be received in the time specified; if claim is dated (a) North America: more than 90 days beyond issue date, (b) all other foreign: more than one year beyond issue date; or if the reason given is "missing from files."

Permission of the American Chemical Society is granted for libraries and other users to make reprographic copies for use beyond that permitted by Sections 107 or 108 of the U.S. Copyright Law, provided that the copying organization pay the appropriate per-copy fee through the Copyright Clearance Center, Inc., 21 Congress St., Salem, Mass. 01970 (617-744-3350). Educational institutions are generally granted permission to copy upon application to Copyright Administrator, Books and Journals Division, ACS, 1155 16th St., N.W., Washington, D.C. 20036.

Advertising Management: Centcom, Ltd., 25 Sylvan Road South, Westport, Conn. 06880 (203) 226-7131

Technical Contents/Briefs ..... 1028 A
Letters ..... 1045 A
Meetings ..... 1092 A
For Your Information ..... 1094 A
New Products ..... 1098 A
Chemicals ..... 1105 A
Manufacturers' Literature ..... 1108 A
Advertising Index ..... 1138 A
Author Index, Future Articles ..... inside back cover





NEWS

FACSS. The Eighth Annual Meeting of the Federation of Analytical Chemistry and Spectroscopy Societies will be held Sept. 20–25 in Philadelphia, Pa.

▶ **The ACS Analytical Division** announces its 1981 fellowship winners

1069 A

ANALYTICAL APPROACH

Reversed phase HPLC in conjunction with mass spectrometry and IR, UV, and NMR spectrometries is used to determine the active ingredients in over-the-counter drug preparations. Choline salicylate, an aspirin substitute, and allantoin, a skin-healing agent, are two of the active components determined

1111 A

BOOKS

Critical reviews. Books on laser methodology, mass spectrometry, and ion-selective electrodes are reviewed by Edward Peipmeier, S. P. Markey, and Richard Durst

1117 A

EDITORS' COLUMN

Computer-aided editorial operation. ANALYTICAL CHEMISTRY is setting up a microcomputer system to improve all phases of the peer review operation. The system will allow a wider choice of reviewers and will automatically generate a list of overdue reviewers for prodding

1048 A

EDITORIAL

The Gordon Research Conferences mark their Golden Jubilee this year. The conferences were started in 1931 by Johns Hopkins University chemistry professor Neil E. Gordon

1313

1981 Subscription prices—including surface postage

	1 yr	2 yr	3 yr
Members:			
Domestic	$15	$25	$36
Canada, Foreign	28	51	75
Nonmembers:			
Domestic	20	34	48
Canada	33	60	87
Other Foreign	43	77	111

Airmail and air freight rates are available from Membership & Subscription Services, ACS, P.O. Box 3337, Columbus, Ohio 43210 (614) 421-7230.

Subscription orders by phone may be charged to Visa or Master Charge. Call toll free at (800)424-6747 from anywhere in continental U.S.; from Washington, D. C., call 872-8065. Mail orders for new and renewal subscriptions should be sent with payment to the Controller, Washington address.

Subscription service inquiries and changes of address (include both old and new addresses with ZIP code and *recent mailing label*) should be directed to the ACS Columbus address noted above. Please allow six weeks for change of address to become effective.

ACS membership information: write Ann Donahue, Washington address.

Single issues, current year, $5.00 except review issue and LabGuide, $6.00; back issues and volumes: *write or call* Special Issues Sales, ACS Washington address (202) 872-4365.

Microfilm and microfiche editions are available by single volume or back issue collection. Send inquiries and payments to Microforms Office, ACS Washington address.

10 MAR 1982

ALL THE SERVICE YOU WANT AND

Call us Beckman Service, Inc. No, we're not changing our name from Beckman Instruments, Inc. But we want to let you know there's another side to us. It's service. The kind you'd expect from a company like Beckman. The best.

And we're not just talking about helping you when something breaks down. We're talking about a wide range of help and support to keep you going, not just get you going. To maximize uptime and do it quickly.

Here's a quick rundown of what we mean:

1. Service Agreements—There are several different service agreements available after the warranty period. These are customized programs designed for you to contain cost and maximize uptime.

2. Technical and Applications Support—Field Service Engineers and highly trained specialists are available to help you keep your Beckman instruments up and running



MORE THAN YOU'LL EVER NEED.

at peak efficiency. And to help you find innovative applications to get more out of those instruments.

3. Seminars and Training Sessions—We offer regularly scheduled classroom training at many of our nationwide facilities. And we'd be more than happy to hold training seminars at your place if that's your need.

4. Hotline (available on a variety of instruments)—If you've got a question—any question—you can call the Hotline number. Anytime, anywhere. And get an answer from a highly trained specialist.

Beckman service. It covers more than you'll ever need. But isn't it nice to know it's there if you want it? For more complete information, write for Bulletin 8514, Analytical Instruments Sales and Service Division, Dept. 962, 2500 Harbor Blvd., Fullerton, CA 92634. Or call: (800) 854-4068. In Calif: (800) 422-4400.

BECKMAN SERVICE.
MORE THAN YOU'LL EVER NEED.

CIRCLE 23 ON READER SERVICE CARD



BECKMAN

Briefs

Verification of Retention and Zone Spreading Equations in Sedimentation Field-Flow Fractionation 1314

Equations for retention and zone spreading are verified experimentally with polystyrene latex beads. Agreement between theory and experiment is within ~1% for retention and within ~5–10% for plate height.

George Karaiskakis, Marcus N. Myers, Karin D. Caldwell, and J. Calvin Giddings*, Department of Chemistry, University of Utah, Salt Lake City, Utah 84112 *Anal. Chem., 53 (1981)*

Conventional Packed Columns vs. Packed or Open Tubular Microcolumns in Liquid Chromatography 1318

A packed column and a capillary column of the same length give approximately the same efficiency (plate number) and the same analysis time if the diameter of the particles in the packed column is half the diameter of the capillary column and both are operated at the optimum flow velocity.

Georges Guiochon, Ecole Polytechnique, Laboratoire de Chimie Analytique Physique, Route de Saclay, 91128 Palaiseau Cedex, France *Anal. Chem., 53 (1981)*

Measurement of Band Broadening in Size Exclusion Chromatography 1325

Total band broadening is measured with "dry" CH_2Cl_2 and interstitial broadening with "wet" eluent in the same column. Band broadening in the pores is obtained by difference.

R. Groh and I. Halász*, Angewandte Physikalische Chemie, Universität des Saarlandes, 6600 Saarbrücken, West Germany *Anal. Chem., 53 (1981)*

High-Resolution Gas Chromatography of Trialkyllead Chlorides with an Inert Solvent Venting Interface for Microwave Excited Helium Plasma Detection 1336

The system incorporates a chemically deactivated, low-volume, valveless fluidic logic gas switching interface for venting large quantities of eluent solvent that would disrupt the helium discharge as sustained by the TM_{010} cylindrical resonance cavity.

Scott A. Estes, Peter C. Uden*, and Ramon M. Barnes, Department of Chemistry, GRC Tower I, University of Massachusetts, Amherst, Mass. 01003 *Anal. Chem., 53 (1981)*

Liquid Chromatographic Elution Characteristics of Some Solutes Used To Measure Column Void Volume on C_{18} Bonded Phases 1341

Injection of sodium nitrate in a methanol–water eluent of sufficient background electrolyte concentration to prevent electrochemical exclusion phenomena produces a consistent V_0 value.

Martha J. M. Wells and C. Randall Clark*, Division of Medicinal Chemistry, Department of Pharmacal Sciences, School of Pharmacy, Auburn University, Auburn University, Ala. 36849 *Anal. Chem., 53 (1981)*

Preparative Liquid Chromatography for Fractionation of Petroleum and Synthetic Crude Oils 1345

The complete operating time is 80 min for the alumina column and 25 min for the silica gel column. Capacity ranges from 1 to 6 g of sample, depending on its composition.

James W. Vogh* and Jane S. Thomson, Bartlesville Energy Technology Center, U.S. Department of Energy, P.O. Box 1398, Bartlesville, Okla. 74003 *Anal. Chem., 53 (1981)*

Chromatographic–Spectrometric Identification of Airborne Polynuclear Aromatic Hydrocarbons 1351

The method involves a combination of gas chromatography, mass spectrometry, liquid chromatography, and ultraviolet spectrometry. A one-step procedure for isolation of PAHs by preparative thin-layer chromatography is reported.

Dilip R. Choudhury* and Brian Bush, Division of Laboratories and Research, New York State Department of Health, Albany, N.Y. 12201 *Anal. Chem., 53 (1981)*

Thin-Layer Chromatography with In Situ Multichannel Image Detection of Fluorescent Compounds 1357

A dynamic range of fluorescence intensity of over 500:1 is measured on a single plate. Detection limit is 3 pg for tetraphenylporphine.

M. L. Gianelli, J. B. Callis*, N. H. Andersen, and G. D. Christian, Department of Chemistry BG-10, University of Washington, Seattle, Wash. 91895 *Anal. Chem., 53 (1981)*

Continuous Flow Alternating Current Polarographic Detection of Nitrazepam in Liquid Chromatography 1362

Effects of mobile phase composition, applied frequency, amplitude, and phase angle are examined. A phase angle of 0° offers the best measurement conditions for batch and flow conditions.

Herman B. Hanekamp, Willem H. Voogt, Roland W. Frei*, and Pieter Bos, Department of Analytical Chemistry, Free University, De Boelelaan 1083, 1081 HV Amsterdam, The Netherlands *Anal. Chem., 53 (1981)*

* Corresponding author.

The Ross™ pH electrode:

A unique internal element system for electrodes has been developed by Dr. James W. Ross, considered by many to be the father of ion-selective electrodes. By replacing the silver chloride or calomel used in conventional electrodes, this system makes possible pH electrodes with extraordinary performance characteristics. Response is fast – readings stable to 0.01 pH are obtained in under 30 seconds even in samples varying from one another by 50°C or more. Over the temperature range of 0 to 100°C using ATC, results are 3 to 5 times more accurate than those obtained with conventional pH electrodes (even the ones we sell!). Drift is virtually unnoticeable at less than 0.002 pH per day, eliminating the need for frequent electrode re-standardization. So if you want pH accuracy ... no matter what ... send for more information right away. Orion Research Incorporated, 840 Memorial Drive, Cambridge, MA 02139, or call (800) 225-1480.

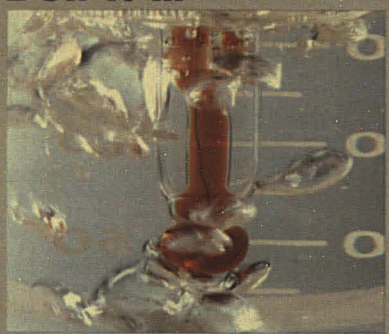


81-01
pH HALF CELL

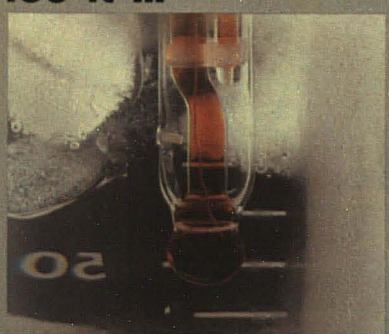
80-05
REFERENCE
HALF CELL

81-02
COMBINATION pH

Boil it ...



Ice it ...





... and it's still in calibration.

See the Ross electrode in action at LABCON '81, Booths 303 & 305.

CIRCLE 156 ON READER SERVICE CARD

Correlation between the Retention Behavior of Mono- and Difunctional Solutes in Binary Solvent–Silica Gel Liquid Chromatography 1365

The correlation between the capacity ratio and solvent composition is determined. The retention of difunctional solutes is estimated on the basis of the retention of two corresponding monofunctional solutes.

Shoji Hara* and Sayuri Miyamoto, Tokyo College of Pharmacy, Horinouchi, Hachioji, Tokyo 192-03, Japan
Anal. Chem., 53 (1981)

Quantitative Resolution of Severely Overlapping Chromatographic Peaks 1369

Peaks with identical retention are resolved as long as the peaks have different shapes. The detector response for each component at various times is fit to a second-order polynomial of the component's concentration. A series of nonlinear simultaneous equations is then solved for the concentration of each component in the mixture.

Jeffrey T. Lundeen and Richard S. Juvet, Jr.*, Department of Chemistry, Arizona State University, Tempe, Ariz. 85281
Anal. Chem., 53 (1981)

Effect of Detector Nonlinearity on the Height, Area, Width, and Moments of Peaks in Liquid Chromatography with Absorbance Detectors 1373

Those properties related to the even moments, such as the area and peak width, are most strongly influenced by detector nonlinearity, whereas odd moments of symmetric (Gaussian) peaks are not altered.

Lynda M. McDowell, William E. Barber, and Peter W. Carr*, Department of Chemistry, Smith & Kolthoff Halls, University of Minnesota, Minneapolis, Minn. 55455 *Anal. Chem., 53 (1981)*

Determination of Cyanide or Thiocyanate at Trace Levels by Derivatization and Gas Chromatography with Flame Thermionic Detection 1377

Cyanide or thiocyanate is methylated with dimethyl sulfate to form acetonitrile or methyl thiocyanate, respectively. Linear calibration curves are obtained in the ranges of 0.05 to 1.00 μg CN^-/mL and 0.25 to 10.0 μg SCN^-/mL.

Koichi Funazo, Minoru Tanaka, and Toshiyuki Shono*, Department of Applied Chemistry, Faculty of Engineering, Osaka University, Yamada-oka, Suita, Osaka 565, Japan
Anal. Chem., 53 (1981)

Reversed-Phase Liquid Chromatographic Resolution of Amino Acid Enantiomers by Mixed Chelate Complexation 1380

The copper(II) complex of optically active *N*-(p-toluenesulfonyl)-L-phenylalanine is the mobile phase. The column eluent is monitored for fluorescence after reaction with *o*-phthalaldehyde.

Noriyuki Nimura, Tsukasa Suzuki, Yoko Kasahara, and Toshio Kinoshita*, School of Pharmaceutical Sciences, Kitasato University, 9-1 Shirokane-5, Minato-ku, Tokyo 108, Japan
Anal. Chem., 53 (1981)

Spurious Peaks in Rapid-Scan Square-Wave Polarography 1383

Spurious peaks arise from a resonance between the electrical frequency of the excitation and the mechanical frequency of oscillation of the dropping mercury electrode.

Adina Lavy Feder and Chaim Yarnitzky, Department of Chemistry, Technion-Israel Institute of Technology, Haifa, Israel, and **John J. O'Dea and Janet Osteryoung*,** Department of Chemistry, State University of New York at Buffalo, Buffalo, N.Y. 14214 *Anal. Chem., 53 (1981)*

Electrochemical Treatment of Pyrolytic Carbon Fiber Electrodes 1386

The treated electrodes, in combination with differential pulse voltammetry, separate ascorbic acid and catechol peaks. Catecholamines are detected at submicromolar levels. Parameters and experimental conditions for the treatment are examined.

F. G. Gonon*, C. M. Fombarlet, M. J. Buda, and J. F. Pujol, INSERM U 171, Département de Médecine Expérimentale, Université Claude Bernard, 8, Avenue Rockefeller, 69008 Lyon, France *Anal. Chem., 53 (1981)*

Derivative Linear Sweep and Derivative Cyclic Voltabsorptometry 1390

The spectroelectrochemical analogs of linear sweep and cyclic voltammetry are described for reversible electrochemical systems. The techniques are insensitive to nonfaradaic charge-consuming processes and exhibit limits of detection below 1×10^{-6} M.

Eric E. Bancroft, James S. Sidwell, and Henry N. Blount*, Brown Chemical Laboratory, University of Delaware, Newark, Del. 19711 *Anal. Chem., 53 (1981)*

Digital Alternating Current Polarography with Microprocessor-Based Instrumentation 1394

All the components of a conventional ac polarograph, except the potentiostat, are simulated with software. Absolute current polarograms at various phase angles as well as phase sensitive fundamental and second harmonic polarograms are in qualitative agreement with theory.

J. E. Anderson and A. M. Bond*, Division of Chemical and Physical Sciences, Deakin University, Waurn Ponds 3217, Victoria, Australia *Anal. Chem., 53 (1981)*

Multielement Analysis of Human Blood Serum by Neutron Activation and Controlled Potential Electrolysis 1398

Fourteen elements are simultaneously determined in a 500-μL sample of blood serum. Limits of determination are 10^{-1} to 10^{-3} μg/L for the nine trace elements investigated.

Kari Jørstad*, Brit Salbu, and Alexis C. Pappas, Department of Chemistry, University of Oslo, Oslo, Norway
Anal. Chem., 53 (1981)

Model for Treatment of Selectivity Coefficients for Solid-State Ion-Selective Electrodes 1401

The model considers the mechanism of metathetic reactions at the membrane surface and describes the sensed surface ion concentrations in terms of the bulk solution concentrations.

Adam Hulanicki and Andrzej Lewenstam*, Department of Chemistry, University of Warsaw, 02-093 Warsaw, Poland
Anal. Chem., 53 (1981)

Where do new ideas in HPLC come from?

New ideas come from the minds of enthusiastic creative people like Jim Burger. Jim has just written an advanced HPLC software program which operates with the Chromatix Real Time Data Acquisition System (RTDAS). With this program and our new multichannel software, you can simultaneously operate up to 16 HPLC detectors, or a combination of GPC, light scattering, and HPLC detectors. You get answers in minutes to a number of complex HPLC analyses, in printed or plotted format, at your option.

You can purchase this multichannel HPLC capability from Chromatix as a complete ready-to-use turnkey system, including the computer. Or if you already have a DEC computer using the RT-11 operating system, you can add our advanced software and peripherals to make up your own system.

By the way, don't worry if one of your analytical instruments is next door or down the hall. Our CMX-10 interface modules handle low level analog signals with no problem.

Want the full story? Contact your Chromatix representative today, or call our new Customer Response Center at the 800 number shown below.



New! 16-channel HPLC software and CMX-10 Interface Modules.

New! CMX-50, a unique UV/VIS spectrophotometric HPLC detector that adds new capability to any HPLC system. Provides up to six full UV/VIS spectra per second. Displays three spectra or three chromatograms. *P.S.—Now you know how we displayed these three chromatograms so easily and neatly.*

chromatix

CIRCLE 32 ON READER SERVICE CARD

560 Oakmead Parkway
Sunnyvale, CA 94086
Phone: 800/538-1595
Calif: 408/736-0300 collect
TWX: 910-339-9291

Heisenbergstrasse 10
8057 Eching b. München
West Germany
Phone: (08165) 5448
Telex: 526512 CHRX

Briefs

Simultaneous Determination of Cadmium and Lead in Whole Blood and in Serum by Computerized Potentiometric Stripping Analysis 1406

Whole blood samples are diluted 1:10 with hydrochloric acid and analyzed directly without prior deoxygenation. Limit of detection after 2 min of preelectrolysis is 25 nM for Cd and Pb. Relative standard deviation is better than 4%.

Daniel Jagner*, Mats Josefson, Stig Westerlund, and Kerstin Årén, Department of Analytical and Marine Chemistry, Chalmers University of Technology and University of Göteborg, S-412 96 Göteborg, Sweden *Anal. Chem., 53 (1981)*

Resolution of Overlapped Electrochemical Peaks with the Use of the Kalman Filter 1410

Quantitative resolution of peaks generated by linear scan voltammetry is possible even when peaks are separated by as little as 2.5 mV. Noise and background are removed by the filter.

Teri F. Brown, Department of Civil Engineering, University of Washington, Seattle, Wash. 98195, and Materials and Molecular Research Division, Lawrence Berkeley Laboratory, Berkeley, Calif. 94720, and **Steven D. Brown*,** Department of Chemistry, University of California, Berkeley, Calif. 94720, and Materials and Molecular Research Division, Lawrence Berkeley Laboratory, 1 Cyclotron Road, Berkeley, Calif. 94720 *Anal. Chem., 53 (1981)*

Multinuclear Nuclear Magnetic Resonance Study of Three Aqueous Lanthanide Shift Reagents: Complexes with EDTA and Axially Symmetric Macrocyclic Polyamino Polyacetate Ligands 1418

The axially symmetric, octadentate lanthanide DOTA complexes are better aqueous shift reagents than lanthanide EDTA or lanthanide aquo complexes.

Charles C. Bryden and Charles N. Reilley*, Kenan Laboratories of Chemistry, University of North Carolina, Chapel Hill, N.C. 27514, and **Jean F. Desreux,** Analytical and Radiochemistry, University of Liege, Sart Tilman, B-4000, Liege, Belgium *Anal. Chem., 53 (1981)*

Dependence of Photoacoustic Signal on Optical Absorption Coefficient in Optically Dense Liquids 1426

The relationship between absorbance and photoacoustic signal amplitude is theoretically derived and experimentally verified. Absolute absorbance values are calculated from normalized photoacoustic signals.

Shmuel Malkin*, Biochemistry Department, The Weizmann Institute of Science, Rehovot 76100, Israel, and **David Cahen,** Department of Structural Chemistry, The Weizmann Institute of Science, Rehovot 76100, Israel *Anal. Chem., 53 (1981)*

Integrated, Microcomputer-Controlled, Adjustable-Waveform Spark Source for Atomic Emission Spectrometry 1432

The spark source has a modular design with unitized discharge circuitry, and incorporates fewer electronic components than previous electronic spark sources. A Commodore PET microcomputer is used to trigger the source.

Steven G. Barnhart, Paul B. Farnsworth, and John P. Walters*, Department of Chemistry, University of Wisconsin, Madison, Wis. 53706 *Anal. Chem., 53 (1981)*

Influence of Instrumental Response Time on Interference Effects in Graphite Furnace Atomic Absorption Spectrometry 1437

The spectrometer has a small time constant and the on-line data acquisition system monitors the signals without distortion. The degree, as well as the sign, of interference effects is influenced by the time constant of the instrument.

Erik Lundberg* and Wolfgang Frech, Department of Analytical Chemistry, University of Umeå, S-901 87 Umeå, Sweden *Anal. Chem., 53 (1981)*

Condensed Phase Photoacoustic Spectroscopic Detection of Porphyrins and Dyes 1442

Performance of the piezoelectric detection system with respect to linearity, solvent effects, and excitation pulse characteristics is experimentally evaluated and compared with theoretical figures of merit. Limits of detection for various porphyrins, laser dyes, and drugs are presented.

Edward Voigtman, Arthur Jurgensen, and James Winefordner*, Department of Chemistry, University of Florida, Gainesville, Fla. 32611 *Anal. Chem., 53 (1981)*

Automated Determination of Ammonia by Gas-Phase Molecular Absorption 1447

Automation is achieved by interfacing an automatic sampler, a multichannel peristaltic pump, an adjustable heating bath, and a gas–liquid separator to an atomic absorption spectrometer. Detection limit is 0.10 μg NH_3/mL.

Prem N. Vijan* and George R. Wood, Laboratory Services Branch, Ontario Ministry of the Environment, 125 Resources Road, Rexdale, Ontario, Canada M9W 5L1 *Anal. Chem., 53 (1981)*

Determination of Mercury at the Ultratrace Level by Atmospheric Pressure Helium Microwave-Induced Plasma Emission Spectrometry 1450

Mercury is generated from solution with the cold vapor generation technique. Limit of detection is 4 pg/mL or 8 pg, and the dynamic range of the calibration curve is 2×10^5.

Kiyoshi Tanabe, Koichi Chiba, Hiroki Haraguchi*, and Keiichiro Fuwa, Department of Chemistry, Faculty of Science, University of Tokyo, Bunkyo-ku, Tokyo 113, Japan *Anal. Chem., 53 (1981)*

Fourier Transforms in the Computation of Self-Deconvoluted and First-Order Derivative Spectra of Overlapped Band Contours 1454

Advantages of Fourier self-deconvolution are demonstrated. A theoretical description of the computation of derivatives with Fourier transforms is presented, and the technique is compared to the method of Savitzky and Golay.

Jyrki K. Kauppinen, Douglas J. Moffatt, Henry H. Mantsch, and David G. Cameron*, Division of Chemistry, National Research Council of Canada, Ottawa, Ontario K1A 0R6, Canada *Anal. Chem., 53 (1981)*

Acids for every application

PRODUCTS
PACKAGING
DISTRIBUTION
THE WINNING COMBINATION

Mallinckrodt.

Wide selection and high quality

You'll find all the popular acids in Mallinckrodt's extensive chemical line. You can be sure we have the acid you require ready for delivery. Mallinckrodt's acids are high-purity products, available in grades suitable for research, medicine, electronics, education, industry and the life sciences.

Packaging variety and innovation

Choose from pints to tank trucks. Our special packaging is designed for a high degree of utility and convenience in the laboratory. For example, Mallinckrodt's PVC-coated Safemor® bottle is less slippery than plain glass, less likely to be dropped. If it is dropped, the tough, polycoating helps hold everything together for prompt disposal. For packaging from the industry's newest and most modern facility, you can depend on Mallinckrodt.



Mallinckrodt's PVC-coated Safemor® bottle

Prompt delivery nationwide

A nationwide network of over 250 fully stocked Mallinckrodt distributors assures prompt delivery of AR® and laboratory chemicals. We're always nearby when you need us...regardless of your present location or where expansion plans take you. Let Mallinckrodt help if you require a new reagent, special purity or nonstandard package sizes. Just call us toll-free at 800-354-2052.

Ask your representative for more information about the complete line of quality chemicals, plasticware, and safety products available from Mallinckrodt.

SCIENCE PRODUCTS DIVISION Mallinckrodt, Inc., St. Louis, Missouri 63134

Mallinckrodt®

© Mallinckrodt, Inc. 1981

CIRCLE 141 ON READER SERVICE CARD

Modulated Differential Reflectance Spectroscopy of Lead Dioxide Films during Growth 1457

A differential reflectivity optical model is presented for linear growth of a PbO_2 film on a reflective Pt substrate. Knowledge of chemical product properties coupled with ac optical techniques enables selective monitoring of surface faradaic processes.

R. J. Gale*, J. Sefaja, and M. Fleischmann, Electrochemistry Group, Chemistry Department, The University, Southampton S09 5NH, England *Anal. Chem., 53 (1981)*

Structure Elucidation from the Hydroxyl Stretching Region of Vapor-Phase Infrared Spectra 1460

Correlations between peak wavelength and functionality are observed for primary, secondary, and tertiary alcohols, phenols, carboxylic acids, and oximes. Peak shifts due to steric crowding and intramolecular hydrogen bonding are seen.

Michael F. Delaney* and F. Vincent Warren, Jr., Department of Chemistry, Boston University, Boston, Mass. 02215 *Anal. Chem., 53 (1981)*

Characterization of Airborne Particulates by Pyrolysis/Mass Spectrometry and Carbon-14 Analysis 1463

The contribution of various pollution sources is determined for the Utah oil shale lands by pyrolysis/mass spectrometry and pattern recognition procedures. Results are discussed in terms of the ^{14}C content of the particulates.

Kent J. Voorhees*, Steven M. Kunen, and Steven L. Durfee, Department of Chemistry/Geochemistry, Colorado School of Mines, Golden, Colo. 80401, and **Lloyd A. Currie and George A. Klouda,** Center for Analytical Chemistry, National Bureau of Standards, Washington, D.C. 20234 *Anal. Chem., 53 (1981)*

Liquid Chromatography with Graphite Furnace Atomic Absorption Spectrometric Detector for Speciation of Organophosphorus Compounds 1466

The method is applied to the speciation of organophosphorus additives dissolved in lubricating oil. RSD is approximately 5–10% for determination at the 2-μg phosphorus level.

Paolo Tittarelli* and Achille Mascherpa, Stazione Sperimentale per i Combustibili, 20097 San Donato Milanese, Italy *Anal. Chem., 53 (1981)*

On Site Continuous Liquid–Liquid Extraction of Nonpolar Organic Compounds in Water 1469

Limits of detection are as follows: 0.2 ng/L, α-1,2,3,4,5,6-hexachlorocyclohexane (α-BHC); 0.7 ng/L, β-BHC; 0.5 ng/L, γ-BHC (lindane); and 0.2 ng/L, hexachlorobenzene.

Burkhard Stachel*, Klaus Baetjer, Mehmet Cetinkaya, Juergen Dueszein, Uwe Lahl, Klaus Lierse, and Wolfram Thiemann, Trinkwassergruppe, Department of Chemistry, Universitaet Bremen, D-2800 Bremen 1, Postfach 330440, Federal Republic of Germany, and **Bernd Gabel, Rosemarie Kozicki, and Angela Podbielski,** Bremen Environmental Institute for the Analysis and Assessment of Hazardous Substances, Colmarer Strasse 22a, D-2800 Bremen 1, Federal Republic of Germany *Anal. Chem., 53 (1981)*

Determination of Hydrocyanic Acid and Free Cyanide in Aqueous Solution 1472

Microgram-per-liter concentrations of HCN in water and wastewater are determined directly by two methods. The linear relationship between pK for HCN (aq) and 1/temperature in degrees Kelvin is defined.

Steven J. Broderius, U.S. Environmental Protection Agency, Environmental Research Laboratory—Duluth, 6201 Congdon Boulevard, Duluth, Minn. 55804 *Anal. Chem., 53 (1981)*

Ion Pair Mobility in Associated Liquid Membranes 1477

Ion pair mobilities in tetraheptylammonium chloride and nitrate membranes are measured by the resistance relaxation method. Results are compared with mobilities calculated from conductometric data.

Claudio Fabiani* and Claudia Cianetti, Material Division, CNEN, CSN-Casaccia, Rome, Italy *Anal. Chem., 53 (1981)*

Determination of Synthetic Amorphous Silica in Industrial Air Samples 1479

The procedure involves thermal conversion of amorphous silica to cristabolite followed by X-ray diffraction. Effects of chemical contaminants are examined.

B. A. Lange, J. C. Haartz*, and R. W. Hornung, National Institute for Occupational Safety and Health, Division of Physical Sciences and Engineering, Cincinnati, Ohio 45226 *Anal. Chem., 53 (1981)*

Microcomputer-Controlled Reagent Preparation System 1484

Reagents are prepared from up to three different stock solutions and one diluent. Concentration precision is ±0.05% and dynamic range is 10^5.

R. Balciunas, F. J. Holler, P. K. Notz, E. R. Johnson, L. D. Rothman, and S. R. Crouch*, Department of Chemistry, Michigan State University, East Lansing, Mich. 48824 *Anal. Chem., 53 (1981)*

Hollow Fiber Ion-Exchange Suppressor for Ion Chromatography 1488

The suppressor is based on a countercurrent regenerated shell and tube device incorporating sulfonated polyethylene ion-exchange hollow fibers. The column allows continuous operation without interference from base line dips, ion-exclusion effects, or chemical reactions.

Timothy S. Stevens* and James C. Davis, Dow Chemical USA, Michigan Division Analytical Laboratories, 574 Building, Midland, Mich. 48640, and **Hamish Small,** Dow Chemical USA, Central Research Laboratories, 1712 Building, Midland, Mich. 48640 *Anal. Chem., 53 (1981)*

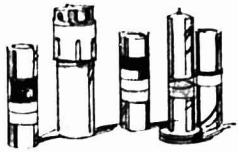
Laser Ionization Mass Spectrometry of Nonvolatile Samples 1492

The sample is electrosprayed onto a moving stainless steel belt for continuous sample introduction. Ionization is produced by focusing the output of a tunable dye laser onto the moving belt.

E. D. Hardin and M. L. Vestal*, Department of Chemistry, University of Houston, Houston, Tex. 77004 *Anal. Chem., 53 (1981)*

No. 450 Gas Stream Purifier

The model 450 purifier with model 454 replaceable cartridge is specially designed for removing the acetone vapor from acetylene. The cartridge contains activated charcoal. It belongs in a AA system. Circle 144



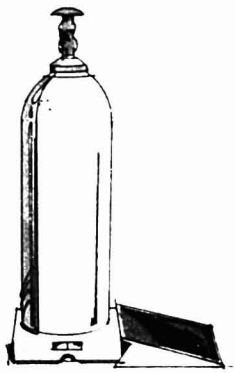
Automatic Regulators 1A-510 and 1L-326

If you are using AA, choose the correct regulators. In the laboratory, use regulators designed for the specific gas. Information on these regulators can be obtained. Circle 145



Cylinder Scale, Model 8510

To judge accurately when a liquefied gas is nearing empty, Matheson has designed and sells a cylinder scale. We recommend this for nitrous oxide because it will let you know ... and it's the only way ... when the cylinder is empty. Invaluable! Circle 146



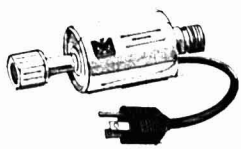
Series 6103 Flash Arrestor

A flash arrestor is installed as a part of the AA system downstream, after the regulator and cylinder. Some instruments have a built-in flash arrestor. If yours does not, two should be installed. Acetylene is highly flammable. Should flashback occur, with the accompanying shock wave, this device will instantly seal off the path to both regulator and cylinder ... preventing an explosion of much greater magnitude in either regulator or cylinder, both of which contain more gas. Flash arrestors are recommended for both fuel gas and oxidizer gas lines. For more information, circle 147



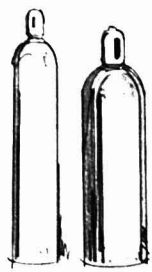
Nitrous Oxide Heater

Because nitrous oxide, frequently used as an oxidizer gas in AA, is liquefied gas, or a gas over liquid in a cylinder, it often cools or ices on expansion, causing problems in automatic control. The heater we offer is installed between cylinder and regulator and eliminates icing and allows for higher flows. Thermostatically controlled, the N_2O is not overheated and the operator can concentrate on his instrument. Works simply with 115 Vac. Circle 148



Acetylene 99.6% and Nitrous Oxide 99.0%

These are pure gases containing less impurities than commercial grades. We recommend them and specially purify them for AA instrument use. The purer the gas, the less interference in final results. Circle 149



Improved Operation Of An Atomic Absorption Spectro-photometer

Chemical analysis by atomic absorption spectroscopy is achieved by converting the sample into an atomic vapor and measuring its absorbance at a selected wavelength. The measured absorbance is proportional to concentration. The analysis is made by comparing this absorbance with a reference sample of known composition under similar conditions.

Atomic absorption lines are so narrow that the use of a conventional monochromator is impractical to measure them. Commercial instruments overcome this by the use of hollow cathode lamps which emit atomic spectral lines of the element to be determined.

Elements are measured after they have been put into solution either aqueous or organic. The solution is then sprayed into a flame, generally, air-acetylene. Some compounds, like the rare earths, require a highly reducing flame. This is done most safely by burning the acetylene in nitrous oxide which gives more available oxygen than air.

For years Matheson has been servicing scientists using AA spectroscopy, not only with gases but with other equipment which makes operation easier, and more important, safer. These items are at left. If you're not familiar with them we will be delighted to rush literature to you.

Matheson

Lyndhurst, N.J. 07071

East Rutherford, NJ 07073
Morrow, Georgia 30260
Bridgeport, NJ 08014
Gloucester, Massachusetts 01930
Joliet, Illinois 60434
Dayton, Ohio 45424
LaPorte, Texas 77571
Cucamonga, California 91730
Newark, California 94560
Dorsey, Maryland 21227
Gonzales, Louisiana 70737
Whitby, Ontario, Canada L1N 5R9
Edmonton, Alberta, Canada T5B 4N6
B 2431 Oevel, Belgium
6056 Heusenstamm, West Germany

HELLMA
... tomorrow's designs today!



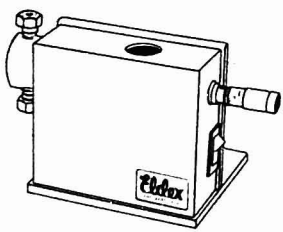
Hellma—the largest assortment of highest precision glass and quartz cells.
Standard · Flow-through · Constant-temperature
Anaerobic · Special Designs
Also available—ULTRAVIOLET LIGHT SOURCES
Deuterium Lamps · Mercury Vapor Lamps
Hollow Cathode Lamps · Power Supplies

HELLMA CELLS, INC.
Write for literature
Box 544
Borough Hall Station
Jamaica, New York 11424
Phone (212) 544-9534

CIRCLE 98 ON READER SERVICE CARD

Eldex LABORATORIES

HIGH PRESSURE METERING PUMPS



HPLC PUMP SPECIALISTS

- Flow Rates from 0.05-100 mL/min.
- Single, Dual & Triple Piston Models
- Priced from $595

ELDEX LABS 3551 Haven Avenue, Menlo Park, CA 94025 (415) 364-8159

CIRCLE 63 ON READER SERVICE CARD

Briefs

Peak Resolution by Semiderivative Voltammetry 1497

Overlapped voltammetric peaks are separated as semiderivatives. Synthetic data are totally resolved with peak separations as small as 25 mV, while real systems are deconvoluted with separations as small as 40 mV.

Jeffrey J. Toman and Steven D. Brown*, Department of Chemistry, University of California, Berkeley, Calif. 94720, and Materials and Molecular Research Division, Lawrence Berkeley Laboratory, 1 Cyclotron Road, Berkeley, Calif. 94720
Anal. Chem., 53 (1981)

Effect of Graphite Furnace Substrate Materials on Analyses by Furnace Atomic Absorption Spectrometry 1504

The porosity of the graphite and the fragility of pyrolytic coatings produce many of the problems reported in the literature. Up to 50 μg of $CaCl_2$ or $CuCl_2$ suppress the Al signal less than 10%.

W. Slavin*, **D. C. Manning, and G. R. Carnrick**, The Perkin-Elmer Corporation, Main Avenue, Norwalk, Conn. 06856
Anal. Chem., 53 (1981)

Determination of Insulin in Serum by Enzyme Immunoassay with Fluorimetric Detection 1509

Total incubation period is 45 min and limit of detection is 7.9 pM (46 pg/mL). Values correlate well with radioimmunoassay ($r = 0.97$).

William D. Hinsberg, III, Kristin H. Milby, and Richard N. Zare*, Department of Chemistry, Stanford University, Stanford, Calif. 94305 *Anal. Chem., 53 (1981)*

Inductively Coupled Plasma–BASIC Programmable Computer-Controlled Double Monochromator for Sequential Multielement Analysis 1512

The monochromator is directly programmable in BASIC through use of a master–slave microcomputer arrangement. Results of analyses of EPA water quality control reference standards and drinking water samples are reported.

James P. McCarthy, Michael E. Jackson, Thomas H. Ridgway, and Joseph A. Caruso*, Department of Chemistry, University of Cincinnati, Cincinnati, Ohio 45221
Anal. Chem., 53 (1981)

Two-Phase Mixed Indicator Titration Method for the Determination of Anionic Surfactants 1516

The method is extended to compounds containing less than 12 carbon atoms in the hydrophobic group by using 2:3 (v/v) chloroform:1-nitropropane as the organic phase and a multiple extraction–titration technique.

Zhi-ping Li and Milton J. Rosen*, Department of Chemistry, Brooklyn College, City University of New York, Brooklyn, N.Y. 11210 *Anal. Chem., 53 (1981)*

Nicolet announces MX-S:

Economical, Compact, Easy-to-Use FT-IR

Nicolet's MX-S now brings you the full analytical power of FT-IR for $26,750.* While offered at a price comparable to many dispersive IR spectrophotometers, the MX-S provides the intrinsic FT advantages of superior sensitivity, rapid sample measurement, absolute wavelength accuracy, and versatile spectral processing. These advantages enhance your analytical productivity and allow you to solve problems you previously found difficult or impossible.



Compact, rugged, durable. MX-S can be conveniently operated from a standard laboratory benchtop, requiring no utilities other than an electrical outlet. Its mechanical simplicity and durable construction provide reliable, trouble-free operation.

Versatile spectral processing. The MX-S incorporates a dedicated microcomputer with five data files, providing capabilities for storage and recall of several sample, reference, and background spectra; simplified multi-level spectral subtractions; automatic baseline correction; and highly versatile spectral plotting.

Friendly operation. You needn't be a computer wizard to become fully familiar with the MX-S. A convenient touch panel gives you access to all measurement, plotting, and data manipulation functions, as well as providing full system diagnostics. For most measurements, you simply insert the sample and press the SCAN function—the MX-S does the rest!

Extend your MX-S capabilities. The MX-S is available with a variety of optional accessories to fit your needs. You can add a Nicolet digital plotter, diskette spectral storage, library searching and quantitative analysis packages. For further data manipulations, spectral comparison, and remote control capabilities, you can interface the MX-S to a Nicolet color-graphics data terminal.

The affordable MX-S offers the performance you've come to expect from Nicolet, the leaders in FT-IR. Contact us for details.

NICOLET ANALYTICAL INSTRUMENTS

5225 Verona Rd. / Madison, WI 53711 / 608/271-3333 / Telex: 910-286-2736

*Introductory U.S. price effective through 1 December 1981. Please inquire for details on educational discounts, quantity discounts, or trade-in discounts.

Circle 152 for literature. Circle 153 for demonstration.

LEADERSHIP
LEADERSHIP
IN
HIGH RESOLUTION
CHROMATOGRAPHY
PRODUCTS



NEW
CATALOG!

- "Durabond" chemically bonded phases
- High Capacity Fused Silica Capillary Columns
- Capillary on-column injection conversions
- Split-splitless conversion kits
- Unique sample extraction/preparation devices
- Gas chromatograph protection systems
- Gas purifier and traps
- Graphite and graphitized Vespel* ferrules
- Stainless steel diaphragm pressure regulators and flow controllers
- and more to come

* Trademark E. I. DuPont

J&W SCIENTIFIC, INC.
SPECIALIZING IN HIGH RESOLUTION CHROMATOGRAPHY
3871 SECURITY PARK DRIVE, RANCHO CORDOVA, CA 95670 (916) 351-0387

CIRCLE 108 ON READER SERVICE CARD

Briefs

Atmospheric Pressure Active Nitrogen Afterglow as a Detector for Gas Chromatography 1519

The system is a selective detector for organomercury, lead, and tin species at trace levels, and a nonselective detector for organic molecules at nanogram levels. Comparison is made to other emission-selective detectors.

G. W. Rice, J. J. Richard, A. P. D'Silva, and V. A. Fassel*, Ames Laboratory and Department of Chemistry, Iowa State University, Ames, Iowa 50011 *Anal. Chem., 53 (1981)*

Adsorption of Sodium Mercaptoacetate on a Mercury Electrode 1523

The extent of adsorption and the surface coverage of the electrode are studied with electrocapillary data, linear sweep voltammetry, and cyclic voltammetry. Mercury(II) and mercury(I) mercaptide are weakly adsorbed, and mercaptoacetic anion is not adsorbed at all.

Robert S. Lawton and Alexander M. Yacynych*, Department of Chemistry, Rutgers, The State University of New Jersey, New Brunswick, N.J. 08903 *Anal. Chem., 53 (1981)*

Stopped-Rotation Voltammetry 1528

A current difference is measured between zero and high rotation speeds. Sensitivity, precision, mass-transport properties, and linearity of response are reported.

Joseph Wang, Department of Chemistry, New Mexico State University, Las Cruces, N.M. 88003 *Anal. Chem., 53 (1981)*

Reversed-Phase Liquid Chromatographic Determination of Phenols in Auto Exhaust and Tobacco Smoke as *p*-Nitrobenzeneazophenol Derivatives 1531

Limits of detection range from 0.02–2 ng. Phenol vapors (except for *p*-chlorophenol) at the low parts-per-million or parts-per-billion level in synthetic air samples are determined with relative standard deviations of less than 6.5%.

Kazuhiro Kuwata*, Michiko Uebori, and Yoshiaki Yamazaki, Environmental Pollution Control Center, 62-3, 1 Chome, Nakarnichi, Higashinari-ku, Osaka City 537, Japan *Anal. Chem., 53 (1981)*

Correspondence

Anion Peak Migration in Ion Chromatography 1535

Dennis Jenke, Montana Energy and MHD Research and Development Institute, P.O. Box 3809, Butte, Mont. 59702 *Anal. Chem., 53 (1981)*

Comparative Precision of Silver Inquartation Techniques 1536

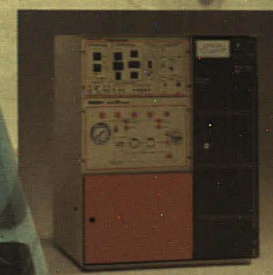
Patrick L. Beaulieu*, Brenda A. Keller, and Tamela R. Wortman, Nevada Mining Analytical Laboratory, Mackay School of Mines, University of Nevada—Reno, Reno, Nev. 89557 *Anal. Chem., 53 (1981)*

STOP LOSING TIME AND MONEY

SAVE TIME AND MONEY.
Now you can stop losing time and money when you do your ion analyses. Dionex Ion Chromatographs™ analyze more than 100 different ions at a fraction of conventional analysis times. The time and labor savings will drive down your costs per ion by 75% and more.

GET MORE OUT OF YOUR ANALYZER.
With multiple-ion analysis per injection and no sample pH limitation, Dionex Ion Chromatographs™ offer you unsurpassed versatility. Best of all, they simplify your procedures. No more complicated sample preparation. No special reagents necessary.

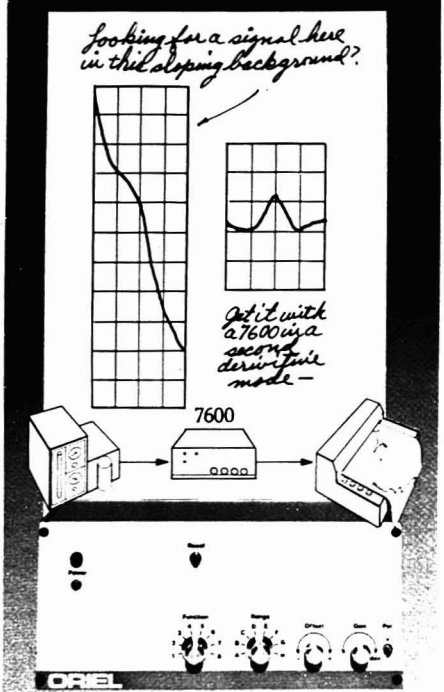
MOVE UP TO DIONEX QUALITY.
When you buy Dionex you are getting instruments of proven accuracy and sensitivity backed up by continuing applications support, complete maintenance services, and a commitment to research and development. To find out how Dionex can help you save time and money, call, write, or circle the reader service number.



DIONEX
Ion chromatography systems
1228 Titan Way, Sunnyvale, CA 94086 U.S.A.
(408) 737-0700 Telex 348-347
Worldwide sales and service
CIRCLE 53 ON READER SERVICE CARD

SEE OUR NEW PRODUCTS AT HET INSTRUMENT AMSTELHAL R-12/S-9.

MULTIFUNCTION
SIGNAL
PROCESSOR
by ORIEL



FUNCTIONS
Low Pass Filter ■ First Derivative
Second Derivative ■ Integrator
Peak Track And Hold ■ Running
Average ■ For Analog Signals
With Response Times Of
2 Milliseconds To 32 Seconds

The MODEL 7600 MULTIFUNCTION SIGNAL PROCESSOR is a simple to use microprocessor based instrument which is inserted between your sensor and display device. Your analog signals are operated on digitally by the microprocessor and converted back to analog for your recorder or other display device. Functions and response times are selectable by front panel switches.



For detailed brochure, write or call...

ORIEL CORPORATION
15 MARKET ST., STAMFORD, CONN. 06902 (203) 357-1600
ORIEL GmbH Im Tiefen See 58, D-6100 Darmstadt, FEDERAL REPUBLIC OF GERMANY Tel (06151) 82076
ORIEL S.A.R.L. 7 Rue Tréfilerie, 75011 Paris, FRANCE Tel 371-00-60
ORIEL SCIENTIFIC LTD. P.O. Box 126, Kingston-upon-Thames, Surrey, KT1 IQU, U.K. Tel 01 549-4525/549-9735
ORIEL S.R.L. Via Val di Sole, 10, 20141 Milano, ITALY Tel 02-5392188

CIRCLE 157 ON READER SERVICE CARD

Briefs

Aids for Analytical Chemists

Thin-Layer Spectroelectrochemical Cell for Nonaqueous Solvent Systems 1539

Rathbun K. Rhodes and Karl M. Kadish*, Department of Chemistry, University of Houston, Houston, Tex. 77004 *Anal. Chem., 53 (1981)*

Analysis of Fish and Sediment for Volatile Priority Pollutants 1541

Michael H. Hiatt, U.S. Environmental Protection Agency, Environmental Monitoring Systems Laboratory, P.O. Box 15027, Las Vegas, Nev. 89114 *Anal. Chem., 53 (1981)*

Standardization of Helium Carrier Gas for Helium Detector Applications 1544

Fikry F. Andrawes*, American Cyanamid Company, Stamford Research Laboratory, 1937 West Main Street, Stamford, Conn. 06904, and **Terry B. Byers**, Lockheed, 1830 NASA Road 1, Houston, Tex. 77058, and **Everett K. Gibson**, SN7/Geochemistry Branch, NASA-Johnson Space Center, Houston, Tex. 77058 *Anal. Chem., 53 (1981)*

Cooling System for High-Power Ion Lasers 1545

S. W. Edwards and J. F. Schetzina*, Department of Physics, North Carolina State University, Raleigh, N.C. 27650 *Anal. Chem., 53 (1981)*

Silanized Carbon Microneedle Emitters for Chemical/Field Ionization 1546

David F. Fraley and Maurice M. Bursey*, William Rand Kenan, Jr., Laboratories of Chemistry, The University of North Carolina, Chapel Hill, N.C. 27514 *Anal. Chem., 53 (1981)*

Elution of Adsorbed Organics from Graphitized Carbon Black 1548

Robert L. Petty, Marine Science Institute, University of California—Santa Barbara, Santa Barbara, Calif. 93106 *Anal. Chem., 53 (1981)*

Sample Introduction and Pressure Measuring System for Chemical Ionization Mass Spectrometers 1551

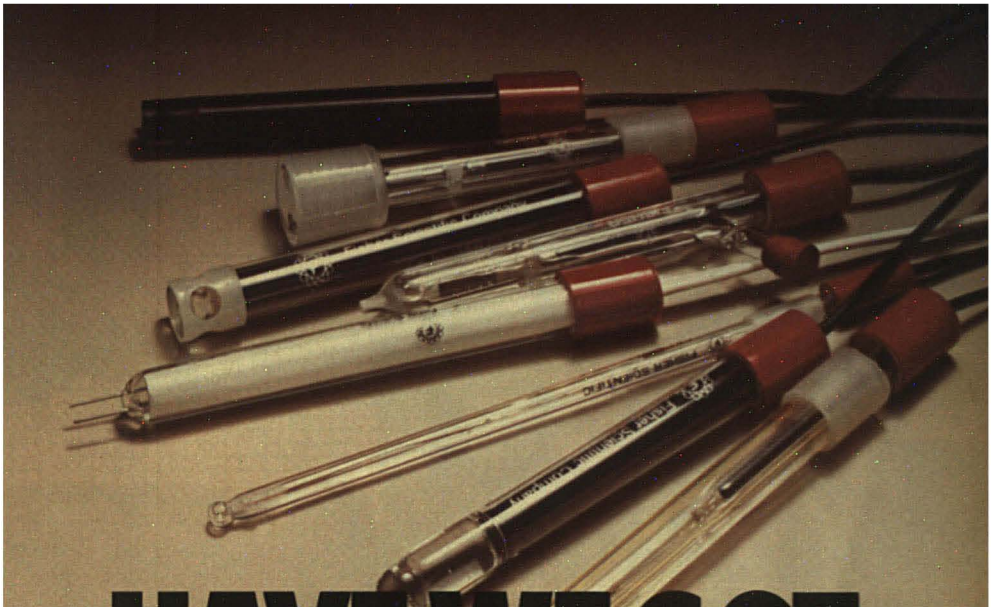
A. J. Illies and M. T. Bowers*, Department of Chemistry, University of California, Santa Barbara, Calif. 93106, and **G. G. Meisels**, Department of Chemistry, University of Nebraska—Lincoln, Lincoln, Neb. 68588 *Anal. Chem., 53 (1981)*

Correction. Smoothing of Digital X-ray Photoelectron Spectra by an Extended Sliding Least-Squares Approach 1552

Andrew Proctor and Peter M. A. Sherwood*, Department of Inorganic Chemistry, University of Newcastle-upon-Tyne, Newcastle-upon-Tyne, NE1 7RU, United Kingdom

Correction. Determination of Atmospheric Sulfur Dioxide without Tetrachloromercurate(II) and the Mechanism of the Schiff Reaction 1552

Purnendu K. Dasgupta*, Kymron DeCesare, and James C. Ullrey, California Primate Research Center, University of California, Davis, Calif. 95616



HAVE WE GOT POTENTIAL!

Indeed we do: fifty-plus specialized electrodes with the potential to give you fast response and precise measurements — right from the first. Made by Fisher with rugged, quality construction — so you can make use of their potential to the fullest.

Potentially perfect. Stringent quality control makes sure that Fisher Electrodes will meet your every expectation. We check 'em at each step of the manufacturing process, as carefully as you monitor your own lab procedures. Any imperfections or structural weakness in raw materials — like tubing or cable — mean immediate rejection. We take all the responsibility for the most critical parameters ourselves: filling solutions are mixed and tested in our own labs, and our pH-sensing glass membranes — made to an exclusive Fisher formula — must meet the strictest specs.

Potentials in action. After assembly, each and every Fisher Electrode is 100% tested in use. So you can be sure of solid, stable performance — and better-than-98% conformity to the theoretical response predicted by the Nernst equation. From the very first measurement you make.

The longevity potential. Our tough testing means we can make you this guarantee of performance: any Fisher Electrode that's properly matched to the sample, and regularly cleaned and maintained, will not fail in normal use due to materials or workmanship for one full year. Or we'll replace it at once.

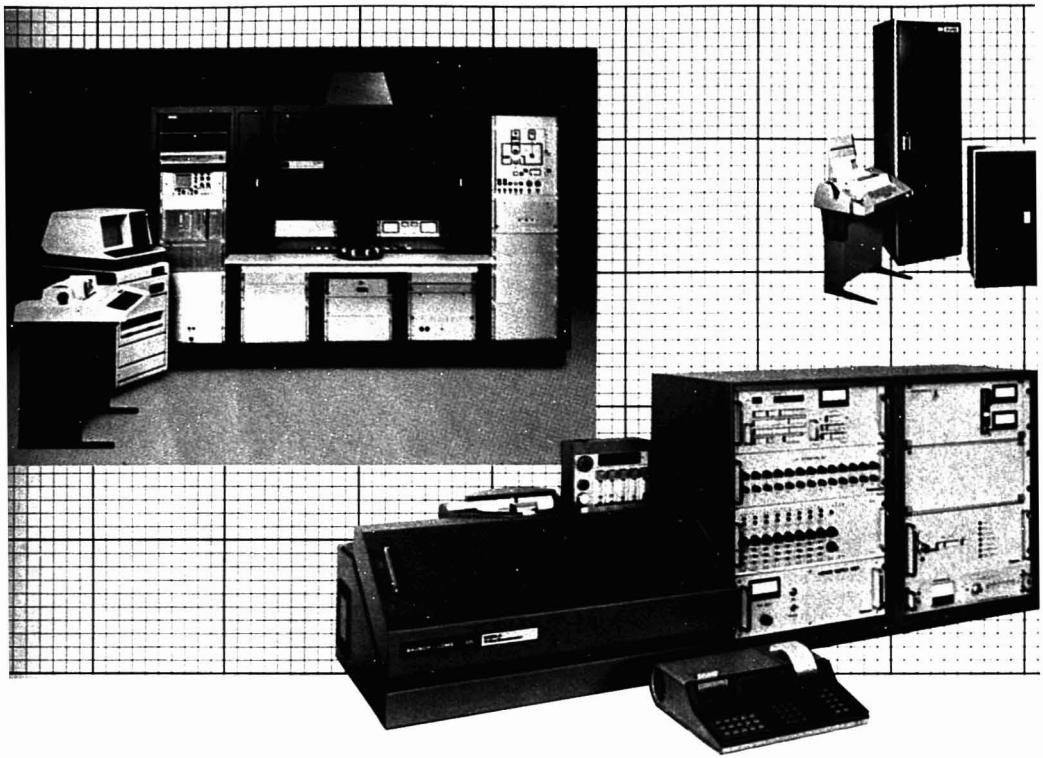
Get full potential from every Fisher Electrode. To get the most out of Fisher Electrodes, just treat 'em right. We'll help you get more measurement mileage — with a copy of the Fisher Electrode Handbook. It has all you need to know to keep your Fisher Electrodes working longer for you.

It tells how to select the right electrodes to match your samples. How to clean, maintain, unblock and even rejuvenate electrodes for renewed performance and extended life. And it includes a concise review of pH basics, plus complete specs for the Fisher Electrode line. It's yours free from the Electrode Experts at Fisher. Just ask your Fisher Representative — or call (412) 562-8543.

Fisher Scientific

CIRCLE 88 ON READER SERVICE CARD

New plot for high



Bausch and Lomb's Applied Research Laboratories Division now offers a comprehensive array of X-ray elemental analysis systems. Whatever your analytical needs — fluorescence or diffraction — you can optimize your instrument configuration and budget by selecting from ARL's complete grouping of modular instruments and support peripherals.

Unrivaled X-ray experience stands behind the world's largest capacity multichannel analyzer, the 72000S with thirty monochromator positions. Internationally, the 72000S has earned an unequalled reputation for reliability and throughput with a record of 98% uptime.

The 10-channel 74000 has proven equally reliable for the cement industry.

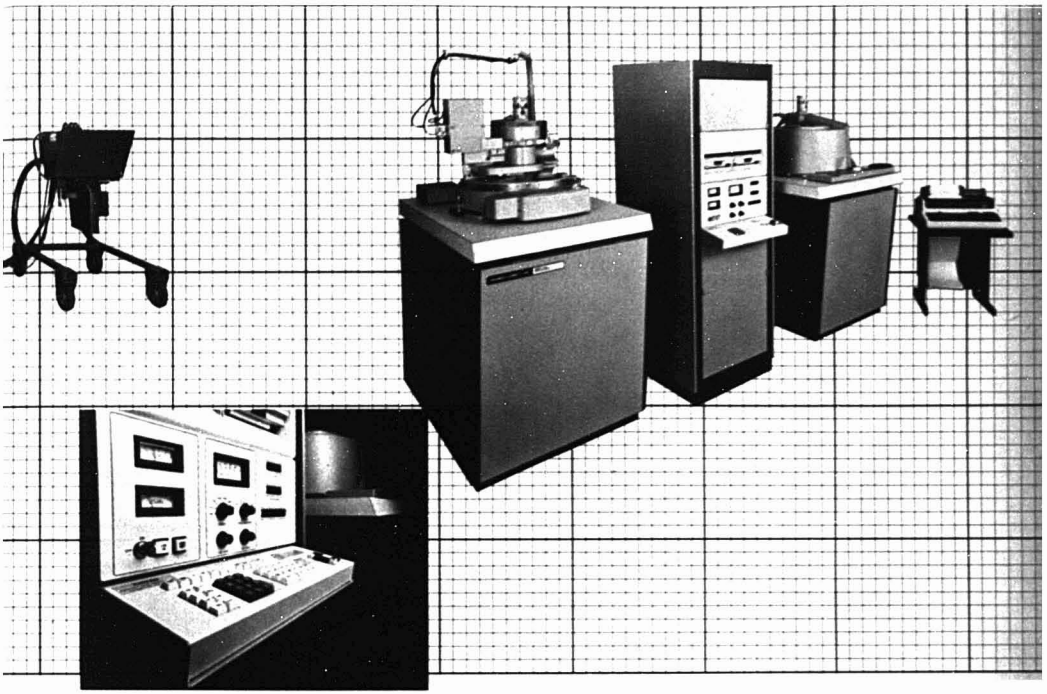
And now the same quality control expertise backs up the Chem-X benchtop unit. This new analyzer offers the accuracy, precision, resolution and speed of a true simultaneous wavelength dispersive instrument for the price **(under $100,000)** of an EDX or sequential spectrometer.

Engineered for maximum analytical efficiency, the Chem-X offers up to eight channels for simultaneous analysis and permits the user to change or add elements with quick, simple plug-in monochromators.

The 8565/8575 is a low cost, versatile sequential spectrometer featuring fully automatic microprocessor control and will perform unattended analysis of either 4 or 10 samples at a time. All instructions are entered simply and quickly on a straightforward keyboard. Printer and strip chart recorder are available as separate options.

The XRD-8535 Automatic X-ray Diffraction System provides precision analysis of compounds in solid or powdered form. Its rugged construction permits samples of up to 100 pounds. It operates at constant speed with continuous step scanning and high speed slewing. An optional sample holder provides automatic unattended analysis of up to 48 samples. Superior electronics include the latest microcircuitry, direct digital readout, keyboard control, microprocessor control and intensity collection.

performance X-ray systems.



Manual, semiautomated and fully-automated versions of spectrometer and diffractometer are available.

The A-6400 Automatic, on-line X-ray Emission Gage (XEG) system is a computerized process control sensor, especially useful for cement or other processes utilizing powdered materials. It keeps process materials under full-time quantitative surveillance on the production line, analyzing nearly 8,000 cc of sample material in an hour. Its great speed lets you take corrective action immediately, saving raw materials and reducing waste and costly out of spec products. Straightforward operation is under the control of a computer to convert sensor signals to weight percent concentrations. Results can be transmitted to a central process control computer for use in overall plant operation.

Modular in nature, many of ARL's X-ray system components can be combined to meet the specific needs of your laboratory or process. Our Aluminum Bath Ratio System for example combines state-of-the-art diffractometer and spectrometer with automatic computer control to greatly increase process efficiency through high speed precision analysis.

But, whether your need is for elemental calcium in under five seconds, benchtop simplicity, or the comprehensive reports of sequential and simultaneous analysis combined your proven source is ARL. Contact us now for full information.

Complete applications assistance, technical service, and scientific suppo are available internationally.

Applied Research Laboratories Division
9545 Wentworth Street
Sunland, California 91040
213-352-6011

En Vallaire
CH-1024 Ecublens
Switzerland
021/349701

BAUSCH & LOMB ARL

CIRCLE 3 ON READER SERVICE CARD



Scientech...The Price/Performance Leader In Electronic Balances

Scientech was first to introduce the beamless electronic balance back in 1968... and the first American company to extend balance capabilities by utilizing microprocessors.

Now Scientech leads again with the introduction of the Series 3300 which sets a new standard for electronic balances in terms of value, accuracy, dependability and ease of use.

There are five models in the series, some with dual ranges. Capacities range from 30g to 5kg with resolutions as fine as 0.001g. All feature instant electronic tare, digital and analog output, plug-in modular circuit boards for easy field servicing, and Scientech's exclusive circuitry that minimizes "digit flutter."

A universal command keyboard is available to enter and store data for complex conversions, averaging, parts counting and more.

Whatever your field, research, industry, quality control, pharmaceuticals or education, you're sure to find a Scientech balance that will help make you a leader too. Write for our brochure now.

SCIENTECH, INC.

5649 Arapahoe Avenue, Boulder, Colorado 80303 • (303) 444-1361 • TWX 910 940 0994

CIRCLE 195 ON READER SERVICE CARD

Letters

The Missionary Work of G. Frederick Smith

Sir: The late Professor G. Frederick Smith would undoubtedly be pleased to see what I believe was his original invention, the reflux cap for Erlenmeyer flasks, republicized (*Anal. Chem.* 1981, *53*, 750–51). He might be less than pleased, however, to learn that not everyone knows that these are available from the company he founded many years ago—the G. Frederick Smith Chemical Company, 867 McKinley Ave., Columbus, Ohio 43223. Two sizes are available—to fit the necks of 250-mL and 500-mL Erlenmeyer flasks.

G. F. Smith was both a pioneer and a missionary for the use of perchloric acid in wet-oxidation procedures to destroy organic matter in samples, a reaction he called the "liquid fire reaction." Those baptized in the perchloric acid faith know that the company he founded sells, in addition to specialty analytical reagents and perchlorates, apparatus for carrying out such digestions, and has published a variety of booklets on the use of those reagents and procedures. The missionary work apparently needs to be strengthened a bit in Idaho.

Laurance A. Knecht
Chemistry Department
Marietta College
Marietta, Ohio 45750

Reply

Sir: I was not "baptized in the perchloric acid faith" because at the time that Dr. Smith was "spreading the word," I was considerably less than 10 years old and had other interests.

However, since my second year of college, I have worked in six different analytical laboratories (government, military, private industry, and academic) and have not seen a reflux cap in use in any of them. Therefore, I believe that I was a reasonably representative member of that "new generation of analyst that seems to be unaware of the advantages of using the caps" (my phrase this time).

When I was faced with the task of developing a quick and efficient method of acid decomposing organic samples about a year ago, I quickly found that open beakers or flasks were not satisfactory digestion vessels. Some simple way of preventing spatter loss, conserving acid, keeping out the dust, and speeding up the operation was needed. After I had tried watch glasses, short stem funnels, etc., etc., for covering these flasks and had not been satisfied with the results, I discussed the problem with H.G. Brinkley (a professional glassblower with almost 30 years of experience) who made me a version of what I later discovered to be Dr. Smith's reflux cap.

It worked so well that I thought that publishing its description would be a service to the analytical community at large. It was only during the literature search undertaken during the writing of the "Aid" that I dug up that 1953 reference to the "liquid fire" reaction and found that I had been "scooped" over a generation ago—a fact duly noted in the article.

I made no claim to originality in the "Aid." Failure to find the caps in the scientific glassware offerings of several purveyors of laboratory supplies indicated to me that their use had never really caught on. Neither the editorial staff of the JOURNAL nor the reviewer(s) had apparent knowledge of the ready availability of these gadgets.

The point in writing the "Aid" was to remind practicing analysts that these caps are useful in simplifying a very commonly required, often tedious laboratory procedure. It is nice that *somebody* is still making the caps commercially; however, they are trivially easy to make in the laboratory itself by anyone with a passing acquaintance with elementary glassblowing (I have made them myself).

Incidentally, other correspondents pointed out that SGA Scientific Company (735 Broad St., Bloomfield, N.J. 07003) and Hach Co. (57th St. and Lindbergh Parkway, Loveland, Colo. 80537) also make similar reflux caps. I'm proud to be carrying on Dr. Smith's missionary work out here in the hinterlands—no one else is.

Darryl D. Siemer
Exxon Nuclear Idaho Company
P.O. Box 2800
Idaho Falls, Idaho 83401

Instrumental Methods vs. Wet Chemical Methods

Sir: In regard to the letter by E.L. Kothny appearing in ANALYTICAL CHEMISTRY, 1981, *53*, 15 A, I must say that there are some points on which I disagree with the author. It is true that wet chemical preparation is still the major time factor in an instrumental analytical procedure. However, these wet chemical steps have also been shortened by instrumentation in some cases.

For instance, despite their complications, electrothermal graphite atomizers can function as digesters to eliminate undesired matrix components before the final detection step, saving the time involved in a classical type of digestion. There are continuous optical and electronic developments in atomic absorption spectrometry for better background correction to render analytical separations unnecessary for some samples. Other instrumental systems could also be mentioned. Chromatograph/spectrometer systems have reduced wet separation procedures by hours, down to minutes in some cases.

After all, it would not be fair to hold instrument manufacturers completely responsible for instrumental developments. Although some companies make important contributions, I prefer to believe that major discoveries and/or developments for analytical instrumentation are still performed in research laboratories other than those of commercial manufacturers.

O. Yavuz Ataman
Department of Chemistry
Middle East Technical University
Ankara, Turkey

Bonded Phases—Users Must Know Changes in Manufacturing Recipe

Sir: Two recent papers by Hansson and Trojer (*J. Chromatogr.* 1981, *207*, 1) and Atwood and Goldstein (*J. Chromatogr. Sci.* 1980, *18*, 650), respectively, have confirmed some of the suspicions of workers using octadecyl bonded silica for liquid chromatography.

Two facts emerge: One is disappointing, the other most disturbing. Atwood and Goldstein show that manufacturers have not yet succeeded in producing consistent materials. Hansson and Trojer produce different evi-

dence from pyrolysis GC of packings that reveals that some differences are produced by changes in the recipe of manufacture, which can only occur by deliberate action.

While we are disappointed (though sympathetic) that manufacturers have failed to control the many production variables well enough, we are extremely disturbed to find evidence of fundamental changes such as different silanes being used.

Have manufacturers considered the implications for users who are trying to follow Good Laboratory Practices? And even those who are not legally bound by such codes face similar difficulties if they are to count themselves professional analysts.

If an analytical method cannot rely at all on the bonded phase material, then each batch used (or each column when using prepacked columns) must be retested for separation and quantitation of all components—the full method validation development procedure. Following this would be catastrophic for sample throughput in a laboratory, and for transfer between laboratories of any pharmacopoeial or other regulatory analytical method.

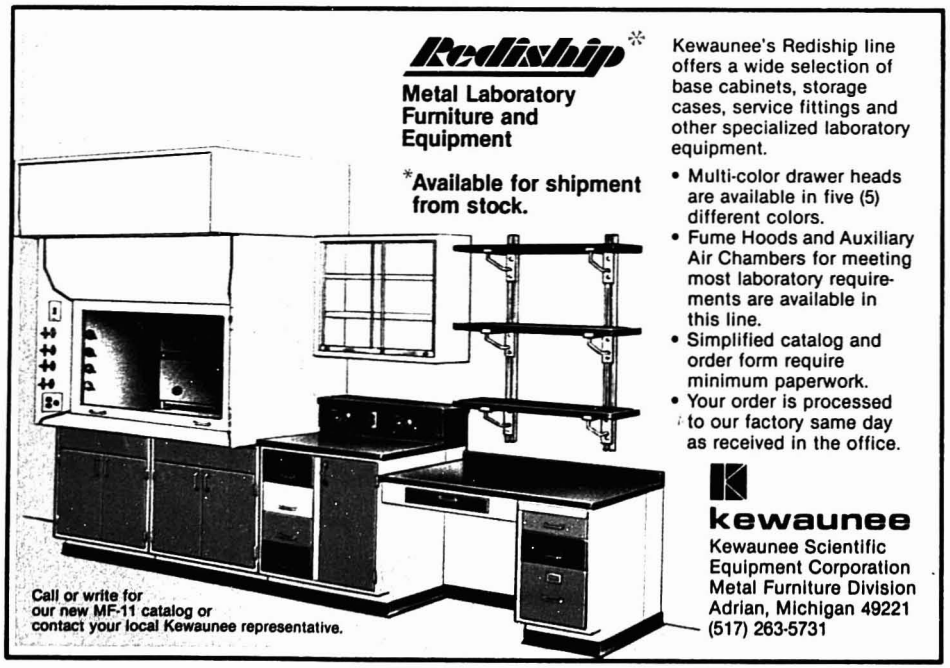
We believe that the profession should censure any manufacturer who knowingly changes its recipe for bonded phases without making this clear to the users, at least by a change in designation. We are not opposed to improvements or changes, but we must know when they are made.

P. A. Bristow
P. N. Brittain
Imperial Chemical Industries Ltd.
Hurdsfield Industrial Estate
Macclesfield Cheshire SK10 2NA
England

Sir: As the authors of one of the papers cited above we strongly support the call by Bristow and Brittain for more information from manufacturers of LC column packing materials concerning changes of recipe. We further believe that manufacturers should publish meaningful lot-to-lot tolerances on the separation factor of each material in a sufficient number of different separations to characterize the lot-to-lot variation of each of its principal retention mechanisms. Users need these data to design rugged analytical methods, but only the manufacturers have access to a sufficiently large number of lots made to the same recipe to obtain the long-term means and standard deviations that result from the recipe.

Our results, referred to by Bristow and Brittain, show that even in material made using the same recipe, different retention mechanisms vary substantially and independently from lot to lot, necessitating tests with a number of well-chosen pairs of compounds to expose all the variations. Ominously, we also found one test pair that not only totally concealed lot-to-lot variation in separation factor for the C_{18} material we tested, but also made five of eight other commercially available C_{18} materials appear identical, while better-chosen test pairs showed that they were widely different. So it is important to deliberately choose test compounds that expose variations. A poorly chosen test pair can conceal even an inadvertent change of recipe.

John G. Atwood
Jane Goldstein
The Perkin-Elmer Corporation
Norwalk, Conn. 06856



CIRCLE 122 ON READER SERVICE CARD

Our pH meters put you out front. Our services back you up.

Introducing our new line of pHI-series meters. With advanced technology that's right on the button.

Like the microprocessor that handles the whole analysis. You don't even have to know the temperature, buffer value or when to take a reading—it's all done automatically. And done faster and less expensively with no sacrifice in precision.

Our pHI-series meters also have a built-in self-diagnostic function that tells you if there is a problem in the procedure, the electrode, or the instrument itself.



There are four meters in the line: the pHI 30, the pHI 60, the pHI 70 and the pHI 71. Each has its own unique features.

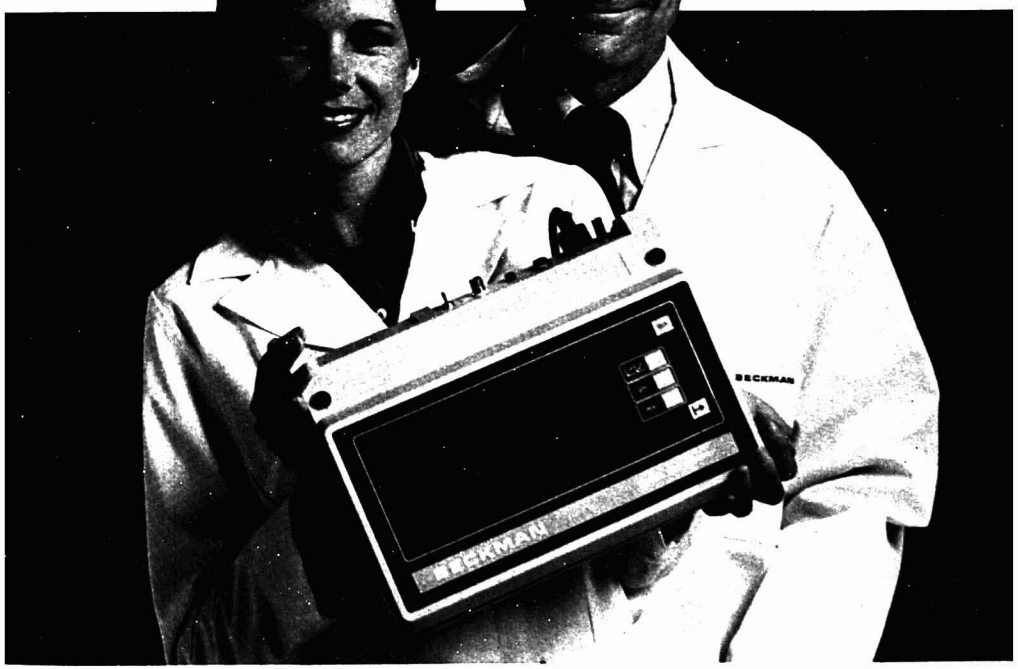
And each is backed up by Beckman's unique brand of sales and service. Which is to say, more extensive than you can get anywhere else.

For openers, there's the Hotline which you can use 24 hours a day to get an answer to your question. And there are applications chemists to help you get more out of your meter.

For closers, there are salespeople who know their business and yours so they can serve you better.

And our extensive experience in pH is behind you all the way. With all this advanced technology and backup going for you, it's no wonder that you're way ahead when you choose a Beckman pHI-series meter.

For more information, contact your local Beckman representative. Or write: Scientific Instruments Division, Beckman Instruments, Inc., Box C-19600, Irvine, CA 92713.



BECKMAN

CIRCLE 25 ON READER SERVICE CARD

"If only I'd known about Scott!"



John Dalton had been able to order Scott gases when formulating his law of partial pressures, he could have spent more time philosophizing about those little things he called atoms.

Today's chemist is better off by far. He need only pick up his Scott Specialty Gases Catalog to obtain any one of 32 pure gases in 5 different grades. Not to mention 129 2-component and 19 3-component mixtures in an infinite number of concentrations.



Or, if one doesn't want to bother with large, heavy cylinders, one can order Scotty® gases in disposable containers: 17 pure gases and 99 stock gaseous mixtures, some with as many as 9 components. And having called Scott, one can return to the bench for continuing researches into one's own modern version of "chemical calculus."

If you have never thought much about who supplies your gases, think about Scott. Scott is a specialist in research gases, calibration gas standards and mixtures, and gas handling equipment. Request your free copy of the 160-page Scott Specialty Gases Catalog today. You will find it a useful tool.

Scott Specialty Gases
a division of Scott Environmental Technology Inc
Plumsteadville, PA 18949 • 215: 766-8861
San Bernardino, CA 92411 • 714: 887-2571
Troy, MI 48084 • 313: 589-2950

3A

CIRCLE 193 ON READER SERVICE CARD

Editors' Column

Computer-Aided Editorial Operation

ANALYTICAL CHEMISTRY is setting up a microcomputer system to improve all phases of its editorial operation. The system was initially developed for *Biochemistry* by Lorrin Garson of the Research and Development Department, ACS Books and Journals Division, and has been in operation there since 1979. Since editorial offices of all peer-reviewed journals have many common features, the system is being adopted with a few minor modifications and improvements to meet some of our unique requirements.

The purpose of automating is to streamline essentially all phases of the peer review operation. But we hope to improve particularly two important areas. With more than 2800 reviewers in our files, it now is almost impossible to make the best use of the information in these files. Inevitably some reviewers who are familiar to the editors are overused and others who are not so familiar are underused. We hope the system will allow a wider choice of reviewers, and thereby relieve overused reviewers. Secondly, the system will enable us to better scrutinize a reviewer's performance. On a weekly basis, it will automatically generate a list of overdue reviewers for prodding. This will be a tremendous improvement over the current practice in which the entire file is manually checked weekly. The system will also allow us a look at a particular reviewer's entire review history.

As a first step, we have developed a classification scheme for the specialty areas of analytical chemistry. The specialty areas are divided into five major designations of: (1) electroanalytical chemistry, (2) separations, (3) spectrometry, (4) other techniques, and (5) applications. And these are subdivided into 197 categories. All of ANALYTICAL CHEMISTRY's reviewers have been asked to fill out a questionnaire consisting of a listing of these 197 categories. Reviewers were asked to designate a maximum of 15 areas of expertise in order of competence. The letter accompanying the questionnaire was mailed on May 4, 1981, and responses are still being received as of this writing although at a somewhat diminished rate. We plan to send a second mailing to nonrespondents as well as to reviewers whose names have been added since the first mailing. Contributors who have not been sent the questionnaire are urged to contact the editorial office for a copy if they wish to participate in the peer review process. The information provided in the questionnaire will be processed and stored in the system to allow a "close matching" of a reviewer's expertise with the subject areas of a given manuscript under review.

"Close matching" here should not be confused with straightforward one-to-one matching. What it means is that the editor in choosing reviewers will be able to recall all reviewers with closely matching expertise. The final selection from the list will as always depend on many factors such as work load, availability, conflict of interest, promptness, familiarity with editorial goals, etc.

The computerized reviewer file will include names, addresses, telephone numbers, area of expertise, editor's comments, dates not available for reviewing, and reviewer recommendations concerning manuscripts. It will also include the manuscript number and dates sent and returned.

The manuscript file will include the manuscript number, the abbreviated title (up to 88 letters), the names and addresses of the corresponding author, the manuscript receipt date, the names of reviewers assigned, the dates sent and returned from the reviewers, the type of revision required, dates sent for revision and returned after revision, and finally, publication date. We will be able to store up to 13 000 manuscript records.

A program will be developed in the near future to access manuscript records via any author and not just by the corresponding author. Some of the other programs we plan to develop after the system is in full operation include a capability to access an individual author or reviewer's publication records for papers published in ANALYTICAL CHEMISTRY and a capability to provide keyword indexing for all papers received.

While the system is being installed and for at least a full year after its implementation, we intend to maintain our current hard copy files. We have no doubt that there will be an initial period of trial and error, but we are confident that ultimately this new system will improve the editorial operation for the benefit of all contributors.

Barbara Cassatt

Gilson and HPLC have come together. We've developed a modular system using our state-of-the-art components...designed for easy set up, operation and maintenance.

Our system is ideally suited to your research needs as well as dedicated routine analyses. And, computer compatible modules will allow future system expansion capabilities.

The key system components are:

New Model 302 Pump. The only microprocessor controlled pump offering flow rates of .005 to 100 ml/min up to 6000 psi with *both* flow and dispense modes.

Model 111 UV Detector. Precision monitoring of LC effluents is a Gilson trademark. This versatile dual beam detector operates at either 254 or 280 nm. A choice of flow cells is available.

Model 801 Service Module. This innovative unit holds 3 solvent vessels. A 4-position stream selection valve allows easy solvent selection for gradient formation or column regeneration. An LED bar graph continuously indicates your system's pressure. A pulse dampener and pressure-limit controls are standard features.

Many other system accessories are available, including sample injection valve and recorders.

Gilson's modular, computer-compatible, and innovative designs will answer your HPLC needs now and in the future. Get in touch!



GILSON
INTERNATIONAL

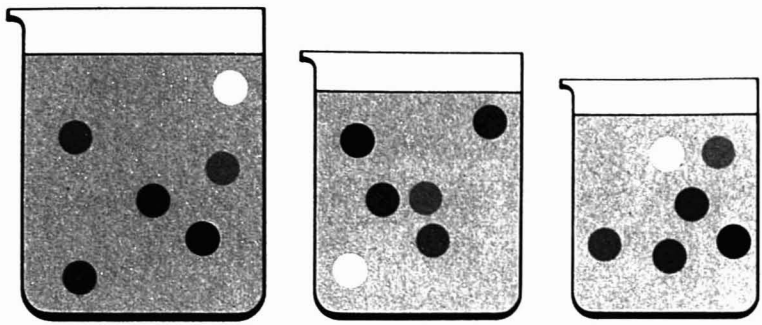
Gilson Medical Electronics
Box 27 • Middleton • WI 53562 • U.S.A. • Telephone (608) 836-1551

Gilson Medical Electronics (France) S.A.
B.P. No. 45, 95400 • Villiers-le-Bel, France • Telephone 990.54.41

When the Warranty runs out on your Gilson, Gilson won't run out on you.

CIRCLE 89 ON READER SERVICE CARD

F. W. Karasek
R. E. Clement
J. A. Sweetman
Chemistry Department
University of Waterloo
Waterloo, Ontario N2L 3G1
Canada



Preconcentration for Trace

To successfully conduct many analyses for organic compounds present at trace concentrations in gas, liquid, or solid samples, it is necessary to selectively extract these compounds and use a concentration step prior to analysis. Many of the techniques developed for preconcentration are described in specialized books and reviews (*1*, *2*); a number appear in works on headspace analysis (*3*). Because of the diversity of this subject, it was felt that an exhaustive review and treatment of all these techniques would not be manageable in this REPORT. Therefore, our discussion will be confined primarily to methods we have found workable and useful for analysis of trace organic constituents in environmental samples.

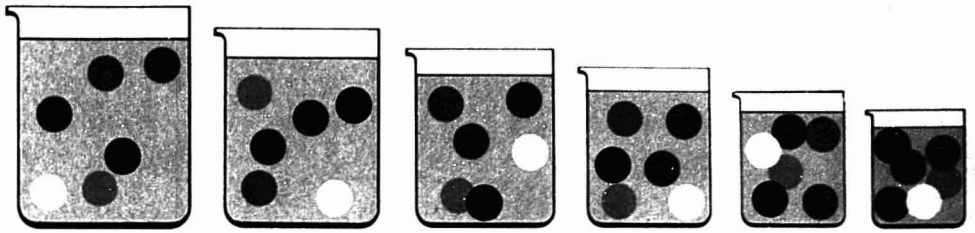
A complete scheme for trace analysis of organic compounds generally consists of sampling, extraction, preconcentration, prefractionation, and analysis by gas chromatography (GC), and gas chromatography/mass spectrometry (GC/MS). Determination of organics at parts-per-trillion (ppt) levels can be performed by combining sensitive and selective detection with sample preconcentration. In many instances, limits of detection can be made arbitrarily small by increasing the degree of preconcentration. The preconcentration step is often an integral part of the sampling and extraction procedure. For example, in the standard method for analysis of atmospheric airborne particulate matter, large volumes of air are drawn through a filter to obtain a sample. This represents simultaneous sampling and preconcentration. After extracting the sorbed organics from the collected particulates, a second preconcentration step is performed before analysis. If interfering components must be removed from the sample matrix, one or more prefractionation steps may be required in the procedure.

Preconcentration procedures are especially important for samples derived from the environment. Many toxic or carcinogenic compounds are distributed in the environment from a wide variety of sources. Because of their serious effects at low levels, it is necessary to achieve the greatest analytical sensitivities possible for these substances to properly assess their environmental impact. In some cases, detection limits as low as a few ppt are required. In addition to the polynuclear aromatic hydrocarbons (PAHs), much attention has been focused on many halogenated pollutants such as pesticides, polychlorinated biphenyls (PCBs), trihalomethanes (THMs), and the polychlorinated dibenzofurans (PCDFs) and dibenzo-*p*-dioxins (PCDDs). Such substances can be found in air, water, and solid and biological samples. Although the extraction and preconcentration procedures may vary for different sample types, problems of sample losses, contamination, interferences, and reproducibility must be considered for all preconcentration methods. Most preconcentration techniques fall into two classes: solvent extraction followed by solvent reduction, or sorbent trapping with subsequent solvent elution or thermal desorption. There are many variations of these methods, and they are frequently used in combination.

Solvent Extraction and Preconcentration

Sample preconcentration by solvent reduction is most frequently performed following the extraction of solid and biological samples by liquid partition. Proper choice of the extracting solvent can often be the critical step in the sample preparation procedure. It is not always correct to assume that a solvent that efficiently removes a compound from one sample matrix will recover the same compound from a different sample type. This was recently demonstrated by a study that compared the relative efficiencies of various solvents for extraction of organic compounds from municipal incinerator fly ash (*4*). Methanol, which had been found to have a very high extraction efficiency for organics on airborne particulate matter (*5*), demonstrated very poor recoveries for organics from fly ash using Soxhlet extraction. Figure 1 illustrates the poor recoveries for the tetrachlorinated dibenzo-*p*-dioxins (TCDDs) from municipal incinerator fly ash using methanol. The top trace of Figure 1 is a GC/MS selected ion monitoring (SIM) analysis of a methanol extract from fly ash using the characteristic 321.9 *m/z* ion of the TCDD isomers. The bottom trace shows results obtained for the same fly ash sample by following the methanol extraction with a benzene extraction. Both extractions were accomplished using a Soxhlet apparatus for 20 cycles with 200 mL of each solvent. This clearly illustrates that no preconcentration step can give adequate re-

0003-2700/81/A351-1050$01.00/0
© 1981 American Chemical Society



Analysis of Organic Compounds

sults for quantitative work unless the initial extraction technique gives high, or at least known and reproducible, recoveries of the desired compounds from the initial sample.

Prior to the GC/MS analyses (shown in Figure 1) of the benzene and methanol extracts from fly ash, each extract was concentrated by a factor of 2000 by removing solvent using a rotary evaporation apparatus. Figure 2 shows one such unit, although several other types are available commercially. Solvent containing the extracted compounds is rotated in a flask partially submerged in a water bath. The water bath can be maintained at temperatures lower than the normal boiling point of the solvent by reducing the internal pressure of the rotary evaporator using aspirator suction. Volatile components will be largely lost in this procedure. However, for many applications the compounds of interest are nonvolatile compared to the extracting solvent. In these applications the rotary evaporation technique is rapid and straightforward, although severe losses of even nonvolatiles can be experienced without careful sample handling. Table I shows the recoveries of components of a standard mixture that was spiked into 200 mL of benzene solvent and then reduced to its original volume (100 μL) by rotary evaporation. Losses of these magnitudes are not uncommon when reducing sample sizes to such small volumes. A major problem exists in the physical handling of the sample. Very small volume losses to the glass walls of the recovery flask or to the disposable glass pipets commonly used for sample transfer may result in significant and nonreproducible component loss.

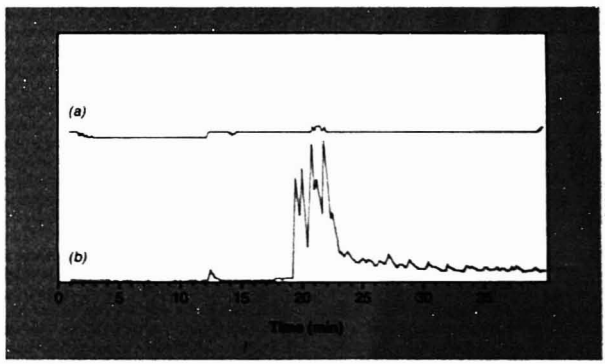


Figure 1. Selected ion monitoring analysis of tetrachlorodibenzo-*p*-dioxins in fly ash; a and b are plotted with the same full-scale values. (a) Methanol extraction. (b) Benzene reextraction of a

Table II shows recoveries of total organic compounds after spiking 200 mL benzene with 100 μL of a concentrated fly ash extract and then concentrating to the original 100-μL volume of the spiked extract by rotary evaporation. The peaks detected by GC were divided into three categories: early-eluting compounds with GC elution temperatures less than 150 °C, middle-eluting compounds (150 to 230 °C), and late-eluting compounds with GC elution temperatures greater than 230 °C. The large losses of the early, more volatile components demonstrate the difficulties of using rotary evaporation preconcentration for compounds of high or medium volatility. To obtain the original concentrated fly ash extract, an initial rotary evaporation step was performed, which caused losses of many of the volatile compounds prior to the additional losses reported in Table III.

Many recovery studies have been reported in the literature. There is a large variation between some studies in which similar preconcentration procedures were employed, even though very reproducible results were obtained for each individual study. Recoveries of PAH compounds, for example, have been reported as being

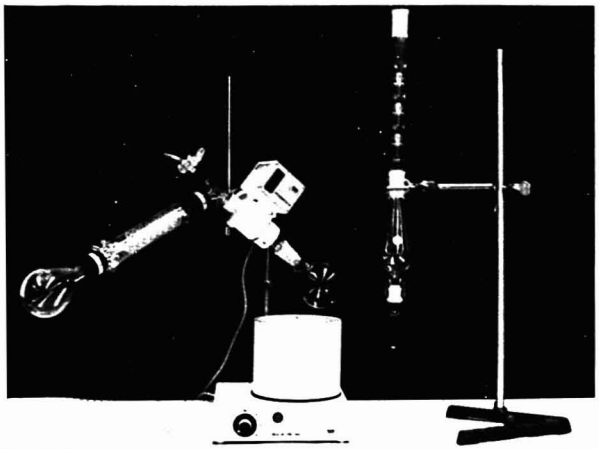


Figure 2. Apparatus used for solvent reduction. Left: rotary evaporator. Right: Kuderna–Danish concentrator with Snyder column

from 70 to 95%. When performing recovery studies, several replicates should be performed. In applications involving frequent analyses, recoveries need to be checked periodically, particularly when modifications to the procedure are made or if the analyses are to be performed by someone inexperienced with the procedure. New batches of solvent should always be checked for levels of trace impurities when used in procedures requiring preconcentration of the solvent extract before analysis.

Several studies have reported the use of correction factors to allow for the organics lost during extraction and preconcentration. For such applications it is important that the range of recoveries for different replicates be examined, and not just the mean recovery and standard deviation. Although the overall recovery may be acceptable, a single experimental value can easily vary by 30–50% from the expected value, especially for the determination of organics at ppb or lower concentrations. One method of coping with this problem is to spike the sample before extraction and concentration with an isotopically labeled standard that is at a concentration similar to the compound to be determined. For example, ^{37}Cl-labeled 2,3,7,8-tetrachlorodibenzo-*p*-dioxin (TCDD) has been used in the determination of this compound (*6*). During the analysis by GC/MS–SIM, the labeled TCDD can be determined with the nonlabeled TCDD by monitoring the *m/z* 321.9 ion (nonlabeled) and the 327.9 ion (labeled TCDD) in a single GC/MS analysis. The use of labeled substances is expensive and not practical for analysis of a large number of compounds, but is well-suited for special applications such as the analysis of TCDD.

Solvent Concentration

Figure 2 also shows the apparatus that is most often used as an alternative to the rotary evaporation method. The Kuderna–Danish evaporative concentrator equipped with a Snyder column also operates by solvent distillation. However, it is a more effective concentrator for compounds of higher volatility. Since the concentrator is operated at ambient pressure, the rising vapors must build up sufficient pressure to force their way past the stage of the Snyder column. Each stage consists of a narrow opening covered by a loose-fitting glass insert. Since the vapors are slow to work their way through the different stages of the Snyder column, there is initially a large amount of condensation of these vapors, which returns to the bottom of the Kuderna–Danish apparatus. Besides continually washing the organics from the sides of the glassware, the returning condensate also contacts the rising vapors and helps to recondense volatile organics. Although this process is slower than the rotary evaporation method, higher recoveries of trace organics can generally be obtained. In Table III recoveries are reported of standard compounds when concentrated from an initial volume of 100 mL to 1 mL using both the rotary evaporation and Kuderna–Danish concentration methods (*7*). The solvent used in this study was chloroform, and 33 μg of each compound in

Table I. Percent Recoveries of Standard Mixture from Rotary Evaporation Using Gas Chromatographic Peak Areas

Compound	Retention time (min)	Percent recoveries
1. n-$C_{12}H_{26}$	1.87	13
2. n-$C_{18}H_{38}$	13.73	70
3. Diethyl phthalate	14.27	73
4. Phenanthrene	16.79	67
5. 9-Fluorenone	17.32	66
6. Methyl anthracene	19.42	71
7. Dibutyl phthalate	22.56	75
8. Fluoranthene	24.01	73
9. Pyrene	25.12	73
10. n-$C_{24}H_{50}$	27.28	74
11. Dioctyl phthalate	34.37	77
12. bis(2-ethylhexyl)-phthalate	37.83	74
13. $C_{30}H_{62}$	38.20	74
14. Benzo[*a*]pyrene	40.67	74
15. n-$C_{36}H_{74}$	52.46	74

Table II. Recovery of Total Organic Compounds in Municipal Incinerator Fly Ash Extract Concentrated by Rotary Evaporation

Sample	Micrograms Detected[1] by GC-FID		
	Early Peaks[2]	Middle Peaks[2]	Late Peaks[2]
Fly ash extract original solution	1600	7500	1300
Original solution after recovery from rotary evaporation	640	6800	1200
Percent recovery	40	91	92

[1] Based on total GC-FID peak areas and estimated average response factor of 400 area counts/ng
[2] Early peaks, elution times <15 min; middle peaks, 15–35 min elution times; late peaks, elution times >35 min

Table III. Recoveries of Organic Compounds Using Rotary Evaporation and Kuderna–Danish Preconcentration Methods (Ref. 7)

Compound	Percent recoveries: Rotary evaporation	Percent recoveries: Kuderna–Danish
n-hexadecane	89	92
Naphthalene	86	91
Phenol	85	90
Acenaphthene	89	91
Dibenzofuran	88	92

Table IV. Percent Recoveries Using GC/MS Analyses of Selected Compounds after Evaporation/Reconstitution of Benzene Extract of Incinerator Fly Ash

Compound	Replicate 1	Replicate 2
Pentadecane	95	96
Octadecane	95	78
Heneicosane	99	92
Tetracosane	98	90
Dibutyl phthalate	92	91
Dioctyl phthalate	86	89
Biphenyl	67	62
Pentachlorobenzene	95	97
Anthracene	95	90
Pyrene	91	88
Benzopyrene	90	98
Tetrachlorinated dibenzodioxins	91	88
Pentachlorinated dibenzodioxins	89	86
Hexachlorinated dibenzodioxins	91	87
Heptachlorinated dibenzodioxins	97	80
Octachlorodibenzo-*p*-dioxin	90	80

Table III was spiked into the initial 100 mL of solvent. Although giving better recoveries than the rotary evaporation method, the Kuderna–Danish apparatus is slower and requires the use of more delicate and specialized equipment. Also, the recovery vessel of the Kuderna–Danish apparatus is more susceptible to violent solvent eruptions that can lead to large sample losses.

Concentration to a final volume of less than 1 mL is seldom accomplished in one step. Samples are usually concentrated to 5–10 mL and then transferred to a micro-Snyder column evaporator to further reduce the volume to 1.0 mL or less. Final volume adjustment or preconcentration to volumes as low as 0.1 mL can be performed by the gas stream–water bath method. This is accomplished by passing a gentle gas stream over the surface of the sample until the desired volume is reached. Gas flow must be gentle to prevent nebulization losses. High-purity air, nitrogen, and helium gases should be used to avoid the introduction of artifacts. During the evaporation, sample cooling will be experienced, and the sample is normally placed in a warm water bath to speed the evaporation process.

Concentration to these low volumes is possible with the micro-Snyder column, but care must be taken that the sample is not boiled to dryness. Large sample losses with the gas stream–water bath method are often associated with organic residues that are left on the glass walls of the concentrating vessel as the solvent level decreases. Once the final volume is reached, it is possible to recover most of these organics by rinsing down the glass surface with the remaining sample using a microliter syringe. Some losses will still be experienced, but will not be critical as long as the composition of the organics remaining on the glass surface is identical to the composition of the organics in solution. Alternatively, sample volume can be reduced to below 100 μL, and small amounts of fresh solvent can be used to wash the glass surface until the desired volume is reached. Measurement of final volumes as low as 0.1 mL can be accomplished by performing the evaporation step after transfer to a graduated vial such as the reacti-vial (Pierce Chemical Co., Rockford Ill.). Several such vials are available commercially. However, the graduations on the vial should be checked by calibration with clean solvent using a microliter syringe.

Many reported preconcentration procedures require the complete evaporation of the initial solvent, usually for the purposes of changing to a second solvent during sample clean-up or for sample storage. Since the largest and most irreproducible losses occur for sample concentration to volumes less than 0.5 mL, reduction below this quantity should be avoided. Even the most gentle evaporation will result in significant sample loss when allowed to continue to dryness. Table IV shows the losses obtained for different compounds when aliquots of a concentrated benzene extract of municipal incinerator fly ash were allowed to evaporate to dryness in a reacti-vial and then were reconstituted to the original volume (8). Evaporation was accomplished using very gentle conditions. The screw caps on the sample vials were loosely fastened, and the vials were allowed to stand in a fume hood at ambient temperatures. To reconstitute the organic residues, fresh solvent was added by washing down the glass surface of the vials. Since no sample handling or transfer was performed, except the initial transfer to the storage vials, the losses reported in Table IV can be attributed to the evaporation to dryness of the benzene extracts. It is not known whether losses are primarily due to volatilization of sample components or irreversible adsorption on the vial walls. If the sensitivity of the instrumental method employed is great enough, it would be best to preconcentrate samples to no less than 1 mL final volume.

Solvent Purity Problems

In addition to the problem of sample losses when preconcentrating trace organics in organic solvents, severe sample contamination may be experienced at any step in the preparation procedure. It is especially important to use the best available solvents, since impurities in the solvent will be concentrated as well as sample components. A recent study compares impurity levels in some commercially available solvents (9). The purity of distilled-in-glass grade solvents was found to be superior to that of pesticide grade solvents. However, the impurity levels for even the distilled-in-glass solvents were observed to vary for different batches from the same manufacturer. Figure 3 shows the impurities revealed by a GC analysis after distilled-in-glass grade cyclohexane was concentrated by a factor of 2000 (200 mL to 100 μL) using rotary evaporation. The concentrations of contaminants are significant enough to interfere in the analysis of organic compounds at the ppb level. The individual impurities are not identical to those observed in other batches of this solvent. Table V shows the nature of impurities identified by GC/MS analysis for solvents from different sources.

Benzene is one of the cleanest solvents available. Because of its toxicity, many laboratories are unable to use benzene. In terms of extraction efficiency, toluene is comparable to benzene, but the batches of toluene tested in this laboratory have all contained high levels of trace organic contaminants. Preconcentrations by a factor of 2000 of distilled-in-glass grade benzene obtained from different manufacturers have consistently produced

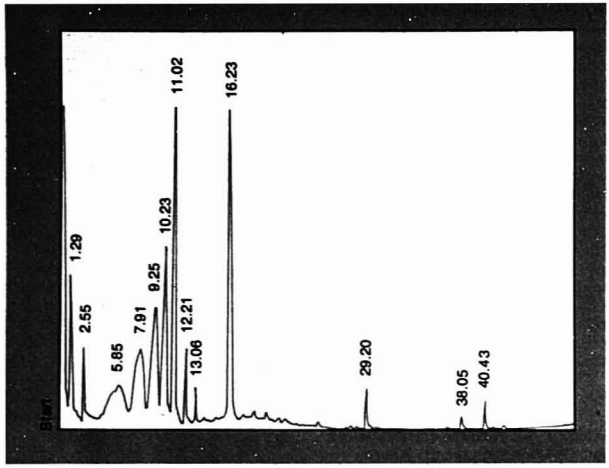


Figure 3. Gas chromatogram of 2000-fold concentrate of distilled-in-glass grade cyclohexane showing solvent impurities

acceptably low levels of impurities during several years of extractions performed in our laboratory. Solvents of initially high purity may become contaminated during storage. This is particularly true for solvents stored in bottles that are not equipped with Teflon liners. It has been demonstrated that organic impurities from the glue holding foil liners to the bottle caps will very rapidly migrate to the solvent (*10*).

Preconcentration with Sorbent Traps

Although the solvent extraction–solvent reduction methods will continue to be important for trace organic analysis of solid samples, there are many applications for which these procedures are not adequate. Most of these other applications are for the analysis of trace organic compounds in air or water. For these sample matrices the sorbent trap preconcentration technique offers combined sampling and preconcentration, and reduced sample handling. In this technique, a hollow tube is filled with an adsorbent material that selectively retains the desired organic compounds as sample volumes of air or water are passed through the adsorbent. Trapped organics can then be eluted from the adsorbent by using a small amount of solvent, or removed by thermal desorption if the compounds have sufficient volatility. Considerable effort has been directed to the study of a wide variety of adsorbent materials for application to the analysis of different compounds in air or water (*11*). Some of the more common adsorbent materials include macroreticular XAD resins, polyurethane foams, activated carbon, and Tenax-GC.

The choice of the proper sorbent material is determined by the compounds of interest, the amount and type of sample, and the desired method of analysis. For water samples, XAD resins have been a popular choice. The XAD series of resins is a product of the Rohm and Haas Company. These resins are hard insoluble spheres of 16–50 mesh available in differing polarities. Each bead is formed from microbeads cemented together during polymerization, giving the resins their macroreticular, controlled pore size structure. XAD-2 and -4 are nonpolar styrene–divinylbenzene copolymers of differing pore size and surface area. XAD-7 and -8 are slightly polar acrylate esters. XAD-2 resins have been found to give good recov-

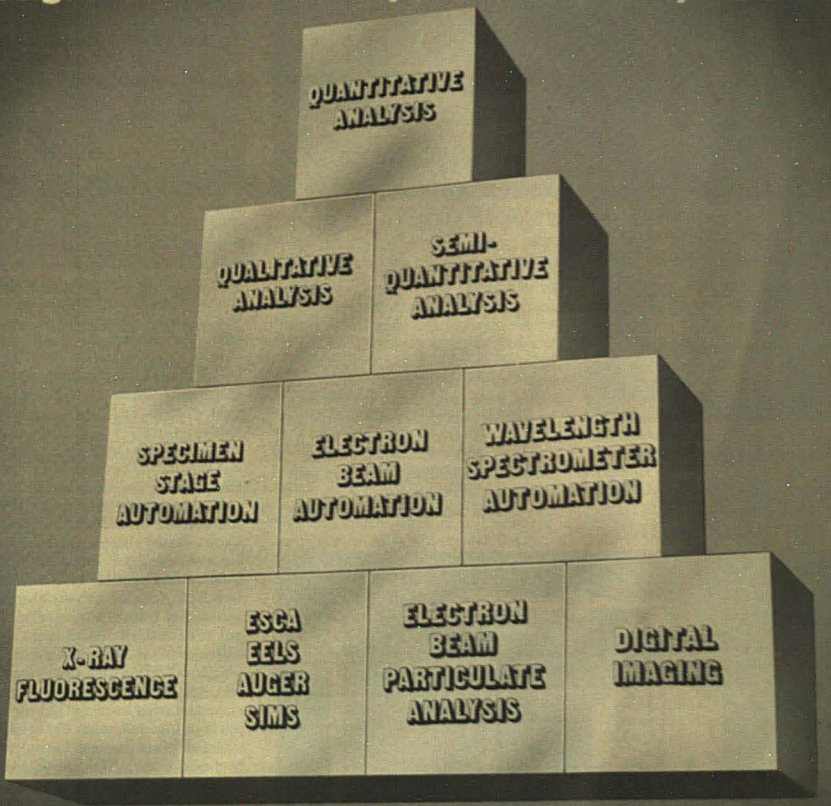
Table V. Identities and Concentrations of Organic Compounds in Solvents by GC/MS after 200-fold Concentration

	A		B		C	
Solvent	Compound	ng/mL	Compound	ng/mL	Compound	ng/mL
Cyclohexane	$C_9H_{12}O$	49	Diethyl phthalate	3.5	*n*-Butyl *n*-butyrate	29
			Dioctyl phthalate	1.8	Tributyl phosphate isomer 1	2.9
					Tributyl phosphate isomer 2	0.9
Methylene chloride	none	—	Diethyl phthalate	0.5	1,1,1-Trichloropropane and	16
			Dibutyl phthalate	7.7	1,2,3-Trichloropropane	
					1,1,1,2-Tetrachloropropane	21
					Tetrachloroethane	1.9
					Phthalic anhydride	0.4
					Dioctyl phthalate	14
Methanol	none	—	none	—	1,4-Bis(methylene)cyclohexane	1.6
					2,6-Dimethylphenol	2.6

A: Caledon Laboratories (Georgetown, Ont. Canada), distilled-in-glass grade; B: Burdick and Jackson (Muskegon, Mich.), distilled-in-glass grade; C: Fisher Scientific (Fairlawn, N.J.), pesticide grade

SYSTEM 2000

The most expandable x-ray microanalysis system ever designed . . . with unsurpassed ease of operation.



Why face tomorrow's challenges with instrumentation designed for yesterday's problems? SYSTEM 2000 incorporates a unique "building-block" design that allows the user to expand capabilities as needs grow . . . from qualitative elemental identification through fully computer-controlled operation.

Tracor Northern

2551 West Beltline Highway
Middleton, Wisconsin 53562
(608) 831-6511
TWX-910-280-2521

TRACOR EUROPA B.V.
P.O. Box 333
3720 AH BILTHOVEN
The Netherlands
Telephone: (030) 780855
Telex: 70775

CIRCLE 206 ON READER SERVICE CARD

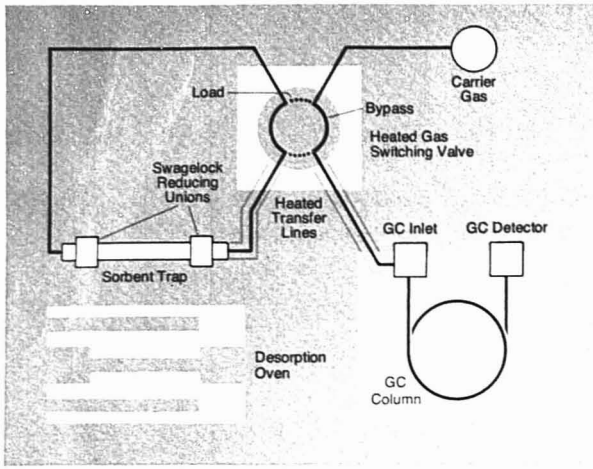


Figure 4. Thermal desorption apparatus used to perform a GC analysis for organic compounds concentrated on sorbent trap

eries for a wide range of neutral compounds in the ppb range in water, including alcohols, PAH, halogen compounds, and, after acidifying the water, organic acids and phenols (*12*). The homogeneous surface of the macroreticular resin with its low energy binding process (van der Waals forces) allows quantitative desorption of the organics sorbed from the water sample. The organics may be readily eluted with a small amount of a water-miscible solvent, usually diethyl ether or methanol. This property contrasts favorably with activated carbon, where physical and chemical adsorption mechanisms may occur on the heterogeneous surface, preventing quantitative desorption.

Since the final eluate volume may be further concentrated, the previous discussions on solvent purity and Kuderna–Danish concentration apply here also. In addition, prior contamination of the resins must be assumed and careful conditioning is necessary.

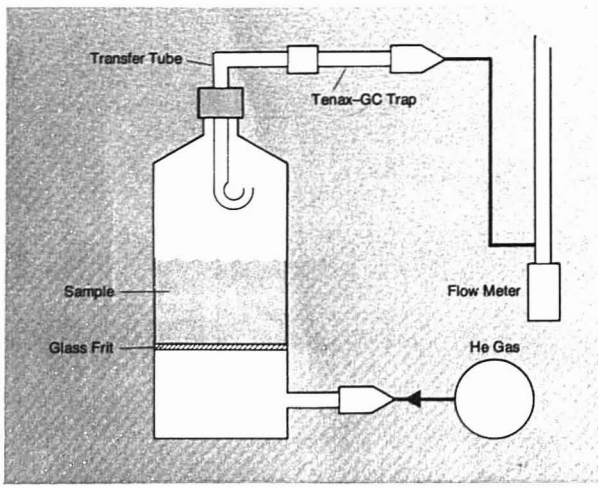


Figure 5. Purge and trap device used to purge and concentrate volatile organic compounds from liquid samples

For the XAD resins, sequential 8-h Soxhlet extractions with methanol, acetonitrile, and diethyl ether have been recommended to remove contaminants. After cleaning, the resins must be kept wet to avoid fracturing of the resin in which new surface contaminants are exposed. Reactions of the resin with inorganic constituents in the sample cannot be overlooked. In a study of organobromine compounds formed during the chlorination of estuarine cooling waters, some of the brominated hydrocarbons found were considered to be artifacts formed by active chlorine, bromide ion, and hydrocarbon impurities from the XAD resins, released by fracturing of the resin during sampling (*13*).

Following sorbent trap concentration with solvent elution of the organic species and solvent reduction, only a small aliquot of the sample is needed for injection into the GC or GC/MS for analysis. Thermal desorption of a sorbent trap directly onto a GC column gives only a single sample of the total collected organics for analysis. For XAD resins used for concentration of organics from water samples, the entrained water presents a problem. Thermal desorption of XAD-2 resin has been accomplished by employing an intermediate Tenax trap (*14*). Tenax–GC is a porous polymer material based on 2,6-diphenyl-*p*-phenylene oxide. The XAD trap is thermally desorbed onto the Tenax tube. A gas flow is maintained until the water exits the hydrophobic Tenax trap, leaving the organics behind.

For many applications, particularly the analysis of trace organic pollutants in air, Tenax alone is used to concentrate the organics. In fact, using this method it is possible to detect several hundred organic compounds in atmospheric air from sampling at almost any urban site. Tenax is more thermally stable than the divinylbenzene polymer XAD resins, which have been reported to outgas extraneous compounds during heating. The air sample is pumped through the trap containing Tenax that has been previously conditioned by heating with an inert gas flow. The trap is sealed and returned to the laboratory for desorption and analysis. A desorption apparatus assembled from readily available parts is shown in Figure 4. The gas switching valve allows carrier gas to flow through the GC column uninterrupted while the sorbent trap is inserted. The desorption oven is made in two sections, allowing it to be quickly clamped around the trap. The carrier gas is then diverted through the trap as it is rapidly heated. Organic compounds are thus desorbed into the inlet of the GC column held at a low temperature. A temperature-pro-

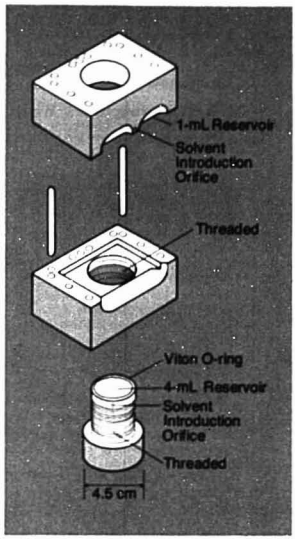


Figure 6. Teflon block apparatus for extraction of organic compounds from particulates collected on small dichotomous filter elements. The filter element is sealed in the block cavity in contact with the solvent reservoirs, and extraction is conducted by ultrasonic agitation. The solvent extract is then removed and concentrated by a factor of 100 or more prior to GC/MS analyses

grammed GC analysis can then be initiated. Uniformly heated transfer lines are critical features of the desorption apparatus. Cold spots will cause condensation of the less volatile compounds, resulting in incomplete transfer and loss of GC resolution.

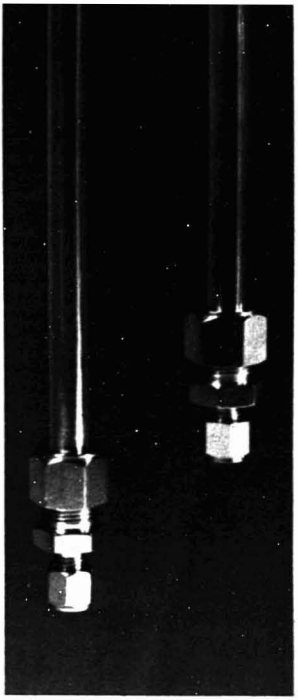
For the analysis of trihalomethanes in water, a purge and trap method followed by thermal desorption has proved to give reliable quantitation (*15*). The method can be used successfully for quantitation of compounds that are <2% soluble in water and with boiling points below 200 °C (*16*). Only qualitative information can be obtained for very water soluble compounds.

Figure 5 shows a simple purge and trap device. The liquid sample chamber is formed by the glass frit, which serves to disperse the inert gas for efficient sparging of the sample. The gas containing the purged organic compounds then exits through the Tenax trap where the organics are retained. The apparatus may be heated to increase the purging of less volatile organics. The required volume of purge gas is a function of the volatility of the compounds of interest and how well the compounds are retained by the Tenax trap. Compounds with low trap retention may saturate the trap and be vented before the high boiling materials are quantitatively purged. Two separate samples with different purging volumes and temperatures may be necessary to analyze a sample containing compounds with a wide boiling range. The trap is desorbed and analyzed as discussed previously. The dynamic nature of the purging technique gives improved precision and sensitivity over the static head space method in which the atmosphere above the sample with its equilibrium partition concentration of organics is analyzed. A variation on the purge and trap technique has been described by Grob (*17*), who used activated carbon as the adsorbent medium and eluted with carbon disulfide.

Conclusion

Preconcentration techniques such as solvent reduction by evaporation, sorbent trapping and desorption, and purge and trap are the basic tools used in sample preparation for trace organic analysis. Other preconcentration methods that have been used include freeze drying, steam distillation, and reverse osmosis. A major problem with all of these techniques is the lack of environmental standards, so that realistic recoveries from the extraction and preconcentration procedures can be determined. In the case of solid samples, simply adding a known quantity of a standard to the sample before sample preparation does not ensure that the added standard will be in the same matrix as sample molecules. A good example of this is incinerator fly ash particles. These particles have been shown to consist of small spheres encapsulated by larger spheres. Added standards will not be able to penetrate the outer surface of these spheres, and therefore may not be representative of organics as they exist in the matrix. No single preconcentration procedure is sufficient for the wide variety of applications in trace organic analysis. However, existing methods are available to give acceptable recoveries of organics for most applications. The methods described here can be used individually, in combination, or may be modified for a particular application. Many variations of these basic methods have been reported.

Work is being performed on the development of sorbent traps for different applications that will selectively trap specific organics and then allow quantitative recovery of these compounds by solvent elution or thermal desorption. Figure 6 illustrates a device currently being developed to provide a sample suitable for GC/MS



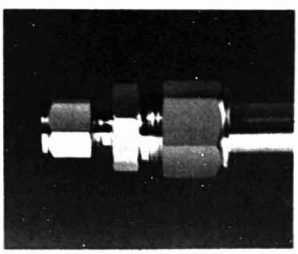
Quality HPLC Columns at a Savings

Quality HPLC Columns for under $100 and off-the-shelf delivery. What could be nicer? Available are silica, CN, NH_2, C8 or C18 columns.

Send for specifications on these HPLC columns and we'll send you a 216 page chromatography catalog that could make your lab life easier.

Call 312 948-8600 or write 2051 Waukegan Road, Deerfield, Illinois 60015

ALLTECH ASSOCIATES

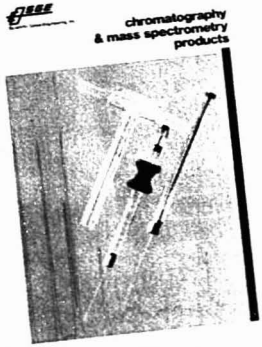


CIRCLE 1 ON READER SERVICE CARD

The Complete Chromatography and Mass Spectrometry Products Catalog

Scientific Glass Engineering's new 1981 product catalog is now available and free for the asking. This new catalog includes the complete line of SGE products for chromatography and mass spectrometry.

- capillary columns
- splitters
- graphite ferrules
- valves
- jet separators
- carrier gas purifiers
- syringes
- GLT



To receive your SGE catalog, contact your nearest Scientific Glass Engineering office or distributor.

SGE

Head Office
Scientific Glass Engineering Pty. Ltd.
7 Argent Place, Ringwood,
Victoria, 3134
Australia
Tel: (03) 874-6333

U.S.A. Sales Office
Scientific Glass Engineering, Inc.
2007 Kramer Lane, Suite 100
Austin, Texas 78758
U.S.A.
Tel: (512) 837-7190

U.K. Sales Office
Scientific Glass Engineering (UK) Ltd.
657 North Circular Road
London, NW27AY
Great Britain
Tel: (01) 452-6244

German (BRD) Sales Office
Scientific Glass Engineering Gmbh.
Fichtenweg 15
D-6108 Weiterstadt 1.
Tel: (06150) 40662

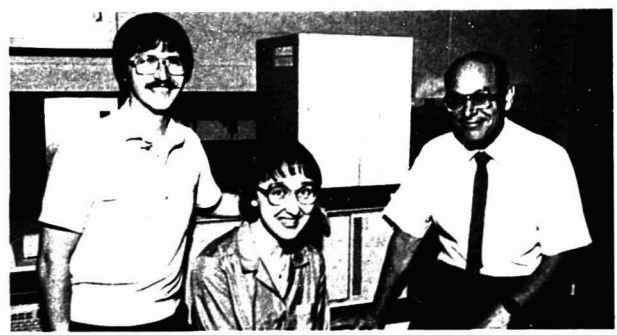
CIRCLE 196 ON READER SERVICE CARD

analysis of the organic constituents of environmental particles collected by the dichotomous filter (*18*, *19*). This is an especially difficult task because the total amount of solid sample available from these small sample elements is in the subnanogram range. The largest problem yet unsolved is reduction of high levels of impurities introduced by a viton O-ring gasket.

There is much room for improvement in existing procedures. Design of the glassware used for rotary evaporation and Kuderna–Danish concentration can be further improved to reduce the inside surface area. Extraction procedures can often be modified to reduce extraction times and the volume of solvent used. Surface adsorption of organics might be reduced by developing truly deactivated glass surfaces. In any given procedure, the analyst must strive for reproducibility, since variability in results is still primarily affected by skill in the basic techniques of sample rinsing, transfer, and consistency during every step of a preconcentration procedure.

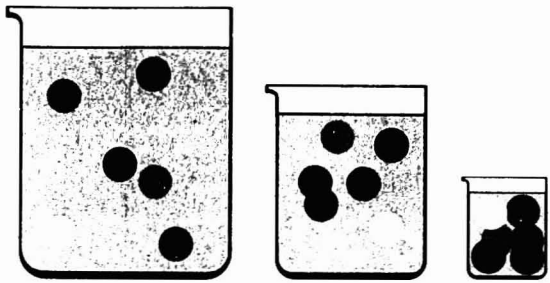
References

(1) Dunges, W. "Prechromatographic Micromethods"; Dr. Alfred Huthig Publishers: New York, in press.
(2) Hertz, H. S.; May, W. E.; Wise, S. A.; Chesler, S. N. *Anal. Chem.* **1978**, *50*, 428 A.
(3) Kolb, B., Ed. "Applied Headspace Gas Chromatography"; Heyden & Son Ltd.: London, 1980.
(4) Clement, R. E.; Cook, R. M.; Karasek, F. W. Paper presented at 1981 Pittsburgh Conference on Analytical Chemistry and Applied Spectroscopy, Atlantic City, N.J., March 9, 1981; Abstract No. 137.
(5) Hill, H. H., Jr.; Chan, K. W.; Karasek, F. W. *J. Chromatogr.* **1977**, *131*, 245.
(6) Harless, R. L.; Oswald, E. O.; Wilkinson, M. K.; Dupuy, A. E., Jr.; McDaniel, D. D.; Tai, H., *Anal. Chem.* **1980**, *52*, 1239.
(7) Webb, R. G. "Isolating Organic Water Pollutants: XAD Resins, Urethane Foams, Solvent Extraction"; EPA Report EPA-660/4-75-003, June, 1975 p 15.
(8) Bowers, W. D.; Parsons, M. C.; Clement, R. E.; Karasek, F. W. *J. Chromatogr.* **1981**, *207*, 203.
(9) Bowers, W. D.; Parsons, M. L.; Clement, R. E.; Eiceman, G. A.; Karasek, F. W. *J. Chromatogr.* **1981**, *206*, 279.
(10) Denney, D. W.; Karasek, F. W.; Bowers, W. D. *J. Chromatogr.* **1978**, *151*, 75.
(11) Keith, L. H., Ed. "Identification and Analysis of Organic Pollutants in Water"; Ann Arbor Science: Ann Arbor, Mich., 1976.
(12) Junk, G. A.; Richard, J. J.; Grieser, M. D.; Witiak, D.; Witiak, J. L.; Arguello, M. D.; Vick, R.; Svec, H. J.; Fritz, J. S.; Calder, G. V. *J. Chromatogr.* **1974**, *99*, 745.
(13) Bean, R. M.; Riley, R. G.; Ryan, P. W. In "Water Chlorination Environmental Impact and Health Effects"; Jolley, R. L.; Gorchev, H.; Hamilton, D. H., Jr., Eds.; Ann Arbor Science, Mich., 1978; Vol. 2, p 223.
(14) Chang, R. C.; Fritz, J. S. *Talanta* **1978**, *25*, 659.
(15) Otson, R.; Williams, D. T.; Bothwell, P. D. *Environ. Sci. Technol.* **1979**, *13*, 936.
(16) Bellar, T. A.; Lichenberg, J. J. *J. Am. Water Works Assoc.* **1974**, *66*, 739.
(17) Grob, K.; Grob, K., Jr.; Grob, G. *J. Chromatogr.* **1975**, *106*, 299.
(18) Karasek, F. W.; Parsons, M. L. "Development of Microextraction Procedures To Analyze Total Carbon and Organic Compounds from Dichotomous Filters"; EPA Grant #R807-028-01, Research Triangle Park, N.C., May 1980.
(19) Bowers, W. D. "Ultratrace Organic Analysis of Dichotomous Filters Using GC and GC/MS Techniques"; PhD Thesis, Arizona State University, May 1981.



Raymond Clement (left) and Janet Sweetman are seen with Francis Karasek in his laboratory at the University of Waterloo, where they work together on analytical methods development for trace organic constituents of environmental samples. Clement, a Natural Sciences and Engineering Research Council (Canada) postdoctoral fellow, received his doctorate at the University of Waterloo; Sweetman's doctorate was earned at the University of Michigan. Current new interests include development of computer software to enhance the selectivity of GC/MS techniques, analysis of atmospheric aerosols for particle size distribution, determination of organic constituents with piezoelectric crystal cascade impact instrumentation, and fundamental studies of ion mobility spectrometry.

Report



Donald E. Leyden
Department of Chemistry
University of Denver
Denver, Colo. 80208

Wolfhard Wegscheider
Institute for General Chemistry, Micro- and Radiochemistry
Technical University of Graz
Graz, Austria

Preconcentration for Trace Element Determination in Aqueous Samples

The need for preconcentration of trace elements or ions in aqueous solution results from the fact that instrumental analytical methods often do not have the necessary selectivity, sensitivity, or freedom from matrix interferences. Certainly it is observed that analytical methods, instrumental and otherwise, often do not meet the specifications claimed by early developers and proponents. This is not to be taken as a condemnation of the other analytical techniques that have been developed in recent decades, but only a statement that, as much as analytical chemists strive to develop the ultimate methodologies, they have to date fallen short of this goal.

In fact, to contradict an earlier statement, the chemistry is not gone from analytical chemistry (*1*). As an illustration of the point, during a recent lecture attended by one of us, the speaker made a great issue over the fact that the standards for his powerful emission spectroscopic technique were prepared without any need to match the matrix of his intended samples. This is indeed an attractive feature of a method. However, as the author described the digestion, the redissolution, and the other procedures involved in preparing the sample, it became increasingly clear that the sample *was* matrix matched to the standard. Again, this is not to criticize the need for such actions, as the results justified the entire procedure.

The point of these comments is to illustrate that there is a need to combine chemical procedures with the powerful instrumentation we use. In our particular research, X-ray spectrometry is used on a routine basis. This technique offers the advantage of well-understood spectroscopic principles and the capability of providing simultaneous multielement determinations. On the other hand, it has the distinct disadvantage that it does not have sufficient sensitivity for the low-level determinations necessary for many of today's analytical problems. The combination of such a well-understood instrument with preconcentration techniques extends the range of application of this instrument in a rather substantial manner. Taking an example such as the inductively coupled plasma optical emission spectrometer, which does provide great sensitivity and large linear dynamic range, one often finds that it is necessary to isolate the analyte from the matrix. The chemical techniques used in preconcentration can provide, in many cases, analyte isolation, as well as enrichment factors. Examples will be given later of the extension of such powerful techniques, both in range of concentration and in the types of matrices that can be investigated.

The concept of sample preconcentration prior to determination should imply many capabilities other than just concentration enrichment. As mentioned above, the minimization of matrix effects may be accomplished. For example, methods that will be discussed below are applicable to the isolation of trace elements from seawater at very low concentrations indeed. Many of the methods of sample enrichment can also be used simultaneously as sampling techniques. Applications of stationary phase concentration tools have been made in the sampling process for the determination of trace elements in seawater. In some cases these stationary phases may be used for the analytical determination directly, and in other cases the elements must be stripped from them. In many cases preconcentration carries a connotation of eliminating the possibility of automated analyses. On the contrary, in some cases preconcentration/sampling techniques can actually lead to the application of simpler instrumentation in the final measurement, thereby facilitating automated analyses. The purpose of this REPORT is not to discuss preconcentration as an alternative to the use of modern instrumentation; rather it is to offer it as a supplement to these methods. This paper will present some of the common methods employed

0003-2700/81/A351-1059$01.00/0
© 1981 American Chemical Society

today for sample preconcentration of trace ions in an aqueous solution prior to their determination. We will attempt to present examples of the application of preconcentration techniques prior to the utilization of a variety of analytical finishes, and will also offer critical comments concerning the various preconcentration methods discussed.

Evaporation of Solvents

Perhaps the simplest method of preconcentration of ions from solution is evaporation of the solvent. This technique has been applied to X-ray spectrometry using conventional wavelength dispersive techniques (2) and proton induced X-ray emission (3). In the case of commercial wavelength dispersive X-ray spectrometry, the potential of evaporation techniques is very limited. Considering a nominal detection limit of 0.1–0.01 μg on a thin film sample, greater than 10–100 mL of water must be evaporated in a confined spot to achieve precise analyses at the ppb level. It is not necessary to take the sample to dryness; however, it is common practice for convenience. In the case of X-ray methods applied to samples where one element is high but variable in concentration (such as iron in certain river waters), evaporation would not be suitable because of the effect of the major element upon the intensity of emission from more minor constituents. Fractional crystallization can lead to microscopically inhomogeneous residues. Matrix effects may be amplified rather than minimized. Therefore, for practical analyses of water samples, evaporation techniques offer little promise, whether X-ray or other instrumental methods are used.

Electrodeposition

A method that would appear to be extremely useful for preconcentration of metal ions is electrodeposition. This technique offers many of the properties described above for a desirable method of preconcentration. Electrodeposition found wide applications several years ago and was used extensively for electrogravimetry (4), an early preconcentration method. Deposition of metals into mercury cathodes, followed by distillation of the mercury to yield the concentrated metals, is one useful approach. Perhaps one of the most valuable and widely applied electrochemical preconcentration techniques is anodic stripping analysis (5). Anodic stripping analysis combines the electrodeposition of metals into a mercury cathode (concentration step) with a current measurement when the mercury electrode is scanned in the anodic direction and the concentrated metal is oxidized. The advantages of electrodeposition are that few reagents need be added and the instrumentation is simple. In some cases, internal electrolysis may be accomplished by preparing a galvanic cell, using the sample solution with an inert electrode as one cell and an electrode of a more electropositive metal as the second cell. Spontaneous deposition of the sample ions occurs when the two electrodes are shorted and the solutions joined by a salt bridge (6). The major disadvantage of the electrodeposition techniques is that they are, by and large, very slow, although very little operator attention is required during the deposition. When fresh water is used, an inert supporting electrolyte must be added to increase the current-carrying capability of the solution. If high currents are forced through the solution to speed up the deposition, gas evolution occurs and loose, mossy deposits of the metal may result.

There have been some successful reports of preconcentration on graphite using laboratory-simulated freshwater samples (7), and using an in situ deposition of metals from sea water (8). In the first study, 2–40 μg each of copper, mercury, zinc, nickel, cobalt, and chromium in 15 mL of solution were electrodeposited on 1 cm-diameter graphite rods, sealed in plastic heat-shrink tubing so that only the end surfaces of the rods were exposed to the solutions. By use of a simple constant current source, a series of solutions was electrolyzed simultaneously. The standard deviation for replicate samples (90-min electrolysis time) was 1–40%. The method was not tested on "real" samples, and it has several important limitations. The current efficiency of a complex sample will be unknown a priori, and therefore trial runs may be required to determine the electrolysis time required for exhaustive deposition. To achieve reasonable deposition rates a supporting electrolyte must be added to freshwater samples, which risks contamination. Electrodeposition from freshwater samples for preconcentration thus would not appear to be a technique of first choice.

Electrodeposition from seawater appears more promising. The saline nature of ocean water provides an excellent, natural electrochemical cell. Small self-contained electrodeposition units have been designed for in situ sampling of seawater (8). Graphite electrodes of various design have been placed in flow cells that can be suspended in the sea at a desired depth. Using the flow technique, exhaustive electrolysis is not required as the rate of deposition of each metal will be proportional to the concentration of that metal. Using a constant current and flow rate for fixed time periods, reproducible deposition from seawater is possible. The major problem is to prepare reference standards that match the samples. The electrodes used for each run may be returned to the laboratory for analysis. X-ray spectrometry or neutron activation techniques can be used directly on the electrodes. Also, the metals can be redissolved by anodic stripping, or the electrodes ashed in low temperature plasma devices and the metals taken up in acid. Either way, techniques such as atomic absorption spectrometry may then be used. Attempts to selectively deposit ions directly in a graphite furnace rod for atomic absorption have been reported (9, 10).

It is well known that enhanced currents may be observed when the electroactive component adsorbs on the electrode surface. This can lead to erroneous analytical results when the adsorption is not reproducible, or when it is significantly affected by other compounds in solution. Recently, however, this phenomenon has been exploited by placing a chemical functional group such as a metal complexing agent on or in the electrode (11). The electroactive analyte is immobilized at the electrode and thereby concentrated from solution. Selective trace element preconcentration may thus be effected simply by inserting the electrode in the sample solution, even at a remote site. The electrochemistry can be performed later on. The procedure is similar to anodic stripping voltammetry, but the deposition step is chemical rather than electrochemical.

Liquid–Liquid Extraction

One of the most extensively studied and most widely used techniques of preconcentration is liquid–liquid extraction, in which a water-immiscible solvent and an aqueous solution containing a chelated metal ion are brought into contact. Most often, the complexing agent forms a nonionic or neutral chelate, which is more soluble in the organic solvent than in water. The result is an extraction of the metal from the water into the organic solvent. The procedure is simple and, if the principles and practice of the technique are well understood by the analyst, liquid–liquid extraction can be powerful both as a separation and as a concentration method. A variety of chelating agents may be used. Some, such as 8-hydroxyquinoline (oxine), diethyldithiocarbamate (DDTC), ammonium pyrrolidinedithiocarbamate (APDC), and β-diketones (acetylacetone [AcAc]), are very general chelating agents which will extract a variety of metal ions. Some others, such as dimethylglyoxime, are

SIEMENS

Two first choices in analytical X-ray.

We were first with many of the significant advances in analytical X-ray ... are first today in the accuracy and reliability that build lasting customer satisfaction.

Each of our two Siemens systems has capabilities that assure top performance in its area. Our SRS 200 is the most cost-effective sequential X-ray spectrometer on the market today. Our MRS 400 high-performance, multichannel spectrometer delivers 28 simultaneous X-ray determinations in as little as 40 seconds.

Siemens people offer exceptional service support, too: software library and frequent updates; service and equipment training seminars; Tele-Service telephone trouble-shooting and consultation; complete contract repair services by Siemens specialists.

So before you invest in spectroscopy, investigate Siemens. We have the equipment you need, backed by generations of experience and a dedication to excellence. Write or call Mr. Pedro Arredondo, Siemens Corporation, Measurement Systems Division, 2 Pin Oak Lane, Cherry Hill, NJ 08034. (609) 424-9210.

For further product information, fill out coupon or attach business card and send to above address.

Name_____

Company_____

Address_____

City_____ State_____ ZIP Code_____

Telephone_____

[AC-881]

E5/3310-001-121

Siemens SRS 200 and MRS 400.

CIRCLE 189 ON READER SERVICE CARD

highly specific. It is interesting that a great deal of research has been performed to develop methods for specific extractions with reagents such as oxine (*12*). Much of this work was performed because the instrumentation at that time was not sufficiently specific and prior separations were required. These methods are still required in some cases. For example, interferences in atomic absorption determinations are not uncommon, and separations by solvent extraction are required. However, for use in conjunction with X-ray fluorescence, a very general extraction procedure would be more useful, as the spectrographic selectivity is excellent. There is no single chelating agent that is a universal extractant. However, Pohl (*13–15*), and others (*16*, *17*) have proposed several multicomponent systems that cover a wide range of elements.

The concentration factor reasonably achieved by solvent extraction on a batch extraction basis has practical limits. Considering that a 100-mL sample extracted with 1 or 2 mL of organic solvent is a practical limit, a concentration factor of 100 is about what one can achieve. Of more potential value to water analysis is some form of continuous or countercurrent extraction, of the type that has been used in preconcentration of organic compounds. In these procedures, a fixed amount of organic solvent is equilibrated with a large volume of sample taken continuously from a reservoir or perhaps directly from a river or stream. In this way a large volume of sample may be extracted by relatively small volumes of organic solvent. The area of continuous extraction would appear to hold much promise. A countercurrent flow system based upon differences in solvent density for in situ sampling would be a powerful concentration method. Some rather novel yet simple devices have been designed (*18*). Such devices should be adaptable to water analysis. A further example is the use of fluoro-β-diketones in solvent extraction combined with gas–liquid chromatography (*19*) or ICP–AES (*20*). These reagents form volatile complexes with many metal ions. Extracts containing these complexes may be injected into a gas chromatograph or gas cell. These techniques have not been sufficiently explored in applications to water pollution analyses to accurately assess their potential. However, they appear to be significant.

Some novel developments in solvent extraction are worthy of note. One of the limitations of the preconcentration factor realized with batch solvent extraction is the difficulty in obtaining a good separation of a small volume of the organic phase from the aqueous sample. Significant portions of the organic solvent may adhere to the walls of the vessel, requiring repeated washings, which decrease the concentration factor. Emulsions may form that are slow to separate. An interesting solution to this problem has been suggested and used in fundamental studies (*21*, *22*) and limited analytical applications (*22*, *23*). The organic phase is one that melts a few degrees above room temperature. A conventional liquid–liquid extraction is carried out at a temperature above the melting point of the organic material. Once the extraction is complete, the mixture is allowed to cool and the organic material solidifies. If the organic material is carefully selected, a solid bead will form upon cooling, and the extract will be retained. The small bead (as little as a few milligrams) may be physically removed from the mixture for determination of the elements. Flaschka (*23*) has used this technique in conjunction with a capillary cell for the spectrophotometric determination of cobalt.

Surface Adsorption

The concept of solvent extraction can be easily translated into that of surface adsorption. Two such applications have been reported. Vanderborght and Van Grieken (*24*) have used the adsorption of neutral 8-hydroxyquinoline (oxine) metal complexes onto the surface of activated carbon as a means of preconcentration of trace ions. The activated carbon bearing the complexes is filtered and analyzed by X-ray fluorescence spectrometry. More recently, oxine complexes formed in seawater samples were adsorbed on a column bed packed with C_{18}-bonded silica gel (*25*). The adsorbed complexes were eluted with methanol. Concentration factors of about 200 were attained, and the saline matrix was eliminated. Inductively coupled plasma atomic emission spectrometry was utilized in the analytical finish.

Precipitation

A method of preconcentration of ions that is of limited use to those analytical techniques requiring liquid samples, but of great value in X-ray spectrometry and neutron activation analysis, is precipitation or coprecipitation. Precipitation is one of the oldest chemical techniques for the separation and concentration of ions. A massive effort has been made over the years to find specific precipitation reagents and to minimize coprecipitation. However, for trace element techniques with high inherent selectivity, selective precipitation is usually not necessary or desirable. The completeness of the precipitation of the ions of interest is much more important. The solubility of many common precipitates is sufficiently great to prevent quantitative precipitation of the ions of interest at concentrations less than a few ppm. For example, nickel in this concentration range cannot be precipitated quantitatively with dimethylglyoxime. In many cases, however, quantitative precipitation may be achieved by the addition of a coprecipitant (*26–28*). When precipitates are formed in exceedingly dilute solutions, several factors may contribute to lack of quantitative recovery in addition to the solubility of the precipitate. The particle size of the precipitate may be very small and the particles may pass through the filter unless much care is used. A supersaturated solution may exist and particles may not form. One of the easiest ways to overcome these problems is to add a carrier ion or coprecipitate that will not only precipitate itself, but will aid in the recovery of the ion of interest. Luke (*26*) has devised an extensive scheme for both general and selective precipitation of metal ions using a variety of reagents. Puschel (*27*) and Watanabe, Berman, and Russell (*28*) have proposed additional schemes using organic precipitants. The major advantages of precipitation methods are that they are simple, and that uniform deposits on a membrane filter can be obtained. A further advantage of precipitation methods is the inherent chemical capacity available. This becomes an important factor when one or more elements is present at a relatively high concentration.

With the possible exception of continuous liquid–liquid extraction, none of the above techniques provides concentration factors of more than 1 or 2 orders of magnitude. It is difficult to determine a concentration factor for precipitation or electrodeposition, as the ions are removed from a homogeneous medium and placed on the surface of a filter or electrode. For X-ray spectrometry, the conversion of the sample to a thin film is a bonus of preconcentration. However, if the sample is to be redissolved for analysis by some other technique, the net gain in concentration may not be great. For example, components can be electrodeposited from 15–25 mL of solution onto a graphite or carbon electrode. However, one may need at least 0.1 mL of solution to dissolve the deposit or to receive the ions by anodic stripping. Therefore, a preconcentration factor of about 250 is achieved. A similar argument can be made about precipitation and batch liquid–liquid extraction.

Ion-Exchange

A series of preconcentration tech-

niques that has been extensively studied and that has potential for much larger concentration factors is that based upon ion-exchange reactions. The major advantage of most ion-exchange methods is that the functional group is immobilized on some type of solid substrate, therefore providing the potential to either batch extract ions from solution or to use the ion-exchange material in a column. Ion-exchange provides the most universal preconcentration technique, as the ions may be analyzed directly upon the solid matrix using X-ray spectrometry (*29*), neutron activation analysis (*30*), or isotopic dilution techniques (*31*). Also, the ions may be eluted from the column and the analysis completed on the resulting solution using methods such as atomic spectrometry (*32*) or inductively coupled plasma emission spectrometry (*33*). Ion-exchange is capable of recovering hydrated ions, charged complexes, and solution components complexed by labile ligands. The recovery efficiency depends upon the distribution ratio of the ion on the ion-exchange material (i.e., the affinity of the material for the ion) and the stability constants of any complexes present in solution. These factors must be carefully considered and tested before use of ion-exchange preconcentration methods (*29*). For a well-chosen ion-exchange material, very large preconcentration factors may be achieved. For example, as much as 4 L of seawater may be passed through a column prepared from 100 mg of ion-exchange material, yielding a concentration factor of $\sim 4 \times 10^4$ (*34*).

The conventional ion-exchange resin formed by a cross-linked styrene-divinylbenzene or other matrix containing ionogenic functional sites is the most obvious ion-exchange material to use. Both batch extraction (*35*) and column techniques (*36*) have been used. The first resins used were the common, commercially available cation and anion exchange materials. These resins operate essentially on an ion association basis, and selectivity and partitioning is frequently a problem. For example, concentration of transition metal ions from seawater is difficult because sodium ions may compete well with the less concentrated transition metal ions. In cases in which alkali metal ions are not of interest, chelating ion-exchange resins may be very effective. These resins contain functional groups that form chelates with the metal ions. Unfortunately, few commercial resins are available, although many varieties have been synthesized (*37*). One chelating ion-exchange resin that is commercially available and has proved very useful in the preconcentration of metal ions from solution is Chelex-100 (Bio-Rad Laboratories). The resin contains iminodiacetic acid functional groups, and its chemical behavior is very similar to ethylenediaminetetraacetic acid (EDTA). This resin has been applied to X-ray spectrometric analysis of geological materials (*38*) and analysis of seawater by X-ray spectrometry (*39*), atomic absorption (*32*), and inductively coupled plasma atomic emission spectroscopy (*40*). Chelex-100 offers several advantages as an ion-exchange concentration material. It generally has very high distribution ratios, which implies that ions (particularly transition metal ions as well as others such as Hg^{2+}, Pb^{2+}, and Bi^{3+}) may be quantitatively recovered from solution using a batch process. It covers a wide range of metal ions, and its chemistry can be accurately predicted by analogy with EDTA. However, there are severe limitations to the applications of Chelex-100. There are samples, such as seawater, or iron- and calcium-laden fresh water, in which major elements will occupy the ion-exchange sites to the exclusion of trace elements. To prevent this, masking agents can be used, or pH or other parameters must be manipulated. At times, control of these parameters may be an advantage. One example is the determination of Cr(III) and Cr(VI) using Chelex-100. Cr(III) is recovered by Chelex-100, whereas Cr(VI) as chromate is not. Therefore Cr(III) may be determined directly by extraction with Chelex-100, and total chromium can be determined on a second aliquot treated with a reducing agent (*41*). Inductively coupled plasma atomic emission spectrometry was employed with a poly(dithiocarbamate) resin for a similar determination (*42*).

Ion-Exchange Impregnated Materials

An interesting modification of the ion-exchange preconcentration approach is the use of ion-exchange impregnated materials. Two major types of materials are used. Ion-exchange resin impregnated papers have found widest use. Campbell and co-workers have performed in-depth studies of the distribution of ions when solutions are filtered through paper disks impregnated with ion-exchange resins (*43*). These materials are very easy to use as the solution is simply filtered through (often repeatedly) the filter disk held in a suitable holder (*44*). Standards are prepared in the same manner as the samples. The disks are well suited for X-ray spectrometric measurements.

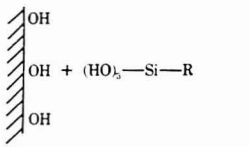
A second type of ion-exchange impregnated material is ion-exchange membranes. These materials are characterized by low capacity and slow rates of ion recovery. In most laboratory analyses they offer no significant advantage over other materials. However, one application of interest has been to take advantage of the slow uptake to essentially integrate the average concentration of metals in a stream over a time period (*45*). The membrane, in principle, will recover ions from solution at a rate proportional to the concentration of the ion in solution. Therefore, exposure of the membrane to a changing concentration should "time average" the concentration. However, careful evaluation of many possible secondary effects must be performed before these membranes can be considered reliable. Competition effects, pH changes, and other parameters must be evaluated. Also, the low capacity of the membrane requires an analytical method with very low limits of detection.

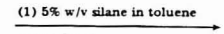
Immobilized Reagents

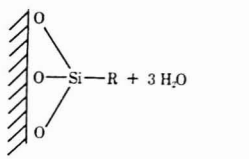
Several recent research efforts have been made to find methods of immobilizing ion-exchange sites to simplify modification of the active functional groups on the sites. Again, a desirable feature is to be able to conduct determinations either directly on the solid ion-exchange material or on solutions eluted from the material. One very important advantage is that the material may be used on a one-time basis and need not have long-term stability. One approach is to absorb a desired chelating agent in a suitable matrix. Some workers have used styrene-divinylbenzene gels (*46*). Commercially available resin beads (Bio-Beads, Bio-Rad Laboratories) are swelled using an organic solvent. The beads are treated with solutions of chelating agents that are absorbed into the pores of the gellike beads. The pores are shrunk by spraying the gel into cold water. The gel may then be used to concentrate metal ions as the ions diffuse into the pores and are trapped by the chelating reagent. This is obviously a simple approach to the preparation of tailor-made immobilized chelating materials. A major limitation of this method is that a very low exchange capacity (1–10 μeq/g) is obtained. There should be some concern given to the possibility of leaching the metal chelate from the gel, as it is not attached by a chemical bond. A similar concept has been proposed by Braun and co-workers (*47*, *48*). These workers used reagents absorbed into open cell polyurethane foam and sealed with plasticizers. These foams are very easily prepared and are effective concentrating agents. Again a major limitation is the very low capacity of 23.4 μeq/g reported for the dithizone-loaded foam (*48*). These materials are recently re-

ported, and a critical evaluation of their potential is not possible. However, it is readily observed that they offer simplicity in the preparation of immobilized reagents and meet a variety of needs. The advantages of these foams have been compared with several other techniques of "trapping" dithizone on substrates (*47*).

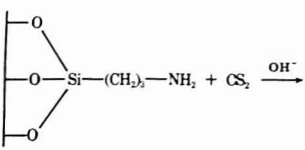
A chemical reaction that has found much use in recent years for a variety of purposes is silylation. This reaction has been used to form volatile derivatives of organic compounds for gas chromatographic work and to immobilize enzymes on substrates. A variety of silylation reagents is available. The reaction is a simple one that can be conducted in water or an organic solvent such as benzene. The reaction may be represented as

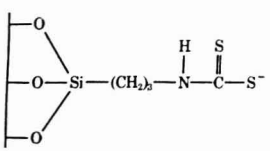






where the polyhydroxyl species may be silica gel or a solid substrate such as glass. Some of the available silylation reagents contain chelating or coordinating functional groups, and modifications are possible.
The modifications are best made after the silylation reaction has been performed. Recent applications of this reaction have shown potential for preconcentration. Hercules and co-workers have silylated fiberglass cloth with a reagent containing an amine and converted the amine to the dithiocarbamate (*49*). Solutions containing as little as 20 ppb of lead were filtered through the treated glass, and the recovered lead was detected by ESCA. The major limitations are a low capacity and the difficulties in quantitation by ESCA. The silylation reaction has been used extensively in the immobilization of chelating agents such as ethylenediamine, ethylenediaminedithiocarbamate, and ethylenediaminetriacetic acid on silica gel (*50*). Chromatographic-grade silica gel is silylated, and modification reactions are conducted. The silica gel may then be used in a batch or column made for concentration, similar to ion-exchange resins. Capacities of 0.5–0.9 meq/g are obtained and, by passing solutions through a column made of 100 mg of the material, metals in the range of 1 ppb may be determined by X-ray spectrometric measurements directly on the packing made into a pellet.





Other Methods

There are many other preconcentration methods of a somewhat specialized nature. Some of these represent interesting applications of chemical reactions and are not strictly preconcentration methods. To attempt a comprehensive list would be of little value, but a few examples may stimulate the reader to think of new solutions to problems. Siggia and co-workers have reported a concentration technique specific to Ag(I), Cu(I), Hg(I), and Hg(II) using precipitation chromatography (*51*). A column prepared with 20% 1-pentadecyne coated on Anakrom AB is treated with an acetate solution of the above ions. These ions form metalloacetylides and are retained on the column. They may be eluted by nitric acid and analyzed. A further example of the use of chemical manipulation to facilitate analysis includes a "chemical amplifier." Orthophosphate is frequently determined in water samples using the blue heteropoly acid known as molybdenum blue. A rapid method to determine phosphate is to extract the phospho-molybdate complex from excess molybdate (*52*) and use the 12:1-Mo:P ratio in the complex to determine the molybdenum. Using a silylated silica gel reagent discussed above to recover the molybdate, as little as 15 ppb phosphate may be determined by X-ray fluorescence determination of the extracted molybdenum. Janauer and coworkers have used an interesting concept which they call "reactive ion exchange" (*53*, *54*). One example presented (*53*) is the use of an anion exchange resin to adsorb chromate ions, followed by in situ reduction of the chromate to chromic ions. The cationic chromic ion is then easily removed by a backwash of the resin. There will probably be many other examples of this technique in the future. X-ray spectrometry has been employed in the determination of organic nitrogen by converting the nitrogen to ammonia using the Kjeldahl reaction and distilling the ammonia from the digested solution. The ammonia distillate is passed through a filter saturated with Nessler's reagent. The excess reagent is washed from the filter and the residual mercury determined by X-ray spectrometry. As little as 0.2 μg of nitrogen may be determined (*55*).

The above comments represent the tip of the iceberg in terms of the methods and applications of preconcentration techniques as applied to trace element determinations. The potential of automated analyses and speciation determination has yet to be fully exploited. It is also important to realize that X-ray spectrometry, atomic absorption spectrometry, neutron activation analysis, and inductively coupled plasma atomic emission spectrometry have each been touted as all-but-ultimate solutions to analytical problems in elemental determinations. Yet, we see in the above brief overview that new applications of these methods to selected analytical problems have been coupled to preconcentration techniques, used as such or as a means toward eliminating undesirable matrix problems. In summary, the ultimate method—highly sensitive, completely selective, with infinite linear dynamic range, capable of determining all elements in their different oxidation states and chemical forms, with no matrix effects—still eludes us. The use of chemical methods of concentration, matrix effect minimization, and species isolation provides an essential supplement to the powerful instrumental techniques available. One naturally hopes to avoid the need for these procedures. Yet the hallmark of a true analytical chemist is the ability to recognize that no two analytical problems are exactly the same and to master the versatility with which they must be approached.

References

(1) Liebhafsky, H. A. *Anal. Chem.* **1962**, *34*(7), 23 A.
(2) Stone, R. G. *Analyst* **1963**, *88*, 56.
(3) Walter, R. L.; Willis, R. D.; Gutknecht, W. F.; Joyce, J. M. *Anal. Chem.* **1974**, *46*, 843.
(4) Lingane, J. J. "Electroanalytical Chemistry", 2nd ed.; Interscience: New York, 1958.
(5) Figura, P.; McDuffie, B. *Anal. Chem.* **1980**, *52*, 1433.

(6) Clarke, B. L.; Wooten, L. A.; Luke, C. L. *Ind. Eng. Chem. Anal. Ed.* **1936**, *8*, 411.
(7) Vassos, B. H.; Hirsch, R. F.; Letterman, H. *Anal. Chem.* **1973**, *45*, 792.
(8) Mark, H. B. "Abstracts of Papers," 162nd National Meeting of the American Chemical Society, Washington, D.C., September 1971.
(9) Torsi, G. *Ann. Chim.* Rome **1977**, *67*, 557.
(10) Torsi, G.; Desimoni, E.; Palmisano, F.; Sabbatini, L. *Anal. Chim. Acta* **1980**, *124*, 143.
(11) Cheek, G. T.; Nelson, R. F. *Anal. Lett.* **1978**, *11*, 393.
(12) Morrison, G. H.; Freiser, H. "Solvent Extraction in Analytical Chemistry"; Interscience: New York, 1967.
(13) Pohl, F. A. *Z. Anal. Chem.* **1953**, *139*, 241.
(14) Pohl, F. A. *Z. Anal. Chem.* **1953**, *139*, 423.
(15) Pohl, F. A. *Z. Anal. Chem.* **1953**, *141*, 81.
(16) Chichilo, P.; Sprecht, A. W.; Whittaker, C. W. *J. Assoc. Off. Anal. Chem.* **1955**, *38*, 903.
(17) Silvery, W. D.; Brennan, R. *Anal. Chem.* **1962**, *34*, 784.
(18) Pan, S. C. *Sep. Sci.* **1974**, *9*, 227.
(19) Ross, W. D.; Sievers, R. E. *Talanta* **1968**, *15*, 87.
(20) Black, M. S.; Browner, R. F. *Anal. Chem.* **1981**, *53*, 249.
(21) Kuznetsov, V. I.; Seryakova, I. V. *Zh. Anal. Khim.* **1959**, *14*, 161.
(22) Fujinaga, T.; Kuwamoto, T.; Nakayama, E. *Talanta*, **1969**, *16*, 1225.
(23) Flaschka, H. A.; Barnes, R.; Paschal, D. *Anal. Lett.* **1972**, *5*, 253.
(24) Vanderborght, B. M.; Van Grieken, R. E. *Anal. Chem.* **1977**, *49*, 311.
(25) Watanabe, H.; Goto, K.; Taguchi, S.; McLaren, J. W.; Berman, S. S.; Russell, D. S. *Anal. Chem.* **1981**, *53*, 738.
(26) Luke, C. L. *Anal. Chim. Acta* **1968**, *41*, 237.
(27) Puschel, R. *Talanta* **1969**, *16*, 351.
(28) Watanabe, H.; Berman, S.; Russell, D. S. *Talanta* **1972**, *19*, 1363.
(29) Blount, C. W.; Leyden, D. E.; Thomas, T. L.; Guill, S. *Anal. Chem.* **1973**, *45*, 1045.
(30) Noakes, J. E.; Harding, J. L.; Spaulding, J. D. 8th Annual Conference of the Marine Technology Society, Preprints, p 415.
(31) Stokes, W. M.; Fish, W. A.; Hickey, F. C. *Anal. Chem.* **1955**, *27*, 1895.
(32) Riley, J. P.; Taylor, D. *Anal. Chim. Acta* **1968**, *40*, 479.
(33) Barnes, R. M.; Genna, J. S. *Anal. Chem.* **1979**, *51*, 1055.
(34) Leyden, D. E.; Patterson, T. A.; Alberts, J. J. *Anal. Chem.* **1975**, *47*, 733.
(35) Van Nickerk, J. N.; DeWet, J. F.; Wybenga, F. T. *Anal. Chem.* **1961**, *33*, 213.
(36) Collin, R. L. *Anal. Chem.* **1961**, *33*, 605.
(37) Helfferich, F. "Ion Exchange"; McGraw-Hill: New York, 1962, p 47.
(38) Leyden, D. E. In "Advances in X-ray Analysis; Grant, C. L.; Barrett, C. S.; Newkirk, J. B.; Ruud, C. O., Eds.; Plenum Press: New York, 1974; Vol. 17, p 293.
(39) Kingston, H.; Pella, P. A. *Anal. Chem.* **1981**, *53*, 223.
(40) Berman, S. S.; McLaren, J. W.; Willie, S. N. *Anal. Chem.* **1980**, *52*, 488.
(41) Leyden, D. E.; Channell, R. E. *Anal. Chem.* **1972**, *44*, 607.
(42) Miyazaki, A.; Barnes, R. M. *Anal. Chem.* **1981**, *53*, 364.
(43) Campbell, W. J.; Spano, E. F.; Green, T. E. *Anal. Chem.* **1966**, *38*, 987.
(44) Hooten, K. A. H.; Parsons, M. L. *Anal. Chem.* **1973**, *45*, 436.
(45) Lochmüller, C. H.; Galbraith, J.; Walter, R. L.; Joyce, J. D. *Anal. Lett.* **1972**, *5*, 943.
(46) Sekizuka, Y.; Kojima, T.; Yano, T.; Ueno, K. *Talanta* **1973**, *20*, 979.
(47) Braun, T.; Farag, A. B. *Anal. Chim. Acta* **1974**, *69*, 85.
(48) Braun, T.; Farag, A. B. *Anal. Chim. Acta* **1974**, *71*, 133.
(49) Hercules, D. M.; Cox, L. E.; Onisick, S.; Nichols, G. D.; Carver, J. C. *Anal. Chem.* **1973**, *45*, 1973.
(50) Leyden, D. E.; Luttrell, G. H. *Anal. Chem.* **1975**, *47*, 1612.
(51) Zeronsa, W. P.; Dobkowski, G.; Siggia, S. *Anal. Chem.* **1974**, *46*, 309.
(52) Leyden, D. E.; Nonidez, W. K.; Carr, P. W. *Anal. Chem.* **1975**, *47*, 1449.
(53) Pankow, J. F.; Janauer, G. E. *Anal. Chim. Acta* **1974**, *69*, 97.
(54) DeLayette-Mills, J.; Karm, L.; Janauer, G. E.; Chan, P.-K.; Bernier, W. E. *Anal. Chim. Acta* **1981**, *124*, 365.
(55) Mathies, J. C.; Lund, P. K.; Eide, W. *Anal. Biochem.* **1962**, *3*, 408.



Leyden



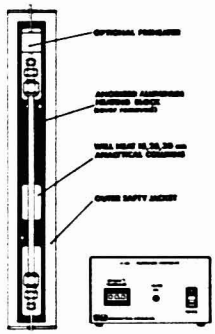
Wegscheider

Donald Leyden received a BS in chemistry from Kent State University and MS and PhD degrees in analytical chemistry from Emory University. He is currently Phillipson Professor of Environmental and Mining Chemistry at the University of Denver. Leyden's research interests include chelating ion-exchange resins, NMR studies of proton exchange reactions, preconcentration of trace ions prior to X-ray fluorescence analysis, and the chemical modification of surfaces.

Wolfhard Wegscheider received his doctorate in technical sciences from the Technical University of Graz, Austria, and worked later under Leyden as a Fulbright scholar. His research interests include sample preparation techniques for multielement analyses and mathematical techniques in analytical chemistry. He is currently universitätsdozent for analytical chemistry at the Technical University of Graz.

TEMPERATURE CONTROL FOR LC COLUMNS

Temperature control in liquid chromatography has generally been neglected. Improved resolution, efficiency, and precision often result from operation of LC columns at controlled temperatures above ambient.



Bioanalytical Systems offers a low cost column heating system based on a metal block heater and solid state controller. The versatile controller can be used with other heating elements and probes for a variety of laboratory applications.

BAS BIOANALYTICAL SYSTEMS INC.

Purdue Research Park
1205 Kent Avenue
West Lafayette, IN 47906
(317) 463-2505

CIRCLE 22 ON READER SERVICE CARD

Tygon.®
Laboratories have placed their confidence in Tygon for over 40 years.

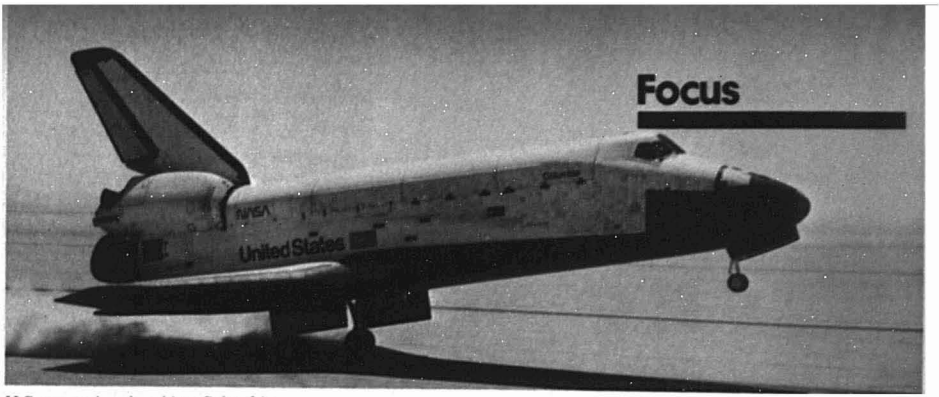


This is Tygon laboratory tubing. It is specifically formulated for use in the laboratory. Tygon laboratory tubing safely handles an exceptionally wide range of chemicals, yet offers outstanding flexibility and long service life. But Tygon offers more. Tygon is used with confidence. Confidence that your analyses of gases or solutions will not be affected. Confidence that your results will be reproducible. Confidence that Tygon laboratory tubing is, in fact, specifically formulated for lab use, and has been for over 40 years. For literature and additional information, contact Norton Plastics and Synthetics Division, P.O. Box 350, Akron, Ohio 44309, or call toll free: 1-800-321-9634. In Ohio, call collect: 216-630-9230.

NORTON

34-058

CIRCLE 155 ON READER SERVICE CARD



U.S. space shuttle orbiter Columbia

Infrared Analyzer Gives Columbia a Passing Grade

Within seconds of the near-perfect landing of the U.S. space shuttle orbiter *Columbia* in April, a team of specialists in space suits approached the craft with a mobile analytical instrument. The instrument was an infrared analyzer, designed specifically to detect and quantitate monomethylhydrazine, hydrazine, and ammonia.

Monomethylhydrazine is one of the fuels utilized in the space shuttle's orbital maneuvering rockets; hydrazine and ammonia are decomposition products of monomethylhydrazine. If any of these gases were leaking from the spacecraft, a spark from an internal combustion engine or any other source could have initiated an explosion. Hence the careful monitoring of the air around the craft after the landing.

Ironically, the National Aeronautics and Space Administration (NASA) was also concerned that the infrared analyzer itself could cause an explosion. That is why the analyzer was encased in a special explosion-proof enclosure and mounted on a nonmotorized cart.

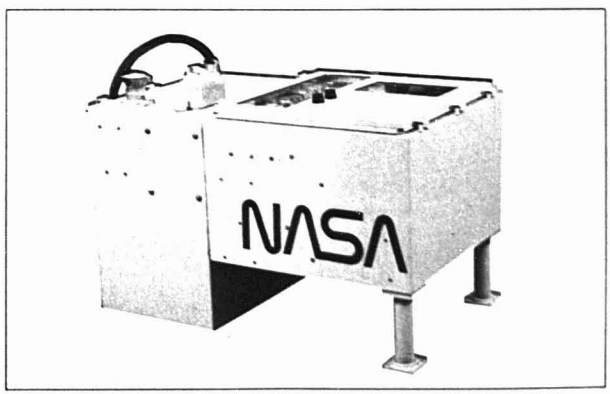
The instrument, designed and constructed by Foxboro Analytical under contract to NASA, is a modified version of Foxboro's MIRAN-80 analyzer, a microcomputer-controlled single-beam infrared spectrometer. The spectrometer's optical system consists of a nichrome wire source, a focusing mirror, a chopper, a circular variable filter, an adjustable slit, a sample chamber, and a detector. The chopper enables the instrument to discriminate between the infrared source and stray light. The circular variable filter operates as a monochromator. Far from being a crude wide-bandpass filter, it has a resolution of 0.05 μm at a wavelength of 3.5 μm (0.5-mm slit width). The overall analytical range is 2.5–14.5 μm, which corresponds to a wavenumber range of 4000–700 cm^{-1}. The analyzer responds to absorbances in the range 0–2.0.

For the space shuttle mission, Foxboro Analytical programmed and calibrated the instrument specifically for the three components NASA was interested in. To determine one of the three analytes, the variable filter wheel isolates a wavelength where the compound absorbs strongly. Air samples are drawn into a stainless steel sample cell, analyzed for all three components, and then exhausted. Concentration data appear on three liquid crystal displays, one for each analyte. The MIRAN-80, on which the NASA instrument is based, is capable of analyzing mixtures of up to 10 components.

The instrument is precalibrated for the dependence of absorption intensity on concentration for each analyte. The absorption of one component at a particular wavelength has to be corrected for interfering absorptions from other components present in the sample, such as the CO_2 and H_2O in air.

On the afternoon of the landing, monitoring the *Columbia* for fuel leaks took less than 10 minutes. After the infrared analyzer gave *Columbia* a clean bill of health, the support vehicles and equipment moved in, and the tumultuous welcome for *Columbia* and its crew proceeded on schedule.

Stuart A. Borman



Foxboro's sniffer cart was used in the shuttle landing. In the left section of the explosion-proof console is a battery-powered pumping system that draws in air samples and passes them to the infrared analyzer (right section)

0003-2700/81/A351-1067$01.00/0
© 1981 American Chemical Society

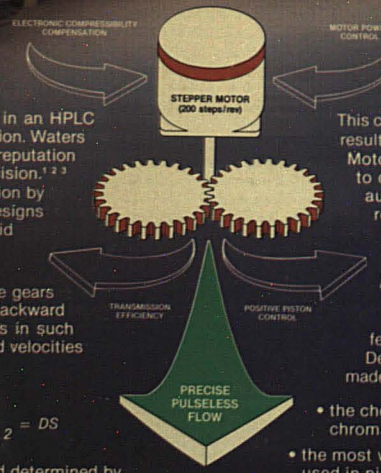
No. 2 in a Series of HPLC Technical Notes.

Waters 2

Subject: Criteria for precise flow in HPLC

Products Designed by Chromatographers for Chromatography





The ultimate measure of quality in an HPLC Solvent Delivery System is precision. Waters Solvent Delivery Systems hold a reputation for the highest flow rate precision.[1,2,3] Waters has achieved this reputation by perfecting a balance of proven designs in mechanics, electronics and fluid pathways.

For example:

Gear Driven Transmission: Precise gears ensure positive forward and backward motion of the piston components in such a way that the sum of the forward velocities $\left(\frac{dx}{dt}\right)$ is always constant,

$$\frac{dx}{dt}_{piston\ 1} + \frac{dx}{dt}_{piston\ 2} = DS$$

where DS is the pump drive speed determined by the compressibility compensation and motor power control circuits.

Electronic Compressibility Compensation: Based on the formula *DS = Flow Rate Set (1 + Solvent Compressibility × Operating Pressure)*, this circuit automatically adjusts DS (Pump Drive Speed) to ensure mass flow accuracy regardless of mobile phase compressibility. Additionally, flow precision is ensured across the entire operating range of the system.

Motor Power Control: An inherent property of pumping systems is production of heat by the drive mechanism. This can cause thermal expansion resulting in variations of flow rate. Motor Power Control enables the system to operate at minimum temperature by automatically adjusting motor current (I_m) in response to changes in system pressure (P):

$$I_m = 2.2\ amps + (3.5 \times 10^{-4})\ Pressure$$

These are but a few of the advanced features included in all Waters Solvent Delivery Systems. Features that have made Waters:

- the choice of over 20,000 chromatographers
- the most widely published systems used in pioneering HPLC applications
- the most precise and accurate systems available in the industry
- the systems that give the greatest value, versatility and control in HPLC.

For more information on Waters Solvent Delivery Systems, call Waters at (617) 478-2000.

[1] R.P.W. Scott, P. Kucera, *J. Chromatogr.*, **185** (1979) 27-41
[2] R.P.W. Scott, *J. Chromatogr. Sci.*, **18** (1980) 49-53
[3] J.H. Olson, et al., *Ind. Eng. Chem. Fundam.*, **16**, 3 (1977) 380-384

MILLIPORE

Waters Associates / The Liquid Chromatography People / 34 Maple St. / Milford, MA 01757 / (617) 478-2000

FACSS•Eighth Annual Meeting



September 20–25, 1981

Philadelphia, Pa.

The eighth annual meeting of the Federation of Analytical Chemistry and Spectroscopy Societies (FACSS) will be held Sept. 20–25, 1981, at the Philadelphia Sheraton Hotel, Philadelphia, Pa. The sponsoring organizations for the meeting are: the Society for Applied Spectroscopy; the Division of Analytical Chemistry of the American Chemical Society; the Association of Analytical Chemists, Inc. (Anachem); the Analysis Instrumentation Division of the Instrument Society of America; and the Chromatography Forum of the Delaware Valley.

Approximately 500 papers on fundamental and applied topics will be presented. The extensive technical program includes symposia on: atomic absorption spectrometry; inductively coupled plasma and DC plasma emission spectrometry; calorimetry; atomic fluorescence spectrometry; gas chromatography; liquid chromatography; electronic spectroscopy; mass spectrometry; electrochemistry; nuclear magnetic resonance spectrometry; photoacoustic spectroscopy; particle size analysis; spectral search; GC/FTIR; LC/FTIR; and photoacoustic FTIR.

Symposia on applications topics include: environmental analysis; forensic chemistry; synfuels; applications of analytical pyrolysis; computers in the analytical laboratory; surface analysis; trace analysis of biological fluids; applications of FTIR and Raman spectrometry; analytical applications of chemically modified electrodes; trace elemental analysis in foods, soils, and plants; clinical chemistry; biomedical spectrometry; polymers; nuclear waste disposal; and system suitability testing in pharmaceutical analysis.



Philadelphia Convention and Visitor Bureau

The Liberty Bell Pavilion is visited by millions of people every year

Two special sessions on the teaching of spectroscopy and on "owning and operating your own business" will be given on Friday, Sept. 25. In addition, Committee E-13 of the American Society for Testing and Materials (ASTM) will sponsor a full-day symposium on Wednesday, Sept. 23, on practical performance testing of spectroscopy instrumentation.

This year's Anachem Award will be presented to Walter McCrone of the McCrone Research Institute in Chicago, Ill. A special symposium on the work carried out at the McCrone Research Institute will follow the award address. In addition, a number of Society for Applied Spectroscopy awards will be presented at a luncheon on Tuesday, Sept. 22.

The American Chemical Society

(ACS) is sponsoring four short courses on the weekend following the FACSS meeting: writing for results; laboratory automation—micro-, mini-, or midicomputers; maintaining and troubleshooting chromatographic systems; and management for the newly appointed supervisor. For information on ACS courses, contact: Dept. of Educational Activities, American Chemical Society, 1155 16th St., N.W., Washington, D.C. 20036, 202-872-4508.

The Society for Applied Spectroscopy (SAS) will offer short courses on plasma emission spectrometry and FTIR. Further information on SAS courses is available from: Peter Griffiths, Dept. of Chemistry, Ohio University, Athens, Ohio 45701, 614-594-6381.

In addition, seven FACSS-sponsored workshops will be given: liquid chromatography of biological and synthetic polymers; analytical techniques using the inductively coupled plasma; ^{13}C NMR: A probe for studying molecular structure dynamics; selected topics in GC/MS; modern practice of capillary column chromatography; practical maintenance, troubleshooting, and repair of electronic lab instrumentation; and the art of sample preparation.

An Employment Bureau will be in operation during the meeting. For information contact: James M. Purcell, USDA, ERRC, 600 East Mermaid Lane, Philadelphia, Pa. 19118, 215-233-6468. An instrument exhibition will also be held. For information on exhibition booth space, contact: Peter N. Keliher, FACSS Exhibit Director, P.O. Box 96, Collegeville, Pa. 19426, 215-489-6721. In addition, a number of special social and recreational events will be offered throughout the meeting.

Housing is available at the Philadelphia Sheraton Hotel. To ensure reservations, room requests should be made three weeks prior to scheduled arrival. For housing information, contact: Reservations Office, Philadelphia Sheraton Hotel, 1725 John F. Kennedy Blvd., Philadelphia, Pa. 19103, 215-568-3300.

Registration hours at the meeting will be: Sunday, Sept. 20, 5:00–9:00 P.M.; Monday through Thursday, 8:00 A.M.–4:30 P.M.; and Friday, 8:00–10:00 A.M. Fees are as follows: $45, preregistration; $55, regular on-site registration; $10, student; $30, single day; $10, Friday only; and spouses' program, complimentary. Deadline for advance registration is Sept. 11. Preregistration information is available from: Jerry Messman, P.O. Box 3235–Diamond Farms Branch, Gaithersburg, Md. 20760. For additional information on the program or on the meeting, contact: Mary A. Kaiser, E.I. du Pont de Nemours & Company, Experimental Station 228/200, Wilmington, Del. 19898, 302-772-3250, or Robert A. Barford, USDA, ERRC, 600 East Mermaid Lane, Philadelphia, Pa. 19118, 215-243-6453.

The complete technical program and list of meeting officers appear on the following pages.

Walter C. McCrone is winner of the 1981 Anachem Award sponsored by the Detroit Association of Analytical Chemists. The award is given annually in recognition of service to analytical chemistry through research administration, teaching, and other activities. McCrone did both his undergraduate and graduate work at Cornell University and in 1956 started his own research laboratory, McCrone Associates, Inc. In 1960, he founded the McCrone Research Institute, devoted to teaching and fundamental research. He served on the Advisory Board of ANALYTICAL CHEMISTRY from 1975–77. He is editor and publisher of *The Microscope*, the international journal of applied microscopy. McCrone's special interests have always been chemical microscopy, crystallography, and ultramicroanalysis. He and his associates have applied these techniques to everything from moon dust to DaVinci's *Last Supper*



1981 Meeting Officers

General Cochairman: *R.A. Barford*, U.S. Department of Agriculture
Program Cochairman: *M.A. Kaiser*, E.I. du Pont de Nemours & Co.
Chairman of the Governing Board: *J.E. Katon*, Miami University (Ohio)

Committee Chairmen
Arrangements: *J.R. Cavanaugh*, U.S. Department of Agriculture
Treasurer and Budget: *D.W. Robinson*, Pennwalt Corp.
Publicity: *R.J. Knauer*, Armco Steel
Registration: *J.D. Messman*, U.S. Geological Survey
Secretary: *E. Murt*, Amchem Products
Exhibits: *P.N. Keliher*, Villanova University
Continuing Education: *P.B. Roush and C.B. Larkey*, Western Electric Co.
Cultural/Social Events: *A. Donnell*, Newtown Square, Pa.
Employment: *J.M. Purcell*, U.S. Department of Agriculture
Student Award: *J. Markham*, Villanova University

FACSS PROGRAM

Monday Morning, Sept. 21

Sample Introduction for Atomic Spectroscopy

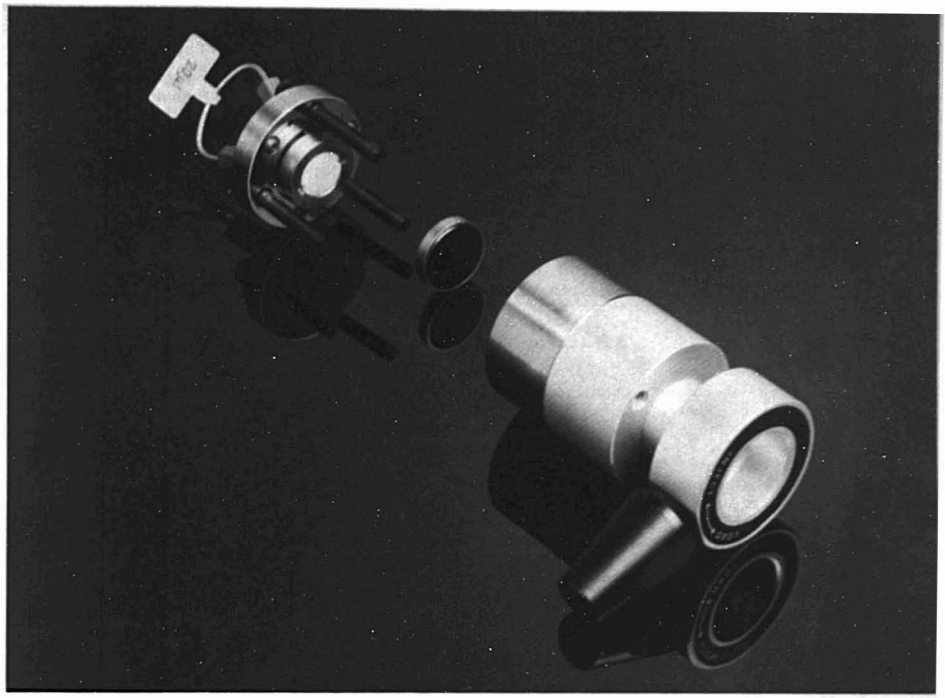
R.F. Browner, *Presiding*

Aqueous Aerosol Production, Transport, Evaluation, Vaporization, and Atomization. R.S. Skogerboe, Colorado State U

Characterization, Conditioning, and Consequences of Pneumatically Generated Liquid Aerosols in AAS. M.W. Routh, Varian Techtron Pty. Ltd.

Evaporation Characteristics of Aqueous Aerosols Using MIE Laser Scattering Techniques. R. Kull, Jr., and R.F. Browner, Georgia Institute of Technology

Nebulizer and Spray Chamber Effects in ICP Spectrometry. C.T. Apel, Los Alamos National Laboratory



The LC disconnection.

A rare peek inside your Rheodyne sample injector.

Chances are your liquid chromatograph has a Rheodyne sample injector. And chances are you've never taken it apart. So we're offering a peek inside and a few tips on how to use it effectively and keep it working perfectly.

The black disc in the center of the picture is the rotor seal. It presses against the white ceramic stator face just to the left of it. If you ever see a leak, you can stop it easily by increasing the force between these two parts. This is done by tightening the three black stator screws, after first loosening the adjacent set screws.

Eventually you may need to replace the rotor seal —a 20-minute task that you can do yourself. Consult your instruction manual. If you've misplaced your manual, we'll send you another one—because we want you to have this helpful information on parts, service and operation. Just contact us, specifying which model number you have.

Another useful publication, Tech Notes 1, describes how to get the best accuracy and precision from your injector. For example, did you know that the volume injected into the column is not always the same as th volume transferred from the syringe? To avoid error when partially filling the loop, load no more than half the loop volume. Tech Notes 2 tells how to use the Model 7125 with a short column in the sample loop. This provides a rapid clean-up technique for eliminating interferences and concentrating samples.

To receive this literature address Rheodyne, Inc., P.O. Box 996, Cotati, California 94928 U.S.A. Phone (707) 664-9050.

RHEODYNE

THE LC CONNECTION COMPANY

CIRCLE 186 ON READER SERVICE CARD

A Computer-Managed Flow-Injection Atomic Absorption System. D.P. Olander, R.S. Lysakowski, and B.E. Jones, U.S. Geological Survey

Jet Impact Nebulization for Sample Introduction in Inductively Coupled Plasma Spectrometry. M.P. Doherty, J.E. Freeman, J.G. Shabushnig, and G.M. Hieftje, Indiana U

Head Space Analysis

R.L. Grob, *Presiding*

The Application of a Gas–Phase Equilibrium Method to Environmental Studies. C.D. McAuliffe, Chevron Oil Field Research Co.

Application of Gas Chromatographic Head Space Analysis to Priority Pollutants. M.E. McNally and R.L. Grob, Villanova U

Determination of Residual Epichlorohydrin in Middle-Cut Alkylglycidyl Ethers by Headspace Gas Chromatography. A.H. Ullman and R. Houston, Procter & Gamble

EPA Purgeable Organics by Equilibrium Headspace Gas Chromatography. C. Sadowski and M. Harter, Perkin-Elmer Corp.

Selected Applications of Headspace Techniques to Priority Pollutants Analysis. G.R. Umbreit and M.J. Loughhead, Greenwood Laboratories

Analytical Applications of Microcalorimetry

H. Taylor, *Presiding*

New Thermochemical Approaches to Biochemical Analysis and Clinical Chemistry. J. Jordan, Pennsylvania State U

Titration Calorimetry as an Analytical Tool. D.J. Eatough, Brigham Young U

Analytical Applications of Microcalorimetry Drug-Macromolecule Interactions. J.H. Perrin, U of Florida

Some Applications of Differential Scanning Calorimetry at the Eastern Regional Research Center, an Agricultural Laboratory. J.W. Hampson, USDA Eastern Regional Research Center

An Engineer Looks at Small Vessel Calorimetry. S.L. Sparks, Tronac, Inc.

Kinetics and Other Selected Partial Area Applications of Differential Scanning Calorimetry. R.L. Blaine and P.F. Levy, Du Pont Co.

The Alpha–Beta Phase Transition in Titanium Alloys by Differential Thermal Analysis. J.S. Fippen, Wyman Gordon Co.

Extensions of Thermoanalytical Techniques: The Impact of the Microprocessor. P. Levy, Du Pont Co.

Atomic Fluorescence Spectroscopy

A.H. Ullman, *Presiding*

Approaches to Multielement Atomic Fluorescence Spectroscopy. A.H. Ullman, Procter & Gamble

Pulsed Hollow Cathode Lamp Excitation of Atomic Fluorescence in the Inductively Coupled Argon Plasma. M.A. Kosinski and J.D. Winefordner, U of Florida

Simultaneous Multielement Analysis of Industrial Samples with an ICP Atomic Fluorescence Spectrometer. D.R. Demers, Baird Corp.

Flame and Plasma Investigations Utilizing Laser-Saturated Fluorescence. G.J. Bastiaans, B.T. Ahn, and F. Albahadily, Texas A&M U

Laser-Excited Atomic Fluorescence in a Glow Discharge. B.W. Smith, C. Van Dijk, and J.D. Winefordner, U of Florida

Absolute Measurements of Heavy Metal Impurities and Hydrogen Atom Densities in the Doublet III Tokamak Using Laser-Induced Fluorescence Spectroscopy. C.H. Muller III and K.H. Burrell, General Atomic Co.

Trace Elements in Biological Fluids

D.C. Warren, *Presiding*

Analysis with Bioselective Membrane Electrodes. G.A. Rechnitz, U of Delaware

Trace Elements in Biological Fluids by Plasma Spectroscopy. R.M. Barnes, P. Fodor, K. Inagaki, and Z. Mian-zhi, U of Massachusetts

Trace Elements in Biological Fluids—Things I Wish I Knew When I Got into This Business. J.M. Fitzgerald, Litton Bionetics, Inc.

Heavy Metals: How Important Are They? R.P. Torrey and S. Seged, Tennessee State U

The Chromium Story—Or How To Start an Entire Field Over. C. Veillon and K.Y. Patterson, USDA Human Nutrition Center

Blood Selenium Levels and Glutathione Peroxidase Activities as Measures of Human Selenium Status. D.C. Warren, Houston Baptist U

Quantitative Surface Analysis

H.S. Gold, *Presiding*

Inelastic Electron Tunneling Spectroscopy. L.J. Hilliard and H.S. Gold, U of Delaware

Surface Analysis by SIMS. N. Winograd, Pennsylvania State U

Comparison of Techniques for Quantitative Surface Analysis Using Auger Electron (AES) and X-ray Photoelectron Spectroscopy (XPS). D.P. Griffis and R.W. Linton, U of North Carolina at Chapel Hill

Problems and Progress in Quantitative Surface Analysis. C.J. Powell, National Bureau of Standards

Quantitative Analysis by Ion Scattering Spectrometry. D.G. Swartzfager, Du Pont Co.

Surface Analysis and Time-Resolved Leaching Studies of Inorganic Species in Airborne Particles. M.E. Farmer and R.W. Linton, U of North Carolina at Chapel Hill

Characterization of Fluidized Bed Aerosols by Auger Microprobe. J.A. King, METC

Influences of the Chemical Composition of the Atmosphere upon Laser Plumes. A.L. Lewis II, G.J. Beenen, and E.H. Piepmeier, Oregon State U

Current Analytical Problems in the Forensic Laboratory

A. A. Cantu, *Presiding*

An Analytical Approach to Determining the Country of Origin of Aviation Gasolines. B.C. Pettitt and Le Tiet, U.S. Customs Service

Identification of Fuels in Arson Debris by Detection of Additives. D.J. Reutter and R.M. Martz, FBI Laboratory

HPLC–ECD (Electron Capture Detection) in the Analysis of Explosive Materials. I.S. Krull, D. Bushee, E.A. Davis, and C. Santasania, Northeastern U, and S. Krauss, A. Bosch, and Y. Bomberger, Israel Police Headquarters

Analysis of Explosives and Explosive Residues by Ion Chromatography. D.J. Reutter and R.C. Buechele, FBI Laboratory

The Use of Electrochemistry in Gunshot and Explosive Residue Detection. R.C. Brimer, S.E. Missouri Regional Crime Laboratory

28 086
14 Si

Petrarch
for
organosilicon
specialties

Silanes for bonded phases

Octyl, octadecyl, amino, cyano and perfluoroalkyl silanes are available from Petrarch for use in preparation of permanently bonded phases for HPLC. We also undertake custom syntheses of non-catalog items for your specific requirements. Send for your information packed, 110 page catalog today—it's free.

PETRARCH SYSTEMS, INC.
Bartram Road
Bristol, PA 19007
215:781-9255
In the Far East:
Chisso Corp., Tokyo

CIRCLE 175 ON READER SERVICE CARD

EASIER DOES IT!



It's easier to make KBr pellets with our new Handi-Press. No need to bother with a separate press. Our die and press are combined in one hand-held unit that weighs only 2½ pounds.

Interchangeable die inserts make it a quick cinch to match the amount of your material with the best pellet size for good spectra. Simply turn the die chamber for the right die pressure for standard 7 mm, 3 mm or 1 mm pellets. Eliminate water bands just by attaching your vacuum pump to the optional vacuum chamber head.

Unexpected savings. Compare the high prices of other KBr pellet-making devices with the far lower cost of our Handi-Press. The savings could surprise you — very pleasantly. Whenever you have an IR problem, call the IR accessories specialist: Barnes Analytical. Easier-does-it in more ways than you might think.

Analytical
BARNES

Barnes Analytical Division, Spectra-Tech, Inc.
652 Glenbrook Road, Stamford, Connecticut 06906
Phone toll free 800-243-9186
In Connecticut, 203-357-7055

CIRCLE 27 ON READER SERVICE CARD

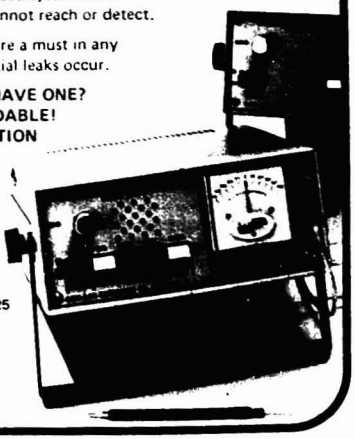
GOW-MAC GAS LEAK DETECTORS

Maximum Response at Modest Prices —
- **DEPENDABLE**
- **SENSITIVE**
- **VERSATILE**
- **EFFICIENT**

GOW-MAC Gas Leak Detectors can ferret out leaks in heated or ambient gas pressurized systems that the usual soap bubble method cannot reach or detect.

GOW-MAC Gas Leak Detectors are a must in any plant or laboratory where potential leaks occur.

**CAN YOU AFFORD NOT TO HAVE ONE?
GOW-MAC MAKES IT AFFORDABLE!
USE THE READER INFORMATION
NUMBER FOR OUR
INFORMATIVE BROCHURE.**



GOW-MAC
INSTRUMENT CO.
P.O. Box 32, Bound Brook, NJ 08825
Telephone: (201) 560-0600

CIRCLE 91 ON READER SERVICE CARD

GC/FTIR: Development and Application

K. H. Shafer, *Presiding*

Optimization of Chromatographic, Spectroscopic, and Computational Parameters for Capillary GC/FTIR. P.R. Griffiths, G. Yifei, and J.N-P. Sun, Ohio U

GC/FTIR/MS and Its Data Reduction. T. Hirschfeld, Lawrence Livermore Laboratory

Chemical Analysis by GC/IR/MS. C.L. Wilkens, U of California

The Development of GC/FTIR for Pollution Analysis. L.V. Azarraga, C. Potter, and R. Williams, U.S. Environmental Protection Agency

An Interferogram-Based Search System for Vapor Phase Infrared Fourier Transform Data. J.A. DeHaseth, U of Alabama

Applications of a Highly Sensitive Capillary GC/FTIR System. D. Keuhl, K. Krishnan, and M. Olsen, Digilab Division of Bio-Rad Laboratories

Monday Afternoon

Sample Introduction for Atomic Spectroscopy

R. F. Browner, *Presiding*

Slurry Atomization Direct Atomic Spectrochemical Analysis. N. Mohamed and R.C. Fry, Kansas State U

Use of a Vortex Ring Generator for Sample Modulation and Aerosol Droplet Size Separation in Atomic Spectrometry. A.W. Steele and G.M. Hieftje, Indiana U

Enhancement and Supression Effects Using a Tandem Nebulization System for Introduction of Sample into the ICP. K.A. Wolnik, F.L. Fricke, and M.H. Hahn, USFDA Elemental Analysis Research Center

Some Observations on the Use of Organic Solvents with a Three-Electrode Direct Current Argon Plasma. W.J. Boyko and P.N. Keliher, Villanova U

Correlations between Aerosol Particle Size and Interference Effects in Atomic Spectrometry. D.D. Smith and R.F. Browner, Georgia Institute of Technology

Powder Introduction in Inductively Coupled Plasma Spectroscopy. G.A. Meyer and R.M. Barnes, U of Massachusetts

Head Space Analysis

G. R. Umbreit, *Presiding*

Analyses and Identification of Organic Impurities in Water by a Headspace Gas Chromatographic Technique. M. Markelov, A. McMaster, and N. Meyer, The Standard Oil Co. (Ohio)

Determination of ppb Solvent Levels in the Atmosphere. S.E. Borodkin, Brooklyn, N.Y.

Gas Chromatographic Headspace Analysis of HCN. W. Reuter, W.B. Caldwell, and B. Singleton, Merck and Co., Inc.

Quantitative Determination of Solvents in Epoxy-Coated Printed Wiring Boards by Gas Chromatographic Headspace Analysis. D.M. La Perriere, K.R. Elmendorf, and J.F. Geibel, Western Electric Co.

The Direct Analysis of Flavors and Fragrances by MS/MS. B. Shushan, Thornhill, Ontario

Progress in Electrothermal Atomization

W. Slavin, *Presiding*

ETA Measurements: A Useful Probe for Surface Investigations? G. Tessari, Istituto di Chimica Analitica, Italy

Surface Effects in Electrothermal Atomizer. T.M. Vickrey, Bowling Green State U

Surface Reactions as a Key to Interferences in Flameless Atomic Absorption Spectroscopy. T.M. Niemczyk, U of New Mexico

Direct GFAAS Determination of Trace Metals in Seawater: A Pyrolysis Mass Spectrometric Investigation. C.G. Flinn, R. Guevremont, and W.D. Jamieson, Atlantic Research Laboratory, National Research Council of Canada

Second Surface Atomization: A Simple Approach for Interference Reduction in GFAA. M. Sheehan and J.A. Holcombe, U of Texas at Austin

Absolute Atomization Efficiency of the Graphite Furnace. R.E. Sturgeon, Division of Chemistry, National Research Council of Canada

Evaluation of AAS Signals for Establishing Atom Formation Processes in GFAAS. W. Frech, E. Lundber, and A. Cedergren, U of Umeå, Sweden

Recent Studies on the Use of the Graphite Furnace as an Atomization Cell in Atomic Absorption Spectroscopy. M.W. Routh, P.S. Doidge, A.G. Wiseman, and T.N. McKenzie, Varian Techtron Pty. Ltd.

Drying Temperature Studies Using Graphite Furnace Atomic Absorption Spectrometry. R.W. Dabeka, Food Research Directorate, Health Protection Branch, Canada

Atomic Fluorescence Spectroscopy

A. H. Ullman, *Presiding*

Recent Studies Using LC/AFS. W.J. Taraszewski and B.D. Pollard, Marquette U

Alternative Atomization Techniques in Atomic Fluorescence Spectrometry. E.M. Heithmar, U of New Orleans

Easily Duplicated Photographic Negative as a Wavelength Encode Wheel for Sequential Atomic Fluorescence Spectrometry. S.K. Hughes, M. van Swaay, and R.C. Fry, Kansas State U

A Zeeman-Effect-Based Scatter Correction System for Multielement Nondispersive Atomic Fluorescence Spectrometry. D.A. Naranjit, B.H. Radziuk, and J.C. Van Loon, U of Toronto

Double Modulation and Its Effect on Accuracy of Atomic Fluorescence Measurements. R.G. Michel, J.T. McCaffrey, and C. Gamper, U of Connecticut

Trace Elements in Biological Fluids

D. C. Warren, *Presiding*

Chromium in Human Serum. K.Y. Patterson and C. Veillon, USDA Human Nutrition Center

Stable Isotope Dilution—GC/MS Determination of Selenium in Biological Materials. D.C. Reamer and C. Veillon, USDA Human Nutrition Center

Influence of Storage Containers and Temperature on the Concentrations of Cadmium and Lead in Whole Human Blood Samples. K.S. Subramanian, J.C. Meranger, and J. Connor, Environmental Health Centre, Health and Welfare Canada

Effect of Selenium Supplementation on Blood Selenium Concentrations and Glutathione-Peroxidase Activities of Patients Undergoing Intravenous Hyperalimentation. D.C. Warren and H.W. Lane, Houston Baptist U

New Instrumental Techniques in Electrochemistry

J. Osteryoung, *Presiding*

Rapid Scan Square Wave Voltammetry. J.J. O'Dea, R. Osteryoung, and J. Osteryoung, State U of New York at Buffalo

Bioselective Membrane Electrodes Using Novel Bacterial Biocatalysts. C.L. Di Paolantonio and G.A. Rechnitz, U of Delaware

Electrochemical Detection of *N*-Nitrosamines and Nitrofurans. G.W. Harrington, H.S. Veale, J. Wang, and S.K. Vohra, Temple U

Voltammetric Determination of Morphine in Poppystraw Concentrate at a Glassy Carbon Electrode. R.S. Schwartz, U.S. Customs Service

Wave-Shape Analysis in Voltammetry Using Deviation–Pattern Recognition. J.F. Rusling, U of Connecticut

Current Analytical Problems in the Forensic Laboratory

A. A. Cantu, *Presiding*

Mass Spectrometry and the Forensic Identification. D. Cooper, Drug Enforcement Administration, Special Testing and Research Laboratory

Applications of Atmospheric Pressure Chemical Ionization Mass Spectrometry for Drug Detection. L.V.S. Hood, B.C. Pettitt, and J.L. Sullivan, U.S. Customs Service

Thin-Layer Immunoassay: A Novel Method for the Detection of Picogram Quantities of Drugs in Biological Samples. M.E. Fredenburg and N.T. Lappas, Dept. of Forensic Sciences, George Washington U

China White—Its Spectroscopic Characteristics and Synthesis Routes. A. Allen, Drug Enforcement Administration, Special Testing and Research Laboratory

On the Uniqueness of Fingernail Ridge Patterns. W.F. Rowe, Dept. of Forensic Sciences, George Washington U

Mathematical Model for Ink Drying and Extraction. A.A. Cantu, Bureau of Alcohol, Tobacco, and Firearms

GC/FTIR: Development and Application

K.H. Shafer, *Presiding*

High Performance GC/FTIR. D.W. Vidrine and S.R. Lowry, Nicolet Instrument Co.

Advances in the Application of GC/FTIR. G. Adams, D. Gerson, and S. Garlock, IBM Instruments, Inc.

Utilizing GC/FTIR and GC/MS Data for Pollution Analysis. R.J. Jakobsen and K.H. Shafer, Battelle Columbus Laboratories

Laser Intracavity Absorption Detector for Gas Chromatography. J.D. Parli and R.B. Green, U of Arkansas

GC/IR of the Aromas of Intact Fruits. J.M. Purcell and P. Magidman, USDA Eastern Regional Research Center

GC/FTIR Applications in Pesticide Chemistry. K.S. Kalasinsky, Mississippi State Chemical Laboratory

Pyrolysis Capillary GC/FTIR Study of Polymers, J.M. Casper, D.J. Gerson, and G.E. Adams, IBM Instruments, Inc.

Hazardous Waste Analysis by GC/FTIR, D. Gurka, D. Sauter, D. Detowski, and G. Meier, USEPA–Las Vegas

Tuesday Morning, Sept. 22

Sample Introduction for Atomic Spectroscopy

R.F. Browner, *Presiding*

Sample Introduction for Atomic Spectroscopy with Electrically Vaporized Thin Metal Films. R. Sacks and J. Goldberg, U of Michigan

Halide Generation—An Approach to Solid Sampling. M.L. Parsons and S.R. Burge, Arizona State U

Microdroplet Sample Application in an Electrothermal Atomizer for Atomic Absorption Spectrometry. J.G. Shabushnig and G.M. Hieftje, Indiana U

Measurement of Nebulization Efficiency with a Furnace Atomizer. R.N. Savage, S.B. Smith, J.J. Sotera, and M.K. Conley, Analytical Instrument Division, Instrumentation Laboratory, Inc.

Rapid ICP Analysis of Soils Extracts and Feed Digests. R.A. Isaac, U of Georgia College of Agriculture

Analysis of Trace Quantities of Silicon by Electrothermal Atomic Absorption Using the Graphite Platform. P.M. Grohse and W.F. Gutknecht, Research Triangle Institute

Automatic Direct Sample Insertion System for Inductively Coupled Plasma Emission Spectrometry. W.W. Pettit and G.E. Horlick, U of Alberta, Canada

Recent Advances in Environmental/ Analytical Chemistry of Priority Pollutants

B.K. Afghan, *Presiding*

Beyond Priority Pollutants. W.L. Budde, U.S. Environmental Protection Agency, Environmental Monitoring and Support Laboratory

The Application of MS/MS to the Rapid Screening and Analysis of Priority Pollutants. S. Tanner, B. Shushan, J. Fulford, and T. Sakuma, SCIEX, Inc.

Analysis of Priority Pollutants in Multimedia Environmental Samples by High Resolution Glass Capillary GC and GC/MS System. P. Bastien, J. Lockwood, D. Wang, R.S. Thomas, and R.C. Lao, Chemistry Division, Air Pollution Control Directorate, Environment Canada

Analysis of Trace Organic Contaminants in Waste Waters and Sludges by GC/MS. S. Lesage, National Water Research Institute, Canada

Very High Speed Liquid Chromatographic Analysis for Priority Pollutants: System and Applications. M.W. Dong, E. Katz, and J.L. DiCesare, Perkin-Elmer Corp.

Factors Influencing Reproducibility in Priority Pollutant Determinations. M.R. Bogdun, Supelco, Inc.

Progress in Electrothermal Atomization

T.M. Vickrey, *Presiding*

The Use of High Temperature Equilibrium Calculations for Establishing Optimum Conditions for AAS Measurements. A. Cedergren, W. Frech, E. Lundberg, and J.A. Persson, U of Umeå, Sweden

Free Atom Generation for AAS with Electrically Vaporized Thin Metal Films. R. Sacks and R. Collins, U of Michigan

Interference Reduction in a Furnace Atomizer by Aerosol Deposition into a Microboat. J. Sotera, M. Conley, and H. Kahn, Instrumentation Laboratory, Inc.

A Critical Study of the Solid Sampling Technique for the Determination of Trace Elements in

Solid Metallurgical Materials by GFAAS. W. Frech and E. Lundberg, U of Umeå, Sweden

Determination of Phosphorous in Steel Using Zeeman Furnace AA. B. Welz, Z. Grobenski, and U. Voellkopf, Bodenseewerk Perkin-Elmer & Co. GmbH, West Germany

Simultaneous Multielement Atomic Absorption Spectroscopy Using Electrothermal Atomization. J.S. Kane, USGS, Branch of Analytical Laboratories, and J.M. Harnly, USDA Nutrient Composition Laboratory

Graphite Furnace Analyses Using Zeeman Effect Background Correction. F.J. Fernandez, M.M. Beaty, and W.B. Barnett, Perkin-Elmer Corp.

A Fundamental Look at Oxygen Ashing of Biological Samples in GFAA. D.K. Eaton and J.A. Holcombe, U of Texas at Austin

Applications of FTIR and Raman Spectroscopy

K.S. Kalasinsky, *Presiding*

FTIR Spectra of Extracts of Sewage Sludge. D. Michael Byler and E.G. Piotrowski, USDA Eastern Regional Research Center

Quantitative Analysis of Kerosenes by Raman Spectroscopy. K.S. Kalasinsky, Mississippi State Chemical Laboratory

Diffuse Reflectance FTIR Spectra of Fossil Fuel-Derived Liquids and the Correlation of Spectral Features with Observed Bioactivity. J.E. Caton, S.H. Harmon, W.H. Griest, and M.R. Guerin, Oak Ridge National Laboratory

FTIR Study of Chemical Reactions Occurring in a Diamond Cell. C.A. Cody and M.T. Hatcher, NL Chemicals/NL Industries, Inc.

Conformational Analysis Utilizing Low Frequency Vibrational Data. J.F. Sullivan and J.R. Durig, U of South Carolina

What Can Raman Spectroscopy Offer to the Industrial Analyst? D.L. Gerrard, British Petroleum, England

FTIR in a Multiple Inexperienced User Situation. M. Baum, Princeton U

Environmental and Forensic Applications of Mass Spectrometry

Jane Gale, *Presiding*

Forensic Applications of Mass Spectrometry. R. Saferstein, New Jersey State Police

Recent Environmental and Forensic Applications of an MS/MS System. W.R. Davidson, Thornhill, Ontario

Screening and Fingerprinting of Fossil Fuels by Chemical Ionization. L.W. Sieck, National Bureau of Standards

Mass Spectral Analysis of Sulfur Compounds in Heavy Petroleum Fraction. C.S. Hsu, T.R. Ashe, J. Kelliher, W.K. Robbins, and F.C. McElroy, Exxon Research and Engineering Co.

Chemical Characterization of Diesel Particulate Matter. J. Yergey, T. Risby, S. Lestz, and R. Yasbin, Johns Hopkins U

Environmental Applications of Secondary Ion Mass Spectrometry. R.W. Linton and M.E. Farmer, U of North Carolina

Thermal Ionization Mass Spectrometry of Quaternary Salts. A.L. Yergey and R.J. Cotter, National Institute of Child Health and Human Development

Analytical Applications of Chemically Modified Surfaces

D.E. Leyden, *Presiding*

Thermometric and Potentiometric Studies of the Reaction of Diamine Modified Glass Surfaces with Aqueous Cu(II). R.J. Kvitek, P.W. Carr, and J.F. Evans, U of Minnesota

An Enthalpimetric Study of the Surface Interactions of Primary Aliphatic Amines on Silica Gel. J.K. Grime and E.D. Sexton, U of Denver

Chemically Modified Electrodes—Approaches to Electron Transfer Catalysis and Catalysis of Coupled Chemical Reactions. C.M. Elliott, J.P. Bickford, R.R. Krebs, C.A. Marrese, and W.S. Martin, U of Vermont

Luminescent Spectroscopy of Chemically Modified Silica Surfaces. C.H. Lochmuller, D.R. Wilder, D.B. Marshall, and P.M. Gross, Duke U

Chemical and Spectroscopic Studies of Modified Surfaces. D. Leyden, L. Burgraff, and D. Kendall, U of Denver

Computers in the Analytical Laboratory

J.L. Glajch, *Presiding*

Laboratory Microcomputers for the Analytical Chemist: A Survey of Available Systems. T.C. O'Haver, U of Maryland

A Laboratory Data Management System. A. Ganz, J.D. Johnson, and B. Gram, Spectrogram Corp.

Instrumentation, Information, and Education. F.A. Settle, Jr., and M.A. Pleva, Virginia Military Institute

Interfacing a Technicon Auto-Analyzer with a Minicomputer and Graphics CRT. R.B. Willis, USDA–Forest Service

Automated and On-Line Gas Chromatography System for Process Engineering Studies. R.L. Cryberg, G.E. Walls, and W.R. Bramstedt, Diamond Shamrock Corp.

Quantitative Analysis of Components Occurring in Biological Extracts with Chromatographic Methods: Computer Simulation and Mathematical Model. W.L. Creten, L. Nagels, and P.M. Vanpeperstraete, Rijksuniversitair Centrum Antwerpen, Belgium

Trace Elemental Analysis in Foods, Soils, and Plants

K. Wolnik, *Presiding*

New Developments in Food and Plant Tissue Certified Reference Materials. R. Alvarez, National Bureau of Standards

Validation of Analysis of Inorganic Nutrients in Foods. W.R. Wolf, USDA Nutrient Composition Laboratory

Contamination Control and Sample Preparation Techniques Required for the Elemental Analysis of Foods. F.L. Fricke, USFDA Elemental Analysis Research Center

Trace Metals Analysis in Plants and Soils Using ICP. R.K. Brown, L. Carrara, V.J. Luciano, L.F. Marciello, and A.F. Ward, Jarrell-Ash Division, Fisher Scientific Co.

ICP–AES Analysis of Plant Tissue Using a Continuous Flow Hydride Generation System. J.E. Borst, Bausch & Lomb, ARL Division, and M. Watson, Ohio State U

Analysis of Elemental Hydrides (Al, Ge, Se, Sb, Sn) at the Parts per Billion Level in Foods by ICP–AES. M.H. Hahn, K.A. Wolnik, F.L. Fricke, , and J.A. Caruso, USFDA Elemental Analysis Research Center

Report on a Workshop on the Determination of Lead in Foods Using Graphite Furnace Atomic Absorp-

tion Spectrometry. R.W. Dabeka, Food Directorate, Health Protection Branch, Canada

Particle Size Analysis

H. Barth, *Presiding*

A Review of Commercially Available Instrumentation for Particle Size Analysis. L.G. Bunville, Hercules, Inc.

Submicron Particle Size Determination. P.E. Plantz, H.N. Frock, and E.C. Muly, Leeds & Northrup Co.

Particle Sizing with Malvern Equipment. B. Weiner, Malvern Scientific Corp.

Particle Size Measurements by Photon Correlation Spectroscopy. G.R. Alms, Du Pont Co.

Application of Photon Correlation Function Profile Analysis to Molecular Weight Distributions of Polymers in Solution. B. Chu and A. DiNapoli, State U of New York at Stoney Brook

Tuesday Afternoon

ICP–DCP Emission Spectroscopy: Fundamentals

G.N. Coleman, *Presiding*

Laser-Induced Fluorescence of Metastable Argon in the Inductively Coupled Plasma. J.W. Carr and G.M. Hieftje, Indiana U

A Study of the Densities of Metastable States in an Argon ICP Using Atomic Absorption Spectroscopy. M.W. Blades and G.M. Hieftje, Indiana U

Influence of the Generator Frequency on the Spectral Characteristics of Inductively Coupled Plasmas. B. Capelle and J.M. Mermet, Laboratoire de Physicochimie Industrielle, France

Atomic Emission with a Skimmed ICP. A. Montaser and V.A. Fassel, Iowa State U

Constriction of a Microwave-Induced Plasma Using a Magnetic Theta Pinch. J.P. Deavor, D.T. Pipes, and S.R. Goode, U of South Carolina

Measurement of Electron Concentrations in DC Plasmas. R.R. Williams and G.N. Coleman, U of Georgia

Calculation of Analyte Level Populations in an ICP Discharge. R.J. Lovett, North Dakota State U

Recent Advances in Environmental/ Analytical Chemistry of Priority Pollutants

B.K. Afghan, *Presiding*

New Development, Preparation, and Application of the First Standard Reference Material for PCB Analysis in Sediment. H.B. Lee and A.S.Y. Chau, National Water Research Institute, Ontario

Priority Pollutant NBS Standard Reference Materials. R. Alvarez, National Bureau of Standards

Methodology for the Extraction and Analysis of Air Particulate Organics. B.D. Barkenbus, W.H. Griest, and B.A. Tomkins, Analytical Chemistry Division, Oak Ridge National Laboratory

Analysis of Volatile Organics in Air Collected in Stainless Steel Sampling Bombs. D.N. Speis, S.C. Stodola, and A. Goldberg, U.S. Environmental Protection Agency

Evaluation of Level I Organic Analysis Procedures. R.K.M. Jayanty, W.F. Gutknecht, A. Gaskill, Jr., and D.E. Lentzen, Research Triangle Institute

Problems of Quantitation in Trace Analysis by Gas Chromatography. J. Novak, Institute of Analytical Chemistry, Czechoslovak Academy of Sciences

Atomic Absorption Applications

M. Kaiser, *Presiding*

Progress in Simultaneous Multielement Atomic Absorption with a Continuum Source (SIMAAC). T.C. O'Haver, U of Maryland

Effect of Wavelength Modulation Frequency on the Signal-to-Noise Ratio of Continuum Source AA. J.M. Harnly, USDA Nutrient Composition Laboratory

A Comparison of Techniques for Determination of Trace Elements in Jet Engine Lubricating Oil. J.Y. Marks, D.E. Fornwalt, and G. G. Welcher, Pratt & Whitney Aircraft

Dynamic Generation of Calibration Gas Standards Using Nebulizer Introduction of Analyte. J.A. Nichols and J. Wallace, U of Denver

Chromium in Biological Fluids by Graphite Furnace Atomic Absorption Spectrometry. C. Veillon, K.Y. Patterson, N.A. Bryden, and D.C. Reamer, USDA, SEA Human Nutrition, Beltsville Human Nutrition Research Center

Analysis of Heavy Matrixed Samples for Trace Levels of Selenium. M.W. Tikkanen, Scientific Laboratory Division, State of New Mexico

Determination of Priority Pollutants by Furnace Atomic Absorption. L.M. Voth, L.M. Covick, and D.E. Shrader, Varian AA Resource Center

The Simultaneous Analysis of 11 Trace Metals in Fruit Juices by Atomic Absorption Spectroscopy. J.M. Harnly, N.J. Miller-Ihli, and W.R. Wolf, USDA Nutrient Composition Lab and U of Maryland

LC/FTIR

D.W. Vidrine, *Presiding*

FTIR Detection in Size Exclusion Liquid Chromatography. R.S. McDonald, General Electric Corporate Research & Development Center

GPC/FTIR of Polybutadienes and Polyurethanes. R. Irwin, ARCO

Functional Group Analysis of Solvent-Refined Coal Fractions Employing HPLC–FTIR. R.S. Brown, C.C. Johnson, P.M. Graham, and L.T. Taylor, Virginia Polytechnic Institute and State U

Pesticide Residue Analysis by LC/FTIR. K.R. Hill, USDA-SEA/AR-AEQI-ACL

High-Sensitivity HPLC/Drift with Solvent Elimination and Solute Extraction: Current Status. P.J. Duff, C.M. Conroy, and P.R. Griffiths, Ohio U

Flow Cell LC/FTIR and GPC/FTIR: Exotic Solvents, Microbore Columns, and Associated Techniques. D.W. Vidrine, Nicolet Instrument Corp.

Separations—Mass Spectrometry

C.W. Polley, Jr., *Presiding*

Analytical Applications of FT-MS. S. Ghaderi and R.B. Spencer, Nicolet Instrument Corp.

GC–ICR. M.T. Nguyen, J. Wronka, B.S. Larsen, and D.P. Ridge, U of Delaware

The Quantitative Characterization of Mixtures Using Soft Ionization Mass Spectrometry. G.E. Hansen, T. Chen, D. Heller, R. Cotter, and C. Fenselau, Johns Hopkins U School of Medicine

Sorption and Release of Organic Molecules by Fly Ash during and

after Heat Treatment. J.E. Caton and W.H. Griest, Oak Ridge National Laboratory

Applications of Fused Silica Capillary Columns in Gas Chromatography/Mass Spectrometry. J. Kananen, Hewlett Packard

Analysis of Diborane, Tetraborane, and Pentaborane in Air at Parts per Billion Levels. M.A. Rudat, Du Pont Co.

Chromatography–Molecular SIMS. K.L. Busch, A. Vincze, S.E. Unger, and R.G. Cooks, Purdue U

MS/MS—Will It Replace the GC/MS? W.R. Davidson, Thornhill, Ontario

Chromatography Forum of the Delaware Valley Student Award

M.J. O'Brien, *Presiding*

Spectrofluorodensitometry of Bile Acids on Thin Layer in Rat Bile. P.J. Carter and J.C. Touchstone, Hospital of the U of Pennsylvania

Evaluation Procedures for LC Pulse Dampeners. J.F. Harris and S.J. Pruskowski, Philadelphia College of Pharmacy and Science

HPLC Analysis of Citral Isomers. G. Facks and J. A. Mangravite, West Chester State College

The Chromatography of Cytochrome P-450 on DEAE Cellulose. L.E. Peterson Archer and J.C. Touchstone, Hospital of the U of Pennsylvania

An Investigation of the Chemistry of Browning Reactions During the Conching of Chocolate. J.C. Hoskin and P.F. Dimick, Pennsylvania State U

Theoretical Explanation of the Relative Rates of Movement of Sterols in Reverse Phase Liquid Chromatography. J.M. Di Bussolo and W.R. Nes, Drexel U

Isolation and Purification of Goat Milk Lipoprotein in Lipase. A.A. DeFeo and P.S. Dimick, Pennsylvania State U

Gas Chromatographic Studies of Adsorption of Hydrocarbons in Soils. P. Kanatharrana and R.L. Grob, Villanova U

Microextraction Studies of Phenols and Phthalate Esters Using GC. L. Olszewski and R.L. Grob, Villanova U

Studies of Modified Carbon Packings in GSC. M.A. Quarry and R.L. Grob, Villanova U

Clinical Chemistry—New Solutions to Old Problems

R.S. Schifreen, *Presiding*

Disposable Potentiometric Gas Sensors for Clinical Analysis. M.E. Meyerhoff, U of Michigan

Kinetic Determination of Glucose in Blood Serum and Plasma Using a Solid Phase Reagent and Reflectance Photometer. R.S. Turk, Ames Division, Miles Laboratories

Coagulation Testing: Going Beyond the Clot. J.F. Perry, Du Pont Co.

A Colorimetric Solid Phase Test for Potassium. S.C. Charlton, R.L. Fleming, and A. Zipp, Ames Division, Miles Laboratories

Automated Multiple Flow Injection Analysis: A New Tool for Clinical Analysis. K.K. Stewart, USDA Nutrient Composition Laboratory

Application of Immobilized Enzymes as Pre- and Post-Column Modification Agents for HPLC. L.D. Bowers and P.R. Johnson, U of Minnesota

HPLC Analysis of Basic Drugs. R. Eksteen, Supelco, Inc., and J.J. Thoma, South Bend Medical Foundation

Rapid Analysis of Cyanocobalamin in Parenteral and Total Parenteral Nutrition Solutions. L.V. Streips and R. Dawe, Travenol Laboratories, Inc.

UV Spectrophotometric Estimations of Quinones of Clinical Importance. N.K. Murty and P.M. Dakshina Murty, Andhra U, India

Trace Elemental Analysis in Foods, Soils, and Plants

F. Fricke, *Presiding*

Quantitative Determination of Lead and Cadmium in Total Diet Market Baskets by Flameless Atomic Absorption. K.C. Faul and B.E. Young, FDA Total Diet Laboratoy

Trace Elements of Nutritional Importance in Jojoba Seeds. W.J. Utz, P.L. O'Connell, and N.W. Bower, Colorado College

Coprecipitation Fluorescence Techniques for Detecting Actinides at Subpicomolar Levels. F. Milanovich, T. Hirschfeld, S. Miller, S. Klainer, and D. Perry, Lawrence Livermore Laboratory

Environmental Analysis by Ion Chromatography. A.W. Fitchett, Dionex Corp.

Trace Element Analysis of Soils. D.E. Baker and D.B. Beegle, Pennsylvania State U

Amount of Birefringence in Defect Crystals Is Proportional to Trace Chemical Concentration—Application to Food Analysis. M.M. Schachter, Chromalcarb Co.

Particle Size Analysis

H. Barth, *Presiding*

A Theoretical and Experimental Examination of Hydrodynamic Chromatography. C.A. Silebi, Lehigh U

Chromatography of Particle Suspensions—Detector Systems. A.E. Hamielec, McMaster U, Canada

Hydrodynamic Chromatography of Rigid Biological Polymers. R.K. Prud'homme, G. Froimann, and D. A. Hoagland, Princeton U

Quantitative Particle Size Distribution Analyses by Sedimentation Field Flow Fractionation. J.J. Kirkland and W.W. Yau, Du Pont Co.

An Overview of Particle Size Distribution Analysis by Disc Centrifuge Photosedimentometry. T. Provder, Gliden Coatings and Resins

Particle Size Analysis by the Radial Dilution Method Using the Disc Centrifuge. I.G. Bunville, Hercules, Inc.

Wednesday Morning, Sept. 23

ICP–DCP Emission Spectroscopy: Fundamentals

G.N. Coleman, *Presiding*

Distributions in a Three Electrode DCP'. R.J. Decker, U of Zimbabwe, Salisbury, Zimbabwe

Application of DC Argon Plasma Emission Spectroscopy to Saline Waters: A Study of Emission Enhancements and Plasma Characteristics. D. Eastwood, M. Schulz Hendrick, and M.H. Miller, U.S. Coast Guard Research & Development Center

Experimental Diagnostics of Electrons and Particulates in High Voltage Sparks. A. Scheeline, M.J. Zoellner, M.A. Lovik, T.V. Tran, and G.J. Kamla, U of Iowa

Simulation of Spark Source and Discharge Properties. A. Scheeline, T.V. Tran, and G.J. Kamla, U of Iowa

Instrumental and Operational Characteristics of an Atmospheric Pressure Microwave-Induced Ni-

trogen Plasma. R.D. Deutsch and G.M. Hieftje, Indiana U

Analytical Characteristics of an Atmospheric Pressure Microwave-Induced Nitrogen Plasma. R.D. Deutsch, J.P. Keilsohn, and G.M. Hieftje, Indiana U

Inductively Coupled Plasma Discharges Sustained in Argon, Nitrogen, and Air. G.A. Meyer and R.M. Barnes, U of Massachusetts

Aerosol Injection Tube Temperature Effects in the ICP Torch. D.H. Tracy and S.A. Myers, Perkin-Elmer Corp.

Recent Advances in Environmental/ Analytical Chemistry of Priority Pollutants

B.K. Afghan, *Presiding*

Preconcentration of Trace Metals from Seawater Using Silica Immobilized 8-Hydroxyquinoline. R. Sturgeon, S. Willie, A. Desaulnierst, and S. Berman, National Research Council, Canada

Applications of Linear Scan and Differential Pulse Anodic Stripping Voltammetries in the Determination of Arsenic in Water Samples. P.C. Leung, J.C. Meranger, and K.S. Subramanian, Environmental Health Centre, Health and Welfare Canada

An Improved Method for Determination of Polynuclear Aromatic Hydrocarbons in Environmental Samples. B.K. Afghan and R.J. Wilkinson, Canada Centre for Inland Waters

The Effect of the Sample Matrix on Capillary Gas Chromatographic Pollutants. M.E. Post, J. Gibs, and I.H. Suffet, Drexel U

Determination and Occurrence of Some Organic Pollutants in Canadian Potable and Raw Water Supplies. R. Otson and D.T. Williams, E.H.C., Tunney's Pasture, Ontario

Solubility of PCBs in Water. T. Stolzenburg, U of Wisconsin

Progress in Electrothermal Atomization—Panel Discussion

J.A. Holcombe, *Presiding*

Interferences in Furnace Atomization: Present Understanding and Future Needs. A. Cedegren, U of Umeå, Sweden; W. Frech, U of Umeå, Sweden; T. Rains, National Bureau of Standards; W. Slavin, Perkin-Elmer Corp.; and R. Sturgeon, National Research Council of Canada

Anachem Award Symposium—Advances in Analytical Microscopy

K. Hutchinson, *Presiding*

Presentation of Anachem Award to Walter C. McCrone, McCrone Research Institute, by K. Hutchinson, President-Elect, Anachem

Anachem Award Address. The Turin "Shroud," W.C. McCrone, McCrone Research Institute

Identifying Nanogram Samples. A. Teetsov, McCrone Associates

Classical Chemical Microscpy in Contemporary Analytical Chemistry. S. Palenik, McCrone Associates

Microanalytical Problem Solving Using MOLE. M. Anderson, McCrone Associates

Frontiers in Biomedical Spectroscopy

R.J. Jakobsen, *Presiding*

Spectrophotometric Bugs: In Vivo and in Vitro Studies of Biomembranes. D.G. Cameron, H.H. Casal, A. Martin, and H.H. Mantsch, National Research Council of Canada

Effects of Intrinsic and Extrinsic Lipid–Protein Associations on Membrane Bilayer Organization; Evidence of Boundry Lipid by Raman Spectroscopy. I.W. Levin, National Institutes of Health

Raman and FTIR Studies of Biopolymers. J. Koenig, Case Western Reserve U

FTIR Studies of Proteins—Surface Absorption. R.J. Jakobsen, R.M. Gendreau, S. Winters, and R. Leininger, Battelle Columbus Laboratories

Multinuclear Cross Polarization Magic-Angle Spinning Solid State NMR

P. Pfeffer, *Presiding*

Magic-Angle Spinning NMR Studies of Surface-Derivatized Samples. G.E. Maciel, D.W. Sindorf, I-S. Chuang, and W. Kolodziejski, Colorado State U

Characterization of Zeolite Molecular Sieves by High Resolution Silicon-29 NMR. M.T. Melchior, Perkin-Elmer Corp.

Solid State NMR of Peptides. M.H. Frey and S.J. Opella, U of Pennsylvania, and L.G. Pease, U of Delaware

Protein Dynamics by Solid State NMR. S.J. Opella, C.M. Gall, T.A. Cross, and J.A. DiVerdi, U of Pennsylvania

C-13 Chemical Shift Anisotrophy and Molecular Motion in Terephthalate-Containing Polymers. L.W. Jelinski and J.J. Dumais, Bell Labs

ASTM E-13 Symposium: Practical Performance Testing of Molecular Spectroscopy Instruments

H.L. Hoover, *Presiding*

Practical Performance Testing of Dispersive IR Spectrometers. R.D. McLochlan, Dow Chemical Co.

FTIR Practical Performance Testing: Where Are We in 1981? T. Hirschfeld, Lawrence Livermore Laboratory

Practical Performance Testing of Raman Instrumentation. M. Bell, National Bureau of Standards

Peak Verification in Liquid Chromatography

B.J. Sliwinski, *Presiding*

LC/FTIR: A Status Report. D.W. Vidrine, Nicolet Instrument Corp.

LC/MS as a Routine Analytical Tool. J. Henion, New York State College of Veterinary Medicine, Cornell U

Proton-NMR; A New Detector for HPLC. J.F. Haw, T. Glass, and H.C. Dorn, Virginia Polytechnic Institute and State U

Aspects of Peak Detection Algorithm for the Quantitation of LC Data. J.D. Mitchell, A.I.D., Inc., and P.B. Fuhrman, Hewlett Packard

Photoacoustics—Methodologies and Applications

C.H. Lochmuller, *Presiding*

Megahertz Photoacoustics: Numerical Modeling and Experiments. R.K. Burnham, R. Trehan, and E.M. Eyring, U of Utah

Photoacoustics for Material-Testing: Photoconductive Dye Films. A.C. Tam, IBM Research Laboratory

Quantitative Photoacoustic Spectroscopy of Intensely Light-Scattering Particulate Samples. L.W. Burggraf and D.E. Leyden, U of Denver

Photoacoustic Spectrometry in

Studies of Chemically-Modified Silica. C.H. Lochmuller and D.B. Marshall, Duke U

PAS Studies of Organic Monolayers on Particulate Materials. G.E. Cabaniss, M.L. Miller, and R.W. Linton, U of North Carolina at Chapel Hill

Vibrational Spectroscopy of Polymers

P.B. Roush, *Presiding*

Microraman Applications in Polymer Analysis. F. Adar, Instruments SA, Inc.

Demonstrating the Multiplex Advantage in Raman Microprobe Spectroscopy. W.R. Steinbach and C.F. Lohrstorfer, McClellan AFB Central Laboratory, and E.S. Etz, NBS Center for Analytical Chemistry

Fourier Transform Infrared Spectroscopy of Polymer Interfaces. Jack L. Koenig, Case Western Reserve U

Comparison of Curing Agents for Triazine Resin. J.L. Markham and M.M. Regn, Western Electric Co.

Phenolic End Group Determination by FTIR. G.D. Guenther, Hooker Research Center

Characterization of the Curing Behavior of Photopolymers by FTIR. T.A. Giversen, Western Electric Co.

Fourier Transform Infared Identification of Off Gases Produced during Thermogravimetric Analysis. C.A. Cody, B.K. Faluseit, and L. DiCarlo, NL Chemicals/NL Industries, Inc.

FTIR Studies of Polymer Degradation. B.J. Bulkin and E.M. Pearce, Polytechnic Institute of New York

Wednesday Afternoon

ICP-DCP Emission Spectroscopy: Optimization and Line Selection

G.N. Coleman, *Presiding*

Cross-Correlation Studies of ICP Emission Signals and System Parameters. G. Horlick and R.M. Belchamber, U of Alberta, Canada

Factors Affecting the Flow Rate of Aerosol Carrier Gas in Sample Introduction to an ICP Emission Source. S.A. Myers and D.H. Tracy, Perkin-Elmer Corp.

Interactions of Organic Solvents with Low-Power Ar ICP Discharges. A.W. Boom and R.F. Browner, Georgia Institute of Technology

Considerations for Obtaining the Utmost in Accuracy Using a DC Plasma. M.S. Epstein and C.G. Blundell, NBS Inorganic Analytical Research Division

New Applications of Argon Plasma Emission Spectroscopy. A.J. Schleisman, R.M. Brown, Jr., S.K. Hughes, and R.C. Fry, Kansas State U

Analytical Advantages of the Vacuum UV Region in ICP Spectroscopy. J. Goulter and H. Sobel, Applied Research Laboratories

Line Selection for the Determination of Trace Elements in Complex Matrices by ICAP—Fact not Fiction. A.F. Ward, Jarrell-Ash Division, Fisher Scientific Co.

The Application of the Internal Standard Technique in Sequential ICPAES. R.G. Schleicher, S.B. Smith, and C. Shapiro, Instrumentation Lab

Spectroscopic Technology for the Infrared and the Ultraviolet-Visible

T.B. Hirschfeld, *Presiding*

Extended Absorbance Range UV-Vis Spectrophotometry. W. Kaye, Beckman Instruments, Inc.

Characterization of Flames and Plasmas by Means of Infrared Emission Spectroscopy. J.E. Freeman, R.D. Deutsch, and G.M. Hieftje, Indiana U

New Optrodes for Long Range Fiber Spectroscopy. T. Hirschfeld and T. Deaton, Lawrence Livermore Laboratory

Use of Linear Response Theory in High-Speed Measurements on Chemical Systems. G.M. Hieftje, T. Lilley, and R.E. Russo, Indiana U, and G.R. Haugen, Lawrence Livermore Laboratory

The Super Scan Infrared Transmission Instrument for Simultaneous Component Analysis of Meat and Other Food Products. W.R. Whitford, Foss America, Inc.

Detection by Two Photon Photoconductivity Measurements. E. Voigtman, A. Jurgensen, and J.D. Winefordner, U of Florida

FTIR-EGA—Finding Out What's Cooking with FTIR. J.O. Lephardt, Philip Morris Research Center

Atomic Absorption Applications

M. Kaiser, *Presiding*

Use of the L'Vov Platform and Matrix Modification for Graphite Furnace Determination of As and Se in Biological Matrices. M.L. Kaiser and E.J. Hinderberger, U of Missouri

The Atomization of Aluminum in a Furnace at Steady State Temperature. D.C. Manning and W. Slavin, Perkin-Elmer Corp.

Elimination of Matrix Interferences in Graphite Furnace Determination of Lead in Tissue Samples with Matrix Modification and the L'Vov Platform. T.W. May and W.G. Brumbaugh, Columbia National Fisheries Research Laboratory

Determination of Chromium and Lead in Groundwater by Furnace Atomic Absorption Spectrometry. M. La Corte, Pennwalt Corp., and B.E. McClellan and R.L. McClellan, Murray State U

Calibration Techniques for Extended Range Multielement AAS. N.J. Miller-Ihli, T.C. O'Haver, and J.M. Harnly, U of Maryland and NCL, USDA

Compromise Flame Parameters for the Simultaneous Analysis of NBS Standard Reference Materials and USGS Standard Rocks by Atomic Absorption Spectroscopy. J.M. Harnley, J.S. Kane, N.J. Miller-Ihli, and T.C. O'Haver, U of Maryland and NCL, USDA

Antimony Analysis at Reduced Sensitivity with Hydride Generation/Cold Vapor Cell. G.H. Newton and J.A. Nichols, Western Zirconium, Inc.

Electronic Spectroscopy: Fluorescence and Dynamics

G.R. Holtom, *Presiding*

Fluorescence of S (B-X) Excited by Fixed Frequency Ultraviolet Lasers. A.L. Smith and J.B. Hopkins, Drexel U

Chemiluminescence from S_2—A Sulfur Detector? E.S. Yeung and S.R. Spurlin, Ames Laboratory, Iowa State U

Photodissociation Dynamics of H_2S and CF_3NO. P.L. Houston, Cornell U

Spectroscopy and Photochemical Separation of Lanthanides in Solution. T. Donohue, Naval Research Laboratory

Nanosecond Absorption Spectroscopy of Hemoglobin. J. Hofrichter, Laboratory of Chemical Physics, National Institutes of Health

Study of Solvation Processes of

Aromatics from Two-Photon Polarization Measurements. M.J. Wirth, C.E. Mohler, and A.C. Koskelo, U of Wisconsin—Madison

Temperature and Energy Dependence of Picosecond Molecular Reorientation. M.J. Wirth, M.J. Sanders, and D.A. Hahn, U of Wisconsin—Madison

System Suitability Testing in Pharmaceutical Analysis

M.J. O'Brien, *Presiding*

Control of Bulk Drug Purity by Liquid Chromatography. W. Caldwell, Merck Sharp and Dohme Research Laboratory

System Suitability Testing—An Aid to the Transfer of Chromatographic Methodology. R. Roman, Merck Sharp and Dohme

System Suitability Tests in the Validation of New Drug Application Methodology. E.B. Sheinin, U.S. Food & Drug Adminstration

System Suitability Testing in USP. S. Sun, U.S. Pharmacopeial Connection, Inc.

A Simple Sample Preparation Procedure for Quantitation of Drugs in Aqueous Methylcellulose by HPLC. L.L. Ng, Merck Sharp and Dohme Research Laboratory

Enhancing the Speed of Analysis and Quality of Chromatographic Results with New Microcomputer Technology and Multicolumn Analyses. B. Suits, Varian Instrument Group

Multinuclear Cross Polarization Magic-Angle Spinning Solid-State NMR

P. Pfeffer, *Presiding*

Solid-State NMR Studies of Bile Acids Bound to Fibers. P.D. Hoagland and P.E. Pfeffer, USDA Eastern Regional Research Center

^{13}C Solid-State Studies of Sludge. E.G. Piotrowski, K.M. Valentine, and P.E. Pfeffer, USDA Eastern Regional Research Center

Solid-State ^{13}C NMR of Humic Substances from Soils. P.G. Hatcher, U.S. Geological Survey, and L.W. Dennis and G.E. Maciel, Colorado State U

Structural Comparisons in Solution and Solids by ^{13}C, ^{31}P, and ^{29}Si NMR. M.J. Albright, JEOL (USA), Inc.

Effects of Water on the Structure and ^{13}C Solid-State Spectra of Carbohydrates. P.E. Pfeffer, W.L. Earl, and K.B. Hicks, USDA Eastern Regional Research Center

ASTM E-13 Symposium: Practical Performance Testing of Molecular Spectroscopy Instruments

K. Whetsel, *Presiding*

Automation of Tests for Spectrophotometer Performance. UV-VIS-Near IR. W. Kaye, Beckman Instruments, Inc.

Finesse of Luminescence Information Content. L.J. Cline Love, Seton Hall U

Practical Performance Testing of Nuclear Magnetic Resonance Spectrometers. T.C. Farrar, U of Wisconsin—Madison

Peak Verification in Liquid Chromatography

B.J. Sliwinski, *Presiding*

Atomic Absorption Detection for Liquid Chromatography. J.D. Messman, U.S. Geological Survey, and T.C. Rains, National Bureau of Standards

Normal and Reversed-Phase Chromatography of Organometallics with Inductively Coupled Plasma Atomic Emission Spectrometer Detection. R.S. Brown, P. Graham, and L.T. Taylor, Virginia Polytechnic Institute and State U

Detection of Optically Active Molecules in HPLC. E.S. Yeung and J.C. Kuo, Ames Laboratory, Iowa State U

LC–Voltammetric Detection for Organic Pollutants. G. Batley and B.K. Afghan, Canada Center for Inland Waters

Photoacoustic FTIR

B.S.H. Royce, *Presiding*

Studies of the Chemistry of Supported Organometallics Using Fourier Transform Infrared Photoacoustic Spectroscopy. J.B. Kinney and R.H. Staley, Massachusetts Institute of Technology

Forensic Analysis and Determination by FTIR-PAS. M.G. Rockley, R. Kroutil, H.H. Richardson, and N. Purdie, Oklahoma State U

Infrared Surface Analysis. M.G. Wisnosky, Owens Corning Fiberglas Technical Center

Recent Applications of Diffuse Reflectance and Photoacoustic Infrared Spectrometry to the Analysis of Bulk Materials and Surfaces. S.A. Yeboah, I.M. Hamadeh, and P.R. Griffiths, Ohio U

Comparison of FTIR and Photoacoustic FTIR in the Characterization of the Curing Behavior of Acrylic-Based Polymers. J. Teng, Princeton U, and J.A. Ors, Western Electric Co.

Applications of Photoacoustic Fourier Transform Infrared Spectroscopy. K. Krishnan, Digilab Division of Bio-Rad Laboratories

Photoacoustic FTIR Including Radiometry and Transduction Efficiency. D.W. Vidrine, Nicolet Instrument Corp.

The Analytical Chemistry of the Nuclear Waste Form

W.P. Reed, *Presiding*

Measurements and Standards for Nuclear Waste Management—An Overview. W.P. Reed, National Bureau of Standards

Leachability Measurement Methodology for Nuclear Waste. J.A. Stone, Du Pont Co.

Analysis of Nuclear Waste Leachates for Trace Elements by Atomic Spectrometry: Problems and Solutions. M.S. Epstein and C.G. Blundell, National Bureau of Standards

The First MCC Leach Test Round Robin Experience. J. Mendel, Battelle Northwest

Nuclear Waste Forms—Design and Characterization Considerations. D.E. Clark, A.R. Jurgensen, and L. Urwongse, U of Florida

The Analytical Constraints that Influence Leachability Measurements and Reference Materials. H.M. Kingston and D. Cronin, National Bureau of Standards

Surface Studies of Leaching and Dissolution in Nuclear Waste Forms. C.G. Pantano, Pennsylvania State U

Thursday Morning, Sept. 24

ICP-DCP Emission Spectroscopy: Instrumentation and Applications

R.C. Fry, *Presiding*

Reduction of Spectral Interferences in Inductively Coupled Plasma Emission Spectrometry by Selective Spectral-Line Modulation. S.W. Downey and G.M. Hieftje, Indiana U

Optimization of ICP Operating Parameters for the Determination of Sulfur in Oils. G.F. Wallace, Perkin-Elmer Corp.

Elemental Analysis with an Atmospheric Pressure Plasma Quadrupole Mass Spectrometer System. D.J. Douglas, F.S.K. Quan, and R.G.G. Smith, SCIEX, Inc.

Evaluation of Silicon Photodiode Array Detector in ICP–AES. F. Graybau and V.A. Fassel, Iowa State U, and Y. Talmi, Consultant, Plainsboro, N.J.

DC Argon Plasma Emission Spectroscopic Detection for Fused Silica Capillary Gas Chromatography. P.C. Uden, J.O. Beyer, and R.M. Barnes, U of Massachusetts

Teflon Nebulizers and Spray Chambers for ICP Samples Containing HF. J.D. Nohe and J.M. Katzenberger, Instruments SA, Inc.

An Optimized Spectrometer for ICPAES. S.B. Smith and R.G. Schleicher, Instrumentation Laboratory, Inc.

Analysis of Aluminum by Inductively Coupled Plasma–Atomic Emission Spectroscopy. R.M. Barnes, L. Fernando, L.S. Jing, and H. Mahanti, U of Massachusetts

Extraction of New Types of Spectroscopic Data

T.B. Hirschfeld, *Presiding*

Advanced Methods of Data Retrieval Using Fourier Transforms. D.G. Cameron, J. K. Kauppinen, D.J. Moffatt, and H.H. Mantsch, National Research Council of Canada

Resonance Raman Spectroscopy of Excited States. R.F. Dallinger, Purdue U

Atomic Emission Spectrochemical Measurements with a Fourier Transform Spectrometer. G. Horlick, U of Alberta, Canada

Fourier Transform Tunable Laser Spectroscopy. T. Hirschfeld, Lawrence Livermore Laboratory

Infrared Macro Group Frequencies. D. Mayo, Bowdoin College, and J. Coates and R.W. Hannah, Perkin-Elmer Corp.

Operating a Self-Learning Algorithm for Quantitative Analysis by NIRA. H. Marks and S. Jackson, Technicon Industrial Systems

Hydride Generation for Atomic Spectroscopy

B.E. McClellan, *Presiding*

Determination of Arsenic and Selenium in Natural Waters, Foods, and Biological Tissues by AAS–Hydride Generation. T.C. Rains, National Bureau of Standards

Some Chemical Insights into the Analytical Hydride Preconcentration. R.M. Brown, Jr., G. Love, and R.C. Fry, Kansas State U

Nondispersive Atomic Fluorescence Hydride Analysis. A. Walsh, K. Braun, and W. Slavin, Perkin-Elmer Corp.

Mutual Interactions of Hydride-Forming Elements in Atomic Absorption. B. Welz and M. Melcher, Bodenseewerk Perkin-Elmer & Co. GmbH, West Germany

Multielement Determination of Arsenic, Antimony, Tin, and Germanium by Hydride Generation–Chromatographically Coupled Emission Spectroscopy. M. Eckhoff,



J. McCarthy, and J.A. Caruso, U of Cincinnati

Continuous Hydride Generation for ICP Analysis. L. Morganthaler, J. Goulter, and D. Painchaud, Applied Research Laboratory

Optimization and Application of Hydride Generation Atomic Absorption. W.B. Hobbins and D.E. Shrader, Varian AA Resource Center

The Determination of Arsenic in Urine by AVA Hydride Generation. J. DuLude, J. Sotera, and H. Kahn, Instrumentation Laboratory, Inc.

Electronic Spectroscopy—Laser Enhanced Ionization (LEI)

G.R. Holtom, *Presiding*

LEI Detection of Potassium and Rubidium by Infrared CW Dye Laser Excitation. G.J. Havrilla and P.K. Schenck, National Bureau of Standards

Stepwise Excitation Laser Enhanced Ionization Spectrometry. G.C. Turk and J.C. Travis, National Bureau of Standards

Optogalvanic Resonance Detection of Pulsed Dye Laser Atomic Absorption. M.A. Nippoldt and R.B. Green, U of Arkansas

Time Evolution of the Depleted Atom Density "Hole" Following Laser Enhanced Ionization in Flames. J.C. Travis, P.K. Schenck, and G.C. Turk, National Bureau of Standards

Measurement of Relative Flame Ion Fractions Using Laser Enhanced Ionization. J.E. Gardner and R.B. Green, U of Arkansas

Multiple-Electrode Interference Removal in Laser Enhanced Ionization Spectrometry. T.O. Trask and R.B. Green, U of Arkansas

Contemporary High Resolution Gas Chromatography

R.D. Dandeneau, *Presiding*

Modification of the Silica Surface Structure for Improved Capillary Column Preparation. M.L. Lee and B.W. Wright, Brigham Young U

Recent Advances in Sampling with Capillary Columns. T.A. Rooney and A. Nohl, Delta Associates

Application of Fused Silica Capillary Columns in Atmospheric Chemistry Studies. M.W. Holdren and C.W. Spicer, Battelle Columbus Laboratories

GC and GC/MS Studies of Coal Liquids. C.G. Scouten, G.D. Dupre, and R.J. Pancirov, Exxon

Novel Applications of NMR: NMR Studies of Surfaces, Coals, Films, and Hydrides

R.G. Pembleton, *Presiding*

Nonchemical Hole Burning in Coals: Advances in C-13 NMR Spectroscopy. B.C. Gerstein and P.D. Murphy, Iowa State U

C-13 NMR Study of the Adsorbed States of Formic Acid. T.M. Duncan, Bell Telephone Labs, and R.W. Vaughan, California Institute of Technology

Structure and Defects in Amorphous Semiconducting Thin Films. J.A. Reimer, IBM

Proton NMR as a Probe of Chemistry and Structure in Solid Metal Hydrides. A.T. Nicol, R&D Associates

Studies of Hydrogen in Metals and Hydrides Using NMR and Magic Angle Sample Spinning. M.E. Stoll, Sandia National Laboratories



Competitive Protein Binding Assays: Radioimmunoassay and Enzyme Immunoassay

M. Medina, *Presiding*

Overview of the Competitive Protein Binding Assays. B. Weintraub, National Institutes of Health

Production and Characterization of Monoclonal Antibodies. K. Bechtol, Wistar Institute

Statistical Evaluation and Computerization of RIA Data. D. Erwin, Micromedic Systems

Criteria for Radioimmunoassay and Enzyme Immunoassay in Regulatory Methods. J. O'Rangers, USFDA

Derivatization for Detection Enhancement for Liquid Chromatography

J.C. Hodgin, *Presiding*

An Improved 2,4-Dinitrophenylhydrazine Method for the Determination of Formaldehyde and Other Aldehyde Species. F. Lipari and S.J. Swarin, General Motors Research Laboratories

Determination of Naturally Occurring Toxins in Foods by Liquid Chromatography and Pre- or Post-Column Derivatization. C.W. Thorpe and A.E. Pohland, Food and Drug Adminstration

Single Pump LC Separation—Post Column Reaction Detection System for Amines and Amino Acids. J.N. LePage, W.R. Grace & Co.

Pre-Column Derivatization of Primary Amino Acids. J.D. Stuart, E.R. Nemergut, M.L. Wu, and D.W. Hill, U of Connecticut

Derivatization of Amines and Amino Acids for Determination by LCEC. W.A. Jacobs and P.T. Kissinger, Purdue U

Pre- and Postcolumn Derivatization Methods for Improved Ultraviolet Detection in Pharmaceutical Analysis. C.R. Clark, Auburn U

Multielement Trace Metal Analysis by Derivatization in HPLC. Y.T. Shih and P.W. Carr, U of Minnesota

High Performance Liquid Chromatography by Derivatization. I. Alkyl Methylphosphonic Acids. P.C. Bossle, J.J. Martin, and E.W. Sarver, Aberdeen Proving Ground

High Performance Liquid Chromatographic Analysis of Acid Chlorides by Prederivatization. J.T. Stoklosa, J.M. Bissinger, K.T. Rullo, C.M. Shearer, and N.J. DeAngelis, Wyeth Laboratories

Determination of Substituted Phenolic Compounds by HPLC Using Phenol as a Fluorescent Probe. J.N. Patterson III, P.R. Dluzneski, and P.N. Keliher, Villanova U

Spectroscopic Techniques Based on Coherent Effects

L.A. Carreira, *Presiding*

Application of Low Frequency CARS. J.W. Fleming, W.T. Barnes, and A.B. Harvey, Naval Research Laboratory

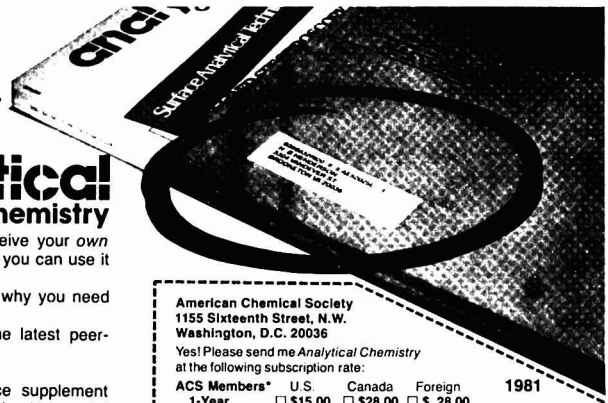
Combustion Diagnostics in Practical Combustor Systems Employing the CARS Technique. L.P. Goss, Systems Research Laboratories, Inc.

Investigations of CARS Spectroscopy for Combustion Applica-

The Mark of the Successful Scientist

An individual subscription to

analytical chemistry



Join the successful scientists and receive your *own* subscription to *Analytical Chemistry* so you can use it when — and how — you want!

There are fifteen important reasons why you need your individual subscription:

Twelve monthly issues filled with the latest peer-reviewed research

plus

The April Review Issue (a reference supplement alternating between applications and fundamentals)

and

Lab Guide (a purchasing directory covering instruments, equipment, chemicals and services)

The fifteenth reason? You get all of this vital professional input for just $20.00 a year ($15.00 if you are a member of ACS)!

Guaranteed!

The American Chemical Society will refund the unused portion of your subscription fee at any time you are not satisfied!

Join the Analytical Chemist VIP set!

Call toll free or use the coupon to order your *individual* subscription now!

American Chemical Society
1155 Sixteenth Street, N.W.
Washington, D.C. 20036

Yes! Please send me *Analytical Chemistry* at the following subscription rate:

ACS Members*	U.S.	Canada	Foreign	1981
1-Year	☐ $15.00	☐ $28.00	☐ $ 28.00	
3-Years	☐ $36.00	☐ $75.00	☐ $ 75.00	Call Toll Free:
Nonmembers				800-424-6747
1-Year	☐ $20.00	☐ $33.00	☐ $ 43.00	(Credit Cards Only)
3-Years	☐ $48.00	☐ $87.00	☐ $111.00	

Name _____

Address _____

City _____ State/Country _____ Zip _____

☐ Bill me ☐ Payment enclosed** *(payable to American Chemical Society)*

Charge my ☐ Master Charge ☐ VISA

Card # _____ Interbank # _____ (Master Charge Only)

Exp. Date _____ Signature _____

*Subscription at ACS Member Rates are for personal use only

**Payment must be made in U.S. Currency, by international money order, UNESCO coupons, U.S. bank draft, or through your subscription agency.

Please allow 60 days for your first copy to be mailed.

tions. A.C. Eckbreth, United Technologies Research Center

Resonance CARS Spectra of Biological Molecules. T.G. Spiro, Princeton U

Inverse Raman Spectra of Solutions. M.D. Morris, U of Michigan

Stimulated Raman Spectroscopy as a High Resolution, Spectroscopic Probe. P. Esherick and A. Owyoung, Sandia National Laboratories

Polarization Detection for Raman and Two-Photon Events. E.S. Yeung and D.R. Bobbitt, Iowa State U

Thursday Afternoon

ICP–DCP: Instrumentation and Applications

A. Scheeline, *Presiding*

Simultaneous Determination of Major, Minor, and Trace Elements in Marine Sediments by ICP–AES. J.W. McLaren, S.S. Berman, V.J. Boyko, and D.S. Russell, National Research Council of Canada

A Study of Digestion Techniques in the Analysis of Samples by Inductively Coupled Argon Plasma Emission Spectroscopy. D.L. Heinrich, Radian Corp.

Properties and Applications of Poly(Acrylamidoxime) Chelating Resin Using Inductively Coupled Plasma Atomic Emission Spectroscopy. R.M. Barnes and W.-Y. Kim, U of Massachusetts

SSEA Analysis of Aluminum Metal Samples. C. Wohlers, R. Belmore, and J. Beaty, Jarrell-Ash

A Versatile Software Package for Sequential Inductively Coupled Plasma Analysis. J. Katzenberger and B. Rosovsky, Instruments SA, Inc.

Application of Inductively Coupled Plasma Atomic Emission Spectrometry for the Determination of Alkali Metals. B.M. Joshi, Ford Motor Co.

Analysis of High-Purity Aluminum. W.J. Kinsey and R.R. Comtois, SpectraMetrics, Inc.

Extraction of New Types of Spectroscopic Data

T.B. Hirschfeld, *Presiding*

Evaluation of Tree-Structured Libraries for the Interpretation of Vapor Phase Infrared Spectra. M.F. Delaney and F.V. Warren, Jr., Boston U

Extraction of Group Environmental Information from Infrared Spectroscopy Obtained at Different Temperatures. J.L. Koenig, Case Western Reserve U

Time-Resolved Studies of Polymers by FTIR. W.G. Fateley, Kansas State U, and D.E. Honigs, Indiana U

FTIR Measurements of Thin Films. R. Curbelo and J.M. Quigley, Bio-Rad Laboratories

Total Luminescence for Improved Selectivity in Multicomponent Analysis. E.L. Inman, Jr., and J.D. Winefordner, U of Florida

Expressing Analytical Results in Terms of Function Rather than Analyte Concentration. J.L. Bernard, Beckman Instruments

Applying Analytical Chemistry Research

M. Margoshes, *Presiding*

The Selection of Research and Development Programs in an Applied Research Environment. T.C. Farrar, U of Wisconsin—Madison

Analytical Research in an Institute Setting. B.L. Karger, Northeastern U

Approaching the Development and Market Realities of a New Product with a Potential Manufacturer. R.A. Dreher, Varian Instruments

Is Industry/University Cooperation the Way? M. Margoshes, Technicon Instruments Corp.

Entrepreneurship and the Academic Chemist. If They Won't Do It, Do It Yourself. P.T. Kissinger, Purdue U and Bioanalytical Systems Inc.

Electronic Spectroscopy: Selection Rules

G.R. Holtom, *Presiding*

Negative Ion Photoelectron Spectroscopy: Design and Applications. C.S. Feigerle and W.C. Lineberger, U of Colorado and National Bureau of Standards



CIRCLE 143 ON READER SERVICE CARD

Analytical Aspects of Two-Photon Spectroscopy. F.E. Lytle, Purdue U

Selection Rules Are Made To Be Broken. M.G. Littman, Princeton U

Forbidden and Allowed Transitions in Conjugated and Unconjugated Dienes. R. McDiarmid, A. Auerbach, and J.P. Doering, Johns Hopkins U

Spectral Search

J. Sprouse, *Presiding*

Which Way to Search? A Review of IR Spectral Search Methods. J.P. Coates and R.W. Hannah, Perkin-Elmer Corp.

Applications of Flexible Multiparameter Infrared Library Search. D.A. Huppler, S.R. Lowry, and C.A. Anderson, Nicolet Instrument Corp.

Advances in Spectral Search. M.L. Olson, Digilab

An Efficacy Study on IR Spectral Search Utility. J.E. Carrol, F.M. Ostrander, and T. Kasky, Analect Instruments

Applications and Versatility of Automated Infrared Spectral Search and Display. J.F. Sprouse, Sadtler Research Laboratories

A Computerized Spectral Search Application to Identification of Industrial Samples. E.V. Miseo and L.W. Guillmette, A.D. Little, Inc.

Novel Applications of Nuclear Magnetic Resonance: Studies of Polymers

Cecil Dybowski, *Presiding*

High Resolution C-13 NMR of Solid Polymers. R.G. Pembleton and L.M. Ryan, Du Pont Co.

Fluorine-19 NMR Spectroscopy of Fluoropolymers. L.M. Ryan, R.G. Pembleton, and R.S. Sudol, Du Pont Co.

Quantitative Analysis of Complex Acrylate Polymers by Carbon-13 FTNMR. T. Sanford, PPG Industries

NMR Studies of Surfactant–Oil–Water Systems. M. Johnson and C.G. Wade, IBM Instruments

NMR Studies of Solubilizates in Micellar Media. J.E. Lacy, K.F. Thompson, A.L. Rockwell, and L.G. Pease, U of Delaware

NMR as a Method for Studying Metal Binding in Metalloproteins. I.M. Armitage, Yale U

Competitive Protein Binding Assays: Radioimmunoassays and Enzyme Immunoassay

M. Medina, *Presiding*

Enzyme Immunoassays: A Critical Review. K. Rubenstein, Syva Research Institute

The Design of Immunoassays for Analyses in Serum. D.B. Berkowitz, USDA–FSQS–Science

Radioimmunoassay Application to Preclinical and Clinical Phases of New Drug Development. M. Hichens, Merck Institute of Therapeutic Research

Radioimmunoassay to Hepatitis B Surface Antigens by Using Monoclonal Antibodies. V. Zurawski, Centacor, Inc.

New Developments in Separations Science

E. F. Hoegger, *Presiding*

Liquid Chromatographic Fractionations of Vanadium Compounds in Venezuelan Crude Oil. C.C. Sommer, W.A. Spencer, E.H. Schmauch, and L.B. Rogers, U of Georgia

HPLC Analysis of Zinc Dialkyldithiophosphates in Used Engine Oils. M. Zinbo, Ford Motor Co.

Liquid Chromatography of Metal Carbonyl Clusters. A.C. Hayman, Du Pont Co., and B. Gates and B. Matrana, U of Delaware

Applications of Multisolvent Liquid Chromatography. A. Goldberg and P. Antle, Du Pont Co.

Practical Use of Microscale LC. N.H.C. Cooke, K. Olsen, A. Berick, C. Schackleford, and B.G. Archer, Altex Scientific

Separation and Characterization of Biopolymers with Capillary Tubing. C.N. Trumbore, R.D. Tremblay, J.T. Penrose, M. Mercer, and F. Kelleher, U of Delaware

Analysis of Surfactants by High Peformance Liquid Chromatography (HPLC)-III. A.C. Hayman and A.J. Mical, Du Pont Co.

Determination of Substituted Phenolic Compounds by High Performance Liquid Chromatography Using Phenol as a Fluorescent Probe. J.M. Patterson III, P.R. Dluzneski, and P.N. Keliher, Villanova U

Enhanced Liquid Chromatographic Selectivity through Multichannel Fluorescence Detection. T.H. Begley and T.C. O'Haver, U of Maryland, and W.E. May, R.A. Velapoldi, and S.A. Wise, NBS

A New Compact Gas Chromatograph. V. Rossiter, Accuspec Ltd., Ireland

Friday Morning, Sept. 25

ICP–DCP: Instrumentation and Applications

G.N. Coleman, *Presiding*

The Application of DC Plasma Emission to Industrial Analysis. L. Shore, Englehard Industries

Speciation Using High Performance Liquid Chromatography Coupled with Inductively Coupled Plasma Emission Spectroscopy. R.N. Savage and S.B. Smith, Instrumentation Laboratory, Inc., and D. Bushee and I.S. Krull, Northeastern U

Application of a DCP–Echelle Spectrometer Technique to Rare Earth Analysis. G.W. Johnson, Molycorp, Inc.

The Determination of Base Extractable Impurities in Organic Uranium Solutions Via Plasma Atomic Emission Spectroscopy. R.R. Comtois and W. Kinsey, SpectroMetrics, Inc.

Industrial Applications of Infrared Spectroscopy

D.B. Chase, *Presiding*

A High-Level Computer Language for the Spectroscopist. J.P. Coates and R.W. Hannah, Perkin-Elmer Corp.

Computer-Assisted Infrared Quantitative Analysis. G.L. McClure, J.P. Coates, and R.W. Hannah, Perkin-Elmer Corp.

Spectrophotometric Analysis by Cross Correlation. C.K. Mann and J.R. Goleniewski, Florida State U

Quantitative Infrared Analysis of Multicomponent Lipids. H. Kinser and C.W. Brown, U of Rhode Island

Diffuse Reflectance FTIR Studies on Catalysts. S.E. Garlock and A.J. Rein, IBM Instruments

Near Infrared Reflectance Analysis in the Laboratory. T. Hirschfeld and E. Stark, Lawrence Livermore Laboratory

Near Infrared Reflectance Anal-

ysis of Dairy Products. E. Stark, K. Luchter, and T. Hirschfeld, Technicon Industrial Systems

Analytical Characterization of Synfuels

B.W. Farnum, *Presiding*

Multimethod Analysis of By-Product Tar from Slagging Fixed Bed Gasification of Lignite. B.W. Farnum, S.A. Farnum, and E.F. Bitzan, Grand Forks Energy Technology Center

Fast-Atom-Bombardment Mass Spectrometry. Application to Nitrogen-Containing Compounds in the Liquid-Fossil-Fuel Cycle. S.E. Scheppele, Q.G. Grindstaff, G.P. Sturm, Jr., and R.D. Grigsby, Bartlesville Energy Technology Center, and L. Taylor, H. Tudge, and S. Evans, Kratos Scientific Instruments, Ltd., England

Characterization of an SRCII Coal Liquid and Upgraded Products. P.L. Grizzle, J.B. Green, J.A. Thomson, R.J. Hoff, S.E. Schepppele, and Q.G. Grindstaff, Bartlesville Energy Technology Center

The Effect of Heteroatom Content on FID Response to Shale Oils and Their Chromatographic Fractions. J.J. Duvall, Laramie Energy Technology Center

Characterization of the Distribution of Organic Materials in Oil Shales Using Scanning Electron Microscopy. J.A. King and E.N. Eisentrout, Morgantown Energy Technology Center

Synfuels Analysis by MS/MS. K.V. Wood, J.D. Ciupek, and R.G. Cooks, Purdue U

The Determination of Nitrogen Base Types in Coal Derived Materials by Nonaqueous Differential Potentiometry. A.W. Wells, H. Schultz, and H.L. Retcofsky, U.S. DOE/PETC

Laser Excited Shpol'skii Effect Spectrometry (LESS) for the Direct Determination of Benzo[*a*]-pyrene in Synfuels: The Application of the Internal Reference Principle. Y. Yang, A.P. D'Silva, and V.A. Fassel, Iowa State U

Applications of Analytical Pyrolysis to Trace Organics

S.A. Liebman, *Presiding*

Pyrolysis of Polyethylene. C.F. Caldwell and A.K. Bhattacharya, Mobil Chemical Co.

Controlled Thermal Degradation Mass Spectrometry. R. Spreen, P. Rudewicz, and B. Munson, U of Delaware

Applications of Pyrolysis GC to Coals. B.K. Hovespian, Du Pont Co.

Applications of Thermal Distillation–Pyrolysis to Petroleum Source Rock Studies and to Analysis of Marine Particles. J.K. Whelan, Woods Hole Oceanographic Institution

Emphasizing Relevant Information in the Mapping of Classified GC and Spectral Data. A.M. Harper, H.L.C. Meuzelaar, D.L. Pope, and D.J. Iwamoto, U of Utah

Pyrolysis–GC for Industrial Polymer Characterization. C.G. Smith, Dow Chemical U.S.A.

Application of Pyrolysis–GC–Mass Spectrometry to Differentiation and Characterization of Cellular Material. T.F. Moran and E. Reiner, Georgia Institute of Technology

The Effect of Polymer Microstructure on Quantitative Analysis. D.H. Ahlstrom and A.H. Evans, Armstrong World Industries, Inc.

Effective Approach to Teaching Analytical Spectroscopy

R.J. Lovett, *Presiding*

Graduate Level Spectroscopy—A Perspective View. M.L. Parsons, Arizona State U

Interface Between the Teaching of Molecular and Atomic Spectroscopy at the Graduate Level. W.G. Fateley, R.M. Hammaker, and R.C. Fry, Kansas State U

A Graduate Program in Spectroscopy: Full Professional Development. J.P. Walters, U of Wisconsin—Madison

Determination of Amines in Physiological Fluids

L. Lakritz, *Presiding*

Overview of the Functions of Biologically Active Amines. R. Buchanan, Drexel U

Factors Influencing the Gas Chromatographic Analysis of Amines. R.R. Freeman, Hewlett-Packard

Analysis of Aliphatic Amines in Human Physiological Fluids. S.R. Dunn and M.L. Simenhoff, Jefferson Medical College

A Rapid Method for the Determination of Ammonia in Tissue. N. Parris, USDA Eastern Regional Research Center

So You Want to Set Up Your Own Business?

L.H. Phifer, *Presiding*

So You Want to Set Up Your Own Business? L. Phifer, Chem Service

The Secret Method for Succeeding in a Business Which You Have Started. W. Supina, Supelco, Inc.

What Business? C. Stanke, Consultant

Financing, Where and How Much—The Importance of Sound Financing. R. Carlow, Hamilton Bank

What Can a Good Accountant Do For You? A. Baker, West Chester, Pa.

Advertising—Where, How Much, and How. T. Bremble, Bremble and Sewforth

Role of the Consultant in the Chemical Industry. E. Beavers, Embarc

Establishing a Small Business/Consulting Lab. R.C. Crippen, Crippen Labs.

The Joy of Being in Business for Yourself. D. Conlon, Instruments for Research and Industry

NSF Grants to Support Computer Science Research

The National Science Foundation has awarded grants to Cornell University, the University of Wisconsin, and the University of Illinois in an effort to provide long-term support for experimental computer science research and research facilities in the U.S.

Over the next five years, the grants (totaling $11.3 million) will support university efforts to purchase or upgrade computing equipment, provide professional and technical support staff, defray graduate student salaries, and cover other costs involved in maintaining experimental computer research facilities. The NSF expects the awards to stimulate an increase in research in computer science and computer engineering and thereby provide greater incentives for students to pursue advanced degrees in those fields.

ACS Analytical Division Announces 1981 Fellowship Winners

The Fellowship Committee of the American Chemical Society Division of Analytical Chemistry has announced the winners of four $7500 full-year awards and nine $2000 summer awards for 1981.

Winners of the full-year awards were: Robert Michael Ianniello, Rutgers University; Vicki Lynn McGuffin, Indiana University; Scott A. McLuckey, Purdue University; and Bob W. Wright, Brigham Young University.

Summer awards were presented to: Christine Ann Ennis, University of Colorado; Karin E. Foley, Pennsylvania State University; Greg Allen Gerhardt, University of Kansas; Linda Moore Hirschy, University of Florida; Stephen Lee Kelly, University of Houston; Lawrence James Murphy, University of Massachusetts; Frederick William Page, University of New Hampshire; Julie Strong Pflug, University of Illinois; and Charles Robert Powley, University of Illinois.

Robert M. Ianniello, sponsored by the Procter and Gamble Company, plans to construct several new immobilized enzyme chemically modified electrodes (IECMEs) for use as potentiometric and amperometric sensors. With research director Alexander M. Yacynych, Ianniello will complete his studies of the catalytic properties of other IECMEs, and will also continue determinations of surface functionality and enzyme loading on carbonaceous materials.

Vicki Lynn McGuffin, working with research director Milos V. Novotny, is constructing a dual-flame detector to measure secondary ionization in capillary column high-performance liquid chromatography. Various parameters and applications will be established once the detector is operational. McGuffin's fellowship is sponsored by the Upjohn Company.

Scott A. McLuckey, sponsored by the Perkin-Elmer Corporation, is using mass spectrometry/mass spectrometry to measure metal ion, hydride, and electron affinities. With research director R.G. Cooks, McLuckey will also investigate varied uses for the MS/MS instrument that result from its modular design.

Bob W. Wright, sponsored by the Procter and Gamble Company and under the direction of Milton L. Lee, is studying fused silica and glass silica surface structures and their influence on capillary column chromatography. The aim of Wright's work is to permit chemical bonding of stationary phases to the column surface with a high degree of deactivation, efficiency, and stability.

Christine A. Ennis has redesigned and rebuilt a mass spectrometry discharge flow apparatus to incorporate OH resonance fluorescence. A second new detection method, negative ion chemical ionization mass spectrometry, is currently being incorporated to enhance use of the discharge flow technique in studying stratospheric reactions. Ennis's research director is John W. Birks, and her work is sponsored by the Society of Analytical Chemists of Pittsburgh.

The Society of Analytical Chemists of Pittsburgh is also sponsoring Karin E. Foley. Working under the direction



Robert Ianniello



Vicki Lynn McGuffin



Scott McLuckey



Bob Wright



Christine Ennis



Karin Foley



Greg Gerhardt



Linda Hirschy



Stephen Kelly



Lawrence Murphy



Frederick Page



Julie Pflug



Charles Powley

of Nicholas Winograd, Foley is using ion mass spectrometry to determine the bonding geometry of CO on nickel crystals. Her work will focus on improving the quality of information obtainable from SIMS.

Greg A. Gerhardt, under the direction of Ralph N. Adams, has constructed microcomputer-controlled instrumentation for in vivo experiments involving the simultaneous use of multiple electrodes. Gerhardt, sponsored by the Analytical Division of the American Chemical Society, is also refining methods for the low-level determination of organic compounds that are electroactive species, such as phenylcyclidine.

Linda M. Hirschy, sponsored by the Dowzard Fund of the Analytical Division of the ACS, is evaluating the analytical potential of laser-enhanced ionization through a critical study of variables. Hirschy and research director J.D. Winefordner will test the newly constructed system on low levels of polyaromatic hydrocarbons.

Stephen L. Kelly is extending his characterization of manganese porphyrins. His study will include the effect of coordinated O_2, CO, NO, and CN^- on the halfwave potential and on electron transfer kinetics. Under the direction of Karl M. Kadish and with support from the Analytical Division of the ACS, Kelly will extend his work to analogous chromium and possibly molybdenum complexes.

Lawrence J. Murphy, whose award is sponsored by the Olin Corporation Charitable Trust, will work on functional group selective–high pressure liquid chromatography, including multidimensional HPLC. His project, under the direction of Sidney Siggia, will include development of new bonded charge transfer phases, with emphasis on nitrogen bases for selective retention of electron acceptor compounds. Murphy's work is directed toward the analysis of environmental samples.

Frederick W. Page, working with research director C. L. Grant, will continue the development of model particulates. Page will study the adsorption of pollutants, such as copper and phosphate, on both model and natural particulates in aqueous solution. Adsorption isotherms of polynuclear aromatic hydrocarbons are also being determined with fluorescence polarization. Page's award is sponsored by the ACS Division of Analytical Chemistry.

Julie S. Pflug, whose research director is Larry R. Faulkner, will study thionine adsorbed onto various electrode surfaces. Fluorescence polarization, both with and without simultaneous electrochemical measurements, will provide information about the system, including possible conformational data. Pflug will work in collaboration with W. Rudolf Seitz and is sponsored by the Society of Analytical Chemists of Pittsburgh.

Charles R. Powley, sponsored by the Federation of Analytical Chemistry and Spectroscopy Societies, is using bipolar pulse conductance to provide fast response measurements with ion-selective electrodes. With research director Timothy A. Nieman, Powley is investigating both the application of the method to the study of luminol and the use of bipolar pulse conductance in determining the critical micelle concentration of nonionic surfactants.

ACS to Conduct Instrumentation Survey

The Joint Board Council Committee on Science of the American Chemical Society will conduct a survey of academic institutions to assess the needs for and current status of chemical instrumentation.

The survey, in response to proposed Reagan Administration budget cuts, will be used to demonstrate to Congress the need for alternate ways to support academic instrumentation. One such alternative would be tax incentives to industry for its support of academic research.

Jordan Bloomfield of the Monsanto Corporation, a member of the ACS committee, hopes to have preliminary information ready for the ACS National Meeting in August and results of the survey by the end of October.



Alfred O.C. Nier, professor emeritus of physics at the University of Minnesota and a pioneer in the field of mass spectrometry, celebrated his 70th birthday on May 26 at a symposium given in his honor by the American Society for Mass Spectrometry (ASMS) at the 29th Annual Conference on Mass Spectrometry and Allied Topics. Burnaby Munson, professor of chemistry at the University of Delaware and president of the ASMS, and Lura J. Powell, research chemist at the National Bureau of Standards, presented Nier with a birthday cake while 250 international scientists serenaded him with strains of "Happy Birthday"

Chakrabarti Wins Fisher Scientific Lecture Award

C.L. Chakrabarti, professor of chemistry at Carleton University, was presented with the Fisher Scientific Lecture Award at the 64th Chemical Conference and Exhibition of the Chemical Institute of Canada, held from May 31–June 3 in Halifax, Nova Scotia. Chakrabarti, whose research interests include atomic spectrometry, trace and ultratrace analysis, and metal–organic interactions in the



C. L. Chakrabarti



SATMAGAN MAGNETIC BALANCE FOR ACCURATE ANALYSIS OF MAGNETITE IN ONE MINUTE

Ideal for analysis of magnetite in iron ores, concentrates and tailings as well as for control of copper and nickel smelting by analysis of magnetite and other ferromagnetic oxides in slag

Measurement easy and accurate, reproducibility better than 0.2 %

Results unaffected by sample dimensions and structure, particle size and packing density — sample weighing unnecessary

Industry's standard instrument — hundreds of satisfied customers all over the world since 1965

☐ MINING ☐ MINERAL PROCESSING ☐ PYROMETALLURGY ☐ HYDROMETALLURGY ☐ METALWORKING ☐ PROCESS AUTOMATION

OUTOKUMPU

OUTOKUMPU OY ENGINEERING DIVISION

Address: P.O. Box 27, SF-02201 Espoo 20, Finland

Representatives in ARGENTINA, AUSTRALIA and NEW ZEALAND, BRAZIL, CANADA, CHILE, INDIA, MEXICO, PERU, PHILIPPINES, SOUTH AFRICA, SPAIN, USA, ZAIRE and ZAMBIA

CIRCLE 159 ON READER SERVICE CARD

Economic, safe membrane filtration. Sartorius has the answer.



sartorius

weighing and filtration
. . . worldwide

Info-Coupon

For the complete range of Sartorius Products please ask for the general catalog.
For specific filtration problems please contact our Product Specialists.

Sartorius Filters Inc.
26575 Corporate Avenue, Hayward, CA 9 45 45
Telefon 4 15-783-66 12, Telex 33 8534

I am especially interested in
☐ Process Filtration ☐ Clinical Chemistry
☐ Laboratory Filtration ☐ Weighing Techniques

Name Position
Company
Address Country

CIRCLE 188 ON READER SERVICE CARD

aquatic environment, was recognized for "distinguished contributions in the field of analytical chemistry."

NSF Announces Cooperative Science Programs

The National Science Foundation has published an 11-page booklet that provides basic information on the Eastern Europe Cooperative Science Programs. These programs are aimed at fostering and supporting scientific cooperation between the U.S. and Bulgaria, Czechoslovakia, East Germany, Hungary, and Romania.

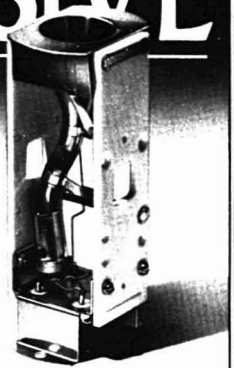
The NSF Division of International Programs coordinates scientific activities undertaken under these programs in the U.S. and maintains liasons with foreign agencies of the cooperating countries. The programs offer support for three types of activities: scientific visits, joint seminars/workshops, and cooperative research. Specific guidelines and requirements apply to each of these programs.

American institutions eligible to participate include universities and colleges, professional societies, and other scientific institutions of the private or public sectors as defined in the NSF publication, "Grants for Scientific Research."

For additional information or to obtain a copy of the program announcement, contact: U.S.–Eastern Europe Cooperative Science Programs, Division of International Programs, National Science Foundation, Washington, D.C. 20550, 202-357-9516.

EXCLUSIVE

GLASS MAKES THE DIFFERENCE IN THE MASS SPECTROMETER DETECTOR



Galileo's Channeltron® ion detectors are more dependable because we gave them a stable glass dynode surface. This simple one-piece component obsoletes the complex metal multidynode detector using a resistive divider.

The glass channel wall provides more accurate and consistent results plus reliability and stability for long-lasting trouble free operation of your mass spectrometer.

A wide selection of detectors is in stock for almost any standard spectrometer. Special mass spectrometer detectors will be designed to meet individual specifications. All are packaged for ease of installation.

Write to us at Galileo Park, Sturbridge, MA 01518 or call (617) 347-9191.

Galileo Electro-Optics Corp.

CIRCLE 90 ON READER SERVICE CARD



James Mitchell

James Mitchell Wins Percy L. Julian Award

James W. Mitchell, head of the analytical chemistry department at Bell Laboratories in Murray Hill, N.J., has received the 1981 Percy L. Julian Outstanding Research Award from the National Organization for the Professional Advancement of Black Chemists and Chemical Engineers.

Mitchell was cited for his "contributions and achievements in advancing the accuracy of trace element analyses." His research at Bell Labs has focused on the development of techniques for identifying contaminants and trace elements in high-purity materials, such as those used to fabricate optical fibers for lightwave communications.

Meetings

■ **12th Congress and General Assembly of the International Union of Crystallography.** Aug. 16–25. Ot-

tawa, Canada. *Contact: K. Charbonneau, Executive Secretary, XIIth I.U.Cr. Congress, National Research Council of Canada, Ottawa, Ontario, Canada, K1A 0R6*

■ **6th International Conference on Fast Ion Beam Spectroscopy.** Aug. 17–20. Quebec, Canada. *Contact: E. J. Knystautas, Dept. de Physique, Univ. Laval, Quebec, Canada, G1K 7P4*

■ **Recent Developments in Instrumental Chemical Analysis.** Sept. 7–9. Kingston upon Thames, England. *Contact: F. A. Burford, School of Chemical and Physical Sciences, Kingston Polytechnic, Penrhyn Road, Kingston upon Thames, KT1 2EE, U.K.*

■ **4th International Conference on Neutron Capture Gamma-Ray Spectroscopy and Related Topics.** Sept. 7–11. Grenoble, France. *Contact: T. von Egidy, Technische Universitat, Munchen, West Germany*

■ **ITA: Department of Commerce Scientific and Medical Laboratory Instruments Exhibition.** Sept. 7–11. Manila, Philippines. *Contact: International Trade Administration, Room 6015, U.S. Department of Commerce, Washington, D.C. 20230*

■ **2nd International Conference on Chemical Analysis: Microanalysis Using Charged Particle Accelerators.** Sept. 8–10. Namur, Belgium. *Contact: Meeting Secretary, Microanalysis Conference, L.A.R.N. rue Muzet 22, B-5000, Namur, Belgium*

■ **International Conference on Advances in Flow Measurement Techniques.** Sept. 9–11. Conventry, England. *Contact: Conference Organizer, BHRA Fluid Engineering, Cranfield, Bedford, U.K.*

■ **2nd International Symposium on Radiopharmacology and Exhibition.** Sept. 9–11. Chicago, Ill. *Contact: Lelio Colombetti, Pharmacology Dept., Loyola University, Stritch School of Medicine, Maywood, Ill. 60153*

■ **Measurement Problems in Medicine and Biology.** Sept. 15–17. Suzdal, U.S.S.R. *Contact: IMEKO Secretariat, H-1371 Budapest, POB. 457, Hungary. Phone (36-1) 324 116, Telex 225792 MTESZ H*

■ **7th International Chemistry Exhibition and MAC 1981.** Oct. 6–10. Milan, Italy. *Contact: Exhibition Secretariat, Viale Premuda 2, 20129 Milano, Italy*

■ **8th ANACHEM Symposium.** Oct. 15–16. Dearborn, Mich. *Contact: T. M. Schmitt, BASF Wyandotte Corporation, Wyandotte, Mich. 48192. 313-282-3300. July, page 981 A*

■ **Workshop on Analytical Chemistry Related to Canada's Nuclear Industry.** Oct. 19–21. St. Jovite, P.Q., Canada. *Contact: R. M. Cassidy, General Chemistry Branch, Station 320C, Atomic Energy of Canada Limited, Chalk River Nuclear Laboratories, Chalk River, Ontario, Canada, K0J 1J0*

■ **Association of Official Analytical Chemists Annual Meeting.** Oct. 19–22, Washington, D.C. *Contact: Kathleen Fominaya, Program Assistant, Box 540, Benjamin Franklin Station, Washington, D.C. 20044*

■ **Workshop on Chemistry and Analysis of Hydrocarbons in the Environment.** Nov. 26–27. Barcelona, Spain. *Contact: Workshop Office, J. Albaiges, Expoquimia, Plaza de España, Barcelona-4, Spain. Telex: 53117 FOMB-E*

■ **American Water Works Association Water Quality Technology Conference.** Dec. 6–9. Seattle, Wash. *Contact: John Hookey, Meeting Di-*

HIGH QUALITY *SPECTROPHOTOMETERS*

Our company specializes in recertified, high quality spectroscopic equipment. Each instrument sold includes a current manufacturer's inspection report indicating it is in excellent operating and cosmetic condition. Upon request, we will run special tests using your samples to guarantee the instrument will fulfill your requirements. A representative listing of our current inventory is as follows:

- **Varian Cary 14's. Price...$9,750 to $12,000 (depending on accessories included and age)**
- **Varian Cary 14 monochrometer. Price... $7,500.**
- **Carl Zeiss — Thin Layer Chromatograph (TLC) spectrophotometer. Price...$5,250.**
- **Gilford Model 2400 spectrophotometer system. Price...$3,750.**
- **Perkin Elmer/Coleman Mod 124D spectrophotometer. Price...$2,750.**
- **Perkin Elmer Mod 241 polarimeter including constant temperature water bath. Price...$7,250.**
- **Varian Cary 15. Price...$6,750.**

Please phone (415) 854-1179 or write Scientific Apparatus Exchange, Box E, Stanford, CA for additional information on the above or if you require other equipment not listed.

SCIENTIFIC APPARATUS

P.O. Box E • Stanford, California 94305 • (415) 854-1179

CIRCLE 194 ON READER SERVICE CARD



...the BEST in a HURRY

Burdick & Jackson local distributors will give you fast delivery on your HPLC solvents from stock locations in or near all these major cities:

East	Central	West
Boston	Detroit	Seattle
Philadelphia	Chicago	Portland
Atlanta	St. Louis	San Francisco
Pittsburgh	Denver	Los Angeles
	Houston	

Call today for information: 616/726-3171

BURDICK & JACKSON LABORATORIES, INC.

1953 SOUTH HARVEY STREET • MUSKEGON, MICHIGAN 49442

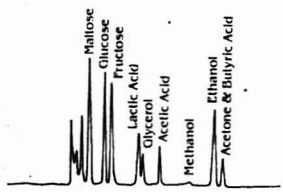
Look for us at ExpoChem '81, Booth 56, at the Shamrock Hilton in Houston, Sept. 1–3.

CIRCLE 24 ON READER SERVICE CARD

When reverse phase doesn't work (not even ours)

Try IMP

Resin based columns for Ion Moderated Partition HPLC



Sample: Fermentation By-Products Model Solution
Column: HPX-87 Organic Acid Analysis 300mm x 7.8mm
IMP separation of fermentation by-products

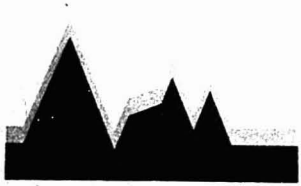
Try this difficult separation on your reverse phase column — it won't work. But it *does* work — time after time — by IMP. This chromatogram proves it.

If you have separations problems, call our HPLC Applications Department. They have the answer.

COMMITTED TO EXCELLENCE IN HPLC

BIO-RAD Laboratories

2200 Wright Avenue • Richmond, CA 94804 USA • Phone (415) 234-4130 Also in Rockville Centre, N.Y., Australia, Austria, Canada, England, Germany, Italy, Japan, The Netherlands, and Switzerland.



CIRCLE 26 ON READER SERVICE CARD

News

rector, 6666 W. Quincy Ave., Denver, Colo. 80235

■ **6th International Conference on Infrared and Millimeter Waves.** Dec. 7–12. Miami Beach, Fla. *Contact: K. J. Button, National Magnet Lab., MIT, 170 Albany St., Cambridge, Mass. 02139*

For Your Information

The National Bureau of Standards has made available **three new Standard Reference Materials.** SRM 469, available for $77, is a 5-mm bead of an aluminum–tungsten alloy for evaluating the resolution of scanning electron microscopes. SRM 1644 is a generator column used for preparing accurate concentrations of anthracene, benzo(*a*)anthracene, and benzo(*a*)pyrene in water. SRMs 1691a–1696, available for $420 each, are seven gas mixtures of sulfur dioxide in nitrogen for calibrating instruments and techniques used in the analysis of stack gases. To order, contact the NBS Office of Standard Reference Materials, Chemistry B311, National Bureau of Standards, Washington, D.C. 20234. 301-921-2045.

Flow General has been appointed distributor for U.S. Gelman products in France and French North Africa. The products include process filtration equipment and supplies, clinical diagnostic supplies, and laboratory filtration goods. Contact Christian Polichard, General Manager, 17/19 Rue deVerdun, 92600 Asnieres, France. Telephone: 793-85-21; telex: 612041 Flow FRA.

"Scientists, Engineers, and Technicians in Private Industry, 1978–80" has recently been released by the National Science Foundation (NSF). The report builds on a series of surveys of private employers conducted for NSF by the Bureau of Labor Statistics and presents data and analyses on employment of technically trained personnel in industry during that period. Copies are available at $2 each from the Superintendent of Documents, U.S. Government Printing Office, Washington, D.C. 20402. Request stock number 038-000-00472-7.

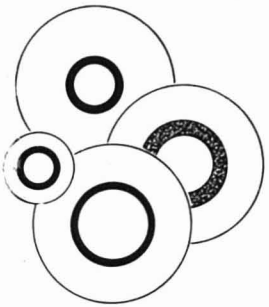
A videotape–workbook training program for instrumentation technicians and plant operators has been announced by Instrument Society of America (ISA). This program provides training in basic technical skills and an understanding of the proper function of process control systems. The first three-tape module is available and covers 12 hours of training on electronic instruments, sensors, indicators, and transmitters. All materials for in-plant training are provided. Contact Don Ellis, ISA, 67 Alexander Dr., Research Triangle Park, N.C. 27709. 919-549-8411.

C22-P, *Proposed Standard for Calibration Materials in Clinical Chemistry*, **and C23-P,** *Proposed Standard for Control Materials in Clinical Chemistry* are available from the National Committee for Clinical Laboratory Standards. These companion publications replace the standard C2-A and provide specifications for the materials that are used to monitor routine or field analytical systems for the measure of analytes and specimens such as serum or urine. Copies are available for $9 each ($10 each for foreign orders) by check or money order in advance from National Committee for Clinical Laboratory Standards, 771 East Lancaster Ave., Villanova, Pa. 19085

The **Mid-South Toxicology Affiliates,** a group representing the tri-state area of Tennessee, Arkansas, and Mississippi, was recently formed. It consists of experts in all aspects of toxicology and includes members from government, industry, and academia. The group's plans include establishment of a toxicology library, promotion of interuniversity educational programs, and coordination of ideas and discoveries between different research groups. Additional information may be obtained from John Autian, College of Pharmacy, University of Tennessee, Memphis, Tenn. 38163. 901-528-6020

An EPA/NIH Mass Spectral Data Base Supplement contains 8807 mass spectra and a completely new index that covers the first four volumes of 25 556 spectra as well. Each spectrum is presented in bar graph format over the full mass range and is accompanied by a *Chemical Abstracts Index* subject name, molecular formula, molecular weight, and *Chemical Abstracts Registry* registry number. The supplemental set is available for $42 from the U.S. Government Printing Office. The stock order number is SN-003-003-02268-3

high esolution capillary columns



All columns are guaranteed to give a specific high efficiency and therefore high peak resolution.

- Flexible vitreous silica columns.
- Glass in WCOT & SCOT.
- Narrow & wide bore in a variety of phases.

SGE also offers a variety of vespel & graphite ferrules, low hold-up unions, splitters and other accessories for capillary column operation.

Write for complete catalog on SGE products.

SGE

Head Office:
Scientific Glass Engineering Pty. Ltd.,
7 Argent Place, Ringwood,
Victoria, 3134 Australia.
Tel: (03) 874 6333

UK Sales Office:
Scientific Glass Engineering (U.K.) Ltd.,
657 North Circular Road,
London NW2 7AY, Great Britain.
Tel: (01) 452 6244

U.S.A. Sales Office:
Scientific Engineering Inc.,
2007 Kramer Lane, Suite 100,
Austin, Texas 78758, U.S.A.
Tel: (512) 837 7190

German (BRD) Sales Office:
Scientific Glass Engineering GmbH.,
Fichtenweg 15,
D-6108 Weiterstadt 1.
Tel: (06150) 40662

CIRCLE 187 ON READER SERVICE CARD



CHEMTECH... because a chemist leads so many lives

There are dozens of journals devoted to chemistry, but only ONE magazine devoted to *chemists* — CHEMTECH. This stimulating monthly magazine reports on world concerns and personal ones — technology, economics, energy, environment, and much more — *as they concern chemists*. And it covers the field of chemistry itself with insight, perspective, a flair for selecting what's important and packaging it in authoritative, readable form.

For a clear-eyed view of *all* the facets of a chemist's life — subscribe to CHEMTECH now!

CALL TOLL FREE: 800-424-8747

CHEMTECH **1981**
American Chemical Society
1155 16th Street, N.W. Washington, D.C. 20036

Sign me up for a one-year subscription to CHEMTECH magazine. I have indicated subscription category and payment preferences below.

	U.S.	Foreign
ACS Members*	☐ $20	☐ $25
Non-Members (Personal)	☐ $25	☐ $30
Institutions, Companies	☐ $100	☐ $105

☐ Bill me ☐ Bill company
☐ Payment enclosed (Make check payable to American Chemical Society)

Charge my ☐ MasterCard ☐ VISA

Card Number _____

Interbank Number _____ Expire Date ____
(MasterCard only)

Signature _____

Name _____

Job Title _____

Employer _____

Address _____

City _____

State, ZIP _____

*Member rates are for personal use only.
Foreign payment must be made in U.S. currency by international money order, UNESCO coupons, U.S. bank draft or order through your subscription agency. Allow 60 days for first copy to arrive.



Purely to meet your needs... Ashland Reagents from 59 locations.

Ashland offers well over 100 quality reagent chemicals through our 59 U.S. distribution centers – one near you. Not a big line, but just about everything basic to wet analysis or synthesis work. More important, we can probably give you one day service on your regular needs. That makes us special.

The range of Ashland® Reagent acids and bases, salts, solvents and specialties meet stringent purity standards, including ACS specifications where they exist. And we offer all the usual sizes of convenient packaging, with specifications published on the labels. In short, we've gone to great lengths to assure you a dependable source of consistently high quality reagents.

Moreover, we've made Ashland Reagents available through our 59 chemical distribution centers, especially for you. We're quite possibly already serving your company from these locations with our full line of industrial chemicals and specialties.

If a quicker source of basic reagents would brighten your day, call the Ashland location, listed under chemicals, in your Yellow Pages. Chances are good they're loading a delivery truck headed your way. And write for our catalog: Industrial Chemicals & Solvents Division, Dept. ARC, P.O. Box 2219, Columbus, Ohio 43216.

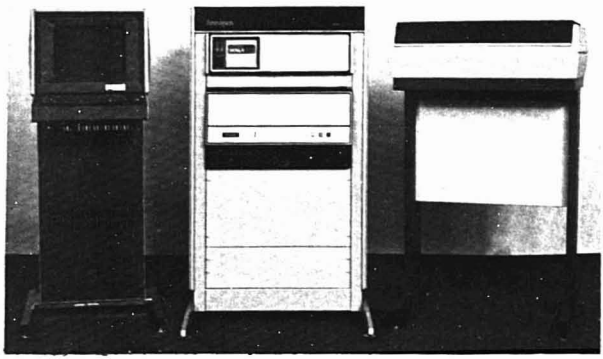
Ashland

Ashland Chemical Company

DIVISION OF ASHLAND OIL, INC.

CIRCLE 2 ON READER SERVICE CARD

New Products



Incos 2100C and 2200C MS Data Control Systems have interfaces designed for quadrupole systems and for magnetic field instruments, respectively. The software features a real-time disk operating system operating in a true priority interrupt foreground/background mode. Options for expansion are available. Finnigan MAT **403**

FTIR Spectrometer

FX-6200FM Spectrometer is a follow-up to the fX-6200 spectrometer. A new feature is the dual 8-in flexible disk storage system utilizing a high-speed proprietary disk controller. Standard software includes a rapid spectral search routine based on the Sadtler Spec-Finder code. Access to the complete Sadtler library in the Analect format can be leased by subscribers to the system. $36 000. Analect Instruments **409**

Electronic Microbalance

M3 Microbalance offers a weighing range of 0–150 mg and is readable to 1 μg; it has a weighing capacity of 3050 mg, a built-in calibration weight, automatic calibration, and a stabilization time of less than 5 s. The balance can be ordered with data output. $7335. Mettler **410**

Water Analysis System

F. I. Analyzer, based on the flow injection principle, can test up to 250 samples/h. Concentrations of phosphate, nitrogen, nitrite, nitrate, silicate, and ammonia are automatically determined in ppm/mg. The analyzer consists of a sampler, an analysis section, a photometer, and a recorder with data system. Cenco Instrumenten B.V. **411**

LC Radioactivity Detector

AN-700 is a dual-channel, microprocessor-controlled radioactivity detector for liquid chromatography that uses either liquid or solid scintillation counting techniques. It is set to count Tritium and ^{14}C but also allows detection of ^{36}Cl, ^{32}P, and ^{125}I and eliminates liquid scintillator vials by using an injected liquid scintillant and on-the-fly detection. It delivers results in real time by generating a histogram as peaks elute from the column. Anspec **408**

HPLC Computing Integrator

Model 302 dual-channel integrator accepts chromatograph data from two detectors simultaneously and allows selection from a variety of computing routines by use of ROM resident BASIC programming language. Its capabilities include area percent, normalization, automatic recalibration, drift and baseline correction, internal/external standards, statistical analysis, and custom reports. Laboratory Data Control **414**

For more information on listed items, circle the appropriate numbers on one of our Readers' Service Cards

Microprocessorized Centrifuge

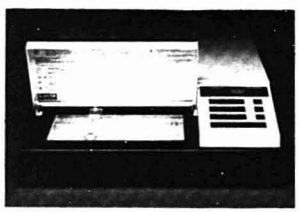
J-6M Microprocessorized Centrifuge has storage space in its memory for 10 programs, a choice of nine acceleration and 10 deceleration rates, automatic temperature compensation after keyboard entry of the name of the rotor to be used, a brushless drive, and a frequency-controlled induction motor. Beckman **412**

Computerized Blood Chemistry Analyzer

K-11 Chemistry Analyzer is capable of performing up to 1020 chemistry results with 180 calculated indexes on up to 60 blood samples/h. Computer features include long-term storage of patient results on the diskette, a report editing program, a flexible parameter file that allows operator changes in the report format, built-in capability that allows interface to a secondary computer system, and remote data transmission to printers. Boehringer Mannheim Diagnostics, Inc. **413**

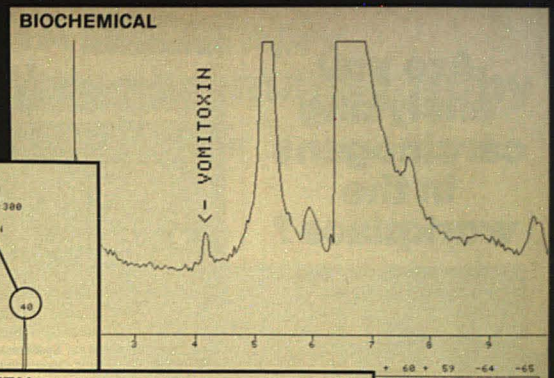
Electronic Top Pan Balances

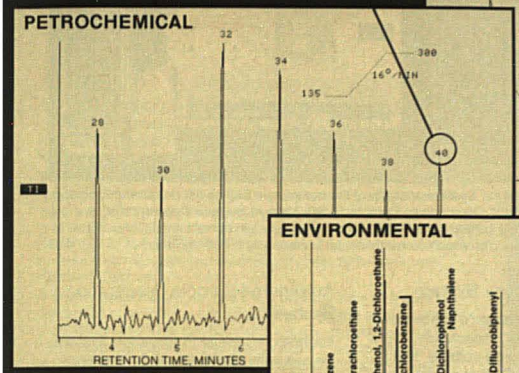
3000C series 3-kg balances read to 0.01 g, comprise state-of-the-art electronics using the vacuum phosphorescent display module, and feature a unique filling-in guide and tare availability indicator. Precisa **428**

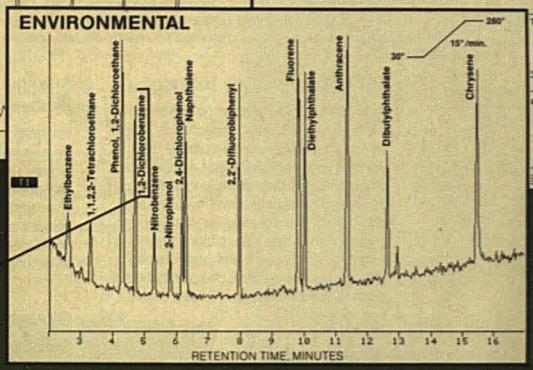


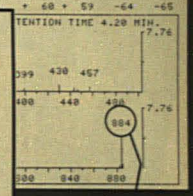
LKB 2202 UltroScan Laser Densitometer for electrofocusing automatically scans high-resolution gels. It features a He–Ne laser source, is microprocessor controlled, and will accommodate gels up to 13 × 27 cm. It will accept polyacrylamide, agarose, and cellulose acetate gels, micro TLC plates, photographs, and autoradiography films. Two cassettes scan tube gels between 2 and 6 mm in diameter. The modular UltroScan may be connected to a variety of potentiometric recorders, integrating printer plotters, or other data-handling systems. LKB **404**

Analysis of a low nanogram mixture C_{28}-C_{40} hydrocarbons made possible by fused silica "open split" interface and the HP 5985B.









Need fast, precise, identification of pollutants? Here, measured with HP 5985B according to new EPA isotopic dilution procedures, is a composite mixture of volatile acid/base neutrals and their isotopically labelled analogs.

Excellent high mass transmission characteristics of the HP 5985B shown by the large molecular derivatized ion (20 ng) at m/z 884.

It's the last word in GC/LC/Mass Spectrometers. Period.



HP 5985B GC/MS System

Whether it's courtroom evidence or positive identification of an elusive component, the HP 5985B GC/MS gives you dependable results like these, even from trace amounts of difficult samples. This system is recognized worldwide for ease of use and day-to-day repeatability of results.

For full data, write to Analytical Group, Hewlett-Packard Co., 1820 Embarcadero Road, Palo Alto, CA 94303. Or call and ask for an HP Analytical Products Representative.
EAST (215) 265-7000,
WEST (408) 988-7000, MIDWEST (312) 255-9800,
SOUTH (404) 955-1500.
CANADA: (416) 678-9430.
EUROPE: (022) 83.81.11. JAPAN: (03) 331-6111.

When performance must be measured by results.

HEWLETT PACKARD

23106/AG

Circle 101 for Literature. Circle 102 to have a HP Representative Contact You.

Are you analyzing carcinogens in the workplace?

Here's help for you from Varian.



Send for these free brochures today!

Instrument Systems. A large selection of gas chromatography, atomic absorption, ultraviolet-visible and liquid chromatography instruments designed to meet the latest standards in air and water pollution analysis.

Application Reports. An ongoing series of Varian application reports on environmental pollution analysis.

Local Support. Hundreds of Varian sales and service representatives and applications scientists located throughout the world. They're on call to give you the help you need, before and after you buy.

Workshops & Training Courses. Local workshops, ranging from elementary training in the analysis of carcinogens to special problem-solving courses tailored specifically for your needs. Lots of instrument training courses, too.

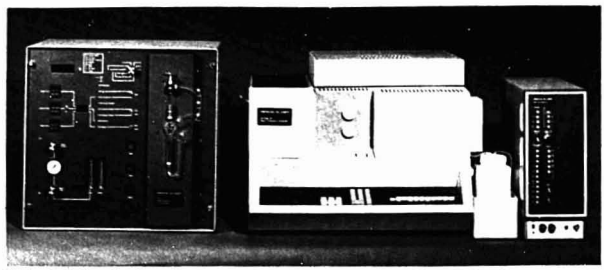
Parts & Supplies. Everything you need to create a total GC, AA, UV-Vis or LC system for environmental pollution analysis.

For literature, circle 240 on the reply card. If you'd be interested in a local "hands-on" workshop, circle 241. Circle 242 for a representative to call.

Varian instrument Group
611 Hansen Way, D-070
Palo Alto, CA 94303

varian

New Products



Water Pollution Analyzer System consists of the company's SIGMA 3B Gas Chromatograph, Model 700A Electrolytic Conductivity Detector, LSC-2 Liquid Sample Concentrator, and the EPA primary analytical column for the determination of four trihalomethanes (chloroform, dichlorobromomethane, dibromochloromethane, and bromoform). Perkin-Elmer **405**

FTIR Spectroscopy System

The 3600C FTIR System's spectrometer features 0.5-cm^{-1} resolution, 1.8-s scan time, small purge volume, and a sample compartment that accommodates virtually any sample-handling accessory. Its data system features a 64K, 20-bit, word programmable processor; an interactive color–graphics raster scan display; and high-density dual-disk storage disk. A spectral data base is also available. Nicolet Instrument Corp. **415**

Automated Sample Preparation System

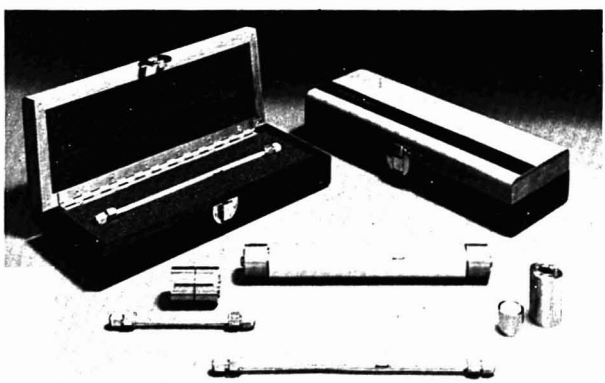
Technicon Sample Preparation System, for use with HPLC, AA, and other techniques, automatically prepares, treats, and collects solid or liquid samples. The system offers filtration, dialysis, solvent extraction, evaporation to dryness, concentration, derivatization, and other capabilities. Technicon **417**

Rapid Ion Analysis

Fast run ion chromatography columns enable seven different ions to be determined in 8 min with sensitivity increased up to a factor of 3 for SO_4 and NO_3. Dionex **422**

Glossmeter

Glossgard IIa Glossmeter is available in 20°, 45°, 60°, 75°, and 85° gloss geometries and conforms with applicable ASTM and international specifications. It has an extended range of 0 to 199 gloss units and a 20 000-h-long life lamp. Pacific Scientific, Gardner Lab Division **424**



Matched Surface Chemistry LC Columns are introduced: C-18 Analytical Reversed-Phase Columns (10 μm) permitting a wide range of flow rates; C-8 Analytical Columns for use when a wide range of sample polarities must be chromatographed; high-speed, high-efficiency LC columns for large numbers of tests in minimum time; and preparative LC columns with distributor plates to spread the injected sample across the full width of the column. Perkin-Elmer **401**

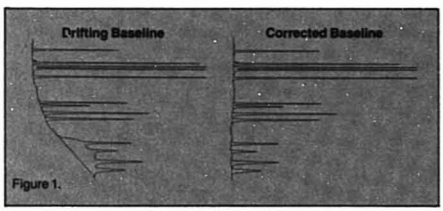
New VISTA 401 simply outsmarts the other chromatography data systems

The new VISTA 401 Chromatography Data System is usefully brilliant. Its powerful interactive CRT/keyboard makes it simple to efficiently handle the data from both GCs and LCs — from any four chromatographs in your lab.

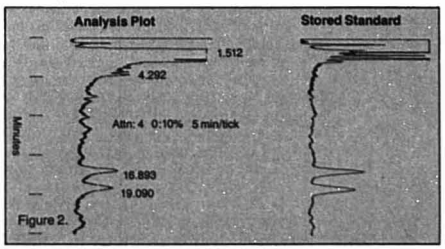
It's more responsive and helpful. When you build a data handling method, the prompted dialog you have with the big interactive CRT is so relaxed and friendly it's almost human. And you can build methods on the CRT while the printer/plotter is reporting an analysis. You don't have to wait. The VISTA 401 even has a "learn" mode in which it scans a chromatogram and automatically selects the best peak measuring parameters for each peak.

A more useful record. On one piece of paper the VISTA 401's fast, fixed-head dual-channel printer/plotter will give you a fully annotated chromatogram and report, both with compound names. Results can be automatically reported in any units of measure desired: ppb, mole %, BTUs, etc. and versatile editing functions help you get clean, clear reports.

Because it's smarter you get better data. In addition to performing all the standard calculations, the VISTA 401 has unique features that help you get better data. It will actually draw the computed baseline on the chromatogram so you can see if each peak is accurately integrated and correct the baseline whenever necessary. To improve the accuracy of data on runs where you get drifting baseline, the VISTA 401 will subtract baseline drift. See Figure 1.



To help you improve data, VISTA 401 subtracts drifting baseline and draws in the computed baseline.



To help you confirm data, the VISTA 401 replots a stored standard alongside an analysis plot.



Floppy disks give you new capabilities. Built-in floppy disks provide convenient on-line data storage with instant random access. Much faster than tape, and smarter. The VISTA 401 will store, directly on disk, all the raw data for an entire chromatogram for replotting and recalculation. It will even replot a standard chromatogram, saved on the disk, alongside another chromatogram on its dual-channel printer/plotter. See Figure 2.

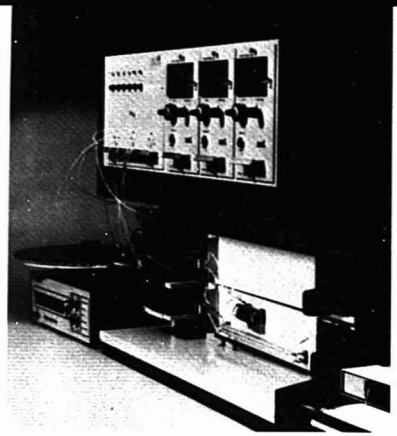
It will grow with you. VISTA 401 provides smart data handling for any four chromatographs in your lab — GC or LC. You can use the VISTA 401 to fully control up to four VISTA chromatographs and it has a standard interface to large and small computers. To help you get the most from your VISTA 401 we offer regularly scheduled user training courses at our regional offices and provide strong service and applications support.

For full information call us (phone numbers below), drop us a line or check these Reader Service Numbers: **238** to have a Varian Representative contact you; **239** for literature.

varian

For immediate assistance contact: • Florham Park, NJ (201) 822-3700 • Park Ridge, IL (312) 825-7772 • Houston, TX (713) 783-1800 • Los Altos, CA (415) 968-8141
Or write 611 Hansen Way, Palo Alto, CA 94303 In Europe: Steinhauserstrasse, CH-6300 Zug, Switzerland

AUTOMATIC WET CHEMICAL ANALYSIS



QuikChem™ System IV Automatic Flow Injection Analyzer

FEATURES

- Automated procedures for colorimetric, fluorimetric, electrochemical and titrimetric analyses.
- Processes 120 to 300 samples per hour
- Determines up to four analytes simultaneously in each sample.
- Demonstrates nominal response time of 30 seconds thus allowing near-real time on-line monitoring as well as sequential and stat operations in the laboratory.
- Microprocessor supports complete control, data reduction and I/O functions for up to four independent analytical systems.
- Micro sample and reagent volumes.

SHORT COURSE INFORMATION

The Lachat *QuikChem*™ System IV Automatic Flow Injection Analyzer will be exhibited at the shows listed below. Short courses will be presented in conjunction with each meeting on the dates indicated.

- **ACS Meeting (Special FIA Symposium)**
  New York-August 24-27
- **LABCON '81**
  Chicago-O'Hare-September 15 & 16
- **AOAC Fall Meeting**
  Washington, DC-October 20
- **Eastern Analytical Symposium**
  New York-November 18

For specific times and locations please contact us.

LACHAT CHEMICALS, INC.
INSTRUMENT DIVISION
10500 N. Port Washington Road
Mequon, Wisconsin 53092 USA
Tel (414) 241-3872 Telex 26-9681

CIRCLE 126 ON READER SERVICE CARD

New Products

LC Column Accessory Products

Mobile Phase Conditioner is a sacrificial column that eliminates the dissolving of silica from analytical or preparative columns during mobile phase conditions of basic pH or high aqueous buffer concentration; it can also prevent column bed collapse. Column end fittings utilize the distributor plate concept, have replaceable porous disks, and increase efficiency by 15% per column. Perkin-Elmer **416**

Laboratory Blender

Stomacher Lab-Blenders minimize contamination of either the sample or the chamber through use of a plastic bag. The process takes about 30 s, and damage to cells and tissues is minimal. The line includes four models, three for sample sizes 5–3500 mL and one with precise temperature control. Tekmar **418**

Disposable Extraction Columns

ChemTube Extraction Columns eliminate the need for centrifugation and aspiration procedures, and prevent the formation of emulsions when using aqueous samples such as wastewater, body fluids, and beverages. Columns are prepacked with an inert, hydrophilic matrix and are available with 50-, 100-, and 300-mL sample capacities. Fisher Scientific Co. **419**

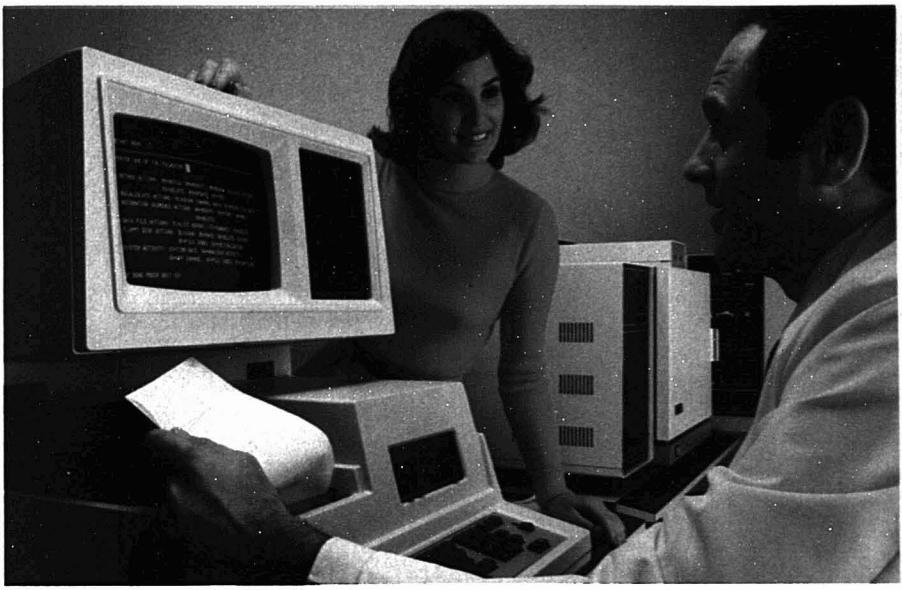
Digital Oscilloscope

4094 Digital Oscilloscope offers a 16K word by 16-bit mainframe memory, the ability to accept one- or two-channel plug-in units, a cursor-interactive waveform coordinate display, and a limited selection of keystroke data manipulation functions. Two available models of plug-in units, the 4562 and 4851 offer ±100-mV and ±64-mV sensitivities, 12-bit and 15-bit resolution, and 2-MHz and 15-bit resolution, and 2-MHz and 100-kHz sampling rates, respectively. Several storage unit and plotter options are available. Nicolet Instrument Corp. **425**

BOD System

60-Second BOD System measures samples precisely in less than 1 min to accuracies comparable to that of the Winkler or electrode methods. No stirring equipment or membrane replacement is required, and no oxygen is depleted from the sample. Acceptable for determining BOD_5 and DO when using approved EPA methodology. Wheaton Instruments **426**

VISTA 44
simply outanalyzes other automatic GC's



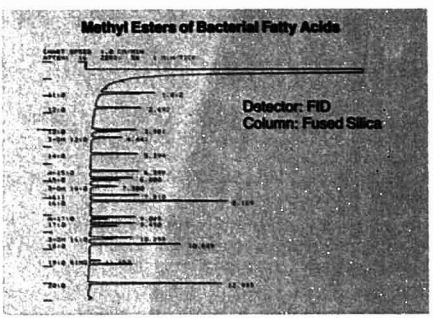
Great gas chromatography results come easier with the new VISTA 44 than with any other GC system you can buy!

The big interactive CRT/keyboard prompts you and helps you monitor the chromatograph and build methods even while the printer/plotter is reporting a fully annotated chromatogram with calculated results.

Everything about the chromatograph is designed for analytical productivity: large convenient column oven and pneumatics compartment, universal injector and detector bases that save time, advanced detectors, easy-to-use capillary systems, and fully controlled AutoSamplers.™

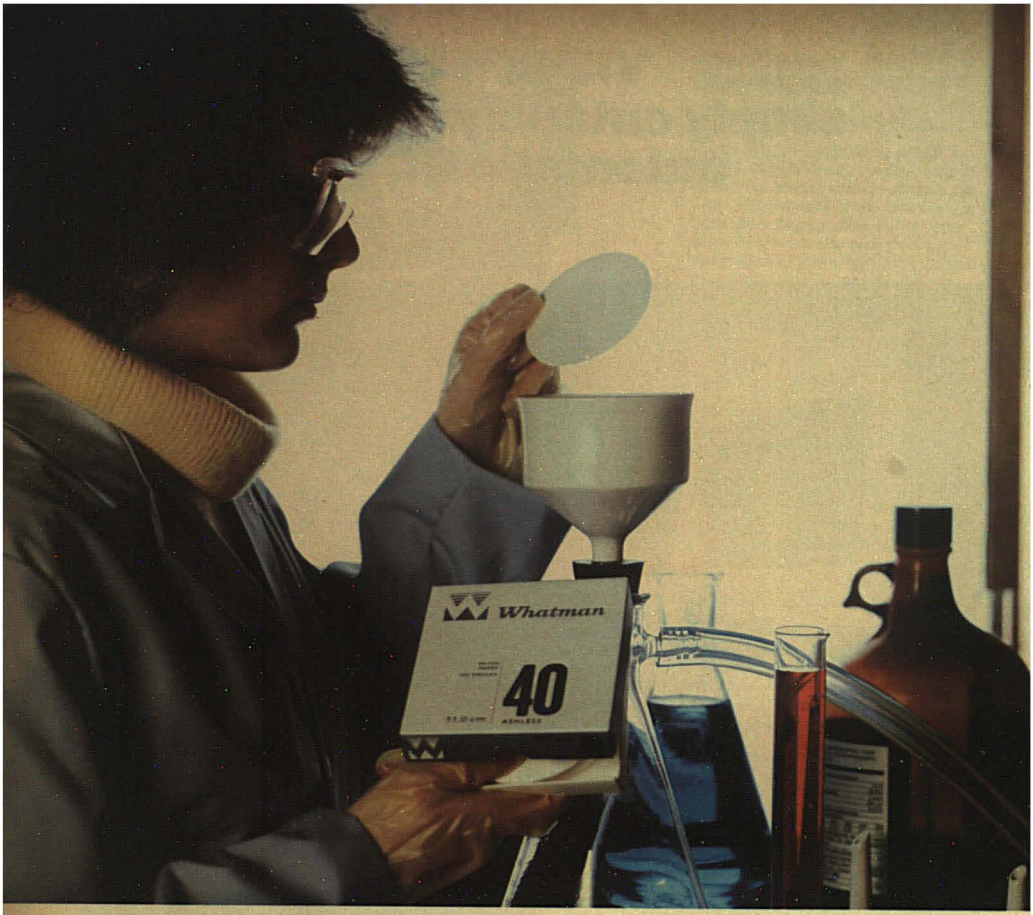
Data and automation channels can be easily added to allow one VISTA 44 to handle up to four chromatographs.

For full information call your nearest Varian Regional Office, the phone number is given below, drop us a line or check these Reader Service Numbers: **243** for literature; **244** if you plan to purchase soon and need current prices; **245** to have a Varian Representative contact you.



varian

For immediate assistance contact: • Florham Park, NJ (201) 822-3700 • Park Ridge, IL (312) 825-7772 • Houston, TX (713) 783-1800 • Los Altos, CA (415) 968-8141
Or write 611 Hansen Way, Palo Alto, CA 94303. In Europe: Steinhauserstrasse, CH-6300 Zug, Switzerland.



Whatman Quantitative Filter Papers. Of Course.

Many times in the course of experiments the filtration step is crucial. Almost invariably the filter paper called upon in these cases is one of the eleven grades of Whatman quantitative filter papers. And this has been so for decades, in laboratories all over the world.

Purity, uniformity, reliability in Whatman quantitative grades are confidently assumed by scientists everywhere and in every kind of analytical laboratory.

As well it should be. No pains are spared to merit that confidence; compromises are unacceptable in producing the finest filter papers in the world. Use of only high purity alpha celluloses, rigorous quality controlled manufacturing, a unique (and proprietary) acid treatment process, use of demineralized water, and many other specialized techniques ensure not only the highest quality but the highest achievable purity and consistency within grade and from grade to grade.

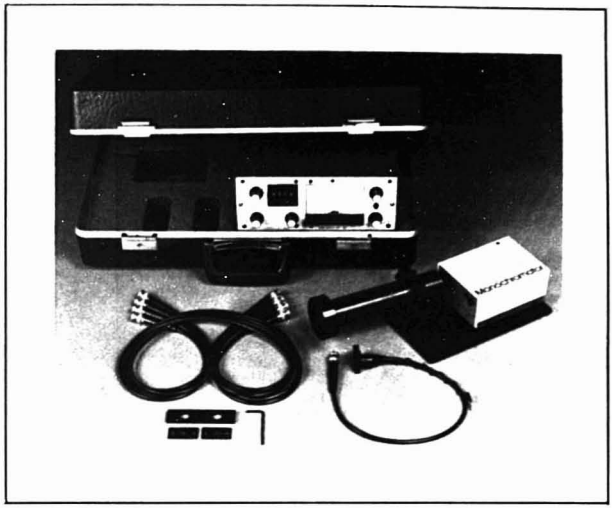
Whatman quantitative filter papers. The world's laboratory standard.

Of course.

Whatman Laboratory Products Inc.
Whatman Paper Division
9 Bridewell Place, Clifton, New Jersey 07014
Tel: (201) 773-5800

Whatman PAPER DIVISION

CIRCLE 227 ON READER SERVICE CARD



Model 6011 Optical Spectrum Analyser displays optical spectra in the region 300–1100 nm on any lab oscilloscope. Features include 0.5-nm wavelength accuracy, up to 2-nm resolution (FWHM), spectral expansion, and a built-in wavelength calibration scale. $2395. Rofin Inc. **402**

Chemicals

Manual Chemistry Kits

Eight manual chemistry kits are introduced: albumin, calcium, chloride, total cholesterol, Glucotall glucose, urea nitrogen, HDL, and total protein. All use minimal sample volumes and are based on the preferred reactions for the individual determinations. Fisher Scientific Co. **421**

Cation Exchange Cellulose

Grade SE 53 acidic cation exchange cellulose is fully ionized and can operate under aqueous–organic as well as under purely aqueous conditions. It is preswollen, and supplied in the sodium form. Its small ion capacity is 2.3 meq/g, protein adsorption value is 1400 mg/g (lysozyme), and it can be used over a pH range of 2–12. Whatman Inc. **433**

HDL Reagent Kit

The kit includes modified magnesium/phosphotungstate reagent, two-part precipitating reagent, human-based control sera, and three aqueous-based cholesterol standards sufficient for 450 determinations. Fisher Scientific Co. **434**

Asbestos Detection Kit

E-C Asbestest, based on a standard chemical colorimetry test, detects the presence of levels of asbestos-bound iron or magnesium as low as 1%. The kit includes chemicals, reaction tubes, controls, and instructions. E-C Apparatus Corp. **431**

Amino Acid Analysis Reagents

This line of analysis reagents offers pH stability of ±0.01 and consists of sodium eluants (pH 3.25, 4.25, and 7.40), diluent, regenerant, chromatographic-grade *o*-Phthalaldehyde (OPA), and OPA diluent. Pickering Laboratories **432**

Luminescence Reagent

Luciferine Luciferase Reagent is for use in bacterial enumeration in urine and biomass studies and is suitable for all standard luminometers. It is available in lyophilized form in 10-, 50-, and 100-mL amounts, or in a 200-test assay kit. Analytical Luminescence Laboratory **435**

Certified Reference Material

CRM 1678 contains 47.2 ± 0.5 ppm carbon monoxide in nitrogen, is EPA certified, and is equal to NBS SRM 1678. It is available in both 30- and 150-ft^3 aluminum cylinders. Scott Specialty Gases **436**

INVOLVED WITH
Pesticides? Toxicology? Environmental Research?



New Corco HPLC-Grade High Purity Solvents Are Double-Distilled-in-Pyrex® for High Reliability and Repeatability with HPLC, Gas Chromatography, Spectrophotometry

Corco double-distills HPLC solvents in Pyrex®—to provide the exceptionally high purity required for reliable and repeatable results in HPLC work.

We've even labeled them HPLC-Grade to distinguish them from other solvents—even from our own ACS grade reagent solvents.

If you're involved in pesticide analysis, toxicology work, environmental research—anywhere you need the reliability and repeatability of true high purity solvents—count on Corco to meet your stringent requirements.

Our Pyrex-double-distilled HPLC-Grade solvents are also ideal for gas chromatography and spectrophotometry.

For complete details call or write Corco today—or circle the number.

CORCO
CORCO CHEMICAL CORPORATION
Manufacturers of Reagent & Electronic Chemicals
Tyburn Road & Cedar Lane • Fairless Hills, PA 19030
(215) 295-5006

®Pyrex registered Trademark, Corning Glass Works
CIRCLE 37 ON READER SERVICE CARD



For environmental standards, make one call– Analabs

Check your requirements against the Analabs complete line of reference standards for food, soil, water and air pollutants.

Choose from PCB's, pure PCB isomers, PBB's, Haloethers, Nitrosamines, Heterocyclic Carcinogens, Polynuclear Aromatics, Chloroaromatics, or Pesticides. Packed individually in kits or in solution as mixtures for environmental monitoring of priority pollutants in accordance with EPA and OSHA guidelines. Custom syntheses available for any chemical for the environmental researcher.

For prompt service, or for information about methodologies and tools for sampling to meet EPA and OSHA requirements, contact us. Call or write for our free Environmental Standards and Accessories Catalog. **Analabs,** A Unit of Foxboro Analytical, 80 Republic Drive, North Haven, CT 06473 (203) 288-8463.

Another dimension in analytical measurement and control

FOXBORO

CIRCLE 87 ON READER SERVICE CARD

Baseball Shirts & Chemist-Tees

Our 50% cotton/50% polyblend in 3 styles to unleash the chemist (and baseball player) in you!



White shirt, navy sleeves, navy and red print. T-shirt blue and red on a light blue shirt

Red and black print on a gray shirt





Multicolored ancient "elements" on a sandy- tone shirt

Sizes: Small *(34)*, Medium *(36–38)*, Large *(40–42)*, Extra-Large *(44)*
Price: T-shirts — 1 to 3 $7.50 each, 4 to 9 shirts $7.00 each, 10 or more $5.95 each
Baseball shirts — 1 to 3 $9.00 each, 4 to 9 $8.50 each, 10 or more $7.95 each
Postage and handling: $1.90 per order
Foreign shipment surcharge: Canada $0.75 per shirt; other countries $1.75 per shirt
Payment: Use **VISA** or **MasterCard** or make checks payable to the American Chemical Society; orders must be prepaid

Send to: Department of Educational Activities, American Chemical Society, 1155 Sixteenth Street, N.W., Washington, D.C. 20036, U.S.A.

Style	S	M	L	XL	Unit Cost	Total
Chemistry Matters—T-shirt						
Experiment with a Chemist—T-shirt						
Chemists have Solutions—T-shirt						
Experiment with a Chemist—Baseball shirt						
	Subtotal					
MasterCard no. _____	In Calif. 6% state tax					
Interbank code _____	Postage and handling					$1.90
Expiration date _____	Foreign shipment					
VISA no. _____	**TOTAL**					
Expiration date _____						

Name _____

Address _____
(Street) (City)

_____
(State) (Zip) (Country)

Please allow 6–8 weeks for delivery

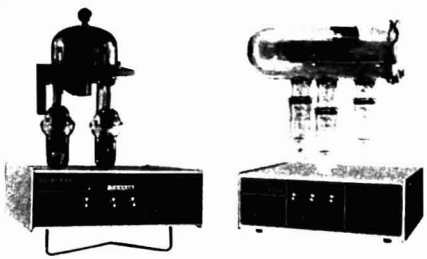
When just the weight isn't enough.

Cahn recording balances measure and record weight changes of as little as 0.0000001 gram under ambient conditions or a variety of controlled environments - including temperature, high vacuum and flowing gases.

Cahn recording balances are currently being used for such diverse analytical techniques as: thermogravimetric analysis, hydration and dehydration studies, magnetic susceptibility determinations, particle size distribution, surface characterizations and thermomagnetic analysis. Add your application to the list!

The most popular recording balances in the world!

Why? Because they use a taut band suspension (not knife edges or jeweled pivots) that results in a rugged, more reliable balance that is not susceptible to vibration and environmental contaminants. Because they are designed with gold plated weighing mechanisms which allow operation in many corrosive atmospheres. Because symmetrical beam construction provides aerodynamic balance, essential for buoyancy and flowing gas studies. Because all electronics are external to the weighing compartment allowing vacuum capabilities to 10^{-7} torr. Because absolute sample weight can be determined at any time during an experiment by the use of push-button range selection and digital thumbwheel switches. Because sample changes can be recorded as weight or as a percentage of the initial sample weight. Because they have the ability to handle heavy samples and still detect extremely small force differences.



The Cahn 1000 offers an unequaled capacity of 100 grams. An automatic range expander permits retention of data normally lost when the recorder pen goes off scale. The Cahn 2000 provides most of the benefits of the Cahn 1000 for those applications that do not require a capacity higher than 2.5 grams.

CIRCLE 38 ON READER SERVICE CARD

TGA System 113

A low cost, full capability thermogravimetric system using the Cahn 2000 Recording Balance. Operates efficiently in high vacuum, purge gas, reactive gas and ambient atmospheres. In addition, it provides the analytical advantages of derivative analysis, automatic range expansion and percent of sample weight readout at no extra cost.



CIRCLE 39 ON READER SERVICE CARD

Accessories

There's a Cahn recording balance and accessories for virtually any application related to gravimetric techniques. Cahn recording balances can be used for either the Gouy or Faraday magnetic susceptibility techniques. The high capacity to sensitivity ratios of Cahn recording balances allows gravimetric adsorption studies such as BET isotherms, heats of adsorption, surface areas and pore size distribution. Accessories for particle size distribution and surface tension studies are also available.

CIRCLE 40 ON READER SERVICE CARD

If you have any questions concerning the applicability of a Cahn recording balance or system to fit your specific needs, please contact our Applications Laboratory at (213) 926-3378.

CAHN...Where weighing a little means a lot.

Cahn Instruments, Inc. 16207 South Carmenita Road, Cerritos, CA 90701 Phone (213) 926-3378 TWX 910-583-4806

Manufacturers' Literature

Airborne Lead Determination. Application note no. AA-5 describes a procedure using an AA spectrophotometer for determination of airborne lead for industrial hygiene purposes. Sensitivity is increased by use of the CRA-90 Carbon Rod Atomizer. 4 pp. Varian **463**

Environmental Sciences Newsletter. 2nd Qtr. 1981, Vol. 7, No. 1 includes articles on analysis of nutrients in water and stream bottom sediment by the USGS, and on EPA approval of alternate test procedures. Technicon **464**

Programmable Multichannel Analyzer. Reviews the basic features, operation, system architecture, setup and display capabilities, data acquisition, and data analysis of the Model 3500 MCA and the series 3500 high-performance input modules. 24 pp. LeCroy Research **465**

Photometry System. Describes the Model 20 Photometer's features—including microprocessor flexibility and autoprotected photomultiplier—and its applications. 7 pp. Turner Designs **437**

Bio-Radiations. The May 1981 (No. 37) issue features methods of improving polyacrylamide gels, and applications of the company's affinity gels, 1405 Immunoelectrophoresis Cell, gel filtration standards, and Enzymobead radioiodination reagent. 8 pp. Bio-Rad Laboratories **438**

Ion Analysis. Model 213A Conductivity Detector, column and guard assembly, and column enclosure convert a liquid chromatograph into an ion analysis system. A cation separation column is described as well. 3 pp. Wescan Instruments Inc. **439**

Multipoint Recorder. Highlights features of Model 306, a 100-mm six-channel multipoint recorder with a "self-annotating" capability. 5 pp. Chessell Corp. **446**

HPLC Quality Control of Multivitamin Preparations. Report LC 114 describes an analysis of six water-soluble vitamins in one step, in less than 30 min, using reverse phase gradient elution. 4 pp. Varian **447**

Mass Flow Meters. Features 505/525/565 Mass Flow Meters with in-line devices, two-wire systems, portable varieties, OEM versions, and air or gas calibrators. Applications include toxicology studies, aerosol testing, and natural and bottled gas monitoring. 6 pp. Kurz Instruments Inc. **440**

Spectrophotometric Detector. Describes the LC-85 Detector and Autocontrol, which permit unattended analytical spectroscopy, wavelength change, and baseline compensation for high-speed LC as well as trace, qualitative, and preparative analysis. 8 pp. Perkin-Elmer **441**

Incubator. Options, performance data, and specifications are detailed for this low-temperature incubator with a range from −10 °C to +45 °C. 2 pp. Astell Hearson **442**

Products for Nucleic Acid and Protein Research. Describes the development of hybridization techniques using membrane-bound DNA; a nitrocellulose membrane hybridization technique; an application to recombinant DNA technology; and related products for molecular biological research. 11 pp. Schleicher & Schuell **443**

GC/MS Systems. Describes the 4500 Series GC/MS system with interchangeable CI and EI ion volumes and automated GC functions. Features advances in ion source design, GC automation, pulsed positive/negative ion mass spectrometry, and liquid chromatography interfacing. 15 pp. Finnigan MAT **444**

Instrumental Application News. Contains articles on analysis of nitrogen-bearing additives in polyolefins by chemiluminescence, and on analysis of nitrogen in agronomic research by pyro-chemiluminescence. Schedules of seminars and training sessions are also included. 7 pp. Antek Instruments, Inc. **445**

For more information on listed items, circle the appropriate numbers on one of our Readers' Service Cards

Catalogs

1981 General Products Catalog. Includes densitometers, electrophoresis equipment, spectrophotometers, column chromatography products, and educational aids. 112 pp. Helena Laboratories **453**

Instruments Catalog. Featured this year is the Mercury-Free McLeod Gage. Major groupings are controls, flow meters, flow meter valve assemblies, gages, pipetters, syringes, syringe pipets, valves, a water still, and a 32-page appendix of reprints and data. 67 pp. Gilmont Instruments, Inc. **455**

Laboratory Filtration Catalog. New products include: Water-I purifier system; disposable capsule filters such as Versacap, Acroflux cross-flow capsule, and Versaflow; new sizes of the Acro 50, 50A, and Acrodisc CR. 48 pp. Gelman Sciences Inc. **456**

Dispensing Systems. Applications, design features, operation, specifications, and available accessories are described for eight precision dispense systems. 18 pp. Tridak **459**

Reactors and Pressure Vessels. Reactor systems with internal stirrers and general purpose pressure vessels are featured. Information about proper selection, construction materials, accessories, and custom modifications also is included. 56 pp. Parr Instrument Co. **460**

1981 Nalgene Labware. An analytical filter unit and filter funnel, syringe filter, membrane filters, filter holders, filter forceps, a pressure adapter and filter cap, specialty test tube racks, and polycarbonate carboys are featured. 75 pp. Nalge Co. **461**

1981–82 BioResearch and Chromatography Products. Includes references, procedures, products, and derivatization methodologies for chromatography, a section on laboratory aids, and a bioresearch section containing updated references and products. 208 pp. Pierce Chemical Co. **462**

A* to Z

* Acetanilide to Zirconyl

(...and a catalog full of others in between)

For over 50 years we have constantly added new chemicals/products to our line. That's our commitment to the industries WE serve.

...and you can still **BUY DIRECT** from the manufacturer and to expect prompt **SERVICE**

Your most DIRECT SOURCE for the finest commercially available ANALYTICAL and FINE CHEMICALS



"Analytical Chemicals Since 1928"

GFS CHEMICALS
867 McKinley Avenue
Columbus, Ohio 43223
614/224-5343
G. FREDERICK SMITH CHEMICAL COMPANY

CIRCLE 198 ON READER SERVICE CARD

Keep That Old GC Working

GOW-MAC Repairs or Makes Replacement Cells for Most GCs Made by the Following:

Abcor, Inc.
Analytical Instrument Development, Inc.
Antek Instruments Inc.
Applied Automation, Inc.
Barber Colman Co.
Baseline Industries, Inc.
Beckman Instruments, Inc.
The Bendix Corp.
Burrell Corp.
Carlo Erba
Chemical Data Systems, Inc.
Chromalytics Corp.
Fisher Scientific Co.
The Foxboro Co.
Glowall Corp.
Hewlett-Packard Co.
Intersmat
Loenco
Micro-Tek Instrument
Mine Safety Appliances Co.
Nester/Faust Manufacturing Co.
Nuclear-Chicago
Packard Instrument Co., Inc.
Packard-Becker
Perkin-Elmer Corp.
Phase Separations Ltd.
Philips Electronic Instruments
Podbielniak, Inc.
Pye Unicam, Ltd.
Sadtler Research Laboratories
Sargent-Welch Scientific Co.
Shandon Scientific Co., Ltd.
Siemens Corp.
Tracor, Inc. (Micro-Tek)
Varian Instrument Group
Victoreen

Just remove your detector from the oven and return the cell to:

GOW-MAC Instrument Co.
Central Jersey Industrial Park South
Kearney Street, Building 26E
Bridgewater, NJ 08807

and we will clean, repair and refilament your cell to the specifications of the original maker for less than $250.

OR, we can supply new replacement cells for most of the above instruments for less than $320.

OR, if you can replace the filaments yourself, we can supply a Quad (set of 4 matched elements) of our famous general purpose WX filaments for only $125.

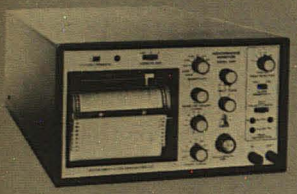
For complete details:

Telex us at 833174 (LAWMAC BRGW ansbk),
Telephone us at (201) 560-0600, or
Write us at P.O. Box 32,
Bound Brook, NJ 08805

GOW-MAC INSTRUMENT CO.

CIRCLE 92 ON READER SERVICE CARD

ISCO upgrades your HPLC



variable wavelength detector

ISCO's Model 1840 should be your first step to improve your liquid chromatograph. With continuous selection from 190-625 nm, you can choose the optimum wavelength for your separation: maximize absorbance for desired compounds, or minimize interference from solvents or impurities. The Model 1840 also offers you:

Triple lamp life. The unique optical and electronic design preserves lamps and tolerates them when they're old and noisy. And it doesn't waste them on overnight warmup.

High sensitivity. Select from ten full scale sensitivity ranges (0.002 to 2.0A), plus %T.

Fast response. 90% response normally takes less than a second.

Peak Separator™. The Model 1840 can be supplied with a built-in Peak Separator, which will operate an associated fraction collector in such a way that separate absorbing peaks are deposited in separate tubes.

Optional built-in 10 cm recorder. It's hard to beat for convenience, and it gives you ½% accuracy. Or use any external recorder.

microprocessor fraction collector

FOXY's microprocessor-controlled collection techniques save you time and expand your research. FOXY can:

1) collect only certain peaks you want.
2) reject void volumes
3) work with your HPLC autosampler.
4) mix tube sizes and volumes during a run.
5) collect from four columns at once.
6) hold containers from 3 to 500 ml.
7) save you $1,000.



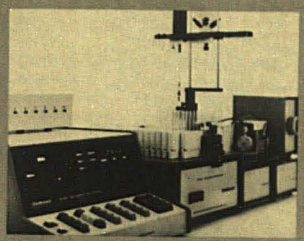
That's right. At $2,795, FOXY costs about $1,000 less than the other microprocessor fraction collectors similarly equipped—and it's smarter.

Check the reply card or send the coupon now to receive our new catalog of innovative instruments. Or phone free [800] 228-4250.

computerized sample preparation

You can completely automate your HPLC analysis, including sample preparation. A ChemResearch™ Model 1560 system is a liquid sample processing unit controlled by a microprocessor-based computer, with the ability to perform virtually any chemical operation that can be accomplished by hand.

Interactive programming with simple chemical commands allows you to use it the day it is installed, even if you have no previous



computer experience. Besides automatic injection, the Model 1560 can automatically dissolve, extract, dilute, derivatize, adjust pH, or even titrate samples before injection. It can also control all aspects of analysis, even deciding to modify and rerun separations which didn't meet your criteria.

™ISCO, Inc.



1981 catalog

ISCO
Box 5347
Lincoln, NE 68505

☐ Please send literature on ISCO and ChemResearch instruments.
☐ Please send the above and have a salesman call.

Name, Dept. _____
Institution _____
Address _____
City _____ State _____ Zip _____
Phone ( ) _____

CIRCLE 115 ON READER SERVICE CARD

Margaret A. Carroll
E. Roderick White
John E. Zarembo
Smith, Kline & French Laboratories
1500 Spring Garden St.
Philadelphia, Pa. 19101

The Analytical Approach

Edited by Jeanette G. Grasselli

Over-the-Counter Drug Analyses with HPLC

The complexity of over-the-counter (OTC) drug preparations makes the identification of their active constituents extremely difficult. Unlike the single compound ethical drug often found in prescription preparations, OTC products are frequently formulations complicated by the numbers and relative quantities of active ingredients as well as by a large variety of excipients. Excipients include antioxidants, emulsifiers, stabilizers, flavoring agents, and buffers.

The most effective analytical approach followed in this laboratory for analyzing OTC products complements high performance liquid chromatography (HPLC) with various spectrometries, specifically the mass spectrometries (electron impact, chemical ionization, field desorption, GC/MS) and IR, UV, and NMR (^{13}C, ^{1}H) spectrometries. Application of these analytical techniques permits the conclusive identifications of compounds required for compliance with safety and efficacy regulations.

The use of HPLC obviates earlier complex, time-consuming, and less specific approaches, viz, liquid–liquid extractions and colorimetric assays. The knowledge obtained in analyzing OTC preparations also serves as a basis for solving other pharmaceutical problems.

Examples of these HPLC approaches to the analyses of OTC preparations are given below. Initially, HPLC was applied to the analysis of ethical products such as antibiotics. HPLC columns used for these assays were packed with medium-efficiency 37-μm pellicular materials. The introduction of high-efficiency 5- and 10-μm packings gave the increased resolution and greater sensitivity required for stability-indicating methods. The development of ion-pairing techniques for reversed phase systems permitted the analysis of many pharmaceutical compounds that were previously difficult to analyze with an ion-suppression reversed phase system because of the pH restrictions (pH 2–8) on the columns. The current method permits the separation of active compounds from their decomposition products, precursors, contaminants, and excipients. One major advantage of the technique is the simplicity of sample preparation, which is due to the high resolving power of HPLC for complex mixtures. Extensive pretreatment is seldom needed, most samples requiring only dissolution, dilution, and injection. The methods are precise ($RSD_{1\sigma} < 1.5\%$) and accurate.

OTC Choline Salicylate Product

One OTC product that was analyzed contained choline salicylate. Choline salicylate is an aspirin substitute and is stable in aqueous solution. The HPLC method developed for the salicylate used camphorsulfonic acid in the mobile phase to completely suppress salicylate ionization.

Since both the starting materials and formulations are viscous liquids, we wanted to establish a procedure for measuring samples volumetrically. This was done by filling a "to contain" pipet to the mark with sample, allowing it to drain into a volumetric flask, and then carefully rinsing the material adhering to the wall of the pipet into the flask with mobile phase liquid. A known amount of internal standard was added, and the sample diluted to volume. To prove that this technique was valid, the precision of the volumetric measurement was compared to that obtained with weighed samples. The average values obtained for both techniques were identical with RSDs of 0.8% and 0.7%, respectively. Thus, no problem appeared to occur with the volumetric measurement.

Attempts were made to decompose choline salicylate in controlled experiments. The sample was subjected to heat, UV radiation, and complexing and oxidizing agents. The HPLC and TLC (thin layer chromatography) chromatograms showed no decomposition products. Thus, salicylate appeared to be exceptionally stable under these conditions.

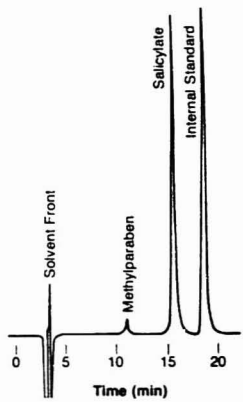


Figure 1. HPLC separation of salicylate in a choline salicylate formulation. Column, Dupont Zorbax C_8 (25-cm × 4.6-mm i.d.); AUFS, 0.04; flow rate, 1.0 mL/min; detector, 280 nm; injection, 10 μL; mobile phase (50:50) methanol: 0.025 M camphorsulfonic acid

A chromatogram of the separation is shown in Figure 1. Methyl paraben is a preservative in the formulation. Ethyl paraben is the internal standard. The purity of the salicylate peak was investigated by an absorbance ratio technique (*1*). Absorbance ratios are determined by measuring the absorbance of the peak at several wavelengths and calculating the ratios of the absorbances. These ratios are con-

0003-2700/81/A351-1111$01.00/0
© 1981 American Chemical Society

stants for pure compounds. The ratios were determined on three samples—a reference standard; a 6-month, 50 °C sample of starting material; and a 6-month, 50 °C formulation. The absorbance ratios of the samples showed no significant variations. While this experiment did not completely eliminate the possible contribution of additional components to the peak, it was strongly indicative that a single entity was present, and we felt that the method had been validated.

Samples were analyzed for several months without any problems. Then, starting material samples that had been stored for 6 months were received. A sample stored at 50 °C assayed 1.9% higher in choline salicylate than did a sample stored at 5 °C. The assay on the 5 °C sample was in agreement with the result on the original sample. If decomposition had occurred at the higher temperature, it probably would have caused low, not high, results. Absorbance ratio measurements and TLC evidenced no decomposition products that might interfere. No inorganic material was present. IR and MS data showed no significant differences. Since the samples were in solution, the possibility of water loss was considered. Karl Fischer analyses for water solved the problem. A material balance was obtained on both samples—99.8% on the 5 °C sample and 99.2% on the 50 °C sample. The change in choline salicylate assay value was compensated for by the change in water content.

OTC Allantoin Product

Another OTC product analyzed was a skin healing and protecting lotion that contained allantoin. The complexity of the matrix precluded the use of frequently applicable colorimetric and titrimetric procedures, and the literature described no appropriate HPLC methods. We therefore developed an HPLC procedure specific for allantoin that included the use of a variable wavelength UV detector set at 220 nm.

The initial investigation included testing a variety of HPLC reversed phase columns, including Waters μBondapak C_{18}, Dupont Zorbax C_8 and C_{18}, and Whatman Partisil-10 ODS-2. Allantoin, however, was not retained on any reversed phase column—even those with very heavy carbon loading. Nor was ion pairing or ion exchange HPLC applicable because allantoin was not retained by any of these columns.

Since none of these approaches was successful, the next step was to investigate bonded normal phase systems. Bonded normal phase columns tolerate water well. The fact that allantoin is very water-soluble and only sparingly soluble in methanol made these columns appear promising for separation of compounds as highly polar as allantoin. Cyano columns, one of the most common types of normal phase columns, were tried first.

Column packings having cyano functionality only did not retain allantoin. One packing, however, Whatman PSX 10/25 PAC, has some amino functionality in addition to cyano, and it retained the compound slightly. We decided to try packings having amino groups.

Both Waters μBondapak and Dupont Zorbax amino columns gave satisfactory retention and peak shape. Figure 2 is a chromatogram of the separation of an allantoin formulation on a Waters column using a water–acetonitrile (11:89) mobile phase. Many components in the formulation also absorb at 220 nm, but these are well separated from allantoin.

The multiplicity of ingredients in the formulations caused other difficulties besides separation problems. Sample preparation is vital to the success of this type of analysis. Large differences in the solubility of components formulated with allantoin presented one of the most difficult problems encountered in the HPLC analysis of these lotions. To successfully assay these preparations, the sample must be completely solubilized or separated from insoluble material by filtration, centrifugation or other means to prevent column blockage by insoluble material at the head of the column. Allantoin lotions were particularly difficult to deal with.

It was observed that certain formulations did not dissolve in the mobile phase which was the preferred diluent. Attempts to solubilize the formulations by heating in methanol were unsuccessful because of decomposition detectable by the presence of extraneous peaks in the chromatogram. Tetrahydrofuran (THF) was a good solvent for the matrix, so mixtures of THF and water were tried. A 30:70 mixture of these solvents kept allantoin in solution and dissolved most of the remaining components. While the solution was slightly cloudy, any undissolved material settled on standing, and the supernatant liquid was suitable for injection. Samples of spiked placebo were assayed to validate the method. The recoveries averaged 99.6% with an RSD of 1.1%.

An additional problem arose when a component in one of the placebo mixtures was found to elute at exactly the same retention volume as allantoin. This interference would have caused allantoin results to be 10% too high. Attempts to modify the chromatographic conditions to solve this problem—first by changing the mobile phase and then by employing a completely new system on a silica column—were not successful. Extractions from acidic, neutral, and basic solutions were also unsuccessful in removing the interference. An attempt was made to identify the source of the problem by investigating the constituents of the placebo. Germall 115, a preservative in the lotion, is a condensation product of allantoin and formaldehyde (2). To determine if this excipient was the source of the HPLC interference, a sample of Germall 115 was injected into the instrument. A small peak eluted at the retention volume of allantoin. To identify the chemical composition of the unknown peak, the placebo was injected, and the unknown peak was collected and examined by mass spectrometry.

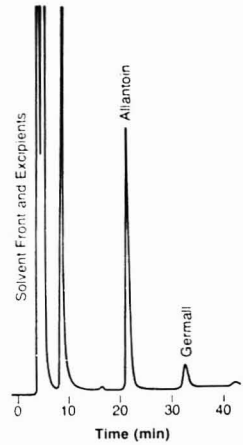


Figure 2. HPLC separation of allantoin in a lotion. Column, Waters μBondapak NH_2 (30-cm × 3.9-mm i.d.); AUFS, 0.08; flow rate, 1.0 mL/min; detector, 220 nm; injection, 25 μL; mobile phase, (11:89) water:acetonitrile

Electron impact (EI) mass spectrometry indicated that the spectrum was essentially identical to that of a reference sample of allantoin. To verify further that the peak was allantoin, a field desorption (FD) mass spectrum was obtained. Since FD is a soft ionization technique, many compounds that are easily fragmented by EI retain their molecular integrity. Field desorption mass spectrometry showed a molecular ion peak at m/e 158, which corresponds to that expected for allantoin. This particular lot of Germall 115 appeared to contain some unreacted precursor.

Many formulations had been prepared with this lot of material, and assays were required. The amount of interference in the placebo was found to



When everything fits together... Now in HPLC

Each component in our HPLC line is designed to operate independently. Or as part of a totally automated HPLC system comprised of Kontron modules.

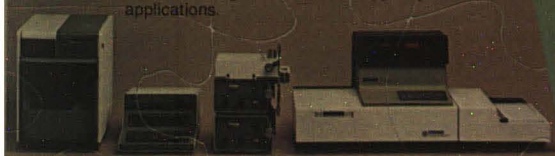
MODEL 410 HIGH PRESSURE PUMP. Fundamental for any HPLC system. Our Model 410 is an extremely dependable pump featuring electronic pulse compensation. The result? Smooth, constant flow for reproducible analysis. Even with high sensitivity detectors. Remote control of the Model 410 provides gradient and flow programming capability in increments of 0.01 ml/min.

MODEL 200 SYSTEM PROGRAMMER. A microprocessor based system controller featuring up to 980 programmable steps of memory and 100 independent files. You get maximum flexibility in gradient selection and automation of your LC analyses.

MODEL MSI 660 AUTOSAMPLER. An easy to use microprocessor based instrument featuring minimum sample wastage, no cross contamination, positive sample identification and up to 120 sample capacity. You get an extremely cost effective instrument for multiple sample analysis.

MODEL 720 LC UV/VIS SPECTROPHOTOMETER AND MODEL 23 LC SPECTROFLUOROMETER. You'll have a choice of detectors to meet a wide variety of HPLC applications. Both offer wavelength scanning for high resolution spectra of eluting peaks. These HPLC components will provide you with superior performance today. And even better performance tomorrow.

In addition to the basic system components, we offer more than 400 accessories. Including columns, fittings and valves to support your HPLC applications.



For literature, an in house demonstration, or details on our full range of UV/VIS products, call or write:

KONTRON ANALYTICAL

630 Price Ave., Redwood City, CA 94063
Phone (415) 381-1017 Toll Free (800) 227-8834

Circle 120 for literature. Circle 121 for demonstration.

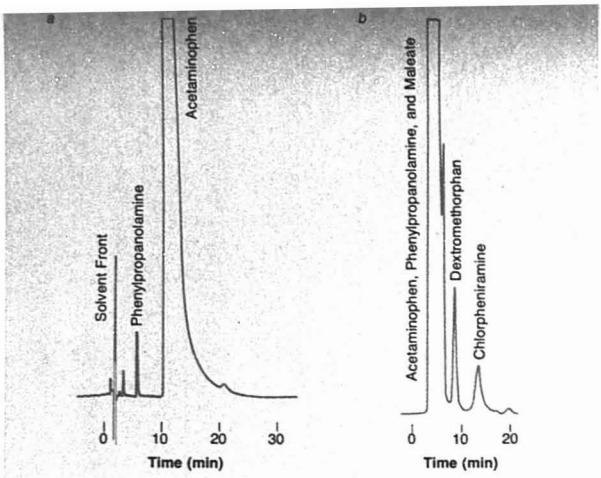


Figure 3. **(a)** HPLC separation of phenylpropanolamine hydrochloride and acetaminophen in a dissolution sample. Column, Whatman PXS-1025 ODS (25-cm × 4.6-mm i.d.); AUFS, 0.02; flow rate, 1.2 mL/min; detector, 256 nm; injection, 20 μL; mobile phase, (9:91) methanol:0.01 M methanesulfonic acid. **(b)** HPLC separation of dextromethorphan hydrobromide and chlorpheniramine maleate in a dissolution sample. Column, Waters μBondapak C_{18} (30-cm × 3.9-mm i.d.); AUFS, 0.02; flow rate, 1.0 mL/min; detector, 262 nm; injection, 100 μL; mobile phase, (75:25) methanol:H_2O (0.02 M dioctylsulfosuccinate sodium salt, 0.1% phosphoric acid)

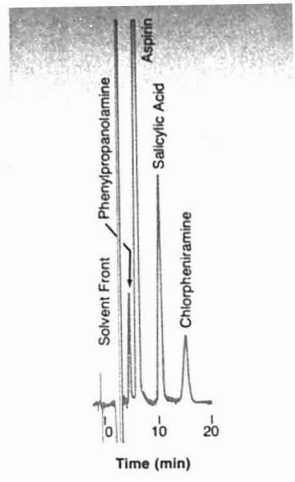


Figure 4. HPLC separation of phenylpropanolamine, aspirin, salicylic acid, and chlorpheniramine in an allergy remedy. Column, Waters μBondapak C_{18} (30-cm × 3.9-mm i.d.); AUFS, 0.04; flow rate, 1.0 mL/min; detector, 256 nm; sample, 20 μL; mobile phase (40:60) methanol:H_2O (0.0125 M camphorsulfonic acid)

correspond to the amount of allantoin expected from the theoretical content of Germall 115. The formulations were corrected by subtracting the equivalent values for allantoin calculated from the Germall concentrations from the total allantoin content of the samples. The placebo was monitored with the stability samples so that any change in allantoin content would be observed and the proper correction made for the samples.

OTC Cough–Cold and Allergy Products

To illustrate the uses of HPLC in the analysis of multicomponent products, ion-pairing reversed phase procedures used for some of these complex formulations are described. One product was a cough–cold remedy that contained phenylpropanolamine hydrochloride, acetaminophen, chlorpheniramine maleate and dextromethorphan hydrobromide. It was necessary to obtain assay and dissolution data on original and stability samples of the solid dosage forms. The extremely dilute (one capsule or tablet/900 mL) solutions of dissolution media were difficult to analyze. To define the solubility characteristics of the preparations, the dissolution medium was sampled at varying time intervals. A large number of samples of low concentration were generated. The HPLC instruments were found to have sufficient sensitivity and stability to assay these solutions successfully. The automated assay procedure permitted samples to be analyzed unattended overnight.

Because of the marked differences in polarity of the four compounds, two HPLC systems were used for the analysis of the cough–cold remedy. Figures 3a and 3b are chromatograms of a dissolution sample at t = 15 min. Depending upon the chain length of the ion-pairing reagent employed and the methanol content, it was possible to have phenylpropanolamine elute before or after acetaminophen. With a short chain reagent (such as methanesulfonic acid) and 9% methanol, phenylpropanolamine eluted before acetaminophen. This was desirable because of differences in concentration and UV response of the two compounds. Phenylpropanolamine and acetaminophen eluted at the solvent front when dioctylsulfosuccinate was used as the ion-pairing reagent in a mobile phase containing 80% methanol. In the same system, the less polar compounds, dextromethorphan and chlorpheniramine, were retained and quantitated.

Another multicomponent product, an allergy remedy, contained phenylpropanolamine hydrochloride, chlorpheniramine maleate, and aspirin. A single HPLC system with a camphorsulfonic acid mobile phase separated these compounds and salicylic acid, the decomposition product of aspirin. A chromatogram of the separation on a Waters μBondapak C_{18} column is shown in Figure 4. Aspirin hydrolyzes rapidly to salicylic acid in an aqueous system and cannot be quantitated in overnight runs. However, it can be quantitated if each sample is prepared shortly before injection. A manual UV assay for aspirin and salicylic acid was found to be more convenient than the HPLC system and required less overall operator time.

To summarize, the reliability of HPLC methods supplemented by other analytical techniques for the analysis of OTC products has been investigated. The examples illustrated in this paper show the utility and advantages of this effort. Large numbers of samples can be assayed automatically and complex mixtures separated into their individual components for qualitative and quantitative determinations. The simplicity of the technique permits its use by both chemists and trained technicians. Mass spectrometry, thin-layer chromatography, and ultraviolet and infrared spectrometries can all be used to complement the HPLC method and to aid in meeting the challenge of over-the-counter drug analysis.

References

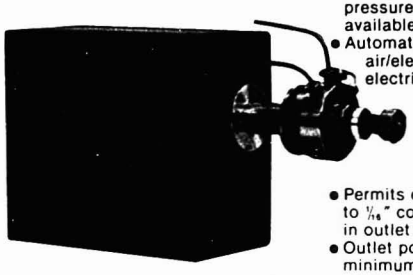
(1) Yost, R.; Stoveken, J.; MacLean, W. *J. Chromatogr.* **1977**, *134*, 73.
(2) Berke, P. A. U.S. Patent 3 248 285, 1966.

HPLC

3 MORE INNOVATIONS FROM VALCO...

DESIGNERS AND MANUFACTURERS OF THE WORLD'S MOST WIDELY USED HPLC INJECTION VALVE - OVER 15,000 SOLD.

SUBMICROLITER INJECTOR FOR HPLC

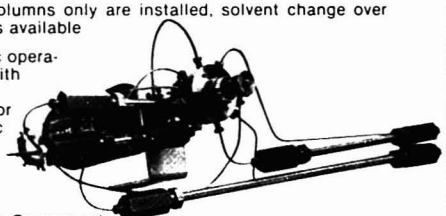


- 0.2, 0.5 or 1.0 μl volumes available
- 5000 psi rated-higher pressure ratings available
- Automatic actuation, air/electronic or electric/electronic
- Permits direct coupling to 1/16" columns with frit in outlet port
- Outlet port is .010" for minimum band-spreading
- See the MICROBORE publications by Scott and Kucera, J. CHROM., 169, 51, (1979), and Scott and Simpson, Pittsburgh Conference, March 1981, #756.

CIRCLE 220 for information on submicroliter injectors

FOUR COLUMN SELECTION VALVE

- Permits up to four columns to be mounted on one valve
- If three columns only are installed, solvent change over position is available
- Automatic operation, air with electronic interface or all electric
- 5000 psi rated
- Cited in "Hardware Components of an Automatic HPLC System", Varghese, Holmes, and Martin, Pittsburgh Conference, March 1981,#798



CIRCLE 221 for information on four column selection valves

10-PORT MULTIFUNCTIONAL INJECTION-SWITCHING VALVE



- Uses standard HPLC syringes without waste (optional)
- Combines two functions into one valve with reduction of band spreading caused by tubing and connections
  Typical examples include:
  - •sample injection followed by backflush of one column
  - •sample injection into two columns simultaneously
  - •sample injection (random access) into either of two columns
  - •sample injection followed by backflush of precolumn
  - •trace enrichment
  - •sample injection followed by backflush to vent of precolumn
  - •alternate sample injection from two streams
  - •two column selection with maintained flow on both columns
- Manual or automatic operation (either air or electric)
- Costs little more than a standard 6-port valve
- Cited in "Sample Injection and Column Switching Using a Multifunctional Valve", Harvey and Stearns, American Laboratory, March 1981 issue, and Pittsburgh Conference, March 1981, #548

CIRCLE 222 for information on 10-port valves

Opening Soon
VICI AG *(Valco Switzerland)*
in Schenkon, Switzerland.

See Valco Products at the following conferences:
LABCON '81, Chicago, Ill., booth 404
ILMAC '81, Basle, Switzerland, Hall 27, booth 651
HET INSTRUMENT, Amsterdam, Netherlands, booth R-7

VICI
Valco Instruments Co. Inc.
P.O. Box 55603 Houston, Texas 77055
(713) 688-9345
TWX 910-881-5550 Telex 79-0033

Swagelok®
WHITEY®
CAJON®
'Sno-Trik®
NUPRO

The most Respected Names in Valves & Fittings

... meeting the industry's requirements for reliability, service, availability.

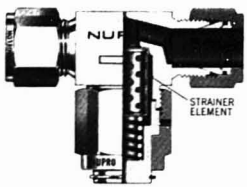
Your local distributor offers over 80 styles of **SWAGELOK** Tube Fittings, **CAJON** Pipe Fittings and Vacuum Components, **SNO-TRIK** Fittings and Valves, **NUPRO** Valves and **WHITEY** Valves to help you build complete, leak-free fluid systems. They're immediately available from stock.



SWAGELOK Tube Fittings
Leak-tight, torque-free connections for vacuum or pressurized systems in sizes to 2" and 18 mm.



High Pressure Fittings
Leak-tight connections on unthreaded heavy wall tubing at pressures to 60,000 psi.



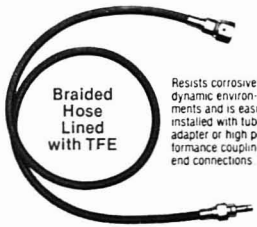
Inline Filters — remove system contaminants, protect components.



Keyed Quick-Connects — positive mechanical lock-out system prevents intermixing of different lines.



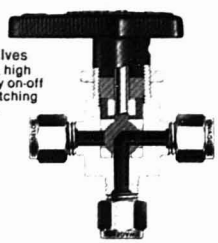
Miniature Quick-Connects — compact design with low dead-space.



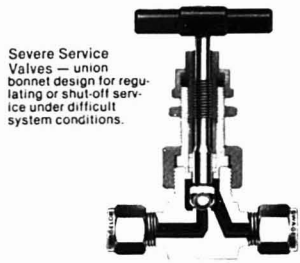
Resists corrosive and dynamic environments and is easily installed with tube adapter or high performance coupling end connections



Bellows Sealed Valves — reliable, packless shut-off and regulating service in extreme environments.



Ball Valves
1/4 turn, high capacity on-off and switching service.



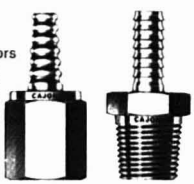
Severe Service Valves — union bonnet design for regulating or shut-off service under difficult system conditions.



Flexible Tubing
321SS tubing with rubber hose flexibility, absorbs vibration, relieves thermal expansion.



Forged Body Valves — low cost, general purpose shut-off and regulating service.



Hose Connectors
Tapered and serrated designs for positive gripping on plastic tubing and rubber hose.

These Products are subjects of patent or patents pending
© 1981 Markad Service Co / all rights reserved FRD1

CIRCLE 35 ON READER SERVICE CARD

New Laser Methodology Previewed

Chemical and Biochemical Applications of Lasers. Vol. V. C. Bradley Moore, Ed. xii + 281 pages. Academic Press, Inc., 111 Fifth Ave., New York, N.Y. 10003. 1980. $23

Reviewed by Edward H. Peipmeier, Department of Chemistry, Oregon State University, Corvallis, Ore. 97331

Volume V of this series contains high-quality introductions to the photochemistry of atoms and small molecules and to laser applications to spectroscopy. The coverage is not meant to be comprehensive; rather it is a timely preview of rapidly advancing fields. Each chapter treats the development of research in its area, typical instrumentation, and the most recent results, usually obtained from the laboratories of the authors. Prospects for future research and applications conclude each chapter. There are from 46 to 105 references at the end of each chapter, enough to direct the reader to more detailed information when desired.

Analytical chemists will find the first chapter on methods for the selective detection of single atoms particularly interesting and worthwhile. This chapter is a well-organized summary of concepts, methods, and results, some of which are not yet commonly used in analytical chemistry. For example, in addition to fluorescence and ionization methods of detecting laser–atom interactions, the method of deflecting the atomic trajectory is discussed. Experimental results are presented that show how detection limits and spectral resolution can be improved by threshold discrimination when observing multiphotoelectron pulses during certain kinds of fluorescence measurements. Atomic photoionization mechanisms are presented. Gas phase sample cell concepts considered include collimated beams and trapped atoms and ions, as well as the more common types used in chemical analysis. In addition to describing methods and current results, the effects of experimental variables are considered in some detail.

Although not always obvious from the titles of the other six chapters, there is a lot of information throughout the book for the analytical chemist interested in new laser measurement methods. For example, in the second chapter on structural studies of transient molecules, several new lasers and measurement methods are discussed, including the advantages and limitations of diode lasers, which have made very high resolution infrared measurements feasible. High resolution sub-Doppler spectrometry is also considered.

The third chapter is devoted to far-infrared laser magnetic resonance, which is a more sensitive method for detecting paramagnetic species than are optical and microwave methods. Spectral resolution is excellent, comparable to optical and microwave methods.

The last four chapters consider kinetic spectroscopy, photochemistry in matrices, laser purification of materials and photochemical separation of elements in solution. The innovative analytical chemist may glean new ideas from these chapters to help solve special analytical problems. For example, laser purification may be the method of choice to purify special materials needed for blanks and standards. As interest develops in the commercial use of selectively excited species to act as reactants and catalysts, better ways to monitor these transient species may be required.

After reading the title, the reader might expect to find both chemical and biochemical applications in this book. However, there are no explicit biochemical applications in this particular volume: The title is for the entire series of books. The lack of chapter numbers in this book, which was produced from camera-ready copy, is only a minor inconvenience. The index is useful and apparently contains all of the chemical species mentioned in the book.

Mass Spectrometry (Part B). Practical Spectroscopy Series. Vol. 3. Charles Merritt, Jr., Charles N. McEwen, Eds. xi + 401 pages. Marcel Dekker, Inc., 270 Madison Ave., New York, N.Y. 10016. 1980. $49.75

Reviewed by S. P. Markey, Department of Health & Human Services, Alcohol, Drug Abuse, and Mental Health Administration, Bethesda, Md. 20205

This is the second volume in a two-part series that is intended to provide timely "how-to" reference material on topics of interest to mass spectroscopists and specialists who want to utilize mass spectrometric techniques. In any expanding field, it is difficult to write summary reviews that are not outdated before the ink is dry on the author's contributed manuscript, much less the publisher's printing press. There are four topics reviewed by specialists in this multiauthored volume—mass spectral approaches to the study of drug metabolism (Reinhold and Costello); chemical derivatization (Vouros); two-dimensional mass spectrometry (Bente and McLafferty); and negative ion chemical ionization mass spectrometry (Haas et al.). The first topic is admirably covered in 90 pages, followed by 37 pages of references (subgrouped by compound or applied technique), all gathered prior to 1978. Because the basic principles of mass spectral studies of drug metabolism have not changed in the interim, this chapter is both relevant and useful to today's students.

The second chapter, covering derivatization techniques, was similarly prepared prior to 1978, and has been somewhat surpassed by several very comprehensive texts on the subject published in the past few years. However, the author stresses and illustrates basic principles in a clear, concise fashion (110 pages).

The third chapter is a short introduction (30 pages) to two-dimensional mass spectrometry. New instrumentation developed during the past three years has exceeded the promise of this preview, and a new, timely review would be welcome.

The fourth chapter is a compilation of 13 papers given at a workshop on negative ion chemical ionization mass spectrometry in 1977. The papers are short, somewhat redundant, outdated, and reveal no evidence of editing.

Editors and publishers of such texts need to be aware that their product is like a perishable fruit—it must arrive in the market and be consumed before it is spoiled by the passage of time.

Ion-Selective Electrodes in Analytical Chemistry. Vol. 2. Henry Freiser, Ed. xi

+ 291 pages. Plenum Press, 227 West 17th St., New York, N.Y. 10011. 1980. $35

Reviewed by Richard A. Durst, Center for Analytical Chemistry, National Bureau of Standards, Washington, D.C. 20234

As the second volume in a series that will eventually provide reviews on all aspects of ion-selective electrodes, this book covers several interesting and important areas of research and application.

The first chapter by K. Kobos on enzyme electrodes is a good general review of the subject and includes useful tabulations of enzyme–electrode reactions. While not providing much detail (e.g., Figure 2 is almost meaningless without reference to the original literature), this chapter presents most of the aspects of this subject necessary to make decisions concerning potential applications to a variety of substrate determinations. It is reasonably current, including references from 1979, such as the first report of a tissue-based enzyme electrode.

Next, a short chapter by the editor treats the subject of coated-wire electrodes. While it is somewhat disappointing that there is still no clear explanation as to how these sensors establish a stable "inner" potential at the membrane–wire interface, there is little doubt that these devices function well and provide an alternate route for sensor fabrication. I was somewhat mystified, however, by the use of δ for activity coefficient and a for the ion-size parameter (instead of the conventionally used γ and $\mathring{a}$), especially since on the same page a is used correctly as the symbol for ionic activity.

Chapter 3 on chemically sensitive field effect transistors (CHEMFET) by J. Janata and R. J. Huber is a very welcome addition to the membrane electrode literature. It provides an excellent review of the theoretical and operational basis for these devices and also includes some results obtained with these sensors. Although the CHEMFET concept was first described about a decade ago, the devices are still very much in the infancy of their development. Only time will tell whether they live up to their potential and provide us with low-cost, miniature, multiprobe sensors.

The final chapter by R. P. Buck, J. C. Thompsen, and O. R. Melroy constitutes more than one-third of this volume and provides a tabular compilation of practical papers on membrane electrodes gleaned from the previous five comprehensive biennial reviews that appeared in ANALYTICAL CHEMISTRY. Papers on theoretical topics have been largely deleted from this compilation, except where they appear in the tabulations on historical developments, books, or reviews. The introduction to this chapter provides a good historical overview and a summary of ion-selective electrode operational principles. Although the authors note that this compilation includes only "membrane" electrodes, they neglected to include a good explanation of what this term connotes. For example, they include citations to papers on coated-wire electrodes but not CHEMFETs, which in my opinion are basically analogous devices.

As with the first volume in this series, the editor achieves his stated purpose of providing up-to-date reviews on various developments in this area. While these volumes will be of consid-

SAMPLE PREPARATION FOR • XRF • AA • ICP • CHEM



CLAISSE FLUXER VI

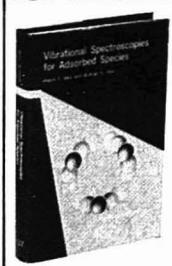
The elegant way to make borate fusions for analysis. The CLAISSE FLUXER VI transforms ores, rocks, cements, slags, etc., into transparent GLASS DISKS or clear SOLUTIONS.

Features:
- Automatic and manual;
- programmable eight-step process;
- makes six glass disks or solutions in ten minutes;
- easy servicing;
- competitive prices;
- designed, manufactured and sold by the inventor of the borate fusion disk technique.

Corporation Scientifique Claisse
1104-7 Place de Mérici,
Québec, Québec
Canada / G1S 4N8
Tél.: (418) 688-8524
Télex 051-3567

CIRCLE 34 ON READER SERVICE CARD

Vibrational Spectroscopies for Adsorbed Species



Twelve chapters provide an update of new techniques used to determine the vibrational structure of molecules adsorbed on surfaces. This volume provides a forum whereby the leading workers in the field interact and rationalize their various approaches.

CONTENTS

The first chapter presents a review of the conventional transmission IR work in surface spectroscopy. Improvements in the sensitivity of transmission IR through the development of the Fourier transform IR spectrometer and through modulation of the incident beam or ellipsometry are detailed. The theory and practice of surface wave spectroscopy are discussed as well as Raman spectroscopy and diffuse reflectance spectroscopy. Reviews of recently developed techniques that provide information about the vibrational states of adsorbed molecules — electron loss spectroscopy, inelastic electron tunneling spectroscopy, and neutron scattering — complete this comprehensive volume.

ACS Symposium Series No. 137

Alexis T. Bell, *Editor*
University of California, Berkeley

Michael L. Hair, *Editor*
Xerox Research Center of Canada

Based on a symposium sponsored by the Division of Colloid and Surface Chemistry of the American Chemical Society.

295 pages (1980) Clothbound $31.00
LC 80-21181 ISBN 0-8412-0585-X

Order from:
SIS Dept. Box 35
American Chemical Society
1155 Sixteenth St., N.W.
Washington, D.C. 20036
or CALL TOLL FREE 800-424-6747

NEW & BEST-SELLING BOOKS from WILEY-INTERSCIENCE

PATTY'S INDUSTRIAL HYGIENE AND TOXICOLOGY, 3rd Ed. Volume 2B: Toxicology

Edited by George D. Clayton and Florence E. Clayton

The third revision of Volume 2 is a completely new review of world literature to be published in three parts. Volume 2B covers industrial toxicology, occupational carcinogenesis, metals, compounds, alkaline materials, ethers and other topics.

Vol. 2A: 1420 pp. (1-16042-3) **1981** $100.00
Vol. 2B: approx. 960 pp. (1-07943-X) **August 1981**
Vol. 2C: approx. 1400 pp. (1-09258-4) **Spring 1982**

AQUATIC CHEMISTRY An Introduction Emphasizing Chemical Equilibria in Natural Waters, 2nd Ed.

Werner Stumm and James J. Morgan

Provides a theoretical basis for the chemical behavior of ocean waters, estuaries, rivers, lakes, groundwaters, and soil water systems, as well as for the processes involved in water treatment. Contrasts models with the behavior observed in real systems. Shows the response of the aquatic environment to chemical perturbation.

780 pp. (1-04831-3) **1981** $45.00 Cloth
780 pp. (1-09173-1) **1981** $27.50 Paper

NONAQUEOUS SOLUTION CHEMISTRY

Orest Popovych and Reginald P.T. Tomkins

A concise, comprehensive reference on the chemistry of solvents other than water, including extensive tabulation and graphic representation of data on nonaqueous solutions.

500 pp. (1-02673-5) **1981** $52.50

ROCK AND MINERAL ANALYSIS, 2nd Ed.

Edited by Wesley M. Johnson and John A. Maxwell
Volume 27 in Chemical Analysis: A Series of Monographs on Analytical Chemistry and Its Applications
Series Editors: P.J. Elving & J.D. Winefordner; Editor Emeritus: I.M. Kolthoff

An updated, completely revised guide to the determination of major, minor, and trace elements in rocks and minerals—from the selection of the sample to the reporting of the results of the analysis. Includes new advances in sampling theory and expanded discussions of standard reference materials and sample decomposition techniques.

approx. 584 pp. (1-02743-X) **September 1981** $40.00 (tent.)

QUALITY CONTROL IN ANALYTICAL CHEMISTRY

G. Kateman and F.W. Pijpers

Techniques for improving the quality of analytical methods, sampling and data handling, along with a discussion of how the organization of the chemical laboratory influences the quality of chemical analysis.

276 pp. (1-46020-6) **1981** $40.00

MAINTAINING AND TROUBLESHOOTING HPLC SYSTEMS: A User's Guide

Dennis J. Runser

Shows users of high performance liquid chromatography how to maintain the system in operating condition, what to look for and how to prevent problems in every facet of the system, and what can be done before calling a service representative.

163 pp. (1-06479-3) **1981** $27.50

FLOW INJECTION ANALYSIS

Jaromir Ruzicka and Elo H. Hansen

Explains the construction and modification of an FIA apparatus. Shows how to automate analytical chemical procedures that employ standard detection methods. 207 pp. (1-08192-2) **1981** $32.50

CIRCLE 229 ON READER SERVICE CARD

CHEMICAL APPLICATIONS OF RAMAN SPECTROSCOPY

Jeanette G. Grasselli, Marcia K. Snavely, and Bernard Bulkin

The first full-scale discussion of virtually every application of modern Raman spectroscopy to chemistry. Gives practicing Raman spectroscopists hands-on guidance in dealing with new areas and enables chemists to determine whether to use Raman spectroscopy to solve a specific problem.

approx. 208 pp. (1-08541-3) **August 1981** $28.00 (tent.)

AFFINITY CHROMATOGRAPHY

William H. Scouten

An introduction to both theory and practice of affinity chromatography that includes descriptions of systems for purifying a wide variety of enzymes, nucleic acids, membranes, virus, glycoproteins, and whole cells.

348 pp. (1-02649-2) **1981** $42.50

PHOTOMETRIC AND FLUOROMETRIC METHODS OF ANALYSIS Nonmetals

Foster D. Snell

Summarizes the methods for determination of the nonmetals, citing procedures and subject references. Each chapter is a quasi-monograph on determination of one nonmetal, including significant forms.

818 pp. (1-81023-1) **1981** $80.00

SEPARATIONS BY CENTRIFUGAL PHENOMENA

Hsien-Wen Hsu
Volume 16 in the Techniques of Chemistry Series
Series Editors: Arnold Weissberger and Edmond S. Perry

Presents all of the important methodology and theory for the various kinds of centrifugation, using the framework of transport phenomena. Arranges topics in order of increasing phase densities: gas, liquid, and solid phases.

approx. 480 pp. (1-05564-6) **October 1981** $49.50 (tent.)

THE THEORY OF VIBRATIONAL SPECTROSCOPY AND ITS APPLICATION TO POLYMERIC MATERIALS

Paul C. Painter and J.L. Koenig

Covers the fundamentals of infrared and Raman spectroscopy and their applications to polymer science and technology. Emphasizes computer techniques to minimize mathematical difficulty.

approx. 560 pp. (1-09346-7) **November 1981** $45.00 (tent.)

REVERSED-PHASE HIGH-PERFORMANCE LIQUID CHROMATOGRAPHY: Theory, Practice and Biomedical Applications

Ante M. Krstulovic and Phyllis R. Brown

A comprehensive, problem-solving approach to reversed-phase high-performance liquid chromatography covering the theoretical aspects and practical information needed in diverse areas of research. Also reviews RPLC applications in the biomedical/biochemical field.

approx. 272 pp. (1-05369-4) **October 1981** $22.50 (tent.)

TREATISE ON ANALYTICAL CHEMISTRY, Vol. 5, 2nd Ed., Part 1: Theory and Practice

Edited by Philip J. Elving; Associate Editor: Eli Grushka; Editor Emeritus: I.M. Kolthoff

CONTENTS/Vol. 5: Decomposition and Dissolution of Samples: Inorganic. Decomposition and Dissolution of Samples: Organic. Principles of Chemical Separations. Mechanical Methods. Membrane Processes. Preparation of Anisotropic Ultrafiltration Membranes. Biochemical and Biomedical Separations Using Liquid Membranes. Crystallization and Precipitation. Adsorptive Bubble Separation Methods. Distillation. Liquid-Liquid Extraction. Countercurrent Distribution.

approx. 800 pp. (1-01837-6) **November 1981** $60.00 (tent.)

DIRECT CHARACTERIZATION OF FINE PARTICLES

Brian H. Kaye

Covers direct examination and assessment of fine particles. Discusses advances in sieving technology, sedimentation methods, automatic image analysis using computers, and methods for shape determination.

approx. 672 pp. (1-46150-4) **August 1981** In Press

Order through your bookstore or write to Nat Bodian, Dept. 2-1161
TOLL-FREE NUMBER FOR BOOK ORDERS only: 800-526-5368
In New Jersey, call collect (201) 797-7809. Order Code # 1161

WILEY-INTERSCIENCE
a division of John Wiley & Sons, Inc.
605 Third Avenue, New York, N.Y. 10158
In Canada: 22 Worcester Road, Rexdale, Ontario
Prices subject to change without notice. 092 2-1161

erable use to practitioners in this field, they will be of much more limited interest to someone merely wanting to learn about the general topic of ion-selective electrodes. For these people, one of several recently published monographs on the subject would probably be more appropriate. But for those analytical chemists and clinical scientists who want to keep abreast of the state of the art, I certainly recommend this series.

Books Received

Advances in Organometallic Chemistry. Vol. 19. F.G.A. Stone, Robert West, Eds. ix + 318 pages. Academic Press, Inc., 111 Fifth Ave., New York, N.Y. 10003. 1981. $42

Supplement to Analytical Toxicology Methods Manual with Cumulative Index. H.M. Stahr, Ed. ix + 311 pages. Iowa State University Press, South State Ave., 112 C Press Office, Ames, Iowa 50010. 1980. $18 (paper)

Ultrafiltration Membranes and Applications. Anthony R. Cooper, Ed. xiv + 707 pages. Plenum Press, 227 West 17th St., New York, N.Y. 10011. 1980. $75

Progress in Macrocyclic Chemistry. Vol. 2. Reed M. Izatt, James J. Christensen, Eds. xi + 347 pages. Wiley Interscience, 605 Third Ave., New York, N.Y. 10158. 1981. $50

Analytical Isotachophoresis. Proceedings of the 2nd International Symposium on Isotachophoresis, Eindhoven, Sept. 9–11, 1980. F. M. Everaerts, F. E. P. Mikkers, Th.P.E.M. Verheggen. Eds., xi + 234 pages. Elsevier/North-Holland, Inc., 52 Vanderbilt Ave., New York, N.Y. 10017. 1981. $58.50

Mass Spectrometry of Priority Pollutants. Brian S. Middleditch, Stephen R. Missler, Harry B. Hines, xii + 308 pages. Plenum Press, 227 West 17th St., New York, N.Y. 10011. 1981. $29.50

Computer Networks in the Chemical Laboratory. George C. Levy, Dan Terpstra, Eds. xv + 221 pages. Interscience, 605 Third Ave., New York, N.Y. 10158. 1981. $27.50

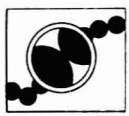
Introduction to Pascal for Scientists. James W. Cooper. xv + 260 pages. Wiley Interscience, 605 Third Ave., New York, N.Y. 10158. 1981. $19.95

Trace Metals in the Environment. Vol. 6. Cobalt. Ivan C. Smith, Bonnie L. Carson, Eds. xxii + 1202 pages. Ann Arbor Science Publishers, Inc., 230 Collingwood, P.O. Box 1425, Ann Arbor, Mich. 48106. 1981. $49.50

Maintaining and Troubleshooting HPLC Systems: A User's Guide. Dennis J. Runser. xiii + 163 pages. Wiley Interscience, 605 Third Ave., New York, N.Y. 10158. 1981. $27.50

Fast Neutron Activation Analysis. Elemental Data Base. John McKlveen. 306 pages. Ann Arbor Science Publishers, Inc., 230 Collingwood, P.O. Box 1425, Ann Arbor, Mich. 48106. 1981. $39.95

Cancer-Causing Chemicals. N. Irving Sax. ix + 466 pages. Van Nostrand Reinhold Co., 135 West 50th St., New York, N.Y. 10020. 1981. $39.95



Advances in Chemistry Series No. 174

Jack L. Koenig, *Editor*
Case Western Reserve University

Based on a symposium cosponsored by the Divisions of Polymer Chemistry and Analytical Chemistry of the American Chemical Society.

Probing Polymer Structures

Polymer chemists . . . this timely, informative volume will be of substantial value in bringing you up to date on the latest available instrumental techniques and sophisticated technology that can be used to detect, identify, and characterize commercial polymeric structures.

The book combines the theoretical and experimental bases of the various techniques and the recent applications of these methods to develop a fundamental understanding of polymer performance, behavior, and microstructural variables in commercial systems.

CONTENTS

Noise Phenomena Associated with Thermal Transitions • Acoustic Emission under Tensile Load • Nanotensiometer • Measurement of Nonlinear Viscoelastic Properties • Stress Mass Spectrometry • Characterization of Organic Polymers Via Pyrolysis-Infrared • Inelastic Electron Tunneling Spectroscopy • FTIR Spectroscopic Studies • Brillouin Scattering • Quasielastic Laser Light Scattering • Multipass Fabry-Perot Spectroscopy • Ion Recombination Luminescence • SBS Block Copolymers and Polyethylene

277 pages (1979) Clothbound $33.00
LC 79-10008 ISBN 0-8412-0406-3

Order from:
SIS/American Chemical Society
1155 16th St., N.W./Wash., D.C. 20036



Advances in Chemistry Series No. 172

Terence H. Risby, *Editor*
Pennsylvania State University

A symposium sponsored by the Division of Analytical Chemistry of the American Chemical Society.

Ultratrace Metal Analysis in Biological Sciences and Environment

With the improved sensitivities of current analytical techniques (inductively coupled plasma, atomic absorption and atomic emission spectrometry, and neutron activation), knowledge of the roles of metals in biochemical processes and in the environment are continually expanding.

This new book contains significant research reports on the collaborated efforts of biochemists, environmental chemists, and analytical chemists who are studying metal concentrations in biological organisms and in air, water, and soil.

CONTENTS

Trace Element Analysis in Nutrition • Multielement Analysis with RF-ICP • Health Implications • Molybdenum in Biological Materials • Analysis of Particulate Matter for Metals • Airborne Metallic Elements • Nickel-Induced Transformation in Tissue Culture • Trace Elements in Urine • Zinc in Biochemical Processes • Cadmium, Lead, Copper, and Iron in Sea Water Derived Samples • Sources of Metals in the Atmosphere • *Bacillus subtilis* Strain 168 • Zinc in Humans • Serum Copper and Age

Order from:
SIS/American Chemical Society
1155 16th St., N.W.
Wash., D.C. 20036

263 pages (1979) Clothbound $36.50
LC 78-31903 ISBN 0-8412-0416-0

The new SCHOTT-GERÄTE automatic titrators offer you ease of operation and maximum precision in titration and dosing.



The piston burette is supplied with interchangeable attachments with cylinders of 1, 5, 10, 20 and 50 ml. The display is coded automatically for each cylinder enabling correct decimal place readings.

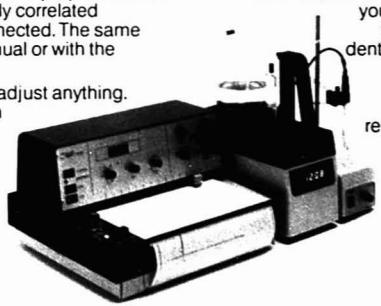
The piston burette is designed for maximum precision under severest laboratory conditions.

The operation of SCHOTT-GERÄTE titrators is so easy and safe that you can concentrate wholly on your analysis.

Whether titrating with the manual titration controller, the end-point titration unit, or the all-purpose titration recorder, all functions are clearly correlated the moment the system is connected. The same applies to dosing whether manual or with the practical dosing programmer.

You don't have to change or readjust anything. You always operate the system from one position only. The operating conditions are indicated – even ommissions.

And SCHOTT-GERÄTE offers you the precision which no other system can at this time, and over a range of volumes up to 50.00 ml.



You will already see how easy it is to work with the SCHOTT-GERÄTE automatic titration systems the moment you fix the interchangeable units of the piston burette.

However, the titration system offers you more than that: you can follow the actual value during the whole process; you have two independent nominal values on the end-point titrating unit. Titration consumption can be recorded by a printer, and the end-point titrating unit can be controlled remotely or by your computer. Automatic paper re-wind on the titration recorder allows easy comparison of several titrations.

SCHOTT-GERÄTE GMBH
Postfach 1130, D–6238 Hofheim a. Ts.
Telefon (06192) 5030 and 8081
Telex 410471 sgh d (West-Germany)

SGH SCHOTT GERÄTE

France: SCHOTT FRANCE SARL., F-89140 Pont s/Yonne,
United Kingdom: SCHOTT GLASS LTD., GB-Stafford ST 16 3 EL,
Netherlands: SCHOTT NEDERLAND B.V., NL-4000 AD Tiel,
Spain: SCHOTT IBERICA S.A., E-Barcelona 13. Sales offices in: Austria, Belgium, Finland, Italy, Portugal, Sweden, Switzerland

sgh 362e

CIRCLE 190 ON READER SERVICE CARD

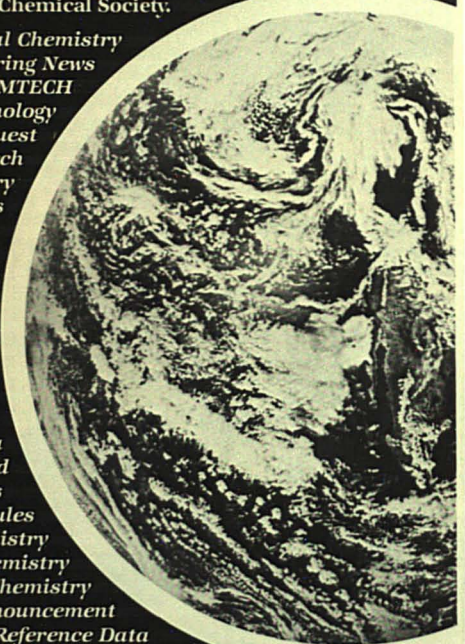
11208

What in the world isn't chemical

—and how do you keep up with it all?

You keep current with developments by subscribing to the timely, authoritative, comprehensive journals published by the American Chemical Society.

Analytical Chemistry
Chemical & Engineering News
CHEMTECH
Environmental Science and Technology
SciQuest
Accounts of Chemical Research
Biochemistry
Chemical Reviews
Industrial & Engineering Chemistry —Process Design and Development
Industrial & Engineering Chemistry —Product R&D
Industrial and Engineering Chemistry —Fundamentals
Inorganic Chemistry
Journal of Agricultural & Food Chemistry
Journal of the American Chemical Society
Journal of Chemical & Engineering Data
Journal of Chemical Information and Computer Sciences
Macromolecules
Journal of Medicinal Chemistry
The Journal of Organic Chemistry
The Journal of Physical Chemistry
ACS Single Article Announcement
Journal of Physical and Chemical Reference Data



TOLL FREE: U.S. New Orders Only (800) 424-6747
Cable Address: JIECHEM — Telex: 440159 ACSP UI or 892582 ACSPUBS

AMERICAN CHEMICAL SOCIETY PUBLICATIONS
1155 Sixteenth Street, N.W., Washington, D.C. 20036 U.S.A.

1120C

Would you like to reduce your sample wastage?



The answer: MSI 660 – Automatic sample injector

Reproducible – no cross-contamination
Easy to use
No contamination
60 samples (30 or 120 as option)
Positive sample identification
System control using modern technology

KONTRON LTD.
Analytic International
Bernerstrasse Süd 169
CH-8048 Zurich, Switzerland

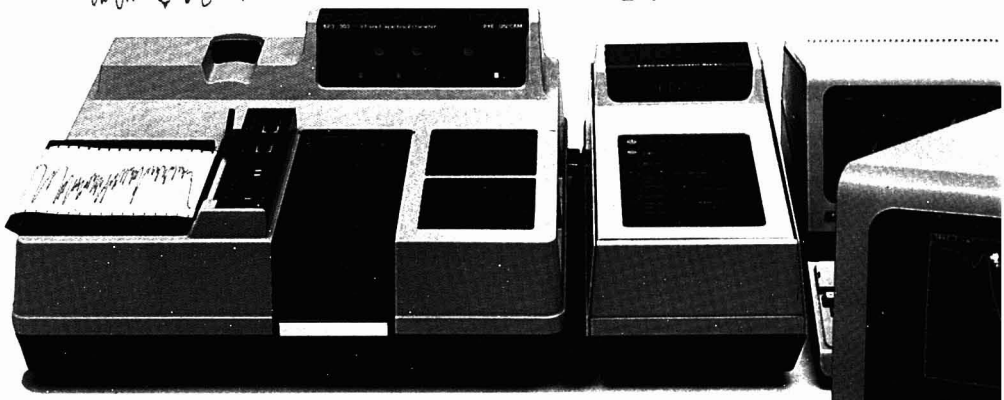
Australia (Sydney)	(02) 9383433	France (Vélizy)	(3) 9469722	Netherlands (Maarssen)	(03465) 60894
Austria (Vienna)	(0222) 945646	Germany (Munich)	(08165)771	Norway (Oslo)	(02) 170390
Belgium (Brussels)	(02) 3444900	Great Britain (St. Albans)	(0727) 66222	Spain (Madrid)	(01) 7348413
Canada (Mississauga)	(416) 6781151	Italy (Milan)	(02) 50721	Sweden (Taeby)	(08) 7567330
Denmark (Ballerup)	(02) 651666	Japan (Tokyo)	(03214) 5371	Switzerland (Zurich)	(01) 62 92 62

U.S.A.: Kontron Electronics Inc., 630 Price Avenue, Redwood City/California 94063, (415) 3611012

CIRCLE 124 ON READER SERVICE CARD

Good news for every spectroscopist, especially thos

Just for you. IR syste more of your ability.



You know Pye Unicam as the maker of *the* low-cost ratio recording IR spectrophotometers.

The SP3 Series. Unbeatable at their price for accuracy, flexibility, simplicity.

Now, Pye Unicam are leading once more, by matching the SP3s with a remarkable data control console, the SP3-080 – a new concept in data systems. Very advanced, easier to use than any other.

You speak to it in English. No codes, no routines. You want it to scan – you press the SCAN button. There's no need to be a typist, or a programmer.

Yet this amazingly powerful instrument can store up to 48 spectra on one cassette. Display the spectral results as they are obtained. Take any spectrum area you select and enlarge it to fill the screen – automatically recalibrating the data in the process.

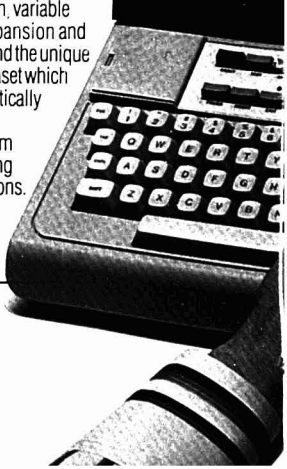
The display will show up three spectra at one time, change from transmittance to absorbance or memorise a display, all at a single keystroke.

The addition of the SP3-080 to the Pye Unicam IR range opens up these superb system possibilities:

SP3-100 spectrophotometer. Like the others it's a ratio recording instrument – in other words, you get exceptional % T linearity and constant response down to 0% T.

Other features include a one-minute high-quality survey scan and a data processor option. All for a "routine" instrument price.

The SP3-200 and 300 offer further sophisticated facilities, including a high resolution slit program, variable %T expansion and offset and the unique Spectraset which automatically selects optimum scanning conditions.



PHILIPS

who aren't programmers or typists.

ms that make

In addition, the SP3-300 has a second grating, which extends its excellent performance from the standard 4000-600 cm^{-1} to 200 cm^{-1}.

Data processor systems are available in three options ranging from conversion of transmittance to absorbance or concentration units through to a microprocessor system for instrument control by teletype, calculator, computer – or the SP3-080 data control console.

With that you can drive two SP3s or one and a printer – completely automatically. Add the SP3-040 automatic sampler and you've got total automation, overnight if you want it.

Also available from Pye Unicam: the SP2000 infrared spectrophotometer which offers considerable flexibility and performance suited to routine or research work.

The full Pye Unicam IR story is contained in a new brochure, available now by circling **reader inquiry number 80**

Like the instrumentation, it's been produced with spectroscopists in mind. And let's face it, who knows more about spectroscopy than Pye Unicam?



New liquid chromatography products.

Pye Unicam's considerable capability in liquid chromatography has been extended further by two new detectors – one electro-chemical, the other a general purpose refractive index detector – which join its world-renowned variable wavelength UV model.



The company can provide isocratic or gradient elution systems, a range of computing integrators and a full columns and accessories service.

Reader inquiry number 81

Big UV scanning range.

There are no fewer than six options in Pye Unicam's SP8 double beam scanning UV/visible spectrophotometer Series.

They all have master holographic gratings which result in exceptionally low stray light levels. The choice of instruments is backed up by a wide range of accessories and attachments for associated techniques.

Reader inquiry number 82

	Inquiry No.
IR spectrophotometry systems	**80**
Liquid chromatography systems	**81**
UV/vis spectrophotometers	**82**

Main Distributors

Australia Philips Industries SIED Ltd. 25-27 Paul Street, North Ryde, NSW. Tel 888 8222 **Belgium** M B L E. SA. 80 Rue des Deux Gares, Brussels 7. Tel. 523000 **Canada** Canadian Laboratory Supplies Ltd. 80 Jutland Road, Toronto, Ontario M8Z 2H4. Tel 416 252 5151 **France** SA Philips Industrielle et Comerciale, 105 Rue de Paris, 93002 Bobigny. Tel. Paris 830 1111 **Holland** Philips Nederland BV. Boschdijk 525, Eindhoven. Tel 788211 **Ireland** P. J. Brennan & Co. Ltd. Unit 61, Shillorgan Industrial Estate, Sandyford, Co. Dublin. Tel 952501 **Italy** Philips SpA. Viale Elvezia 2, 20052 Monza. Tel. 361441 **India** Preco Electronics & Electricals Ltd., Shivsagar Estate, Block A Dr. Annie Besant Road, Worli, Bombay 400 018. Tel 391431 **Japan** Nihon Philips Corp., Shuwa Shinagawa Bldg. 7th Floor, 26-33, Takanawa 3-Chome, Minato-Ku, Tokyo 108. Tel. 448 5611 **New Zealand** Philips Electrical Industries of NZ Ltd., P.O. Box 2097, 181 Wakefield Street, Wellington. Tel. 859-859. **Portugal** Philips Portuguesa SARL, Av. Eng. Duarte Pacheco 6, Lisbon 1. Tel. 683121 **Spain** Philips Iberica SAE, Martinez Villergas 2, Madrid 27. Tel. 404 22 00. **Scandinavia** Svenska AB Philips, S-115 84 Stockholm. Tel. 63500000 **Switzerland** Philips AG, Allmendstrasse 140, Postfach, CH-8027 Zurich. Tel. 43211 **South Africa** South African Philips (Pty) Ltd., P.O. Box 7703, Johannesburg 2000. Tel. 614041. **West Germany** Philips GmbH, 35 Kassel – B. Miramstr. 87. Tel. 0561 50111

Pye Unicam Ltd
York Street, Cambridge, England CB1 2PX.
Tel: (0223) 358866 Telex 817331

Pye Unicam

A SCIENTIFIC INSTRUMENT COMPANY OF PHILIPS

SP8–500: complete UV/Visible spectrum



The latest addition to the SP8 Series, the SP8–500 spectrophotometer, is truly the master of all it surveys. It has both the versatility and performance to tackle almost any UV/Visible assay, yet its introduction signals a new era in ease of operation and convenience.

The versatility of the SP8–500 is illustrated by its array of standard features which include:

PHILIPS

mastery of the



- 190 – 900nm range
- integration
- autoconcentration
- baseline correction
- overlaid spectra
- cycle timer
- 10 wavelength selection
- rate calculation
- fault diagnostics
- RS 232C output

Not only have Pye Unicam packaged all this at a price that will be hard to resist, but we have added an extra that will send competitors scurrying to their drawing boards:–

Synchroscan + is an innovation that eliminates the need to compromise scan speed for either throughput or resolution. *Synchroscan +* constantly adjusts the scan speed to zip through flat areas of spectrum but slows so peaks are not cropped or shifted. *Synchroscan +* aligns the chart and monochromator for spot-on calibration.

Don't try it unless you're prepared to be hooked!

The SP8–500 joins the comprehensive Pye Unicam UV/Visible range with its SP6, SP7 and SP8 families catering for all applications and every budget.

The four SP6 models with choice of Visible or UV/Visible range and digital or analogue display have proved themselves the perfect single beam work-horses in thousands of labs.

Another newcomer is the SP7–500 spectrophotometer which is just the job for both routine colorimetric and scanning assays with its built-in printer and XY recorder.



SP7-500 spectrophotometer

The SP8 Series now stretches from the ultra-simple operation of the low cost SP8–300 and SP8–400, through the mastery of the SP8–500 to the research performance SP8–200 and double monochromator SP8–250.

Few can match the breadth of the Pye Unicam UV/Visible range. None will match its excellence!

Reader inquiry no 78

New meters expand electrochemistry range



PW 9509 conductivity meter

Two new conductivity meters have just been announced by Philips.

The PW 9509 will measure accurately all electrolytic conductivities you are ever likely to meet in any application. The instrument automatically adjusts itself to the range being measured and displays the answer as 4 digits with the correct units. Where contamination or polarisation is a problem, 4-point measurement can be used.

Another new conductivity meter is the PW 9506, which has a 3½ digit LED display. Philips electrochemistry know-how is also reflected in a range of versatile pH meters.

And for ion-selective analysis the PW 9416 Ion-Selective Analyser takes full advantage of microprocessor technology giving the choice of 8 measurement and 4 calibration methods; step by step introduction on the VDU to carry them out and automatic calculation and display of the answer, with printout.

Reader inquiry no 79

Circle the appropriate inquiry number for further information about Philips and Pye Unicam products.

	Inquiry No.
UV/visible spectrophotometers	**78**
Electrochemistry	**79**
Infrared spectrophotometers	**80**
Liquid chromatography systems	**81**
AA spectrophotometers	**83**
Gas chromatography systems	**84**

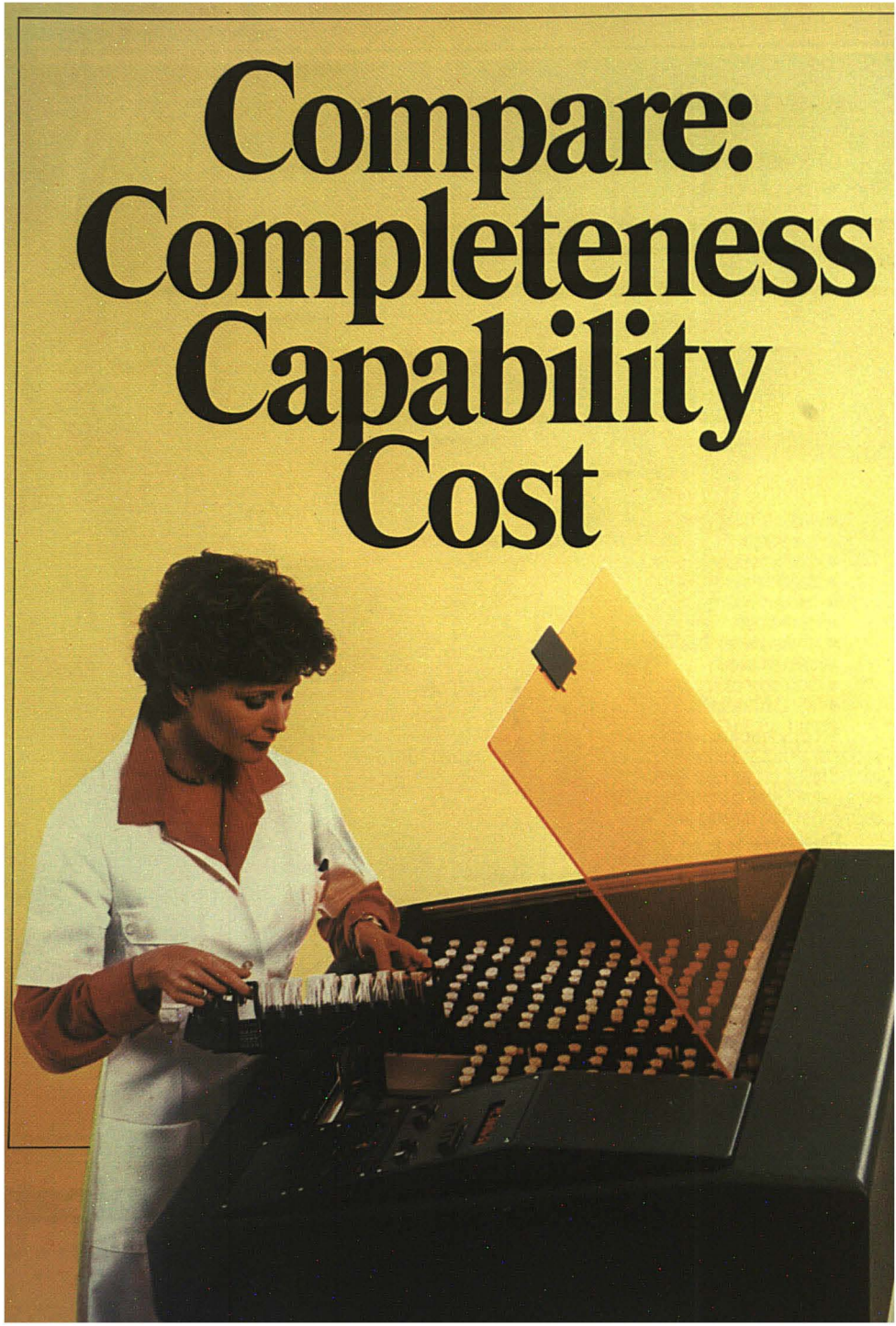
For the address and telephone no. of your Pye Unicam agent see the other Pye Unicam advertisement in this issue.

Pye Unicam Ltd
York Street, Cambridge, England CB1 2PX
Tel (0223) 358866 Telex 817331

Pye Unicam

A SCIENTIFIC INSTRUMENT COMPANY OF PHILIPS

Compare: Completeness Capability Cost



and you'll find the Philips range of Automatic Gamma Counters are unbeatable

Completeness

Philips Automatic Gamma Counters, the most complete on the market. Unlike other manufacturers, Philips include in their standard instruments all those features which normally cost extra – digital display, built-in microcomputer with 15 measuring programs, automatic gain calibration, spectrum scan and plot, multi-user facility, etc.

Complete suitability for your application. Available as a general purpose or dedicated RIA instrument, with a choice of detector sizes, shielding and with a sample capacity of 310, 620 or 480 vials.

Philips also offer completeness of another type. Complete service, around the world. Complete technical and aftersales back-up. And, of course, a complete guarantee!

Capability

Combining sophisticated analytical capability with reliable, easy operation. Accurate and consistent results with high sample through-put and multi-user operation. For demanding life-science research or strenuous routine RIA, Philips Gamma Counters meet every requirement.

Philips Gamma Counters use individually programmable sample-trays, whereby sample identification and selected measuring program are entered on the sample tray. This gives positive sample identification and allows multi-user operation. In fact, the Philips tray-loading and sample-changing system is so effective that it has been copied by many other manufacturers.

Up to 15 different measuring programs can be stored in the built-in micro-computer, any of which can be addressed by any individual sample tray.

Each program includes parameters, such as: isotope window settings, replicates, background to be subtracted, low count reject, normalisation factors, preset time, preset count, repeat count, output mode, etc.

Each of these programs can perform a special function, such as: RIA counting for single and dual labelled samples, with % bound calculations (via bound or free fractions), or general purpose gamma counting functions with DPM and % reference calculations.

To further extend the capability of Philips Gamma Counters an optional low-cost calculator is available, permitting an extensive range of calculations, e.g. RIA curve plots, concentration calculations for single and dual labelled samples (via bound or free fractions), comparison between entered and calculated concentrations, replicate averaging with % coefficient of variation, curve optimisation in area of interest, automatic elimination of faulty standards. Giving complete calculating capability for each of the 15 programs.

Cost

Despite their advanced performance and capability, Philips Gamma Counters are realistically priced. In fact, the cost of the standard Philips Gamma Counter is lower than the list price of any comparable instrument. And then, consider the cost of 'optional extras' which are needed to make other instruments remotely comparable.

Philips also helps keep operating costs down. By guaranteeing the availability of spares and service for 10 years. By having local service immediately available. And by providing the sort of back-up you would expect from a company of Philips' reputation.

All in all Philips Gamma Counters are unbeatable. For completeness. For capability. For cost. So send in the coupon and get the full details. It could save you a lot of time and money.

Coupon

Please send me full details on the unbeatable Philips Gamma Counters.

Name

Position

Addres

Telephone

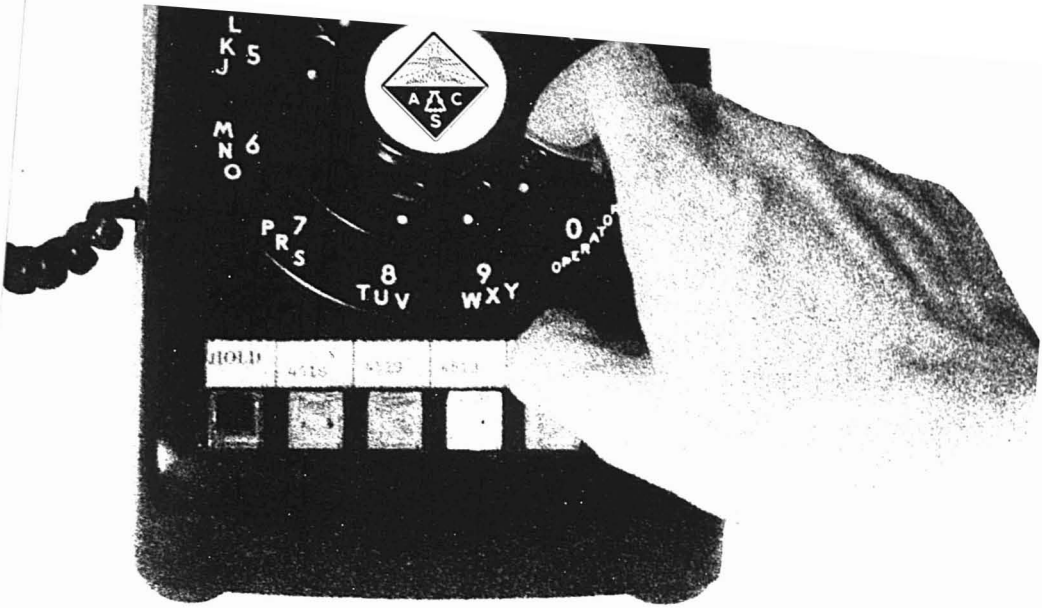
Company

Send coupon to: Nuclear Analysis Manager, Philips Industries, S&I Division, Lelyweg 1, 7602 EA Almelo, The Netherlands. Telephone: 05490-18291, Telex 36591

PHILIPS

PHILIPS

CIRCLE 176 ON READER SERVICE CARD



DIAL TOLL FREE
(1) 800-424-6747

From anywhere in the continental United States
D.C. Area Call 202-872-8065

TO ORDER AMERICAN CHEMICAL SOCIETY PRIMARY PUBLICATIONS

master charge

Call ACS Sales Office
Books and Journals Division
Kenneth Phillips, Sales Manager

VISA

MICROFILM, MICROFICHE, and PRINTED EDITIONS

Analytical Chemistry
Chemical & Engineering News
CHEMTECH
Environmental Science and Technology
SciQuest
Accounts of Chemical Research
Biochemistry
Chemical Reviews
I&EC Process Design and Development
I&EC Product Research and Development
I&EC Fundamentals
Inorganic Chemistry
Journal of Agricultural and Food Chemistry
Journal of the American Chemical Society
Journal of Chemical and Engineering Data
Journal of Chemical Information and Computer Sciences
Macromolecules
Journal of Medicinal Chemistry
The Journal of Organic Chemistry
The Journal of Physical Chemistry

BOOKS and TAPE RECORDINGS

Advances in Chemistry Series
ACS Symposium Series
ACS Monograph Series
Data Reference Books
Other Technical Books
The Chemical Society's Specialist Periodical Reports

Cassette Tapes
Science Symposia Series
Lab Professionals Series

Office Hours are 8:30 A.M. to 5:00 P.M. Eastern Time
After 5:00 P.M., automatic answering and recording service



DURAN®. The best technician is only as good as his tools.

SCHOTT

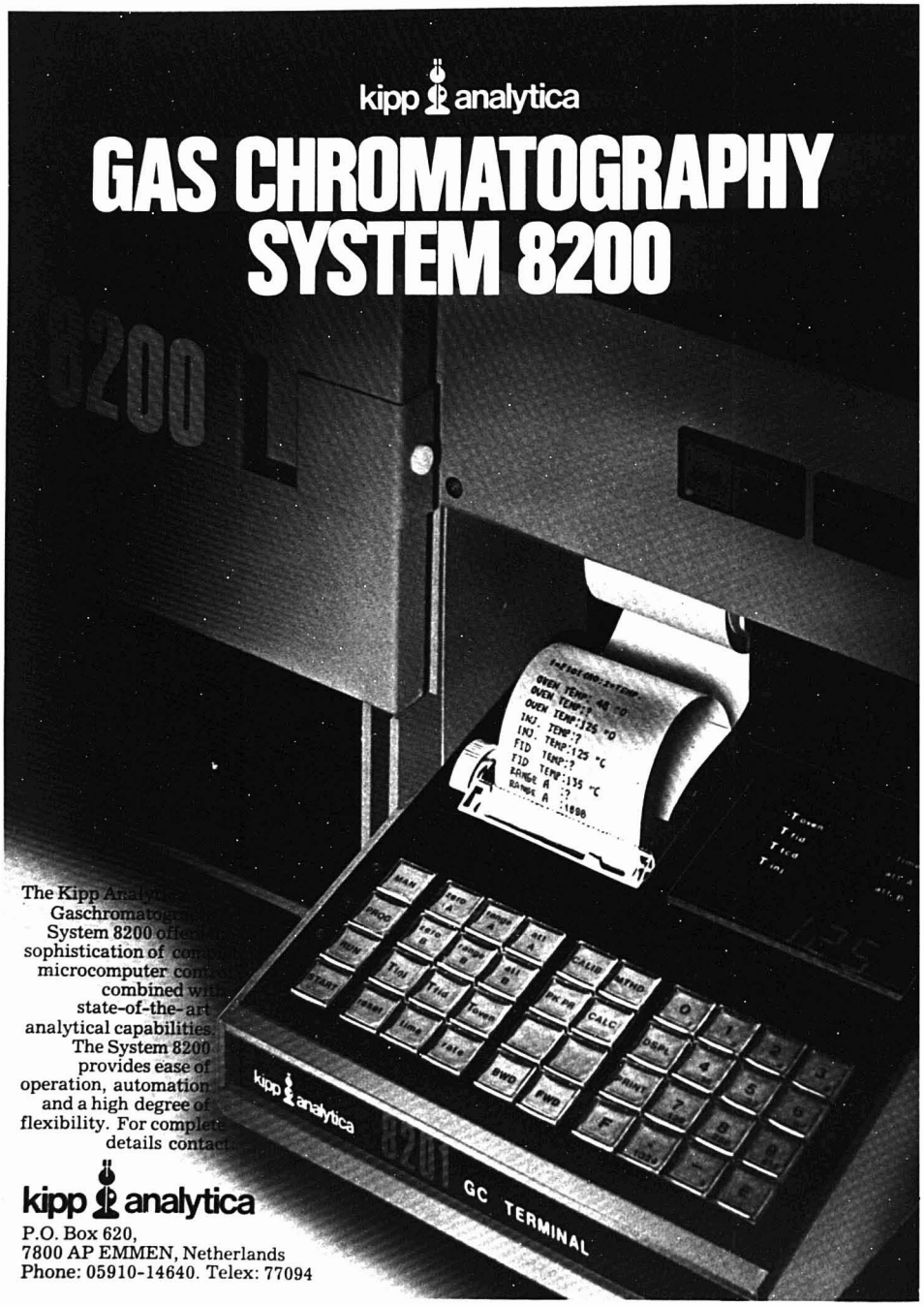
Chemical Division, Product Group Laboratory Glassware,
P.O. Box 2480, D-6500 Mainz 1, Telephone (0 61 31) 6 61, Telex 4 187 379 smz d.

CIRCLE 104 ON READER SERVICE CARD

1120L

kipp analytica

GAS CHROMATOGRAPHY SYSTEM 8200



The Kipp Analytica Gaschromatograph System 8200 offers the sophistication of computer microcomputer control combined with state-of-the-art analytical capabilities. The System 8200 provides ease of operation, automation and a high degree of flexibility. For complete details contact:

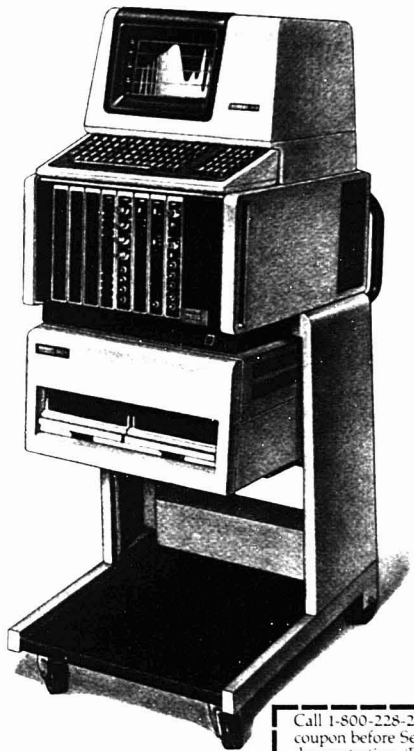
kipp analytica

P.O. Box 620,
7800 AP EMMEN, Netherlands
Phone: 05910-14640. Telex: 77094

CIRCLE 123 ON READER SERVICE CARD

1120M

In less than 2 hours, you can start saving hundreds of lab hours with a MINC-23 computer.



Learn how Digital's MINC-23 lab computer can be installed by you and working in your lab in less than 2 hours. Simply wheel it in. Plug it in. The graphics and system software have been pre-programmed and pre-written for you. The MINC-23 interfaces with a variety of lab instruments. And it's efficient, saving you time and money.

The MINC-23 is just what you need to solve your laboratory research problems. And it's just what you'd expect from Digital, the world's leading manufacturer of lab computers.

Call 1-800-228-2028, ext. 31, toll-free, or mail in this coupon before September 1, 1981, for your free demonstration. (Please include your business card or letterhead with coupon.)

Mail to: Digital Equipment Corporation, Laboratory Data Products Group MR 2-4/M16, One Iron Way, Marlboro, Mass. 01752 (13A 8/81)

Name _____

Job Title _____

Company _____

Company Address _____

Company Phone _____

digital

We change the way the world thinks.

© 1981, Digital Equipment Corporation

A Handheld Colorimeter ...in a water test kit!

Now from Hach—**a pocket colorimeter** that will give you instant test results—without the errors of color comparisons. For example, imagine an accurate chlorine test you can do right on site in minutes. The complete test set, including reagents and apparatus in a durable lightweight case, is only $145.00.

The new DR-100 pocket colorimeter is also available for 19 additional water parameters, each with direct readout in concentration.



Use reader service card for more information or call 800-525-5940

Available DR 100 Test Kits.

Ammonia	Nitrate High Range
Chlorine	Nitrate Low Range
Hexavalent Chromium	Nitrite High Range
COD High Range*	Nitrite Low Range
COD Low Range*	Phosphate
Copper	Silica High Range
Cyanide	Silica Low Range
Fluoride	Sulfate
Hydrazine	Zinc
Iron	
Manganese	*reagents separate

HACH COMPANY
P.O. Box 389
Loveland, CO 80537

CIRCLE 97 ON READER SERVICE CARD

Repeating Dispensers?

Pistolpet™

Solvent* Unit Handles All Reagents

***Autoclavable* Unit Ideal for All Sterile Dispensing**



New precision dispensers mount directly on almost all standard chemical bottles. Unique design gives great stability. Reagent being dispensed comes into contact with only teflon and glass in Solvent Unit. Autoclavable Unit constructed of polypropylene, glass and silicone. Supplied with 16 oz. 38 mm neck bottle. Available: adapter kit to fit 28 or 33 mm bottles, and undercounter remote dispensing attachment.

Pistolpet™

0.8 ml capacity • 8.5 ml capacity
20 ml capacity

Manostat!

For complete bulletin, contact Manostat

519 Eighth Ave., New York, N.Y. 10018 • Tel: (212) 594-6262
Or ask your dealer

CIRCLE 139 ON READER SERVICE CARD

PCR 81 82 PCR



PCR PRODUCTS

A general catalog listing physical properties and prices is available, free. This catalog lists:

Organofluorine Compounds
Organosilicon Compounds
Derivatizing Reagents
Mass Spec Standards
NMR Reference Compounds
Crown Ethers
Synthetic Reagents
Fine Organic Intermediates
Terpenes

If you are interested in any of the above products, you should have your own copy of our catalog.

Write or call for your free copy today.

PCR RESEARCH CHEMICALS, INC.
P.O. BOX 1778 GAINESVILLE, FLORIDA 32602 (904) 376-7522
SCM ORGANIC CHEMICALS DIVISION, SCM CORPORATION

CIRCLE 170 ON READER SERVICE CARD

Direct Digital Readout Pipet?



Digipet . . .
is capable of dispensing as little as 0.0002 µl and is the most accurate dispenser available. The newly redesigned case is comfortable for use as a hand held unit or is available mounted on a stand for use as a buret. Both units feature an easy reset digital direct readout.

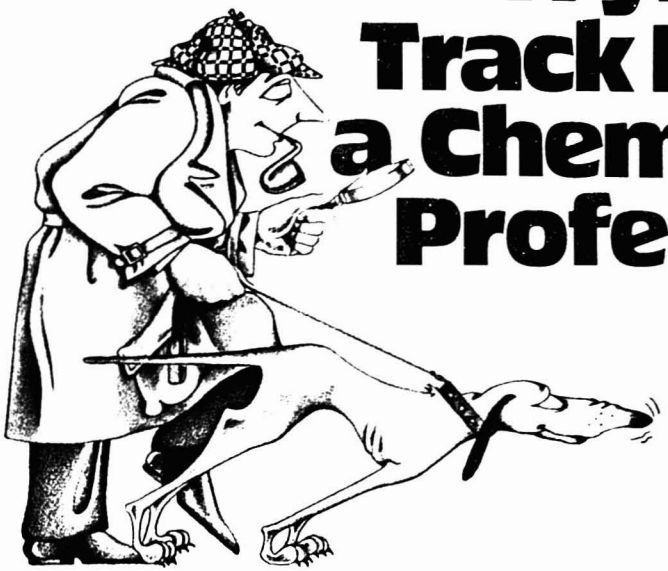
Manostat!

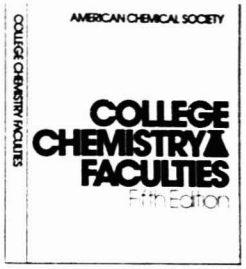
For complete bulletin, contact **Manostat**

519 Eighth Avenue
New York, N.Y. 10018
Tel: (212) 594-6262
Or ask your Dealer

CIRCLE 140 ON READER SERVICE CARD

Trying to Track Down a Chemistry Professor?





With the new fifth edition of COLLEGE CHEMISTRY FACULTIES you can be hot on the trail of any of the 17,000 faculty members in the chemical sciences in the U.S., Canada, and Mexico.

Have you heard about some interesting research that you'd like to learn more about, but don't know how to locate the researcher?

Do you have trouble reaching that special segment of the academic community that needs your products and services?

When the trail is cold and clues are hard to find, the solution is in the American Chemical Society's fifth edition of **College Chemistry Faculties.**

This thorough, up-to-date directory of college chemistry faculties is conveniently organized to quickly provide the information you need to find:

- Major field(s) of teaching for each faculty member: analytical, biochemistry, chemical engineering, inorganic, organic, physical, or polymer
- Faculty listed by college or university so you know at a glance who's who in any chemistry, biochemistry, chemical engineering, or medicinal chemistry department, including the present chair
- Alphabetical index of the 17,000 faculty members and their current affiliation
- Departmental telephone numbers and addresses to help make contacting professors easy
- Name, academic rank, and highest degree for all faculty members

Since institutions are listed by state, it's easy to see who's nearby when planning meetings or looking for a consultant. For marketers, it's ideal for planning sales and service territories.

Listings of over 17,000 chemistry, biochemistry, chemical engineering, and medicinal chemistry teachers at 2,000 two-year colleges, four-year colleges, and universities

College Chemistry Faculties, published by the American Chemical Society, is one of the major reference sources in the academic chemical world. If you move around in that world or want to contact people who do, you shouldn't be without it.

American Chemical Society Department 3D 1155 Sixteenth Street, N.W. Washington, D.C. 20036

Please send _____ **copies of COLLEGE CHEMISTRY FACULTIES @ $25.00.**

☐ Payment enclosed (payable to American Chemical Society)

☐ Bill me ☐ Bill company (add $1.50 billing costs) Charge my ☐ Master Card ☐ Visa

Card # _____ Interbank # _____ (Master Card Only)

Exp. Date _____ Signature _____

Name _____

Company _____

Address _____

Billing Address _____

City _____ State _____ Zip _____

Or ORDER BY CALLING TOLL FREE: (800) 424-6747



Finnigan MAT 4500 Series GC/MS Systems:

TOP QUALITY EI AND CI ANALYSES, CONSISTENTLY!

As the art of combined gas chromatography/mass spectrometry (GC/MS) advances, so do the demands today's analysts place on the instrument's capabilities. The new Finnigan MAT 4500 Series GC/MS is designed to address analytical needs such as these:

- Analyzing samples which can easily contaminate your ion source.
- Performing analyses which benefit from chemical ionization (CI) with corrosive reagent gases.
- Doing routine analyses amenable to extensive automation, such as GC control, autosampler operation and automatic data analysis.
- Obtaining optimized quality of both electron impact (EI) and CI spectra.

The Features That Benefit You

The 4500 Series meets these demands. To give you high quality, reproducible EI and CI spectra, it features replaceable ion volumes geometrically optimized for EI and CI analyses of solid, liquid and gaseous samples.

Ion source contamination problems are minimized, because of the ease with which you can replace a dirty source. Also, the 4500 lens assembly design greatly simplifies source cleaning.

An optional discharge ionization system allows you to perform CI using "problem" reagent gases which are corrosive or oxidizing.

Add to this:

- Complete computer control of the GC/MS system and analysis of results by the Incos™ data system,
- Proven GC and quadrupole analyzer design, and
- A host of accessories

and you have the new 4500 Series: versatile, modular and responsive to your analytical needs.

Plus User Support

The 4500 Series is supported in every aspect by Finnigan MAT, the world's most experienced mass spectrometry company. For service, parts and technical advice, all you need to do is pick up your telephone. And for training, the Finnigan MAT Institute offers the most complete selection of maintenance and operator training courses available.

Contact us for information about our full line of GC/MS and MS systems for organic and inorganic analysis, laboratory data systems, and training courses. We're Finnigan MAT — dedicated to serving the mass spectrometry community worldwide.

Finnigan MAT

Sunnyvale Operations
845 West Maude Ave.
P.O. Box 459
Sunnyvale, CA 94086
(408) 732-0940

Finnigan MAT GmbH
Barkhausenstr. 2
Postfach 14 40 62
D-2800 Bremen 14
(0421) 54 93 -1

CIRCLE 86 ON READER SERVICE CARD

R. Mark Wightman
Department of Chemistry
Indiana University
Bloomington, Ind. 47405

Microvoltammetric Electrodes



In every area of analytical chemistry it seems that smaller is better. For example, capillary columns for gas and liquid chromatography are rapidly replacing the conventional columns because they lead to increased resolution. Mini-inductively coupled plasma torches have been developed that result in considerable savings in operating expense. Microcomputers, with their increased capabilities, are rapidly becoming the method of choice for laboratory automation. As will be shown, small also has many advantages in voltammetry. Disk-shaped voltammetric electrodes of less than 10-μm radius have recently been fabricated. These electrodes are approximately 10 times smaller in diameter than a human hair, and because of their very small size they exhibit very different voltammetric properties than do electrodes of conventional size. In this REPORT, these very small chemical sensors will be referred to as microvoltammetric electrodes.

One may well ask, why in the world would you want to make such a small electrode? An obvious answer is that if you have a very small place in which you wish to make a chemical measurement, you have a need for such a device. Our particular interest in microvoltammetric electrodes arose because of our desire to make measurements of chemical concentrations inside the mammalian brain. The specific compounds that we, as well as a number of other groups, are interested in measuring are a class of small molecules referred to as neurotransmitters.

Neurotransmitters have a very important role in the brain since they are the key link in communication between neurons. Four of the known neurotransmitters, dopamine, norepinephrine, epinephrine, and serotonin, are easily oxidized at carbon electrodes and, thus, in vivo voltammetry provides a unique way to monitor chemical changes arising from neuronal actions. These four neurotransmitters are of special interest to researchers in neuroscience since several different types of drugs, such as amphetamine, cocaine, and various neuroleptics, are known to have their sites of action in the brain, where these neurotransmitters operate. They have also been implicated in various disease states. A review that describes the function of neurotransmitters in greater depth has appeared in this JOURNAL (*1*). As will be shown later in this REPORT, very interesting information concerning drug-induced changes in concentration of chemical compounds in the mammalian brain can be obtained by using microvoltammetric electrodes.

Besides the unique size of microvoltammetric electrodes, there are several other features that make them useful in various forms of chemical analysis. We have investigated many of these since it is absolutely necessary that an analytical tool be well understood before it is used in a unique en-

This work was supported by the National Institutes of Health and the National Science Foundation.

0003-2700/81/A351-1125$01.00/0
© 1981 American Chemical Society

vironment such as the mammalian brain. One notable feature of microvoltammetric electrodes is that they enable time-independent currents to be easily monitored. This feature simplifies measurements and facilitates their use under conditions where variations in potential are disadvantageous. The currents at these electrodes are extremely small, and the electrodes are, therefore, virtually nondestructive of the species being electrolyzed. Furthermore, because of the small currents, the electrodes can be used in solutions of very high resistance. The equations describing these features of microvoltammetric electrodes have been recognized for a number of years. Thus, one of the advantages of working in this field is that detailed derivations for the expected current–voltage response are given in the literature, and these can be directly applied to chemical systems. However, only recently have microvoltammetric electrodes been constructed.

Current–Voltage Curves

Effects of Diffusion. The goal of most voltammetric experiments, including in vivo electrochemistry, is to generate a current–voltage curve from which the chemist can extract a half-wave potential, which can be used to identify the species in solution; the amplitude of the current can be related directly to the concentration of the species in solution. Unfortunately, these parameters are not easy to obtain in a straightforward fashion in most electrochemical experiments done in stationary solutions.

Let's first consider cyclic voltammetry at a microvoltammetric electrode done at a relatively fast scan rate (10 V/s). In cyclic voltammetry, the voltage is scanned in a triangular fashion, and the resulting current measured. Most cyclic voltammograms have a peak-shaped current–voltage curve as shown for the oxidation of ferrocene in acetonitrile in Figure 1a. The initial potential, 0.0 V in this example, is selected as a place where no electrochemistry is occurring. As the potential is scanned in a positive direction, the half-wave potential for ferrocene is approached and the current starts to increase. However, as electrolysis of the compound decreases its concentration at the electrode surface, the current returns toward the baseline after reaching a maximum. This occurs because the electrolysis rate greatly exceeds the rate at which the species can diffuse to the electrode surface. At these rapid time scales, the majority of the diffusion is perpendicular to the electrode surface (Figure 2) (2). Therefore, both diffusion and concentration information are convoluted in the current–voltage curve. On the reverse

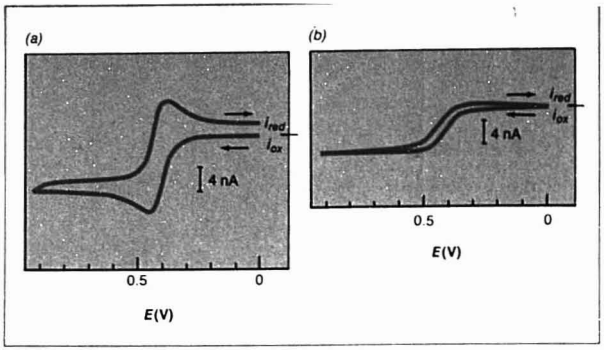


Figure 1. Cyclic voltammogram of ferrocene (1.0 mM) in acetonitrile with 0.1 M tetra-*n*-butylammonium perchlorate at a gold microdisk electrode (r = 6.5 μm). (a) 10 V s^{-1} scan rate. (b) 0.1 V s^{-1} scan rate

half of the triangular voltage sweep, the electrolysis products (ferricinium ions in this example) can be reduced, resulting in current flowing in the opposite direction. Although the data given in Figure 1a were obtained at a microvoltammetric electrode, this type of response is also obtained at an electrode of conventional size (radius $\simeq$1 mm).

If we do the experiment again, but at a slower sweep rate, the results given in Figure 1b are obtained. Again, the potential was scanned from 0.0 V toward positive potentials. The increase in current in the vicinity of the half-wave potential is still well-defined but, under these conditions, the current at more positive potentials is essentially steady-state and, thus, is easier to use for measuring concentration. The steady-state current arises because the electrolysis rate is approximately equal to the rate of diffusion of molecules to the electrode surface. At the slower scan rate, radial diffusion to the edges of the surface of the disk-shaped electrode as well as diffusion perpendicular to the surface becomes important (Figure 2). When the direction of the potential sweep is reversed, the current essentially follows that obtained with the initial scan because the products of electrolysis have diffused away from the electrode. At an electrode of larger size, this type of effect is difficult to observe because the scan rate must be very slow for the radial diffusion to contribute appreciably to the current (see below).

In both voltammograms shown in Figure 1, diffusion plays an important role in the shape of the current–voltage curve. Theoretically, one can carry this argument even further. If an electrode of 10-nm diameter could be constructed and used at the same sweep rates as shown in Figure 1, the resulting current would be an exponential function of potential. At these very small electrodes, the rate of elec-

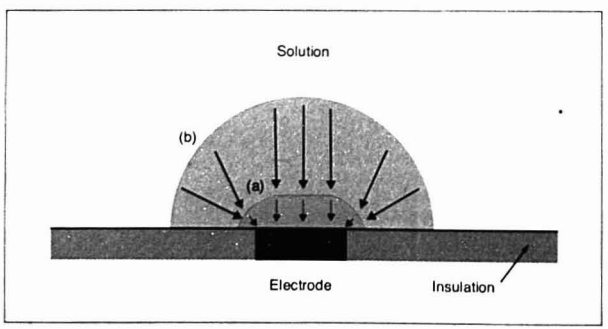


Figure 2. Diffusion profile of electrolyzed species at a microvoltammetric electrode. (a) Profile at short times as in rapid cyclic voltammetry (10 V s^{-1}). (b) Profile at longer times as with slower scan rate cyclic voltammetry (0.1 V s^{-1})

Some people will do anything to sell you their pH meters...



except make them as good as Radiometer does.

Introducing two new additions to the Radiometer pH family, created with the same dedication to quality and craftsmanship as fine Danish porcelain.

The PHM83 Autocal pH Meter with the unique simplicity of auto calibration and advanced operator information.

- Micro processor controlled for precise measurement of pH, mV and temperature.
- One key calibration with automatic recognition of specified buffer.
- 20 Character alpha-numeric display.
- Permanent memory retains calibration data even when power is switched off.
- Built-in test and service programs.
- Optional output module for connection to printer, recorder and titration systems.

The PHM80 Portable pH Meter.

- Measures pH and mV.
- 4 digit LCD display.
- 800 hour battery life.

See the new PHM83 and all the fine quality Radiometer pH meters in our new "pH Family" brochure. Get your copy today. Call (800) 321-9484. In Ohio, Alaska and Hawaii call (216) 871-8900. The London Company, subsidiary of Radiometer Copenhagen, 811 Sharon Drive, Cleveland, Ohio 44145.

RADIOMETER COPENHAGEN

When you can't afford to be wrong.

CIRCLE 184 ON READER SERVICE CARD

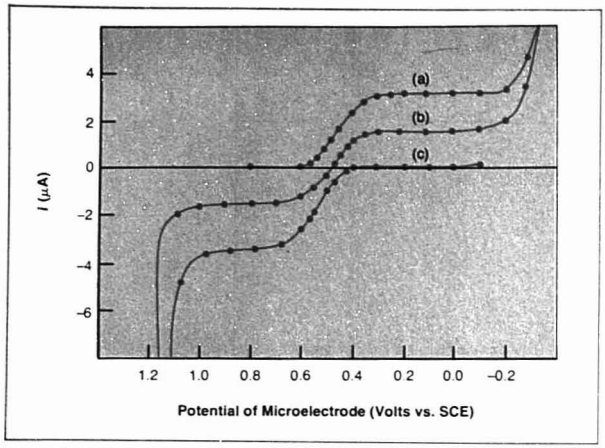


Figure 3. Electrolysis of ferrous chloride and ferric chloride in 0.5 N hydrochloric acid. Curve a, 0.002 M $FeCl_3$; curve b, 0.001 M $FeCl_2$, 0.001 M $FeCl_3$; curve c, 0.002 M $FeCl_2$. Reprinted by permission

trolysis of molecules would be so reduced relative to the rate of diffusion of molecules to the electrode that electrolysis would become the rate-determining step, and the current–voltage curve for a reversible system would be given by the Nernst equation.

The steady-state contributions to the current have been colloquially referred to as edge effects (or, at spherical electrodes, as spherical effects) and have been recognized by electrochemists for a number of years. In fact, in 1941, Laitinen and Kolthoff introduced the term *voltammetry* to describe steady-state current–voltage curves (*3*). Working with disk electrodes of the size commonly used in the electrochemical laboratory today (diameter ≃3 mm), they obtained the curves shown in Figure 3. Each point on these curves was measured at a fixed, applied potential that was monitored for "two or three minutes" so that the time-dependent effects of diffusion would be minimized. The current was then recorded and the voltage changed to the next desired value. This procedure was necessary at this larger-size electrode because the ratio of the number of molecules diffusing perpendicular to the electrode relative to those diffusing in at the edges is much greater at an electrode of this size, and the steady-state response is not observed for a much longer time. This approach to voltammetry often gives irreproducible results because natural convection also affects transport of molecules to the surface at these time scales.

As shown above, the measurement of sigmoidally shaped voltammograms at electrodes in stationary solutions is not new—it is simply easier to do with the newly developed microvoltammetric electrodes. These microvoltammetric electrodes do not have to be disk-shaped. Cylinders, spheres, rods, and virtually any other geometry of electrode of small enough size will also give the same result.

The time scale of the measurement and the radius of the electrode affect the type of voltammogram that one obtains in stationary solutions. At fast time scales, or at electrodes of large radius, peak-shaped voltammograms are obtained, whereas with small radius or with long time scales of measurement, steady-state voltammograms are obtained. Electrodes of intermediate size (or measurements at intermediate scan rates), of course, give intermediate results: Time-dependent and time-independent currents are superimposed.

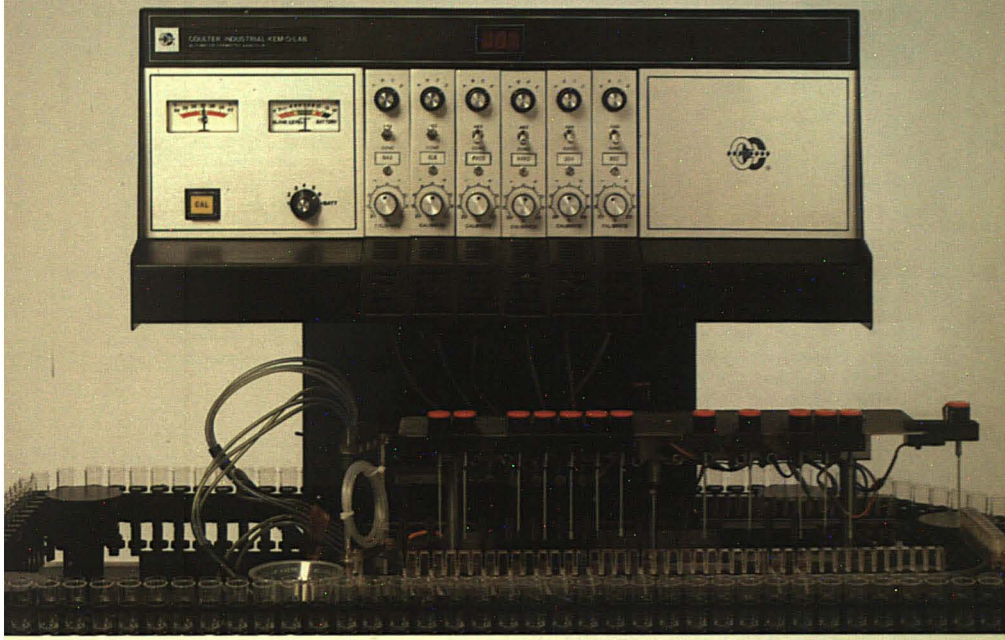
Effects of Chemical Rate Constants. The rates of chemical reactions occurring in solution and the rate of electron transfer with the electrode can also affect the shape of the current–voltage curve. If the rate of electron transfer of the species in solution with the electrode is slow, this can distort the current–voltage curve, giving a drawn-out response. Fleischmann's research group at Southampton has extensively studied the rate of electron transfer at small electrodes and finds it to be comparable to that of electrodes of conventional size (*4*). However, because the effect of diffusion on the electrochemical signal is less pronounced, faster heterogeneous rate constants can be measured at microvoltammetric electrodes. Although this is interesting from a fundamental electrochemical point of view, to the practicing electroanalytical chemist it simply means that the rate of electron transfer may distort the current–voltage curve even more at microvoltammetric electrodes than at electrodes of larger size. To get rid of this distortion, the electrochemist can do little except change electrode materials, change the solution conditions, pick another compound to analyze by electrochemical techniques, or, perhaps, chemically modify the surface of the electrode.

An effect of equal concern to analytical use of electrochemistry is the presence of chemical reactions that precede or follow the initial electron transfer and that also contribute to the current, since these may also distort the predicted current–voltage curve. The theoretical effect of this type of reaction has been extensively studied and several of the derivations of the current response have been compiled by Galus (*5*). Fortunately for chemists working with microvoltammetric electrodes, these derivations have been considered for electrodes of all sizes. These derivations show that chemical processes that follow the initial electron transfer and are of moderate rate will have much less of an effect on the current at microvoltammetric electrodes than at larger electrodes. To see why this is true, let's examine a reaction of the type

$$O \xrightarrow{ne} R \xrightarrow{k_c} O + Y$$

This reaction is referred to as a catalytic reaction because the initially reduced species, O, is regenerated by a chemical reaction with a pseudo-first-order rate constant, k'_c. At a large electrode, this regenerated O will return to the electrode surface, resulting in an increased current. However, at a microvoltammetric electrode with moderate values for k'_c, very little enhanced current is obtained. This result is easily rationalized when one realizes that the average distance into solution that R diffuses before reacting to form O, given by $(Dt)^{1/2}$, where t is the half-life of the reaction and D is the diffusion coefficient, is larger than the radius of a microvoltammetric electrode. Thus, while the distance that R diffuses is not far, at a microvoltammetric electrode a large part of the regenerated oxidant is removed from the vicinity of the electrode surface and, thus, a minimal catalytic contribution to the current is observed. The decreased effect that a catalytic reaction has at microelectrodes has been demonstrated for the oxidation of dopamine in the presence

High speed water chemistries





- Up to 240 results per hour.
- Up to six methods per sample.
- 12 methods presently available.
- Unattended operation.
- Digital printout and computer interface.

The COULTER® Industrial Kem-O-Lab is an automated, water chemistry analyzer designed for the busy laboratory. Up to six tests may be run at the same time on each set of samples. The most important feature of all is that it can operate continuously with very limited attention.

And the Kem-O-Lab is economical to operate. It performs only those tests requested and uses only the reagents necessary for the tests performed. Reagent consumption per test is minimal and never exceeds 5 ml per test.

For more information on what the COULTER® Industrial KEM-O-LAB™ can do for you, call the Coulter or Curtin Matheson Scientific office nearest you.

Coulter... Quality Counts.

COULTER ELECTRONICS, INC.
590 West Twentieth Street
Hialeah, FL 33010

CIRCLE 36 ON READER SERVICE CARD

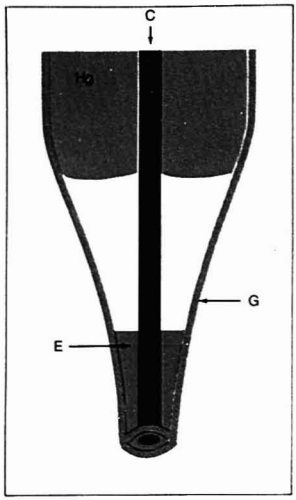


Figure 4. Glass capillary, disk-shaped microvoltammetric electrode. C, carbon fiber; G, glass; E, epoxy to prevent leakage; Hg, mercury for electrical connection

of ascorbic acid, conditions at which catalytic reaction is known to occur (*6*). This reaction is of importance in the measurement of dopamine in the brain since ascorbic acid is present in large concentrations in extracellular fluid and thus could distort measurement of extracellular dopamine.

The same qualitative arguments can be made for other types of chemical reactions following the electron transfer. This is important in chemical analysis, since determinations are often made in solutions of unknown composition (especially in vivo) where these types of reactions are likely to occur.

Electrodes and Instrumentation

We have employed carbon fibers, obtained from various commercial sources such as Hercules, Inc., Union Carbide Corporation, and Courtauld, Ltd., in the construction of microelectrodes. These fibers have diameters in the range of 6–12 μm (*6*, *7*). They are formed from the high temperature pyrolysis of materials such as polyacrylonitrile or pitch and are intended for use in golf clubs, bicycle frames, etc. Our method of construction is relatively simple and results in the fiber being sealed with epoxy in a glass capillary (Figure 4). Approximately 50% of the electrodes constructed are useful for electroanalysis. Double-barreled pipets can also be constructed, with the second barrel used as the reference electrode or as a second carbon fiber electrode (*6*).

Several other types of microvoltammetric electrodes have been described in the literature. Ponchon et al. were the first to use carbon fibers for microvoltammetric electrodes (*8*). Their electrodes have approximately 500 μm of the fiber protruding from the glass capillary, resulting in a cylindrical electrode. This design results in a larger faradaic current, but the voltammograms exhibit non-steady-state behavior at 300 mV s^{-1}. Swan has described micro-disk electrodes fabricated from platinum and tungsten wires (*4*). These wires were electrochemically etched to form electrodes with diameters as small as 1 μm as determined by the limiting diffusion currents. McCreery has constructed cylindrical microvoltammetric electrodes from carbon fibers and 7-μm-radius gold wires for use in spectroelectrochemical applications (*9*).

Microvoltammetric electrodes connected in parallel maintain the features of single microvoltammetric electrodes with the advantage of increased current amplitudes. These have been fabricated using thin film technology (*10*) or photoetching techniques (*11*). As expected, the steady-state current is maintained, but the current is increased by the sum of the small electrodes.

An obvious limitation in the use of single microvoltammetric electrodes is that very small currents must be measured. For electrochemical measurements in the millisecond time range, where very little electronic filtering can be employed, we make all of our measurements in a faraday cage. The EG&G Princeton Applied Research Corporation Model 174A is useful for measurements down to 10 pA. For measurements of dilute concentrations at slow scan rates, commercial picoammeters can be used. We recently built a current transducer capable of low noise subpicoamp measurements, which is ideal when rapid potential pulses (92 ms) are employed. Using this repetitive pulse waveform, we can measure concentration changes of 1×10^{-7} M for the $2e^-$ oxidation of dopamine in pH 7.4 buffer. In these measurements, the current is integrated over 34 ms, during which time only about 60 000 molecules are oxidized! Obviously, measurements of much lower concentration at microvoltammetric electrodes are going to require a new approach to potentiostat design.

Other Features of Microvoltammetric Electrodes

The concentration is perturbed by electrolysis only a very small distance from the microvoltammetric electrode (approximately six times the radius under totally steady-state conditions) (*12*). Therefore, microelectrodes are not greatly affected by movement in solution. In fact, the steady-state current density observed at microvoltammetric electrodes of 4-μm radius is equivalent to that observed at a rotating disk electrode operated at 500 rps, a relatively fast rotation speed. This feature is of particular importance in applications of "polarographic" oxygen electrodes in biological systems, where variable convective rates may occur.

Microvoltammetric electrodes show great potential utility for very fast measurements since double-layer charging currents should be proportional to the electrode area. This prediction of decreased charging current times is important since this parameter determines the shortest time at which meaningful measures of faradaic current can be made. For a potential pulse, the charging current (i_{DL}) is

$$i_{DL} = \frac{\Delta E}{R} e^{-t/RC} \qquad (1)$$

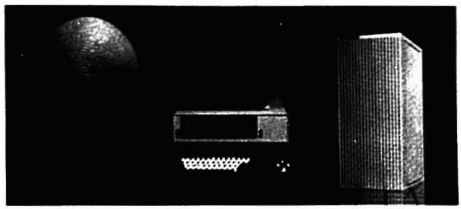
where ΔE is the amplitude of the pulse, R is the resistance of the electrochemical cell, C is the double layer capacitance, and t is the time measured from application of the pulse. The double-layer capacitance decreases exponentially with a decrease of the area, while the time-dependent faradaic current decreases linearly with area. Thus, the faradaic/charging current ratio should be increased at a microvoltammetric electrode. For a disk electrode of 4-μm radius, the double layer should be 99% charged within 3 μs, even assuming a 100 μF cm^{-2} double-layer capacitance and a cell resistance of 10 kΩ. With this response, very rapid time-dependent measurements of chemical events could be made. Unfortunately, we have not been able to experimentally verify this prediction. Nonfaradaic currents at carbon fiber electrodes are observed that restrict faradaic measurements to the millisecond time domain. Possible sources of this residual current are microcracks in the carbon formed during the process of fabrication, or surface oxides on carbon. A clever approach to these problems has been taken by McCreery, who ignores the current and uses spectroelectrochemistry to monitor electrolysis on carbon fiber electrodes (*9*). Using a laser with a highly aligned optical system, he has observed electrochemically generated products along the axis of a carbon fiber within 5 μs of a potential pulse.

An area in which microvoltammetric electrodes should be of great importance is in the study of redox systems in highly resistive solvents. Electrochemical currents at disk electrodes of 4-μm radius are 4 to 5 orders

COMPUTER AIDED CHEMISTRY

The concept that is revolutionizing laboratory productivity.

Perkin-Elmer is leading a revolution in productivity, in laboratory management, in manpower use and economics...a revolution called Computer Aided Chemistry.



LEVEL 1—INSTRUMENTS THAT PUT PEOPLE BACK TO WORK ON CHEMISTRY.
At the heart of Computer Aided Chemistry is the same tiny microprocessor that is transforming commercial and industrial electronics. Built into analytical instruments, it makes possible an awesome jump in their efficiency. Setup and calibration, methods, autosampling, sample identification and data reduction are all controlled electronically.

The broadest line. Perkin-Elmer offers the world's broadest line of microprocessor controlled analytical instruments. *Almost every analytical instrument Perkin-Elmer offers is microprocessor controlled.* If your laboratory uses one or more of them, you are already working with Computer Aided Chemistry.

LEVEL 2—DATA STATIONS MAKE INSTRUMENTS AND ANALYSTS MORE PRODUCTIVE.
The microprocessor also opens ways for instruments to interact with advanced control devices, such as Perkin-Elmer Data Stations.

A Data Station is actually a microcomputer system through which operator and instrument communicate. Programmable in BASIC, it can order and compare analyses, record and manipulate data. Results can be displayed on a CRT or as hard copy on a printer.

Result: More savings in time, another increase in productivity.

Consider the Perkin-Elmer SMS/200 Sample Management System, for instance. Basic hardware is a Model 3600 Data Station. But Perkin-Elmer software enables the Data Station to function either full time as a stand-alone computer, or part time as a computer and part time as an instrument controller.

Result: An immensely flexible small laboratory system that can perform sample log-in and tracking, data draw-off and archiving, backlog analyses and report generation, and much more.

Software—The Perkin-Elmer advantage.
The catalyst for communication at every level of Computer Aided Chemistry is software. And Perkin-Elmer offers the broadest repertoire of proven ready-to-use software in the analytical field. More than 50 software programs for Computer Aided Chemistry are available now, and cover the full range of analytical disciplines.

LEVEL 3—LIMS/2000 UNLOCKS THE FULL POTENTIAL OF COMPUTERIZATION.
LIMS/2000—Laboratory Information Management System—consists of advanced software and a broad array of instruments and Data Stations interacting with a powerful 32-bit Perkin-Elmer minicomputer.

LIMS/2000 not only fosters a quantum leap in productivity, it gives the manager of even the largest laboratory total control over the flow of work.

A single source. Perkin-Elmer Computer Aided Chemistry integrates instruments, computers, and software through a single, reliable source. This means you can begin a system with instruments, add Data Stations as workload grows, and a minicomputer still later *without* obsoleting any hardware or software purchased in the process.

Let Perkin-Elmer show you.
Perkin-Elmer will make a free survey of your laboratory and show you how Computer Aided Chemistry can improve productivity and efficiency. We also have a brochure on Computer Aided Chemistry.



Ask for a copy. Just write or call:

Perkin-Elmer Corp., Analytical Instruments, Main Ave. (M S 12), Norwalk, CT 06856 U S A. Tel. (203) 762-1000.

Bodenseewerk Perkin-Elmer & Co., GmbH, Postfach 1120, 7770 Ueberlingen, Federal Republic of Germany. Tel. (07551) 811

Perkin-Elmer Ltd., Post Office Lane, Beaconsfield, Bucks HP9 1QA, England. Tel: Beaconsfield (049 46) 6161.

PERKIN-ELMER
Responsive Technology

Circle 171 for literature. Circle 172 for sales call.

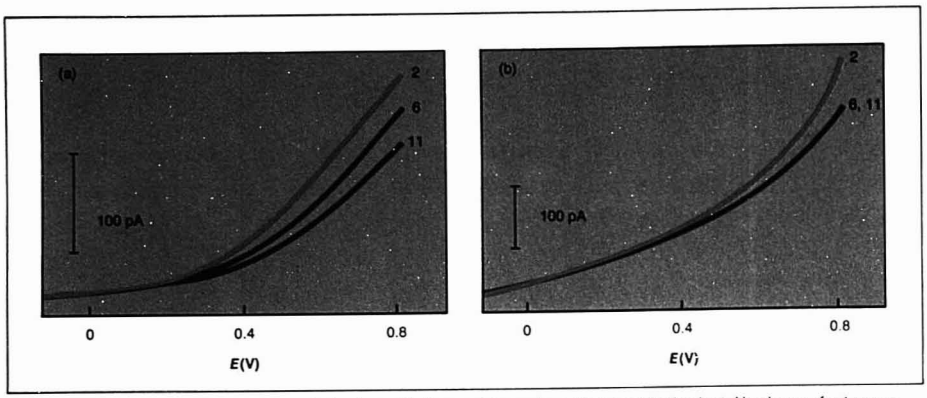


Figure 5. Voltammograms from an electrode implanted in the caudate nucleus of an anesthetized rat. Numbers refer to scan after implantation. 20 mV s^{-1} scan rate. (a) Linear sweep voltammetry. (b) Back-step corrected normal pulse voltammetry

of magnitude smaller than those seen at electrodes of conventional size. Since less current is passed, iR problems are much less severe, as previously noted. We have recently examined the oxidation of ferrocene in acetonitrile with low concentrations of tetra-*n*-butylammonium perchlorate as supporting electrolyte. Nernstian behavior is observed with a disk electrode of 6.5-μm radius even with supporting electrolyte and depolarizer both at 10^{-3} M. With the same conditions, the cyclic voltammogram at a Pt electrode of 400-μm radius has 240 mV peak separation! (Ideal behavior is 59 mV peak separation for $n = 1$.) These results demonstrate that electrochemistry without correction for iR effects is now feasible in solutions of very high resistance.

Applications

As previously discussed, microvoltammetric electrodes have an advantage over conventionally sized electrodes in such applications as voltammetry in resistive solutions and the determination of oxygen under conditions of varying convective mass transport. Interest in the area of microvoltammetric electrodes originally arose for the accurate measurement of diffusion coefficients. Although measuring diffusion coefficients is not a particularly stimulating research endeavor, it is of fundamental importance since the knowledge of the values of diffusion coefficients is necessary to interpret electrochemical results. In these types of experiments, a pulsed waveform is generally employed so that the current is measured at a single fixed potential, usually selected so that the surface concentration of the species being oxidized will be zero. Under these conditions at a spherical electrode, the current is given by

$$i = 4\pi rnFCD\left[r\left(\frac{1}{D\pi t}\right)^{1/2} + 1\right] \quad (2)$$

where n is the number of electrons involved in the electrode reaction, F is the faraday, D is the diffusion coefficient, C is the concentration, and r is the radius of the electrode. Inspection of Equation 2 shows that, at sufficiently long times, the current is independent of time. It is also apparent that the time when the steady-state current becomes significant is dependent on the radius of the electrode. Expressions have been derived for electrodes of other geometries, including a disk (*9*), a hemisphere (*6*), and a cylinder (*2*).

As stated at the beginning of this review, our primary interest in microvoltammetric electrodes is to use them as sensors of changes in chemical concentrations of neurotransmitters in the mammalian brain. Obviously, small electrodes are necessary for these in vivo measurements so that the electrode does not destroy the brain region in which measurements are being made. Nerve terminals have diameters in the 1-μm range, so even the electrode shown in Figure 4 is large with respect to these cells. Nevertheless, these electrodes appear to be essentially nonperturbational in brain tissue since the measured current does not change significantly with repetitive potential pulses—a criterion of tissue damage that has been established on theoretical considerations (*13*). Another parameter that is essential for meaningful in vivo measurements is that the electrode response remain constant for long periods of time. The electrode must be implanted in the brain and monitored for at least 8 h in most experiments, so opportunities are not available for electrode resurfacing. Our experience has shown that pulsed waveforms, similar to those used in normal pulse voltammetry, are best for maintaining electrode stability in the extremely complex environment of the mammalian brain. We have designed an instrument that is tailor-made for pulse voltammetry at microvoltammetric electrodes and even provides a method of residual current correction (*14*). Normal pulse voltammograms are steady-state when 92-ms pulses are used. Examples of voltammograms in a region of the brain (the caudate nucleus) containing dopamine, using a linear sweep and a pulsed waveform, are given in Figure 5. As shown in the upper half of Figure 5, the current response decreases with successive linear potential sweeps, indicating the instability of the electrode. However, as shown in the lower part of Figure 5, enhanced stability is observed using the pulse technique.

The potential range of the scans given in Figure 5 includes the half-wave potential for the oxidation of dopamine. Voltammograms of dopamine are sigmoidal, but dihydroxyphenylacetate, a major dopamine metabolite, and ascorbic acid both give drawn-out voltammograms as a result of their slow rate of charge transfer with carbon fiber electrodes (*6*). Thus, although these three compounds have a very similar formal potential and are all present in this brain region, the carbon fiber electrodes that we use are most sensitive to dopamine at 0.3 V because of the difference in charge transfer rates. As mentioned previously, interference via the dopamine–ascorbate catalytic reaction is also minimized at these electrodes. Since in

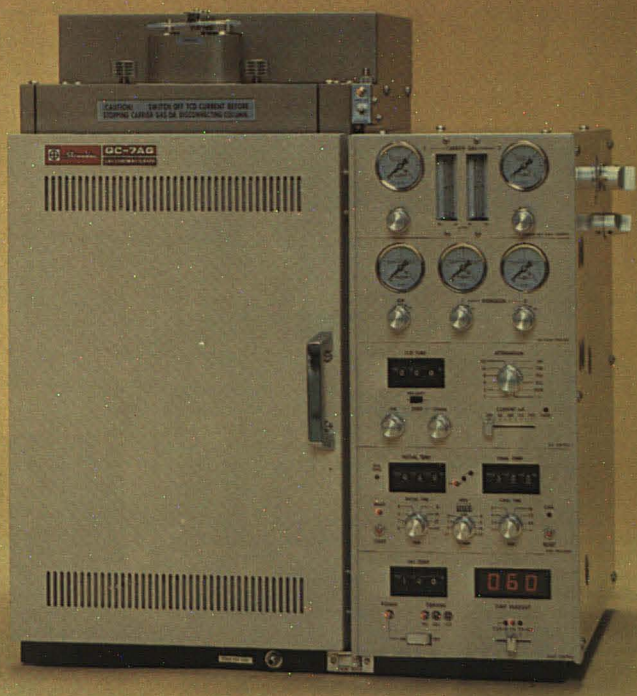
TRY GHOST-CUT INJECTION

WITH SHIMADZU GC-7A GAS CHROMATOGRAPHS*

The unique Shimadzu Ghost-Cut sample injection port eliminates ghost peaks and baseline fluctuations caused by the substances evolved from the rubber septum and the volatile substances absorbed by the sample residue on the inner surface of the injection port. Thus, contamination of the injection port is reduced and the meantime between cleanings is lengthened, resulting in more efficient operation.

This new GC also features a low heat capacity column oven to ensure rapid cooling, interchangeable column, dependable automatic wall sensor cooling mechanism, and dual column/dual flow system. Simultaneous installation of 4 detectors for multi-purpose versatility; constant current TCD with filament protection circuit featuring excellent stability in temperature programmed GC. new FID with improved sensitivity and stability, new linear ECD with expanded dynamic range, and new direct heated FTD. Automatic digital scanning display, foolproof digital temperature setting, and complete protection against temperature runaway are also included.

*US PATENT 3985016



• *Write today for more information on these and other Shimadzu instruments.*

SHIMADZU
SCIENTIFIC INSTRUMENTS, INC.

SHIMADZU SCIENTIFIC INSTRUMENTS, INC.
9101-D Red Branch Road, Columbia, MD 21045, U.S.A. Phone: (301)993-0267 Telex:87669

SHIMADZU (EUROPA) GmbH
4000 Düsseldorf 1, Duisburger Straße 58, F.R. Germany. Phone: (0211)33951 Telex:8586679

SHIMADZU CORPORATION INTERNATIONAL MARKETING DIV.
Shinjuku-Mitsui Building, 1-1, Nishishinjuku 2-chome, Shinjuku-ku, Tokyo 160, Japan
Phone: Tokyo(03)346-5641 Telex: 0232-3291 SHMDT J

CIRCLE 191 ON READER SERVICE CARD

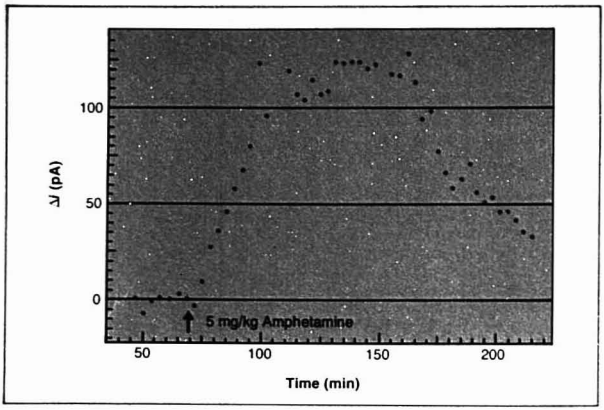


Figure 6. Change in current (Δi) at a microelectrode implanted in the caudate nucleus of an anesthetized rat for repetitive potential steps to 0.35 V vs. SCE following intraperitoneal amphetamine administration

vivo electrochemistry is a relatively new technique, this partial selectivity is important because it is unclear whether dopamine, dihydroxyphenylacetate, ascorbic acid, or some other electroactive compounds change in concentration with neuronal stimulation (*15, 16*). The in vivo voltammograms from anesthetized, unstimulated rats (Figure 5) appear very similar to those obtained for ascorbate in a conventional electrochemical cell and show no evidence for the presence of extracellular dopamine.

To determine whether the electrode would sense changes in chemical composition in this brain region, we administered the drug amphetamine to anesthetized rats. This drug is known to cause the displacement of dopamine from nerve terminals when it is injected into the intraperitoneal cavity of the rat. As shown in Figure 6, the current at our electrode near the dopamine nerve terminal certainly does increase following administration of amphetamine. Since amphetamine itself is not electroactive, the increase in this signal is definitely due to a change in the chemical composition of endogenous species in the extracellular fluid of rat brain. However, careful analysis of the voltammograms obtained after amphetamine injection does not indicate any substantial signal arising from dopamine. These results suggest that some substance other than dopamine increases in concentration to such a significant extent that the signal from any dopamine that is released is simply masked. The identity of the compound or compounds giving rise to this signal is currently unknown. In contrast to the results shown here, Gonon et al., using a chemically modified electrode, found that the electrochemical signal from the same brain region decreases following amphetamine administration (*15*). Since their electrode had different sensitivities to the compounds suspected to be in brain tissue, these results imply that at least two compounds alter in concentration with amphetamine administration. Thus, while the interpretation of in vivo electrochemical experiments is currently undergoing a revision, it is important to note that the electrochemical signals do correlate with behavioral and electrophysiological measures. This suggests that chemical manifestations of neuronal activity can be measured by this method.

Many applications of microvoltammetric electrodes other than in vivo electrochemistry are just starting to appear. Very recently, Cushman and Anderson showed that carbon fiber electrodes are useful in anodic stripping applications (*17*). Schroeder has digitally simulated the results of the stripping experiment at micromercury drops and has found that very high concentrations of metal ions are obtained in the drop simply during the time for the cathodic scan (*18*). This means that the waiting time for metal deposition in the mercury can be greatly minimized. In addition to the "accelerated" mass transport at microvoltammetric electrodes, features such as low current and rapid time response should lead to increased use of microvoltammetric electrodes in a variety of applications. Since a tremendous amount of literature concerning the theoretical limits and capabilities of microvoltammetric electrodes already exists, this new tool for electroanalytical chemists should rapidly expand in use.

Acknowledgment

The clever insights and enthusiastic research of my students have been the major source of our progress in this new area.

References

(1) Adams, R. N. *Anal. Chem.* **1976**, *48*, 1126 A–1138 A.
(2) Adams, R. N. "Electrochemistry at Solid Electrodes"; Marcel Dekker: New York, 1969; Bard, A. J.; Faulkner, L. R. "Electrochemical Methods, Fundamentals and Applications"; J. Wiley and Sons: New York, 1980.
(3) Laitinen, H. A.; Kolthoff, I. M. *J. Phys Chem.* **1941**, *45*, 1062–79.
(4) Swan, P. N. Ph.D. Dissertation, University of Southampton, 1980.
(5) Galus, Z. "Fundamentals of Electrochemical Analysis"; Halsted Press: New York, 1976.
(6) Dayton, M. A.; Ewing, A. G.; Wightman, R. M. *Anal. Chem.* **1980**, *52*, 2392–96.
(7) Dayton, M. A.; Brown, J. C.; Stutts, K. J.; Wightman, R. M. *Anal. Chem.* **1980**, *52*, 946–50.
(8) Ponchon, J.-L.; Cespuglio, K.; Gonon, F.; Jouvet, M.; Pujol, J.-F. *Anal. Chem.* **1979**, *51*, 1483–86.
(9) Robinson, R. S.; McCreery, R. L. *Anal. Chem.*, in press.
(10) Siu, W.; Cobbold, R. S. C. *Med. Biol. Eng.* **1976**, *14*, 109–21.
(11) Osteryoung, J.; Aoki, K. *J. Electroanal. Chem.*, in press.
(112) Saito, Y. *Rev. Pola.* **1968**, *15*, 178–87.
(13) Cheng, H. Y.; Schenk, J.; Huff, R.; Adams, R. N. *J. Electroanal. Chem.* **1979**, *100*, 23–31.
(14) Ewing, A. G.; Withnell, R.; Wightman, R. M. *Rev. Sci. Instrum.* **1981**, *52*, 454–8.
(15) Gonon, F.; Buda, M.; Cespuglio, R.; Jouvet, M.; Pujol, J.-F., *Nature* **1980**, *286*, 902–4.
(16) Conti, J. C.; Strope, E.; Adams, R. N.; Marsden, C. A. *Life Sci.* **1978**, *23*, 2705–16.
(17) Cushman, M. R.; Anderson, C. W. *Anal. Chim. Acta*, in press.
(18) Schroeder, R. R., personal communication.



R. Mark Wightman is assistant professor of chemistry at Indiana University. His training in electroanalytical chemistry was with Royce Murray (Univ. of North Carolina) and with Ralph N. Adams (Univ. of Kansas). His research interests include electron transfer at carbon electrodes, microvoltammetric electrodes, liquid chromatography with electrochemical detection, and the rate and mechanisms of neurotransmitter release from brain tissue.

NEW WEIGHING VERSATILITY

SHIMADZU ELECTRONIC BALANCE

LIBROR EB SERIES

SHIMADZU announces new microprocessor-based electronic balances that WEIGH, COUNT, CONVERT, CALCULATE, SOUND, CONTROL

In addition to the original weighing (function),

- ***Multi-control (linked with EP-40 digital printer)***
  1. Automatic zeroing
  2. Automatic printer
  3. Setting and printout of date or lot number
  4. Classification of signals into 5 groups
  5. Ready buzzer and signal
  6. Peak value detection signal
- ***Conversion Function***
  1. Piece counting or percentage display
  2. Specific gravity (density) measurement
  3. Moisture content display
  4. Constant multiplication (linked with EP-40 digital printer)
- ***Multi-function (Super Models)***
  1. Averaged data
  2. Automatic stabilizing
  3. Holding of stabilized value
  4. Animal weighing
  5. Peak value detection
  6. Holding of peak value
  7. High-speed display
  8. Automatic printout of peak value
  9. Automatic memory
  10. Automatic memorizing and display zeroing
- ***Statistical Calculation (Super Models)***
  1. Total
  2. Maximum value
  3. Minimum value
  4. Range
  5. Number of samples
  6. Average
  7. Variance
  8. Standard deviation
  9. Standard error
  10. Coefficient of variation



Write today for more information on these and other Shimadzu instruments.

SHIMADZU SCIENTIFIC INSTRUMENTS, INC.

SHIMADZU (EUROPA) GmbH

SHIMADZU CORPORATION INTERNATIONAL MARKETING DIV.

SHIMADZU
SCIENTIFIC INSTRUMENTS, INC.

CIRCLE 192 ON READER SERVICE CARD

Can Your GC Analyze Solids?

It Can With A Pyroprobe.®

The Pyroprobe expands the capabilities of your GC, GC/MS or GC/IR by allowing you to analyze most solids including synthetic polymers, geo-polymers and bio-polymers. And that's not all. A Series 120 Pyroprobe can perform:

- **Analytical Pyrolysis**
- **Headspace Analysis of Volatile Organics**
- **Simulated Combustion Studies**
- **Simulated Thermal Analysis**

Pyroprobe®... The Solid Solution



CDS

Chemical Data Systems, Inc.
7000 Limestone Road
Oxford, PA 19363
Phone 215-932-3636
Telex 83-5308

CIRCLE 41 ON READER SERVICE CARD

Want to Receive Your ANALYTICAL CHEMISTRY *Faster?*

Try

AIR FREIGHT

Join other readers who have chosen **Air Freight** service. Receive your copy of *Analytical Chemistry* in Europe and the Far East in 3 to 10 days.

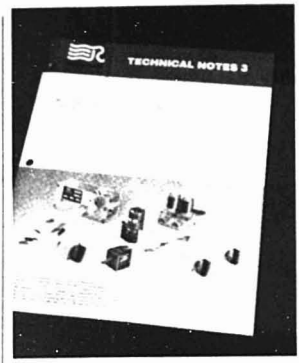
One full year of foreign **Air Freight** service is only $35. Service can be started at any time and the cost will be prorated based on your expiration date.

To begin **Air Freight** service immediately, please fill in the coupon below and include your current mailing label. We will bill you for the appropriate amount based on your subscription expiration date.

American Chemical Society
Attn: Circulation Development
1155 16th St., N.W.
Washington, D.C. 20036

☐ **YES!** I would like to begin AIR FREIGHT service immediately on my *ANALYTICAL CHEMISTRY* subscription. I understand you will bill me for the appropriate amount. I have attached a recent mailing label of *ANALYTICAL CHEMISTRY.*

PLACE CURRENT MAILING LABEL HERE



How to simplify HPLC using low-pressure valves.

Rheodyne's Technical Note 3 shows eight ways of using low-pressure switching valves to simplify method development and routine analysis in high-pressure liquid chromatography.

These economical 2-position and 6-position Teflon valves can be inserted before the pump or after the column.

Among uses described in detail are switching between reservoirs to select the correct mobile phase for a particular routine analysis. Switching between several different solvents during method development when seeking maximum selectivity. Switching to a flushing solvent. Switching effluent back to the reservoir to conserve solvent. And switching effluent to a fraction collector.

Send for Tech Note #3

All techniques are fully described in this well-illustrated 6-page technical note. Contact Rheodyne, Inc., P.O. Box 996, Cotati, Calif. 94928, U.S.A. Phone (707) 664-9050.

RHEODYNE
THE I.C. CONNECTION COMPANY

CIRCLE 185 ON READER SERVICE CARD

NEW ENVIRONMENTAL BOOKS FROM ACS

Chemical Hazards in the Workplace
State of the art and future directions of monitoring and measurement procedures for the occupational environment.
ACS Symposium Series 149
628 pages (1981) Cloth $43.00

Monitoring Toxic Substances
State-of-the-art techniques for identifying contaminants by nature, concentration, source and biological effects.
ACS Symposium Series 94
289 pages (1979) Cloth $26.50

Particulates in Water: Characterization, Fate, Effects and Removal
Latest research on improved modeling tools for water quality managers and designers of pollution control and water treatment facilities.
Advances in Chemistry Series 189
401 pages (1980) Cloth $59.50

Pesticide Analytical Methodology
Covers the latest analytical techniques for determining small levels of pesticides and their residues.
ACS Symposium Series 136
406 pages (1980) Cloth $38.00

Petroleum in the Marine Environment
Presents analytical methodology and applications that will be of major interest to environmentalists and energy conservationists.
Advances in Chemistry Series
371 pages (1980) Cloth $42.00

Biomass as a Nonfossil Fuel Source
Latest research on biomass production, liquid fuels, gaseous fuels, economics and energetics, and systems analysis.
ACS Symposium Series 144
564 pages (1981) Cloth $42.00

Analytical Techniques in Occupational Health Chemistry
State-of-the-art review of new and improved instrumental methods for analyzing potentially hazardous chemicals in the workplace.
ACS Symposium Series 120
318 pages (1980) Cloth $28.00

Cleaning Our Environment
Contains information on the nature and sources of pollutants in air, water, and solid wastes, and recommends action in each area.
457 pages (1978) Paper $9.50

Order from:
SIS Dept. 65, American Chemical Society
1155 Sixteenth St., N.W., Washington, D.C. 20036
or CALL TOLL FREE 800-424-6747 and use your credit card.

CLASSIFIED SECTION ■ POSITIONS OPEN

CLASSIFIED ADVERTISING RATES

Rate based on number of insertions used within 12 months from date of first insertion and not on the number of inches used. Space in classified advertising cannot be combined for frequency with ROP advertising. Classified advertising accepted in inch multiples only.

Unit	1-T	6-T	12-T	24-T	48-T
1 inch	93	87	83	76	72

(Check Classified Advertising Department for rates if advertisement is larger than 10".)

SHIPPING INSTRUCTIONS:

Send all material to
Analytical Chemistry
Classified Advertising Department
25 Sylvan Rd. South, Westport, CT 06881

CAREER OPPORTUNITIES

Exxon Production Research Company, located in Houston, Texas, has openings for a variety of well-qualified personnel interested in a challenging career in petroleum geochemistry.

•ORGANIC GEOCHEMISTS (PhD/MS)
To evaluate source rock potential and address problems of maturation and migration. Appreciable analytical laboratory experience together with strong geological and physical chemistry backgrounds preferred.

•ANALYTICAL CHEMISTS (PhD/MS)
Applicants should have a thorough knowledge of multiple chromatographic techniques (GC, LC, TLC) and column technology, and familiarization with state-of-the-art instrumentation. A lab supervisor role would be considered in the future. Prior experience is desirable.

•MASS SPECTROSCOPISTS (PhD/MS)
An instrument-oriented mass Spectroscopist to participate in crude-oil characterization. Applicant would participate in the development and application of new analytical and data-reduction methods within an expanding research program. Applicant must be adept in the operation and maintenance of modern state-of-the-art instrumentation. Responsibilities include analytical mass spectrometry, isotope-ratio mass spectrometry, and prepration and analysis of hydrocarbon samples.

We offer an outstanding employee benefit program and excellent opportunities for advancement and travel. Salaries commensurate with education and/or experience. Please send resume (and copies of transcripts if available) to:

J.J. Hedgemon
Exxon Production Research Company
Dept. 301
P.O. Box 2189
Houston, Texas 77001
An Equal Opportunity Employer, m/f

EXXON PRODUCTION RESEARCH
EXXON

LABORATORY SERVICE CENTER

Aluminon • ϵ-Aminocaproic Acid • Caffeic Acid • Cesium Chloride
Chalcone • m-Cresyl Methyl Ether • Cuprous Bromide • p-Cyanobenzaldehyde
Diacetylmonoxime • Dibenzoylmethane • Dimethylacetonedicarboxylate
Dimethyl Glyoxime & Sodium Salt • N,N'-Diphenylbenzidine • Dulcitol
Esculin • HHSNN • Methyl Acetate • p-Naphtholbenzein • Ninhydrin
Orcinol • pH Indicators • p-Phenylenediamine DiHCl • Phloroglucinol
Protocatechuic Acid • Sodium Tetraphenylboron • Sulfosalicylic Acid
Tetramethyl Ammonium Chloride & Hydroxide • n- & iso-Valeraldehydes

Write for our Products List of over 3000 chemicals

Tel: 516-273-0900 TWX: 510-227-6230

EASTERN CHEMICAL
Division of GUARDIAN CHEMICAL CORP.

P.O. Box 2500
DEPT AC
SMITHTOWN, N.Y. 11787

USE LABORATORY SERVICE CENTER

Laboratory Service Center (Equipment, Materials, Services, Instruments for Leasing). Maximum space — 4 inches per advertisement. Column width, 2-3/16"; two-column width, 4-9/16". Artwork accepted. No combination of directory rates with ROP advertising. Rates based on number of inches used within **12** months from date of first insertion. Per inch: **1" — $85; 12" — $84; 24" — $81; 36" — $78; 48" — $77.**

CALL OR WRITE BARBARA AUFDERHEIDE

ANALYTICAL CHEMISTRY
25 Sylvan Road South
Westport, Ct. 06881
203-226-7131

INDEX TO ADVERTISERS IN THIS ISSUE

CIRCLE INQUIRY NO.	ADVERTISERS	PAGE NO.
1	* Alltech Associates, Inc. — Chromad Agency	1057A
3	* Applied Research Laboratories — J. B. Talmadge & Company, Inc.	1042A-1043A
2	Ashland Chemical Company — Marsteller, Inc.	1097A
27	Barnes Analytical Div./Spectra-Tech — Lorenz Hansen	1073A
23	Beckman AIS Div. — NW Ayer ABH International	1026A-1027A
25	Beckman SID — NW Ayer ABH International	1047A
22	* Bioanalytical Systems, Inc. — Kissinger Advertising Associates	1065A
26	* Bio-Rad Laboratories-Chemical Division — Fred Schott & Associates	1094A
19, 20	* Sybron/Brinkmann — Hanson, Fassler & Associates-Blatt Health	OBC
24	Burdick & Jackson Lab., Inc. — Studio 5 Advertising, Inc.	1093A
38-40	* Cahn Instruments — Brigham/Scully, Inc.	1107A
41	* Chemical Data Systems — Levy Associates	1136A
32	* Chromatix — David R. McClurg	1031A
37	Corco Chemical Corporation — SIT/COM	1105A
34	Corp Scientifique Claisse — Pierre Tremblay Publicite, Inc.	1118A
36	Coulter Electronics — Gary Singer Communications, Corp.	1129A
35	Crawford Fitting — Falls Advertising Company	1116A
XX	Digital Equipment — Benton & Bowles	1121A
52-53	* Dionex — Dionex Communications	1039A
50	* Dohrmann — Fred Schott & Associates	1023A
63	Eldex Laboratories — Eli Media	1036A
86	* Finnigan Corporation — F & M Advertising	1124A
88	* Fisher Scientific Co.	1041A
87	* Foxboro Analytical — STG Marketing Communications, Inc.	1106A
90	Galileo Electro-Optics Corp. — Edward E. Heske Associates	1092A
89	* Gilson Medical Electronics — Fred Schott & Associates	1049A
91, 92	Gow-Mac — Kenyon Hoag Associates	1073A, 1109A
97	Hach Company — Art Service/Technical Promotions	1122A
96	* Hamilton Company — Mealer & Emerson	1082A-1083A
98	* Helma International — Miller Advertising Agency, Inc.	1036A
101-102	* Hewlett-Packard Company — Corporate Marketing Communications	1099A

INDEX TO ADVERTISERS IN THIS ISSUE

CIRCLE INQUIRY NO.	ADVERTISERS	PAGE NO.
99-100	* **Houston Instruments Div. of Bausch & Lomb** Cooley & Shillinglaw, Inc.	IFC
115	* **ISCO, Inc.-Environmental Division** Farneaux Associates	1110A
108	**J & W Scientific**	1038A
122	**Kewaunee Scientific** Communications Concepts	1046A
123	** **Kipp Analytica** Reclame Adviesbureau	1120M
120-121	**Kontron Electronics, Inc.**	1113A
124	** **Kontron Ltd.** Kontron Analytic	1120D
126	**Lachat Chemicals, Inc.** Consulting Associates	1102A
141	**Mallinckrodt, Inc.-Science Products Div.** Abelson Taylor, Inc.	1033A
139-140	**Manostat Corporation** KAS Studios Inc.	1122A
144-149	* **Matheson** Kenyon Hoag Associates	1035A
143	* **Mitsubishi Chemical Industries** Global Advertising Co., Ltd	1085A
152-153	* **Nicolet Instrument Corp.** Technical Communications	1037A
155	* **Norton Company** The Jayme Organization, Inc.	1066A
157	**Oriel Corporation of America** Oriel Advertising	1040A
156	* **Orion Research, Inc.** OBC Advertising	1029A
159	**Outokumpu OY** Erva-Latvala OY	1090A
170	**PCR Research Chemicals** Media Marketing	1122A
171-172	* **Perkin-Elmer Corporation** Marquardt & Roche, Inc.	1131A
175	**Petrarch Systems, Inc.** The Matlin Company, Inc.	1073A
176	** **Philips Science & Industry** Vaz Dias Internationale	1120I-1120J
78-84	** **Pye Unicam** Rory Connors Publicity	1120E-1120H
181	**Quantachrome Corporation**	1140A
184	**Radiometer America, Inc.** Forte Communications	1127A
185, 186	* **Rheodyne** Bonfield Associates	1071A, 1136A
188	**Sartorius GMBH** Werbestudio Baars	1091A
104	** **Schott** Werbeagentur Frenz	1120L
190	** **Schott Gerate GmbH** Werbeagentur Frenz GmbH	1120R
195	* **Scientech, Inc.** Karsh & Hagan Advertising	1044A
194	**Scientific Apparatus Exchange**	1093A
187, 196	* **Scientific Glass Engineering, Inc.** Arden Advertising Agency	1058A, 1095A
193	**Scott Specialty Gases** The Matlin Company	1048A
191-192	* **Shimadzu Corporation** General Advertising Agency, Inc.	1133A, 1135A
189	* **Siemens Corporation** Hogan Gazzara Associates	1061A
198	* **G. Frederick Smith Chemical Company** Andrew Show Advertising	1109A
206	**Tracor Northern, Inc.**	1055A
220-222	* **Valco Instrument Company, Inc.** Cooley & Shillinglaw, Inc.	1115A
238-245	* **Varian Instrument Division** Moran Lanig & Duncan Advertising	1100A, 1101A, 1102A
235	**Waters Associates**	1068A
227	**Whatman Laboratory Products, Inc.** J. S. Lanza & Associates	1104A
229	* **John Wiley & Sons, Inc.** 605 Advertising Group	1119A

** See ad in ACS Laboratory Guide*

*** Company so marked has advertisement in Foreign Regional edition only.*

Advertising Management for the American Chemical Society Publications

CENTCOM, LTD.

Thomas N. J. Koerwer, President; James A. Byrne, Vice President; Alfred L. Gregory, Vice President; Clay S. Holden, Vice President; Benjamin W. Jones, Vice President; Robert L. Voepel, Vice President; 25 Sylvan Rd. South, Westport, Connecticut 06881 (Area Code 203) 226-7131

ADVERTISING SALES MANAGER
James A. Byrne

SALES REPRESENTATIVES

Atlanta, GA . . . Don Davis, CENTCOM, LTD. Telephone: 203-226-7131

Boston, MA . . . Don Davis, CENTCOM, LTD. Telephone: 203-226-7131

Chicago . . . Bruce E. Poorman, CENTCOM, LTD., 540 Frontage Rd., Northfield, Ill. 60093, 312-441-6383

Cleveland . . . Bruce E. Poorman, CENTCOM, LTD., 17 Church St., Berea, Ohio 44017, 216-234-1333

Houston . . . Robert LaPointe, CENTCOM, LTD., 415-781-3430

Denver . . . Clay S. Holden, CENTCOM, LTD., 213-325-1903

Los Angeles . . . Clay S. Holden, CENTCOM, LTD., Newton Pacific Center, 3142 Pacific Coast Highway, Suite 200, Torrance, CA 90505, 213-325-1903

New York . . . Dean A. Baldwin, Don Davis, CENTCOM, LTD., 60 East 42nd St., 212-972-9660, New York, N.Y. 10165

Philadelphia . . . Dean A. Baldwin, Jerry Naab, CENTCOM, LTD., GSB Building, Suite 425, 1 Belmont Avenue, Bala Cynwyd, Pa. 19004. Telephone: 215-667-9666

San Francisco, CA . . . Robert E. LaPointe, CENTCOM, LTD., Suite 303, 211 Sutter Street, San Francisco, CA 94108. Telephone: 415-781-3430

Westport, CT . . . Don Davis, CENTCOM, LTD., 25 Sylvan Rd. South, Westport, Ct. 06881. Telephone: 203-226-7131

United Kingdom
Lancashire, England . . . Technomedia Ltd., c/o Meconomics Ltd., Meconomics House, 31 Old Street, Ashton Under Lyne, Lancashire, England.
Reading, England . . . Malcolm Thiele, Technomedia Ltd., Wood Cottage, Shurlock Row, Reading RG10 OQE. Berkshire, England. Telephone: 073-581-302

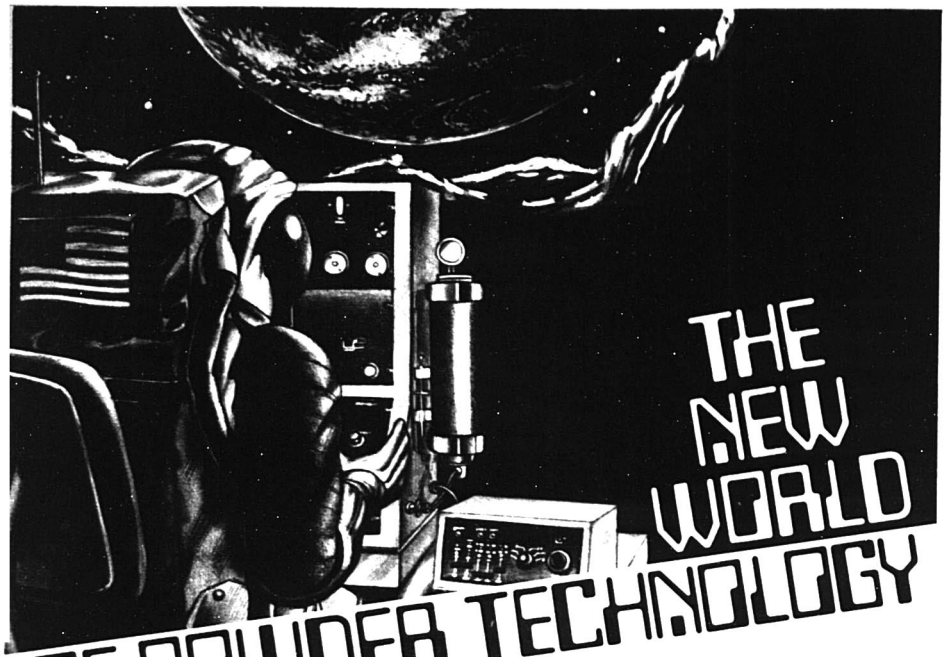
Tokyo, Japan . . . Shigeo Aoki, International Media Representatives Ltd., 2-29 Toranomon, 1-Chome Minato-ku Tokyo 105 Japan. Telephone: 502-0656

Continental Europe . . . Andre Jamar, Rue Mallar 1, 4800 Verviers, Belgium. Telephone: (087) 22-53-85, Telex #49263

PRODUCTION DEPARTMENT

Production Director
Joseph P. Stenza

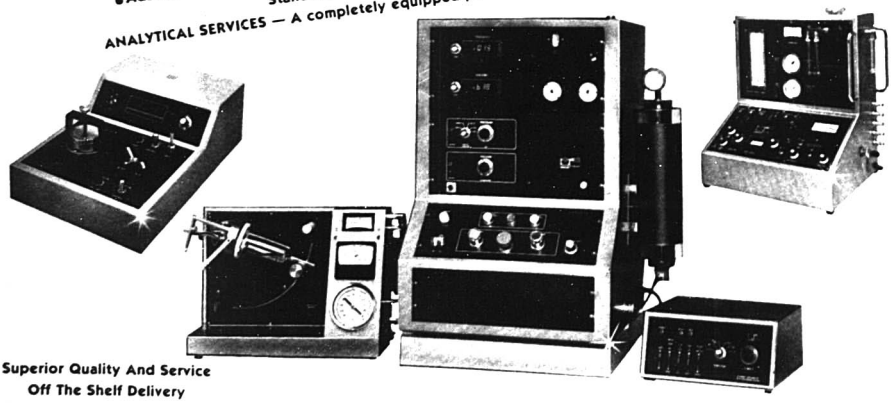
Advertising Production Manager
Barbara Aufderheide



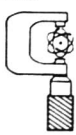
SUPERIOR INSTRUMENTS FOR

• Surface Area • Pore Size Distribution by Mercury Intrusion and Gas Adsorption • Outgassing
• Adsorption/Desorption Isotherms • Chemisorption Studies • True Powder Density • Riffling
Standard Reference Materials for Surface Area Analyses

ANALYTICAL SERVICES — A completely equipped powder technology laboratory to serve your needs.



Superior Quality And Service
Off The Shelf Delivery



QUANTACHROME
CORPORATION POWDER INSTRUMENTATION

Six Aerial Way, Syosset, NY 11791
TWX: 510 221 2239 • TEL: 516-935-2240

CIRCLE 181 ON READER SERVICE CARD

One reason to have your own subscription to analytical chemistry



is that it won't be worn, torn, and several months late when you see it. And besides, you can always clip your own copies . . . and refer to back issues when you want!



Subscribe now, you'll receive FOURTEEN information-packed issues including THE ANNUAL LABORATORY GUIDE TO INSTRUMENTS, EQUIPMENT, AND CHEMICALS and the special APRIL ANNUAL REVIEWS . . . **no wonder it's called the greatest bargain in chemical literature today!**

Fill in the order form now – we'll do the rest!

Please send me ANALYTICAL CHEMISTRY at the following subscription rate:	ACS Members*	U.S.	Canada	Foreign**
	1-Year	☐ $15.00	☐ $28.00	☐ $ 28.00
	3-Years	☐ $36.00	☐ $75.00	☐ $ 75.00
	Nonmembers			
	1-Year	☐ $20.00	☐ $33.00	☐ $ 43.00
	3-Years	☐ $48.00	☐ $87.00	☐ $111.00

CALL TOLL FREE: NEW ORDERS: 800-424-6747 **1981**

☐ Bill me ☐ Bill company ☐ Payment enclosed** (payable to American Chemical Society)

Charge my ☐ Master Card ☐ VISA

Card # _____ Interbank # _____ (Master Card Only)

Exp. Date _____ Signature _____

Name _____

Job Title _____

Your Employer _____
☐ Home
Address ☐ Business _____

City _____ State _____ Zip _____
Employer's Business ☐ Manufacturing ☐ Academic
☐ Government ☐ Other _____

If manufacturing type of products produced _____

*Subscriptions at ACS Member Rates are for personal use only.
**Payment must be made in U.S. Currency, by international money order, UNESCO coupons, U.S. bank draft, or through your subscription agency.

Please allow 60 days for your first copy to be mailed. 1110K

Please send me ANALYTICAL CHEMISTRY at the following subscription rate:	ACS Members*	U.S.	Canada	Foreign**
	1-Year	☐ $15.00	☐ $28.00	☐ $ 28.00
	3-Years	☐ $36.00	☐ $75.00	☐ $ 75.00
	Nonmembers			
	1-Year	☐ $20.00	☐ $33.00	☐ $ 43.00
	3-Years	☐ $48.00	☐ $87.00	☐ $111.00

CALL TOLL FREE: NEW ORDERS: 800-424-6747 **1981**

☐ Bill me ☐ Bill company ☐ Payment enclosed** (payable to American Chemical Society)

Charge my ☐ Master Card ☐ VISA

Card # _____ Interbank # _____ (Master Card Only)

Exp. Date _____ Signature _____

Name _____

Job Title _____

Your Employer _____
☐ Home
Address ☐ Business _____

City _____ State _____ Zip _____
Employer's Business ☐ Manufacturing ☐ Academic
☐ Government ☐ Other _____

If manufacturing type of products produced _____

*Subscriptions at ACS Member Rates are for personal use only.
**Payment must be made in U.S. Currency, by international money order, UNESCO coupons, U.S. bank draft, or through your subscription agency.

Please allow 60 days for your first copy to be mailed. 1110K

NO POSTAGE
NECESSARY
IF MAILED
IN THE
UNITED STATES

BUSINESS REPLY CARD
FIRST CLASS PERMIT NO. 10094 WASHINGTON, D.C.

POSTAGE WILL BE PAID BY ADDRESSEE

AMERICAN CHEMICAL SOCIETY
Circulation Dept.
1155 Sixteenth Street, N.W.
Washington, D.C. 20036

NO POSTAGE
NECESSARY
IF MAILED
IN THE
UNITED STATES

BUSINESS REPLY CARD
FIRST CLASS PERMIT NO. 10094 WASHINGTON, D.C.

POSTAGE WILL BE PAID BY ADDRESSEE

AMERICAN CHEMICAL SOCIETY
Circulation Dept.
1155 Sixteenth Street, N.W.
Washington, D.C. 20036

analytical chemistry

EDITOR: **GEORGE H. MORRISON**

EDITORIAL HEADQUARTERS
1155 Sixteenth St., N.W.
Washington, D.C. 20036
Phone: 202-872-4570 Teletype: 710-8220 151

Executive Editor: Josephine M. Petruzzi
Managing Editor: Barbara Cassatt
Associate Editor: Stuart A. Borman
Editorial Assistants:
Marcia Cohen, Jacquelyn Danes, Rani A. George
Production Manager: Leroy L. Corcoran
Art Director: John V. Sinnett
Staff Artist: Linda M. Mattingly
Copy Editor: Gail M. Mortenson
Circulation Manager: Cynthia G. Smith

Journals Dept., Columbus, Ohio
Associate Head: Marianne Brogan
Assistant Editor: Rodney L. Temos

Advisory Board: L.S. Birks, Donald D. Bly, Richard Durst, Shizuo Fujiwara, Georges Guiochon, Wilbur I. Kaye, Bruce R. Kowalski, Robert A. Libby, Robert S. McDonald, Royce W. Murray, Richard S. Nicholson, Janet Osteryoung, Robert E. Sievers, Walter Slavin, Rudolph H. Stehl, John P. Walters

Instrumentation Advisory Panel: Nelson L. Alpert, Edward Chait, Stuart P. Cram, Martin S. Frant, Tomas Hirschfeld, Fred E. Lytle, Carter L. Olson, Thomas H. Ridgway, Yair Talmi

Contributing Editor, The Analytical Approach: Jeanette G. Grasselli

The Analytical Approach Advisory Panel: Edward C. Dunlop, Robert A. Hofstader, Wilbur D. Shults

Regulatory Affairs, Analytical Division Committee: Fred Freeberg (Chairman)

Published by the
AMERICAN CHEMICAL SOCIETY
1155 16th Street, N.W.
Washington, D.C. 20036

Books and Journals Division
Director: D. H. Michael Bowen
Journals: Charles R. Bertsch
Production: Elmer Pusey, Jr.
Marketing & Sales: C. K. Robinson
Research and Development: Seldon W. Terrant

Manuscript requirements are published in the January 1981 issue, page 139. Manuscripts for publication (4 copies) should be submitted to ANALYTICAL CHEMISTRY at the ACS Washington address.

The American Chemical Society and its editors assume no responsibility for the statements and opinions advanced by contributors. Views expressed in the editorials are those of the editors and do not necessarily represent the official position of the American Chemical Society.

The Gordon Research Conferences—Golden Jubilee

This year marks the Golden Jubilee of the Gordon Research Conferences, which have become a unique and vital medium for the exchange of ideas and information. The conferences, which were started by Johns Hopkins University chemistry professor Neil E. Gordon, have grown in number from one in 1931 to 115 this year. Each brings together about 100 researchers for five days in an environment that encourages informality and maximum interaction. Conferees include scientists from academia, industry, and government who are active at the frontiers of an expanding field. Most of the conferences are held during the summer on campuses of private schools in rural New Hampshire. A limited number of talks are scheduled, and ample time is allowed for discussion. To encourage open exchange of ideas, the talks and discussions are not recorded.

The first conferences of direct interest to analytical chemists were those on "Instrumentation" starting in 1946 and "Ion Exchange" starting in 1949. In 1950, the first conference on "Current Trends in Analytical Chemistry" was held, with leading speakers such as N.H. Furman, H.S. Strain, R.H. Müller, Charles E. White, Grant Wernimont, W.J. Youden, J.J. Lingane, W.E. Campbell, and C.W. Gould covering the topics of instrumental analysis, chromatographic adsorption, fluorescence analysis, statistical methods of analysis, electrical methods of analysis, and organic analysis.

To mark the Golden Jubilee year, the theme of the conference on "Analytical Chemistry," being held this month at the New Hampton School, is "Research Trade-off To Achieve Selectivity in Analyses, Sensitivity of Detection, and Speciation in Determinations." The conference chairman, Frederick Brech, has organized an excellent program (see the May issue of ANALYTICAL CHEMISTRY, p 713 A) that properly reflects the health and vigor of the discipline.

There is no shortage of meetings today for the oral communication of research results; however, the Gordon Conferences are something special. They provide a forum where young researchers and graduate students have an opportunity to meet and interact with established leaders in the field. Over the years, many careers have been launched, and lifelong friendships established at these conferences. More importantly, new ideas generated at these conferences have had a profound influence on the future of analytical chemistry.

G. H. Morrison

Verification of Retention and Zone Spreading Equations in Sedimentation Field-Flow Fractionation

George Karaiskakis,[1] Marcus N. Myers, Karin D. Caldwell, and J. Calvin Giddings*

Department of Chemistry, University of Utah, Salt Lake City, Utah 84112

It is argued that accurate characterization of complex particle and macromolecule populations by field-flow fractionation (FFF) hinges, in large part, on the agreement between FFF theory and experiment with respect to retention and zone spreading. After briefly reviewing past comparisons of theory and experiment, we summarize the relevant theoretical equations. Two sedimentation FFF systems are described and results are presented for polystyrene latex beads that are presumably well characterized. Very close (~1%) agreement in retention measurements and theory for some samples contrasts strongly with cases having serious discrepancies. It is suggested that the discrepancies are due to the inaccurate specifications given for particle diameters. The zone spreading (plate height) measurements verify this, demonstrating rather uniform consistency with the retention measurements but not with some reported diameters. It is concluded that theory and experiment agree very well (a few percent) for retention parameters and within 5–10% for plate height parameters.

One of the analytical strengths of field-flow fractionation (FFF) is that separation occurs in a channel of such simple geometry, within which there is flow of such uniform profile, that exact equations can be developed relating such component's retention and zone spreading to underlying physicochemical parameters. Presumably, then, the measurement of a solute's behavior in an FFF channel can be used to deduce these physicochemical parameters, thus helping characterize or identify the solute material. It is therefore important to determine the closeness of the agreement between theory and experiment in FFF to assess the potential accuracy of this procedure. Consequently, a number of studies of retention and zone spreading have been made by using various subtechniques of FFF (*1–8*). Generally, the retention equations have been well verified, often accurate to within a few percent. Zone spreading measurements are subject to larger relative uncertainties than retention measurements. In the most meticulous of previous studies, using linear polystyrene polymers in 11 different thermal FFF channels, the departure from theory averaged approximately 30% (*8*).

Sedimentation FFF, using polystyrene latex beads as sample probes, would appear to be an ideal combination to test the agreement between theory and experiment. Such beads are used as standards in electron microscope measurements and the necessary size, density, and polydispersity parameters are available from the manufacturer. Earlier experiments with such beads verified the applicability of the FFF retention equations but encountered large discrepancies in zone spreading (*2*). In this study we will reconfirm the retention studies and then attempt to improve zone spreading measurements to a level of accuracy where meaningful comparisons with theory can be made.

[1] Present address: Department of Chemistry, Univeristy of Patras, Patras, Greece.

THEORY

The theory of FFF has been developed and refined in several papers (*6, 9–11*). Below we summarize the basic relationships which govern retention and zone spreading in FFF systems, with particular focus on sedimentation FFF.

Retention. The basic retention equation for FFF shows retention ratio R to be uniquely related to the reduced layer thickness of the zone, λ, in the following manner

$$R = 6\lambda[\coth 1/2\lambda - 2\lambda] \quad (1)$$

Retention ratio R is determined experimentally as the ratio of the column void volume V° to the retention volume V_r of the component zone

$$R = V^\circ / V_r \quad (2)$$

Under conditions of high retention the solute layer is strongly compacted, leading to small values for parameter λ. Under these circumstances the value of the bracketed term in eq 1 approaches unity, and we have

$$\lim_{\lambda \to 0} R = 6\lambda \quad (3)$$

In the special case of sedimentation FFF the reduced layer thickness takes the form

$$\lambda = \frac{kT}{Gm(1 - \rho/\rho_s)w} \quad (4)$$

where G is the acceleration (gravitational) field imposed on solute particles of mass m and density ρ_s, ρ is the carrier density, w is the thickness of the flow channel, T is the temperature, and k the Boltzmann constant. In the case of spherical solute particles, λ can be expressed in terms of particle diameter d

$$\lambda = \frac{6kT}{\pi d^3 \Delta\rho G w} \quad (5)$$

where $\Delta\rho$ is the density difference between solute and solvent, $\rho_s - \rho$.

Plate Height. Zone spreading is measured by plate height H exactly as in chromatography. The factors influencing plate height in field-flow fractionation can be summarized in a relationship similar to the equation governing chromatography in capillary tubes (*12*)

$$H = \frac{2D}{R\langle v\rangle} + \chi\frac{w^2\langle v\rangle}{D} + \sum H_i = \frac{B}{\langle v\rangle} + C\langle v\rangle + \sum H_i \quad (6)$$

where D is the diffusion coefficient of the solute in the solvent or carrier fluid, $\langle v\rangle$ the mean linear fluid velocity, and χ the λ-dependent nonequilibrium coefficient which has the following limit at high retention (*6*):

$$\lim_{\lambda \to 0} \chi = 24\lambda^3 \quad (7)$$

The substitution of eq 5 into 7 and the latter into eq 6, combined with the Stokes–Einstein equation for D, leads to the following coefficient of $\langle v\rangle$ for the second term:

0003-2700/81/0353-1314$01.25/0 © 1981 American Chemical Society

$$C = \frac{15552}{\pi^2} \frac{\eta(kT)^2}{w(\Delta\rho G)^3} \frac{1}{d^8} \quad (8)$$

The first term on the right-hand side in eq 6 describes zone spreading due to longitudinal diffusion, the second accounts for nonequilibrium or mass transfer effects, and the third is a composite term which includes any disturbances due to imperfect channel design, relaxation processes (initial establishment of the zonal equilibrium distribution), width of the injection slug, end effects, polydispersity, etc.

In practical work, the first term of eq 6 is negligible because of the sluggish diffusion of large solute species. If stop-flow procedures are used, the relaxation contribution to plate height is negligible. With proper equipment design and careful procedures, all contributions to $\sum H_i$ except polydispersity can be practically eliminated, leaving $\sum H_i$ as a measure of the polydispersity of the sample.

If the sample is indeed polydisperse, its different components experience different degrees of retention in the channel due to differences in mass, and as a result the composite zone is broadened. The polydispersity contribution to peak variance σ_p^2 can be calculated as (2)

$$\sigma_p^2 = \left(\frac{dX}{dd}\right)^2 \sigma_d^2 \quad (9)$$

where X is the distance migrated by a particle of diameter d in a given time, and σ_d^2 is the variance in the particle diameter within the sample. This equation can be converted to a plate height expression based on FFF parameters in a series of simple steps (2). For a well-retained peak ($\lambda \to 0$) in a uniform channel of length L the expression becomes

$$H = 9L(\sigma_d/d)^2 \quad (10)$$

If we assume that polydispersity and nonequilibrium are the only important plate height terms, H assumes the following simple form, linear in velocity $\langle v \rangle$:

$$H = C\langle v \rangle + H_p \quad (11)$$

By using eq 8 and 10 in conjunction with eq 11, it is possible to make quantitative comparisons between experimental and theoretical nonequilibrium and polydispersity contributions to the zone spreading in sedimentation FFF.

Secondary Flow. The foregoing theoretical equations hinge on the presence of a uniform, axially directed parabolic flow in the channel in which edge effects are neglected. However, it is known that fluid flowing in a spinning duct is subject to a nonaxially directed secondary flow (*13*), which, if it is strong enough, will circulate the solute over the channel cross section. Significant circulation would be expected to hinder retention and increase plate height, causing important departures from the theoretical equations noted above. However, as noted in an early paper (2), secondary flow is inhibited by a rectangular channel of large breadth to thickness ratio ($\sim 10^2$), such as we routinely use. Nonetheless, some secondary flow will exist. Its effects are expected to be quite different if the flow and spin directions are the same (parallel) rather than acting in opposition (antiparallel). If the former, there will be a gradual motion of solute (in the case where solute is compressed toward the outer wall of the channel) toward the channel edges. If the latter, the solute will move toward the midway plane dividing the channel breadth a. Figure 1 shows a schematic representation of the former. The true situation can be more complex, with the lateral flow profile dividing into additional cells under some circumstances.

There is some possibility that a mild secondary flow under antiparallel flow-spin conditions would remove solute from the edges of the channel where, normally, a perturbation from parabolic flow occurs. However, this benefit may be offset by the "updraft" at the center tending to carry solute to higher than calculated elevations and by an undue concentration of solute near the midway plane. These factors require theoretical attention. Our emphasis here is on qualitative aspects of secondary flow as a prelude to some empirical tests to follow.

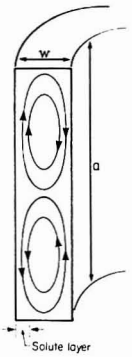


Figure 1. Secondary flow in a sedimentation FFF channel in which the direction of flow and spin are the same. The arrows are reversed when the directions of flow and spin are opposite.

EXPERIMENTAL SECTION

The general characteristics of our experimental sedimentation FFF device have been described (*14*). Two sedimentation FFF systems which differed mainly with respect to channel thickness were used in this study. The dimensions of channel I were $w = 0.0254$ cm, length $L = 83.3$ cm, and breadth $a = 2.00$ cm; channel II had $w = 0.0127$ cm, $L = 79.4$ cm, and $a = 2.00$ cm. The rotor radius was 7.7 cm for each of the two instruments. Control of rotation for the channel I system was provided by equipment designed and built in this laboratory, while the channel II system was controlled by a D-C motor speed control, type DPM-6130 E, from Bodine Electric Co., Denver, CO. The rates of rotation were determined in both cases by an in-house built digital counter.

The carrier fluid was degassed at 80 °C and pumped through channel II by a Model Minipuls 2 metering pump from Gilson Medical Electronics, Middleton, WI, and through channel I by a metering pump of type CMP-1 from Laboratory Data Control Inc., Riviera Beach, FL. Following channel II was a UV monitor Model 1205 also from Laboratory Data Control, Inc., Riviera Beach, FL, while the effluent from channel I was monitored by an Altex Analytical UV detector, Model 153, from Beckman Instruments, Inc., Berkeley, CA. Both detectors used a wavelength of 254 nm, and their respective signals were fed to Omniscribe recorders from Houston Instrument, Inc., Austin, TX.

The samples employed in this study were spherical polystyrene latex beads from Dow Diagnostics Indianapolis, Inc., nominal particle diameters of 0.220, 0.357, 0.481, 0.620, and 0.945 μm, respectively. The standard deviations in these diameters were given as 0.0065, 0.0056, 0.0018, 0.0076, and 0.0064 μm, respectively. All beads were assumed to have a density of 1.05 g/cm^3. The samples, as supplied by the manufacturer, were all suspensions of 10% (by weight) solids in an aqueous detergent.

The carrier solutions were doubly distilled water containing FL-70 detergent from Fisher Scientific Co., Pittsburgh, PA, 0.5% FL-70 in the case of channel II, and 0.1% in the case of channel I. To both carriers was added a small amount (0.02%) of sodium azide as a bacterocide.

The samples were introduced by means of microsyringes (10 and 25 μL) from Hamilton Co., Reno, NV. In all exper-

Table I. FFF Retention Data for Polystyrene Latex Spheres[a]

d (nominal value, in μm)	rpm	v, mm/s	w, μm	R_{expt}	λ (from R_{expt})	R_{calcd}	$(R_{expt} - R_{calcd})/R_{calcd} \times 100$
0.220	1440	0.3-3.3	254	0.191 ± 0.004	0.032	0.186	+2.7
0.357	1500	1.8-7.4	127	0.085 ± 0.001	0.014	0.084	+1.2
0.357	880	0.1-3.4	254	0.124 ± 0.002	0.021	0.120	+3.3
0.481	500	0.3-3.3	254	0.122 ± 0.003	0.020	0.150	−18.7
0.620	600	0.8-7.6	127	0.101 ± 0.002	0.017	0.100	+1.0
0.945	400	1.4-7.7	127	0.080 ± 0.001	0.013	0.064	+25.0

[a] The calculated values of R, R_{calcd} are based on nominal (manufacturer's) d values using eq 5 combined with eq 1. The runs were made at 25 °C in a carrier with density $\rho = 1.00$ g/mL.

riments the injected sample was 1 μL. The injection was immediately followed by a 12-min stop-flow period to allow for relaxation.

Retention ratio R was measured as the volume of a nonretained peak (acetone) divided by the elution volume recorded for the sample peak. Both volumes were corrected for the dead volume encountered between channel exit and detector cell. These dead volumes were 0.15 mL for channel II and 0.20 mL for channel I.

Plate height calculations were based on the measured peak width at half-height on the recorder tracing.

RESULTS AND DISCUSSION

Retention. The results from retention measurements are reported in Table I. The two different channels employed are indicated by their different thickness, w, 254 and 127 μm, respectively. The experimental R values were obtained as an average of five to ten individual values calculated at different flow velocities extending over the range shown under the $\langle v \rangle$ column.

The overall agreement between experimental and calculated R values is reasonably good, and in some specific cases, excellent. However, in other cases the departures are substantial. Because the various FFF retention experiments appeared to be quite consistent with one another, we have investigated the possibility that the reported particle diameters might be in error, thus leading to the observed discrepancy. We have noted substantial discrepancies in previous studies with latex beads from another manufacturer (*3*).

The diameter and polydispersity of the latex spheres were determined by the manufacturer from electron microscopic observations. However, as indicated by independent electron microscopy studies on other polystyrene latex preparations from Dow, there are, in some instances, substantial discrepancies between results obtained by different observers (*15*, *16*). The impact of the electron beam apparently causes a noticeable shrinkage of latices, which in turn makes recorded particle diameters highly dependent on the microscopic procedure used to obtain such data.

The size distribution for any given sample is recorded from micrographs of 10^2–10^3 beads per picture. As these beads are all exposed to the electron beam in a uniform manner, it is reasonable to assume a uniform shrinkage of all particles. The relative standard deviation in size should thus be a reasonably reliable number, particularly for samples where the number of measured beads approaches 10^3.

Because of the excellent agreement between measured and calculated retention in three of the six systems studied, and the self-consistency of the results reflected in the low standard deviations in R values and the very close agreement of two separate channels with the calculated values for 0.357-μm beads, it appears that retention in sedimentation FFF can be predicted quite accurately under the experimental conditions used here. The annoying discrepancies found for three other systems can, we have found, possibly be traced to errors in reported bead diameters.

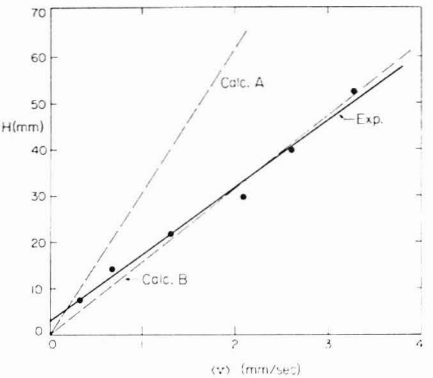


Figure 2. Plate height vs. flow velocity plots for nominal 0.481-μm polystyrene latex beads.

Fortunately, the study of peak spreading, which we initially undertook as an independent investigation, can be used to produce additional evidence bearing on this matter. This is a consequence of the fact that both retention (eq 1 and 3) and the nonequilibrium contribution to plate height (eq 7) depend solely on λ, thus linking the two together with a common, size-dependent (eq 5) parameter.

Zone Spreading. Equation 11 suggests that the plate height–flow velocity relationship is linear, with slope C and intercept H_p. This conclusion is substantially verified by our data, an example of which we have plotted in Figure 2. In that H_p and C are calculable for a well-defined particle sample using eq 8 and 10, the experimental plot can be compared with a theoretical plot, the latter shown as "calculated, A" in Figure 2. The figure shows that the discrepancy between the two is substantial, the slope of the experimental line being very much lower. Since all $\sum H_i$ terms add to the plate height, neglect of important velocity-dependent terms would result in too low a value for the calculated slope. Our observed plate heights are in this case substantially lower than the calculated values, indicating that some other problem must exist.

Next we examine the possibility that the discrepancy is caused by an incorrect particle diameter. The slope C would reflect this error dramatically because of the 8 power dependence of C on d (eq 8). In order to check this possibility, we have used λ values from the retention data of Table I to calculate C ($C = 24\lambda^3 w^2/D$ with D calculated from $D = kT/3\pi\eta(6kT/\pi\lambda w\Delta\rho G)^{1/3}$) rather than eq 5 which requires some preassumed d value. When C is calculated on this basis, the slope is in better agreement with the data, as shown by the line "calculated, B" in Figure 2. This lends very strong support to the contention that the reported particle diameter is in error and is responsible for the discrepancy. The con-

Table II. Plate Height Parameters for Polystyrene Latex Spheres (Temperature 25 °C, carrier viscosity 0.01 P)

d (nominal value, in μm)	slope C, s				intercept, mm	
	w, μm	exptl	B^c	A^d	exptl	expected from manufacturer's data
0.220	254	28.27 ± 1.78	30.70	33.53	2.8 ± 3.5	6.5
0.357	127	0.93 ± 0.04	0.96	0.88	1.5 ± 0.2	1.8
0.357	254	11.93 ± 0.15	12.53	11.38	2.5 ± 0.3	1.8
	254	(11.72 ± 0.15)p[a]			(2.5 ± 0.3)p	
	254	(11.71 ± 0.14)a[b]			(3.5 ± 0.3)a	
0.481	254	14.26 ± 0.94	17.48	30.80	3.0 ± 1.9	0.1
0.620	127	2.80 ± 0.12	2.84	2.68	1.8 ± 0.5	1.1
0.945	127	1.78 ± 0.05	1.99	1.05	1.4 ± 0.2	0.3

[a] Parallel spin flow. [b] Antiparallel spin flow. [c] Values calculated from retention values. [d] Values calculated from nominal d values.

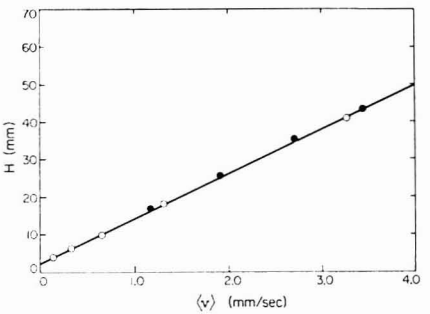


Figure 3. Experimental plate height vs. flow velocity plot for 0.357-μm nominal beads under conditions of parallel (open circles) and antiparallel (solid circles) spin flow.

sistency of the two top lines in Figure 2 also verifies that the observed plate height is in good agreement with theoretical predictions.

Table II shows the relevant results for all of the latex beads measured. Columns A and B under the "slope C" heading correspond to calculated lines A and B in Figure 2. A comparison of the "experimental" column and B shows agreement with 10% in all cases and down to about 5% in several cases. In all but two of the six cases the "B" calculations lie within 2 standard deviations of the experimental slope. Thus the discrepancy between the two is neither large nor particularly systematic. The results suggest that observed plate height values are indeed calculable, if one has the correct parameter for the particles, within 5–10%. This is considerably better than previous results.

The experimental intercept values to Table II show considerably more scatter than the slope values. This is a consequence of the smallness of the intercepts, which reflects the extremely low polydispersity of the latex beads. The reliability of the intercepts appears to be ~1 mm, which corresponds to a polydispersity, σ_d/d of only about 1%. The tendency for the intercepts to be somewhat larger than predicted may indicate a small plate height contribution due to dead volume effects, etc., or it may reflect an error in the reported polydispersity of the latex spheres. Unfortunately, there is no second approach for determining the reliability of the manufacturer's polydispersity values, as there is for mean particle diameter values.

With respect to evaluating the influence of secondary flow, we obtained plate height measurements for the 0.357-μm nominal beads under both parallel and antiparallel spin-flow conditions. The results are shown in Figure 3 and summarized in the terms in parentheses in Table II. No systematic difference between parallel and antiparallel conditions can be discerned from the figure. The slopes reported in Table II are also in near perfect accord, although some noticeable difference is found in the intercepts. We conclude that secondary flow does not have a very significant effect under present experimental conditions, but we leave open the question of its importance under other circumstances.

We note that we have found conditions under which there are signficant departures of theory and experiment. The problem is particularly severe for the larger beads at high flow rates. We are presently studying these departures in order to better define the range over which good theoretical–experimental agreement can be found.

In conclusion, we find that we can obtain very good self-consistency between theoretical and observed retention and plate height values in sedimentation FFF in our normal range of operations despite the lack of well-characterized particles. In fact, our results suggest that FFF data may be more reliable and exacting than data from other sources (such as the electron microscope) in reflecting the properties of particle populations, and thus in characterizing particles. We intend to pursue this avenue of investigation in future work.

LITERATURE CITED

(1) Smith, L. K.; Myers, M. N.; Giddings, J. C. *Anal. Chem.* **1977**, *49*, 1750.
(2) Giddings, J. C.; Yang, F. J. F.; Myers, M. N. *Anal. Chem.* **1974**, *46*, 1917.
(3) Giddings, J. C.; Myers, M. N.; Moellmer, J. F. *J. Chromatogr.* **1978**, *149*, 501.
(4) Giddings, J. C.; Lin, G. C.; Myers, M. N. *J. Colloid Interface Sci.* **1978**, *65*, 67.
(5) Myers, M. N.; Caldwell, K. D.; Giddings, J. C. *Sep. Sci.* **1974**, *9*, 47.
(6) Hovingh, M. E.; Thompson, G. H.; Giddings, J. C. *Anal. Chem.* **1970**, *42*, 195.
(7) Giddings, J. C.; Martin, M.; Myers, M. N. *J. Polym. Sci.* **1981**, *19*, 815.
(8) Martin, M.; Myers, M. N.; Giddings, J. C. *J. Liq. Chromatogr.* **1979**, *2*, 147.
(9) Giddings, J. C. *J. Chem. Phys.* **1968**, *49*, 1.
(10) Giddings, J. C. *J. Chem. Educ.* **1973**, *50*, 667.
(11) Giddings, J. C. *Sep. Sci.* **1973**, *8*, 567.
(12) Giddings, J. C. "Dynamics of Chromatography, Part I"; Marcel Dekker: New York, 1965.
(13) Benton, G. S.; Boyer, D. *J. Fluid Mech.* **1966**, *26*, 69.
(14) Giddings, J. C.; Myers, M. N.; Caldwell, K. D.; Fisher, S. R. In "Methods of Biochemical Analysis"; Glick, D., Ed.; Wiley: New York, 1980; p 79.
(15) Heard, M. J.; Wells, A. C.; Wiffen, R. D. *Atmos. Environ.* **1970**, *4*, 141.
(16) Porstendörfer, J.; Heyder, J. *Aerosol Sci.* **1972**, *3*, 141.

RECEIVED for review January 19, 1981. Accepted April 30, 1981. This project was supported by National Science Foundation Grant No. CHE 79-19879.

Conventional Packed Columns vs. Packed or Open Tubular Microcolumns in Liquid Chromatography

Georges Guiochon

Ecole Polytechnique, Laboratoire de Chimie Analytique Physique, Route de Saclay, 91128 Palaiseau Cedex, France

The results of a comparison between the performances of chromatographic columns can be drastically influenced by some changes in the conditions of the separation. The influence of the maximum pressure available as well as of the diameter of the particles or capillary tubes used is stressed. It is shown that a packed column and a capillary column of the same length give approximately the same efficiency (plate number) and the same analysis time if the diameter of the particles in the packed column is half the diameter of the capillary column and both are operated at the optimum flow velocity. Capillary columns must be only a few microns in diameter just to be competitive with conventional packed columns. Enormous technological difficulties must be solved to achieve high efficiencies with capillary columns. Finally, it is shown that whereas capillary columns are much faster than packed columns in gas chromatography, a similar advantage does not exist in liquid chromatography. Because the liquid phase compressibility is negligible compared to that of the gas phase, the much larger permeability of the open tubular column bears no consequence on the average velocity at which the column is operated.

There is currently a major effort to develop very efficient columns for liquid chromatography, columns which would have a much larger efficiency than the classical 20-30 cm long ones in current use (*1-6*). These columns would offer the possibility of analyzing very complex mixtures, an increasing necessity in petroleum studies, biochemical and clinical analysis, control of fermentation processes (*1*), water pollution analysis, etc. Such an analysis of mixtures containing more than 100 components can be achieved in gas chromatography, if open tubular columns 100 m long or more, with 100-300 μm inner diameter are used (*7-10*). There is no way yet to practically carry out these separations in LC.

Three main different approaches have been used: true open tubular columns (OTC), also called capillary columns (*2, 3*); packed capillary columns (PCC) (*11*); and conventional packed columns (PC) (*1, 12*). The last approach, which is currently far beyond the development stage (*1, 13*), has been the most successful one, as it is the only one which has supplied true, practical analyses. The purpose of this paper, then, is to compare the results which can be expected from the first two approaches to the results already achieved by simply increasing the length of conventional packed columns (*1, 12, 13*). These results can be predicted by the extrapolation of experimental results obtained on 20-50 cm long conventional packed columns (*5*).

I. THEORETICAL FRAMEWORK FOR COMPARISON AMONG THE PERFORMANCES OF VARIOUS COLUMN TYPES

The optimization of such complex processes as chromatographic separation is difficult and involved. Using an identical approach and the same equations, two theoreticians can arrive at quite different conclusions if they make only slight different assumptions regarding which parameters are kept constant during the comparison process, which numerical values are chosen as most representative of the studied phenomena, or how those parameters which hide behind the famous phrase "everything else remaining the same" are chosen.

For example, Knox and Gilbert recently published a comparison between the expected performances of open tubular columns and the actual performances of packed columns (*4*). The presentation of their results sounds very optimistic since the authors announce that "if [the standard deviation of the unretained solute is kept at least] equal to 1 nL, then capillaries of 10 μm bore are required and are faster than packed columns when $N > 30{,}000$. For example, the time, t_m, for a peak of $N = 10^6$ theoretical plates is 2 hours with the capillary compared with 55 hours with the packed columns" (summary of ref 4). We note in passing that the difficult problem of the marked decrease in the efficiency of open tubular columns with increasing column capacity factor, k', has been elegantly solved by referring all column efficiencies to the plate number of $k' = 3$, thus slightly underestimating the performances of the OTC. Table II of the paper (*4*) illustrates the results obtained for OTC and compares them to the performances of a good packed column. We feel, however, that *the conditions of the comparison are not realistic because of the arbitrary decision to operate the two columns at the same inlet pressure* of 100 atm. We want to present here a more detailed discussion of the relationship between column performance and maximum pressure available. The set of equations used to optimize the design and operation parameters of LC columns, irrespective of their type, has been established and discussed in several papers (*4, 5, 14-17*). They are given in Table I. The equations for the liquid flow velocity (eq 1), the analysis time (eq 2) and the column plate number (eq 3) can be transformed by using the reduced plate height (eq 4) and reduced velocity (eq 5) into eq 6 and 7 which are the fundamental equations used for the optimization of column performances. Numerical calculations need the relationship between reduced plate height and velocity, the plate height equation (*14*). This equation is different for PC (eq 8) and OTC (eq 9). The equations used by Knox and Gilbert (eq 10 and 11) are equivalent to our equations.

Simple numerical calculations show that Knox and Gilbert (*4*) compare in their Table II the ability to generate 1×10^6 plates of a 9.5 μm i.d. 14 m long OTC to that of a 40 m long PC, packed with 20 μm particles. The diameter of the OTC selected is determined by the condition that the standard deviation of the unretained peak is 1 nL, which permits the use of a 1-nL cell volume detector without excessive band broadening at $k' > 1$. This is a quite reasonable assumption. On the other hand, the unusually large particle size of PC is imposed by the arbitrary decision to operate both columns at the same inlet pressure, 100 atm. As the only clear and undisputed advantage of open tubular columns over packed ones in LC is their large permeability, it is not surprising that the result of this comparison turns out to be in favor of the open tubular columns. The suprise in fact is that under these

0003-2700/81/0353-1318$01.25/0 © 1981 American Chemical Society

Table I[a]

Basic Equations for LC Performances

$$u = \frac{k_o d_p^2 \Delta P}{\eta L} \quad (1) \qquad N = \frac{k_o}{\eta D_m}\frac{d_p^2}{h\nu}\Delta P \quad (6)$$

$$t_R = \frac{L}{u}(1 + k') \quad (2) \qquad t_R = N\frac{1 + k'}{D_m}\frac{h}{\nu}d_p^2 \quad (7)$$

$$L = NH \quad (3) \qquad \text{PC } h = \frac{B}{\nu} + A\nu^{1/3} + C\nu \quad (8)$$

$$H = hd_p \quad (4) \qquad \text{OTC } h = \frac{2}{\nu} + C\nu \quad (9)$$

$$\nu = \frac{ud_p}{D_m} \quad (5)$$

Equations Used by Knox and Gilbert

$$\phi = \frac{\Delta P t_m d_p^2}{\eta L^2} \quad (10)$$ equivalent to eq 1 except $\phi = 1/k_o$

$$t_m = \frac{N^2 h^2 \phi \eta}{\Delta P} \quad (11)$$ equivalent to a combination of eq 6 and 7 arranged to eliminate d_p^2/D_m

$$t_m = \left[\frac{16\phi\eta\sigma_v^2 C^2}{\pi^2 \Delta P D_m^3}\right]^{1/4} N \quad (12)$$ diameter of an OTC and breakthrough time when the standard deviation of the inert peak, σ_v, is determined by cell volume consideration (*4*)

$$d_c = \left[\frac{16\phi\eta D_m \sigma_v^2}{\pi^2 C \Delta P}\right]^{1/8} \quad (13)$$

[a] All equations are valid for PC or OT columns as well, except eq 8 and 9. For PC columns ϕ = 500–1000; for OT columns ϕ – 32.

conditions the advantage of OTC over PC is rather moderate.

There are many other approaches to optimize or compare column performances (*15*), two of which are used here. First we can compare the performances of PC many meters long, extrapolated from the best ones currently prepared in many laboratories to that of the best possible OTCs conceivable. This will give us an idea of the real incentive to develop an entirely new technology. Second the performance of an OTC can be compared to that of a PC packed with particles having half the diameter of the OTC, since in gas chromatography (GC) the classical diameter of OTC is 0.25 mm and that of particles used to make the PC is around 0.125 mm.

II. COMPARISON BETWEEN THE PERFORMANCE OF OPEN TUBULAR COLUMNS AND PACKED COLUMNS

The best possible OTC which can be prepared is probably the one described by Knox and Gilbert (*4*) and used by them in their comparison between OTC and PC. The main difference between that one and the one actually prepared and operated by Tsuda and Novotny (*2*) is in the inner diameter, 10 μm in the first case and 60 μm in the second. There are reasons discussed in the following section which make it probable that, assuming that that kind of small bore OTC can be used at all, the minimum practical diameter will hardly be much smaller than 10 μm. One of these reasons has been discussed in details (*4*), this is the need of a very small cell volume.

The optimum reduced velocity of a good OTC is 5 and the corresponding minimum reduced plate height 0.8, assuming $C = 0.08$ in eq 9. Although this seems to be a reasonable value

Table II. Performances of Capillary Columns[a] (d_c = 10 μm)

ν	h	L, m	u, cm/s	ΔP, atm	t_m, s	t_A,[b] h	N	n[c]
5	0.8	8	0.05	13	16.000	33	1×10^6	500
		20		32	40.000	82	2.5×10^6	790
		60		96	120.000	246	7.5×10^6	1370
10	1.0	20	0.10	64	20.000	41	2×10^6	707
		30		96	30.000	62	3×10^6	866
18	1.5	14	0.18	90	8.300	17	1×10^6	500
20	1.7	15	0.20	96	7.500	15.4	0.88×10^6	470
100	8	80	1.0	2560	8.000	16	1×10^6	500

[a] Same numerical values of the parameters as used by Knox (*4*): $D_m = 1 \times 10^{-5}$ cm/s; η = 1 cP; $k_o = 1/32$. [b] $t_A = 7.4 t_m$ (*5*). [c] n is the peak capacity for $k' = 6.4$, i.e., $N^{1/2}/2$ (*20*).

which is in agreement with some experimental data (*18*), it is worth noting that in GC it is very rare that reduced plate heights below 1 are achieved in practical situations (*6–9*). This is because for real solutes the resistance to mass transfer in the stationary phase cannot easily be made negligible. Hopefully it will prove easier in LC than in GC. For a 10 μm i.d. OTC, the plate height is thus 8 μm and the velocity 0.05 cm/s for $D_m = 1 \times 10^{-5}$ cm/s. Thus an 8 m long column allows the achievement of 1×10^6 theoretical plates with t_m = 4 h and 27 min. The values given by Knox and Gilbert (L = 14 m, t_m = 2 h) are achieved with a larger reduced velocity (ν = 18) and a larger reduced plate height (h = 1.5). The use of long OTC and/or large velocities is permitted by the large permeability of these columns.

With such a constraint as a standard deviation for the unretained solute of 1 nL, the potential performances are already quite impressive for the 10 μm i.d. columns (Table II). The operation of this type of column requests a relatively moderate pressure, easy to achieve except in the last case considered. The use of eq 12 and 13 (eq 24 and 25 of ref 4) shows that a 6.5 μm i.d., 98 m long column would generate 10×10^6 plates with t_m = 19 h. and t_A = 6 days, if it could be used with a 1000-atm inlet pressure.

In this table and in the following we define the analysis time as 7.4 times the dead time, t_m since it has been shown that the optimum analytical performances are obtained when the last compound of the mixture is eluted at $k' = 6.4$ (*5*); otherwise the peak capacity (*19*) can be increased by changing the column length and the elution strength of the solvent to keep the same analysis time. Then the peak capacity of the column is $N^{1/2}/2$ (*5*). Thus the liquid holdup time of the columns, t_m, and the analysis time ($t_A = 7.4 t_m$) are important. With this definition, the analysis time for an OTC delivering peaks with an efficiency of 1×10^6 theoretical plates is around 1 day, and mixtures with several hundred components can be reasonably well resolved provided a system can be found which spread these compounds rather uniformly over a k' range of 0–6.4. It is difficult to exceed these performances markedly and we find again the old dilemma of chromatography: large separation power *or* short analysis time, or in other words separation takes time (*4, 5, 14, 20–22*). The past decade of marked technological progress has partially offset that relationship, but it should not be totally forgotten.

With PCs the column wall is metal and it is possible to find tubing which can withstand pressures up to 3 kbar at least. Although some solvents become solid at ambient temperature under moderate pressure, like cyclohexane around 230 atm (*12*), most classical solvents and especially mixtures of water, methanol, and acetonitrile remain liquid at such high pressures, although their viscosity increases markedly, an effect which is not considered in the following, although it is not

Table III. Comparison between the Characteristics of OTC and PC[a]

	d_p or d_c, μm	L, m	ΔP, atm	cell volume,[b] μL	t_m, s	t_A, h
			300 000 Plates			
PC	1.7	1	3000	1.5	600	1.2
OTC	10	8.2	100	0.001	2546	5
			1×10^6 Plates			
PC	4	8	3000	6	6667	14
OTC	10	15	100	0.001	7200	15
			3×10^6 Plates			
PC	5.5	33	3000	15	60 000	123
OTC	8	36	300	0.001	19 000	40
			10×10^6 Plates			
PC	10	200	3000	50	670 000	1350
OTC	5	98	1000	0.001	68 000	140

The particule size for the PC does not seem realistic. With $d_p = 3$ μm, however, we have $\Delta P = 1000$ bar and $t_m = 1800$ s. For a breakthrough time of 1800 s, a 7.7 μm i.d. OTC should be used with a detector having a 0.5-nL cell volume and an inlet pressure of 100 atm. For a breakthrough time of 600 s, a 4.4 μm i.d. OTC should be used similarly with a 0.05-nL cell.

The use of 3-μm particles for the PC, at optimum velocity, would require an unrealistic inlet pressure of 33 kbar while providing a breakthrough time of 60 000 s, approximately equal to that of the OTC.

[a] PC operated at the optimum flow velocity, $\nu = 3$, $h = 2$, $\phi = 500$; OTC operated at $\nu = 18$, $h = 1.5$. [b] PC has 1 mm i.d. Cell volume is equal here to 1 standard deviation of the inert peak, hence a 25% loss of efficiency for that peak. Calculations are made by using eq 25-27 of ref 4 for the OTC with $\sigma_v = 1$ nL.

quite negligible (*23*). The melting points of liquids increase usually by about 20 °C/kbar. Columns have been operated at pressures of several kilobars. Pumps for LC capable of delivering a steady flow of solvent at pressures up to 5 kbar are available. An inlet pressure of 3–4 kbar is thus a realistic value and a value of 3 kbar is used in the following calculations (with current technology, injection should be made by using the stop-flow technique).

It is immediately apparent from eq 11 that if nothing is changed to the other assumptions made by Knox and Gilbert (*4*) but the available pressure is increased from 100 to 3000 bar, the analysis time with a PC will be reduced by a factor of 30. In such a case eq 7 shows that to achieve this result the particle size has to be reduced by a factor of $30^{1/2} = 5.5$; i.e., with particles approximately 4 μm in diameter, a breakthrough time of 2 h is observed for a peak of $N = 10^6$ plates, which is equal to the values observed for the 10 μm OTC.

It so happens that with the assumptions made, i.e., the performance of the OTC is limited by the requirement that the standard deviation of the inert peak is 1 nL but there is no pressure limitation, while the inlet pressure of the PC is limited to 3 kbar, with no restriction on peak volume, both columns give almost the same breakthrough time and analysis time for 1×10^6 plates. The other characteristics (particle or column diameter, column lengths, inlet pressure for the OTC, peak volume for the PC) seem quite acceptable (cf. Table III).

Should we raise our demand to 10×10^6 plates, with the same limitations we find a breakthrough time of 19 h for a 6.5 μm OTC and 185 h (7.7 days!) for a PC (10 μm particles). For that kind of performance the first is quite reasonable, the second is not, which again illustrates the major role of the available pressure in controlling the analysis time. In fact increasing the column inlet pressure from about 10 torr to several hundred atmospheres was the essence of the technological revolution in LC which occurred in the late 60s (*15*).

The performance of PC designed and operated in various ways are given in Table IV. The relative ease with which PC permits the achievement of 3×10^5 plates (Table III) contrasts with the extreme difficulty with which 1×10^6 plates can be generated.

At this stage the conclusion is that the operation of conventional PC columns providing a few hundred thousand plates in a few hours does not require any unusual performance from the equipment or stationary phase needed; 3–10 μm particles, 1–10 m long columns, 1 to a few mm i.d. columns, a few hundred to a few thousand atm inlet pressure, and a few to 10 μL cell volume detector are specifications which are

Table IV. Maximum[a] Performances of Packed Columns[b]

d_p, μm	ν	h	L, m	u, cm/s	$t_m \times 10^3$, s	t_A, h	$N \times 10^6$ plates	n^c
			(A) Using the Maximum Pressure Available to Generate 1×10^6 Plates (i.e., ΔP – 3000 atm)					
3	1.5	2.2	6.5	0.05	13	27	1	500
4	3	2	8	0.08	11	22	1	500
5	4.4	2.1	10	0.09	12	24	1	500
10	13.2	2.9	29	0.13	22	45	1	500
20	34.5	4.3	87	0.17	50	102	1	500
			(B) Using This Maximum Pressure to Generate the Largest Possible Plate Number					
3	3	2	3.4	0.10	3.4	7	0.56	375
4	3	2	8	0.08	11	22	1.0	500
5	3	2	16	0.06	26	53	1.6	625
10	3	2	125	0.03	(417)	(856)	6.2	1250
20	3	2	1×10^3	0.015	(6.7×10^3)	(13704)	25	2500
			(C) Using Columns Working at Optimum Flow Velocity to Generate 1×10^6 Plates					
								ΔP, atm
3	3	2	6	0.10	6	12.5	1	(5333)
4	3	2	8	0.08	11	22	1	3000
5	3	2	10	0.06	16	33	1	1920
10	3	2	20	0.03	67	137	1	480
20	3	2	40	0.015	(267)	(548)	1	120

[a] Using the present packing technology. All numbers rounded up. [b] Experimental conditions: $\eta = 1.0$ cP; $D_m = 1 \times 10^{-5}$ cm/s; $k_o = 1/800$, i.e., $\phi = 800$. This value, less favorable to PC that the one used by Knox (*4*) seems more realistic to this author. [c] Peak capacity ($k' = 0$–6.4).

easy to meet with products available presently on the market. On the other hand, the operation of OTC with comparable performances is made extremely difficult by the specification that the detector cell volume should be less than 1 nL. This and other practical problems discussed below makes quite questionable the interest of OTC in that range of performance (a few 10^5 plates in a few hours).

It is almost as clear, from this theoretical discussion that the generation of 1×10^6 plates in 1 day or so is about the best performance we can expect from PC. Exceeding this limit would require the use of pressures in the 10 kbar range or more which, although not impossible is clearly extremely difficult and expensive. If 10×10^6 plates or more are needed and ever generated, it is most probable that an OTC will provide them. The technical problems, however, are enormous, as seen below, and it is not clear at that stage whether the separations offered will be worthwhile. There might be other ways to apply the brute force approach to separation.

The calculations carried out by Halasz are more complex and detailed than ours or those by Knox (*4*) as they consider the variation of the HETP with increasing retention and the exact effect of the resistance to mass transfer in the stationary phase (*6*). He, however, comes to the same conclusion: open tubular columns cannot compete with currently available packed columns unless they are made extremely narrow, less than 5 μm in diameter, which requests the development of detectors with cell volume of 0.1–0.3 nL depending on the pressure available (eq 13).

Finally there is a last way to compare the performances of PCs and OTCs. Let us assume that we want to generate the same plate number in the same time, with the same system. Assuming that the phase ratios can be adjusted so that the k's are about the same with the two columns, eq 7 shows that the following relationship should apply:

$$\left[\frac{h}{\nu} d_p^2\right]_{PC} = \left[\frac{h}{\nu} d_c^2\right]_{OTC} \tag{14}$$

At the optimum we have considered that for a good PC, $h = 2$ and $\nu = 3$; for a good OTC we have $h = 0.8$, $\nu = 5$. Then we obtain

$$(d_c)_{OTC} = 2.1(d_p)_{PC} \tag{15}$$

In the conditions selected by Knox and Gilbert, to partially offset the influence of the detector cell volume, we have $(d_c)_{OTC} = 2.8(d_p)_{PC}$. This is of course why a 10 μm i.d. OTC gives performances comparable to those of a PC made with 5 μm particles. The OTC can achieve better performance only if its diameter is markedly below twice the particle diameter which happens only if a small enough detector cell can be used or if the pressure available for the PC is not large enough, as explained above.

III. RANGE OF VALIDITY OF THE THEORY

Obviously the results of the above discussion are valid only as long as the theoretical framework over which it is based rests on firm ground. This problem has different aspects for PC and OTC columns.

In the case of PCs difficulties can arise from deviations at high pressures between actual results and extrapolation of our measurements made at low or moderate pressures. The compressibility of liquids over the range 0–3000 atm is far from negligible (*23*). The viscosity of liquids increases with increasing pressure and the diffusion coefficient decreases (*23*). Hardly anything is known of a possible variation of k_0 (or ϕ) at very high pressures. Clearly some serious difficulties may be experienced at large pressure. The actual performances of PC will probably be somewhat less than expected, but probably not much, most of these effects being actually small and some compensating for the others (*23*). The most serious problems should be expected from the solidification of some solvents under high pressure, preventing the use of these pure solvents, and a variation in the equilibrium constant with the pressure, since

$$\partial(\Delta G)/\partial P = \Delta V \tag{16}$$

ΔG and ΔV being the variation of the Gibbs free energy and the partial molar volume associated with the retention phenomenon used. This effect has been used by Rogers to improve the relative retention of compounds or alter their elution order (*25*). It could have a useful or detrimental influence on the separation, depending on the particular case but will not impede seriously the development of PCs operated at large pressures.

If the situation is quite satisfactory for PC, it is still somewhat more ambiguous with OTC. The effects of high pressure described above will also act on the OTC performance much as on the PCs, which appears to be of little consequence actually, but it should be clear that all of the above discussion rests on the assumption of the validity of the Golay equation (*4*, *6*). This equation is valid for straight tubes, with cylindrical cross section, and laminar flow.

It has been shown that operating the OTC in the turbulent flow does not improve the performances *for retained solutes* (*26*) whereas it does provide narrower zones for the inert peak, which is in agreement with the results observed in GC (*27*). Anyway the pressure cost of operating an OTC in turbulent flow conditions is too enormous to warrant its consideration for analytical application. It has been shown by Tijssen that coiling a capillary tube into a tight coil (coil diameter below ca. 10 times the column diameter) reduces markedly the width of inert peaks (*28*). This is in agreement with the experimental results by Doué et al. (*29*) who, unfortunately, have shown that this effect becomes much smaller for retained peaks and that for $k' > 1$ the efficiency of a tightly coiled column is smaller than that of a normal coil. No dimensional analysis of the system has been made and the derivation of an extended Golay equation for coiled tubes seems to be a very complex task indeed, so it is not impossible that a tightly coiled OTC or an OTC with a noncylindrical cross section (a twisted elliptical cylinder for example) proves to offer better performances than a conventional one, but this author is very skeptical about this possibility. Recent results by Halasz (*30*) on OTC with periodical cross section points to narrow inert peaks but wider retained peaks than conventional, circular OTC with same cross section area.

IV. PRACTICAL CONSIDERATIONS

The development of long, efficient PCs with the ability to deliver any kind of performance in the range of 1 to 10×10^5 plates with analysis times between a few hours and a couple of days is presently well advanced. Performing analyses requiring a few hundred thousand plates is now possible. Equipment manufacturers are busy working on the development of the necessary apparatus, but pumps delivering up to 5 kbar are available, as well as sampling valves working at up to 1 kbar (above we still have to use stop flow injections). Packing 1 m long columns with silica particules has been proved possible by Scott and Kucera (*1*, *13*) and reduced performances comparable to those of the conventional 10–30 cm long columns (i.e., $h = 2$, $\nu = 3$) can be obtained (*12*). Reversed-phase particules are much more difficult to pack (*12*), but Kucera has proven it possible (*24*). All the associated problems are under intense study in many laboratories and the operation of such columns will be considered as routine in a couple of years. It is quite possible that 4 mm i.d. columns will prove as efficient as 1 mm i.d. ones as there is no reason why the efficiency should decrease with increasing diameter

Table V. Sample Size and Detection Limits in LC

	column diameter	external porosity,[a] ϵ	sample size,[b] ng	N	detection limit,[c] fg	peak volume,[d] μL	detection limit,[e] ng/mL
PC	4 mm	0.4	10^6	10^4	10^7	200	75
	1 mm	0.4	2×10^5	10^5	2×10^5	40	7.5
	1 mm	0.4	6×10^5	10^6	6×10^4	125	0.75
OTC	60 μm	0.87	50	10^4	500	1	2
	10 μm	0.7	30	10^6	3	0.01	0.25
	5 μm	0.6	30	10^7	0.3	0.004	0.07

[a] The column porosity for OTC depends on the thickness of the phase layer. Assuming a layer of constant thickness d_f, we have $\epsilon = 4d_f/d_c$. We assume a layer of 2 μm for the 60 μm i.d. column, 0.75 μm for the 10 μm 1.d. one, and 0.5 μm for the last column. Those figures are consistent with other results and give a small enough contribution to band broadening of the resistance to mass transfer in the stationary phase. [b] Assuming $m = \lambda(1 - \epsilon)d_c^2N^{1/2}$, a maximum sample size proportional to the mass of stationary phase in a column section of unit length, and increasing with the square root of column length (5). Here $\lambda = 1 \times 10^5$ ng/cm^3. [c] Assuming $\mu = m/10N$, which is arbitrary but gives sound results. [d] Peak base width, in volume unit, for a compound with $k' = 3$. [e] $c = \mu N^{1/2}/V_R(2\pi)^{1/2} = 4\lambda(1 - \epsilon)/(1 + k')hd_p\pi(2\pi)^{1/2} \times 1/10N$. d_p particle (PC) or column (OTC) diameter. $h = 1.5$ for OTC.

if narrow size distribution particules are packed homogeneously.

The development of capillary columns is much less advanced. The best capillary columns prepared for LC have 60 μm (2) or 45 μm (31). Their performances are reasonably close to those predicted by the theory (18), which confirms the validity of the Golay equation applied to OTC in LC. The analyses reported are, of course, slower and less efficient than those obtained currently with PC, which is a direct consequence of the use of a large inside diameter column and a relatively large velocity of about 1 cm/s for a 50 μm i.d. column ($t_m \simeq 8$ min (3)); this corresponds to $\nu = 500$ for $D_m = 1 \times 50^{-6}$ cm^2/s. At that reduced velocity, with $C = 0.08$, $h = 40$, thus a 5 m long column gives 2500 plates. (The plate number measured from figure 10 of ref 31 is approximatively 2200 for $k' = 1$.) A PC 25 cm long, packed with 5 μm particles, operated at 0.1 cm/s (i.e., $\nu = 5$) would give 25 000 plates with $t_m = 250$ s or 10 times as many plates in half the time. In another experience, a 21 m long 43 μ i.d. column is operated at 0.3 cm/s (i.e., $t_m = 6500$ s, in agreement with the chromatogram Figure 9). The reduced velocity is about 130; hence $h \simeq 11$ and $N \simeq 45\,000$. The value estimated from the chromatogram is about 30 000 for $k' = 1$.

These performances show that even with extreme care it is difficult to approach the theoretical performances but also that it is possible to prepare satisfactory OTC with various types of stationary phases. It certainly seems easier to prepare an OTC several meters or tens of meters long than a PC of the same length which is a marked advantage. On the other hand there are a number of serious technological problems. The flow rate at $\nu \simeq 20$ for a 10 μm i.d. OTC is 9 nL/min making the design of a reciprocating pump more than difficult. The use of syringe pumps is not recommended because of the serious difficulties encountered with their use which have led to their surrender (32). Unfortunately the drawbacks of syringe pumps are not related to the size of either the pump cylinder or the flow rate delivered. It thus seems that OTC should be operated with constant inlet pressure, not constant flow rate, a source of serious problems if the column is plugged as it will not be easy to measure the flow rate.

The difficulty in preparing a suitable layer of porous silica on the inner wall of a glass tube and to bond the desired chemical groups densely enough to obtain a suitable phase for reversed-phase LC should not be underestimated, although similar problems have been solved in gas chromatography, using either glass tubes (33) or aluminum tubes (34). The maximum pressure that a glass tube can withstand before bursting is not well-known. In this laboratory etched glass tubes, 100 μm i.d. burst around 200 atm. Novotny (35) claims that he can operate 60 μm tubes at 1000 atm but it seems those are not etched, and etched tubes are certainly more brittle than those with a smooth surface since the pores made during the leaching process can be the origin of microfactures. Although this is a potential source of difficulties in the search for extremely high efficiencies, when pressures around 1 kbar will become necessary, it is sure that etched glass OTC could be operated up to 100–200 bars.

Sampling is not a major problem as the use of splitting devices is always possible (36). On the other hand as pointed out by Knox and Gilbert (4) and explained above, the detector cell volume is of critical importance. The detector must have a very small volume as dilution by a flow of makeup or scavenger liquid is too detrimental for the detection limits. A cell volume of 1 nL is an absolute maximum for the use with 10 μm i.d. OTC offering performances competitive with or exceeding those of conventional PC. Very small cells have been made already. Using two quartz fibers, Gruska (37) has achieved a 0.06-μL cell, but what is the sensitivity of a UV cell with a 0.5-mm path length? To illustrate the difficulty of the task, we note that a 1-nL cell volume is the volume of a 1.3 cm long section of a 10 μm i.d. tube. Laser-induced fluorescence (38) or MS/MS could probably satisfy most of the requirements. Nonetheless, the sample size of the column is small and the sensitivity required is high. The sample size acceptable on a 60 μm i.d. column was shown to be of the order of 50 ng for a compound with $k' = 1.22$ (2). On a 10-μm column with identical performance [10^4–10^5 plates] the maximum sample size would be of the order of 1 ng. Thus the positive identification of a major compound would be very difficult with present day mass spectrometers. The identification of impurities at significant concentration (below 0.1%) would be impossible; they would be barely detectable in single ion monitoring. Capillary columns are not the solution for trace analysis in GC/MS. They are not too attractive in LC/MS, as long as the ion yield of MS sources has not been improved by several orders of magnitude. The loading capacity of PC and OTC columns is compared in Table V. A 10 μm i.d. column having a very large resolution power would have a loadability around 30 ng.

Furthermore the sensitivity required is better when the column efficiency increases: the high separation power is required for the analysis of very complex mixtures. If we want to separate a 500-component mixture we certainly require a lower detection limit than for the analysis of a 10-component mixture. An order of magnitude of the detection limit is also given in Table V where it has been assumed, somewhat arbitrarily, because of the lack of suitable data, that the detection limit required is inversely proportional to the plate number. In the discussion of such figures only orders of magnitude are important. Thus the analysis of a 500-component mixture, requiring 1×10^6 plates would request a detector with a detection limit of 100 ppb. With a 30-ng

Table VI. Basic Equations for GC Performances

$$u_o = \frac{k_o d_p^2}{2\eta L P_o}(P_i^2 - P_o^2) \quad (17) \qquad N = \frac{k_o}{2\eta D_m}\frac{d_p^2}{h\nu}\frac{P_i^2 - P_o^2}{P_o} \quad (19)$$

$$t_R = \frac{4\eta L^2}{3k_o d_p^2}(1 + k') \times \frac{P_i^3 - P_o^3}{(P_i^2 - P_o^2)^2} \quad (18) \qquad t_R = \frac{4\eta N^2 h^2}{3k_o}(1 + k') \times \frac{P_i^3 - P_o^3}{(P_i^2 - P_o^2)} \quad (20)$$

$$L = NH \quad (3) \qquad \text{PC} \quad h = \frac{B}{\nu} + A\nu^{1/3} + C\nu \quad (8)$$

$$H = hd_p \quad (4) \qquad \text{OT} \quad h = \frac{2}{\nu} + C\nu \quad (9)$$

$$\nu = ud_p/D_m \quad (5)$$

A combination of eq 19 and 20 gives

$$t_R = \frac{2}{3}N\frac{h}{\nu}\frac{d_p^2}{D_m}\frac{P_i^3 - P_o^3}{P_o(P_i^2 - P_o^2)} \quad (21)$$

For very efficient packed columns and for extremely long open tubular columns, P_o^2 can be neglected compared to P_i^2. Equations 17–21 are then simplified accordingly.

sample size, the sensitivity of the detector must be of the order of 3 fg to make such an analysis worthwhile. For a compound of molecular weight 300, this means only 6×10^6 individual molecules. For narrower bore OTC, another source of problems would be encountered rapidly, the limit of conventional chromatography: chromatograms are statistical distributions of residence times. For sample sizes with a small number of molecules, statistical fluctuations would become another source of noise. The relevance of the analyzed sample to the actual mixture of interest would also have to be studied. There is not a fundamental roadblock here as the situation is similar to the one met with in the extraction of heavy transuranide metal ions by ion-exchange chromatography. The development of detection systems working on a one molecule at a time basis is probably not more difficult than the development of detectors for elementary particles. Clearly this is an economical problem whose solution will long remain beyond the reach of most analysts.

V. COMPARISON BETWEEN LC AND GC

It is striking that OTCs are so useful and widely used in GC while they seem much less attractive in LC as shown by the previous discussion. When OTCs were still a rarity in analytical practice, this author has repeatedly insisted on their marked advantages over PC, using the same theoretical approach as the one developed here (*39-41*). There are two answers to this question.

Besides the problems related to the different orders of magnitude of the diffusion coefficients in the two phases, which makes the entire development of a new generation of submicro instruments necessary, another fundamental reason comes from the markedly different values of the compressibility of gases and liquids.

It is easy to derive a set of equations for gas chromatography (Table VI) similar to those used above for LC (Table I). These equations relate the inlet and outlet pressures, the plate number, and the analysis time to the column characteristics. The difference with the corresponding equations for LC results from the large difference in compressibility between gases and liquids.

In GC, if the inlet pressure is large compared to the outlet pressure, eq 19 and 20 simplify and it becomes possible to eliminate P_i between them. This gives

$$t_R = \left(\frac{8\eta N^3 h^3}{k_0 P_0 D_m \nu}\right)^{1/2}\frac{(1 + k')d_p}{3} \quad (22)$$

To obtain the same efficiency in the same time, we need to choose the diameters of the OTC and of the particles of the PC so that

$$\left[\left(\frac{h^3}{k_0\nu}\right)^{1/2} d_p\right]_{PC} = \left[\left(\frac{h^3}{k_0\nu}\right)^{1/2} d_c\right]_{OT} \quad (23)$$

The open tubular column has a specific permeability (k_0) 25 times larger than the packed column (800/32). The theoretical performance characteristics of an OTC, assuming very fast mass transfer in the stationary phase, are $h_{min} = 0.80$, $\nu_0 = 5$. This compares to those of a good PC ($h_{min} = 2$, $\nu_0 = 3$). According to eq 23 the OTC must have a diameter 26 times larger than the particles used to pack the PC.

This is a major difference with the situation which prevails in LC since we have shown above that the same analysis time and plate number are obtained when the OTC diameter is twice the diameter of the particles of the PC. If the PC is compared to a more conventional OTC with $h_{min} = 1.25$ and $\nu_0 = 3.2$, a ratio of 11 is obtained. In this case the OTC would be 7 times longer (eq 3 and 4 with the different values of h), and the actual mobile phase velocity at column outlet would be 10 times slower (eq 5) in spite of the fact that the analysis times and plate numbers are the same. Thus a PC made with 100–125-μm particles is as fast as an OTC having an i.d. between 1.2 and 2.7 mm. This explains why some authors have found marked advantages in wide bore OTC, having i.d. between 0.5 and 1 mm. The performance of such columns still compares quite favorably to those of conventional PCs (*42*).

Alternatively, if a PC is compared to an OTC with $d_c = d_p$, to achieve a given efficiency, hence a given resolution between two compounds with a given chromatographic system, the PC will yield an analysis time 10–20 times that for the OTC.

Still if we operate the OTC and the PC with the same inlet pressure, eq 23 shows that the OTC will give about as many plates per unit time as the PC (if $d_c = 2d_p$), but the OTC will give about 36 times as many plates while the analysis time will be 36 times longer, since to operate an OTC at its optimum velocity with the same inlet pressure as a PC we need to use a much longer column. Since eq 22 shows that the time necessary to achieve a given plate number increases faster that this plate number in GC, the advantage of OTC is again obvious.

The reason for this dramatic difference in behavior between LC and GC is to be found in the difference between eq 1 and 17, hence between eq 7 and 20. Practically the compressibility of liquids can be neglected to calculate retention times in LC (*23*) while the compressibility of gases is inversely proportional to the pressure ($\chi = (1/v)dv/dp) = 1/p$). Thus, the velocity profile along the LC column is a horizontal straight line (u = constant); the velocity profile along a GC column is parabolic. If an OTC is compared with a PC with $d_p = d_c$ and the same outlet velocity for a given value of ν, the actual inlet velocity will be much larger with the OTC which is more permeable and requires a lower inlet pressure than the PC in gas chromatography, while in LC the velocity will be the same all along the two columns. Consequently the analysis time, which depends on the average velocity, will be much shorter in GC with the OTC than with the PC. This is why k_0 takes place in eq 23 and not in the similar 14. The specific permeability is of great importance to control analysis time in GC. It is not in LC (*43*). There is no similar effect in LC columns, and this is why an OTC in LC is only about as fast as the PC which gives the same plate number and has $d_p = d_c/2$. For this reason, and this reason alone, we may conclude that even if they can be prepared and operated properly, 10 μm i.d. OTC will not have the importance in LC that 0.25 mm i.d. OTC have in GC.

Table VII. Performances of Packed Open Tubular Columns[a]

d_p,[c] μm	ν	L, m	u,[b] cm/s	ΔP,[b] atm	t_m, h	t_A, h	N
30	2	11	7×10^{-3}	1.3	45	333	10^5
	50	30	0.17	92	5	37	10^5
	200	210	0.67	2500	10	74	10^5
10	2	36	0.02	120	50	370	10^6
	50	100	0.50	(8250)	5.6	41	10^6
5	2	18	0.04	475	12.5	92	10^6

[a] Data taken from ref 11: $h = 3.6$, $\nu = 2$; $h = 10$, $\nu = 50$; $h = 70$, $\nu = 200$. [b] $\eta = 1$ cP, $D_m = 1 \times 10^{-5}$ cm²/s, $k_0 = 1/165$. [c] The column inner diameter should be around $2.5 d_p$ (11).

VI. PACKED OPEN TUBULAR COLUMNS

These columns are loosely packed columns obtained by drawing glass tubes previously packed with a stationary phase which can stand the softening point of the glass used (44). They have been used in GC to a limited extent, their only successful, practical application being the analysis of light hydrocarbon gases (C_1–C_5). In this case a large efficiency is required, but conventional liquid phases do not offer a sufficiently large retention. Packed open tubular columns drawn with alumina or silica are an excellent compromise. Similar columns have been prepared by using Chromosorb which is coated after drawing (45). Their efficiency is good as long as the ratio of the particle diameter to the column diameter is between 0.3 and 0.15. Strong radial mixing due to flow unevenness compensates the effect of the marked variation of the local flow velocity over the column cross section due to the heterogeneity of the packing. The contribution to band broadening due to the resistances to radial mass transfer in the mobile gas phase remains of the same order of magnitude as the resistance to mass transfer in the gase phase inside a particle.

The reduced plate height remains acceptable—usually between 3 and 5 (42–46).

The main advantage of these packed capillary columns (PCC) is in their large specific permeability, intermediate between that of PC and OTC. They are more difficult to prepare than PC and more difficult to deactivate than OTC; however, their only practical advantages over the faster OTC are their larger loadability, useful in GC/MS applications, and the easy possibility of using adsorbents.

The application of this column type in LC has been studied recently by Tsuda and Novotny (11) who have found that the best HETP plots were obtained for 70 μm i.d. columns packed with 30-μm particles. When the ratio of particle to column diameter becomes smaller, the packing structure is unstable and collapses under the influence of the sheer forces generated by the viscous flow, a phenomenon not observed in GC, and clogging of the column occurs. The minimum reduced plate height is around 3.6, and the optimum reduced velocity is a few units (47). The efficiency decreases markedly with increasing retention, however. This decrease may be related to the large particle diameter used. These columns demonstrate performance characteristics markedly inferior to those of conventional packed columns. The efficiency data for the 30-μm-particle column of Tsuda and Novotny (11) can be accounted for approximatively by eq 8 with $A = 3$ and $C = 0.2$ within the precision of measurement of data from this figure. In spite of expectations coming from previous work in GC (45, 46), we observe that the permeability is rather low. The only clear data derives from the caption of Figure 8, ref 11, and gives $k_0 = 1/165$, only 5–6 times larger than for a conventional PC but 5 times smaller than for an OTC. The combination of these results using the method described above leads to performance characteristics much less attractive than those of conventional packed columns (Table VII). The large drop in efficiency with increasing k' as illustrated by Figures 2 and 3 of ref 47, where the plate number decreases by 60% when k' increases from 0.1 to 0.5, is not taken into account and points out to a very pessimistic conclusion.

Furthermore any progress in efficiency of this type of column could be obtained only by a reduction in the column diameter which must be 2 to 2.5 times larger than the particle diameter. It is clear that PCC can have efficiency and performances comparable to those of conventional PC only if they are made with the same particles, so the contributions of resistances to mass transfer in the stationary and the stagnant phases are the same. The advantage of PCC 12–15 μm i.d., packed with 5-μm particles over OTC 10 μm i.d. with a 1-μm layer of silica is doubtful. Finally, this approach cannot help much in solving the problems of equipment dead volumes or sample size associated with the use of very narrow bore columns.

CONCLUSION

The most fruitful approach at present to generate very high efficiency columns is in the extension of modern HPLC technology toward the coupling of a number of 0.5 to 1 m long columns packed separately and the use of very high inlet pressures. There is nothing very spectacular in this development which comes in a straightforward way from recently published work (1, 13), but success is guaranteed as long as the analyst has the patience to wait for the end of the analysis.

The development of open tubular columns faces formidable technological difficulties and, although wrong conclusions derived by superficial analogies between gas and liquid chromatography seem to point to the opposite, the reward for this work will be very limited until columns with an inner diameter in the 5–10-μm range can be operated routinely using 1-nL cell volume detectors. The permeability advantage of OTC will then allow the achievement of performances which are merely impossible with PC.

Packed capillary columns are not an interesting compromise in spite of their extreme ease of preparation because the positive effect of their increased permeability is more than offset by poor efficiency at moderate or large retention and by difficulties in using the small particles which would be necessary.

LITERATURE CITED

(1) Scott, R. P. W.; Kucera, P. *J. Chromatogr.* **1979**, *169*, 51–72.
(2) Tsuda, T.; Novotny, M. *Anal. Chem.* **1978**, *50*, 632–634.
(3) Ishii, D.; Asai, K.; Hibi, K.; Jonokuchi, T.; Nagaya, M. *J. Chromatogr.* **1977**, *144*, 157–168.
(4) Knox, J. H.; Gilbert, M. T. *J. Chromatogr.* **1979**, *186*, 405–418.
(5) Guiochon, G. *J. Chromatogr.* **1979**, *185*, 3–26.
(6) Halasz I. *J. Chromatogr.* **1979**, *173*, 229–247.
(7) Schomburg, G.; Dielmann, R.; Husmann, H.; Weeke, F. *J. Chromatogr.* **1976**, *122*, 55–72.
(8) Maskarinec, M. P.; Alexander, G.; Novotny, M. *J. Chromatogr.* **1976**, *126*, 559–568.
(9) Grob, K.; Grob, G.; Grob K., Jr. *Chromatographia* **1977**, *10*, 181–187.
(10) Guiochon G. *Anal. Chem.* **1978**, *50*, 1812–1821.
(11) Tsuda, T.; Novotny, M. *Anal. Chem.* **1978**, *50*, 271–275.
(12) Colin, H.; Jandera, P., Palaiseau, France, unpublished work, 1980.
(13) Scott, R. P. W. *J. Chromatogr. Sci.* **1980**, *18*, 49–54.
(14) Knox, J. H.; Saleem, M. *J. Chromatogr. Sci.* **1969**, *7*, 614–622.
(15) Martin, M.; Eon, C.; Guiochon, G. *J. Chromatogr.* **1974**, *99*, 357–376.
(16) Martin, M.; Eon, C.; Guiochon, G. *J. Chromatogr.* **1975**, *108*, 229–241.
(17) Martin, M.; Eon, C.; Guiochon, G. *J. Chromatogr.* **1975**, *110*, 213–232.
(18) Knox, J. H. *J. Chromatogr. Sci.* **1980**, *18*, 453–461.
(19) Gushka, E. *Anal. Chem.* **1970**, *42*, 1142–1147.
(20) Giddings, J. C. *Anal. Chem.* **1964**, *36*, 1890–1892.
(21) Giddings, J. C. *Anal. Chem.* **1965**, *37*, 60–63.
(22) Knox, J. H. *J. Chem. Soc.* **1961**, 433–441.
(23) Martin, M.; Blu, G.; Eon, C.; Guiochon, G. *J. Chromatogr. Sci.* **1973**, *11*, 641–654.
(24) Kucera, P. *J. Chromatogr.* **1980**, *198*, 93–109.
(25) Prukop, G.; Rogers, L. B. *Sep. Sci.* **1978**, *13*, 59–78.
(26) Martin, M.; Guiochon, G., to be submitted for pubication in *J. Chromatogr.*

(27) Doue, F.; Guiochon, G. Sep. Sci. 1970, 5, 197–218.
(28) Tijssen, R. Sep. Sci. Technol. 1978, 13, 681–702.
(29) Doue, F.; Merle D'Aubigne, J.; Guiochon, G. Chim. Anal. (Paris) 1971, 53, 363–374.
(30) Hofmann, K.; Halasz, I. J. Chromatogr. 1980, 199, 3–22.
(31) Ishii, D.; Takeuchi, T. J. Chromatogr. Sci. 1980, 18, 462–472.
(32) Martin, M.; Blu, G.; Eon, C.; Guiochon, G. J. Chromatogr. 1974, 112, 399–414.
(33) Mohnke, M.; Saffert, W. In "Gas Chromatography, 1962"; Van Swaay, M., Ed.; Butterworths: London, 1962; pp 216–221.
(34) Desty, D. Adv. Chromatogr. (N. Y.) 1965, 199–228.
(35) Novotny, M., Bloomington, IN, unpublished results, 1981.
(36) Hirata, Y.; Novotny, M. J. Chromatogr. 1979, 186, 521–528.
(37) Grushka, E. Jerusalem, Israel, unpublished work, 1980.
(38) Hershberger, C. W.; Calis, J. B.; Christian, G. D. Anal. Chem. 1979, 51, 1444.
(39) Guiochon, G.; Chovin, P. Bull. Soc. Chim. Fr. 1965, 3396–3403.
(40) Guiochon, G. Anal. Chem. 1966, 38, 1020–1030.
(41) Guiochon, G. Adv. Chromatogr. (N. Y.) 1969, 8, 179–270.
(42) Nikelly, J. G. Anal. Chem. 1976, 48, 987–989.
(43) Halasz, I.; Hartmann, K.; Heine, E. In "Gas Chromatography 1964"; Goldup, A., Ed.; British Petroleum Institute: London, 1965; pp 38–61.
(44) Halasz, I.; Heine, E. Adv. Chromatogr. 1967, 4, 207–263.
(45) Landault, C.; Guiochon, G. In "Gas Chromatography 1964"; Goldup, A., Ed.; British Petroleum Institute: London, 1965; pp 121–139.
(46) Landault, C.; Guiochon, G. Chromatographia 1968, 1, 119–132.
(47) Hirata, Y.; Novotny, M.; Tsuda, T.; Ishii, D. Anal. Chem. 1979, 51, 1807–1809.

RECEIVED for review January 16, 1981. Accepted March 6, 1981.

Measurement of Band Broadening in Size Exclusion Chromatography

R. Groh and I. Halász*

Angewandte Physikalische Chemie, Universität des Saarlandes, 6600 Saarbrücken, West Germany

The interstitial band broadening in silica filled columns has been determined experimentally. The pores were filled with water, which is impenetrable to the benzene and polystyrene samples. Total band broadening, h, was measured with "dry" CH_2Cl_2 eluent and the interstitial broadening with "wet" eluent in the same column. The band broadening in the pores was obtained by difference (Δh). The interstitial band broadening is about 10 times smaller than those obtained with accessible pores. The reduced interstitial band broadening is at least a factor 2 smaller than reported earlier. The diffusion coefficients of polystyrenes in CH_2Cl_2 as a function of M_w were measured in packed columns by a stopped flow method. It is shown that restricted diffusion is not only a function of M_w of the samples but also of the pore size distribution and specific pore volume of the support. Extremely high specific pore volumes, theoretically desirable in SEC, lead in practice to undesirable high mass transfer terms. Packing structures in dry and slurry packed columns are discussed.

Band broadening is of particular interest in size exclusion chromatography (SEC) because separation occurs in a strictly limited range of the elution volume (V_e)

$$V_e = V_z + KV_{p,max} = V_z + V_p \qquad (1)$$

where K is the exclusion chromatographic "partition coefficient" always lying between 0 and 1 (see list of symbols at the end of the paper for the other symbols). Consequently peak capacities (*1*) in SEC are much smaller than in other forms of chromatography. A further reason for interest in band broadening in SEC is that proper calculation of the molecular weight distributions (MWD) of polymers is only possible, after correction for the different sources of band broadening (*2*).

In this paper an experimental method will be described to measure the interstitial peak broadening in columns packed with porous materials. Band broadening in SEC has been discussed from both a theoretical and an experimental point of view. It is sometimes possible to approach the problem from diametrically opposing points of view and to end up with mathematical treatments which are remarkably similar.

The Theoretical HPLC Approach. The van Deemter equation (*3*) is the most common expression used to describe the h vs. u curve

$$h = A + \frac{B}{u} + Cu \qquad (2)$$

Dimensionless parameters are often used to describe hydrodynamic phenomena. The ones appropriate to chromatography are reduced plate height ($h_{red} = h/d_p$) and reduced linear velocity ($u_{red} = ud_p/D$). Reduced parameters sometimes permit better comparisons of chromatographic systems with differing d_p and D.

The simplified form of the van Deemter equation

$$h = A' + C'u \qquad (3)$$

is often used in LC, and here in SEC, since the B/u term is only of importance when the flow rate is uninterestingly low.

Some experimental h vs. u_z curves have a concave ascending branch and therefore cannot be described by the van Deemter equation. In order to account for such h vs. u_z curves, several theories have been proposed (*4–19*).

Giddings and Mallik (*7*) pointed out that the flow velocity can, with advantage, be described in terms of the interstitial velocity

$$u_z = u\frac{V_o}{V_z} = u\frac{\epsilon_t}{\epsilon_z} = u\alpha = \frac{L}{t_z} \qquad (4)$$

where α is a constant.

This can be measured with a totally excluded inert sample (eq 4). Furthermore, they (*7*) also proposed an obstruction factor (γ_s) describing the ratio of the restricted diffusion inside the particles (D_s) and the diffusion in the interstitial volume (D_m), which they assumed to be constant

$$\gamma_s = \frac{D_s}{D_m} = \frac{2}{3} \qquad (5)$$

The Experimental HPLC Approach. Heitz (*20*) measured h vs. u curves for olygophenols in columns packed with polystyrene and poly(vinyl acetate) gels (d_p = 100–500 μm). All his results were describable by the van Deemter equation. The author states (*21*) (our translation): "While Giddings (*7*) assumed, that mass transfer in the stationary phase is rela-

0003-2700/81/0353-1325$01.25/0 © 1981 American Chemical Society

tively unimportant in band broadening, today it can surely be held, that this is the most important contribution."

Kelley and Billmeyer (*10, 12-14*) studied band broadening in columns packed with nonporous glass beads, porous silicas, and porous polystyrene gels, all other parameters being held as constant as possible. For the porous packings they concluded that, for silica (d_p = 115 μm), mass transfer effects inside the pores predominated, whereas for polystyrene gels (d_p = 50 μm) band broadening was mainly caused by interstitial effects.

van Kreveld and van den Hoed (*18*) measured the h vs. u curve of toluene in a column packed with silica (d_p = 125 μm). The ascending branch of the curve was linear. In contrast polystyrene samples gave, in the same column, a concave ascending branch. From these experiments, obstruction factors were calculated, which decreased with increasing molecular weight, ranging from γ = 0.7 for toluene to γ_s = 0.1 for polystyrene (M_w = 160 000).

Knox and McLennan (*22, 23*) measured the h vs. u curves of polystyrene samples on silica (d_p = 7 μ) in columns with different lengths. Obstruction factors were calculated, γ_s = 0.1 for polystyrene of M_w = 20 000. They also showed, using a monodisperse oligomer of styrene, that the band broadening due to "kinetic" effects is proportional to $L^{1/2}$ in SEC as it is in retentive chromatography. On the other hand the difference in retention volume of two monodisperse substances is proportional to L. On the basis of these considerations their experimental results were used to calculate polydispersities.

Dawkins et al. (*24, 25*) measured band broadening for spherical silicas and polystyrene gels. They concluded that plate height decreased not only with decreasing d_p but also with narrowing particle size distribution. Dawkins and Yeadon (*26*) describe a method to calculate polydispersities of polymers from plate height measurements at low velocities.

The Approach of Polymer Chemists. Moore et al. (*27*) introduced an experimental method for eliminating band broadening caused by polydispersity. The sample is allowed to run only half way along the column, when the direction of flow is reversed and the sample is eluted at the inlet end of the column. Peak broadening caused by polydispersity is thus eliminated, while the kinetic peak broadening is the same as if the sample had passed along the entire column length.

Hendrickson (*28*) used the method of Moore to measure band broadening on polystyrene gels (d_p = 40 μm). Excluded substances had the same peak volumes (i.e., the same h values), although the ratios of their molecular weight were as much as 100. Consequently it was assumed that interstitial band broadening is independent of the diffusion coefficient of the sample. Partially excluded peaks at constant flow rate showed a maximum in the h vs. M_w curve. This must be caused by kinetic (mass transfer) effects, because the effects of polydispersities are eliminated by this technique. The h vs. u curves were, on the other hand, linear.

Bly (*29, 30*) found that the peak volume, when corrected for polydispersity, was constant in the linear part of the calibration curve (log M_w vs. V_e). Consequently $n^{1/2}$ is proportional to V_e.

Basedow et al. (*31*) found that the band broadening of nearly monodisperse dextran fractions in water on porous glass at u_z = 0.008 mm/s was nearly independent of the molecular weights.

The maximum in the h vs. M_w curve described by Hendrickson (*28*) has been confirmed for polystyrene gels by Tung and Runyon (*32*) and Yau et al. (*33*) and for dextran gels by Povey and Holm (*34*). Smit et al. (*35*) found, however, that h increased monotonicly with increasing M_w.

The seemingly contradictory findings of Smit (*35*) and of Tung and Runyon (*32*), which were both obtained by the reversed flow technique (*27*), can be explained by Kubin's (*36*) "sphere-model" of SEC, which assumes that only a given depth of the porous stationary particle is available to the polymer sample.

Both sphere models (*36, 37*) predict a maximum in the h vs. M_w curve, as a consequence of two opposing effects. Band broadening is increased as M_w increases (because of decreasing of diffusion coefficients) and it is decreased with increasing M_w.

Berger (*38*) has demonstrated, with the aid of radioactively labeled polystyrene samples, that as far as the elution volume is concerned, a polydisperse sample behaves like a mixture of many monodisperse substances. This is also true for h, as long as there are no big differences in diffusion coefficients.

From the above it can be seen that the causes of band broadening in SEC are *qualitatively* well understood. The major ones are, in the *interstitial volume*, (a) longitudinal diffusion, (b) eddy diffusion, and (c) mass transfer effects and in the pore volume (d) mass transfer effects and (e) polydispersity of the sample.

The *quantitation* of the above contributions to band broadening is extremely difficult. Theory is formulated in terms of independent effects, whereas an experiment always yields the sum of several terms (*39*).

In the main, four experimental approaches have been used to isolate the various contributions to band broadening in SEC:

(1) The measurement of h vs. u curves with different combinations of particle size, eluent, and monodisperse sample. This is the classical approach to chromatographic kinetics.

(2) The reversed flow method of Moore (*27*), which eliminates band broadening caused by the polydispersity of the sample.

(3) Experiments with porous and with nonporous packing materials, under as nearly as possible identical chromatographic conditions. Peak broadening in the pores being calculated by difference from measurement in two different columns (*10, 12-14*).

(4) On the basis of theoretical considerations, columns of different length allow the isolation of peak broadening due to polydispersity (*22, 23*).

In this paper, we propose an experimental method which allows the direct measurement of interstitial band broadening in columns packed with porous materials. The same column can also be used to measure the total band broadening. Thereby overcoming the problem of calculating band broadening inside the pores from data obtained with different columns that never pack identically (*39*). This is done by filling the pores of the stationary phase with a different liquid phase, as in liquid-liquid chromatography (*40*). Any sample, which cannot penetrate the stationary liquid phase, which fills the pore volume, can have its interstitial band broadening measured. The total peak broadening of polystyrene samples on a porous silica column was measured using "dry" dichloromethane as eluent. If the column is equilibrated with water-saturated dichloromethane ("wet" eluent), the total pore volume is filled with water, producing a heavily loaded column (*41-44*). Since the pore volume is now inaccessible to polystyrene samples, it is possible to measure their interstitial band broadening.

EXPERIMENTAL SECTION

Supports and Packing Procedures. The silicas used are described in Table I. Supports 1, 8, 9, and 10 were used as delivered. The support for column 2 was dry sieved and freed from fines by repeated sedimentation in water. Columns 3-7 were packed with material prepared from a single batch of Lichrosorb SI 500 of a sieve fraction 63-200 μm. Packings 3 and 4 were obtained by dry sieving. In order to obtain packings 5-7, we ground the original material in an achat mill, support 5 was obtained from the ground material by sieving and 6 and 7 by

Table I. Properties of Silica Packed Columns

support or column no.	silica	origin	d_p,[a] μm	O_{sp},[b] m^2/g	$V_{p,sp}$,[b] cm^3/g	ϕ,[b] Å	columns L, cm	i.d.,[c] mm	V_K, cm^3	d_p,[d] μm
1	Lichrosorb Si 100	e	10	330	1.0	94	27.8	4	4.076	9.4
2			150-200				50	8	25.10	170
3	Lichrosorb Si 500	e	100-125	100	0.75	390	102	4	12.302	110
4			63-71				45	4	5.540	67
5			25-32				30	4	4.233	28.5
6							23	4	2.995	13.8
7							17.7	4	2.452	6.5
8	Spherical silica	f	7-11	205	1.8	260	27.8	4	3.876	7.4
9	Lichrosorb Si 100	e	7	330	1.04	94	25	4.5	4.030	7.8
10	Spherisorb S5W	g	5	280	0.54	79	25	4.5	4.030	5.7

[a] Sieve fraction. [b] Measured and calculated according to ref 64. [c] Nominal i.d. [d] As calculated from the permeability (*45*), or from our sieve fraction. [e] E. Merck A.G., Darmstadt. [f] Kindly donated by K. Unger, Technical University, Darmstadt. [g] Phase Separation Ltd., Queensferry, Clwyd, U.K.

countercurrent sedimentation in acetone.

Silicas with $d_p \geq 40$ μm were dry packed (*44*, *46*). The best results were obtained when the silica was dried overnight at 130 °C and was packed while still warm.

Of the various slurry techniques described in the literature (*47–51*) a modified viscosity method (*47*) was chosen, with mixtures of cyclohexanol, 2-propanol, and carbon tetrachloride as the suspending medium. Column packing techniques have been well reviewed (*50*, *51*), nevertheless, we found it necessary to establish the optimum conditions for each silica and for each sieve fraction by trial and error.

Samples and Eluents. Polystyrene sample standards (PSt) of narrow molecular weight distribution were obtained from Waters Associates Inc. (Milford, MA) and from Pressure Chemical Co. (Pittsburgh, PA). In this paper we have designated, for example, a PSt with M_w = 111 000 as PSt 111. Benzene and 1,3-diphenylbutane were also used as samples. The later compound, with a molecular weight of 210, is designated as 0.21. The samples were dissolved in dichloromethane (concentration: 0.1–0.5%).

The dichloromethane eluent was continuously recycled. To obtain "dry" conditions, we included a moisture control system (*52*) and a column packed with 5-Å molecular sieve in the eluent circuit. The water content of the "dry" dichloromethane so obtained was less than 5 ppm. For the production of water-saturated dichloromethane ("wet" eluent), a temperature-controlled reservoir, where the eluent was stirred in contact with water, was included in the eluent circuit. The water content of the "wet" dichloromethane was approximately 2200 ppm.

With a new eluent the whole chromatographic system was always equilibrated for at least 12 h. A heat exchanger was installed between the pump and the injection system.

The column itself was enclosed in a thermostated water jacket. The temperature was controlled to 22 ± 0.1 °C.

The water content of the eluent was determined by Karl Fischer titration (Metrohm, Herisau, Switzerland), before and after each measurement.

Apparatus. The equipment was assembled from commercially available and homemade units. Special attention was paid to the connection between injection system, column, and detector to minimize extra column band broadening, which may yield misleading results in HPLC (*9*, *53*, *55*, *56*, *62*) and in SEC (*10*, *54*, *57*, *58*). For the same reason samples were injected on the top of the small volume columns (*59–61*) through a septum. Samples were introduced onto the larger volume columns by means of a sample loop (either Rhenodyne type 7 120, Kontron Technik, Eching or type U6K, Waters Associates). A Waters M 6000 syringe pump or an M3 (Orlita, Giessen) membrane pump were used. The UV detector (254 nm, cell volume 8 μL) was homemade (*47*, *62*). Columns were made from drilled out (*47*) stainless steel tubes (nominal i.d. 4 mm or 8 mm) and modified Swagelock fittings. Empty column volumes (V_k) were determined by weighing the column empty and filled with water.

Presentation of Data. Linear velocities are always quoted in terms of u_z, the linear velocity of a totally excluded sample.

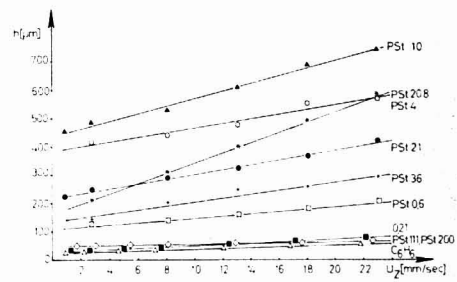


Figure 1. h vs. u_z curves for column 1 (SI 100, 10 μm) in "dry" CH_2Cl_2: $\epsilon_z = 0.454$, $\epsilon_p = 0.382$.

The shape of the plate height vs. linear velocity curve is the same, whether u or u_z is used. However, the constants of the equations describing it, such as the van Deemter equation, will be changed by the transposition.

The h values were calculated from the intercept of the tangents to the point of inflection, assuming Gaussian peaks. The constants of the h vs. u_z curves, eq 3, were calculated by the least-squares method.

RESULTS AND DISCUSSION

The h vs. u Curves Obtained with "Dry" and with "Wet" Dichloromethane. The change in pore volume experienced on changing from "dry" to "wet" eluent can be expressed in terms of the dimensionless porosities (*63–65*)

$$\epsilon_z = V_z/V_k \quad (6)$$

$$\epsilon_p = V_{p,max}/V_k \quad (7)$$

$$\epsilon_t = \epsilon_z + \epsilon_p = (V_z + V_{p,max})/V_k \quad (8)$$

The h vs. u_z curves for eight polystyrenes, 1,3-diphenylbutane, and benzene obtained on column 1 (Lichrosorb SI 100, d_p = 10 μm) using "dry" CH_2Cl_2 are shown in Figure 1. The descending branches of this and of most other curves were not determined, because of the very low u_z which would have been involved. The h vs. u_z curves in Figure 1 are linear. The two excluded polymers, PSt 111 and PSt 200, together with the two monomers, have the lowest, and very similar, h values, which are almost independent of u_z. The partially excluded polystyrenes disclose no obvious relationship between h values, C terms, and M_w.

The h vs. u_z curves of the same samples, on the same column, are, however, quite different, when the eluent is "wet" CH_2Cl_2, as shown in Figure 2. The pore volume here is almost totally filled with water and is not accessible for the samples

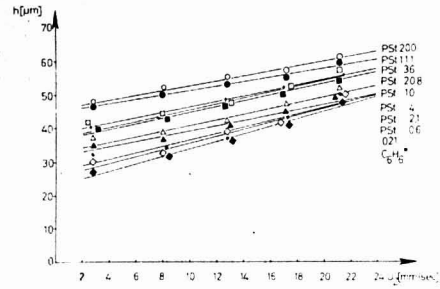


Figure 2. h vs. u_z curves for column 1 in "wet" CH_2Cl_2: $\epsilon_z = 0.446$, $\epsilon_p = 0.010$. The samples are listed in the order of their A' values.

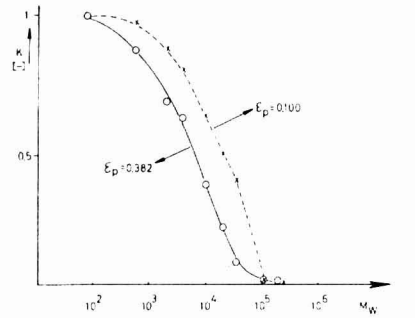


Figure 3. Calibration curves for column 1 with "dry" and "moist" CH_2Cl_2: (solid line) "dry" CH_2Cl_2 (<5 ppm H_2O), $\epsilon_p = 0.382$; (broken line) "moist" CH_2Cl_2 (0.2% H_2O), $\epsilon_p = 0.100$.

($\epsilon_p = 0.01$). Now for all flow velocities the h values increase with increasing M_w. It can be seen that, at a given velocity, the h values differ at most by a factor of 2, while in Figure 1 the h values for PSt 10 were at least 15-fold greater than those for benzene.

By accurately controlling the water content of the eluent (*52*), it is possible to produce a partial filling of the pores, so that the ϵ_p lies between that obtained in Figure 1 and that in Figure 2. However, it should be recognized, that in this case not only the pore volume but also the mean pore size change. Figure 3 shows the calibration curves (K vs. log M_w) for "dry" eluent ($\epsilon_p = 0.382$) and for such a partially loaded system ($\epsilon_p = 0.100$). Figure 4 shows the h vs. u_z curves of this system. In comparison with Figure 1 (the data for "dry" eluent) lower h values were obtained for permeating polystyrenes. The sequence of the curves is also changed.

When silica of similar type but much larger particle size (150–200 µm) is used, then the shape of the h vs. u_z curves changes. Column 1 (Figure 1–4) was filled with SI 100, d_p = 10 µm, column 2 (Figures 5 and 6) was packed with SI 100, d_p = 150–200 µm, which was not from the same batch of silica. Figure 5 was obtained by using "dry" CH_2Cl_2. In contrast to Figure 1 most of the curves are not straight. The contrast between Figure 6 and Figure 2, both obtained by using "wet" CH_2Cl_2, is much more striking. The h vs. u_z curves in Figure 2 are linear, while those in Figure 6 are concave. It is remarkable, that the lowest plate height measured for benzene in this column was 175 µm, corresponding to the mean particle diameter. As is to be expected, the band broadening obtained with "dry" CH_2Cl_2 is about 10-fold greater than that obtained with "wet" eluent. Consequently h is sometimes expressed,

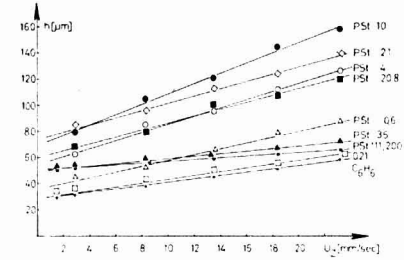


Figure 4. h vs. u_z curve for column with "semiwet" CH_2Cl_2: water content of the eluent, 0.2%; $\epsilon_z = 0.437$, $\epsilon_p = 0.100$.

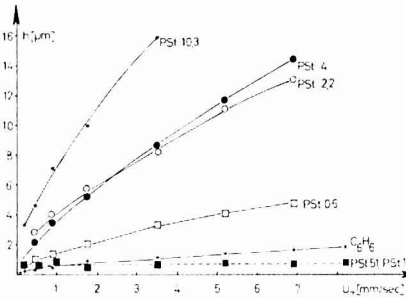


Figure 5. h vs. u_z curves for column 2 (SI 100, 150–200 µm) in "dry" CH_2Cl_2: $\epsilon_z = 0.365$, $\epsilon_p = 0.443$.

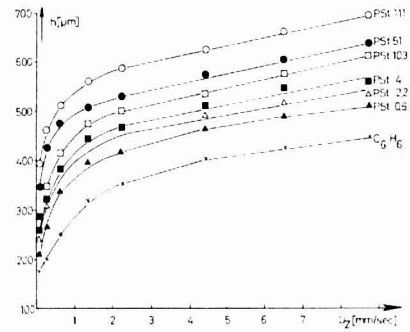


Figure 6. h vs. u_z curves for column 2 in "wet" CH_2Cl_2: $\epsilon_z = 0.365$, $\epsilon_p = 0.005$.

in the figures, in millimeter instead of micrometer units.

The effect of particle size on the h vs. u_z curves obtained with "wet" and with "dry" CH_2Cl_2 was also studied by using silicas of different particle size ranges prepared from the same batch of silica, columns 3–7, as described in Table I. The average pore size of this silica was 390 Å in contrast to that in columns 1 and 2 (Figures 1–6), where the average pore size was 94 Å. As before the h vs. u_z curves for the smaller particles were straight and for the larger concave.

The h vs. u_z curves obtained in column 4 (SI 500, 63-71 µm) are illustrated in Figures 7 and 8. The curves for PSt 111 and for PSt 55 in "dry" eluent, which are indicated by broken lines in Figure 7, have no meaning, since peaks for these substances were nonsymmetrical and the h values were

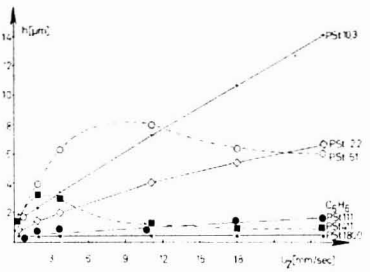


Figure 7. h vs. u_z curves for column 4 (SI 500, 63–71 μm) in "dry" CH_2Cl_2: $\epsilon_z = 0.352$, $\epsilon_p = 0.311$.

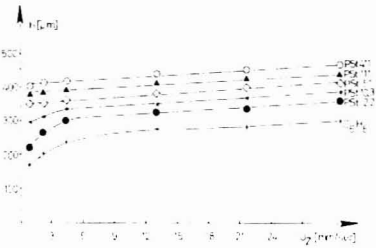


Figure 8. h vs. u_z curves for column 4 in "wet" CH_2Cl_2: $\epsilon_z = 0.352$, $\epsilon_p = 0.005$.

evaluated by the tangent method and thus erroneous (*55*). For these two samples the elution volume defined by the peak maximum decreased with increasing flow rate, while remaining constant for the other samples.

Similar curves to those shown in Figures 7 and 8 were obtained by using columns 3 and 5, filled with particles greater in size than 25 μm.

When the particle size of the SI 500 was 13.8 μm or 6.5 μm, and the column was wet packed, then the h vs. u_z curves were always linear, as is usual in HPLC.

It was not possible to measure h vs. u_z curves for column (SI 500, 6.5 μm) in "wet" CH_2Cl_2, because if the pore volume was filled with water and then flushed with "wet" eluent at 1 mL/min for 12 h, almost 20% of the water was washed out of the pores. With a flow rate of 7.5 mL/min over 90% of the water was washed out in the same time.

One explanation of this behavior could be erosion by eddies in the entrance to the pores, as postulated by van Kreveld and van den Hoed (*18*). On the other hand, since the pressure drop per unit length of column increases quadratically with decreasing particle size, the pressure drop across a particle is inversely proportional to particle size. It is possible, therefore, that with decreasing particle size (6.5 μm) and increasing pore diameter (390 Å) the eluent will begin to move in the pores, as postulated in the "separation by flow" models of gel permeation chromatography (*66–69*).

Such movement of the eluent in the pores of small particles may be of importance in HPLC in the isocratic mode, when using binary or ternary eluent mixtures of widely differing polarities, where one component of the eluent is enriched in the pores. This enrichment could be a function of particle size, pore size, and flow rate, causing changes in absolute and relative retentions with time after equilibration.

It was also not possible to fill the pores of column 8, packed with spherical silica (7.4 μm, 260 Å), with water using "wet" CH_2Cl_2. The probable reason is, that since this material is produced from organosilanes, its surface is rather hydrophobic. We have noticed similar effects in other silicas, where organic material was involved in the production. Column 8 packed with the spherical silica had values of $\epsilon_z = 0.333$ and $\epsilon_p = 0.531$. The high pore volume per unit column volume is theoretically desirable for SEC. However, with dry eluent the column produced unusually high mass transfer C terms for its particle size.

Table II. Constants of Equation 9 $D_m = kM_w^{-b}$ for Polystyrenes

authors	citation	solvent	k, cm²/s	b
Hendrickson	28	toluene	6.85×10^{-4}	0.57
Ouano-Barker	37	chloroform	5×10^{-4}	0.60
Kreveld-Hoed	18	tetrahydrofuran	2.45×10^{-4}	0.54
Knox	23	dichloromethane	4.53×10^{-4}	0.595

Calculation of Diffusion Coefficients. It is necessary to know the diffusion coefficients (D_m) of the samples in the eluent, if h vs. u_z curves are to be interpreted. The diffusion coefficients of homologous polymers can be described empirically by

$$D_m = kM_w^{-b} \tag{9}$$

where k and b are empirical constants. Some constants for this equation are given in Table II. The D_m values of Hendrickson (*28*) were plotted by us against M_w. Ouano and Barker (*37*) used D_m data from the literature (*70*) to calculate the constants; van Kreveld and van den Hoed (*18*) measured D_m by small angle light scattering.

Diffusion coefficients for gases (*72*) and for liquids (*73*) can be calculated from chromatographic data in open tubes, using the equation of Taylor (*74*). Giddings (*39*) determined D_m for one polystyrene ($M_w = 4000$) in four different solvents, by this means.

We have calculated D_m for polystyrene in CH_2Cl_2 at 22 °C from the B terms of the h vs. u_z curves for a packed column (column 9, SI 100, 7 μm), using the method of Jansen (*75*). "Dynamic" and "static" measurements were made. The lowest flow rate, where the conventional "dynamic" method can be used, is determined by the quality of pump. We obtained the lowest constant flow rate with a combination of the M 6000 pump and the M 660 flow programmer (Waters Associates). Extremely small flow rates, down to 0.001 mm/s, were simulated by the "static" method. In this method the residence time of the sample in the column is increased, by stopping the flow for a given time, sometime after the sample has been introduced into the column. The elution volume is independent of the residence time. Consequently plate heights can be calculated from peak volumes. The "average linear velocity (u)" of the eluent was calculated as the ratio between the column length and the time elapsed between injection and detection of the sample. The interstitial velocity (u_z) was calculated by substituting the values of ϵ_z and ϵ_t in eq 4. The longest residence time of a sample in the column was more than a week.

The h vs. u_z curves, obtained in this way, for benzene and PSt 111, in dry CH_2Cl_2, are shown in Figure 9. As can be seen, the agreement between "dynamic" (open symbols) and "static" (solid symbols) measurements is good.

An analogous equation to that of van Deemter can be written relating h and u_z

$$h = A + \frac{B_z}{u_z} + C_z u_z \tag{10}$$

where $B_z = B/\beta$ and $C_z = C\beta$.

From the h vs. u_z curves of benzene and three polystyrenes, B_z values were calculated. The B_z term is proportional to D_m.

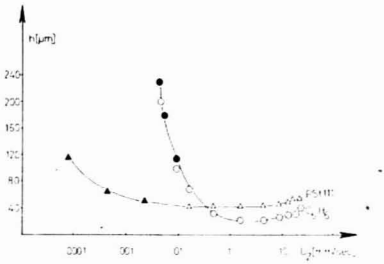


Figure 9. Low velocity h vs. u_z curves for column 8 (SI 100, 7 μm) in "dry" CH_2Cl_2: $\epsilon_z = 0.463$, $\epsilon_p = 0.400$; (solid symbols) "static" method, (open symbols) "dynamic" method.

Longitudinal diffusion only takes place during the residence of the sample in the interstitial volume, consequently

$$B_z \sim D_m \frac{\epsilon_i}{\epsilon_z} \tag{11}$$

Combining eq 9 and 11

$$B_z \sim \frac{\epsilon_i}{\epsilon_z} M^{-b} \tag{12}$$

where ϵ_i is the total porosity available to a given sample and is a function of M_w.

If $B_z\epsilon_z/\epsilon_i$ is plotted against M_w in log–log format, from the slope of the straight line it can be calculated, that

$$D_m \sim M_w^{-0.6} \tag{13}$$

This is in good agreement with the figure calculated by Knox (*23*) if we used the Wilke–Chang eq (*71*). From Figure 12 it can also be calculated, for polystyrene samples in CH_2Cl_2 eluent, that

$$B_z\epsilon_z/\epsilon_i = (6 \times 10^{-4})M_w^{-0.6} \tag{14}$$

Band Broadening in the Interstitial Volume. All the more sophisticated attempts (over and above the A and B terms in eq 2) to describe band broadening in the interstitial volume, resemble the coupling term of Giddings (*6*). However, Giddings himself (*39*) has written: "The coupling expression is simply an approximation to a very complex interaction between diffusion and convection. The process has been formulated rigorously, but the boundary conditions for real granular beds are so complex, that meaningful solutions have not yet been obtained."

We shall try to describe our experimental results in terms of empirical equations with only a few constants. It is not likely that each of these constants will be ascribable to a single physical effect.

Synder (*15*) described total band broadening in adsorption chromatography by the empirical equation

$$h = \text{const } u^m \tag{15}$$

Knox (*16*, *76*) used a similar empirical form, when describing interstitial band broadening in terms of reduced parameters.

$$h_{red} = \text{const } u_{red}^{1/3} \tag{16}$$

In Figures 10–12 h_{red} is plotted against $u_z d_p M_w^{0.6}$ in log–log terms, that is, a quasi-reduced presentation. Only data obtained with "wet" CH_2Cl_2 are presented, and consequently here $u_z = u$.

If D_m is assumed to be about $(5 \times 10^{-4})M_w^{-0.6}$ cm²/s, then

$$u_{red} = \text{constant } u_z d_p M^{0.6} \tag{17}$$

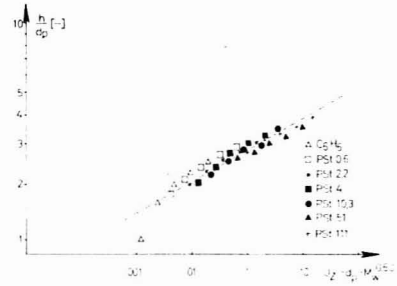


Figure 10. h_{red} vs. u_{red} (quasi) for column 2 (SI 100; 150–200 μm) in "wet" CH_2Cl_2.

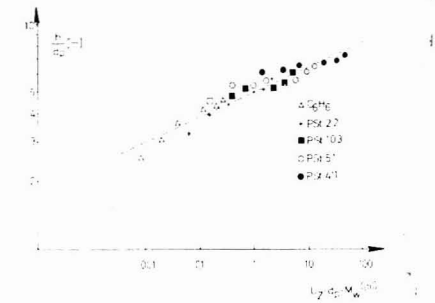


Figure 11. h_{red} vs. u_{red} (quasi) for column 4 (SI 500; 63–71 μm) in "wet" CH_2Cl_2.

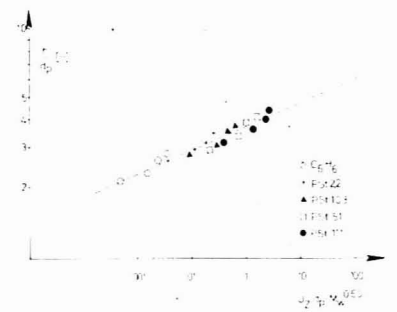


Figure 12. h_{red} vs. u_{red} (quasi) for column 6 (SI 500; 13.8 μm) in "wet" CH_2Cl_2.

Thus to obtain u_{red} from the abscissas of our plot, it must be multiplied by a constant factor, whose value is about 2000.

The plots in Figures 10–12 show a considerable amount of scatter, not all of which can be attributed to experimental error. They also diverge from linearity. Therefore we concur with other authors (*77*, *78*), who stated that the concept of reduced parameters alone is not sufficient to describe band broadening in the interstitial volume of a packed column.

The corresponding equation to eq 16 of Knox for ot quasi-reduced velocity is

$$h_{red} = A^*(u_z d_p M_w^{0.6})^m \tag{18}$$

The value of A^* is a good measure of the efficiency of a column (*79*), because it defines plate height when $u_z d_p M^{0.6} = 1$. The

Table III. The Constants of Equation 18 together with ϵ_z for Various Columns

column no.	packing	d_p, μm	A^*	m	ϵ_z[a]
1	SI 100	10	5.6	0.10	0.454 (s)
2		150–200	2.8	0.14	0.365 (d)
3	SI 500	100–125	6.7	0.09	0.393 (d)
4		63–71	4.9	0.11	0.352 (d)
5		25–32	5.5	0.15	0.466 (s)
6		13.8	3.8	0.10	0.501 (s)

[a] Key: d = dry packing; s = slurry packing.

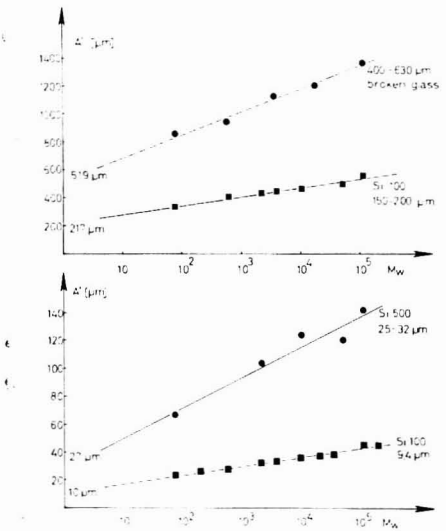


Figure 13. A' (from eq 5) vs. log M_w plots in "wet" CH_2Cl_2 for columns 1, 2, and 5 and for a column filled with broken glass. The figure to the left of each plot is the value of its intercept.

packing structure mainly determines A^*. The values of the constants for this equation are given in Table III. As can be seen the exponent m lies between 0.09 and 0.15 and is therefore more than a factor of 2 less than the value 0.33 proposed by Knox (*16*), which is most likely a consequence of differing packing technique.

The Quality of Column Packing. As can be seen from Table III ϵ_z is lower, consequently the packing density is higher, for those columns which were dry packed than is the case for those which were slurry packed. For dry packed column ϵ_z approaches the value of 0.36, calculated by Le Fevre (*80*) for randomly packed spheres. The relatively high ϵ_z = 0.393 in column 3 is probably a consequence of is small aspect ratio (δ), which is less than 40 (*14*, *37*, *81–86*).

From the systematic variation of ϵ_z it seems likely that the packing structure of dry and slurry packed columns is different. This conclusion is supported by the facts that column efficiency increases with increasing packing density for dry packed columns (*87*). With slurry packed columns, however, it is our experience, that very loose packing leads to extraordinarily efficient columns, which are unfortunately short lived.

It is, on the other hand, well established, that dry packed small particle size columns ($d_p \sim 10$ μm) are not efficient, even

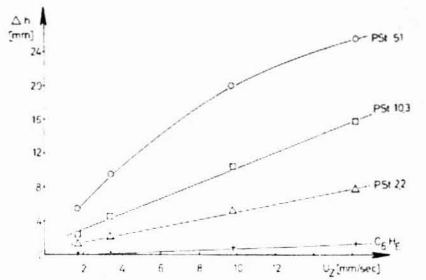


Figure 14. Δh vs. u_z curves for column 3 (SI 500, 100–125 μm).

Table IV. $\Delta A'$ and $\Delta C'$ (Equation 3) for Column 2 (SI 100, 150–200 μm)

	$\Delta A'$, μm	$\Delta C'$, ms
benzene	97	177
PSt 0.6	425	570
PSt 2.2	1800	1650
PSt 4	1280	1840
PSt 10.3	2740	3600

though high packing densities are obtained.

The constants of the simplified van Deemter equation (eq 3) were calculated, using "wet" CH_2Cl_2, for silicas of various sizes (10–200 μm) and for broken glass (500 μm). The A' values for large particle size columns were obtained by extrapolating the quasi-linear, high-velocity, part of the curve to zero. When A' is plotted vs. log M_w, a straight line is obtained for a "well-packed" column. Surprisingly the intercept of this plot is d_p, as is shown in Figure 13 for columns no. 1, 2, and 5 and a column packed with broken glass. This phenomenon has also been confirmed for aqueous eluents with dextran samples (*88*).

Band Broadening inside the Pores (Δh vs. u_z). The difference between the measured h vs. u_z curves obtained with "dry" and "wet" eluents (Δh vs. u_z) corresponds to the band broadening inside the pores. Such curves for column 3 are shown in Figure 14. With one exception, Δh vs. u_z curves are linear for all particle sizes and all samples and can be described in terms of the simplified van Deemter equation, independent of the shape of the original h vs. u_z curves. The exception occurs in Figure 14 with PSt 51, which, as described previously, gave nonsymmetrical peaks. For this sample the low velocity part of the h vs. u_z curves was used to calculate the constants $\Delta A'$ and $\Delta C'$ of eq 3, where the original h vs. u_z are nearly linear. The relative errors in this case are, of course, large. Values of the constants $\Delta A'$ and $\Delta C'$ are given for column 2 (Si 100, 160–200 μm) in Table IV and for columns 3–6 (Si 500, various particle sizes) in Table V. The errors for benzene in Table V are large, because the original h values were small.

The h vs. u_z data for column 1 are presented in Figure 2 for "wet" CH_2Cl_2 (ϵ_p = 0.010), in Figure 4 for "semiwet" eluent (ϵ_p = 0.100), and in Figure 1 for "dry" CH_2Cl_2 (ϵ_p = 0.382). In the "semiwet" eluent the pores are partially filled with water. Subtracting the "wet" h vs. u_z curve from each of the other ones, two Δh vs. u_z curves are obtained. The values of $\Delta A'$ and $\Delta C'$ so obtained are given in Table VI. The calculation of these terms was facilitated by the fact that for this column all the original h vs. u_z curves, even those for high M_w samples, were linear.

The $\Delta C'$ terms are proportional to the mass transfer effects inside the pores. The $\Delta C'$ values given in Table VI are plotted vs. log M_w in Figure 15. As can be seen, both curves pass

Table V. $\Delta A'$ and $\Delta C'$ (Equation 3) for Columns 3–6 (SI 500)

	column 6 13.8 μm		column 5 25–32 μm		column 4 63–71 μm		column 3 100–125 μm	
	ΔA, μm	ΔC, ms	ΔA, μm	ΔC, ms	ΔA, μm	ΔC, ms	ΔA, μm	ΔC, ms
benzol	−2	1.1	−6	7.6	157	47	−102	87
PSt 2.2	43	7.5	57	45	853	227	607	456
PSt 10.3	70	15	147	77	1092	512	1180	911
PSt 51	105	29	403	125	1275	1250	1408	2405
PSt 111	100	29						

Table VI. The Variation of $\Delta A'$ and $\Delta C'$ with M_w in Column 1 (SI 100, 10 μm) with " Dry" (ϵ_p = 0.382) and with "Semiwet" (ϵ_p = 0.100) Eluent

	ϵ_p = 0.382		ϵ_p = 0.100	
	$\Delta A'$, μm	$\Delta C'$, ms	$\Delta A'$, μm	$\Delta C'$, ms
PSt 200	5	0	5	−0.1
PSt 111	3	0	6	−0.1
PSt 36	101	6.0	12	0.1
PSt 20.8	123	17.1	22	1.7
PSt 10	401	12.4	33	3.0
PSt 4	185	7.7	22	2.3
PSt 2.1	350	7.5	42	2.0
PSt 0.6	82	3.0	9	1.2
0.21	1	1.3	3	0.4
benzene	0	0.3	5	0.2

through a maximum. This supports the previously mentioned theory of Ouano and Barker (*37*), who proposed, that this term is determined by two opposing factors, having opposite effects. The two factors are decreasing diffusion coefficients (increasing $\Delta C'$ terms) and decreasing diffusion distances, caused by exclusion effects (decreasing $\Delta C'$ terms) with increasing M_w. For totally excluded samples $\Delta C'$ is zero, by definition, because then there is no mass transfer inside the pores.

If κ is defined as the ratio of the probabilities of the sample being in the pore volume or in the interstitial volume, then

$$\kappa = \frac{K\,V_{p,max}}{V_z} = \frac{V_p}{V_z} = \frac{\epsilon_p}{\epsilon_z} \tag{19}$$

then eq 1 can be rewritten as

$$V_e = V_z + V_p = V_z(1 + \kappa) \tag{20}$$

Thus κ is the analog in SEC of the capacity ratio in retentive chromatography. The mass transfer term in the nonmobile phase, i.e., the C_s term in the retentive chromatogrpahy, is the analog of the mass transfer term in the pore volume $\Delta C'$ in SEC. Different theoretical approaches assume explicitly or implicitly the proportionality of the $\Delta C'$ to the κ containing term.

The following proportionality term was originally proposed by van Deemter (*3*) and by Golay (*89*) and has been cited by many authors (*6*, *9*, *11*, *17*, *90*, *91*)

$$\Delta C' \sim \frac{\kappa}{(1 + \kappa)^2} \tag{21}$$

while Ouano and Barker (*37*) proposed

$$\Delta C' \sim (1 - (1 - K)^{1/3})^2 \tag{22}$$

and Kubin (*36*)

$$\Delta C' \sim \frac{\kappa(1 - \epsilon_z)/\epsilon_p}{(1 + \kappa(1 - \epsilon_z)/\epsilon_p)^2} \tag{23}$$

Our measured $\Delta C'$ terms were divided by each of the proportionality terms in eq 21–23, respectively, to yield three different values of $\Delta C'_{adj}$. These C'_{adj} terms are different theoretical attempts to produce a term which only depends

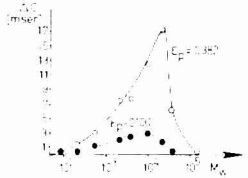


Figure 15. $\Delta C'$ vs. log M_w curves for column 1 (SI 100, 10 μm) as calculated by using "dry" (ϵ_p = 0.382) and "semiwet" (ϵ_p = 0.100) CH_2Cl_2 as eluent: (solid line) ϵ_p = 0.382, (dotted line) ϵ_p = 0.100.

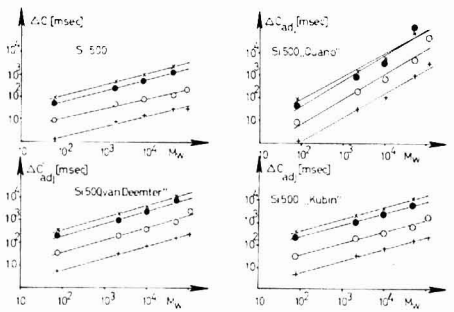


Figure 16. $\Delta C'$ and $\Delta C'_{adj}$ vs. M_w lines on silica SI 500 of the same batch and different sieve fractions: column 3 (100–125 μm), ×; column 4 (63–71 μm), ●; column 5 (25–32 μm), ○; column 6 (13.8 μm), +.

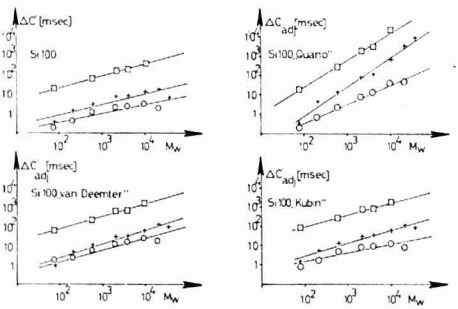


Figure 17. $\Delta C'$ and $\Delta C'_{adj}$ vs. M_w on silica 100 with different sieve fractions and different ϵ_p: column 2 (150–200 μm), □; column 1 (10 μm, ϵ_p = 0.382), +; column 1 (10 μm, ϵ_p = 0.100), ○.

on the restricted diffusion coefficient (D_s) of the sample in the pores. In Figure 16 $\Delta C'$ and the three different values of $\Delta C'_{adj}$ are plotted against M_w, for silica SI 500 of various sieve fractions. Similar plots for silica 100 of different sieve fractions

Table VII. Slopes and Relative Errors (±%) of the Best Straight Lines for Figures 16 and 17

	unadjusted		van Deemter equation (27)		Ouano equation (28)		Kubin equation (29)	
d_p, μm	slope	% error	slope	% error	slope	% error	slope	% error
			SI 500					
13.8	0.463	11	0.539	3	1.071	7	0.509	5
25-32	0.439	8	0.547	11	1.124	14	0.495	10
63-71	0.504	4	0.554	12	1.133	20	0.501	6
100-125	0.503	5	0.536	9	1.020	16	0.501	6
			SI 100					
10 (0.382)	0.533	24	0.714	10	1.399	5	0.665	12
10 (0.100)	0.436	26	0.524	17	0.988	5	0.438	25
150-200	0.620	7	0.644	6	1.545	6	0.613	6

and different ϵ_p values are shown in Figure 17. The slopes and relative errors (as percentages) of the best straight lines for the curves shown in Figures 16 and 17 are given in Table VII. As can be seen from this table, deviations from linearity are largest for column 1 (SI 100, 10 μm). This is reasonable, because in this column measurements were made with samples of high M_w, and hence low κ value. In this range the correction functions are very sensitive to small changes of κ. Furthermore the large molecular volume following on high M_w may lead to unusually hindered diffusion.

The calculated $\Delta C'_{adj}$ are inversely proportional to D_s; if it is assumed that

$$D_s = \text{const } M_w^{-b_s} = \gamma_s D_m \tag{24}$$

then the slope of a log $\Delta C'_{adj}$ vs. log M_w plot, as given in Table VII, is the constant b_s. As can be seen in Table VII the b_s values (i.e., the slopes), no matter which theoretical approach is used, depend upon the average particle size.

Most authors prefer to use the obstruction factor γ_s, as defined in eq 5 and repeated in eq 24, to describe mass transfer controlled by restricted diffusion in the pores. This factor (γ_s) was originally regarded as a constant (*7*, *92*). Later van Kreveld and van den Hoed (*18*) and Knox and McLennan (*23*) found that γ_s decreased with increasing M_w. As shown here b_s, and consequently γ_s, is also a function of the pore size distribution and of the specific pore volume. It is thus not surprising, that in ref (*18*) and (*23*) quite different factors were obtained by using different types and sieve fractions of silica.

In order to investigate the dependence of $\Delta C'_{adj}$ (i.e., D_s) on particle size, for the columns packed with SI 500, we plotted the intercepts of the plots in Figure 16 vs. d_p, as given in Table I; see Figure 18. The uncorrected and the three theoretically corrected approaches are each represented by one plot in Figure 18. The values of the slopes are given along side each plot in parentheses. It can be seen that, independent of the approach, $\Delta C'_{adj}$ is proportional to d_p^2.

Calculation of Polydispersities of the Polystyrene Samples from the $\Delta A'$ Term. The $\Delta A'$ term is the contribution to band broadening of a polymer standard sample, caused by its polydispersity, and is independent of the flow velocity. The molecular weight distribution of the polystyrene standard samples can, because of their method of production, be described, to a good approximation, by a normal Gaussian distribution.

If the standard deviation of the sample peak (in volume units) due to the polydispersity of the sample ($P = M_w/M_n$) is designated σ_v(MWD), then

$$\Delta A' = L\left(\frac{\sigma_v(\text{MWD})}{V_e}\right)^2 = L\left(\frac{\Delta K V_{p,max}}{V_e}\right)^2 \tag{25}$$

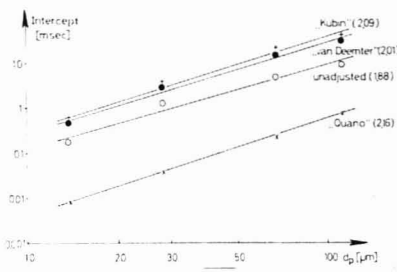


Figure 18. Intercepts from Figure 19 vs. particle size in columns filled with SI 500 silica. The slopes of the curves are given in parentheses.

This expression allows the calculation of ΔK from the experimental data. The value of K can be obtained from eq 1. From the log M vs. V_e (or K) calibration curve, the molecular weights corresponding to $K + \Delta K$ and $K - \Delta K$ can be calculated. Half of the difference between these two molecular weights is taken as the standard deviation (σ_m) of the molecular weight distribution.

According to Ousterhoudt and Ray (*93*) and later Knox (*22*) the polydispersity (P) can be calculated from

$$P = 1 + \left(\frac{\sigma_m}{M_n}\right)^2 = 1 + \left(\frac{\sigma_m}{M_w/P}\right)^2 \tag{26}$$

The $\Delta A'$ values obtained with column 1 (SI 100, 10 μm) and column 6 (SI 500, 13.8 μm) were used to calculate P for polystyrene samples. The molecular weight differences were determined from small elution volume differences by using the semilogarithmic calibration curve, hence errors will be large. It is questionable whether this source of error could be avoided by an analytical formulation of the calibration curve. Our polydispersities, together with those of other authors, are listed in Table VIII. The agreement is surprisingly good, especially since the same batches of the standards were not used. This can be taken as a tribute to the technology used in the preparation of such standards.

Pore Structure and Band Broadening inside the Pores. It is a well-known fact that for partially excluded substances the h vs. M_w curve passes through a maximum. Werner and Halász (*97*) showed that this maximum corresponds to the maximum in the pore size distribution, as determined by SEC (*63*, *64*), where the probability of a particular pore size (ϕ) is proportional to $\Delta\epsilon_i/\Delta \log \phi$. In Figure 19 the variation of $\Delta C'$, $\Delta A'$ and the pore size probability is plotted against M_w. The maximum in the $\Delta C'$ value (dotted line in Figure 19) was

Table VIII. Polydispersities of the Polystyrene Samples

M_w	Knox (94)	Dawkins (26)	Kato (95)	Tung (96)	this work
600					1.4
2 000	1.036				
2 100					1.8
2 350		1.16			
4 000	1.003				1.07
9 800		1.08			
10 000	1.063		1.04		1.06
10 300			1.06	1.08	1.12
19 800			1.05	1.07	
20 000	1.015				
20 800					1.02
33 000	1.008				
35 000		1.02			
36 000					1.02
37 000			1.01		
51 000			1.02	1.03	1.03
110 000			1.01		
111 000					1.01
200 000		1.06			

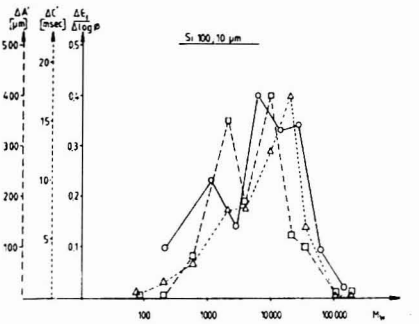


Figure 19. The variation of $\Delta A'$, $\Delta C'$, and the pore size distribution with the M_w of the sample: data from column 1 (SI 100, 10 μm); $\Delta A'$, dashed line; $\Delta C'$, dotted line; pore probability ($\Delta\epsilon_i/\Delta \log \phi$), solid line.

discussed in Figure 15. The maximum in the $\Delta A'$ values is caused by the fact that most samples have very similar polydispersities (see Table VIII), and hence band broadening is nearly proportional to the slope of the calibration curve.

CONCLUSION

The interstitial band broadening in silica filled columns has been determined experimentally. The pores were filled with water, which is impenetrable to the benzene and polystyrene samples. By variation of the controlled water content of the CH_2Cl_2 eluent the pores could be empty ("dry" eluent), semifilled ("semiwet" eluent), or filled up ("wet" eluent). Total and interstitial band broadening was thus measured directly in the same column. The band broadening in the pores was obtained by difference (Δh). Velocities are expressed in terms of interstitial velocity (u_z), which is appropriate to SEC. The ascending branches of the h vs. u_z curves are all linear, when the reduced velocities are small enough, which is usual in HPLC and SEC, i.e., $d_p < 15$ μm. With larger particles, i.e., bigger reduced velocities in routine work, the curves can be concave. The h values obtained with water-filled pores are 10 times smaller than those obtained with accessible pores. For one column ($d_p = 170$ μm) $h = d_p$ was measured with benzene, when the pores were filled with water. The dependence of the various sorts of band broadening on d_p has been studied by using supports of differing d_p from the same batch of silica ($\phi = 390$ Å). The diffusion coefficients of polystyrenes in CH_2Cl_2 as a function of M_w were measured in a packed column by a stopped flow method, with residence times of up to 1 week ($D_m \sim (6 \times 10^{-4}) M_w^{-0.6}$ cm²/s). The directly measured reduced interstitial band broadening is proportional to the reduced velocity raised to the power of 0.09–0.15, which is a factor of at least 2 smaller than reported earlier (16). Band broadening inside the pores was calculated from the Δh vs. u_z curves. The mass transfer term here ($\Delta C'$) passes through a maximum as M_w is increased, because the effect of the decreasing diffusion coefficient opposes that of the decreasing diffusion distance. The $\Delta C'$ term is a function of the restricted diffusion coefficient (D_s) and of κ, which is the SEC analog of the capacity ratio in retentive chromatography. Three different published suggestions as to the form this function takes were used to calculate different estimates of D_s and of the obstruction factor (γ_s). It is shown that restricted diffusion, described in terms of D_s or γ_s, is not only a function of M_w of the samples but also of the pore size distribution and specific pore volume of the solid. The polydispersity of polystyrene samples was calculated from the $\Delta A'$ terms. These values agree well with published ones.

The following results have implications for HPLC in general. Columns of small particle size (7.4 μm), whose pores (ϕ = 260 Å) are loaded with water, are not stable; as the flow rate is increased the water is washed from the pores. In isocratic HPLC methods, where the composition of eluent in the pores differs from that in the bulk, a similar effect will occur, causing changes in the retentions as a function of time after equilibration. Spherical silicas made from organosilanes are less hydrophylic than the conventional. Extremely high pore volumes, theoretically desirable in SEC, lead in practice to undesirably high mass transfer terms. The efficiency of a dry packed column usually increases with increasing packing density, i.e., with decreasing interstitial porosity (ϵ_z). Typically for irregular silica $\epsilon_z = 0.36$, which is close to the theoretical value for randomly packed spheres. In contrast to a slurry packed column $\epsilon_z > 0.45$. The difference in the packing structure is not understood.

ACKNOWLEDGMENT

Our special thanks are due to F. Hampson for extensive discussions during the preparation of the manuscript.

GLOSSARY

A	eddy diffusion constant
A'	eddy diffusion constant
A^*	constant
$\Delta A'$	A' for "dry" eluent minus A' for "wet" eluent
B	longitudinal diffusion constant
B_z	longitudinal diffusion constant
b	constant
b_s	constant
C	mass transfer constant
C'	mass transfer constant
C_z	mass transfer constant
$\Delta C'$	C' for "dry" eluent minus C' for "wet" eluent
$\Delta C'_{adj}$	$\Delta C'$ adjusted for κ containing term
D	diffusion coefficient
D_m	D in interstitial volume
D_s	D in the pores
d_c	column i.d.
d_p	mean particle diameter
h	height equivalent to the theoretical plate
h_{red}	h/d_p reduced plate height
Δh	h for "dry" eluent minus h for "wet" eluent
K	exclusion chromatographic partition coefficient
k	constant
L	column length
M_n	number averaged molecular weight
M_w	weight averaged molecular weight
m	constant
n	number of theoretical plates
O_{sp}	specific surface area

P	M_w/M_n polydispersity
t_z	elution time of a totally excluded inert peak
u	time averaged linear velocity of the eluent
u_z	linear velocity of a totally excluded inert sample
u_{red}	$u\,d_p/D$ reduced linear velocity
V_e	elution volume
V_k	empty column volume
V_o	elution volume of a totally penetrating inert sample
V_p	pore volume
$V_{p,max}$	pore volume available to smallest inert sample
V_z	interstitial volume
α	constant
β	ϵ_t/ϵ_z
γ_s	D_s/D_m obstruction factor
δ	d_c/d_p aspect ratio
ϵ_i	V_e/V_k total porosity available to a polymer of a given molecular size
ϵ_p	V_p/V_k pore porosity
ϵ_t	$\epsilon_z + \epsilon_p$ total porosity as measured by the smallest inert sample
ϵ_z	V_z/V_k interstitial porosity
κ	$\epsilon_p/\epsilon_z = V_p/V_z$
σ_m	standard deviation of the molecular weight distribution
σ_V	standard deviation in volume units
ϵ_v(M-WD)	ϵ_V caused by MWD
ϕ	diameter of a pore

LITERATURE CITED

(1) Giddings, J. C. *Anal. Chem.* **1967**, *39*, 1027.
(2) Tung, L. H.; Moore, J. C. In "Fractionation of Synthetic Polymers"; Tung, L. H., Ed., Marcel Dekker: New York, Basel, 1977.
(3) Deemter, J. J.; Zuiderweg, F. J.; Klinkenberg, A. *Chem. Eng. Sci.* **1956**, *5*, 271.
(4) Walton, H. F. In "Chromatography"; Heftmann, E., Ed., Reinhold: New York, 1961.
(5) Sternberg, J. C.; Poulson, R. E. *Anal. Chem.* **1964**, *36*, 1492.
(6) Giddings, J. C. "Dynamics of Chromatography, Part 1, Principles and Theory"; Marcel Dekker: New York, 1965.
(7) Giddings, J. C.; Mallik, K. L. *Anal. Chem.* **1966**, *38*, 997.
(8) Sie, S. T.; Rinjders, G. W. A. *Anal. Chim. Acta* **1967**, *38*, 3.
(9) Huber, J. F. K.; Hulsman, J. A. R. J. *Anal. Chim. Acta* **1967**, *38*, 305.
(10) Billmeyer, F. W.; Johnson, G. W.; Kelley, R. N. *J. Chromatogr.* **1968**, *34*, 316, 322.
(11) Huber, J. F. K. *J. Chromatogr. Sci.* **1969**, *7*, 85.
(12) Kelley, R. N.; Billmeyer, F. W. *Anal. Chem.* **1969**, *41*, 874.
(13) Kelley, R. N.; Billmeyer, F. W. *Anal. Chem.* **1970**, *42*, 399.
(14) Kelley, R. N.; Billmeyer, F. W. *Sep. Sci.* **1970**, *5*, 291.
(15) Snyder, L. R. In "Gaschromatography 1970"; Stock, R., Perry, S. G., Eds.; Institute of Petroleum: London, 1971.
(16) Done, J. N.; Knox, J. H. *J. Chromatogr. Sci.* **1972**, *10*, 606.
(17) Horvath, C.; Lin, H. J. *J. Chromatogr.* **1976**, *126*, 401.
(18) van Kreveld, M. E.; van den Hoed, N. *J. Chromatogr.* **1978**, *149*, 71.
(19) Johnson, G. W. Ph.D. Thesis, Rensselaer Polytechnic Institute, Troy, NY, 1967.
(20) Heitz, W.; Coupek, J. *Makromol. Chem.* **1967**, *105*, 280.
(21) Heitz, W. *Z. Anal. Chem.* **1975**, *277*, 323.
(22) Knox, J. H.; McLennan, F. *Chromatographia* **1977**, *10*, 75.
(23) Knox, J. H.; McLennan, F. *J. Chromatogr.* **1979**, *185*, 289.
(24) Dawkins, J. V.; Taylor, G. *Polymer* **1974**, *15*, 687.
(25) Dawkins, J. V.; Stone, T.; Yeadon, G. *Polymer* **1977**, *18*, 1179.
(26) Dawkins, J. V.; Yeadon, G. *J. Chromatogr.* **1980**, *188*, 333.
(27) Tung, L. H.; Moore, J. C.; Knight, G. W. *J. Appl. Polym. Sci.* **1966**, *10*, 1261.
(28) Hendrickson, J. G. *J. Polym. Sci., Polym. Phys. Ed.* **1968**, *6*, 1903.
(29) Bly, D. D. *J. Polym. Sci., Part C* **1968**, *21*, 13.
(30) Bly, D. D. *J. Polym. Sci., Polym. Chem. Ed.* **1968**, *6*, 2085.
(31) Basedow, A. M.; Ebert, K. H.; Ederer, H.; Hunger, H. *Makromol. Chem.* **1976**, *177*, 1501.
(32) Tung, L. H.; Runyon, J. R. *J. Appl. Polym. Sci.* **1969**, *13*, 2397.
(33) Yau, W. W.; Malone, C. P.; Suchan, H. L. *Sep. Sci.* **1970**, *5*, 259.
(34) Povey, N.; Holm, R. A. *J. Chromatogr.* **1970**, *46*, 33.
(35) Smit, J. A. M.; Hoogenvorst, C. J. P.; Staverman, A. J. *J. Appl. Polym. Sci.* **1971**, *15*, 1479.
(36) Kubin, M. *J. Chromatogr.* **1975**, *108*, 1.
(37) Quano, A. C.; Barker, J. A. *Sep. Sci.* **1973**, *8*, 673.
(38) Berger, K. C. *Makromol. Chem.* **1975**, *176*, 399.
(39) Giddings, J. C.; Bowman, L. M.; Myers, M. N. *Macromolecules* **1977**, *10*, 443.
(40) Martin, A. J. P.; Synge, R. L. M. *Biochem. J.* **1941**, *35*, 1358.
(41) Halász, I.; Engelhardt, H.; Asshauer, J.; Karger, B. L. *Anal. Chem.* **1970**, *42*, 1460.
(42) Engelhardt, H.; Weigand, N. *Anal. Chem.* **1973**, *45*, 1149.
(43) Engelhardt, H.; Asshauer, J.; Neue, U. D.; Weigand, N. *Anal. Chem.* **1974**, *46*, 336.
(44) Engelhardt, H. "High Performance Liquid Chromatography"; Springer: Berlin, Heidelberg, New York, 1979.
(45) Halász, I.; Schmidt, H.; Vogtel, P. *J. Chromatogr.* **1976**, *126*, 19.
(46) Halász, I.; Naefe, M. *Anal. Chem.* **1972**, *44*, 76.
(47) Asshauer, J.; Halász, *J. Chromatogr. Sci.* **1974**, *12*, 139.
(48) Kirkland, J. J. *J. Chromatogr. Sci.* **1971**, *9*, 206.
(49) Strubert, W. *Chromatographia* **1973**, *6*, 50.
(50) Martin, M.; Guiochon, G. *Chromatographia* **1977**, *10*, 194.
(51) Elgass, H.; Engelhardt, H.; Halász, I. *Fresenius Z. Anal. Chem.* **1979**, *294*, 97.
(52) Engelhardt, H.; Böhme, W. *J. Chromatogr.* **1977**, *133*, 67.
(53) Halász, I.; Gerlach, H. O.; Kroneisen, A.; Walkling, P. *Z. Anal. Chem.* **1968**, *234*, 97.
(54) Ouano, A.; Biesenberger, J. A. *J. Chromatogr.* **1971**, *55*, 145.
(55) Kirkland, J. J.; Yau, W. W.; Stocklosa, H. J.; Dilks, C. H. *J. Chromatogr. Sci.* **1977**, *15*, 303.
(56) Halász, I.; Engelhardt, H.; Groh, R.; Vogtel, P. *Erdöl* Kohle **1977**, *30*, 88; Compendium 76/77, 936.
(57) LePage, M.; Beau, R.; de Vries, A. J. *J. Polym. Sci., Part C* **1968**, *21*, 119.
(58) Ouano, A.; Biesenberger, J. A. *J. Appl. Polym. Sci.* **1970**, *14*, 471, 483.
(59) Hupe, K. P.; Bayer, E. *J. Chromatogr. Sci.* **1967**, *5*, 197.
(60) Halász, I.; Kroneisen, A.; Gerlach, H. O.; Walkling, P. *Z. Anal. Chem.* **1968**, *234*, 81.
(61) Scott, R. P. W.; Lawrence, J. G. *J. Chromatogr. Sci.* **1970**, *8*, 65.
(62) Deininger, G.; Halász, I. *J. Chromatogr. Sci.* **1971**, *9*, 83.
(63) Halász, I.; Martin, K. *Ber. Bunsenges.* **1975**, *79*, 731.
(64) Halász, I.; Martin, K. *Angew. Chem.* **1978**, *90*, 954; *Angew. Chem., Int. Ed. Engl.* **1978**, *17*, 901.
(65) Halász, I.; Vogtel, P. *Angew. Chem., Int. Ed. Engl.* **1980**, *19*, 24.
(66) DiMarzio, E. A.; Guttman, C. M. *J. Polym. Sci., Part B* **1969**, *7*, 267.
(67) DiMarzio, E. A.; Guttman, C. M. *Macromolecules* **1970**, *3*, 131.
(68) Guttman, C. M.; DiMarzio, E. A. *Macromolecules* **1970**, *3*, 681.
(69) Verhoff, F. H.; Sylvester, N. D. *J. Macromol. Sci. Chem.* **1970**, *4*, 979.
(70) Brandrup, I.; Immergut, E. H., Eds., "Polymer Handbook"; Wiley: New York, 1966.
(71) Wilke, C. R.; Chang, P. *AIChE J.* **1955**, *1*, 261.
(72) Giddings, J. C.; Seager, S. L. *Ind. Eng. Chem. Fundam.* **1962**, *1*, 277.
(73) Grushka, E.; Kikta, E. J. *J. Phys. Chem.* **1974**, *78*, 2297.
(74) Taylor, G. *Proc. R. Soc. London, Ser. A* **1953**, *219*, 186; **1954**, *223*, 446; **1954**, *225*, 473.
(75) Jansen, Th. Diplomarbeit, Saarbrücken, 1975.
(76) Kennedy, G. J.; Knox, J. H. *J. Chromatogr. Sci.* **1972**, *10*, 549.
(77) Cluff, J. R.; Hawkes, S. J. *J. Chromatogr. Sci.* **1976**, *14*, 248.
(78) Huber, F. J. K. Lecture 4th International Symposium on Liquid Chromatography, Boston, MA, May 1979.
(79) Synder, L. R.; Kirkland, J. J. "Introduction to Modern Liquid Chromatography"; Wiley-Interscience: New York, 1974.
(80) LeFevre, E. J. *Nature (London) Phys. Sci.* **1972**, *235*, 20.
(81) Halász, I.; Heine, E. *Nature (London)* **1962**, *194*, 971.
(82) Halász, I.; Hartmann, K.; Heine, E. "Gas Chromatography 1964"; Goldup, A., Ed.; Institute of Petroleum: London, 1965.
(83) Sternberg, F. C.; Poulson, R. E. *Anal. Chem.* **1964**, *36*, 1492.
(84) Halász, I.; Heine, E. In "Advances in Gas Chromatography"; Giddings, F. C., Keller, R. A., Eds.; Marcel Dekker: New York, 1967, Vol. 4, p 206.
(85) Edwards, M. F. *Anal. Chem.* **1969**, *41*, 383.
(86) Knox, J. H.; Parcher, J. F. *Anal. Chem.* **1969**, *41*, 1599.
(87) Yau, W. W.; Malone, C. P.; Suchan, H. L. *Sep. Sci.* **1970**, *5*, 259.
(88) Hofmann, K. personal communication.
(89) Golay, M. J. E. *Anal. Chem.* **1957**, *29*, 928.
(90) Knox, J. H. *J. Chromatogr. Sci.* **1977**, *15*, 352.
(91) Knox, J. H., Ed. "High Performance Liquid Chromatography"; Edinburgh University Press: Edinburgh, 1978.
(92) Horowitz, S. B.; Fenichel, I. R. *J. Phys. Chem.* **1964**, *68*, 2229.
(93)Ousterhoudt, W.; Ray, L. N. *J. Polym. Sci., Part C* **1968**, *21*, 5.
(94) Knox, J. H. Lecture given at the 4th *International Symposium on Liquid Chromatography*, Boston, MA, May 1979.
(95) Kato, Y.; Kido, S.; Hashimoto, T. *J. Polym. Sci., Polym. Phys. Ed.* **1973**, *11*, 2329.
(96) Tung, L. H.; Runyon, J. R. *J. Appl. Polym. Sci.* **1973**, *17*, 1589.
(97) Werner, W.; Halász, I. *Chromatographia* **1980**, *13*, 271.

RECEIVED for review October 28, 1980. Accepted April 27, 1981. This paper is part of the Ph.D. Thesis of R. Groh, Universität des Saarlandes, Saarbrücken, 1979. The authors are indebted to the Deutsche Forschungsgemeinschaft, Bad Godesberg, for financial support.

High-Resolution Gas Chromatography of Trialkyllead Chlorides with an Inert Solvent Venting Interface for Microwave Excited Helium Plasma Detection

Scott A. Estes, Peter C. Uden,* and Ramon M. Barnes

Department of Chemistry, GRC Tower I, University of Massachusetts, Amherst, Massachusetts 01003

A gas chromatograph interfaced to a microwave induced and sustained atmospheric pressure helium plasma for element selective and sensitive detection is described. It incorporates a chemically deactivated, low-volume, valveless fluidic logic gas switching interface, to vent large quantities of eluent solvent which would disrupt the helium discharge as sustained by the TM_{010} cylindrical resonance cavity. The inertness and venting characteristics of the interface are demonstrated for chemically active and thermally sensitive trialkyllead chlorides for which analysis in spiked tap water is investigated in the range of 10 ppb to 10 ppm. The detection system features a low-resolution scanning monochromator with a quartz refractor plate background corrector directly after the entrance slit to improve selectivity ratios of elements whose emission wavelengths occur in the cyanogen background region. Use of the plasma as a nonselective universal organic compound detector is desmonstrated by monitoring a carbon atomic emission line.

Previous studies have demonstrated the need for a gas chromatographic solvent venting interface (*1-3*) for the microwave excited atmospheric pressure helium discharge (GC-MED), as sustained by the Beenakker TM_{010} cylindrical resonance cavity (*4-6*). The first GC-MED systems described were based on either atmospheric pressure (*7*) or various types of reduced pressure cavities (*8, 9*). The reduced pressure system made impractical the implementation of a solvent venting interface between the gas chromatograph operating at atmospheric pressure and the reduced pressure of the MED. As a result, reduced pressure plasma reignition was continually required due to disruption by the solvent. The TM_{010} cavity not only eliminates the need for bulky vacuum equipment but also makes practical the implementation of atmospheric pressure solvent venting interfaces. In addition, plasma emission light resulting from the fragmentation of analyte molecules and subsequent excitation and decay of their constituent elements can be viewed axially rather than transversely through the discharge tube walls. Thus, the severe reproducibility problems caused by the inevitable obscuring of the transversely viewed optical window, due to carbonaceous and metallic oxide deposition on the discharge tube walls and devitrification of the quartz by the action of the plasma, are circumvented.

Quimby et al. (*1*) described the first of such solvent venting interfaces which consisted of a small auxiliary oven containing a high-temperature stainless steel valve for venting. Interface tubing was of small bore $^1/_{16}$ in. stainless steel to maintain minimal dead volume. This interface proved to be suitable for the determination of relatively stable and chemically inert volatile organometallics of Pb, Mn, and Hg (*1*) as well as volatile organic compounds of Si (*1, 10*), S, P, and the halogens (*1-3*). However, a hot stainless steel surface is too chemically active to permit passage of low levels of chemically active and thermally unstable volatile compounds, and an interface thus composed of a high-temperature stainless steel valve and stainless steel tubing may sometimes prove inadequate.

In this paper, the design of a GC-MED system incorporating a chemically deactivated low dead volume heated interface oven, which is capable of venting solvent via a nonvalve fluidic logic gas switching network, is described. The inertness and venting characteristics of the interface are demonstrated for the chemically active and thermally unstable trimethyl- and triethyllead chlorides. In addition, the universal detection capability of the MED is illustrated for carbon-containing compounds.

Organically bound lead is a minor but important contributor to total lead intake by humans and animals. It has been shown that alkyl lead salts such as trialkyllead carbonates, nitrates, and/or sulfates arising in tissues from rapid metabolic dealkylation of tetraalkyllead compounds are important in lead toxicity (*11*). For their specific determination as chlorides at biological and environmental trace levels, gas chromatography has received only one report (*12*) where nanogram levels were claimed eluted from a packed polyester column. There have been no further successful reports of such analysis and it may be that observed peaks were those of degradation products of these very reactive compounds. The combination of high resolution and great inertness of fused silica columns now allows the elution of the trialkyllead chlorides to subnanogram levels, thus substantiating some other recent observations (*10*).

EXPERIMENTAL SECTION

Gas Chromatographic Systems. Varian 1200 (Walnut Creek, Ca) and Shimadzu (Columbia, MD) G. C.-Mini 2 gas chromatographs with hydrogen flame ionization detectors (FID) were used with SP-2100 fused silica WCOT capillary columns (12.5 m × 0.3 mm o.d. × 200 μm i.d.) (Hewlett-Packard Co., Avondale, PA) and a 30 m × 1 mm o.d. × 350 μm i.d. OV-101 SCOT glass capillary column.

Combination injection port liner–splitters were designed for each gas chromatograph consisting of quartz injection port liners attached to $^1/_4$ in. to $^1/_{16}$ in. brass Swagelok reducers. The reducer had a $^1/_{16}$ in. hole drilled through its side into which a piece of 12 in. by $^1/_{16}$ in. o.d. × 0.02 in. i.d. stainless steel tubing was silver soldered. A Nupro brass fine metering valve fitted to the end of the stainless steel tubing served to adjust the injection split ratio.

Spectrometer. A Heath 703 (McPherson Instruments, Acton, MA) 0.350 m *f*/6.8, Czerny-Turner mount scanning monochromator, was used. The grating had 1180 lines/mm and was blazed for the first-order maximum at 2500 Å. The scan range was from zeroth order to 10000 Å with a reciprocal linear dispersion of 20 Å/mm at the exit slit. The monochromator was fitted with an oscillating quartz refractor plate ($^1/_8$ in. × $^1/_2$ in. × 1 in.) background correction device (*13*) which was mounted in an inverted position directly after and onto the entrance slit baffle (Figure 1). The refractor plate motor's drive was operated at the full deflection voltage. Entrance and exit slit widths were either 25 or 50 μm and the full 12 mm entrance and exit slit heights were used. The axially viewed plasma image was focused onto the entrance slit of the monochromator by a 5.4-cm focal length biconvex quartz lens which was held in an X-Y positioning holder

0003-2700/81/0353-1336$01.25/0 © 1981 American Chemical Society

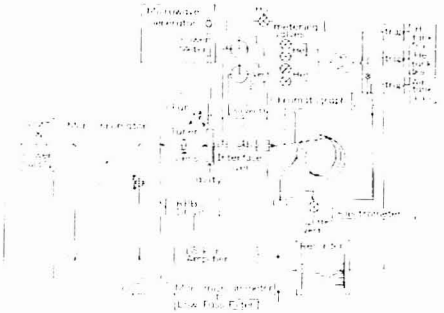


Figure 1. Block diagram of the GC-MED system.

and stand (Monolux, Japan). The photomultiplier tubes (1P28 or 4832 RCA) were maintained at 700 and 1100 V, respectively, by the Heath 703 power supply. The photomultiplier photocurrent was monitored by a Model 414 micromicroammeter (Keithley Instruments, Cleveland, OH), the voltage output being filtered through a passive low-pass filter before display on a Houston Instruments (Houston, TX) Omniscribe dual channel stripchart recorder; a 0.1 s time constant was used throughout. When the background correction device was in use, the photocurrent was monitored by a lock-in amplifier (Princeton Applied Research, Princeton, NJ, Model 120), which was set to 148 Hz, the frequency of the Quartz refractor plate.

Microwave Power Train. The microwave generator (microwave diathermy generator, Microtherm Model CMD 5, Raytheon Co., Waltham, MA) utilized had a 0–125 W, 2.45-GHz microwave power output. The TM_{010} cavity (J and D. Instrument Co., Lexington, MA) was of aluminum after the description of Beenakker (*4*). The cavity had an inner diameter of 87 mm, an inner axial cavity depth of 10 mm, a radial wall thickness of 20 mm, a 1 mm diameter copper wire coupling loop depth of 28.5 mm from the inner wall, a total external diameter of 127 mm, and a total axial wall thickness of 25.4 mm; it was silver plated to a thickness of 7×10^{-4} in. and then gold plated to a thickness of 5×10^{-6} in. The UG-58 connector was mounted on the cavity without further change. The initial reflected power could be tuned to a minimum, with the quartz discharge tube in place, by the face plate copper tuning screw and a 3 in. × 6.5 mm o.d. × 0.5 mm i.d. quartz tuning rod wrapped with Teflon, which extended radially into the side of the cavity. These adjustments provided a permanent rough-tuning of the cavity (*1*). Final daily frequency and impedance matching/tuning of the cavity to the microwave generator for ignition of the helium plasma was accomplished by a coaxial stub stretcher Model SL-1ON (Microlab/FXR, Livingston, NJ) which was affixed directly to the UG-58 connector of the cavity. The tuning of the cavity was monitored by a VSWR forward-reverse coaxial power meter (#725.3, Raytheon Co., Waltham, MA) which was connected directly to the output microwave power stub of the diathermy unit. The VSWR power meter and coaxial stub stretcher were connected by a 1.3 m. length of 50 Ω impedance coaxial cable and a type LN(M) to N(F) coaxial adapter (Opthos Instrument Co., Rockville, MD). With this arrangement, typical atmospheric pressure helium plasma discharge ignition parameters were 6–10 W reverse/reflected microwave power and 60–80 W forward input microwave power (*14*). After the plasma discharge commenced, the stub stretcher was readjusted to give a reflected power of ca. 0 W and a forward input power of 45–75 W as needed (*15*). During plasma discharge operation the coaxial stub stretcher and the cavity were continuously cooled by a 11-cm muffin fan aimed directly at them (see Figure 1). This reduced the chance of melting the interior of the tuner by over heating due to conduction of heat from the discharge to the cavity and then to the tuner. When the plasma discharge tube became overly carbonized, a small amount of hydrogen (instead of oxygen (*1*)) (ca. 0.5–1 mL/min) could be bled into the plasma via a Whitey fine metering valve with micrometer adjustment ($^1/_4$ in. no. 316 stainless steel) for a short period of time.

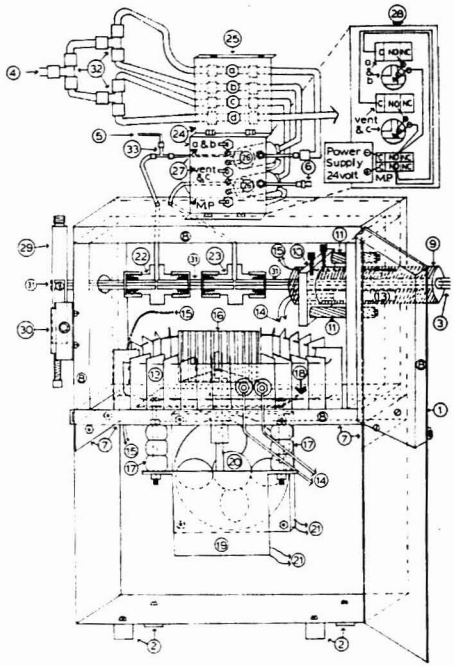


Figure 2. Interface oven: (1) hinged interface door with latch; (2) rubber feet; (3) column effluent inlet; (4) "interface He" inlet; (5) hydrogen inlet; (6) vent; (7) galvanized sheet metal divider; (8) $^1/_2$ in. thick fiberglass insulation; (9) cylindrical aluminum transfer block; (10) aluminum bracket; (11) ceramic electrical insulators; (12) Kolfin heating element; (13) cartridge heater; (14) connections to Variacs; (15) thermocouples; (16) cylindrical fan; (17) rubber shock mounts; (18) aluminum floating mount plate; (19) fan motor; (20) muffin fan; (21) connections to 120-V, 60-Hz house current; (22) front interface tee; (23) rear interface tee; (24) rear interface tee; (24) 3 in. × $5^1/_2$ in. × $^1/_{32}$ in. mounting plates; (25) $^1/_8$ in. brass Nupro fine metering valves: (a) high helium flow rate for venting, (b) adjustable plasma helium flow rate, (c) low helium flow rate, (d) column makeup helium flow rate; (26) electrical solenoid valves; (27) microswitches: top, helium flow (b) when "off" and (a) when "on", bottom, main power (M.P.) "off" plasma and "on" venting, for simultaneous switching when top and middle are "on"; (28) circuit diagram for microswitches and solenoid valves; (29) cavity; (30) cavity X-Y positioner–holder; (31) discharge and interface quartz capillary tubing; (32) $^1/_8$ in. brass Swagelok tees; (33) $^1/_{16}$ in. brass Swagelok tee.

If necessary continuous hydrogen doping of the plasma could be carried out.

Interface. The GC-MED system is shown in Figure 1. As with the previous instrumental system (*1–3*), both the FID and the MED could be simultaneously used with packed and glass capillary columns. This was accomplished by an easily installed (Varian 1200) column effluent gas makeup and splitter system, which consisted of two $^1/_{16}$ in. S.G.E. (Austin, TX) zero dead volume makeup tees and short pieces of $^1/_{16}$ in. o.d. × 0.01 in. i.d. stainless steel tubing. The first tee was used as a makeup tee to raise the carrier gas flow rate to 45–60 mL He/min. The second tee served as a "natural" 1 to 1 splitter between the FID and MED. When the fused silica capillary column was used, the MED served as the sole detector. The extremely mechanically flexible column could be threaded through the interface tubing to within 1–5 mm of the helium plasma (*15, 16*).

The basic interface oven design is shown in Figure 2, the rationale being that discussed earlier (*1*). Instead of a heated transfer

Table I. GC-MED Operating Parameters for Lead and Carbon

parameters	for lead	for carbon
column		
packing material	SP-2100 WCOT fused silica Carbowax pretreated	OV-101 SCOT glass capillary
dimensions	12.5 m × 300 μm 0.d. × 200 μm i.d.	30 m × 1 mm 0.d. × 350 μm i.d.
injection split	100 to 1	25 to 1
carrier gas flow rate (helium)	1 mL/min	4 mL/min
temperatures		
column or program	140–165 °C	60–220 °C at 4 °C/min
injector	180 °C	250 °C
transfer block	180 °C	240 °C
interface oven	180 °C	235 °C
total plasma flow rate	125 mL/min	75 mL/min
PMT tube & voltage	RCA 1P28, 700 V	RCA 1P28, 700 V
entrance & exit slit		
widths	25 μm	50 μm
height	12 mm	12 mm
microwave input power	54 W	55 W
wavelength obsd	405.8 nm	247.9 nm
picoammeter time constant	0.10 s	0.10 s

line for the gas-phase transfer of effluent to the isolated interface oven, a 1.5 in. diameter × 5 in. long cylindrical aluminum transfer block, heated by a Model C-382 J4, 50-W 120-V, 60-Hz ITT Vulcan cartridge heater, was employed. The interface oven was a sheet metal box (10 in. × 10 in. × 14.75 in.) refinished with high-temperature automotive paint, divided horizontally by a suitably sized piece of galvanized sheet metal bolted to the box; the upper portion was insulated with $^1/_2$ in. thick pieces of fiberglass to form the oven. The cylindrical aluminum transfer block was held in an aluminum bracket fixed to the wall of the box by ceramic electrical insulators. The upper portion of the interface was heated by a 9 in. o.d. × 6 in. i.d. 1950-W, 120-V, 60-Hz koilfin heating element (Chromalox, Pittsburgh, PA) which rested tightly on the insulated dividing plate. Variacs provided electrical power and temperature regulation of the interface oven and transfer block heaters, and even heat distribution throughout the oven was maintained by the 3 in. cylindrical fan in the center of the koilfin heating element. The fan motor in the lower portion of the interface was shock mounted to the metal dividing plate by two 2.75 in. bolts, six 1 in. diameter × $^1/_3$ in. thick rubber shock mounts, and a $^1/_{32}$ in. × 4.25 in. × 4.25 in. aluminum floating mount plate, which rested on the $^1/_2$ in. thick layer of fiberglass insulation. The oven fan motor was cooled by a 4.5-in. muffin fan mounted in the lower middle portion of the box. Interface temperatures were monitored by iron–constant thermocouples placed within the aluminum transfer block and the interface oven. The double arrangement of zero dead volume tees made from $^1/_4$ in. stainless steel unions drilled through $^1/_4$ in. and with a $^1/_{16}$ in. hole drilled in each served as the basis for the fluidic logic nonvalve gas switching system. The front tee (closest to the discharge) had a 2 ft × $^1/_{16}$ in. o.d. × 0.01 in. i.d. stainless steel tube silver soldered into it and the rear tee had a 2 ft × $^1/_{16}$ in. o.d. × $^1/_{32}$ in. i.d. stainless steel tube silver soldered into it. Each tube passed to a 24-V dc three-way electrical solenoid gas switching valve (Clippard, Cincinnati, OH) outside the oven, driven by an adjustable regulated power supply (Model LH 125 Lambda Electronics Corp., Melville, NY) and provided with various input helium flow rates by brass $^1/_8$ in. Nupro fine metering valves (Figure 2). The front tee could have a high input helium flow rate of ca. 300 mL/min and an adjustable helium flow rate of 40–800 mL/min. The rear tee could have a low input helium flow rate of 10–20 mL/min or could serve as a vent to atmosphere. The interface and plasma discharge tubing was 6.5 mm o.d. × 0.5 mm i.d. quartz capillary (Quartz Scientific). The discharge tube, 3 in. long, was held rigidly in place by the aluminum transfer block, so that no additional fastening to the plasma cavity was needed. All interface quartz-to-metal gastight connections were made by $^1/_4$ in. graphite ferrules. The TM_{010} cavity was attached to an aluminum X-Y positioner–holder shock mounted to the interface box. Exact X-Y plasma imaging was by the lens, X-Y positioning holder, and stand. The overall interface, which rested on thick rubber feet, was sufficiently heavy that activity around it did not disturb the optical alignment.

Materials. Trimethyllead chloride and triethyllead chloride were obtained from the Ethyl Corp. (Ferndale, MI), *n*-octane, *n*-nonane, *n*-decane, *n*-undecane, *n*-tridecane, *n*-tetradecane, and *n*-pentadecane from Eastman Kodak Co. (Rochester, NY), dichlorodimethylsilane from Ventron Alfa Division (Danvers, MA), and the solvents from Fisher Scientific Co. (Fairlawn, NJ). Commercial grade helium was purified through a silica gel and molecular sieve 3A trap.

Procedure. The general GC-MED operating parameters for lead and carbon are given in Table I (*15*). For fused silica capillary column separations, when injection volumes did not exceed 0.1 μL and the injection split was 100 to 1, solvent venting was unnecessary. Thus, the fused silica was threaded through the interface to within 1–5 mm of the helium discharge to maintain the highest chromatographic efficiency (*15, 16*). When glass capillary, large or small bore fused silica capillary, and packed columns were in use, for which solvent levels did not exceed 1 μg/s through the helium discharge (due to large injection volumes or low split ratios), the solvent had to be vented to preclude disruption of the discharge. Fused silica capillary columns were placed 1–5 mm behind the rear interface tee. Solvent venting was accomplished by simultanesouly activating the electrical solenoid valves causing a high helium flow (ca. 300 mL/ min) to be introduced at the front interface tee and creating a vent to atmosphere at the rear interface tee. The high helium flow rate of the front tee was split approximately equally between the plasma discharge and the vent. This caused all helium effluent from the column containing solvent to exit the vent, while maintaining sufficient helium for the discharge. The passage of the solvent could be monitored with the FID response. When this returned back onto the recorder scale, the electrical solenoid valves were simultanesously deactivated. This returned the front and rear interface tees to their preset plasma flow rates, and the remaining separated compounds eluting from the column could enter the discharge.

Analytical Method. Five-hundred-milliliter samples of tap water were spiked with trimethyllead chloride and/or triethyllead chloride in the range from 10 ppb to 10 ppm. The mixture was stirred for 10 min with a magnetic stirring bar and the sodium chloride concentration was then raised to 300 mg/mL (*17*). If the pH was not between 5 and 7, it was adjusted with hydrochloric acid or sodium hydroxide (*17*). The resulting mixture (500 mL) was extracted with 50 mL of "spectrograde" benzene in a 1-L separatory funnel and allowed to separate for 20 min. The benzene was drawn off and placed in a 100-mL round-bottom flask (14/20 ground glass joint). The volume of benzene was vacuum reduced to between 0.25 and 4 mL. A sample of the final benzene volume (2–5 μL) was analyzed with the GC-MED. The total extraction and vacuum reduction required approximately 2.5 h.

RESULTS AND DISCUSSION

Carbon Detection. The microwave excited atmospheric pressure helium discharge has proven to be a very versatile

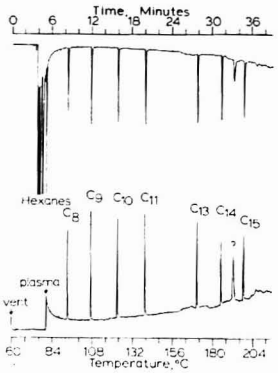


Figure 3. Dual detection chromatogram of an *n*-alkane mixture: top, F.I.D., attenuation 128; bottom MED monitoring C I at 247.9 nm, gain 1 $\times 10^{-6}$ A; 30 m OV-101 glass SCOT column, 0.2 μL injected, split 25 to 1.

element selective detector for gas chromatography (*1–3*, *15*, *16*). However, it is not limited in this regard. By specific element monitoring of the carbon I 247.9-nm atomic emission line, the MED can be utilized as a universal organic compound detector behaving similarly to the flame ionization detector (*16*, *18*), except that the MED is not limited by the combustibility of the analyte molecule but rather by its carbon content. Figure 3 depicts a dual detection separation of *n*-alkanes with flame ionization detection and the MED monitoring simultaneously. The MED trace indicates the point at which "solvent venting" is started and the point at which it is discontinued and the effluent is once again directed to the "plasma". The tailing edge of the solvent peak can be seen at the beginning of the MED trace immediately after column effluent is directed back to the plasma. The FID trace indicates an unknown combustible impurity, peak "?", in the *n*-alkane mixture and the MED verifies that carbon is present.

Interface Characteristics. In order to ascertain the chemical activity of the interface, we determined a standard solution of triethyllead chloride in benzene in the following ways: (i) with the fused silica column threaded directly up to the helium discharge (*15*, *16*) and (ii) with the fused silica pulled back behind the rear interface tee or in the venting position.

Two replicates of the response to the standard sample with the column at the plasma are seen in Figure 4A. The first spike (s) is the solvent, the second (a) a small quantity of tetraethyllead impurity in the triethyllead chloride, and the third (b) the triethyllead chloride. At the 2-ng level of triethyllead chloride, the MED gave an excellent signal for lead, monitoring the lead I 405.8-nm atomic emission line. An identical sample of the standard with the column at the venting position is seen in Figure 4B. The triethyllead chloride response is greatly reduced while the tetraethyllead response is unchanged. The loss of triethyllead chloride and the accompanying unchanged response of tetraethyllead indicates the drastic decomposition of the triethyllead chloride within the interface. This interface chemical activity could be due to uncapped silanol groups on the surface of the capillary quartz tubing or an unexpected surface activity from the modified stainless steel unions utilized to produce the zero dead volume tees.

In order to address this problem, the quartz injection port liner, quartz discharge tube, and the quartz interface tubing were removed and silanized by passing 100% dichlorodi-

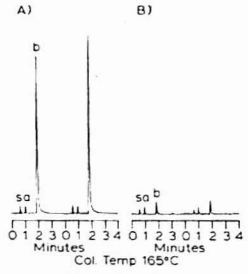


Figure 4. Detection of Et_3PbCl with unsilanized quartz interface tubing, MED monitoring Pb I at 405.8 nm, gain 3 $\times 10^{-6}$ A: (A) fused silica column pushed up to the helium discharge; (B) fused silica column pulled back behind the rear interface tee, venting position; 0.1 μL injection of 2.0 μg/μL solution of Et_3PbCl in benzene, split 100 to 1; s = solvent, a = $(C_2H_5)_4Pb$, b = $(C_2H_5)_3PbCl$.

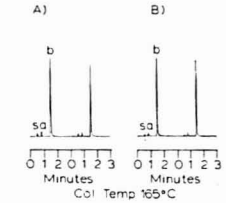


Figure 5. Detection of Et_3PbCl with silanized quartz interface tubing, MED monitoring Pb I at 405.8 nm, gain 3 $\times 10^{-6}$ A: (A) fused silica column at the discharge; (B) fused silica column at the venting position; 0.1 μL injection of 1 μg/μL Et_3PbCl in benzene, split 100 to 1; s = solvent, a = $(C_2H_5)_4Pb$, b = $(C_2H_5)_3PbCl$.

methylsilane through the tubing. The tubing was placed in an airtight container flushed with nitrogen and allowed to react for 30 min. The tubes were washed with a large quantity of "spectrograde" methanol in order to quench any remaining chlorosilane bonds and dried at 250 °C for 1 h while being flushed with helium. This was followed by helium flushing at room temperature overnight. Figure 5 shows the determination of 1 ng of triethyllead chloride in benzene standard after silanization of the quartz interface tubing. It is quite evident that the differences in triethyllead chloride response from the "at plasma" and "venting" column positions was now negligible. Thus, the loss of triethyllead chloride when utilizing the nonsilanized quartz interface tubing was due to the chemically active quartz surface and not the modified stainless steel unions. The unions presented a minimum of active surface. If it were necessary, the stainless steel unions could be eliminated and a solid deactivated quartz or fused silica double tee arrangement substituted to maintain the most chemically inert gas chromatographic surface possible.

The lead response at 405.8 nm for a standard solution was investigated as a function of retention time from the time at which column effluent is directed back to the discharge. Column temperatures were varied from 145 to 165 °C. It was found that the maximum response was at a retention time of approximately 1.5–2 min or more from switching. Retention times less than 1.5 min resulted in reduced lead response for the same level of lead. This behavior is attributable to the plasma discharge returning to excitation equilibrium for the elements as the plasma gas flow rates return to normal after venting. This behavior occurs because "plasma" and "venting" helium discharge flow rates are not the same. The plasma flow rate equilibration is responsible for the broad malformed peak after venting has ceased, since changes in flow rate tend

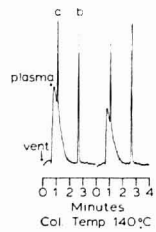


Figure 6. Detection of Me_3PbCl and Et_3PbCl at 3.0 ppm and 2.6 ppm in tap water, respectively. MED monitoring Pb I at 405.8 nm, gain 3 × 10^{-7} A. Final benzene extract = 5 mL, 2 μL injected split 100 to 1.

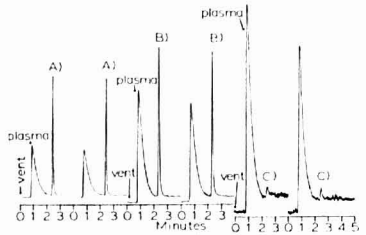


Figure 7. Extraction of Et_3PbCl from spiked tap water. MED monitoring Pb I at 405.8 nm, SP-2100 fused silica column at vent position: (A) 5.8 ppm Et_3PbCl in tap water, final benzene extract = 2 mL, 2 μL injected, split 100 to 1, gain 5 × 10^{-6} A; (B) 400 ppb Et_3PbCl in tap water, final benzene extract = 0.25 mL, 2 μL injected, split 100 to 1, gain 3 × 10^{-7} A; (C) 34 ppb Et_3PbCl in tap water, final benzene extract = 0.5 mL, 5 μL injected, split 100 to 1, gain 3 × 10^{-8} A.

to alter the plasma continuum background dramatically (*19*). The broad peak is not the tailing edge of the solvent, for it was totally vented at least 10 s before initiation of "plasma".

The selectivity ratio of 2.0 × 10^5 for lead over carbon at this wavelength supports this conclusion (*15*). This time for equilibration of the discharge after venting of the solvent to maintain maximum elemental response has also been observed for the determination of chlorine in ether solutions containing methylated tri- and dichloracetic acid (*20*), using a stainless steel valve for venting (*1*).

Analysis of Spiked Tap Water. Figure 6 shows chromatograms for the analysis of a sample of tap water spiked at the 3.0 and 2.6 ppm levels of trimethyllead chloride and triethyllead chloride, respectively. The trimethyllead chloride is more volatile than triethyllead chloride and elutes long before the discharge has returned to equilibrium. Therefore, although trimethyllead chloride is at a higher level than triethyllead chloride, the latter compound gives the stronger signal.

Chromatograms for various concentrations of triethyllead chloride extracted from spiked tap water are given in Figure 7. The detection limit is at the 10–30 ppb level of triethyllead chloride in tap water under the chromatographic and extraction–vacuum reduction procedures utilized. The extraction–vacuum reduction procedure was determined to be approximately 50% efficient for triethyllead chloride but probably less efficient for the trimethyl compound. The loss of sample is probably a result of decomposition of the trialkyllead chlorides on the glass walls of the round-bottom flask during benzene vacuum reduction, since the compounds will not sublime. We are presently investigating extraction–concentration procedures which eliminate the vacuum reduction step in the hopes of increasing the overall efficiency of the method.

It has been shown that this interface will pass very chemically reactive and thermally unstable compounds affording advantage in situations where stainless steel high-temperature valves are unacceptable. It can accommodate all types of columns (packed, glass capillary, large or small bore fused silica capillary columns) and ideally features chemical inertness, since all tubing is deactivated quartz. If the deactivation quartz tubing becomes permanently contaminated it can easily be replaced. In addition, this type of solvent venting interface cannot only be applied to the problem of solvent disruption of the MED but also to the solvent disruption of flame photometric detectors and the solvent overloading of the electron capture or the nitrogen/phosphorus detectors by solvents of an interfering nature which cannot be avoided or may even be more desirable in analytical workup procedures. The application to the very testing example of the trialkyllead chlorides promises to make available a specific trace determination method for these compounds in a variety of matrixes; such studies are presently being pursued.

ACKNOWLEDGMENT

We thank Manuel Brandt of the Ethyl Corp., Ferndale, MI, for providing the alkyllead chlorides and Charles D. Allemand for the loan and helpful suggestions on the use of the spectral components. We thank Richard Willis and the Perkin-Elmer Corp. for providing quartz plates for the RPBC. We thank Daniel Keedy, Gerhard Meyer, and Christopher T. Estes for help in design and construction. We extend our appreciation to Bruce D. Quimby of Hewlett-Packard Co., Avondale, PA, for providing a fused silica capillary column, the three-way 24-V electrical solenoid valves, and helpful suggestions concerning their use and the construction of the interface. We thank R. K. Brehm, J. and D. Instrument Co., Lexington, MA, for the donation of the microwave cavity.

LITERATURE CITED

(1) Quimby, B. D.; Uden, P. C.; Barnes, R. M. *Anal. Chem.* **1978**, *50*, 2112–2118.
(2) Quimby, B. D.; Delaney, M. F.; Uden, P. C.; Barnes, R. M. *Anal. Chem.* **1979**, *51*, 875–880.
(3) Quimby, B. D.; Delaney, M. F.; Uden, P. C.; Barnes, R. M. *Anal. Chem.* **1980**, *52*, 259–263.
(4) Beenakker, C. I. M. *Spectrochim. Acta, Part B* **1976**, *31B*, 483–486.
(5) Beenakker, C. I. M. *Spectrochim. Acta, Part B* **1977**, *32B*, 173–187.
(6) Beenakker, C. I. M.; Boumans, P. W. J. M. *Spectrochim. Acta*, **1978**, *33*, 53–54.
(7) McCormack, A. J.; Tong, S. C.; Cooke, W. D. *Anal. Chem* **1965**, *37*, 1470–1476.
(8) McLean, W. R.; Stanton, D. L.; Penketh, G. E. *Analyst (London)* **1973**, *98*, 432–442.
(9) Fehsenfeld, F. C.; Evenson, K. M.; Broida, H. P. *Rev. Sci Instrum.* **1964**, *36*, 294–298.
(10) Estes, S. A.; Poirier, C. A.; Uden, P. C.; Barnes, R. M. *J. Chromatogr.* **1980**, *196*, 265–277.
(11) Hayakawa, K. *Nippon Eiseigaku Zasshi* **1972**, *26*, 526–535.
(12) Hayakawa, K. *Nippon Eiseigaku Zasshi* **1971**, *26*, 377-385.
(13) Snelleman, W.; Rains, T. C.; Yee, K. W.; Cook, H. D.; Menis, O. *Anal. Chem.* **1970**, *42*, 394–398.
(14) Outred, M. *Spectrochim. Acta. Part B* **1980**, *35B*, 447–450.
(15) Estes, S. A.; Uden, P. C.; Barnes, R. M., to be submitted to *Anal. Chem.*
(16) Estes, S. A.; Uden, P. C.; Rausch, M. D.; Barnes, R. M. *HRC CC J. High Resolut. Chromatogr. Chromatogr. Commun.* **1980**, *3*, 471–472.
(17) Bolanowska, A. W. *Chimie Anal. (Warsaw)* **1967**, *12*, 121–429.
(18) Wasik, S. P.; Schwartz, P. *J. Chromatogr. Sci.* **1980**, *18*, 660–663.
(19) Mulligan, K. J.; Caruso, J. A.; Fricke, F. L. *Analyst (London)* **1980**, *105*, 1060–1067.
(20) Miller, J. W.; Uden, P. C., unpublished work.

RECEIVED for review February 19, 1981. Accepted May 8, 1981. This work was supported by an A.C.S. Analytical Division Summer Fellowship sponsored by the Olin Corp. Charitable Trust, by an A.C.S. Analytical Division Full-Year Fellowship sponsored by the Proctor & Gamble Co. (S. Estes), and by The Ethyl Corp.

Liquid Chromatographic Elution Characteristics of Some Solutes Used To Measure Column Void Volume on C_{18} Bonded Phases

Martha J. M. Wells[1] and C. Randall Clark*

Division of Medicinal Chemistry, Department of Pharmacal Sciences, School of Pharmacy, Auburn University, Auburn University, Alabama 36849

The liquid chromatographic elution characteristics of some solutes commonly used to measure column void volume on hydrocarbonaceous stationary phases are described. The elution characteristics of tartrazine, sodium benzenesulfonate, sodium nitrate, potassium dichromate, acetone, uracil, *N,N*-dimethylformamide, and the mobile phase components were determined by using four C_{18} columns with aqueous methanol eluents. The results indicate that the volume required to elute acetone, *N,N*-dimethylformamide, methanol, and uracil increases as the organic modifier in the mobile phase decreases. The elution volumes of the ionic solutes are independent of mobile phase composition (nonbuffered) but dependent on the concentration of the injected solute. When the aqueous component of the mobile phase was replaced by a phosphate buffer, the elution volume of the organic ionic solutes became independent of amount injected and dependent on organic modifier content of the mobile phase. The inorganic ionic solutes were independent of both amount injected and eluent composition in buffered eluent.

In liquid chromatography (LC), the capacity factor (k') is commonly used to define retention (*1*). If the volume required to elute the peak maximum is V_R for a retained solute and V_0 for a nonretained compound, the capacity factor can be defined by eq 1. The elution of a solute on different columns

$$k' = \frac{V_R - V_0}{V_0} \quad (1)$$

is not correctly described by V_R, since V_R varies with the inter- and intraparticulate volumes associated with the column packing, as well as with differences in tubing dimensions, guard columns, or other hardware placed between the points of injection and detection. Proper measurement of the column void volume (V_0) is essential for the calculation of solute k' values. The need for research into the problem of determining the column V_0 when reversed-phase high-performance liquid chromatographic (RPHPLC) columns are used has been discussed by Colin et al. (*2*). Many different solutes are used to determine V_0 in RPHPLC; moreover, a large amount of k' data is reported without describing the method used to determine the column void volume. In this study we have investigated the elution characteristics of several solutes used for determining the column V_0 in RPHPLC.

EXPERIMENTAL SECTION

Apparatus. The liquid chromatograph consisted of a Waters Model 6000A solvent pump, Model U6K injector, Model 440 UV absorbance detector, an Alltech Associates (Deerfield, IL) HPLC column water jacket, and a Hitachi or a Beckman recorder. RI measurements were determined on an Erma (Tokyo, Japan) refractometer. Constant temperature in both the HPLC column water jacket and the refractometer was maintained by a Haake (Saddle Brook, NJ) Model FE constant-temperature circulator.

Reagents and Chemicals. All chemicals were of reagent grade quality or better and were used as purchased without further purification. Sodium nitrate, *N,N*-dimethylformamide, spectrophotometric grade methanol, potassium phosphate monobasic, and potassium phosphate dibasic were obtained from Fisher Scientific Co. (Fair Lawn, NJ). Sodium benzenesulfonate and uracil were obtained from Eastman Kodak Co. (Rochester, NY). Potassium dichromate and spectrophotometric grade acetone were purchased from Mallinckrodt, Inc. (St. Louis, MO). Tartrazine was obtained from Aldrich Chemical Co. (Milwaukee, WI). Doubly distilled water was further purified by pumping (Waters Model 6000 solvent pump) through a 7 cm by 2.1 mm i.d. column dry packed with Whatman CO:PELL ODS (30–38 μm) prior to preparation of solvent mixtures.

Mobile Phase Characteristics. The mobile phase solvent mixtures were prepared and allowed to equilibrate for at least 1 h before use. The specific gravity and refractive index were measured for each batch of HPLC solvent (methanol–water). The specific gravity of the mobile phase was determined by adding an aliquot of the solvent mixture to a 25-mL Kimax specific gravity bottle equipped with a thermometer, side arm, and a side tube cap with vent. The bottle and contents were weighed (±0.1 mg) at 25 °C. The refractometer was calibrated to a value of 1.3325 at 25 °C using the purified water. Refractive index values of the prepared mobile phase solutions were determined at 25 °C. Phosphate buffer solutions (0.1 M) were prepared by mixing equal volumes of 0.1 M potassium phosphate monobasic and 0.1 M potassium phosphate dibasic which produced a solution of pH 6.91 prior to mixing with methanol.

Chromatographic Procedures. Four analytical HPLC columns were used in this study. A 25 cm by 4.6 mm i.d. Partisil ODS (10 μm, irregular, porous particle) column, 1F3583, and a 25 cm by 4.6 mm i.d. Partisil ODS-2 (10 μm, irregular, porous particle) column, 1H3213, were purchased from Whatman, Inc. (Clifton, NJ). Two 15 cm by 4.6 mm i.d. Ultrasphere ODS (5 μm, spherical, porous particle) columns (UE795 and UE2588N) were obtained from Altex Scientific, Inc. (Berkeley, CA). In operation, the Partisil ODS-2 and Ultrasphere ODS columns were preceded by guard columns 7 cm by 2.1 mm i.d. dry packed with Whatman CO:PELL ODS (30–38 μm). The guard column and analytical column were contained inside a column jacket and maintained at 25.0 ± 0.2 °C by circulating water from a constant-temperature bath through the column jacket. The Partisil ODS column was operated at ambient temperature and without a guard column. The mobile phase consisted of mixtures of water and methanol or phosphate buffer (0.1 M) and methanol at a flow rate of 1.5 mL/min. The ultraviolet detector was operated at 254 nm and varied over five sensitivities (0.5, 0.1, 0.02, 0.01, and 0.005 AUFS) for studies of retention as a function of solute concentration. Solutions of sodium nitrate, *N,N*-dimethylformamide, sodium benzenesulfonate, potassium dichromate, acetone, and tartrazine were prepared in water. Solutions of uracil were prepared in methanol.

RESULTS AND DISCUSSION

The movement and band spreading of unsorbed solutes on glass beads have been discussed by Horvath and Lin (*3*). Even though a solute is unsorbed, measurements of the column void

[1] Present address: USDA Forest Service, Southern Forest Experiment Station, George W. Andrews Forest Sciences Laboratory, Auburn University, AL 36849.

0003-2700/81/0353-1341$01.25/0 © 1981 American Chemical Society

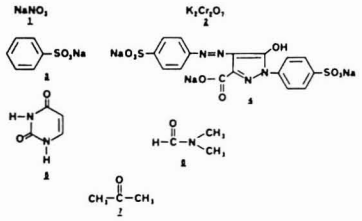


Figure 1. Compounds included in this study: (1) sodium nitrate; (2) potassium dichromate; (3) sodium benzenesulfonate; (4) tartrazine; (5) uracil; (6) *N,N*-dimethylformamide; (7) acetone.

volume can vary according to the molecular size of the solute and its ability to penetrate the intraparticulate pores of the column packing material. This situation is then described by eq 2. The elution volume of an unsorbed solute, V_M, is the

$$V_M = V_e + \phi Vi \quad (2)$$

sum of two factors, the interstitial fluid volume, V_e, and the intraparticulate fluid volume explored by the solute, ϕVi. In the extreme case in which $\phi = 0$, the unsorbed solute is completely excluded from the pores of the packing material, and when $\phi = 1$, the solute undergoes total pore penetration. When there is incomplete pore penetration by the solute, $0 < \phi < 1$. The ability of silica gels which are used for adsorption chromatography to also exhibit exclusion properties has been discussed by Scott and Kucera (*4*).

For the unsorbed solutes, the shortest elution time will be exhibited by solutes for which $\phi = 0$, and the longest elution time by those having $\phi = 1$, according to eq 2. Solutes which undergo only partial pore penetration elute at volumes between the two extremes of V_e and $(V_e + V_i)$.

A search of the literature for a solute suitable to use in determining V_0 for RPHPLC columns reveals that many materials have been used for this purpose. Several authors have used components of the mobile phase to determine the column V_0, i.e., water (*5*), deuterium oxide (*6*), methanol (*7, 8*), acetonitrile (*9*), or water–organic modifier solutions of a composition different to that of the mobile phase (*10, 11*) in nonbuffered solvent systems, or the solvent front (*12*) in buffered solvents. Among the organic solutes (other than components of the mobile phase) used to measure V_0 in nonbuffered eluents are uracil (*10*) and acetone (*13*), while *N,N*-dimethylformamide (*14*) has been used in buffered solvents. The organic salts sodium benzenesulfonate (*15*) and tartrazine (*16*) as well as the inorganic salts potassium dichromate (*17*) and sodium nitrate (*18*) have been used in nonbuffered eluents. Sodium nitrate (*19*) has also been used with buffered mobile phases to determine V_0. (Structures are shown in Figure 1.) Hemetsberger et al. (*20, 21*) have used an equation developed by Halasz to calculate the elution time of a nonretained component. This relationship has also been used by Lochmuller and Wilder (*18*) to verify the elution time they obtained by using sodium nitrate.

Initial experiments with nonionic organic compounds (acetone, uracil, *N,N*-dimethylformamide, and methanol) showed the elution characteristics of these solutes to be dependent on mobile phase composition and independent of the amount injected. A plot of measured elution volume vs. mobile phase composition for acetone, uracil, and methanol is shown in Figure 2. The average elution volume for all solute concentrations injected is plotted for acetone and uracil. A 10-μL sample was consistently injected for methanol. Methanol is not detectable over the entire mobile phase composition range. The elution behavior of *N,N*-dimethylformamide is almost identical to that of acetone in this experiment. Similar results

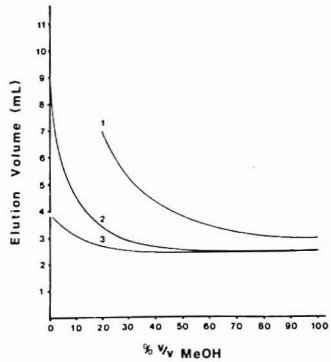


Figure 2. Elution volume vs. eluent composition on Partisil ODS-2: (1) acetone; (2) uracil; (3) methanol.

were obtained on all columns tested and show that the elution volumes for these solutes increase with decreasing concentration of organic modifier. Thus, these compounds appear to be retained according to the typical reversed-phase process and would not be suited for use in measuring the column void volume.

Chromatograms illustrating the elution upon variation of the mobile phase composition (nonbuffered) are given in Figure 3. These chromatograms further illustrate that nonionic organic solutes such as acetone, uracil, *N,N*-dimethylformamide and methanol are not suitable for determining V_0 in RPHPLC. Figure 3 illustrates the elution of sodium nitrate, uracil, and acetone over the entire range of mobile phase composition. Figure 3A was obtained in pure methanol and Figure 3E was produced by using pure water as eluent. The increased separation observed between these solutes as the concentration of organic modifier is decreased would indicate reversed-phase retention. Furthermore, Figure 3E shows a peak for methanol (solvent for the uracil sample) between peaks 1 and 2. On this column, acetone and *N,N*-dimethylformamide were inseparable over the entire water–methanol composition range. The elution volume for sodium nitrate remains constant in this series of chromatograms.

The elution behavior of the ionic solutes was observed to be extremely dependent on the background electrolyte composition in the mobile phase. In nonbuffered eluent, determination of individual elution volumes suggests these solutes should be separable when injected concomitantly. The separation of similarly detectable amounts of sodium nitrate and sodium benzenesulfonate from the water in which they were dissolved (Figure 4) illustrates this point. It can be observed that the separation between peaks 1 and 2 is greater in Figure 4B. The observed elution volume for sodium nitrate was 2.00 mL and 1.78 mL for sodium benzenesulfonate. When these ionic species are injected together in a nonbuffered eluent, it is not possible to obtain a separation. Furthermore, the results in Figure 4 are misleading due to the difference in detectability of these two solutes. When similar concentrations are injected, the resulting retention volumes are the same for both solutes. Water is not detectable over the entire solvent composition range.

Chromatograms presenting the results from both buffered and nonbuffered mobile phases are shown in Figures 5 and 6. Figure 5A represents the chromatography of tartrazine, sodium nitrate, sodium benzenesulfonate, and potassium dichromate in nonbuffered 50% v/v methanol, while Figure 5B,C was obtained in 50% v/v methanol buffered with 0.1

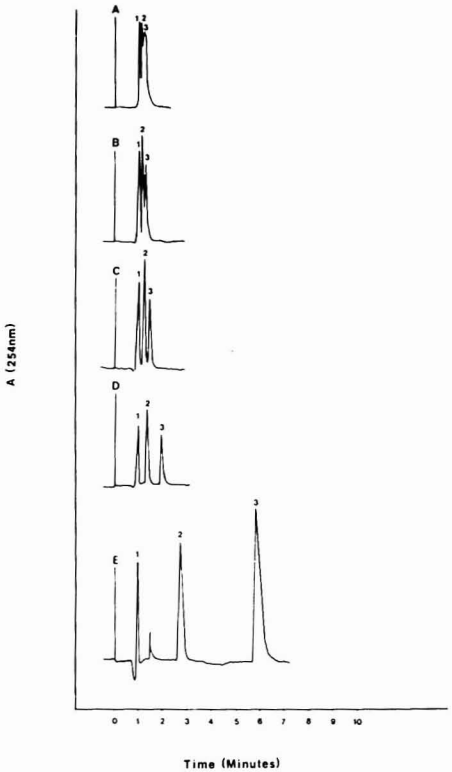


Figure 3. RPHPLC elution on Ultrasphere ODS (UE795) in methanol–water: (A) 100:0, (B) 80:20, (C) 50:50, (D) 20:80, (E) 0:100; (1) sodium nitrate, (2) uracil, (3) acetone.

M phosphate (pH 6.91). Comparison of Figure 5B and Figure 5C (both obtained with buffered mobile phase) demonstrates that under these conditions potassium dichromate elutes after tartrazine and prior to sodium nitrate thereby obscuring the separation of these two solutes. The elution characteristics of these solutes in nonbuffered and buffered mobile phases containing 20% v/v methanol are presented in Figure 6. The separations in 50% v/v methanol–phosphate buffer and in 20% v/v methanol–phosphate buffer are quite different (Figures 5B,C and 6B). In the buffered mobile phase, tartrazine and sodium benzenesulfonate exhibit a dependence upon the concentration of the eluent which implies that these two solutes are being chromatographed under these conditions.

Explanation of these results is facilitated by conclusions drawn from gel permeation (or size exclusion) chromatography (GPC). Experiments on the electrolyte effects of salts in aqueous GPC (22, 23) have established that when an unbuffered solution contains two or more different ionic species, a Donnan salt-exclusion effect occurs, and one of the solutes is blocked from regions penetrable by the others. The presence of a salt in the eluent is used to prevent interference from the Donnan equilibrium. Thus, in the concomitant injection of sodium nitrate and sodium benzenesulfonate in unbuffered eluents, the Donnan salt-exclusion effect results in the equilibration of the level of sodium ions inside and outside

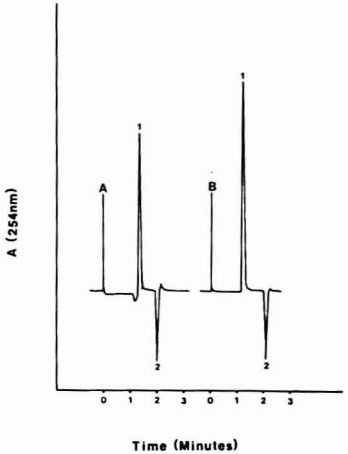


Figure 4. RPHPLC elution on Partisil ODS in methanol/water (50:50): A (1) sodium nitrate, (2) water; B (1) sodium benzenesulfonate, (2) water.

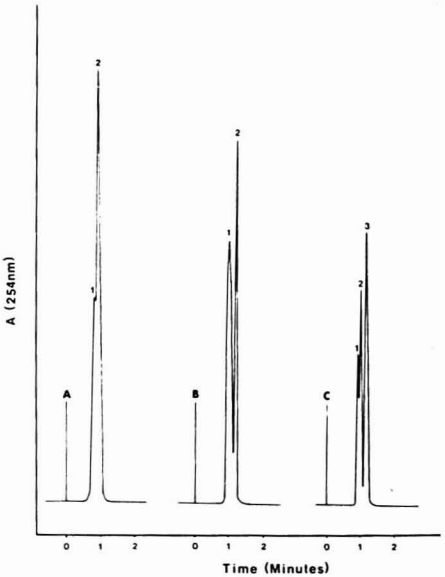


Figure 5. RPHPLC elution on Ultrasphere ODS (UE2588N) in: A, methanol–water (50:50) (1) tartrazine, (2) sodium nitrate, sodium benzenesulfonate, and potassium dichromate; B, methanol–phosphate buffer (50:50) (1) tartrazine, potassium dichromate, and sodium nitrate, (2) sodium benzenesulfonate; C, methanol–phosphate buffer (50:50) (1) tartrazine, (2) sodium nitrate, (3) sodium benzenesulfonate.

the bonded silica particles. This causes these solutes to elute together. When the Donnan effect was masked by the presence of phosphate buffer, it was possible to obtain a separation of the ionic solutes.

Comparisons of the elution data as a function of the amount of solute injected are presented in Figures 7 and 8. These

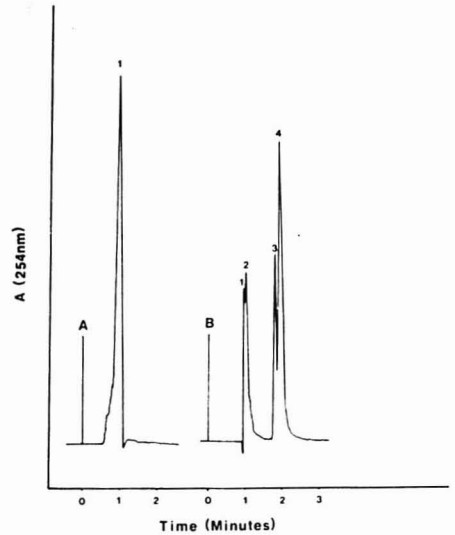


Figure 6. RPHPLC elution on Ultrasphere ODS (UE2588N) in: A, methanol–water (20:80) (1) tartrazine, potassium dichromate, sodium nitrate, and sodium benzenesulfonate; B, methanol–phosphate buffer (20:80) (1) potassium dichromate, (2) sodium nitrate, (3) tartrazine, and (4) sodium benzenesulfonate.

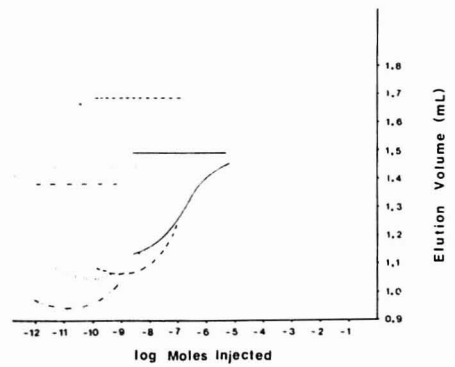


Figure 7. Elution volume vs. moles of solute injected on Ultrasphere ODS (UE2588N). Curves were determined in methanol–water (50:50), while horizontal lines were obtained in methanol–phosphate buffer (50:50): (—) sodium nitrate; (- - -) sodium benzenesulfonate; (···) potassium dichromate; (·-·) tartrazine.

figures are complicated by the differences in UV detectability among the solutes. Plots were prepared for all mobile phase compositions and columns studied and only a representative example is presented. These plots show that the elution volumes of the ionic solutes increased with increasing amounts injected as long as the mobile phase was not buffered. Experiments in GPC have shown that exclusion can occur with molecules of the correct size if they possess the same charge as groups on the surface of the support (*24*). This results in limited pore penetration. Buytenhuys and van der Maeden (*23*) conducted gel permeation chromatography on unmodified

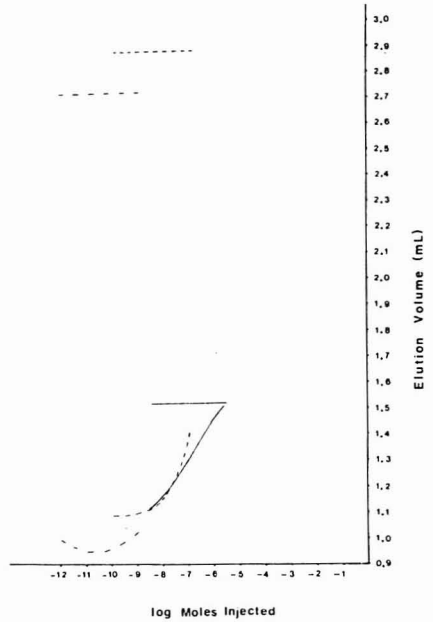


Figure 8. Elution volume vs. moles of solute injected on Ultrasphere ODS (UE2588N). Curves were determined in methanol–water (20:80), while horizontal lines were obtained in methanol–phosphate buffer (20:80): (—) sodium nitrate; (- - -) sodium benzenesulfonate; (···) potassium dichromate; (·-·) tartrazine.

silica gel with aqueous solvents and demonstrated an ion exclusion effect resulting from a negative charge on the surface of silica gel. The effect was suppressed by using an aqueous buffer to shield the negative charges of the silica. The concentration dependence observed in Figures 7 and 8 in unbuffered eluents can then be understood on the basis of this ion exclusion effect. On the basis of studies with reversed-phase supports, Berendsen et al. (*25*) suggested that at low electrolyte concentration in unbuffered eluents, a salt is excluded from the pores of the packing, presumably due to electrical charges on the phase surface. With increased electrolyte concentration in the mobile phase, the ion exclusion effect is suppressed and the pores become accessible to the salt. Thus, injection of trace amounts of a salt in nonbuffered eluents yields the interstitial or exclusion volume, V_e, in eq 2. When the mobile phase is buffered with 0.1 M phosphate, the ionic solutes do not exhibit any solute concentration dependence, yet sodium benzenesulfonate and tartrazine are dependent upon eluent composition as shown in Figures 5B,C and 6B. From these studies it is apparent that the solutes can be separated into three groups: group I, methanol, uracil, acetone, *N,N*-dimethylformamide; group II, sodium nitrate, potassium dichromate; group III, sodium benzenesulfonate, tartrazine. For those solutes in group I, elution is dependent on the mobile phase composition yet independent of the amount of solute injected. The solutes in group II are relatively independent of solvent composition in both buffered and nonbuffered eluents but demonstrate a concentration dependence in nonbuffered eluents which disappears in the presence of phosphate buffer. Group III solutes exhibit a concentration dependence–solvent composition independence

in nonbuffered methanol solutions, but they are concentration independent–solvent composition dependent in methanol–phosphate buffer mixtures.

From the foregoing discussion, solutes in groups I and III can be eliminated as suitable for use in determining the column void volume. Discrimination between the group II solutes, sodium nitrate and potassium dichromate, can be made on the basis of the elution order for equimolar quantities of these solutes in buffered eluent. That solute which undergoes a greater pore penetration of the silica gel backbone is expected to have a greater elution volume, e.g., sodium nitrate. Therefore, according to eq 2, sodium nitrate more nearly represents the case of $\phi = 1$ than does potassium dichromate.

CONCLUSIONS

On the basis of the evidence presented for the solutes examined, acetone, *N,N*-dimethylformamide, methanol, and uracil appear to be unsuitable for determining column void volume on hydrocarbonaceous stationary phases. When buffered methanol eluents are used, the injection of any detectable amount of sodium nitrate produces a good estimate of the column void volume in RPHPLC. In unbuffered aqueous methanol, the column void volume can be estimated by an injection of approximately 3×10^{-6} mol or greater of sodium nitrate. Perhaps the most important conclusion is that the identity and concentration of the solute used to determine the column void volume must accompany all reported k' data in RPHPLC studies.

LITERATURE CITED

(1) Heftmann, Erich "Chromatography: A Laboratory Handbook of Chromatographic and Electrophoretic Methods"; Van Nostrand Reinhold: New York, 1975; p 49.
(2) Colin, Henri; Ward, Norman, Guiochon, Georges *J. Chromatogr.* **1978**, *149*, 169–197.
(3) Horvath, Csaba; Lin, Hung-Jye *J. Chromatogr.* **1978**, *126*, 401–420.
(4) Scott, R. P. W.; Kucera, P. *J. Chromatogr.* **1977**, *125*, 251–263.
(5) Scott, R. P. W.; Kucera, P. *J. Chromatogr.* **1977**, *142*, 213–232.
(6) McCormick, R. M.; Karger, B. L. *Anal. Chem.* **1980**, *52*, 2249–2257.
(7) Schabron, J. F.; Hurtubise, R. J.; Silver, H. F. *Anal. Chem.* **1978**, *50*, 1911–1917.
(8) Roumeliotis, P.; Unger, K. K. *J. Chromatogr.* **1978**, *149*, 211–224.
(9) Melander, Wayne R.; Chen, Bor-Kuan; Horvath, Csaba *J. Chromatogr.* **1979**, *185*, 99–109.
(10) Karger, Barry L.; Gant, J. Russel; Hartkopf, Arleigh; Weiner, Paul H. *J. Chromatogr.* **1976**, *128*, 65–78.
(11) Gant, J. R.; Dolan, J. W.; Snyder, L. R. *J. Chromatogr.* **1979**, *185*, 153–177.
(12) Baker, John K.; Ma, Cheng-Yu *J. Chromatogr.* **1979**, *169*, 107–115.
(13) Johnson, Howard J., Jr.; Cernosek, Stanley F., Jr.; Gutierrez-Cernosek, Rose Mary *J. Chromatogr.* **1979**, *177*, 297–311.
(14) Unger, Stefan H.; Feuerman, Tony F. *J. Chromatogr.* **1979**, *176*, 426–429.
(15) Bakalyar, Stephen R.; McIlwrick, Rod; Roggendorf, Elizabeth *J. Chromatogr.* **1977**, *142*, 353–365.
(16) Bakalyar, Stephen R.; Henry, Richard A. *J. Chromatogr.* **1976**, *126*, 327–345.
(17) Schoenmakers, P. J.; Billiet, H. A. H.; Tijssen, R.; de Galan, L. *J. Chromatogr.* **1978**, *149*, 519–537.
(18) Lochmuller, C. H.; Wilder, D. R. *J. Chromatogr. Sci.* **1979**, *17*, 574–579.
(19) Horvath, Csaba; Melander, Wayne; Molnar, Imre *J. Chromatogr.* **1976**, *125*, 129–156.
(20) Hemetsberger, H.; Maasfeld, W.; Ricken, H. *Chromatographia* **1976**, *9*, 303–310.
(21) Hemetsberger, H.; Kellerman, Marlene; Ricken, H. *Chromatographia* **1977**, *10*, 726–730.
(22) Neddermeyer, P. A.; Rogers, L. B. *Anal. Chem.* **1969**, *41*, 94–102.
(23) Buytenhuys, F. A.; van der Maeden, F. P. B. *J. Chromatogr.* **1978**, *149*, 489–500.
(24) Krejci, M.; Kourilova, D.; Vespalec, R.; Slais, K. *J. Chromatogr.* **1980**, *191*, 3–7.
(25) Berendsen, Gert E.; Schoenmakers, Peter J.; de Galan, Leo; Vigh, Gyula; Varga-Puchony, Zita; Inczedy, Janos *J. Liq. Chromatogr.* **1980**, *3*, 1669–1686.

RECEIVED for review December 29, 1980. Accepted April 27, 1981. We sincerely appreciate the support of the American Foundation for Pharmaceutical Education Silas M. Burroughs Memorial Fellowship for M. J. M. Wells.

Preparative Liquid Chromatography for Fractionation of Petroleum and Synthetic Crude Oils

James W. Vogh* and Jane S. Thomson

Bartlesville Energy Technology Center, U.S. Department of Energy, P.O. Box 1398, Bartlesville, Oklahoma 74003

The procedures for routine preparative liquid chromatographic separation of hydrocarbon classes in high boiling petroleum and coal liquid samples have been improved by use of high-performance liquid chromatography techniques. Separations were carried out on alumina and silica gel to produce sample fractions equivalent to those obtained with older methods. The columns are reusable following suitable solvent backwashing and provide stable performance and good hydrocarbon class resolution over an extended series of runs. The complete operating time, including regeneration to starting conditions, is 80 min for the alumina column and 25 min for the silica gel column. Capacity ranges from 1 to 6 g of sample, depending on its composition.

One of the primary steps in the detailed characterization of petroleum and similar materials has been the adsorption column separation of hydrocarbon classes. The principal methods have been the silica–alumina gel procedure developed under the API-60 program or variations of this procedure (*1*). The subsequent steps through gel permeation and characterization by mass spectrometric and other methods depend largely on the success of the adsorption column separation.

The silica–alumina procedure in common use is a conventional open column chromatographic method. It was developed through a procedure of step gradient displacements of a series of model compounds. This became a set procedure depending on the dimensions of the column, the quality and activation of the adsorbants, and the volumes and flow rate of the eluting solvents. Sample capacity varied from 4 to 15 g depending on the amount or nature of the more strongly adsorbed components. The procedure does not permit an easy change of scale of equipment unless the column is coupled to a liquid chromatography monitor.

The silica–alumina column method usually provides a good separation of the hydrocarbon classes; however, there are difficulties and inconvenient aspects in this procedure. As a method conceived for routine use, the most severe problem is the requirement for an unbroken 50-h operation. Other

This article not subject to U.S. Copyright. Published 1981 by the American Chemical Society

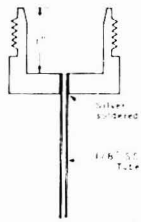


Figure 1. Column end fitting prepared by modification of Swagelok cap SS-2000-C.

problems in the method are associated with lack of a detection system. Overloading of the column may not be detected until succeeding separations or characterizations are carried out.

There is a large background of information on alumina column chromatography, especially in procedures developed by Snyder (*2*), based on water deactivated alumina for separations of petroleum samples and many hydrocarbon classes. Detailed studies of structural and other effects in separations on alumina were carried out (*3*), and it was shown that deactivation of alumina results both in improved column efficiency and in increased linear capacity. The latter effect is particularly important in preparative chromatography.

Other studies (*4*) on deactivated alumina have shown the effects of molecular shape, alkylation, and acid–base interactions of a large variety of hydrocarbons. A routine for adsorbant activity control has been worked out (*5*). Highly active alumina is infrequently used in high-performance liquid chromatography separations, but it has been applied in gradient mode for analyses of lubricant base oils (*6*). In this method, the column was reactivated for the succeeding run at 250 °C while purging with nitrogen.

There is some inconvenience in maintaining a fixed level of deactivation with water or in holding a highly active state by thermal activation. It has been shown that various polar solvents may be used in place of water (*2*) so that it seemed desirable to select a solvent combination that would allow more convenient control of the alumina activity level.

Alumina can separate saturate from monoaromatic hydrocarbons only in the highly activated state. Silica is more satisfactory for this separation since it provides good resolution without need for high activation. In addition, it has a much higher sample capacity than does activated alumina.

Generally, the group separation obtained with the silica–alumina column has been satisfactory when carried out properly, and these adsorbants were retained as the basis of the separation method in the development of an improved procedure. Continued use of group separation by alumina and silica gel adsorption also allows the other separation and characterization procedures to be continued without change.

The major change sought in the improved procedure was development of efficient, high-speed, reusable preparative columns. Current techniques of liquid chromatography provide the basis for the development of this type of column.

EXPERIMENTAL SECTION

The column tubing and fittings were prepared from conventional stainless steel pipe and Swagelok fittings. Tubing was 30-cm lengths of 3.18 cm (1.25 in.) o.d. and 2.75 cm i.d. pipe, and the interior of the tubing was polished by means of a cylinder hone. The end fitting is shown in Figure 1. These were Swagelok 1.25 in. caps, type SS-2000-C, machined to a flat interior base leaving an end wall about 7 mm thick. A length of 0.125-in. o.d. stainless tubing was silver soldered through the center of the end wall. A slurry packing reservoir of 150-cm length was prepared from the 1.25-in. pipe and was attached to the column by a drilled out Swagelok union. Columns and the reservoir were tested at 2000 psi before the columns were packed.

A disk of porous polyethylene (Bel Art, Pequannock, NJ, 35 μm) was cut to fit tightly in the end of the column by means of a sharp-edged punch prepared from the tubing stock. Stainless steel screen (150 mesh, Small Parts, Inc., Miami, FL) and polytetrafluoroethylene filter element (Millipore, Bedford, MA, type FHLP, 0.5-μm porosity) were cut to approximately the outer diameter of the column and were placed in the end fitting. The Millipore element was placed against the polyethylene frit.

Adsorbants were prepared from thin-layer grade materials (Merck alumina 60 PF-254, type E, and Merck silica gel H, type 60, EM Laboratories, Inc., Elmsford, NY). These adsorbants are not suitable for column chromatography as received and must be processed to remove the very small particle material. For refining of the silica gel, about 200 g of the adsorbant was suspended in 2 L of 0.04 N NH_4OH, the mixture was allowed to settle about 5 min, and the supernatant suspension was siphoned off. This was repeated three or four times with the last rinse being carried out with deionized water. The silica was dried and activated at 110 °C.

The alumina was first soaked in ethyl acetate a minimum of 48 h, with occasional stirring, for removal of binder material. It was then washed with successive portions of ethyl acetate and acetone and finally with deionized water. Fine particulates were removed by suspension, first in 0.04 N acetic acid and subsequently in deionized water. The supernatant suspension was siphoned off after 30 min of settling. Typically, seven to eight rinses with deionized water were used. Drying and activation were at 200 °C.

All column packing was done by a pressurized viscous slurry technique. The slurry was prepared as a suspension of about 215 mL of the adsorbant (about 20% excess of the column volume) in about 500 mL of pharmaceutical-grade mineral oil plus 25–60 mL of pentane. The pentane causes a substantial reduction in the viscosity of the mineral oil slurry. The amount added should not be sufficient to allow visible settling of the adsorbant but should be enough to make the mixture quite fluid. About 25 mL of mineral oil was placed in the column, the slurry was introduced, and the remaining space in the reservoir was filled with pentane.

The slurry was forced into the column under the pressure of pentane from a Haskel (Burbank, CA) air driven pump, Model 28645. About 1600 psi pressure was applied by the pump during the packing and about 20–60 min were required for completion of the packing. Two liters of pentane were then pumped rapidly through the packing assembly.

After the slurry packing was completed, the column and reservoir tubes were carefully separated to avoid excessive disturbance of the adsorbant bed. The exposed adsorbant was scraped out of the end of the column to allow insertion of a polyethylene frit. The column was closed with a fitting including a wire gauze and Millipore filter in the same manner as the opposite end.

After packing and closure of the columns they were washed with about 500 mL of pentane, allowed to stand for 18–24 h, and again washed with more pentane. This procedure was found to be necessary for complete removal of the mineral oil. After the second washing the silica column was ready for use in examination of samples. The alumina column required washing with 10% (vol) of ethyl ether in pentane. About 2–4 L of this mixture was passed through the column followed by about 500 mL of 1% (vol) ether in pentane to prepare it for use.

Figure 2 shows the schematic flow system used when the columns were operated in the preparative mode by gradient elution. For solvent gradient operation a pair of 500-mL mixing vessels (Glenco, Houston, TX, type 3130) were used. Linear gradients were formed in this system. The system included a Fluid Metering, Inc., Oyster Bay, NY, solvent pump (Model RP3DSS). This pump was capable of pumping up to 110 mL min^{-1} at pressures up to 200 psi. Refractive index (Waters Associates, Milford, MA, Model R401) and ultraviolet (254 nm, Waters) detectors were used with the silica column. Effluent from the silica column was split, with the major part of the flow going to waste or sample receivers and the minor part of those detectors. This splitting of the solvent stream prevented development of excessive back-pressure in these analytical-type detectors. A flow-through cuvette-type cell of 1.5-mm path length (Helma Cells,

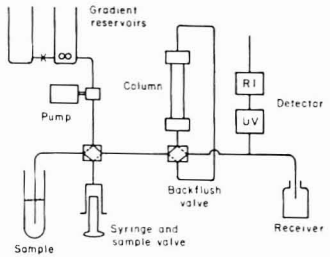


Figure 2. Schematic of preparative liquid chromatography system.

Jamaica, NY, Model 176.52) was used in an ultraviolet–visible spectrophotometer (Beckman Instruments, Fullerton, CA, Model 25) as detector for the alumina column. No signifciant backpressure was developed by this flow-through cell so that solvent stream splitting was not needed. Large sample introduction and column back-flushing were accomplished with Altex four-way slider valves.

The alumina column was commonly operated in the solvent gradient elution mode. In the usual preparative separation routine, the sample was introduced in the stop-flow mode by syringe injection through the slider valve. It was then washed onto the column with 150 mL of 1 vol% of ethyl ether in either pentane, hexane, or heptane. This was followed by 800 mL of 1–10% ether linear gradient and back-washing with 400–800 mL of 20% ether in the same hydrocarbon solvent. To prepare the column for further use, it was then washed in the forward direction with 400–600 mL of 1% ether solution. Cut points for fraction collection were taken at the chromatogram minima, if these were evident and at the beginning of the backflush. Complex or unusual samples that did not show the typical hydrocarbon class chromatograms were cut at points determined from model compound studies. Prior to preparative separations, an analytical size sample of the particular oil was chromatographed on the alumina column to aid in location of exact cut points and to detect any unusual character of the oil. The first cut from the alumina column contains both saturate and monoaromatic hydrocarbon classes. This sample cut was concentrated to a suitable volume for introduction to the silica column for further separation. The following cuts from the alumina column contained diaromatic and polyaromatic-polar classes and were not subjected to silica column separation.

The silica gel column was operated in a similar forward and backflush manner but without solvent gradient. Pentane was the commonly used solvent, and no regeneration of the column was required before a succeeding run. The forward and backwash volumes for the silica column were determined by the detector response to the saturate and monoaromatic hydrocarbon classes.

In some cases it was found desirable to carry out preparative separations at elevated temperatures. For this purpose the column was placed in a regulated-temperature water bath. The upper temperature limit was set at the boiling point of the solvent in the column.

Hydrocarbon solvents (Phillips Petroleum Co., Bartlesville, OK, commercial and pure grades) were distilled and passed through columns of activated 3A molecular sieve. Anhydrous, alcohol-free ethyl ether (Fisher Scientific, Pittsburgh, PA) was used as received. Tetrahydrofuran was used in mixtures with pentane or heptane for displacement of strongly held materials or for occasional regeneration of the columns.

Hydrocarbon model compounds listed in the discussion were used as received. Petroleum and coal liquid samples from characterization studies were examined for comparison with previous separation results.

RESULTS AND DISCUSSION

Figure 3 shows a chromatogram of some model compounds at analytical levels on an alumina column. This run was made under the conditions described earlier of gradient elution and backwash. On the time axis of Figure 3, the zone A–B was

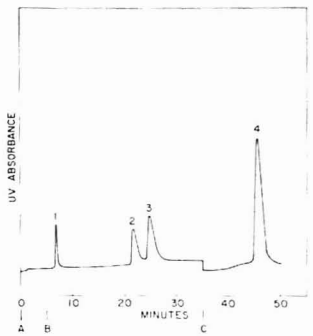


Figure 3. Chromatogram of hydrocarbons on preparative alumina column: (1) toluene, (2) 2,6-dimethylnaphthalene, (3) acenaphthene, (4) pyrene. UV detection, flow rate, 28 mL/min. The solvent gradient zones are as follows: A–B, 1% ether in hexane; B–C, 1–10% ether linear gradient; C (backflush), 20% ether.

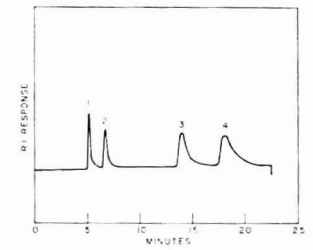


Figure 4. Chromatogram of hydrocarbons on preparative silica column: (1) cyclohexane, (2) 2-methyl-1-pentene, (3) toluene, (4) 6-methyltetralin. Refractive index detection, pentane solvent, flow rate, 28 mL/min.

the initial isocratic stage of 1% ethyl ether in hexane and zone B–C the linear gradient stage of 1–10% ether in hexane. At C the flow direction was reversed to backflush remaining material from the column with 20% ether in hexane. The point B was selected for development of a well-resolved chromatogram and was not related to fraction collection. C, however, represents the initial collection of the backflush on polar class fraction. Figure 4 shows a similar chromatogram for the silica column. This chromatogram was prepared with forward flow only and without gradient. It is evident that the performance of these columns in the analytical mode is not that of the best LC systems. However, it can be useful in preliminary analytical examination of samples as well as in the preparative separations.

Figure 5 shows a chromatogram from the alumina column of a 1-g sample of the 370–535 °C distillate of Gach Saran crude. This chromatogram was carried out in the conventional gradient and backflush manner described for Figure 3. The zones of aromatic hydrocarbon classes for this as well as other oil samples appear somewhat earlier than expected on the basis of model compound studies. This is not an overload effect since the chromatograms are not altered if analytical size samples are injected. The first peak in this chromatogram is the UV response for monoaromatic hydrocarbons. Saturate hydrocarbons elute before and with the monoaromatics so that this fraction must be resolved later on the silica column. The alumina column in this procedure could not be maintained in a sufficiently active state to provide a useful separation of

Table I. Capacity Factors (K') of Hydrocarbons on Silica and Alumina Columns

	silica[a]	alumina[b]		silica[a]	alumina[b]
dotriacontane	0.00	0.00	butylbenzene	1.51	
isopentane	0.05		benzylcyclohexane	1.63	
pristane	0.06		ethylbenzene	1.74	
cyclohexane	0.10		toluene	1.98	0.67
decalin	0.10		cyclohexylbenzene	2.14	
cyclododecane	0.10		1,3,5-trimethylbenzene	2.19	
perhydroanthracene	0.10		*p*-xylene	2.26	
7-tetradecene	0.20		indan	2.55	
1-hexadecene	0.23		tetralin	2.72	
2-hexene	0.39		6-methyltetralin	2.88	0.80
2-methyl-1-pentene	0.43		tetrahydroacenaphthene	2.92	1.26
4-methylcyclohexene	0.47		naphthalene	3.24	4.55
nonadecylbenzene	1.06		1,2,4,5-tetramethylbenzene	3.29	1.05
tridecylbenzene	1.19		dodecahydrotriphenylene	4.30	2.51
			hexamethylbenzene	4.75	2.94

[a] Pentane solvent. [b] Hexane, 1% ether solvent. Capacity factors were determined only for compounds with listed values.

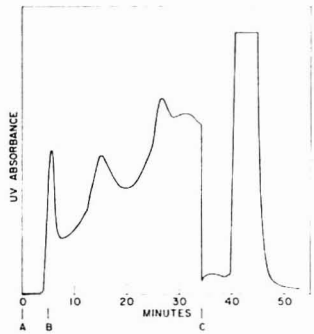


Figure 5. Chromatogram of Gach Saran crude distillate, 370–535 °C, 1.01 g, on alumina column. For conditions see Figure 3.

saturate from monoaromatic hydrocarbons.

The columns were ordinarily operated at a flow rate of about 28 mL min^{-1}, which was about as fast as possible for convenient sample collection. If an automated, detector-coupled, sample collection apparatus was available, columns should operate well at much higher flow rates. Figure 6 shows the trend of plate height (HETP) with flow rate for toluene and 2-butylbiphenyl on alumina. The column was at 25 °C, and the solvent was 1% ether in heptane. Figure 6 also shows the same trend for cyclohexane and toluene on silica at 25 °C with pentane solvent. It is apparent that both columns will give useful separation and stable behavior at flow rates to 80 mL min^{-1}. At the time of this HETP rating, both of these columns were several months old and had been subjected to backflush operation so that these results represent the properties of well-stablized columns.

The apparent low resulution of the chromatogram in Figure 5 compared to the other chromatograms is due the complexity of that high-boiling sample rather than any failure of the column to resolve individual compounds efficiently. Variation of capacity factors for model compounds in a class is discussed below. Because of this, class separations do not benefit very much from high plate numbers and should be only slightly less complete when carried out at high flow rates.

Table I shows capacity factors for a variety of saturate and aromatic hydrocarbons on the silica gel column. There is a slight retention of some cyclic saturates, but it is not sufficient to provide useful separation in this class. Alkenes are sufficiently resolved from saturates to allow their detection in

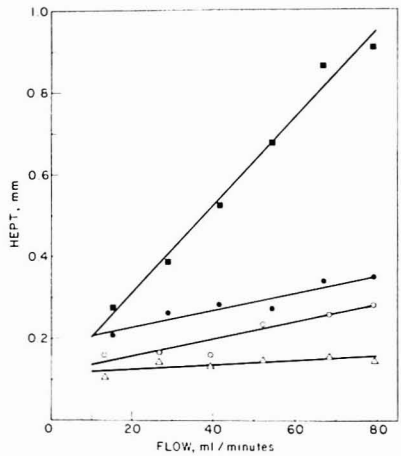


Figure 6. Trends of plate height (HETP) with flow rates. Upper two lines represent alumina column, 1% ether in heptane solvent: (■) 2-butylbiphenyl, (●) toluene. Lower two lines represent silica column, pentane solvent: (○) toluene, (△) cyclohexane.

analytical samples. For preparative separations of alkenes from saturates, the column must be cooled to −10 °C or lower to increase retention sufficiently to offset the peak blending effect of large sample volumes. If large amounts of normal paraffins are present in the sample, they will tend to crystallize from solution at this temperature and interfere with flow through the column. In this situation, a procedure based on a mixed fluorinated solvent and aliphatic solvent system (7) might be preferable. That procedure was not examined in this work, however. Capacity factors of monoaromatic hydrocarbons show the same general patterns that have been observed in other work (8, 9). The monoaromatic hydrocarbon class is well separated from the saturates but tends to overlap the diaromatic hydrocarbons. For this reason, the silica gel column is used mainly for separation of saturate from monoaromatic hydrocarbons in mixtures containing only these two classes.

Table II shows the effect of temperature and solvent on capacity factors of the silica column. Most of this effect is due to temperature. Ordinarily no special benefit is gained by operating at elevated temperature, but waxy samples may

Table II. Influence of Temperature and Solvent on Capacity Factors

Silica Column, Isocratic Mode

	capacity factors	
	room temp pentane	44 °C heptane
nonadecylbenzene	1.06	0.70
pentylbenzene	1.42	1.05
toluene	1.98	1.35
cyclohexylbenzene	2.14	1.35
tetralin	2.72	1.59

Alumina Column, Gradient Mode

	capacity factors		
	1–10% ether in hexane, 22 °C	1–10% ether in heptane 22 °C	1–10% ether in heptane, 35 °C
2-butylbiphenyl	2.2	1.8	1.8
naphthalene	3.5	3.4	3.1
2,6-dimethylnaphthalene	4.3	3.7	3.4
1-phenylnaphthalene	5.5	4.9	4.5
fluorene	BF[a]	BF	7.2
2,6-dimethylanthracene	BF	BF	BF

[a] Backflush.

Table III. Capacity Factors (K') of Hydrocarbons on the Alumina Column[a]

2-butylbiphenyl	2.19	1-phenylnaphthalene	5.46
1-butylnaphthalene	3.08	fluorene	BF[b]
naphthalene	3.54	2-phenylnaphthalene	BF
hexahydropyrene	3.79	2,6-dimethylanthracene	BF
1,2-diphenylethane	4.16	phenanthrene	BF
1,5-dimethylnaphthalene	4.24	chrysene	BF
biphenyl	4.36	pyrene	BF
acenaphthene	5.00		

[a] Gradient mode, 1–10% ether in hexane. [b] Backflush.

require higher temperature for adequate solubility.

Table I contains capacity factors for some model compounds in the mono- and diaromatic hydrocarbon classes on the alumina column. These capacity values were determined in isocratic mode operation with 1% ether in hexane, that is, without gradient operation. Although resolution efficiency is less for the alumina than for the silica gel column, the separations of aromatic hydrocarbon classes are more satisfactory on alumina since the capacity factors of members of an aromatic class are less dispersed than on silica gel. The last three monoaromatic hydrocarbons in this list would elute after naphthalene on the silica column but are well retained in the monoaromatic class on alumina. These retention values follow the same patterns that have been observed in other work (*4*).

Table III shows capacity factors of a number of diaromatic and polyaromatic hydrocarbons on alumina under gradient operation. Most of the diaromatics elute between capacity factor values of 3 and 5. Only the sterically crowded 2-butylbiphenyl falls significantly outside this range. The triaromatic 1-phenylnaphthalene elutes just after the diaromatic zone and much before any other model triaromatic compound. This is expected since the hydrogens of the 2-phenyl and 8-naphthyl positions of this compound crowd each other. The other polyaromatics examined all elute at essentially the same zone in the backflush.

Table II shows the effect of temperature and solvent on capacity factors on alumina under gradient operation. Alumina shows less sensitivity than silica, but the appearance of fluorene in the forward wash near the end of the solvent program at 35 °C indicates a possible effect on sample fraction composition.

A number of samples originating from petroleum, coal liquids, and shale oil sources have been processed by this system. Each of the samples was first introduced to the alumina column at analytical level. Sample size was then increased until the chromatogram showed signs of overloading as indicated by smearing or substantially early appearance of the peaks. The acceptable quantities varied among the different samples and fell in the range of 1–6 g per injection. It seemed in several cases that the polar and polyaromatic materials could occupy a sufficient fraction of the column capacity so that the diaromatic and earlier polyaromatic hydrocarbons were crowded forward in the chromatogram at the overload condition. For this reason, the usual overload rating based on HETP at increasing single compound injection (*10*) was not used.

Some of the samples studied were duplicates of those run by the API-60 method (*1*) either in that program or in later residue or coal liquid studies at the Bartlesville Energy Technology Center. The first of these is the 370–535 °C

Table IV. Recovery of Hydrocarbon and Polar Class Fractions

	Gach Saran crude 370–535 °C dist (acid and base free)		South Swan Hills crude 370–535 °C dist (acid and base free)		Utah coal syncrude 200–370 °C dist	
fraction	API-60 method[a]	this report	API-60 method	this report	API-60 method[c]	this report[d]
saturate	51.03	48.81	65.94	64.75	28.1	27.32
monoaromatic	17.72	20.64	12.55	13.65	30.0	28.85
diaromatic	12.32	10.42	6.27	6.67	14.7	16.89
diaromatic-second		5.86		3.02		2.67
PAP-backflush	18.93	12.17	10.82	9.99	5.2	3.49
BF (THF)[b]		0.00		.26		0.65
acids					10.8	10.47
bases					0.6	5.50
solids					3.4	
(total)	100.00	97.90	95.58	98.34	92.8	95.84

[a] Data had been normalized to 100%. [b] Backflush with tetrahydrofuran. [c] Acid and base materials were extracted from the initial PAP fraction. In the extraction procedure, solids amounting to 3.4% of total sample were also recovered. [d] Acid and base materials were extracted from the distillate.

Table V. Comparison of Mass Spectrometric Saturate Class Analysis, South Swan Hills, 370–535 °C

	API-60 method	this report
0-ring	28.8	29.5
1-ring	31.1	28.3
2-ring	14.6	17.1
3-ring	9.2	9.3
4-ring	8.1	8.1
5-ring	4.5	4.6
6-ring	3.8	3.2
monoaromatic	0.0	0.0

distillate of Gach Saran (Iran) crude (*11*) shown in Table IV. Both runs were carried out on acid- and base-free material. Yields from the two methods are in reasonable agreement for the saturate, monoaromatic, and diaromatic classes. In this and the following samples, the eluant following the diaromatic zone was collected separately from the backflush (PAP) material. The yield of this (DA-2, Diaromatic-Second) plus the backflush (BF) approximates the PAP fraction of the API-60 method. In several samples the yield of the DA-2 fraction was fairly substantial in comparison to the backflush fraction. Since the DA-2 appears by mass spectrometric examination to be largely diaromatic, characterization of it apart from the polar components of the backflush material should improve analytical results. Analysis of the saturate fraction by mass spectrometry showed it to correspond well to the old saturate fraction.

The Gach Saran sample was a fairly typical high-boiling distillate of petroleum crude. It responded well to both separation processes and, according to the yields shown in Table IV, produced well-defined hydrocarbon concentrates.

The second part of Table IV shows the yields from separation of the 370–535 °C distillate of South Swan Hills (Alberta, Canada) crude (*12*). Both runs were carried out on acid- and base-free material. Again the yields of the saturate, monoaromatic, and diaromatic concentrates are in good agreement. The combined DA-2 and backflush yields are somewhat greater than the PAP yield of the old method, which probably indicates improved sample recovery by the backflush operation.

The South Swan Hills distillate is somewhat higher in saturates than the usual crude. It separated to the several concentrates by both methods without difficulty.

The analysis of the saturate fractions of both the old and new separations of South Swan Hills distillate is shown in Table V. The MS analysis of the old fraction was repeated concurrently with the analysis of the new sample.

The last part of Table IV shows results obtained on a coal liquid. This was the 200–370 °C distillate of a Utah syncrude (*13*) produced by the COED process from Utah A-seam coal and supplied by FMC Co. (Chicago, IL). This was a fairly complex material containing a relatively large amount of polar material. Also, the hydrocarbon material was highly aromatic. The sample processed by the API method did not have acids and bases removed before the hydrocarbon class separation; therefore, these as well as some solids were recovered from the PAP fraction. The sample processed in this work was treated by extraction for removal of acids and bases before the column separations.

Despite the considerable difference in sample handling, the hydrocarbon class yields for the Utah Syncrude are quite comparable for the two methods. The low overall yields by both methods may be partly due to loss of the more volatile components boiling near 200 °C.

The experience gained in processing a number of samples has shown the advantages as well as the need for certain cautions. Solvent mixtures more polar than 10% tetrahydrofuran in heptane should probably not be used in the alumina column. Both pure tetrahydrofuran and methanol in heptane appear to have been damaging to alumina and should be avoided if possible. The need for washing alumina with strongly polar solvents arises when the column has been used for an extended series of highly polar samples. In this condition, the column will show diminished capacity and retention volume. Ordinarily, extended recycle washing with 10% tetrahydrofuran with a tube of conventional activated alumina in line will correct this problem. Solvents and samples should be free of water if possible, but washing with 10% tetrahydrofuran will reactivate the column. Particulate matter in the samples either may be caught on the polyethylene frit or may be passed through and lodged on the end of the adsorbent bed. This may be repaired without harm to the column by removing the frit, scraping out the particulate and a small amount of the packing, and replacing with a new frit.

Silica appears to be immune to these problems. The silica column prepared originally for this study is still in use.

Several advantages have been achieved by use of this separation procedure. An obvious advantage is the saving of time. At the flow rates used in most of this work, the alumina column requires 80 min for a complete cycle and the silica column about 25 min. Samples equal in size to those processed in the old, open-column method can be prepared in a series of runs scheduled at convenient times, rather than in a continuous 50-h run. Small samples may be processed in a lesser number of runs with proportional saving of time, whereas the open-column run time cannot be shortened.

The use of the columns to produce a reference analytical chromatogram has been helpful in identifying unusual composition of samples and problems that may result. For example, comparison of chromatograms prepared during preparative runs with the reference analytical chromatogram can indicate possible overload conditions.

Both the silica and alumina columns are reusable and stable through an extended series of sample separations. The reusable chracter of the columns saves a considerable amount of time activating adsorbents and cleaning and repacking columns. More important than the saving of time is the reliably good resolution and repeatability of the columns. Column reproducibility over a long time period has been important in the development of an efficient separation procedure.

LITERATURE CITED

(1) Hirsch, D. E.; Hopkins, R. L.; Coleman, H. J.; Cotton, F. O.; Thompson, C. J. *Anal. Chem.* **1972**, *44*, 915–919.
(2) Snyder, L. R.; Saunders, D. L. "Chromatography in Petroleum Analysis"; Altgelt, K. H., Gouw, T. H., Eds.; Marcel Dekker: New York, 1979; Chapter 10.
(3) Snyder, L. R. "Principles of Adsorption Chromatography"; Marcel Dekker: New York, 1968; Chapters 10, 11.
(4) Popl, M.; Dolansky, V.; Mostecky, J. *J. Chromatogr.* **1974**, *91*, 649–658.
(5) Engelhardt, H.; Wiedemann, H. *Anal. Chem.* **1973**, *45*, 1641–1646.
(6) Matsunaga, A.; Yagi, M. *Anal. Chem.* **1978**, *50*, 753–756.
(7) Suatoni, J. C.; Swab, R. E. *J. Chromatogr. Sci.* **1980**, *18*, 375–378.
(8) Snyder, L. R. *J. Chromatogr.* **1963**, *11*, 195–227.
(9) Popl, M.; Dolansky, V.; Mostecky, J. *J. Chromatogr.* **1976**, *117*, 117–127.
(10) DeStefano, J. J.; Beachell, H. C. *J. Chromatogr. Sci.* **1972**, *10*, 654.
(11) Dooley, J. E.; Hopkins, R. L.; Hirsch, D. E.; Coleman, H. J.; Thompson, C. J. Bureau of Mines Report of Investigations RI 7770; Bartlesville Energy Technology Center: Bartlesville, OK, 1973.
(12) Dooley, J. E.; Hirsch, D. E.; Coleman, H. J.; Thompson, C. J. Bureau of Mines Report of Investigations RI 7821; Bartlesville Enegy Technology Center: Bartlesville, OK, 1973.
(13) Dooley, J. E.; Sturm, G. P., Jr.; Woodward, P. W.; Vogh, J. W.; Thompson, C. J. BERC/RI-75/7; Bartlesville Energy Technology Center: Bartlesville, OK, 1975.

RECEIVED for review November 20, 1980. Accepted May 11, 1981.

Chromatographic–Spectrometric Identification of Airborne Polynuclear Aromatic Hydrocarbons

Dilip R. Choudhury*[1] and Brian Bush

Division of Laboratories and Research, New York State Department of Health, Albany, New York 12201

An integrated approach comprising a combination of glass capillary gas chromatography (GC), mass spectrometry (MS), liquid chromatography (LC), and ultraviolet (UV) spectrometry has been used for unambiguous identification of polynuclear aromatic hydrocarbons (PAH) in airborne particulates. Liquid chromatography with on-line ultraviolet spectral scanning was particularly valuable for differentiation and positive identification of isomeric and coeluting PAHs. The advantages of this approach over GC/MS alone are illustrated. Parent PAHs containing three to seven rings were found in most samples examined, some alkyl- and alkoxy-PAHs were also detected. A simple, one-step procedure for isolation of PAHs by preparative thin-layer chromatography is also reported.

Polynuclear aromatic hydrocarbons (PAH) are nearly ubiquitous in the environment because they originate from various combustion effluents, tobacco smoke, petroleum distillates, emissions from energy generation processes, and automobile exhausts. Many PAHs are either known or suspected carcinogens and mutagens (*1*). The carcinogenicity of a PAH is dependent on its structure, which determines the reactivity of the ultimate carcinogenic metabolites. While benzo[*a*]pyrene (B[*a*]P) is a potent carcinogen, the isomeric benzo[*e*]pyrene (B[*e*]P) is only a weak carcinogen. Consequently it is important to identify unambiguously the individual PAHs in each environmental sample.

The analytical techniques (*2–8*) currently employed to identify airborne PAHs are gas chromatography, gas chromatography–mass spectrometry (GC-MS), and, to a lesser extent, liquid chromatography (LC), GC-MS being the most common. The analysis step is usually preceded by extraction from the sample matrix and separation of the crude sample into subgroups based on polarity and functionality.

Many procedures of varying complexity have been described for isolation of PAHs from interfering substances in crude environmental samples (*5, 6, 9*). Some are too complex, resulting in loss of material, others are limited in scope. Gas chromatography using conventional packed columns cannot separate many important isomeric pairs, such as B[*a*]P and B[*e*]P. Recently certain nematic liquid crystals have been used successfully to separate many three to five ring compounds (*10, 11*). However, these stationary phases are not satisfactory for analysis of samples containing PAHs of a wide range of molecular weights. Capillary GC seems to offer the best choice in this regard.

Analysis of trace PAHs in environmental samples is an enormously difficult task and even when a large sample is available, a complete analytical resolution of PAHs exceeds the capability of any single analytical technique (*12*). Because a large number of PAHs, including many isomeric ones, are frequently present in air particulate extracts, definitive identification of individual PAHs in such samples may necessitate combined use of several powerful separation and detection techniques.

As part of a study initiated in 1977 on the characterization of mutagenic organic compounds in airborne particulates, we have attempted a comprehensive characterization of airborne PAHs by a combination of existing techniques such as capillary GC, GC-MS, LC, and a relatively new technique, on-line millisecond-scan LC-ultraviolet (UV) spectrometry. In this paper we report qualitative identifications of PAHs, frequency of their occurrence at several sites in New York State, and a simple procedure for isolating the PAHs from interfering substances in the crude particulate extract. We emphasize the importance of LC/UV spectrometry as a means of achieving isomer-specific identification of PAHs.

EXPERIMENTAL SECTION

Materials. Glass-distilled, UV-grade solvents for LC were purchased from Burdick and Jackson Laboratories, Inc. (Muskegon, MI), Nanograde quality solvents for other purposes from Mallinckrodt, Inc. (St. Louis, MO), and glass-fiber filters from Mine Safety Appliance Co. (Pittsburgh, PA). Silica gel thin-layer chromatography (TLC) plates (G1500) were purchased from Schleicher and Schuell, Inc. (Keene, NH), and were used without further activation.

PAH reference compounds were obtained from Aldrich Chemical (Milwaukee, WI), Eastman Organic (Rochester, NY), and K&K Laboratories (Plainview, NY). Commercial standards were checked for purity and, if necessary, were purified further by column chromatography on silica gel and recrystallization from an appropriate solvent. Standard solutions were prepared by dissolving the weighed amounts in a small volume of chloroform or tetrahydrofuran and diluting to the required volume with methanol. The solutions were protected from light and stored in the cold (4 °C).

Apparatus. A Hewlett-Packard 5840A gas chromatograph equipped with a capillary inlet system and flame ionization detector was used. The glass capillary column (40 m × 0.35 mm) was drawn from Pyrex glass tubing on a Shimadzu GDM-1 capillary-drawing machine (Shimadzu Scientific Instruments, Inc., Columbia, MD). After three washes with methanol, concentrated hydrochloric acid, and methanol, the column was silanized with a 5% solution of 1,1,3,3,3-hexamethyldisilazane in toluene, washed again with toluene and methanol, and allowed to dry. It was coated dynamically by passing 2 mL of 0.5% SE30 solution in chloroform through it under a constant pressure of nitrogen (3–4 psi). The column showed virtually no adsorptivity for PAHs.

A Finnigan Model 4000 GC-MS system equipped with an INCOS 2300 data system was used for mass spectrometry. The instrument was operated at 70 eV and scanned from 50 to 400 amu every 2 s.

LC was performed on a Waters Associates (Milford, MA) liquid chromatograph comprising two Model 6000A solvent delivery systems, a Model 660 solvent programmer, and a Model 440 dual absorbance detector. A Hewlett-Packard 3385A data system was used for recording the chromatogram and for integration of peaks.

Sample Collection and Preparation. At representative sites throughout New York state, air particulate samples were collected on glass fiber filters using standard high-volume samplers (General Metal Works, Cleveland OH), operated at an average flow rate of 1.70 m^3/min for 24 h. The filters containing the particulates were Soxhlet-extracted with benzene (100 mL) for 6 h, concentrated to ca. 10 mL, and refiltered through a medium-porosity

[1] Present address: Vick Divisions Research and Development, Richardson Vicks Inc., 1 Bradford Road, Mount Vernon, NY 10553.

0003-2700/81/0353-1351$01.25/0 © 1981 American Chemical Society

fritted filter. The solvent was completely evaporated at 60 °C in a gravity convection oven, and the residue was cooled in a desiccator under vacuum and carefully weighed. Several filter extracts from the same site were combined to give a sample of workable size. Two composite samples were fractionated into acidic, basic, and neutral fractions by liquid–liquid partitioning. The sample was first partitioned between chloroform and aqueous H_2SO_4 (10%) and aqueous KOH (10%) to extract the bases and acids, respectively, in the aqueous phases. The basic and acidic compounds were subsequently back-extracted into chloroform after a pH adjustment of the aqueous phases. The organic layer, which was left after extraction of acids and bases, was washed with water and dried over anhydrous sodium sulfate, and the solvent was evaporated to obtain the neutral fraction.

TLC Isolation of PAHs. A dichloromethane solution of the neutral fraction (15–17 mg), which contains the PAHs, was applied as a thin continuous streak 1 cm from the bottom of the TLC plate. After air-drying of the solvent, the plate was placed in a developing tank containing 160 mL of cyclohexane–benzene (1:1) mixture. The plate was developed to 1 cm from the top, air-dried, and observed immediately under UV light. The region containing the PAHs as determined by R_f values of naphthalene and coronene was marked, and adsorbent from this region was carefully scraped out and placed in a small glass column (9.5 × 0.6 cm). The adsorbed compounds were eluted with ether, which was subsequently evaporated to obtain the PAH fraction. A similar procedure was followed when the whole benzene extract was used instead of the neutral fraction. Recovery of several representative PAHs by the TLC procedure was greater than 85%.

GC and GC-MS. For GC analysis the PAH sample was dissolved in a small volume of $CHCl_3$ (0.1–0.5 mL) and 1–2 μL aliquots were injected with stream splitting (30% split). The injector temperature was held at 230° C, and the oven temperature was programmed from 190 °C (2 min) to 290 °C at 5 °C/min. This temperature program produced optimum resolution and the minimum analysis time; the fluorene peak was clearly observable outside and solvent front. Nitrogen was used as both carrier and makeup gas.

For mass spectral analysis, an SF-96 glass capillary column (30 m × 0.3 mm i.d.) was connected to the mass spectrometer via a jet separator; helium was used as the carrier gas.

LC and LC-UV Spectrometry. LC in reversed-phase mode was performed with a Zorbax ODS (C_{18}) column (4.6 mm × 25 cm, DuPont Instruments, Wilmington, DE). The mobile phases were filtered and degassed before use. A solvent gradient was essential for best separation. With a flow rate of 1.6 mL/min and two solvent systems, (A) methanol–water (20–80) and B) methanol, optimum resolution and minimum analysis time were achieved by starting elution with 80% B (84% MeOH–H_2O) and continuing for 20 min. A gradient to 100% MeOH over 20 min was then initiated. For certain samples the gradient was spread over 25 min for better separation of poorly resolved compounds.

The UV spectra of the LC eluates were obtained by interfacing a millisecond-scan UV spectrophotometer to the LC instrument. The spectrometer (Figure 1) comprised a hydrogen continuum hollow cathode lamp, 10-μL flow-through LC cell (path length = 1 cm), and a detection system using a UV-enhanced silicon target vidicon (STV) tube mounted in the exit slit of a 0.25-m grating monochromator (295 grooves/mm) (Jerrel-Ash, Waltham, MA) and coupled to a Model 1205 optical multichannel analyzer (OMA) (Princeton Applied Research, Princeton, NJ). The grating used can provide a theoretical spectral range of 168 nm. The flow cell was connected in series with the flow cell of the Waters detector thus allowing the spectra to be assigned to different LC peaks. The 500 channel detector target was scanned every 32 ms; 125 scans were accumulated to obtain a well-defined spectrum. To obtain the UV spectrum of an LC eluate, the solvent spectrum (Io) is recorded and stored electronically in the first memory unit (A). When the solute elutes, its spectrum (I) is recorded and stored in the second memory unit (B). A push-button operation enabled us to determine the difference (A – B), and the eluate spectrum (Io – I) was observed on the oscilloscope. A cursor control allows accurate determination of wavelength of any peak. The analog output displayed on the oscilloscope was recorded on a chart recorder; the read out rate was 50 s for the 500-channel spectrum. The latter can be as fast as 16.4 s. For compounds eluting isocratically the solvent background (Io) taken at the beginning of the chromotgraphic run is used. For compounds eluting during the gradient part to the run Io was recorded at convenient points (where no constituent apparently eluted) before the component of interest starts eluting. Sometimes this resulted in minor distortion of spectral base line of components eluting under gradient conditions.

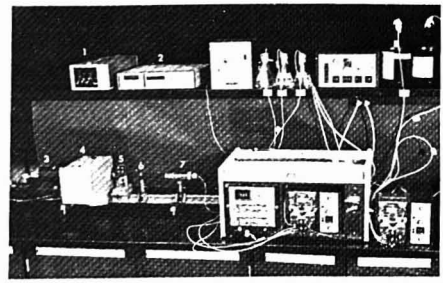


Figure 1. Millisecond-scan ultraviolet spectrometer interfaced to liquid chromatograph: (1) oscilloscope, (2) multichannel analyzer, (3) vidicon tube, (4) monochromator, (5) flow cell, (6) quartz lens, (7) hydrogen hollow cathode lamp, (8) LC eluate.

RESULTS AND DISCUSSION

To identify PAHs conclusively, first it is essential to separate them from the numerous interfering compounds that are always present in a complex mixture like airborne particulate extract. Although a cleanup method containing many steps can generate cleaner samples for final analysis, extra steps result in unavoidable loss of material and long sample-processing time. Our initial fractionation by liquid–liquid partitioning was a simple procedure by which neutral, acidic, and basic fractions were separated from the crude extract. In a typical sample, neutral compounds made up 94% (by weight) of the total benzene extractable; acidic and basic compounds constituted 4 and 2%, respectively.

In early stages of the present work we found that the PAHs could be isolated by preparative TLC of the neutral fraction. Subsequently we observed that acid–base fractionation was not essential for isolation of PAH fraction; the whole extract could be applied directly for TLC fractionation. The PAH fractions isolated by both methods gave identical GC profiles. The one-step cleanup procedure was therefore used for all but two samples reported in this study. We emphasize this method which is simple and particularly convenient for analyzing small samples of air particulates—an important advantage in view of the difficulty of collecting large samples. No interfering compound was detected in any PAH fraction by GC-MS.

Dong et al. (8) has used TLC with a different ratio of solvents as used by us to separate PAH fraction from airborne particulate extract. Katz (*13*) used a two-stage TLC method in which the PAHs are first partially separated on aluminum oxide and then on acetylated cellulose and finally isolated and identified by fluorescence monitoring. More recently Daisy and Leyko (*14*) used TLC on acetylated cellulose to isolate three PAH subfractions for subsequent GC analysis. Our procedure has the potential to separate the PAH fraction from aliphatics and other polar compounds, including the strongly basic nitrogen heterocycles, amines, and acidic and phenolic compounds. In addition to the aliphatics and PAHs, we have isolated two fractions exhibiting mutagenic properties (*15*) and their characterization is presently in progress.

The SE-30 capillary column was evaluated with difficult-to-separate PAH groups, such as, B[*a*]P and B[*e*]P. GC profiles of the PAH fractions of two air particulate extracts

Table I. GC Peak Identities in Figure 3

no.	compound	no.	compound
1	fluorene	25	benz[*a*]anthracene
2	methoxyfluorene	26	phenylfluorene
3	methoxyfluorene	27	naphthanthrene, methylbenzo[*ghi*]fluoranthene
4	phenanthrene	28	methylchrysene/benz[*a*]anthracene/triphenylene
5–7	dimethoxyanthracene/phenanthrene	29	phenylphenanthrene/anthracene, binaphthyl
8	cyclopenta[*def*]phenanthrene	30	benzo[*b*]fluoranthene
9, 10	dimethoxyanthracene/phenanthrene	31	benzo[*j*]fluoranthene
11	2-phenylnaphthalene	32	benzo[*k*]fluoranthene
12	fluoranthene	33	methylphenylphenanthrene/anthracene
13	pyrene	34	benzo[*e*]pyrene
14, 15	methylphenylnaphthalene	35	benzo[*a*]pyrene
16	methylpyrene/fluoranthene	36	methylbenzofluoranthene/benzopyrene
17	benzo[*a*]fluorene	37	quaterphenyl
18	benzo[*b*]fluorene	38, 39	methylbenzofluoranthene/benzopyrene
19	methylpyrene/fluoranthene	40	indeno[1,2,3-*cd*]pyrene
20	dimethylphenylfluorene, trimethylchrysene/benz[*a*]anthracene	41	dibenz[*a,h*]anthracene
21	terphenyl, dimethylpyrene/fluoranthene	42	benzo[*ghi*]perylene
22	benzo[*ghi*]fluoranthene	43	1,2,3,4-dibenzopyrene
23	triphenylene	44	coronene
24	chrysene		

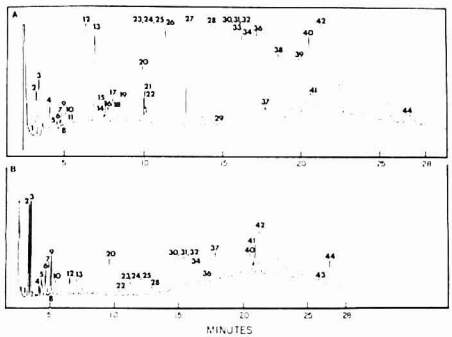


Figure 2. Gas chromatogram of PAH fractions of air particulate extracts from (A) Niagara area and (B) Mount Vernon.

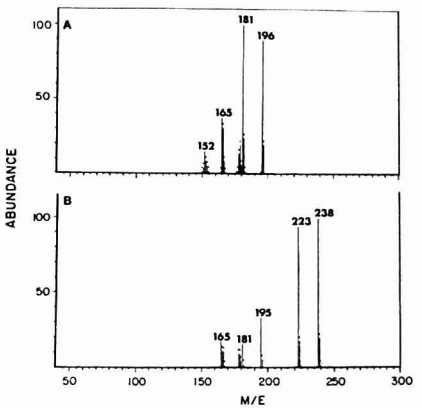


Figure 3. Mass spectra of (A) peak 3, methoxyfluorene, and (B) peak 6, dimethoxyanthracene/phenanthrene (from Figure 2A).

are shown in Figure 2. Retention times of chromatographic peaks were compared with those of representative parent PAHs and compounds containing from three to seven rings were identified (Table I). Coronene (seven rings) eluted in less than 30 min (Figure 3), in contrast to the more than 80 min elution time reported elsewhere (*16*). Phenanthrene and anthracene were easily separated by the capillary column used. Chrysene, benz[*a*]anthracene (B[*a*]A), and triphenylene (peaks 23–25) could not be resolved completely on the present column although the first two had a retention time difference of 0.1 min. Three isomeric benzofluoranthenes (peaks 30–32) were not completely resolved by the capillary column used in this work; several variations of chromatographic conditions did not improve the separation of these isomers (*17*). Other investigators have reported difficulties in separating these two groups of compounds (*16*). B[*a*]P and B[*e*]P were base-line resolved by this column. The occurrence of two separate peaks was dependent on the relative concentrations of the two compounds present in a sample. In most samples because B[*e*]P was present in much higher concentration than B[*a*]P, one peak with a distinct shoulder was observed. The major constituents observed in the chromatogram in Figure 3 were present in all of the air particulate PAH fractions we examined.

The GC-separated components were further characterized by GC-MS with a glass capillary column. Because of the instrumental limitations, chromatographic conditions for the GC-MS work were optimized separately for best resolution. PAHs exhibit strong molecular ions on electron impact, which permits reliable measurement of molecular weight and hence identification of a particular PAHs ring system. m/e values of parent ions of all peaks observed in the reconstructed ion chromatogram were determined. Mass chromatograms of the parent ions and their significant fragment ions (very few for PAHs) were generated, and computer-assisted background substraction was used to obtain clean spectra. These spectra were compared with those of reference compounds when available, otherwise they were compared with the computer-stored library spectra.

By GC-MS most components were confirmed to be parent PAHs; however, some alkyl-PAHs were detected in most samples. Several methoxy-PAHs were detected in all samples examined: although no reference standards were available, the mass spectral fragmentation pattern was characteristic of the structures assigned. For example, the parent ion in the mass spectrum of (Figure 3A) peak 3, identified as methoxyfluorene, gave strong fragment ions corresponding to the loss of a CH_3 group and CH_2O group. Mass spectrum of peak 6, identified as dimethoxyanthracene/phenanthrene, showed

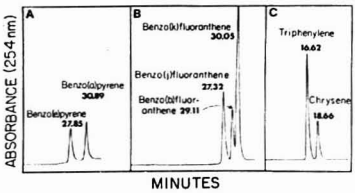


Figure 4. Liquid chromatogram of (A) benzo[*a*]pyrene and benzo-[*e*]pyrene, (B) benzo[*b*]fluoranthene, benzo[*j*]fluoranthene, and benzo[*k*]fluoranthene, and (C) triphenylene and chrysene.

Table II. LC Peak Identities in Figure 6

no.	compound	no.	compound
1	phenanthrene	9	benzo[*b*]fluoranthene
2	fluoranthene	10	benzo[*k*]fluoranthene
3	pyrene	11	benzo[*a*]pyrene
4	triphenylene	12	dibenz[*a,h*]anthracene
5	chrysene	13	benzo[*ghi*]perylene
6	benz[*a*]anthracene	14	indeno[1,2,3-*cd*]pyrene
7	benzo[*j*]fluoranthene	15	coronene
8	benzo[*e*]pyrene		

fragments characteristic of this structure (Figure 3B). All compounds characterized by GC-MS are listed in Table I.

Although GC-MS is the single most powerful technique commonly applied to identify constituents of a complex mixture, electron impact (EI) mass spectra of PAHs lack significant fragmentation. Consequently the spectra cannot differentiate between structural isomers of PAHs such as chrysene and B[*a*]A—a limitation particularly when chromatographic separation is lacking. Additional independent evidence for isomer-specific identification is important particularly since carcinogenicity of PAHs is isomer dependent.

Several authors have reported satisfactory results from application of LC to analysis of PAHs (*7, 8*). The Zorbax ODS column used in this study performed excellently with a methanol–water mobile phase gradient.

LC retention times were criteria for preliminary identification. By our method triphenylene was well separated from chrysene or B[*a*]A (Figure 4), although the latter two were only partially resolved when present together. Elevated column temperature of up to 35° C did not improve this separation. Similar difficulty has been experienced by other authors (*8, 18*). B[*a*]P and B[*e*]P were well separated by LC (Figure 4), as were benzo[*j*]fluoranthene (B[*j*]F), benzo[*b*]-fluoranthene (B[*b*]F), and benzo[*k*]fluoranthene (B[*k*]F). B[*k*]F was clearly separated from B[*e*]P or B[*a*]P, although some authors have reported failure in these separations (*18*). We did not obtain adequate separation between B[*e*]P and B[*b*]F in a multicomponent mixture; this pair always appeared as an unresolved peak. LC profiles of two PAH fractions, typical of all samples examined, are shown in Figure 5. Peak identities are listed in Table II.

Chromatographic conditions were optimized for best separation and minimum analysis time. In our work coronene eluted in 42 min, some authors have reported elution times of greater than 100 min for this compound (*8*). Variation of flow rate or mobile-phase composition did not noticeably improve resolution.

Other analytical approaches are possible. For example, Das and Thomas (*18*) have used a Zorbax ODS column with acetonitrile–water as a mobile phase. They attempted the separation of nine PAHs, using the more selective fluorescence detection system. With the appropriate excitation and emission wavelengths one component of a coeluting pair was detected in preference to the other. Thus B[*a*]A was monitored in the presence of chrysene, although the two were not chromatographically separated. However, a number of chromatographic runs would still be needed to detect a wide range of PAHs.

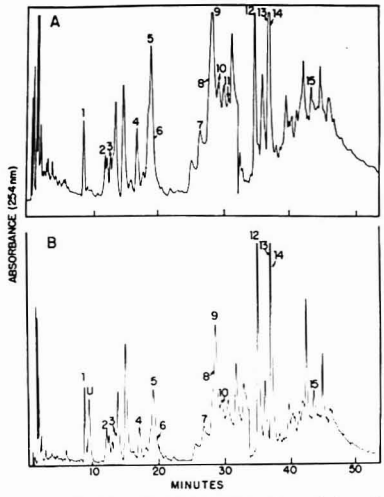


Figure 5. Liquid chromatogram of PAH fractions of air particulate extracts from (A) City College of New York and (B) Mount Vernon.

In another recent study, Ogan et al. (*19*) separated 16 synthetic PAHs using a Perkin-Elmer HC-ODS reversed-phase column with acetonitrile–water as a mobile phase and a programmable fluorescence detection system. Separation of chrysene and B[*a*]A was reported but not of B[*j*]F from B[*b*]F or B[*k*]F. The late-eluting peaks were slightly broader compared to similar peaks in our work presumably because Zorbax ODS packing has 6-μm particles as compared to the 10-μm particles present in the HC-ODS column packing. The same authors have also compared the ability of a number of commercial ODS columns to separate isomeric PAHs (*20*). Recently Wilkinson et al. reported similar results for analysis of PAHs in aqueous effluents (*21*). We are presently evaluating the separation capability of the HC-ODS column for complex PAH mixtures.

Except for a few difficult-to-separate pairs, our present method can separate a wide range of PAHs normally encountered in environmental samples using a commonly used UV detector. The column can handle relatively large size samples without losing any resolution and reproducibility—an advantage in analyzing very complex mixtures.

Retention time data as generated from use of a single wavelength detector does not, however, provide adequate confirmation for identity of PAHs particularly when the sample has a complex compositon. Since PAHs possess strong and distinctive absorbance in the UV region and since the spectra of isomers are significantly different, UV spectra of LC eluates generated in real time can be invaluable for fingerprinting of the eluates. We have utilized a millisecond scan UV spectrometer enabling determination of spectra of LC eluates in a continuous flow mode, a distinct advantage over many commercial scanning UV detectors which require stopping of column flow or collecting fractions and determining UV spectra. Some investigators have used vidicon and diode array spectrometer to determine absorbance and fluorescence spectra of LC eluates (*22–24*). A recent review describes possible applications of various optoelectronic image

detectors (25). A few rapid-scan spectrometers have recently become commercially available (26). In the present study, the spectral window of the instrument which is adjustable was calibrated for 204–348.7 nm using the atomic spectral lines of Zn and Hg. One nanogram or lower amount of most PAHs produced distinctive UV spectra.

To confirm the identity of the constituents, we compared the UV spectrum of the eluate with that of the suspected reference compound. A superimposable spectrum was the criterion for identification of a single component peak. For coeluting compounds presence of essential spectral features was considered adequate. For example, the retention time of peak 5 (Figure 5B) corresponded to that of both chrysene and B[*a*]A, but the UV spectra of this isomeric pair are distinctly different (Figure 6). Scanning of the central part of peak 5 gave a spectrum (Figure 6) superimposable on the UV spectrum of chrysene. Scanning of the trailing edge (peak 6) gave a spectrum (Figure 6) which contained the essential features of the spectra of both chrysene and B[*a*]A. Thus the presence of both compounds in this sample was unequivocally established despite lack of chromatographic separation. The spectrum of the leading edge of the peak was not readily identifiable.

As mentioned earlier, B[*e*]P, B[*b*]F, and perylene were not sufficiently resolved by the LC method used. The retention time of peak 9 suggested that this peak may represent any or all three of these compounds. A scan of the leading edge of the peak (no. 8) gave a spectrum (Figure 6) superimposable on that of B[*e*]P. Another scan of the center of the peak (no. 9) produced a spectrum (Figure 6) superimposable on that of B[*b*]F. Scans at several other parts of the peak failed to establish the presence of perylene. The unidentified peak (U) in Figure 5B had a retention time which corresponds accurately to that of anthracene, but its UV spectrum was clearly different than that of anthracene. UV spectra of all peaks having retention times corresponding to available authentic standards were determined and compared with spectra of reference standards. The three benzofluoranthenes—B[*b*]F, B[*j*]F, and B[*k*]F—not completely resolved by GC were separated by LC, and their UV maxima were sufficiently different to enable their definite identification. UV spectra of compounds eluting under gradient conditions did not show any significant base line distortion.

The high resolving power of LC coupled with the fingerprinting power of UV spectrometry enabled isomer-specific identification of PAHs. Determination of peak purity is also important for quantitation purpose. Confirmed identification by this novel technique can be achieved preferably when an authentic standard of the compound in question is available. Comparison of the spectrum of an unknown sample component with a literature spectrum may sometimes be inconclusive. However, computer interfacing of the vidicon spectrometer could allow generation of spectral library and search programs can be developed to compare LC eluate spectra with library spectra. Computer interfacing will also permit continuous spectral acquisition during a chromatographic run, displaying a chromatogram at optimal wavelength for various components, enhanced detectability by integrating spectral output for the whole range, and subtraction of more accurate solvent background by storing spectra for blank gradient run prior to running the sample.

The LC-UV method was applied to 14 air particulate samples collected from several parts of New York state and the UV spectral data in conjunction with LC retention time, GC retention time, and GC-MS data enabled unambiguous characterization of 15 PAHs (Table III) in most samples. The majority of these PAHs are proven carcinogens and mutagens. Many other PAHs were characterized with less certainty by

Table III. Polynuclear Aromatic Hydrocarbons Confirmed in Airborne Particulates by LC/UC and GC/MS

site (year)	phenanthrene	fluoranthene	pyrene	triphenylene	chrysene	benz[*a*]anthracene	benzo[*j*]fluoranthene	benzo[*e*]pyrene	benzo[*b*]fluoranthene	benzo[*k*]fluoranthene	benzo[*a*]pyrene	dibenz[*ah*]anthracene	benzo[*ghi*]perylene	indeno[1,2,3-*cd*]pyrene	coronene
City College of NY (1975)	+	+	+	+	+	+	+	+	+	+	+	+	+	+	+
Eisenhower Park (1975)	+	+	+	+	+	+	+	+	+	+	+	+	+	+	+
Garden City (1975)	+	+	+	+	+	?[a]	+	+	+	+	+	+	+	+	+
Garden City (1976)	+	+	+	+	+	+	+	+	+	+	+	+	+	+	+
Mamaroneck (1975)	+	+	+	+	+	+	+	+	+	+	+	+	+	+	+
Massena (1976)	+	+	+	+	+	?[a]	+	+	+	?[a]	?[a]	+	+	+	+
Mt. Vernon (1975)	+	+	+	+	+	+	+	+	+	+	?[a]	+	+	+	+
Mt. Vernon (1976)	+	+	+	+	+	+	+	+	+	+	?[a]	+	+	+	+
Mt. Vernon (1977 neutral)	+	+	+	+	+	+	+	+	+	+	+	+	+	+	+
New Rochelle (1975)	+	+	+	+	+	+	+	+	+	+	+	+	+	+	+
Niagara (1975)	+	+	+	+	+	+	+	+	+	+	+	+	+	+	+
Niagara (1975 neutral)	+	+	+	+	+	+	+	+	+	+	?[a]	+	+	+	+
Roosevelt Island (1975)	+	+	+	+	+	+	+	+	+	+	+	+	+	+	+
Whiteface Mountain (1976)	+	+	+	+	+	+	+	+	+	+	+	+	+	+	+

[a] UV spectra were not completely satisfactory.

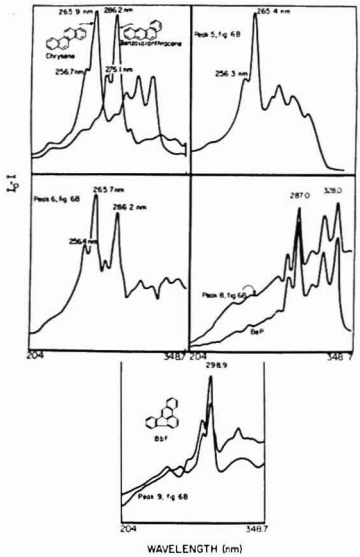


Figure 6. Ultraviolet spectra LC eluates (from chromatogram in Figure 5B) and some PAH standards.

GC-MS. It is noteworthy that the 15 compounds listed in Table III were present in ambient air even at the top of Whiteface Mountain (elevation ca. 5000 ft), although their concentrations were presumably lower than in samples from industrial areas.

ACKNOWLEDGMENT

We thank R. Parillo and E. LeGere for technical assistance and P. Dymerski for assistance in mass spectral work.

LITERATURE CITED

(1) Freudenthal, R., Jones, P. W., Eds. "Polynuclear Aromatic Hydrocarbons: Chemistry, Metabolism and Carcinogenesis"; Raven Press: New York, 1976.
(2) Lao, R. C.; Thomas, R. S.; Oja, H.; Dubois, L. *Anal. Chem.* **1973**, *45*, 908.
(3) Karasek, F. W.; Denney, D. W.; Chan, K. W.; Clement, R. E. *Anal. Chem.* **1978**, *50*, 82.
(4) Lao, R. C.; Thomas, R. S.; Monkman, J. L. *J. Chromatogr.* **1975**, *112*, 681.
(5) Lee, M. L.; Novotny, M.; Bartle, K. D. *Anal. Chem.* **1976**, *48*, 1566.
(6) Cautreels, W.; Van Cauwenberghe, K. *Atmos. Environ.* **1976**, *10*, 447.
(7) Fox, M. A.; Stanley, S. W. *Anal. Chem.* **1976**, *48*, 992.
(8) Dong, M.; Locke, D. C.; Ferrand, E. *Anal. Chem.* **1976**, *48*, 368.
(9) Novotny, M.; Lee, M. L.; Bartle, K. D. *J. Chromatogr. Sci.* **1974**, *12*, 607.
(10) Janini, G. M.; Muschik, G. M.; Zielinski, W. L., Jr. *Anal. Chem.* **1976**, *48*, 1879.
(11) Janini, G. M.; Muschik, G. M.; Zielinski, W. L., Jr. *Anal. Chem.* **1976**, *48*, 809.
(12) Blumer, M.; Giger, W. *Anal. Chem.* **1974**, *46*, 1633.
(13) Katz, M.; Sakuma, T.; Ho, A. *Environ. Sci, Technol.* **1978**, *12*, 909.
(14) Daisy, J. M.; Leyko, M. A. *Anal. Chem.* **1979**, *51*, 24.
(15) Choudhury, D. R.; Bush, B.; Miller, T.; Wolin, M. J., unpublished work.
(16) Giger, W.; Schaffner, C. *Anal. Chem.* **1978**, *50*, 243.
(17) We have recently developed capillary columns that can base-line-resolve chrysene, B[*a*]A and B[*b*]F, B[*b*]F, B[*k*]F. However, in the presence of triphenylene and B[*j*]F, respectively, only partial separation of the components in the two groups can be achieved.
(18) Das, B. S.; Thomas, G. H. *Anal. Chem.* **1978**, *50*, 967.
(19) Ogan, K.; Katz, E.; Slavin, W. *Anal. Chem.* **1979**, *51*, 1315.
(20) Ogan, K.; Katz, E. *J. Chromatogr.* **1980**, *188*, 115.
(21) Wilkinson, J. E.; Strup, P. E.; Jones, P. W. In "Polynuclear Aromatic Hydrocarbons"; Jones, P. W., Leber, P., Eds.; Ann Arbor Science Publishers: Ann Arbor, MI, 1979; p 217.
(22) McDowell, W. E.; Pardue, H. L. *Anal. Chem.* **1977**, *49*, 1171.
(23) Jadamec, J. R.; Saner, W. A. *Anal. Chem.* **1977**, *49*, 1977.
(24) Milano, M. J.; Lam, S.; Savonis, M.; Pautler, D. B.; Pav, J. W.; Grushka, E. *J. Chromatogr.* **1978**, *149*, 599.
(25) Talmi, Y. *ACS Symp. Ser.* **1979**, *No. 102*, 1.
(26) James, G. E. Paper presented at the Pittsburgh Conference on Analytical Chemistry and Applied Spectroscopy, paper no. 164, March 1981.

RECEIVED for review October 8, 1980. Resubmitted February 18, 1981. Accepted May 6, 1981. This work was partially supported by New York State Health Research Council Grant HR414. Part of this work was presented at the 176th National Meeting of the American Chemical Society, Miami Beach, FL, Sept 1978.

Thin-Layer Chromatography with in Situ Multichannel Image Detection of Fluorescent Compounds

M. L. Gianelli, J. B. Callis,* N. H. Andersen, and G. D. Christian

Department of Chemistry BG-10, University of Washington, Seattle, Washington 98195

A multichannel detector for in situ analysis of fluorescent materials on thin-layer plates is evaluated. Optical system 1 is designed to obtain a fluorescence spectrum from each position along the elution axis of a one-dimensional plate without need for mechanical scanning. By use of tetraphenylporphine (H_2TPP) and octaethylporphine (H_2OEP) as test materials, it is shown how overlapping spots can be resolved into their components. Optical system 2 is designed to obtain a quantitative two-dimensional fluorescence image of a single, two-dimensional chromatogram or of multiple, one-dimensional chromatograms. A dynamic range of fluorescence intensity of over 500:1 can be measured on a single plate, and the detection limits extend as low as 3 pg for H_2TPP. Imaging detectors allow rapid, in situ qualitative and quantitative information on fluorescent materials to be obained and might allow the analyst to take full advantage of the parallel processing capabilities of thin-layer plates for routine assays.

Recent advances in separation power coupled with methodology for elimination of active sites have so greatly improved the capacilities of thin-layer chromatography that the term "high-performance thin-layer chromatography" (HPTLC) does not appear at all unwarranted (*1*). At the same time, advances in technology have made quantitative analysis of the plates possible in situ by scanning densitometry (*2*). Fluorescence densitometry in particular has proven to be of significant value in many applications due to its sensitivity and selectivity (*3–5*).

In clinical and environmental analysis, the use of HPTLC is especially appealing compared to gas–liquid chromatography (GLC) or high-performance liquid chromatography (HPLC) because it is quite feasible to develop many plates/samples simultaneously. Unfortunately, there still remains the difficulty of quantitatively analyzing the plates. The present generation of mechanical scanners simply do not provide the high throughput desired; moreover, any attempt to speed up mechanical scanning is likely to suffer a signal-to-noise degradation inversely proportional to the decreased time spent in the scanning process.

One possible solution to this problem is to use an imaging detector to quantitatively measure light reflected or emitted from the plate. The capabilities of imaging detectors are by now well appreciated in the scientific community and their usefulness in chemistry has been amply demonstrated (*6*). We have been especially impressed with these devices as fluorescence detectors (*7–11*).

In this paper, we report on the use of a digital imaging photometer based upon a SIT vidicon as a two-dimensional fluorescence detector. We have used this device in two ways: (a) in conjunction with a monochromator to analyze both the wavelength of emission and retention time of each spot on a one-dimensional chromatogram and (b) in conjunction with a simple optical filter to analyze either two-dimensional chromatograms or multiple one-dimensional chromatograms simultaneously. In both approaches no mechanical scanning is required. The results contained herein demonstrate the feasibility of this approach.

EXPERIMENTAL SECTION

Apparatus. Two different optical configurations were used and are presented schematically in Figure 1. Both systems used a 150-W Xenon arc lamp as excitation source. Light from the arc was collected by a quartz $f/1.0$ lens focused to infinity to produce nearly uniform illumination of the entire plate. A band of excitation wavelengths was selected by means of various Corning glass filters; infrared light was eliminated by means of a Schott KG-3 glass filter. In the first configuration (Figure 1) a Jarrell-Ash 82-415 quarter-meter Ebert monochromator equipped with a 295 1/mm grating blazed at 400 nm was used to analyze the emitted light. The exit slit and holder were removed from the housing and the entire exit plane image was focused onto the SIT vidicon by means of an $f/2.5$ lens with 2:1 demagnification. In the second configuration, Figure 1 minus the monochromator and fixed lens, various Corning and Schott glass filters were used to isolate the fluorescence emission from the thin-layer plates and the resultant fluorescence image was focused directly onto the photo surface of the vidicon with an $f/2.5$ lens with approximately 2:1 demagnification.

The digital SIT vidicon and computer system has been previously described (*7*).

Reagents. For spotting on the thin-layer plates, chromatographically pure free base octaethyl-, etio- and tetraphenylporphines were dissolved in spectroquality dichloromethane from Matheson, Colem and Bell.

Thin-Layer Chromatography. Porphyrin mixtures were chromatographed on Whatman KC_{18} reversed-phase microslides. The two-porphyrin mixture was developed in methanol–acetone (80:20); the three-porphyrin mixture was developed in the same manner, dried, and then redeveloped in 100% acetonitrile. All development solvents were spectroquality reagents from Matheson, Coleman and Bell.

Data Acquisition and Analysis. Fluorescence images were collected with the digital photometer operated at a resolution of 64×64 elements. A total of 512 successive images were summed together for improvement of the signal-to-noise ratio. An automatic shutter was then closed and 512 successive "dark" images were subtracted from memory to eliminate dark noise arising from systematic variation of leakage current from element to element. Data were then analyzed with a PDP 11/04 computer using a series of programs described in the Ph.D. thesis of Johnson (*12*). Data were displayed on a video monitor or Tektronix 4006 terminal.

For rank analysis and hard copy graphics display, the data were transmitted via phone line to the University Computer Center where it was analyzed with programs developed by Warner et al. (*13*).

THEORY

Optical System 1. The optical system of Figure 1 was designed to produce an emission spectrum from every point along the retention axis of a one-dimensional chromatogram *without any mechanical scanning*. The manner in which this was accomplished is given in Figure 2. Suppose that we have a two-component mixture of fluorophores a and b whose fluorescence spectra (Figure 2A) and relative retention profiles (Figure 2B) are highly overlapping. A mixture of these components when chromatographed will produce a thin-layer plate

0003-2700/81/0353-1357$01.25/0 © 1981 American Chemical Society

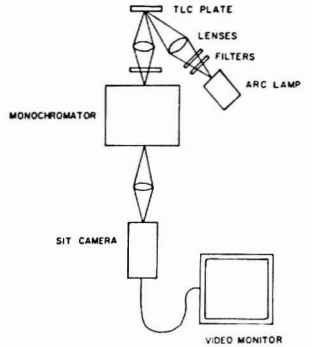


Figure 1. Optical system 1 for producing emission spectra from materials on thin-layer plates. A two-dimensional fluorescence image of a thin-layer plate is obtained by removal of the monochromator and focal lens and replacing with a filter (optical system 2).

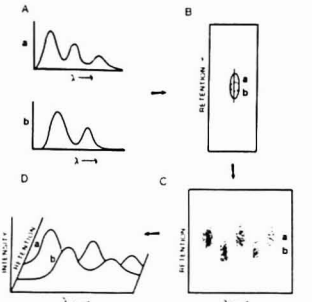


Figure 2. Concept for producing emission spectra from materials on thin-layer plates without mechanical scanning: (2A) emission spectra of components a and b; (2B) image of thin-layer plate spotted with a and b; (2C) image of video monitor of 2B; (2D) isometric projection of 2C.

which, when viewed under a uniform excitation light, would have the appearance of Figure 2B, a single unresolved spot. Suppose that a lens of appropriate focal ratio is used to project a fluorescent image of the thin-layer plate onto the entrance slit of an analyzing monochromator such that the long axis of the slit is aligned parallel with the thin-layer development axis and such that the center of the spots is centered on the slit. Suppose further that the exit slit assembly has been removed from the monochromator to allow the two-dimensional detector to view the resultant image. From our previous work (7) it is known that the monochromator faithfully preserves the information concerning the distribution of fluorescence along the long axis of the slit. Thus, the y axis of the exit plane image represents the retention axis of the thin-layer plate, while the x axis represents the wavelength of the fluorescence. The expected image for the compounds of Figure 2A is shown in Figure 2C as it might appear on a television monitor display. Once the image is captured quantitatively, various data analysis and display modes may be invoked; for example, Figure 2D shows how the data might appear when formated as an isometric projection with the vertical axis representing fluorescence intensity and all hidden lines removed for clarity.

The data from the above experiment are most conveniently represented as a matrix M of intensity values which are a function of position along the retention axis indexed by i and a function of wavelength of emission indexed by j. In the case where the number of photons absorbed is small and concentrations of interacting species are low, interaction between components is negligible, and energy transfer rates are low, one may write

$$\mathbf{M} = [m_{ij}] = \sum_{k=1}^{r} \alpha^k t_i^k y_j^k = \sum_{k=1}^{r} \alpha^k \mathbf{t}^k \otimes \mathbf{y}^k \qquad (1)$$

In this expression we have assumed that r fluorescent species have been chromatographed (indexed by k) and that each has a unique fluorescence spectrum characterized by a vector $\mathbf{y}^k \equiv [y_j]$ and a retention time characterized by a vector $\mathbf{t}^k \equiv [t_i]$ which expresses the relative concentration of the particular fluorophore along the retention axis. The scalar, α^k, contains the concentration dependence of the fluorescence intensity and is proportional to the fluorescence quantum efficiency as well. The symbol $\otimes$ denotes the outer product operation.

The bilinear form of eq 1 suggests that certain powerful theorems of linear algebra may be used to analyze the data. Indeed there is an obvious similarity between eq 1 of this paper and eq 4 of Warner et al. (*13*) wherein data from a video fluorometer in the form of an emission excitation matrix is discussed. In analogy with that work, we can assert that: (a) the rank of $\mathbf{M}$ is a lower bound to the number of independently emitting species on the plate, and (b) the eigenvectors of the real square symmetric matrices $\mathbf{M}^T\mathbf{M}$ and $\mathbf{M}\mathbf{M}^T$ are linearly related to the fluorescence and retention vectors. Thus one can obtain a rather exhaustive qualitative analysis of the materials if they are unknowns. In the case of known components, the techniques of least squares (*13*, *14*) and rank annihilation may be used for quantitative analysis (*15*, *16*).

In practice, the use of a multichannel imaging device produces distortions of the data in a characteristic manner which requires correction. This point has been carefully considered by our astronomer colleagues (*17*). It is easily shown that eq 1 must be modified as follows:

$$\mathbf{M}^{\text{obsd}} = \sum_{k=1}^{r} \alpha^k t_i^k y_j^k \sigma_{ij} + p_{ij}\sigma_{ij} + d_{ij} \qquad (2)$$

where σ_{ij} is the relative sensitivity of each pixel, p_{ij}, the background fluorescence of the plate as imaged onto the detector, and d_{ij}, the dark signal from each pixel. Corection for the dark signal is easily obtained by closing a shutter in front of the camera and collecting a "dark frame" $\mathbf{D} \equiv [d_{ij}]$ averaged over the same time as the light frames. A "blank frame" $\mathbf{B}$ is also obtained from the plate prior to spotting and developing, and stored in the computer for later substraction. Obviously

$$\mathbf{B} = [p_{ij}\sigma_{ij} + d_{ij}] \qquad (3)$$

Correction for the variation in pixel to pixel relative sensitivity can be obtained by means of a "flat field" correction F obtained by shining a white light source onto the plate and collecting the radiation from it. In this case

$$\mathbf{F} = [\beta u_i v_j \sigma_{ij} + d_{ij}] \qquad (4)$$

where u_i is the relative intensity collected along the long axis of the slit. v_j is the relative spectral output of the lamp and a constant of proportionality. With the above data in hand, one obtains a corrected matrix $\mathbf{M}^{\text{corr}}$ as follows

$$\mathbf{M}^{\text{corr}} = (\mathbf{M}^{\text{obsd}} - \mathbf{B})/(\mathbf{F} - \mathbf{D}) = \sum_{k=1}^{r} \alpha^k o_i q_j \qquad (5)$$

where $\gamma^k = \alpha^k/\beta$, $o_i = t_i/u_i$ and $p_j = x_k/v_j$. Obviously eq 5 and 1 are identical for the purposes of rank analysis, and our previous work may be taken over unmodified.

Optical System 2. The optical system of Figure 1 was modified to obtain a two-dimensional fluorescent image of the

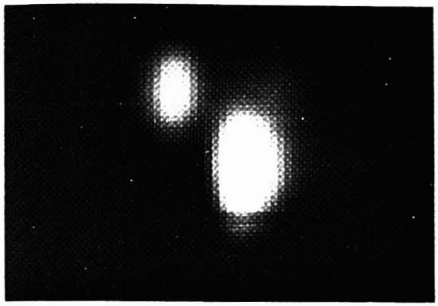


Figure 3. Image of a thin-layer chromatagram of a mixture of H_2OEP and H_2TPP produced by optical system 1, raw data as displayed on a video monitor.

plate by removal of the monochromator and isolating the fluorescence by introducing colored glass filters in front of the detector. In this case, the ability to obtain wavelength information is forfeited in favor of simultaneously analyzing several one-dimensional chromatograms or one two-dimensional chromatogram. Our previous comments regarding flat field, dark field, and blank field corrections apply to optical system 2, and a strategy similar to that of the previous section must be used to obtain a quantitative analysis.

Unfortunately, due to irreproducibility in positioning the plate for background dark and flat field frames, there remained a small background signal which without further correction frustrated analysis at the subnanogram level. We found it sufficient to use a simple interactive level thresholding algorithm in which the operator determined the spot size and the computer obtained the background signal per pixel from an average of all of the pixels immediately adjacent to the spot. For quantitative purposes, we assumed that concentration was proportional to the total fluorescence from the spot minus the total background signal estimated for the spot.

RESULTS AND DISCUSSION

Optical System 1. We evaluated optical system 1 for its ability to provide a qualitative analysis of a thin-layer plate using rank analysis reduction of the data. Accordingly, a mixture of free base tetraphenylporphine (H_2TPP) and free base octaethylporphine (H_2OEP) was chromatographed so that it exhibited only a single unresolved spot similar to Figure 2B. Figure 3 shows a video monitor display of the output image from the monochromator. Only the upper half of the retention axis was imaged onto the entrance slit of the analyzing monochromator. The single spot has now been resolved into two distinct species with the added dimension of wavelength of emission. The substance with the largest R_f value is H_2OEP which is confirmed by the emission peaks at 624 and 686 nm. The substance with the lesser R_f value is H_2TPP which is confirmed by the emission peaks at 652 nm and the shoulder at 718 nm. Figure 4 shows contour map representations of the raw data, the blank, the flat field, the data minus the blank, and the fully corrected data according to eq 5. Figure 5 shows linear plots of the total emission spectra and total elution data, together with selected rows and columns providing spectra and retention profiles, respectively, of each compound.

Examination of Figures 3–5 shows that the optical system of Figure 1 does indeed provide us with data in the manner shown in Figure 2. One can quite clearly observe that two components are present. Reference to Figure 4B shows that the blank fluorescence was not at all negligible for porphyrins at the concentrations used while reference to Figure 4C shows that the plate is not irradiated uniformly nor is the pixel–pixel sensitivity uniform.

Table I gives the results of a rank analysis of the data of Figure 4A,E. It can be seen that the first two eigenvalues of

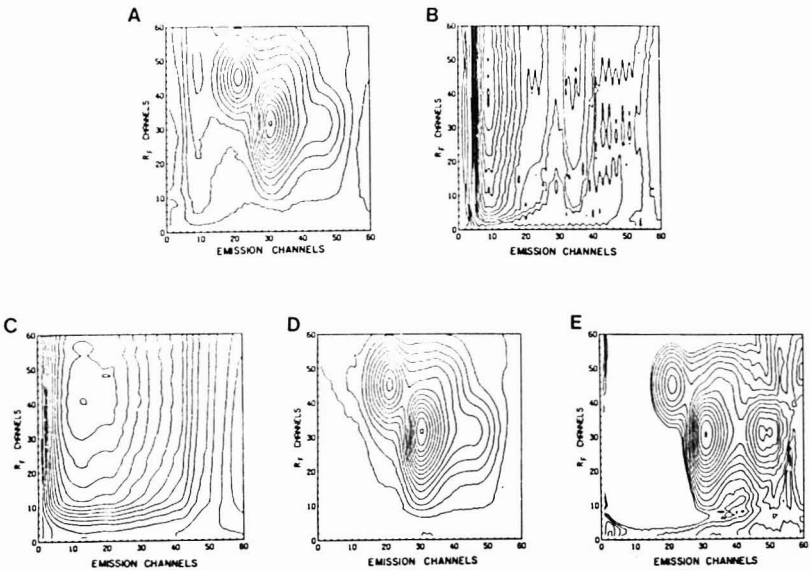


Figure 4. log contour maps of data acquired by optical system 1: (A) data of Figure 3; (B) blank for plate; (C) flat field; (D) raw data with blank subtracted; (E) data corrected for blank and flat field. The ratio of the most intense pixel of A to the intense pixel of B is 7.26.

Table I. Eigenvalues[a]

	first	second	third	2/3
two components 60 × 60	1.99×10^{11}	2.99×10^{10}	1.65×10^{8}	181
two components 40 × 40	4.38×10^{12}	6.13×10^{11}	1.04×10^{9}	589
two components 40 × 40 flat field corrected	1.13×10^{11}	7.50×10^{9}	3.17×10^{7}	237

[a] Noise at the edges was deleted by cropping to a 40 × 40 matrix.

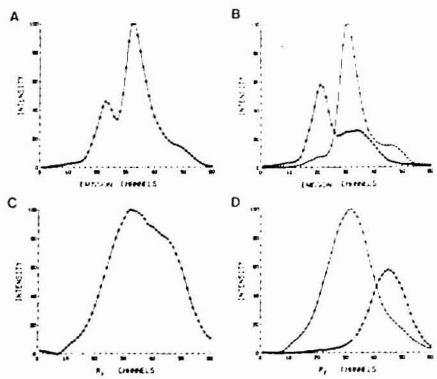


Figure 5. Linear plots of both emission and retention data of Figure 4D: (A) scan of total emission spectra, sum of all the rows; (B) scan of emission of H_2TPP and H_2OEP by selecting two individual rows of pixels; (C) total retention data, sum of all the columns; (D) chromatographic profiles of H_2TPP and H_2OEP by scanning two individual columns by pixels.

of the retention-time matrix are rather larger than the third (and succeeding) eigenvalues demonstrating that rank analysis may be a useful tool in determining the number of compounds spotted on the plate. A comparison of the ratio of eigenvalues with and without flat field corection shows that this potential source of error is negligible compared to others. Also, we found that data from the edges of the thin-layer plate contributed only noise, and accordingly such data were eliminated from the rank analysis.

Clearly, the multichannel capability of optical system 1 offers an advantage over conventional thin-layer plate scanners. All mechanical scanning of the plate has been eliminated while taking the spectrum of every spot along the retenion axis. One may also choose to focus in on only one or two unresolved spots by changing the focal point of the lens between the plate and the monochromator and readjusting the plate accordingly.

Disadvantages of our system are (a) that correction must be made for pixel-pixel variation in sensitivity and (b) that only a limited central region of each spot is analyzed. The pixel-pixel variation may be partially overcome by suitable flat field correction. Disadvantage (b) may be overcome, at least partially, by means of a cylindrical lens system which images more of each spot onto the entrance slit of the analyzing monochromator by compressing the focus of the spot in the X direction while maintaining the spatial resolution in the retention direction.

A possible compromise optical system would use a stepper motor to drive the thin-layer plate past the entrance slit of the analyzing system. The optics would be devised so that the retention axis of the plate would be normal to the long axis of the slit. This configuration would be identical with the conventional scanners except that all spectral information would be acquired at once using a multichannel detector. We

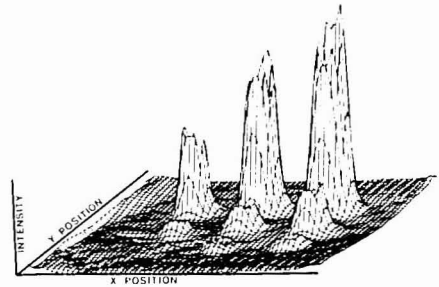


Figure 6. Dynamic range study. Various concentrations of H_2TPP were spotted on a thin-layer plate, and their fluorescent image was obtained with optical system 2. Isometric projections of fully corrected data.

are currently building such a system to test this approach.

Our feasibility study shows that rank annihilation is likely to be of great value in analyzing retention-emission data. In its present form, the algorithm does have the disadvantage that it cannot successfully separate two substances which have identical or similar emission characteristics, even though they might have rather different retention times. For example, a three-component mixture of H_2TPP, H_2Etio (free base etioporphine), and H_2OEP porphyrins yields a retention-time matrix which has only two principal components, based on eigen analysis. This happens because the spectra of H_2Etio and H_2OEP are nearly identical. However, if the algorithm were to be modified to recognize the fact that each component elutes as a single spot of predictable half-width, the separation into three components is quite straight forward (*18*).

Optical System 2. We evaluated system 2 for its ability to provide a quantitative analysis of a thin-layer plate in two dimensions. We were particularly interested in the capability to operate over a wide dynamic range with very small amounts of materials. As a test of this, we placed nine spots of H_2TPP at amounts varying from 3 pg to 1.5 ng. Figure 6 gives the fully corrected data as isometric projections.

It can be safely concluded that quantitation is quite feasible in the picogram region and that at least a 2.5 orders of magnitude range of H_2TPP can be quantitated on one plate. The only disappointment is that the calibration curves are not quite linear. While the correlation coefficient was very high (0.996), the slope of a log-log plot was only 0.779. For a truely linear relationship, the value of the slope should have been equal to 1.0. This nonlinearity could be due to aggregation of the compound on the plate, allowing self-quenching to occur and thus lowering the fluorescence at higher concentrations. Uchiyama and Uchiyama (*19*) have shown that spraying the plate with a suitable nonviscous solvent can often prevent self-quenching due to aggregation. The linearity of the multichannel detector has been carefully checked (*7*) and this has been eliminated as a source of error.

To ensure that development of the plate does not somehow prevent quantitation, we have placed three spots of H_2TPP (3 pg, 9 pg, 15 pg) on a second plate and developed it. An isometric projection of the image is shown in Figure 7. While

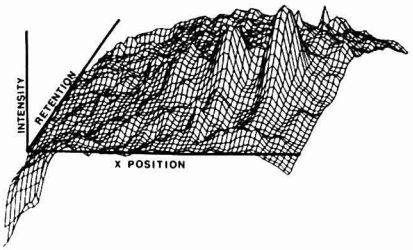


Figure 7. Thin-layer chromatogram of H_2TPP at three different concentrations; isometric projection.

it is difficult to observe the 3-pg spot by eye, summation of the pixels at the R_f value expected for H_2TPP and correction for the background gave a signal considerably above the noise level for the plate. The linear correlation coefficient in this case was greater than 0.999. In this case, the limit of visual detection probably lies somewhere between 3 and 9 pg. Increased amounts of fluorescent compounds may also be measured until saturation of the camera has occurred. When this happens, suitable neutral density filters may be placed in front of the camera to cut down the intensity of light reaching it.

Further studies (*20*) have been carried out with prostaglandins derivatized by the method of Dunges (*21*). Under chromatography conditions optimized for separation of prostaglandin derivatives and their metabolites, we again obtained excellent calibration profiles extending from 100 pg to 20 ng and reconfirmed the necessity for background and flat field corrections.

Optical system 2 is perhaps the most useful apparatus for routine determinations of fluorescent compounds on thin-layer plates. We have demonstrated that in situ quantitation of fluorescent materials at the picogram level is feasible. Moreover, a dynamic range of 500:1 may be covered on the same plate. We believe that a number of improvements can be made to further decrease the detection limits and increase the precision of the analysis. At present, the major problem is the high blank values of the plate. Some of this blank obviously arises from undesired fluorescence of impurities in the plate; hopefully, this will be remedied by manufacturers in the future. Another contributor to the blank fluorescence of the plate arises from excitation light leaking through the analyzing filter. Specially constructed interference filters on fluorescence-free glass could eliminate much of this problem. Finally, the blank problem was greatly increased by our inability to reposition the plate after chromatography. With the present blank fluorescence, we must operate the camera at sensitivities 2 orders of magnitude less than its ultimate sensitivity. Indeed, if blank fluorescence could be elimated entirely, we calculate that as few as 10^5 molecules per spot could be detected.

We shall leave for future studies the important questions of resolving and quantitating overlapping spots using optical system 2. Here, we merely point out that four variables provide separation of components on a two-dimensional chromatogram: wavelength of emission, wavelength of excitation, retention value along the first elution axis, and retention value along the second axis. Such data may be conveniently thought of as a tensor of rank 4. Strategies for evaluation of such data are currently under development in our laboratories.

Finally, we should mention the applicability of multichannel detectors to other problems in spatially resolved analytical chemistry. Obviously one can use multichannel detectors for UV–Vis, IR, and Raman imaging of thin-layer plates as well. One exciting development in our laboratory involves use of an improved multichannel detector for two-dimensional scintillation autography. Also one can use our system for other problems as well, such as the spatial mapping of catecholamines in brain slices and the enumeration of proteins with two-dimensional gel electrophoresis.

ACKNOWLEDGMENT

We are indebted to Biswanath De for his experimental assistance and to Niels Andersen and Ernest Davidson for useful discussion. We would also like to thank Leon Hershberger and Chu-Ngi Ho for their technical assistance and helpful advice. The chromatographically pure free base octaethyl-, etio-, tetraphenylporphines were the kind gift of Martin Gouterman.

LITERATURE CITED

(1) Zlatkis, A.; Kaiser, R. E. "High Performance Thin Layer Chromatography", Elsevier Scientific: Amsterdam, 1977.
(2) Touchstone, J. C.; Sherma, J. "Densitometry in Thin Layer Chromatography"; Wiley: New York, 1979.
(3) Haefelfinger, P. *J. Chromatogr.* **1979**, *162*, 215–222.
(4) Gupta, R. N.; Eng, F.; Lewis, D. *Anal. Chem.* **1978**, *50*, 197–199.
(5) Doss, M. In "Progress in Thin-Layer Chromatography and Related Methods"; Niederwieser, A., Pataki, G., Ed.; Ann Arbor Science: Ann Arbor, MI, 1972, Vol. III, pp 145–176.
(6) Talmi, Y., Ed. *ACS Symp. Ser.* 1979, *No. 102*.
(7) Johnson, D. W.; Gladden, J. A.; Callis, J. B.; Christian, G. D. *Rev. Sci. Instrum.* **1979**, *50*, 118–126.
(8) Warner, I. M.; Fogarty, M. P. Shelly, D. C. *Anal. Chim. Acta* **1979**, *109*, 361–372.
(9) Talmi, Y.; Baker, D. C.; Jadamec, J. R.; Saner, W. A. *Anal. Chem.* **1978**, *50*, 936A–952A.
(10) Vo-Dinh, T.; Johnson, D. J.; Wineforner, J. D. *Spectrochim. Acta, Part A* **1977**, *33A*, 341–345.
(11) Curtis, T. G.; Seitz, W. R. *J. Chromatogr.* **1977**, *134*, 513–516.
(12) Johnson, D. W. Ph.D. Dissertation, University of Washington, Seattle, WA, 1978.
(13) Warner, I. M.; Callis, J. B.; Davidson, E. R.; Christian, G. D. *Clin. Chem.* **1976**, *22*, 1483–1492.
(14) Warner, I. M.; Davidson, E. R.; Christian, G. D. *Anal. Chem.* **1977**, *49*, 2155–2159.
(15) Ho, C. N.; Christian, G. D.; Davidson, E. R. *Anal. Chem.* **1978**, *50*, 1108–1113.
(16) Ho, C. N.; Christian, G. D.; Davidson, E. R. *Anal. Chem.* **1980**, *52*, 1071–1079.
(17) McCord, T. B.; Frankston, M. J. *Appl. Opt.* **1975**, *14*, 1437–1446.
(18) Appeloff, C.; Davidson, E. R., unpublished results.
(19) Uchiyama, S.; Uchiyama, M. *J. Chromatogr.* **1978**, *153*, 135–142.
(20) Andersen, N. H. submitted for publication in Proceedings of the U.S.-Italian Joint Symposium on Prostaglandins and Cardiovascular Disease, Houston, TX, Nov 1979.
(21) Dunges, W. *Anal. Chem.* **1973**, *45* 963.

RECEIVED for review October 6, 1980. Accepted April 24, 1981. This research was supported in part by National Institutes of Health Grant GM-22311.

Continuous Flow Alternating Current Polarographic Detection of Nitrazepam in Liquid Chromatography

Herman B. Hanekamp, Willem H. Voogt, Roland W. Frei,* and Pieter Bos

Department of Analytical Chemistry, Free University, De Boelelaan 1083, 1081 HV Amsterdam, The Netherlands

The potential of alternating current polarography for detection of reducible organics in continuous flow systems is explored. Systematic studies in batch and in dynamic flow conditions have been carried out with the model compound nitrazepam. Parameters such as influence of mobile phase composition, applied frequency, amplitude and phase angle on the signal were studied. Although striking differences were found between batch and flow conditions for the influence of the adjusted phase angles, a phase angle of 0° seems to offer the best measurement condition in both instances. The detection limit is in the order of 5-20-fold lower than for previously reported DME detectors. The AC polarographic cell assembly for continuous flow conditions was tested for the detection of four benzodiazepines after reversed-phase chromatographic separation. The enhanced selectivity of this detection mode makes it promising for organic trace analysis in complex matrices.

The usefulness of electrochemical detectors in high-performance liquid chromatography (HPLC) has already been recognized (*1-3*). Especially solid-state electrode detectors are able to detect quantities at the subnanogram level (*1, 4-13*). Mercury possesses several advantages as an electrode material. However, the relatively low sensitivity of polarographic detectors obstructed the introduction of this type of detector.

Some of the problems have been overcome by the construction of a fast dropping mercury electrode (DME) detector with a conically ground horizontal capillary (*14*). With direct current amperometry good results can be obtained with such a detector (*15*). The fast DME system, however, does not allow the application of techniques with enhanced sensitivity and selectivity such as (differential) pulse techniques, which require a synchronization between the electronics and the drop lifetime. This necessary synchronization has recently been achieved by means of a potential pulse supplied to a horizontal DME with a partially conical glass capillary (*16*). The advantages of pulse techniques become apparent only if the content of electrochemically active impurities (oxygen, trace metals, etc.) in the eluent stream is very low. These impurities cause a background current and are actually determining the noise in the base line and hence the attainable detection limit (*11, 16-19*). As purging with nitrogen is not sufficient, the impurities have to be removed by reduction in a flow-through cell with porous silver electrodes (*19*). Thus, a favorable detection limit is obtainable with normal pulse amperometry (*18*).

An other approach can be the use of sampled alternating current (AC) polarography (*20*). In AC polarography a sinusoidal voltage of small amplitude is superimposed on the usual DC potential. The resulting polarogram is peak shaped and consequently possesses a better selectivity than DC measurements. The total measured alternating current exhibits a shift in phase angle relative to the superimposed voltage. By means of a phase-sensitive readout the faradaic component of the current can be distinguished from the capacitive current. The latter is primarily responsible for the noise, and its elimination results in an improved detection limit (*21*).

It is also possible to measure the change in the capacity at the mercury drop. Thus, adsorbing but nonelectroactive compounds can be determined too. This tensiometric type of detection has been demonstrated by Lankelma and Poppe (*22*) and Kemula and Kutner (*23*). In addition AC measurements could be very useful to investigate electrode kinetics (*24, 25*).

In the present work it was our aim to examine to what extent employment of this technique can improve the sensitivity and selectivity of a DME detector in continuous-flow systems.

EXPERIMENTAL SECTION

The first experiments were performed in batch and compared to the corresponding measurements under flow conditions. Nitrazepam was chosen as test compound as used in earlier work (*18*).

The detector used in this work was identical with the one developed for the application of pulse techniques (*16, 18*). As the drop lifetime and electronics can be synchronized by using this cell, a sampled AC measurement was applied. All measurements in the chromatographic system were made with the electrochemical eluent scrubber as an indispensable part of the instrumentation (*19*).

Apparatus. In all experiments a Bruker modular polarograph (E 310 M, Bruker Spectrospin, N.V., Brussels, Belgium) was used. The chromatographic system consisted of a PE 601 pump (Perkin-Elmer), the electrochemical eluent scrubber, an injection valve (25 μL loop) (Valco Instruments Co., Houston, TX) and a column (ss, 10 cm × 4.6 mm i.d.) packed with ODS hypersil 5 μm (Shandon, Rumcorn, U.K.). The electrochemical scrubber and the polarographic detector were constructed in our workshop and have been extensively described elsewhere (*16, 19*).

The electrical currents were measured with the Bruker and recorded on a XY recorder (BD 30, Kipp en Zonen, Delft, The Netherlands). All potentials and electrical currents were checked on a Tektronix 5103 N oscilloscope (Tektronix, Beverton, OR). The applied potential was always measured vs. an Ag|AgCl| 1 M LiCl, methanol-water (50/50% v/v) reference electrode.

Chemicals. In all measurements water-methanol mixtures, which contained 0.1 M KNO_3 and 10^{-3} M HNO_3 or 0.02 M H_2SO_4, were used as eluent. The stock solution was deaerated for several hours by purging with nitrogen (A 28).

Nitrazepam was supplied by Nogefa (Haarlem, The Netherlands). All other chemicals were analytical-reagent grade (Baker "Analyzed" or Merck P.A.) and used without further purification. Water was demineralized and distilled. Samples were deaerated by purging with nitrogen for 10 min.

RESULTS AND DISCUSSION

Batch Experiments. These experiments were performed in a classical polarographic setup. The DC polarogram of nitrazepam (1,3-dihydro-7-nitro-5-phenyl-2*H*-1,4-benzodiazepin-2-one, mol wt 281.26) exhibits two waves. The more positive one is the reduction of the nitro group and the more negative one that of the azomethine function. On comparison

0003-2700/81/0353-1362$01.25/0 © 1981 American Chemical Society

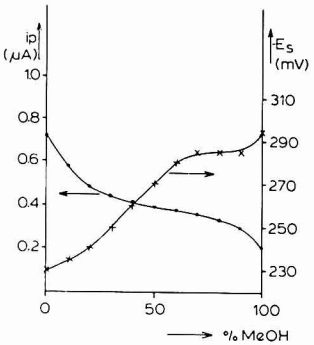


Figure 1. The peak height and summit potential as a function of the percentage of methanol: 10^{-4} M nitrazepam, f = 35 Hz, amplitude = 7 mV eff, scan rate = 2 mV s^{-1}, drop time = 1 s, h_{Hg} = 50 cm, ϕ = 0°.

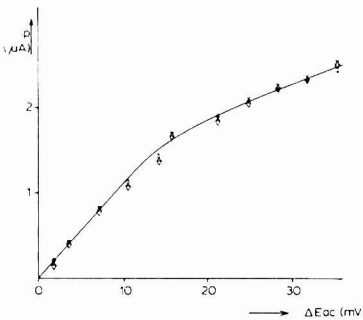


Figure 2. The peak height vs. the applied amplitude: (●) f = 11.6 Hz, (×) f = 35 Hz, (▽) f = 116 Hz. For further conditions see Figure 1.

of the DC and AC polarograms, the half-wave and summit potentials for the nitro group are equal within 5 mV. For the azomethine function the summit potential is 25 mV more negative than the half-wave potential. However, in this work we paid attention mainly to the behavior of the nitro group as most interesting functional group for flow-through detection.

In order to establish the influence of the eluent as used in reversed-phase chromatography, we measured the peak height and summit potential as a function of the percentage methanol (see Figure 1). From this plot it is obvious, that the highest peak currents occur in the low methanol percentage range and that the summit potential is dependent on the eluent composition. Further, the summit potential depends on the pH. In a pH range of 2–6.5 (Britton-Robinson buffers) a linear relation of −58 mV per pH unit was found.

From a logarithmic plot of $(i_d - i)i^{-1}$ vs. the potential in the rising part of a DC polarogram, a value of 2.0 can be calculated for αn. As this is a four-electron electrode reaction, it appears that the reaction is not reversible and a value for α of 0.5 can be assumed.

The plot of the peak height vs. the root of the applied frequency indicates a fairly irreversible behavior in AC polarography. A constant value for the peak height is reached already at a rather low frequency. As there is no gain in using high frequencies, it is attractive to apply a low frequency, where the capacitive current will be small.

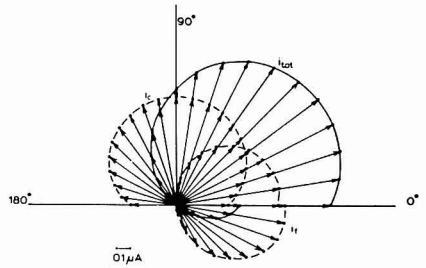


Figure 3. The peak height vs. the adjusted phase angle; for conditions see Figure 1.

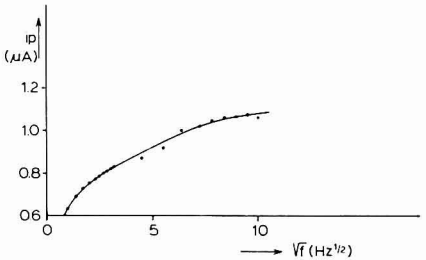


Figure 4. The peak height vs. the root of the applied frequency in flow conditions: 10^{-4} M nitrazepam, amplitude = 7 mV eff, scan rate = 2 mV s^{-1}, cycle time = 0.4 s, h_{Hg} = 50 cm, ϕ = 0°, flow rate = 1 mL min^{-1}.

The dependence of the peak height upon the applied amplitude has been measured at three frequencies. The response is actually the same for all frequencies (see Figure 2). Up to 15 mV the peak height increases linearly with the amplitude, but up to 35 mV an important gain in signal can be achieved. Another interesting feature of AC measurements is the phase angle between the applied voltage and the resulting current. In Figure 3 a vectorial representation is given of the current for nitrazepam as function of the adjusted phase angle. In this batch experiment an expected pattern is found and a phase angle of 0° offers the best ratio between faradaic and capacitive currents.

For a concentration range of 10^{-4}–10^{-6} M a calibration line was computed via the method of least squares. A sensitivity of 6.99×10^{-3} A L mol^{-1} was found with a regression coefficient of 0.9977. At higher concentrations the sensitivity is slowly decreasing and the response is no longer linear. A concentration of 10^{-6} M can be estimated as the lower detection limit.

Experiments in a Flow System. These experiments were carried out with the DME detector, at a flow rate of 1 mL min^{-1}. The eluent contained a constant level of 10^{-4} M nitrazepam and the electrochemical scrubber cannot be used.

In the AC polarogram the summit potential for the nitro group has shifted 30 mV in cathodic direction compared to the half-wave potential measured under the same conditions. The plot of the peak height as function of the root of the applied frequency exhibits the same form as in the corresponding batch experiments. Only at very low frequencies does the peak height increase with the frequency, but a plateau is soon reached (see Figure 4). Again the dependence of the peak height upon the applied amplitude was measured at two frequencies (see Figure 5). In contrast to the behavior in the batch experiment there is a difference in response for the two

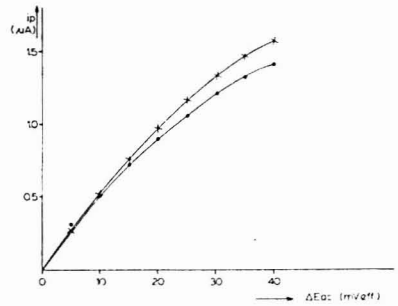


Figure 5. The peak height vs. the applied amplitude in flow conditions: (●) f = 10 Hz, (×) f = 40 Hz. For further conditions see Figure 4.

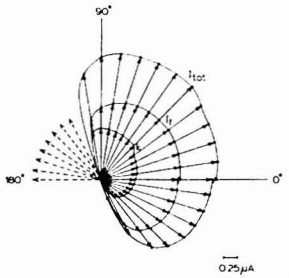


Figure 6. The peak height vs. the applied phase angle in flow conditions, f = 10 Hz. For further conditions see Figure 4.

frequencies used. But equally, the peak height increases linearly with the amplitude up to 15 mV, while up to 35 mV there is a favorable gain in signal.

In the measurement of the peak height as a function of the adjusted phase angle the difference between batch and flow conditions is striking. In Figure 6 a vectorial representation of the total, capacitive and faradaic currents is given. Especially the relation for the capacitive current differs greatly with that under nonflow conditions. Probably a phase angle shift due to the geometry and construction of the cell could be held responsible for this phenomenon. However, a phase angle of 0° still offers the best distinction of the faradaic component of the total current from the capacitive current.

Performance as Detector for HPLC. For the measurement of the linearity of response, sensitivity, and detection limit an actual chromatographic system was adapted. The oxygen present in the sample can easily be separated chromatographically from nitrazepam. The indication potential was fixed at the summit potential of the nitro group. At a flow rate of 1 mL min^{-1} (water–methanol, 50/50% (v/v), 0.1 M KNO_3, 10^{-3} M HNO_3) the capacity factor for nitrazepam was 4.5 and the effective plate number of the column was 1500.

A linear dynamic range of 4 orders of magnitude was found (10^{-4}–4×10^{-8} M). The calibration line was computed via linear regression with the method of least squares; a sensitivity of 5.1×10^{-3} A L mol^{-1} (or 200 A mol^{-1} injected) with a regression coefficient of 0.9995 was found. With a noise of 0.05 nA (peak-to-peak variation in the base line), the detection limit (3× noise) was 0.7 pmol (or 0.2 ng) per injection of 25 μL (see Figure 7). Calculated from the chromatographic data this would represent a least detectable amount (for an ideal plug injection of 25 μL) of 1×10^{-15} mol (or 0.3 pg). This is a 5-fold improvement in detection limit in comparison to pulse polarographic detection and about 20-fold compared to the fast DME system (*18*).

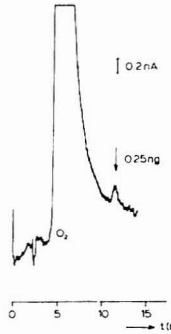


Figure 7. Determination of nitrazepam near the detection limit: flow rate = 1 mL min^{-1}, eluent water–methanol (50/50% (v/v)), 0.1 M KNO_3, 10^{-3} M HNO_3, f = 11.7 Hz, amplitude = 7 mV eff, ϕ = 0°, cycle time = 0.4 s, h_{Hg} = 50 cm.

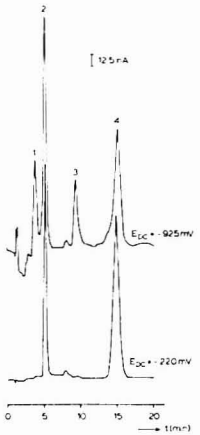


Figure 8. Chromatograms of four benzodiazepines at two detection potentials: (1) bromazepam, (2) nitrazepam, (3) diazepam, (4) clonazepam; 1 μg of each injected. HNO_3 replaced by 0.02 M H_2SO_4. For further conditions see Figure 7.

To demonstrate the selectivity of the detector, another well-known advantage of AC measurement, we chromatographed a mixture of four benzodiazepines: bromazepam, nitrazepam, diazepam, and clonazepam. Two of them contain a nitro group (nitrazepam and clonazepam) and all four possess, of course, the azomethine function. If the potential is fixed at a certain value, only compounds having a summit potential within the window defined by the AC amplitude will be detected. So, the first two compounds can be selectivity detected at the summit potential of the nitro group. All of the benzodiazepines can be recorded at the summit potential of the azomethine group (see Figure 8) without interference from the nitro groups or other compounds with summit potentials different from the one for the azomethine group.

CONCLUSION

Phase-sensitive sampled alternating current measurement appears to be a powerful analytical technique. Especially when used in polarographic detection for HPLC a very low detection

limit for nitrazepam can be found. The added selectivity of this type of detection can be advantageous in separations of complex mixtures. Also the possibility of electrokinetic investigations makes AC measurement highly interesting.

ACKNOWLEDGMENT

We wish to thank H. G. de Jong for technical assistance.

LITERATURE CITED

(1) Kissinger, P. T. *Anal. Chem.* **1977**, *49*, 448.
(2) Brunt, K. *Pharm. Weekbl.* **1978**, *113*, 689.
(3) Rucki, R. J. *Talanta* **1980**, *27*, 147.
(4) Kissinger, P. T.; Refshauge, C.; Dreiling, R.; Adams, R. N. *Anal. Lett.* **1973**, *6*, 259.
(5) Bollet, C.; Oliva, P.; Caude, M. *J. Chromatogr.* **1977**, *149*, 625.
(6) Cox, J. A.; Przyjazny, A. *Anal. Lett.* **1977**, *10*, 869.
(7) McCrehan, W. A.; Durst, R. A.; Bellama, J. M. *Anal. Lett.* **1977**, *10*, 1175.
(8) Sasa, S.; Leroy Blank, C. *Anal. Chem.* **1977**, *49*, 354.
(9) Lores, E. M.; Bristol, D. W.; Moseman, R. F. *J. Chromatogr. Sci.* **1978**, *16*, 358.
(10) Carr, R. S.; Neff, J. M. *Anal. Chem.* **1980**, *52*, 2428.
(11) McCrehan, W. A. *Anal. Chem.* **1981**, *53*, 74.
(12) Blaedel, W. J.; Wang, J. *Anal. Chem.* **1981**, *53*, 78.
(13) Beauchamp, R.; Boinay, P.; Fombon, J. J.; Tacussel, J.; Breant, M.; Georges, J.; Porthault, M.; Vittori O. *J. Chromatogr.* **1981**, *204*, 123.
(14) Hanekamp, H. B.; Bos, P.; Brinkman, U. A. Th.; Frei, R. W. *Fresenius' Z. Anal. Chem.* **1979**, *297*, 404.
(15) Hanekamp, H. B.; Bos, P.; Frei, R. W. *J. Chromatogr.* **1979**, *186*, 489.
(16) Hanekamp, H. B.; Voogt, W. H.; Bos, P. *Anal. Chim. Acta* **1980**, *118*, 73.
(17) Greenberg, M. S.; Mayer, W. J. *J. Chromatogr.* **1979**, *169*, 321.
(18) Hanekamp, H. B.; Voogt, W. H.; Bos, P.; Frei, R. W. *J. Liq. Chromatogr.* **1980**, *3*, 1205.
(19) Hanekamp, H. B.; Voogt, W. H.; Bos, P.; Frei, R. W. *Anal. Chim. Acta* **1980**, *118*, 81.
(20) Hanekamp, H. B.; Bos, P.; Vittori, O., submitted for publication in *Anal. Chim. Acta*.
(21) Jee, R. D. *J. Electroanal. Chem.* **1976**, *69*, 109.
(22) Lankelma, J.; Poppe, H. *J. Chromatogr. Sci.* **1978**, *14*, 310.
(23) Kemula, W.; Kutner, W. *J. Chromatogr.* **1981**, *204*, 131.
(24) Smith, D. E. *Electroanal. Chem.* **1966**, *1*.
(25) Sluyters-Rebach, M.; Sluyters, J. H. *Electroanal. Chem.* **1970**, *4*.

RECEIVED for review March 3, 1981. Accepted May 11, 1981. Sandoz (Basle) is thanked for financial support.

Correlation between the Retention Behavior of Mono- and Difunctional Solutes in Binary Solvent–Silica Gel Liquid Chromatography

Shoji Hara* and Sayuri Miyamoto

Tokyo College of Pharmacy, Horinouchi, Hachioji, Tokyo 192-03, Japan

To systematize the optimization of the binary solvent for multifunctional solutes in liquid–solid chromatography, we determined the correlation between the logarithms of capacity ratio vs. molar fraction of the stronger eluent by employing 3- and 17-mono- and 3,17-disubstituted androstanes containing the same functions at the same positions of the steroid nucleus. According to the linear relationship, it became possible to estimate the retention of difunctional solutes on the basis of the retention of two corresponding monofunctional solutes.

In the liquid chromatographic separation of a given sample mixture, optimization of the stationary and mobile phases is the major and most important process. The technique of separating mixtures by solvent system selectivity in liquid–solid chromatography has been widely utilized, especially in the field of organic chemistry, and much data related to the optimization of chromatographic systems has been accumulated. Snyder has determined the parameters for the adsorption energies of functional groups of solute molecules and the solvent strength parameters for the mobile phase on the basis of the theoretical and experimental investigations (*1*). The quantitative relationship between the retentions and the binary solvent compositions has been exploited by Soczewinski and found to be useful for the selection of the mobile phase (*2*, *3*). In these studies, silica gel–binary solvent systems containing a diluent and a stronger solvent have been the most commonly employed. Consequently, the retention behavior of a given sample in a binary solvent for silica gel chromatography has come to be predictable if the hydrogen bonding of the functional groups in the solute molecules with the silanol groups on the silica gel surface is evaluated (*4–6*).

However, when the number of functional groups present in the solute increases, difficulty arises in applying directly such procedures. In order to predict the retention behavior of a multifunctional compound and to optimize the chromatographic system based on the data obtained from the corresponding monofunctional solutes, a series of model compounds having typical substituents on the same nucleus was selected and their retention behaviors were compared. In this paper, three series of mono- and disubstituted solutes were prepared. In the sample compounds, acetoxyl, keto carbonyl, and hydroxyl groups, chosen as the most common functions in organic compounds having medium polarity, were located on the 3 and/or 17 position of a steroid nucleus. Various binary solvent systems were adapted as mobile phases and capacity ratios of the solutes related with the solvent composition were quantitatively determined.

EXPERIMENTAL SECTION

Samples. 3- and 17-Monosubstituted and 3,17-disubstituted steroids were prepared by a standard procedure from 17β-hydroxy-5α-androstan-3-one and 3β-hydroxy-5-androsten-17-one which were commercially available. Monosubstituted androstane derivatives were obtained by deoxygenation of one of the oxygen functions in the disubstituted androstanes. A keto group in hydroxyandrostanone was converted to the methylene group via tosylhydrazone by Wolff–Kishner reduction. The remaining hydroxyl function was modified to the acyloxy group by acylation or to the keto group by chromium oxide or Oppenauer oxidation. Isolation and purification of the products were carried out by employing a direct fractionation procedure previously proposed by Hara (*7*, *8*). Compounds were characterized and identified according to spectral data and compared directly with standard samples.

Adsorbent and Columns. Irregular-shaped silica gel, with a pore size of 70 Å, and particle diameter of 10 μm, Wakogel LCH-10, obtained from Wako Pure Chemicals Co., Osaka, was packed into glass tubes, 4 mm i.d. × 20 cm length. A CIG column system described in a previous report (*9*) was utilized.

Chromatographic Procedure. Flow rate of the mobile phase

0003-2700/81/0353-1365$01.25/0 © 1981 American Chemical Society

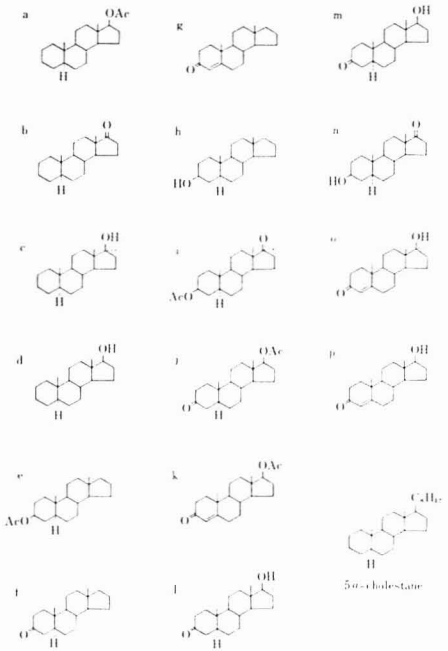


Figure 1. Structures of the steroids investigated.

was 1 mL/min. Holdup volume V_0 was measured by injecting cyclohexane as a standard sample, and retention volume V_R was obtained at ambient temperature, ca. 15 °C. Capacity ratio k' was calculated by the equation $k' = (V_R - V_0)/V_0$. The liquid chromatograph system was assembled with a reciprocal pump, KP-9H, Kusano Scientific Co., Tokyo, and refractive index detector, R 401, Waters Associates, MA.

RESULTS AND DISCUSSION

For examination of retention behaviors of mono- and difunctional solutes, medium polar compounds having hydroxyl, keto, and acyloxyl groups which are distributed widely as common functional groups in the nonionic organic compounds were selected. 3- and 17-Monosubstituted androstane derivatives were prepared by deoxygenation of 3,17-dioxyandrostanes and by conversion of their functional groups. The structural formulas are shown in Figure 1.

The capacity ratios of the samples were determined by employing systematically prepared solvent systems containing a diluent and a stronger eluent. Solvents were classified according to their hydrogen bonding activity as mentioned previously (*4*, *9*). The diluents were *n*-hexane (O), benzene (P), and dichloromethane (N), and stronger solvents were basic and acidic/basic compounds such as diethyl ether (B_1), ethyl acetate (B_2), acetone (B_3), and 2-propanol (AB). The symbols used to represent the solvents were proposed by Hara (*4*, *9*). Binary systems were classified as O + B or AB, P + B or AB, and N + B or AB types. A log–log plot was made of the capacity ratios vs. molar fractions for the solvent mixtures. Linear relations were yielded, and the data were found to be in exact agreement with eq 1 as follows (*4–6*, *9*, *10*):

$$\log k' = c - n \log X_s \qquad (1)$$

where c and n are constants, k' is the capacity ratio, and X_s is the mole fraction of the stronger solvent in the binary system. Experimental values for samples a–d (17-monosubstituted), e–h (3-monosubstituted), and i–p (3,17-disubstituted androstanes) in O + B and AB systems are given in Figure 2. The intercept c and slope n for all systems were calculated by the least-squares procedure and are listed in Table I.

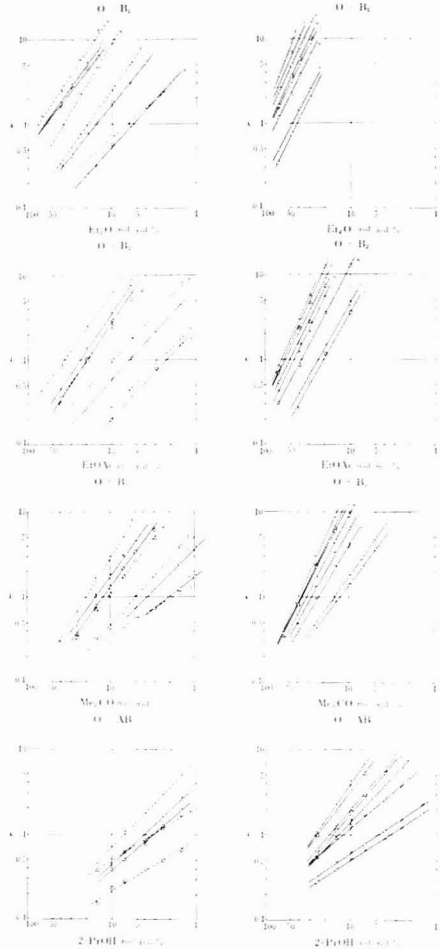


Figure 2. Logarithm of capacity ratios on silica gel as a function of the logarithm of the stronger solvent concentration in *n*-hexane–stronger solvent binary systems. Samples are as in Figure 1.

Retention Behavior of Monosubstituted Derivatives. From a stereochemical view point, the adsorption activity of a given functional group may vary according to its position in the androstane nucleus. However, the retention behavior of two series of positional isomers having the same substituent at the 3 or 17 position of the steroid nucleus such as the pairs of compounds a–e, b–f, and d–h were found to be similar. Constants c and n in eq 1 obtained for both positional isomers were approximately equal. The retention behavior of the solutes basically depended on the substituent but not on the location of the function. The retention data of some 3-substituted cholestanes which contain the same functional group

Table I. Constants of the Linear Relationship between Retention and Solvent Composition

	O + B$_1$[a]		O + B$_2$		O + B$_3$		O + AB		P + B$_1$		P + B$_2$	
sample[c]	c[b]	n[b]	c	n	c	n	c	n	c	n	c	n
a	0.83	1.11	0.37	1.07	0.23	0.78			−0.16	0.72	−0.11	0.90
b	1.49	1.26	0.86	1.10	0.56	1.00			0.10	0.69	0.14	0.84
c	2.31	1.31	1.94	1.50	1.44	1.33	0.43	0.86	0.85	0.71	1.04	1.02
d	2.51	1.40	2.03	1.47	1.60	1.37	0.58	0.93	0.86	0.70	1.13	1.03
e	0.68	0.85	0.41	0.96	0.14	0.59			−0.21	0.61	−0.10	0.83
f	1.82	1.42	1.07	1.09	0.77	1.10	−0.06	0.62	0.34	0.82	0.42	0.93
g	2.67	1.70	1.72	1.34	1.31	1.27	0.34	0.62	0.77	0.82	0.92	1.00
h	2.81	1.49	2.18	1.39	2.02	1.57	0.86	1.02	1.14	0.69	1.30	0.92
i	3.23	2.00	2.33	1.79	1.46	1.32	0.36	0.64	0.74	0.96	0.86	1.15
j	3.22	1.92	2.40	1.74	1.64	1.41	0.46	0.67	0.92	1.05	1.08	1.28
k	3.72	1.98	3.00	1.90	2.34	1.72	0.93	0.83	1.36	1.10	1.53	1.29
l	3.92	2.02	3.46	2.10	2.61	1.83	1.23	1.07	1.47	0.96	1.67	1.21
m	4.13	2.14	3.58	2.12	2.93	1.95	1.44	1.21	1.53	0.96	1.75	1.21
n	4.44	2.16	3.63	2.07	3.11	2.00	1.48	1.18	1.53	0.85	1.70	1.10
o	4.70	2.33	4.07	2.31	3.31	2.13	1.83	1.33	1.83	1.00	1.97	1.31
p	5.07	2.46	4.12	2.29	3.57	2.25	2.06	1.44	2.32	1.29	2.10	1.31

	P + B$_3$		P + AB		N + B$_1$		N + B$_2$		N + B$_3$		N + AB	
sample	c	n	c	n	c	n	c	n	c	n	c	n
a					−0.53	0.48	−0.42	0.68			−0.96	0.72
b	0.05	0.99			−0.10	0.84	0.00	0.85	−0.24	0.74	−0.89	1.17
c	0.70	0.96	0.14	1.02	0.46	0.52	0.54	0.65	0.39	0.74	−0.10	0.92
d	0.79	1.00	0.19	1.06	0.51	0.52	0.60	0.66	0.45	0.71	0.00	0.87
e					−0.39	0.72	−0.41	0.73			−0.94	0.78
f	0.09	0.93			0.09	0.81	0.20	0.86	−0.09	0.82	−0.60	0.96
g	0.52	1.00	0.09	1.28	0.66	0.99	0.79	1.01	0.46	1.06	−0.10	1.22
h	0.91	0.86	0.44	0.96	0.73	0.50	0.94	0.75	0.67	0.71	0.23	0.91
i	0.70	1.54	0.10	1.22	0.48	1.22	0.58	1.09	0.20	1.13	−0.52	1.27
j	0.78	1.50	0.13	1.28	0.56	1.16	0.78	1.22	0.30	1.09	−0.40	1.38
k	1.19	1.45	0.29	1.31	1.11	1.32	1.23	1.23	0.81	1.27	0.08	1.40
l	1.29	1.22	0.46	1.17	0.88	0.85	1.18	1.00	0.79	0.94	0.16	1.13
m	1.40	1.28	0.58	1.19	1.06	0.97	1.17	0.99	0.90	0.98	0.26	1.13
n	1.52	1.24	0.66	1.12	1.11	0.84	1.12	0.89	0.93	0.87	0.39	1.05
o	1.70	1.38	0.78	1.27	1.18	0.84	1.44	1.01	1.11	1.04	0.41	1.37
p	1.94	1.53	0.88	1.30	1.34	1.00	1.51	1.03	1.26	1.11	0.60	1.36

[a] Solvents: O = n-hexane; P = benzene; N = dichloromethane; B$_1$ = diethyl ether; B$_2$ = ethyl acetate; B$_3$ = acetone; AB = 2-propanol. [b] c and n are constants for eq 1. [c] Samples as in Figure 1.

as androstanes were reported previously (*4*). The structural formula of cholestane is given in Figure 1. The behaviors of these two classes of compounds in binary solvent systems were compared. Cholestane is a homologue of androstane and has an additional eight-carbon side chain. The lipophilic part of the solute usually has a slight effect on the retention behavior in liquid–solid chromatography. Retention behaviors of 3-substituted cholestane and androstane derivatives were found to be very similar, as was expected.

According to the adsorption mechanism discussed in the literature (*3*), the following relationship is assumed. When a combination of a solute and a solvent having the same active function is used in a n-hexane (O)–binary system, the number of solute and polar solvent molecules exchanged on the adsorbent surface may be nearly identical; i.e., $n = 1$. This assumption was consistent with the data previously reported (*4*) and is also supported by the experimental results for O + B and O + AB systems as shown in Table IIa of this article.

If the polarity of the diluent W increases, the exchange ratio of the stronger solvent and solute molecules may decrease because the participation of the diluent molecules increases. When the O component was changed to P or N, the values of n tended to be smaller than in O + B or O + AB systems as shown in Table IIb.

In a comparison of the eluotropic sequence of stronger solvents with the same diluent and same solute, the strength was in the increasing order of $B_1 < B_2 < B_3 < AB$. The values of constants c and n decreased in this order. This can be explained by the fact that the increase of the stronger solvent localization on active sites of the adsorbent surface leads to a decrease in the exchange ratio of solute and solvent S molecules.

Table II. Slopes (n) for the Binary Solvent Systems

Part a

solute	solvent system	n[a]
acetate	O + B$_2$	1.07 (a), 0.96 (e)
ketone	O + B$_3$	1.00 (b), 1.10 (f)
alcohol	O + AB	0.93 (d), 1.02 (h)

Part b

solute	solvent system	n[a]	solvent system	n[a]
acetate	P + B$_2$	0.90 (a), 0.83 (e)	N + B$_2$	0.68 (a), 0.73 (e)
ketone	P + B$_3$	0.99 (b), 0.93 (f)	N + B$_3$	0.74 (b), 0.82 (f)
alcohol	P + AB	1.06 (d), 0.96 (h)	N + AB	0.87 (d), 0.91 (h)

[a] Sample in parentheses.

Constants provided for a sample having a particular substituent was then compared. It was clearly shown that both constants decreased in the order of hydroxyl, keto, and acetoxyl compounds in O + B and O + AB systems containing n-hexane as a diluent. When a P or N type diluent was employed instead of an O type, constant c also decreased in a similar manner; however, no regular relation between the

Table III. Coefficients for Difunctional Solutes in Binary Solvent Systems

a. Coefficient for Less Active Functional Group, β

solvent system	sample i	j	k	l	m	n	o	p
O + B_1	0.87	0.45	0.25	0.46	0.51	0.53	0.48	0.54
O + B_2	0.72	0.61	0.52	0.55	0.60	0.62	0.60	0.61
O + B_3	0.54	0.40	0.58	0.45	0.53	0.43	0.63	0.69
O + AB				0.34	0.45		0.76	0.82
P + B_1	0.44	0.32	0.39	0.20	0.20	0.23	0.25	0.67
P + B_2	0.37	0.39	0.32	0.20	0.19	0.21	0.29	0.28
P + B_3				0.28	0.30	0.38	0.40	0.53
P + AB							-0.01	0.02
N + B_1	0.53	0.73	0.69	0.08	0.31	0.00	0.29	0.02
N + B_2	0.33	0.53	0.32	0.22	0.20	0.05	0.00	0.03
N + B_3				0.16	0.23	0.18	-0.03	0.07
N + AB	0.13	0.58	0.25	0.18	0.20	0.13	0.16	0.16

b. Average Coefficient, γ

solvent system	sample i	j	k	l	m	n	o	p
O + B_1	0.95	0.76	0.70	0.74	0.76	0.79	0.77	0.79
O + B_2	0.87	0.81	0.79	0.81	0.83	0.83	0.81	0.81
O + B_3	0.83	0.75	0.84	0.75	0.79	0.78	0.82	0.85
O + AB				0.72	0.78		0.90	0.93
P + B_1	0.74	0.68	0.71	0.63	0.63	0.62	0.65	0.85
P + B_2	0.69	0.70	0.68	0.62	0.62	0.63	0.65	0.65
P + B_3				0.65	0.66	0.67	0.70	0.77
P + AB							0.55	0.56
N + B_1	0.78	0.90	0.90	0.64	0.73	0.63	0.56	0.66
N + B_2	0.69	0.79	0.73	0.66	0.65	0.56	0.61	0.62
N + B_3				0.60	0.64	0.60	0.58	0.63
N + AB	0.65	0.82	0.72	0.60	0.62	0.50	0.64	0.65

c. Mean Value and Standard Deviation of the Coefficient

solvent system (diluent)	β, mean value	std dev	γ, mean value	std dev
O	0.56	0.13	0.81	0.06
P	0.30	0.14	0.67	0.06
N	0.20	0.23	0.67	0.09

constant n and polarity of the functional group in the solute was observed.

Retention Behavior of Disubstituted Solutes. For determination of the correlation between the retentions of mono- and difunctional solutes, data obtained by 3,17-disubstituted androstanes were compared with those of 3- and 17-monosubstituted compounds having corresponding functional groups.

Two series of monosubstituted compounds and the corresponding disubstituted compounds having two active functions x_1 and x_2 at the 1 and 2 positions of a lipophilic nucleus P are represented as x_1-P, P-x_2, and x_1-P-x_2. The constants c_1, c_2, c_{12}, n_1, n_2, and n_{12} are the intercepts and the slopes of these three classes of the samples.

The slope in eq 1, constant n, represents the area fraction of the solvent and the solute molecules on the surface of the adsorbent according to the mechanistic consideration of adsorption chromatography (*3*). In a bifunctional compound, when the more active group at position 1 is adsorbed by the silanol group, the weaker group at position 2 is only partially adsorbed. In such cases, the constant n_{12} is given as

$$n_{12} = n_1 + \beta n_2 \tag{2}$$

where β is the diminution coefficient of the less active function. It should be noticed that $n_1 > n_2$ and $\beta < 1$.

If neither of the functional groups plays a predominant role in the adsorption, the diminution of adsorption of the two groups is evaluated as a mean value as follows:

$$n_{12} = \gamma(n_1 + n_2) \tag{3}$$

where γ is designated as the average coefficient.

On the basis of such a mechanistic assumption, the following pairs of mono- and difunctional samples having the same substituent at the same position of the steroid nucleus were chosen:

i–b, e j–a, f k–a, g l–c, f m–d, f
n–b, h o–c, g p–d, g

Experimental results revealed that both constants c and n for disubstituted solutes were always larger than those for either monosubstituted solute. First, the coefficient β and average coefficient γ were calculated by using the experimental values of constant n. These coefficients are shown in Table III. The standard deviations of the data are also listed in the table.

It was indicated that the scattering for the coefficient β was larger than that of γ. Consequently, the use of the average coefficient γ is more reliable when calculating the constant n of a difunctional solute from the corresponding values of monofunctional solutes.

The coefficient γ for the disubstituted solutes in *n*-hexane (O)–, benzene (P)–, and dichloromethane (N)–binary systems were ca. 0.8, 0.7, and 0.7, respectively. As the elution strength

of the solvent increases, dimunution of the coefficient in this sequence was observed.

Next, let us consider constant c. The sums of c_1 and c_2 were calculated for all combinations of samples and were compared with the constant c_{12} of the corresponding disubstituted solutes.

The results showed that the values of c_{12} were roughly equal to the sum of c_1 and c_2. In many cases, c_{12} was slightly larger than the sum of c_1 and c_2. This cannot be explained by theoretical consideration; however, it seems to be useful for the prediction of the retention behavior of the disubstituted solutes by using the data on the corresponding monosubstituted solutes, because an approximate value of c_{12} is afforded simply by the addition of c_1 and c_2.

In summary, the capacity ratio for disubstituted solutes can be expressed by the retention behaviors of the two corresponding monosubstituted solutes, the mole fraction of the stronger solvent in a binary system, and the average coefficient as

$$\log k'_{12} = (c_1 + c_2) - \gamma(n_1 + n_2) \log X_s \qquad (4)$$

In this work, a procedure simply using the mean values of constants c and n in eq 1 was employed and any selectivity due to interaction between the solute and the solvent molecules was disregarded. Therefore, eq 4 described above seemed not to be applicable to the precise prediction of the retention behavior for an individual sample. However, in spite of the ambiguity of this treatment, the practical procedure described in this article could be useful in order to optimize chromatographic systems using disubstituted solutes on the basis of the retentions of the two corresponded monosubstituted solutes.

LITERATURE CITED

(1) Snyder, Lloyd R. "Principles of Adsorption Chromatography"; Marcel Dekker: New York, 1968.
(2) Soczewinski, Edward Anal. Chem. 1969, 41, 179-182.
(3) Snyder, Lloyd R. Anal. Chem. 1974, 46, 1384-1393.
(4) Hara, Shoji; Fujii, Yumiko; Hirasawa, Mamiko; Miyamoto, Sayuri J. Chromatogr. 1978, 149, 143-159.
(5) Hara, Shoji; Ohsawa, Akiko J. Chromatogr. 1980, 200, 85-94.
(6) Hara, Shoji; Hirasawa, Mamiko; Miyamoto, Sayuri; Ohsawa, Akiko J. Chromatogr. 1979, 169, 117-127.
(7) Hara, Shoji; Nakahata, Masaaki J. Liq. Chromatogr. 1978, 1, 43-54.
(8) Hara, Shoji; Fukasaku, Noboru J. Org. Chem. 1979, 44, 893-894.
(9) Hara, Shoji J. Chromatogr. 1977, 137, 41-52.
(10) Hara, Shoji; Yamauchi, Noriko; Nakae, Chizuko; Sakai, Shinichiro Anal. Chem. 1980, 52, 33-38.

RECEIVED for review August 11, 1980. Resubmitted January 30, 1981. Accepted April 27, 1981.

Quantitative Resolution of Severely Overlapping Chromatographic Peaks

Jeffrey T. Lundeen and Richard S. Juvet, Jr.*

Department of Chemistry, Arizona State University, Tempe, Arizona 85281

A method is proposed to mathematically resolve severely overlapping chromatographic peaks. This method is successful even for the case in which the two peaks have identical retention as long as the peaks have different shape. Compounds with identical chromatographic peak shape may also be analyzed if a slight difference exists in retention. The detector response for each component at various times is fit to a second-order polynomial of the component's concentration. A series of nonlinear simultaneous equations are then solved for the concentration of each component in the mixture. Two computer simulation studies are presented.

The inability to completely separate component peaks becomes an increasingly troublesome problem as more complex systems are investigated chromatographically. The accurate, quantitative analysis of natural products, for example, in which many hundreds or thousands of components are typically present, is a challenge to the resourcefulness of the analytical chemist. The need for such analyses has led over the years to the development of high-resolution chromatographic columns, a detailed knowledge of methods for choosing the best stationary phase, and an intense study of the theory of chromatography which enables the knowledgeable chromatographer to choose the optimum experimental conditions to produce the highest separation efficiency possible for a given system. With the best of technique, however, unresolved peaks in complex mixtures commonly occur, greatly reducing the normal accuracy expected, or often completely preventing quantitative determination in the case of severely overlapping chromatographic peaks—those in which no shoulder or other indication of a mixed peak occurs.

If chromatographic peaks are partially resolved, mathematical resolution has been an alternative to "brute-force" separation attempts. Some methods of mathematical resolution now in common use may lead to enormous errors, however, and must be used with caution. Several means have been proposed to apportion the area under the curve of a mixture into its constituent components. These methods include geometric methods, curve fitting, principal component analysis, and the solution of simultaneous equations.

When the degree of peak overlap is only moderate, geometric methods such as perpendicular drop at a valley, triangulation, and extrapolation under a shoulder have been used. These are the methods most commonly used in commercial integrating systems. When the degree of overlap increases or when a large difference in peak size exists, these methods give progressively worse results or fail completely.

Curve fitting methods have been proposed assuming the peak to be a predefined shape, often Gaussian (*1-3*). It is well-known, however, that chromatographic peaks are not truly Gaussian in shape (*4-6*), and exponentially modified Gaussian (*4*, *7*), bi-Gaussian (*5*, *8*), Poisson (*5*), Gram-Charlier (*9*), and a combination of Gaussian, exponential, and hyperbolic tangent (*6*) have been applied. Grushka and co-workers (*10*, *11*) have shown that compounds with varying functional groups have different peak shapes. Moreover, as will be shown in the present work, peak shape changes with sample size. Therefore any curve fitting procedure which assumes that all components have the same peak shape (Gaussian or otherwise) or that the peak shape remains constant at different concentrations is subject to error.

Principal component analysis as well as factor analysis have also been used in studying mixtures of overlapping components (*12*). Principal component analysis assumes that the

0003-2700/81/0353-1369$01.25/0 © 1981 American Chemical Society

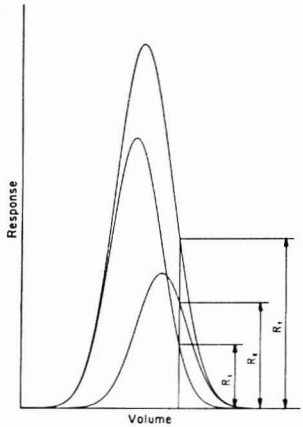


Figure 1. Computer-simulated overlapping chromatographic peaks and shoulderless composite peak. Response shown for composite peak and individual peaks at volume *i*.

curves from each of the components are the eigen vectors of a response matrix, composed of the curves of various mixtures of the two components. These eigen vectors when linearly combined will fit the curve of the mixture. The method does not assume a peak shape. It does, however, assume constant peak shape. Moreover, Macnaughtan et al. (*12*) found that a precision chromatograph, in which the flow rate and column temperature were precisely controlled, was required.

Mori (*13*) proposed the use of linear simultaneous equations in which the detector response at a particular time is assumed to vary linearly with concentration. Gourlia and Bordet (*14*) have used a method of simultaneous equations according to the proposal of Goldberg (*15*) for the analysis of overlapping components. These methods assume the detector response at any time varies linearly with concentration, which is shown in this paper not to be the case except near the peak maximum.

None of these methods are applicable when there is no resolution between the components of the mixture. Baudisch and co-workers (*16*) observed that peak fronts and half-widths do not change significantly with sample size, but the peak maxima and peak shape do vary with sample size. Thus, assuming a constant peak shape or a response at a particular time that is directly proportional to concentration is inaccurate over much of the peak. The present study is based on relating the response at a particular time to a second degree polynomial in concentration. The response from the mixture may then be expressed as a series of nonlinear simultaneous equations which may be solved to give the concentration of the components of the mixture with a high degree of accuracy even for the case in which the retention is identical for two components or for the case in which peak shapes are identical but a slight difference exists in retention.

THEORY

Figure 1 shows a computer-simulated chromatogram of a two-component mixture in which the individual component peaks are so close in retention that only a single composite peak is produced and that peak shows no shoulder. Such a system obviously cannot be analyzed by the perpendicular drop method or by the tangential approach since in these cases a valley between the peaks or, at least, a well-developed shoulder must be present on the composite peak.

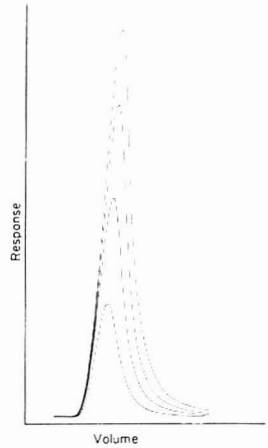


Figure 2. Analysis of 1, 2, 3, and 4% *n*-dodecane in hexane (hexane peak not shown). Column was 12% Carbowax 20M on 60/80 mesh Chromosorb WAW at 100 °C. Injection port temperature was 260 °C.

A basic assumption of the method being proposed is that the response from the mixture is equal to the sum of the responses from each component. Inherent in this statement is the assumption that the components do not interact with each other at the low concentrations of the solutes in the liquid phase. Experimental data to be published elsewhere show that this is generally a correct assumption. A data envelope containing peaks of interest is divided into evenly spaced volume increments. Volume increments are used rather than time increments since account must be made of variations in the flow rate of the mobile phase and variations in the column temperature during the period of analysis, both of which would alter the peak position. Either the flow rate and column temperature must be held constant so that the peak position does not vary or else these parameters must be accurately measured and the peak position adjusted to the position it would have had had these parameters not changed. Accurate, continuous measurement of flow rate and column temperature thus becomes an essential part of the successful use of the proposed method. The computer-assisted measurement of these parameters for liquid chromatography and for isothermal and programmed temperature gas chromatography is the subject of articles to be published elsewhere.

If R_{Ti} is the total response from the mixture at volume i and R_{1i} and R_{2i} are the responses at volume i from component 1 and 2, respectively, then

$$R_{Ti} = R_{1i} + R_{2i} \tag{1}$$

It is important to realize that generally peak shape changes with sample size as shown in Figure 2, a series of chromatograms of *n*-dodecane on a Carbowax 20M column at 100 °C. If the response at a particular volume is plotted against concentration, calibration curves similar to those shown in Figure 3 are obtained. Since peaks generally increase in asymmetry as concentration increases and a relatively sharp front with tailing is common, the leading edge of the peak does not change in proportion to sample size and calibration curves measured before the peak maximum are concave downward. Calibration curves obtained near the peak maximum are more linear. Tailing increases with sample size, and calibration curves after the peak maximum are concave upward. Asym-

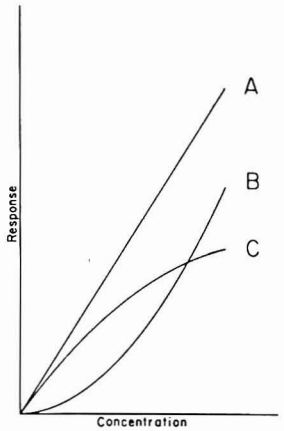


Figure 3. Calibration curves for various regions of a typical asymmetric chromatographic peak: (A) near peak maximum; (B) tailing portion of peak; (C) leading portion of peak.

etry is an indicator of nonlinear isotherms.

Let x_j be the concentration of component 1 in standard solution j and R_{1ij} be the response of component 1 at volume i and concentration x_j. The calibration curves of Figure 3 may then be represented by a second degree polynomial

$$R_{1ij} = a_i x_j^2 + b_i x_j \tag{2}$$

There is no constant term included in the polynomial because when there is no sample present, there should be no response above base line. The best least-squares estimates for a_i and b_i are

$$a_i = \frac{\sum_j x_j R_{1ij} \sum_j x_j^3 - \sum_j x_j^2 R_{1ij} \sum_j x_j^2}{(\sum_j x_j^3)^2 - \sum_j x_j^2 \sum_j x_j^4} \tag{3}$$

and

$$b_i = \frac{\sum_j x_j^2 R_{1ij} \sum_j x_j^3 - \sum_j x_j R_{1ij} \sum_j x_j^4}{(\sum_j x_j^3)^2 - \sum_j x_j^2 \sum_j x_j^4} \tag{4}$$

For each volume, i, at which calibration data have been obtained, a set of a and b values are computer derived to fit the response. At these same volume increments calibration curves are also made for component 2 and fit to the relationship

$$R_{2ij} = c_i y_j^2 + d_i y_j \tag{5}$$

where y_j is the concentration of component 2 in standard solution j and R_{2ij} is the response for this concentration at volume i. Equations similar to eq 3 and 4 can be derived for c_i and d_i, respectively.

In the mixture, the response of each component at any volume can be related to its concentration by

$$R_{1i} = a_i x^2 + b_i x \tag{6}$$

and

$$R_{2i} = c_i y^2 + d_i y \tag{7}$$

where x and y are the concentrations of components 1 and 2 in the mixture, respectively. Substituting eq 6 and 7 into eq 1 yields

$$R_{Ti} = a_i x^2 + b_i x + c_i y^2 + d_i y \tag{8}$$

The response at any particular time for the mixture is related to the amounts of each component in the mixture by the previously evaluated constants. Each equation will have some error associated with it, and it is desired to minimize these errors. Lam et al. (*17*), proposed several different error equations that can be minimized. In the present study we choose to minimize the sum of the squares of these errors

$$S = \sum_i (R_{Ti} - a_i x^2 - b_i x - c_i y^2 - d_i y)^2 \tag{9}$$

To minimize this equation, its partial deviations with respect to x and y are set equal to zero

$$\delta S/\delta x = k(x,y) =$$
$$-2x\sum_i a_i R_{Ti} - \sum_i b_i R_{Ti} + 2x^3\sum_i a_i^2 + 3x^2\sum_i a_i b_i + x\sum_i b_i^2 + 2xy^2\sum_i a_i c_i + y^2\sum_i b_i c_i + 2xy\sum_i a_i d_i + y\sum_i b_i d_i = 0 \tag{10}$$

$$\delta S/\delta y = g(x,y) =$$
$$-2y\sum_i c_i R_{Ti} - \sum_i d_i R_{Ti} + 2y^3\sum_i c_i^2 + 3y^2\sum_i c_i d_i + y\sum_i d_i^2 + 2x^2 y\sum_i a_i c_i + x^2\sum_i a_i d_i + 2xy\sum_i b_i c_i + x\sum_i b_i d_i = 0 \tag{11}$$

The problem of solving a set of equations similar to eq 8 has now been reduced to solving two nonlinear equations, eq 10 and 11, in two unknowns. These equations can be solved by Newton's method (*18*). Expanding $k(x,y)$ and $g(x,y)$ in Taylor series about some initial estimate of the concentration of each component, x_0 and y_0, and neglecting the higher order terms gives

$$k(x,y) = k(x_0,y_0) + (x - x_0)\delta k/\delta x(x_0,y_0) + (y - y_0)\delta k/\delta y(x_0,y_0) = 0 \tag{12}$$

$$g(x,y) = g(x_0,y_0) + (x - x_0)\delta g/\delta x(x_0,y_0) + (y - y_0)\delta g/\delta y(x_0,y_0) = 0 \tag{13}$$

where $k(x_0,y_0)$, $\delta k/\delta x(x_0,y_0)$, $\delta k/\delta y(x_0,y_0)$, and the corresponding g terms are the function and its partial derivatives evaluated at the point (x_0,y_0), respectively.

Solving eq 12 and 13 for $(x - x_0)$ and $(y - y_0)$ yields

$$x - x_0 = \frac{g(x_0,y_0)\delta k/\delta y(x_0,y_0) - k(x_0,y_0)\delta g/\delta y(x_0,y_0)}{\delta k/\delta x(x_0,y_0)\delta g/\delta y(x_0,y_0) - \delta g/\delta x(x_0,y_0)\delta k/\delta y(x_0,y_0)} \tag{14}$$

and

$$y - y_0 = \frac{k(x_0,y_0)\delta g/\delta x(x_0,y_0) - g(x_0,y_0)\delta k/\delta x(x_0,y_0)}{\delta k/\delta x(x_0,y_0)\delta g/\delta y(x_0,y_0) - \delta g/\delta x(x_0,y_0)\delta k/\delta y(x_0,y_0)} \tag{15}$$

Because the higher powers of the Taylor series were ignored, eq 14 and 15 will not give the values of x and y that satisfy eq 10 and 11 initially. However, by setting up iteration equations the values of x and y may be progressively improved.

$$x_{i+1} = x_i + \frac{g(x_i,y_i)\delta k/\delta y(x_i,y_i) - k(x_i,y_i)\delta g/\delta y(x_i,y_i)}{\delta k/\delta x(x_i,y_i)\delta g/\delta y(x_i,y_i) - \delta g/\delta x(x_i,y_i)\delta k/\delta y(x_i,y_i)} \tag{16}$$

$$y_{i+1} = y_i + \frac{k(x_i,y_i)\delta g/\delta x(x_i,y_i) - g(x_i,y_i)\delta k/\delta y(x_i,y_i)}{\delta k/\delta x(x_i,y_i)\delta g/\delta y(x_i,y_i) - \delta g/\delta x(x_i,y_i)\delta k/\delta y(x_i,y_i)} \tag{17}$$

The iteration process can be judged complete when

$$\frac{|x_{i+1} - x_i|}{x_i} < \epsilon \text{ and } \frac{|y_{i+1} - y_i|}{y_i} < \epsilon$$

or

$$|x_{i+1} - x_i| < \epsilon \text{ and } |y_{i+1} - y_i| < \epsilon$$

Table I. Average of Three Analyses of Two Gaussian Peaks of Equal Half-Width at Various Resolutions (1% Noise Added)

resolution	actual amt of comp 1	calcd amt of comp 1	actual amt of comp 2	calcd amt of comp 2
0.8	3.00	3.00	3.00	3.00
0.8	5.00	5.00	0.50	0.50
0.6	3.00	3.00	3.00	3.00
0.6	5.00	5.00	0.50	0.50
0.4	3.00	3.00	3.00	3.00
0.4	5.00	5.01	0.50	0.49
0.2	3.00	3.00	3.00	3.00
0.2	5.00	5.00	0.50	0.50
0.1	3.00	3.00	3.00	3.00
0.1	5.00	4.97	0.50	0.53

where ϵ is the relative or absolute acceptable correction term. For this study the second set of criteria was chosen. Each iteration involves very small amounts of computing time since only eq 16 and 17 need to be reevaluated, and all the summations need only be done once. Total data analysis time is a matter of a few seconds.

RESULTS AND DISCUSSION

The proposed method involves the solution of a set of nonlinear simultaneous equations having the general form of eq 8. These can be solved to give the concentration of each component in the mixture provided that the equations have a unique solution. This will be the case either if the peak shapes of the two components are different or if there retention times are different. A very small difference in retention is sufficient for quantitative determination. Mott and Grushka (*11*) have shown that peak shape varies with the class of a compound. If two compounds have the same functional groups, their retention times should vary. Thus one of the two conditions for the method can almost always be met.

Two computer simulation studies were run to evaluate the effect of variations in random noise, resolution, and peak shape on the accuracy of the method. Standard curves were simulated for each of the components at various concentrations by assigning them some functional form and adding 1% of full scale random noise to all points. The data envelope was adjusted to contain $\pm 3\sigma$ of each peak. The envelope was divided into 100 retention volume increments, and four standards were used to make the calibration curves. A mixture was generated by superimposing two of these standard curves, one from each component, and again adding 1% random noise.

Table I shows the results of the analysis of two curves of equal half-width at various degrees of resolution. For convenience in computer generation of these curves, a Gaussian function was chosen. A resolution of 1 indicates a 4σ separation (base line resolution) while a resolution of 0 indicates identical retention for the two peaks. A mixture containing equal amounts of both components and one in which component 2 is only 10% of component 1 were analyzed in each case. The errors do not vary significantly with resolution and even at a resolution of 0.1 excellent results are obtained. Errors are introduced by noise and increase as the noise increases. Errors diminish as the number of volume increments within the peak is increased. In the simulated studies reported here, 100 points appears to be adequate. Individual analysis errors were typically ca. 1% but ranged as high as 9% for the smaller component at the lowest resolution of 0.1. In the unrealistic case of two perfectly Gaussian curves being superimposed, no answer is calculable when the resolution is 0.0 since an infinite number of solutions to the series of simultaneous equations is generated.

Table II. Average of Three Analyses of Gaussian and Cauchy Peaks of Identical Retention and Half-Widths (1% Noise Added)

actual amt of Gaussian	calcd amt of Gaussian	actual amt of Cauchy	calcd amt of Cauchy
3.00	3.01	3.00	2.99
4.00	3.97	2.00	2.04
5.00	4.95	1.00	1.08
5.00	4.98	0.50	0.53
2.00	2.00	4.00	4.00
1.00	1.06	5.00	4.91
0.50	0.56	5.00	4.91

Quantitative determination is possible, however, even at a resolution of 0.0 when peak shapes are not identical. To demonstrate this point, a computer simulation study was made at a resolution of 0 using, for convenience, a computer-generated Gaussian peak and a Cauchy (Lorentzian) peak superimposed. Random noise at a level of 1% of full scale was added as in the previous experiment, and the results are shown in Table II. Errors for an individual analysis averaged ca. 3% but ranged as high as 16% for the smallest concentrations. When the concentration of the smaller component is only 10% of full scale at its maximum, a noise level of 1% of full scale corresponds to 10% of the smaller peak at its maximum and even more in the wings of the peak. It is not surprising that the error increases significantly as the sample peak approaches the level of background noise. If a smaller amount of noise is superimposed on the peaks, the errors diminish accordingly.

LITERATURE CITED

(1) Roberts, S. M. *Anal. Chem.* **1972**, *44*, 502–507.
(2) Scott, C. D.; Chilcote, D. D.; Pitt, W. W., Jr. *Clin. Chem. (Winston-Salem, N.C.)* **1970**, *16*, 637–642.
(3) Bartlet, J. C.; Smith, D. M. *Can. J. Chem.* **1960**, *38*, 2057–2065.
(4) Anderson, A. H.; Gibb, T. C.; Littlewood, A. B. *J. Chromatogr. Sci.* **1970**, *8*, 640–646.
(5) Grushka, E.; Myers, M. N.; Giddings, J. C. *Anal. Chem.* **1970**, *42*, 21–26.
(6) Chesler, S. N.; Cram. S. P. *Anal. Chem.* **1973**, *45*, 1354–1359.
(7) Gladney, H. M.; Dowden, B. F.; Swalen, J. D. *Anal. Chem.* **1969**, *41*, 883–888.
(8) Buys, T. S.; de Clark, K. *Anal. Chem.* **1972**, *44*, 1273–1275.
(9) Grubner, O. *Anal. Chem.* **1971**, *43*, 1934–1937.
(10) Grushka, E. *Methods Protein Sep.* **1975**, *1*, 161–192.
(11) Mott, S. D.; Grushka, E. *J. Chromatogr.* **1976**, *126*, 191–204.
(12) Macnaughtan, D., Jr.; Rogers, L. B.; Wernimont, G. *Anal. Chem.* **1972**, *44*, 1421–1427.
(13) Morl, Y. *J. Chromatogr.* **1972**, *66*, 9–18.
(14) Gourlia, J. P.; Bordet. J. *J. Chromatogr. Sci.* **1981**, *19*, 35–39.
(15) Goldberg, B. *J. Chromatogr. Sci.* **1971**, *9*, 287–292.
(16) Baudisch, J.; Papendick, H. D.; Schlöder, V. *Chromatographia* **1970**, *3*, 469–477.
(17) Lam. C. F.; Forst, A.; Bank, H. *Appl. Spectrosc.* **1979**, *33*, 273–278.
(18) Conte, S. D.; de Boor, C. "Elementary Numerical Analysis: An Algorithmic Approach", 2nd ed.; McGraw-Hill: New York, 1972, pp 84–90.

RECEIVED for review March 2, 1981. Accepted May 11, 1981. This work was supported in part by the National Science Foundation under Grant CHE 76-81583.

Effect of Detector Nonlinearity on the Height, Area, Width, and Moments of Peaks in Liquid Chromatography with Absorbance Detectors

Lynda M. McDowell, William E. Barber, and Peter W. Carr*

Department of Chemistry, Smith & Kolthoff Halls, University of Minnesota, Minneapolis, Minnesota 55455

The effect of nonlinear absorbance detectors on chromatographic peak height, area, centroid, and second moment is experimentally investigated. In accord with theory developed previously, those properties related to the even moments, such as the area and peak width, are most strongly influenced by detector nonlinearity, whereas odd moments of symmetric (Gaussian) peaks are not altered. This is in contrast to the behavior of the effect of nonlinear isotherms which shift the position of the peak centroid as well as alter peak symmetry. We have shown that even with relatively narrow spectral slit widths (2 nm) absorbance detectors can be quite nonlinear even at low concentration (1 mM) and at absorbances considerably below the stray radiation limits of the instrument.

In a previous paper (*1*) we have shown that nonlinear detectors can have a substantial effect on the area and *even* central moments of Gaussian chromatographic peaks. It was also shown that the *odd* central moments (peak position, skew) of *symmetric* peaks are not altered by detector nonlinearity. These "chromatographic" characteristics of the effect of a nonlinear detector on a peak contrast sharply with the effect of a nonlinear isotherm. For example, an isotherm of the Langmuir type causes the peak centroid to shift to longer time and the peak to become increasingly tailed as the sample concentration is increased. A very general model of peak linearity based on the use of an infinite power series relationship between the sample concentration in the detector and the detector response was employed in the previous paper. The purpose of the present work is to demonstrate that such effects are indeed observable under reasonable chromatographic conditions. We chose to investigate the effect of absorbance detectors of the type used in liquid chromatography based on the report of Stewart (*2*) whose calculations indicate that such detectors can be rather nonlinear even at low absorbances if the slit widths are too wide relative to the width of the spectral band. Many other types of detectors, e.g., the fluorescence (*3*) and refractive index devices (*4*) are known to be nonlinear but are not as commonly used as is the absorbance detector.

There are a number of potential sources of nonlinearity in photometric detectors. Assuming that chemical nonlinearity due to solution equilibria (dimerization, etc.) as well as nonlinear column effects (sample decomposition, irreversible adsorption, nonlinear isotherm, etc.) can be dismissed, then the chief sources of nonlinearity in the context of LC detectors will be stray light and lack of source monochromaticity (*2*). Of course, the electronics per se may be nonlinear, for example, amplifiers may saturate and logarithmic conversion circuits may not function perfectly. Indeed the effect of photoamplifier bias will act to cause nonlinearity in the same way as stray light. Although it is possible to arrive at a closed form expression for the effect of stray radiation on detector nonlinearity, the relationship in the case of polychromatic radiation is not available in closed form. In this instance the relationship between the observed absorbance and the sample concentration will depend upon the wavelength, the spectrometer slit function, as well as the shape, width and position of the absorption spectrum of the sample. Nonlinearity will be greatest when the slits are wide and when the solution absorbance is a strong function of wavelength, i.e., when $dA/d\lambda$ is large. It is also evident that no matter how polychromatic the radiation is, the limiting value of the absorbance (at infinite sample concentration) will be set by the stray radiation and photoamplifier bias currents. Thus the effects of stray radiation and polychromatic radiation must be considered simultaneously.

Due to the above complications we decided not to generate theoretical calibration curves such as those shown by Stewart (*2*). Rather an experimental calibration curve was generated and then the peak moments were computed by assuming that the *concentration* profile at the detector was Gaussian.

EXPERIMENTAL SECTION

Instrumentation. All experiments were carried out with a Perkin-Elmer (Norwalk, CT) Series 3B liquid chromatograph operated in the isocratic mode (80% acetonitrile and 20% water by volume) at a flow rate of 1.0 mL/min. A Perkin-Elmer LC-55 variable-wavelength detector was used for all results reported here. This instrument has a bandwidth of 2 nm and a cell path length of 6 mm. The stray light specification of the instrument is stated to be 0.1% at an absorbance of 220 nm when used with a conventional cuvette and not an HPLC flow cell. The manufacturer does not provide the stray light figure of the flow cell plus the detector. All measurements were carried out at 212 nm (see Figure 1). The column employed in this work was 12.5 cm long × 4.6 mm in diameter and was packed with 10 μm Lichrosorb RP-18. Samples were introduced to the column via a Rheodyne 7125 sample injection valve fitted with a 20-μL loop. The volume of sample was defined by the loop size.

The signal was recorded simultaneously on a 10-mV recorder and transmitted to a data acquisition system comprised of a high-speed analog to digital converter and laboratory computer system (Data General Corp., NOVA II). In all the experiments reported here care was taken to ensure that no component of the detection system or the data system was saturated; thus the nonlinear effects reported here are spectroscopic in origin and not electronic. It should be noted that the amplifier bias currents are totally negligible with this detector; i.e., with the light source totally blocked the apparent absorbance is much greater than the maximum values observed with a sample in place.

Reagents. The sample in all cases was biphenyl (Aldrich, Milwaukee, WI) and was used without further purification. Samples were dissolved in the mobile phase. Water was purified by use of a Continental demineralization system, it was then passed over a column of XAD-2 resin (Rohm & Haas, Philadelphia, PA) to remove trace organics and passed through a 0.5 μm Millipore filter prior to use. HPLC grade acetonitrile (Mallinckrodt, Paris, KY) was used in all experiments.

Computations. All data were obtained at a rate of 150 ms per point. Each concentration was run at least three times. The various concentrations and individual runs at each concentration were run in random order. The moments reported here were

0003-2700/81/0353-1373$01.25/0 © 1981 American Chemical Society

Table I. Effect of Sample Concentration on Measured Peak Characteristics

concn,[a] mM	peak height, A	peak area, $A \cdot s$	centroid (m_1), s	second central moment ($\bar{m}_2$), s^2
0.1	0.187 ± 0.02	1.580 ± 0.02	202.9 ± 0.2	11.8 ± 0.6
0.5	0.810 ± 0.01	6.912 ± 0.1	202.8 ± 0.2	12.0 ± 0.1
1.0	1.39 ± 0.02	12.08 ± 0.1	202.7 ± 0.2	12.7 ± 0.08
2.5	2.46 ± 0.02	24.98 ± 0.6	202.4 ± 0.4	14.2 ± 0.5
5.0	2.62 ± 0.04	33.43 ± 0.6	202.9 ± 0.3	19.1 ± 0.8
10.0	2.66 ± 0.005	40.38 ± 0.4	203.0 ± 0.4	25.5 ± 0.7
25.0	2.68 ± 0.03	49.34 ± 0.9	203.9 ± 0.5	39.6 ± 1.9

[a] Concentration injected.

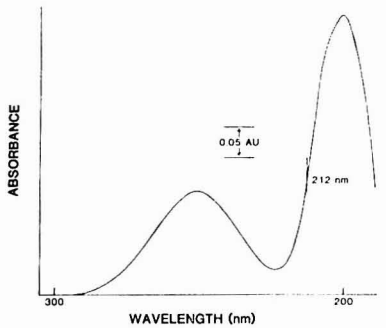


Figure 1. UV spectrum of biphenyl. Conditions: 0.01 mM solution in 80:20 acetonitrile/water. Note the position of the 212-nm wavelength on the spectrum.

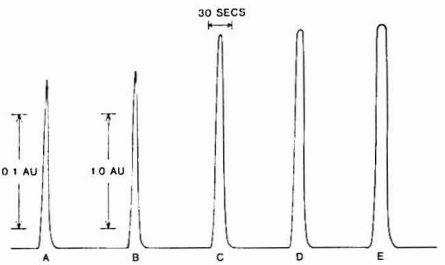


Figure 2. Experimental chromatograms: curve A, 0.1 mM; curve B, 1.0 mM; curve C, 2.5 mM; curve D, 10 mM; curve E, 25 mM. All conditions are described in the text. Note the changes in absorbance scales at 0.1 and 1.0 mM.

obtained by simple statistical summation techniques. Peak height was computed by fitting the topmost 15 data points to the equation of a parabola via Gram polynomials as described by Rogers (5). We also attempted to avoid the enormous problems caused by noise in the measurement of the higher central moments (6) by use of the Yau algorithm for asymmetric peaks (7). We found, as anticipated, that this approach failed because of the lack of fit of the peak shapes (see Figure 2) to the exponentially modified Gaussian model which is the basis of Yau's approach. Thus we are not able to report the third and fourth central moments due to their extreme imprecision.

RESULTS

A spectrum of biphenyl is shown in Figure 1. All chromatographic results were obtained on the shoulder at 212 nm in order to maximize the effect of nonlinearity. The calibration curve (Figure 3) is evidently extremely nonlinear at concentrations in excess of 1.0 mM. Note that the absorbance is only slightly in excess of 1.4 when a noticeable nonlinearity occurs in the calibration curve. A theoretical calibration curve can be computed on the basis of eq 1 which describes the effect

$$A_{obsd} = -\log \frac{10^{-A} + \theta}{1 + \theta} \qquad (1)$$

of stray monochromatic radiation. In this equation, A is the true absorbance of the sample, θ is the ratio of the intensity of the stray radiation to the intensity of the *monochromatic* radiation incident upon the sample cell, and A_{obsd} is that which would be measured by the electronics in the presence of the stray radiation. The fraction θ is easily calculated from the limiting value of the observed absorbance at very high concentration. For our experimental system θ calculates to be 2.1×10^{-3}. A theoretical calibration curve (not shown) based on eq 1 and the experimental estimate of the stray light indicate that stray light is not the sole source of nonlinearity, i.e., nonmonochromatic light is acting to decrease the observed absorbance below that expected based on the stray light effect.

A series of chromatographic peaks obtained at various concentrations of samples but otherwise under identical conditions are shown in Figure 2. Peak broadening is evident at concentrations in excess of 2.5 mM. It is important to note that peak symmetry is not significantly altered until the sample concentration exceeds at least 10 mM. At a concentration of 25 mM a slight but definite tail is observed in the peak. This indicates that the partition isotherm is linear until rather high concentrations (see below).

The experimental peak height, area, centroid, and second central moments are given in Table I along with estimates of their standard deviations. The response in terms of peak height is essentially constant from 2.5 mM upward but the peak area continues to increase because the peaks become progressively wider. This is in accord with the general results of the previous work (1) where it was shown that the relative change in the peak area was less sensitive to detector nonlinearity than is the change in peak height.

The position of the peak centroid (m_1) is remarkably reproducible in view of the fact that all samples were run in random order. As predicted by the previous work, the centroid of a perfectly symmetric peak is not altered by detector nonlinearity. The position of the centroid is essentially invariant from 0.1 to 10 mM sample concentration.

It could be argued that the calibration curve nonlinearity shown in Figure 3 is not due to the detector response but rather to a nonlinear chromatographic process, e.g., a nonlinear isotherm. This, however, is not the case since a direct and inescapable consequence of a nonlinear isotherm is first to distort peak symmetry and then broaden the peak and shift the position of the peak centroid (8). Inspection of the chromatograms of Figure 2 provides no evidence whatsoever of alteration of peak symmetry at sample concentrations less than 25 mM whereas the detector response is essentially flat (saturated) just above 2.5 mM.

It might be argued that the nonlinearity of the calibration curve is related to irreversible adsorption of part of the sample. This position is also untenable because this effect would be

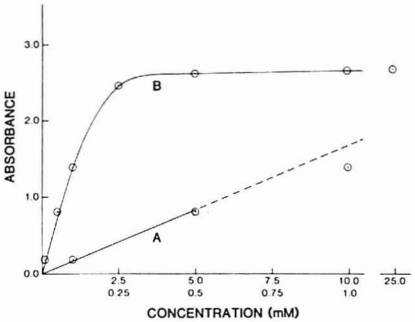


Figure 3. Experimental calibration curve for biphenyl: (curve A) expanded scale to show linearity at low concentration; (curve B) full data range. All conditions are described in the text.

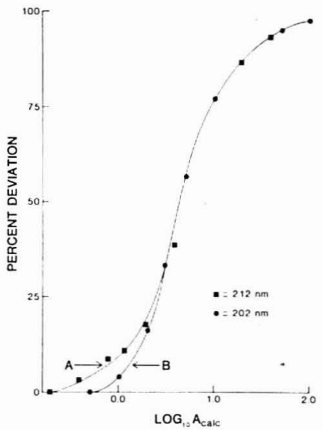


Figure 4. Results of the open tube experiment. All conditions are described in the text. Curve A (■) 212 nm (% deviation = $(A_{obsd} - 3.90C)/3.90C$). Curve B (●) 202 nm (% deviation = $(A_{obsd} - 10.68C)/10.68C$).

most serious at *low* concentration whereas our calibration curve is linear at low concentrations and passes through the origin. Secondly, biphenyl is an ideal sample for reversed-phase chromatography on an octadecylsilane bonded phase; it is totally aromatic and contains no heteroatoms which could interact strongly with bare silanol groups. Finally, the fact that the area is less effected by the calibration curve than is the height, as predicted by previous work (*1*), argues against the loss of a fraction of the sample which is not eluted from the column. If a given amount of material does not elute and the remainder elutes via a linear isotherm, then peak area and height would be equally altered and would be proportional to one another.

The fact that the effects reported here are not chromatographic in origin but are due to the detector was proved by replacing the column with a short length of HPLC tubing. The maximum absorbance of a series of dilute solution of biphenyl (0.05–10 mM) was recorded. These results are summarized in Figure 4. The percent deviation of the response from linearity was calculated as $100(A_{obsd} - A_{calcd})/A_{calcd}$ and plotted vs. the decadic logarithm of the calculated absorbance. The calculated absorbance was estimated from the known concentration and the molar absorptivity measured at a concentration of 0.05 mM. This figure shows a clear monotonic increasingly negative deviation from linearity. One should note that the detector is linear to higher absorbances at 202 nm than at 212 nm which is an expected result due to the contribution of the nonmonochromaticity to detector nonlinearity when one works on a shoulder of a spectral peak.

Table II. Calculated Values of Peak Characteristics as a Function of Sample Concentration

concn, mM	A_{max},[a] A	area,[b] $A \cdot s$	second central moment,[c] s^2
0.1	0.183	1.40	11.9
0.5	0.796	7.01	11.9
1.0	1.35	13.8	12.6
2.5	2.64	25.3	14.8
5.0	3.05	34.6	17.9
10.0	3.19	40.7	22.6
25.0	3.63	47.7	29.4

[a] Computed from eq 5. [b] Computed from eq 9. [c] Computed from eq 10.

The above results indicate that the partition isotherm is quite linear up to 10 mM. The barely significant increase in the position of the centroid at a sample concentration of 25 mM is in agreement with the development of a slight but definite tail in the peak (see Figure 2, curve E).

It is clear that the pumping system is much more reproducible than is our ability to inject and quantitate the size of the signal. The precision of m_1 at a given concentration, which as pointed out above were not run sequentially, indicates that the long term average flow rate is constant to approximately ±0.2%. The *relative* standard deviation in peak height decreases with sample concentration. This is symptomatic of noise limitations. In contrast the relative standard deviation in area is approximately constant.

The measurement precision is quite good enough to allow reproducible estimation of the second central moment. Table I indicates that the second central moment is constant where the detector is linear (0.1, 0.5 mM) but increases significantly as soon as a *negative* deviation from linearity occurs (1 mM). This is also in qualitative accord with our previous results (*1*). Although we calculated the third and fourth central moments from our data, the reproducibility was extremely poor and the slight trend in $\overline{m_4}$ predicted by the general model of the effect of nonlinear detectors could not be verified.

Table II shows the results of some predictions of peak height, area, and second central moment based on the assumption that the actual *concentration profile* in the detector is Gaussian at all concentrations. If one assumes that at the lowest concentrations used the detector is linear (see Figure 3, curve A) and that the peak is Gaussian one arrives at the following relationships:

$$A_{max} = \epsilon b C^\circ V^\circ / \sqrt{2\pi}\sigma_v \tag{2}$$

$$\int_0^\infty A \, dt = \epsilon b C^\circ V^\circ / F \tag{3}$$

where ϵ is the molar absorptivity, b the path ceil length, C° the injected concentration, V° the volume injected, σ_v the square root of the variance due to the column per se (in volume units), and F the mobile phase flow rate. Chromatographic theory indicates for a pure Gaussian peak

$$\overline{m_2} \text{ (time units)} = (\sigma_v/F)^2 \tag{4}$$

Thus for a Gaussian peak the above equations lead to

$$A_{max} = \int_0^\infty A \, dt / (2\pi\overline{m_2})^{1/2} \tag{5}$$

Values for A_{max} were computed from the measured peak area and second central moment at each concentration and are summarized in Table II. The first two entries (at 0.1 and 0.5 mM) are in good agreement with measured peak absorbance values and areas. Note that the second central moment at these lowest concentrations is constant and corresponds to a σ_v of 57.5 μL. This agreement verifies that the peak is essentially Gaussian. The calculated value of A_{max} at 1.0 mM also agrees with the measured value but only if one uses the *measured second central moment*, $\overline{m_2}$, which is definitely larger than the value at the lower concentrations. Above 1.0 mM the agreement between calculated and measured values of the absorbance at the peak maximum worsens progressively as the signal peaks become less Gaussian (see Figure 2).

On the basis of a value of 57.5 μL for σ_v and a 20-μL sample volume, one calculates from eq 6 that any sample will be

$$C_{max} = C^\circ V^\circ / \sqrt{2\pi}\sigma_v \tag{6}$$

diluted to 0.138 times its initial concentration upon arrival at the detector. The calibration curve shown in Figure 3 can now be transformed to a plot of absorbance vs. the concentration of solute in the detector cell. This plot constitutes a graphical representation of the functional relationship between A and C as embodied in eq 7.

$$A = f(C) \tag{7}$$

The area and second central moment can be calculated assuming that the concentration as a function of time in the detector is Gaussian, i.e.

$$C(t) = 0.138C^\circ \exp[(t - m_1)^2/2\sigma_t^2] \tag{8}$$

where σ_t^2 is the variance due to the column in time units. This leads to the results

$$\text{area} = \int_0^\infty A(t)\,dt = \int_0^\infty f(C(t))\,dt \tag{9}$$

$$\overline{m_2} = \int_0^\infty A(t)(t - m_1)^2\,dt = \int_0^\infty f(C(t))(t - m_1)^2\,dt \tag{10}$$

In the data reported in Table II the above integrals were carried out by use of a 16 point Gauss–Legendre integration technique (*9*). Values of the absorbance were estimated based on a piecewise linear interpolation between each data point. Values of σ_t were obtained from eq 11. The greatest discrepancy (14%) between a calculated and measured area occurs at a concentration of 10 mM. The average absolute deviation is 5%.

$$\sigma_t = \sigma_v/F \tag{11}$$

The calculated second central moments are also shown in Table II. Agreement with experiments is very good except for the highest concentration where the discrepancy is nearly 25%. We believe that this may be due to the tail which starts to develop at this very high (25 mM) concentration.

We believe that the experimental work presented here indicates that chromatographic detectors can produce quite nonlinear calibration curves. Such nonlinearity leads primarily to distortion of the even central moments of symmetric peaks. Clearly detector nonlinearity is not an insurmountable analytical problem since one can rerun the sample after dilution to move to a linear part of the curve. Detector nonlinearity evidently has some impact on the experimental measurement of the resolution of overlapping peaks and in the area of steric exclusion chromatography can lead to erroneous estimates of molecular weight distributions. Obviously any attempt to build algorithms into chromatographic data systems to correct for nonlinear detectors must take into consideration the fact that nonlinearity will alter the peak's shape as well as its area and height. Finally, it should be noted that the detector used in this work has a spectral bandwidth of only 2 nm. Many other commercial variable wavelength LC detectors have bandwidths of 5 to 20 nm and therefore can potentially be nonlinear at lower absorbances than reported in this work.

LITERATURE CITED

(1) Carr, P. W. *Anal. Chem.* **1980**, *52*, 1746–1750.
(2) Stewart, J. E. *J. Chromatogr.* **1979**, *174*, 283–290.
(3) Hercules, D. M. *Anal. Chem.* **1966**, *38* (12), 29A–43A.
(4) Meggs, R. J. In "Practical High Performance Liquid Chromatography"; Simpson, C. F., Ed.; Heyden: London, 1976; p 279.
(5) Pauls, R. E.; Rogers, L. B. *Sep. Sci.* **1977**, *12*, 395–413.
(6) Chesler, S. N.; Cram, S. P. *Anal. Chem.* **1971**, *43*, 1922–1933.
(7) Yau, W. W. *Anal. Chem.* **1977**, *49*, 395–398.
(8) Littlewood, A. B. "Gas Chromatography, Principles, Techniques and Applications"; 2nd ed.; Academic Press: New York, 1970; p 12.
(9) Atkinson, K. E. "An Introduction to Numerical Analysis"; Wiley: New York, 1978; p 231.

RECEIVED for review December 9, 1980. Accepted April 23, 1981. This work was supported in part by a grant from the National Institute of Occupational Safety and Health (5 R01 OH00876-02). Summer support for W.E.B. from the Uniroyal Corp. is gratefully acknowledged.

Determination of Cyanide or Thiocyanate at Trace Levels by Derivatization and Gas Chromatography with Flame Thermionic Detection

Koichi Funazo, Minoru Tanaka, and Toshiyuki Shono*

Department of Applied Chemistry, Faculty of Engineering, Osaka University, Yamada-oka, Suita, Osaka 565, Japan

A new gas chromatographic method is described for the determination of cyanide or thiocyanate in aqueous matrices. Cyanide or thiocyanate is quantitatively methylated with dimethyl sulfate to form acetonitrile or methyl thiocyanate, respectively. The resulting acetonitrile or methyl thiocyanate is extracted into ethyl acetate and determined by gas chromatography with flame thermionic detection. Good linear calibration curves are obtained in the ranges of 0.05–1.00 μg CN^-/mL and 0.25–10.0 μg SCN^-/mL which are low enough to detect these anions in environmental and biological matrices. This method is not affected by inorganic anions which commonly coexist with cyanide or thiocyanate, except for ferricyanide and ferrocyanide anions which positively interfere with the cyanide analysis. Cyanide in wastewater samples was determined by both the gas chromatographic and the colorimetric methods. Good agreement was found between the methods. The recoveries of cyanide and thiocyanate added to human urine samples are over 90%.

Cyanide (CN^-) has been known for its extreme toxicity to human beings, animals, and aquatic life. On the other hand, thiocyanate (SCN^-) plays a biologically important role in living organisms. Therefore, the determination of these anions in various matrices is of great importance. A large number of reports have been published for the determination of CN^- (*1–3*) and SCN^- (*4, 5*). The recommended standard method for the determination of CN^- (*6*) is the pyridine–pyrazolone method developed by Epstein (*7*), which is a modification of the pyridine–benzidine method reported by Aldridge (*8*). The pyridine–benzidine method can also be used for the determination of SCN^-. For the determination of SCN^-, several colorimetric methods have also been reported which are based on the formation of a red-brown complex with iron(III) cation (*6, 9*) and a green complex with copper(II) cation and pyridine (*10*). Electrochemical methods based on the use of ion-selective electrodes are also used for the determination of CN^- or SCN^-. However, they are subject to several interferences.

Much of analytical work has been carried out which involves the use of analytical derivatization prior to gas chromatographic analysis—derivatization gas chromatography. Several reviews have been published for derivatization gas chromatography (*11–14*). We have investigated the determination of inorganic anions by using derivatization gas chromatography (*15, 16*). Derivatization gas chromatographic methods for the determination of CN^- and/or SCN^- (*17–20*) have been reported. In these methods, CN^- and/or SCN^- are derivatized to cyanogen halide by bromine or chloramine T, and the resulting cyanogen halide is subsequently determined by gas chromatography with electron capture detection. Total amount of CN^- plus SCN^- can be determined by using this gas chromatographic method.

This paper describes a new method to determine CN^- or SCN^- by derivatization gas chromatography. In this method, CN^- or SCN^- was methylated with dimethyl sulfate to form acetonitrile or methyl thiocyanate, respectively. The reactions are formulated as

$$CN^- + (CH_3O)_2SO_2 \rightarrow CH_3CN + CH_3OSO_3^- \quad (1)$$

$$SCN^- + (CH_3O)_2SO_2 \rightarrow CH_3SCN + CH_3OSO_3^- \quad (2)$$

The resulting acetonitrile or methyl thiocyanate was determined sensitively by gas chromatography with a flame thermionic detector (FTD).

EXPERIMENTAL SECTION

Apparatus. A Shimadzu GC-6AM gas chromatograph equipped with a FTD (Kyoto, Japan) was used. A glass column (1 m × 3 mm i.d.) was packed with 80–100 mesh Porapak Q. Nitrogen was used as the carrier gas at a constant flow rate of 45 mL/min. The detector and injection port temperatures were kept at 250 °C. The column temperature was maintained at 155 °C for the determination of acetonitrile derivatized from CN^- and at 205 °C for that of methyl thiocyanate from SCN^-. The peak areas were measured by a digital integrator (Shimadzu Chromatopac-E1A, Kyoto, Japan).

Reagents. All reagents were of analytical reagent grade and were used without further purification unless otherwise stated. Dimethyl sulfate used was a commercial grade reagent (98% up) purchased from Tokyo Kasei Kogyo Co. Ltd. (Tokyo, Japan). Deionized water was distilled before use.

Procedure. The recommended procedure for the determination of CN^- or SCN^- was as follows. Dimethyl sulfate (0.1 mL) was added to a 1.0-mL aliquot of neutral aqueous sample in a reaction vessel (ca. 10 mL) with a glass stopper. When CN^- was methylated in this case, 2.0 N KOH aqueous solution (0.1 mL) was added before adding dimethyl sulfate. On the other hand, in the case of methylation of CN^- in wastewater samples, dimethyl sulfate (0.1 mL) was added to a 1.1-mL aliquot of wastewater sample with no addition of 2.0 N KOH aqueous solution, because the basicity of wastewater samples was adjusted to the optimum one (see "wastewater" section). Then the vessel was shaken for 20 min in an incubator controlled at 70 °C. At the end of the reaction period, 1.0 mL of ethyl acetate solution containing an internal standard (4.0×10^{-6} M) was added to the cooled reaction solution. As an internal standard, propionitrile was used in the analysis of CN^-; ethyl thiocyanate was used in the analysis of SCN^-. Then the derivatized product, "acetonitrile or methyl thiocyanate", was extracted by shaking for 10 min at room temperature of 18 °C, and the organic layer was separated from the aqueous layer. An aliquot (1.0 μL) of the organic layer was injected into the gas chromatograph and derivatized acetonitrile or methyl thiocyanate was determined with a FTD.

Samples. *Wastewater.* The samples were collected from plating and metal refining factories. Instantly after collection, 10 mL of 2.0 N KOH aqueous solution was added to 100 mL of each water sample to avoid the evolution of hydrogen cyanide and also to obtain the optimum basicity for methylation. The samples were filtered to remove turbidity. By both the colorimetric method (*6*) and this gas chromatographic method, the filtered water samples were analyzed directly and after distillation of hydrogen cyanide. The distillation was carried out according to the standard method (*6*) in order to reduce interferences.

Human Urine. The samples were diluted 5-fold with water and were directly used for analysis, as soon as collected.

RESULTS AND DISCUSSION

Optimum Derivatization Conditions. For the optimum derivatization conditions, the overall yields (= derivatization yield × extractability) of acetonitrile and methyl thiocyanate were examined in various cases. The overall yield of aceto-

0003-2700/81/0353-1377$01.25/0 © 1981 American Chemical Society

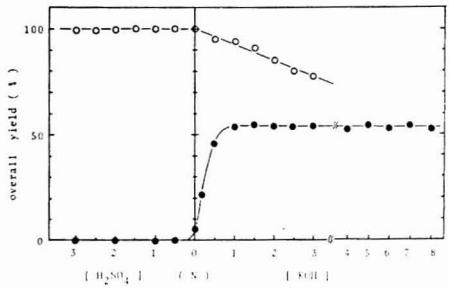


Figure 1. Effect of normality of added acid or base on overall yields of acetonitrile (●, 1.0 μg/mL) and methyl thiocyanate (○, 10.0 μg/mL).

nitrile was estimated as follows. The peak area of acetonitrile extracted into ethyl acetate from the reaction mixture was compared with that of the acetonitrile standard solution. This standard solution contains acetonitrile in ethyl acetate at just the same molar concentration as that of CN^- in the aqueous solution used for derivatization. Similarly, the overall yield of methyl thiocyanate was also estimated from the peak area of methyl thiocyanate.

In order to ascertain the optimum derivatization conditions, we examined the effects of pH, reaction temperature, and reaction time on the overall yield. In this series of studies to find the optimum derivatization conditions, 1.0 μg CN^-/mL and 10.0 μg SCN^-/mL aqueous solutions were used as the samples. The effect of pH was examined as follows. To 1.0 mL of each aqueous solution of CN^- and SCN^-, KOH or H_2SO_4 aqueous solution (0.1 mL) with different concentrations was added before adding dimethyl sulfate. Then the methylation reaction was carried out by shaking at 70 °C for 20 min. After extraction with ethyl acetate, the overall yield was estimated by the method mentioned above. Figure 1 shows the effect of KOH and H_2SO_4 concentrations added to the samples on the overall yields of acetonitrile and methyl thiocyanate. By the addition of H_2SO_4 (0.5–3.0 N), the yield of acetonitrile was reduced down to zero, whereas the derivatization of SCN^- proceeded quantitatively. In the case of KOH addition, the yield of methyl thiocyanate decreases linearly with an increase in KOH concentration, while the yield of acetonitrile increases and reaches a constant value of 55% at the KOH concentration of about 1.0 N. From these results, a 2.0 N KOH solution was added to the sample before adding dimethyl sulfate in the CN^- analysis. On the other hand, dimethyl sulfate was directly added to the sample in the analysis of SCN^-.

The effects of reaction temperature on the overall yields of acetonitrile and methyl thiocyanate were investigated. The yields do not vary between reaction temperatures of 20–70 °C. However, when methylation was carried out at lower temperatures than 50 °C, a broad peak with a longer retention time appeared on the gas chromatogram. This peak always appeared by the injection of dimethyl sulfate. To avoid troubles from dimethyl sulfate fluctuating the base line and deteriorating the column, we fixed the reaction temperature at 70 °C.

The effects of reaction time were also examined. The term "reaction time" means the period for which the reaction solution was shaken in an incubator controlled at 70 °C. In both cases, methylation completes within about 10 min. The reaction time, therefore, was fixed at 20 min.

Derivatization Yields and Calibration Curves. Table I shows the results of derivatization of CN^- and SCN^- under the optimum conditions described in the Experimental Section. The direct injection of the reaction mixtures into the gas chromatograph gave rise to the great fluctuating base line. Therefore, an appropriate pretreatment, liquid–liquid extraction, distillation, or column cleanup was inevitable. The distillation and column cleanup procedures did not bring reproducible results and were, moreover, time-consuming. It was very difficult to extract the resulting acetonitrile from the aqueous mixture into organic solvents. Of common organic solvents tested, ethyl acetate gave the highest extractability (ca. 60%). Acetonitrile was not extracted quantitatively. However, this extraction procedure gave the reproducible results as in Table I provided that it was performed under the controlled conditions where the volumes of ethyl acetate and reaction mixture and the extraction temperature were kept constant. The corrected derivatization yields for extraction loss were calculated by using the extractability and are listed in Table I together with the overall yields. The corrected derivatization yields show that CN^- and SCN^- are quantitatively methylated.

Table I. Derivatization Yields and Extraction Loss[a]

	CN^- [b] (%)	SCN^- [b] (%)
overall yield	55.5 ± 1.5	99.7 ± 4.2
extractability of CH_3CN or CH_3SCN [b,c]	58.9 ± 1.9	99.5 ± 2.6
corrected derivatization yield	94.5 ± 2.2	100.2 ± 4.4

[a] Mean ± standard deviation of five replicate analyses is shown. [b] The concentration of CN^- or SCN^- and that of CH_3CN or CH_3SCN are 2.0×10^{-4} M. [c] In the extraction of CH_3CN, the volumes of water and organic layers are 1.1 and 1.0 mL, respectively, whereas in the case of CH_3SCN, the volumes of both layers are 1.0 mL.

A calibration curve was constructed by plotting the peak area of methylated product vs. the concentration of CN^- or SCN^-. A good linear relationship is obtained in the concentration range of 0.05–1.00 μg CN^-/mL or 0.25–10.0 μg SCN^-/mL. According to the extractabilities shown in Table I, a two times better detection limit for SCN^- than that for CN^- should be expected. Actually, the detection limit (the concentration of anion solution which gives a signal twice that of the average background noise) is 0.01 μg CN^-/mL (= 3.85×10^{-1} μM) or 0.1 μg SCN^-/mL (= 1.72 μM). This phenomenon can be explained as follows: the response of acetonitrile to a FTD is about 2.5 times great as that of methyl thiocyanate, and the background noise is higher in the case of methyl thiocyanate chromatographed at 205 °C than in the case of acetonitrile at 155 °C. These determination levels and detection limits are low enough to determine these anions in various environmental and biological matrices.

Interference Study. The interferences of some anions on the determination of CN^- and SCN^- are shown in Table II. The anions selected are those normally found in environmental and biological samples. The concentrations of anions added are much higher than those in environmental and biological samples. These anions do not appear to interfere with this analysis except for ferricyanide and ferrocyanide anions which positively interfere with the CN^- analysis.

Applications. A few wastewater samples were analyzed both by this gas chromatographic method and by the pyridine–pyrazolone method (6), which has been used widely as the standard method for the determination of CN^-. These wastewater samples were collected from plating and metal refining factories and made alkaline (see Experimental Section). The samples were filtered and distilled before analysis. The distillation was performed to liberate CN^- from tightly bonded metal cyanide complex in the sample. Therefore, total CN^- in the sample was determined by using the distilled sample and free CN^- was done by analyzing directly. The

Table II. Interference Study

anion[a]	added as	peak area[b] acetonitrile	peak area[b] methyl thiocyanate
standard		100.0 ± 3.0	100.0 ± 2.5
SCN^-	KSCN	101.7 ± 1.8	
CN^-	KCN		99.7 ± 1.5
F^-	NaF	101.7 ± 5.1	100.6 ± 1.5
Cl^-	NaCl	99.0 ± 4.7	99.1 ± 1.2
Br^-	NaBr	98.5 ± 2.6	99.1 ± 1.0
I^-	NaI	101.1 ± 2.9	101.4 ± 2.1
CH_3COO^-	CH_3COOK	98.9 ± 2.2	98.6 ± 1.4
NO_2^-	$NaNO_2$	102.4 ± 2.1	100.1 ± 1.5
S^{2-}	Na_2S	102.2 ± 3.6	102.2 ± 1.9
NO_3^-	$NaNO_3$	100.7 ± 4.6	99.7 ± 2.8
CO_3^{2-}	Na_2CO_3	101.2 ± 3.5	100.6 ± 3.2
$H_2PO_4^-$	KH_2PO_4	100.8 ± 2.3	99.9 ± 1.5
$Fe(CN)_6^{3-}$	$K_3Fe(CN)_6$	114.0 ± 2.7	99.3 ± 4.4
$Fe(CN)_6^{4-}$	$K_4Fe(CN)_6$	109.9 ± 1.7	100.6 ± 2.8

[a] Concentration of anions added is 100 μg/mL. CN^- and SCN^- concentrations are 1.0 μg CN^-/mL and 10.0 μg SCN^-/mL. [b] Mean ± standard deviation of four replicate analyses is shown.

Table III. Intercomparison Study for the Determination of CN^-

wastewater sample[a]	GC-method[b] (μg CN^-/mL)	colorimetric method[c] (μg CN^-/mL)
A[d]	0.29 ± 0.01	0.30
A	0.28 ± 0.02	0.29
B[d]	0.20 ± 0.01	0.20
B	0.20 ± 0.02	0.21
C[d]	0.05 ± <0.005	0.04
C	0.02	N.D.[e]

[a] Sample A was collected from a metal refinery, and B and C were from plating factories. [b] Mean ± standard deviation of five replicate analyses is shown. [b] Pyridine–pyrazolone method. [d] The samples were distilled before analysis and others were analyzed directly. [e] N.D. = not detected.

results thus obtained are shown in Table III, and Figure 2a shows the gas chromatogram of derivatized CN^- in wastewater sample A (analyzed without distillation). The values measured by the two methods agree well. The relative standard deviations of the gas chromatographic analyses are less than 10%. These samples were filtered to remove the turbidity. This pretreatment is inevitably necessary for the colorimetric method but unnecessary for the gas chromatographic method. The CN^- concentration values by the gas chromatographic method are the same within the experimental errors whether or not this pretreatment is performed. In these analyses, the wastewater samples did not contain acetonitrile. Acetonitrile can accidentally be present in wastewater, because it is a common solvent. In that case, however, the presence of acetonitrile should be excluded by running a chromatogram of an ethyl acetate extract of wastewater, without addition of dimethyl sulfate (i.e., blank).

In the determination of SCN^-, the method based on the formation of iron thiocyanate complex is used widely as a standard method (6). However, this method is not sufficiently sensitive to determine SCN^- in human urine samples. Therefore, the recovery test for SCN^- added to human urine samples was performed by this gas chromatographic method. The results are shown in Table IV, and the gas chromatogram obtained for the urine sample (no. 1) is given in Figure 2b. The recoveries of SCN^- are all over 90%. Table IV also shows that the relative standard deviations are less than 4%.

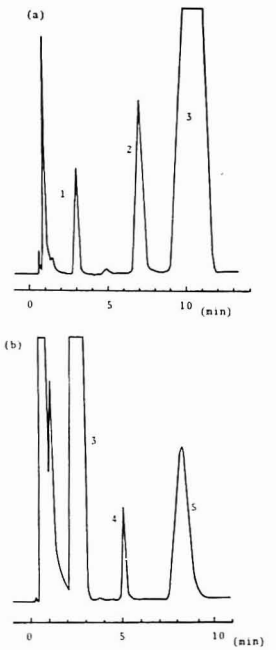


Figure 2. (a) Gas chromatogram obtained in the analysis of wastewater sample (A). (b) Gas chromatogram obtained in the analysis of human urine sample (no. 1). Peak: 1 = acetonitrile, 2 = propionitrile (internal standard), 3 = ethyl acetate, 4 = methyl thiocyanate, 5 = ethyl thiocyanate (internal standard).

Table IV. Results of Analyses of Human Urines with SCN^- Recovery Test[a]

urine no.	amt added, μg SCN^-/mL	amt found, μg SCN^-/mL	recovery, %
1	0.0	(5.2 ± 0.2)[b]	
	5.0	10.5	106
	10.0	14.5	93
	15.0	20.5	102
	20.0	24.6	97
2	0.0	(3.8 ± 0.1)[b]	
	5.0	8.9	102
	10.0	14.0	102
	15.0	18.4	99
	20.0	24.3	103
3	0.0	(3.1 ± 0.1)[b]	
	5.0	7.7	92
	10.0	13.2	101
	15.0	16.6	90
	20.0	22.3	96

[a] Urine and SCN^- added urine samples were diluted 5-fold with water. [b] Mean ± standard deviation of five replicate analyses is shown in parentheses.

Similarly, both CN^- and SCN^- were added to the human urine sample (no. 3 in Table IV) and recovered. As shown in Table V, the recoveries of CN^- and SCN^- are also over 90%. We hope this method can be applied to a variety of real samples after some modification and/or additional manipulation, if necessary.

Table V. Results of Analyses of Human Urines with CN^- and SCN^- Recovery Test[a]

amt added, μg/mL		amt found, μg/mL		recovery, %	
CN^-	SCN^-	CN^-	SCN^-	CN^-	SCN^-
0.00	0.0	0.00	3.1[b]		
1.00	5.0	0.94	7.9	94	96
2.00	10.0	1.81	13.6	91	105
3.00	15.0	3.31[c]	16.8	110	91
4.00	20.0	3.98	21.5	100	92

[a] The sample was no. 3 in Table IV. [b] Mean of five replicate analyses, standard deviation = 0.1. [c] Mean of five replicate analyses, standard deviation = 0.31.

ACKNOWLEDGMENT

Authors thank Y. Tsugita, Y. Matsushita, and H. Iida of the Environmental Protection Research Center (Nishi-ku, Osaka, Japan) for their assistance to collect wastewater samples.

LITERATURE CITED

(1) Bark, L. S.; Higson, H. G. *Analyst (London)* **1963**, *88*, 751-760.
(2) Guilbault G. G.; Kramer, D. N. *Anal. Chem.* **1965**, *37*, 1395-1399; **1966**, *38*, 834-836.
(3) Darr, R. W.; Capson, T. L.; Hileman, F. D. *Anal. Chem.* **1980**, *52*, 1379-1380.
(4) Deshmukh, G. S.; Tatwawadi, S. V. *J. Sci. Ind. Res., Sect B* **1960**, *19*, 195-198.
(5) Pettigrew, A. R.; Fell, G. S. *Clin. Chem. (Winston-Salem, N.C.)* **1972**, *18*, 996-1000.
(6) "Standard Methods for the Examination of Water and Wastewater", 14th ed.; American Public Health Association, American Water Works Association, and Water Pollution Control Federation: New York, 1975; pp 367-372, pp 383-386.
(7) Epstein, J. *Anal. Chem.* **1947**, *19*, 272-274.
(8) Aldridge, W. N. *Analyst (London)* **1944**, *69*, 262-265; **1945**, *70*, 474-475.
(9) Butts, W. C.; Kuehneman, M.; Widdowson, G. M. *Clin. Chem. (Winston-Salem, N.C.)* **1974**, *20*, 1344-1348.
(10) Danchik, R. S.; Boltz, D. F. *Anal. Chem.* **1968**, *40*, 2215-2216.
(11) Ahuja, S. *J. Pharm. Sci.* **1976**, *65*, 163-182.
(12) Dorozd, J. *J. Chromatogr.*, **1976**, *113*, 303-356.
(13) Knapp, D. R. "Handbook of Analytical Derivatization Reactions"; Wiley: New York, 1979.
(14) Blau, K., King, G. S., Eds. "Handbook of Derivatives for Chromatography"; Heyden: London, 1978.
(15) Funazo, K.; Tanaka, M.; Shono, T. *Chem. Lett.* **1979**, 309-310; *Anal. Chem.* **1980**, *52*, 1222-1224.
(16) Funazo, K.; Kusano, K.; Tanaka, M.; Shono, T. *Anal. Lett.* **1980**, *13*, 751-757.
(17) Nota, G.; Palombari, R. *J. Chromatogr.* **1973**, *84*, 37-41; **1976**, *123*, 411-413.
(18) Valentour, J. C.; Aggarwal, V.; Sunshine, I. *Anal. Chem.* **1974**, *46*, 924-925.
(19) De Brabander, H. F.; Verbeke, R. *J. Chromatogr.* **1977**, *138*, 131-142.
(20) Thomson, I.; Anderson, R. A. *J. Chromatogr.* **1980**, *188*, 357-362.

RECEIVED for review March 12, 1981. Accepted May 13, 1981. This work was partially supported by a Grant-in-Aid for Scientific Research from the Ministry of Education of Japan.

Reversed-Phase Liquid Chromatographic Resolution of Amino Acid Enantiomers by Mixed Chelate Complexation

Noriyuki Nimura, Tsukasa Suzuki, Yoko Kasahara, and Toshio Kinoshita*

School of Pharmaceutical Sciences, Kitasato University, 9-1 Shirokane-5, Minato-ku, Tokyo 108, Japan

Separation of enantiomers of amino acids by reversed-phase liquid chromatography has been accomplished by using the copper(II) complex of optically active *N*-(*p*-toluenesulfonyl)-L-phenylalanine (TosPhe) as the mobile phase. The stereoselectivity is ascribed to the differences in the stability of the ternary complex of enantiomeric amino acids with the TosPhe-Cu(II) reagent. The column eluent is monitored for fluorescence after reaction with *o*-phthaladehyde. Amino acids are detectable up to picomole range.

The many attempts to resolve the enantiomeric amino acids by high-performance liquid chromatography (HPLC) have followed two general approaches: precolumn derivatization converting amino acids into diastereomers (*1*) or the use of a chiral stationary phase (*2*) or mobile phase containing chiral additive(s) (*3*). The chiral derivatization methods for the resolution of enantiomeric amino acids by reversed-phase HPLC have been described in a previous report (*4*). Resolution of enantiomeric Dns or DNP derivatives of amino acids have also been developed by using a chiral stationary phase (*5*) or chiral eluant (*6-8*), but the procedures for precolumn derivatization such as dansylation can be tedious.

In contrast, various metal chelate additives to the mobile phase have been used for the separation of underivatized amino acid enantiomers on commerically available stationary phases. Recently, Grushka et al. (*9*) have separated underivatized D,L-amino acids on a reversed-phase column containing the chiral reagent L-aspartylcyclohexylamidecopper(II). However, conventional postcolumn reaction for the highly sensitive detection of amino acids is not applicable to their system since L-aspartylcyclohexylamide has a free amino group. Gil-Av et al. have reported the methods for the resolution of free amino acid enantiomers on an ion-exchange column (*3*) and reversed-phase column (*10*) using a chiral eluant containing a copper-proline complex accompanied by sensitive fluorometric detection using *o*-phthalaldehyde (OPTA) reagent.

The present paper describes a method for separating free D- and L-amino acids on a reversed-phase column using mobile phases containing the chiral reagent *N*-(*p*-toluenesulfony)-L-phenylalaninecopper(II) [TosPhe-Cu(II)]. TosPhe is readily prepared by the reaction of L-phenylalanine with *p*-toluenesulfonyl chloride in alkaline media. The resolution was accomplished on a short column 10 cm long filled with a *n*-octylsilyl bonded silica gel, and amino acids were monitored by fluorescence postcolumn reaction using OPTA reagent.

EXPERIMENTAL SECTION

Reagent. Amino acids and other reagents were purchased from Wako Pure Chemical Industries (Osaka, Japan) and Tokyo

0003-2700/81/0353-1380$01.25/0 © 1981 American Chemical Society

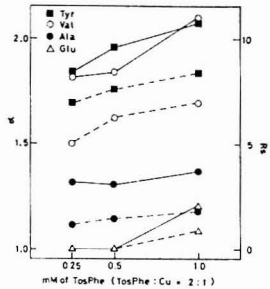


Figure 1. Influence of TosPhe-Cu(II) concentration on separation factor (α, solid line) and resolution value (Rs, dashed line): mobile phase, aqueous solution containing TosPhe-Cu(II) in concentration as given in the figure; pH 6.0.

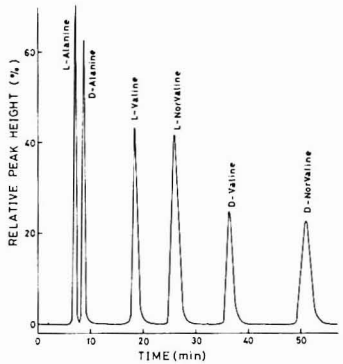


Figure 2. Separation of D,L-amino acids with TosPhe-Cu(II) eluent: mobile phase, aqueous solution containing 1 mM TosPhe and 0.5 mM $CuSO_4 \cdot 5H_2O$; pH 6.0. Approximately 0.5 nmol of each amino acid was injected.

Chemical Industry Co. (Tokyo, Japan). Chemically bonded *n*-octylsilyl silica gel Develosil C8 (particle size; 5 μm) was obtained from Nomura Chemical (Seto-shi, Japan), and its unreacted accessible silanol groups were capped with trimethylsilane (*11*) in our laboratory. Water and acetonitrile were distilled by using glass apparatus before use.

TosPhe was prepared as described by McChensney and Swann (*12*).

The mobile phase consisted of acetonitrile–water containing TosPhe and $CuSO_4 \cdot 5H_2O$ in 2:1 molar ratio. The pH of the mobile phase was adjusted with 5% aqueous sodium carbonate solution. The OPTA reagent containing EDTA·2Na (2.5 g/L) for postcolumn derivatization was prepared as described by Hare and Gil-Av (*3, 13*).

Chromatographic System. Both mobile phase and postcolumn reagent were delivered at a constant flow rate of 1.0 mL/min using a double plunger pump (Sanuki Industry Co., Tokyo, Japan). Trimethylsilyl-treated Develosil C8 was packed in the stainless steel column tube (10 cm × 4.0 mm i.d.) in our laboratory by the conventional slurry packing technique. The column was operated at 30 °C utilizing a Taiyo thermo unit C-600 (Taiyo Scientific Industry Co., Tokyo, Japan). The column eluate was mixed with the OPTA reagent in a mixing T-piece and a PTFE-tubing reaction coil (50 cm × 0.5 mm i.d.). Fluorescence intensity of the effluent was measured at 455 nm; excitation of fluorescence was achieved at 340 nm, using an RF-500 LCA spectrofluoromonitor (Shimadzu Seisakusho Ltd., Kyoto, Japan) equipped with a xenon discharge lamp.

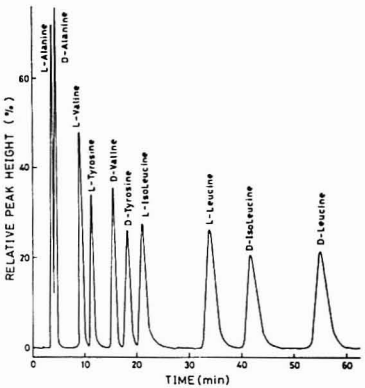


Figure 3. Separation of D,L-amino acids with TosPhe-Cu(II) eluent: mobile phase, 10% acetonitrile in an aqueous solution containing 1 mM TosPhe and 0.5 mM $CuSO_4 \cdot 5H_2O$; pH 6.0. Approximately 0.5 nmol of each amino acid was injected.

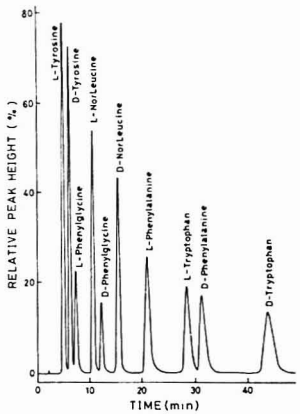


Figure 4. Separation of D,L-amino acids with TosPhe-Cu(II) eluent: mobile phase, 15% acetonitrile in an aqueous solution containing 1 mM TosPhe and 0.5 mM $CuSO_4 \cdot 5H_2O$; pH 6.0. Approximately 0.5 nmol of each amino acid was injected.

RESULTS AND DISCUSSION

In the following discussion, the symbols k', α, and Rs represent capacity ratio, separation factor, and resolution value, respectively. These values changed with alteration of the pH and the concentrations of TosPhe-Cu(II) complex and acetonitrile in the mobile phase.

k' and α increased with the increase in the pH in the range from pH 5 to pH 7, so most amino acids can be resolved in this pH range. However, the racemic pairs of alanine, aspartic acid, glutamic acid, and asparagine were resolved at pH 6 or above. Moreover, the Rs values markedly decreased at pH 7 due to the tailing of chromatographic peaks (Table I). Therefore, the pH of the mobile phase was adjusted to 6.

The dependence of α and Rs on the concentration of TosPhe-Cu(II) is shown in Figure 1. Both α and Rs increased as the concentration of TosPhe-Cu(II) increased. The resolution of glutamic acid enantiomers could be achieved at 1

Table I. Capacity Ratio (k'), Separation Factor (α), and Resolution Value (Rs) as a Function of pH[a]

amino acid		pH 5.0 k'	pH 5.0 α	pH 5.0 Rs	pH 6.0 k'	pH 6.0 α	pH 6.0 Rs	pH 7.0 k'	pH 7.0 α	pH 7.0 Rs
glutamic acid	D	1.60	1.00	0.00	2.20	1.20	0.80	2.70	1.26	0.48
	L	1.60			2.63			3.40		
alanine	L	2.00	1.00	0.00	2.40	1.35	1.87	3.60	1.39	1.65
	D	2.00			3.24			5.00		
valine	L	3.00	1.27	1.38	8.25	2.05	6.85	11.20	2.08	2.45
	D	3.80			16.90			23.30		
tyrosine	L	6.44	1.30	2.52	10.51	2.08	8.25	16.25	2.24	3.89
	D	8.38			21.86			36.40		

[a] Mobile phase: aqueous solution containing 1 mM TosPhe and 0.5 mM $CuSO_4 \cdot 5H_2O$.

Table II. Capacity Ratio (k'), Separation Factor (α), and Resolution Value (Rs) as a Function of Acetonitrile Concentration
Acetonitrile Concentration[a]

amino acid		0% acetonitrile k'	0% acetonitrile α	0% acetonitrile Rs	10% acetonitrile k'	10% acetonitrile α	10% acetonitrile Rs	15% acetonitrile k'	15% acetonitrile α	15% acetonitrile Rs
aspartic acid	D	1.44	1.39	1.10	0.10	2.90	0.64	0.05	1.00	0.00
	L	2.00			0.29			0.05		
glutamic acid	D	2.20	1.20	0.80	0.28	2.07	0.90	0.10	1.00	0.00
	L	2.63			0.58			0.10		
asparagine	D	2.70	1.09	0.39	0.60	1.00	0.00	0.18	1.00	0.00
	L	2.93			0.60			0.18		
glutamine	D	3.52	1.00	0.00	0.68	1.00	0.00	0.20	1.00	0.00
	L	3.52			0.68			0.20		
alanine	L	2.40	1.35	1.87	0.78	1.41	1.21	0.12	1.00	0.00
	D	3.24			1.10			0.12		
valine	L	8.25	2.05	6.85	3.70	1.73	4.32	1.00	1.54	1.71
	D	16.90			6.40			1.54		
tyrosine	L	10.51	2.08	8.25	4.50	1.78	5.56	1.20	1.58	2.21
	D	21.86			8.00			1.90		
norvaline	L	12.00	2.08	7.35	5.20	1.78	4.75	1.22	1.61	2.06
	D	25.00			9.24			1.96		
phenylglycine	L	22.81	2.28	10.85	9.20	2.37	8.57	2.60	1.92	5.45
	D	52.00			21.80			5.00		
isoleucine	L		[b]		9.40	2.10	7.39	2.60	1.69	3.33
	D				19.74			4.40		
leucine	L		[b]		16.00	1.66	4.53	3.82	1.48	3.15
	D				26.60			5.64		
norleucine	L		[b]		16.80	1.88	5.88	4.10	1.61	3.79
	D				31.50			6.60		
phenylalanine	L		[b]		37.40	1.90	6.04	9.50	1.55	4.30
	D				71.20			14.70		
tryptophan	L		[b]			[b]		13.20	1.58	4.14
	D							20.80		

[a] Mobile phase: acetonitrile in an aqueous solution containing 1 mM TosPhe and 0.5 mM $CuSO_4 \cdot 5H_2O$, pH 6.0. $t_0 \simeq 2.0$ min. [b] Not measured as the amino acid was retained over 1 h.

mM TosPhe and 0.5 mM Cu(II) (Figure 1).

The separation of the amino acids was dependent on acetonitrile concentration (Table II). When acetonitrile was omitted, leucine, phenylalanine, and tryptophan were retained on the column for over an hour. Addition of acetonitrile at a concentration from 10% to 15% enabled rapid separation of a several amino acid isomers (Table II, Figures 2–4).

TosPhe does not interfere with the detection of amino acids with OPTA which reacts with primary but not with secondary amines and amides. Precipitation of copper ions by the alkaline OPTA reagent is prevented by adding EDTA in the reagent (*3*). Consequently, picomole levels of amino acids are detected.

In the mobile phase, TosPhe and copper(II) ion can be assumed to form a binary complex [$(TosPhe)_2CuII$] as shown in Figure 5.

Recently, Karmen et al. (*8*) have reported a method for separating D- and L-Dns derivatives of amino acids by adding Cu(II) complexes of proline and arginine. Their study suggests that *N*-sulfonylamino acid, free amino acid, and copper(II) form a ternary complex. Accordingly free amino acid, TosPhe,

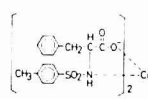


Figure 5. Proposed structure of binary complex of TosPhe with copper(II).

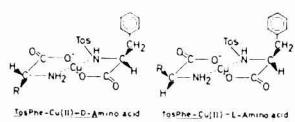


Figure 6. Proposed structure of ternary complexes formed from D- and L-amino acid with TosPhe and copper(II).

and copper(II) appear to form a ternary complex. Enantiomeric pairs of amino acids may form complexes of different conformation. The ternary complex of D-amino acid may assume trans conformation around the Cu(II) ion and that of L-isomer cis conformation (Figure 6). These molecular

models support the fact that L-amino acid was eluted before the D-isomer except for acidic amino acids since the trans isomer is thermodynamically more stable than the cis one (*13*).

The difference in mobility among amino acid appears to be based on different hydrophobic and steric interaction between the alkyl substituent on the α-carbon of the amino acid and *n*-octyl residue on the bonded phase silica gels. Consequently, amino acids which have higher hydrophobic alkyl substituents were retained longer than those having lower hydrophobic moiety. For isomers with an equal number of carbon atoms, those pairs with the branched side chain such as valine and leucine are eluted faster than those with a linear side chain such as norvaline and norleucine. These results agreed with the results of Grushka et al. (*9*) and Karmen et al. (*7*).

A preliminary test showed that TosPhe does not react with ninhydrin. This fact suggests that proline may also be detected after separation by the present system with slight modifications although it is not detectable when copper–proline complex is used as the mobile phase (*3*, *10*).

LITERATURE CITED

(1) Tamegai, T.; Ohmae, M.; Kawabe, K.; Tomoeda, M. *J. Liquid Chromatogr.* **1979**, *2*, 1229–1250.
(2) Davankov, V. A.; Rogozhin, S. V. *J. Chromatogr.* **1971**, *60*, 280–283.
(3) Hare, P. E.; Gil-Av, E. *Science* **1979**, *204*, 1226–1228.
(4) Nimura, N.; Ogura, H.; Kinoshita, T. *J. Chromatogr.* **1980**, *202*, 375–380.
(5) Pirkle, W. H.; House, D. W.; Finn, J. M. *J. Chromatogr.* **1980**, *192*, 143–158.
(6) Lindner, W.; LePage, J. N.; Davies, G.; Seitz, D. E.; Karger, B. L. *J. Chromatogr.* **1979**, *185*, 323–344.
(7) LePage, J. N.; Lindner, W.; Davies, G.; Seitz, D. E.; Karger, B. L. *Anal. Chem.* **1979**, *51*, 433–435.
(8) Lam, S.; Chow, F.; Karmen, A. *J. Chromatogr.* **1980**, *199*, 295–305.
(9) Gilon, C.; Leshem, R.; Grushka, E. *Anal. Chem.* **1980**, *52*, 1206–1209.
(10) Gil-Av, E.; Tishbee, A.; Hare, P. E. *J. Am. Chem. Soc.* **1980**, *102*, 5115–5117.
(11) Evans, M. B.; Dale, A. D.; Little, C. J. *Chromatographia* **1980**, *13*, 5–10.
(12) McChensney, E. W.; Swann, W. K., Jr. *J. Am. Chem. Soc.* **1937**, *59*, 1116–1118.
(13) Jozefonvidz, J.; Muller, D.; Petit, M. A. *J. Chem. Soc., Dalton Trans.* **1980**, 76–79.

RECEIVED for review February 6, 1981. Accepted April 6, 1981.

Spurious Peaks in Rapid-Scan Square-Wave Polarography

Adina Lavy Feder and Chaim Yarnitzky

Department of Chemistry, Technion-Israel Institute of Technology, Haifa, Israel

John J. O'Dea and Janet Osteryoung*

Department of Chemistry, State University of New York at Buffalo, Buffalo, New York 14214

Square-wave polarography can exhibit spurious peaks due to a resonance between the frequency of the applied potential and the mechanical frequency of oscillation of the dropping mercury electrode. The peak heights can correspond to signals arising from the faradaic response of solution in the concentration range 10^{-7}–10^{-6} M. The resonant frequency is a function of the drop mass and can be estimated from a semiempirical equation, $f = (1/2\pi)(a/M + b/M^{1/3})^{1/2}$ where $a = 1.51 \times 10^5$ mg and $b = -2.64 \times 10^5$ mg$^{1/3}$.

Square-wave voltammetry at high scan rates provides peak-shaped signals which appear well-suited to both physical chemical investigation and analysis (*1*–*5*). We have designed a One-Drop Square-Wave Analyzer (ODSWA) for the special purpose of using the rapid-scan square-wave waveform at the dropping mercury electrode (DME) for analysis (*6*). Work with this instrument has shown that the sensitivity is typically greater than that for differential pulse polarography for normal operating conditions, and of course the scan of potential is accomplished in much shorter time for square-wave polarography (*7*). In addition, the cost of constructing commercially an instrument with parameters similar to those of the one-drop square-wave analyzer should be comparable to that of other routine instrumentation for pulse voltammetry (e.g., the PARC Model 174 polarographic analyzer). Therefore there is interest in defining carefully the characteristics of this technique, especially those which might arise from instrumental artifacts or from physical phenomena neglected in the development of theory.

Here we report on a phenomenon not previously seen, a spurious peak which arises from a resonance between the frequency of the applied potential and the mechanical frequency of oscillation of the growing mercury drop of the DME. This peak could be misinterpreted as arising from an unidentified analyte or could interfere with measurement of the peak current for an analyte which is present. Thus although the phenomenon itself is a laboratory curiosity, it can have important practical consequences for the user of square-wave voltammetry.

EXPERIMENTAL SECTION

The potential–time waveform applied in square-wave voltammetry consists of a staircase with tread width equal to the square-wave period on which is superimposed a symmetrical square wave. In the first half of each period, the square-wave pulse is in the same direction as the riser of the staircase; this is the forward pulse, and the current measured during this pulse is the forward current. Correspondingly during the second half period the square-wave pulse is in the opposite or reverse direction and the current is the reverse current. The usual signal output is the forward current minus the reverse current and is referred to as the net current. The parameters of this technique are the square-wave frequency, f, the step height of the base staircase, ΔE, the amplitude of the square-wave pulse, E_{sw}, and the delay time, t_d, at the initial potential, E_i.

Two different kinds of instrumentation were used in these experiments. The first is the one-drop square-wave analyzer already described (*6*). This instrument was operated at a fixed frequency of 25 Hz, and the current was sampled and integrated over the last 10 ms of each pulse. (Note that the version described in ref 6 is designed for mains frequency of 60 Hz and therefore operates at 30 Hz.) The second is based on a Digital Equipment Corp. PDP 8/e minicomputer with homemade interface and analog electronics and is described more fully elsewhere (*8*). The current was sampled and integrated over the last one-third of each pulse.

0003-2700/81/0353-1383$01.25/0 © 1981 American Chemical Society

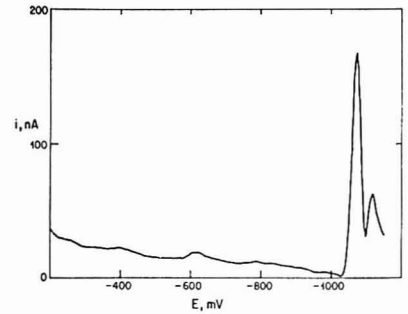


Figure 1. Square-wave polarogram in 0.1 F KCl showing the spurious peak. E_{sw} = 25 mV; f = 45 Hz, ΔE = 5 mV; m = 1.685 mg s^{-1}; t_d = 0.1 s; computer system.

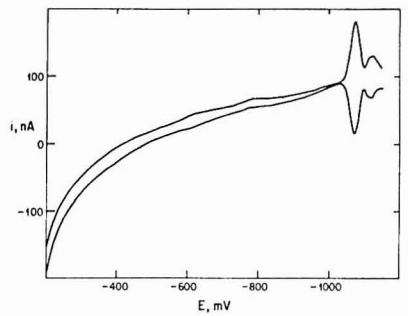


Figure 2. Forward (upper curve) and reverse (lower curve) currents; same experiment as Figure 1.

Triple-distilled mercury and reagent grade chemicals were used without further purification. Experiments were carried out at 22 ± 2 °C. All potentials were measured and are reported vs. SCE.

RESULTS AND DISCUSSION

The spurious peak is displayed in Figures 1 and 2 which show the net and the forward and reverse currents, respectively. Trace contamination with Cd(II) and Pb(II) produces small peaks at −0.4 and −0.6 V in Figure 1, but the main features are the spurious peaks at −1.07 and −1.11 V. These peaks are clearly seen also in both the forward and reverse currents where they appear to be nearly equal in magnitude but opposite in sign when measured with respect to the curved background due to the growth of the drop during the scan. The magnitude of the net current peak is that to be expected for the reduction of a substance in a reversible two-electron process at a concentration in the range 10^{-7}–10^{-6} M. Chemical contamination and instrumental artifact were quickly eliminated as possible causes of the effect. At the DME the peak potential was found to be a function of initial potential, scan rate, square-wave frequency, and mercury flow rate. Similar peaks have been observed in a variety of electrolytes but never very near the point of zero charge or with very small (<1 mV) pulse amplitudes. The details of these observations are as follows.

Figure 3 displays the dependence of the peak shape, position, and height on delay time with other parameters constant. From the peak position and delay times the lifetime of the drop at the peak is found for these data to be nearly constant, 12.8 ± 0.4 s.

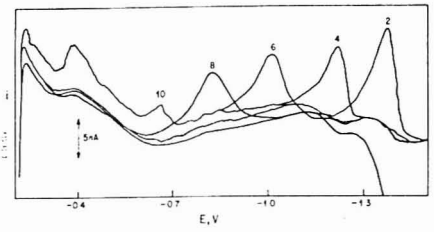


Figure 3. Square-wave polarograms in 0.1 F HCl. Numbers on the peaks are the delay times in seconds. E_{sw} = 25 mV; ΔE = 5 mV; m = 0.274 mg s^{-1}; ODSWA.

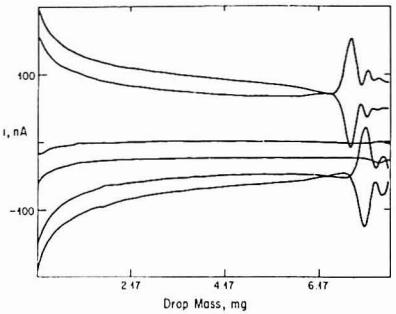


Figure 4. Forward (upper curve in each pair) and reverse (lower curve in each pair) square-wave currents in 0.1 F KCl at the DME. Computer system; f = 45 Hz, E_{sw} = 25 mV; t_d = 0.1 s; m = 1.685 mg s^{-1}, ΔE = 0.05 mV (the base staircase potential changes by less than 2 mV). Upper pair of curves, E_i = −1.50 V; center pair, −0.40 V; lower pair, −0.20 V.

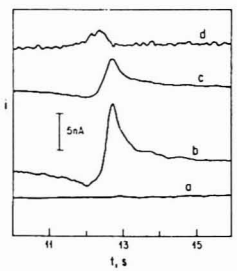


Figure 5. Square-wave currents at the DME in 0.1 F KCl at DC potential of −1.4 V. m = 0.274 mg s^{-1}; ODSWA: (a) E_{sw} = 0; (b) E_{sw} = 0 but mechanical vibration at 25 Hz; (c) E_{sw} = 25 mV; (d) optical signal obtained in (c) from a photocell positioned on one side of the drop and directed toward a small lightbulb on the other side.

The effect of DC potential is illustrated in Figure 4, which shows forward and reverse currents for square-wave voltammograms near to and far from the potential of zero charge. The peak amplitude decreases markedly near the pzc.

Figure 5 illustrates the qualitative equivalence of vibration induced electrically and mechanically. In Figure 5a neither electrical nor mechanical excitation is employed, and no peak appears. In Figure 5b,c the growing mercury drop is excited at a frequency of 25 Hz, in the former case mechanically and in the latter electrically; similar peaks appear. In the case of electrical excitation the resulting vibration of the drop can be observed directly as shown in Figure 5d. As might be

Table I. Drop Mass at Peak Current for Various Frequencies of Square-Wave Excitation[a]

freq, Hz	drop mass, mg: m = 1.685 mg s^{-1}	m = 0.7560 mg s^{-1}
20	5.223[b]	5.179[b]
30	2.915[b]	2.926[b]
40	1.887[b]	1.852[b]
45	6.871	6.781
50	6.403	6.305
60	5.308	5.239
70	4.314	4.287
80	3.606	3.561
90	3.033	2.979
100	2.578	2.548

[a] E_{sw} = 25 mV, DC potential −1.0 V, ΔE = 0.05 mV, 0.1 F KCl (computer system). [b] Observed peaks are the harmonics at 60, 90, and 120 Hz.

expected, other experiments showed that these phenomena are sensitive to the angle of the capillary from the vertical.

It appears from the forgoing that these spurious peaks are caused by resonant mechanical vibration of the mercury drop at the frequency of the pulse. Changes in drop shape cause changes in area which in turn require flow of current to maintain constant charge density at fixed potential. Because the surface tension and charge density depend on potential and the drop mass at a given potential depends not only on the flow rate of mercury but also on the initial potential and the step height, the behavior of the phenomenon is quite complex. An estimation of the resonant frequency as a function of drop mass is possible by the use of an empirical relationship

$$f = (1/2\pi)(a/M + b/M^{1/3})^{1/2} \quad (1)$$

where f is the frequency (Hz), M is the drop mass (mg), and a and b are constants. The rationale for the mathematical form of eq 1 follows directly from the example of two pendulums coupled by a spring in which two forces act to restore the system to mechanical equilibrium (*9, 10*). At the DME, these forces are surface tension and gravity. The constant a should be proportional to the surface tension of the drop, while b should be proportional to the acceleration due to gravity. A more rigorous approach based upon the calculation of the drop shape should yield an expression for f as a function of the fundamental quantities, mass, gravity, and surface tension. Table I presents the results of experiments carried out over the range 20–100 Hz and for two different flow rates. Fitting these data to eq 1 produced the values $a = 1.51 \times 10^6$ mg and $b = -2.64 \times 10^5$ mg$^{1/3}$. The quality of the results can be expressed in terms of the linear regression of the values of frequency calculated from eq 1 on the experimental values. The slope of the regression line is 0.99, the intercept 0.30 Hz, and the correlation coefficient 0.9995. Thus although the details of the effects of mechanical vibration are obscure the general notions which form the basis of eq 1 appear to be substantiated. The dependence of the value of a on surface tension was not investigated. However, in normal practice surface tension should not differ from 400 dyn cm^{-1} by more than 10%; thus eq 1 should provide a fairly general description of the resonance phenomenon.

As pointed out in Table I some of the observed frequencies are harmonics of the fundamental frequency. The curves of Figures 3 and 5 which were obtained with the one-drop square-wave analyzer at 25 Hz show peaks with a relatively small amplitude which arise from the natural mechanical oscillation at 75 Hz. Figures 1, 2, and 4 were obtained with the computer-controlled system at higher frequency and capture the fundamental which naturally exhibits much greater amplitude.

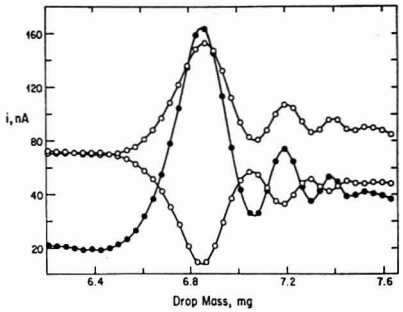


Figure 6. Forward (upper curve) and reverse (lower curve) (○) and net (●) square-wave currents at the DME at DC potential of −1.0 V. ΔE = 0.05 mV; other conditions are those of Figure 1.

The phenomenon of ringing or underdamped oscillation is shown in Figure 6. Here the fundamental frequency is 45 Hz (45.3 Hz predicted from eq 1) but ringing occurs as the drop mass continues to increase at nearly constant potential.

In order for these sorts of effects to be observed it is necessary for either the mass of the drop or its potential to be changing with time. One would not expect to see these peaks in AC voltammetry at a stationary drop electrode under typical steady-state conditions. However, if the frequency of the AC excitation signal were changed rapidly with time one would expect a peak to occur when the frequency of the AC modulation coincided with the mechanical frequency of vibration of the drop. We have observed such peaks using a hanging mercury drop electrode in conjunction with a standard potentiostatic circuit with rapid scan of the frequency of the sine wave modulation from 100 to 10 Hz. The frequencies at which the peaks occurred agreed with those calculated from eq 1 within 5%. For these experiments the amplitude of the modulation was 50 mV (peak-to-peak), the DC potential was −1.0 V, and the solution was 0.1 F H_2SO_4.

These observations show that this resonance phenomenon is pronounced and can be expected to occur for square-wave polarography under the range of conditions normally employed. The mass of the drop and the parameters of the square-wave experiment are related in the following way. The mass, M, at time t after the drop growth begins is given by $M = mt$, where m is the flow rate of mercury. The time is given by $t = t_d + t_s$ where t_d is the delay time before initiation of the scan and t_s is the duration of the scan. Thus $t_s = (E(t_s) - E_i)/f\Delta E$ where $E(t_s)$ is the potential of the electrode at time t_s, E_i is the initial potential (the potential during the period t_d), f is the square-wave frequency, and ΔE is the step height of the base staircase. Combination of these relations with eq 1 gives

$$4\pi^2 f^2 = \frac{a}{\left[mt_d + \frac{m(E_p - E_i)}{f\Delta E}\right]} - \frac{b}{\left[mt_d + \frac{m(E_p - E_i)}{f\Delta E}\right]^{1/3}} \quad (2)$$

where E_p is the potential at which the peak occurs. For sufficiently large values of the quantity $t_d f\Delta E/(E_p - E_i)$ this becomes simply

$$f = \frac{1}{2\pi}\sqrt{\frac{a}{mt_d} - \frac{b}{(mt_d)^{1/3}}} \quad (3)$$

and for typical values (m = 1 mg s^{-1}, t_d = 6 s) f = 52 Hz. It should always be possible, therefore, to eliminate the peak by increasing the square-wave frequency. For instruments which operate at fixed frequency, the peak position should move as the flow rate, delay time, initial potential, or step height are changed. As none of these parameters influence the peak position for a faradaic response, their systematic variation should identify unambiguously peaks due to the resonance phenomenon. Consider the instrument which operates at 25 Hz. From eq 2 at 25 Hz

$$E_p - E_i = \Delta E \frac{1.31}{m} - t_d \quad (4)$$

For reasonable values of m and t_d (m = 1.31 mg s^{-1}, t_d = 6s), $E_p - E_i = -5\Delta E$. Thus the peak position is not influenced strongly by changes in step height for normal operating conditions. To the extent the electrochemical system permits, the best way to move the resonant peak from the potential region of interest is to change the initial potential. The ability to influence the phenomenon through choice of parameters should ensure that in most practical applications it can be avoided.

LITERATURE CITED

(1) Ramaley, C.; Krause, M. S., Jr. *Anal. Chem.* **1969**, *41*, 1362-1365.
(2) Krause, M. S., Jr.; Ramaley, L. *Anal. Chem.* **1969**, *41*, 1365-1369.
(3) Christie, J. H.; Turner, J. A.; Osteryoung, R. A. *Anal. Chem.* **1977**, *49*, 1899-1903.
(4) Turner, J. A.; Christie, J. H.; Vucovic, M.; Osteryoung, R. A. *Anal. Chem.* **1977**, *49*, 1904-1908.
(5) O'Dea, John J.; Osteryoung, R. A.; Osteryoung, Janet *Anal. Chem.* **1981**, *53*, 695-701.
(6) Yarnitzky, Chaim; Osteryoung, R. A.; Osteryoung, Janet *Anal. Chem.* **1980**, *52*, 1174-1178.
(7) Stojek, Z.; Osteryoung, Janet *Anal. Chem.* **1981**, *53*, 847-851.
(8) Brumleve, Timothy R.; O'Dea, John J.; Osteryoung, R. A.; Osteryoung, Janet *Anal. Chem.* **1981**, *53*, 702-706.
(9) French, A. P. "Vibrations and Waves"; W. W. Norton and Co.: New York, 1971; p 121.
(10) Forham, S. *Proc. R. Soc. London, Ser. A* **1948**, *A194*, 1.

RECEIVED for review March 23, 1981. Accepted May 15, 1981. This work was supported in part by Grant CHE7917543 from the National Science Foundation.

Electrochemical Treatment of Pyrolytic Carbon Fiber Electrodes

F. G. Gonon,* C. M. Fombarlet,[1] M. J. Buda, and J. F. Pujol

INSERM U 171, Département de Médecine Expérimentale, Université Claude Bernard, 8, Avenue Rockefeller, 69008 Lyon, France

Pyrolytic carbon fiber electrodes improved by electrochemical treatment appeared very useful for in vivo studies of dopamine metabolism in brain tissue. These treated electrodes used in combination with differential pulse voltammetry were capable of separating ascorbic acid from catechols and exhibited a very high sensitivity for some catechols. Parameters and experimental conditions of this electrochemical treatment were explored.

In order to investigate the functional significance of brain catechols, it is of great interest to monitor their endogenous level from the brain tissue of live, freely moving animals and thus to avoid tissue sampling postmortem or tissue perfusion. Several in vivo voltammetric techniques have been developed for detection of catechol compounds which are synthesized by dopaminergic neurons (*1-7*). However, the major problem was the presence in brain tissue of high levels of ascorbic acid (AA) which oxidizes on untreated carbon electrodes at the same potential as several catechols.

Improvements of pyrolitic carbon electrodes by various treatments have been already reported. Kuwana and coworkers have treated pyrolytic graphite electrodes by radio frequency plasma in oxygen (*8*) and subsequent attachment of benzidine (*9*) or various quinones (*10*). Improvements of oxidation reaction of AA and of several other compounds have been demonstrated (*9, 10*). Blaedel and Mabbott (*11*) described electrochemical and chemical treatments of a pyrolytic carbon film electrode and thus obtained well-defined, reproducible current voltage curves. Various pyrolytic carbon fiber electrodes for in vivo application in brain tissue have been recently developed (*2, 7, 12, 13*). The active surface of our electrode is a pyrolytic carbon fiber 8 μm thick and 0.5 mm long. In recent reports (*14-17*) we have shown that it is possible to resolve AA from catechols by means of this electrochemically treated carbon fiber electrode used in combination with differential pulse voltammetry. Then the catechol signal obtained in vivo from dopaminergically innervated tissue had been identified as the direct metabolite of dopamine (DA), i.e., 3,4-dihydroxyphenylacetic acid (DOPAC) (*14-17*). Thus it appeared that this technique might be a valuable tool to study in vivo DA function.

However, these in vivo studies give rise to several questions from the point of view of the electrochemistry. Actually, the separation of AA from catechol resulted from the electrochemical treatment which moved the AA signal to a more negative potential than that of the catechol signal. Moreover, the sensitivity of the treated carbon fiber electrode appeared 10 times higher for DOPAC than for AA and almost 100 times higher for DA than for DOPAC. Such improvement of sensitivity and selectivity of carbon fiber electrodes required very precise treatment conditions. This led us to explore in this paper several parameters of this treatment.

MATERIALS AND METHODS

Recording of the Voltammograms. A conventional three-electrode system was connected to a pulse voltammetric system (PRG5 Tacussel, Villeurbanne, France). The auxiliary electrode was a platinum wire. The Ag/AgCl reference electrode was prepared by stripping a 10 mm length of Teflon-coated silver wire (ϕ 0.25 mm, Medwire Corp., Mt. Vernon, NY) and anodizing (+0.6 V for 1 min) in 1 M hydrochloric acid. During experiments this AgCl-coated silver wire was directly immersed in the solutions. A commercially available Ag/AgCl reference electrode (C6 Tacussel, Lyon) has been occasionally used. Both electrodes obtained identical results. The potential of such reference electrodes slightly (+20 mV) differed from this of a calomel saturated electrode. The carbon fiber electrodes were prepared as previously described (*7*).

[1] Present address: Laboratoire de Chimie Organique et Cinétique, Institut de Chimie et Physique Industrielles, 69002 Lyon, France.

0003-2700/81/0353-1386$01.25/0 © 1981 American Chemical Society

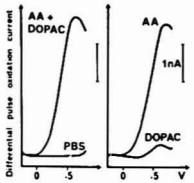


Figure 1. Voltammograms obtained with an untreated carbon fiber electrode. AA (200 μM) and DOPAC (20 μM) were added to a PBS solution.

In order to obtain a complete polymerization of the resin, we kept these electrodes at 60 °C for 24 h.

The parameters of the differential pulse voltammetry used here were scan rate 10 mV/s and pulse modulation +50 mV in amplitude, 48 ms in duration, and 0.2 s in period. When phosphate buffered saline (PBS) solutions (KCl, 0.2 g/L; KH_2PO_4, 0.2 g/L; $MgCl_2$, 0.047 g/L; NaCl, 8 g/L; Na_2HPO_4, 1.15 g/L; pH 7.4) contained AA and/or DOPAC, the concentrations of these compounds was always 200 μM (AA) and 20 μM (DOPAC). The solutions were generally not deaerated since identical results were obtained with or without deaeration of solutions. AA, DA, and DOPAC solutions were tested at 25 °C within an hour following their preparations in order to avoid the influence of spontaneous oxidation.

Electrochemical Treatments. Carbon fiber electrodes were immersed in the PBS solution. The first treatment was achieved by applying an alternating potential of a triangular wave form to the working electrode. In the standard conditions (as used in ref 14–17 and Figures 2 and 5A), the parameters of this treatment were the following: frequency of the alternating potential, 70 Hz; lower potential limit, 0 V, upper potential limit, +3 V, duration, 20 s. Several of these parameters have been independently investigated. The effect on the AA + DOPAC signal of various upper potential limits is shown in Figure 3 and the duration effect is in Figure 4. In these studies other parameters values were those of the standard conditions. In all these treatments the triangular wave form potential was applied via the PRG5 to the three-electrode system. For this purpose the "pilot tension input" of the PRG5 was supplied by a conventional function generator (FG 600, Feedback Instruments Ltd., England; output impedance, 600 Ω).

During the treatment the resulting current occurring through the working electrode was measured by means of an oscilloscope, the first channel of which was connected to the working electrode output in the back panel of the PRG5. The potential measured at this output is directly proportional to the current measured by the current–voltage amplifier of the PRG5 without filtering or damping. The second channel was connected to the pilot potential output to control the potential applied to the working electrode.

The second treatment was always applied after the first one described above (standard conditions). It was achieved by applying to the working electrode a continuous potential of +1.5 V vs. the reference electrode for 20 s. This was performed by means of the PRG5 alone, the "initial potential" of which was set at +1.5 V.

RESULTS

Untreated carbon fiber electrodes gave poorly defined peaks at +550 mV for DOPAC and +600 mV for AA (Figure 1). Moreover, these peak potentials varied from one electrode to another. The sensitivity of such electrodes was almost equal for AA and DOPAC (Figure 1). Mixed solutions of AA and DOPAC exhibited only one peak, which rapidly decreased in successive scans.

When the standard treatment (0 to +3 V, 20 s) was applied to a carbon fiber electrode, voltammograms obtained from AA and DOPAC solutions exhibited two well-resolved peaks (Figure 2). AA peaked at −80 mV and DOPAC at +70 mV. Both peaks increased during successive scans until an

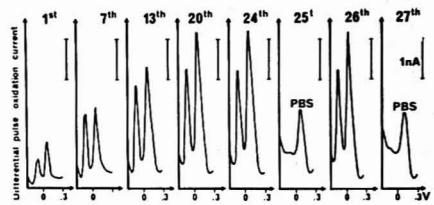


Figure 2. Equilibration of a carbon fiber electrode just after a standard treatment. Numbers indicate the order of the successive voltammograms recorded every 1 min (AA 200 μM and DOPAC 20 μM excepted when "PBS" is mentioned).

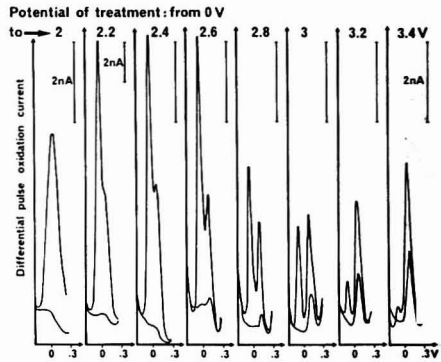


Figure 3. Effect of various upper potential limits on the AA + DOPAC signal. For each treated electrode, voltammograms are recorded after equilibration (see Figure 2) first in AA + DOPAC solution (higher traces) and second in PBS solution (lower traces).

equilibration of the electrochemical response was reached at the 20th scan. Subsequent AA and DOPAC signals were stable. Then, when the electrode was immersed in PBS solution without AA or DOPAC, the voltammogram exhibited a remaining peak at +70 mV. This remaining peak did not change when several voltammograms were recorded from PBS solution. If the electrode was tested again in AA + DOPAC solution, the previous AA and DOPAC peaks were immediately obtained without the need for equilibration. Finally, as regards peak heights, Figure 2 shows that this treatment slightly decreased the sensitivity of the electrode for AA, while that for DOPAC increased by 1 order of magnitude.

For each electrode the current induced by the standard treatment was measured. It reached a maximum value which was 296 ± 28 μA (mean ± standard deviation, 10 experiments). The standard treatment was also performed by using various solutions: deaerated PBS solution (by means of N_2), PBS solution at pH 2.5 and at pH 8. These treated electrodes were then tested in the same conditions as in Figure 2. The voltammograms thus obtained from the test solution (AA + DOPAC in PBS solution at pH 7.4) did not differ significantly from standard experiments.

Figure 3 shows the effect of increasing upper potential limit of the treatment on the AA + DOPAC signal. The effect of the lowest treatment (0 to +2 V) was, first, to move the DOPAC and AA signals to +70 mV and, second, to improve the AA + DOPAC peak definition. However, these effects progressively disappeared following successive scans. It appeared that a potential equal to or higher than +2.6 V was required to obtain a valuable separation of AA and DOPAC peaks. This separation arose from the moving of the AA peak from

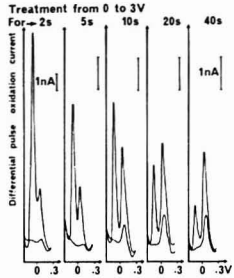


Figure 4. Effect of various treatment durations on the AA + DOPAC signal (test conditions as in Figure 3).

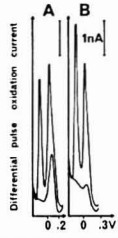


Figure 5. Effect of the second treatment. Voltammograms were obtained: (A) after the standard treatment, (B) after the second one (test conditions as in Figure 3).

+70 to −80 mV. When the upper limit of the potential applied during the treatment was increased, the AA signal decreased and the DOPAC peak increased. But if the remaining blank peak appearing at +70 mV in PBS solution was subtracted, then the signal due to DOPAC had the same amplitude when tested after every treatment (from +2.6 to +3.4). When the upper potential limit was extended to +3.6 V, the electrode was broken by this treatment. During these various treatments, the current occurring through each carbon fiber electrode was measured. The values of the maximum current were found to be 50, 80, 130, 210, 260, 310, 350, and 410 μA when the upper limit of the treatment increased from +2 to +3.4 V, respectively.

The influence of the frequency of the triangular wave potential has been explored from 10 to 1000 Hz. In all cases a 0 to +3 V potential was applied to the working electrode for 20 s. This parameter slightly affected the resulting test voltammograms. When a 10-Hz frequency treatment was applied, the subsequent test voltammogram was very similar to that recorded after a 70-Hz treatment, the upper limit of which was equal to +3.2 V (Figure 3). The test voltammogram obtained after a 1000-Hz frequency treatment was almost identical with that obtained after a 0 to +2.8 V treatment applied at 70 Hz (Figure 3).

Various durations of the standard treatment (0 to +3 V, 70 Hz) were tested (Figure 4). In all cases the separation between AA and DOPAC occurred. This parameter mainly acted on the sensitivity of the carbon fiber electrode to AA. When the treatment was extended up to 60 s, the electrode was broken.

In order to decrease the amplitude in the remaining blank peak at +70 mV, we performed a second treatment after the standard one (Figure 5). Two durations of this treatment were tested (5 s and 20 s), but the resulting voltammograms were very similar. Moreover, this second treatment slightly improved the sensitivity of the electrode to AA. Such double

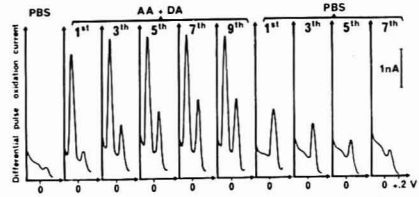


Figure 6. DA measurement with a double treated electrode. Numbers indicate the order of successive voltammograms recorded every 1 min (DA 0.1 μM and AA 200 μM in PBS solution).

treated electrodes were used in vivo and then calibrated in vitro for DOPAC and AA (*17*). The DOPAC peak height linearly increased with DOPAC concentration (5–50 μM) and did not depend on the AA concentration in the solution (from 0 to 400 μM). The AA peak height linearly increased with AA concentration (50–400 μM) but was slightly depressed when the DOPAC concentration exceeded 20 μM.

Chemical treatments of the carbon fiber electrode were also tried. The working electrode was immersed for 20 min in HNO_3, H_2SO_4, H_2O_2, and concentrated acid dichromate solution. In all these cases the resulting test voltammograms (AA + DOPAC in PBS) showed only one poorly defined peak. However, this peak moved to a less positive potential and its height was increased. The best results were obtained with concentrated acid dichromate solution. In this case the resulting voltammograms were very similar to those obtained after a 0 to +2 V electrochemical treatment (Figure 3).

Finally, electrochemically treated carbon fiber electrodes were used for in vitro detection of submicromolar DA concentrations in the presence of 200 μM AA (Figure 6). As previously reported (*14–17*) DA peaked at the same potential as DOPAC and other unmethylated or unconjugated catechols such as norepinephrine, L-3,4-dihydroxyphenylalanine, and 3,4-dihydroxyphenylethylene glycol. But the sensitivity for DA was about 100 times higher than for DOPAC. Figure 6 shows that the maximum peak height for DA was not immediately obtained. In fact this DA peak took 10–20 min (with or without voltammetric recordings) to reach a maximum. Consequently, and in contrast to DOPAC or AA measurement, every time the DA concentration was modified, about 15 scans (recorded every minute) were necessary to obtain a steady-state signal. However, the electrode used in Figure 6 was tested as described in Figure 6 with increasing DA concentrations (from 50 nM to 1 μM) and a linear response of the steady-state signal was observed from 50 nM to 0.5 μM. For higher concentrations the maximum peak height measured at the steady state still increased but not as much as predicted with a linear response.

DISCUSSION

The test voltammograms obtained from electrodes which were treated in the standard manner were not identical (compare Figures 2, 3, 4, and 5A). Moreover, the current which occurred through the carbon fiber electrode had a standard deviation of 10%. This latter variation can, however, be correlated to the resulting aspects of the test voltammograms. In fact the lowest maximum currents observed during standard treatments (in the range of 260–270 μA) correspond to treated electrodes which then exhibited tested voltammograms similar to those obtained with a 0 to +2.8 V treatment (Figure 3). This suggests that the relative lack of reproducibility could be due to some variation in the impedance of the carbon fiber electrodes. This suggests that the maximal density current, which reached about 2.5 A/cm^2 during standard treatment, could be a parameter as important as the applied potential

(Figure 3). However, since the duration of the treatment greatly influenced the resulting signals (Figure 4), it might be suggested that the total amount of current occurring through the electrode during the treatment could also be a significant factor.

The effect of chemical and electrochemical treatments on the pyrolytic carbon film electrode has already been reported (*11*). It has been shown that dichromate solution as well as electrochemical treatment (−4 V to +4 V applied using a square-wave generator for 4 min) improved the sensitivity and the reversibility in ferricyanide–ferrocyanide systems. However, electrochemical measurements were reported to be unreproducible except when the electrode was pretreated again just before each scan. These results are very close to ours with regard to chemical treatment as well as with the lowest electrochemical treatment (0 to +2 V, Figure 3). The fact that their −4 to +4 V electrochemical treatment gave results similar to our 0 to +2 V treatment could be explained by the fact that their electrode surface was more than 2000 times larger than ours. Thus, the current density applied to their electrode was presumably smaller than that which occurred during our standard treatment.

The most interesting feature of our electrochemically treated electrode is its ability to resolve catechols from AA which is achieved by moving AA redox potential to −80 mV. This potential corresponds very closely to the reversible formal potential given by Milazzo (*18*).

As regards peak heights (compare Figures 1 and 5A) the increase in sensitivity following electrochemical treatment was more than 1 order of magnitude for DOPAC. This sensitivity improvement is probably related to the DOPAC peak shifting and could be due to the improvement of the reversibility and consequently of the efficiency of the DOPAC oxidation reaction. With regard to DA, the increase in sensitivity was higher (more than 2 orders of magnitude). But in this case an adsorption mechanism might be suspected since a very progressive equilibration phenomenon occurred every time the DA concentration was modified. Finally the AA peak height was increased by the less aggressive treatments (left part of Figures 3 and 4) but was depressed by the most aggressive ones (right part of the Figures 3 and 4).

In light of these results, much more work is needed to support a valuable hypothesis about the mechanism by which such treatments act. However, it might be suggested that some unknown surface functionalities could be attached to the electrode surface during the treatment. The resulting improvement of sensitivity, reversibility, and selectivity could then be explained by a catalytic mechanism similar to that described by Kuwana and co-workers (*9*, *10*): the oxidation of the compound present in the solution could be initiated by the previous oxidation of the surface functionalities. However, this study underlines the importance of the current which occurred through the carbon fiber electrode during the treatment. Moreover, these data might be very useful for obtaining desirable performance from pyrolytic carbon electrodes used for in vivo neurochemistry or for other purposes.

ACKNOWLEDGMENT

We thank R. N. Adams for his helpful discussion and criticism of this work.

LITERATURE CITED

(1) Adams, R. N. *Anal. Chem.* **1976**, *48*, 1126A–1137A.
(2) Gonon, F.; Cespuglio, R.; Ponchon, J. L.; Buda, M.; Jouvet, M.; Adams, R. N.; Pujol, J. F. *C. R. Hebd. Seances Acad. Sci.* **1978**, *286*, 1203–1206.
(3) Lane, R. F.; Hubbard, A. T.; Blaha, C. D. *Bioelectrochem. Bioenerget.* **1978**, *5*, 506–527.
(4) Conti, J. C.; Strope, E.; Adams, R. N.; Marsden, C. A. *Life Sci.* **1978**, *23*, 2705–2716.
(5) Lane, R. F.; Hubbard, A. T.; Blaha, C. D. *J. Electroanal. Chem.* **1979**, *95*, 117–122.
(6) Lane, R. F.; Hubbard, A. T.; Fukunaga, K.; Blanchard, R. J. *Brain Res.* **1976**, *114*, 346–352.
(7) Ponchon, J. L.; Cespuglio, R.; Gonon, F.; Jouvet, M.; Pujol, J. F. *Anal. Chem.* **1979**, *51*, 1483–1486.
(8) Evans, J. F.; Kuwana, T. *Anal. Chem.* **1977**, *49*, 1632–1635.
(9) Evans, J. F.; Kuwana, T. *J. Electroanal. Chem.* **1977**, *80*, 409–416.
(10) Chi-Sing, D.; Kuwana, T. *Anal. Chem.* **1978**, *50*, 1315–1318.
(11) Blaedel, N. J.; Mabbott, G. A. *Anal. Chem.* **1978**, *50*, 933–936.
(12) Dayton, M. A.; Brown, J. C.; Stutts, K. J.; Wightman, R. M. *Anal. Chem.* **1980**, *52*, 946–950.
(13) Armstrong-James, M.; Millar, J.; Kruk, Z. L. *Nature (London)* **1980**, *288*, 181–183.
(14) Buda, M.; Gonon, F.; Cespuglio, R.; Jouvet, M.; Pujol, J. F. *C. R. Hebd. Seances Acad. Sci.* **1980**, *290*, 431–434.
(15) Gonon, F.; Buda, M.; Cespuglio, R.; Jouvet, M.; Pujol, J. F. *Nature (London)* **1980**, *286*, 902–904.
(16) Buda, M.; Gonon, F.; Cespuglio, R.; Jouvet, M.; Pujol, J. F. *Eur. J. Pharmacol.*, in press.
(17) Gonon, F.; Buda, M.; Cespuglio, R.; Jouvet, M.; Pujol, J. F. *Brain Res.*, in press.
(18) Milazzo, G. In "Electrochimie"; Dunod Ed.: Paris, 1969.

RECEIVED for review February 3, 1981. Accepted May 11, 1981. This research was supported by DGRST (Grants No. 7870156 and 7872788), INSERM U 171 and CNRS La 162.

Derivative Linear Sweep and Derivative Cyclic Voltabsorptometry

Eric E. Bancroft, James S. Sidwell, and Henry N. Blount*

Brown Chemical Laboratory, University of Delaware, Newark, Delaware 19711

A new spectroelectrochemical technique has been developed which couples linear and cyclic linear potential sweep perturbation of an optically transparent electrode (OTE) with optical monitoring of the light-absorbing product of the electrode reaction. For the O + ne^- = R couple, the absorbance of the product of the electrode reaction (A_R) is differentiated with respect to the linearly varying potential (dA_R/dE) and is displayed as a function of sweep potential. The techniques are termed *d*erivative *l*inear *s*weep *v*olt*a*bsorptometry (DLSVA) and *d*erivative *c*yclic *v*olt*a*bsorptometry (DCVA). The dA_R/dE vs. E waveforms are morphologically identical with the ideal linear sweep or cyclic voltammetric responses for the electrochemical process. The analytically significant derivative optical peak amplitude is given by $(dA_R/dE)_p = \beta n^{1/2}\epsilon_R D_O^{1/2} C_O^* \nu^{-1/2}$ where $\beta = -0.0881\ mV^{-1/2}$. This functional form has been experimentally verified by using four well-characterized electrochemical systems. For the two-electron oxidation of *o*-tolidine at a gold OTE in pH 2.00 phosphate buffer, the limit of detection of this technique has been found to be 3.8×10^{-7} M at a scan rate of 2.5 mV/s.

Since its inception in the mid-60s (*1*), the technique of absorption spectroelectrochemistry has been widely utilized to study the redox chemistry of numerous systems. This methodology which combines electrochemical perturbation of an optically transparent electrode (OTE) with simultaneous absorption spectrophotometric monitoring of the solution adjacent to the electrode surface has been successfully applied to the delineation of kinetic parameters characteristic of homogeneous chemical reactions which are coupled to the primary electrode process as well as to the evaluation of thermodynamic system parameters (*2–6*). Indirect coulometric titrations with optical monitoring have provided significant data on formal potentials and n values of biological redox components (*4, 5*). Potential step absorption spectroelectrochemistry (chronoabsorptometry) has also proven to be a viable tool for the determination of heterogeneous electron transfer kinetic parameters at both normal (*6*) and chemically modified (*7, 8*) OTEs.

Apart from indirect coulometric titrations (*4, 5*), absorption spectroelectrochemistry has enjoyed virtually no analytical applications. This is principally due to the morphology of the absorbance–time transient which is observed when potential step excitation techniques are employed. For the electrode process represented by

$$O + ne^- = R \tag{1}$$

application of a potential step of sufficient amplitude to cause reaction 1 to proceed at a diffusion-controlled rate results in the time-dependent absorbance of R given by (*9*)

$$A_R(\lambda,t) = 2\epsilon_R(\lambda) D_O^{1/2} C_O^* t^{1/2}/\pi^{1/2} \tag{2}$$

where ϵ_R (λ) is the molar absorptivity of R, D_O is the diffusion coefficient of O, and C_O^* is the bulk concentration of O. This functional form is analogous to that noted for the faradaic charge passed under the same experimental conditions, namely (*10*)

$$Q(t) = 2nFAD_O^{1/2} C_O^* t^{1/2}/\pi^{1/2} \tag{3}$$

where F is the Faraday constant and A is the electrode area.

Both $A_R(\lambda,t)$ and $Q(t)$ represent the integral of the flux of eq 1. It follows, then, that the derivative of the absorbance with respect to time is analogous to that of the charge with respect to time, namely, the current. Thus $dA_R(\lambda,t)/dt$ provides an alternative measure of the flux of the process of interest and does so with both the molecular specificity attendant to the use of optical monitoring and insensitivity to nonfaradaic charge-consuming processes (*11*). Moreover, the absorbance derivative suggests numerous analogues of electroanalytical techniques which can be expected to offer many advantages for the analysis of low concentrations of materials, the analysis of mixtures, the diagnosis of mechanisms of coupled chemical reactions as well as the evaluation of kinetic parameters which are characteristic of those reactions, and the determination of heterogeneous electron transfer kinetic parameters.

This report describes the optical analogue of linear sweep and cyclic voltammetry in which the absorbance of the product of the electrode reaction (A_R, eq 1) is differentiated with respect to the linearly varying scan potential and is displayed as a function of the scan potential. The resulting dA_R/dE vs. E waveforms are *morphologically* identical with their ideal current–potential analogues (Figure 1) and the methods are termed *d*erivative *l*inear *s*weep *v*olt*a*bsorptometry (DLSVA) and *d*erivative *c*yclic *v*olt*a*bsorptometry (DCVA).

THEORY

For the electrode process given by eq 1, the faradaic current observed under conditions of linear potential scan ($E = E_i - \nu t$) may be expressed as (*12, 13*)

$$i = nFAD_O^{1/2} C_O^* \nu^{1/2} \xi^{1/2} \pi^{1/2} \chi(x) \tag{4}$$

where ν is the rate of potential sweep, $\xi = nF/RT$, and the transcendental function $\pi^{1/2}\chi(x)$ (also known as the current function where $x = nF(E_{1/2} - E)/RT$) may be represented in series form as (*14*)

$$\pi^{1/2}\chi(x) = -\sum_{j=1}^{\infty} (-1)^j j^{1/2} \exp(j\xi\nu t - j\xi\Delta E) \tag{5}$$

where $\Delta E = E_i - E_{1/2}$, E_i is the initial potential, and $E_{1/2}$ is the polarographic half-wave potential. Substitution of eq 5 into eq 4 and subsequent integration afford the charge observed under conditions of linear potential scan, namely

$$Q = -nFAD_O^{1/2} C_O^* \xi^{-1/2} \nu^{-1/2} \sum_{j=1}^{\infty} (-1)^j j^{-1/2} [\exp(j\xi\nu t - j\xi\Delta E) - \exp(j\xi\Delta E)] \tag{6}$$

The absorbance of R is related to the charge passed in producing R according to

$$A_R = 10^3 \epsilon_R Q/nFA \tag{7}$$

Substitution of eq 6 into eq 7 and subsequent differentiation with respect to the electrode potential, E, and rearrangement

0003-2700/81/0353-1390$01.25/0 © 1981 American Chemical Society

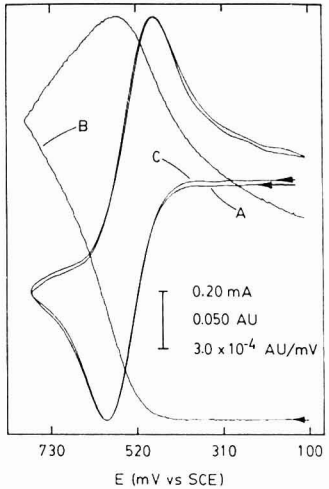


Figure 1. Simultaneously acquired current-potential (A) and absorbance-potential (B) responses for the cyclic linear sweep oxidation of 3.16 mM TAA at a platinum OTE in acetonitrile/0.100 M TEAP at ν = 551 mV/s. Trace (C) is the derivative of trace (B) with respect to scan potential. AU = absorbance unit; arrows indicate initial scan direction.

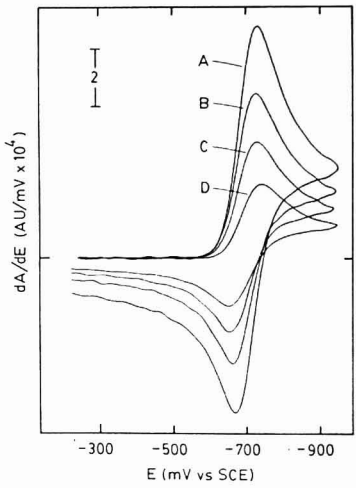


Figure 2. Variation of DCVA response with scan rate for 1.55 mM MV^{2+} at tin oxide OTE in pH 7.00 phosphate buffer. Scan rates are as follows: A, 25.0 mV/s; B, 50.0 mV/s; C, 97.2 mV/s; D, 265 mV/s.

gives rise to the functional form of the derivative optical signal shown in eq 8. Although the series representation of the dA_R/dE =

$$\epsilon_R D_O^{1/2} C_O^* \nu^{-1/2} \xi^{1/2} \sum_{j=1}^{\infty} (-1)^j j^{1/2} \exp(j\xi\nu t - j\xi\Delta E) \quad (8)$$

current function given in eq 5 is mathematically convenient for the manipulations described above, it is not well behaved for $x > 0$ which includes the analytically significant region of the voltammetric peak. Oldham (*15*) has recently reported several alternative series representations of the current function which are well behaved for all values of x. One particularly useful form is (*15*)

$$\pi^{1/2}\chi(x) = L + Mx - Nx^2 + (\pi/2)^{1/2} \sum_{k=1}^{\infty} (\gamma - x)^{1/2}(\gamma + 2x)/\gamma^3 - (8b^2 + 12bx - 15x^2)/8b^{7/2} \quad (9)$$

where $L = 0.380\,104\,813$, $M = 0.118\,680\,871$, $N = 0.043\,920\,560$, $\gamma = [(2k-1)^2\pi^2 + x^2]^{1/2}$, and $b = (2k-1)\pi$. At the voltammetric peak ($x = 1.1090$), $\pi^{1/2}\chi(x)$ is numerically equal to 0.44629 at 25 °C (*15*, *16*). Substitution of this value into eq 8 gives rise to the optical analogue of the Randles-Sevcik equation, namely

$$(dA_R/dE)_p = \beta n^{1/2} \epsilon_R D_O^{1/2} C_O^* \nu^{-1/2} \quad (10)$$

where $\beta = -0.088\,10\ mV^{-1/2}$, the concentration is in mol/L, and the scan rate is in mV/s.

EXPERIMENTAL SECTION

Materials. Potassium ferrocyanide (Mallinckrodt, Analytical Reagent) was used as received. Solutions of this reagent were prepared gravimetrically in pH 2.50 glycine buffer (0.50 M). Methyl viologen (Aldrich) was recrystallized three times from absolute ethanol and vacuum dried prior to preparation of sample solutions in pH 7.00 phosphate buffer (Titrisol, Merck) containing 0.100 M sodium chloride (Fisher). *o*-Tolidine (Fisher) was recrystallized three times from absolute methanol and vacuum dried (mp 130.5–131.5 °C, lit. (*17*) 130 °C). Solutions of this reagent were prepared in pH 2.00 phosphate buffer (0.50 M). Tri-*p*-anisylamine was prepared after the manner of Wieland and Wecker (*18*). Sources of and purification procedures for acetonitrile and tetraethylammonium perchlorate (TEAP) have been reported elsewhere (*19*, *20*). Deionized, glass distilled water was used in the preparation of all aqueous solutions. All sample solutions were prepared immediately prior to use and were deoxygenated with prepurified nitrogen (Linde) which had been passed over hot copper turnings and presaturated with the appropriate solvent. Concentrations of methyl viologen, *o*-tolidine, and tri-*p*-anisylamine were determined spectrophotometrically.

Apparatus. All electrode potentials are reported relative to the aqueous saturated calomel electrode (SCE) and were controlled by a potentiostat of conventional design (*6*). Fluoride-doped tin oxide (PPG Industries, Pittsburgh, PA), vapor deposited gold (*21*), and vapor deposited platinum (*21*) OTEs were fitted to cells which are similar in design to those already reported (*22*, *23*).

Both the potentiostat and the single-beam spectroelectrochemical apparatus (*24*) were interfaced to a dedicated NOVA 1200 (Data General Corp.) computer system (*25*) for both the simultaneous acquisition of electrochemical and optical signals and subsequent data processing. All measurements were made at 25.0 (±0.6) °C.

Computational Algorithms. Following data acquisition, the potential-dependent optical intensity was converted to an absorbance-potential file. The absorbance elements of this array were then subjected to two passes of a five-point moving average smoothing routine (*26*) followed by differentiation of the optical absorbance (*26*) with respect to potential. The resulting dA/dE vs. E waveform was then displayed as shown in Figures 2 and 3.

RESULTS AND DISCUSSION

To demonstrate that the dA/dE vs. E and i vs. E waveforms are morphologically identical, absorbance and current data were simultaneously acquired as a function of linearly varying potential for the monoelectronic oxidation of tri-*p*-anisylamine (TAA) to its corresponding cation radical ($TAA^{+\cdot}$) and subsequent reduction of $TAA^{+\cdot}$ back to TAA at a platinum OTE in acetonitrile containing 0.100 M TEAP. Shown in Figure 1 are the observed current-potential and cation radical absorbance-potential responses together with the derivative optical (dA_{TAA^+}/dE vs. E) waveform. The cyclic voltammetric (CV) and derivative optical (DCVA) responses are in excellent agreement.

Table I. Properties of Electrochemical Systems of Interest to This Work

precursor	medium	D,[a] $cm^2 s^{-1} \times 10^6$	OTE	electrode reaction	species monitored	λ_{max}, nm	$\epsilon(\lambda_{max})$, $M^{-1} cm^{-1} \times 10^{-4}$
MV^{2+}	aqueous phosphate (0.06 M) buffer, pH 7.00, 0.10 M NaCl	4.84	tin oxide	$MV^{2+} + e^- = MV^{+\cdot}$	$MV^{+\cdot}$	605	1.25[b]
$Fe(CN)_6^{4-}$	aqueous glycine (0.50 M) buffer, pH 2.50	6.55	tin oxide	$Fe(CN)_6^{4-} = Fe(CN)_6^{3-} + e^-$	$Fe(CN)_6^{3-}$	420	0.102[c]
TAA	acetonitrile, 0.10 M TEAP	10.1	platinum	$TAA = TAA^{+\cdot} + e^-$	$TAA^{+\cdot}$	715	3.30[d]
OT	aqueous phosphate (0.50 M) buffer, pH 2.00	5.62	gold	$OT = OT^{2+} + 2e^-$	OT^{2+}	437	6.20[e]

[a] Determined from single potential step spectroelectrochemical responses (9) and known molar absorptivities (see above). [b] Reference 27. [c] Reference 9. [d] Reference 2. [e] Reference 28, 29.

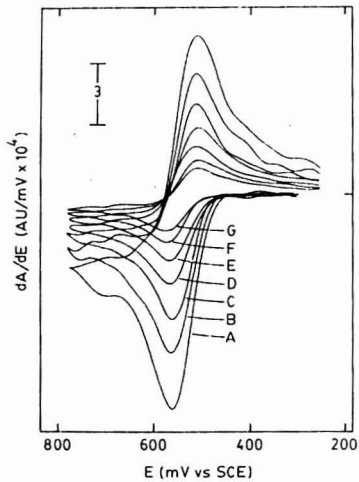


Figure 3. Variation of DCVA response with scan rate for 9.23×10^{-5} M OT at gold OTE in pH 2.00 phosphate buffer. Scan rates are as follows: A, 2.72 mV/s; B, 4.87 mV/s; C, 8.99 mV/s; D, 15.5 mV/s; E, 27.1 mV/s; F, 48.6 mV/s; G, 90.6 mV/s.

Examination of eq 10 reveals two unique features of the functional form of the derivative optical peak value. These are the *inverse* square root scan rate dependence and the dependence of $(dA/dE)_p$ on the n value of the system. The dependence of the derivative optical signal on the molar absorptivity of the electrode reaction product and on the concentration and diffusion coefficient of the electroactive species is to be expected.

In order to establish the validity of eq 10, several experimental systems have been characterized using the DLSVA and DCVA techniques. The salient features of these systems are summarized in Table I.

The dependence of the dA/dE waveform on scan rate has been established for all systems shown in Table I. Typical of these dependencies are those shown in Figure 2 for the derivative cyclic voltabsorptometric reduction of methyl viologen dication (MV^{2+}) to the corresponding cation radical ($MV^{+\cdot}$) and subsequent reoxidation at a tin oxide OTE in aqueous pH 7.00 phosphate buffer. The $(dA/dE)_p$ value for the reduction of MV^{2+} is clearly dependent upon the inverse square root of the scan rate as shown in Table II.

The concentration dependence of $(dA/dE)_p$ has been evaluated for each of the experimental systems listed in Table I. Typical of these data are those for the oxidation of TAA in acetonitrile (Table III) which indicate linear dependence of $(dA/dE)_p$ on concentration from 2.5×10^{-6} M to 2.5×10^{-3} M.

Table II. Dependence of $(dA/dE)_p$ on Scan Rate for the Reduction of MV^{2+} [a,c]

ν, mV/s	$\nu^{-1/2}$, $(mV/s)^{-1/2}$	$(dA/dE)_p$, AU/mV $\times 10^5$ [b]
2.50	0.632	235.
4.94	0.450	169.
15.0	0.258	97.2
25.0	0.200	75.0
50.0	0.141	54.2
97.2	0.101	36.9
158.	0.0796	28.4
265.	0.0614	22.1

[a] $[MV^{2+}] = 1.55 \times 10^{-3}$ M; $\epsilon_{MV^{+\cdot}} D^{1/2}_{MV^{2+}} = 27.5\ M^{-1}\ s^{-1/2}$ at 605 nm; solution conditions given in Table I. [b] Mean of triplicate determinations. [c] Regression statistics for plot of $(dA/dE)_p$ vs. $\nu^{-1/2}$: slope = 3.74 (±0.02) × 10^{-3}; intercept = −0.15 (±0.67) × 10^{-5}; coefficient of correlation = 0.999 90.

Table III. Dependence of $(dA/dE)_p$ on Concentration for the Oxidation of TAA [a,c]

[TAA], M × 10^5	$(dA/dE)_p$, AU/mV × 10^5 [b]
2.52	3.21
12.6	16.7
25.5	32.9
31.6	41.9
63.2	82.5
149.	198.
255.	331.

[a] $\nu = 50$ mV/s; $\epsilon_{TAA^{+\cdot}} D^{1/2}_{TAA} = 105\ M^{-1}\ s^{-1/2}$ at 715 nm; solution conditions given in Table I. [b] Mean of triplicate determinations. [c] Regression statistics for plot of $(dA/dE)_p$ vs. [TAA]: slope = 1.303 (±0.008); intercept = 0.45 (±0.90) × 10^{-5}; coefficient of correlation = 0.999 91.

The dependence of $(dA/dE)_p$ on the molar absorptivity of the electrode reaction product and the diffusion coefficient of the precursor has been evaluated through an examination of $(dA/dE)_p$ at a common scan rate for experimental systems having the same n value but widely differing $\epsilon_{product} D^{1/2}_{precursor}$ values. These are ferrocyanide oxidation in pH 2.50 glycine buffer, MV^{2+} reduction in pH 7.00 phosphate buffer, and TAA oxidation in acetonitrile. As shown in Table IV, the peak derivative optical signal is linearly dependent upon the product $\epsilon_{product} D^{1/2}_{precursor}$ over a 40-fold range of this parameter.

In order to test the n value dependence of $(dA/dE)_p$ predicted by eq 10, an experimental system which undergoes a

Table IV. Dependence of $(dA/dE)_p$ on $\epsilon_{product}D^{1/2}_{precursor}$[a,d]

precursor	$\epsilon_{product}D^{1/2}_{precursor}$, $M^{-1}\ s^{-1/2}$ [b]	$(dA/dE)_p$, AU/mV $\times 10^5$ [c]
$Fe(CN)_6^{4-}$	2.61 (±0.01)	3.23
MV^{2+}	27.5 (±0.1)	34.5
TAA	105 (±1)	129.

[a] Substrates present at 1.00 mM; ν = 50 mV/s; solution conditions given in Table I. [b] Determined from single potential step spectroelectrochemical responses. [c] Mean of triplicate determinations. [d] Regression statistics for plot of $(dA/dE)_p$ vs. $\epsilon_{product}D^{1/2}_{precursor}$: slope = 1.226 (±0.007) × 10^{-5}; intercept = 0.35 (±0.45) × 10^{-5}; coefficient of correlation = 0.999 98.

Table V. Dependence of $(dA/dE)_p$ on Scan Rate for Oxidation of OT[a,c]

ν, mV/s	$\nu^{-1/2}$, $(mV/s)^{-1/2}$	$(dA/dE)_p$, AU/mV $\times 10^4$ [b]
2.72	0.606	10.4
4.87	0.453	7.66
8.99	0.334	5.78
15.5	0.254	4.33
27.1	0.192	3.18
48.6	0.143	2.39
90.6	0.105	1.74

[a] [OT] = 9.23 × 10^{-5} M; $\epsilon_{OT^{2+}}D^{1/2}_{OT}$ = 147 $M^{-1}\ s^{-1/2}$ at 437 nm; solution conditions given in Table I. [b] Mean of triplicate determinations. [c] Regression statistics for plot of $(dA/dE)_p$ vs. $\nu^{-1/2}$: slope = 1.73 (±0.01) × 10^{-3}; intercept = −0.078 (±0.018) × 10^{-4}; coefficient of correlation = 0.999 83.

reversible, concerted two-electron transfer at the electrode to produce an absorbing product was examined by DLSVA and DCVA. At pH 2.00, *o*-tolidine (OT) is known to undergo a concerted two-electron oxidation to the corresponding quinonediimine (*28*) (OT^{2+}). The derivative optical response for this system as a function of scan rate is shown in Figure 3. For this $n = 2$ system, $(dA/dE)_p$ is also inversely dependent upon the square root of the scan rate as shown in Table V. The validity of the n-value dependence predicted by eq 10 has been established by comparing the ratios of the theoretical and experimentally determined $\beta n^{1/2}$ values for $n = 1$ and $n = 2$ systems. The dependence of $(dA/dE)_p$ on C^*, $\epsilon D^{1/2}$, and ν has been established (Tables II–V). Therefore the ratio

$$\frac{\left[\dfrac{(dA/dE)_p}{\epsilon D^{1/2}C^*\nu^{1/2}}\right]_{n=2}}{\left[\dfrac{(dA/dE)_p}{\epsilon D^{1/2}C^*\nu^{-1/2}}\right]_{n=1}} = \frac{\beta(2)^{1/2}}{\beta(1)^{1/2}} \qquad (11)$$

affords the necessary test relationship. For the three $n = 1$ systems, experimental results obtained for all scan rates and concentrations examined give rise to $\beta n^{1/2} = -0.087$ (±0.001). For the $n = 2$ system, $\beta n^{1/2}$ is expected to be $(2)^{1/2}$ times greater than this or −0.123. The experimental value of $\beta n^{1/2}$ for $n = 2$, determined with the OT system for all scan rates and concentrations examined, is −0.122 (±0.001) which is in excellent agreement with the expected value of −0.123. Thus the n-value dependence of the peak derivative optical signal is as predicted by eq 10. The experimentally determined value of β, based on 195 experiments conducted on four electrochemical systems at 19 concentrations and 27 scan rates is −0.087 (±0.002) $mV^{-1/2}$ and agrees well with the theoretical value of −0.0881 $mV^{-1/2}$ calculated at 25 °C.

Table VI. Effect of Scan Rate on DCVA and CV Peak Potential Separation[a]

ν, mV/s	$\Delta E_p(n = 1)$, mV [b]		$\Delta E_p(n = 2)$, mV [c]	
	DCVA	CV	DCVA	CV
2.50	58	59		
2.72			31	31
4.87			34	32
4.94	58	59		
8.99			34	36
15.0	58	59		
15.5			35	38
25.0	60	61		
27.1			37	39
48.6			38	41
50.0	62	63		
90.6			42	46
97.2	70	71		
150.			54	65
158.	74	75		
265.	82	84		

[a] Uncertainty in ΔE_p measurement ≃ ±1 mV. [b] $[MV^{2+}]$ = 1.55 × 10^{-3} M; solution conditions given in Table I. [c] [OT] = 1.75 × 10^{-4} M; solution conditions given in Table I.

The peak potential separation observed in both DCVA and CV responses increases with scan rate. This effect is reflected in the simultaneously acquired DCVA and CV data shown in Table VI. Although the peak potentials of the DCVA and CV responses are altered due to the ohmic resistances of the OTEs (*29*, *30*), the amplitude of $(dA/dE)_p$ is not perceptibly diminished over the scan ranges examined in this work as evidenced by the linear dependence of $(dA/dE)_p$ on $\nu^{-1/2}$ (Tables II and V). Like its optical counterpart, the normalized peak current ($i_p/\nu^{1/2}$) is, within experimental error, independent of scan rate. This invariance of the normalized current parameter indicates that the surface resistance of the OTEs, rather than double layer charging current, is the dominant contributor to the peak separations shown in Table VI. It is noteworthy that in the limit of slow scan rates, the peak separations observed in both DCVA and CV responses approach the expected values of 58 mV and 29 mV for $n = 1$ and $n = 2$, respectively (*31*).

The limit of detection ($S/N = 2$) of the linear sweep derivative optical methods is a function of the n value and $\epsilon D^{1/2}$ of the system under examination, the scan rate, and the performance characteristics of the spectrophotometer employed. Taking as representative those values for the TAA system ($n = 1$, $\epsilon_{TAA^{+\cdot}}D^{1/2}_{TAA} = 105$) and a nominal scan rate of 10 mV/s, the limit of detection has been experimentally evaluated in this present work as 1.5 × 10^{-6} M. This limit will decrease with increasing value of n and $\epsilon D^{1/2}$ and decreasing scan rate. For the OT system, for example ($n = 2$, $\epsilon_{OT^{2+}}D^{1/2}_{OT} = 147$), at the minimum scan rate employed in this work (2.50 mV/s), the limit of detection has been determined to be 3.8 × 10^{-7} M.

The dependence of the derivative optical response on scan rate makes this technique quite complementary to linear sweep and cyclic voltammetry. Depending upon the molar absorptivity of the monitored species, the derivative optical response may afford a more sensitive analytical tool than linear sweep voltammetry at the same rate of potential scan. At reduced scan rates, the analytical utility of DLSVA would be more favorable. The species selectivity attendant to the use of optical monitoring makes the derivative optical technique an attractive approach to the rapid quantitation and n-value determination of a single species of interest in systems which are not electrochemically "clean", i.e., systems where more

than one faradaic process is on-going. The insensitivity of the technique to nonfaradaic charge-consuming processes suggests its use in the determination of analytes in matrices such as physiological fluids which normally exhibit high background currents (32). The use of DLSVA and DCVA with multiple wavelength detection permits simultaneous multicomponent analysis with a single potential scan (32).

The DCVA technique also holds considerable promise for mechanism diagnosis and kinetic characterization of homogeneous chemical reactions which are coupled to the primary electrode reaction (33). In addition, heterogeneous electron transfer kinetic parameters can also be evaluated with DLSVA and DCVA (33).

ACKNOWLEDGMENT

Stimulating discussions with P. F. Seelig and the experimental assistance of E. R. Summers are gratefully acknowledged. This work was supported in part by grants from the University of Delaware Center for Catalytic Science and Technology, the University of Delaware Institute of Neuroscience (NIH Biomedical VII), and the North Atlantic Treaty Organization.

LITERATURE CITED

(1) Kuwana, T.; Darlington, R. K.; Leedy, D. W. *Anal. Chem.* **1964**, *36*, 2023.
(2) Kuwana, T.; Winograd, N. *Electroanal. Chem.* **1974**, *7*.
(3) Kuwana, T. *Ber. Bunsenges. Phys. Chem.* **1973**, *77*, 858.
(4) Kuwana, T.; Heineman, W. R. *Acc. Chem. Res.* **1976**, *9*, 241.
(5) Heineman, W. R. *Anal. Chem.* **1976**, *50*, 390A.
(6) Albertson, D. E.; Blount, H. N.; Hawkridge, F. M. *Anal. Chem.* **1979**, *51*, 556.
(7) Bowden, E. F.; Hawkridge, F. M.; Blount, H. N. *Bioelectrochem. Bioenerg.* **1980**, *7*, 447.
(8) Bowden, E. F.; Wang, M.; Bailey, J. W.; Hawkridge, F. M.; Blount, H. N. *J. Electrochem. Soc.*, in press.
(9) Winograd, N.; Blount, H. N.; Kuwana, T. *J. Phys. Chem.* **1969**, *73*, 3456.
(10) Delahay, P.; Charlot, G.; Laitinen, H. A. *Anal. Chem.* **1960**, *32* (6), 103A.
(11) Armstrong, N. R.; Vanderborgh, N. E.; Quinn, R. K. *J. Phys. Chem.* **1976**, *80*, 2740.
(12) Randles, J. E. B. *Trans. Faraday Soc.* **1948**, *44*, 327.
(13) Sevcik, A. *Collect. Czech. Chem. Commun.* **1948**, *13*, 349.
(14) Reinmuth, W. H. *Anal. Chem.* **1962**, *34*, 1446.
(15) Oldham, K. B. *J. Electroanal. Chem.* **1979**, *105*, 373.
(16) Nicholson, R. S.; Shain, I. *Anal. Chem.* **1964**, *36*, 706.
(17) *Beilstein*, E III 13, 484.
(18) Weiland, H.; Wecker, E. *Ber. Dtsch. Chem. Ges.* **1910**, *43*, 699.
(19) Evans, J. F.; Blount, H. N. *Anal. Lett.* **1974**, *7*, 445.
(20) Shang, D. T.; Blount, H. N. *J. Electroanal. Chem.* **1974**, *54*, 305.
(21) von Benken, W.; Kuwana, T. *Anal. Chem.* **1970**, *42*, 1114.
(22) Grant, G. C.; Kuwana, T. *J. Electroanal. Chem.* **1970**, *24*, 11.
(23) Hawkridge, F. M.; Kuwana, T. *Anal. Chem.* **1973**, *45*, 1021.
(24) Strojek, J. W.; Kuwana, T. *J. Electroanal. Chem.* **1968**, *16*, 471.
(25) Evans, J. F.; Blount, H. N. *J. Phys. Chem.* **1976**, *80*, 1011.
(26) Savitzky, A.; Golay, M. J. E. *Anal. Chem.* **1964**, *36*, 1627.
(27) Ito, M.; Kuwana, T. *J. Electroanal. Chem.* **1971**, *32*, 415.
(28) Kuwana, T.; Strojek, J. W. *Discuss. Faraday Soc.* **1968**, *45*, 134.
(29) Petek, M.; Neal, T. E.; Murray, R. W. *Anal. Chem.* **1971**, *43*, 1069.
(30) Osa, T.; Yildiz, A.; Kuwana, T. *J. Am. Chem. Soc.* **1969**, *91*, 3994.
(31) Matsuda, H.; Ayabe, Y. *Z. Elektrochem.* **1955**, *59*, 494.
(32) Blount, H. N.; Bancroft, E. E., unpublished work.
(33) Blount, H. N.; Sidwell, J. S., unpublished work.

RECEIVED for review February 17, 1981. Accepted May 4, 1981.

Digital Alternating Current Polarography with Microprocessor-Based Instrumentation

J. E. Anderson and A. M. Bond*

Division of Chemical and Physical Sciences, Deakin University, Waurn Ponds 3217, Victoria, Australia

The technique of digital ac polarography is described. In this technique, a small amplitude digital sine wave is applied to the cell instead of an analog sine wave. This signal is obtained from a microprocessor-based function generator and data acquisition system. Assuming that the 36-step sine wave produces a response similar to that in conventional ac polarography, current data are collected every 10° relative to the applied signal. By simulating the various electronic components found in conventional ac instruments, phase-sensitive detection of fundamental and second harmonics is also possible. A qualitative comparison between the absolute current polarograms and of the phase-sensitive fundamental harmonics is in excellent agreement with ac polarographic theory for a reversible system.

The instrumentation used to perform ac polarography is somewhat more extensive than that used in other forms of polarography. Even in the wide variety of pulse polarographic techniques which have emerged, the only additional circuitry required (besides a basic potentiostat) is a sample and hold amplifier if a microprocessor-based function generator is used. With the exception of the more recently developed fast Fourier transform (FFT) techniques (*1*, *2*) most ac instruments must also be equipped with: (1) a small amplitude ac signal source (and reference signal), (2) a high pass filter or tuned amplifier input, (3) a lock-in amplifier (phase sensitive detector), (4) phase shifting circuitry (if phase-sensitive detection is used), and finally (5) a low pass filter output (*3–5*). Although more and more instrument companies are providing these features as options to their polarographic instruments, they are often inflexible (with respect to ac amplitude, frequency, and phase selectivity) as well as costly. The use of on-line FFT in ac polarography is quite different from the above approach in that the only analog components which remain are the potentiostat and a low pass filter(s) (*1*). This technique is quite elegant and a wealth of information may be obtained from a single experiment. However, at present the necessity of a minicomputer or the equivalent in computing power still restricts the number of users of this technique.

We report on here the technique of digital ac polarography which uses a microprocessor data acquisition system to mimic the analog devices mentioned above which are necessary for conventional ac polarography. As in the FFT technique, the only analog component of the instrument is the potentiostat. Unlike the FFT technique, the software required is quite simple and may be easily accomplished in assembler language.

0003-2700/81/0353-1394$01.25/0 © 1981 American Chemical Society

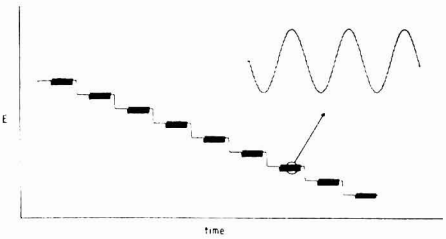


Figure 1. Waveform used in digital ac polarography.

It is apparent that the components necessary to perform digital ac polarography are the same as are required to perform the pulse techniques. From a commercial viewpoint, the cost and ease of use of this ac technique are essentially the same as for the pulse methods.

It should be mentioned that the software simulation of the electronic components in ac polarography has previously been suggested by Smith (*4*). However, this branch in the evolution of ac polarography was bypassed by this worker in favor of the FFT techniques.

EXPERIMENTAL SECTION

Instrumentation. The microprocessor-based instrumentation used in this work is identical with that used to perform variable-amplitude normal-pulse polarography (*6*) except that it was necessary to increase the memory capabilities to 16K of RAM. This system based on a Motorola 6800 D2 microprocessor "kit" has also been described in part elsewhere (*7*). Two 12-bit digital to analog converters (DAC) (Analog Devices DAC80-CB1-V) and a 12-bit analog to digital converter (ADC) (Analog Devices AD74JD) were interfaced to the system via three peripheral interface adapters (PIA). One of the DACs was used to generate the staircase ramp potential and the other to generate the digital ac sine wave as described later. The ADC was used to collect current data during the experiment. A homemade potentiostat was used in all experiments (*6*). Further information on the hardware or software may be obtained by writing to the authors.

Data were recorded on a Y-t recorder (Houston Instruments Model 2000) via the DAC after the experiments. A static mercury drop electrode (SMDE) Model 303 from E.G.+G. Princeton Applied Research Corp., Princeton, NJ, was used in all experiments. A platinum auxiliary electrode and a Ag/AgCl (saturated KCl) reference electrode were used in conjunction with the SMDE.

Reagents. Analytical reagent grade chemicals were used throughout as was distilled water. All solutions were degassed 4 min with high-purity nitrogen (two distilled water bubblers) prior to undertaking polarographic experiments. All polarograms were recorded at ambient temperatures of 21 (±1) °C.

RESULTS AND DISCUSSION

Figure 1 illustrates the digital sine wave superimposed on to a staircase ramp potential waveform. The two waveforms were summed via the summing amplifier type controller of the potentiostat. In addition, the output of the sine wave generated was scaled down from 8.19 V p-p to 0.0819 V p-p by the summing amplifier to reduce significant losses in resolution. Additional scaling of the sine wave may be achieved by software division by two (81.90, 40.95, 20.48, 10.24, 5.12 mV). Alternatively, intermediate amplitudes of sine waves could be obtained by adjusting the gain of the DAC output amplifier.

Each cycle of the digital sine wave was made up of 36 potential steps. The sine wave was obtained by stepping through a look-up table containing the appropriate codes for the DAC. This method was found to be faster than calculating the appropriate code prior to each step. This procedure could be carried out as many times as desired to produce multiple cycles. Each potential step in the sine wave consisted of: (1) a software delay, (2) sampling of the resulting current, and (3) a software delay (same as 1). The frequency of the resulting sine wave could be changed by varying the software delay times. Since the current was sampled once per step, 36 current measurements were made per cycle.

Assuming that this waveform adequately approaches a true sine wave, the collection of data may be considered to be in the frequency domain rather than in the time domain. This means the current is measured once every 10° with respect to the applied potential (360°/36 steps). Therefore in the following discussion the sampling of the current will be considered to be at a particular phase angle rather than at a particular position or step on the sine wave. However, from an instrumental point of view, time domain measurements are being made which have parallels with those in dc and pulse techniques. In subsequent discussion this mode of measurement is referred to as total alternating current polarography.

As is apparent from Figure 1, more than one cycle was applied at each ramp potential. In the work presented here a total of 18 cycles were applied on each ramp step. This was done for the twofold purpose of allowing the ac current to reach equilibrium after the initial application of the digital sine wave and for signal averaging purposes. It was assumed that transients would have vanished and that equilibration was achieved after two cycles of the sine wave and data collected during these cycles was discarded. The data from the remaining 16 cycles (576 points) were averaged as described below to eliminate the dc current and to improve the signal to noise ratio.

Since the dc component of the signal is a function of time ($t^{-1/2}$ with the SMDE) (*8*, *9*), it is difficult to obtain a mean dc current to subtract from the signal, particularly at low frequencies. To obtain the mean dc current, we averaged the data from one cycle (36 points) and subtracted from each of the individual points making up that particular cycle. This procedure was carried out on each of the 16 cycles of data. The data from the 16 cycles were then averaged to obtain a representative value (36 data points) at the given applied potential ramp step. This approach to eliminating the dc component assumes that the dc component is constant during the time of one cycle and will obviously be most effective at high frequencies. However, this filtering technique appeared to be quite effective in the frequency range studied (5–102 Hz). In analogy to conventional ac polarographic instrumentation, this procedure represents the high pass filter or tuned amplifier at the input. The data manipulation described above is summarized in the flow diagram in Figure 2.

Three factors determine the minimum drop time which may be achieved by using this procedure: (1) time before the sinusoidal signal is applied (determined by the staircase ramp generator), (2) time required to apply the sine waves, and (3) time required for data manipulation. By use of a 0.5 s delay before the sine wave was applied, a minimum drop time of ~1 s (total) could be used at 102 Hz. At 5 Hz the minimum drop time was ~3.5 s. These drop times are determined primarily by the time required to apply 18 cycles. Further experiments indicate that the number of cycles averaged could be reduced to eight or four without seriously lowering the signal to noise ratio. This approach could be useful in decreasing the total time required to perform an experiment. Indeed, this reduction in cycles may be necessary if this digital ac technique is used to study electrode kinetics. Since the surface concentration in other than reversible systems may still be time dependent, it may be necessary to know the time of measurement more accurately (rather than an average time).

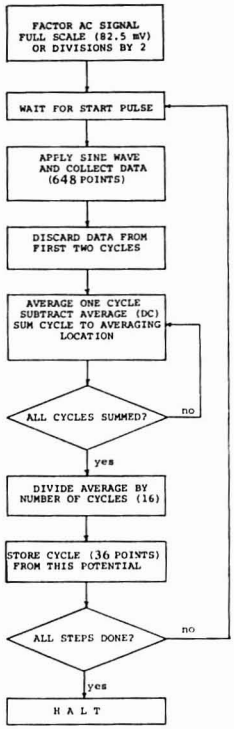


Figure 2. Flow diagram of software used in digital ac polarography.

As mentioned above, the maximum frequency studied was 102 Hz. This maximum frequency is a limitation of the microprocessor and data acquisition system used. In this case, the Motorola 6800 based system used has a 614.4-kHz clock. More recent experiments indicate that the use of a 1-mHz clock in the same system increases the maximum frequency to ~194 Hz. Although this frequency is still quite low compared to the capabilities of analog ac polarographic instrumentation, the work presented here was to test the basic concept of digital ac polarography. Analytical work in fact is usually confined to frequencies less than 100 Hz. Higher frequencies could easily be obtained by using a faster processor with a more extensive instruction set and faster data acquisition (ADC, etc.). The use of direct memory access or even decreasing the number of steps per sine wave are but two other possibilities. Therefore, the limited frequency range of the particular system described in this work should not be considered anywhere near the upper limit of this technique.

Once a particular experiment has been completed according to the potential region scanned, the data may be displayed in a number of ways via the DAC and Y-t (X-Y) recorder.

Figure 3 shows 37 polarograms which are obtained from a single scan from 0.5 to −0.8 V vs. SCE with 2 mV ramp steps of 5×10^{-4} M Cd(II) in 1.0 M KCl. In this display method, the phase angle was set to 0° (step 1 on the sine wave) and the current data from 0° from each ramp step is successively output via the DAC. Once the data from the entire scan has been output, the phase angle is incremented by 10° to display the next polarogram. The complete curve in Figure 3 consists

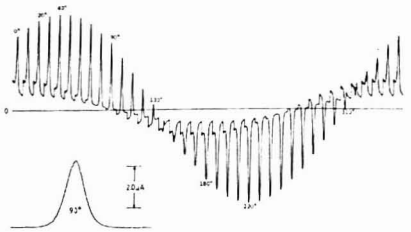


Figure 3. Digital total current ac polarograms at 0 to 360°; 5×10^{-4} M Cd(II) in 1.0 M KCl. Digital sine wave frequency of 83.3 Hz with an amplitude of 6.3 mV peak-to-peak. Dc potential scan from −0.45 to −0.85 V vs. Ag/AgCl with 2 mV ramp steps. Electrode area was 0.0156 cm^2. The solid horizontal line is the point of zero current. Also shown is the expanded ac polarogram at 90° relative to the applied potential.

of 7200 points. It is also apparent that in this digital approach the reference ac signal and the applied signal are one in the same. Also shown in Figure 3 is an expanded polarogram at 90°. In this case, the phase angle was specified and only one polarogram output (at a slower speed). Two important aspects of Figure 3 are that: (1) the amplitude of the charging current is at a maximum at ~0° and ~180° (zero at ~90° and ~270°, note solid line at zero current), (2) the amplitude of the faradaic current is at a maximum at ~45° and ~225° (zero at ~135° and ~315°). These observations are consistent with polarographic theory (for a reversible system) (*4*, *5*). It is possible some phase shift may exist in our data from *iR* drop since a positive feedback circuit to eliminate uncompensated resistance was not used. The use of the difference in phase of the capacitance and faradaic current is the basis of phase-sensitive detection as a means of minimizing the capacitance current from faradaic measurements (*3*).

The above technique of ac polarography measures what we refer to as total alternating current in a slightly different mode to that normally associated with ac polarography. An alternate method of displaying the data involves the use of software to mimic the last two components of a conventional phase-selective ac polarograph: a lock-in amplifier and finally a low pass filter. Up to this point the dc component and some unwanted frequencies have been minimized by averaging (high pass filter).

Lock-in amplifiers provide a very effective means of frequency discrimination in measurement systems and are presently used in most commercial ac polarographs. The lock-in amplifiers operation was simulated by summing the first 18 points with the 2 s complement of the last 18 points of a given cycle and dividing by 36. This operation is more closely related to synchronous rectification of the signal followed by application of a low pass filter. It may also be considered as multiplying the data of a cycle by a square wave of the same frequency with an amplitude of ±1.0 followed by averaging of the resulting 36 points. In this case the square wave is the reference signal. The net result of this operation enables the phase-selective ac polarograms to be produced with an improved signal to noise ratio.

As in the previous output method, the phase relationship between the signal and reference may be changed via software (phase shifter) and phase-sensitive detection achieved. Figure 4 shows the fundamental harmonic polarograms at phase angles of 0° to 180° using data shown in Figure 3. Again as expected, the capacitance current is now essentially zero at ~0° and ~180° and at a maximum amplitude at ~90° and ~270°. A comparison of Figures 3 and 4 indicates the expected decrease in noise obtained by using the lock-in am-

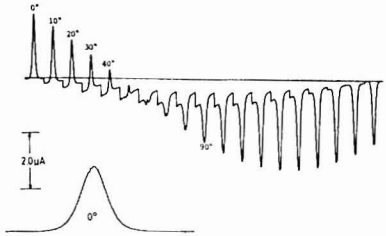


Figure 4. Phase selective fundamental harmonic digital ac polarograms at 0 to 180° using simulated lock-in amplifier. Same conditions as in Figure 3. Also shown is the fundamental harmonic at 0° expanded along the potential axis.

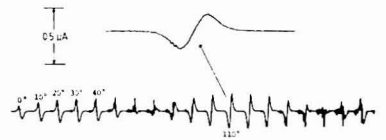


Figure 5. Phase selective second harmonic digital ac polarograms at 0 to 180°. Same conditions (data) as in Figure 3 and 4. In expanded form is the second harmonic response at 110°.

plifier approach. The Faradaic current now has its maximum amplitude at ~135° and ~315°. This technique is referred to as phase-selective ac polarography, because of its close relationship to the conventional analog instrumentation. In essence, the data are shifted -90° with respect to the total ac current version and the response is slightly decreased in amplitude.

Carrying the "lock-in amplifier" approach one step further, one may obtain higher harmonics of the ac polarogram by multiplying the signal by a reference square wave an integer multiple of the signal frequency. Since the digital sine wave used consisted of 36 steps, harmonics higher than the third may not be readily obtained. However, harmonics higher than the second are seldom of any practical use. The nonlinearity of the faradaic response which gives rise to higher harmonics is not shared by the capacitance component so the second harmonic is often of interest because of the near absence of this capacitance component (*3*). Figure 5 shows the second harmonic response of the data (in Figures 3 and 4) at various phase angles. It is clear that the capacitance current is absent in the second harmonic at all phase angles and that the appropriate wave shape is obtained for phase-sensitive second harmonic ac polarography. When the third harmonic was observed, it was apparent that the wave shape was not as predicted (derivative of the second harmonic). Due to the smaller amplitude of the third harmonic, the output had to be expanded to the point where the resolution of the ADC and DAC distorted the data. Therefore, the third harmonic is not shown here.

It should be noted that up to this point no mention has been made concerning the assumption that the digital sine wave used adequately simulates an analog sine wave. Qualitatively, the results suggest that the digital sine wave gives the predicted results for the fundamental and second harmonics based on a theoretical model assuming a pure sine wave. It is undoubtedly at higher harmonics that the deviation caused by the use of a step function will first appear. Apparently resolution based upon 36 steps is inadequate for accurate resolution of the third harmonic.

Quantitative comparison between the digital ac method and ac theory for the fundamental harmonic indicates excellent

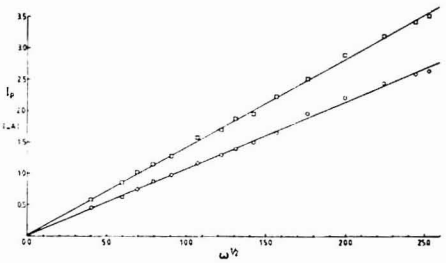


Figure 6. Plot of peak current (I_p) of total ac current (90°) and phase-selective fundamental harmonic (0°) polarograms vs. the square root of the angular velocity ($\omega^{1/2}$): total current, □; phase-selective fundamental harmonic, O; 5 × 10^{-4} M Cd(II) in 1.0 M KCl. Sine wave amplitude was 6.3 mV peak to peak.

agreement. Figure 6 shows a plot of peak ac current vs. the square root of the angular velocity for both methods of measurement with the Cd(II) system. As expected for a reversible system (in this frequency range) a straight line is obtained with a zero intercept (*3*). Cd(II) reduction is known to show this behavior in conventional ac polarography in this frequency range. Finally, an additional check for reversibility is a plot of E vs. $\log [(I_p/I)^{1/2} \pm ((I_p - I)/I)^{1/2}]$ which should be linear, where I_p is the peak current (*3*). This procedure is based on the fact that for a small applied ac potential, the shape of the ac response appears as the first derivative of the dc wave. These plots of the absolute current at 90° and the in-phase first harmonic of digital ac data yield slopes of 61 and 59 mV, respectively, compared to the theoretical value of 118.2/n mV (*3*). These features, coupled with the observation of the expected phase-angle response are indicative of a close approximation to results obtained with a conventional analog ac polarograph.

CONCLUSIONS

The technique of digital ac polarography appears to yield results in excellent qualitative agreement with its theoretical analog counterpart. The microprocessor-based instrumentation required is the same as that for the various pulse polarographic techniques. Therefore, the software simulation of the components of ac instrumentation reduces the hardware requirements necessary for ac polarography. It is also apparent that much more information is collected in a single digital ac experiment than is possible using analog instrumentation. For example, once an experiment has been performed either the total current or fundamental ac polarograms may be examined. The phase angle may then be easily adjusted to minimize the charging current. This technique is somewhat more closely related to FFT ac polarography in that the only analog circuitry needed is the potentiostat. Although the FFT approach has many advantages, it is at present out of the range of most users' financial resources and therefore it is only used in a very limited number of laboratories.

The digital ac polarographic technique described appears to be a viable intermediate between analog and FFT ac polarography primarily becuase of its simplicity and low cost.

ACKNOWLEDGMENT

The authors thank Fred L. Walter and Howard B. Greenhill for their work on the hardware and helpful discussion.

LITERATURE CITED

(1) Smith, D. E. *Anal. Chem.* **1976**, *48*, 221A–240A.
(2) Smith, D. E. *Comput. Chem. Instrum.* **1972**, *2*, 369–422.
(3) Smith, D. E. In "Electroanalytical Chemistry"; Bard, A. J., Ed.; Marcel Dekker, New York, 1966; Vol. I, Chapter 1.
(4) Smith, D. E., *CRC Crit. Rev. Anal. Chem.* **1971**, *2*, 247–343.

(5) Bond, A. M. "Modern Polarographic Methods in Analytical Chemistry"; Marcel Dekker: New York and Basel, 1980; Chapter 7.
(6) Anderson, J. E.; Bond, A. M. *Anal. Chem.* **1981**, *53*, 504-508.
(7) Anderson, J. E.; Bagchi, R. N.; Bond, A. M.; Greenhill, H. B.; Henderson, T. L.; Walter, F. L. *Am. Lab. (Fairfield, Conn.)* **1981**, *13*(2), 21-32.
(8) Bond, A. M.; Jones, R. D. *Anal. Chim. Acta* **1980**, *121*, 1-11.
(9) Anderson, J. E.; Bond, A. M.; Jones, R. D. *Anal. Chem.* **1981**, *53*, 1016-1020.
(10) Bond, A. M.; O'Halloran, R. J.; Ruzic, I.; Smith, D. E. *J. Electroanal. Chem.* **1978**, *90*, 381-388.

RECEIVED for review December 29, 1980. Accepted April 20, 1981. The financial assistance of the Australian Research Grants Committee in support of this work is gratefully acknowledged.

Multielement Analysis of Human Blood Serum by Neutron Activation and Controlled Potential Electrolysis

Kari Jorstad,* Brit Salbu, and Alexis C. Pappas

Department of Chemistry, University of Oslo, Oslo, Norway

The combination of neutron activation analysis and controlled potential electrolysis has proved itself to be a useful multielement method for the determination of 14 elements in a 500-μL sample of human blood serum. After freeze-drying and irradiation, the samples are decomposed and electrolyzed for 3 h. The radioactive species deposited on the mercury cathode allow simultaneous determination of eight elements (Ag, Au, Cd, Co, Fe, Hg, Sb, Zn). Another six elements (Br, Ca, Cs, Na, Rb, Sc) are determined by measuring the activities in the residual solution. Data illustrating the precision of the method are given. The determination limits are of the order 10^{-1}–10^{-3} μg/L for the nine trace elements investigated.

According to the World Health Organization (*1*) 14 trace elements, i.e., Co, Cr, Cu, F, Fe, I, Mn, Mo, Ni, Se, Si, Sn, V, and Zn, are considered to be essential to the human organism. Several other elements (e.g., Br, Ba, Sr) are supposed to be added to the list as more knowledge about their metabolic functions is obtained.

The concentrations of the trace elements in body tissues and fluids are frequently in the parts-per-billion range or lower. The metabolism of a healthy individual maintains the concentrations of trace elements within narrow limits. In addition, the concentration ranges between essential and toxic levels for different chemical forms of elements are rather narrow. Moreover, species of several elements (e.g., As, Cd, Hg, Pb) are assumed to be hazardous even in very low concentrations. Thus, investigation of trace elements in human tissues and body fluids has become a field of great emphasis in recent years, and attempts have been made to relate changes in concentration of specific elements to various diseases. In some cases such relationships are firmly established (*2-6*).

Human blood serum supplies all parts of the body with necessary components, and it can be obtained easily and frequently in routine procedures. Thus, analysis of human blood serum is very useful in studies of trace elements in man (*5-8*).

However, the number of useful methods for multielement analysis of human blood serum is rather limited, due to the low concentrations involved and to interfering effects of the matrix.

Application of instrumental neutron activation analysis (INAA) to whole blood and serum has recently been reported (*8-12*). After irradiation with thermal neutrons, whole blood and blood serum show a γ-spectrum in which the predominant nuclide 15.0 h ^{24}Na prevents determination of other elements. The background activity is also increased by the presence of 35.4 h ^{82}Br and 14.3 days ^{32}P (bremsstrahlung).

Most applications are therefore hampered by these effects and the resulting necessity of singling out groups of elements. This requires many samples, a variety of irradiation times (10 s–10 days) and decay times (10 s–6 months), or introduction of radiochemical separation procedures. In this way only, a number of elements can be determined by neutron activation analysis; however, it is expensive and time-consuming.

The elimination of Na, Br, and P without affecting the concentration of activation products of other elements of interest would not only permit simultaneous determination of a greater number of trace elements but also reduce the irradiation time and avoid the long decay times mentioned above.

The present paper describes a technique based on a combination of neutron activation and controlled potential electrolysis for the simultaneous determination of eight elements (Ag, Au, Cd, Co, Fe, Hg, Sb, Zn) in human blood serum 3 days after irradiation. During the electrolysis, reducible species in solution will be deposited on the cathode, while the interfering elements Na, Br, and P will remain in solution. In addition, another six elements (Br, Ca, Cs, Na, Rb, Sc) may be determined in the residual solution of the sample by means of their activation products, 3-4 weeks later.

Table I. Elemental Content of Seronorm, Batch No. 139

element	certified values (*13*)	this work
Ag (μg/L)		3.64 ± 0.07
Au (μg/L)		0.72 ± 0.02
Br (mg/L)		1.48 ± 0.04
Ca (mg/L)	109	108 ± 3
Cd (μg/L)		9.2 ± 0.3
Co (μg/L)		1.39 ± 0.03
Cs (μg/L)		2.68 ± 0.09
Fe (mg/L)	1.54	1.54 ± 0.05
Hg (μg/L)		2.67 ± 0.08
Na (g/L)	3.06	3.06 ± 0.03
Rb (μg/L)		350 ± 7
Sb (μg/L)		0.85 ± 0.02
Sc (μg/L)		0.053 ± 0.003
Zn (μg/L)	804	803 ± 9

METHOD OF ANALYSIS

Reference Standard. Seronorm (batch no. 139, standard reference material from NYCO, Oslo (*13*)) with certified values for Fe, Zn, Ca, and Na was used as a standard. On the basis of

0003-2700/81/0353-1398$01.25/0 © 1981 American Chemical Society

Table II. Elements Determined by Neutron Activation and Controlled Potential Electrolysis of Human Blood Serum

element	nuclide	half-life	most abundant γ-ray, keV
	Deposited on the Mercury Electrode		
Ag	^{110m}Ag	250.4 days	657.7
Au	^{198}Au	2.7 days	411.8
Cd	^{115}Cd	2.2 days	527.9
Co	^{60}Co	5.26 years	1332.5
Fe	^{59}Fe	44.6 days	1099.3
Hg	^{203}Hg	46.6 days	279.2
Sb	^{122}Sb	2.7 days	564.1
Zn	^{65}Zn	243.8 days	1115.5
	Left in Solution		
Br	^{82}Br	35.4 h	554.3
Ca	^{47}Ca-^{47}Sc	4.54 + 3.40 days	159.4
Cs	^{134}Cs	2.05 years	604.7
Na	^{24}Na	15.0 h	1368.6
Rb	^{86}Rb	18.6 days	1078.8
Sc	^{46}Sc	83.9 days	889.3

standard solutions, the Seronorm concentrations of the above mentioned four elements, and of Ag, Au, Br, Cd, Co, Cs, Hg, Rb, Sb, and Sc, were determined, using the present method and INAA. As seen from Table I, the values obtained for Fe, Zn, Ca, and Na are in full agreement with their certified values. Thus, this batch of Seronorm serves as a multielement standard for all the elements in question.

Sample Preparation. Samples of human blood serum and Seronorm (500 μL) are pipetted into quartz ampules, using Eppendorf pipets, as described by Medina et al. (*14*). The samples are freeze-dried for 5 h under a pressure of 0.05 torr, which has been shown to be a convenient drying procedure for biological samples, including blood serum (*15*). The ampules are then heat-sealed.

Irradiation. Samples of human blood serum and of Seronorm are irradiated for 3 days at a fixed position in the reactor JEEP II, Institute for Energy Technology, Kjeller, Norway, at a thermal neutron flux of 1.5×10^{13} neutrons cm^{-2} s^{-1}.

Controlled Potential Electrolysis. After a decay time of 3 days, the freeze-dried samples of human blood serum and Seronorm are decomposed by 0.5 mL of concentrated H_2SO_4 and 1 mL of concentrated HNO_3, and diluted to 20 mL with distilled water. Tests have shown that the usual addition of carrier is unnecessary in the present procedure.

The electrolysis used is a modification of the method reported by Jørstad and Salbu (*16*) for the determination of 28 elements in seawater. The main modification is that the magnetic stirrer is replaced by a synchronous electric stirrer, to avoid the deviation from a first-order kinetic expression when minute concentrations are reached during the electrolysis (*16*).

Controlled potential electrolysis is performed by means of a potentiostat especially contructed for this purpose (*17*). Mercury is used as cathode material (area 8 cm^2), a platinum coil serves as counterelectrode, and the reference electrode is a saturated Ag/AgCl electrode. The applied potential is −1.5 V, the volume of electrolyte 20 mL, and the temperature 22 ± 2 °C. For further details, reference is given to Jørstad and Salbu (*16*).

Each sample of human blood serum and of Seronorm is electrolyzed for 3 h, which is shown to be sufficient for maximum deposition of the electroactive forms of the elements in question. The mercury cathode is then transferred into an especially constructed container for measurement of the radionuclides deposited on the mercury electrode. The residual solution is transferred to a counting vial in order to measure the nonelectroactive species.

Counting and Data Processing. In the present study, the radioactivity measurements were based on Ge(Li) γ-spectrometry (efficiency of 20.7% and resolution of 1.89 keV, defined by means of the 1332.5-keV γ from ^{60}Co). The elements determined, their corresponding radionuclides, and the γ energies used in the measurements are given in Table II. Peak location and calculation of peak areas were performed by means of GAMANL, a computer program developed by Gunnink et al. (*18*) and adjusted to the CDC-CYBER 74 computer at the University of Oslo by Scheidemann (*19*).

The concentrations of Ag, Au, Cd, Co, Fe, Hg, Sb, and Zn were determined by measuring the γ-spectrum of the mercury electrode. As seen from Figure 1, which shows a typical spectrum, matrix elements (i.e., ^{24}Na, ^{82}Br, ^{32}P) are no longer interfering. Thus, a simultaneous determination of the above mentioned elements is obtained.

Determination of Br, Ca, Cs, Na, Rb, and Sc was carried out by γ-spectrometry of the residual solution 1 week (Br, Na) and 3–4 weeks (Ca, Cs, Rb, Sc) after irradiation.

RESULTS AND DISCUSSION

The described method has been tested and applied to serum samples from individuals in a healthy state.

The results obtained for the 14 elements are in good agreement with literature values compiled by Iyengar et al. (*20*) and results for Norwegian individuals reported by Blekastad et al. (*21*) (Table III).

In order to investigate the reproducibility of the method, we analyzed four aliquots of human blood serum. The results obtained, together with the maximum deviation from the mean value for each element, are listed in Table IV. The precision varies from 3% (Ag, Fe, Br, Ca, Cs, Na) to 7% (Sc).

The determination limits (n_Q) (Table V) of the present method are calculated by using the GAMANL (*18, 19*) criterion of the least possible registerable peak area, as described by Salbu et al. (*22*). The determination limits are of the order 10^{-1}–10^{-3} μg/L for the nine trace elements investigated. The

Table III. Content of Some Elements in Human Blood Serum

element	this work		Iyengar et al. (*20*)		Blekastad et al. (*21*)
	mean value	range	mean value	range	mean value
		Deposited on the Mercury Electrode			
Ag (μg/L)	6.60	5.17–7.84		2.9–200	
Au (μg/L)	0.32	0.17–0.44	0.08		
Cd (μg/L)	10.07	8.11–12.91		2.3–12	
Co (μg/L)	0.67	0.32–1.04		0.22–14	
Fe (mg/L)	1.35	1.04–1.67	1.09	0.87–1.87	1.7 ± 1.4
Hg (μg/L)	8.38	7.18–9.74	12		1.3 ± 0.8
Sb (μg/L)	2.82	2.43–3.33		2.5–3.2	≤0.3 ± 0.2
Zn (mg/L)	1.38	1.02–1.72	1.15	0.67–1.83	0.84 ± 0.14
		Left in Solution			
Br (mg/L)	2.24	1.92–2.73	3.9	1.04–7.5	2.4 ± 0.8
Ca (mg/L)	106.01	98.16–113.41	97	92–109	
Cs (μg/L)	1.60	1.48–1.74		1.33–60	1.5 ± 0.9
Na (g/L)	3.11	2.97–3.21	3.251	3.130–3.70	3.21 ± 0.12
Rb (μg/L)	169.76	159.13–192.64	200	40–580	250 ± 60
Sc (μg/L)	0.074	0.052–0.096	0.15		

Table IV. Data Obtained by Analysis of Four Aliquots of Human Blood Serum

element	parallel 1	parallel 2	parallel 3	parallel 4	mean value	max dev from mean value, %
			Deposited on the Mercury Electrode			
Ag (μg/L)	5.33	5.31	5.11	5.37	5.28	3
Au (μg/L)	0.42	0.42	0.39	0.41	0.41	5
Cd (μg/L)	12.58	13.22	12.73	11.87	12.60	6
Co (μg/L)	0.56	0.60	0.61	0.59	0.59	5
Fe (mg/L)	1.22	1.16	1.20	1.17	1.19	3
Hg (μg/L)	7.96	7.73	8.17	8.34	8.05	4
Sb (μg/L)	2.71	2.53	2.47	2.65	2.59	5
Zn (mg/L)	1.06	1.05	0.99	0.97	1.02	5
			Left in Solution			
Br (mg/L)	1.98	2.04	1.95	2.07	2.01	3
Ca (mg/L)	115.52	111.31	117.26	115.43	114.88	3
Cs (μg/L)	1.38	1.45	1.47	1.47	1.43	3
Na (g/L)	3.08	2.94	2.98	3.12	3.03	3
Rb (μg/L)	161.15	175.63	182.19	165.63	171.15	6
Sc (μg/L)	0.060	0.057	0.054	0.059	0.058	7

Table V. Determination Limits of the Present Method Applied to Samples of Human Blood Serum

element	determination limit, n_Q, μg/L	background level, counts/channel
	Deposited on the Mercury Electrode	
Ag	0.81	70
Au	0.004	200
Cd	0.25	120
Co	0.004	40
Fe	36.30	80
Hg	0.012	500
Sb	0.014	90
Zn	40.90	80
	Left in Solution	
Br	2.33	5000
Ca	54.79	240
Cs	0.20	40
Na	46.73	1700
Rb	0.89	10
Sc	0.0023	20

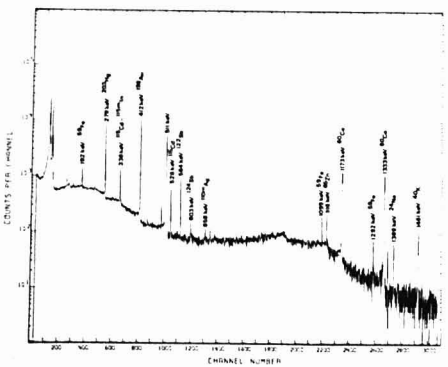


Figure 1. γ-spectrum of the mercury electrode after electrolyzing human blood serum for 3 h.

remaining five elements (Fe, Zn, Br, Ca, Na) occur in human blood serum as major elements.

A comparison between the results obtained by the present method and by conventional instrumental neutron activation analysis (INAA) is given in Table VI. Ag, Au, Cd, and Sb cannot be determined by INAA. The results obtained by using

Table VI. Elements Determined by Controlled Potential Electrolysis and by INAA

element	controlled potential electrolysis[a]	INAA[a]
	Deposited on the Mercury Electrode	
Co (μg/L)	0.59 ± 0.03	0.63 ± 0.04
Fe (mg/L)	1.19 ± 0.03	1.13 ± 0.05
Hg (μg/L)	8.1 ± 0.3	7.8 ± 0.4
Zn (mg/L)	1.02 ± 0.05	1.09 ± 0.06
	Left in Solution	
Br (mg/L)	2.01 ± 0.06	2.02 ± 0.05
Ca (mg/L)	115 ± 4	119 ± 6
Cs (μg/L)	1.43 ± 0.05	1.50 ± 0.08
Na (g/L)	3.03 ± 0.09	2.94 ± 0.06
Rb (μg/L)	171 ± 11	180 ± 14
Sc (μg/L)	0.058 ± 0.004	0.056 ± 0.006

[a] Mean values based on analysis of four aliquots.

Table VII. The Fractional Deposition of Some Elements after Electrolyzing for 3 h

element	% deposition: human blood serum	% deposition: Seronorm
Co	92.3	92.1
Fe	73.1	72.6
Hg	81.2	80.9
Zn	88.1	88.8

controlled potential electrolysis as here described are in good agreement with those obtained by using INAA. However, a decay time of 3–4 weeks is required when using INAA, as compared to 3 days when using the present method. Hence, introduction of controlled potential electrolysis as a chemical separation step not only eliminates the long decay time required by INAA but moreover allows determination of a greater number of elements, without affecting the concentration of the elements remaining in solution after the electrolysis.

Measurements of the residual solution allow determination of the fractions of Co, Fe, Hg, and Zn not deposited on the mercury electrode during electrolysis. The fractional deposition of these four elements in human blood serum and Seronorm is given in Table VII. As no further deposition takes place during 12 h of electrolysis, small amounts of these elements most likely occur in nonelectroactive forms. This may be caused by an incomplete decomposition of the irradiated sample. However, tests including different destruction

procedures show no change in the nonelectroactive fractions.

Emphasis should also be placed on the fact that no contamination problems occur during electrolysis, as only radioactive species are being measured, deposited on the electrode, or left in the solution.

CONCLUSIONS

The present paper shows that the combination of neutron activation and controlled potential electrolysis is a very convenient analytical method for determination of 14 elements in a 500-μL sample of human blood serum. The method may also be used in multielement analysis of other human body tissues and fluids having high content of interfering elements.

Biologically active trace elements in body fluids are often associated with particular compounds (e.g., organic ligands). Thus, in combination with biochemical separation techniques, trace element analysis as described in the present paper may elucidate associations to fractions of proteins, and information of chemical states of different trace elements are obtained.

As measurable changes in the trace element content in body fluids and tissues occur with certain diseases, determination of trace elements and their chemical states may give valuable information for diagnostic work and in treatment planning.

ACKNOWLEDGMENT

The authors are indebted to E. Jellum, Norwegian State Hospital, Oslo, for kindly providing the serum samples.

LITERATURE CITED

(1) Trace Elements in Human Nutrition *W. H. O. Tech. Rep. Ser.* **1973**, *No. 532*.
(2) Schroeder, H. A.; Nason, A. P. *Clin. Chem.* **1971**, *17*, 461–474.
(3) Danielsen, A.; Steinnes, E. *J. Nucl. Med.* **1970**, *11*, 260–264.
(4) Mulay, I. L.; Roy, R.; Knox, B. E.; Suhr, N. H.; Delaney, W. E. *J. Natl. Cancer Inst.* **1971**, *47*, 1–11.
(5) Nuryagdyev, S. K. *Vopr. Onkol.* **1971**, *17*, 7–12.
(6) Arsagova, N. S. *Vopr. Onkol.* **1971**, *17*, 53–56.
(7) Nakahara, H.; Nagame, Y.; Yoshizawa, Y.; Oda, H.; Gotoh, S.; Murakami, Y. *J. Radioanal. Chem.* **1979**, *54*, 183–190.
(8) Zdankiewicz, D. D.; Fasching, J. L. *Clin. Chem.* **1976**, *22*, 1361–1365.
(9) Fritze, K.; Robertson, R. *J. Radioanal. Chem.* **1968**, *1*, 463–473.
(10) Anovski, T.; Memedovic, T.; Rastvovac, M. *J. Radioanal. Chem.* **1972**, *12*, 483–489.
(11) Behne, D.; Jürgensen, H. *J. Radioanal. Chem.* **1978**, *42*, 447–453.
(12) Ward, N. I.; Ryan, D. E. *Anal. Chim. Acta* **1979**, *105*, 185–197.
(13) Seronorm, Batch no. 139, Nyegaard & Co. AS, Oslo, 1977.
(14) Medina, F.; Cheong, V.; Peck, C.; Bensinger, T. A. *Clin. Chem.* **1977**, *23*, 1188–1189.
(15) Iyengar, G. V.; Kasperek, K.; Feinendegen, L. E. *Sci. Total Environ.* **1978**, *10*, 1–16.
(16) Jorstad, K.; Salbu, B. *Anal. Chem.* **1980**, *52*, 672–676.
(17) Knutsen, P. D. Thesis, Department of Chemistry, University of Oslo, 1979.
(18) Gunnink, R.; Levy, H. B.; Niday, B. UCID-15140, 1967.
(19) Scheidemann, O. Internal report no. 1, Department of Chemistry, Nuclear Chemistry Division, University of Oslo, 1970.
(20) Iyengar, G. V.; Kollmer, W. E.; Bowen, H. J. M. "The Elemental Composition of Human Tissues and Body Fluids"; Verlag Chemie: Weinheim and New York, 1978.
(21) Blekastad, V.; Jonsen, J.; Steinnes, E. "Concentrations of Trace Elements in Human Blood Serum from different Places in Norway Determined by Neutron Activation Analysis", manuscript submitted for publication, University of Oslo, Feb 1981.
(22) Salbu, B.; Steinnes, E.; Pappas, A. C. *Anal. Chem.* **1975**, *47*, 1011–1016.

RECEIVED for review March 3, 1981. Accepted April 4, 1981. Karl Jostad and Brit Salbu are indebted to the Norwegian Research Council for Science and the Humanities for fellowships provided.

Model for Treatment of Selectivity Coefficients for Solid-State Ion-Selective Electrodes

Adam Hulanicki and Andrzej Lewenstam*

Department of Chemistry, University of Warsaw, 02-093 Warsaw, Poland

The model presented provides an explanation of the observed variability among selectivity coefficients of the solid-state ion-selective electrodes (ISE). This model considers the mechanism of metathetic reactions at the membrane surface and describes the sensed surface ion concentrations in terms of the bulk solution concentrations. The influence of various parameters such as bulk concentrations, time, temperature, and stirring rate on determined selectivity coefficients is discussed. Currently existing models are shown to be limiting cases of the presented model. The AgCl|Br^-, AgBr|Cl^-, and LaF_3|OH^- systems were chosen as representatives of the solid-state ISEs.

The selectivity coefficient for an ion-selective electrode (ISE) is of great interest from both theoretical and empirical points of view. Theoretical interpretations of this parameter first appeared in the works of Dole (*1*) and Nikolsky (*2*). More empirical approaches have been reviewed recently (*3*).

It is well-known that empirically determined values of selectivity coefficients may be different, depending on the method of determination (separate or mixed solutions), the measurement technique (the time elapsed for observing potential, stirring, etc.) chemical conditions in the solution (composition, levels of ion concentration), the character and kinetics of electrode reaction, the influence of interfering processes besides ion-exchange like leaching, corrosion, redox processes, adsorption, and electrode history (all phenomena acting to create the present state of the membrane surface).

This complexity of factors not only results in a divergence of empirical selectivity coefficients but also creates some difficulties in theoretically describing ISE action and interpreting and predicting values for the selectivity coefficients.

Existing and generally accepted models usually predict definite, discrete values of the selectivity coefficients. The coefficient is usually expressed in the case of solid membrane electrodes as the ratio of solubility products of the respective salts of the main and interfering ions. This assumes that mobility of interfering ions in the membrane phase equals zero. If this is not so, the selectivity coefficient includes mobility terms (*4–6*). The selectivity coefficients predicted on this basis are occasionally not equal to those measured experimentally. This fact was pointed out in some papers (Table I) but until

0003-2700/81/0353-1401$01.25/0 © 1981 American Chemical Society

Table I. Literature Data on the Selectivity Coefficients of the Discussed System

authors or firms	$K^{pot}_{Cl,Br}$	$K^{pot}_{Br,Cl}$	$K^{pot}_{F,OH}$
Activion,[a] Beckman[a]	3×10^2	2.5×10^{-3}	0.1
Corning,[a] Radelkis[a]			
Amel[a]	4.0	1×10^{-2}	
Radiometer[a]	2.0	$(5\text{-}6) \times 10^{-3}$	0.2
Phillips[a]	1.2	6×10^{-3}	
Tacussel[a]	1.2		
Havas et al. (7)	2×10^2		
Havas (8)	40		
Rechnitz and Kersz (9)	15	1×10^{-2}	
Pungor and Tóth (5)		1.8×10^{-2}	
Hulanicki and Lewenstam (10,11)	2.1-3.1 $\times 10^2$	$(2.9\text{-}5.6) \times 10^{-3}$	9×10^{-3}-2
Rhodes and Buck (12)	10-4.5 $\times 10^2$		
Butler (13)			~0->1

[a] Manufacturers data.

now has not been fully explained. This paper attempts to present a more comprehensive explanation of observed facts based on a generalized approach, which combines existing models.

EXPERIMENTAL SECTION

Mera 101 Cl chloride, Radelkis OP-Br-711 bromide, and Orion 94-09 fluoride electrodes were used in the measurements. Potentials were registered with respect to a saturated calomel electrode with a 1 M potassium nitrate bridge, by means of a Radiometer pHM-64 pH meter and Servograph REC 61 recorder. The potential readings were taken at 25 and 50 °C. All measurements were done in solutions with ionic strength $\mu = 1.0$ (KNO_3). Solutions were prepared with potassium salts.

THEORETICAL SECTION

Two cases will be distinguished and treated separately. The first is without diffusion in the membrane phase as occurs in the $AgCl/Cl^-$, Br^- or $AgBr/Br^-$, Cl^- systems and the second case is with diffusion in the membrane phase, as represented by the LaF_3/F^-, OH^- system.

In the considerations which follow, a set of general and typical ISE model assumptions will be made. These are zero-current condition, total electroneutrality, rapidity, and reversibility of all ion-exchange processes, constancy of chemical standard potentials, mobilities, and diffusion coefficients of ion in relevant regions (5, 14). All electrochemical potentials are assumed to change only in a direction perpendicular to the planar membrane surface. Linear concentration changes within diffusion regions and steady-state distribution of ions for defined moments are also assumed. Finally it is accepted that concentrations of all ions in solution, in the vicinity of membrane are not disturbed by "independent" processes such as dissolution of membrane, leakages, and adsorption. For simplification, activity coefficients of all species under consideration are assumed to equal one.

System without Diffusion in the Membrane. The total equilibrium model (4, 5, 15, 16) is based on the solubility product principle. In this model two additional assumptions have been introduced: (i) the compound formed in the metathetic reaction forms a mixed phase with the electrode-active component of the membrane and (ii) the ion concentrations at the membrane surface and in the bulk solution are equal. This is equivalent to the statement that the compound formed is electrode active and the system membrane–solution remains in thermodynamic equilibrium. The potential E_B at the AgCl membrane–solution interface is given by the equation

$$E_B = E^\circ_{Ag^+/Ag} + \frac{RT}{F} \ln K_{so(AgCl)} + \frac{RT}{F} \ln \frac{\bar{N}_{(AgCl)}}{[Cl^-]} \quad (1)$$

in which all symbols have their usual meaning and $\bar{N}_{(AgCl)}$ represents the mole fraction of silver chloride participating in the ion exchange. The exchange reaction $AgCl + Br^- \rightleftharpoons AgBr + Cl^-$ is characterized by the constant

$$K_{Cl,Br} = \frac{K_{so(AgCl)}}{K_{so(AgBr)}} = \frac{\bar{N}_{(AgBr)}[Cl^-]}{\bar{N}_{(AgCl)}[Br^-]} \quad (2)$$

The number of active centers of silver ions which take part in the exchange is constant and can be described as

$$\bar{N}_{(AgCl)} + \bar{N}_{(AgBr)} = 1 \quad (3)$$

The final expression which follows from eq 1–3 has the form

$$E = E^\circ_{Ag^+/Ag} + \frac{RT}{F} \ln K_{so(AgCl)} - \frac{RT}{F} \ln ([Cl^-] + K_{Cl,Br}[Br^-]) \quad (4)$$

in which the selectivity coefficient has a constant numerical value $K^{pot}_{Cl,Br} = K_{so(AgCl)}/K_{so(AgBr)}$ which is independent of conditions of measurement. That relation holds for all values of the exchange reaction constants as was initially indicated by Pungor and Toth (5).

The steady-state (diffusion layer) model developed for soluble products only (17–19) and extended for precipitate formation (10, 20) is based on different assumptions. It is assumed that (i) the precipitate of silver bromide formed in a metathetic reaction at the membrane surface is not electrode active and does not form a mixed phase with silver chloride. It is also assumed that (ii) the concentrations at the electrode surface and in the bulk solution are not equal. The ion concentrations in the bulk remain constant. Inequality of concentrations in bulk and at the electrode surface (index 0) requires that the ion flux is given by the equation

$$D_{Cl}([Cl^-]_0 - [Cl^-]) = D_{Br}([Br^-] - [Br^-]_0) \quad (5)$$

The exchange reaction constant is given as before by the ratio of solubility products

$$K_{Cl,Br} = \frac{K_{so(AgCl)}}{K_{so(AgBr)}} = \frac{[Cl^-]_0}{[Br^-]_0} \quad (6)$$

but referred to surface concentrations. Both compounds, silver chloride and silver bromide, which participate in the exchange are present as pure phases and therefore their mole fractions are equal to 1: $\bar{N}_{(AgCl)} = \bar{N}_{(AgBr)} = 1$. Because the electrode senses the surface ion concentration, $[Cl^-]_0$, and $K_{Cl,Br} \gg 1$, it follows from eq 1, 5, and 6 that the potential is expressed by

$$E = E^\circ_{Ag^+/Ag} + \frac{RT}{F} \ln K_{so(AgCl)} - \frac{RT}{F} \ln \left([Cl^-] + \frac{D_{Br}}{D_{Cl}}[Br^-] \right) \quad (7)$$

In this model the selectivity coefficient should also have a constant value $K^{pot}_{Cl,Br} = D_{Br}/D_{Cl}$. However, if the exchange reaction constant is smaller than 1 (case $AgBr/Br^-$, Cl^-) this value is the same as in the total equilibrium model.

The presented models assume two different mechanisms of formation of a slightly soluble precipitate as a result of the metathetic reaction. In the total equilibrium model a mixed phase is formed with both compounds being electrode active. In the diffusion layer model the product of the exchange reaction is not electrode active. These two mechanisms may therefore be called "electroactive mixed phase formation" and "dissolution–precipitation". A similar distinction has been

previously proposed by Armstrong (*21*) in his study of metal passivation.

It might be expected that electrode active mixed phase formation is preferred whenever the thermodynamic force is large or it is being acted on for a sufficiently long time period. In these conditions the selectivity coefficient is expressed only by solubility products. On the other hand the dissolution–precipitation mechanism is favored if the ion concentration is small, if the system is stationary, and if the interaction time is short. In these conditions the transport phenomena should influence the value of the selectivity coefficient.

In the generalized model the electrode active mixed phase formation and the dissolution–precipitation mechanisms represent two limiting cases.

In real systems which correspond to intermediate conditions both mechanisms influence the electrode response. Such intermediate conditions may be described in the following way. The potential of the AgCl membrane electrode is given in the form of an equation for surface conditions described by

$$E = E^{\circ}_{Ag^+/Ag} + \frac{RT}{F} \ln K_{so(AgCl)} + \frac{RT}{F} \ln \frac{\bar{N}_{o(AgCl)}}{[Cl^-]_0} \quad (8)$$

Correspondingly in the case of the AgBr membrane electrode

$$E = E^{\circ}_{Ag^+/Ag} + \frac{RT}{F} \ln K_{so(AgBr)} + \frac{RT}{F} \ln \frac{\bar{N}_{o(AgBr)}}{[Br^-]_0} \quad (9)$$

Consequently the equilibrium constant is expressed by

$$K_{Cl,Br} = \frac{K_{so(AgCl)}}{K_{so(AgBr)}} = \frac{\bar{N}_{o(AgBr)}[Cl^-]_0}{\bar{N}_{o(AgCl)}[Br^-]_0} \quad (10)$$

or

$$K_{Br,Cl} = \frac{K_{so(AgBr)}}{K_{so(AgCl)}} = \frac{\bar{N}_{o(AgCl)}[Br^-]_0}{\bar{N}_{o(AgBr)}[Cl^-]_0} \quad (11)$$

The mole fractions of both silver salts taking part in the reaction of the electroactive solid phase formation fulfill the condition

$$\bar{N}_{o(AgCl)} + \bar{N}_{o(AgBr)} = 1 \quad (12)$$

in which the contribution of both salts is described introducing an apparent coverage factor

$$s = \bar{N}_{o(AgBr)} \quad (13)$$

In the case of the bromide electrode, the apparent coverage factor is respectively given by the mole fraction of silver chloride. The factor s can vary in the range $s \in (0, 1)$. When $s \to 0$ the interference is of the dissolution–precipitation type. As stated previously, the diffusion flux is given by eq 5. From eq 5 and 8–13 it follows that the potential of the chloride electrode is given by the equation

$$E = E^{\circ}_{Ag^+/Ag} + \frac{RT}{F} \ln K_{so(AgCl)} - \frac{RT}{F} \ln \frac{K_{Cl,Br}}{s(D_{Br}/D_{Cl}) + (1 - s)K_{Cl,Br}} \left([Cl^-] + \frac{D_{Br}}{D_{Cl}}[Br^-] \right) \quad (14)$$

A similar expression with appropriate parameters may be given for the bromide-selective electrode. These equations enable one to predict the variability of selectivity coefficients as a function of apparent coverage of the membrane with silver bromide or silver chloride, respectively. However, these changes are possible only in limits given by the two limiting models.

Assuming the proper approximations, the generalized model is reduced either to the total equilibrium model or to the steady-state model.

If the equilibrium between the membrane surface and the bulk solution is assumed and when the ion exchange proceeds by the electroactive solid phase formation, then the apparent coverage factor for chloride electrode is given as

$$s = s_{eq} = \frac{K_{Cl,Br}[Br^-]}{[Cl^-] + K_{Cl,Br}[Br^-]} \quad (15)$$

which when substituted into eq 14 results in an equation identical with eq 4. A corresponding expression can be written for the bromide electrode with chloride interference.

Assuming a steady-state with a concentration gradient between the membrane surface and bulk solution and a dissolution–precipitation mechanism, eq 10 is reduced to eq 6, and finally eq 7 for a diffusion layer model is obtained. A similar result is possible by assuming $s \to 0$ in eq 14.

System with Diffusion Potential in the Membrane. The total equilibrium model (*4*, *22*), besides the general assumptions for ISE considerations, assumes that (i) the interfering ion as a result of exchange reaction can penetrate into the membrane phase with a mobility larger than zero and (ii) concentrations at the membrane solution interface are equal to those in the bulk solution. This means that the system membrane–solution remains in a thermodynamic equilibrium.

Considering the interference of hydroxyl ions on the fluoride selective electrode, the boundary potential is given by the equation

$$E_B = \text{const} - \frac{RT}{F} \ln \frac{[F^-]}{[\bar{F}^-]} \quad (16)$$

where a symbol with a bar refers to the membrane phase.

The diffusion potential in the membrane is given as

$$E_D = \text{const} - \frac{RT}{F} \ln \left([\bar{F}^-] + \frac{\bar{U}_{OH}}{\bar{U}_F}[\overline{OH}^-] \right) \quad (17)$$

in which $\bar{U}_{OH}$ and $\bar{U}_F$ represent mobilities in the membrane phase of corresponding ions. One may assume that in the ion exchange reaction only one fluoride ion in the lanthanum fluoride "molecule" is exchanged for hydroxyl ion or that more fluoride ions per one lanthanum atom participate in the reaction. However, this influences only the numerical values of the reaction constant and therefore has no influence on the principles of the discussed model. For simplicity, the reaction $LaF_3 + OH^- \rightleftharpoons LaF_2(OH) + F^-$ is considered with a constant

$$K_{F,OH} = \frac{[F^-][\overline{OH}^-]}{[\bar{F}^-][\overline{OH}^-]} \quad (18)$$

From eq 16–18 it follows that the total electrode potential equals

$$E = \text{const} - \frac{RT}{F} \ln \left([F^-] + \frac{\bar{U}_{OH}}{\bar{U}_F} K_{F,OH}[OH^-] \right) \quad (19)$$

In this model the selectivity coefficient has a constant value $K^{pot}_{F,OH} = (\bar{U}_{OH}/\bar{U}_F)K_{F,OH}$, independent of the measurement conditions or the electrode pretreatment.

Several authors (*13*, *23–26*) have pointed out that the response of the fluoride-selective electrode is limited by the diffusion processes. The presence of the hydrated layer at the electrode surface has been confirmed by independent techniques (*23*). For a more general description of the functioning of the electrode it should be assumed that the ion concentrations in the interface region may not be equal to those in the bulk of both phases.

With those assumptions the potential at the boundary of the hydrated membrane–solution is expressed by

$$E_D = \text{const} - \frac{RT}{F} \ln \frac{[F^-]_0}{[\bar{F}^-]_0} \quad (20)$$

The diffusion potential in the membrane equals

$$E_D = \text{const} - \frac{RT}{F} \ln \left([\bar{F}^-]_0 + \frac{\bar{U}_{OH}}{\bar{U}_F} [\overline{OH}^-]_0 \right) \quad (21)$$

The ion-exchange constant refers to concentrations at the electrode surface and therefore has the form

$$K_{F,OH} = \frac{[F^-]_0 [\overline{OH}^-]_0}{[\bar{F}^-]_0 [OH^-]_0} \quad (22)$$

The number of active sites is constant

$$[\bar{F}^-]_0 + [\overline{OH}^-]_0 = \text{const} \quad (23)$$

so the relative contributions which correspond to particular ions may be expressed by the apparent site-filling factor

$$s = \frac{[\overline{OH}^-]_0}{[\bar{F}^-]_0 + [\overline{OH}^-]_0} \quad (24)$$

The diffusional flux is as usual expressed by the equation

$$D_F([F^-]_0 - [F^-]) = D_{OH}([OH^-] - [OH^-]_0) \quad (25)$$

Thus the final equation is obtained from eq 20–25 in the form

$$E = \text{const} - \frac{RT}{F} \ln \frac{(1-s)K_{F,OH} + s(\bar{U}_{OH}/\bar{U}_F)K_{F,OH}}{s(D_{OH}/D_F) + (1-s)K_{F,OH}} \left([F^-] + \frac{D_{OH}}{D_F} [OH^-] \right) \quad (26)$$

This equation presents the interpretation of the selectivity coefficients as a variable, dependent on the value of the apparent site-filling factor.

When an equilibrium exists between the interface and the bulk solution, eq 26 is reduced to eq 19 of the total equilibrium model. In such a case the value of s is assumed to be

$$s = s_{eq} = \frac{K_{F,OH}[OH^-]}{[F^-] + K_{F,OH}[OH^-]} \quad (27)$$

RESULTS AND DISCUSSION

The final eq 14 and 26 of the generalized model indicate the dependence of the electrode potential, and as a consequence, of the selectivity coefficients, on the apparent coverage (or site-filling) factor. The graphical presentation of such a relationship in the case of the bromide interference on the chloride ISE ($K \gg 1$) is based on the assumptions that the diffusion coefficient ratio equals one and the solubility product ratio equals 3×10^2 (Figure 1a). According to the generalized model the selectivity coefficient may change from $K^{pot}_{Cl,Br} = D_{Br}/D_{Cl}$ to $K^{pot}_{Cl,Br} = K_{so(AgCl)}/K_{so(AgBr)}$, which is close to experimental observation (Figure 1b). This change is attributed to the electroactive mixed phase formation mechanism, i.e., to the miscibility of silver bromide formed in the membrane phase.

If the bromide ISE with chloride interference ($K \ll 1$) is concerned when using reciprocal values of constants, one can predict the selectivity coefficient change from $K^{pot}_{Br,Cl} = D_{Cl}/D_{Br}$ to $K^{pot}_{Br,Cl} = K_{so(AgBr)}/K_{so(AgCl)}$.

This should occur in the case of the electroactive mixed phase formation mechanism (Figure 2a). Experimentally it was observed that the selectivity coefficient remains constant and equal to the solubility product ratio (Figure 2b). This suggests that the dissolution-precipitation mechanism governs the process because according to this mechanism the selectivity

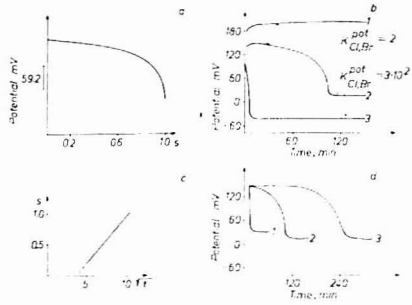


Figure 1. The bromide interference on chloride electrode: (a) calculated change of potential vs. apparent coverage factor (eq 14), $[Cl^-]$ = 0, $[Br^-]$ = const; (b) experimental curve, potential vs. time (1) in 10^{-4} M, (2) in 10^{-3} M, (3) in 10^{-2} M stirred solutions of bromides; (c) apparent coverage factor as a function of square root of time, calculated from curve 2, Figure 1b; (d) experimental curve, potential vs. time in 10^{-3} M bromide (1) stirred solution at 50 °C, (2) stirred solution at 25 °C, (3) unstirred solution at 25 °C.

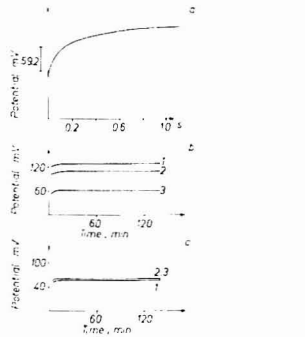


Figure 2. The chloride interference on the bromide electrode: (a) calculated change of potential vs. apparent coverage factor (eq 14), $[Br^-]$ = 0, $[Cl^-]$ = const; (b) experimental curve, potential vs. time (1) in 10^{-3} M, (2) in 10^{-2} M, (3) in 10^{-1} M stirred solution of chlorides; (c) experimental curve, potential vs. time in 10^{-1} M chloride (1) stirred solution at 50 °C, (2) 10^{-1} M stirred solution at 25 °C, (3) unstirred solution at 25 °C.

coefficient is predicted to be constant and equal $K^{pot}_{Br,Cl} = K_{so(AgBr)}/K_{so(AgCl)}$.

The fluoride electrode interference by hydroxyl ions is known as a system in which the diffusion potential within the membrane phase cannot be neglected. In such case the selectivity coefficient depends on site filling and changes from D_{OH}/D_F to $(\bar{U}_{OH}/\bar{U}_F)K_{F,OH}$. The potential change as a function of site filling factor was calculated when the diffusion coefficient ratio in aqueous phase $D_{OH}/D_F = 3.6$ and the bulk concentration of hydroxyl ion is constant. Because the value of the ion mobilities in the membrane and the exchange constant, $K_{F,OH}$, are not known exactly, the calculations were performed for several probable values of $(\bar{U}_{OH}/\bar{U}_F)K_{F,OH}$ ranging from 0.001 to 0.1 (Figure 3a). The experimental record of potential change with time (Figure 3b) confirms the expected variation of selectivity coefficient.

The discrepancies among experimentally determined selectivity coefficients according to the generalized model are due to the distance of the system from equilibrium. In systems in which the equilibration proceeds through electroactive mixed phase formation mechanism or site-filling mechanism

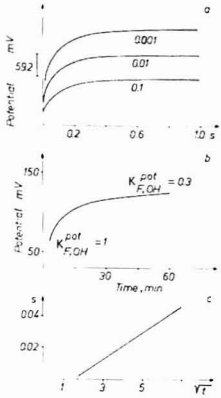


Figure 3. The hydroxyl interference on the fluoride electrode: (a) calculated change of potential vs. apparent site-filling factor (eq 26), $[F^-]$ = 0, $[OH^-]$ = const, the value $\bar{U}_{OH}K_{F,OH}/\bar{U}_F$ is indicated at the respective curves; (b) experimental curve, potential vs. time, $[F^-]$ = 10^{-5} M, and $[OH^-]$ = 10^{-3} M, unstirred solution at 25 °C; (c) apparent site-filling factor as a function of square root of time calculated on the basis of the curve on Figure 3b assuming $\bar{U}_{OH}K_{F,OH}/\bar{U}_F$ = 0.01.

the distance from the total equilibrium is given by the difference $|s - s_{eq}|$ and changes with time, $ds/dt \neq 0$. At total equilibrium $|s - s_{eq}| = 0$ and $ds/dt = 0$ the composition of the surface layer is described by eq 2 or 18. This implies usually that the bulk concentration is insignificantly influenced by the process of equilibration.

In the case when equilibrium proceeds through the dissolution–precipitation mechanism, the composition of the membrane surface is not changing and therefore $ds/dt = 0$ at each moment. Equilibrium may be attained on this way as well, but an appropriate change of solution composition must occur.

The actual value of s may be calculated for each time instant from the empirical relationship, $E(t)$ and eq 14 or 26. The recorded $E(t)$ curves for various concentrations, at a fixed temperature and mixing rate indicate that the apparent coverage factor ($AgCl/Br^-$ system) is proportional to the square root of time (Figure 1b,c). Similar results were obtained in the case of the LaF_3/OH^- system (Figure 3b,c). As was mentioned, in the $AgBr/Cl^-$ system, the potential does not depend on solution conditions and $K^{pot}_{Br,Cl}$ remains constant (Figure 2b,c). The increase of concentration, rise of temperature, and stirring rate shorten the time of reaching the total equilibrium (Figure 1d) for studied systems, except the system $AgBr/Cl^-$.

The correlations between the experimental findings and the principles of the generalized model are as follows: (i) The model predicts for all three cases discussed that $dE/ds \neq 0$, if mixed phase formation ($E_D = 0$) or site-filling mechanism ($E_D \neq 0$) prevails. Thus when $ds/dt \neq 0$, i.e., when the system is not in total equilibrium ($s > 0$) or dissolution–precipitation mechanism ($s = 0$) does not prevail: $dE/dt = (dE/ds)(ds/dt) \neq 0$. This agrees with experimental findings. (ii) Because the transport processes determine the equilibration rate therefore the rate of conversion of the membrane surface layer (ds/dt) is related to the flux of interfering ions (J_c)

$$J_c \propto \frac{ds}{dt} \tag{28}$$

As follows from the Fick laws the ion flux is inversely related to the square root of time (27)

$$J_c \propto A \cdot t^{-1/2} \tag{29}$$

and thus is a function of square root of time which is in accordance with our measurements and confirms the validity of the generalized model.

ACKNOWLEDGMENT

The authors thank E. Ghali, Laval University at Quebec, and R. P. Buck, University of North Carolina at Chapel Hill, for their kind interest and valuable discussions.

LITERATURE CITED

(1) Dole, M. *J. Am. Chem. Soc.* **1931**, *53*, 4260–4280.
(2) Nikolsky, B. P. *Zh. Fiz. Khim.* **1937**, *10*, 495–503; *Chem. Abstr.* **1938**, *32*, 1166(9).
(3) Buck, R. P. *Anal. Chem.* **1978**, *50*, 17R–29R.
(4) Buck, R. P. *Anal. Chem.* **1968**, *40*, 1432–1439.
(5) Pungor, E.; Toth, K. *Analyst (London)* **1970**, *95*, 625–648.
(6) Wuhrman, H. R.; Morf, W. E.; Simon, W. *Helv. Chim. Acta* **1973**, *56*, 1011–1038; *Chem. Abstr.* **1973**, *79*, 72861k.
(7) Havas, J.; Papp, B.; Pungor, E. *Acta Chim. Acad. Sci. Hung.* **1968**, *58*, 9–21; *Chem. Abstr.* **1969**, *70*, 83910r.
(8) Havas, J. *Proc. Conf. Appl. Phys. Chem., 2nd* **1971**, 361–368.
(9) Rechnitz, G. A.; Kersz, M. R. *Anal. Chem.* **1966**, *38*, 1786–1788.
(10) Hulanicki, A.; Lewenstam, A. *Talanta* **1977**, *24*, 171–175.
(11) Hulanicki, A.; Lewenstam, A. "Ion Selective Electrodes, Conference, 1977"; Pungor, E., Buzas, I., Ed.; Elsevier: Amsterdam, 1978; pp 395–402.
(12) Rhodes, R. K.; Buck, R. P. *Anal. Chim. Acta* **1980**, *113*, 78–90.
(13) Butler, J. N. *NBS Spec. Publ. (U.S.)* **1969**, *No. 314*, Chapter 5.
(14) Helfferich, F. *Discuss. Faraday Soc.* **1956**, *21*, 83–94.
(15) Covington, A. K. *NBS Spec. Publ. (U.S.)* **1969**, *No. 314*, Chapter 3.
(16) Buck, R. P. "Ion-Selective Electrodes in Analytical Chemistry"; Freiser, H., Ed.; Plenum: New York, 1978; Chapter 1.
(17) Evans, D. H. *Anal. Chem.* **1972**, *44*, 875–876.
(18) Bound, G. P.; Fleet, B.; von Storp, H.; Evans, D. H. *Anal. Chem.* **1973**, *45*, 788–789.
(19) Morf, W. E.; Kahr, G.; Simon, W. *Anal. Chem.* **1974**, *46*, 1538–1543.
(20) Hulanicki, A.; Lewenstam, A. *Talanta* **1976**, *23*, 661–665.
(21) Armstrong, R. D. *Corros. Sci.* **1971**, *11*, 693–697.
(22) Eisenman, G. *NBS Spec. Publ.* **1969**, *No. 314*, Chapter 1.
(23) Brand, M. J. D.; Rechnitz, G. A. *Anal. Chem.* **1969**, *41*, 1185–1191.
(24) Vesely, J.; Stulik, K. *Anal. Chim. Acta* **1974**, *73*, 157–166.
(25) Cammann, K.; Rechnitz, G. A. *Anal. Chem.* **1976**, *48*, 856–862.
(26) Hawkings, R. C.; Corriveau, L. P. V.; Kushnerluk, S. A.; Wong, P. Y. *Anal. Chim. Acta* **1978**, *102*, 61–83.
(27) Galus, Z. "Fundamentals of Electrochemical Analysis"; Ellis Horwood, Ltd.: Chichester, 1976; Chapter 5.

RECEIVED for review October 9, 1979. Resubmitted February 3, 1981. Accepted April 2, 1981.

Simultaneous Determination of Cadmium and Lead in Whole Blood and in Serum by Computerized Potentiometric Stripping Analysis

Daniel Jagner,* Mats Josefson, Stig Westerlund, and Kerstin Arén

Department of Analytical and Marine Chemistry, Chalmers University of Technology and University of Göteborg, S-412 96 Göteborg, Sweden

A simple electroanalytical technique for the simultaneous determination of cadmium and lead in whole blood and in serum has been developed. Contrary to voltammetric stripping techniques, the potentiometric stripping technique does not suffer from interferences from electroactive species which might be present in the sample. The limit of detection after 2 min of preelectrolysis is equal to 25 nM for both elements and the relative standard deviation is better than 4%. Sample volumes down to 25 μL can be handled. Due to the computerized registration of the stripping curve and the background curve a throughput of 12 samples/h is possible. This is considerably more than in hitherto voltammetric stripping techniques. The accuracy of the potentiometric stripping technique has been tested by comparison with the results obtained by 52 other laboratories on 12 different international standards.

Electroanalytical determination of cadmium and lead in whole blood and in serum by means of either anodic stripping voltammetry or differential pulse anodic stripping voltammetry has been attempted by several authors (*1–10*). Since, however, these techniques suffer from interference from all electroactive constituents present in the blood sample, it has been necessary to modify the matrix prior to analysis. The most frequently used technique is wet digestion with mineral acids, but low-temperature ashing has also been attempted (*11*). The simplest sample pretreatment technique hitherto suggested is the use of the very expensive ion-exchange reagent Metexchange (*7*). As pointed out by Oehme and Lund (*12*), this reagent cannot eliminate ghost peaks in the vicinity of the lead stripping peak which may cause erroneous results. Moreover, the blood sample must be diluted to such an extent that cadmium cannot be determined.

Potentiometric stripping analysis (*13–16*) resembles the anodic stripping techniques in that the trace metal analytes are preconcentrated in a mercury film on a glassy-carbon electrode by means of potentiostatic deposition according to

$$M^{n+} + ne^- \rightarrow M(Hg) \quad (1)$$

The stripping (oxidation) step in potentiometric stripping analysis is, however, fundamentally different from that in the anodic stripping techniques in that stripping is achieved chemically by

$$M(Hg) + \text{oxidant} \rightarrow M^{n+} \quad (2)$$

and the transport rate of oxidant to the electrode surface is kept constant by means of constant rate rotation of the electrode both during preelectrolysis and stripping. By monitoring the potential vs. time behavior of the working electrode during stripping, well-defined stripping plateaus can be registered for each reversibly amalgamated element (*13–15*). Since no current is drawn through the working electrode during potentiometric stripping, electroactive species present in the sample will not interfere with the stripping plateaus. Consequently the potentiometric stripping technique is better suited to the analysis of complex samples than are all those techniques which are based on the anodic stripping principle. Hitherto potentiometric stripping analysis has, however, suffered from the drawback that stripping according to reaction 2 occurs very rapidly in samples containing high concentrations of oxidants. In order to be able to register the stripping plateaus on a normal speed strip-chart recorder, very long potentiostatic deposition times were necessary when the trace element analyte concentration was below 10 μg L^{-1} in the sample. This problem has been overcome by means of the microcomputer system described in detail elsewhere (*17*).

The purpose of this work is to show how computerized potentiometric stripping analysis can be used for the simultaneous determination of cadmium and lead in whole blood and serum after a very simple sample pretreatment and without deoxygenation of the sample prior to analysis, dissolved oxygen and mercury(II) ions being used as oxidants (*15*).

EXPERIMENTAL SECTION

Instrumentation. A Radiometer ISS 820 ion scanning system (*16*) was used in combination with a laboratory-constructed microcomputer system using an Intel 8085 8-bit processor (*17*).

Electrodes and Electrochemical Cell. A Radiometer TTA 80 titration assembly with polyethylene cells of total volume 35 mL was used. The stirring motor of the TTA 80 was used to rotate the glassy-carbon working electrode at a constant rate of approximately 2000 rpm. The glassy-carbon electrode was manufactured by pressure-fitting a 15-mm glassy-carbon rod, with a diameter of 2.1 mm, into a 80 mm Teflon rod with a diameter of 12 mm. The center of the glassy-carbon rod was placed 4 mm from the center of the Teflon rod. A platinum foil was used as counterelectrode and a saturated calomel electrode as reference (Radiometer P 101 and K 4040, respectively).

Chemicals. All chemicals used were of analytical grade with the exception of the mineral acids (Suprapur, Merck). Stock solutions containing 1 g L^{-1} of the metal analytes were prepared in 0.1 M nitric acid. Working standards were prepared every week by dilution with triply distilled water.

Samples. All samples had been haemolyzed with heparin and deep frozen prior to analysis. During thawing the blood samples were homogenized by means of careful shaking.

Mercury Preplating Solution. The solution contained 100 mg L^{-1} of mercury(II) nitrate in 0.1 M hydrochloric acid solution.

Sample Dilution Solution. This solution contained 75 mg L^{-1} of mercury(II) nitrate in 0.5 M hydrochloric acid.

Mercury Preplating Procedure. A 20-mL portion of the mercury preplating solution was placed in the electrochemical cell, and rotation of the working electrode was started. The potentiostatic circuitry was adjusted to −0.5 V vs. SCE and preelectrolysis for 1 min was started. After the sample was stripped, which takes less than 0.1 s, the potentiostat was set at −0.6 V and another minute of preelectrolysis was started. This procedure was repeated at −0.7, −0.8, and −0.9 V vs. SCE. At −0.9 V vs. SCE the 1-min preelectrolysis/stripping cycle was repeated three times making the total preelectrolysis time for mercury preplating equal to 8 min. Once mercury preplated, the electrode could be used for several days, provided that it was carefully rinsed and stored in doubly distilled water. When the electrode is used

0003-2700/81/0353-1406$01.25/0 © 1981 American Chemical Society

Table I. Comparison between the Results Obtained by Potentiometric Stripping Analysis (PSA) for Lead in Whole Blood Samples and the Results Obtained by Four Other Techniques on the Same Intercalibration Samples[a]

this work (PSA)	carbon rod		Delves cup		dithizone extraction		anodic stripping	
conen, μM	no. of labs	conen, μM ± std dev	no. of labs	conen, μM ± std dev	no. of labs	conen, μM ± std dev	no. of labs	conen, μM
0.63	13	0.62 ± 0.15	21	0.69 ± 0.12	5	0.97 ± 0.45		
0.87	21	0.89 ± 0.14	27	0.91 ± 0.14	5	0.86 ± 0.36		
1.45	26	1.42 ± 0.16	28	1.53 ± 0.26	5	1.19 ± 0.17	1	1.55
1.52	22	1.62 ± 0.16	29	1.57 ± 0.18	4	1.42 ± 0.36	1	1.55
2.32	19	2.24 ± 0.18	22	2.30 ± 0.17	4	2.27 ± 0.08	1	2.25
2.51	22	2.46 ± 0.22	23	2.54 ± 0.22	6	2.52 ± 0.30		
2.77	20	2.92 ± 0.15	24	3.00 ± 0.22	4	3.02 ± 0.47		
2.94	16	3.05 ± 0.23	25	2.98 ± 0.27	4	2.81 ± 0.21	1	3.29
3.01	23	2.99 ± 0.33	26	2.98 ± 0.23	4	2.75 ± 0.64	1	2.80
3.33	16	3.43 ± 0.20	22	3.37 ± 0.33	4	3.58 ± 0.52		
3.69	20	3.68 ± 0.33	22	3.44 ± 0.26	5	3.54 ± 0.63		
4.20	20	3.92 ± 0.31	22	3.74 ± 0.40	5	3.44 ± 0.38	1	3.37

[a] The samples were diluted 1:20 prior to analysis.

continuously, mercury preplating once a day is recommended. Occasional cleaning of the mercury-coated electrode with acidified 50% ethanol is recommended. The same mercury preplating solution could be used for a large number of mercury preplatings. Prior to mercury preplating, the glassy-carbon working electrode was polished for 10–20 s with 3 μm diamond paste and rinsed carefully with ethanol.

Analytical Procedure for Cadmium and Lead in Whole Blood. One milliliter of whole blood is pipetted into a 9-mL sample dilution solution and mixed by gentle shaking. The samples should be analyzed within 3 h of mixing. Adjust the preelectrolysis potential to −1.2 V vs. SCE and the preelectrolysis time to 2 min and register the first preelectrolysis/stripping cycle. The working electrode is rotated at a constant rate during preelectrolysis and stripping. Add one or two standard aliquots of lead and cadmium and repeat the preelectrolysis/stripping cycle after each addition. The length of the stripping plateaus are evaluated as is shown in Figure 1. The concentrations of lead and cadmium are evaluated by means of the normal equations for standard addition.

If only lead is to be determined, the preelectrolysis time can be decreased to 1 min which is the minimum on the instrumental setup used in this investigation. Alternatively, the sample can be diluted to 1:40 without significant loss of precision. If low levels of cadmium are to be determined the preelectrolysis time has to be increased to 4 or 8 min.

Analytical Procedure for Cadmium and Lead in Serum. Four milliliters of serum is pipetted into a 6-mL sample dilution solution and mixed by gentle shaking. The sample is preelectrolyzed for 4 or 8 min at −1.2 V vs. SCE prior to the registration of the potentiometric stripping curve. The cadmium and lead concentrations are evaluated by means of standard addition.

Analytical Procedure Used in the Preliminary Experiments for Copper Determination. One milliliter of whole blood on serum is pipetted into 9 mL of sample dilution solution and mixed by gentle shaking. The preelectrolysis potential is adjusted to −0.9 V vs. SCE and the preelectrolysis time to 2 min. The copper concentration is evaluated by means of standard addition.

RESULTS

Potentiometric Stripping Curves in Diluted Whole Blood Samples. Figure 1 shows potentiometric stripping curves registered after 2 min of preelectrolysis at −1.2 V vs. SCE in a whole blood sample diluted 1:10. The undiluted sample contained 0.37 μM of lead and 116 nM of cadmium. This corresponds to a normal lead value for unexposed persons and an elevated cadmium value. A stripping curve registered after the addition of a standard aliquot corresponding to 1 μM of lead in the undiluted blood sample is also shown in Figure 1.

As can be seen from Figure 1, well-shaped potentiometric stripping plateaus can be obtained for both cadmium and lead in the diluted blood samples.

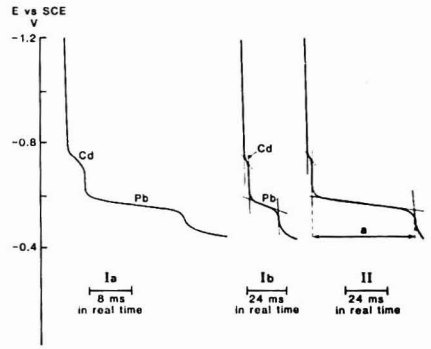


Figure 1. Potentiometric stripping curves registered after 2 min of preelectrolysis at −1.2 V vs. SCE in a whole blood sample containing 0.37 μM of lead and 110 nM of cadmium. Curves Ia and Ib have been transferred from the microcomputer to the strip-chart recorder at different rates. Curve II shows the potentiometric stripping curve registered under the same experimental conditions after the addition of 1 μM of lead. The blood sample was diluted 1:10 prior to analysis. Distance a in curve II is the length of the stripping plateau for lead.

Determination of Lead in International Calibration Standards. Accuracy. In order to investigate the accuracy of the potentiometric stripping technique in the concentration range of interest, 0.4–4 μM of lead, we analyzed 12 different samples. These samples had been used in an international calibration scheme (*18*) and had been analyzed by several different techniques at a large number of laboratories. In Table I the results obtained by potentiometric stripping analysis have been compared with the results obtained by the three most frequently used techniques: carbon rod, Delves cup, and dithizone extraction. Also included in Table I are the results obtained by the only laboratory using anodic stripping voltammetry. As can be seen from Table I, the potentiometric stripping results agree satisfactorily with the results obtained by the other techniques throughout the whole concentration range investigated. A more detailed report, summarizing the results from more than 60 reference samples can be obtained on request.

Determination of Lead in Lead-Exposed Persons. Precision. The results obtained in Table I have been derived from blood samples spiked with inorganic lead. In order to ascertain that the potentiometric stripping technique responds to lead in samples which have been "naturally" elevated due to lead exposure, we analyzed on such sample, containing

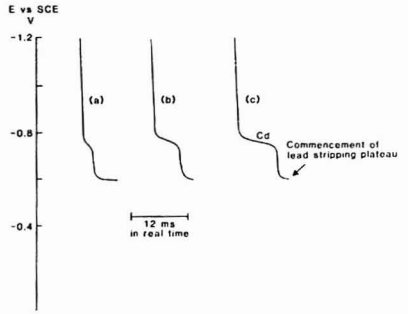


Figure 2. Potentiometric stripping analysis for cadmium in a whole blood sample containing 120 nM of cadmium (curve a), preelectrolysis for 2 min at −1.2 V vs. SCE. Curves b and c have been registered after the addition of 180 and 360 nM of cadmium, respectively.

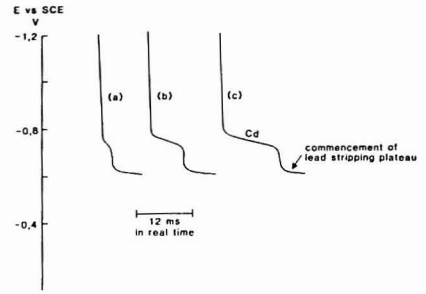


Figure 3. Potentiometric stripping curve registered after 16 min of preelectrolysis at −1.2 V vs. SCE in a whole blood sample containing 16 nM of cadmium (curve a). Curves b and c have been registered under the same experimental conditions after the standard addition corresponding to 45 and 90 nM of cadmium in the whole blood sample.

according to carbon-rod analysis 2.4 μM of lead. Ten repetitive analyses of this sample yielded the result 2.37 μM with a standard deviation of ±0.07 μM. Ten repetitive analysis of a sample originating from an unexposed person gave the result 0.37 μM of lead with a standard deviation of ±0.02 μM. The corresponding carbon rod value was 0.4 μM. As expected, the potentiometric stripping technique responds to the total concentration of lead in the blood samples, irrespective of its origin.

Most of the preliminary experiments were performed with a stationary electrode and using a three-edged polypropylene rod as stirrer (*16*). With this setup the relative standard deviation of the lead determination was approximately 12%. The introduction of the rotating electrode decreased the relative standard deviation to 3% in the concentration range 1–4 μM of lead.

Determination of Lead by Means of a Calibration Plot. All lead determinations reported in this work have been performed by means of the standard addition technique. When a large number of samples are to be analyzed, it is sometimes advantageous to use a calibration plot instead of the more time-consuming standard addition technique. In order to be able to do this it is, however, necessary that individual variations in the blood samples do not affect the analytical signal. Moreover, the sensitivity of the working electrode should not change with time and each new mercury preplating should give approximately the same sensitivity. In order to investigate the possibility of using a calibration plot in the lead determinations in whole blood, we plotted the potentiometric stripping signal registered in the sample prior to standard addition against the lead concentration value obtained by the standard addition technique. The results obtained from 23 different blood samples diluted 1:20 or 1:10 showed a linear relationship between signal and concentration. Obviously a calibration plot procedure could be used instead of a standard addition procedure.

Determination of Cadmium in Whole Blood. Normal concentrations of cadmium in human blood are of the order of magnitude 5–50 nM, i.e., considerably less than the lead concentration. Consequently, if normal cadmium values are to be determined, a preelectrolysis of more than 2 min must be used. If, however, only elevated cadmium values are of interest, a preelectrolysis time of 2 min is sufficient. This is illustrated in Figure 2 where a blood sample containing 20 nM of cadmium and spiked with 100 nM of cadmium has been preelectrolyzed for 2 min at −1.2 V vs. SCE. Also shown in Figure 2 are the potentiometric stripping curves registered after two standard additions of cadmium. As can be seen from the figure, well-shaped stripping plateaus are obtained for cadmium in diluted whole blood samples. The detection limit, after 2 min of preelectrolysis, can be estimated from Figure 2 to be approximately 25 nM of cadmium in the undiluted blood sample.

Table II. Potentiometric Stripping Analysis for Cadmium[a]

amt of Cd added, nM	preelectrolysis time, min	amt of Cd found (total ± std dev), nM	amt of Cd found corrected for zero value, nM
0	8	16 ± 4	-
25	4	46 ± 2	30
50	4	66 ± 7	50
100	2	118 ± 3	102
150	2	155 ± 3	139
200	2	208 ± 6	192
300	2	302 ± 7	286
400	2	407 ± 2	391
500	2	512 ± 7	496

[a] Each sample was analyzed 4 times.

Figure 3 shows the potentiometric stripping curve registered after 16 min of preelectrolysis at −1.2 V vs. SCE in a blood sample containing 16 nM of cadmium. By comparison with Figure 2, it can be concluded that the length of the cadmium stripping plateau is proportional to the preelectrolysis time in the interval 2–16 min. Consequently, the detection limit for cadmium after 16 min of preelectrolysis is approximately 4 nM.

The accuracy of the potentiometric stripping technique for cadmium was tested by analyzing whole blood samples spiked with inorganic cadmium. These samples had previously been used as standards for atomic absorption spectroscopy using the heated graphite technique. The unspiked blood sample contained approximately 16 nM of cadmium. The results are summarized in Table II. Although each sample was analyzed only four times, it can be concluded that the relative standard deviation in the concentration range 100–500 nM is better than 4%.

Determination of Cadmium and Lead in Serum. Figure 4 shows the potentiometric stripping plateaus registered after 8 min of preelectrolysis at −1.2 V vs. SCE in a serum sample diluted 1:2.5. Also shown in the figure is the potentiometric stripping curve registered after the addition of a cadmium aliquot corresponding to 18 nM of cadmium in the serum sample.

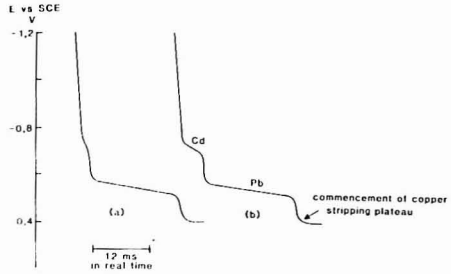


Figure 4. Potentiometric stripping curves registered after 8 min of preelectrolysis at −1.2 V vs. SCE in a serum sample diluted 1:2.5 (curve a). Curve b was registered under the same experimental conditions after a standard addition of cadmium corresponding to 18 nM cadmium in the undiluted serum sample.

As seen from Figure 4, well-shaped stripping plateaus for cadmium and lead can be obtained in serum samples diluted only 1:2.5. Obviously lead could be determined with a shorter preelectrolysis time. The cadmium content in the serum, as evaluated by standard addition, was equal to 3 nM, i.e., very close to the reagent blank value of approximately 2 nM. The lead content in serum was evaluated as 0.026 μM after correction for a reagent blank approximately equal to 0.002 μM of lead. Since no reference analytical technique for the determination of lead and cadmium in serum was available, the accuracy of the determination could not be checked. The results do, however, indicate the possibility of determining the lead content of serum.

Determination of Copper in Whole Blood. Most of the copper in whole blood is present in the enzyme caeruloplasmin (*19*). In order to investigate whether or not the potentiometric stripping technique responded to copper in the enzyme, a known aliquot of the enzyme was diluted in the sample dilution solution. The copper content was determined by means of standard addition after preelectrolysis for 4 min at −0.95 V vs. SCE. The copper recovery was 96 ± 5% assuming a molecular weight of 130 000 and eight copper atoms per enzyme molecule.

Figure 5 shows the potentiometric stripping curve registered in a dilute whole blood sample after preelectrolysis for 2 min at −0.95 V. The figure also shows the potentiometric stripping curves registered after a standard addition corresponding to 8.0 μM of copper in the undiluted whole blood sample. Ten consecutive determinations of copper in a whole blood sample yielded a mean value of 12.1 μM with standard deviation of 1.8 μM. The unsatisfactorily low precision was due to two samples which, for unknown reasons, differed considerably from the eight others. Obviously more work is necessary to make the determination reliable.

DISCUSSION AND CONCLUSIONS

Comparison between Potentiometric Stripping Analysis and the Anodic Stripping Techniques. The computerized potentiometric stripping technique has a number of advantages compared with the anodic stripping techniques, the main advantage being that the sample pretreatment procedure is simpler and the risk for interference due to electroactive organic constituents, e.g., pharmaceutical metabolites, in the sample is eliminated. Nor is sample deoxygenation necessary in potentiometric stripping analysis. Furthermore shorter preelectrolysis times can be used, and the registration of a potentiometric stripping curve is made within a couple of milliseconds. Potentiometric stripping analysis for lead and cadmium in whole blood and serum does not seem to have any disadvantages compared with anodic stripping voltammetry or differential pulse anodic stripping voltammetry.

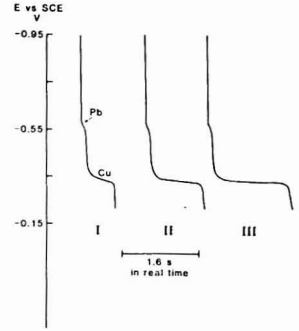


Figure 5. Potentiometric stripping analysis for copper in a whole blood sample. Preelectrolysis for 2 min at −1.2 V vs. SCE (curve I). Curves II and III have been registered under the same experimental conditions after the standard addition of 8.0 and 16 μM of copper, respectively.

Comparison between Potentiometric Stripping Analysis and the Atomic Absorption Techniques. The main advantage of the potentiometric stripping technique over the three atomic absorption techniques, specified in Table I, is that the potentiometric stripping technique can be used to determine the lead and cadmium concentrations simultaneously. Moreover, the potentiometric stripping technique can be used for the determination of the low lead concentrations in serum. Other important advantages are that the instrumentation is small in size, has very low power demand, and does not have any special installation requirements such as ventilation, cooling, or supply of gas. Furthermore, the instrument is simple to operate in that very few instrumental parameters have to be adjusted prior to analysis. None of the parts of the instrument need to be replaced regularly; the sensor electrode can be used almost indefinitely, provided that it is properly polished and cleaned and that it is mercury precoated at regular intervals.

The time for one whole blood analysis with potentiometric stripping is slightly longer than with, e.g., the carbon-rod technique. Assuming a preelectrolysis time of 2 min and one standard addition, the total time for one analysis will be approximately 5 min. Since, however, the potentiometric stripping analyzer operates semiautomatically, most of this time can be used for preparation of the next sample and evaluation of the results of the previous analysis. Thus a throughput of 12 analyses/h is feasible. If only lead and very high cadmium concentrations are to be determined, the preelectrolysis time can be decreased to 1 min, which would permit 20 analyses/h. If a large number of samples are to be analyzed, it may sometimes be advantageous to use a calibration plot instead of the standard addition technique.

The potentiometric stripping procedure, as it has been reported in this paper, requires more sample than does, e.g., the carbon-rod technique. It is, however, quite feasible to decrease the sample volume from 10 to 5 mL and, probably, even further. If only lead is to be determined, the sample could be diluted down to 1:50 and by increasing the preelectrolysis time to, e.g., 8 min, a sample dilution of 1:200 is feasible. For such an analysis only 25 μL of the blood sample is required.

In the potentiometric stripping technique it is necessary to handle solutions containing ionic mercury. Since only very dilute solutions have to be handled, this is not hazardous for the personnel. Ther mercury waste from the diluted blood

samples can be estimated to correspond to 1 cm^3 of liquid mercury per 50 000 analyses if sample volumes of 5 mL are used. This is negligible compared with other sources of mercury waste in chemical or clinical laboratories.

Since no computerized potentiometric stripping analyzer is commercially available, it is not possible to compare the instrumental cost between this technique and atomic absorption techniques. The computerized potentiometric stripping analyzer is, however, a much less complicated instrument that is, e.g., a carbon-rod atomizer and it is thus reasonable to assume that its cost would be considerably less than that of atomic absorption instrumentation.

ACKNOWLEDGMENT

The authors wish to thank J. Pedersen, Yrkesmedicinskt Centrum, Göteborg, for helpful advice and for placing the blood reference samples at their disposal.

LITERATURE CITED

(1) Cernik, A. A. *Proc. Anal. Div. Chem. Soc.* **1976**, *13*, 227.
(2) Copeland, R.; Osteryoung, R. A.; Skogerboe, R. K. *Anal. Chem.* **1974**, *46*, 2093.
(3) Duic, L.; Szechter, S.; Srinivacan, S. *J. Electroanal. Chem. Interfacial Electrochem.* **1973**, *41*, 89.
(4) Herheuval, X.; Maso, J.-L.; Baudot, P.; Hutin, M.-F.; Burnel, D. *Pathol. Biol.* **1975**, *23*, 379.
(5) Kisser, W. *Arch. Toxicol.* **1975**, *34*, 237.
(6) Lopez Fonseca, J. M.; Sanz Pedrero, P.; Bugeiro, M. T. *An. Quim.* **1976**, *72*, 485.
(7) Morrell, G.; Giridhar, G. *Clin. Chem.* **1976**, *22*, 221.
(8) Peter, F.; Reynolds, R. G. *Anal. Chem.* **1976**, *48*, 2041.
(9) Pinchin, M. J.; Newham, J. *Anal. Chim. Acta* **1977**, *90*, 91.
(10) Searle, B.; Chan, W., Davidow, B. *Clin. Chem.* **1973**, *19*, 76.
(11) Valenta, P.; Rützel, H.; Nürnberg, H. W.; Stoeppler, M. *Fresenius' Z. Anal. Chem.* **1977**, *285*, 25.
(12) Oehme, M.; Lund, W. *Fresenius' Z. Anal. Chem.* **1979**, *298*, 260.
(13) Jagner, D.; Årén, K. *Anal. Chim. Acta* **1979**, *100*, 375.
(14) Jagner, D. *Anal. Chem.* **1978**, *50*, 1924.
(15) Jagner, D. *Anal. Chem.* **1979**, *51*, 342.
(16) Graaback, A. M.; Jensen, O. J. *Ind. Res./Dev.* **1979**, *21*, 124.
(17) Granéli, A.; Jagner, D.; Josefson, M. *Anal. Chem.* **1980**, *52*, 2220.
(18) Whitehead, T. P. In "Quality Control in Clinical Chemistry"; Wiley: New York, London, Sydney, 1977.
(19) Sunderman, F. W., Jr. In "Chemical Diagnosis of Disease"; Brown, S. S., Mitchell, F. L., Young, D. S., Eds., Elsevier: Amsterdam, 1970.

RECEIVED for review March 2, 1981. Accepted April 27, 1981. Financial support from the Swedish Work Environment Fund is gratefully acknowledged.

Resolution of Overlapped Electrochemical Peaks with the Use of the Kalman Filter

Teri F. Brown[1]

Department of Civil Engineering, University of Washington, Seattle, Washington 98195, and Materials and Molecular Research Division, Lawrence Berkeley Laboratory, Berkeley, California 94720

Steven D. Brown*[1]

Department of Chemistry, University of California, Berkeley, California 94720, and Materials and Molecular Research Division, Lawrence Berkeley Laboratory, 1 Cyclotron Road, Berkeley, California 94720

A major limitation in the use of electrochemical techniques for the quantitative analysis of mixtures is the difficulty of resolving overlapped peaks. This problem is further complicated by the low signal-to-noise ratios often encountered in trace analysis and by the use of electrochemical techniques that produce broad, asymmetric waveforms. This paper demonstrates the use of the Kalman filter for multicomponent analysis of linear sweep voltammograms. Even with the broad, asymmetric linear sweep voltammetry waveform, synthetic data runs show that a peak separation of as little as 2.5 mV is sufficient for peak deconvolution in the presence of random noise. Besides separating overlapped peaks, the method also filters the noise from the signal and can be used to separate the capacitive current component from the faradaic current component. The method is validated further by using the Cd(II)/In(III) and Cd(II)/In(III)/Pb(II) systems which show peak separations of 40–200 mV. The use of the techniques with two other voltammetric waveforms is also demonstrated.

Electrochemical techniques show great promise for the analysis of complex mixtures because of their ability to determine both concentrations and stability constants. Unfortunately, the methods are limited by the difficulty of resolving overlapped peaks. Recent techniques have been able to separate peaks which are similar in height and have half-wave potentials as close as 30–40 mV using either semiderivative voltammetry (*1*) or square-wave voltammetry (*2*) combined with modern data analysis techniques. This paper presents a new technique based on the Kalman filter which has the ability to resolve peaks which are much closer together and which is applicable to a wide variety of waveforms.

Three other approaches have been used for the deconvolution of overlapped electrochemical peaks. The first approach fits the data to a previously defined functional shape such as the $sech^2$ function used in convolution voltammetry (*1*) or the empirical functions used by Perone and co-workers in stationary electrode polarography (*3*) and in square-wave voltammetry (*2*). In this method, the peak shape of each component is defined by the general functional shape and three to nine parameters. This procedure may be used to reduce the noise in a single component system or to separate peaks and reduce noise in a multicomponent system. Besides the general problem of choosing the correct functional shape, there are three important limitations to the method: (1) the correct number of components must be specified, (2) the peaks must be separated enough to be distinguishable (this is usually expressed as a minimum separation per unit width of the wider peak), and (3) the computational load is heavy, i.e., to fit a four-parameter system would require the iterative determination of 12–36 parameters.

The second approach, which is less mathematical in nature, uses a microprocessor-controlled polarograph to subtract a background solution from the multicomponent solution (*4*). Aliquots of all but one of the components are added into the

[1] Present address: Department of Chemistry, Washington State University, Pullman, WA 99164.

0003-2700/81/0353-1410$01.25/0 © 1981 American Chemical Society

background solution, and the polarographic measurement is repeated until visual inspection of the difference polarogram shows the complete removal of all but one peak. Not only is this method extremely time-consuming but the background subtraction increases the noise in the difference polarogram from which the peak height is determined.

The last approach uses linear parameter estimation to determine the concentration of each component in a mixture and is exemplified by Binkley and Dessy (5) working with square-wave voltammetry (SWV). This method uses single-component SW voltammograms which have been normalized by dividing by their concentration to define the line shapes and positions of the components. A linear model is assumed in which the products of each component's concentration times its line shape are added to yield the mixture voltammogram. The individual concentrations are treated as unknown parameters and are determined through a batch minimization process. Binkley and Dessy performed the linear parameter estimation in the Fourier frequency domain instead of in the time domain because this greatly reduced the size of the matrices used in the algorithm.

The peak separation technique presented in this paper uses the Kalman filter, a recursive digital filtering algorithm, for linear parameter estimation of multicomponent voltammetry data in the time domain. The mathematical formulation of the Kalman filter eliminates the problem of manipulating large matrices; this makes it possible to perform time domain calculations rapidly on small laboratory computers. Additionally, the algorithm yields not only optimal estimates of the variables but also their covariance matrix. A discussion of the notation used in linear parameter estimation theory and three simple chemical examples can be found in a recent review of the subject (6).

THEORY

The Kalman filter is a specific algorithm derived by Kalman in the early 1960's (7–9), which can be used for linear parameter estimation. Its application requires more stringent assumptions about the structure of the electrochemical noise than do the other least-squares algorithms (6, 8), but if these assumptions are met, the Kalman filter estimate is the optimal estimate, in either the least-squares or the maximum likelihood sense, of both the system parameters and their covariance matrix (10). Additionally, the algorithm is fast, easy to program, and, because it is recursive, does not require much computer memory.

Application of the Kalman filter requires formation of the problem in state-space notation. The general approach requires the specification of (1) a model of the system dynamics, (2) a measurement function that relates the measurables of the system (such as current or potential) to the state variables of the system (such as concentration), and (3) initial guesses of the variables. Table I is a summary of the Kalman filter equations for the discrete time case. The system model equation defines how the system would evolve in time. Its first term is a model of the system dynamics; the second term represents the effect of random fluctuations on the model. The measurement function also has two terms: the first to define the relationship between measurables and state variables, and the second to handle the noise present in the measurements. Since the algorithm is not self-starting, it is necessary to specify initial guesses of the state variables; for a statistically robust system, the final estimate of the state variables should be very nearly independent of the initial guess. The next three equations in Table I are the noise assumptions; they state that the noise contained in the system model and in the measurements must be defined by noise processes which have mean values of zero and known variances and which are uncorrelated with each other in time. In simpler words, the equations require that the noise be from independent, white noise processes.

Table I. Summary of the Kalman Filter Equations for Discrete Time Measurements

Defining Equations	
system model	$\mathbf{X}(k) = H(k,k-1)\cdot\mathbf{X}(k) + G(k)\cdot\omega(k)$
measurement model	$\mathbf{Z}(k) = S(k)\cdot\mathbf{X}(k) + \nu(k)$
initial conditions	$E[\mathbf{X}(0)] = \bar{\mathbf{X}}$
	$E[(\mathbf{X}(0) - \bar{\mathbf{X}})(\mathbf{X}(0) - \bar{\mathbf{X}})] = P$
noise assumptions	$\omega(k) = N(0,Q_k)$
	$\nu(k) = N(0,R_k)$
	$E[\omega(k)\cdot\nu(j)] = 0$ for all k,j
Algorithm Equations	
state estimate extrapolation	$\mathbf{X}(k\|k-1) = H(k,k-1)\cdot\mathbf{X}(k-1\|k-1)$
error covariance extrapolation	$P(k\|k-1) = H\cdot P(k-1\|k-1)\cdot H^{\mathrm{T}} + Q(k)$
Kalman gain equation	$K(k) = P(k\|k-1)\cdot S^{\mathrm{T}}(k)\cdot[S\cdot P(k\|k-1)\cdot S^{\mathrm{T}} + R]^{\mathrm{T}}$
state estimate update	$\mathbf{X}(k\|k) = \mathbf{X}(k\|k-1) + K(k)\cdot[\mathbf{Z}(k) - S\cdot\mathbf{X}(k\|k-1)]$
error covariance update	$P(k\|k) = [I - K(k)\cdot S(k)]\cdot P(k\|k-1)$

where

- $\mathbf{X}(k)$ = the vector of state variables of length N at time k
- $\mathbf{Z}(k)$ = the vector of measurables of length M at time k
- $\omega(k)$ = the vector of model noise of length L at time k
- $\nu(k)$ = the vector of measurement noise of length M at time k
- $H(k,k-1)$ = the state transition matrix (N by N) between times $k-1$ and k
- $S(k)$ = the measurement function matrix (M by N) at time k
- $G(k)$ = the model noise matrix (N by L) at time k
- $P(k)$ = the state covariance matrix (N by N) at time k
- $K(k)$ = the gain or weight matrix (N by M) at time k

and where the notation

- $A(k|j)$ ≡ the most probable value of A at time k conditioned on information from times up to and including j
- $E[A]$ = the expectation value of A
- $N(A,B)$ ≡ a noise process with a mean value of A and a variance of B
- A^{T} = the transpose of the matrix A

The next five equations in Table I are the equations of the actual Kalman filter algorithm. The first two equations are calculated prior to each measurement; they determine the optimal estimate of the state vector, **X**, and its covariance matrix, **P**, based on the system dynamics alone. The next three equations add the information contained in the measurement, **Z**, to form the optimal estimates of **X** and **P** based on both the system dynamics and the latest measurement.

The Kalman filter contains one last criterion that must be met—observability. This verifies that there is enough information contained in the measurement vector, **Z**, so that it is possible to determine the state vector, **X**. Mathematically, this involves showing that the observability matrix, χ, is of rank n, where n is the number of state variables. χ is defined as

$$\chi(t) = \left[\, S^{\mathrm{T}} \,\vdots\, H^{\mathrm{T}}\cdot S^{\mathrm{T}} \,\vdots\, H^{\mathrm{T}}\cdot H^{\mathrm{T}}\cdot S^{\mathrm{T}} \,\vdots\, \cdots \,\vdots\, (H^{\mathrm{T}})^{t-1}\cdot S^{\mathrm{T}} \,\right] \qquad (1)$$

Rigorous application of this equation is difficult for time-dependent matrices. However, a conceptually simple example of when the observability criterion is not met is when the value

Table II. The Kalman Filter Equations for the Analysis of Multicomponent Voltammograms

Defining Equations	
system model	$\mathbf{X}(k) = I \cdot \mathbf{X}(k-1)$
measurement model	$Z(k) = \mathbf{S}^T(k) \cdot \mathbf{X}(k) + \nu(k)$
initial conditions	$\mathbf{X}_0$
	$P_0 = I \cdot \sigma_z^2$
noise assumptions	$\omega(k) \simeq 0$
	$\nu(k) \simeq N(0, \sigma_z^2)$
Algorithm Equations	
state estimate extrapolation	$\mathbf{X}(k\|k-1) = \mathbf{X}(k-1\|k-1)$
error covariance extrapolation	$P(k\|k-1) = P(k-1\|k-1)$
Kalman gain equation	$\mathbf{K}(k) = P(k\|k-1) \cdot \mathbf{S}^T(k) \cdot [\mathbf{S} \cdot P \cdot \mathbf{S}^T + \sigma_z^2]$
state estimate update	$\mathbf{X}(k\|k) = \mathbf{X}(k-1\|k-1) + \mathbf{K} \cdot [Z - \mathbf{S} \cdot \mathbf{X}]$
error covariance update	$P(k\|k) = [I - \mathbf{K} \cdot \mathbf{S}] \cdot P(k-1\|k-1)$

of $S(t)$ for two different components is the same for all time. When this is so, the two components are not linearly independent and $\chi(t)$ will be singular.

The Kalman filter was formulated originally with time as the independent variable; a formulation that still permeates the literature. However, any other independent variable is acceptable as long as the noise assumptions can be met in terms of that variable. For electrochemical techniques using linear scan mechanisms to scan potential, the transformation is simple because the new independent variable, potential, is linear with time.

For the example of a voltammogram with overlapped peaks, the state vector consists of the concentration (or peak height) of each component, and the independent variable is potential. The system model equation has the identity matrix as the state transition matrix because the bulk concentration of each component is constant throughout the run. The measurement function model is given by

$$Z(E) = S_1(E) \cdot X_1 + S_2(E) \cdot X_2 + \ldots + S_N(E) \cdot X_N + \nu(E) \quad (2)$$

or, in state-space notation

$$Z(E) = \mathbf{S}^T(E) \cdot \mathbf{X} + \nu(E) \quad (3)$$

where $Z(E)$ is the value of the current at potential E, $\nu(E)$ is the noise in the measurement of the current, $\mathbf{X}$ is the column vector of the concentrations of each component, and $\mathbf{S}^T$ is the row vector defining the measurement function. The Kalman filter equations for this example are given in Table II. Because there is only one measurable quantity, current, the dimensionality of the problem is greatly reduced. The only matrix that remains is the symmetric covariance matrix, and the matrix inversion required for the filter gain matrix (which is now a vector) determination has been reduced to a scalar divide. Additionally, the system model is assumed to be noise free. This will cause the state covariance matrix to be slightly underestimated by the filter, as can be seen by comparing the covariance matrix extrapolation equations in Tables I and II.

The measurement function, $\mathbf{S}(E)$, is calculated from the single-component voltammograms that have been normalized by dividing by their concentrations. Figure 1 shows a sample input for a two-component system; here, $Y1(E)$ is a single-component scan of 8.36×10^{-5} M Cd(II), $Y2(E)$ is a single-component scan of 8.09×10^{-5} M In(III), and $Z(E)$ is an unknown mixture of Cd(II) and In(III). The measurement function for this example would be calculated as

$$\mathbf{S}(E) = \begin{bmatrix} Y1(E)/(8.36 \times 10^{-5}) \\ Y2(E)/(8.09 \times 10^{-5}) \end{bmatrix} \quad (4)$$

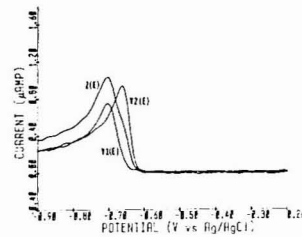


Figure 1. Input voltammograms: Y1(E) is the single-component Cd(II) voltammogram; Y2(E) is the single-component In(III) voltammogram; and Z(E) is an unknown mixture of Cd(II) and In(III).

There is noise in the single-component scans, $Y1(E)$ and $Y2(E)$; yet, the Kalman filter derivation assumes that the measurement function is known exactly. For the case where the measurement function does contain noise, the measurement model would be better described by

$$Z(E) = \mathbf{S}^T(E) \cdot \mathbf{X} + \mathbf{F}^T(E) \cdot \omega(E) + \nu(E) \quad (5)$$

where $\omega(E)$ is the vector of random noise of $\mathbf{S}(E)$ and $\mathbf{F}^T(E)$ is the vector of weights for the measurement function noise components. Although it is possible to determine the covariance matrix of $\omega(E)$ from the variance of the noise in the single-component voltammograms, it is very difficult to determine the form of the $\mathbf{F}(E)$ vector. For this reason, $\mathbf{F}(E)$ is assumed to be the identity vector, which has the effect of assuming equal weights. Additionally, it is necessary for the noise processes in the single-component data to be independent, white noise processes. With these assumptions, the measurement function model equation can be rewritten as

$$Z(E) = \mathbf{S}^T(E) \cdot \mathbf{X} + \omega_1(E) + \omega_2(E) + \ldots + \omega_N(E) + \nu(E) \quad (6)$$

or if the random variables are added together to get an effective noise component, $\nu'(E)$, as

$$Z(E) = \mathbf{S}^T(E) \cdot \mathbf{X} + \nu'(E) \quad (7)$$

For independent noise processes, the variance of the sum is the sum of the variances of the components. The variance of a voltammogram at each point can be found by averaging many replicate voltammograms; this is a long and tedious process. Fortunately, we found that the magnitude of the variance was independent of the potential and that it could be estimated from the high-frequency components of the Fourier power spectrum (*11*).

Poulisse and co-workers have (*12 14*) used a similar formulation of the Kalman filter to separate the overlapped ultraviolet spectra of organic compounds. Their work used a different formulation of the effective variance of the spectra, in part, because of the problem of determining the variance of a UV spectrum. Additionally, they propose using the Kalman filter for on-line drift compensation (*14*). This same approach could be used to remove the capacitive current component in voltammetry in those cases where it is approximately linear over the scan. Instead, we chose to treat the capacitive current as though it were another peak and used the background scan to generate the necessary term in the measurement function. This process avoided the assumption of linear capacitive current.

EXPERIMENTAL SECTION

Reagents. Stock solutions of approximately 1.0×10^{-2} M Pb(II) and Cd(II) were made by dissolving AR grade metallic lead and cadmium, respectively, in AR grade nitric acid and then diluting with quartz distilled water. The In(III) solution was made in an analogous manner from 99.95% In_2O_3 dissolved in a minimum

amount of hot 72% $HClO_4$. Aliquots of these solutions were titrated with a standard EDTA (ethylenediaminetetraacetic acid) solution, and the following stock concentrations were determined: [Pb(II)] = 1.96×10^{-2} M; [Cd(II)] = 2.09×10^{-2} M; and [In(III)] = 2.02×10^{-2} M. All solutions were made 0.58 M in AR grade HCl, which had been further purified by subboiling distillation in a Teflon still (*15*).

Cells, Electrodes, and Equipment. The cell used for all runs was the standard Princeton Applied Research (PAR) polarographic cell and cell holder, thermostated to 24.9 ± 0.1 °C. The working electrode was a PAR 9323 HMDE. The reference electrode was a Ag/AgCl electrode with a 1.0 M $NaClO_4$/0.1 M NaCl salt bridge; its potential was +40 mV vs. SCE. The counterelectrode was a length of heavy gauge platinum wire. All solutions were degassed by using purified argon to remove oxygen. A PAR 173 potentiostat was used to apply potentials to the cell. The scans were controlled with either a PAR 175 ramp generator or a 16-bit digital-to-analog (D/A) converter optically coupled to the parallel interface provided on the computer. A Digital Equipment Corp. MINC-11B computer, equipped with a 12-bit A/D converter, four 12-bit D/A converters, a programmable real time clock, a parallel I/O interface, and a serial I/O interface was used to control the experiment and collect the data. The central processing unit (CPU) was an LSI 11/2 unit with 30K words of usable memory.

Control of the linear sweep voltammetry (LSV) experiment was performed by MACRO-11 assembly language routines linked with a FORTRAN driver and other MACRO and FORTRAN subroutines for graphics and data storage. The routines were run under the RT-11 monitor. The data were stored on floppy disk for later processing on a separate LSI-11/23 processor. Data processing included noise reduction using fast Fourier filtering techniques (*16*) and background subtraction to remove the capacitive current component (*17*). Semidifferentiation to produce semiderivative voltammograms (SDV) (*18*) and semiintegration to yield neopolarograms (*19*) were available with the G1 algorithm based on Grünwald's definition of differintegration (*20*). All programs except the fast Fourier transform (FFT) subroutine were written by our group; the FFT subroutine, based on the Cooley–Tukey algorithm, was obtained from the Digital Equipment Corp. Laboratory Applications-11 Software package. Data processing, without differintegration, took less than 1 min per file; differintegration required an additional 80 s.

Laboratory Procedure. Six series of LSV standard addition experiments were performed; they were (1) standard additions of Cd(II) to supporting electrolyte solution, (2) standard additions of In(III) to supporting electrolyte solution, (3) standard additions of Pb(II) to supporting electrolyte solution, (4) standard additions of Cd(II) to supporting electrolyte solution which was 5.88×10^{-5} M in In(III), (5) standard additions of In(III) to supporting electrolyte solution which was 8.36×10^{-5} M in Cd(II), and (6) standard additions of Cd(II) to supporting electrolyte solution which was 8.09×10^{-5} M in In(III) and 7.86×10^{-5}M in Pb(II). The additions were made from the stock solutions using Eppendorf pipets. After each solution was degassed with purified argon, a potential of −0.200 V vs. Ag/AgCl reference electrode was applied to the cell. The potential was then scanned to −0.900 V using a linear ramp; the scan rate was 1 V/s and 512 uniformly spaced points were taken and stored on disk. Standardization curves were made from the three runs of single-component data; the three linear least-squares fits gave correlation coefficient values of 0.9998, 0.9996, and 0.9988, respectively.

Synthetic Data Generation. Synthetic LSV data were generated from tabulated values of the χ(at) function described by Nicholson and Shain (*21*) for reversible systems. Given the χ(at) function, the half-wave potential ($E_{1/2}$), the number of electrons (n), and the concentration (C), synthetic voltammograms were constructed by a FORTRAN program using

$$i(E) = \beta \cdot C \cdot n \cdot \chi(E - E_{1/2}) \tag{8}$$

where β was a constant which included the scan rate, the temperate, and the diffusion coefficient. Single-component voltammograms were added together point by point to produce multicomponent voltammograms. Additionally, white noise constructed from a 12-point Gaussian pseudorandom number generator could be added by specifying the desired signal-to-noise

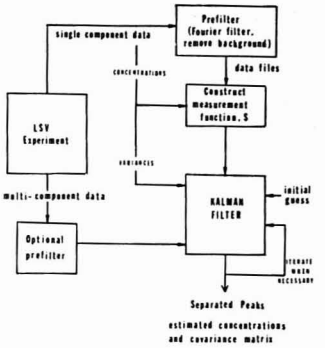


Figure 2. Flow chart of peak separation using the Kalman filter.

(S/N) ratio. Synthetic semiderivative voltammograms were constructed to test the effect of line shape on the Kalman filter and to determine the value of semidifferentiation of the data. The semiderivative voltammograms were constructed in a manner similar to the linear sweep voltammograms, except that the defining equation for the semiderivative wave was given by

$$e(E) = \gamma \cdot n \cdot C \text{ sech}^2 \langle n \cdot f \cdot (E - E_{1/2}) \rangle \tag{9}$$

where $f = F/2RT$ and γ includes the scan rate, the temperature, and the diffusion coefficient.

Peak Separation Procedure. Peak separation was performed by using a FORTRAN program, KFMCA, which was based on the Kalman filter algorithm but which was written specifically to perform peak deconvolution rapidly. The program first calculated the measurement function from the single-component voltammograms and their concentrations (or peak heights). Next the multicomponent voltammogram data file was read in and the effective variance calculated as the sum of its variance and the variances of the single-component voltammograms. Lastly, initial guesses of the concentration and the variance of each component were needed to start the algorithm. Although either concentration or peak height could be used as the state variable, it was important to choose a unit system such that most of the values fell between 10^{-2} and 10^{+2} in order to avoid computer round-off error. In this paper, peak heights in microamperes were used. The program output consisted of the optimal estimates of the concentrations of each component and their covariance matrix; additionally, four measures of overall goodness of fit were calculated—the variance of the fit, the average relative error, the squared correlation coefficient, and the coefficient of determination (*22*). The coefficient of determination is given by

$$\text{CD} = 1.0 - \frac{\sum_{i=1}^{N} (Y_i - Y(X_i))^2}{\sum_{i=1}^{N} Y_i^2} \tag{10}$$

where Y_i is the experimental curve, $Y(X_i)$ is the fit curve, and N is the number of data points. For best results the single-component voltammograms should be Fourier filtered and background subtracted; this process is helpful but not necessary for the multicomponent data. Since the final estimate was found to depend slightly on the initial guess, the program was allowed to iterate up to 5 times through the data points, using the final estimate as the initial guess on the next iteration. For a two-component, 512 point system each iteration took 10 s. This whole procedure is pictured in Figure 2.

RESULTS AND DISCUSSION

The peak separation technique was tested with synthetic LSV data, synthetic SDV data, and real LSV data from two-component Cd(II) and In(III) systems and from a three-component Cd(II)/In(III)/Pb(II) system. The method

Table III. Comparison of Synthetic LSV and SDV Results for a Two-Component System

	semiderivative data				linear sweep data			
file	E9	E10	E14	E15	A9	A10	A14	A15
ΔV[a]	25	25	10	10	25	25	10	10
pk ht[b]	1:1	1:1/10	1:1	1:1/10	1:1	1:1/10	1:1	1:1/10
S/N[c]	5.0	5.0	5.0	5.0	10.0	10.0	10.0	10.0
$X(1)$[d]	0.999	0.999	0.997	0.995	1.004	1.002	1.004	1.001
$X(2)$	1.003	0.105	1.001	0.092	0.998	0.100	0.999	0.100
$P(1,1)$[e]	$2.0E-5$	$2.3E-5$	$3.0E-5$	$4.5E-5$	$4.3E-7$	$2.5E-5$	$2.4E-6$	$4.4E-5$
$P(1,2)$	$-7.8E-6$	$-1.7E-5$	$-1.1E-5$	$-3.2E-5$	$-4.1E-7$	$-2.2E-5$	$-2.3E-6$	$-4.2E-5$
$P(2,2)$	$2.0E-5$	$2.6E-5$	$3.0E-5$	$4.8E-5$	$4.6E-7$	$2.6E-5$	$2.4E-6$	$4.5E-5$
VAR[f]	$2.1E-2$	$2.1E-2$	$2.1E-2$	$2.1E-2$	$2.9E-2$	$9.1E-3$	$3.0E-2$	$9.3E-3$
CD[f]	0.9901	0.9703	0.9981	0.9711	0.9975	0.9975	0.9974	0.9974
$\%e_1$[f]	0.1	0.1	0.3	0.5	0.4	0.2	0.4	0.1
$\%e_2$	0.3	5.0	0.1	8.0	0.2	0.0	0.1	0.0

[a] Difference in peak potentials of the two components (in mV). [b] Ratio of peak heights of the two components. [c] Signal to noise ratio. [d] Estimated peak heights for the two components. [e] Estimated covariance matrix; $P(1,2) = P(2,1)$. [f] Four measures of the fit: the variance of the fit, the coefficient of determination of the fit, and the percent error in each component.

is applicable to a wide range of wave forms, but the broad, asymmetric LSV waveform and the narrow, symmetric SDV wave form represent extremes of those typically encountered in electrochemistry. Additionally, a brief application of the method to neopolarographic waves was demonstrated. Four measures of the overall fit were tried: the variance of the fit, the average relative error, the squared correlation coefficient, and the coefficient of determination. The squared correlation coefficient was very close in value to the coefficient of determination (CD) but was tedious to calculate and contained large round-off errors. The average relative error, even with a modified denominator, tended to increase to unrealistic values. The variance of the fit and the CD were useful measures of different aspects of the fit. The CD was independent of the properties of the system being fit and allowed for rapid comparison of widely different systems. However, the variance of the fit was much more sensitive to changes in parameters, in the structure of the model, and in the measurements but less sensitive to round-off errors. However, its magnitude depends both on the magnitude of the signal and on the signal-to-noise ratio; this limits its use for intersystem comparisons. Perone and co-workers (*2*, *3*) also recommend using these two values as measures of goodness of fit. For systems with moderate amounts of noise, the variance elements of the estimated peak heights were much smaller than the variance of the fit; this was a good indication of the successful removal of the random noise and showed the importance of calculating the covariance matrix.

The synthetic data were used to determine the sensitivity of the method to different peak shapes, to differences in peak height and position, to the S/N of the data, and to errors in the input parameters or in the model. The results and a few examples follow.

Effect of Peak Shape. In general, better results were obtained with the LSV data than with the SDV data, even for the same systems. This effect is shown in Table III; the terms of the covariance matrix and the percent error in the components were smaller for the LSV data than for the SDV data. The variances of the fit do not show this effect as clearly because the magnitude of the LSV signal is larger than the the SDV signal. This preference for the LSV data is in direct contrast to most other fitting techniques which prefer narrow, symmetric peaks because of decreased peak overlap and fitting parameters. However, asymmetric peaks contain more information than their symmetric analogues; i.e., more moments are necessary to describe them. Because our technique stores all line shape information in the measurement function, this extra information does not increase the number of parameters nor the computational load and, therefore, is effectively free.

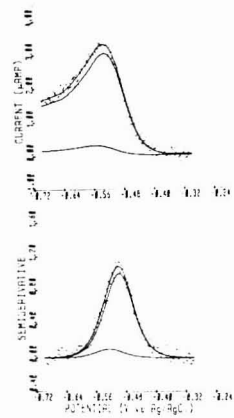


Figure 3. Comparison of synthetic LSV and SDV data.

Figure 3 shows a comparison of the separation of a two-component system using LSV data and SDV data. Both systems were two-component systems with peak potential separations of 25 mV and peak height ratio of 1:1/10. All charge transfer reactions were 1 electron reactions. S/N = 40.0 for the LSV data and 20.0 for the SDV data because semidifferentiation doubles the magnitude of the noise. In general, the fits of the semiderivative voltammograms gave errors that were 1–100% larger than the LSV fits.

Effect of Peak Separation. To determine the minimum difference in peak potential of the two peaks, which allowed for a quantitative resolution of the two peaks, a series of runs was made with two equal height peaks separated by 50, 25, 10, 5, and 2.5 mV. The minimum difference was found to depend on the point density of the scans, i.e., on the number of observations per unit of the potential scan. For 512 point scans over a 0.50-V range, a 2.5 mV separation of the peak potentials was sufficient to give fits with less than 0.1% error in the estimated peak heights. When the peaks were of unequal heights, the error in the smaller peak was seen to increase; but for peaks with height ratios of 1 to 10, quantitative resolution was still possible at 2.5 mV peak separation. Table IV summarizes these results. The 2.5 mV separation is a factor of 10 improvement over reported values using other techniques and could be further decreased by increasing the

Table IV. Separation of Synthetic LSV Peaks of Equal Heights

	S/N = 100				S/N = 10			
$\Delta E_{1/2}$ [b]	%e$_1$ [b]	%e$_2$	VAR [c]	CD [d]	%e$_1$	%e$_2$	VAR	CD
50	0.00	0.00	4.1E − 8	1.000	0.5	0.3	2.6E − 2	0.9976
25	0.00	0.00	3.9E − 8	1.000	0.4	0.2	2.9E − 2	0.9975
10	0.00	0.00	5.0E − 8	1.000	0.4	0.1	3.1E − 2	0.9974
5	0.00	0.00	4.4E − 8	1.000	0.1	0.4	3.1E − 2	0.9974
2.5	0.00	0.01	4.0E − 8	1.000	0.6	0.9	3.1E − 2	0.9974

[a] Separation of peak potentials in mV. [b] Percent error found in each component. [c] Variance of the fit. [d] Coefficient of determination of the fit.

Table V. Detection of Peak Shifts between Single-Component and Multicomponent Voltammograms

peak shift, mV	%e$_1$	%e$_2$	VAR	CD	
+10.0	23.	21.	7.5E − 3	0.9993	shift increased
+5.0	10.	9.	1.9E − 3	0.9998	apparent
+2.5	5.	4.	5.5E − 4	0.9999	overlap
0.0	0.0	0.0	4.1E − 8	1.000	
−2.5	4.	4.	5.2E − 4	1.000	shift decreased
−5.0	9.	8.	1.9E − 3	0.9998	apparent
−10.0	16.	15.	7.3E − 3	0.9993	overlap

point density in the critical range. This improvement is not possible with most other techniques, since they do not depend on the point density. Improvement might be possible with the technique of Binkley and Dessy (5), if the increased point density has the effect of increasing the information in Fourier space.

Effects of Errors in Peak Position. With the ability to separate fused peaks with peak potentials as close as 2.5 mV, the problem of peak shifts between the single-component voltammograms used to generate the measurement function and the multicomponent voltammogram became appreciable. This shift may be caused by an inability to match the backgrounds, by ligand concentration effects, or by unknown synergistic effects in the mixture. An initial study to estimate the magnitude of this problem showed that a shift of 7.5 mV in the mixture voltammogram from its original position was sufficient to increase the errors in the estimated concentrations to greater than 50% for peaks within 30 mV of each other. In an attempt to circumvent this problem, a synthetic voltammogram of a two-component system which contained two peaks with half-wave potentials of −0.500 and −0.550 V was examined. The single-component voltammogram for component two has a peak at −0.550 V; but for component one a series of single-component voltammograms was tried with peak potentials from −0.490 V to −0.510 V. The results are presented in Table V. Note the very sharp decrease in the variance of the fit when the correct half-wave potential was found. This behavior was seen in noise corrupted scans, also. The sensitivity of the variance to the peak potential position allowed for a determination of a probable shift and an accurate measurement of its magnitude.

Effect of Errors in the Initial Guess. The next study dealt with the detection of one peak between two large peaks with various initial guesses. Table VI shows the results of four runs in which the three peaks were separated by 25 mV from each other and had peak height ratios of 1:1:1 or 1:$^1/_{10}$:1. As expected, the worst case was with a small middle peak and low S/N. However, even in this case, and with an initial guess of the presence of only the two larger components, the filter algorithm was able to separate the peaks and estimate the peak heights of the two outside peaks to within 5%. The percent error in the estimate of the height of the middle peak was greatly reduced when the accuracy of the initial guess was

Table VI. Effect of the Initial Guess on a Strongly Overlapped Three-Component System

True Peak Height Ratio: 1:1:1 S/N = 100					
guess	%e$_1$	%e$_2$	%e$_3$	VAR	CD
1.0:0.0:1.0	+4.3	−8.5	+4.4	9.0E − 5	1.000
1.0:0.5:1.0	+2.2	−4.2	+2.2	2.8E − 5	1.000
1.0:1.0:1.0	0.00	0.00	0.00	1.1E − 7	1.000
True Peak Height Ratio: 1:$^1/_{10}$:1 S/N = 100					
guess	%e$_1$	%e$_2$	%e$_3$	VAR	CD
1.0:0.0:1.0	+0.4	−8.4	+0.4	9.7E − 7	1.000
1.0:0.5:1.0	−1.8	+34.	−1.8	1.4E − 5	1.000
1.0:0.1:1.0	0.0	+0.1	0.0	6.6E − 8	1.000
True Peak Height Ratio: 1:1:1 S/N = 10					
guess	%e$_1$	%e$_2$	%e$_3$	VAR	CD
1.0:0.0:1.0	+11.	−21.	+10.	6.0E − 2	0.9975
1.0:0.5:1.0	+8.5	−16.	+7.8	6.0E − 2	0.9974
1.0:1.0:1.0	+5.0	−9.0	+3.4	5.8E − 2	0.9981
True Peak Height Ratio: 1:$^1/_{10}$:1 S/N = 10					
guess	%e$_1$	%e$_2$	%e$_3$	VAR	CD
1.0:0.0:1.0	+4.0	−60.	+1.9	2.8E − 2	0.9981
1.0:0.5:1.0	−11.	+240.	−15.	2.8E − 2	0.9981
1.0:0.1:1.0	+0.9	+1.8	−1.4	2.8E − 2	0.9981

improved. This study presented a worst case situation; for less overlapped systems, the initial guess could be incorrect by a factor of 10 to 100 without affecting the value of the final estimate. Strangely, for very strongly overlapped systems, extremely poor initial guesses were sometimes found to cause more rapid convergence to the correct value.

Effect of Peak Width and Changes in Peak Width. The effect of peak width on the minimum difference in peak potential for quantitative resolution was minimal up to a peak width of 60–70 mV. At peak widths of greater than 90 mV the minimum separation was nearer to 5.0 mV. The effect was stronger, the lower the S/N of the voltammogram. A more critical effect occurred when the peak width changed between the single-component voltammogram and the multicomponent voltammogram. This study was done with synthetic SDV data because of the difficulty of modifying the LSV data to peak widths corresponding to nonintegral electron transfer or irreversible reactions; the results with LSV data would be expected to give slightly lower errors. Table VII shows the results from a series of runs where either peak broadening or narrowing occurred between the single-component and multicomponent runs. These runs were chosen to represent a worst case, because the peaks are only separated by 10 mV and the peak height ratio is 1 to 10 with the larger peak going through the peak width changes. When the large peak was broadened, the error in the small peak was very large because the filter was unable to attribute the large increase in overlap to the large peak and attempted to assign it to the smaller.

Since the synthetic data runs showed that the LSV data with high S/N gave the best results, the real data was Fourier

Table VII. Effect of Changes in Peak Width between Single-Component and Multicomponent Voltammograms[a]

file	SC fwhm[b]	MC fwhm[c]	Δfwhm	%e_1	%e_2	VAR	CD
E25	0.030	0.050	0.020	37.	600.	$2.3E-2$	0.9675
E26	0.045	0.050	0.005	5.6	200.	$2.2E-3$	0.9969
E27	0.050	0.050	0.000	1.5	15.	$1.2E-5$	1.000
E28	0.055	0.050	0.005	5.6	7.2	$2.2E-3$	0.9969
E29	0.060	0.050	0.010	15.	67.	$7.8E-3$	0.9890
E30	0.070	0.050	0.020	39.	370.	$2.2E-2$	0.9691

[a] Conditions: 10 mV peak potential separation; peak height ratio of 1:10; peak width changes in larger peak only. [b] Peak width of half-maximum in the single-component voltammogram. [c] Peak width at half-maximum in the multicomponent voltammogram.

Table VIII. Results for the Cadmium/Indium Systems with Allowed Peak Shifts of ±5 mV

cadmium				indium					
concn[a]	pk ht[b]	pk ht_e[c]	%e	concn	pk ht	pk ht_e	%e	VAR	CD
8.36	0.747	0.787	5.4	0.00	0.002	0.032		$1.0E-4$	0.9995
8.36	0.747	0.783	4.8	1.62	0.187	0.193	3.4	$1.4E-4$	0.9995
8.36	0.747	0.761	1.9	3.24	0.372	0.411	1.0	$1.9E-4$	0.9996
8.36	0.747	0.758	1.4	4.85	0.550	0.577	5.0	$2.6E-4$	0.9995
8.36	0.747	0.748	0.2	6.47	0.740	0.778	5.1	$4.4E-4$	0.9994
8.36	0.747	0.818	9.5	8.09	0.924	0.889	−3.8	$2.7E-4$	0.9997
0.00	0.002	0.001		5.88	0.670	0.675	0.7	$3.7E-5$	0.9998
1.67	0.150	0.161	6.5	5.88	0.670	0.664	−0.9	$5.3E-5$	0.9998
3.34	0.300	0.292	−2.9	5.88	0.680	0.655	−2.2	$7.0E-5$	0.9997
5.01	0.448	0.474	5.8	5.88	0.670	0.667	−0.4	$1.1E-4$	0.9997
6.68	0.597	0.583	−2.3	5.88	0.670	0.661	−1.4	$1.4E-4$	0.9997
8.36	0.747	0.745	−0.4	5.88	0.670	0.662	−1.1	$1.8E-4$	0.9997

Peak Shifts

Cd(II) 4 mV from 0.702 to 0.706 V vs. Ag/AgCl
In(III) −3 mV from 0.662 to 0.665 V vs. Ag/AgCl

[a] Concentrations in 10^{-3} M. [b] Theoretical peak heights based on single-component standard addition curves. [c] Kalman filter estimate of peak heights.

filtered and background subtracted before peak separation but not semidifferentiated nor semiintegrated. The actual procedure of peak separation and estimation of component concentrations consisted of four steps: (1) making standard addition curves from the single peak data for each component, (2) using the highest concentration run from the standard addition curve as the single-component voltammogram to form the measurement function, (3) running the filter to estimate the peak height, and (4) using the peak heights and the standard curves as determine the concentration. Visual inspection of the results, as in Figure 4, showed that small peak shifts were occurring between the single-component and multicomponent voltammograms. This shift increased the variance of the fit, the percent error in each component, and the covariance matrix of the estimated peak heights. Additionally, it caused the innovations sequence of the Kalman filter to be correlated, an indication of nonoptimal performance by the Kalman filter (*10*). This can be seen in Figure 4 by looking at the sinusoidal shape of the residuals of the fit, which are related to the innovations sequence. The KFMCA program was modified to allow for shifts of ±5 mV about the single-component value, in increments of about 1.2 mV. The variance of the fit and the flatness of the residuals were used to determine an improved fit. Figure 5 shows the results using the modified program on the same system shown in Figure 4. Note that the residuals of the fit (or the innovations sequence) look much flatter and less correlated.

Table VIII is a summary of the results for the two-component systems of Cd(II) and In(III) using the modified Kalman filter routine. The coefficient of determination was better than 0.9995 for all fits. The percent error in the estimated concentration included errors caused by experimental technique, by changes in the standard addition curve, and by the fitting algorithm. Table IX presents the results for the

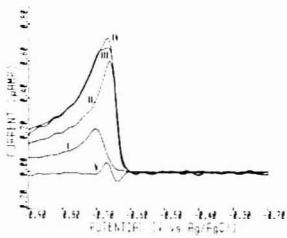


Figure 4. Peak separation of a two-component Cd(II)/In(III) system: (I) Cd(II) wave, (II) In(III) wave, (III) sum of Cd(II) and In(III) waves, (IV) the original voltammogram, and (V) the residuals of the fit (also called the innovations sequence).

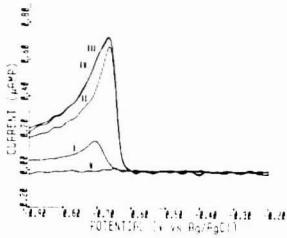


Figure 5. Peak separation of the same Cd(II)/In(III) as shown in Figure 4 using the modified KFMCA routine.

three-component Cd(II)/In(III)/Pb(II) system. Again, the filter gave quantitative resolution of the peaks, accurate es-

Table IX. Results for the Three-Component Cd(II)/In(III)/Pb(II) System with ±5 mV Peak Shifts Allowed

cadmium				indium				lead					
concn[a]	pk ht[b]	pk ht$_e$[c]	%e	concn	pk ht	pk ht$_e$	%e	concn	pk ht	pk ht$_e$	%e	VAR	CD
0.00	0.002	0.004		8.09	0.924	0.915	0.9	7.86	0.814	0.852	4.7	$3.4E-4$	0.9995
1.67	0.150	0.162	8.0	8.09	0.924	0.887	4.0	7.86	0.814	0.846	3.9	$3.0E-4$	0.9991
3.34	0.300	0.311	3.7	8.09	0.924	0.875	5.3	7.86	0.814	0.841	3.3	$3.0E-4$	0.9992
5.01	0.448	0.455	1.6	8.09	0.924	0.883	4.4	7.86	0.814	0.848	4.2	$3.4E-4$	0.9992
6.68	0.597	0.603	1.0	8.09	0.924	0.891	3.6	7.86	0.814	0.828	1.7	$3.6E-4$	0.9993
8.36	0.747	0.780	4.4	8.09	0.924	0.903	2.3	7.86	0.814	0.846	3.9	$2.8E-4$	0.9996

Peak Shifts

Cd(II) −1.4 mV from −0.702 to −0.703
In(III) −1.4 mV from −0.662 to −0.663
Pb(II) −4.1 mV from −0.498 to −0.502

[a] Concentrations in 10^{-5} M. [b] Theoretical peak heights based on single-component standard addition curves. [c] Kalman filter estimate of the peak heights.

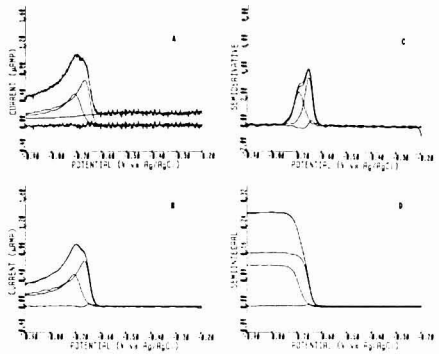


Figure 6. Demonstration of the peak separation for a two-component Cd(II)/In(III) system using four different procedures: (A) raw data with capacitive current treated as a third component; (B) prefiltered data; (C) prefiltered and semidifferentiated data; and (D) prefiltered and semintegrated data. Each graph contains plots of the original voltammogram, the separated component voltammograms, and their sum and the residuals of the fit.

timates of the concentrations, and estimates of the peak shifts in the mixture.

As a final comparison, Figure 6 shows the results of the fits of a two-component Cd(II)/In(III) voltammogram using four different procedures: (1) multicomponent data file was left unmodified, single-component data files were Fourier filtered and background subtracted, and a scan of the background was used to model the capacitive current prior to peak separation; (2) all data files were Fourier filtered and background subtracted prior to peak separation; (3) all data files were Fourier filtered, background subtracted, and semidifferentiated prior to peak separation; (4) all data files were Fourier filtered, background subtracted, and semiintegrated prior to peak separation. In all four procedures quantitative resolution of the peaks was possible. Procedure one (Figure 6A) used the Kalman filter to separate the current response into a capacitive current component, two faradaic current components, and noise which is contained in the innovation sequence. Procedure two (Figure 6B) shows the effect of background subtraction and Fourier filtering prior to peak separation; the capacitive current component is gone and the slight structure in the innovation sequence is caused by small errors in the model and by low-frequency noise. (In our case, it was mostly low-frequency noise from a particle accelerator in the next building.) Procedures three and four were used to demonstrate the versatility of the Kalman filter for a variety of waveforms.

ACKNOWLEDGMENT

The authors would like to thank another member of our group, Jeff Toman, for allowing us to use his Cd(II)/In(III)/Pb(II) data in our paper.

LITERATURE CITED

(1) Toman, J. J.; Brown, S. D. *Anal. Chem.* **1981**, *53*, 1497–1504.
(2) Boudreau, P. A.; Perone, S. P. *Anal. Chem.* **1979**, *51*, 811–817.
(3) Gutknecht, W. F.; Perone, S. P. *Anal. Chem.* **1970**, *42*, 906–917.
(4) Bond, A. M.; Grabaric, B. S. *Anal. Chem.* **1978**, *48*, 1624–1628.
(5) Binkley, D. P.; Dessy, R. E. *Anal. Chem.* **1980**, *52*, 1335–1344.
(6) Brubaker, D. P.; Tracy, R.; Pomernacki, C. L. *Anal. Chem.* **1978**, *50*, 1017A–1024A.
(7) Kalman, R. E. *J. Basic Eng.* **1960**, *82*, 34–45.
(8) Kalman, R. E.; Bucy, R. S. *J. Basic Eng.* **1961**, *83*, 95–107.
(9) Kalman, R. E. In "Proceedings of the First Symposium on Engineering Applications of Random Function Theory and Probability"; Bagdanoff, J. L., Kozin, F., Eds.; Wiley: New York, 1963; pp 270–388.
(10) Gelb. A., Ed. "Applied Optimal Estimation"; M.I.T. Press: Cambridge, MA, 1974; Chapter 4.
(11) Brown, T. F.; Brown, S. D. Pittsburgh Conference on Analytical Chemistry and Applied Spectroscopy, Atlantic City, NJ, 1981; paper 184.
(12) Poulisse, H. N. J. *Anal. Chim. Acta* **1979**, *112*, 361–374.
(13) Didden, C. B. M.; Poulisse, H. N. J. *Anal. Lett.* **1980**, *13*, 921–935.
(14) Poulisse, H. N. J.; Engelen, P. *Anal. Lett.* **1980**, *13*, 1211–1234.
(15) Mattison, J. M. *Anal. Chem.* **1972**, *44*, 1715–1716.
(16) Hayes, J. W.; Glover, D. E.; Smith, D. E.; Overton, M. W. *Anal. Chem.* **1973**, *45*, 277.
(17) Brown, S. D.; Kowalski, B. R. *Anal. Chim. Acta* **1979**, *107*, 13–27.
(18) Goto, M.; Ishii, D. J. *J. Electroanal. Chem.* **1975**, *61*, 361–365.
(19) Grenness, M.; Oldham, K. B. *Anal. Chem.* **1972**, *44*, 1121–1129.
(20) Oldham, K. B.; Spanier, J. "Fractional Calculus" (Vol 111 in Math. in Science and Eng. Series); Academic Press: New York, 1974; Chapter 8.
(21) Nicholson, R. S.; Shain, I. *Anal. Chem.* **1964**, *36*, 706–723.
(22) Mosteller, F.; Tukey, J. W. "Data Analysis and Regression"; Addison Wesley: Reading, MA, 1977; Appendix A.

RECEIVED for review January 19, 1981. Accepted April 27, 1981. This work was supported by the Director, Office of Energy Research, Office of Basic Energy Sciences, Chemical Sciences Division of the U.S. Department of Energy under Contract No. W-7405-ENG-48.

Multinuclear Nuclear Magnetic Resonance Study of Three Aqueous Lanthanide Shift Reagents: Complexes with EDTA and Axially Symmetric Macrocyclic Polyamino Polyacetate Ligands

Charles C. Bryden[1] and Charles N. Reilley*

Kenan Laboratories of Chemistry, University of North Carolina, Chapel Hill, North Carolina 27514

Jean F. Desreux

Analytical and Radiochemistry, University of Liege, Sart Tilman, B-4000, Liege, Belgium

Lanthanide complexes with the macrocycles 1,4,7,10-tetraazacyclododecane-N,N',N'',N'''-tetraacetate (DOTA) and 1,4,7-triazacyclononane-N,N',N''-triacetate (NOTA) and with ethylenediaminetetraacetate (EDTA) were prepared in D_2O solution; ten paramagnetic lanthanide ions and one or two diamagnetic lanthanide ions were complexed with each ligand. The shift reagent properties of these three types of complexes were studied with positively charged (Na^+), neutral (D_2O), and negatively charged (Cl^-) substrates, using ^{23}Na, ^2H, ^{17}O, and ^{35}Cl NMR. The axially symmetric octadentate Ln(DOTA)$^-$ complexes are the best shift reagents, as the paramagnetic ^2H, ^{23}Na, and ^{35}Cl shifts measured in these solutions were purely dipolar. However, the best fit of the ^{23}Na shifts to the theoretical dipolar shifts was obtained for Na^+ in LnNOTA solutions, indicating that the axially symmetric hexadentate LnNOTA complexes are best for positively charged substrates. Proton NMR spectra of the organic substrates 1-butanol, *n*-butylammonium cation, and *n*-valerate anion in Tm(DOTA)$^-$ solution all showed paramagnetic shifts.

Lanthanide aquo ions have frequently been used as shift reagents for water-soluble molecules (*1–6*); more recently, lanthanide EDTA complexes have been used for the same purpose (*7–9*). The LnEDTA complexes were introduced to alleviate the problems of low solubility (*7*) and hydroxide precipitation (*8*) encountered with the aquolanthanides. The applicability and utility of aqueous shift reagents could be further increased if problems such as limited pH range, presence of higher than 1:1 complexes, contact shifts, and nonaxial symmetry could be overcome.

As is well-known, the use of the aquolanthanides is restricted due to precipitation of hydroxides above about pH 6. The LnEDTA complexes are useful at higher pHs, although hydroxide coordination to the metal (*10*) can produce a change in the chemical shift of the substrate above pH 9 (*8*), limiting the use of LnEDTA shift reagents to pHs below about 9.

Another problem that is frequently confronted when aqueous (or nonaqueous) shift reagents are used is the formation of higher than 1:1 adducts with substrate molecules, making the calculation of the chemical shift of the bound substrate more difficult. The aquolanthanides are known to form mixtures of 1:1 and 2:1 adducts in solution (*5, 8*), and this possibility must be considered for LnEDTA complexes as well, since EDTA is only six-coordinate, with 3 ± 1 water molecules occupying the remaining coordination sites on the lanthanide ion (*11–14*). More than one substrate molecule might displace these water molecules and bind to the LnEDTA complex (depending on the charge and size of the substrate), producing higher than 1:1 adducts.

The possible contribution of contact shifts to the paramagnetic shift of the substrate is a third problem which complicates the application of shift reagents, both aqueous and nonaqueous. The paramagnetic shift is a combination of a contact (through-bonds) shift and a dipolar (through-space) shift, expressed by the equation

$$\delta = F\langle S_z \rangle + GC^D \qquad (1)$$

where the measured shift in parts per million is δ, the first term on the right-hand side represents the contact shift as the product of a ligand-dependent parameter F and a lanthanide ion dependent parameter $\langle S_z \rangle$, and the second term on the right-hand side represents the dipolar shift as the product of a ligand-dependent parameter G and a lanthanide ion dependent parameter C^D (*15*). The lanthanide-dependent parameters $\langle S_z \rangle$ and C^D have been calculated for all the lanthanides (*16–19*) and will be referred to respectively as theoretical contact shifts and theoretical dipolar shifts. It is the dipolar shift that is usually of interest, since it contains structural information. A number of methods for separating contact and dipolar shifts have been developed (*20*), but a shift reagent which produces purely dipolar shifts would be the best solution to this problem.

Even when the paramagnetic shift of a particular nucleus in a substrate molecule is known to be purely dipolar, the shift reagent–substrate adduct must have axial symmetry (at least a threefold symmetry axis) if geometric information about the substrate is to be easily obtained (*20*).

With the above requirements in mind, we decided to investigate the shift reagent properties of the lanthanide complexes of two ligands, one a derivative of a tetraaza macrocycle and the other a derivative of a triaza macrocycle, and compare them to the LnEDTA shift reagents. We prepared 11 or 12 lanthanide complexes with each of the ligands 1,4,7,10-tetraazacyclododecane-N,N',N'',N'''-tetraacetate (DOTA), 1,4,7-triazacyclononane-N,N',N''-triacetate (NOTA), and ethylenediaminetetraacetate (EDTA), the structures of which are shown in Figure 1. The complexes with NOTA have a C_3 (threefold) symmetry axis (Figure 4), while the complexes with DOTA have a C_4 symmetry axis (Figure 2); both complexes thus have axial symmetry. The LnDOTA complexes are eight-coordinate and are unlikely to form higher than 1:1 adducts with substrate molecules. Potentiometric titrations show that LnDOTA complexes do not coordinate OH^- even above pH 13 (*21*). These features suggest that LnNOTA and LnDOTA complexes might be superior to LnEDTA as

[1] Present address: Research Center, Hercules Inc., Wilmington, DE 19899.

0003-2700/81/0353-1418$01.25/0 © 1981 American Chemical Society

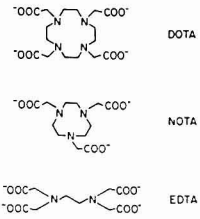


Figure 1. Structures of the three ligands.

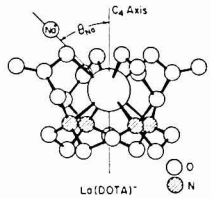


Figure 2. Model of the lanthanum DOTA complex, showing the C_4 symmetry axis and illustrating the dipolar angle for the case of a sodium ion (the position of the sodium ion is arbitrary). The plane of the four coordinated oxygens is above the lanthanum ion.

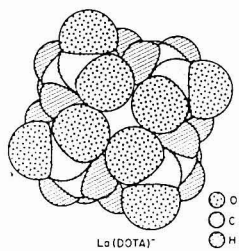


Figure 3. Space-filling model of the LaDOTA complex.

aqueous shift reagents (especially the LnDOTA complexes). To determine the relative utility of the three types of complexes as aqueous shift reagents with respect to positively charged, neutral, and negatively charged substrates, we measured the ^{23}Na shifts of Na^+, the ^2H and ^{17}O shifts of deuterated water, and the ^{35}Cl shifts of Cl^- in solutions of all 35 complexes. We were particularly interested in determining which (if any) of these substrates would show significant paramagnetic shifts, and if so, what was the contact contribution to the shifts. Also, for those species where the contact contribution was negligible (Na^+, at least, would have no contact shift contribution), it would be important to compare the shifts to the theoretical dipolar shifts (C^D values). A close correspondence of the measured shifts to the theoretical dipolar shifts would be evidence that the crystal field coefficients were constant along the lanthanide series, that the shift reagent–substrate stability constant did not vary along the series, and that the shift reagent–substrate adducts were isostructural.

EXPERIMENTAL SECTION

Chemicals and Solutions. The ligand DOTA was prepared as described previously (22), and the ligand NOTA was prepared as the trisodium salt according to ref 23. The tetrasodium salt of EDTA was purchased from Sigma Chemical Co., and the disodium salt of EDTA was purchased from Aldrich Chemical Co. The 0.1 M LnDOTA solutions were prepared in D_2O as in ref 22; the 0.1 M LnEDTA and LnNOTA solutions were prepared in D_2O from anhydrous lanthanide chlorides and adjusted to pH 7.5–8.0 with NaOD (not corrected for deuterium isotope effect). The EuEDTA, GdEDTA, and TbEDTA complexes had lower solubilities, and their solutions were prepared at 0.03, 0.038, and 0.05 M concentrations, respectively. All solutions contained 0.15 M dioxane (1.25%) as an internal heteronuclear reference. LuDOTA, LuEDTA, LuNOTA, LaEDTA, and LaNOTA were prepared for use as diamagnetic references. The Na^+ concentration was 0.35–0.63 M in LnDOTA solutions, 0.36–0.44 M in LnEDTA solutions, and 0.73–0.79 M in LnNOTA solutions; the Cl^- concentration was 0.30–0.39 M in LnDOTA solutions, 0.30–0.31 M in LnEDTA solutions, and 0.78–0.79 M in LnNOTA solutions.

Table I. NMR Experimental Conditions

nucleus obsd	obsd freq, MHz	pulse[a] width, μs	acq time, s	no. of transients	half-height[b] line width, Hz
^{23}Na	26.47	170 (170)	0.20	600	10–30
^{13}C	25.16	16 (47)	0.80	500	2–3
^2H	15.36	200 (200)	1.00	50	2–5
^{17}O	13.57	200 (200)	0.05	10000	60–90
^{35}Cl	9.81	500 (800)	0.10	4000	20–50

[a] The 90° pulse width is in parentheses. [b] Typical line widths in paramagnetic solutions (except for solutions of Gd complexes, where the line widths are usually much larger).

NMR Measurements. All spectra were obtained on a Varian XL-100/12 NMR spectrometer modified for multinuclear observation as described previously (24). The spectra were recorded at an ambient probe temperature of 28 ± 2 °C, using 2–3 mL of solution in 10-mm NMR tubes, spinning for ^{13}C and ^2H spectra, nonspinning for ^{35}Cl, ^{23}Na, and ^{17}O spectra. The ^{13}C spectra of the dioxane internal reference were obtained with low power, 200-Hz bandwidth ^1H decoupling to minimize heating of the solutions. The ^{13}C spectra of dioxane, and the ^{23}Na spectra of Na^+ were obtained twice, once with internal deuterium lock and once with ^{19}F external lock; the ^{35}Cl spectra of Cl^-, the ^{17}O spectra of water, and the ^2H spectra of water were all obtained by using ^{19}F external lock. Other experimental conditions are listed in Table I.

The shift due to the bulk paramagnetic susceptibility of each solution was accounted for by subtracting the ^{13}C shift of dioxane in parts per million from the ^{23}Na, ^2H, ^{17}O, or ^{35}Cl shift in parts per million. This is the same procedure that is routinely followed with ^1H spectra using Me_4Si (homonuclear internal reference), except that in our case, the observe nucleus is different from the reference nucleus (heteronuclear internal reference). The paramagnetic shift for a given nucleus was then obtained by subtracting the shift measured in the diamagnetic LuDOTA, LuEDTA, or LuNOTA solution. All shifts for a given nucleus measured in LuDOTA, LuEDTA, LuNOTA, LaEDTA, and LaNOTA solutions, and in a 0.4 M NaCl in D_2O solution were virtually identical, indicating a very small diamagnetic shift in every case.

For the 100-MHz ^1H spectra of *n*-butylammonium ion, 1-butanol, and *n*-valerate ion, 0.05 mmol of each substrate was dissolved in 0.5 mL of D_2O and in 0.5 mL of 0.1 M TmDOTA solution in D_2O. The pH of the solutions containing the *n*-butylammonium and *n*-valerate ions were adjusted with NaOD or DCl to the values indicated in Figures 9 and 11 (not corrected for deuterium isotope effect). Dioxane was already present in the three solutions containing TmDOTA but was added to the other three solutions and was assigned a shift of 3.53 ppm vs. Me_4Si for all six solutions, thus correcting for the bulk paramagnetic susceptibility of the TmDOTA solutions.

In the discussion which follows, positive shifts are to higher frequency (lower field).

THEORY

Equation 1 is the expression for the measured paramagnetic shift, which is the average of the shifts of the free and bound substrate. In the following sections, we will be interested in the paramagnetic shift of the bound substrate

$$\left(\frac{\Delta\nu}{\nu}\right)_b = F_b\langle S_z\rangle + G_bC^D \tag{2}$$

Here $\Delta\nu$ and ν are both in hertz (i.e., the bound shift is *not* expressed in parts per million). F_b and G_b are related to F and G as follows:

$$F_b = 10^{-6}\frac{C_S}{nC_{SR\text{-}S}}F \tag{3}$$

$$G_b = 10^{-6}\frac{C_S}{nC_{SR\text{-}S}}G \tag{4}$$

where n is the coordination number of the substrate in the shift reagent–substrate adduct, $C_{SR\text{-}S}$ is the concentration of the shift reagent–substrate adduct in moles per liter of solution, and C_S is the total concentration of substrate (free + bound) in moles per liter of solution. Geometric information is contained in the ligand-dependent parameter G_b

$$G_b = \frac{2\beta^2}{60k^2T^2}\left(\frac{\langle r^2\rangle A_2{}^0(3\cos^2\theta - 1)}{r^3} + \frac{\langle r^2\rangle A_2{}^2(\sin^2\theta\cos 2\phi)}{r^3}\right) \tag{5}$$

where $\langle r^2\rangle A_2{}^0$ and $\langle r^2\rangle A_2{}^2$ are two crystal field coefficients, and r, θ, and ϕ are the spherical coordinates of the observed nucleus with respect to the lanthanide ion at the origin of the coordinate system (*18*). When the shift reagent–substrate complex is axially symmetric or has effective axial symmetry because of motional averaging, eq 5 simplifies to

$$G_b = \frac{2\beta^2}{60k^2T^2}\left(\frac{\langle r^2\rangle A_2{}^0(3\cos^2\theta - 1)}{r^3}\right) \tag{6}$$

Equation 6 can be used to find r and θ for several nuclei in (and hence the solution structure of) the substrate molecule and is clearly preferable to eq 5 for this purpose. As has been pointed out by Sherry, Yang, and Morgan (*25*), a linear correlation between the observed shifts and the theoretical C^D values is not proof of axial symmetry, as such a correlation can be obtained with G represented by either eq 5 or eq 6. For the same reason, constancy of the shift ratios of two nuclei for several lanthanides is not proof of axial symmetry. Consequently, experimental proof of effective axial symmetry is difficult to obtain, and it is therefore desirable to have a shift reagent which is axially symmetric and which can be expected to form axially symmetric adducts with substrate molecules.

Where contact shifts might be expected, we used the procedures designated in ref 20 as "method A_1" and "method A_2" to separate the contact and dipolar shifts. In method A_1, which was used when contact shifts were dominant, eq 1 was rearranged to

$$\frac{\delta}{C^D} = F\frac{\langle S_z\rangle}{C^D} + G \tag{7}$$

and δ/C^D was plotted against $\langle S_z\rangle/C^D$. In method A_2, which was used when dipolar shifts were dominant, eq 1 was rearranged to

$$\frac{\delta}{\langle S_z\rangle} = G\frac{C^D}{\langle S_z\rangle} + F \tag{8}$$

and $\delta/\langle S_z\rangle$ was plotted against $C^D/\langle S_z\rangle$. The slope (F for method A_1 and G for method A_2) and the intercept (G for method A_1 and F for method A_2) were calculated by using the linear least-squares technique, with shifts measured in solution for ten paramagnetic lanthanide complexes.

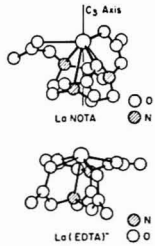


Figure 4. Models of the lanthanum NOTA and lanthanum EDTA complexes. The plane of the coordinated oxygens is below the lanthanum ion in both complexes.

Coupling constants and spin densities were calculated by using the following equations (*20*):

$$\frac{A}{h} = -10^{-6}\frac{3kT}{2\pi\beta}\gamma F_b \tag{9}$$

$$\rho = -40\frac{|\Psi_H(0)|^2}{|\Psi(0)|^2}F_b \tag{10}$$

where A/h is the electron–nucleus coupling constant in megahertz, γ is the magnetogyric ratio of the nucleus, and ρ is the electron spin density at the nucleus. Values of $|\Psi(0)|^2/|\Psi_H(0)|^2$ are tabulated in ref 26. When the substrate is the solvent (D_2O), $C_{SR\text{-}S}$ can be replaced by C_{SR}, the concentration of the shift reagent in moles per liter of solution.

Theoretically one could observe dipolar paramagnetic shifts, even when the shift reagent does not form a complex with the substrate, through what we call the "excluded volume effect". This effect can occur in complexes where the lanthanide ion is closer to one periphery of the complex. Under such circumstances, the substrate would be able to approach the lanthanide ion more closely in one region of the molecule, and the dipolar shift may no longer average to zero as a result of random motion. Figures 2 and 4 show that the effect can occur for all three complexes, with the substrate approaching the lanthanide ion more closely in the region above each complex. To determine whether the effect was important for the LnDOTA, LnEDTA, and LnNOTA shift reagents, we plotted the ^{13}C shifts of dioxane vs. the paramagnetic susceptibilities of the lanthanide aquo ions. As dioxane does not complex with these shift reagents, the dioxane shifts will correlate well with the magnetic susceptibilities provided the excluded volume effect is negligible (and provided the ligands do not significantly alter the paramagnetic susceptibilities of the aquo ions). The correlation coefficient was 0.99 or better in all three cases, demonstrating that the excluded volume effect was indeed negligible.

RESULTS

The ^{35}Cl, ^{17}O, ^{23}Na, and ^{2}H shifts for each set of lanthanide complexes are plotted in Figures 5–7, along with scaled theoretical dipolar (*19*) or contact (*17*) shifts (solid line in figures). The theoretical shifts were scaled by using the zero-intercept least-squares slope of the line fitting the observed shifts to the unscaled theoretical shifts. A table of the observed shifts is given in Table II. In Figure 8, the theoretical shifts (solid line) have been scaled to fit previously measured ^{17}O and ^{1}H shifts of H_2O in lanthanide aquo complexes (*16*, *27*); the shifts have been extrapolated down to 0.1 M for comparison to the shifts in Figures 5–7.

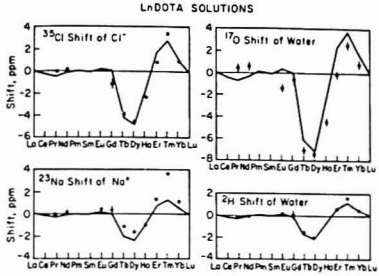


Figure 5. Measured vs. theoretical dipolar NMR shifts in 0.1 M LnDOTA solutions.

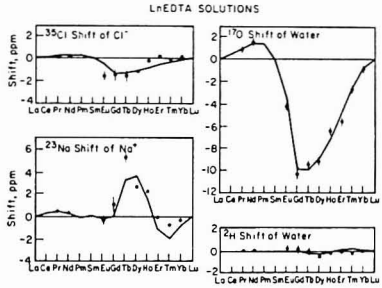


Figure 6. Measured vs. theoretical contact (^{35}Cl, ^{17}O) or dipolar (^{23}Na, ^{2}H) NMR shifts in 0.1 M LnEDTA solutions.

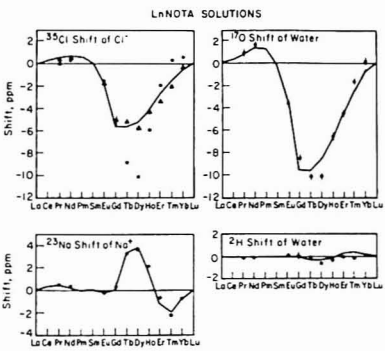


Figure 7. Measured vs. theoretical contact (^{35}Cl, ^{17}O) or dipolar (^{23}Na, ^{2}H) NMR shifts in 0.1 M LnNOTA solutions. In the plot of ^{35}Cl shifts, ● = observed shift and ▲ = shift after calculated dipolar shift was subtracted.

Table III gives the results when separation method A_1 or A_2 was applied to each set of ^{17}O, ^{2}H, ^{1}H, and ^{35}Cl shifts, except where the relative error in shift measurement was large (^{2}H shifts for water in LnEDTA and LnNOTA solutions, ^{35}Cl shifts for chloride ion in LnEDTA solutions). The ^{17}O shift of water in the Sm aquo complex (reported in ref 16) was excluded, as the measured and theoretical contact shifts of Sm are very small and thus have large relative uncertainties; the ratio of the two $(\delta/\langle S_z \rangle)$ used in the separation has an even larger relative error. In Table IV, the Sm ^{17}O shift was again excluded. In Tables III and IV, N is the number of lanthanides

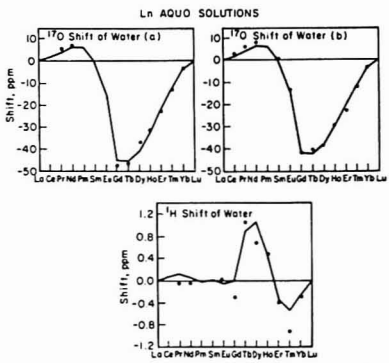


Figure 8. Measured vs. theoretical contact (^{17}O) or dipolar (^{1}H) NMR shifts in 0.1 M Ln aquo complexes. The ^{1}H shifts, and the ^{17}O shifts labeled (a) are from ref 27; the ^{17}O shifts labeled (b) are from ref 16.

Table II. Paramagnetic Shifts in Parts per Million for Cl^-, Na^+, and D_2O in 0.1 M Solutions of LnDOTA, LnNOTA, and LnEDTA Complexes

Ln	^{17}O shifts	^{2}H shifts	^{35}Cl shifts	^{23}Na shifts
		LnDOTA		
La				
Pr	0.34	−0.18	−0.14	−0.02
Nd	0.54	−0.08	0.09	0.13
Eu	−1.44	0.13	0.04	0.29
Gd	−0.76	0.06	−1.13	0.28
Tb	7.06	−1.52	−3.96	−1.11
Dy	−7.41	−2.01	−4.80	−1.68
Ho	−4.66	−1.02	−2.54	−1.01
Er	−0.23	0.59	0.82	1.25
Tm	2.43	1.54	3.38	3.56
Yb	0.83	0.47	0.85	1.04
Lu	0.00	0.00	0.00	0.00
		LnNOTA		
La	−0.07	0.01	−0.25	0.03
Pr	0.99	−0.08	−0.02	0.49
Nd	1.65	−0.05	0.16	0.23
Eu	−3.74	0.08	−1.70	−0.13
Gd	−8.60	0.06	−5.03	0.27
Tb	−10.25	−0.18	−9.04	3.16
Dy	−10.21	−0.77	−10.22	3.68
Ho	−6.22	−0.33	−6.04	2.16
Er	−4.40	−0.11	−1.97	−0.79
Tm	−1.74	−0.14	0.23	−2.26
Yb	0.14	0.06	0.57	−0.84
Lu	0.00	0.00	0.00	0.00
		LnEDTA		
La	0.03	0.01	−0.22	0.05
Pr	0.84	0.03	0.05	0.55
Nd	1.58	0.02	0.11	0.32
Eu[a]	−1.25	0.05	−0.51	−0.07
Gd[b]	−3.86	0.08	−0.57	0.21
Tb[c]	−4.77	0.00	−0.83	2.78
Dy	−9.11	−0.56	−1.14	2.73
Ho	−6.44	−0.16	−0.23	2.24
Er	−5.49	−0.08	0.11	0.03
Tm	−2.85	−0.22	−0.05	−0.84
Yb	−0.87	0.00	0.14	−0.18
Lu	0.00	0.00	0.00	0.00

[a] 0.03 M. [b] 0.0375 M. [c] 0.05 M.

used in the separation and r is the correlation coefficient.

The shifts measured in EuEDTA, GdEDTA, and TbEDTA solutions were linearly extrapolated to 0.1 M for comparison

Table III. Separation of Contact and Dipolar Shifts[a]

complex		^{17}O shifts	^{2}H shifts	^{35}Cl shifts
LnDOTA	N	10[c]	10[c]	10[c]
	F	0.116 (25%)	−0.00197 (320%)	0.0269 (82%)
	G	0.0489 (15%)	0.0228 (7.1%)	0.0470 (12%)
	r	0.921	0.980	0.947
LnEDTA	N	9[b]		
	F	0.375 (2.9%)		
	G	−0.00787 (140%)		
	r	0.997		
LnNOTA	N	9[b]		10[c]
	F	0.348 (3.0%)		0.174 (9.8%)
	G	0.00289 (360%)		0.0433 (10%)
	r	0.997		0.961
Ln aquo[e]	N	8[b]	10[c,d]	
	F	1.50 (2.2%)	−0.00157 (570%)	
	G	−0.0352 (48%)	−0.0119 (19%)	
	r	0.9985	−0.898	
Ln aquo[f]	N	10[b]		
	F	1.35 (4.0%)		
	G	−0.0900 (57%)		
	r	0.994		

[a] Relative standard deviations in parentheses. [b] Separation method A_1. [c] Separation method A_2. [d] ^{1}H shifts. [e] Shifts from ref 27. [f] Shifts from ref 16.

to the shifts for the other lanthanides. The validity of this extrapolation was verified by measuring shifts in 0.025, 0.05, and 0.10 M HoEDTA solutions.

DISCUSSION

Oxygen-17 Shifts. The ^{17}O shifts of water in LnDOTA solution tend to follow the scaled theoretical dipolar shifts (Figure 5), although there appears to be a small contact shift contribution. The substantial dipolar contribution to the water ^{17}O shifts in LnDOTA solution means that at least one water molecule must have a preferred orientation with respect to the LnDOTA complex and must approach the lanthanide ion fairly closely. If there were no preferred orientation, the $3\cos^2\theta - 1$ term in eq 6 would average to zero, and there would be no dipolar shift. A molecular model (Figure 2) shows that the distance of closest approach is for a water molecule approaching the lanthanide ion along the C_4 symmetry axis from above, so that it is equidistant from the four coordinated carboxylate oxygens. A space-filling model (Figure 3) shows that only one water molecule at a time can closely approach the lanthanide ion from above.

As there is a contact contribution to the water ^{17}O shifts in LnDOTA solution, a water molecule must be coordinated to the lanthanide ion at least some of the time. However, the water molecule above the complex cannot approach the lanthanide ion as closely as the coordinated water does in lanthanide aquo complexes as long as all four carboxylate oxygens are rigidly coordinated. Thus the complex must be sufficiently flexible that a water molecule can coordinate to the complex a large fraction of the time.

The ^{17}O shifts of water in solutions of LnEDTA, LnNOTA, and Ln aquo complexes all closely follow the scaled theoretical contact shifts (Figures 6–8); thus water must be coordinating to the metal in each of these three types of complexes. Given

Table IV. Separation of Contact and Dipolar ^{17}O Shifts for Light and Heavy Lanthanide Complexes[a]

complex		light lanthanides	heavy lanthanides
LnDOTA	N	3[c]	6[c]
	F	0.131 (5.7%)	0.0923 (17%)
	G	0.00481 (70%)	0.0527 (6.3%)
	r	0.817	0.992
LnEDTA	N	3[b]	6[b]
	F	0.405 (2.6%)	0.319 (3.3%)
	G	0.0425 (42%)	−0.00853 (46%)
	r	0.9997	0.998
LnNOTA	N	3[b]	6[b]
	F	0.350 (2.9%)	0.278 (7.5%)
	G	−0.00463 (370%)	0.0139 (55%)
	r	0.9996	0.989
Ln aquo[d]	N	2[f]	6[b]
	F	1.46	1.43 (1.9%)
	G	−0.100	−0.0137 (74%)
	r		0.9993
Ln aquo[e]	N	4[b,g]	6[b]
	F	1.23 (6.6%)	1.37 (2.1%)
	G	−0.316 (37%)	−0.0235 (46%)
	r	0.996	0.9991

[a] Light lanthanides are Pr, Nd, and Eu, except as noted. Heavy lanthanides are Tb, Dy, Ho, Er, Tm, and Yb. [b] Separation method A_1. [c] Separation method A_2. [d] Shifts from ref 27. [e] Shifts from ref 16. [f] No Eu shift available. [g] Includes Ce.

the large ^{17}O dipolar shifts in LnDOTA solutions (e.g., a −4.9 ppm dipolar shift for DyDOTA using separation method A_2), it is surprising at first to see little dipolar contribution to the ^{17}O shifts in Ln aquo, LnEDTA, and LnNOTA solutions. However, rapid ligand exchange averages the dipolar ^{17}O shifts of Ln aquo complexes to zero, while water dipolar angles in LnEDTA and LnNOTA solutions are near the magic angle of 54.7°, resulting in small dipolar shifts.

The close correspondence of the ^{17}O shifts of water to the theoretical contact shifts in solutions of Ln aquo and LnEDTA complexes means that the electron–nucleus coupling constant does not vary along the lanthanide series; this coupling constant can be calculated given the water coordination number n. Although there is controversy as to whether n changes along the lanthanide series in Ln aquo and LnEDTA complexes (*14*), there is general agreement that n is constant in both cases for the heavy lanthanides (Tb–Yb). If n for the heavy lanthanides is taken to be eight for the Ln aquo solutions (*28*) and three for the LnEDTA solutions (*14*), then the coupling constants can be calculated for these two systems using eq 3, 4, and 9 (with water as the substrate, $C_{SR\text{-}S} = C_{SR} = 0.1$ M, while $C_S = 55.5$ M). For the Ln aquo complexes, using a average F of 1.40 (mean of 1.43 and 1.37; see Table III), and taking the temperature to be 300 K, $A/h = 0.75$ MHz. If n is taken to be nine (*12*, *14*), $A/h = 0.67$ MHz. For LnEDTA, using $F = 0.319$, and a temperature of 300 K, $A/h = 0.46$ MHz. We see that the coupling constant decreases at least 0.21 MHz, or 31% when the lanthanide ion is chelated with EDTA. Thus the coupling constant can change significantly when the complex is varied, in contrast to the result when the lanthanide ion is varied.

If the coupling constant did not vary from complex to complex, we could reverse the above process for the LnDOTA and LnNOTA complexes and calculate n for the heavy lanthanides from the known contact shifts in these solutions. Unfortunately, the coupling constant does vary; however, some useful estimates can still be made if we assume that the coupling constants in LnDOTA and LnNOTA complexes vary no more than 33% from the LnEDTA complexes (i.e., $A/h = 0.46 \pm 0.15$ MHz). Using $F = 0.278$ for the ^{17}O shifts of

water in LnNOTA solutions (Table III), we can estimate a water coordination number of 3 ± 1 for the heavy lanthanides. For LnDOTA solutions, using $F = 0.0923$, we estimate a water coordination number of 1 ± 0.3 for the heavy lanthanides.

Sodium-23 Shifts. The ^{23}Na shifts of Na^+ in LnDOTA solutions follow the theoretical dipolar shifts, which means that the sodium ion must have a preferred orientation with respect to the LnDOTA complex. If there were no preferred orientation of the sodium ion, it would experience all possible dipolar shifts equally, with a resultant average (observed) dipolar shift of zero. The sign of the ^{23}Na shifts is the same as the water ^2H shifts and the dipolar part of the water ^{17}O shifts; since the dipolar angles for water (θ_O and θ_D) are less than 54.7°, the dipolar angle θ_{Na} must also be less than 54.7°. The sodium ion must prefer one or both of the cones (defined by $0° \leq \theta \leq 54.7°$) above or below the LnDOTA complex. The lower portion of the LnDOTA complex is hydrophobic, and there is no reason for charged or polar species to associate closely with this region of the complex. There are four carboxylate oxygens in the vicinity of the upper cone, and as we expect to find the positively charged sodium ion near the negatively charged carboxylate oxygens, the sodium ion undoubtedly prefers the upper cone. We also expect the carboxylate groups to attract the sodium ion away from the C_4 symmetry axis, so that its preferred position will be in a cone about the axis, making θ_{Na} substantially greater than zero. We emphasize that the geometric terms such as θ_{Na} and r_{Na} refer only to the *weighted dipolar average* position of the sodium ion (or other substrate).

Given that θ_{Na} is large in LnDOTA solutions, we can easily explain the change in sign of the ^{23}Na shifts in LnEDTA and LnNOTA solutions. The ^{23}Na shifts in LnEDTA and LnNOTA solutions also follow the theoretical dipolar shifts, but with a change in sign relative to the ^{23}Na shifts in LnDOTA solution. It is clear from the sign change that the dipolar angle θ_{Na}, already large in LnDOTA solution, is greater than 54.7° in LnEDTA and LnNOTA solutions. X-ray structures and molecular models show that it is reasonable for θ_{Na} to be larger in LnEDTA and LnNOTA solutions. For LaEDTA and DyEDTA, X-ray crystal structures show that the four carboxylate oxygens form a plane below the lanthanide ion (*11, 13*). A model of LaNOTA (Figure 4) shows that the three carboxylate oxygens in this complex also form a plane below the lanthanide ion. However, a model of LaDOTA clearly demonstrates that the four carboxylate ions form a plane *above* the lanthanide ion (Figure 2). Since the sodium ion will be attracted to the carboxylate oxygens in each complex, the sodium ion will have a larger dipolar angle in LnEDTA and LnNOTA solutions than in LnDOTA solutions. Consequently it is not surprising to find that the ^{23}Na NMR results show that $\theta_{Na} > 54.7°$ in LnEDTA and LnNOTA solutions and $\theta_{Na} < 54.7°$ in LnDOTA solutions. (It could be argued that the crystal field coefficients change sign in LnEDTA and LnNOTA complexes, but the ^{35}Cl results show that this does not happen.)

Deuterium Shifts. From Figure 5, it can be seen that the ^2H shifts of water in LnDOTA solutions closely follow the theoretical dipolar shifts. We conclude that the crystal field coefficient, $\langle r^2 \rangle A_2^0$, is constant along the lanthanide series and that the deuterium dipolar angle θ_D and the Ln–D distance r_D do not change appreciably, despite the decrease in radius from La to Lu. The sign of the ^2H shifts is the same as for the dipolar portion of the ^{17}O shifts, as expected.

The ^2H shifts in LnDOTA solutions are twice as large as the proton shifts in Ln aquo solutions, which also follow the theoretical dipolar shifts, although not as closely (Figure 8). The shifts in LnDOTA solutions are even larger if the comparison is adjusted to reflect the different water coordination numbers in the two complexes. As discussed earlier, only one water molecule can closely approach the lanthanide ion in LnDOTA complexes; if we take the coordination number of water in Ln aquo complexes to be 9, the ratio of water coordination numbers in the two complexes is 9:1, and the shift per water molecule in LnDOTA solutions is $2 \times 9 = 18$ times the shift per water molecule in Ln aquo solutions. Large dipolar shifts are expected for LnDOTA solutions, as the closest water molecule is located on the C_4 symmetry axis, and the dipolar angle θ_D for water deuterons must therefore be small ($3 \cos^2 \theta - 1$ large). On the other hand, small dipolar shifts are expected for Ln aquo solutions as a result of the averaging process discussed in the section on ^{17}O chemical shifts. From the crystal structures of $Pr(H_2O)_9^{3+}$, $Nd(H_2O)_9^{3+}$, and $Yb(H_2O)_9^{3+}$ (*29, 30*), 12 protons should have $\theta_H < 54.7°$, and their instantaneous dipolar shift will be opposite to the six protons of the equatorial water molecules, which have θ_H near 90°. Rapid exchange will lead to a small average (observed) shift. (If there is an outer sphere contribution (*31*), there will be a similar averaging process.) Since large shifts are expected for LnDOTA solutions, and small shifts per water molecule are expected for Ln aquo solutions, the LnDOTA/Ln aquo shift ratio of 18 per water molecule is not surprising.

The ^2H shifts of water in LnDOTA solutions are not only larger but also opposite in sign to the proton shifts in Ln aquo solutions, which could be the result of a change in sign of $\langle r^2 \rangle A_2^0$. However, the difference in sign may simply be due to geometry. The six hydrogens of the equatorial water molecules (θ_H near 90°) in the aquo complex have dipolar shifts opposite in sign to the hydrogens of water in LnDOTA solutions (θ_H small). If the other 12 hydrogens in the Ln aquo complex have $\theta_H > 45°$, the six equatorial hydrogens will dominate the average (observed) shift, which will then be opposite in sign to the shifts in LnDOTA solutions.

In contrast to the large ^2H shifts observed in LnDOTA solutions, the ^2H shifts in LnEDTA and LnNOTA solutions are very small (Figures 6 and 7). These results are similar to the ^{17}O results for the two complexes, where the dipolar contributions to the shifts are also very small. Again, the best explanation for the small shifts is that the dipolar angle θ_H is near 54.7° for water hydrogens in LnEDTA and LnNOTA solutions.

Chlorine-35 Shifts. The ^{35}Cl shifts of chloride ion in LnDOTA solutions closely follow the scaled theoretical dipolar shifts (Figure 5), which means that Cl^-, like Na^+ and D_2O, must have a preferred orientation with respect to the LnDOTA complex. The close correspondence to the theoretical dipolar shifts also shows that $\langle r^2 \rangle A_2^0$, the chloride dipolar angle θ_{Cl}, and the Ln–Cl distance r_{Cl} are constant along the lanthanide series in LnDOTA solutions.

The sign of the ^{35}Cl shifts in LnDOTA solutions is the same as the ^{23}Na shifts, the ^2H shifts, and the dipolar portion of the ^{17}O shifts in LnDOTA solutions, so the Cl^- ion must have a preferred orientation near the Na^+ ion above the LnDOTA complex where $0° \leq \theta \leq 54.7°$. The chloride ion will be repelled by the four negatively charged carboxylate oxygens and attracted by the positively charged lanthanide ion, so the chloride ion should be located on the C_4 axis equidistant from the carboxylate oxygen, i.e., θ_{Cl} should be near zero.

Given a θ_{Cl} near 0°, we can account for the fact that the ^{35}Cl shifts have the same magnitude as the ^{23}Na shifts in LnDOTA solution. The Cl^- ion should be farther away from the negatively charged LnDOTA complex than the Na^+ ion, and on this basis should have a smaller dipolar shift. However, we previously concluded that Na^+ has a large dipolar angle, and this decreases the ^{23}Na shifts relative to the ^{35}Cl shifts to the point where the ^{35}Cl shifts are comparable to (and for some lanthanides larger than) the ^{23}Na shifts in LnDOTA solutions.

The ^{35}Cl shifts in LnDOTA solutions, unlike the ^{17}O shifts, show little or no evidence of a contact contribution. The Cl–Ln interaction, like the D_2O–Ln interaction, could have some small covalent character, which would then give rise to a contact contribution to the ^{35}Cl shifts. Indeed, there is a substantial contact contribution to the ^{35}Cl shifts in LnNOTA solutions (see below), and there is a contact contribution to the ^{17}O shifts in all three complexes; however, there is little or no contact contribution to the ^{35}Cl shifts in LnDOTA solutions. We conclude that the chloride ion is farther away from the lanthanide ion in LnDOTA solutions than in LnNOTA solutions, so that the Cl–LnDOTA interaction is entirely ionic. These results are consistent with the ^{17}O results, where a much smaller contact contribution was observed for water in LnDOTA solutions than in LnEDTA or LnNOTA solutions. It must be that the region above the LnDOTA complex is quite crowded, preventing the chloride ion or water molecule from approaching the lanthanide ion as closely as in Ln aquo, LnEDTA, or LnNOTA complexes. The chloride ion, because of its negative charge and larger radius, cannot approach the negatively charged LnDOTA complex as closely as the water molecule and experiences a negligible contact shift.

In LnNOTA solution, the ^{35}Cl shifts follow a pattern which is clearly a sum of contact and dipolar shifts. When the dipolar shifts obtained by using separation method A_2 (G = 0.0433) are subtracted from the measured shifts, the residual shifts fit the scaled theoretical contact shifts quite closely (Figure 7); the good fit demonstrates that the ^{35}Cl–electron coupling constant does not vary much along the lanthanide series. Chlorine-35 contact shifts have been observed previously for chloride ion in aqueous $LnCl_3$ solutions (*32*). A contact contribution to the LnNOTA ^{35}Cl shifts means that the chloride ion is coordinated to the lanthanide ion in LnNOTA complexes at least some of the time. Although a number of studies show no detectable inner sphere chloride in Ln aquo complexes (*28*, *33*), NMR contact shifts can be observed even when only a very small amount of inner sphere complex is present. If we assume that 1% of the LnNOTA complexes have one chloride ion in the inner sphere (i.e., $C_{SR\text{-}S}$ = 1% of 0.1 M, or 0.001 M), then using eq 3, 4, and 10, we can estimate the spin density ρ_{Cl} at the ^{35}Cl nucleus required to produce the observed contact shifts. The chloride ion concentration is 0.78 M, and F is 0.174 (Table III); using $C_{SR\text{-}S}$ = 0.001 M, and n = 1, we obtain $\rho_{Cl} = -1.6 \times 10^{-4}$. This spin density is similar to that obtained for directly coordinated nuclei in other systems; for example, $\rho_O = -1.15 \times 10^{-4}$ for ^{17}O of water in LnEDTA solutions (taking n = 3), and $\rho_N = -2.6 \times 10^{-4}$ for ^{14}N of pyridine in $Ln(dpm)_3$ adducts (*20*). Thus the observed ^{35}Cl contact shifts can be accounted for by a very small amount of chloride ion in the inner coordination sphere.

The signs of the dipolar contribution to the ^{35}Cl shifts are the same in LnNOTA and in LnDOTA solutions, but the signs are opposite for the ^{23}Na shifts in the two solutions. If we tried to account for the opposite signs of the ^{23}Na shifts on the grounds that $\langle r^2 \rangle A_2^0$ was of opposite sign in the two complexes, then the signs of the dipolar ^{35}Cl shifts should be opposite also. Since in fact the dipolar ^{35}Cl shifts have the same sign, it is clear that a change in sign of $\langle r^2 \rangle A_2^0$ cannot be the reason for the opposite signs of the ^{23}Na shifts. The best explanation is that $\theta_{Na} < 54.7°$ in LnDOTA solutions, and $\theta_{Na} > 54.7°$ in LnNOTA solutions, as stated in the section on ^{23}Na shifts, and that $\theta_{Cl} < 54.7°$ for both LnDOTA and LnNOTA solutions.

Aqueous Shift Reagent Utility. As all of our studies were on inorganic substrates, we felt it would be useful to include some organic molecules, thus verifying the utility of the LnDOTA complexes for organic substrates. To determine the extent to which LnDOTA complexes would induce paramagnetic shifts in organic substrates, we measured the ^1H shifts in TmDOTA solution of three molecules containing the n-butyl group. Figures 9–11 show the results for the positively charged n-butylammonium ion (pK_a = 10.6), the neutral 1-butanol, and the negatively charged n-valerate ion (valeric acid pK_a = 4.8). Paramagnetic shifts were observed for all three

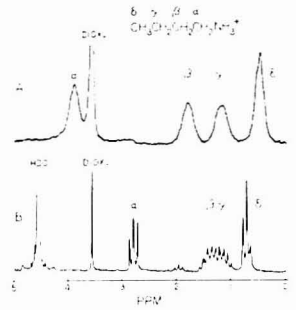


Figure 9. The ^1H spectra of 0.1 M n-butylammonium ion in D_2O, with dioxane reference: (A) in 0.1 M TmDOTA, pH 9.0 (the HDO resonance is at 6.13 ppm. The small resonances due to excess DOTA ligand are under the α-proton and dioxane resonances); (B) no addition, pH 9.1.

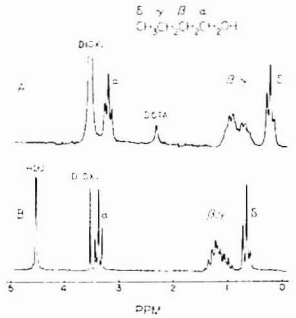


Figure 10. The ^1H spectra of 0.1 M 1-butanol D_2O, with dioxane reference: (A) in 0.1 M TmDOTA (the HDO resonance is at 6.19 ppm. One of the resonances due to free DOTA is under the left portion of the α-proton multiplet); (B) no additions.

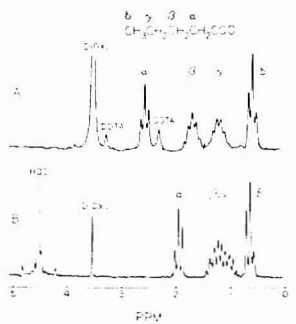


Figure 11. The ^1H spectra of 0.1 M n-valerate in D_2O, with dioxane reference: (A) in 0.1 M TmDOTA, pH 11.0 (the HDO resonance is at 6.26 ppm); (B) no additions, pH 11.9.

charge types, with the two charged molecules showing the largest shifts. The ^1H shift of HDO was also measured and, as expected, was the same as the ^2H shift of D_2O.

For the *n*-butylammonium ion (Figure 9), the shifts of the α and β protons are to high frequency (the same direction as the water protons), while the shift of the δ protons is to lower frequency. This result shows that the association of the *n*-butylammonium ion with the TmDOTA complex is similar to that of the Na^+ ion. The positively charged alkyl ammonium ion is located near the negatively charged carboxylate oxygens of the TmDOTA complex, so that the protons closest to the nitrogen (the α and β protons) are in the same region as the Na^+ ion ($\theta < 54.7°$) and have paramagnetic shifts of the same sign as the ^{23}Na shifts of the Na^+ ion in TmDOTA solution. The end of the alkyl chain extends down into the equatorial shift cone, so that the δ protons have $\theta > 54.7°$ and experience a paramagnetic shift opposite in sign to the α and β protons and to the water protons.

The shifts of the 1-butanol protons (Figure 10) are small, and in the *opposite* direction to the water proton shift, with the δ protons experiencing the largest shift. Clearly, the 1-butanol molecule does not compete with water for the region above the TmDOTA complex, but instead hydrogen bonds to the carbonyl oxygens, with the alkyl chain extending down into the region where $\theta > 54.7°$. The 1-butanol molecule is thus farther away from the TmDOTA complex than the water molecule at θ near 0°, which accounts for the smaller shifts, as well as the opposite sign of the shifts. The δ protons, having θ_H nearest 90°, have the largest shift.

The opposite direction of the 1-butanol and water shifts suggests an application of LnDOTA complexes for solutions prepared in H_2O, namely, shifting the large H_2O peak away from the alkyl resonances for better qualitative and quantitative analysis.

In contrast to the 1-butanol results, the paramagnetic shifts of the *n*-valerate protons (Figure 11) are in the *same* direction as the water protons, with the protons nearest the carboxylate group having the largest shifts. This result shows that the association of the *n*-valerate ion with the TmDOTA complex is similar to that of the Cl ion. The valerate carboxylate group is located above the TmDOTA complex, so that the alkyl chain is in the axial shift cone; the valerate protons thus have paramagnetic shifts of the same sign as the Cl^- ion and the water protons. In this case, the α protons, which have θ_H nearest 0° and are closest to the carboxyl group of the valerate ion, have the largest shift.

In all three spectra, the β and γ resonances are partially or completely resolved, but our proposed analytical application of the LnDOTA and LnNOTA complexes has nothing to do with the resolution of overlapping resonances. The application is to the determination of the structure of molecules in solution, and for this purpose we would prefer to start with a spectrum having all multiplets resolved (e.g., obtain the ^1H spectrum at 360 MHz) and then add an axially symmetric shift reagent to obtain purely dipolar paramagnetic shifts. The dipolar shifts of the substrate (if rigid) can then be fitted to the dipolar surface, and r and θ can be calculated for each proton (and carbon if ^{13}C spectra are obtained) in the substrate molecule.

As outlined in the introduction, our major objective was to find an aqueous shift reagent whose adducts with substrate molecules were axially symmetric and which induced only dipolar shifts in the substrate. Other desirable features were 1:1 stoichiometry and a wide pH range. The LnDOTA complexes satisfy these requirements. They are axially symmetric, induce only dipolar shifts in Na^+, Cl^-, and the ^2H nuclei of D_2O, and induce largely dipolar shifts in the ^{17}O nuclei of D_2O. In contrast to the Ln aquo, LnEDTA, and LnNOTA complexes, where hydroxide coordination is a problem in the basic pH region, LnDOTA complexes are usable to pH 13 or higher. Additionally, the eight-coordinate LnDOTA complexes are unlikely to form higher than 1:1 complexes with substrate molecules.

ACKNOWLEDGMENT

The authors thank Dennis S. Everhart and Ronald F. Evilia for providing the trisodium salt of NOTA.

LITERATURE CITED

(1) Barry, C. D.; North, A. C. T.; Glasel, J. A.; Williams, Robert J. P.; Xavier, Antonio V. *Nature (London)* **1971**, *232*, 236–245.
(2) Desreux, Jean F.; Reilley, Charles N. *J. Am. Chem. Soc.* **1976**, *98*, 2105–2109.
(3) Elgavish, Gabriel A.; Reuben, Jacques *J. Am. Chem. Soc.* **1977**, *99*, 5590–5591.
(4) Sherry, A. Dean; Pascual, E. *J. Am. Chem. Soc.* **1977**, *99*, 5871–5876.
(5) Fazakerley, G. Victor; Linder, Peter W.; Reid, David G. *Eur. J. Biochem.* **1977**, *81*, 507–514.
(6) Izumi, Kunihiko *Agric. Biol. Chem.* **1980**, *44*, 1623–1631.
(7) Dobson, Christopher M.; Williams, Robert J. P.; Xavier, Antonio V. *J. Chem. Soc., Dalton Trans.* **1974**, 1762–1764.
(8) Elgavish, Gabriel A.; Reuben, Jacques *J. Am. Chem. Soc.* **1976**, *98*, 4755–4759.
(9) Geraldes, C. F. G. C. *J. Magn. Reson.* **1979**, *36*, 89–98.
(10) Southwood-Jones, Rosalind V.; Merbach, Andre E. *Inorg. Chim. Acta* **1978**, *30*, 77–82.
(11) Nassimbeni, Luigi R.; Wright, M. Robert W.; van Niekerk, Jill C.; McCallum, Pamela A. *Acta Crystallogr., Sect B* **1979**, *B35*, 1341–1345.
(12) Lee, Byungkook, Ph.D. Thesis, Cornell University, 1967.
(13) Hoard, J. L.; Lee, Byungkook; Lind, M. D. *J. Am. Chem. Soc.* **1965**, *87*, 1612–1613.
(14) Horrocks, William Dew., Jr.; Sudnick, Daniel *J. Am. Chem. Soc.* **1979**, *101*, 334–340.
(15) Reilley, Charles N.; Good, Bennie W.; Desreux, Jean F. *Anal. Chem.* **1975**, *47*, 2110–2116.
(16) Lewis, W. Burton; Jackson, Jasper A.; Lemons, Joe Fred; Taube, Henry *J. Chem. Phys.* **1962**, *36*, 694–701.
(17) Golding, R. M.; Halton, Margaret P. *Aust. J. Chem.* **1972**, *25*, 2577–2581.
(18) Bleaney, B. *J. Magn. Reson.* **1972**, *8*, 91–100.
(19) Golding, R. M.; Pyykkö, P. *Mol. Phys.* **1973**, *26*, 1389–1396.
(20) Reilley, Charles N.; Good, Bennie W.; Allendoerfer, Robert D. *Anal. Chem.* **1976**, *48*, 1446–1458.
(21) Desreux, Jean F.; University of Liege, 1979, personal communication.
(22) Desreux, Jean F. *Inorg. Chem.* **1980**, *19*, 1319–1324.
(23) Everhart, Dennis S.; Evilia, Ronald F., unpublished work, University of New Orleans.
(24) Good, Bennie W., Ph.D. Thesis, University of North Carolina, 1978.
(25) Sherry, A. Dean; Yang, Ping P.; Morgan, Leon O. *J. Am. Chem. Soc.* **1980**, *102*, 5755–5759.
(26) McGarvey, B. R.; Kurland, R. J. "NMR of Paramagnetic Molecules", La Mar, Gerd N., Horrocks, William DeW., Holm, R. H., Eds., Academic Press, New York, 1973; p 559.
(27) Reuben, Jacques; Fiat, Daniel *J. Chem. Phys.* **1969**, *51*, 4909–4917.
(28) Habenschuss, Anton; Spedding, Frank H. *J. Chem. Phys.* **1980**, *73*, 442–450.
(29) Albertsson, Jörgen; Elding, Inga *Acta Crystallogr., Sect. B* **1977**, *B33*, 1460–1469.
(30) Helmholz, L. *J. Am. Chem. Soc.* **1939**, *61*, 1544–1550.
(31) Zaev, E. E.; Khalilov, L. M. *Zh. Strukt. Khim.* **1980**, *21*, 53–58.
(32) Barbalat-Rey, Francoise *Helv. Phys. Acta* **1969**, *42*, 515–538.
(33) Choppin, G. R. *Pure Appl. Chem.* **1971**, *27*, 23–41.

RECEIVED for review January 14, 1981. Accepted May 11, 1981. We gratefully acknowledge research support from the National Science Foundation and the F.R.N.S. of Belgium.

Dependence of Photoacoustic Signal on Optical Absorption Coefficient in Optically Dense Liquids

Shmuel Malkin*

Biochemistry Department, The Weizmann Institute of Science, Rehovot 76100, Israel

David Cahen

Department of Structural Chemistry, The Weizmann Institute of Science, Rehovot 76100, Israel

A quantitative investigation of the photoacoustic (PA) signal amplitude on the exponential optical absorption coefficient, β (=absorbance × (ln 10)/cm), in thermally thick liquid samples is presented. Experimental results agree with a practical approximation to the Rosencwaig–Gersho theory of the PA effect. The experimental results fit the theoretical predictions from values of β of about 0.005 × (thermal diffusion length)$^{-1}$ upward. The effect of the direct acoustic coupling probably limits the usefulness of the Rosencwaig–Gersho theory at low values of $\mu\beta$—theoretically, below values of about 0.03 for fairly opaque samples (having absorbancies of about 1 or more). A normalized PA signal (ratio between signal and the maximal, saturation, value) is used for comparison with β. Values for β are measured directly, rather than estimated or extrapolated by using Beer's law. A straight-forward method to extract optical absorption data in absolute units from the PA signal amplitude only is presented and applied to concentrated samples.

The photoacoustic (or optoacoustic) method (*1*, *2*) is essentially the detection of modulated heat resulting from the absorption of modulated light in a given sample. In its most common configuration the modulated heat produces an acoustic wave in the gas phase surrounding the sample, which is sensed by a microphone connected to a lock-in amplifier. The signal obtained is proportional to the exciting light intensity. It depends monotonically on the optical absorption coefficient (β) and obviously on the geometry, elastic and thermal properties of the sample, and the adjacent phases (*3–7*).

It was recognized (*3–5*) that the main mechanism contributing to the photoacoustic signal in solid samples (and presumably also in liquids) starts with the generation of a modulated thermal wave, by the conversion of absorbed light into heat. The thermal wave travels in the medium and reaches the surface, where periodic heating and cooling of the surrounding gas phase occurs, inducing periodic expansion and contraction of the gas. Another mechanism may become important at low values of β and at high modulation frequencies, in which the local heating and cooling generates periodic expansion and contraction in the sample itself. An elastic wave is thus formed, which travels through the sample and is ultimately transmitted into the gas phase (direct elastic coupling mechanism (*6*, *7*)).

Several theoretical treatments have been presented for the heat transfer mechanism or the combined elastic coupling and heat mechanisms for various geometries (*3–10*). In the following we will consider mainly the heat transfer mechanism. Theoretical approaches to this mechanism consider each element of the sample to be a source of heat in proportion to the light absorbed in it. For a geometry in which the cross section of the sample is large compared to the optical path and is uniformly illuminated, Rosencwaig and Gersho (RG) (*4*) gave a general solution for a unidimensional heat transfer mechanism and computed the photoacoustic signal as a function of β, the chopping frequency, the thermal properties of the sample, and the backing (supporting) material as well as the thermal and elastic parameters of the gas phase. The resulting mathematical expression given by them (ref 4, eq 21) is quite complex in relation to the parameters involved and needs considerable simplification in order to be useful in practice. A common approximation (*3*) is to consider the case where the thermal diffusion length μ (cf. Theory) of the sample is small compared to the optical path through it (i.e., a thermally thick sample). This is a common situation, since the thermal diffusion length at ordinary modulation frequencies (>10 Hz) is usually small (in the order of microns). For such a case it was shown that the photoacoustic signal is linear with β for small β values but finally tends to saturation at higher values of β. The ratio of the initial slope of the signal amplitude vs. β to the saturation value can be obtained from (*4*) and is equal to $(2^{1/2}/2)\mu$. Poulet et al. (*11*) examined the thermally thick sample case and showed that the RG equation can be simplified further (considering that many expressions can be neglected). The final form obtained for the amplitude of the photoacoustic signal (PAS) was

$$(\mathrm{PAS}) = \frac{A\mu\beta}{[(\mu\beta)^2 + (\mu\beta + 2)^2]^{1/2}} I_0 \qquad (1)$$

This expression retains the predicted ratio of initial slope to saturation value of $(2^{1/2}/2)\mu$. An expression was also given for the phase angle (*11*), but this will not be considered here as its usefulness for obtaining β values from actual experimental data is severely limited by practical considerations. In eq 1, I_0 is the amplitude of the modulated component of the incident light and A is a constant (independent of β) which can be divided into three independent factors $A = A_1 \cdot A_2 \cdot A_3$. Using only A_1 instead of A in eq 1 gives the surface temperature modulation amplitude. Further multiplication by A_2 gives the amplitude of the acoustic wave. A_3 takes care of the microphone sensitivity. A_1 may be written as

$$A_1 = \frac{1}{(\pi f)^{1/2}} \frac{1}{(\kappa \rho C_p)^{1/2}} \qquad (2)$$

A_2 can be obtained by the piston model of Rosencwaig and Gersho (*4*)

$$A_2 = \frac{1}{(2\pi f)^{1/2}} \frac{\gamma P_0 (\alpha_g)^{1/2}}{l_g T_0} \qquad (3)$$

Here, f is the modulation frequency. The sample parameters are as follows: κ the heat conductivity, ρ density, and C_p the heat capacity. γ is the ratio of specific heats (C_p/C_v) in the gas, $\alpha_g = \kappa_g/\rho_g C_{pg}$ is the thermal diffusivity of the gas (sub-

0003-2700/81/0353-1426$01.25/0 © 1981 American Chemical Society

script g denotes gas parameters), l_g is the thickness of the (gas) medium, and P_0 and T_0 are the ambient pressure and temperature.

For our purposes A serves as a (frequency dependent) instrumental factor and its actual dependence will not be further analyzed.

In spite of many recorded photoacoustic spectra only a few critical direct tests of the connection between β and PAS under the conditions specified above have been reported. McClelland and Knisley (*12*) demonstrated the general behavior of the PAS vs. β behavior for an aqueous methylene blue solution, particularly the approach to saturation at large values of β and the effect of the frequency on that behavior. However, there did not seem to be a clear correspondence between theory and experiments. Teng and Royce (*13*) calculated β values for aqueous solutions of $KMnO_4$ from both amplitude and phase of the PAS by computerized curve fitting procedures to the theoretical curve. The agreement is good in general, but there are deviations in certain parts of the spectrum. Also, this cannot be considered as a good direct test as one needs to check the dependence of both amplitude and phase on β separately. Wetsel and McDonald (*14*) calculated β from their experimental data of PAS vs. frequency by a curve fitting procedure to the most general equation obtained from RG theory (*4*). In another article, where they develop the theory of the combined elastic and thermal wave mechanisms (*6*) they again test their theory by a curve fitting procedure. Although such procedures are consistent with the theory they are not practical for obtaining spectroscopic data in the laboratory. Furthermore, it is important to be able to test each part of the theory separately, i.e., eq 1 with respect to the β dependence, eq 2 for A_1, and eq 3 for A_2. A direct test for eq 1 was made by Poulet et al. (*11*) (cf. their Figure 1). They were interested mainly in obtaining β values from phase measurements. This is not necessary, and often not practical for the following reasons: eq 1 allows calculation of absolute β values from the PAS amplitudes only, as we show here; calculation of β from phase measurements seems to require an arbitrary correction by a certain constant phase factor (*11*); the relation between β and the PAS phase is trigonometric (*11*) and the experimental range of validity for β determination is limited. All these factors severely decrease the attractivity of use of the PAS phase from routine experimental data.

In testing eq 1, it was very important to determine β at the *same* concentrations as used in photoacoustic spectroscopy. This was not usually done previously; a general practice was to estimate β values by extrapolation to orders of magnitude higher concentrations from measurements on diluted samples. However, serious deviations from the Beer–Lambert law usually occur at high concentrations and distort the results (cf., e.g., Figure 8 and ref 11).

One of our purposes is to improve the tests made on eq 1 and to suggest a procedure to obtain absolute β values. The optical measurements of the absorption coefficients were done at the same concentrations used for the photoacoustic work by using special spectrophotometric cells of very small optical lengths, thus avoiding possible changes of chemical composition and other interactions due to very high concentrations.

Liquid samples were tested under a variety of conditions, in which many parameters were varied: we used two different solvents (i.e., different thermal parameters), several absorbing solutes, and a range of modulation frequencies. The experimental results were compared directly to the analytical predictions (using linear plots and comparing slopes and intercepts).

While mainly concentrating on the thermal mechanism it was of importance to consider the effect of the direct acoustic coupling. It will be shown that under most circumstances considered here (i.e., photoacoustic signal within about 2 orders of magnitude smaller than the saturation value) the direct acoustic coupling effect is small, compared to the accuracy of our data.

THEORY

Consideration of the Thermal Mechanism. Equation 1, as derived by Poulet et al. (*11*), serves as our starting point. This equation is an approximation to the RG equation (*4*) under the following specified set of conditions: (a) The sample is "thermally thick" (i.e., the total optical path (length of the sample), l, is much longer than the thermal-diffusion length, μ defined below). (b) The ratio $g = (k_g/\mu_g)(\mu/k)$ is much smaller than 1. There are no further approximations considering the thermal coupling only. These approximations are not severely restrictive and apply to many real situations. For practical frequencies ($f > 10$ Hz) μ in many liquids and solids is less than about 30 μm and decreases as the inverse square root of the frequency. Thus, a 1-mm thick sample is already considered as thermally thick. The g ratio was calculated for many materials (*11*) and found to be in the order of 10^{-2} or less (3×10^{-3} for water).

We have examined the physical meaning of the above approximations by deriving eq 1 in a different way. In this derivation it is assumed that each element of the sample is a generator of a pure hormonic thermal wave propagating to the surface. Each elementary wave (cf. Figure 1) is described by the following equation

$$T \propto \exp\left[-\left(\frac{x-\xi}{\mu}\right)\right] \sin\left(2\pi ft - \frac{x-\xi}{\mu} + \delta\right) \quad (4)$$

The amplitude of each such wave is proportional to the light absorbed in an element δx, which is $I_0\beta \exp(-\beta x)\delta x$. The parameter μ in eq 4 is called the thermal diffusion length. It describes the attenuation of the amplitude as the wave propagates through the sample (by a factor of $1/e$ over one thermal diffusion length) and equals $1/2\pi$ times the wavelength. μ is a function of the thermal parameters and modulation frequency is given by

$$\mu = \left(\frac{\kappa}{\pi\rho C_p f}\right)^{1/2} \quad (5)$$

By considering the continuity of T and the heat flux in each boundary layer it is possible to show that each wave, as expressed by eq 4, is partly transmitted and partly reflected at the boundary. Reflection and transmission coefficients at the boundary can be expressed by using the thermal parameters of the materials at each side of the boundary. The (modulated) temperature at the sample/air interphase was calculated as a superposition of all the elementary waves produced by light absorption. Such integration led directly to eq 1 under the following conditions: the boundary conditions between the sample and the air, as usually introduced (*4*), were replaced by the reflection and transmission coefficients. Reflected thermal waves from the air/walls or from the backing material/walls were neglected at the sample/air boundary. This is justified since the distances between this boundary and the walls are sufficiently large (several thermal diffusion length units) to damp these waves efficiently. This derivation will be presented elsewhere.

Using eq 1 and normalizing the maximal saturation signal to 1, we can write the β dependence of the normalized signal amplitude R as

$$R = \frac{2^{1/2}\mu\beta}{[(\mu\beta)^2 + (\mu\beta + 2)^2]^{1/2}} \quad (6)$$

Equation 6 can be tested as follows: (a) Probing the linear part of R vs. β this has a slope given by

$$\left(\frac{\delta R}{\delta \beta}\right)_{\text{small } \beta} = \frac{2^{1/2}}{2}\mu \approx 0.707\mu \tag{7}$$

(b) Equation 6 can be written also as

$$\beta\left(\frac{1}{R^2} - 1\right) = \frac{2}{\mu} + \frac{2}{\mu^2\beta} \tag{8}$$

Hence by plotting $\beta(R^{-2} - 1)$ as a function of $1/\beta$ we should get a linear plot with intercept $2/\mu$ and a slope $2/\mu^2$. It should be borne in mind, that eq 8 is most useful in the intermediate range of β vs. PAS where deviations of the experimental curve from the extrapolation of the low β part and from the high β saturation value are measurable. (For the low β linear part the accuracy is lost for the estimation of the intercept, and for the saturation part the accuracy is lost for the estimation of both slope and intercept.) Hence a test by eq 8 probes the behavior of the approach to saturation over the most interesting part of the functional dependence of R and β.

Other checks of consistency are as follows: The (PAS) raw data (not necessarily normalized) are plotted vs. β. If a line with a slope equal to $2/10^{1/2}$ ($\approx$0.633) times the initial slope of the (PAS) vs. β curve is drawn from the origin, it will intersect the (PAS) vs. β curve at a point $(\beta_1$:$(\text{PAS})_1)$, such that

$$\beta_1 = \mu^{-1} \tag{9}$$

(cf. eq 1), and

$$(\text{PAS})_1 = (\text{PAS})_{\text{saturation}}/5^{1/2} \tag{10}$$

Hence μ can be calculated from eq 9 and the saturation value of (PAS) from eq 10. Stated somewhat differently, eq 9 and 10 show that at the point $\beta = 1/\mu$ the normalized photoacoustic signal is $1/5^{1/2} \approx 0.447$. Conversely, for a given normalized photoacoustic signal plot finding the β value (β_1) corresponding to $R \approx 0.447$ enables us to calculate μ, by eq 10.

The Effect of the Direct Acoustic Coupling. In their composite piston model McDonald and Wetsel (*6*) treat the photoacoustic signal as a linear superposition of two waves, one generated by the thermal wave exactly as treated by RG theory (*4*) and the second as generated by the direct acoustic coupling. The second wave amplitude is approximately proportional to the total light energy absorbed in the sample and therefore its β dependence is described by the factor $(1 - \exp(-\beta l))$ in which l is the total optical path (length) of the sample. Since generally $l \gg \mu$ (thermally thick samples) the β dependence of the direct acoustic-coupling wave is saturated at a considerably lower value of β than the direct thermal wave. It is of interest to compare the relative amplitudes of the two waves: In (*6*) a formula is given for the (complex) surface displacement (eq 39) δx_m of the acoustic wave from which the amplitude $|\delta x_m|$ can be written as $|\delta x_m| = (\beta_T/\omega\rho C_p)(1 - \exp[-\beta l])I_0$, where I_0 is the amplitude of the modulated light intensity component (expressed by $I_0 \cos \omega t$), ω is the angular frequency $(= 2\pi f)$, and β_T is the (volume) coefficient of thermal expansion. The amplitude of the pressure variation δp_m due to δx_m is given (*6*) through multiplication by $\gamma P_0/l_g$ (cf. our eq 3 for definitions). The amplitude of the pressure variation δp_l due to the thermal wave is given by our eq 1, 2, and 3 as $A_1 \cdot A_2 \cdot \mu\beta/[(\mu\beta)^2 + (\mu\beta + 2)^2]^{1/2}$. The ratio of the two amplitudes is then

$$\beta_T T_0\left(\frac{\kappa}{\rho C_p} \cdot \frac{\rho_g C_{pg}}{\kappa_g}\right)^{1/2} \frac{1 - \exp[-\beta l]}{2^{1/2}\mu\beta[(\mu\beta)^2 + (\mu\beta + 2)^2]^{-1/2}} \tag{11}$$

The first factor is the β-independent part of this ratio, the second is the ratio of the normalized β-dependent signals due to the two different mechanisms. Insertion of the numerical factors gives a value of about 5×10^{-3} for the first factor (for water, $\beta_T = 2.1 \times 10^{-4}$ deg^{-1}, $\kappa = 1.4 \times 10^{-3}$ cal cm^{-1} deg^{-1} s^{-1}, $\rho = 1$ g cm^{-3}, $C_p = 1$ cal deg^{-1} g^{-1}; other parameters, $T_0 = 294$ K, $\alpha_g = 0.3$ cm^2 s^{-1}). At photoacoustic saturation the contribution of the effect of direct acoustic coupling is therefore negligible (around 0.5%). It becomes progressively more important at decreasing values of β as $[1 - \exp(-\beta l)]$ may still be close to 1 while the contribution of the thermal effect decreases monotonically. One can arrive at a simplified estimation of the contribution of the direct acoustic coupling. For small β values the two contributions tend to be in 45° phase difference (*6*). The square of the combined amplitude was calculated from the two (vector) contributions for a case where the thermal mechanism was still dominant; the amplitude was then simplified by expanding the square root expression in Taylor's series, taking the first expansion term. This leads to the following expression for the normalized (with respect to saturation) photoacoustic signal

$$R(\text{thermal and direct acoustic coupling}) \simeq R(\text{thermal only}) + \frac{5 \times 10^{-3}}{2^{1/2}}(1 - \exp[-\beta l]) \tag{12}$$

For a reasonable deviation of less than ~15% from the prediction of the thermal mechanism alone, this leads to $[R]_{\text{thermal}} \gtrsim 0.023$ or $\mu\beta \lesssim 0.03$. (If l is small such that $\exp[-\beta l]$ can be significantly above zero, the estimated minimum $\mu\beta$ value is even smaller than the above.) For a common case of an opaque sample such that $\beta l \gg 1$ with $[R]_{\text{thermal}}$ still in the linear range eq 12 can be approximated roughly to a variant of eq 7

$$R \simeq 0.707\mu\beta + 3.54 \times 10^{-3} \tag{13}$$

where the second term represents the (constant) contribution of the direct acoustic coupling.

In the case where the sample is not optically thick, one must consider also the relative magnitude of its thickness compared to the thermal diffusion length, in order to establish the range of $\mu\beta$ where the effect of the direct acoustic coupling has to be considered. In any case one has to be aware of this effect, particularly when dealing with transparent samples.

It is worthwhile to point out, with regard to the methods developed previously for the thermal mechanism case, that the initial slope method is the more sensitive one to the effect of the direct acoustic coupling, as it is based on measurements in a range of small $\mu\beta$. The point giving a relative signal of 0.447, being at $\beta = \mu^{-1}$, is virtually unaffected.

EXPERIMENTAL SECTION

Our photoacoustic cell and experimental arrangement were described previously (*15*). The cell is sketched again in Figure 1 with the approximate dimensions. The experimental arrangement is conventional, with 450-W Xe-arc illumination, monochromator, and light guide optics. We compared samples with known optical attenuation coefficient β for their photoacoustic responses. β values were obtained by scanning through wavelength and were carefully determined in a Cary 1605 spectrophotometer for exactly the *same* concentrations used in the photoacoustic cell (by this we ensured the same chemical identity—extrapolation from low to high concentrations is not usually allowed for the high concentrations used in the photoacoustic work, since dimers and trimers of the soluted pigments are easily formed at high concentrations). For these measurements optically thin cells (0.1 mm) were used (NSG, Japan). The Cary spectrophotometer had the capability of zero suppression by 1.9 units of absorbance. For absorbancies higher than about 4, calibrated neutral density filters were placed in the reference compartment which acted as zero suppressors. By this it was

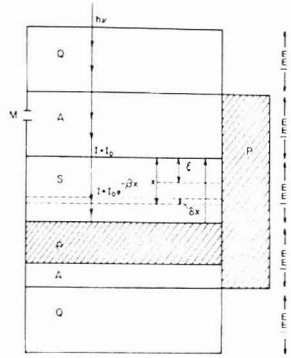


Figure 1. Schematic sketch of the photoacoustic cell (cf. ref 15): Q, quartz cover; A, air phase; S, sample; P, plastic support; M, microphone. Light of incident intensity I_0 (at the surface of S) travels through the sample and is attenuated according to the Beer–Lambert law. Each absorbing element, δx, is a generator of a modulated temperature field (thermal wave), calculated at any location ξ. The value of the total temperature field at the surface is calculated as a superposition of all elementary waves resulting in eq 1 and 2.

possible to reach absorbance values around 7. Alternatively, the same solution was placed between two glass plates giving a very small optical path of measurable absorbance over the whole wavelength range. The absorbancies appropriate to known optical paths were calculated by comparison from the data at wavelengths of measurable absorbancies with the 0.1-mm cell. The absorbance readings were converted to specific absorption β by multiplying by $100 \times \ln 10$ ($\approx$230).

Several solutes were used, hexaamminecobaltic(III) chloride ($Co(NH_3)_6Cl_3$), Gentian violet, malachite green, water soluble chlorophyll (chlorophyllin), methylene blue, and Waterman blue ink. Parker black ink (Queen) was also used as a reference and to obtain the maximal signal in water. Carbon black suspension was used for the same purpose in glycerol. β was varied by changing the wavelength. μ was calculated from the thermal parameters of the solvents (*16*) (water or glycerol) and the frequency. In the absence of any information no account was taken in this work for the change of the thermal parameters with the solute concentration, although it is planned to take it into account in future work. It is felt that this is only a secondary effect, due to the small ratio of solute/solvent even for the higher concentrations used.

The sample volume in the photoacoustic cell was 18–25 μL, giving a liquid depth around 1 mm. The photoacoustic signal was processed by a Brookdeal lock-in amplifier 9502 SC operated in the vector mode (i.e., the amplitude of the signal was recorded). Background correction was applied by taking the signal from cells filled with pure solvent and normalizing it to that of the sample in wavelengths outside the absorption region. The raw data for the photoacoustic spectrum were taken by a slow scanning through the wavelength as in the transmission spectroscopy experiment. Relative variations of the incident light intensity with the wavelength were taken care of by recording a spectrum of carbon black at low frequency (i.e., at photoacoustic saturation) and then dividing the spectrum of the sample by that of the carbon black reference. Care was taken to calibrate both the photoacoustic monochromator and the Cary spectrophotometer with respect to the wavelength. It is felt that a possible serious source of error is the different slit width used in photoacoustic and transmission spectrophotometry. This was experimentally hard to avoid: the slit width was larger for the photoacoustic work so as to obtain a reasonable signal/noise ratio; in the Cary it was impossible to increase the slit beyond a certain value set by its design for optimal signal. However, a check for several wavelengths in the spectrophotometer showed that probably for the ascending or descending parts of the absorption band this did not give appreciable discrepancies but could be reduced compared to the photoacoustic signal at the peak, by a few percent.

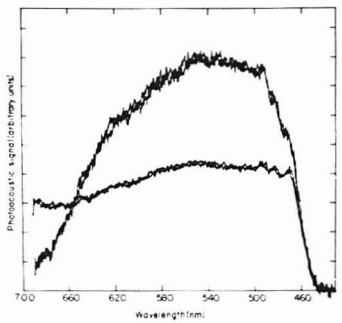


Figure 2. Raw data for photoacoustic spectrum: (upper curve) Gentian violet, concentrated solution in water; (lower curve) black ink. The black ink spectrum represents the saturated signal, proportional to I_0, and is used to correct the Gentian violet spectrum for light intensity variations. Modulation frequency is 45 Hz.

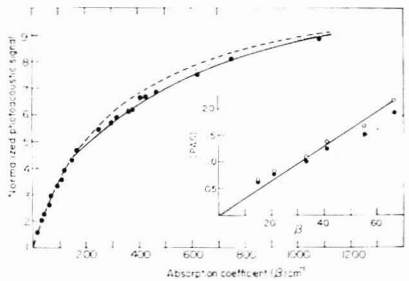


Figure 3. Normalized photoacoustic signal vs. the absorption coefficient β (in cm^{-1}): chlorophyllin in water, modulation frequency 31 Hz; (insert) the linear part expanded; (closed points) raw data; (open points) after correction (cf. text); (solid line, insert) the best fit initial slope line to the PAS vs. β data; (dotted line, insert) the theoretical line with initial slope corresponding to $\mu = 3.85 \times 10^{-3}$ cm; (solid curve, main figure) the smooth curve passing through the experimental points; (dotted curve, main figure) the theoretical curve corresponding to $\mu = 3.85 \times 10^{-3}$ cm; (dashed curve, main figure) the theoretical curve corresponding to the observed initial slope (4.6×10^{-3} cm).

Figure 2 shows an example of the raw photoacoustic spectrum in one of the experiments, specifically designed for high spectral resolution (sacrificing signal/noise) to allow a better comparison with the transmission spectrophotometric data. Although the photoacoustic spectrum seems somewhat noisy (in Figure 2 it is a superposition of two identical scannings), the estimation of the photoacoustic signal is more accurate than the noise figure, as the spectrum contour is relatively smooth and one can draw a smooth line through the middle of the trace. In more advanced instrumentation the noise can be eliminated through repeated scanning and proper electronic averaging.

For analysis of the data we had to determine the saturation value of the photoacoustic signal. This was done by a comparison to a saturated ink solution. It was felt, however, that due to interchange of samples this was not of sufficient accuracy. Alternatively, the data were treated by intersecting with a line of slope $2/10^{1/2}$ the initial slope, as described in the end of the previous section, thus finding the saturation value independently.

RESULTS AND DISCUSSION

Figure 3 shows the relation between the photoacoustic signal and the absorption coefficient β for one case study (chlorophyllin in water; chopping frequency 31 Hz). As expected, for low values of the absorption coefficient the relation is

Table I. μ Values from the Photoacoustic and Absorbance Data

material	solvent	frequency, Hz	μ_{exptl}	μ_{theo}	remarks
Gentian violet	glycerol	38	2.75×10^{-3}	2.95×10^{-3}	initial slope
Gentian violet	water	44	3.4×10^{-3}	3.25×10^{-3}	initial slope
Gentian violet	water	500	0.99×10^{-3}	0.96×10^{-3}	initial slope
$Co(NH_3)_6^{3+}$	water	140	1.6×10^{-3}	1.8×10^{-3}	initial slope
$Co(NH_3)_6^{3+}$	water	280	1.25×10^{-3}	1.25×10^{-3}	initial slope
malachite green	water	38	3.9×10^{-3}	3.4×10^{-3}	initial slope
methylene blue	water	600	1×10^{-3}	0.86×10^{-3}	initial slope
Waterman blue ink	water	13.3	6.2×10^{-3}	5.9×10^{-3}	initial slope
Waterman blue ink	water	625	8.4×10^{-3}	8.6×10^{-3}	initial slope
chlorophyllin	water	31	4.6×10^{-3}	3.85×10^{-3}	initial slope cf. text
chlorophyllin	water	31	4.2×10^{-3}	3.85×10^{-3}	from $\beta(R^{-2} - 1)$ vs. β
chlorophyllin	water	31	3.8×10^{-3}	3.85×10^{-3}	from β at $R = 0.447$

linear, tending ultimately to saturation at high absorption. At saturation the photoacoustic signal is given the value 1. The initial linear part (Figure 3, insert) was drawn in such a way as to take into account the small deviation from linearity, which increases progressively as β increases. This was done by adding a certain small correction term to the signal at each point, as calculated from eq 1 for each value of the normalized photoacoustic signal. The value for the thermal diffusion length calculated from the slope is close but higher than that calculated directly from the thermal parameters (4.6×10^{-3} cm vs. 3.85×10^{-3} cm). It seems, however, by other criteria that the initial slope is abnormally high. For example, the thermal diffusion length calculated from the reciprocal of the β value corresponding to a normalized photoacoustic signal of about 0.447 is 3.8 ($\pm$0.2) $\times 10^{-3}$ cm which is in excellent agreement with the calculated value. In the main Figure 3, the experimental points of the normalized photoacoustic signal R vs. β and the theoretical curve (based on $\mu = 3.85 \times 10^{-3}$ cm) are in quite good agreement.

It could be thought that the higher initial slope reflects the effect of the direct acoustic coupling. Considering eq 13 which corrects for the effect of the direct acoustic coupling, a line with the same slope corresponding to $\mu = 3.85 \times 10^{-3}$ but with an intercept $\simeq 0.00354$ has to be drawn. However, this is such a (relatively) small intercept that it does not improve the fit significantly, in this case (cf. later).

Figure 4 shows a different possibility to analyze the same data. On the basis of eq 8 we expect a linear plot of $\beta(R^{-2} - 1)$ vs. β^{-1} having a slope and intercept such that the ratio of the square of the intercept to the slope is exactly 2. A family of lines having this last property with initially chosen different intercepts was drawn in order to fit the experimental points. The fit to the experimental points was determined by attaining a minimum in the sum, $\sum$, of the percent deviations of the experimental ordinate value from the selected line. It should be noted that the observed $\beta(R^{-2} - 1)$ vs. β^{-1} is very sensitive to rather small inaccuracies in either R or β, which explains the scattering of the points. From this plot a value for the thermal diffusion length is estimated to be 4.2 ($\pm$0.3) $\times 10^{-3}$ cm, again in agreement with the value obtained by the previous method. It is not clear yet why the initial slope in Figure 3 was so much higher than expected. However, this was not typical for all other samples. (Cf. later and Table I.) Mostly μ values agreed within 10% and less, with occasional larger deviations.

The analysis described above was repeated for various other samples over a broad range of frequencies and gave essentially similar results. In some cases where the saturation value was not achieved or was uncertain we applied the method of intersecting the raw (unnormalized) PAS vs. β curve with a line drawn from the origin having a slope of approximately 0.633 times the initial slope and determining μ and the PAS saturation value, as described in the Theoretical section. The μ value obtained by the last method was always close to the μ value obtained by the other methods. One of the above cases of study is that of Gentian Violet in water; data for two chopping frequencies for this case are given in Figure 5. There is a fit of μ values to those calculated from the thermal parameters within less than 5%. Other cases are summarized in Table I. The parameter μ is frequency dependent, as expressed in its defining equation (cf. Theoretical section), being inversely proportional to the square root of the frequency. This is exemplified in Figure 5 and shown numerically in Table II. In all the other cases of Table I the raw data were obtained with no special care to use small slits and to check the saturation value. Nevertheless, it clearly demon-

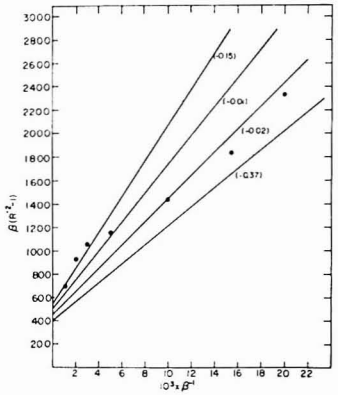


Figure 4. Plot of $\beta(R^{-2} - 1)$ vs. β^{-1} (eq 8). Data are from Figure 3. Several lines were drawn to correspond to the experimental points, with same ratio of (intercept)^2/slope = 2. The sum of weighted vertical deviations of the points is indicated in parentheses.

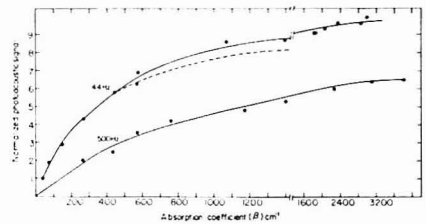


Figure 5. Normalized photoacoustic signal vs. β, Gentian violet in water. μ values were deduced from β values corresponding to (PAS) = 0.447; $\mu = 3.45 \times 10^{-3}$ cm for 44 Hz (theoretical value 3.23×10^{-3} cm for which the dashed line was calculated) and $\mu = 1.06 \times 10^{-3}$ cm for 500 Hz (theoretical value 0.96×10^{-3} cm).

Table II. Relation between the Initial Slope of the Normalized PAS vs. β and the Reciprocal of the Square Root of the Modulation Frequency ($f^{-1/2}$)[a]

frequency, (f), Hz	$f^{-1/2}$	10^3 × initial slope (R vs. β)	10^3 × ratio of initial slope to $f^{-1/2}$	theoretical expected ratio (×10^3)
14	0.267	3.80	14.2	15.1
54	0.136	2.10	15.4	15.1
625	0.040	0.60	15.0	15.1

[a] Data from blue ink—cf. Experimental Section.

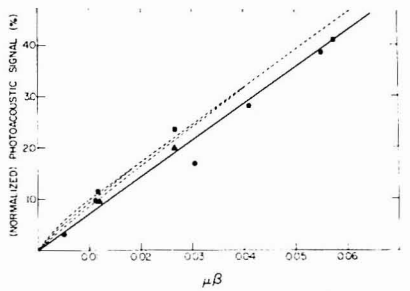


Figure 6. Normalized photoacoustic signal R vs. $\mu\beta$ for the lowest range of $\mu\beta$ attainable, Gential violet in water at three sets of measurements, 190 Hz (■), 900 Hz (△), and 4950 Hz (●) (the last frequency corresponds to resonance condition): (continuous line) theoretical prediction from the thermal mechanism alone; (dashed lines) theoretical curves for the combined thermal and direct acoustic coupling mechanisms for the above three frequencies (from bottom to top, respectively).

strates the fit to the theoretical prediction with similar precision.

Figure 6 represents an experimental study of a range of small $\mu\beta$, where one expects that the direct acoustic coupling would become exceedingly important. Both theoretical predictions for the "composite piston model" and the thermal mechanism alone (cf. Theory) are plotted and compared to experimental points achieved for low values of β. As the data stand in the figure, it does not give clear support to the predicted extent of the direct acoustic coupling effect and the predictions of the composite piston model. The data for the highest frequency (ca. 5000 Hz), for which the direct acoustic coupling should be more noticeable, agree with the predictions of the thermal mechanism alone, down to a $\mu\beta$ value of about 0.005. It must be admitted, however, that the scattering of data points and the uncertainty in background correction, which is a considerable fraction of the signal at low $\mu\beta$ values, do not permit a more confident conclusion with regard to the direct acoustic coupling, at the moment, for sample configurations as studied here.

We would like to stress, however, the utility of photoacoustic spectroscopy in obtaining absolute absorbance data for very highly concentrated solutions. In the example given in Figure 7 (methylene blue) an absolute absorbance spectrum is obtained from the PAS. The spectrum of the concentrated solution is quite different from that of the dilute sample, due to formation of dimers. It will be rather difficult to obtain the spectrum for the highly opaque sample (i.e., absorptivity/cm in the order of 100–1000) by conventional spectrophotometry (e.g., special sample cells, use of neutral density filters) while for such a case the photoacoustic method is straightforward. It is particularly useful for spectral study

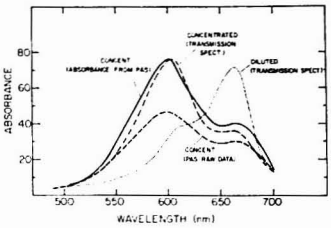


Figure 7. Comparison between the spectrum of methylene blue obtained by regular transmission (- - -) and photoacoustic spectroscopy for a concentrated sample and by transmission spectroscopy (···) for a dilute sample. The concentrated sample was prepared such as to have a specific optical density at 600 nm of 76.5 cm^{-1} and was measured with a cell of 0.1-mm optical path. The diluted sample (×200) was measured with a regular 1-cm path cell. The PAS raw data (- - -; the units are arbitrary in the figure) were treated according to eq 1 to calculate β and the absorbance spectrum (—).

of interactions resulting from high concentrations (*17*, *18*).

Another (reciprocal) application of photoacoustic spectroscopy is the measurement of the thermal diffusion length μ, by the method outlined here, for samples with known β. Besides being a goal by itself this would be particularly useful in following changes in a given medium (e.g., phase changes) into which an absorbing material is introduced as a marker.

It is felt, by the scattering of values in Table I, that there is no appreciable *systematic* error if one averages the results of all experiments. It could be that a systematic error exists in each one of the samples studied, and we suspect that mainly the spectral slit difference contributes to deviations between the transmission and photoacoustic spectra. This will seriously affect the results particularly at the "tail" part of the spectrum, where most of the points for the initial slope come from. Simultaneous determination of the photoacoustic and transmitted signal may overcome this problem.

In conclusion, the results obtained here demonstrate that absorbance values obtained by photoacoustic spectrometry can become quite accurate, and useful information is obtained from the amplitude measurements alone. A possible suggested procedure to obtain absolute β vs. wavelength is first to scan at high frequency, far from saturation and close to the linear range. This will result in relative β values. For the calibration of β on an absolute basis a low-frequency scan is done in which the maximal PAS value can be approached as a saturation value (or else saturation values can be obtained with concentrated ink solutions). From the known ratio $PAS/PAS_{max} = R$ and a known value for μ, β can be easily estimated from eq 6.

ACKNOWLEDGMENT

The authors wish to thank F. A. McDonald for his comments.

LITERATURE CITED

(1) Pao, Y. H. "Optoacoustic Spectroscopy and Detection"; Academic Press: New York, 1977.
(2) Rosencwaig, A. *Adv. Electron. Electron. Phys.* **1978**, *46*, 207–311.
(3) Bennett, H. S.; Forman, R. A. *Appl. Opt.* **1976**, *15*, 1313–1321.
(4) Rosencwaig, A.; Gersho, A. *J. Appl. Phys.* **1976**, *47*, 65–69.
(5) Parker, J. G. *Appl. Opt.* **1973**, *12*, 2974–2977.
(6) McDonald, F. A.; Wetsel, G. C., Jr. *J. Appl. Phys.* **1978**, *49*, 2313–2322.
(7) McDonald, F. A. *Appl. Opt.* **1979**, *18*, 1363–1367.
(8) Aamodt, L. C.; Murphy, J. C.; Parker, J. C. *J. Appl. Phys.* **1977**, *48*, 927–933.
(9) Afromowitz, M. A.; Yeh, P.-S.; Yee, S. *J. Appl. Phys.* **1977**, *48*, 209–211.
(10) Quimby, R. S.; Yen, W. M. *Appl. Phys. Lett.* **1979**, *35*, 43–45.
(11) Poulet, P.; Unterreiner, R.; Chambron, J. *J. Appl. Phys.* **1980**, *51*, 1738–1742.
(12) McClelland, J. F.; Kinsley, R. N. *Appl. Opt.* **1976**, *15*, 2658–2663.
(13) Teng, Y. C.; Royce, B. S. H. *J. Opt. Soc. Am.* **1980**, *70*, 557–560.

(14) Wetsel, G. C., Jr., McDonald, F. A. Appl. Phys. Lett. 1977, 30, 252-254.
(15) Cahen, D.; Garty, H. Anal. Chem. 1979, 51, 1865-1867.
(16) Hodgman, C. D., Ed. "Handbook of Chemistry and Physics", 44th ed.; The Chemical Rubber Publishing Co.: Cleveland, OH, 1963.
(17) Cahen, D.; Garty, H.; Becker, R. S. J. Phys. Chem. 1980, 84, 3384-3389.
(18) Garty, H.; Caplan, S. R.; Cahen, D., submitted for publication.

RECEIVED for review October 20, 1980. Accepted April 22, 1981. Partial support from the U.S.-Israel Binational Science Foundation, Jerusalem, Israel, is gratefully acknowledged.

Integrated, Microcomputer-Controlled, Adjustable-Waveform Spark Source for Atomic Emission Spectrometry

Steven G. Barnhart, Paul B. Farnsworth, and John P. Walters*

Department of Chemistry, University of Wisconsin, Madison, Wisconsin 53706

Electrical schematics, construction details, and performance examples for an electronic, adjustable-waveform spark source are given. The source is operable under computer control, and an example of such using a PET microcomputer is presented. The source operates at high voltage, is series switched with a hydrogen thyratron, produces long-duration, pulsating unidirectional current waveforms, and does not require high-voltage diodes in parallel with the spark gap or thyratron for current wave shaping. The circuitry and mechanical construction allowing this are illustrated.

Spark excitation continues to be a popular method for rapid spectrochemical analysis of metals and alloys without the necessity of sample dissolution. In practical situations, it is important that the spark source be under automatic control and requires a minimum of attention. In research work, the same requirements are added to the need for fine adjustments in the current waveform, synchronization to other experimental events, and mechanical integration with diverse spectroscopic optics. In methods development work, exploration of stabilized discharges attacking electrodes in computer-controlled spark stands at variable repetition rates requires all of the above, plus an absolute minimum of radio-frequency interference at the spark stand. In addition, the study of unpredictable combinations of samples, e.g., stainless or resulfurized steels intermixed with nonferrous alloys, mandates the source operate at high voltage so that precise spark formation can occur to "dirty" electrode surfaces. Lastly, to use time-gated methods of detection (*1*, *2*) for enhanced spectroscopic sensitivity, the discharge current should have a pulsating unidirectional waveform and last as long as possible. In all classes of work the maximum source resistance should be in the analytical spark gap (*3*) to maximize sample erosion.

To the best of our knowledge, a source meeting all of the above requirements has yet to appear, including previous work reported from this laboratory (*4*-*9*). We report such a development now and emphasize the following features. The circuit is much simpler than previous sources, with shorter leads and better grounding. This minimizes radio-frequency transients. Precise electronic switching at voltages up to 15 kV is accomplished with a rugged and inexpensive type 5C22 glass-envelope hydrogen thyratron. For a long discharge, high-quality, glass-mica transmitting capacitors are used instead of oil-filled or ceramic devices. These are fixed in value, and the current waveform is adjusted inductively (*6*). By proper component arrangement and grounding, and by floating both electrodes in the analytical gap, the diodes in parallel with the thyratron and analytical gap are both eliminated, removing substantial resistance from the discharge portion of the circuit. Leads are shortened by building the stand inside the source proper and building the high-voltage ac supply external to it. Lastly, the source diodes, capacitor base-plates, and thyratron cathode are all firmly fixed to a massive, grounded, heat-sink plate, made light by using magnesium and machined with a vee-and-flat on its base for optical alignment on our rail and experiment bed system (*10*, *11*).

We have several types of computers in laboratory use for spark-source control. However, it is clear from economics alone that the new 8-bit microcomputers are best for controlling analytical instrumentation. To capitalize on this remarkable cost situation, and to meld this source into our research direct-reading spectrometers, we integrated a Commodore PET 6502-based microcomputer into its electronics for firing control (*12*, *13*).

The net effect of all of these developments has been to produce a source that is simpler, easier to build, more reliable, and more efficient than any that we have worked with previously, at about two-thirds the cost of our earlier units. It is analytically significant on these counts alone and is now being tested for practical analysis of steel alloys with positionally stable discharges and time-gated photoelectric detection.

CONSTRUCTION

The source is separated in two physical components: a charging module and a discharge module. The charging module provides the ac high-voltage power, power controls, and safety interlock for the source. The discharge module contains the high-voltage capacitors, diodes, thyratron, inductors, and spark stand. Separation of the charging and discharge functions in this manner permits a unitized design that allows all the discharge components to be grouped together on a single experiment-bed rider (*11*). In addition to generating less radio frequency interference (RFI), the unitized nature of the source allows it to be completely enclosed thereby further reducing radiated RFI from the spark stand and providing ready portability. The enclosure helps minimize source breakdown from dirty or moist lab air, and the large heat sink provided by the magnesium rider base eliminates the need for circulating outside cooling air to the source. A small vent easily exhausts hot air from the thyratron. The source thus can be used in dirty environments.

0003-2700/81/0353-1432$01.25/0 © 1981 American Chemical Society

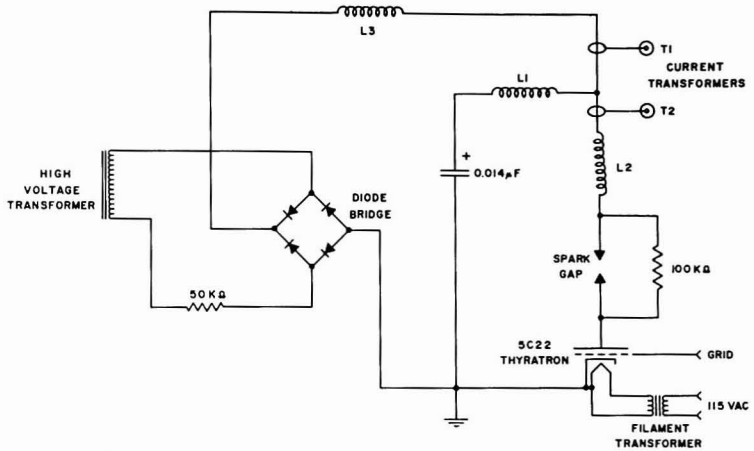


Figure 1. Electrical schematic of the adjustable-waveform spark source. Components are listed in Table I.

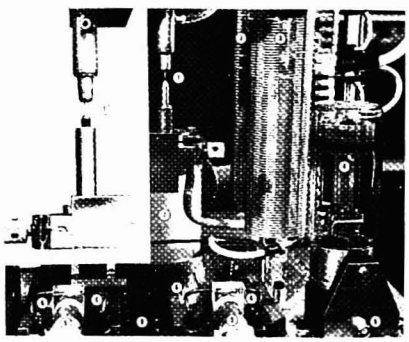


Figure 2. Adjustable-waveform discharge module: (1) spark gap with flow jet-tungsten anode and sample pin, (2) inductor L2, (3) inductor L3, (4) 5C22 hydrogen thyratron, (5) power input jacks from charging module, (6) rectifying bridge diodes, (7) energy storage capacitor, (8) magnesium heat sink component rider, (9) thyratron grid connection.

Table I. Components for Figure 1—Adjustable-Waveform Spark Source

component	description
diodes	4 FMC Catalog No. ER*H16, 16 kV max. PRV
L1	air core inductor, residual to approximately 85 μH, selected taps are available
L2	air core inductor, residual to approximately 87 μH, selected taps are available
L3	air core inductor, residual to approximately 137 μH, selected air taps are available
HV capacitor	2 parallel-connected 0.007 μF glass–mica transmitting capacitors, type 1980-300, peak working voltage: 20 kV, Aerovox Inc.
T1, T2	current transformer, Model 110, 0.100 V/A, Pearson Electronics Inc.
100 kΩ resistor	Ohmite No. 0422, 100 kΩ, 50 W
5C22 thyratron	ITT 5C22 hydrogen thyratron or equivalent
50 kΩ resistor	4 parallel-connected 200 K, 200-W resistors, Ohmite, Inc.
HV transformer	unmarked surplus component

Charging Module. The charging module of the source contains the circuitry necessary to provide the discharge module with alternating current, high-voltage power. Primary power to the module is provided from a 110-V isolated power source. After being fused and switched, this power is fed to a variable autotransformer, the secondary of which feeds the primary windings of a high-voltage transformer. The high-voltage transformer has a turns ratio of approximately 134 giving an upper limit of 18 kV RMS with the 140-V variable autotransformer used. This 18 kV RMS limit cannot be realized at present due to the limitations of the glass-envelope 5C22 hydrogen thyratron used as the switching element in the discharge module, although steady operation at 14 kV is practical. It probably is best to limit the charging module voltage to less than 20 kV to keep long-distance transmission problems simple.

For full computer control of the source, the ac mains voltage feeding the high-voltage transformer should be switched on with solid-state devices such as a zero-crossing TRIAC. We are not reporting that here because current work is focused on feedback control over both the line voltage and frequency.

To characterize its independent performance, we chose to switch the ac primary with a three-pole relay. Both the hot and neutral lines are switched, while the third leg provides a holding loop to the relay coil. Power and safety switches control the actuation of this relay.

Also contained within the charging module are four, 200-kΩ, 200-W wire-wound resistors that limit the charging current and isolate the charging module from the discharge circuitry during firing periods. In addition, the module contains a filament transformer for the hydrogen thyratron, plus two fans for internal cooling, and a volt and ammeter.

Discharge Module. The discharge module contains the necessary circuitry to accept the alternating-current high-voltage power from the charging module and produce an adjustable-waveform high-voltage spark. A schematic diagram of the discharge circuit is given in Figure 1 with the components listed in Table I. All the components of this module are mounted directly on the large magnesium rider as part



Figure 3. Adjustable-waveform discharge module component placement; (1) 100-kΩ spark gap resistor, (2) rectifying bridge diodes, (3) power input jacks from charging module, (4) magnesium heat sink component rider, (5) power lead to inductor L3, (6) 5C22 hydrogen thyratron, (7) inductor L3, (8) inductor L2, (9) glass–mica energy storage capacitors, (10) inductor L1, (11) spark stand.

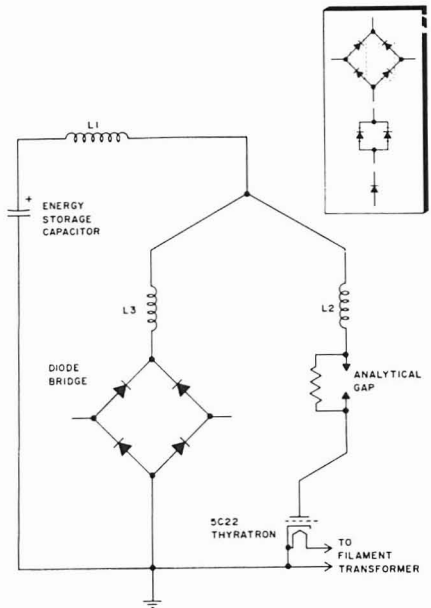


Figure 4. Schematic diagram illustrating the spark gap and diode paths for capacitor discharge. Inset shows a schematic representation of the diode bridge acting as a single shunt diode.

of the optical experimental bed (*11*). The physical placement of the various components is shown in Figures 2 and 3. This source has one side of the energy-storage capacitor grounded, as well as the thyratron cathode. However, there is neither a diode in parallel with the thyratron nor a diode in parallel with the analytical gap. Instead, the rectifying bridge diodes serve a multiple purpose. They rectify the ac power from the charging module, in addition to acting as a single shunt diode (Figure 4) in parallel with both the analytical gap and the thyratron switching element. The diode shunting action for current waveform generation has been described previously (*4*, *6*) and will not be treated here. It is instructive, however, to examine the current paths in this source design during the charging and discharging portions of a line half-cycle.

Waveform Generation. During the charging cycle, the 5C22 hydrogen thyratron is not in conduction and effectively produces an open circuit in the loop containing the spark gap (refer to Figure 4). With the thyratron turned off, the 0.014 μF high-voltage capacitor charges from the high-voltage transformer through the 50-kΩ charging resistor and the full-wave-rectifying bridge. The capacitor continues to charge until its voltage equals the instantaneous rectified voltage from the high-voltage transformer. This voltage limit can be adjusted with the variable autotransformer in the charging module. Application of a positive trigger pulse to the thyratron grid fires the tube and begins the discharge cycle as an electrical "short" in the circuit loop containing the spark gap. This directly connects the spark gap with the high voltage on the storage capacitor. If the proper conditions exist (primarily electrode geometry, capacitor voltage, and support gas) a spark discharge will form between the electrodes.

Once the thyratron has been fired and current conduction has begun, there are two circuit loops by which the energy-storage capacitor can discharge. One path is through the analytical spark gap, and the second is through the rectifying bridge. The relative impedance of these two paths determines the magnitude of the current in each. Initially, the oscillatory discharge voltage is positive, placing the diodes of the bridge in a reverse bias condition. This creates a high impedance path to ground in the diode loop, and the path through the spark gap is favored on this first half-cycle of the parent oscillatory discharge. On the second half-cycle of the discharge, the polarity changes and the rectifying diodes become forward biased, creating a low impedance path to ground to pass a larger fraction of the discharge current. The 50-kΩ resistor in the charging module isolates the high-voltage transformer from this shunting action of the bridge.

The various inductors in the discharge path can be adjusted to give full unidirectional current wave shaping. Inductor L2 can be balanced against L1 and L3 to make the discharge current continuously adjustable from a pulsating to a smoothly decaying unidirectional waveform. In these cases, the thyratron remains in conduction and does not require reignition during the oscillatory, capacitor-discharge cycle. If L2 is made too small, the spark current will attempt to oscillate and be series-clipped by the thyratron. We understand this to shorten the tube lifetime (*6*) and avoid this mode.

ELECTRICAL PERFORMANCE

Due to the combination of low-loss glass–mica capacitors, fewer circuit components, and unitized design, the pulsating-unidirectional current waveform can be sustained for 200 μs at 13 kV with the gap shorted and for 165 μs with it open. This is the proper type of waveform damping for analytical work. The long duration with an open gap is presently being exploited for time-gated direct-reading spectrometry and will be discussed in a future article.

Microcomputer Control. Because the spark is a pulsed, short duration discharge, many of the measurements of its properties must be made stroboscopically. This dictates that a research spark source must be capable of producing trains of stable, identical sparks. This requires in turn that the

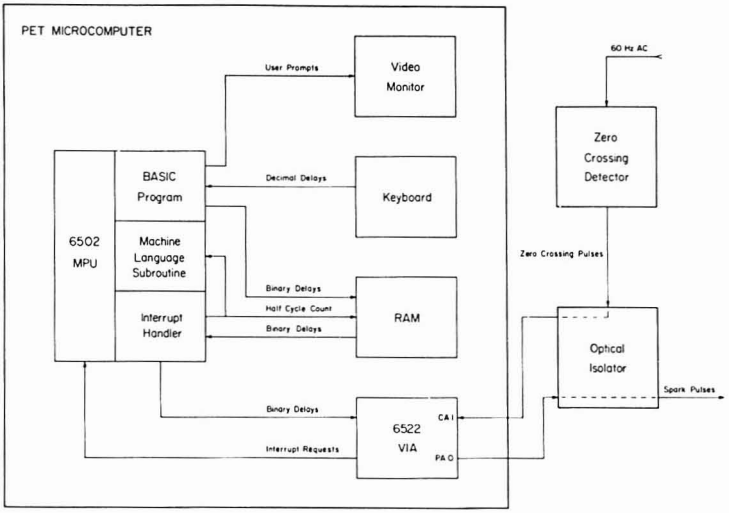


Figure 5. Schematic representation of the PET microcomputer operation for spark source control.

ignition of the discharge be synchronized with the ac charging circuit, so that the breakdown of the spark gap will always occur at a predictable set of voltages. In a separate paper (*14*) we describe how this is accomplished by a laboratory minicomputer interfaced to a zero-crossing detector and a digital delay generator. For this spark source the functions of the minicomputer and the delay generator are combined in the form of a Commodore PET microcomputer. While this substitution introduces some minor limitations in discharge timing, which will be described later, it provides satisfactory performance in most situations at a price that is less than one-tenth that of the minicomputer system. The cost of the microcomputer is low enough that it becomes practical to dedicate the computer to control of the spark and integrate it into the spark source.

The operation of the PET computer is outlined schematically in Figure 5. A simple I/O routine written in the machine's resident BASIC prompts the user to enter the pertinent burn parameters. These include the number of breaks per half cycle of the ac charging voltage, the delay of each discharge from either the zero-crossing reference or the previous discharge, and the duration of the burn. The burn duration, in the form of the number of half cycles in the burn, and the delay times are converted by BASIC into two-byte binary numbers and are stored in a table in memory for later access by a machine language subroutine and an interrupt handler. Once the discharge parameters have been specified, control is passed to the machine language subroutine, which sets up the interrupt logic for the VIA chip and also monitors the half-cycle count as the source is fired.

The PET logic board includes one 6522 VIA that is only partially used by the computer. Complete descriptions of this chip are available in ref 15 and 16. (Both ref 15 and 16 contain errors. The bit assignments for the auxiliary control register are incorrect in ref 15 and correct in ref 16, whereas the bit assignments for the peripheral control register are incorrect in ref 16, but correct in ref 15.) This application uses the following chip features: (1) a latched 16-bit counter (timer 1) that is decremented by the 1-MHz computer clock, (2) an edge sensitive input, CA1, that can generate an interrupt on either the leading or trailing edge of an input signal, (3) one pin of the eight-bit A port, and (4) the four interrupt and control registers. CA1 is configured to generate an interrupt on the leading edge of the zero-crossing signal. The service routine for this interrupt loads the first delay time into time 1, starts it, and decrements the half-cycle count. Timer 1 is operated in the one shot mode, which means that upon timing out it will generate an interrupt and then remain inactive until loaded with another delay. The interrupt from the timer is serviced by a routine that fires the spark, loads the next delay time, and restarts the timer. This process is repeated until all of the stored delay times have been loaded. The machine then waits for the next zero crossing pulse.

All hardware interrupts for the PET are vectored through a section of code that saves the 6502 registers on the stack and then performs an indirect jump to a location stored at hexadecimal locations $90 and $91 ($219 and $21A in the 2001 series machines). Normally this address is that of a keyboard and clock routine. This routine is activated every sixtieth of a second by an interrupt generated on the PET logic board. In order to use the interrupts for accurate timing, it is necessary to make two changes. First, the 60-Hz PET interrupt is disabled. This interrupt is not synchronous with the line voltage and could thus cause unpredictable interference with the spark timing. The interrupt is disabled by storing 0 in hex location $E813. Because disabling this interrupt also disables the keyboard, it must be done after all keyboard I/O functions are completed. Second, the interrupt handler for timer 1 and CA1 is stored in an open section of memory (we used the machine's second cassette buffer), and the vector at locations $90 and $91 is changed to point to it. Such an interrupt handler must include statements pulling the accumulator and the index registers off the stack. Once the burn is complete, normal machine operation is restored by storing the original PET vector ($E62E) in locations $90 and $91 and storing $3D in location $E813.

Several machine language instructions are executed between the occurrence of an interrupt and the loading of a delay time. This makes it necessary to subtract a constant value from the delays as they are entered and dictates the mimimum value

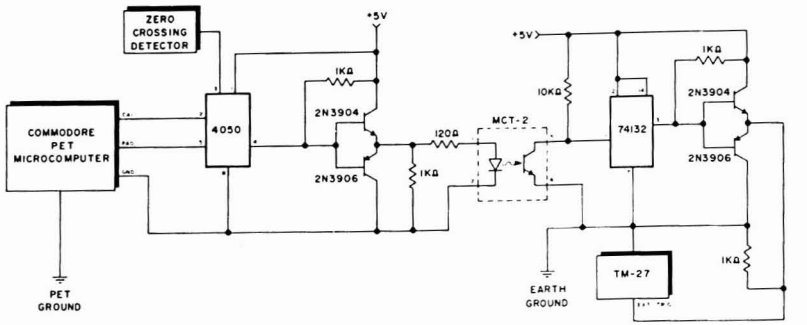


Figure 6. Electrical schematic of the PET isolation circuit.

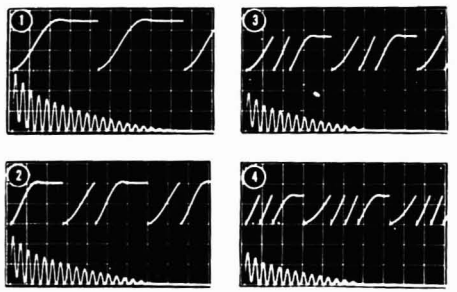


Figure 7. Examples of source operation at 1, 2, 3, and 4 breaks per half-cycle. The top traces represent the capacitor voltage with an ordinate of 5 kV/division and an abscissa of 2 ms/division. The bottom traces illustrate the current waveform in the spark gap with an ordinate of 50 A/division and an abscissa of 20 μs/division.

of a delay time. The minimum values are 140 μs for the first delay and 90 μs for subsequent delays. Once corrected, the delays are accurate to ±3 μs for the first delay and 1 μs for subsequent delays. The jitter in the first delay time of ±3 μs results from the fact that the zero crossing interrupt can occur at any time during the execution of an instruction and is not serviced until the instruction is completed. Later delays are jitter free with respect to the first. All factors considered, such noncumulative jitter is acceptable for most practical source uses. In those research applications where more exact synchronization of other parts of the experiment with source firing is needed, a minicomputer and external programmable timer are used.

Because this microcomputer employs CMOS integrated circuitry, it is highly sensitive to radio-frequency interference. For stable operation of the computer and spark source an optical isolator was placed between port A of the PETs 6522 and the thyratron driver (EG and G type TM-27, Boston, MA). A schematic of this isolation circuit is given in Figure 6. This circuit completely isolates the PET signal from the thyratron driver, as well as from the power supplies and grounds. All circuit components on the PET side of the MCT-2 optical isolator are powered by a power supply derived from the PET power supply. Those components on the source side of the circuit are powered by a separate power supply originating from the isolated power used to power the thyratron driver and spark source. Model CD 4050 CMOS buffers are used to couple between CMOS and TTL circuit components, and a 74132 Schmitt trigger is used to sharpen the trigger signal and to help eliminate noise pulses. The complementary transistor pair totem pole drivers are used to boost the respective signals.

Example Waveforms. Some representative waveforms which illustrate the operation of the source under control by the PET are given in Figure 7. Waveforms for one, two, three, and four breaks per half-cycle are illustrated. All traces were taken by using an argon flow-jet with a tungsten pin as the anode and an iron pin as the cathode. The top trace in each case represents the voltage at the capacitor using a 2 ms per division time base. The bottom trace shows the current through the spark gap using a 20 μs/division time base. Note in the multiple break cases that the break times have been set such that the source is fired at the same capacitor voltage each time. This is further illustrated by the current waveforms, where every discharge waveform is superimposed upon the previous one. A wide variety of break patterns can be achieved by software manipulation of the number of breaks per half-cycle and the time at which each occurs (e.g., ref 13).

ACKNOWLEDGMENT

The assistance of Russ Riley and Ken Spielman in fabrication of portions of the hardware is appreciated. Discussions with David Coleman, Alex Scheeline, John Bernier, Bob Watters, and John Norris during the design phases of this work were valuable and are acknowledged.

LITERATURE CITED

(1) Walters, J. P.; Malmstadt, H. V. *Anal. Chem.* **1965**, *37*, 1484.
(2) Walters, J. P. *Anal. Chem.* **1968**, *40*, 1672.
(3) Farnsworth, P. B.; Walters, J. P. *Spectrochim. Acta, Part B* **1980**, *35B*, 315.
(4) Walters, J. P. *Anal. Chem.* **1968**, *40*, 1672.
(5) Walters, J. P. *Anal. Chem.* **1969**, *41*, 1990.
(6) Coleman, D. M.; Walters, J. P. *Spectrochim. Acta, Part B* **1976**, *31B*, 547.
(7) Rentner, J. R.; Uchida, T.; Walters, J. P. *Spectrochim. Acta, Part B* **1977**, *32B*, 125.
(8) Coleman, D. M.; Walters, J. P.; Watters, R. L., Jr. *Spectrochim. Acta, Part B* **1977**, *32B*, 287.
(9) Araki, T.; Walters, J. P. *Appl. Spectrosc.* **1979**, *33*, 463.
(10) Walters, J. P. In "Contemporary Topics in Analytical and Clinical Chemistry"; Hercules, D. M., Hieftje, G. M., Snyder, L. R., Evenson, M. A., Eds.; Plenum Press: 1978; Vol. 3, pp 91–151.
(11) Coleman, D. M.; Walters, J. P. *Spectrochim. Acta, Part B* **1978**, *33B*, 127.
(12) Walters, J. P.; Coleman, D. M. U.S. Patent 4 055 783, Nov 18, 1977.
(13) Scheeline, A.; Coleman, D. M.; Walters, J. P. *Appl. Spectrosc.* **1978**, *32*, 215.
(14) Ekimoff, D.; Mathews, S. E.; Walters, J. P., in preparation.
(15) Osborne, Adam; Kane, Jerry "An Introduction to Microcomputers"; Adam Osborne: Berkeley, CA, 1928; Vol. 2.
(16) Zaks, Rodney, "6502 Applications Book", Sybex, 1979.

RECEIVED for review January 26, 1981. Accepted May 12, 1981. Portions of this work were funded by the National Science Foundation under Grant CHE-79-15195 and the Graduate School of the University of Wisconsin.

Influence of Instrumental Response Time on Interference Effects in Graphite Furnace Atomic Absorption Spectrometry

Erik Lundberg* and Wolfgang Frech

Department of Analytical Chemistry, University of Umeå, S-901 87 Umeå, Sweden

The influence of instrumental response time on observed interference effects in graphite furnace atomic absorption spectrometry was illustrated by the systems lead in sodium chloride or sodium nitrate and manganese and beryllium in aluminum nitrate. For the accomplishment of these studies, a spectrometer with a small time constant and an on-line data acquisition system was used. It is shown that concomitants can affect the vaporization characteristics of the analyte by changing (i) the atomization interval and/or (ii) the rate of atom formation. From the experimental results it is concluded that such changes cannot be established adequately when the detector/readout system has a too slow response time, which is the case in many commercial instruments. This means that many empirical studies of interference effects reported in the literature, where such instruments have been used, are of limited value.

The degree of observed interference effects in graphite furnace atomic absorption spectrometry (GFAAS) is determined by two different categories of factors which should be considered separately. The first category concerns the basic principles which underlie this technique and includes all factors which bring about changes in the efficiency of free atom formation or which alter the temporal as well as spatial distribution of free atoms within the measuring cell. Interference effects belonging to this category originate from changes in the chemical or physical properties of the sample or the measuring cell and are referred to as chemical and physical interferences.

The second category is instrumental in origin and includes (i) the ability of the spectrophotometer to discriminate the specific absorbance from the absorbance caused by particles, molecules, or atoms and (ii) changes in peak shapes as well as displacements of peak maxima arising from a too slow temporal response of the detector/readout system. The absorption signal obtained during the vaporization of atoms in the cell is time dependent and can be monitored with a relatively small error (<2%) only if the overall RC-time constant of the readout system is 10 times shorter compared with the temporal half-width of the peak (*1*). This means that changes of the evaporation characteristics of an element will not be reflected adequately by the recorded signal if the RC-time constant is too large.

Normally there is an interaction between instrumental imperfections and chemical or physical interference effects so that signals are affected by both at the same time. Little information on the effects of inadequate RC-time constants on observed interference effects in GFAAS is available. A theoretical evaluation of the influence of the temporal response of the detection system upon other transient atomic absorption signals has been given by Piepmeier and de Galan (*2*). Recently Siemer (*3*) has evaluated the influence of slow instrumental response on the accuracy of GFAAS determinations. The effect of low pass filtering on integrated absorbance values before and after logarithmic conversion of the signal was treated and it was shown that the RC-time constant did not alter the integrated value if filtering was done after the logarithmic conversion.

In this paper we have investigated the errors produced by a large RC-time constant in the recorded peak height and peak area absorbances. Such large constants are used in many commercial instruments. Special emphasis was given to the influence of instrumental response on observed chemical as well as physical interference effects in liquid samples. To realize this type of study, we used a spectrometer with small time constant and an on-line data acquisition system sufficiently fast to monitor the signals without distortion.

EXPERIMENTAL SECTION

Instrumentation. A Varian-Techtron AA-6 atomic absorption spectrophotometer provided with background correction was fitted with a carbon rod atomizer (CRA 63). The original transformer of the CRA 63 power supply was replaced by a more powerful transformer with secondary voltages of 3, 5, 12, and 15 V, capable of delivering 7.5 kW. To this transformer was connected a Varian CRA 90 workhead (normally at 12 V) or a Perkin-Elmer HGA 74 (normally at 15 V), the latter with a modified mounting base to fit the optical rail of the AA-6. The CRA 63 power supply was modified to provide an "outburning" step immediately after the atomization step. Facilities for close temperature control of the graphite tube of each furnace were installed. A fiber optic cable, directed toward the outer surface of the tube, was mounted on each furnace and the light emitted from the tube was monitored with a photodiode sensitive to infrared radiation. The principle for this optical feed-back control has been described earlier (*4*). By adjusting the gain in the feed-back circuit, it was also possible to vary the heating rate during atomization. Temperature settings referring to the inner surface of each graphite tube were calibrated with a NiCr-Ni thermocouple (below 1000 °C) and with an optical pyrometer (Keller Spezialtechnik Pyro Werk GmbH, Model PB06AF3) for higher temperatures. Separate gas control units were connected to each furnace in order to maintain suitable gas flows and to reduce gas consumption (*5*).

The hollow cathode lamps were modulated at 285 Hz, resulting in a new absorbance value every 3.5 ms. The signal damping of the AA-6 readout module was modified to obtain a faster response time of the electronics. The value of the DAMP *A* time constant was thus altered from the original 260 ms to 10 ms and the DAMP *B* time constant from 1290 ms to 270 ms, as described earlier (*6*).

An Alpha LSI minicomputer with 32K bytes memory was used for data acquisition. To the computer was connected a 2 × 256K byte floppy disk for program and data storage, a teletype and a 16-channel 12-bit A/D + 2-channel 12-bit D/A interface card (DT 1732, Data Translation Inc.). One of the A/D channels was connected to the readout module of the AA-6. The recorder output of the AA-6 was not used, however, since its output impedance was high and the signal level low (100 mV for 100% *T*). Instead, TP 301 and TP 308 (common) on PCB No. 02-100251-00 (see manual) were connected to the computer, resulting in a 5-V signal with low output impedance. In this way the S/N ratio was significantly improved. Another A/D channel was connected to the output signal from the photodiode sensing the temperature. The D/A channels were used to feed out atomic absorption and temperature signals to the X-Y recorder (Model 2000, Houston Instrument). The triggering signals obtained from the CRA 63 power supply for the ashing and atomization steps were used to

0003-2700/81/0353-1437$01.25/0 © 1981 American Chemical Society

Table I. Instrumental Parameters, CRA 90

	lead			manganese		
	time, s	temp, °C	heating rate, °C s⁻¹	time, s	temp, °C	heating rate, °C s⁻¹
drying	25	110	6	25	110	6
ashing	40	570	64	40	570	64
atomization[a]	2.5	1670	1460[b]	3	1880	1660

	lead	manganese
wavelength, nm	283.3	279.5
spectral bandwidth, nm	0.5	0.5
lamp current, mA	5.0	9.0
hydrogen lamp current (scale division)	9.0	9.0
argon flow, L min⁻¹	4.5	5.5

[a] Temperature controlled heating (4). [b] For some experiments a heating rate of 470 °C s⁻¹ was used.

Table II. Instrumental Parameters, HGA 74

	lead			beryllium			manganese		
	time, s	temp, °C	heating rate, °C s⁻¹	time, s	temp, °C	heating rate, °C s⁻¹	time, s	temp, °C	heating rate, °C s⁻¹
drying	25	110	7	25	110	7	25	110	7
ashing	40	500	22	40	575	22	40	500	22
atomization[a]	3.5	1740	1740[b]	5	2250[c]	1940	4	1950	1940
outburning	0.5	2200		2	2600		2	2600	

	lead	beryllium	manganese
wavelength, nm	283.3	234.9	279.5
spectral bandwidth, nm	0.5	1.0	0.5
lamp current, mA	5.0	5.3	9.0
hydrogen lamp current (scale division)	9.0	1.5	9.0
argon flow, L min⁻¹			
internal[d]	0.34	0.34	0.34
external	1.00	1.00	1.00

[a] Temperature controlled heating (4). [b] For some experiments a heating rate of 530 °C s⁻¹ was used. [c] For nonpyrolytically coated tubes the temperature was 2400 °C. [d] Gas stop during atomization.

initiate data acquisition, as will be described below.

Data Processing. The AA-6 readout module was always operated in the transmission mode in order to obtain the fastest possible response time. Logarithmic conversion to absorbance was then performed by the computer.

At the end of the ashing step the I_0 value was measured, averaged during 2 s, and stored. In this way any offset from 100% T could be corrected for and it was not necessary to "zero" the instrument between runs. During atomization 1000 AA values and 1000 temperature values were transferred to the memory. The time lag between corresponding AA and temperature values was 40 μs. The sampling interval, i.e., the time between successive measurements, was set in the program and could be varied from 0.1 ms to 1 s. Typically, the atomization time was 2–5 s and, hence, the sampling interval was set to 2–5 ms. After atomization, log I_0/I was calculated, and peak height and peak area values were printed on the teletype. The AA and temperature signals were then plotted on the X-Y recorder and could in addition be stored (as raw data) on a diskette for future use. The programs for input and output data transmission were written in high-speed assembler language, whereas the other programs were written in BASIC.

Signals obtained from the temperature sensor were voltages corresponding to certain temperatures. These voltages were converted into absolute temperatures by means of temperature vs. voltage calibration curves, one for each furnace (stored on a diskette).

Normally 100 values (out of 1000) were displayed on the recorder. Every 10th value was fed out in order to see the signal time dependence for the whole atomization time. However, by feeding out 100 successive values to the recorder, 10 times temporal scale expansion of a suitable portion of the signal could be achieved.

The digitized AA and temperature signals fed to the recorder were subjected to some kind of data smoothing to reduce noise and thus facilitate interpretation. This was accomplished by using spline functions, i.e., piecewise polynomials with continuity conditions (7), or by calculating weighted moving mean values. The shape of a peak was not distorted by this operation.

Procedure. For each series of experiments a new graphite tube was used, conditioned by repeated blank firings. We always started with pure standard solutions and continued with solutions containing the matrix in order of increasing concentrations. All measurements were made with two time constants, 10 ms (DAMP A) and 270 ms (DAMP B), and were made at least in triplicate. The instrumental parameters are given in Table I and II. The background corrector was always used.

Reagents. Reagent grade reagents were used except for sodium chloride and nitric acid, which were of ultrapure quality. Stock solutions were prepared from $Pb(NO_3)_2$, MnO_2, and $BeSO_4$. All standard solutions were made immediately before use, acidified with 0.01 M HNO_3, and stored in acid-washed polyethylene bottles. The concentrations of the elements investigated were found to be below their detection limits in NaCl, $NaNO_3$, and $Al(NO_3)_3$.

Pyrolytically coated graphite tubes were used for CRA 90 and nonpyrolytically as well as pyrolytically coated tubes for HGA 74.

RESULTS AND DISCUSSION

Response Time Considerations. As was discussed by McWilliam et al. (1) the overall time constant of a detector/readout system must be 0.1 times the temporal half-width of a Gaussian-shaped transient signal in order to correctly monitor the signal. The shortest half-width obtained in this study was 120 ms. Considering this half-width a time constant of 10 ms was regarded as sufficient for the present work. Using an even smaller time constant would merely increase the noise

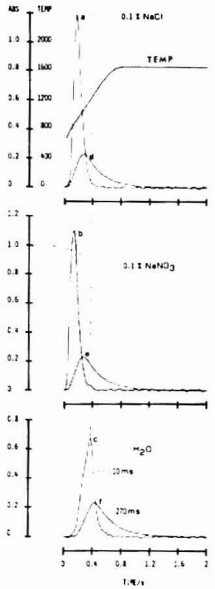


Figure 1. Signal transients for lead in H_2O, 0.1% $NaNO_3$, and 0.1% NaCl obtained with CRA 90 for time constants 10 ms (a–c) and 270 ms (d–f). The variation in temperature with time is also shown.

level. For comparisons the original time constant of the instrument, 270 ms, was used.

The modification of the time constant was performed at a point in the signal processing where the signal is not linearly related to the amount of analyte (6), i.e., before conversion into absorbance. Consequently, the spectrometer is incapable of accurately measuring either peak areas or peak heights when the time constant is 270 ms (3).

Correlation between Absorbance Evaluation Mode and Number of Atoms. The peak height is a measure of the total number of atoms only if they are present at the same time and uniformly distributed throughout the absorbing cell. This is not the case with commercial atomizers like CRA 90 and HGA 74 (8). As a consequence, the magnitude of the peak height will be affected by, e.g., changes in rate of atom formation and atomization interval. If such changes are introduced by a matrix, the peak height method cannot be used to compare the number of atoms in matrix-free and matrix-containing samples.

The peak area (Q) is a measure of the total number of atoms (N_0) only if their mean residence time (τ_2) is not changed during the atomization according to

$$Q = N_0\tau_2 \tag{1}$$

The atoms are formed during heating of the graphite tube, i.e., at nonisothermal conditions. τ_2 is at atmospheric pressure given by

$$\tau_2 = \frac{l^2}{8D_0}\left(\frac{T_0}{T}\right)^n \tag{2}$$

where l is the length of the tube, D_0 is the diffusion coefficient, n is a constant that varies between 1.5 and 2, and T is the temperature (ref 9, p 220). This means that τ_2 varies during the heating of the tube. If the atomization interval is changed by a matrix, the mean residence time of atoms will also change.

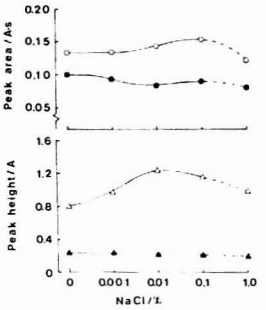


Figure 2. The variations in lead peak height and peak area values for different concentrations of NaCl (CRA 90): (unfilled symbols) 10 ms; (filled) 270 ms. The lines between 0.1 and 1.0% NaCl are dashed because the background corrector was not able to correct for the nonspecific absorption caused by 1.0% NaCl.

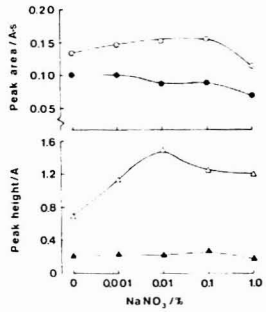


Figure 3. The variations in lead peak height and peak area values for different concentrations of $NaNO_3$ (CRA 90): (unfilled symbols) 10 ms; (filled) 270 ms.

Hence, the peak area method cannot be used to compare the number of atoms in matrix-free and matrix-containing samples. For simplicity, only pure diffusion processes through the tube openings have been considered.

Pb in NaCl and $NaNO_3$. When commercial instruments with relatively large time constant are used, NaCl is known to have a suppressing effect on lead signals. We have observed this suppression for the CRA 90 as well as for the HGA 74 regardless of whether the peak height or the peak area was evaluated. However, as was discussed in a preceding paragraph, a slow response time introduces an error in signal processing which makes the results difficult to interpret.

Results Obtained with CRA 90. Figure 1 shows the signal time dependence for 0.6 ng of Pb in H_2O, 0.1% $NaNO_3$, and 0.1% NaCl for the two different time constants. As can be seen, there is a severe distortion in peak shape when the larger time constant is used, giving rise to a decreased peak height and a shift in peak maximum. In agreement with results reported earlier, the peak height decreases slightly in the presence of the matrices (Figure 1d–f). However, when the undamped mode is used (Figure 1a–c), the peak heights are significantly increased and the peak maxima as well as the appearance times are shifted to lower temperatures. This means that the degree as well as the sign of the obtained interference effects are strongly influenced by the time constant of the system.

The variations in peak height as well as peak area for different concentrations of the mentioned sodium salts are

Table III. The Effects of Varying the CRA 90 Heating Rate on Observed Interferences from Sodium Nitrate on the Lead Signal, Using the Two Time Constants

heating rate, °C s⁻¹	RC, ms	peak height (rel sensitivity)			peak area (rel sensitivity)		
		0% $NaNO_3$	0.001% $NaNO_3$	0.1% $NaNO_3$	0% $NaNO_3$	0.001% $NaNO_3$	0.1% $NaNO_3$
470	10	100 ± 7.1	100 ± 6.2	162[a] ± 1.8	100 ± 8.7	106 ± 8.2	104 ± 6.2
	270	100 ± 3.4	114 ± 1.5	103 ± 1.8	100 ± 3.7	120 ± 6.3	94 ± 5.2
1460	10	100 ± 1.3	160 ± 8.3	177[b] ± 7.1	100 ± 1.5	112 ± 2.5	116 ± 1.7
	270	100 ± 1.3	103 ± 2.5	97 ± 2.6	100 ± 1.0	100 ± 3.0	88 ± 0.7

[a] Temporal half-width 190 ms. [b] Temporal half-width 120 ms.

Table IV. The Effects of Varying the HGA 74 Heating Rate on Observed Interferences from Sodium Nitrate on the Lead Signal, Using the Two Time Constants

heating rate, °C s⁻¹	RC, ms	peak height (rel sensitivity)			peak area (rel sensitivity)		
		0% $NaNO_3$	0.001% $NaNO_3$	0.1% $NaNO_3$	0% $NaNO_3$	0.001% $NaNO_3$	0.1% $NaNO_3$
530	10	100 ± 2.5	84 ± 1.4	79[a] ± 0.3	100 ± 0.8	94 ± 0.9	89 ± 2.2
	270	100 ± 0.9	98 ± 1.8	93 ± 0.3	100 ± 1.1	98 ± 2.5	93 ± 0
1740	10	100 ± 2.9	82 ± 4.0	58[b] ± 2.3	100 ± 1.9	86 ± 2.0	72 ± 0
	270	100 ± 0.4	96 ± 2.3	85 ± 2.5	100 ± 0.7	92 ± 1.2	82 ± 1.2

[a] Temporal half-width 730 ms. [b] Temporal half-width 210 ms.

seen in Figure 2 and 3 for both time constants. Results obtained with the 10-ms time constant represent a correct reflection of the atom concentration in the absorbing cell at any instant of time. Even the presence of minute amounts of sodium salts gives rise to increased signals. With conventional response times this increase cannot be detected.

As was discussed above, the increased signals observed in the presence of the matrices do not allow any conclusions to be drawn about the relative number of atoms formed. For example, in the presence of 0.1% NaCl the peak area is increased by 16%, with a shift in the atomization interval toward lower temperatures; see Figure 4. This shift means that the diffusion rate of atoms will be lower when the solution contains sodium chloride, which partly explains the increased area. In addition to this physical effect, the atoms might be formed in a quite different chemical environment, e.g., with other partial pressures of potential interfering elements like oxygen and chlorine.

Results Obtained with HGA 74. In order to investigate if the findings with the CRA 90 were valid also for the HGA 74 (a semienclosed furnace with larger graphite tube), we repeated the experiments with the latter. Figure 5 shows the signal time dependence for 0.6 ng of Pb in H_2O, 0.1% $NaNO_3$, and 0.1% NaCl for the two different time constants. In the presence of a matrix, the peaks are shifted to lower temperatures. In contrast to the results obtained for CRA 90, the peak heights decreased for the fast response time.

The signal variation for various concentrations of NaCl and $NaNO_3$ is given in Figures 6 and 7. The differences seen between Figures 2–3 and 6–7 can at present not be explained, but from the results it becomes evident that also in this furnace the time constant will have a strong influence on the observed signals.

Effects of Heating Rate. The maximum heating rate of the commercial version of CRA 90 is 800 °C/s, whereas the experiments reported above were performed with a modified version with a heating rate of 1460 °C/s. To investigate if the severe distortion in peak characteristics remain for the large time constant if a slower heating rate corresponding to the commercial one is used, we repeated some of the earlier experiments with a heating rate of 470 °C/s. The results given in Tables III and IV show that the degree of distortion has not decreased significantly. It can also be seen from the tables that the extent of matrix effects are strongly dependent on the applied heating rate (RC = 10 ms). Therefore, it is essential to consider this parameter when investigating interference effects.

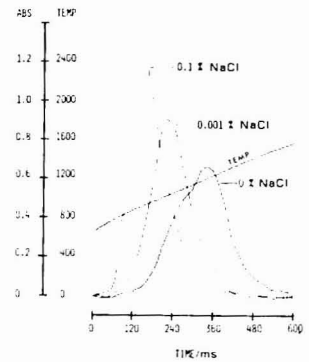


Figure 4. Signal transients for lead in H_2O, 0.001% NaCl, and 0.1% NaCl obtained with CRA 90 (time constant = 10 ms). The variation in temperature with time is also shown.

Table V. Observed Interference Effects from Aluminum Nitrate on the Manganese Signal for Two Time Constants Using CRA 90

RC, ms	peak height (rel sensitivity)		peak area (rel sensitivity)	
	H_2O	0.05% Al	H_2O	0.05% Al
10	100 ± 3.8	128 ± 10.0	100 ± 0.5	100 ± 1.2
270	100 ± 0.4	103 ± 3.0	100 ± 0	90 ± 0.8

Mn and Be in $Al(NO_3)_3$. The influence of $Al(NO_3)_3$ on the atomization behavior of Mn and Be has been studied by Maessen et al. (*10*). They showed that in the presence of this matrix, the peaks were shifted toward higher temperatures and increased in height. A time constant of 10 ms was used. In order to establish the errors introduced by using a large time constant with regard to observed interference effects, we repeated some of their experiments with the CRA 90.

The change in peak characteristics we obtained were in agreement with the findings of Maessen et al. The peak

Table VI. Observed Interference Effects from Aluminum Nitrate on the Manganese Signal for Two Time Constants Using HGA 74

RC, ms	peak height (rel sensitivity)			peak area (rel sensitivity)		
	H_2O[a]	0.05% Al[a]	0.05% Al	H_2O[a]	0.05% Al[a]	0.05% Al
10	100 ± 3.0	131 ± 13.0	120 ± 6.4	100 ± 5.0	105 ± 5.8	94 ± 5.6
270	100 ± 0.6	117 ± 3.3	99 ± 0.3	100 ± 1.0	119 ± 1.5	87 ± 2.3

[a] Pyrolytically coated tubes.

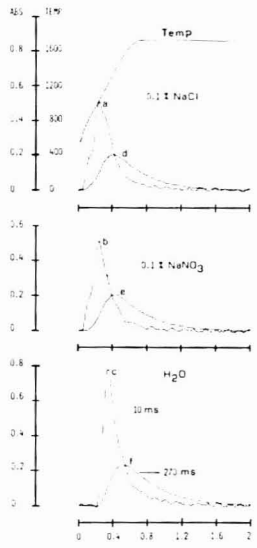


Figure 5. Signal transients for lead in H_2O, 0.1% $NaNO_3$, and 0.1% NaCl obtained with HGA 74 for time constants 10 ms (a–c) and 270 ms (d–f). The variation in temperature with time is also shown.

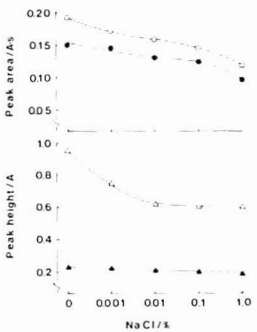


Figure 6. The variations in lead peak height and peak area values for different concentrations of NaCl (HGA 74): (unfilled symbols) 10 ms; (filled) 270 ms. The lines between 0.1 and 1.0% NaCl are dashed because the background corrector was not able to correct for the nonspecific absorption caused by 1.0% NaCl.

heights as well as the peak areas obtained when using the two time constants are given in Table V. If an investigation of this system had been made with an instrument with slow response time, no interference effect would have been observed. In fact, however, the addition of Al gives rise to an increase in the maximum concentration of atoms in the tube. Corresponding results obtained with HGA 74 can be seen in Table VI for Mn and Table VII for Be. Considering peak heights, the pattern for observed interference effects is similar to that seen in Table V when using the different time constants.

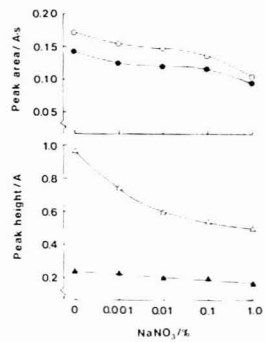


Figure 7. The variations in lead peak height and peak area values for different concentrations of $NaNO_3$ (HGA 74): (unfilled symbols) 10 ms; (filled) 270 ms.

Table VII. Observed Interference Effects from Aluminum Nitrate on the Beryllium Signal for Two Time Constants Using HGA 74

RC, ms	peak height (rel sensitivity)		peak area (rel sensitivity)	
	H_2O[a]	0.05% Al[a]	H_2O[a]	0.05% Al[a]
10	100 ± 0.8	219 ± 14.9[b]	100 ± 5.1	160 ± 3.2
270	100 ± 2.4	135 ± 3.0	100 ± 1.5	117 ± 2.1

[a] Pyrolytically coated tubes. [b] The shift in appearance time and peak position was 100 ms toward higher temperatures compared with water solution.

Table VIII. Observed Interference Effects from Sodium Chloride on the Beryllium Signal for Two Time Constants Using HGA 74

RC, ms	peak height (rel sensitivity)		peak area (rel sensitivity)	
	H_2O[a]	0.1% NaCl[a]	H_2O[a]	0.1% NaCl[a]
10	100 ± 1.4	230 ± 10.9	100 ± 1.2	150 ± 12.3
270	100 ± 1.1	125 ± 2.3	100 ± 4.9	133 ± 1.1

[a] Pyrolytically coated tubes.

Be in NaCl. Table VIII gives the results obtained for Be in the presence of NaCl. For this matrix, the Be signal was shifted 60 ms toward lower temperatures and increased significantly in height. These effects were not observed when

ordinary graphite tubes were used instead of pyrolytically coated ones.

CONCLUSIONS

As has been shown in this paper, concomitants can affect the vaporization characteristics of the analyte so that (i) the atomization interval is shifted toward lower or higher temperatures and (ii) the rate of atom formation is changed. Such effects cannot be established when the detector/readout system has a too slow response time. This means that many empirical studies of interference effects reported in the literature, where such instruments have been used, are of limited value.

Even if a fast response time is used the relative number of free atoms formed cannot be determined if the atomization interval is changed, whether the peak height or the peak area is measured. The degree of interference effects can therefore only be established accurately if the atomization interval is unchanged and, moreover, if peak areas are evaluated.

LITERATURE CITED

(1) McWilliam, I. G.; Bolton, H. C. *Anal. Chem.* **1969**, *41*, 1755-1762.
(2) Piepmeier, E. H.; de Galan, L. *Spectrochim. Acta, Part B* **1976**, *31B*, 163-177.
(3) Siemer, D. D.; Baldwin, J. M. *Anal. Chem.* **1980**, *52*, 295-300.
(4) Lundgren, G.; Lundmark, L.; Johansson, G. *Anal. Chem.* **1974**, *46*, 1028-1031.
(5) Lundberg, E.; Lundmark, L. *Chem. Biomed. Env. Instrum.* **1979**, *9*, 91-93.
(6) Lundberg, E. *Chem. Instrum.* **1978**, *8*, 197-204.
(7) Wold, S. *Technometrics* **1974**, *16*, 1-11.
(8) van den Broek, W. M. G. T.; de Galan, L. *Anal. Chem.* **1977**, *49*, 2176-2186.
(9) L'vov, B. V. "Atomic Absorption Spectrochemical Analysis"; Adam Hilger: London, 1970.
(10) Maessen, F. J. M. J.; Balke, J.; Massee, R. *Spectrochim. Acta, Part B* **1978**, *33B*, 311-324.

RECEIVED for review February 2, 1981. Accepted April 27, 1981.

Condensed Phase Photoacoustic Spectroscopic Detection of Porphyrins and Dyes

Edward Voigtman, Arthur Jurgensen, and James Winefordner*

Department of Chemistry, University of Florida, Gainesville, Florida 32611

A simple piezoelectric detection system suitable for performing highly sensitive liquid-phase photoacoustic spectroscopy is presented. Performance of the system with respect to linearity, solvent effects, and excitation pulse characteristics is experimentally evaluated and compared with theoretical figures of merit. Limits of detection for various porphyrins, laser dyes, and drugs are presented.

Although photoacoustic detection has been previously employed in the study of condensed phase materials, the technique employed has most often been of the type studied by Rosencwaig and Gersho (*1*): a photothermalacoustic detection. Absorption of modulated light by a condensed medium leads to modulated diffusion of resultant heat into the surrounding confined buffer gas which then undergoes modulated pressure fluctuations. The fluctuations are detected with a sensitive capacitance microphone. The slowness of thermal diffusion, signal saturation effects (*2*), and possibility of scattered light artifacts (*3*) partially annul the very high sensitivity of the technique. Consequently, other photoacoustic spectroscopy (PAS) schemes have been investigated in hopes of retaining the sensitivity while eliminating the aforementioned difficulties.

In 1969, Callis et al. (*4*) adapted a capacitance microphone to the study of triplet yields of anthracene and acridine orange in ethanol solutions using pulsed broad band excitation. In 1977, Hordvik and Schlossberg (*5*) studied absorption coefficients in fluorite crystals using attached and nearby piezoelectric transducers with differential amplification and lock-in amplifier detection. They measured absorptivities approaching 10^{-5} cm^{-1}. Lahmann et al. (*6*) used a frequency-shift keyed (FSK) argon ion laser together with piezoelectric transducer and lock-in detection to achieve a detection limit of 54 ppt (80 pg cm^{-3}, 2.2×10^{-5} cm^{-1}) for β-carotene in chloroform. Also in that year, Bonch-Bruevich et al. (*7*) used laser excitation and a piezoelectric transducer to study single and multiple photon absorption in dye solutions. Sensitivities of 1 μJ were achieved with oscilloscopic detection.

In 1978, Farrow et al. (*8*) exploited the acoustic impedence matching advantage of piezoelectric transducers when used with condensed media and demonstrated the feasibility of obtaining excellent PAS spectra with both chopped CW and pulsed laser excitation of various Nd^{3+}-containing samples. Also in 1978, Oda et al. (*9*) achieved a detection limit for cadmium as cadmium dithiozonate of 14 ppt (20 pg cm^{-3}) in chloroform. They employed a chopped 514.5-nm argon ion laser line with piezoelectric transducer and phase sensitive detection. Tam and Patel (*10*), in 1979, used a "submersed" lead zirconate titanate (PZT) piezoelectric transducer, gated integrator detection, and pulsed laser excitation to measure absorptivities approaching 10^{6} cm^{-1} with incident pulse energies of approximately 1 mJ thus yielding a thermalized energy sensitivity near 1 nJ. Additional studies undertaken by Patel and co-workers with their system included nonlinear Raman gain spectroscopy (*11*), C-H stretch overtones in benzene (*12*), and evaluation of a cuvette cell and "C-clamp" transducer mounting scheme (*13*).

The origin of the photoacoustic effect underlying the above results has been heuristically derived by Tam and Patel (*10*) and rigorously derived by Atalar (*14*); it is summarized briefly below. Absorption of light produces heat in the illuminated region which then expands, assuming a positive coefficient of expansion. The expansion pulse impinges on the lightly damped transducer producing a ringing damped output. The

0003-2700/81/0353-1442$01.25/0 © 1981 American Chemical Society

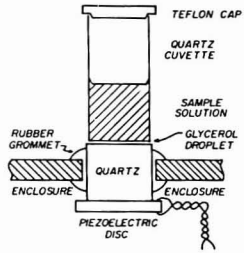


Figure 1. Schematic of the liquid-phase photoacoustic cell.

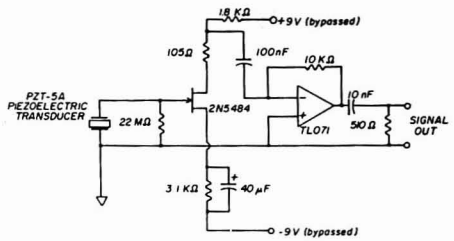


Figure 2. Photoacoustic preamplifier circuit schematic.

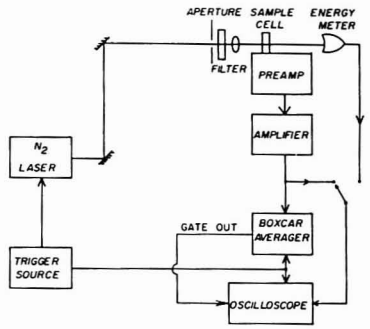


Figure 3. Nitrogen laser excited photoacoustic detection scheme.

transducer output, S, in V, is proportional to both incident pulse energy E_P, in mJ, and to sample optical absorptivity α, in cm^{-1}, for small absorptivities. The proportionality constant R, in $V/(mJ\ cm^{-1})$, is called the responsivity and is shown to be dependent on the detection system geometry. The responsivity is also proportional to the solvent thermal expansion coefficient β, in K^{-1}, and solvent speed of sound c, in cm s^{-1}, and inversely proportional to the solvent specific heat C_P, in cal/(g-mol K).

If the limiting detectable absorptivity, α_L, is defined as the absorptivity of the solute at the limiting detectable concentration C_L, where $S/N = 3$, then it is apparent that higher pulse energy lasers may allow lower C_L and α_L values to be achieved without improvement in the PAS cell or signal processing. Therefore, α_L values, though widely used as figures of merit of the sensitivity, are actually misleading. A much better figure of merit for comparison of the sensitivities of two PAS systems is the limiting detectable thermalized energy E_L, defined as $\alpha_L l E_p$, where α_L is as above, l is the illuminated path length, in cm, and E_p is the incident laser pulse energy, in J. This figure of merit is implicit in the work of Bonch-Bruevich et al. (*7*) and is explicitly used by Tam et al. (*15*) as ϵ_{min}. Physical processes liberating more than E_L of thermalized energy per excitation pulse would be expected to be observable with the PAS system.

The cell design used by Tam and Patel (*10*), though quite sensitive by the above criteria, consists of a stainless steel cylinder with quartz windows, "O"-ring seals, and side ports for the transducer and sample admission. Though well-suited to their studies, it would be useless for rapid analysis of potentially hazardous materials and difficult to clean thoroughly. Consequently, they developed a sensitive "C-clamp" arrangement for holding their PZT transducer assembly in contact with a standard 1-cm cuvette (*13*). Unfortunately, we found that the various "C-clamp" cell versions we built were quite sensitive, but offered poor signal reproducibility when the cuvette was removed from the clamp assembly and then replaced. Signal amplitudes frequently varied by factors of 2. In addition, stray incident light and scattered light impinging on the "C-clamp" itself generated acoustic transients which could not be temporally resolved from the genuine PAS signal. Therefore, we developed an extremely simple photoacoustic detection system by simplifying the designs used by previous investigators. Our design, which employs a "submersed" PZT transducer and a standard 1-cm Suprasil fluorescence cuvette, does not appreciably suffer from the aforementioned difficulties.

This paper details our cuvette PAS system and preamplifier electronics and their use in detecting various porphyrins, laser dyes, and drugs. Calibration data establishing the approximate thermalized energy sensitivity of the system are presented and several pulsed laser systems are compared with respect to pulse energy and pulse width effects in our system. Since the magnitude of the photoacoustic effect utilized here is dependent on certain solvent physical properties, data are presented comparing the magnitude of the observed signals in the normal alkanes (C_5–C_9), methanol, ethanol, acetonitrile, carbon tetrachloride, and water.

EXPERIMENTAL SECTION

The simple cuvette/transducer arrangement is shown in Figure 1. Standard Suprasil fluorescence cuvettes are employed and the transducer is PZT-5A composition with 0.5 in. diameter, 0.12 in. thickness, and 200 kHz fundamental mechanical resonant frequency (no. 8125, Vernitron Piezoelectric Division, Bedford, OH). The transducer is attached to the bottom of a fused quartz flat with cyanoacrylate adhesive while the cuvette is placed on the upper surface of the flat. A drop of glycerol on the flat greatly improves acoustic coupling efficiency and is much easier to remove than vacuum grease. Prior to using this arrangement, we found that a "C-clamp" arrangement was unsatisfactory for the reasons given above. To eliminate the attendant acoustic artifacts, we replaced the "C-clamp" with a simple arrangement in which a PZT transducer was cemented to one end of an Alnico rod magnet and a polished steel disk was cemented to the bottom of a Suprasil cuvette. Magnetic attraction provided a reproducible coupling force. We found that use of a coupling fluid was much more important in obtaining a sensitive and reproducible signal than the use of a relatively strong coupling force. Opaque flats made of stainless steel and tantalum were then used until it became clear that scattered light artifacts would not be problematic. The transducer is shielded from external electrical fields since the quartz flat is thick enough (0.5 in.) to breach the preamplifier enclosure wall. A rubber gasket reduces acoustic coupling between the enclosure wall and the quartz flat. No other attempts were made to acoustically or thermally shield the apparatus.

Figure 2 shows the preamplifier circuit employed. It is a slight modification of the preamplifier circuit used by Tam and Patel (*10*). Frequency response is 28–400 kHz (–3 db), voltage gain is 37.5, and noise is 4 μV rms. Nine-volt alkaline batteries are used to power the preamplifier to avoid power line hum pickup. The transducer is located as close to the preamplifier input as feasible (1 in.) and the leads are carefully soldered to the transducer

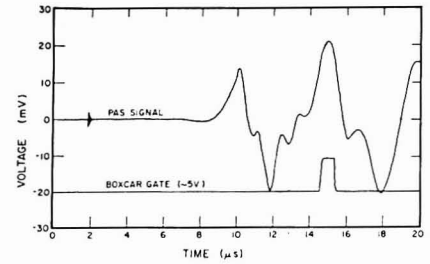


Figure 4. Photoacoustic signal produced by 12.85 ppm of tris(2,4-pentadiono)chromium(III) and excitation pulse energy of ~15 μJ at λ = 337.1 nm.

although we have also used nickel–silver terminals from a solderless breadboard socket (Continental Specialties Corp., New Haven, CT) to effect a removable electrical connection to the transducers.

A block diagram of the primary configuration of our experimental system is shown in Figure 3. The excitation illumination is provided by an unfiltered Molectron UV-14 N_2 laser producing pulses of approximately 1.3 mJ at a repetition rate of 20 Hz. The laser pulse width of 10 ns (fwhm) is obtained by using a Hamamatsu streak camera system with C979 temporal disperser. Pulse energies are measured with a Molectron Model J3-05 pyroelectric energy meter. The predominant laser output wavelength is 337.1 nm. The laser beam is passed through an adjustable aperture, usually set at 1 in. diameter, is attenuated, if necessary, by high-quality neutral density filters (Corion Corp., Holliston, MA), is focused with an *f*/2 1.5 in. diameter quartz lens, and passes through the cuvette to the energy meter or a beam stop. The beam is focused 1 cm in front of the cuvette and 0.5 cm above the bottom of the cuvette. Sample size is approximately 1 cm^3 in all cases. Prefocusing the beam gives lower (3×) signals but better stability in the preamplifier output. Beam positioning is not especially critical.

The preamplifier output is amplified by a Tektronix 26A2 differential amplifier with selected frequency response of 10–300 kHz and adjustable gain from 1 to 1000. the amplifier output is processed by a PAR Model 160 boxcar averager (EG&G Princeton Applied Research, Princeton, NJ) with gate duration of 0.5–1.5 μs and gate delay of 12–14 μs. The second positive excursion of the signal is usually selected for processing as explained below. The nitrogen laser, boxcar averager, and Tektronix Model 454 oscilloscope used for setup and monitoring of the signal during the experiment are triggered with a Wavetek Model 802 pulse generator. Instrumental time constant for the boxcar averager is 100 μs giving an observed time constant of 5 s. Stock solution absorptivities were measured with a Varian 634 spectrophotometer (Varian, Palo Alto, CA). Additional laser excitation sources were (i) a Garching nitrogen laser (Garching, West Germany), (ii) a CMX-4 flash-lamp-pumped tunable dye laser (Chromatix, Sunnyvale, CA), and (iii) a Molectron DL-400 nitrogen laser-pumped tunable dye laser (Molectron Corp., Sunnyvale, CA).

The signal waveform, shown in Figure 4, is very similar to that exhibited by Tam and Patel (*10*). It consists of a damped ($\tau \sim$ 20 μs) ringing at the mechanical resonant frequency of the transducer and also contains contributions from other resonances and reflections. With the nitrogen laser operating, but with the laser output blocked, a short duration (~1 μs) RFI transient is observed with the fast oscilloscope. With a cuvette and solvent on the quartz flat and illumination unblocked, a small artifact is observed in the first 5–10 μs of the oscilloscope trace. This artifact is found to be due to scattered light; although it was feared initially that scattered light would prove to be a major problem with our "naked" transducer, this was not found to be the case. The introduction of a thin, highly light absorbing layer between the cuvette and quartz flat had no effect on the delay in the solute-generated signal. The addition of various laser dyes to the glycerol coupling fluid showed that very little scattered light

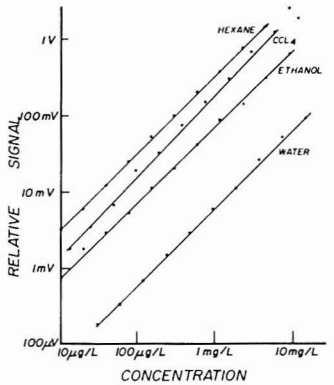


Figure 5. Photoacoustic signal vs. solute concentration for tris(2,4-pentadiono)chromium(III).

normally impinges on the transducer. In any event, the artifact could always be avoided by simply using the second positive excursion of the signal waveform for processing. Had scattered light been problematic, it would still have been possible to proceed either with a quartz piezoelectric transducer, which is not pyroelectric (*16*), or with gated damping of the transducer output with a suitable high speed switch, such as the General Electric H11F3 optically isolated bilateral analog FET switch.

As mentioned previously, 1-cm^3 liquid samples are measured, and the cuvette is removed and replaced several times to provide an average signal value. Sixteen blank values are measured and blank standard deviations are 2–4%. The % RSD values are approximately 4%. In order to set the boxcar averager gate delay, which varies with solvent due to speed of sound variations, a relatively concentrated sample solution (10–100 ppm) is used in one cuvette and the freshly prepared dilutions are then measured in a matched cuvette.

Cuvettes are cleaned by rinsing them well and immersing them in concentrated nitric acid in a beaker in a fume hood. A small (0.3 mL) quantity of absolute ethanol is added to the nitric acid which causes a vigorous boiling. The cuvettes are then copiously rinsed with large quantities of distilled, demineralized water (Barnstead Sybron Corp., Boston, MA) rinsed with absolute ethanol, and dried.

The laser dyes used are supplied by Exciton Chemical Co., Inc., Dayton, OH. The porphyrins are obtained from Sigma Chemical Co., St. Louis, MO. Privine HCl and Nupercaine HCl are supplied by Ciba-Geigy, Summit, NJ.

RESULTS AND DISCUSSION

In order to verify that the simple phenominological results derived by Tam and Patel (*10*) are applicable to our PAS system, we measured the responsivity of our system as a function of solvent. Responsivities were measured by dividing the input-referred amplitude of the first positive signal waveform excursion by the product of the incident laser pulse energy and the extrapolated solution absorptivity. The compound tris(2,4-pentadiono)chromium(III) was chosen as the solute since it is soluble in the disparate solvents used, is stable, does not luminesce, absorbs well at 337.1 nm, and is readily available in high purity (triple recrystallized). Binary dilutions were prepared and measured as indicated above. The results are shown in Figure 5. Although the preamplifier output signal, which is proportional to the responsivity, is seen to be linearly proportional to solute concentration, as expected, the hexane result is anomalously good. Consequently, solutions of tris(2,4-pentadiono)chromium(III) were prepared in 10 solvents at concentrations of approximately 1 ppm. Absorptivities were measured on the 10 ppm solutions from which

Table I. Photoacoustic Responsivities of Tris(2,4-pentadiono)chromium(III) in Several Solvents with 337.1-nm Excitation

no.	solvent	responsivity, R, mV/(mJ cm^{-1})	R_x/R_{H_2O}[b]	predicted ratios at 20 °C
1	ethanol	12.	7.8	6.0
2	methanol	17.	11.	5.6
3	carbon tetrachloride	30.	20.	14.4
4	acetonitrile	19.	13.	
5	water	1.5	1	
6	*n*-pentane	22.	15.	
7	*n*-hexane	8.5	5.8	7.7
8	*n*-heptane	17.	11.	
9	*n*-octane	14.	9.3	
10	*n*-nonane	18.	12.	

[a] R_x is the responsivity for solvent X and R_{H_2O} is the responsivity of water.

Table II. Limiting Detectable Energies, E_L, and Solution Absorptivities, α, for Several Photoacoustic Calibration Standards in Aqueous Solution with 337.1-nm Excitation (Smoky Quartz Is Included for Comparison)

compound	α, cm^{-1}	E_L, nJ
tris(2,4-pentadiono)-chromium(III)	0.665 at 15.5 ppm	230
potassium permanganate	0.095 at 13.0 ppm	31
potassium chromate	0.072 at 12.1 ppm	83
potassium dichromate	0.077 at 10.8 ppm	400
tetraamminoruthenium hydroxychlorochloride	0.022 at 10.0 ppm	97
rhodium ammonium chloride	0.002 at 13.2 ppm	80
smoky quartz		250

the 1 ppm solutions were prepared by dilution. Table I gives the measured responsivities, their ratios with that of water, and calculated values (*17*) of several of these ratios. Since the solutions were concentrated enough to afford high signal to noise ratios, blank correction was dispensed with and oscilloscopic rather than boxcar averager detection was employed. Laser pulse energy was continually monitored by using a 50% beam splitter modification of our experimental apparatus. Note that the use of ratios of solvent responsivities with respect to that of water is somewhat misleading since the responsivity of water is strongly temperature dependent. This is due to the temperature dependence of the thermal expansion coefficient of water.

In addition to the 10 solvents studied above, several others were found to be unsatisfactory for various reasons. Diethyl ether produced severe fluctuations in the preamplifier output, pyridine absorbed too strongly at 337.1 nm, and carbon disulfide was spectacularly unsuited for use as a solvent at 337.1-nm excitation wavelength. Since the laser power employed is well above the threshold for beam self-focusing in carbon disulfide (~2 kW (*18*)) and carbon disulfide is strongly absorbing at 337.1 nm, a number of unusual effects occur: the liquid bubbled vigorously, a loud clicking sound is produced, a bluish white "laser plasma" is produced, and the Suprasil cuvette is conchoidally fractured on the inner surface nearest the beam focus.

Examination of the results in Table I shows that our measured responsivity ratios agree moderately weil with the predicted ratios. The discrepancies are most likely due to variations in illuminated sample volume, variations in beam prefocusing distance, and use of first peak oscilloscopic detection rather than second peak boxcar averager detection.

Though responsivities are useful figures of merit for condensed phase PAS detection systems, the limiting detectable thermalized energy, E_L, is preferable since it contains information concerning the system noise level. These E_L values are obtained by measuring the corrected PAS signal vs. solute concentration and dividing the least-squares slope of the resulting line into three times the standard deviation of the blank; concentrations are converted to equivalent absorptivities by performing absorbance measurements on the stock solutions of the solutes. The value of E_L is then obtained by multiplying the limiting absorptivity value, α_L, by cell length, l, and by incident laser pulse energy, E_p. Alternatively, the signal may be measured vs. incident pulse energy (using neutral density filters) and the least-squares slope may be divided into three times the electronic noise level, as was done for the smoky quartz sample in Table II. The results of such calibrations are given in Table II. Although it is expected that dilute solutions of different absorbing solutes should give the same E_L value, assuming the same solvent is used, this is not seen to be verified by our data. It is possible that the discrepancies in our calibration data are due to ambient temperature changes (samples were not run on the same day) or they may be similar in origin to the aforementioned responsivity discrepancies.

Accordingly, investigations are continuing in order to determine the cause of the imprecision in the measured values of the figures of merit discussed above.

The effects of laser excitation pulse energy and pulse duration were examined and the results are shown in Table III. Considering first the effect of laser pulse duration, note that the DL-400 dye laser output is 100 times shorter than the CMX-4 dye laser output but of approximately equal pulse energy. The responsivity and E_L values are about twice as good for the DL-400 system as they are for the CMX-4 system. Although this seems to contradict the results of Atalar (*14*) that higher signal to noise ratios may be obtained by using shorter laser pulses, this result assumes that system bandwidth is commensurate with the laser pulse durations used. With the preamplifier we have used, system bandwidth is approx-

Table III. Laser Excitation Source Comparison of Limiting Detectable Energy, E_L, Responsivity, R, and Limiting Detectable Absorptivity, α_L, for Tris(2,4-pentadiono)chromium(III) in Hexane[a]

	Molectron UV-14 N_2 laser E_p = 1.6 mJ[b] τ = 10 ns[c] λ = 337.1 nm[d]	Garching N_2 laser E_p = 7 μJ τ = 1 ns λ = 337.1 nm	Molectron DL-400 dye laser E_p = 54 μJ τ = 10 ns λ = 595 nm	Chromatix CMX-4 dye laser E_p = 47 μJ τ = 1 μs λ = 595 nm
E_L, nJ	6.	5.	3.	6.
R, V/(mJ cm^{-1})	0.10	0.08	0.12	0.077
α_L, cm^{-1}	4. × 10^{-6}	7. × 10^{-4}	6. × 10^{-5}	1. × 10^{-4}

[a] Solution absorptivities were 0.460 cm^{-1} at 10 ppm (λ_{ex} = 337.1 nm) and 0.013 cm^{-1} at 100 ppm (λ_{ex} = 595 nm). [b] Incident pulse energy. [c] Incident pulse duration. [d] Excitation pulse wavelength.

Table IV. Nitrogen Laser Excited Photoacoustic Characteristics of Porphyrins and Laser Dyes at 298 K

compound	solvent	slope[a]	LOD,[b] ng/mL
bacteriochlorophyll a	ethanol	0.81	1.
bilirubin[c]	ethanol	0.62	2×10^1
biliverdin	water	1.10	0.9
chlorophyll a	ethanol	0.94	0.9
chlorophyll b	ethanol	1.06	0.3
chlorophyll water sol	water	0.98	5.
chlorophyllin	water	1.01	3.
coproporphyrin III tetraethyl ester[c]	ethanol	0.72	2.
coumarin 120[c]	ethanol	0.74	1.
cytochrome c	water	0.96	3×10^1
eosin Y	water	0.98	4.
fluorescein disodium	water	0.99	3.
hematin	water	1.06	1.
hematoporphyrin	ethanol	1.02	0.3
hemoglobin	water	0.99	7×10^1
mesoporphyrin IX dimethyl ester	ethanol	1.05	0.5
nupercaine HCl	water	0.95	1×10^1
oxazine perchlorate[c]	ethanol	0.51	3.
privine HCl	water	1.01	9×10^1
protoporphyrin IX dimethyl ester	ethanol	1.17	0.09
protoporphyrin disodium	water	0.94	1.
rhodamine 6G	water	1.00	2.
riboflavine	water	0.97	1×10^1
tetraphenylporphine[d]	ether		6.
uroporphyrin I ethyl ester[c]	ethanol	0.53	2.
vitamin B_{12}	water	1.02	4.

[a] Slope of the linear portion of the blank-corrected log-log plot of relative photoacoustic signal vs. concentration. [b] The limit of detection is equal to three times the standard deviation of the blank divided by the sensitivity. [c] Data obtained by using oscilloscopic peak detection instead of boxcar averager detection. [d] LOD estimated from a single data point with oscilloscopic peak detection. Thermal instabilities in the solvent were severe.

imately 400 kHz. Hence, the expected improvement in going from a 1-μs pulse to a 10-ns pulse is approximately

$$100(1 - e^{-[(10\text{ ns})(2 \times 400\text{ kHz})]})/(1 - e^{-[(1\ \mu\text{s})(2 \times 400\text{ kHz})]}) = 1.45$$

Our results are in reasonable agreement with the above estimate.

The results in Table III also indicate that the responsivity and E_L figures of merit are relatively unaffected by incident laser pulse energy while the limiting absorptivity values are strongly dependent on pulse energy. The α_L value shown for the UV-14 nitrogen laser system having $E_P = 1.6$ mJ is commensurate with the lowest detectable absorptivity (3.9×10^{-6} cm^{-1} at $S/N = 3$ and $E_P = 1$ mJ) given by Atalar (*14*).

Having characterized our condensed phase PAS system, we determined a number of limiting detectable concentrations for various porphyrins, laser dyes, drugs, and vitamins. The results are shown in Table IV. The materials selected were chosen for their general importance and because they exhibit widely varying luminescence yields. Since sample fluorescence could possibly cause an artifact similar to the small observed scattered light artifact, we did not expect spectacular results from such substances as Rhodamine 6G. Nevertheless, the best limit off detection concentration achieved, i.e., ~90 ppt for protoporphyrin IX dimethyl ester, is quite good despite the rather high slope of the analytical curve. Our detection limit for vitamin B_{12} was 4 ppb (3×10^{-9} M) which is commensurate with the reported value of 2×10^{-9} M by chemiluminescence (*19*). Our value of 0.5 ppb (9×10^{-10} M) for mesoporphyrin IX dimethyl ester is commensurate with the value of 1.2×10^{-9} M ($S/N = 3$) reported by Hershberger et al. (*20*) using a windowless flow cell arrangement.

Although we do not expect to surpass fluorescence detection techniques, we have demonstrated that nonluminescing substances may be conveniently detected at the parts-per-billion level or below, depending on laser pulse energy, in a simple, easily cleaned PAS cell.

ACKNOWLEDGMENT

The authors would like to acknowledge the kind assistance of Andrew Tam, who supplied the preamplifier schematic from which our circuit was adapted. We also which to thank C. K. N. Patel for bringing the "C-clamp" mounting arrangement for a cuvette cell to our attention at the 1979 FACSS meeting in Philadelphia.

LITERATURE CITED

(1) Rosencwaig, A.; Gersho, A. *J. Appl. Phys.* **1976**, *47*, 64–69.
(2) Lin, J. W.-p.; Dudek, L. P. *Anal. Chem.* **1979**, *51*, 1627–1632.
(3) McClelland, J. F.; Kniseley, R. N. *Appl. Opt.* **1976**, *15*, 2967–2968.
(4) Callis, J. B.; Gouterman, M.; Danielson, J. D. S. *Rev. Sci. Instrum.* **1969**, *40*, 1599–1605.
(5) Hordvik, A.; Schlossberg, H. *Appl. Opt.* **1977**, *16*, 101–107.
(6) Lahmann, W.; Ludewig, H. J.; Welling, H. *Anal. Chem.* **1977**, *49*, 549–551.
(7) Bonch-Bruevich, A. M.; Razumova, T. K.; Starobogatov, I. O. *Opt. Spectrosc.* **1977**, *42*, 45–48.
(8) Farrow, M. M.; Burnham, R. K.; Auzanneau, M.; Olsen, S. L.; Purdie, N.; Eyring, E. M. *Appl. Opt.* **1978**, *17*, 1093–1098.
(9) Oda, S.; Sawada, T.; Kamada, H. *Anal. Chem.* **1978**, *50*, 865–867.
(10) Tam, A. C.; Patel, C. K. N. *Appl. Opt.* **1979**, *18*, 3348–3358.
(11) Patel, C. K. N.; Tam, A. C. *Appl. Phys. Lett.* **1979**, *34*, 467–470.
(12) Patel, C. K. N.; Tam, A. C.; Kerl, R. J. *J. Chem. Phys.* **1979**, *71*, 1470–1474.
(13) Tam, A. C.; Patel, C. K. N. *Opt. Lett.* **1980**, *5*, 27–29.
(14) Atalar, A. *Appl. Opt.* **1980**, *19*, 3204–3210.
(15) Tam, A. C.; Patel, C. K. N.; Kerl, R. J. *Opt. Lett.* **1979**, *4*, 81–83.
(16) Neubert, H. K. P. "Instrument Transducers"; Oxford at the Clarendon Press, Oxford, 1963.
(17) "CRC Handbook of Chemistry and Physics", 49th ed.; The Chemical Rubber Co.: Cleveland, OH, 1968.
(18) Yariv, A. "Quantum Electronics", 2nd ed.; Wiley: New York, 1975.
(19) Sheehan, T. L.; Hercules, D. M. *Anal. Chem.* **1977**, *49*, 446–450.
(20) Hershberger, L. W.; Callis, J. B.; Christian, G. D. *Anal. Chem.* **1979**, *51*, 1444–1446.

RECEIVED for review January 2, 1981. Accepted May 6, 1981. This work was supported by NIH-GM11373-17 and by DOE-AS05-78EV06022 MOD A00E.

Automated Determination of Ammonia by Gas-Phase Molecular Absorption

Prem N. Vijan* and George R. Wood

Laboratory Services Branch, Ontario Ministry of the Environment, 125 Resources Road, Rexdale, Ontario, Canada M9W 5L1

Strong absorption at 197.2 nm by traces of ammonia in a continuous stream of nitrogen forms the basis of this method. Automation is achieved by interfacing an automatic sampler, a multichannel peristaltic pump, an adjustable heating bath, and a gas–liquid separator to an atomic absorption spectrophotometer. Ammonium ions react with a strong base and release ammonia which is purged out of solution and passed through a windowless heated absorption cell. The absorbance is recorded. The method is relatively free from interferences and has a sensitivity of 0.26 and a detection limit of 0.10 μg NH_3/mL, respectively. The calibration curve is linear between 0 and 40 ppm. Chemical conversion into ammonium form is a prerequisite for determining total organic nitrogen. Typical results obtained on some environmental samples for ammonium and total organic nitrogen are presented. Twenty samples can be analyzed in 1 h.

The most widely used routine methods for determining ammonia are based on the formation of colored complex compounds with hypochlorite–phenate (*1*) and Nessler's reagent (*2*). More recently, gas-sensing electrodes (*3*), ion chromatography (*4*), and gas diffusion (*5*) methods have been used for this purpose. The colorimetric methods are susceptible to interference by heavy metals and colored organic species present in sample solutions. A pretreatment step in the procedure is required to eliminate such interferences. The other two methods require strict pH control and can tolerate only a low concentration of heavy metal cations and organic compounds. The gas diffusion method is time-consuming and not quite so sensitive.

Cresser (*6–8*) utilized the well-known characteristic UV absorption bands of gaseous ammonia for its determination in solutions. His method is manual and involves considerable manipulation, including a 30-min thermostating of the prepared sample solution prior to the measurement step. The conversion/evolution efficiency of ammonium ions to ammonia gas is poor at the near ambient temperature used. His method is highly dependent on variables such as bubbler design, bubbler depth, and slit width. Muroski and Syty (*9*) confirmed the findings of Cresser whereas Takahashi et al. (*10*) improved the sensitivity by using a 1 m long absorption cell, a higher temperature for generating ammonia gas, and a nitrogen trap for separating ammonia from water vapor.

This paper concentrates on automation and further refinement of Cresser's approach and also its application to the determination of ammonia in environmental samples including heavily contaminated waste waters and effluents.

EXPERIMENTAL SECTION

Apparatus. A Varian Techtron Model AA-5 atomic absorption spectrophotometer (Varian Associates, Palo Alto, CA) equipped with a Corning 840 recorder was used for absorption measurements. An arsenic hollow cathode lamp was used as a source of radiation. A hydrogen lamp was used as a continuum light source for scanning the absorption spectrum of ammonia. A windowless quartz "T" cell, 10 cm × 0.6 cm i.d. with a 16 cm × 0.3 cm i.d. inlet tube, was used as an absorption cell. The cell was wound with 4 m of No. 7 Chromel "C" wire (Fisher scientific) to which approximately 10 V were applied by means of a variac transformer to maintain a temperature of 160 °C. A 100-W heating tape was used to heat the inlet tube of the "T" cell. The latter was fastened to the burner head and aligned with the hollow cathode lamp and the monochromator using the burner controls. The Technicon autoanalyzer (Terrytown, N.Y.) proportioning pump, sampler, and heating bath (20 ft glass coil) modules were used to automate the chemical procedure. The gas–liquid separator used is described elsewhere (*11*). A precision flow meter was used to control the carrier gas flow rates. The schematic of the instrumental setup is shown in Figure 1.

Table I. Operating Conditions

Spectrophotometer	
wavelength setting, 197.2 nm	
mode, absorbance	
response time, 5 s	
lamp current, 7 mA	
spectral bandwidth, 1 nm	
Recorder	
sensitivity, 1 and 10 mV full scale	
chart speed, 30 cm/h	
Proportioning Pump and Automatic Sampler	
sampling cycle, 1 min	
wash cycle, 2 min	
Heating Bath	
temperature, 98 °C	

Reagents. All chemicals used were of A.R. grade. Sodium hydroxide used was a 50% w/w solution supplied by Fisher Scientific Co. A 1000 μg NH_3/mL stock standard was prepared by dissolving 3.1573 g of NH_4Cl (Baker Analyzed Reagent 99.5%) in water and making up to 1 L. Working standards were prepared by serial dilution. Purified compressed argon and nitrogen were used as carrier gases.

Procedure. The operating parameters for the various parts of the instrument are shown in Table I. The hollow cathode lamps, the "T" cell, and the heating bath are allowed sufficient time to warm up and reach equilibrium temperature conditions. The manifold tubes of the proportioning pump are lowered into the appropriate reagent bottles and the solutions are allowed to flow until a stable base line is established on the recorder.

Sample Preparation. For the determination of free ammonia in sewage samples, a 10-mL aliquot of the clear supernatant is acidified with a few drops of concentrated nitric acid, boiled, and brought back to the same volume. The samples thus prepared are transferred to the autoanalyzer cups for analysis. For determining total organic nitrogen in sewage, sediment, and vegetation samples, aliquot portions are digested according to Kjeldahls' procedure. This procedure is essentially the same as described by Muroski and Syty (*9*). Hi-Vol filter aliquots are extracted with hot 1% sulfuric acid solution prior to analysis. The handling and treatment of these air particulate filters are adequately covered in ref 11. Precipitation samples require no preparation at all. A set of calibration standards is run along with each set of samples, and the concentrations of ammonia are read from a standard curve of peak heights vs. concentrations.

RESULTS AND DISCUSSION

The Autoanalyzer AAS System. The reagent and sampling part of the system consists of Technicon autoanalyzer sampler and proportioning pump modules. Sequencing and timing of the sample and wash cycles are controlled by the two-lobe cam. The proportioning pump is a seven-channel

0003-2700/81/0353-1447$01.25/0 © 1981 American Chemical Society

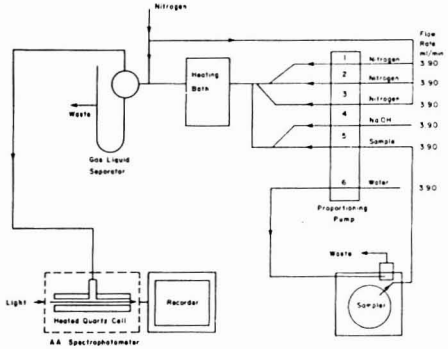


Figure 1. Schematic of autoanalyzer–AAS system for ammonia.

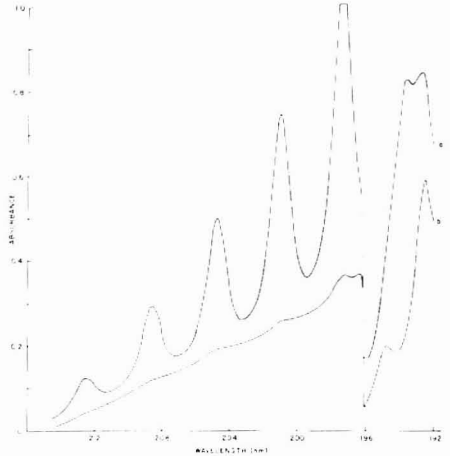


Figure 2. Scan of the absorption spectra: (a) with ammonia, (b) without ammonia.

model and works by forcing liquid through flexible tubes pinched between a pressure plate and a movable roller system. Six identical channels are used, each capable of pumping 3.90 mL/min of solution.

The sample stream (channel 5) and the reagent stream (channel 4) merge on leaving the pump. The resulting mixture at this point contains 37.4% WV NaOH. Nitrogen is next introduced through channels 1, 2, and 3. The nitrogen segments the liquid stream and helps to push it through the heating bath. The 98 °C temperature of the bath aids in the conversion of ammonium ion to ammonia gas as well as its subsequent evolution from solution. Downstream from the heating bath a flow controlled nitrogen stream (145 mL/min) is introduced which sweeps the mixed gas–liquid stream into a separator. The sweep gas containing ammonia is directed into the heated "T" cell while the liquid portion is emptied into a waste container. During the wash phase the cam activates the probe causing it to enter the wash reservoir for 2 min. This establishes a base line between sampling cycles.

Condensation of water vapor in the inlet tube of the "T" cell reabsorbs ammonia and obstructs the smooth flow of gases, thus causing base line drift, peak distortion, and tailing. The optimum temperature of the horizontal limb of the "T" cell was found to be 160 °C in order to overcome this problem.

If fully automatic operation is not desired, the user may manually present the solution to the sample channel and, thus, do away with the automatic sampler.

Figure 2 represents the absorption spectrum of ammonia between 190 and 215 nm using a hydrogen hollow cathode lamp as the source of radiation. Sharp absorption bands, 3.8 nm apart, are seen at 193.4, 197.2, 201.0, 204.8, 208.6, and 212.4 nm. The scans appear to be somewhat different in appearance from those reported by Cresser (6) as well as Muroski and Syty (9). These authors recorded their spectra with UV spectrophotometers equipped with compensating reference channels. The scans shown in Figure 2 are seen by the single beam measuring instrument. Curve "a" is the characteristic absorption spectrum of ammonia in air, uncorrected for background absorption. Curve "b" shows absorption characteristic of the carrier gas which is largely air, since the light beam travels a long distance through air before reaching the detector. The split peaks shown by Cresser are not seen in curve "a".

The first two absorption peaks happen to coincide with the two principal resonance lines of arsenic. Therefore, an arsenic hollow cathode lamp can be used as a suitable light source at 193.7 and 197.2 nm. This was also demonstrated by Cresser (7). However, contrary to his observation, we found that the radiant output of the arsenic lamp at a given lamp current and slit width was greater than the hydrogen lamp. Also, it performed equally well at both wavelengths. This may be attributed to the differences in the condition and characteristics of the lamps used. The lower curve in Figure 2 was obtained with the exclusion of ammonia from the gas stream. The half-widths of the absorption peaks of ammonia were found to be very similar to those of the emission lines from the arsenic lamp, recorded under identical instrument conditions. Gases other than ammonia absorb strongly at wavelengths shorter than 193.7 nm (curve "b"). On the longer wavelength side, an absorption minimum is reached at 215 nm. The differences between on-peak and off-peak absorptions for all absorption bands in Figure 2 are large enough to be of analytical value. The sensitivities of ammonia measurement, at the above stated absorption maxima, expressed as ratio of the sensitivity at 193.4 nm are 1.0, 0.80, 0.60, 0.34, and 0.16 in the order of increasing wavelengths. For this work 197.2 nm was chosen because it satisfies the sensitivity requirements and yet is favorably removed from an equally sensitive and usable 193.4-nm line. The absorption spectrum allows a wide choice of wavelengths to suit the concentration range of different types of samples.

A maximum available spectral band width (SBW) of 1 nm was used in this work to allow for the use of a lower instrument gain setting. Cresser (7) stated that the slit width was very critical. We found that, using a hydrogen lamp, the sensitivities at SBW of 1.0, 0.75, and 0.35 are only 20, 10, and 5% lower than at 0.15 nm. Figure 3 shows a few typical absorption peaks of calibration standards. The standard curve is linear up to 40 μg NH_3/mL and then starts bending toward the concentration axis. The base line is stable enough to allow 10-fold expansion of the signal for better accuracy at low concentrations.

The Effect of Sodium Hydroxide Concentration. The absorption at 197.2 nm by ammonia molecules increases linearly with the increase in concentration of sodium hydroxide solution from 10% to 50%. The absorbance signal obtained by the use of 10% sodium hydroxide was approximately 2.5 times less than the one obtained by 50%. Further increases beyond this concentration were not attempted as the solution becomes too viscous to be handled conveniently by the proportioning pump. The sodium hydroxide solution is mixed

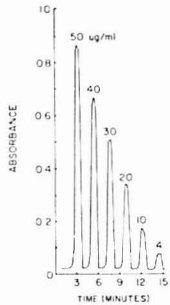


Figure 3. Absorbance peaks of calibration standards at 10 mV full scale recorder setting.

in a 1:1 ratio with the sample solution, and therefore its effective concentration is 37.4% compared with 40% used by Cresser (*6*), in his manual method. Such a comparison, however, is unfair because of the basic differences between the two approaches and the fact that the absorption maximum was the combined result of reaction temperature, carrier gas flow rate, and sodium hydroxide concentration. Because of the lubricating nature of the sodium hydroxide solution, it is important that the various connections between glass parts and manifold tubings are well secured by twisting pieces of wire around them.

Effect of Temperature. The temperature of the sodium hydroxide and sample solution has a substantial effect on the rate of evolution of ammonia and, hence, on its absorbance signal. Cresser (*6, 7*) has adequately demonstrated this fact. However, because of the condensation problem in his method, he was unable to use the optimum temperature. Muroski and Syty (*9*) used no heat at all which explains an order of magnitude lower sensitivity of their method (3.92 vs. 0.37 μg/mL) compared with Cresser's improved method (*7*). The proposed method is approximately twice as sensitive as Cresser's after accounting for the use of a 33% longer absorption cell.

An optimum temperature of 98 °C was used in our method. Higher temperatures resulted in blowouts, thus making smooth operation of the system difficult. The absorbance of a 10 μg NH_3/mL solution decreased almost linearly as the temperature was reduced to 50 °C. Similar observations were made by Cresser (*6*).

Carrier Gas. Nitrogen was used as the carrier gas in this work. Substitution of nitrogen by more expensive argon did not offer any advantage. Ammonia-free air may also be used for this purpose. The optimum flow rate for maximum signal was found to be 145 mL/min. An accurate control of carrier gas flow is necessary for precise results. An increase in nitrogen flow from 145 to 580 mL/min causes a 25% reduction in the absorbance signal. Lower flow rates result in larger base line drift. Introduction of the carrier gas upstream from the heater module tends to push the reagents too rapidly and is not desirable. Nitrogen is also drawn in at the rate of 11.7 mL/min by the proportioning pump which serves to segment the liquid stream and carries liberated ammonia through the heater coil. Three nitrogen lines furnish smoother absorption peaks as opposed to one or two lines.

Interference. Various amounts of a composite heavy metal solution were added to a 20 μg NH_3/mL standard solution to give final concentrations of: 5 ppm each of zinc, copper, nickel, lead, cobalt, manganese, chromium; 20 ppm of nickel and iron; and 1 ppm of cadmium and 1000 ppm of potassium. These levels of the metals specified produced no interference. Volatile organic compounds, such as methanol and acetone, interfere by absorbing the UV radiation. Boiling the acidified sample solution prior to analysis completely removed this interference. This is demonstrated by the results obtained on boiled and unboiled samples (Table II). The unboiled samples obviously contain volatile organic compounds which absorb at the same wavelength as ammonia. Hydrazine (250 μg/mL) did not interfere. However high concentrations of nitrogenous compounds such as plasma proteins which may evolve ammonia on reaction with strong NaOH at high temperatures will likely interfere.

Table II. Free Ammonia in Sewage Effluents (μg NH_3/mL)

GMPA[a] method		
raw	boiled	Conway method
34.0	32.4	35.0
38.9	24.8	27.8
11.6	11.0	11.8
8.9	8.2	9.0
8.7	8.2	10.7
43.0	45.6	42.0
10.9	10.9	10.8
13.9	13.8	13.0
20.0	19.7	17.7

[a] Gas-phase molecular absorption.

Table III. Spike Recovery of Ammonia (μg/mL)

sample	present	added	found	% recovery
1	1.13	2.00	3.20	103.5
2	0.57	2.00	2.72	107.5
3	0.49	2.00	2.59	105.0
4	1.16	2.00	3.23	103.5
5	0.95	2.00	3.08	106.5
6	0.49	2.00	2.51	101.0
av recovery				103.7

Table II also demonstrates good agreement between gas-phase molecular absorption (GPMA) and Conway methods. The method described in ref 5 is an improved version of the Conway method. This method is based on the slow diffusion of gaseous ammonia from an alkylated ammonium solution into a standard acid solution. The excess acid is titrated with standard alkali by means of a microburet. The whole operation takes place inside a container called the "Conway dish" (Fisher Scientific) with three concentric chambers.

Table III contains the results of a recovery study. The data show a slight bias toward the higher side. A mean recovery of 103.7% is quite satisfactory in view of the fact that the concentrations of ammonium ions present in the samples and those added from outside were low.

A study was carried out to establish the extent of conversion and evolution of ammonia gas from ammonium ions in solution under the optimized experimental conditions. Ammonia evolved from a standard solution was absorbed in a known volume of standard hydrochloric acid, and the excess acid was back-titrated with a standard alkali solution. A conversion efficiency of 62.5% was obtained.

Table IV contains data obtained on sediments digested by the Kjeldahl method. Ammonia was determined by the present method and the indophenol blue method by two different laboratories. The agreement is satisfactory and does not show bias.

Table V contains some typical results obtained on Hi-Vol air filters and precipitation samples.

Precision, Sensitivity and Detection Limit. The relative standard deviation of 10 measurements taken at 20 μg NH_3/mL and 4 μg NH_3/mL were 1.23% and 0.91%, respectively. The practical as well as the calculated detection limits

Table IV. Nitrogen in Kjeldahl Digested Sediments (μg/g)

present method	indophenol blue method	present method	indophenol blue method
1.96	2.20	2.78	2.70
6.21	6.50	0.27	0.30
1.67	1.70	2.30	2.30
3.31	3.40	0.25	0.30
2.47	2.40	0.21	0.20

Table V. Ammonia in Environmental Samples

amt of NH_3 as particulate[a] in air, μg/m³	amt of NH_3 in rainwater, μg/mL
0.44	0.59
5.80	0.50
0.70	0.38
6.55	0.57
0.50	0.15
5.63	0.82
0.35	0.39
0.65	1.77
5.79	0.14
0.49	0.10
0.54	0.10

[a] Collected on Hi-vol filters.

(twice the standard deviation at or near zero concentration) are close to 0.10 μg/mL). The sensitivity as calculated from the slope of the standard curve is 0.26 μg NH_3/mL. It may be further increased by using a longer absorption cell.

Comparison of Proposed Method with Manual Methods. The sensitivity of the automated method is significantly greater than that of Muroski and Syty's manual method and 27% greater than Cresser's improved method. The base line stability is superior. The ammonia absorption signals can be recorded with equal ease and sensitivity at the 193.7- and 197.3-nm arsenic lines. The proposed method is faster and more sensitive than Cresser's improved method which requires 30 min of thermostating and is subject to the effect of variables such as configuration, depth and dead volume of the bubbler, slit width, heat of neutralization, etc. Although Muroski and Syty's manual method (*9*) is fast, it is 15-fold less sensitive. As opposed to the transient signals generated by the manual methods, the proposed method produces steady-state signals and provides complete recording of sequential events in a continuous manner. This feature is very useful in assessing the performance of the system. The appearance of signal peaks and base line assists in diagnosing problems, if any should arise. The most desirable feature of the automated method is its manipulation-free unattended operation. The system is very rugged, and up to 140 determinations can be performed in 1 man day. The sampler module can be eliminated if fully automatic operation is not desired. In this mode, the sample can be presented manually to the sample probe.

LITERATURE CITED

(1) Crowther, J.; Evans, J. *Analyst (London)* **1980**, *105*, 841.
(2) Vogel, A. I. "A Textbook of Quantitative Inorganic Analysis", 3rd ed.; London W-1, 1961; p 783.
(3) Orion Research "Analytical Methods Guide", 9th ed.; 1978; p 33.
(4) Bouyoucos, S. A. *Anal. Chem.* **1977**, *49*, 409.
(5) Obrink, K. J. *Biochem. J.* **1955**, *59*, 134.
(6) Cresser, M. S. *Anal. Chim. Acta* **1976**, *85*, 253.
(7) Cresser, M. S. *Lab. Pract.* **1977**, 19.
(8) Cresser, M. S. *Analyst (London)* **1977**, *102*, 99.
(9) Muroski, C. C.; Syty, A. *Anal. Chem.* **1980**, *52*, 143.
(10) Takahashi, M.; Tanabe, K.; Saito, A.; Matsumoto, K.; Haraguchi, H.; Fuwa, K. *Can. J. Spectrosc.* **1980**, *25*, 25.
(11) Vijan, P. N.; Wood, G. R. *At. Absorpt. Newsl.* **1974**, *13*, 33.

RECEIVED for review January 30, 1981. Accepted April 20, 1981.

Determination of Mercury at the Ultratrace Level by Atmospheric Pressure Helium Microwave-Induced Plasma Emission Spectrometry

Kiyoshi Tanabe, Koichi Chiba, Hiroki Haraguchi,* and Keiichiro Fuwa

Department of Chemistry, Faculty of Science, University of Tokyo, Bunkyo-ku, Tokyo 113, Japan

Atmospheric pressure helium microwave-induced plasma emission spectrometry has been applied to the determination of mercury, where the cold vapor generation technique was employed for generation of mercury from the solution. The detection limit was 4 pg/mL or 8 pg, and the dynamic range of the calibration curve was 2×10^5. The relative standard deviation of 10 replicate measurements using 100 pg/mL standard solution was about 2%. The interferences of some cations with the mercury determination were negligible except for Pt^{2+} and Pd^{2+}. The present method was applied to the determination of mercury in bovine liver (SRM 1577 from NBS), and analytical data were consistent with the certified value.

Current environmental concern with the danger of mercury pollution has accelerated progress of analytical methods for mercury. Especially in the field of atomic absorption spectrometry, the cold vapor generation technique has been developed to determine mercury at the sub-part-per-billion (ng/mL) level (*1–4*), and such a method has been extensively applied to mercury analysis in various samples. Furthermore, such a technique has also been used for atomic fluorescence spectrometric determination of mercury, and has also provided great detection capability of mercury at the sub-part-per-billion level (*5, 6*). In spite of extensive studies, the cold vapor generation technique utilizing the amalgamation trap for preconcentration has been required for the determination of mercury in some natural samples (e.g., seawater), which contain mercury only at a few parts-per-trillion (pg/mL) level (*7–9*). However, this kind of preconcentration methods has many chances of loss or/and contamination of mercury. Therefore, improved methods are required for the direct determination of mercury at such low-level concentrations without resorting to tedious preconcentration procedures.

0003-2700/81/0353-1450$01.25/0 © 1981 American Chemical Society

Recently, the present authors reported vacuum-ultraviolet (VUV) atomic absorption spectrometry of mercury with cold vapor generation technique (*10*), where the resonance line at 185.0 nm used for the absorption measurements. The VUV atomic absorption spectrometry was more sensitive by about 5 times than the conventional methods utilizing the atomic line at 253.7 nm. This method, however, was still not sensitive enough to determine mercury directly at the parts-per-trillion level.

On the other hand, in the field of atomic emission spectrometry, various types of plasmas, such as inductively coupled plasma (ICP), microwave-induced plasmas (MIP), and direct current plasma (dc plasma), have been used for the determination of mercury (*11–21*). The use of the cold vapor generation technique has also improved the analytical sensitivity of mercury by plasma emission spectrometry. Lichte and Skogerboe reported the detection limit of 60 pg (6 pg/mL) by argon MIP emission spectrometry with the cold vapor generation technique (*15*), and Braman obtained the detection limit of 0.4 ng (4 pg/mL) by dc helium plasma emission spectrometry with the membrane probe cold vapor generation technique (*17*).

In 1976, a new type of cavity (TM_{010} type) for MIP was developed (*22*) and the helium plasma at atmospheric pressure sustained by the cavity has been investigated as an excitation source for both metallic and nonmetallic elements (*21, 23–29*). According to these investigations, the excitation efficiency of this new helium MIP is generally about an order of magnitude higher for most elements than those of the plasmas previously used for atomic emission spectrometry. Quimby et al. used the atmospheric pressure helium MIP as an element-selective detector for gas chromatography and obtained the detection limit of 1 pg/s for mercury (*21*). However, the determination of ultratrace mercury in solution by atmospheric pressure helium MIP emission spectrometry with the cold vapor generation technique has not been investigated yet. Hence, the present authors applied the atmospheric pressure of helium MIP to the determination of mercury with the cold vapor generation technique to realize the direct determination of mercury at the parts-per-trillion level without any preconcentration method.

EXPERIMENTAL SECTION

Chemicals. A stock solution of mercury (10 μg/mL) was prepared by dissolving mercury(II) chloride in 3% (w/v) hydrochloric acid. All the standard solutions were obtained by properly diluting the mercury stock solution with 1% HCl solution, while standard solutions with concentrations lower than 10 ng/mL were diluted with subboiling water to avoid contamination from hydrochloric acid. All the mercury solutions prepared were analyzed within 6 h. A 3% $SnCl_2$ in 1% HCl solution was used as the reducing agent.

Instrumentation. For the present experiment, the measurement system used previously for the determination of nitrogen was employed without any modification (*28*). The microwave generator (Model MR-3S from Ito Chotanpa Co., Ltd., Japan), which provided 20–200 W of microwave power at 2.45 GHz, was generally run at 75 W forward power in the present experiment. Reflected power could be tuned to a minimum (13 W) with the tuning screws on the cavity, and no additional tuning device was used. The carrier helium gas for the gas generation was commonly used as the plasma gas. The flow rate of helium gas was in the range of 0.25–1.0 L/min, when a silica tube of 6 mm o.d. and 3 mm i.d. was used for the plasma discharge tube. The cavity (laboratory constructed) was mounted on a pedestal which could move both vertically and horizontally for the adjustment of the observation position. The 1:1 image of the plasma (axially viewed) was focused on the entrance slit of the monochromator (Model JE-50E from Nippon Jarrell-Ash Co., Ltd.). The slit width and height of the entrance slit were 10 μm and 1.5 mm, respectively, and those of the exit slit were 10 μm and 10 mm, respectively. In the present system, the spectral band pass of the monochromator was 0.02 nm. The mercury atomic line at 253.7 nm was used for the analysis. The time constant of the readout system was 0.3 s.

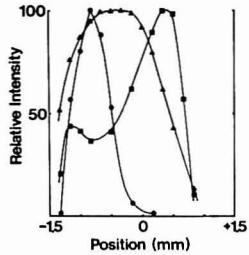


Figure 1. Spatial distributions of emission intensities of He I, Hg I, and Hg II: (●) He I 388.9 nm, (■) Hg I 253.7 nm, (▲) Hg II 194.2 nm.

Procedures. At first, the carrier gas was flowed through the bypass. Then the washed reaction vessel was connected to the gas generation system, and the carrier gas was directed to the reaction vessel by switching the two synchronous electromagnetic three-way valves. First, the plasma was extinguished by the excess air in the vessel, and so the gas flow was switched back from the reaction vessel to the bypass. After a few seconds, self-initiation of the plasma occurred, and then the carrier gas was directed again to the reaction vessel. This procedure had to be repeated a few times until the air was almost completely removed and the plasma could be stably sustained with the carrier gas flowing through the vessel. Next, 0.5 mL of the reducing solution (the tin chloride solution) was injected with a syringe into the reaction vessel through the side wall rubber septum and was bubbled with helium gas from about 15 s to remove mercury and air dissolved in the reducing solution. The completion of the degassing was confirmed by monitoring the emission signal at 253.7 nm. After the degassing, 2 mL of sample solution was injected with a syringe into the vessel through the side wall septum. The generated mercury vapor was led into the plasma with carrier helium gas (which was also the plasma gas at the same time) and the emission signal was observed. The signal was measured as the peak height on the recorder chart. The silicone rubber septum could be used for about 50 measurements.

RESULTS AND DISCUSSION

Spacial Distributions of Emission Intensities in the Plasma. The spacial distributions of the emission intensities of the mercury atomic line (Hg I; 253.7 nm), mercury ionic line (Hg II; 194.2 nm), and helium atomic line (He I; 388.9 nm) in the plasma were investigated in order to find the optimum position for the measurement. During the measurement of the emission intensity distributions, mercury vapor was constantly introduced into the plasma by the vaporization of metallic mercury at room temperature with flowing the carrier/plasma helium gas (0.5 L/min). The results are illustrated in Figure 1. The abscissa of Figure 1 indicates the distance from the center of the discharge tube; 0 mm corresponds to the center, ±1.5 mm corresponds to the wall of the discharge tube. It should be noted that the emission intensities in Figure 1 are not real ones, i.e., they are normalized by taking the maximum intensity for each line as 100. As can be seen from the figure, the center of the plasma, at which the helium atomic line was most intense, was slightly apart from the center of the discharge tube (*30*).

The emission intensity profile of the mercury atomic line was broad as twice as that of the helium atomic line and provided two peaks. It showed the large dip near the center of the plasma. The large dip of the emission profile, which means the less population of mercury atoms, may be caused by extensive ionization of atoms near the center of the plasma. Therefore, the position for the measurement of mercury atomic line was preferable near 0.5 mm from the center of the

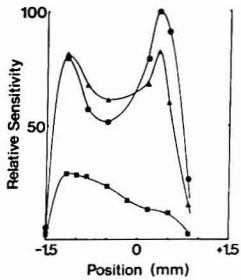


Figure 2. Dependence of analytical sensitivity on the measurement position investigated at three different helium gas flow rates: (▲) 0.25 L/min, (●) 0.5 L/min, (■) 1 L/min.

discharge tube at which the mercury atomic line was most intense.

On the other hand, the emission intensity profile of the mercury ionic line which was also broad similar to that of the atomic line has only one peak near the center of the plasma. However, the actual intensity of the ionic line was about 2 orders of magnitude weaker than that of the atomic line. Thus, the mercury ionic line could not be used for the analysis.

Optimization of Experimental Conditions. According to the previous works employing mercury cold vapor generation techniques (*2–4*), the influences of the carrier gas flow rate, the solution volume in the reaction vessel, and the volume of the reaction vessel on the analytical sensitivity must be generally taken into account. Furthermore, it has been reported that the sensitivity of the helium MIP emission spectrometry is significantly dependent on the plasma gas flow rate (*23, 24, 28*). Therefore, the experimental conditions for the cold vapor generation and the plasma parameters were examined to achieve better analytical sensitivity for mercury analysis.

Volume of the Reaction Vessel. In general, the use of the smaller volume reaction vessel provided better sensitivity in the gas generation experiment. This may be due to less dilution of generated mercury vapor in the dead space of the reaction vessel. Therefore, a 20-mL reaction vessel was used in this experiment.

Solution Volume. Using the smaller solution volume is generally advantageous to obtain better sensitivity. It was reported in the previous paper (*28*) that the use of solutions more than 3 mL made the sensitivity worse in the analysis of nitrogen with the similar experimental system. Consequently, the volumes of the reducing solution and the sample solution were made up to be 0.5 and 2 mL, respectively.

Flow Rate of Helium Gas. The dependence of analytical sensitivity on the measurement position in the plasma was investigated at three different flow rates of helium gas, i.e., 0.25, 0.5, and 1 L/min, where the 0.5 ng/mL mercury standard solution was used. The results are shown in Figure 2. The results obtained at the flow rates of 0.25 and 0.5 L/min are almost identical with each other. At the flow rate of 1 L/min, however, analytical sensitivity was significantly decreased at any point in the plasma. Particularly, the sensitivity was poor near the center of the discharge tube, at which the maximum sensitivity was obtained at the lower flow rates. This may be interpreted by the cooling effect of helium gas on the plasma or by the short residence time of mercury in the plasma because of too rapid gas flow near the center of the discharge tube.

The optimum measurement position was near 0.3 mm from the center of the discharge tube in both cases of the flow rates of 0.25 and 0.5 L/min. However, at the former flow rate, the analytical signal profiles were broad and the standard deviation of the measurements was not good. Therefore, the flow rate of carrier/plasma helium gas was chosen to be 0.5 L/min.

Table I. Detection Limits and Standard Deviations at Different Helium Gas Flow Rates

He gas flow rate, L/min	detection limit, pg/mL	std dev,[a] %
0.25	4.2 (8.4 pg)[b]	3.1
0.5	4.1 (8.2 pg)	1.9
1.0	6.4 (12.8 pg)	6.1

[a] Standard deviation obtained at 0.1 ng of Hg/mL.
[b] Detection limit represented by the absolute amount of mercury.

Detection Limit and Dynamic Range. The detection limits (defined as the signal level of mercury corresponding to twice the standard deviation of the blank signal) and dynamic ranges were investigated at three different flow rates of helium gas. The results are summarized in Table I. As can be seen from Table I, the best detection limit and the dynamic range of 8 pg (or 4 pg/mL) and 2×10^5, respectively, were obtained at the gas flow rate of 0.5 L/min. The detection limit of 4 pg/mL may be the best one obtained in the measurement system without any preconcentration. The dynamic range of 2×10^5 is about 3 orders of magnitude wider than that obtained with atomic absorption spectrometry (*28*). The relative standard deviation of 10 repeated measurements using the 0.1 ng/mL mercury standard solution was about 2%.

Blank Problems. When the analysis is preformed at extremely low concentration, the blank from the solutions, reagents, and environments significantly influence the analytical results. Furthermore, the blank restricts the detection limit of the method. In the helium MIP emission spectrometry of mercury, there are two possibilities for blank contributions, i.e., contaminated mercury and dissolved nitrogen in the solutions. The latter provides the emission of the NO band near 253.7 nm. Actually, 2 mL of distilled water gave the apparent signal equivalent to about 0.03 ng of mercury. In order to elucidate the origin of this blank signal, the spectral profiles of the blank signal and the signal of 0.5 ng/mL mercury standard solution were measured. The results are shown in Figure 3 (top). The spectral profile of the blank signal had no peak at 253.7 nm, but it showed some background emission which decreased toward the shorter wavelength. The characteristics of the profile indicates that the blank signal is mainly due to the band emission. As can be seen in Figure 3 (bottom), the interfering band emission is ascribed to that of NO double-headed bands in the "γ system", which have the band heads at 255.0, 255.9, 258.8, and 259.6 nm.

This problem can be overcome by injecting the solutions in the reverse order as follows (see Experimental Section): First, sample solution should be taken in the reaction vessel and degassed for about 10 s. Then, the reducing solution previously degassed should be injected into the vessel.

As an alternative method to reduce the influences of the band emission due to the dissolved nitrogen, simultaneous background correction may be taken into account. If the problem of the NO band emission could be avoided, the detection limit of the present method may be improved to less than 1 pg (<0.5 pg/mL).

Interferences. The effects of various salts and cations possibly coexisting in natural waters or disgested biological samples were examined to know their interferences with mercury determination. The samples containing 0.5 ng of Hg/mL were analyzed in the presence of NaCl (2%), KCl (1%), Mg^{2+} (1000 μg/mL), Ca^{2+} (1000 μg/mL), Cu^{2+} (200 μg/mL), Ni^{2+} (200 μg/mL), Pd^{2+} (10 or 1 μg/mL), or Pt^{2+} (10

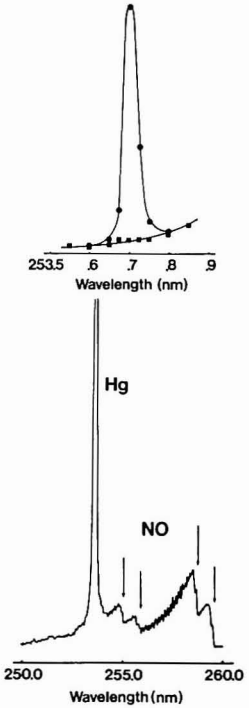


Figure 3. (Top) Spectral profiles of blank and mercury emission signals: (■) blank signal, (●) the signal for mercury standard solution (0.5 ng/mL). (Bottom) MIP emission spectrum near the mercury analytical line at 253.7 nm.

or 1 μg/mL). The results obtained were similar to those reported previously for mercury atomic absorption spectrometry with the cold vapor generation technique. As described in the previous paper (*31*), palladium and platinum at high concentrations interfered with mercury analysis. This result suggests that there exist some chemical interferences in the generation of mercury vapor from the solution. However, in general, the contents of these elements are very low in natural waters and digested biological samples, and so the interferences of them may be negligible in the analysis of real samples.

Application. The present helium MIP emission spectrometric method was applied to the determination of mercury in bovine liver (SRM 1577) from the NBS. About 1 g of the sample was digested with 7 mL of HNO_3 for about 72 h, and the digested solution was filled up to 100 mL. The analytical result was 15 ± 2 ng/g, which was almost consistent with the certified value (16 ± 2 ng/g).

ACKNOWLEDGMENT

The authors thank J. Takahashi of the Department of Chemistry, University of Tokyo, for his valuable discussion. We also express our thanks to M. Imai of the University of Tokyo for his construction of the microwave cavity.

LITERATURE CITED

(1) Hatch, W. R.; Ott, W. L. *Anal. Chem.* **1968**, *40*, 2085–2087.
(2) Gilbert, T. R.; Hume, D. N. *Anal. Chim. Acta* **1973**, *65*, 461–465.
(3) Hawley, J. E.; Ingle, J. D., Jr. *Anal. Chem.* **1975**, *47*, 719–723.
(4) Yamazaki, S.; Doklya, Y.; Hayashi, T.; Toda, S.; Fuwa, K. *Nippon Kagaku Kaishi* **1977**, *8*, 1148–1152; *Chem. Abstr.* **1977**, *87*.
(5) Caupell, J. E.; Hendrikse, P. W.; Bongers, J. S. *Anal. Chim. Acta* **1976**, *81*, 53–60.
(6) Nakahara, T.; Tanaka, T.; Musha, S. *Bull. Chem. Soc. Jpn.* **1978**, *51*, 2020–2024.
(7) Omang, S. H. *Anal. Chim. Acta* **1971**, *53*, 451–419.
(8) Olafsson, J. *Anal. Chim. Acta* **1974**, *68*, 207–211.
(9) Matsunaga, K.; Nishimura, M.; Konishi, S. *Nature (London)* **1975**, *258*, 224–225.
(10) Tanabe, K.; Takahashi, J.; Haraguchi, H.; Fuwa, K. *Anal. Chem.* **1980**, *52*, 453–457.
(11) Fassel, V. A. *Science* **1978**, *202*, 183–191.
(12) Kirkbright, G. F.; Ward, A. F.; West, T. S. *Anal. Chim. Acta* **1973**, *64*, 353–362.
(13) Skogerboe, R. K.; Coleman, G. N. *Appl. Spectrosc.* **1976**, *30*, 504–507.
(14) Layman, L. R.; Hieftje, G. M. *Anal. Chem.* **1975**, *47*, 194–202.
(15) Lichte, F. E.; Skogerboe, R. K. *Anal. Chem.* **1972**, *44*, 1321–1323.
(16) Watling, R. J. *Anal. Chim. Acta* **1975**, *75*, 281–288.
(17) Braman, R. S. *Anal. Chem.* **1971**, *43*, 1462–1467.
(18) Bricker, J. L. *Anal. Chem.* **1980**, *52*, 492–496.
(19) Bache, C. A.; Lisk, D. J. *Anal. Chem.* **1971**, *43*, 950–952.
(20) Talmi, Y. *Anal. Chim. Acta* **1975**, *74*, 107–117.
(21) Quimby, B. D.; Uden, P. C.; Barnes, R. M. *Anal. Chem.* **1978**, *50*, 2112–2118.
(22) Beenakker, C. I. M. *Spectrochim. Acta, Part B* **1976**, *31B*, 483–486.
(23) Beenakker, C. I. M. *Spectrochim. Acta, Part B* **1977**, *32B*, 173–187.
(24) Quimby, B. D.; Delaney, M. F.; Uden, P. C.; Barnes, R. M. *Anal. Chem.* **1979**, *51*, 875–880.
(25) Quimby, B. D.; Delaney, M. F.; Uden, P. C.; Barnes, R. M. *Anal. Chem.* **1980**, *52*, 259–263.
(26) Zander, A. T.; Hieftje, G. M. *Anal. Chem.* **1978**, *50*, 1257–1260.
(27) Mulligan, K. J.; Hahn, M. H.; Caruso, J. A; Fricke, F. L. *Anal. Chem.* **1979**, *51*, 1935–1938.
(28) Tanabe, K.; Matsumoto, K.; Haraguchi, H.; Fuwa, K. *Anal. Chem.* **1980**, *52*, 2361–2365.
(29) Tanabe, K.; Haraguchi, H.; Fuwa, K. *Spectrochim. Acta, Part B* **1981**, *36B*, 119–127.
(30) Tanabe, K. Ph.D. Thesis, University of Tokyo, 1981.
(31) Ure, A. M.; Shand, C. A. *Anal. Chim. Acta* **1974**, *72*, 63–77.

RECEIVED for review January 5, 1981. Accepted April 21, 1981. This research has been supported by the Grant-in-Aid for Developmental Scientific Research under Grant No. 584022 from the Ministry of Education, Science and Culture (1980) and also partly by a grant from the Kurata Science Foundation (1980).

Fourier Transforms in the Computation of Self-Deconvoluted and First-Order Derivative Spectra of Overlapped Band Contours

Jyrki K. Kauppinen,[1] Douglas J. Moffatt, Henry H. Mantsch, and David G. Cameron*

Division of Chemistry, National Research Council of Canada, Ottawa, Ontario K1A 0R6, Canada

Fourier self-deconvolution is compared to first-order derivatives as a method for studying intrinsically overlapped band contours. A number of advantages of Fourier self-deconvolution are demonstrated. A short theoretical description of the computation of derivatives using Fourier transforms is given, and advantages of this technique are discussed as compared to the method of Savitzky and Golay.

A variety of spectroscopic techniques have developed to the point where the major problem is the determination of the individual components of intrinsically overlapped band contours. One must then resort to mathematical methods such as band fitting, factor analysis, first-order derivatives, and deconvolution.

In earlier papers we have developed a Fourier self-deconvolution technique (*1*) and studied the way in which self-deconvolution changes the signal-to-noise ratio, S/N, of the spectrum (*2*). In this publication we compare the Fourier self-deconvolution method to first-order derivative techniques and demonstrate the facility of self-deconvolution and computation of derivatives when Fourier transforms are employed. It is shown that deconvolution and derivation are limited in a similar way by the noise in the spectrum (*2*) and concluded that self-deconvolution is the most advantageous technique. We also consider the optimum derivative for a spectrum with a given S/N ratio and discuss the advantages of the use of Fourier transforms for derivation compared with other methods, such as the Savitzky–Golay technique (*3*).

THEORY

Description of Fourier Self-Deconvolution. According to our notations (*1*, *2*) a spectrum, $E(\nu)$, and an interferogram, $I(x)$, are a pair of Fourier transforms; that is

$$E(\nu) = \int_{-\infty}^{\infty} I(x) \exp(i2\pi\nu x)\, dx = \mathcal{F}\{I(x)\} \quad (1)$$

and

$$I(x) = \int_{-\infty}^{\infty} E(\nu) \exp(-i2\pi\nu x)\, d\nu = \mathcal{F}^{-1}\{E(\nu)\} \quad (2)$$

where $\mathcal{F}\{\}$ and $\mathcal{F}^{-1}\{\}$ are the Fourier and inverse Fourier transforms, respectively.

Fourier self-deconvolution involves the multiplication of an interferogram, the inverse Fourier transform of the spectrum to be deconvoluted, by $D_g(x)/\mathcal{F}^{-1}\{E_0(\nu)\}$, where $D_g(x)$ is an apodization function and $E_0(\nu)$ is the intrinsic line shape function of the spectrum $E(\nu)$. The self-deconvoluted spectrum, $E'(\nu)$, is then the Fourier transform of the new interferogram, $I'(x)$. The division by $\mathcal{F}^{-1}\{E_0(\nu)\}$ results in the self-deconvolution and $D_g(x)$ determines the line shape function, $\mathcal{F}\{D_g(x)\}$, and hence the spectral resolution, in the deconvoluted spectrum. An equivalent operation is to smooth the spectrum by $\mathcal{F}\{D_g(x)\}$ and then self-deconvolute the smoothed spectrum.

In practice, the intrinsic line shape is approximated by a Lorentzian line, i.e.

$$E_0(\nu) = \frac{\sigma/\pi}{\sigma^2 + \nu^2} \quad (3)$$

$$\mathcal{F}^{-1}\{E_0(\nu)\} = \exp(-2\pi\sigma|x|) \quad (4)$$

where 2σ is the half-width (the width at half-height) of $E_0(\nu)$.

The efficiency of the operation is given by the parameter, K, the ratio of the line width before self-deconvolution to that after. That is

$$K = 2\sigma/\Delta\nu_{1/2} \quad (5)$$

where $\Delta\nu_{1/2}$ is the half-width of $\mathcal{F}\{D_g(x)\}$.

First-Order Derivatives by Fourier Transforms. From eq 1 the nth derivative of $E(\nu)$ is given by

$$d^nE(\nu)/d\nu^n = \int_{-\infty}^{\infty} (i2\pi x)^n\, I(x) \exp(i2\pi\nu x)\, dx \quad (6)$$

Thus the nth derivative of the spectrum is the complex Fourier transform of the interferogram apodized by a complex function

$$A_n(x) = (i2\pi x)^n \quad (7)$$

In the case of the even order derivatives the apodization function is real and even, and is given by

$$A_n(x) = (-1)^{n/2}(2\pi x)^n \qquad n \text{ is even} \quad (8)$$

Thus, as the new interferogram $A_n(x)\cdot I(x)$ is real, even, and symmetric, the right-hand side of eq 6 is real and the derivative is the Fourier cosine transform of the new interferogram.

In the case of odd order derivatives we have an imaginary apodization given by

$$A_n(x) = (-1)^l\, i(2\pi x)^n \qquad n \text{ is odd} \quad (9)$$

where $n = 2l + 1$ and l is an integer. Consequently, $A_n(x)\cdot I(x)$ is imaginary and odd (antisymmetric), the right-hand side of eq 6 is real and hence the derivative is the Fourier sine transform of the apodized interferogram given by

$$I'(x) = (-1)^{l+1}(2\pi x)^n\, I(x) \quad (10)$$

In practice, due to the noise it is also necessary to smooth the spectrum before the derivatives are computed. The most elegant way to do this is to use Fourier transforms, as smoothing of the spectrum is simply a particular apodization of the interferogram. If we multiply the interferogram by $S(x)$, the spectrum is smoothed by $\mathcal{F}\{S(x)\}$. Hence, we can simultaneously achieve both smoothing and derivation by including such apodization, i.e.

$$A_{sn}(x) = S(x)\, A_n(x) \quad (11)$$

[1] NRCC Fellow (1980). Permanent address: Department of Physics, University of Oulu, 90570 Oulu 57, Finland.

0003-2700/81/0353-1454$01.25/0 © 1981 American Chemical Society

It is apparent that the best smoothing function, $\mathcal{F}\{S(x)\}$, is a sinc ((sine x)/x) function, i.e., boxcar apodization in the interferogram space, given by

$$S(x) = \begin{cases} 1, & |x| \leq L \\ 0, & |x| > L \end{cases} \quad (12)$$

The optimum truncation point, L, of $S(x)$ is the point in the interferogram where the signal of the line is equal to the noise. This means that the distortions of the line due to the truncation of the interferogram are smaller than the noise in the spectrum. In the case of a Lorentzian line the above situation is approximately valid when

$$\exp(2\pi\sigma L) = 2\pi\sigma L_0(S/N)_0 \quad (13)$$

and hence

$$L = \frac{1}{2\pi\sigma} \ln [2\pi\sigma L_0(S/N)_0] \quad (14)$$

where $(S/N)_0$ is the signal-to-noise ratio of the original spectrum and L_0 is the length of the whole interferogram. L_0 is also related to the sampling interval, $\Delta\nu_0$, in the spectrum in the following way:

$$L_0 = \frac{1}{2\,\Delta\nu_0} \quad (15)$$

General Properties of First Order Derivatives and Self-Deconvoluted Spectra. There are several distinctly different properties of first-order derivatives compared to self-deconvoluted spectra.

A general property of first-order derivatives is that the integrated intensity of the line is zero. This is easily demonstrated in interferogram space, since, from eq 6 and 7

$$A_n(x)\ I(x) = \mathcal{F}^{-1}\left\{\frac{\mathrm{d}^n E(\nu)}{\mathrm{d}\nu^n}\right\} = \int_{-\infty}^{\infty} \frac{\mathrm{d}^n E(\nu)}{\mathrm{d}\nu^n} \exp(-i2\pi\nu x)\ \mathrm{d}\nu \quad (16)$$

Hence, setting $x = 0$ in the above equation we have

$$\int_{-\infty}^{\infty} \mathrm{d}^n E(\nu)/\mathrm{d}\nu^n\ \mathrm{d}\nu = A_n(0)I(0) = 0 \quad (17)$$

In contrast, the integrated intensity of the self-deconvoluted spectrum, $E'(\nu)$, is given by

$$\int_{-\infty}^{\infty} E'(\nu)\ \mathrm{d}\nu = D_g(0)\exp(2\pi\sigma 0)\ I(0) = I(0) = \int_{-\infty}^{\infty} E(\nu)\ \mathrm{d}\nu \quad (18)$$

That is, the integrated intensity is exactly the same after self-deconvolution as it is before.

A second property of the nth derivative of a line is that it has $n + 1$ positive or negative peaks, and n zero crossings. The positions of the zero crossings are fixed (depending mainly on the half-width 2σ). If n is odd, there is one zero crossing exactly at the line position and the "line shape" is antisymmetric around the line position. If n is even, the "line shape" is symmetric around the line position and the strongest "peak" is at the line position.

In contrast, the line shape in a self-deconvoluted spectrum (2) is $\mathcal{F}\{D_g(x)\}$, and hence we can select the desired line shape and half-width.

Generally, the even order derivative spectra are comparable to self-deconvoluted spectra, and the optimum order of the derivative depends mainly on the signal-to-noise ratio, $(S/N)_0$, in the original spectrum. The signal-to-noise ratios, $(S/N)_A$, in the derivative and self-deconvoluted spectra can be easily derived from our general formula, in ref 2:

$$(S/N)_A = \left[\nu_0^{1/2}\, 2 \int_0^L A(x)\mathcal{F}^{-1}\{E_0(\nu)\}\ \mathrm{d}x\right] \Big/ \left[(\overline{n^2})^{1/2}\left(\int_0^L A^2(x)\ \mathrm{d}x\right)^{1/2}\right] \quad (19)$$

where $A(x)$ is a general apodization function, $(\overline{n^2})^{1/2}$ is the root-mean-square value of the noise in the interferogram, and ν_0 is the width of a wavenumber region which defines the sampling interval, $1/2\nu_0$, in the interferogram. Using $A(x) = (2\pi x)^n S(x)$ and $A(x) = D_g(x)/\mathcal{F}^{-1}\{E_0(\nu)\}$ in the above equation we can calculate the signal-to-noise ratios for even order derivation and self-deconvolution, respectively. Examination of the second, fourth, and sixth derivatives of a line shows that the derivatives are respectively 2.7, 3.9, and 5.3 times narrower than the line, using the peak-to-peak value as the peak height when determining $\Delta\nu_{1/2}$ of the derivative line. That is, in our terminology, $K = 2.7$, 3.9, and 5.3 for the second, fourth, and sixth derivatives, respectively. Computation of $(S/N)_A$ shows that the signal-to-noise ratios in the even order derivative spectra are approximately the same as those in self-deconvoluted spectra with the same K values, a Lorentzian line shape, and $D_g(x) = D(x)\ \mathrm{sinc}^2(\pi x/L)$. Further, the maximum practical K value of a derivative or self-deconvoluted spectrum is related to $(S/N)_0$ in the following way:

$$K \approx \frac{4\sigma L}{1.207} = \frac{2}{\pi\ 1.207} \ln [2\pi\sigma L_0(S/N)_0] \gtrsim \frac{2}{\pi\ 1.207} \ln [(S/N)_0] \quad (20)$$

The above relationship is similar to eq 23 in ref 2. Using eq 20 we find that for $K = 2.7$, 3.9, and 5.3, $(S/N)_0 \approx 167$, 1630, and 23 100, respectively. Hence, the optimum derivations for spectra with $(S/N)_0 \approx 200$, ≈ 2000, and $\approx 20\,000$ are the second, fourth, and sixth, respectively. This means that if, for example, $(S/N)_0 = 2000$, the highest spectral resolution, i.e., K value, in conjunction with a reasonable signal-to-noise ratio, is achieved with the fourth derivative. The next even derivative, the sixth, has an S/N ratio which is an order of magnitude lower. It is possible to compute higher order derivatives by employing apodizations other than boxcar (e.g., triangular) in the smoothing operation. However, the resultant "derivative" is broadened and distorted and has a smaller K value than predicted. That is, it is no longer a true derivative of the recorded spectrum.

EXAMPLES

Figure 1 shows a Lorentzian line

$$E(\nu) = \frac{1}{\sigma^2 + (\nu - \nu_0)^2} \quad (21)$$

its first four derivatives, and a self-deconvoluted line, $E'(\nu)$, with $K = 4$ and $D_g(x) = D(x)\ \mathrm{sinc}^2(\pi x/L)$ (2). The derivatives and $E'(\nu)$ are computed by using Fourier transforms. The derivatives can be expressed as shown in eq 22 and the curves

$$\begin{cases} \mathrm{d}E(\nu)/\mathrm{d}\nu = -2(\nu - \nu_0)E^2(\nu) \\ \mathrm{d}^2E(\nu)/\mathrm{d}\nu^2 = -2E^2(\nu) + 8(\nu - \nu_0)^2E^3(\nu) \\ \mathrm{d}^3E(\nu)/\mathrm{d}\nu^3 = 24(\nu - \nu_0)E^3(\nu) - 48(\nu - \nu_0)^3E^4(\nu) \\ \mathrm{d}^4E(\nu)/\mathrm{d}\nu^4 = 24E^3(\nu) - 288(\nu - \nu_0)^2E^4(\nu) + 384(\nu - \nu_0)^4E^5(\nu) \end{cases} \quad (22)$$

in Figure 1 accurately fit these expressions. The complexity of the derivative "line shape" contrasts with the line shape resulting from self-deconvolution. Further, the derivative "line shapes" are essentially fixed, the only flexibility being that they can be broadened by smoothing the spectrum with $\mathcal{F}\{S(x)\}$. On the other hand, as Figure 1 shows, the line shape of the deconvoluted spectrum, $E'(\nu)$, is very good. This results

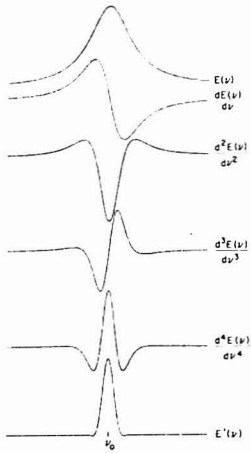


Figure 1. Comparison of the first, second, third, and fourth derivatives of a Lorentzian line, $E(\nu)$, with the self-deconvoluted spectrum, $E'(\nu)$, obtained by using $K = 4$ and $D_g(x) = D(x)\ \mathrm{sinc}^2\ (x/L)$.

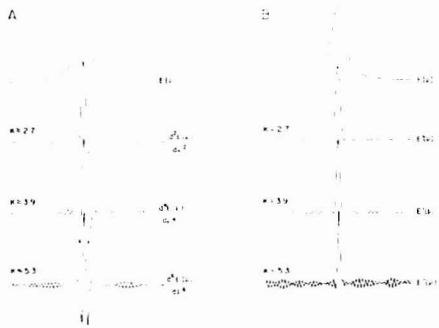


Figure 2. Behavior of noise in even order derivation and self-deconvolution: (column A) a Lorentzian line, $E(\nu)$, with $(S/N)_0 = 200$, and the second, fourth, and sixth derivatives of the Lorentzian lines with $(S/N)_0$ of 200, 2000, and 20 000, respectively; (column B) self-deconvoluted spectra of the corresponding noisy Lorentzian lines when using K values of 2.7, 3.9, and 5.3.

from the fact that the width (spectral resolution) and shape of the line shape function is completely determined by $\mathcal{F}\text{-}[D_g(x)]$, and hence user selectable (*1*, *2*).

Figure 2 illustrates the behavior of the signal-to-noise ratio of even order derivatives (column A) compared to that of self-deconvoluted spectra (column B). In column A are shown the second, fourth, and sixth derivatives of a Lorentzian line to which noise has been added so that $(S/N)_0 \approx 200$, 2000, and 20 000, respectively. Hence, when truncation points derived from eq 14 are used, each derivative gives the optimum situation predicted by eq 20. Self-deconvolution of the same Lorentzian lines using $K = 2.7$, 3.9, and 5.3 gives the spectra shown in column B. As predicted from eq 19, the S/N ratios in all of the derivative and deconvoluted spectra are approximately the same, the S/N ratios of derivative spectra change, as a function of K, in much the same way as do those of self-deconvoluted spectra. Figure 2 shows very clearly that, in order to proceed from the nth to the $(n + 2)$th derivative,

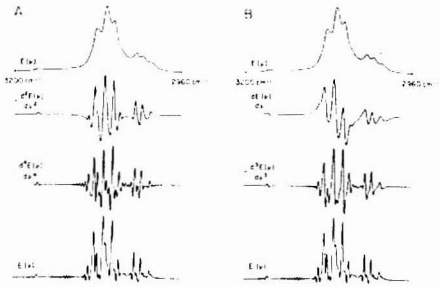


Figure 3. Comparison of the infrared spectrum, $E(\nu)$, of chlorobenzene with the self-deconvoluted spectrum, $E'(\nu)$, and with the second and fourth (column A) and the first and third (column B) derivatives.

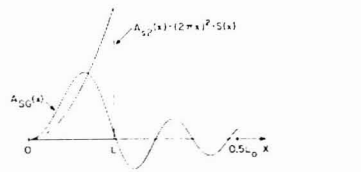


Figure 4. Comparison of our apodization function, $A_{s2}(x) = (2x)^2\ S(x)$, with the corresponding Savitzky–Golay function, $A_{SG}(x)$, obtained by taking the inverse Fourier transform of the fourth order polynomial 25 point second derivative convoluting function (*4*). In the function $A_{s2}(x)$, $S(x)$ is a boxcar function with the truncation point L.

one requires an increase of an order of magnitude in $(S/N)_0$.

The advantages of self-deconvolution are further illustrated in Figure 3, where we show the infrared spectrum, $E(\nu)$ (top), of chlorobenzene in the CH stretching region (3200–2960 cm^{-1}) recorded on a Digilab FTS-11 spectrometer with an instrumental resolution of about 1.2 cm^{-1}, boxcar apodization and $(S/N)_0 \approx 3000$, along with the self-deconvoluted spectrum $E'(\nu)$ (bottom), computed by using $2\sigma = 9.8\ cm^{-1}$, $K = 3.6$, and $D_g(x) = D(x)[1 - (x/L)^2]^2$. $D_g(x)$ is a boxcar function truncated at $x = L$. Figure 3 also shows the first four derivatives of the spectrum $E(\nu)$ smoothed by $|S(x)|$, where $S(x)$ is a boxcar apodization function with $L = 0.35$ cm. For a better comparison, the even order derivatives (column A) are displayed separately from the odd order derivatives (column B).

It is apparent from Figure 3 that the Fourier self-deconvolution method yields the maximum information regarding the band structure. With $(S/N)_0$ higher than 1000 the first, second, and third derivatives provide little information other than that which can be obtained by a careful examination of $E(\nu)$. Further, the interpretation of the odd order derivatives is difficult. As Figure 3 shows, when $(S/N)_0 \approx 3000$ the fourth derivative is of potential value as a supplement to the self-deconvoluted spectrum in that it may assist in deciding on the validity of some of the extremely weak features. However, as a stand-alone technique its value is limited due to the interpretive problems discussed in the foregoing section.

Finally it is of interest to compare the Fourier transform method of derivative computation with the Savitzky–Golay technique (*3*, *4*). Figure 4 shows our apodization function, $A_{s2}(x) = (2\pi x)^2 S(x)$, where $S(x)$ is a boxcar function, and the corresponding Savitzky–Golay apodization function, $A_{SG}(x)$, obtained by taking the inverse Fourier transform of the fourth-order polynomial 25 point second derivative Savitzky–Golay convoluting function (*4*). Two main points are evident. While $A_{s2}(x)$ is exactly correct for $|x| < L$, the Savitzky–Golay function, $A_{SG}(x)$, deviates and as a consequence

will lead to a slightly distorted second derivative curve; i.e., the result is only approximately the second derivative. In contrast, the distortions in derivative spectra obtained by means of the Fourier transform method are smaller than the noise in such spectra. This results from the truncation just below the point in the interferogram when the noise dominates, as computed with eq 14. Consequently, the derivatives resulting from the Fourier transform method are very close to those given by eq 22. Secondly, while $A_{*2}(x) = 0$ for $|x| > L$, $A_{SG}(x)$ oscillates about zero. This results in an increase of noise in the derivative spectrum. Similar effects result from the use of the other Savitzky–Golay convoluting functions.

SUMMARY

We have described the computation of derivative and self-deconvoluted spectra using Fourier transforms and carried out a comparison of first-order derivatives with Fourier self-deconvoluted spectra.

There are two main advantages in the use of Fourier transforms to compute the first-order derivatives. Firstly, distortions in the derivatives are smaller than the noise. Secondly, the computation is very easy, as there is only one parameter, L, used in the smoothing function, and this parameter depends mainly on the signal-to-noise ratio in the original spectrum.

The signal-to-noise ratio also defines the highest utilizable derivative of the spectrum. In the case of the more useful even order derivatives, the use of the sixth order is restricted to spectra with $(S/N)_0 \gtrsim 10000$, the fourth order to spectra with $(S/N)_0 \gtrsim 1000$, and the second order to spectra with $(S/N)_0 \gtrsim 100$.

Generally, Fourier self-deconvolution yields by far the highest degree of information regarding the band structure, particularly when the bandwidths of the individual component bands are similar. In the case where bandwidths in the region of interest differ substantially, the advantages of Fourier self-deconvolution will not be immediately apparent due to the restrictions imposed by the narrower lines. However, by employment of the band separation technique (*1*) to remove such lines the full advantages can readily be achieved.

LITERATURE CITED

(1) Kauppinen, J. K.; Moffatt, D. J.; Mantsch, H. H.; Cameron, D. G. *Appl. Spectrosc.* **1981**, *35*, 271–276.
(2) Kauppinen, J. K.; Moffatt, D. J.; Cameron, D. G.; Mantsch, H. H. *Appl. Opt.* **1981**, *20*, 1866–1879.
(3) Savitzky, A.; Golay, M. J. E. *Anal. Chem.* **1964**, *36*, 1627–1639.
(4) Steinier, J.; Termonia, V.; Deltour, J. *Anal. Chem.* **1972**, *44*, 1906.

RECEIVED for review February 2, 1981. Accepted April 24, 1981. NRCC Publication No. 19286.

Modulated Differential Reflectance Spectroscopy of Lead Dioxide Films during Growth

R. J. Gale,*[1] J. Sefaja,[2] and M. Fleischmann

Electrochemistry Group, Chemistry Department, The University, Southampton S09 5NH, England

External reflectance spectroscopy has been used to study the dynamic growth of electrochemical lead dioxide films on a platinum substrate. The reflectance–time and pulse modulated reflectance–time relations have been recorded simultaneously during film formation and theoretical models are proposed to account for the experimental results. Optical and coulometric estimations of the film thicknesses were in satisfactory agreement. A normalized differential reflectivity simulation has been made for the linear accumulation of absorbing and nonabsorbing product material in a three-phase optical model. It is demonstrated that ac optical techniques coupled with a knowledge of chemical product properties enable selective monitoring of surface faradaic processes.

Specular reflectance spectroscopy (SRS) is particularly suitable for in situ film formation studies, and in this paper we report a novel procedure and analysis for the differential reflectivity of a dynamically growing PbO_2 film on a platinum substrate. Admittance spectroscopy techniques using sweep frequency correlation methods are becoming increasingly important for characterizing electrode (metal and semiconductor)/electrolyte interphases. Coupled with optical probes, such techniques should form a powerful means of resolving potential-modulated surface properties. Relatively few optical studies have been made of lead dioxide films despite their importance for the lead acid battery and diverse electrode applications. Lappe (*1*) has determined the absorption spectrum of the rutile form of PbO_2 films by transmission and found the band edge to be approximately 2.0 eV. The optical absorption, resistivity, and Hall effect properties of electrodeposited α- and β-PbO_2 films have been investigated by Mindt (*2*). Optical band gaps were reported as 2.0 and 1.7 eV for the α- and β-forms, respectively. From an X-ray photoelectron spectral study of the lead oxides, Kim et al. (*3*) proposed that two kinds of adsorbed water are found on electrodeposited PbO_2.

Additionally, the energy band structure of PbO_2 was investigated experimentally by Thomas and Tricker (*4*) and evaluated theoretically in semiempirical calculations by Jacquemin and Bordure (*5*). Recently, Peter and Sefaja have investigated the photoelectrochemical properties of partially reduced α-PbO_2 films by interferometry and photocurrent measurements (*6*). Our purpose in this paper is to demonstrate that ac polarographic theoretical advances may be coupled to absorption spectroscopy of interphases to provide a means of resolving faradaic processes at electrodes.

EXPERIMENTAL SECTION

Lead dioxide films were produced by using potentiostatic pulse techniques, following the procedure outlined by Fleischmann and

[1] Present address: Chemistry Department, Colorado State University, Fort Collins, CO 80523.
[2] Present address: Faculty of Mining and Metallurgy, University of Pristina, Kosovska Mitrovica, Yugoslavia.

0003-2700/81/0353-1457$01.25/0 © 1981 American Chemical Society

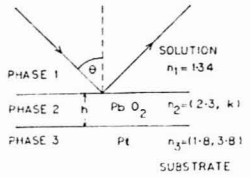


Figure 1. Optical model for computer simulations.

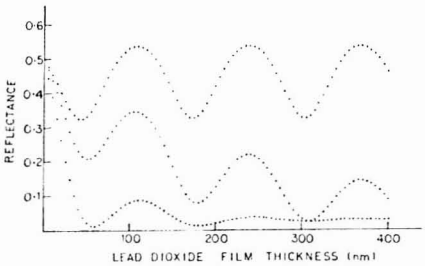


Figure 2. Calculated reflectivity variation with film thickness. Optical parameters are $\lambda = 546$ nm, 45° incidence, p-polarization, $n_2 = (2.3, 0.0$ (upper); 0.1 (middle); 0.5 (lower)).

Liler (7). The electrolyte, prepared from triply distilled water and analytical reagent chemicals, contained 1 M lead acetate, 1 M sodium acetate, and 1 M acetic acid. The platinum substrate electrode, a disk of area 0.126 cm^2 sealed in Pyrex glass, was polished with alumina pastes of successively finer grades (5, 1, 0.3 μm) prior to use. After the solution in the SRS cell was deoxygenated with purified N_2 gas for 30 min, the rest potential was selected by nulling the current follower reading, usually at ~0.80 V SCE. Reflected light was detected by using a solid-state photodiode. Alternatively, normalized spectra could be recorded with continuous scanning of the wavelength using a photomultiplier and filtered feedback system. The modulation and recording equipment have been described elsewhere (8).

RESULTS

1. Reflectance Behavior during Film Growth. Specular reflectance variations with increasing thickness (h) for an isotropic, homogeneous layer may be simulated by using stratified layer theory (9). The reflectance, $\mathcal{R}$, is given by

$$\mathcal{R} = \frac{r_{12}^2 + r_{23}^2 + 2r_{12}r_{23}\cos 2\beta}{1 + r_{12}^2 r_{23}^2 + 2r_{12}r_{23}\cos 2\beta} \qquad (1)$$

in which r_{12} and r_{23} are the Fresnel coefficients for the appropriate polarization states (complex for absorbing interphases) and the phase difference $\beta = 2\pi n_2 h \cos\theta_2/\lambda$. The three-phase optical model chosen for computer calculations is shown in Figure 1 and computational methods are given in the Appendix. Optical constants are taken from the International Critical Tables. Any effects introduced by platinum oxide on the metallic substrate have been disregarded for the purpose of these calculations. Simulated reflectance variations as a function of the optical layer thickness are illustrated in Figure 2. The reflectance is a periodic function of the film thickness for a nonabsorbing layer ($k = 0.0$) and increasing absorptivity causes the first minimum to shift to greater thicknesses. The position of the first maximum is not affected appreciably by k values in the range 0.0–0.5.

Lead dioxide films were prepared by the potential-step method and the current–time (i–t), the reflectance–time ($\mathcal{R}$–t), and the differential reflectance–time ($d\mathcal{R}/dt$) relations were recorded simultaneously during their growth. A typical data

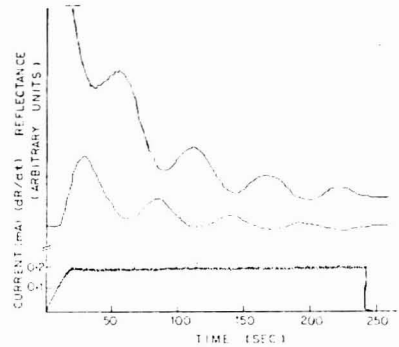


Figure 3. Experimental reflectance, differential reflectance (unnormalized) and current–time curves for PbO_2 film growth. Electrochemical conditions are bias potential +0.83 V, pulse +1.05 V (SCE), modulation 10 mV/120 Hz square wave. Optical conditions are $\lambda = 546$ nm, p-polarization, 56° incidence.

set is shown in Figure 3. The initial rise portion of the i–t transient depended markedly on the state of preparation of the Pt electrode and the nucleation transients could become quite pronounced on fresh and highly polished substrates. These effects may be minimized, however, by reusing the electrode after solely an etch clean in dilute nitric acid or by the use of a short nucleation prepulse. After the passage of about 44 mC charge, the reflectance value decreased to about 3–4% of the initial value by a sequence of damped oscillations. From a comparison of the experimental reflectances with the theoretical simulations, electrochemically formed PbO_2 appears to be absorbing at λ values in the range 400–600 nm, and the magnitude of k is between 0.1 and 0.5. Iterative computing procedures might be employed to determine more precise values for the extinction coefficient of films if reliable data exist for the substrate material.

Attempts to determine the thickness of absorbing layers by optical procedures of this type are fraught with problems (10). Firstly, the optical constants of a thin slice of material may differ from its bulk values. Secondly, absorption may diminish the intensity of the reflected radiation and thereby introduce considerable errors in measurements. Thirdly, the applicability of specular reflectance theory may be questionable due to surface disorder and the inhomogeneity of real films may give rise to practical problems for obtaining reliable (material) data. Nevertheless, as Schopper demonstrated for Sb_2S_3 films of 0–200 nm thickness (11), appropriately chosen values of n and k can be used to compute reasonably good fits to the reflectance and transmittance curves obtained experimentally. It is of interest to estimate the film thicknesses of PbO_2 layers optically and to compare these with the coulometric estimations based on bulk properties. By integration of the i–t responses and with the assumption that the density of β-PbO_2, $\rho = 9.38$, is a reasonable value (cf. ref 6), thicknesses derived from the inflection points of the experimental reflectivity curves may be compared to the coulometric thicknesses. We assume 100% faradaic efficiency for the deposition reaction

$$Pb + 2H_2O - 4e^- \rightleftharpoons PbO_2 + 4H^+ \qquad (2)$$

The first minimum in Figure 1 occurs at $h \sim 43$ nm ($k = 0.0$) and shifts to about 35% greater thickness as k is increased to 0.5; the first maximum is affected less by the magnitude of k, at ≈110 nm, and therefore is more useful for obtaining the approximate optical thickness. Table I contains a sum-

Table I. Comparison of Optical Thicknesses of First Maxima, h_{max}, and Coulometric Thicknesses, h_q

λ/nm	h_{max}/nm	h_q/nm
435	88	75
577	116	101

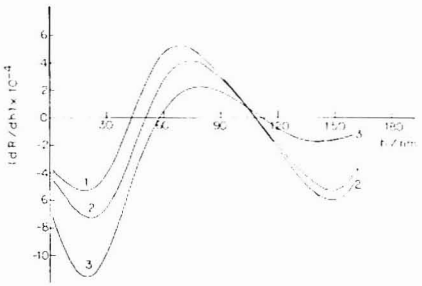


Figure 4. Numerical simulation of derivative of reflectivity function with increasing PbO_2 film thickness. Optical conditions are as given in Figure 2: curve 1, $k = 0.0$; curve 2, $k = 0.1$; curve 3, $k = 0.5$.

mary of the experimental coulometric thicknesses and the theoretical optical values at wavelengths λ = 435 nm and 577 nm. The ratio of the experimental values of the coulometric thicknesses (1.35) agrees reasonably well with the wavelength ratio (1.33). Thickness estimates from the first maxima and coulometric data differ by ~16%. This discrepancy is reasonable considering the simplicity of the three-phase model and the approximate physical constants that were used in the calculations. Nevertheless, it is possible too that because of voids or irregularities in the film, the packing density is slightly less than that of bulk β-PbO_2. Such a condition would modify the optical constants for the film with respect to those of bulk material, as well as density.

2. Differential Reflectance Spectroscopy. The differential reflectance function is readily calculable if the phase-detected signal arises primarily from fluctuations of film thickness (integral concentration) due to the small electrical modulation. In other words, $\mathcal{R} = f(h,t)$ and $d\mathcal{R}/dt = (d\mathcal{R}/dh)(dh/dt)$ and it is assumed that (dh/dt) is constant. Such modulation of the layer thickness implies that the faradaic reaction in question is sufficiently rapid with respect to the imposed signal frequency and that other modulation effects (e.g., space-charge modulations) are constant with film thickness. In general, the faradaic reaction may or may not be reversible to the applied modulation, but a small superimposed ac pulse in this case is considered to modulate the growing layer thickness in a constant manner. Figure 4 is a computer simulation of the derivative of the reflectance–thickness function obtained by differentiating the reflectance expression with respect to the layer thickness. The initial peak in this function may be useful for thickness estimations in the early stages of film growth because it occurs at a smaller layer thickness than the first inflection in the reflectance function. Figure 5 shows the simulated curves for $(d\mathcal{R}/dh)\mathcal{R}^{-1}$ vs. film thickness. This function is accessible experimentally using a feedback arrangement to normalize the reflected light intensity. Such damped functions, like the reflectivity–time curves, may be useful diagnostically or for extracting optical information. More importantly, it should be possible to extract optical information from a product film grown by a faradaic reaction, for example, due to its unique molecular properties. This could aid in the delineation of superimposed, frequency-dependent processes. More precise experimental

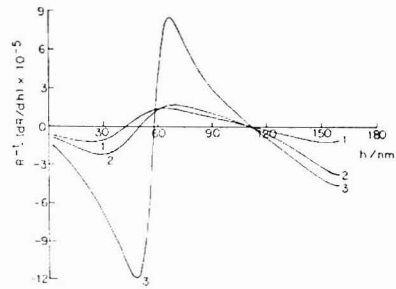


Figure 5. Computer form of $(d\mathcal{R}/dt)\mathcal{R}^{-1}$ vs. film thickness for conditions of Figures 2 and 4.

measurements, especially in the early stages of film growth, will be required to ascertain the value of the derivative technique for obtaining solid film information.

ACKNOWLEDGMENT

We are grateful to A. Bewick for the use of experimental facilities and to L. Peter for helpful discussion. R.J.G. acknowledges the support of a Research Fellowship at Southampton and recent support from the Solar Energy Research Institute, Golden, CO, and the Chemistry Department, Colorado State University. Paul Beaulieu, Chemistry Department, Colorado State University, aided with computer operation and figure preparation.

APPENDIX

Reflectance–thickness relationships may be calculated from the modulus of the square of the Fresnel coefficient for the three-layer model

$$\mathcal{R} = |r_{123}|^2 = U/V \tag{3}$$

$$r_{123} = \frac{r_{12} + r_{23}e^{2i\beta}}{1 + r_{12}r_{23}e^{2i\beta}} \tag{4}$$

in which $\beta = 2\pi n_2 h \cos\theta/\lambda$. Both n_2 and the angle θ will be complex for absorbing layer 2. For a numerical simulation of the derivative, these expressions were expanded to obtain the squared modulus and then differentiated with respect to the layer thickness h. Let $2\beta = (x + iy)h$, $r_{12} = (x_1 + iy_1)$, and $r_{23} = (x_2 + iy_2)$, then

$$U = x_1^2 + y_1^2 + e^{-2yh}(x_2^2 + y_2^2) + 2e^{-yh}(x_1x_2 + y_1y_2)\cos xh + 2e^{-yh}(y_1x_2 - x_1y_2)\sin xh$$

$$V = 1 + e^{-2yh}(x_1^2x_2^2 + y_1^2y_2^2 + y_1^2x_2^2 + x_1^2y_2^2) + 2e^{-yh}(x_1x_2 - y_1y_2)\cos xh - 2e^{-yh}(x_2y_1 + x_1y_2)\sin xh$$

$$dU = 2e^{-yh}[-ye^{-yh}(x_2^2 + y_2^2) - (x_1x_2 + y_1y_2)(y\cos xh + x\sin xh) - (y_1x_2 - x_1y_2)(y\sin xh - x\cos xh)]$$

$$dV = 2e^{-yh}[(x_1^2x_2^2 + y_1^2y_2^2 + y_1^2x_2^2 + x_1^2y_2^2) - ye^{-yh} - (x_1x_2 - y_1y_2)(y\cos xh + x\sin xh) - (x_2y_1 + x_1y_2)(x\cos xh - y\sin xh)]$$

The derivative is computed from $(V\,dU - U\,dV)V^2$.

LITERATURE CITED

(1) Lappe, F. *J. Phys. Chem. Solids* **1962**, *23*, 1563.
(2) Mindt, W. *J. Electrochem. Soc.* **1969**, *116*, 1076.
(3) Kim, K. S.; O'Leary, T. J.; Winograd, N. *Anal. Chem.* **1973**, *45*, 2214.
(4) Thomas, J. M.; Tricker, M. J. *J. Chem. Soc., Faraday Trans. 2* **1975**, *71*, 329.
(5) Jacquemin, J. L.; Bordure, G. *Solid State Commun.* **1972**, *11*, 1583; *J. Phys. Chem. Solids* **1975**, *36*, 1081.

(6) Peter, L. M.; Sefaja, J. *Surf. Sci.*, in press.
(7) Fleischmann, M.; Liler, M. *Trans. Faraday Soc.* **1958**, *54*, 1370.
(8) Bewick, A.; Robinson, J. *Surf. Sci.* **1976**, *55*, 349. Bewick, A.; Gale, R. J., paper in preparation.
(9) Born, M.; Wolf, E. "Principles of Optics", 5th ed.; Pergamon Press: New York, 1975; Chapter 13.
(10) Heavens, O. S. "Optical Properties of Thin Solid Films"; Academic Press: New York, 1955; Chapter 5.
(11) Schopper, H. *Z. Phys.* **1952**, *131*, 215.

RECEIVED for review January 27, 1981. Accepted May 5, 1981.

Structure Elucidation from the Hydroxyl Stretching Region of Vapor-Phase Infrared Spectra

Michael F. Delaney* and F. Vincent Warren, Jr.

Department of Chemistry, Boston University, Boston, Massachusetts 02215

The hydroxyl stretching region of over 400 vapor-phase infrared spectra is examined. Correlations between peak wavelength and functionality are observed for primary, secondary, and tertiary alcohols, phenols, carboxylic acids, and oximes. Peak shifts due to steric crowding and intramolecular hydrogen bonding are seen. The use of the tabulated results for identification of compounds separated by gas chromatography is discussed.

The use of vapor-phase infrared spectrometry (VPIR) directly interfaced to gas chromatography (GC) continues to develop as a viable alternative or complement to mass spectrometry (MS) for identifying the separated components. VPIR can facilitate isomeric assignments which are difficult or impossible by MS, and the instrumentation based on Fourier transform spectrometry (FTIR) has pushed detection limits down to nanogram levels (*1*). Applications of GC-FTIR have recently been reviewed (*2*).

The interpretation of IR spectra can be approached in several ways, depending upon the needs and time constraints of the laboratory being served, the available instrumentation, the skill and experience of the chemist, and the availability of a large body of reliable and computer-accessible spectra. The capabilities of computerized spectral interpretation methods are rapidly progressing. Automated approaches range from systems employing artificial intelligence techniques, designed to mimic a chemist's strategy (*3*), to the more abstract and mathematically based pattern recognition (*4*) and library searching (*5*) methods.

Manual and artificial intelligence based spectra interpretation both employ some form of a "correlation table" which relates the wavelength of spectral peaks to specific structural fragments in the simple molecule. The interpretation consists of identifying the stuctural fragments present and combining these together to yield the correct structure. Recently a theory has been proposed (*6–8*) which seeks to firmly define the function and structure of a correlation table using information theoretic concepts to optimize the division of the wavelength axis into functional group categories. This theory is expected to formalize and improve the interpretation systems, both under development (*3*) and commercially available (*9*), which identify possible structure units using a correlation table.

While structure elucidation by IR is routine in many laboratories and extensive correlations between structure and IR adsorption wavelength have been published (*10*), there are significant differences in the vapor phase, primarily due to the absence of intermolecular interactions. As an example, Figure 1 compares a portion of the VPIR spectra of 2-isopropylphenol with the same region of the liquid-phase IR spectrum. The hydroxyl stretching band is seen to be quite broad in the condensed phase due to extensive intermolecular hydrogen bonding, while the gas-phase O–H band is considerably sharper.

Published correlations for vapor-phase spectra (*11*) are based on only few examples due to the previous lack of suitable instrumentation. The focus of our research (*12–15*) has been to facilitate the use of VPIR to identify components separated by GC by providing a reliable computerized interpretation system. Reported herein are our observations of structural correlations for various hydroxyl group containing compounds drawn from a large commercial library of VPIR spectra measured on a FTIR instrument. Using a commercially available, high-quality spectral library with extensive "biographical" information provided for each spectrum and with computerized data handling, we were able to rapidly compile functional group categories and to study these spectral correlations extensively for a large number of spectra.

EXPERIMENTAL SECTION

The spectral library available was the Sadtler Research Laboratories VPIR collection (Sadtler Research Laboratories, Inc., Philadelphia, PA). Five thousand spectra were obtained on magnetic tape. Each spectrum was measured from 4000 to 450 cm^{-1} at a sampling rate of 2 cm^{-1} and a resolution of 4 cm^{-1} using a Digilab FTS-14 spectrometer and a CIRA GC (Sadtler Research Laboratories, Inc., Philadelphia, PA). The resulting spectrum contains 1842 data points which are background corrected with intensities digitized in milliabsorbance units.

For compounds numbered 2001–4000, the information record, which contains the compound number, molecular formula, Chemical Abstracts Service (CAS) name and registry number, etc., were text searched by computer to find hydroxyl group containing compounds. For each compound the Wiswesser line notation (WLN) (*16*) was examined by computer to place spectra into the categories: primary, secondary, and tertiary alcohol, phenolic, oxime, and carboxylic acid. The members of each category were examined by using the CAS name to verify correct category assignments. In this manner 416 hydroxyl-containing compounds were found.

For each compound, the spectral zone from 3400 to 3800 cm^{-1}, encompassing the hydroxyl group stretching region, was examined. Each spectrum was studied by using several programs to prepare tabulations of spectral information. The location of peak maximum positions using maximum absorbance and a peak picking algorithm (*15*) was examined, as were average spectra and a histogram of peak positions vs. number of spectra, for each functional group class. A visual assessment of a large fraction

0003-2700/81/0353-1460$01.25/0 © 1981 American Chemical Society

Table I. Observed Position of Hydroxyl Stretching Bands for Several Functional Groups

	this work				Welti (*11*)	
functional group	no. of spectra	steric crowd. limit, cm^{-1}	regular range, cm^{-1}	intramol H bond limit, cm^{-1}	no. of spectra	regular range, cm^{-1}
primary alcohol	91	*a*	3676-3666	3429	5	~3670
benzyl alcohol		*a*	3664-3649	3639		
secondary alcohol	84	3668	3658-3645	3529	9	~3660
tertiary alcohol	24	*a*	3644-3640	3545	2	~3640
phenolic	101	3670	3657-3645	3402	16	3655-3650
oxime	6	*b*	3647-3640	*b*		
carboxylic acid						
saturated	68	*a*	3580-3568	*a*	14	3575-3570
$\alpha\beta$-unsaturated[c]	42	*a*	3586-3581	3572	11	3585-3580

[a] Minimal effect observed. [b] Insufficient data. [c] Includes aromatics.

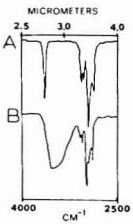


Figure 1. Liquid- and gas-phase IR spectra for 2-isopropylphenol: (A) vapor phase, (B) neat liquid.

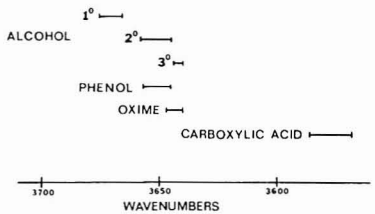


Figure 2. Correlation of hydroxyl functional group type with peak maximum location.

of the spectra was facilitated by display on a Tektronix graphics terminal. A cursor was used to cross check computer derived vs. manual peak location.

RESULTS AND DISCUSSION

The major correlations between peak location and hydroxyl functional group type from this work and from the study by Welti (*11*) are reported in Table I. A graphical representation is presented in Figure 2. The most obvious observation is that the carboxylic acids give peaks in a region well separated from the alcohols and phenols. All functionalities studied are noted to be shifted to frequencies 20–60 cm^{-1} higher than corresponding absorptions in condensed phase spectra due to the elimination of intermolecular interactions in the gas phase. The hydroxyl region is also well separated from the vapor-phase amine and amide stretching frequencies which range from 3330 to 3500 cm^{-1} and which are often of low intensity (*11*).

As demonstrated below, the position of the O–H stretching band can be shifted due to intramolecular interactions of two major types:

1. Steric Crowding. For many of the functional group categories, shifts to slightly higher frequencies (larger wavenumbers) are observed when the hydroxyl group is surrounded by nonpolar side chains. This steric crowding results in restricted movement of the hydroxyl group, increasing the apparent force constant for the vibration, which produces a higher energy absorption.

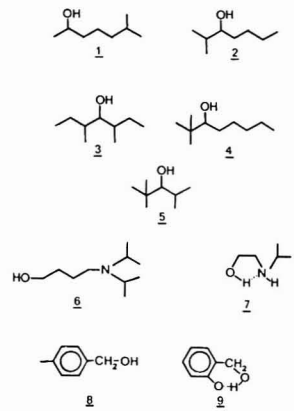


Figure 3. Representative compounds discussed in the text.

2. Intramolecular Hydrogen Bonding. While intermolecular interactions are virtually eliminated in the vapor phase, intramolecular interactions are still routinely observed. For molecules which can intramolecularly hydrogen bond to form five- and six-membered rings, a new absorption is usually observed. The O–H bond is slightly weakened by hydrogen bonding, so the new peak is seen at lower frequency since the apparent force constant is decreased. This effect will often produce a new peak in addition to the nonhydrogen bonded form, and the spectral shifts are usually much larger than for steric crowding effects.

Alcohols. In the absence of steric hindrance and hydrogen bonding, the O–H stretching regions for primary, secondary, and tertiary alcohols are seen to be resolvable, facilitating spectral identification. Only for secondary alcohols were steric crowding effects observed with shifts to higher frequency of about 10–15 cm^{-1}. A correlation between the degree of steric crowding and the O–H peak location is seen. For example, the unhindered 6-methyl-2-heptanol, **1** (Figure 3), absorbs at 3655 cm^{-1}, while 2-methyl-3-heptanol, **2**, peaks at 3658 cm^{-1}, 3,5-dimethyl-4-heptanol, **3**, at 3662 cm^{-1}, 2,2-dimethyl-3-octanol, **4**, at 3664 cm^{-1}, and 2,2,4-trimethyl-3-pentanol, **5**, at 3668 cm^{-1}.

Displacement of peaks to lower energy by intramolecular hydrogen bonding can be up to 100 cm^{-1} or more and are

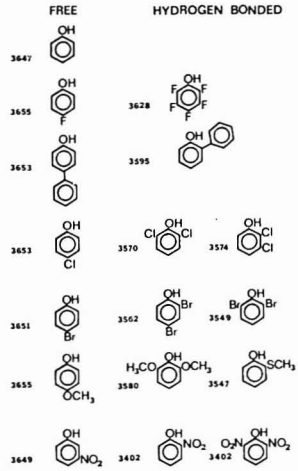


Figure 4. Comparison of the O–H stretching frequency for free vs. hydrogen bonded phenols.

observed routinely when five- or six-membered rings involving electonegative atoms or double bonds can be formed. For example, 4-diisopropylaminobutanol, **6** (Figure 3), exhibits a free O–H stretch at 3670 cm^{-1}, while 2-isopropylaminoethanol, **7**, has a peak at 3566 cm^{-1} due to the formation of a hydrogen bonded six-membered ring.

In contrast to Welti's observation (*11*) that the bonded O–H band is usually more intense, we found a fairly even distribution with the free O–H peak being the more intense in about half of the observed spectra. However, these relative peak intensities are expected to be a function of both the gas temperature and the strength of the hydrogen bond. Higher temperatures will favor the free O–H while a stronger hydrogen bond will favor the bound peak.

Benzyl alcohols as a group exhibit a free O–H peak at somewhat lower frequencies than normal alcohols due to the inductive effect of the aromatic ring (*10*). The O–H stretch for benzyl alcohols can also be shifted by hydrogen bonding. For example, 4-methylbenzyl alcohol, **8** (Figure 3), has a free O–H peak at 3653 cm^{-1}, while 2-hydroxybenzyl alcohol, **9**, has a peak at 3639 cm^{-1} due to the formation of a six-membered ring.

Phenols. The hydroxyl stretching region for phenols closely parallels that for secondary alcohols, being from 3645 to 3657 cm^{-1} for unshifted compounds. Steric hindrance moves the peak up to 3670 cm^{-1} in 2,6-di-*tert*-butylphenol. Substantial shifts to smaller energies are seen for ortho-substituted phenols. As seen in Figure 4, this "ortho effect" is quite well-behaved, with the magnitude of shift for the bonded O–H being: F < phenyl < OCH_3 < Cl < Br < SCH_3 < NO_2. Compounds doubly ortho-substituted show only a slight tendency to move to lower frequencies relative to the corresponding mono-ortho-substituted analogues.

Oximes. The small number of oximes included were observed to be at the same frequency as tertiary alcohols, from 3647 to 3640 cm^{-1}. In addition to the utilization of other spectral features, oximes can be distinguished from tertiary alcohols since the hydroxyl stretching band is seen to be much more intense for oximes.

Carboxylic Acids. The carboxylic acid O–H stretching bands range from 3586 to 3568 cm^{-1}, in a spectral region well separated from the hydroxyl stretching of alcohols. This can presumably be ascribed to inductive effects (*10*). A careful examination of the acid O–H bands shows that the region can be further subdivided, to distinguish aliphatic from aromatic carboxylic acids. Aromatic and $\alpha\beta$-unsaturated compounds have O–H peaks from 3586 to 3581 cm^{-1} while saturated acids have peaks from 3580 to 3568 cm^{-1}. For example, dodecanoic acid absorbs at 3576 cm^{-1}, while 2-dodecenoic acid has a peak at 3586 cm^{-1} and 3-bromobenzoic acid peaks at 3583 cm^{-1}. Although the difference in peak location for these two subgroups is small, it is expected to be of utility in structure elucidation due to the sharpness of these bands in the vapor phase.

Only small spectral shifts, if any, were observed for carboxylic acids. For example, benzoic acid peaks at 3585 cm^{-1}, while hydrogen bonding shifts the band to 3576 cm^{-1} for 2-chlorobenzoic acid and 3572 cm^{-1} for 2-trifluoromethylbenzoic acid.

ACKNOWLEDGMENT

Acknowledgment is made to the donors of the Petroleum Research Fund, administered by the American Chemical Society, for the support of this research.

LITERATURE CITED

(1) Coffey, P.; Mattson, D. R.; Wright, J. C. *Am. Lab.* (*Fairfield, Conn.*) **1978**, *10*, 126.
(2) Erickson, M. D. *Appl. Spectrosc. Rev.* **1979**, *15*, 261.
(3) Woodruff, H. B.; Smith, G. M. *Anal. Chem.* **1980**, *52*, 2321.
(4) Kowalski, B. R.; Jurs, P. C.; Isenhour, T. L.; Reilley, C. N. *Anal. Chem.* **1969**, *41*, 1945.
(5) Grotch, S. L. *Anal. Chem.* **1974**, *46*, 526.
(6) Veszpremi, T. J.; Csonka, G. I. *J. Mol. Struct.* **1980**, *60* 249.
(7) Veszpremi, T.; Csonka, G. J. *Chem. Inf. Comput. Sci.* **1980**, *20*, 234.
(8) Veszpremi, T.; Csonka, G. *J. Chem. Inf. Comput. Sci.* **1980**, *20*, 239.
(9) Anacreon, R. E.; Pattachini, S. C. *Am. Lab.* (*Fairfield, Conn.*) **1980**, *12*, 97.
(10) Bellamy, L. J. "The Infra-red Spectra of Complex Molecules", 2nd ed.; Wiley: New York, 1958.
(11) Welti, D. "Infrared Vapour Spectra"; Heyden: New York, 1970.
(12) Delaney, M. F.; Uden, P. C. *Anal. Chem.* **1979**, *51*, 1242.
(13) Delaney, M. F.; Denzer, P. C.; Uden, P. C.; Barnes, R. M. *Anal. Lett.* **1979**, *12A*, 963.
(14) Delaney, M. F.; Uden, P. C. *J. Chromatogr. Sci.* **1979**, *17*, 428.
(15) Warren, F. V.; Delaney, M. F., submitted to *Appl. Spectrosc.*
(16) Smith, E. G. "The Wiswesser Line-Formula Chemical Notation"; McGraw-Hill: New York, 1968.

RECEIVED for review January 12, 1981. Accepted May 11, 1981.

Characterization of Airborne Particulates by Pyrolysis/Mass Spectrometry and Carbon-14 Analysis

Kent J. Voorhees,* Steven M. Kunen, and Steven L. Durfee

Department of Chemistry/Geochemistry, Colorado School of Mines, Golden, Colorado 80401

Lloyd A. Currie and George A. Klouda

Center for Analytical Chemistry, National Bureau of Standards, Washington, D.C. 20234

Pyrolysis/mass spectrometry (Py/MS) has been used to characterize the composition of organics in an ambient air particulate sample from the eastern Utah oil shale lands. The procedure involved collection of the individual contributors, pyrolysis of these samples, and finally a least-squares fitting of the individual contributor spectra to the pyrolysis mass spectrum of the ambient sample. The Py/MS results were verified by using ^{14}C analysis.

The use of pyrolysis/mass spectrometry (Py/MS) coupled with pattern recognition procedures (*1*) has been demonstrated as a method for differentiating airborne particulate matter arising from various formation sources (*2*). The results of this study presented evidence to substantiate that the kerogen-like polymeric material is unique for each formation process and that it may be possible to use these polymeric materials to identify sources of air particulates (*3*).

Fausett and Weber (*4*) recently developed a pattern recognition procedure for the determination of mixture constituents and their relative concentrations by low-resolution MS. The technique requires that a reference set of mass spectra be available for the pure components which are suspected of being present in the mixture. These spectra are fitted to the experimental mixture spectrum by computer using a least-squares approach which minimizes the sum of squares of the residuals. The procedure has been successfully applied on a number of known test mixtures containing as many as 20 components (*4*).

The ability of Py/MS technique to differentiate various airborne particulates and the utility of the Fausett–Weber program for determining the constituents in the mixture spectrum of hydrocarbons have led to the results of this paper which describes the analysis of an ambient particulate sample for determining the concentration of the various source components. Special emphasis has been placed on establishing the validity of the results of the Py/MS pattern recognition procedure by comparison to ^{14}C analysis of the contemporary carbon content in the ambient particulate sample.

EXPERIMENTAL SECTION

Sampling Sites and Procedures. A site in the eastern Utah oil shale tracts (near Bonanza, UT) was chosen for the collection of the ambient sample. The remoteness of this site eliminated any significant urban particulate contribution. The local atmospheric particulate contributors were assessed as being vegetive emissions, oil shale, dust, and soil. A survey of the region showed that pine, sage, and juniper were the major vegetations of the area. Soil dust could not be completely segregated from the other collections; however, most soil samples have extremely low concentrations of organics. In addition, the amount of soil in the individual samples was minimized by collecting during periods of low wind velocity. Particulates representing the various vegetive species were collected in areas in which a particular species was dominant. Sampling sites were (sage) Birdseye, UT, (pine) High Uintas, UT, and (juniper) Cedar Mountain, UT.

All air particulate samples were collected on Pallflex quartz-fiber filters (Pallflex Products Corp., Putnam, CT) using a Sierra Hi-Vol sampler (Sierra/Misco, Berkeley, CA) with an automatic flow controller. A flow rate of 1.2 m^3/min was used with collection periods of 48 h for the pine and sage samples, 18 h for the juniper, and 168 h for the ambient sample. Shale samples were prepared directly by grinding the oil shale to pass an 80/100 mesh (0.14–0.18 mm) sieve. Meteorological data were recorded during collection of the ambient sample.

Pyrolysis Sample Preparation. The Hi-Vol filter samples were prepared for pyrolysis by removal and grinding of the top layer of the filter containing the particulate material. The ground particulate material (~50 mg) was suspended by ultrasonification in 1 mL of methanol and was then applied directly to a rotating Curie-Point wire (Fischer, Kottenforst, West Germany) (*5*). After evaporation of the solvent at room temperature, the sample (~15 μg) on the wire was transferred to the Curie-Point pyrolyzer (Fischer, Kottenforst, West Germany).

^{14}C Analysis Sample Preparation. Counting gas (CO_2) was prepared by means of a combustion purification system which allowed the sample to be combusted, purified, and collected in one operation (*6*). The combustion purification train included an after-burner to decompose and oxidize the organics, a CuO furnace to oxidize CO, and a furnace packed with silver wool to remove interfering vapors containing sulfur or halogen species. The trapping procedure utilized three traps: the first at −78 °C to remove water and the second and the third at liquid nitrogen temperature (−196 °C) to collect CO_2. Following combustion, the CO_2 was sublimed, repurified over Cu-wool (700 °C), and volumetrically regulated for counting.

Pyrolysis/Mass Spectrometry/Pattern Recognition. The pyrolysis was conducted by using the Fischer Curie-Point pyrolyzer (1.5 kW, 1.1 MHz power supply) in conjunction with an Extranuclear SpectrEL quadrupole mass spectrometry system (Extranuclear Laboratories Inc., Pittsburgh, PA). Curie-Point wires composed of Fe, Ni, and Co (510 °C final temperature) were used throughout the study, and low-energy (14 eV) electron impact was used for ionization. A scan rate of 1000 amu/s was employed for all analyses. The Extranuclear pulse counting system was used for ion detection. All mass spectral data were collected on a Tracor Model 1700 multichannel analyzer (MCA) (Tracer Northern, Inc., Middleton, WI). Data from the MCA were transferred to a PDP System 10 computer system (Digital Equipment Corp., Marlboro, MA) for the statistical calculations. The data were normalized by expressing the intensity of each peak as a fraction of the total ion intensity.

Two pattern recognition programs have been used for the data calculations. ARTHUR, obtained from Informetrix Inc., Seattle, WA, was used for multivariate analysis subroutines (*7–11*). The analysis procedure using ARTHUR was similar to those described by Meuzelaar et al. (*1*). Following normalization, the data were autoscaled and Fisher weighted (*12*). A point in *n*-dimensional space was calculated for each spectrum followed by the determination of the Euclidian distance between points. In addition, a nonlinear map (*13*, *14*) in two dimensions and dendrogram representation were made. The composition analysis of the ambient sample was accomplished by using a program supplied by the Department of Energy's Laramie Energy Technology Center, Laramie, WY (*4*). The least-squares option in the program using the oil shale and vegetive pyrolysis mass spectra as the reference spectra was utilized for all reported calculations.

0003-2700/81/0353-1463$01.25/0 © 1981 American Chemical Society

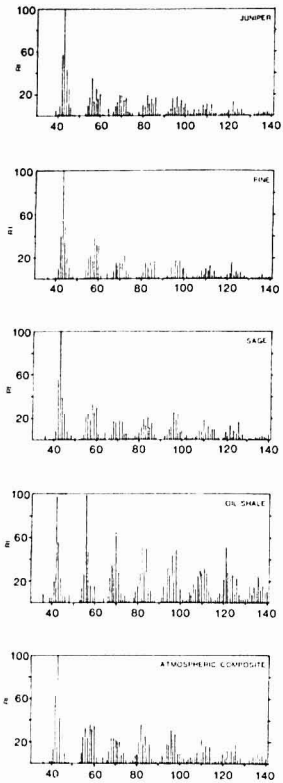


Figure 1. Summary of Py-MS data for various air particulates.

^{14}C Measurement. Radiocarbon measurements were performed in a specially designed low-level gas proportional counting system which permitted the "dating" of samples containing only a few milligrams of carbon (*6*, *15*). The practical sample sizes available in studies of atmospheric pollutants are about 10^3 times smaller than in conventional radiocarbon dating, thus necessitating the special system (*16*). Methods of achieving improvements in sensitivity are described in the above references and include the use of miniature high-purity (quartz) counting tubes, radioactively pure massive shielding, anticoincidence cancellation of cosmic ray muons, plus pulse shape analysis to discriminate against spurious electronic events. The resulting background rate, ca. 0.07 counts/min using the 5-mL quartz counter, represents a reduction of a factor of 200 compared to that without the above precautions.

Independent measurements of the ambient sample were performed in two of the minicounters, having volumes of 15 mL (counter-M) and 5 mL (counter-N). In order to ensure the absence of chemical or isotope fractionation, the carbonaceous particulate material was oxidized quantitatively to CO_2 which was subsequently transferred completely to the respective counter. Maximum counting efficiency was obtained by stringent purification measures. The counting efficiency and overall amplification (gain) were monitored on-line by analysis of the μ-mesons.

RESULTS AND DISCUSSION

Each of the four particulate samples and the ground oil shale sample were analyzed in triplicate, generating a total of 15 spectra. Representative spectra for each sample are shown in Figure 1. The major peaks in the oil shale samples arise primarily from a series of alkenes, alkanes, and alkynes with m/z 56 as the largest peak in the spectrum. In general, the largest peaks associated with a homologous series in the oil shale spectrum were postulated to be alkenes. The largest peak in all the vegetive emission samples was found at m/z 43. One can detect major visual differences between the oil shale and vegetive emission spectra; however, differences between the three vegetive samples are much more difficult to visually discern. The ARTHUR program has the capability to provide a data format from these spectra in a form which will show the various differences and similarities. A distance table calculation including Fisher weights was performed by using the ARTHUR program. These data are summarized in Table I. The diagonal represents an average of three duplicate runs of each sample and gives an estimate of the reproducibility of the Py/MS process. The nonlinear map of the distance table is presented in Figure 2. As expected from visual examination, the vegetive samples were clearly different from the oil shale samples. Interestingly, the ambient sample seemed to resemble the vegetive samples more than the oil shale sample. This suggests that a higher concentration of vegetive material was present in the composite sample. A hierarchical clustering dendrogram verified these observations (Figure 3). This plot shows the poor correlation of the oil shale spectra with the other samples. On comparison of the vegetive samples, sage and pine have the highest similarity values with the composite sample.

The ions with the highest Fisher weight (ions responsible for highest degree of separation) are summarized in Table II. Since the Fisher weight partially reflects the intensity dif-

Table I. Distance Matrix for the Py/MS Results of Air Particulates

	oil	sage	juniper	pine	composite
oil	9.9	182.	158.	216.	152.
sage		24.3	62.7	60.9	60.4
juniper			50.1	103.	83.2
pine				30.1	81.1
composite					19.0

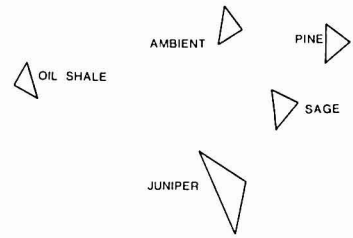


Figure 2. Nonlinear map of various Py-MS data.

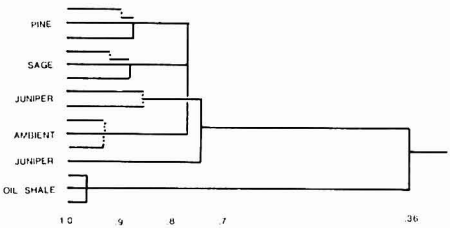


Figure 3. Dendrogram representation of Py-MS data.

Table II. Summary of Mass Spectral Peaks with Highest Fisher Weights

peak	possible assignment	Fisher weight	greatest intensity[a]
59	C_3H_7O	194	vegetive
50	C_4H_2	101	vegetive
70	C_5H_{10}	90	oil shale
109	C_8H_{13}	88	approx equal[b]
58	C_4H_{10}	76	approx equal
44	C_2H_4O, CO_2	76	vegetive
43	C_3H_7	59	vegetive
106	C_8H_{10}	54	oil shale
136	$C_{10}H_{16}$	54	oil shale
111	C_8H_{15}	49	oil shale
56	C_4H_8	47	oil shale

[a] Sample type with greatest peak intensity. [b] Not clear in which sample type peak is highest.

Table III. Summary of Factor Analysis Calculation

species	percentage[a]
oil shale	24.2 ± 2.3
sage	64.3 ± 2.5
pine	11.3 ± 1.8
juniper	00

[a] 95% confidence level.

ferences between peaks of the same mass, a high value indicates an important peak for discriminating between the oil shale and the vegetive sample. For example, m/z 57, 70, 106, 111, and 136 are considerably more intense in the oil shale sample and when combined with m/z 92 and 120 which also have high Fisher weight, these peaks become an important factor in differentiating the oil shale from the vegetive samples. While fairly unimportant in the oil shale spectrum, the m/z 43, 44, 50, and 59 are major peaks in the vegetive samples. Examination of the remainder of the ions with high Fisher weights establishes the fact that compound classes are present which appear to make factor analysis a viable approach for the compositional determination.

The least-squares analysis has been used to determine the composition of the ambient sample. The results of this analysis using an average of the three spectra in each source category are summarized in Table III. The results indicate that a major portion of the organic particulate material originated from plant emissions. The meteorological data recorded during the collection period of the composite sample showed no dominant wind direction; therefore, one would expect mixing of the various vegetation types. Sagebrush grows uniformly in the entire area. The pine grows in a defined location, while sparse outcroppings of juniper occur in most of the area. It is speculated, therefore, that the high sagebrush contribution resulted because of the population dominance and higher terpene emission of sagebrush (*17*) over the other species in the area. The oil shale dust results primarily because of wind entrainment. The maximum wind speed recorded during collection was 13 mph which indicates even at low wind speed, fairly large amounts of oil shale dust are constantly being introduced into the atmosphere.

As an independent assessment of the oil shale contribution in the ambient sample, the ^{14}C content was analyzed. The results of this analysis are summarized in Table IV. These results were derived from two measurements in counter-M, and four in counter-N. By use of a direct comparison with the "Modern Standard" for radiocarbon dating and the current (1979) nuclear testing excess (~28%) for atmospheric radiocarbon, a value for the percent contemporary (f_c) was calculated (last column of the table). The two counters yielded consistent estimates with the mean being $f_c = 63.5 \pm 4.4\%$. We interpret this to mean that approximately two-thirds of the carbonaceous material collected originated from living matter (vegetation), and the remaining third originated from fossil carbon (*18*). The observed ^{14}C content (63.5 ± 4.4%) seems lower than would be predicted from Py/MS results (75.7 ± 3.1%); however, comparing the present ambient ^{14}C content of 63.5 ± 4.4% to a previous desert sample ^{14}C content of 88 ± 16% (*19*), a ratio constant (ambient/desert) of 73 ± 14% is calculated. This value is consistent with the Py/MS results of 75.7 ± 3.1%.

Table IV. Radiocarbon Results for the Ambient Sample[a]

counter	net rate,[b] counts/min	f_m,[c] %	f_c, %
M (15 mL)	0.153 ± 0.016	83 ± 8	65 ± 6
N (5 mL)	0.094 ± 0.006	80 ± 8	62 ± 6

[a] Uncertainties represent 1σ due to Poisson counting statistics. [b] Background rates were 0.184 (M) and 0.062 (N). [c] Percent of "Modern" carbon, f_m, was based on the international radiocarbon dating standard (NBS oxalic acid SRM No. 4990B).

ACKNOWLEDGMENT

We wish to thank H. L. C. Meuzelaar and Don W. Fausett for their helpful discussions. Assistance of the staff of the White River Shale Project, Vernal, UT, is also gratefully acknowledged.

LITERATURE CITED

(1) Eshuis, W.; Kistemaker, P. G.; Meuzelaar, H. L. C. In "Analytical Pyrolysis"; Jones, C. E. R., Cramers, C. A., Eds.; Elsevier: Amsterdam, 1977; pp 151–166.
(2) Voorhees, K. J.; Kunen, S. M.; Hileman, F. D. "Proceedings of the 26th Annual Conference on Mass Spectrometry"; St. Louis, MO, June 1978; p 437.
(3) Kunen, S. M.; Burke, M. L.; Bandurski, E. L.; Nagy, B. *Atm. Environ.* **1976**, *10*, 913.
(4) Fausett, D. W.; Weber, J. H. *Anal. Chem.* **1978**, *50*, 722.
(5) Meuzelaar, H. L. C.; Hileman, F. D. "Pyrolysis Mass Spectrometry of Biomaterials"; Elsevier: Amsterdam, in press.
(6) Currie, L. A. "Environmental Radiocarbon Measurements", Proceedings of the First Conference on Radiocarbon Datings with Accelerators"; Gove, H., Ed.; University of Rochester, 1978, p 372.
(7) Isenhour, T. L.; Kowalski, B. R.; Jurs, P. C. *Crit. Rev. Anal. Chem.* **1975**, *4*, 1.
(8) Jurs, P. C.; Isenhour, T. L. "Chemical Application of Pattern Recognition"; Wiley-Interscience: New York, 1975.
(9) Kowalski, B. R.; Bender, C. F. *J. Am. Chem. Soc.* **1972**, *94*, 5632.
(10) Kowalski, B. R., Bender, C. F. *J. Am. Chem. Soc.* **1973**, *95*, 686.
(11) Kowalski, B. R. *Anal. Chem.* **1975**, *47*, 1152A.
(12) Fisher, R. A. *Ann. Eugen.* **1936**, *7*, 179.
(13) Kruskal, J. B. *Physchoetrika* **1964**, *29*, 115.
(14) Sammon, J. W. *IEEE Trans. Comput.* **1968**, *C–18*, 401.
(15) Currie, L. A.; Murphy, R. B. *NBS Spec. Publ.* **1977**, *No. 464*, 439.
(16) Currie, L. A.; Noakes, J. A.; Breiter, N. A. *Proc. Int. Conf. Radiocarbon Dating, 9th* **1979**, 158.
(17) Rasmussen, R. A. *J. Air Pollut. Control Assoc.* **1972**, *22* 537.
(18) Currie, L. A.; Klouda, G. A.; Copper, J. A. *Radiocarbon* **1980**, *22*, 349.
(19) Currie, L. A.; Kunen, S. M.; Voorhees, K. J.; Murphy, R. B.; Koch, W. F. Report LBL 1979; Lawrence Berkeley Laboratory, Berkeley, CA.

RECEIVED for review December 17, 1980. Accepted April 27, 1981. This work was supported by the Colorado Energy Research Institute, the Office of Environmental Measurements, National Bureau of Standards, and the Energy-Environment Program (EPA-IAG-D6-E684), U.S. Environmental Protection Agency. Use of commercial product names is for accuracy in technical reporting and does not constitute endorsement of the product by the United States Government.

Liquid Chromatography with Graphite Furnace Atomic Absorption Spectrometric Detector for Speciation of Organophosphorus Compounds

Paolo Tittarelli* and Achille Mascherpa

Stazione Sperimentale per i Combustibili, 20097 San Donato Milanese, Italy

Reversed-phase high-performance liquid chromatography (HPLC) is used to separate organophosphorus compounds. The detection of the various phosphorus species in the chromatograph effluent is performed by graphite furnace atomic absorption (GFAA). The use of GFAA as specific detector enables not only compound identification but also the quantitative determination of each compound. The phosphorus values obtained by GFAA compare well with the known amounts introduced into the liquid chromatograph. The detection limit of GFAA for phosphorus is about 0.3 mg/L (with 20-μL introductions in the furnace). This compares with the detection limits of emission spectrometry methods used for phosphorus specific detection in HPLC. The proposed method is applied to the speciation of organophosphorus additives dissolved in lubricating oil.

The speciation of organometallic compounds has received increasing attention in the last years because of the extent of use of these compounds in commercial products and because of the environmental problems connected with this use (*1*).

High-performance liquid chromatography (HPLC) has been proved to be a useful analytical tool for the separation of organometallic compounds (*2*). A wide range of detectors can be employed for HPLC, and the choice of the detector is usually based on the structural features of the separated molecules (*3*).

Atomic absorption spectrometry is an element-specific analytical technique capable of detecting organometallic compounds separated by HPLC. A number of applications are reported in review articles dealing with the coupling of atomic absorption and HPLC (*4, 5*). Flame atomic absorption (FAA) can be coupled directly with HPLC through the nebulizer capillary if the effluent flow from the liquid chromatograph and the nebulizer uptake rate are similar (*6*). When the flow rate through the nebulizer exceeds that of the column, dropwise monitoring of the effluent can be done by collecting the latter in a Teflon cup attached to the nebulizer (*7*). When the concentration of the metal in the effluent is too low for FAA detection, graphite furnace atomic absorption (GFAA) can be used because of the improved sensitivity compared to FAA (up to 3 orders of magnitude). Coupling of GFAA detectors with HPLC involves a number of problems because of the stepwise operational characteristics of the commercially available flameless atomizers and because only small volumes can be injected into the atomizers each time. Vickrey et al. (*8*) described a peak storage procedure to analyze the chromatographic peak off-line, suitable for routine determination of organometallic compounds with known retention time.

Phosphorus sensitivity is poor by FAA but can be determined with good sensitivity by GFAA. An important industrial use of phosphorus is as an organophosphorus additive in lubricating oils because of its oxidation inhibiting and antiwear capabilities (*9*). An accurate and sensitive method for determining the various species of phosphorus in such samples is required.

The determination of phosphorus by GFAA is usually performed by a matrix modification technique. Lanthanum nitrate (*10, 11*) or organolanthanum compounds (*12, 13*) are added to the solution containing phosphorus to obtain useful atomic absorption signals. A GFAA method has also been reported, involving the direct ashing and atomization of phosphorus compounds without matrix modification (*14*).

Emission spectrometric methods have been reported for the detection of phosphorus compounds separated by HPLC. Kirkland et al. employed the flame emission of phosphorus (HPO molecules) at 526 nm to detect inorganic phosphates and monophosphate nucleotides separated by anion-exchange HPLC (*15*). Fraley et al. evaluated the use of inductively coupled plasma optical emission spectrometry (ICP) (*16*).

This investigation has been carried out to study the applicability of HPLC–GFAA coupling for the simultaneous speciation and determination of organophosphorus compounds in comparison with the emission spectrometry couplings cited above. The determination of phosphorus additives in lubricating oils is also reported.

EXPERIMENTAL SECTION

Apparatus. The apparatus consists of a liquid chromatograph coupled with an atomic absorption spectrometer. A Perkin-Elmer Series 3 dual pump high-performance liquid chromatograph is used. Samples are introduced via a Rheodyne 7105 Septumless injector valve from a Hamilton 801 microsyringe. The column for reversed-phase chromatography is a 0.26 cm i.d. × 25 cm long stainless steel tube packed with octadecylsilane bonded on silica ODS-HC Sil-X-1. A Perkin-Elmer Model LC 55B UV-Vis spectrophotometer is employed as "first stage" continuous detector of the chromatograph effluent. The effluent is collected by a fraction collector ISCO Model 1850 (Instrumentation Specialties Co., Lincoln NE).

The atomic absorption spectrometer is Perkin-Elmer Model 5000, equipped with an HGA 76-B flameless atomizer and AS-1 autosampler. The GFAA signals are displayed on a Perkin-Elmer Model 56 strip-chart recorder.

Reagents. The organophosphorus compounds used are the following: trimethyl phosphite (TMPi), tributyl phosphate (TBP), and tri-*p*-cresyl phosphate (TCP), E. Merck, Darmstadt, West Germany; triphenyl phosphite (TPPi), trimethyl phosphate (TMP), and triethyl phosphate (TEP), EGA Chemie, Steinheim, West Germany; di-*n*-butylphosphoric acid (DBP), Riedel-De Haën, Hannover, West Germany; triphenyl phosphate (TPP), SRM no. 1071b NBS, Washington, DC.

Xylene, methyl isobutyl ketone (MIBK), and lanthanum nitrate were obtained from Carlo Erba RP, Milan, Italy.

The lubricating oil additive containing 9.5% (w/w) phosphorus as zinc dialkyl dithiophosphate (ZTP) is Lubrizol 1395, Rouen, France.

Methyl alcohol, Lichrosolv E. Merck, Darmstadt, West Germany, and deionized water ($\simeq 18 \times 10^6\ \Omega\ cm^{-1}$ resistivity) are employed as HPLC eluents.

Procedure. Each organophosphorus compound listed above is diluted with xylene or MIBK to obtain phosphorus concentrations ranging from 500 to 2000 mg/L. These solutions are

0003-2700/81/0353-1466$01.25/0 © 1981 American Chemical Society

Table I. Experimental Parameters

wavelength	213.6 nm
bandwidth	0.2 nm
lamp	EDL, 8 W
background	D_2 correction
purge gas	argon (gas stop during atomization)
(1) drying cycle	30 s, 100 °C
(2) charring cycle	30 s, 1300 °C
(3) atomization cycle	10 s, 2700 °C
heating rate from (1) to (2)	60 °C/s
sample volume	20 μL
lanthanum addition	0.5 mg
detection limit	6 ng
sensitivity (0.0044 A)	5 ng

employed to determine the retention time of each compound. ZTP is dissolved in lubricating oil together with TCP and TPP. Phosphorus concentrations in the oil are respectively 3500 mg/L as ZTP, 2000 mg/L as TCP, and 2300 mg/L as TPP. The oil is then diluted (1 + 3) with xylene.

Four microliters of the solutions is introduced into the liquid chromatograph. Two solvent programs are employed. Solvent program A: The gradient elution is started with 50% methyl alcohol and continued to 100% methyl alcohol in a linear manner within 25 min. Solvent program B: The elution is started with 20% methyl alcohol in an isochratic manner for 10 min and then the methyl alcohol content is increased to 100% within 30 min. The column is purged with 100% methyl alcohol for 15 min at the end of both programs.

The effluent flow is set to 1 mL min^{-1} and UV detection is performed at 260 nm. After UV detection, portions of the effluent are collected at constant intervals in the AS-1 sampling cups by means of the fraction collector. The cups are then transferred in the AS-1 sample tray for phosphorus detection.

The GFAA detection of phosphorus in each portion is performed by the matrix modification technique as follows. The experimental parameters are listed in Table I.

Twenty microliters of 2.5% (w/v) lanthanum nitrate aqueous solution is introduced into the furnace before each atomization cycle.

The determination of the quantities of phosphorus in the effluent portions is obtained by calibration with methyl alcohol solutions of TPP having phosphorus content variable from 3 to 30 mg/L and by area measurement of the atomization peaks.

The furnace is purged by high-temperature heating every five cycles to avoid memory effects.

RESULTS AND DISCUSSION

A preliminary investigation was carried out to fix the conditions for GFAA detection of the compounds listed above. The application of the method suggested by Prevot and Gente-Jauniaux (*14*) does not give satisfactory results, because of low sensitivity obtained with TPP standards.

Also the procedures given in ref 12 and 13, which involve the addition of organolanthanum compounds to the phosphorus-containing solutions, yield poor atomization efficiency (in comparison with TPP) for some of the compounds. These phosphorus compounds (TMP, TEP, TBP, TMPi) volatilize from the furnace during the drying and ashing stages because of their low boiling points.

When 0.5 mg of lanthanum, as lanthanum nitrate, is added for each heating cycle, the atomization of the low boiling point phosphorus compounds is complete. In this case all phosphate and phosphites form thermally stable compounds with lanthanum during the drying stage (*17*). In this way the GFAA detector provides species-independent signals for phosphorus in the effluent. The quantity of phosphorus in each portion is plotted vs. the retention time and the GFAA histogram is compared with the UV chromatogram. The UV and GFAA chromatograms (solvent program A) of a xylene solution of TPP (500 mg/L phosphorus) are shown in Figure 1. The GFAA histograms (full line) are obtained with two different

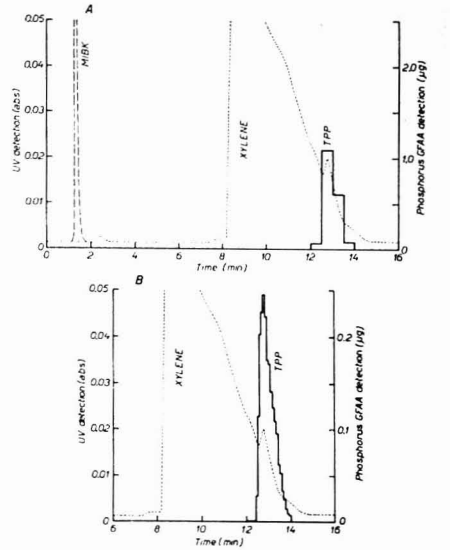


Figure 1. (A) GFAA and UV chromatograms of TPP solution with 30 s collection time (500 mg/L phosphorus): UV detection, dotted line; GFAA detection, full line. (B) GFAA and UV chromatograms of TPP solution with 5 s collection time (500 mg/L phosphorus): UV detection, dotted line; GFAA detection, full line.

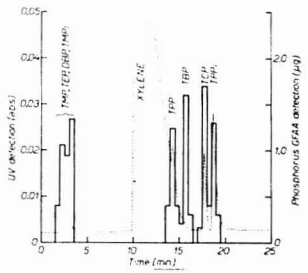


Figure 2. GFAA and UV chromatograms of organophosphorus compounds solution (250 mg/L phosphorus as TMP, TEP, DBP, and TMPi, 500 mg/L phosphorus as TPP, TBP, TCP, and TPPi): UV detection, dotted line; GFAA detection, full line.

collection times: 30 s (Figure 1A) and 5 s (Figure 1B).

The UV detector measures a broad and intense peak ascribed to the presence of xylene in the effluent and a peak ascribed to the phenyl rings of TPP. As the UV peaks of TPP and xylene are overlapped partially, MIBK can substitute xylene as the solvent, as indicated in Figure 1A.

The 30-s collection time is usually employed to detect the number of organophosphorus compounds separated by the column while the 5-s collection time enables a more precise evaluation of the retention time of a known phosphorus compound. In both cases GFAA acts as a element specific detector. As can be seen (Figure 1), the GFAA chromatogram is not influenced by the presence of UV absorbing molecules (xylene and the organo part of the phosphorus molecule). The determination of the total quantity of phosphorus in the chromatographic peak is performed by addition of all partial phosphorus quantities determined in each effluent portion.

Table II. Phosphorus Recoveries with GFAA Detection (n = 3)

figure	amt of phosphorus introduced in the chromatograph, μg	amt of phosphorus determined by GFAA, μg	std dev
1A	2.00 (TPP)	2.02	0.15
1B	2.00 (TPP)	2.04	0.06
2	4.00 (TMP + TEP + DBP + TMPi)	3.74	0.15
	4.00 (TPP + TBP)	3.94	0.11
	4.00 (TCP + TPPi)	3.78	0.09
3	6.00 (TMP)	5.90	0.13
	6.00 (DBP + TEP)	6.25	0.19
4	2.30 (TPP)	2.45	0.19
	2.00 (TCP)	1.96	0.09
	3.50 (ZTP)	3.61	0.25

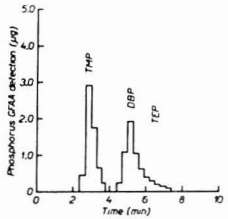


Figure 3. GFAA chromatogram of TMP, DBP, and TEP solution (1500 mg/L phosphorus as TMP, 1000 mg/L as DBP, 500 mg/L as TEP).

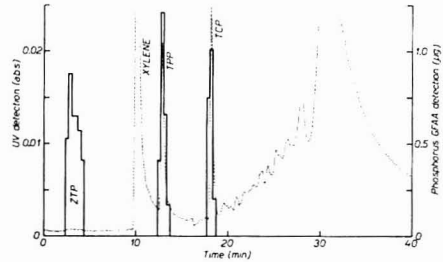


Figure 4. GFAA and UV chromatograms of lubricating oil (575 mg/L phosphorus as TPP, 500 mg/L as TCP, 875 mg/L as ZTP): UV detection, dotted line; GFAA detection, full line.

Figure 2 shows UV and GFAA chromatograms of a xylene solution containing all phosphorus compounds (solvent program A). The UV detection is not effective for the phosphite and phosphates which have organic groups not absorbing in the range 200–350 nm (TMP, TEP, DBP, TBP, TMPi). Only the GFAA detection shows the presence of these organophosphorus compounds in the column effluent. The identification of the GFAA and UV chromatographic peaks is done with reference to retention times determined previously for each phosphorus compound. The UV detection allows evaluation of the separation efficiency of the solvent program only in the case of TPP, TCP, and TPPi. The other phosphorus compounds are not revealed by the UV detector. GFAA detection shows that some of the most polar phosphates and phosphite (TMP, TEP, DBP, and TMPi) have a retention time very close to the "dead" time of the column and that they cannot be separated by the solvent program A.

The partial overlapping of TPP with TBP and TCP with TPPi can be avoided by reduction of the collection time (from 30 to 5 s). The separation of TMP, TEP, and DBP can be improved when the solvent program B is employed. Figure 3 shows that TMP and DBP are separated while DBP and TEP are overlapped partially. The reduction of methyl alcohol content in the mobile phase allows the separation of the most polar compounds in reversed-phase chromatography. However, at the same time the retention time and the width of the chromatographic peaks increase.

The results of the application of the proposed procedure to the analysis of a lubricating oil are shown in Figure 4. A xylene solution of lubricating oil containing ZTP (anticorrosion agent), TCP (antiwater agent), and TPP was injected into the chromatograph and the solvent program A was followed.

Figure 4 shows clearly that the GFAA detector is effective for the three phosphorus compounds in the oil. On the other hand the UV detector does not indicate the presence of ZTP, although it gives strong absorption for a wide range of compounds in the oil in this area of the chromatogram.

The recoveries of phosphorus, i.e., the quantities of phosphorus determined by GFAA in comparison with the quantities introduced into the chromatograph are reported in Table II for all GFAA histograms together with the standard deviations of triplicate measurements.

The GFAA detection limit of phosphorus, i.e., the amount of phosphorus which yields an atomization peak height twice the height of the base-line peak to peak noise, is about 6 ng when 20 μL of methyl alcohol solution of TPP is introduced in the graphite furnace and detected with the operating parameters reported in Table I.

The chromatographic detection limit (CDL) of phosphorus in the stepwise collection of the HPLC effluent, i.e., the quantity detectable in each portion, depends on the collection volume. The CDL can be calculated as

$$\text{CDL (ng)} = D(V_c/V_i) \quad (1)$$

where D is the GFAA detection limit of phosphorus (6 ng), V_c is the collection volume (μL), and V_i is the volume introduced in the furnace (20 μL). The CDL coincides with the GFAA detection limit only if the volume introduced in the furnace coincides with the collected volume and becomes poorer increasing the collection time. With the solvent program described in procedure A the volumes containing the chromatographic peak range from 0.7 to 2 mL when 2 μg of phosphorus is introduced into the chromatograph. The GFAA detection limit (0.3 mg/L) compares well with the detection limit obtained by ICP (0.29 mg/L) (*16*) but is much poorer than that obtained by HPO flame emission (0.02 mg/L) (*15*).

Phosphorus GFAA detection is independent of interferences of the eluents listed above, thus suitable for reversed-phase liquid chromatography and for organophosphorus speciation. HPO flame emission suffers from interferences of organic solvents which can deprime the emission intensity of species to be detected (*15*).

The use of element-specific GFAA detection offers a distinct advantage compared with UV detection usually employed in reversed-phase HPLC. The signal obtained is dependent only on the presence of phosphorus and is independent of structural features of the molecules. Moreover the stepwise collection

of the liquid chromatograph effluent allows the detection and determination of phosphorus compounds in a single run.

The coupling between the liquid chromatograph and flameless atomizer described in this work cannot be considered a "true" coupling, as the effluent is analyzed off-line. The chromatographic analysis time (25–40 min) is shorter than the element-specific analysis time (approximately 2 min for each portion, i.e., 100–120 min).

It has been shown that reversed-phase HPLC can be employed in the separation of organophosphorus compounds dissolved in high boiling point matrix and that GFAA represents an effective detector in spite of the "coupling" limitation reported above.

LITERATURE CITED

(1) Thayer, J. S. *J. Organomet. Chem.* **1974**, *76*, 265–295.
(2) Brinckman, F. E.; Blair, W. R.; Jewett, K. L.; Inverson, W. P. *J. Chromatogr. Sci.* **1977**, *15*, 493–503.
(3) Maggs, R. J. "Practical High Performance Liquid Chromatography", 1st ed.; Heyden & Son: London, 1978; Appendix 1.
(4) Van Loon, J. C. *Anal. Chem.* **1979**, *51*, 1139A–1150A.
(5) Fernandez, F. J. *At. Abs. Newsl.* **1977**, *10*, 33–36.
(6) Jones, D. R.; Tung, H. C.; Manahan, S. E. *Anal. Chem.* **1976**, *48*, 7–10.
(7) Slavin, W.; Schmidt, G. J. *J. Chromatogr. Sci.* **1979**, *17*, 610–613.
(8) Vickrey, T. M.; Howell, H. E.; Paradise, M. T. *Anal. Chem.* **1979**, *51*, 1880–1883.
(9) Larson, C. M.; Larson R. "Petroleum Products Handbook", 1st ed.; McGraw-Hill: New York, 1960; Section 2, pp 32–38.
(10) Ediger, R. D.; Knott, A. R.; Peterson, G. E.; Beaty, R. D. *At. Abs. Newsl.* **1978** *17*, 28–32.
(11) Driscoll, D. J.; Clay, D. A.; Rogers, C. H.; Jungers, R. M.; Butler, F. E. *Anal. Chem.* **1978**, *50*, 767–769.
(12) Tittarelli, P. XXI Colloquium Spectroscopicum Internationale, Abstract Handbook; Cambridge, U.K., 1979; p 450.
(13) Slikkerveer, F. J.; Baard, A. A.; Hendrikse, P. W. *At. Spectrosc.* **1980**, *1*, 30–32.
(14) Prevot, A.; Gente-Jauniaux, M. *At. Abs. Newsl.* **1978**, *17*, 1–3.
(15) Julin, B. G.; Vanderborn, H. W.; Kirkland, J. J. *J. Chromatogr.* **1975**, *112*, 443–453.
(16) Fraley, D. M.; Yates, D.; Manahan, S. E. *Anal. Chem.* **1979**, *51*, 2225–2229.
(17) Tittarelli, P., unpublished data, 1980.

RECEIVED for review July 15, 1980. Accepted April 21, 1981.

On Site Continuous Liquid–Liquid Extraction of Nonpolar Organic Compounds in Water

Burkhard Stachel,* Klaus Baetjer, Mehmet Cetinkaya, Juergen Dueszeln, Uwe Lahl, Klaus Lierse, and Wolfram Thiemann

Trinkwassergruppe, Department of Chemistry, Universitaet Bremen, D-2800 Bremen 1, Postfach 330440, Federal Republic of Germany

Bernd Gabel, Rosemarie Kozicki, and Angela Podbielski

Bremen Environmental Institute for the Analysis and Assessment of Hazardous Substances, Colmarer Strasse 22a, D-2800 Bremen 1, Federal Republic of Germany

We have modified the continuous liquid–liquid extraction apparatus introduced by Ahnoff and Josefsson for pesticide analysis in water. By the installation of an electronically directed water level regulator, we succeeded in measuring chlorinated organic compounds in on site, composite sampling of water. The systematic and statistical errors of the modified procedure were analyzed for the α isomer of 1,2,3,4,5,6-hexachlorocyclohexane (α-BHC), β-BHC, γ-BHC (lindane), and hexachlorobenzene (HCB). For these substances we found the following recoveries in a laboratory test procedure: α-BHC, 77.0%; lindane, 73.8%; sum of β-BHC and HCB, 44.7%. The analysis of mean concentrations of the compounds listed above in the lower reaches of the Weser River (Weser, km 361, F.R.G.) from May to November 1980 gave the following results: α-BHC, 3.3 mg/L; lindane, 11.6 ng/L; HCB, 0.4 ng/L. The sampled water volume on the average was about 500 L, no β-BHC was detected within the limits of detection. Limits of detection are as follows: α-BHC, 0.2 ng/L; β-BHC, 0.7 ng/L; lindane, 0.5 ng/L; HCB, 0.2 ng/L.

From an ecological point of view, the mean values of measurements which are analytically integrated over a long period are of particular importance for the study of pollution in a stream. In pesticide analysis the well-known method of continuous liquid-liquid extraction is often used (*1*, *2*). This method provides the acquisition of the *time integrated* samples and extremely low detection limits. However, in our field experiments using this method in on site mode, the lowering of the water level in both extractors, even as far as the complete removal of the solvent phase, made the operation of the apparatus difficult. The cause was found to be the escape of gases from the water during extraction. This phenomen has been also seen when sampled water was sucked from a level below *and* above the extractors. Even in winter, when there is no remarkable temperature difference between sampled water and environment, the fall of the water level also occurred. The water level remained constant only if water was degased before extraction or when extracted water in circuit was used. Because of these facts, the use of this method was unreliable.

EXPERIMENTAL SECTION

As reported previously by Ahnoff and Josefsson (*1–3*), the apparatus consisted of a watertight stainless steel box containing a 12-V dc peristaltic pump, two magnetic stirrers, two governors, and a 12-V battery. There are two cylindrical extractors attached to the box and linked with a Teflon tube. The extractors are constructed solely of glass and Teflon (see Figure 1).

The water samples were taken from a station placed at the Weser River near Bremen, where the river water was constantly pumped with a submersible pump. In the station, pH, redox potential, temperature, and conductivity were continuously recorded. The sampled water volume was on the average of about 500 L.

0003-2700/81/0353-1469$01.25/0 © 1981 American Chemical Society

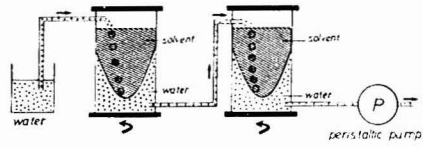


Figure 1. Schematic diagram of the extractors for continuous liquid–liquid extraction (curved arrow indicates = magnetic stirrer).

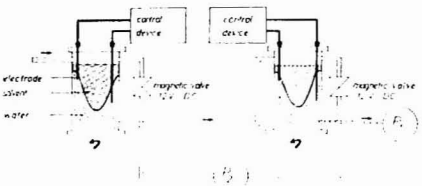


Figure 2. Schematic diagram of the extractors with electronic control regulation of the water level: curved arrow indicates magnetic stirrer, P_1 = peristaltic pump (12 V dc), P_2 = pneumatic pump (12 V dc).

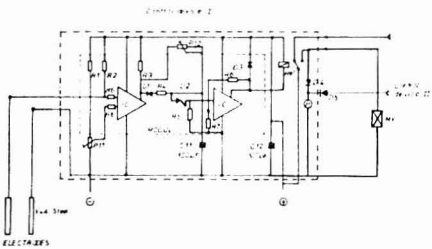


Figure 3. Wiring diagram of the control device: R1 = 4.7 kΩ; R2 = R6 = 82 kΩ; R3 = 2 kΩ; R4 = 330 Ω; R5 = 1 MΩ; R7 = 15 kΩ; P11 = 5 kΩ; P12 = 220 kΩ; D1 = D3 = 1 N 4148; D2 = BZX 7.5; D4 = D5 = 1 N 4003; IC = TAA 2761; Rel. = 12 V dc; MV = magnetic valve 12 V dc; P = pneumatic pump 12 V dc.

Apparative Modifications. Because of the problems mentioned above, it was necessary to provide an electronically directed regulator for the water level in both extractors (see Figure 2).

In each extractor there are two electrodes of different length made of V4A-steel. The long electrode is 110 mm and the short one is 40 mm; both have a diameter of 4 mm. Both electrodes penetrate the extractors through holes where they are connected to the regulator by cables. If the water level sinks to a given depth, a magnetic valve opens and a battery-driven air pump creates a weak vacuum thus pumping more water into the extractor until the desired water level is obtained. The electronic regulator with its (variably) adjustable detector sensitivity and retardation time causes the adjustment of water levels in the extractors and the duration of the pumping to match the conditions. The wiring diagram of the control device can be seen in Figure 3. The diode D5 was additionally installed to prevent the simultaneous opening of *both* valves, if the water level falls in only *one* extractor.

Choice of Solvent. Different solvents have been proposed for the liquid–liquid extraction of nonpolar substances of water samples: *n*-hexane, cyclohexane (*1*), and *n*-pentane (*4*). As solvent losses might occur in the on site mode because of the modification of the extraction apparatus, we chose *n*-pentane as a solvent (*5*) in order to be sure that our procedure was reliable. Even in the summer days (temperature 26–28 °C), after 11 days of extraction, solvent losses did not exceed 20%.

Method. The identification of single substances was carried out by gas chromatography with an electron-capture detector by the method of standard addition, using two of the following three columns: (a) 50 m glass-capillary column, OV-101, Fa. Werner Guenther Analysentechnik; (b) 6 ft packed column, Apiezon L 15% on Chromosorb; (c) 50 m flexible capillary column, SP 2100, Hewlett-Packard. The final identification of the compounds was done by using GC/MS-techniques.

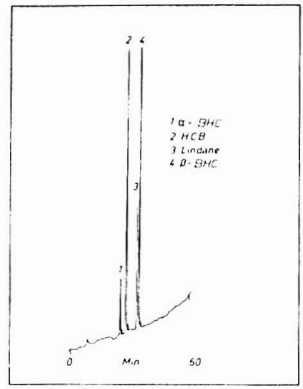


Figure 4. Separation of α-BHC, β-BHC, lindane, and HCB on a 50-m flexible capillary column (SP 2100, Hewlett-Packard).

The gas chromatograph was a GC 5840A Hewlett-Packard fitted with an automatic liquid sampler (ALS) 7671A and using He as a carrier gas. The make-up gas consisted of an Ar/methane (95:5) mixture, the ^{63}Ni electron-capture detector had the following specifications: dynamic range $1:10^4$, automatic pulse frequency direction, and a sensitivity of 10^{-12} g of lindane. The mass spectrometer was a CH5 Varian MAT combined with a computer system Spectro System 100 MS.

In a test of long duration (3 weeks) 1.055 L of tap water was extracted with 0.3 L of *n*-pentane in each extractor. Before the GC analysis (analyzed on flexible capillary column, SP 2100, Hewlett-Packard, length 50 m) the pentane extract was cleaned by Florisil (60–100 mesh) and concentrated in the Kuderna–Danish evaporator to 5 mL. This procedure was also used for cleaning the pentane extracts obtained from the field experiments.

The separation of the four analyzed compounds was achieved with a flexible capillary column (minimum of 4000 theoretical plates per meter at a column capacity ratio $k \geq 4.5$ tested using a normal hydrocarbon at 130 °C; SP 2100, Hewlett-Packard) as shown in Figure 4, whereas the separation of β-BHC and HCB was incomplete with other columns.

RESULTS

Recovery of Some Added Organo–Chlorine Compounds. The following mixture is made in a 200-L polyethylene barrel by adding a standard solution. The barrel has been filled with 200 L of pesticide-free water. The concentrations in water sample before treatment were 10 μg of α-BHC, 32.6 μg of β-BHC + HCB, and 24 μg of lindane. 40–60% of the added amounts of the substances are adsorbed by the inner surface of the barrel and are therefore not available for extraction. This was experimentally verified by independent analysis. For each substance the amount adsorbed is rather constant, but different substances are not equally adsorbed (*6*). The entire volume of water (200 L) with the added organo–chlorine compounds was extracted with the modified apparatus using 0.2 L of *n*-pentane. A pump rate of 1.8 L/h was used for the extractions. Because of mechanical problems the rate was not constant but varied insignificantly between 1.6 and 1.9 L/h. The results are shown in Table I. As derived from Table I, the recovery of the sum of β-BHC and HCB is relatively low. Assays showed that in once-extracted water more than 30% of the original amount of β-BHC was detectable. This demonstrates the breakthrough of this substance. The recovery is calculated by taking as 100% the

Table I. Recovery of Some Organo-Chlorine Compounds Using the Modified Continuous Liquid-Liquid Extraction Apparatus (solvent, 0.2 L of *n*-pentane; number of extractions, $N = 7$)

	amt of α-BHC, μg	amt of β-BHC + HCB, μg	amt of lindane, μg
1st extractor	$\bar{x}_1 = 6.51$	$\bar{x}_1 = 10.31$	$\bar{x}_1 = 13.15$
std dev	±1.14	±4.13	±2.07
confidence interval 95%	$\bar{x}_1 \pm 1.06$	$\bar{x}_1 \pm 3.82$	$\bar{x}_1 \pm 1.92$
2nd extractor	$\bar{x}_2 = 1.22$	$\bar{x}_2 = 4.26$	$\bar{x}_2 = 4.52$
std dev	±0.34	±2.05	±0.71
confidence interval	$\bar{x}_2 \pm 0.31$	$\bar{x}_2 \pm 1.90$	$\bar{x}_2 \pm 0.66$

recovery	% α-BHC	% β-BHC + HCB	% lindane
1st extractor	65.0	31.6	55.0
2nd extractor	12.0	13.1	18.8
Σ	77.0	44.7	73.8

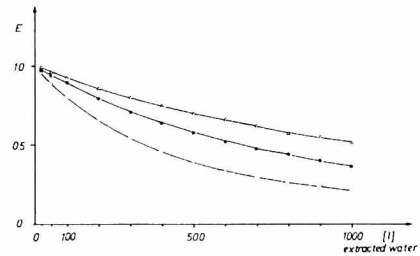


Figure 5. Extraction efficiency E as a function of the extracted water volume: △, HCB; ●, α-BHC; ○, lindane.

amount of organo-chlorine compounds which are ultimately dissolved in water.

Limit of Detection. The substances α-BHC, β-BHC, lindane, and HCB could not be detected in the range of sensitivity of our method in tap water in Bremen. Assuming that the recoveries were the same as those found above (see Table I), the limits of detection were as follows: α-BHC, 0.2 ng/L; β-BHC, 0.7 ng/L; lindane, 0.5 ng/L; HCB, 0.2 ng/L.

Field Procedure. The Weser River is one of the largest in West Germany and originates over a wide, agriculturally developed area. Where the river flows by the city of Bremen (Weser, km 361) the nonpolar compounds given in Table II have been found in the period May to November 1980. In addition, Figure 6 shows the course of the lindane concentration in the Weser River during the same period, including the water flux of the river at the sampling station. The sampled water volume on the average was about 500 L. No β-BHC was detected within the limits of detection.

DISCUSSION

From the theory the extraction process in one extractor can be described as follows (*1*):

$$\text{extraction efficiency } E = (V_{org}K/V_{aq})(1 - e^{-V_{aq}/V_{org}K}) \quad \text{(I)}$$

V_{org} is the volume of the organic phase, V_{aq} is the volume of the extracted water, and K is the distribution constant. The distribution constants of the substances α-BHC, lindane, and HCB for the system *n*-pentane/water were determined as proposed by Voerman (*7*); see Table III. The extraction

Table II. Determination of α-BHC, Lindane and HCB Extracted from the Weser River with 0.2 L *n*-Pentane during the Period from May-November 1980[a]

date of sampling	concentration α-BHC	HCB	lindane
11.05-16.05	4.2	0.1	21.0
16.05-20.05	3.4	0.2	8.9
27.05-04.06	5.5	0.4	24.6
05.06-16.06	4.7	0.6	39.5
16.06-22.06	n.d.	n.d.	0.8
26.06-04.07	3.3	0.2	1.1
10.07-18.07	n.d.	n.d.	0.4
28.07-04.08	0.8	0.2	1.7
04.08-12.08	0.7	0.2	6.2
12.08-20.08	4.7	0.9	18.4
20.08-28.08	2.9	1.1	13.8
28.08-05.09	4.0	0.7	16.0
06.09-14.09	n.d.	n.d.	3.0
15.09-22.09	3.3	0.2	12.5
22.09-06.10	1.8	0.2	8.8
06.10-15.10	3.8	0.3	18.6
22.10-29.10	n.d.	n.d.	6.9
21.11-01.12	n.d.	n.d.	5.8

[a] Concentrations are in ng/L. Determined with a 50-m flexible capillary column, SP 2100, Hewlett-Packard.

Table III. Distribution Constants K of Some Organo-Chlorine Compounds[a]

	α-BHC	HCB	lindane
N	5	3	4
$\bar{C}_o$	0.492	0.329	0.963
std dev	±0.012	±0.017	±0.123
C_i	997	1093	1037
K	2030	3220	1080

[a] C_i = initial concentration, C_o = concentration in the organic layer (μg/mL *n*-pentane), N = number of assays.

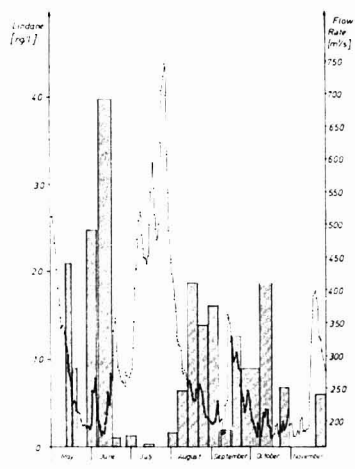


Figure 6. Concentration of lindane extracted from the Weser River with *n*-pentane and the water flux during May-November 1980.

efficiency of the above mentioned assays, calculated from eq I and using the experimentally determined distribution constants are shown in Table IV. Figure 5 shows extraction efficiencies for the substances α-BHC, lindane, and HCB as

Table IV. Calculated Extraction Efficiencies E of Some Organo-Chlorine Compounds[a]

	α-BHC	HCB	lindane
E	0.79	0.86	0.65

[a] V_{aq} = 200 L, V_{org} = 0.2 L of n-pentane.

a function of the volume of extracted water.

Ahnoff and Josefsson (1) recovered nearly 100% of the added amount of lindane while using a pump rate corresponding to 2 L/h. However, the volume of water which was extracted amounted to only 8 L. The determination of recovery in Table I is important for practical reasons because a large amount of water containing a small concentration of organo-chlorine compounds was extracted.

ACKNOWLEDGMENT

We wish to thank H. Siemer whose cooperation and assistance in modifying the apparatus made this work possible.

LITERATURE CITED

(1) Ahnoff, M.; Josefsson, B. *Anal. Chem.* **1974**, *46*, 658-662.
(2) Ahnoff, M.; Josefsson, B. *Anal. Chem.* **1976**, *48*, 1268-1269.
(3) Manual for Continuous Extraction Unit; Tellusond Ltd. Box 21014, S-10031 Stockholm 21, Sweden.
(4) Bauer, U. "Halogenkohlenwasserstoffe im Trink- und Oberflächenwasser. Messergebnisse 1976/77 in der BRD" (Trinkwasser aus 100 Städten, Oberflächenwasser aus Ruhr, Lippe, Main, Rhein); WaBoLu Bericht 3/1978, 64-74, Berlin (West), F.R.G.
(5) Baetjer, K.; Faust, J.; Gabel, B.; Koschorrek, M.; Lahl, U.; Lierse, K.; Stachel, B.; Thiemann, W. *Chromatographia* **1979**, *12*, 742-744.
(6) Friedrich, Klaus J. "Modelluntersuchungen über die Eliminierung von Lindan aus Rohwasser mit Hilfe von Polymergranulaten", MS Thesis, 1977, Institut für technische Hygiene, Giessen.
(7) Voerman, S. *Bull. Environ. Contam. Toxicol.* **1969**, *4* (2), 64-67.

RECEIVED for review September 9, 1980. Resubmitted February 10, 1981. Accepted April 24, 1981. This work is part of the MS thesis at the University of Bremen of B. Stachel.

Determination of Hydrocyanic Acid and Free Cyanide in Aqueous Solution

Steven J. Broderius

U.S. Environmental Protection Agency, Environmental Research Laboratory—Duluth, 6201 Congdon Boulevard, Duluth, Minnesota 55804

Microgram-per-liter concentrations of HCN in aqueous solutions were determined directly by two methods: bubbling compressed air through a solution to displace a small quantity of HCN, which was collected in a glass bead concentration column, or allowing some HCN to diffuse from an enclosed solution into dilute NaOH in a dish suspended above the solution. The separated and concentrated cyanide was determined colorimetrically. The HCN concentration was calculated from linear calibration curves that related the determined HCN displacement rate or quantity of HCN collected to the known concentration of HCN for standard cyanide solutions. The linear relationship between pK for HCN (aq) and 1/temperature in degrees Kelvin was defined. Thus the fraction of free cyanide (i.e., HCN + CN^-) as HCN for specific conditions of temperature and pH could be determined. These procedures for determining HCN in various waters and wastewaters were accurate, precise, and not susceptible to common interfering substances.

Cyanides are formed and extensively used in industrial processes and occur in effluents from various sources. Simple cyanides (e.g., NaCN) readily react with certain heavy-metal salts, forming complex cyanides. Hydrocyanic acid (HCN) is formed in solutions of these salts through dissociation or decomposition of the complex metallocyanide anions and hydrolytic reaction with water by the liberated cyanide ions. The acute toxicity to aquatic organisms of dilute solutions of various simple cyanides and metal-cyanide complexes is usually attributed almost entirely to the concentration of HCN (*1*, *2*), with minimal contribution from the cyanide ion (CN^-) and most metallocyanide anions.

The concentration of free cyanide (i.e., HCN + CN^-) in less stable metal cyanide complex solutions and that of HCN alone cannot be accurately determined by conventional analytical methods for cyanide. Blaha's (*3*) mathematical approach of computing the concentration of HCN in natural water is of questionable accuracy because the accepted equilibrium constants of the metallocyanide ions may be inaccurate. Also, the kinds and concentrations of metallic compounds and complex ions present, and the degree of their equilibration, are uncertain. Since a determination of total cyanide may not be a reliable index of cyanide toxicity, a need exists to measure directly the concentration of HCN in the microgram-per-liter range in evaluating the adverse effects on aquatic biota of cyanide wastes discharged to natural waters.

Methods have been proposed to estimate free cyanide in an aqueous sample by using the Roberts and Jackson distillation procedure (*4*), a microdiffusion cell (*5*, *6*), or a gas-permeable membrane (*7*) to isolate and concentrate HCN in dilute alkali. These methods, however, require acidification of the sample with the conversion to HCN of simple cyanides and most likely some portion of certain metallocyanides.

Several methods have been described for the direct determination of HCN in aqueous solution. Methods based on establishing a distribution equilibrium between the concentration of HCN in water and in air or nitrogen bubbled through the water were described by Worley and Browne (*8*), Schneider and Freund (*9*), Claeys and Freund (*10*), and Nelson and Lysyj (*11*). The methods differ in the ways in which the displaced HCN is trapped and then measured. Montgomery et al. (*12*) developed a procedure for determining HCN whereby a small proportion of HCN is extracted with 1,1,1-trichloroethane, transferred into sodium pyrophosphate, and determined colorimetrically. In a relatively untested method (*13*, *14*) molecular HCN is allowed to diffuse for a fixed time period from a sample in an airtight container into weak alkali contained in an open, shallow dish exposed to the atmosphere above the sample. The cyanide content in the alkali solution is then determined colorimetrically.

This article not subject to U.S. Copyright. Published 1981 by the American Chemical Society

The methods in which vapor-phase equilibration is used require costly and special analytical apparatus and a fairly large sample size. The extraction method uses a hazardous organic solvent, and its applicability for determining HCN in certain metal cyanide complex solutions is questionable. Therefore, the main objective of this study was to develop a convenient and generally interference free analytical procedure for the direct determination of microgram-per-liter concentrations of HCN in water and wastewater.

EXPERIMENTAL SECTION

Determination of Cyanide. Cyanide was determined by titration with silver nitrate and by a slightly modified colorimetric method which uses chloramine-T and pyridine–barbituric acid reagents (*15*). The titrimetric procedure was used to standardize stock cyanide solutions prepared from sodium cyanide (NaCN). Dilute cyanide solutions were prepared by quantitative dilution of a standardized stock. The reagents used in the colorimetric method were prepared as directed (*15*) except that the pH of the NaOH absorbent solution was reduced to about 5.6 with acetic acid just before addition of the chlormine-T reagent. Standard cyanide solutions were prepared and analyzed spectrophotometrically to establish a calibration curve for each set of test conditions. Since varying the NaOH concentration, reagent volumes, etc. may affect color development, an effort was made to maximize the sensitivity of the method by adjusting test conditions. A Beckman DB-G spectrophotometer equipped with digital display and 1-cm cell-path length was used to measure color intensity.

Direct Determination of HCN. Methods based upon solution–air distribution of HCN and analysis of the displaced and concentrated HCN were used to eliminate interference from most components in solution and interaction between the color-development reagents and complex cyanides. With both procedures the proportion of HCN extracted from a test solution was so small (less than 4%) that the complex equilibria involving other cyanide forms was not appreciably altered.

The apparatus used to determine HCN by the vapor-phase-equilibration method was previously described by Broderius and Smith (2), where they used a similar procedure for the direct determination of H_2S. The method for determining HCN uses a gas regulator and flow meter, a temperature regulated sparging chamber, and a glass bubbler through which finely dispersed air is bubbled at 25–300 mL/min in 20 L of test solution. A glass bead concentration column coated with about 0.4 mL of 1.0 N NaOH is used to collect the displaced HCN, and a water displacement bottle measures the volume of air dispersed in the sample and passed through the column. At the end of the collection period the cyanide absorbed in the concentration column is washed off with three 5-mL washings of deionized water into a 25-mL volumetric flask for colorimetric analysis.

The HCN concentration in a solution is calculated from the quantity of HCN collected in a column and by reference to a calibration curve relating the micrograms of HCN displaced per liter of air dispersed with the known HCN concentration in standard solutions of the same temperature. The standard HCN test solutions were prepared by diluting stock cyanide solutions with deionized water and then lowering the pH with HCl to about 5.5, where essentially all the free cyanide is present as HCN. The actual concentration of free cyanide in these standard solutions was determined by the direct colorimetric procedure during the bubbling period.

The apparatus used to determine HCN by the diffusion method consists of a 2.8-L Fernbach flask (Corning 4420) fitted with an airtight No. 13 neoprene rubber stopper and the bottom section of a petri dish (Corning 3160, 60 × 15 mm) attached by silicone cement to a solid glass support rod (Figure 1). The isolation and concentration of HCN from an aqueous solution is accomplished by adding 1.5 L of sample to the flask and sealing with a stopper. After a short equilibration period either 8.5 or 20.5 mL of 0.02 N NaOH is pipetted through a small hole in the large stopper into the petri dish suspended in the air space above the sample. The system is sealed, and the HCN diffusing from the surface of the test solution is absorbed into the alkali solution. The air space between the sample and alkali serves to separate the nonvolatile and ionic species in solution from the collected HCN. A 2-h collection period is generally sufficient to allow for an analytically measurable amount of HCN to be transferred from the sample to the NaOH. The small stopper in the lid is then removed, and an 8- or 20-mL aliquot of alkali absorbent containing the dissolved HCN is transferred to a 10- or 25-mL volumetric flask, respectively. The solution is acidified to about pH 5.6 with 3 or 6 drops of 2.25 N acetic acid, respectively. Four drops of chloramine-T solution (1.0 g/100 mL) are added, mixed, and allowed to stand for about 2 min. A single solution combining a phosphate buffer and chloramine-T can be used to lower the pH of the 0.02 N NaOH and to halogenate the cyanide (*15*). Then 1.0 or 2.5 mL, respectively, of the pyridine–barbituric acid reagent is added and mixed, and the volume is made to the mark with deionized water. After about 10 min the intensity of color produced is measured at 582 nm against a blank. The cyanide content expressed as HCN is determined from a suitable calibration curve.

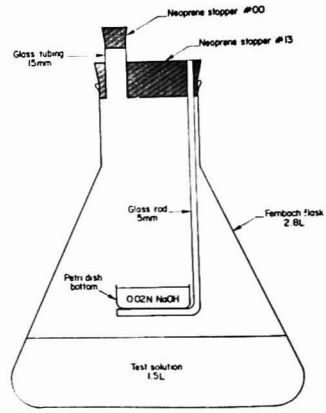


Figure 1. Apparatus used to isolate and concentrate molecular hydrogen cyanide by the diffusion procedure.

The concentration of HCN in a sample is determined from a calibration curve defined from tests performed with standardized NaCN solutions prepared with deionized water and at about pH 6. The tests with the standard solutions are conducted at the same time and under the same conditions as those for the unknown samples. In this way standard solutions are treated as samples, and slight changes in factors that may affect the diffusion of HCN from a test solution would be reflected in the calibration curve. A constant-temperature water bath may be used to ensure temperature control of the test solutions during the collection period.

Nickel and silver cyanide complex stock solutions were prepared by adding Ni(II) or Ag(I) salt solutions to concentrated NaCN solutions until the first definite but persistent turbidity due to precipitated metal cyanide was observed.

RESULTS AND DISCUSSION

Direct Determination of HCN. The concentration of HCN in an aqueous solution was determined by either of two methods of separating a small portion of HCN from a sample and collecting the evolved cyanide in an alkaline solution. Experiments with the vapor-phase-equilibration method demonstrated that with a constant air-flow rate of 50 mL/min there was essentially no effect on HCN displacement rate when the dispersion depth for a glass frit of medium or coarse porosity ranged from 15 to 90 cm. During any determination the column height varied at most only a few centimeters within this range. The efficiency of HCN displacement from a solution by a disperser at a depth of 50 cm was essentially constant when the rate of air flow varied between 25 and 300 mL/min.

Table I. Reproducibility in Amount of HCN Collected by the Diffusion Procedure from Standard Cyanide Solutions

HCN concn, μg/L	HCN collected,[a] μg		
	mean	std dev	RSD
	8.5 mL 0.02 N NaOH		
1.31	0.0809	0.004 55	5.62
2.14	0.118	0.005 76	4.89
4.46	0.218	0.012 3	5.62
7.86	0.416	0.023 3	5.60
27.2	1.08	0.043 7	4.06
38.9	1.35	0.063 6	4.71
	20.5 mL 0.02 N NaOH		
3.46	0.174	0.013 0	7.46
4.80	0.262	0.014 1	5.36
10.1	0.555	0.021 2	3.81
26.9	1.36	0.060 4	4.45
52.4	2.78	0.128	4.58

[a] HCN collected by 8.5 or 20.5 mL of 0.02 N NaOH in 2 h from 1.5-L solutions at 22 °C. Results are for six replicate determinations at each HCN concentration.

The rate at which HCN is displaced by dispersed air was determined at six temperatures for each of six different solutions containing known HCN concentrations ranging from about 0.01 to 0.20 mg/L. The mean distribution coefficients relating the micrograms of HCN displaced per liter of air dispersed through a solution to the known HCN concentration in milligrams-per-liter for mean temperatures of 5.0, 10.1, 15.0, 20.0, 24.9, and 30.0 °C were 1.955, 2.372, 2.897, 3.513, 4.112, and 4.922, respectively. The corresponding standard deviations were 0.0641, 0.0715, 0.0639, 0.0620, 0.131, and 0.0519. These values correspond to a precision estimate expressed as an overall mean relative standard deviation of 2.42 ± 0.90%. The lower limit of detection of this method is governed by the bubbling time and rate. With a 3-h collection period at a dispersion rate of 100 mL/min and selecting 0.020 as an easily measured absorbance change for a 1-cm path length, the detection limit is approximately 1.3 μg HCN/L.

The distribution coefficients (Y) are log linear with temperature in degrees Celsius (X), and a regression equation defining this relationship with $R^2 = 0.994$ is $\log Y = 0.2153 + 0.01608X$. This equation was used to calculate the concentration of HCN in a test solution when temperature and micrograms of HCN displaced per liter of air dispersed through the solution were determined.

The isolation and concentration of cyanide by the diffusion procedure were shown to be particularly suitable as a simple and convenient method for the determination of low concentrations of HCN in aqueous solution. The reproducibility of HCN measurements, as defined by the relative standard deviation in amount of HCN collected, was determined for a 2-h diffusion period from 1.5-L solutions at 22 °C. The results for collection volumes of 8.5 or 20.5 mL of 0.02 N NaOH from six replicate determinations at each of several known HCN concentrations are presented in Table I. In the concentration range of about 1–50 μg HCN/L the precision of this method expressed as an overall mean relative standard deviation is 5.08 ± 0.64% and 5.13 ± 1.41% for 8.5- and 20.5-mL collection volumes, respectively. The linear relationships between the quantities (μg) of HCN collected (Y) by 8.5- and 20.5-mL volumes and the HCN concentration (μg/L) in a test solution (X) at 22 °C can be represented by $Y = 0.0758 + 0.0342X$, $R^2 = 0.989$, and $Y = -0.0035 + 0.0527X$, $R^2 = 0.999$, respectively (Table I). The lower limit of detection is governed by the diffusion time and test temperature. When the collection period is 2 h for solutions at 22 °C, and 0.020 is selected as an easily measured absorption change for a 1-cm path length, the detection limit is approximately 1.0 and 1.6 μg HCN/L for the 8.5- and 20.5-mL collection volumes, respectively.

The amount of HCN collected by the diffusion procedure is temperature dependent. This effect is minimal, however, in the temperature range of 15 °C to about 22 °C. At higher temperatures the rate of HCN displacement increases rapidly. Determinations were made on solutions that gradually warmed up during the HCN collection period from an initial temperature of about 9.5 °C to a final temperature of 14 °C. The precision of these measurements was comparable with that for solutions held at a constant temperature of 22 °C. Therefore, refrigerated samples need not be warmed to a constant temperature but can be transferred to a test apparatus for immediate HCN analysis. Under all circumstances, however, it is essential that standard cyanide solutions be run under the same test conditions along with the unknown solutions to define an appropriate calibration curve relating the quantity of HCN collected to the known HCN concentration.

When the time from addition of a test solution to a Fernbach flask to initiation of a 2-h collection period was varied from near 0 to 2 h, the quantity of HCN collected was virtually the same. An equilibration time of 15–30 min was normally used, however, just before a 2-h collection period. When making cyanide determinations on solutions of very low HCN concentration a longer collection period may be needed to concentrate enough cyanide to make an accurate colorimetric determination. The amount of HCN collected from a test solution was shown to be directly and linearly related to the duration of the collection period. When the test solution volume was between 250 and 1500 mL, the quantity of HCN collected was essentially constant. The displacement of HCN from a solution is apparently not markedly affected by surface area since for this volume change the surface area for the test solutions decreases from about 300 to 250 cm^2.

The results with the diffusion collection system were at least as satisfactory as those with the vapor-phase-equilibration system. The diffusion procedure appears well suited to the routine measurement of HCN since it requires a minimum of sample manipulation, requires no special apparatus, serves to reduce chances of interfering chemical reactions by isolating and concentrating evolved HCN, and has adequate sensitivity and precision.

pK for HCN. The thermodynamic equilibrium constant (pK) of HCN in aqueous solution was determined as a function of temperature over the range of 5–30 °C. The three test solutions at each temperature used to define this relationship contained free cyanide concentrations of about 100 μg/L as HCN. The solutions were prepared with deionized water and had borate buffered pH values of approximately 9.0, 9.3, and 9.7. The HCN displacement rate was determined for each test solution by the vapor-phase-equilibration method, and the molecular HCN concentration was calculated from the appropriate distribution coefficient. The apparent mean pK values for HCN(aq) determined for various cyanide solutions with mean temperatures of 5.1, 10.0, 14.9, 20.1, 25.0, and 30.0 °C were 9.629, 9.533, 9.421, 9.337, 9.220, and 9.145, respectively. The corresponding standard deviations were 0.0135, 0.0048, 0.0066, 0.0039, 0.0150, and 0.0109.

The rate of HCN displacement was approximately the same for similar solutions prepared with deionized water or various natural waters. Therefore, the proposed relationship between the apparent ionization constant of HCN and temperature should be applicable to most fresh waters of normal ionic strength (i.e., μ less than 0.01). The relationship between pK and 1/temperature in degrees Kelvin is an adequate and theoretically justifiable representation of the temperature dependence of the pK for HCN over the experimental tem-

Table II. Fraction of Free Cyanide (HCN + CN^-) as Hydrocyanic Acid (HCN) in Aqueous Solutions of Low Ionic Strength (μ less than 0.01)

temp, °C	pH 6.0	pH 6.2	pH 6.4	pH 6.6	pH 6.8	pH 7.0	pH 7.2	pH 7.4
5	1.000	1.000	0.999	0.999	0.999	0.998	0.996	0.994
6	1.000	1.000	0.999	0.999	0.998	0.998	0.996	0.994
7	1.000	1.000	0.999	0.999	0.998	0.997	0.996	0.994
8	1.000	1.000	0.999	0.999	0.998	0.997	0.996	0.993
9	1.000	1.000	0.999	0.999	0.998	0.997	0.996	0.993
10	1.000	1.000	0.999	0.999	0.998	0.997	0.995	0.993
11	1.000	1.000	0.999	0.999	0.998	0.997	0.995	0.992
12	1.000	0.999	0.999	0.999	0.998	0.997	0.995	0.992
13	1.000	0.999	0.999	0.999	0.998	0.997	0.995	0.992
14	1.000	0.999	0.999	0.999	0.998	0.996	0.994	0.991
15	1.000	0.999	0.999	0.999	0.998	0.996	0.994	0.991
16	1.000	0.999	0.999	0.998	0.998	0.996	0.994	0.990
17	1.000	0.999	0.999	0.998	0.997	0.996	0.994	0.990
18	1.000	0.999	0.999	0.998	0.997	0.996	0.993	0.989
19	1.000	0.999	0.999	0.998	0.997	0.996	0.993	0.989
20	1.000	0.999	0.999	0.998	0.997	0.995	0.993	0.988
21	1.000	0.999	0.999	0.998	0.997	0.995	0.992	0.988
22	0.999	0.999	0.999	0.998	0.997	0.995	0.992	0.987
23	0.999	0.999	0.999	0.998	0.997	0.995	0.992	0.987
24	0.999	0.999	0.999	0.998	0.996	0.994	0.991	0.986
25	0.999	0.999	0.999	0.998	0.996	0.994	0.991	0.986
26	0.999	0.999	0.998	0.998	0.996	0.994	0.990	0.985
27	0.999	0.999	0.998	0.997	0.996	0.994	0.990	0.984
28	0.999	0.999	0.998	0.997	0.996	0.993	0.990	0.984
29	0.999	0.999	0.998	0.997	0.996	0.993	0.989	0.983
30	0.999	0.999	0.998	0.997	0.995	0.993	0.989	0.982
temp, °C	pH 7.6	pH 7.8	pH 8.0	pH 8.2	pH 8.4	pH 8.6	pH 8.8	pH 9.0
5	0.991	0.986	0.977	0.964	0.945	0.915	0.872	0.811
6	0.990	0.985	0.976	0.963	0.942	0.911	0.866	0.804
7	0.990	0.984	0.975	0.961	0.939	0.907	0.861	0.796
8	0.989	0.983	0.974	0.959	0.937	0.903	0.855	0.788
9	0.989	0.982	0.973	0.957	0.934	0.899	0.849	0.780
10	0.988	0.982	0.971	0.955	0.931	0.894	0.842	0.771
11	0.988	0.981	0.970	0.953	0.928	0.890	0.836	0.763
12	0.987	0.980	0.968	0.951	0.924	0.885	0.829	0.754
13	0.987	0.979	0.967	0.949	0.921	0.880	0.823	0.745
14	0.986	0.978	0.965	0.946	0.918	0.875	0.816	0.737
15	0.985	0.977	0.964	0.944	0.914	0.870	0.809	0.727
16	0.985	0.976	0.962	0.941	0.910	0.865	0.802	0.718
17	0.984	0.975	0.961	0.939	0.906	0.860	0.794	0.709
18	0.983	0.974	0.959	0.936	0.903	0.854	0.787	0.699
19	0.982	0.972	0.957	0.934	0.899	0.848	0.779	0.690
20	0.982	0.971	0.955	0.931	0.894	0.842	0.771	0.680
21	0.981	0.970	0.953	0.928	0.890	0.836	0.763	0.671
22	0.980	0.969	0.951	0.925	0.886	0.830	0.755	0.661
23	0.979	0.967	0.949	0.922	0.881	0.824	0.747	0.651
24	0.978	0.966	0.947	0.918	0.877	0.818	0.739	0.641
25	0.977	0.964	0.945	0.915	0.872	0.811	0.730	0.631
26	0.976	0.963	0.942	0.912	0.867	0.804	0.722	0.621
27	0.975	0.961	0.940	0.908	0.862	0.798	0.713	0.611
28	0.974	0.960	0.938	0.905	0.857	0.791	0.704	0.601
29	0.973	0.958	0.935	0.901	0.852	0.784	0.696	0.591
30	0.972	0.956	0.933	0.897	0.846	0.777	0.687	0.580

perature range. This relationship can be represented by the regression equation $pK = 3.658 + 1662/T$ with $R^2 = 0.995$ and was used to define pK at various temperatures in subsequent calculations. The pK value determined in the present study, 9.232 at 25 °C, is in good agreement with that determined by Ang (*16*), 9.22, and by Izatt et al. (*17*), 9.21. However, the relationship calculated from data by Izatt et al. (*17*) for the temperature interval 10–30 °C, and as represented by the equation $pK = 1.620 + 2268/T$ with $R^2 = 0.998$, is slightly different from that determined in this study.

The relationship between [HCN]/[free cyanide] is equal to the factor $[H^+]/(K_1 + [H^+])$ or $1/(10^{pH-pK} + 1)$. When both molecular HCN and free cyanide are expressed as HCN, an HCN concentration divided by the appropriate factor will give the free cyanide concentration. Factors presented in Table II define the fraction of free cyanide as molecular HCN at 1.0 °C intervals from 5 to 30 °C and pH values from 6.0 to 9.0 in 0.2-unit intervals.

HCN Determinations in Waters and Wastewaters. The feasibility of directly determining HCN concentrations in water samples was evaluated by use of the diffusion technique. Several ions, two gases, and a few organic compounds commonly found in natural waters and wastewaters were investigated for possible interference with this method.

A substance that would directly interfere with the measurement of HCN must have a significant vapor pressure above its solution, must be collected by an alkaline solution, and must affect the colorimetric determination of cyanide.

Table III. Quantity of HCN Collected by the Diffusion Procedure from Standard Cyanide Solutions of Different pH

buffered pH value[a]	HCN collected,[b] μg	
	predicted[c]	determined
5.99	1.31	1.31
7.62	1.28	1.12
8.45	1.14	1.11
8.71	1.04	1.08
9.07	0.816	0.846
9.29	0.654	0.714
9.36	0.601	0.646
9.50	0.499	0.587
9.67	0.385	0.412

[a] pH controlled with phosphate or borate buffers. [b] HCN collected by 20.5 mL of 0.02 N NaOH in 2 h from 1.5-L solutions containing 25 μg/L free cyanide and at 22 °C. [c] Predicted values based on pK_a = 9.289 at 22 °C.

The colorimetric reaction between cyanide and pyridine, however, is a relatively specific reaction and not very subject to interferences. The presence of ammonia at 50 mg/L NH_3-N, sulfide at 0.50 and 1.0 mg/L S, and phenol at 50 mg/L resulted in only about an 8%, 3%, 13%, and 0% reduction, respectively, in the color developed by the pyridine–barbituric acid method for solutions containing 40 μg/L HCN. Thiocyanate, however, severely affects the determination of cyanide since it is halogenated directly just as free cyanide. The presence of silver and nickel cyanide complexes also gave a positive interference in the direct determination of free cyanide.

A substance could indirectly interfere with the measurement of HCN by contributing free cyanide to the system or affecting the rate at which HCN diffuses from a test solution. The displacement of HCN by diffusion from 1.5-L test solutions containing 25 μg HCN/L was virtually unaffected by the individual presence of the following chemicals: 130 mg/L Cl^-,

Table IV. Determination of HCN by the Diffusion Procedure for Phosphate-Buffered Cyanide Solutions at 20 °C and Containing Complexing Metals

test solution[a]	pH value	amt of total cyanide present (as HCN), μg L^{-1}	HCN concn, μg L^{-1}	
			expected	determined
$ZnSO_4$ + 4NaCN	7.35	25.3	25.3	24.3
$CdSO_4$ + 4NaCN	7.50	24.7	24.7	20.1
$Pb(NO_3)_2$ + 4NaCN	7.50	26.4	26.4	26.0
$K_4Fe(CN)_6$	7.72	1000	~0.0	1.67
$K_4Fe(CN)_6$ + 25 μg/L HCN	7.74	1025	~25.0	25.9
$K_3Fe(CN)_6$	7.74	1000	~0.0	1.53
$K_3Fe(CN)_6$ + 25 μg/L HCN	7.74	1025	~25.0	25.7
$AgNO_3$ + 2NaCN	7.68	500	5.82[b]	4.63
$AgNO_3$ + 2NaCN	7.43	10000	12.3[b]	14.0
$NiSO_4$ + 4NaCN	7.07	5000	190[b]	149
$NiSO_4$ + 4NaCN	7.06	10000	200[b]	154

[a] Iron cyanide solutions were shielded from light. [b] Concentrations based on results for similar solutions as reported by Broderius (*19*).

Table V. Determination of HCN by the Diffusion Procedure for NaCN Spiked Water and Wastewater Samples at 20 °C

sample	pH value	amt of total cyanide added (as HCN), μg L^{-1}	HCN concn, μg L^{-1}	
			expected[a]	determined
Natural Waters				
well	7.92	27.2	26.2	18.8
spring	7.38	27.2	26.9	27.0
creek	6.53	27.2	27.1	26.2
lake	7.85	27.2	26.3	23.4
pond	8.57	27.2	23.1	20.6
Industrial and Muncipal Treatment Effluent				
Plant A[b]				
100% effluent	7.00	0.0	0.0	~0.0
100% effluent	6.80	27.5	27.4	15.9
50% effluent	6.90	27.5	27.4	19.1
25% effluent	7.00	27.5	27.4	23.3
Plant B[c]				
100% effluent	7.55	0.0	0.0	~0.0
100% effluent	7.55	27.0	26.6	11.0
50% effluent	7.65	27.0	26.4	11.3
25% effluent	7.70	27.0	26.4	16.8
Oil Refinery Effluent[d]				
100% effluent	5.90	0.0	0.0	7.8
100% effluent	5.95	28.5	36.3	41.0
50% effluent	6.05	28.5	32.4	33.9
25% effluent	6.15	28.5	30.4	31.2

[a] Expected concentration is equal to that added as NaCN plus that present in the effluent portion; all values adjusted for pH and temperature. [b] Effluent from the Western Lake Superior Sanitary District Treatment Plant, Duluth, MN. [c] Effluent from Mill Creek Wastewater Treatment Plant, Cincinnati, OH. [d] Effluent from the catalytic cracking of Canadian crude oil before any treatment and not including the cooling water portion of the total effluent.

7.4 mg/L SO_4^{2-}, 3.0 mg/L NO_3^-, 100 mg/L SCN^-, 50 mg/L NH_3-N, 0.1 mg/L Na_2S-S, 50 mg/L phenol, 50 mg/L *o*-cresol, 5 mg/L Zn^{2+}, 5 mg/L Cd^{2+}, 5 mg/L Pd^{2+}, 1.0 mg/L $Fe(CN)_6^{4-}$ or $Fe(CN)_6^{-3}$ as CN in the dark, 100 mL of $^1/_{15}$ M phosphate or borate buffers, and 33 mg/L granular or 0.15 mL/L liquid detergent.

Sulfide at concentrations of 1.0 mg/L Na_2S-S extensively interfered with the determination of HCN. Since it was observed that such a concentration will only have minimal effect on the direct colorimetric procedure for cyanide determination, the interference process must occur in the test solution itself. Possibly sulfide oxidation products, especially polysulfides, react with cyanide to produce thiocyanate (*18*). Therefore, sulfide should be removed from a sample as soon as possible after collection to prevent its potential interaction with cyanide. Recommended procedures for sulfide removal suggest the addition of either lead or cadmium salts (*15*).

The performance of the diffusion method was evaluated with a variety of water and wastewater samples by determining the recovery of cyanide from samples spiked with NaCN and complex cyanides. A summary of the tests with various waters is presented in Tables III–V.

The quantity of HCN collected in NaOH from deionized water solutions buffered at various pH values and containing 25 μg/L free cyanide was generally lower than, but satisfactorily agreed with, the values predicted from a calculated pK value of 9.289 for 22 °C (Table III). The results for solutions containing iron cyanide complexes, which are essentially undissociated in the dark, and for those with zinc, cadmium, and lead, which are virtually completely dissociated at dilute concentrations, are in accordance with expectations (Table IV). The results for silver and nickel cyanide complex solutions, in which only a fraction of the total cyanide exists as HCN, are also in reasonable agreement with expected values as determined from earlier work (*19*), which utilized the vapor-phase equilibration procedure for HCN measurement.

The type of sample was most important in determining the percentage recovery of spiked simple cyanide (Table V). For natural water samples, with the exception of very hard well water (296 mg/L as $CaCO_3$), the determined HCN concentrations were essentially equal to the expected values. In most cases the recoveries from spiked effluents were lower than from pure water samples, which resulted in lower determined HCN concentrations than expected. This response may be due to free cyanide-complexing components and other chemical and biological reactions making a portion of the spiked cyanide not present or unavailable for measurement. Therefore measuring the recovery of cyanide added to certain samples is not necessarily a reliable means of studying the suitability of the method for natural water samples. In no instance, however, was a marked positive interference detected when HCN was expected to be absent or in low concentration (Table V). This was also true for an effluent from a copper, cadmium, and zinc plating plant in which no free cyanide was determined following a spike of about 25 μg/L.

The vapor-phase-equilibration method was not deemed as useful as the diffusion procedure in determining low concentrations of HCN. The diffusion method appears to be suitable for the determination of HCN in the microgram-per-liter range since considerable direct and indirect evidence indicates that the method can be used for many types of samples. Even when it is necessary to analyze for HCN in the field, the diffusion method provides a feasible approach.

LITERATURE CITED

(1) Doudoroff, P. EPA-600/3-76-038; U.S. Environmental Protection Agency: Duluth, MN, 1976.
(2) Broderius, S. J.; Smith, L. L., Jr. *Anal. Chem.* **1977**, *49*, 424–428.
(3) Blaha, J. *Water Res.* **1976**, *10*, 815–819.
(4) Roberts, R. F.; Jackson, B. *Analyst (London)* **1971**, *96*, 209–212.
(5) Kruse, J. M.; Thibault, L. E. *Anal. Chem.* **1973**, *45*, 2260–2261.
(6) American National Standards Institute. "Method for Determining Free Cyanide in Photographic Effluents"; American National Standards Institute: New York, 1978; ANSI PH 4.41.
(7) Durst, R. A. *Anal. Lett.* **1977**, *10*, 961–978.
(8) Worley, F. P.; Browne, V. R. *J. Chem. Soc., Trans.* **1917**, *111*, 1057–1062.
(9) Schneider, C. R.; Freund, H. *Anal. Chem.* **1962**, *34*, 69–74.
(10) Claeys, R. R.; Freund, H. *Environ. Sci. Technol.* **1968**, *2*, 458–460.
(11) Nelson, K. H.; Lysyj, I. *J.-Water Pollut. Control Fed.* **1971**, *43*, 799–805.
(12) Montgomery, H. A. C.; Gardiner, D. K.; Gregory, J. G. G. *Analyst (London)* **1969**, *94*, 284–291.
(13) Great Britain, Ministry of Technology "Water Pollution Research 1966"; H. M. Stationery Office: London, 1967; pp 152–154.
(14) Brown, V. M.; Shurben, P. G.; Shaw, D. *Water Res.* **1970**, *4*, 363–382.
(15) American Public Health Association et al. "Standard Methods for the Examination of Water and Wastewater", 14th ed.; American Public Health Association; Washington, DC., 1975.
(16) Ang, K. P. *J. Chem. Soc.* **1959**, 3822–3825.
(17) Izatt, R. M.; Christensen, J. J.; Pack, R. T.; Bench, R. *Inorg. Chem.* **1962**, *1*, 828–831.
(18) Luthy, R. G.; Bruce, S. G., Jr. *Environ. Sci. Technol.* **1979**, *13*, 1481–1487.
(19) Broderius, S. J. "Determination of Molecular Hydrocyanic Acid in Water and Studies of the Chemistry and Toxicity to Fish of Metal-Cyanide Complexes", Ph.D. Thesis, Oregon State University, Corvallis, OR, 1973.

RECEIVED for review December 5, 1980. Accepted April 14, 1981.

Ion Pair Mobility in Associated Liquid Membranes

Claudio Fabiani* and Claudia Cianetti

Material Division, CNEN, CSN-Casaccia, Rome, Italy

The ion pair mobilities of the site–counterion associated species in liquid membranes formed by tetraheptylammonium salts dissolved in different organic solvents are measured by means of the resistance relaxation method. The results are compared with the mobilities of the same species calculated from conductometric data. The conclusion is reached that the two methods give different mobility values especially in moderately associated membranes.

The use of liquid ion exchange and carrier membranes for separation processes with industrial applications has been demonstrated (*1*, *2*). The development of selective and economical separation processes, useful in the areas of metal recovery and treatment of hazardous nuclear and nonnuclear wastes, are the objective of many research programs on free and solid supported liquid membranes. The liquid membranes studied for these purposes are characterized by the presence in the membrane phase of a carrier molecule, i.e., a chemical species which selectively transports an ion through the membrane by forming a complex or, more generally, an associated uncharged species. Therefore the mobilities of the uncharged species which are formed into the membrane phase are of relevant importance because they contribute to determine

0003-2700/81/0353-1477$01.25/0 © 1981 American Chemical Society

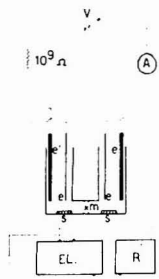


Figure 1. Scheme of the measuring cell and circuit: batteries (V), picoammeter (A), electrodes pairs (ee, e'e'), membrane (m), stirrers (s), electrometer (EL), and recorder (R).

both the selectivity and the transport behavior of the membrane (*3*, *4*). However, very often, these mobilities are not measured directly, but their values are computed from the conductivities of the ions which constitute the uncharged complex. A very simple method for measuring ion pair mobilities in associated liquid ion exchange membranes has been proposed by Sandblom (*3*). The method is based on the measurement of the relaxation time needed by the electrical resistance of an associated liquid membrane to reach its steady-state value when a step change in the external aqueous solutions is produced (*3*). Following this external solution change the membrane potential immediately assumes its steady-state value. On the contrary the resistance changes according to the establishment of the new steady-state concentration profiles in the membrane interior.

In this report the ion pair mobilities in tetraheptylammonium chloride and nitrate membranes have been measured according to this method, and the results are compared with the ion pair mobilities computed from conductivity data (*4*, *5*). The effect of the solvent on the ion pair mobilities has also been taken into account.

EXPERIMENTAL SECTION

Tetraheptylammonium chloride (THACl) and nitrate (THA-NO_3) were prepared from tetraheptylammonium iodide (supplied by Fluka) as reported in ref 6. All other chemicals were Carlo Erba (Milan, Italy) purity grade reagents and were used as received. The liquid membrane was of the type

KCl (0.1 M)/THANO_3 (0.1 M) (organic solvent)/KCl (0.001 M), KNO_3 (0.1 M) (A)

and similarly for the THACl system. The membrane solvents were monochlorobenzene, *o*-dichlorobenzene, and nitrobenzene. The membrane was formed in a small hole (diameter 0.8 mm) drilled into a PTFE disk (thickness d = 0.4 mm) interposed between the two arms of a U-shaped cell. The cell was thermostated at 25.0 ± 0.1 °C and the aqueous solutions were vigorously stirred at a constant rate. It is worth noting that the rate of stirring seems to have no effect on the experimental results. A constant small current of 0.002 μA supplied by standard batteries connected via a 10^9-Ω resistor was passed through the membrane by means of two Ag,AgCl electrodes. Another pair of similar electrodes was used to measure the potential difference across the membrane and hence the membrane resistance (Figure 1). The Ag,AgCl electrodes, prepared according to the classical method of ref 7, were used only if the asymmetry was less than ±0.2 mV. As the membrane was preequilibrated only with the reference solution (KCl 0.1 M) the step change in the external conditions was obtained when the test solution (KCl, KNO_3) contacted the membrane phase.

RESULTS AND DISCUSSION

When the membrane phase is put into contact with the external aqueous solutions, the steady-state membrane potential is immediately observed while a certain time, τ, is needed for the membrane resistance to reach its steady-state value (*3*). In associated liquid membranes, the kinetic behavior is determined by the diffusion of the associated species, and hence it depends on the ion pair mobilities. Sandblom (*3*) has deduced the following relation for the relaxation time

$$\tau = (d^2/\pi^2 D) = (d^2F^2/RT\pi^2\lambda_0) \qquad (1)$$

where d is the membrane thickness, D is the diffusion coefficient, λ_0 is the ion pair conductivity, and R, T, and F have their usual meaning. As a consequence of eq 1, provided the assumptions made on deriving it are fulfilled as in the case of our tetraheptylammonium membranes (*5*), a measure of τ allows a direct determination of the ion pair mobility (λ_0). In the case of a biionic system like system A, the hypothesis is made that due to the dimensional difference between the ionic membrane trapped sites (THA^+) and the counterions (Cl^-, NO_3^-) the ion pair mobilities are very similar for THA-Cl and THA-NO_3. It must also be remembered that in associated liquid membranes the ion pairs are the predominant species (*4*, *5*). In Figure 2 the registered resistance relaxation curves for the THANO_3 membranes are reported as examples. In Table I the relaxation times τ and steady-state resistance R are collected. The reported data are the mean values of at least three curves, shown in Figure 2. From these data it is seen that for a given ion exchanger the relaxation time increases with the membrane association, i.e., decreases with the membrane solvent dielectric constant. Therefore according to eq 1 the ion pair mobility increases in the order monochlorobenzene < *o*-dichlorobenzene < nitrobenzene. As expected the steady-state resistance is higher when the liquid membrane is more associated. These trends are observed both for THACl and THANO_3. As already supposed the difference between the ion pair mobilities for THACl and THANO_3 are small. In Table II together with the dissociation constants (k_{is}), site and counterion mobilities (λ_i), and ion pair mobilities ($\bar{\lambda}_{is}$) as evaluated from conductivity data (*4*, *5*), the ion pair mobilities (λ_{is}) from relaxation measurements are reported for THACl and THANO_3 in the three solvents used. The $\bar{\lambda}_{is}$s are evaluated according to Sandblom et al. (*8*) as $\bar{\lambda}_{is} = (2\lambda_i\lambda_s/\lambda_i + \lambda_s)$ being λ_s the site mobility. From these data it is evident that the same correlation between association and ion pair mobilities is shown by the conductometric mean value $\bar{\lambda}_{is}$ and the corresponding relaxation data λ_{is}. However, for a given membrane system the λ_{is} and $\bar{\lambda}_{is}$ values are very different from each other particularly in the *o*-dichlorobenzene case. These

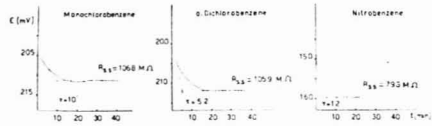


Figure 2. Recorded curves for the resistance relaxation in THANO_3 liquid membranes in the reported solvents. $R_{s.s}$ is the steady-state resistance of the membrane after the relaxation time τ (min). The current is I = 0.002 μA.

Table I. Relaxation Times, τ, and Steady-State Resistance, R, for THACl and THANO_3 Liquid Membranes

	THACl		THANO_3	
solvent	τ, min	$10^{-6}R$, Ω	τ, min	$10^{-6}R$, Ω
monochlorobenzene	11	107.2	10	106.8
o-dichlorobenzene	6	105.3	5	105.2
nitrobenzene			1	79.8

Table II. Equilibrium and Transport Parameters for THACl and $THANO_3$ Liquid Membranes

		monochloro-benzene	o-dichloro-benzene	nitro-benzene
k_{is}[a]	$THANO_3$	3.3×10^{-7}	1.52×10^{-5}	0.019
	THACl	1.1×10^{-7}	1.62×10^{-6}	0.018
λ_i[a]	THA^+	8.9	9.5	9.2
	NO_3^-	1.1	15.5	25.2
	Cl^-	1.2	36.0	35.6
$\bar{\lambda}_{is}$[a]	$THANO_3$	2.0	11.8	13.5
	THACl	2.1	15.1	14.6
λ_{is}	$THANO_3$	1.01	2.03	11.12
	THACl	0.92	1.69	

[a] Data are taken from ref 4. Mobilities are expressed in conductivity units Ω^{-1} cm^2 mol^{-1}.

differences cannot be due to convective or kinetics effects because the membranes are convection-free and in steady-state conditions as demonstrated by their zero current potentiometric behavior (*3*, *5*). Therefore it must be inferred that the computation of ion pair mobilities as a mean value of the limiting constituting ion mobilities is a rough approximation specially in moderately associated membranes. Similar differences can be found also in the Sandblom paper concerned with a bis(2-ethylhexyl)phosphoric acid in amyl alcohol membrane (*3*). These conclusions demonstrate that a direct measurement of the associated species mobility is needed especially when membrane transport properties are requested for characterizing the liquid membrane in separation applications. Nevertheless this difference in ion pair mobilities seems less important when a potentiometric characterization of the membrane is pursued (i.e., in ion specific electrode research) because the membrane potentiometric selectivity depends on the ratio of the mobilities of the diffusing species (*8*). In fact on comparison of the λ_{is} and $\bar{\lambda}_{is}$ ratios for THACl and $THANO_3$ liquid membranes in the examined solvents, very small differences appear. Possibly these conclusions may not be true if two very different counterions were present in the membrane phase. In this case a direct experimental measurement of the ion pair mobilities should be necessary.

LITERATURE CITED

(1) Lee, K. H.; Evans, D. F.; Cussler, E. L. *AIChE J.* **1978**, *24*, 860–868.
(2) Baker, R. W.; Tuttle, M. E.; Kelly, D. J.; Lonsdale, H. K. *J. Membr. Sci.* **1977**, *2*, 213–233.
(3) Sandblom, J. *J. Phys. Chem.* **1969**, *73*, 257–264.
(4) Fabiani, C. *Anal. Chem.* **1976**, *48*, 865–868.
(5) Fabiani, C.; Danesi, P. R.; Scibona, G.; Scuppa, B. *J. Phys. Chem.* **1974**, *78*, 2370–2375.
(6) Danesi, P. R.; Magini, M.; Scibona, G. "Solvent Extraction Research"; Kertes, A. S., Marcus, Y., Eds.; Wiley: New York, 1965; p 185.
(7) Ives, D. J.; Janz, G. J. "Reference Electrodes"; Academic Press: New York, 1961; Chapter 4.
(8) Sandblom, J.; Eisenman, G.; Walker, J. L., Jr. *J. Phys. Chem.* **1967**, *71*, 3862–3869.

RECEIVED for review November 3, 1980. Accepted April 13, 1981.

Determination of Synthetic Amorphous Silica in Industrial Air Samples

B. A. Lange,[1] J. C. Haartz,* and R. W. Hornung

National Institute for Occupational Safety and Health, Division of Physical Sciences and Engineering, Cincinnati, Ohio 45226

A method has been developed for the determination of small quantities of airborne synthetic amorphous silica. The analytical procedure utilizes X-ray diffraction following conversion of the amorphous silica to cristobalite by heating. The method is characterized by specificity for amorphous silica, linear calibration curves, good precision, and similar responses for three different types of amorphous silica. The method has been shown to be "rugged" relative to procedural variability and has the potential for partial automation. In the course of the study the effects of chemical contaminants were examined, and samples collected in an industrial environment were analyzed.

Synthetic amorphous silica, or vitreous silica (*1*), is a material that finds wide use in a diverse range of industrial applications including food processing and pharmaceutic preparations and in the manufacture of paper, paints and varnishes, and rubber products. Use of the material in the rubber industry provides increased tensile strength, hardness, and abrasion resistance while its chief function in the food and pharmaceutical industry is to improve flowability and provide moisture protection. Paper products treated with amorphous silica exhibit better opacity and printability and it is used to control thixotropy, flatting, and corrosion resistance in protective coatings. The potential for worker exposure is high not only because such massive amounts of the material are used but also because the particle size is such that a high percentage of it is in the respirable range. As a result, concern has been expressed about worker exposure to amorphous silica.

Determination of amorphous silica in workplace atmospheres is complicated by the existence of different occupational safety and health permissible exposure limits (OSHPEL) for the various chemical forms of SiO_2 (*2*). The permissible levels for cristobalite and tridymite are the lowest, that for quartz is intermediate, while those for amorphous silica and natural diatomaceous earth are the highest. Additionally, the allowable levels are dependent upon the percent SiO_2 in the atmosphere. For amorphous silica, the permissible average, 8-h exposure for a worker is given by the formula

$$\text{OSHPEL} \leq \frac{80\ \text{mg/m}^3}{\%\ \text{SiO}_2}$$

A variety of analytical methods exist for the determination of quartz, cristobalite, and tridymite in workplace atmospheres (*3*). The present study was undertaken to develop a method which would be specific for determining the airborne con-

[1] Present address: W. R. Grace & Co., 62 Whittemore Ave., Cambridge, MA 02140.

This article not subject to U.S. Copyright. Published 1981 by the American Chemical Society

centration of amorphous silica.

The gravimetric method used heretofore for amorphous silica was simply the determination of the weight of sample collected for a known volume of air. This technique obviously lacks specificity, for not only are concomitants included but also the adsorbed water content, which varies considerably with the type of amorphous silica as well as with the atmospheric conditions. The general approach applied in the method development involved conversion of the amorphous silica to cristobalite by heating to high temperatures; the cristobalite is in turn determined by using X-ray diffraction (XRD). If the sample contains a crystalline form as well as amorphous SiO_2, the crystalline components can be determined by using existing XRD methods (*3*) prior to conversion. Earlier work (*4–9*) indicated that quantitative conversion was possible, although no evidence exists suggesting that it has been employed as an analytical technique for the determination of amorphous silica. The development of a method was complicated by the fact that there are three different major techniques used in the preparation of commercial amorphous silica, each leading to a product with somewhat different properties, i.e., particle size, water content, density, and level of impurities. The vapor-phase hydrolysis of a silicon halide such as $SiCl_4$ at elevated temperatures produces fumed amorphous silica. In a second process, the reaction between sodium silicate and an acid is used to produce a gel which is then heated and ground to give a dry powder. In the third process, sodium silicate is destabilized in solution by the addition of acid causing precipitation of very fine, amorphous silica particles which are subsequently washed and dried. In this paper these three types will be referred to as Silica F, Silica G, and Silica P, respectively; parallel studies were carried out by using all three types to ensure general applicability of the techniques developed.

The primary objectives of this research were to develop a method that would be specific for amorphous silica, i.e., free of chemical interferences, be applicable to the three types of amorphous silica and to the sample sizes (~2–5 mg) that would be collected in industrial environments under the present Occupational Safety and Health Permissible Exposure Limits (OSHPEL) (2), and be statistically rugged relative to procedural variability.

EXPERIMENTAL SECTION

Apparatus. X-ray diffraction measurements were made with an automated powder diffractometer (APD-3500) in combination with an X-ray generator (XRG-3000) and a scintillation counter (Philips Electronic Instruments, Inc.). Integrated peak areas were measured through the use of a step-scanning mode. Silver membrane filters (0.45 μm pore size, Selas Flotronics, Huntingdon Valley, PA) were used as a support for the samples which, along with a pulse height selector and a focusing graphite monochromator, served to reduce background radiation levels. All measurements were obtained by using a long fine focus copper X-ray tube (Philips) run at a power level of 1400 W (40 kV, 35 mA). The instrumental configuration employed in this study included a 1° receiving slit and a 2θ compensating divergence slit. The positions (2θ) of the analytical peaks for the various chemical species examined, along with the associated scan ranges, step increments, and count times per step increments are summarized in Table I.

All thermal measurements were made in platinum crucibles under dry air at atmospheric pressure using a Mettler thermoanalyzer, Model TA-1. Samples were heat treated by use of a furnace (Anter Laboratories, Pittsburgh, PA, Model S42) specially constructed to maintain (±1 °C) preset temperatures over the range 100–1500 °C. The filters used in the chemical contamination study were ashed in a low-temperature plasma asher (International Plasma Corp., Hayward, CA, Model IPC 4005) for 3 h at a radio frequency (rf) power level of 100 W with an oxygen flow of 40 cm^3/min. This ashing procedure was introduced to simulate the treatment that would be used for field samples suspected of containing a chemical contaminant.

Table I. Measurement Parameters

component	analytical peak[a] (°2θ)	scan range (°2θ)	step increment (°2θ)	time/step increment, s
cristobalite	21.93	20.10–23.00	0.02	2.0
silver	38.03	37.03–39.03	0.02	0.5
α-quartz reference stone	26.66	26.41–26.91	0.01	0.6

[a] Cu Kα radiation (1.541 78 Å).

Reagents. Samples of Silica F, Silica P, and Silica G were obtained from Cabot Corp., Boston, MA, PPG Industries, Pittsburgh, PA, and Davison Chemical, Baltimore, MD, respectively. The water content of each type of amorphous silica was determined by using thermogravimetric analysis at temperatures and heating rates identical with those used in the experimental procedures. Replicate analyses showed the weight losses for Silica F, Silica P, and Silica G to be 0.1%, 9.3%, and 9.8%, respectively. From these data, the theoretical weight of cristobalite could be calculated from the initial weight of amorphous silica used in subsequent experiments. Other reagents used in this study were reagent grade or the highest purity obtainable and included: kaolin (J. T. Baker Co.), quartz (Min-u-sil 10, Pennsylvania Glass Sand Co.), and talc, which was prepared by IIT Research Institute (ITTRI) under NIOSH Contract 210-75-0043 (*10*). Reference cristobalite samples were obtained from Tem-Pres (State College, PA), C-E Refractories (Valley Forge, PA), and IITRI (*10*).

Preparation of Suspensions and Samples. A weighed amount of amorphous silica (Silica F, P, or G) was placed in 50 mL of 2-propanol and the mixture subjected to an ultrasonic cell disruptor (Ultrasonics Inc., Model W140) at an output level of 5 W until good dispersion was obtained. The resulting suspensions were diluted with 2-propanol to 1 L in a standard volumetric flask to give a final concentration of ~0.2 mg/mL. Aliquots (2–25 mL) of the appropriate suspension were filtered through 37 mm diameter membrane filters using a procedure described previously (*11*). For the preparation of samples containing both amorphous silica and other components, the aliquot was placed in a beaker with the desired concomitant and, after ultrasonic dispersement, the mixed suspension was filtered onto a membrane filter. The filters used for these studies included polycarbonate membrane filters (type N 060, 0.6 μm pore size, Nuclepore Corp., Pleasanton, CA) as well as two different poly(vinyl chloride) (PVC) membrane filters (type FWS-D, 0.5 μm pore size, MSA Co., Pittsburgh, PA, and type BD, 0.6 μm pore size, Millipore Inc., New Bedford, MA).

Collection of Field Samples. Samples of airborne amorphous silica were collected at a manufacturing facility using 37-mm filter cassettes with PVC (type FWS-B, 5.0 μm pore size, MSA Co.) filters. Both battery powered personal sampling pumps (Model G, MSA Co.) and a large vacuum pump equipped with a manifold capable of taking multiple, simultaneous samples were used at flow rates of approximately 1.7 L/min. Each sampling system was individually calibrated; air flow through the personal pumps was regulated with rotameters, while critical orifices were used with the large vacuum pump. To enable a comparison of the amorphous silica concentration of the respirable fraction of the dust with that of the total dust, we equipped half of the cassettes used with the personal sampling pumps with 10-mm nylon cyclones. These cyclones function as particle size discriminators allowing only particles less than 10 μm (respirable fraction) to enter the filter cassette. The remaining cassettes, which were not equipped with cyclones, collected samples representative of the total dust.

Preparation of Samples for X-ray Analysis. The filters having amorphous silica deposits were folded and placed in platinum crucibles for conversion of the amorphous silica to cristobalite by heating. Initially, the temperature was increased slowly (ca. 50 °C/min) to 500 °C to ash the filters. After the filters were ashed, the temperature was increased to the desired final

temperature level at the maximum rate possible. At the end of the predetermined time period for heating, the samples were cooled at the natural cooling rate of the furnace. The residue remaining after heat treatment was transferred to an agate mortar and pestle and interground with approximately 10 mg of NaCl which acted both as a grinding aid and as a carrier for the small amounts of heated amorphous silica (cristobalite). The resulting powder was quantitatively transferred to a beaker, the NaCl dissolved in distilled water, and the insoluble residue deposited on a silver membrane filter for the XRD measurements.

RESULTS AND DISCUSSION

Preliminary Conversion Studies. Numerous studies concerning the transformation of quartz to cristobalite (see ref 12) have shown that the conversion is feasible and that the yields approach 100%. The *rate* of transformation has been reported to be dependent on a number of factors, including particle size, temperature, and the presence of impurities, or "mineralizers". The latter term is applied to substances which are added to increase the rate of conversion of one phase to another and includes substances as diverse as carbonates, tungstates, and water. Although fewer in number, reported investigations of the amorphous silica–cristobalite transformation also indicate that the rate dependence on particle size (*1*), temperature (*1*, *4–7*), and mineralizers (*5*, *7*, *9*, *14*, *15*) is similar to that observed for the quartz–cristobalite transformation. The extent of sample packing has also been reported to influence the conversion rate (*9*). The effects of temperature are extreme, and reported conversion rates vary widely over the temperature range 900–1700 °C. The transformation is reported to proceed rapidly at temperatures greater than 1400 °C (*7*), require more than 24 h at 1100–1300 °C (9) and be unappreciable at 1000 °C under most laboratory conditions (*1*). More recently, pure cristobalite was prepared by heating silica gel for 20 h at 1770 °C (*13*).

To determine the extent to which the various types (F,P,G) of amorphous silica were converted to cristobalite by heat treatment, we compared the diffraction peaks from samples heated at various temperatures over the range 1200–1500 °C for varying periods of time with those of six available reference samples of cristobalite. The cristobalite sample obtained from IITRI has been carefully analyzed and studied (*10*); the chemical and phase purity have been shown to be 100% for this sample. Independent studies and comparisons of this cristobalite by another laboratory also indicate that the material is ~100% cristobalite with a high degree of crystallinity (*16*). Although we have relatively little independent information as to the purity and crystallinity of the cristobalite samples obtained from Tem-Pres and from C-E Refractories, XRD scans do not indicate the presence of any impurities or of any other silica phases in these samples. The XRD data for the samples heated to 1500 °C are included in Figure 1 wherein the dashed line indicates the average cristobalite peak intensity found for these "reference" samples and the dotted lines indicate 1 standard deviation on either side of this average. The greatest response (net normalized counts/3 mg of sample) was obtained for the IITRI material [$(10.7 \pm 0.01) \times 10^4$] and the lowest for that from Tem-Press [$(9.5 \pm 0.3) \times 10^4$], while that from C-E refractories was intermediate [$(10.1 \pm 0.3) \times 10^4$]. Three other "reference" samples of cristobalite available to our laboratory but of undocumented origin were also investigated; data from these samples were not included in Figure 1. Two of these samples were shown by XRD and DTA to contain α-quartz and thus are not suitable for reference use. The size reduction techniques (grinding) used on the third sample apparently caused some degradation of the crystallinity (*16*) of the cristobalite or creation of an amorphous surface layer. This effect has been described previously for α-quartz (*17*). As might have been

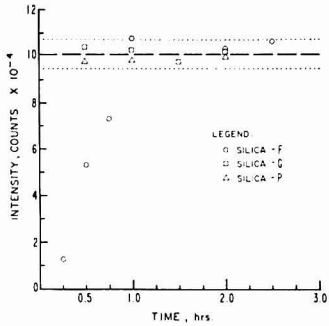


Figure 1. Integrated intensity of XRD peak (4.05 Å) for 3-mg samples of amorphous silica converted to cristobalite, as a function of heating time. Lines indicate average intensity ±1 standard deviation for reference samples of cristobalite.

expected, lower responses [$(5.4–7.4) \times 10^4$] were obtained for these cristobalite samples.

Plotted in Figure 1 is the XRD response obtained for cristobalite as a function of heating time (T = 1500 °C) for each of the three types of amorphous silica. From these data, it may be seen that the cristobalite diffraction intensities for each of the three types are essentially equal after 1 h at 1500 °C and are effectively the same as those found for the reference samples. The mean intensity for the group of three reference samples of cristobalite was compared with the mean intensities (three each for Silica F and P, four for Silica G) for the cristobalite formed from amorphous silica in a one-way classification analysis of variance (*18*). No significant difference among these four groups was found (P = 0.148), indicating that the conversion of amorphous silica to cristobalite is quantitative under these conditions. The data also indicate that the conversion of amorphous silica to cristobalite is rapid at 1500 °C; in all cases the conversion was complete after 1 h or less of heating. That Silica F was the slowest to convert is probably a consequence of the fact that this material is extremely pure with trace element and water levels far lower than those found with Silica P and Silica G. The presence of impurities, including water, has been found to have a marked effect on conversion rate (*1*, *7*, *9*, *14*, *15*). Although some oxides have a restraining effect on conversion rates, water vapor has been reported to accelerate the conversion (*1*).

Although conversion rates and yields were acceptable at 1500 °C, it was felt that most laboratories would not have access to a furnace which could reach and maintain that temperature. Consequently, in an effort to effect conversion at lower temperatures, various time/temperature combinations were explored until it was found that heating at 1100 °C for 6 h brought about the same degree of conversion as that found using 1500 °C for 1 h. The 1100 °C/6 h firing procedure was used in the remainder of this study.

Analytical Results. Having shown that amorphous silica can be quantitatively converted to cristobalite, we generated calibration curves using samples of Silica F, G, and P. Samples over the range 0.4–5.0 mg/filter were prepared, fired, and redeposited on silver membrane filters in the manner described in the Experimental Section. Five weights of amorphous silica, with triplicate determinations at each level, were used for each curve. The data are plotted in Figure 2 (open symbols). For purposes of comparison, data obtained in the study of conversion rates (Figure 1) are also included (solid symbols). The calibration curve parameters, given in Table II, indicate that the procedure yields calibration curves with good precision and that the slopes obtained for the

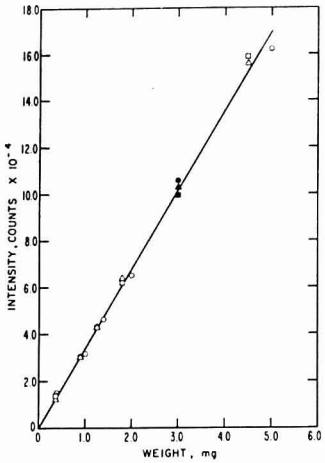


Figure 2. Integrated intensity of XRD peak (4.05 Å) for cristobalite as a function of weight of amorphous silica converted: O, Silica F; □, Silica G; △, Silica P.

Table II. Calibration Curve Parameters

type of amorphorus silica	slope, counts/mg	RSD, %
G	34828	2.0
F	30745	2.8
	32507[a]	1.9
P	33501	2.8
	34657[a]	2.0
pooled data	33987	1.5

[a] Based on 44 determinations (see text); all other slopes are based on 45 determinations.

cristobalite response for each of the three types of amorphous silica are similar. Since the samples for each curve were prepared by using a single suspension of a given type of amorphous silica, the component of variance due to preparation of the suspension had to be estimated in order to make a statistically meaningful comparison between the curves. This estimate was obtained by using data from the study in which optimum heating times were determined (Figure 1), wherein aliquots from several suspensions were used for replicate X-ray diffraction measurements. This estimated component of variance was then used in conjunction with the error terms from the replicate samples for the statistical comparison of the three calibration curves. The results indicated that the slope for Silica F was statistically significantly lower than that obtained for either Silica P or Silica G ($P < 0.05$), while the slopes for Silica P and G were not significantly different from each other.

However, the data for Silica P and Silica F showed an unusually large amount of variability for replicates at the highest weight (~5 mg). In both cases, this high degree of variability was caused by one measurement which was substantially lower than that for the other two replicates. Elimination of these two suspected outliers changed the calculated slope for the calibration curves (Table II) and decreased the magnitude of the differences between the slopes. However, a statistical comparison of these slopes indicates that the slope for Silica F is still statistically significantly lower ($P < 0.05$) than that of Silica P or Silica G, which are not significantly different from each other. It should be noted that this statistical significance resulted from the unusually good precision of replicates in the experimental data. While the slope for Silica F is statistically significantly lower than the slopes for the other two types, because it appears to be within the range of usual experimental error, a pooled calibration curve with slope of 3.40×10^4 counts/mg (RSD = 1.5%) was constructed by using these data, disregarding the significant statistical test. As may be seen from Figure 2, this line represents an acceptable fit for all of the data. Thus, from a realistic point of view, a calibration curve derived either from pure cristobalite or from one type of amorphous silica can be used for analysis of samples of any of the three types of amorphous silica. In terms of practicality, the low moisture content and the ensuing negligible weight loss upon heating of Silica F make this type of amorphous silica the most convenient for use as a standard.

The detection limit found for heated amorphous silica (cristobalite) in these studies is 3 μg, i.e., the amount of material required to give a net diffracted X-ray intensity equal to the average background plus three times the standard deviation of the background (*19, 20*). The data also show that the lower limit for quantitative determination, i.e., that quantity which can be determined with an RSD of 10% is 40 μg, an amount far lower than would be collected in atmospheres meeting the present OSHPEL. (*2*).

Concern existed that, in the application of this method by other laboratories, errors would result from variations in the time and temperature of heat treatment or from the use of filters other than those employed in this study. To examine the effects of these variables, we employed a two-level, three-factor experimental design wherein the two levels for time were 5 and 7 h, for temperature were 1050 °C and 1150 °C, and for filter type were polycarbonate (Nuclepore N-060) and PVC (MSA FWS-D). The results of these experiments showed that neither the variations in time, nor temperature, nor filter type nor any combination of these variables had any effect on the results at a significance level of 0.05 for any of the three types of amorphous silica. Because earlier studies of filters in this laboratory had indicated that silica background levels of some PVC filters were high and variable (*21*), the use of another PVC filter (Millipore B-D) was investigated. The high levels of silica (~1 mg/filter) found indicate that this filter is unsuitable for use in determination of amorphous silica. Because amorphous silica is used as a binder or filler in polymers, the use of other filter types should be preceded by suitable blank determinations.

Interferences. A number of studies concerning the effects of impurities on the conversion of quartz or of amorphous silica to cristobalite have shown that these impurities can accelerate, retard, or have no effect on the conversion rate. In general, oxides are reported to accelerate the conversion (*9, 12, 14, 15*) although Al_2O_3 has a retarding effect on the conversion of amorphous silica to cristobalite. The effect of impurities on the conversion of amorphous silica is an area of concern which is particularly germane for samples collected in those industrial environments where amorphous silica is used in conjunction with other materials.

To simulate chemical contamination and study the effects thereof on the conversion under the conditions used in this study, we combined samples of each of the three types of amorphous silica with a contaminant (2:1 w/w) and then heated as described above. The substances studied and results are listed in Table III. Examination of the data indicates that the amorphous silica to cristobalite conversion is somewhat sensitive to the presence of contaminants, especially at these relatively high levels of contamination. It is not clear why the extent of interference varied with the type of

Table III. Effect of Chemical Contaminants on the Conversion of Amorphous Silica to Cristobalite

interferant	Silica F		Silica P		Silica G	
	av response[a]	RSD, %	av response[a]	RSD, %	av response[a]	RSD, %
carbon black	0.970	0.72	1.048	0.79	1.055	6.38
ZnO	0.906	7.75	0.992	6.50	0.940	2.00
TiO_2	0.872	0.31	1.067	4.12	0.998	3.00
talc	1.009	3.14	1.136	1.18	1.116	0.41
quartz	1.256	4.72	1.426	2.47	1.279	0.20
kaolin	0.103	12.7	0.564	3.61	0.095	0.65
Al_2O_3	0.213	43.6	0.889	0.55	0.145	11.85
Cr_2O_3	0.789	1.94	1.087	0.51	1.021	12.60
Fe_2O_3	0.775	6.76	0.991	3.42	1.035	6.33
$SrCO_3$	0.800	2.00	0.749	2.46	0.850	5.52
$BaCO_3$	[b]		[b]		[b]	
MgO	0.865	7.20	0.850	4.02	0.895	3.95
CaO	0.516	5.87	0.532	15.64	0.520	3.01
CaO[c]	1.006	10.69	0.972	2.15	1.004	3.37

[a] Average of three samples containing interferant (2 mg amorphous silica/1 mg contaminant) divided by the response expected for a pure sample. [b] The final product was a mixture of $Ba_2Si_2O_5$ and cristobalite which could not be quantitated. [c] Acid washed prior to heat treatment (see text); average of four samples.

amorphous silica. Although in general the effect of a contaminant on conversion was greatest for Silica F, the data are not unequivocal. Since the scope of this study was more concerned with the ultimate effect than with the cause, delineation of these relationships was not pursued.

Two materials, carbon black and ZnO, which are often used with amorphous silica in industrial applications, had the least effect on the conversion of all three types of amorphous silica. The effect of TiO_2 addition was also relatively small although both TiO_2 and carbon black are reported to have a strong inhibiting effect on the conversion of quartz to cristobalite (*15*). As expected, the greatest positive interference was observed for quartz, which undoubtedly is partially converted to cristobalite at the temperatures used. The formation of quartz from cristobalite is reported to be very slow below 1200 °C (*12*); quantitative conversion would require longer heating times or higher temperatures. Interferences posed by quartz in the analysis of samples for amorphous silica could be alleviated by the preliminary determination of quartz using XRD followed by sufficient heating to ensure quantitative conversion of both quartz and amorphous silica to cristobalite and, finally, subtraction of the initial weight of quartz from the total cristobalite found. It should be noted that if quartz is present in sufficient quantities to seriously bias the analytical results for amorphous silica, then a significant health hazard is being posed by the quartz (*2*) and it should be the analyte of interest. The greatest negative interferences were found for the aluminum-containing compounds (Al_2O_3, kaolin) and the alkaline earth oxides, all of which either restrain the rate of conversion or, in the case of $BaCO_3$, reacted with the silica to form a metal silicate mixture.

The detrimental effect of these oxides prompted the development of a sample pretreatment step to be used if these compounds are known or suspected to be present in a sample. CaO was selected as a representative contaminant for these studies. Filter samples containing amorphous silica and CaO (2:1) were ashed in the LTA, and the residue was either treated with 50 mL of 2% HCl or carried through the usual suspension technique with 2-propanol prior to redeposition on polycarbonate filters. Thus, in the first set of filters, the CaO was removed prior to heat treatment. The results, which are included in Table III, indicated that the acid treatment eliminated the negative interference posed by CaO. Since most metal oxides are soluble in acid, use of an acid pretreatment step should eliminate many potential interferences.

In applications of this technique, preliminary identification of potential interferences using XRD scans of representative samples is essential. If interferences are identified, a more definitive study of the extent of interference and the efficacy of a pretreatment step should be investigated in greater detail.

Table IV. Determination of Airborne Amorphous Silica Concentrations in an Industrial Environment

location	sample type[a]	av concn, mg/m	N	RSD, %
1	total dust	56.5	6	3.3
2	total dust	14.3	5	1.8
3	total dust	29.6	3	7.5
	respirable dust fraction	2.2	2	13.5
4	total dust	74.5	3	3.8
	respirable dust fraction	12.5	3	7.9
5	total dust	10.7	3	18.4
	respirable dust fraction	2.1	3	9.7

[a] Locations 1 and 2 were sampled by using a manifold attached through critical orifices to a vacuum pump. All other locations were sampled by using battery-operated pumps and sampling cassettes which were equipped with 10-mm nylon cyclones only for collection of respirable fraction.

Analysis of Samples Collected in an Industrial Environment. As a test of the developed methodology using "real" samples, 28 dust samples were collected at a facility manufacturing amorphous silica. Because this was a methods development study, high dust levels were deliberately sought to assure that sufficient quantities of amorphous silica would be collected to allow determination of the reproducibility and practicality of the method. Samples were collected in particularly dusty areas unoccupied by workers, and therefore these results do not represent an industrial hygiene evaluation of a specific workplace atmosphere. The collected samples were ashed, heat treated, and redeposited on silver membrane filters using the techniques described in the experimental section. The analytical results are summarized in Table IV. The samples collected with the large vacuum pump show excellent precision for replicate samples, indicating that the analytical reproducibility is acceptable. The samples collected by using the battery powered personal pumps also showed acceptable reproducibility (pooled RSD = 11.0%) considering that the flow rate error associated with these pumps is inherently greater than that obtained by using a large pump and critical orifices. Federal regulations (*22*) require that the reproducibility (calibration and flow rate consistency over an 8-h period) of these pumps be ±5%; laboratory data indicate

that, at room temperatures, the pumps do meet that criterion (23). However, from data obtained in a simulated field sampling experiment (24), the volume correction for personal sampling pumps under conditions of actual use was found to be 0.99 ± 10.3% (N = 128). Thus a higher RSD for the samples collected in areas 3-5 (Table IV) is not unexpected. The large differences between total and respirable dust levels found in locations (3-5) is not surprising. Size distribution data for this type of amorphous silica (Silica F) indicate a mean particle size of 9 μm. Since the 10-mm nylon cyclone passes only about 10% of 9-μm particles, a much higher concentration of total dust is expected.

ACKNOWLEDGMENT

The authors express their appreciation to D. D. Dollberg and M. T. Abell for helpful discussions not only during the course of the work but also in the preparation of the manuscript.

LITERATURE CITED

(1) Sosman, R. B. "The Phases of Silica"; Rutgers University Press: New Brunswick, NJ, 1965; Chapter 7.
(2) Title 29, Part 1910: "Occupational Safety and Health Standards" *Fed. Regist.* **1971**, *36*, (no. 157), 15 101.
(3) Taylor, D. G., Ed. "NIOSH Manual of Analytical Methods", 2nd ed.; Cincinnati, OH, 1977; No. 106, 109, 110, 259, S315.
(4) Day, A. L.; Shepherd, E. S. *J. Am. Chem. Soc.* **1906**, *28*, 1089.
(5) Rieke, R.; Endel, K. *Silik. Z.* **1913**, *1*, 6.
(6) Endell, K.; Rieke, R. *Tschermaks Mineral. Petrogr. Mitt.* **1912**, *31*, 501.
(7) Verduch, A. G. *J. Am. Ceram. Soc.* **1958**, *41* (11), 427.
(8) Das, S. K.; Mookerjee, S. K.; Niyogi, S. K.; Thakur, R. L. *J. Therm. Anal.* **1976**, *9*, 43.
(9) Austrheim, I. T. *J. Br. Ceram. Soc.* **1977**, *76* (6), 134.
(10) Graf, J. L.; Ase, P. K.; Draftz, R. G. "Preparation and Characterization of Analytical Reference Minerals"; DHEW (NIOSH Publ. No. 79-139); Cincinnati, OH, 1979.
(11) Lange, B. A.; Haartz, J. C. *Anal. Chem.* **1979**, *51*, 520.
(12) Sosman, R. B. "The Phases of Silica"; Rutgers University Press: New Brunswick, NJ, 1965; Chapter 6.
(13) Thompson, A. B.; Wennemer, M. *Am. Mineral.* **1979**, *64*, 1018.
(14) Ekstrom, T.; Tiley, J. D. *J. Cryst. Growth* **1977**, *38*, 197.
(15) Taylor, N. W.; Lin, C.-Y. *J. Am. Ceram. Soc.* **1941**, *24*, 57.
(16) Lang, H. U.S. Bureau of Mines, Bruceton, PA, personal communication, 1979.
(17) Edmonds, J. W.; Henslee, W. W.; Guerra, R. E. *Anal. Chem.* **1977**, *49*, 2196.
(18) Walpole, R. E. "Introduction to Statistics"; MacMillan Co: New York, 1968; p 291.
(19) Birks, L. S. "X-Ray Spectrochemical Analysis"; Interscience: New York, 1959; p 54.
(20) Jenkins, R.; DeVries, J. L. "Worked Examples in X-Ray Analysis"; Springer-Verlag: New York, 1970; p 51.
(21) Haartz, J. C. In "Proceedings of the Symposium on Silica"; Industrial Health Foundation: Pittsburgh, PA, 1976; pp 38-55.
(22) Title 30, Part 74: "Coal Mine Dust Personal Sampler Units" *Fed. Regist.* **1970**, *35*, (No. 51), 4326.
(23) Parker, C. D.; Lee, M. B.; Sharpe, J. C. "An Evaluation of Personal Sampling Pumps in Sub-Zero Temperatures"; DHEW (NIOSH Publ. No. 78-117); Cincinnati, OH, 1977.
(24) Marks, G. E.; Knutson, E. O. "Complete Testing of the NIOSH Method for the Determination of Trace Metals by Atomic Absorption Spectrophotometry"; Final Report, Contract No. CDC 99-74-48, NIOSH, Cincinnati, OH, 1975.

RECEIVED for review July 10, 1980. Resubmitted April 17, 1981. Accepted April 17, 1981.

Microcomputer-Controlled Reagent Preparation System

R. Balciunas, F. J. Holler,[1] P. K. Notz,[2] E. R. Johnson,[3] L. D. Rothman,[4] and S. R. Crouch*

Department of Chemistry, Michigan State University, East Lansing, Michigan 48824

The design, operation, and evaluation of a microcomputer-controlled, syringe-based reagent preparation system with a dilution range of up to 5 orders of magnitude is reported. Reagents are prepared from up to three different stock solutions and one diluent. Reproducibility of the delivered stock solutions and of the diluted reagent is better than that of class A glassware for all cases tested. The results of several chemical complexation and kinetics studies are presented as a demonstration of the precision and utility of the system.

The microelectronics revolution that we are witnessing is spawning a new generation of automated laboratory instruments that, because of microprocessors, are intelligent, versatile, easily programmable, and highly reliable. This new breed of scientific instruments promises to enhance greatly the efficiency with which instrumental measurements can be carried out in the laboratory. Despite the high degree of automation of the measurement steps in UV-visible spectrophotometers, atomic absorption spectrometers, gas chromatographs, electrochemical analyzers, and other instruments, the chemist in most laboratories is still faced with the tedious, time-consuming, and error-prone task of manually preparing the solutions to be used for chemical studies and chemical analyses.

With automated instrumental systems, the preparation of solutions can easily be the step that limits the rate of information production. In stopped-flow chemical kinetics studies in our laboratory, for example, we commonly prepare for a single experimental session 10 or more solutions each containing two or more reagents often in buffered or constant ionic strength media. The mixing of the two reactant solutions and the recording of data that describes the reaction progress can be accomplished in our automated stopped-flow apparatus (*1-3*) in a few seconds or less for rapid reactions. Complete kinetics studies involving replications and several levels of reactant concentrations can often be carried out in an hour or less once the requisite solutions are prepared. However, preparing even moderately complex reaction mixtures usually requires a good deal more time than the mixing and measurement steps. In analytical procedures, the preparation of standard solutions for constructing calibration curves, for implementing standard addition methods, and for evaluating and optimizing instrumental performance can easily require

[1] Present address: Department of Chemistry, University of Kentucky, Lexington, KY 40506.
[2] Present address: Getty Oil Co., Houston, TX 77099.
[3] Present address: Departments of Chemistry and Psychology, Wayne State University, Detroit, MI 48202.
[4] Present address: Analytical Laboratories, The Dow Chemical Co., Midland, MI 48640.

0003-2700/81/0353-1484$01.25/0 © 1981 American Chemical Society

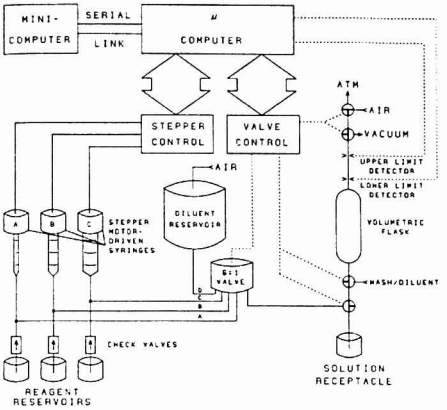


Figure 1. Schematic diagram of automated reagent preparation system. Capacity of syringes: A, 1 mL; B, 5 mL; C 50 mL.

more time than data acquisition, analysis, and interpretation.

Several automated reagent preparation systems have been previously reported (*4–12*) and many are reviewed elsewhere (*3, 12*). These have been classified by Stieg and Nieman (*12*) as continuous-flow systems or discrete-manipulation systems. The discrete systems are further divided into volume-based (*4–7, 9–11*) or weight-based (*8*) systems. In general, the systems that have been described have a rather limited dynamic range with a dilution ratio of 1:100 being the largest reported. While these systems are satisfactory for some analytical procedures and limited-range optimizations, many investigative studies require a much wider dynamic range of dilution.

In this report we describe a microcomputer-automated, volume-based solution preparation system that features highly accurate dilutions and a dynamic range of 10^5. The system can deliver and mix up to three reagents and a diluent, with a typical delivery and dilution precision of 0.05% RSD. The instrument is first described and then the results of several chemical tests that were made to evaluate its performance in laboratory studies are presented.

EXPERIMENTAL SECTION

System Description. The reagent preparation system shown in Figure 1 is composed of three stepper motor-driven syringes of 1, 5, and 50 mL capacities (motors, Model 23D6102, Computer Devices, Santa Fe Springs, CA; syringes, home-built), a zero dead volume six-way selector valve (Model B6031V6A, Altex, Berkeley, CA), four three-way flow selector valves (Model 201-14, Altex), and a volumetric flask with two optical meniscus detectors made from optointerrupters (Model no. 13B1, General Electric, Syracuse, NY). The volumetric flask can be of any convenient volume (10 mL to 1 L). A flask of 100 mL volume, constructed locally, was used throughout this study. The flasks used were identical in size and shape to volumetric pipets. The necks of the flasks were made from no. 6 glass tubing to mate with HPLC connectors. The system is under the direct control of a microcomputer, based on the IM 6100 microprocessor (Intersil Corp., Cupertino, CA), with 4096 words of random-access memory (RAM). The microcomputer performs all of the control and sensing functions. It is linked to a PDP 8/e (Digital Equipment Corp., Maynard, MA) minicomputer that carries out the necessary calculations and serves as the host computer for software development and data storage.

The entire reagent preparation sequence is controlled by the microcomputer. The user initially loads a control routine into the microcomputer from the minicomputer and initializes the system. A routine, executed by the minicomputer, calculates the number of steps each stepper motor should turn from the desired concentrations entered by the user. Once all of the parameters are transmitted to the microcomputer, the minicomputer is released and is free to perform other tasks. The controlling routine running in the microcomputer then takes over and initializes the solution preparation system by washing and filling the syringes and washing the dilution vessel. The remainder of the information required to make the desired dilutions resides in RAM in the microcomputer.

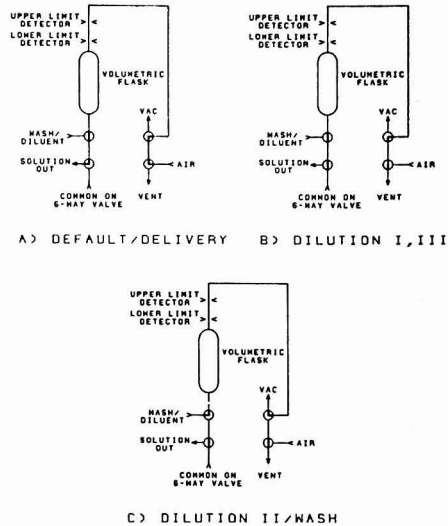


Figure 2. details of valve positions for various stages in solution preparation.

Reagent Preparation Sequence. As shown in Figure 2, the preparation of a single solution or series of solutions is straightforward. An appropriate volume of reagent is delivered from each of the syringes through the six-way selector valve into a central volumetric delivery vessel (dilution step I in Figure 2). A small volume (~10 mL) of diluent is then washed through the common line to flush out any reagent(s) into the volumetric flask (dilution step I). The flow-control valves then switch to allow 90% of the diluent volume to be rapidly drawn up through the wash/diluent valve into the volumetric flask by a vacuum until the solution reaches the lower meniscus limit detector (dilution step II in Figure 2). The valves switch again to allow a slower flow of diluent through the six-way valve common line into the volumetric flask until the upper limit detector is reached (dilution step III in Figure 2). Finally, the valves switch to deliver the diluted solution to an appropriate solution receptacle (delivery in Figure 2). The default/delivery position in Figure 2 leaves all of the three-way valves in the deactivated state and disconnected from the six-way valve common line. The microcomputer ascertains whether or not enough reagent remains in each of the syringes for preparation of the next solution and fills those syringes that are too low. The six-way valve turns to allow a small quantity of diluent to flush out the common line. This wash solution is then expelled, followed by the flow of another volume of diluent. The remaining wash sequence is similar to that followed in the dilution process described earlier. The entire washing process is performed twice before the next reagent is prepared. Upon completion of an entire dilution series, the user has the option of having the system repeat the entire series or reprepare individual solutions. The turbulence created by the uptake of diluent in dilution step II is used to mix the reagents and diluent. In cases where difficult to mix reagents or small dilution factors are involved, a stirrer could readily be added to the solution receptacle of Figure 1.

Table I. Syringe Resolution and Precision

syringe (fig 1)	total capacity, mL	resolution, μL	% RSD for delivery of total syringe volume
A	1	0.25	0.04
B	5	0.5	0.008
C	50	2.5	0.004

Reagents. All chemicals were reagent grade and were used without further purification. All solutions were prepared with distilled water.

The stock solutions for the mole ratio study were 0.3969 M Cu(II) prepared from $CuCl_2 \cdot 2H_2O$, 0.019 84 M EDTA prepared from the disodium salt, and acetate-buffer diluent that was 0.1 M in sodium acetate and adjusted to pH 2.2 with 10% HCl solution.

The stock reagents for the continuous variations study included 0.015 00 M Fe(II) solution prepared from $FeSO_4(NH_4)_2SO_4 \cdot 6H_2O$, 0.015 00 M 1,10-phenanthroline prepared from the monohydrate, and a combination buffer–reducing agent solution that was 0.056 M citric acid, 0.089 M hydroxylamine hydrochloride, and 0.02 M sodium hydroxide.

The stock solutions used in the kinetics study were 0.099 97 M Fe(III) prepared from $Fe(NO_3)_3 \cdot 9H_2O$, 0.025 19 M NaSCN, 1.003 M $NaClO_4$, and perchloric acid standardized to 1.094 M.

Procedures. The spectrophotometric measurements for the mole ratio and the mole fraction studies were done by using a single-beam molecular absorption spectrophotometer (EU-701A GCA McPherson Corp., Acton, MA) with a current-to-voltage converter (Model 427, Keithley Instruments, Inc., Cleveland, OH) interfaced to a 12-bit analog-to-digital converter (Model ADC-HZ12BGC, Datel Systems, Inc., Canton, MA). The solutions prepared in the two studies were analyzed with precision spectrophotometric measurements (*13*).

The Fe(III)–SCN kinetics studies were performed with an automated stopped-flow apparatus (*1*). The reaction was monitored at 450 nm. All of the data collection, averaging, and analyses were done by using the PDP 8/e minicomputer.

RESULTS AND DISCUSSION

The components of the reagent preparation system were tested as stand-alone devices and as an assembled unit. Each reagent syringe was calibrated by weighing the amount of distilled–deionized water displaced during a complete delivery cycle. The volume of water delivered was then computed from the density of water at the temperature of the calibration. The delivery precision and resolution for each syringe is shown in Table I. Over the course of 1 year, it was observed that unless the ambient temperature changed drastically, i.e., by more than 10 °C, the error in delivery volume due to changes in solution density was negligible compared to the error in weighing at the time of calibration.

Calibration of the dilution system (the volumetric flask with optical limit detectors) was performed by delivering distilled–deionized water into the volumetric flask until the upper limit sensor indicated that the flask was full. As before, the weight of water expelled into a weighing vessel was converted to volume using the appropriate density. The delivery precision of the 100-mL volumetric flask was found to be ±0.04% RSD. This figure, combined with a typical syringe delivery precision of ±0.01% RSD, gives the precision of the concentration of a given dilution of ±0.05% RSD, neglecting the uncertainty involved in the preparation of the stock reagents.

In normal use with a 100-mL dilution vessel, stock reagents delivered from the 1- and 5-mL syringes can be diluted by factors as large as 1:10 000 with 0.1% RSD. This dilution range can be readily extended by an order of magnitude by use of a 1-L dilution vessel, although solution preparation times become long with the 1-L vessel. The dilution range for solutions delivered from the 50-mL syringe with 0.1% RSD is limited by the coarseness of the lead screw that drives the syringe plunger to a factor of 1:4000 (100 mL dilution vessel). The 50-mL syringe is normally used to deliver buffer solutions or to make ionic strength adjustments where a large dilution range is not required. For cases where more than two reagents must be diluted by factors up to 1:10 000, two additional 1- or 5-mL syringes can be added to the unused ports of the six-way selector valve.

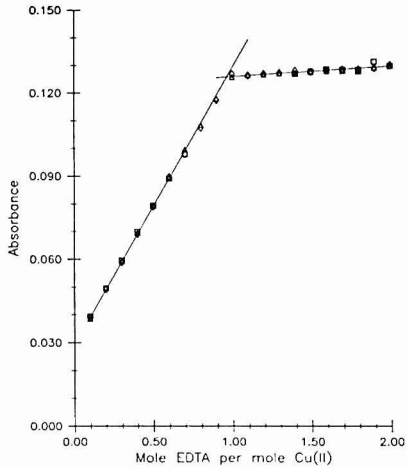


Figure 3. Mole ratio plot for Cu(II)–EDTA complex. Absorbance at 710 nm is plotted vs. mole ratio EDTA/Cu(II) in solutions prepared automatically. Three separate solutions prepared automatically at each mole ratio are indicated by △, ◇, and □.

The automatic reagent preparation system was critically evaluated by determining the stoichiometry of two complexation reactions. Initially, the simple 1:1 reaction of copper and EDTA was studied by the mole ratio method (*14*). Three series of 20 solutions were prepared, each containing a constant concentration of copper and varying amounts of EDTA and each at a constant pH. The absorbance of the resulting solutions was measured at 710 nm. The resulting plot of absorbance of the complex vs. mole ratio of EDTA/copper is shown in Figure 3. The intersection of the extrapolated linear portions of the curve occurs at a mole ratio of 0.987 ± 0.044, as is expected for this type of complex. The variation in the absorbance value of a replicate preparation of a solution of a given mole ratio was negligible compared to the imprecision of the individual absorbance measurements.

A more rigorous evaluation of the system performance was done by using the iron–*o*-phenanthroline complexation reaction in a continuous variations study (*15*). In this case, three series of 14 solutions each were prepared, all containing a constant molar quantity of iron and *o*-phenanthroline and all at a constant pH of 4.0. The absorbance of the complex was measured at 510 nm. The plot of absorbance vs. mole fraction of *o*-phenanthroline is presented in Figure 4. Here the variation of the absorbance of the individual solutions in each series was expected to be larger than that observed in the copper–EDTA study because of the small volumes of reagents that were delivered: 25–900 μL of iron solution from the 5-mL syringe and 100–1000 μL of *o*-phenanthroline from the 1-mL syringe. This particular arrangement was chosen in order to observe the performance of the 5-mL syringe in delivering small reagent volumes. As can be seen in Figure 4, the imprecision of the absorbance of each solution for a given mole fraction is small and was observed to be within the absorbance

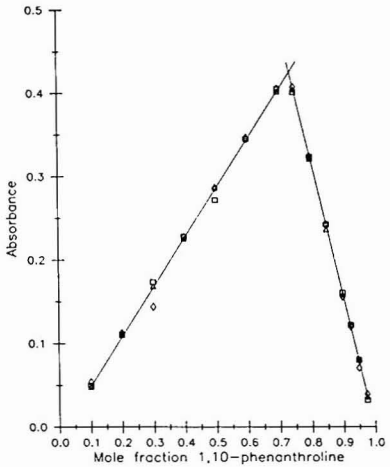


Figure 4. Continuous variations plot for Fe(III)-*o*-phenanthroline complex. Absorbance measured at 510 nm. Three separate solutions prepared automatically at each mole fraction are indicated by △, ◊, and □.

measurement error for most of the solutions. The extrapolated linear portions of the curve intersect at a mole fraction of *o*-phenanthroline of 0.75 giving a complexation number of 3.0 ± 0.1 as is expected.

The automated reagent preparation system has also been used to prepare solutions at constant ionic strength for kinetics studies of the iron(III)-thiocyanate reaction. These studies were made to evaluate the system performance using a "real" laboratory problem, i.e., to prepare a series of solutions to be used in the generation of initial rate vs. reactant concentration curves. The conditions and procedures for the study were similar to those reported previously (*16*, *17*). Two sets of reagents were prepared: the first consisted of varying concentrations of iron at a constant perchloric acid concentration. The second consisted of varying concentrations of thiocyanate with sufficient quantities of sodium perchlorate added to adjust the total molar ionic strength of the reaction mixture in the stopped-flow observation cell to 0.4. log-log plots of initial rate vs. reactant concentration, with one reagent at a fixed concentration, were linear and gave reaction orders of 0.9794 ± 0.0006 for thiocyanate and 0.997 ± 0.008 for iron, both in good agreement with pseudo-first-order kinetics.

With a 100-mL dilution vessel, the automated reagent preparation system requires nearly the same amount of time as would be required to prepare the solutions manually. However, because a solution can be prepared without operator intervention, the operator is free to perform other tasks, and gross errors due to mishandling of reagents are eliminated. Further automation of the system, e.g., addition of a reagent turntable, would totally free the operator from any attendance to the system while a complete series of solutions are being made. Construction details for the reagent preparation system are available (*18*).

LITERATURE CITED

(1) Beckwith, P. M.; Crouch, S. R. *Anal. Chem.* **1972**, *44*, 221-227.
(2) Notz, P. K., Ph.D. Thesis, Michigan State University, East Lansing, MI, 1977.
(3) Crouch, S. R.; Holler, F. J.; Notz, P. K.; Beckwith, P. M. *Appl. Spectrosc. Rev.* **1977**, *13*(2), 165-259.
(4) Deming, S. N.; Pardue, H. L. *Anal. Chem.* **1971**, *43*, 192-200.
(5) Mueller, K. A.; Burke, M. F., *Anal. Chem.* **1971**, *43*, 641-645.
(6) Toren, E. C.; Carey, R. N.; Sherry, A. E.; Davis, J. E. *Anal. Chem.* **1972**, *44*, 339-343.
(7) Gregory, R. P.; Lowry, J. D.; Malmstadt, H. V. *Anal. Chem.* **1977**, *49*, 1608-1615.
(8) Renoe, B. W.; O'Keefe, K. R.; Malmstadt, H. V. *Anal. Chem.* **1976**, *48*, 661-666.
(9) Malmstadt, H. V.; McCraken, M. S.; Krottinger, D. L. *J. Autom. Chem.* **1978**, *1*, 15-21.
(10) Malmstadt, H. V.; Wu, A. H. B. *Anal. Chem.* **1978**, *50*, 2090-2096.
(11) Mieling, G. E.; Taylor, R. W.; Hargis, L. G.; English, J.; Pardue, H. L. *Anal. Chem.* **1976**, *48*, 1686-1693.
(12) Steig, S.; Nieman, T. A. *Anal. Chem.* **1980**, *52*, 796-800.
(13) Rothman, L. D.; Ingle, J. D.; Crouch, S. R. *Anal. Chem.* **1975**, *47*, 1226-1233.
(14) Skoog, D. A.; West, D. M. "Fundamentals of Analytical Chemistry"; Holt, Rinehart, and Winston: New York, 1976.
(15) Vosburgh, W. C.; Cooper, G. R. *J. Am. Chem. Soc.* **1941**, *63*, 437-442.
(16) Willis, B. G.; Bittikofer, J. A.; Pardue, H. L.; Margerum, D. W. *Anal. Chem.* **1970**, *42*, 1340-1349.
(17) Mieling, G. E.; Pardue, H. L. *Anal. Chem.* **1978**, *50*, 1333-1337.
(18) Balciunas, R., Ph.D. Thesis, Michigan State University, East Lansing, MI, 1981.

RECEIVED for review March 23, 1981. Accepted May 15, 1981. This work was supported in part by National Science Foundation Grants GP-18123, MPS 75-03650, CHE 76-81203, and CHE 79-26490.

Hollow Fiber Ion-Exchange Suppressor for Ion Chromatography

Timothy S. Stevens* and James C. Davis

Dow Chemical USA, Michigan Division Analytical Laboratories, 574 Building, Midland, Michigan 48640

Hamish Small

Dow Chemical USA, Central Research Laboratories, 1712 Building, Midland, Michigan 48640

A suppressor for ion chromatography based on a countercurrent regenerated shell and tube device incorporating sulfonated polyethylene ion-exchange hollow fibers is described. Compared to the conventional ion-exchange resin bed packed suppressor column, the hollow fiber suppressor allows continuous operation without varying interference from base line dips, ion-exclusion effects, or chemical reactions. Conventional suppressor columns were found to have less band spreading and this resulted in slightly poorer resolution of early eluting ions with the use of the hollow fiber suppressor.

Ion chromatography is widely used for the determination of organic and inorganic ions in wastewaters, process streams, rainwaters, air samples, and food products (*1*). It is a unique analytical system using two ion-exchange columns in series followed by a flow-through electrical conductivity detector. The first column separates the ions in the injected sample while the second column suppresses the conductance of the electrolyte in the eluant while enhancing the conductance of the separated anions since they are detected as the acid moiety (*2*). The second column, called the "stripper" or the "suppressor", complicates the use of ion chromatography relative to the practice of conventional liquid chromatography. These complications include the need to periodically replace or regenerate the suppressor column, varying elution time of weak acid anions or weak base cations due to ion-exclusion effects (*3*) in the unexhausted portion of the suppressor column (*2*), apparent reaction of some ions such as nitrite with the unexhausted portion of the suppressor column resulting in varying response depending on the percent exhaustion of the suppressor column (*4*), and interference from the varying elution time of a characteristic base line upset (*5*). Finally, there is some band spreading in the suppressor column.

The ion-exchange resin packed suppressor column is not the only alternative for suppressing the conductivity of the eluant electrolyte. We have discovered that ion-exchange hollow fibers can be used in a suppressor device that eliminates most of the problems of the conventional suppressor column.

EXPERIMENTAL SECTION

The ion chromatograph used was a preproduction prototype of the Model 10 unit available from Dionex Corp., Sunnyvale, CA. The eluant used was 0.003 M $NaHCO_3$ and 0.0024 M Na_2CO_3 at a flow rate of 64 mL/h and a pressure of about 300 psig at room temperature. The analytical column was 2.8 × 100 mm filled with a proprietary resin resulting in equivalent separations as the 2.8 × 500 mm Dionex column but at half the eluent flow rate. The injection loop volume was 50 μL. When suppressor columns were used they were either 2.8 × 300 mm or 9 × 110 mm filled with Dowex 50 W×16 ion-exchange resin, 200–400 mesh size, and were regenerated off-line with 1 N H_2SO_4. When the hollow fiber suppressor was used, the regeneration pump was used to continuously supply 0.02 N H_2SO_4, at a flow rate of 64 mL/h. A "seven ion standard" was prepared from reagent grade salts containing 3.3 ppm F^-, 4 ppm Cl^-, 20 ppm NO_2^-, 54 ppm PO_4^{3-}, 10 ppm Br^-, 34 ppm NO_3^-, and 50 ppm SO_4^{2-}.

The low-density polyethylene hollow fibers used were extruded from Dow no. 4005 resin to a size of about 300 μM i.d. and about 380 μM o.d. and were sulfonated using 10% chlorosulfonic acid, 90% methylene chloride, v/v, at about 42 °C (the reflux temperature of the mixture) for 30 min. The ion exchange capacity of the fibers was 1 mequiv/g. A bundle of eight hollow fibers 6 ft in length was used.

The hollow fiber suppressor was constructed using a coiled section of 2 mm i.d., 1/8 in. o.d., 316 stainless steel tubing as shown in Figure 1. The high-pressure liquid chromatography (HPLC) end fittings were used without frits and the $^1/_{16}$ in. bore of the fitting on the inside end was chamfered with a twist drill to about 2.5 mm so as not to block the flow of fibers positioned on the side of the bore of the sealing tube. The hollow fibers were sealed in the sealing tube with Dow Corning room temperature vulcanizing silicone rubber bathtub caulk.

RESULTS AND DISCUSSION

The theory of operation of the hollow fiber suppressor used for the determination of anions with an eluant electrolyte of sodium carbonate is shown in Figure 2. The sulfonated polyethylene fiber wall allows sodium ion to permeate out and hydrogen ion to permeate in. Carbonate ions and sulfate ions do not permeate the fiber wall because of Donnan exclusion forces (*6*). Sample anions also do not permeate the wall while the cations do. Thus, the highly conducting sodium carbonate of the eluant is converted to feebly conducting carbonic acid and the sample anions emerge with enhanced conductivity because they elute in the acid form. The sulfuric acid regenerant is converted to sodium sulfate.

Several limitations are seen with the system. If the flow rate of sodium carbonate solution through the device is too fast, there will not be enough time for sodium ion to diffuse from the center of the fiber flow stream to the fiber wall and incomplete suppression will occur. The device reported here could suppress a maximum eluent flow rate of 80 mL/h. The number of mequiv/min of sodium ion into the device must be matched by at least as many mequiv/min of hydrogen ion flowing countercurrent around the outside of the fibers. Some excess of hydrogen ion is usually required. The device used in this work required at least a 10% excess of regenerant. Donnan exclusion forces are not always sufficient to prevent "leakage" of regenerant into the eluent stream, especially at relatively high regenerant concentration. However, no detectable leakage of regenerant was seen with 0.02 N H_2SO_4.

Comparison with Conventional Suppressor Columns. Two suppressor columns were compared to the hollow fiber device. The first was 2.8 mm × 300 mm containing about 1.8 mL of resin. This is a small suppressor column having a lifetime, under the conditions listed, of about 6 h. The second suppressor column tested was 9 mm × 110 mm containing about 7 mL of resin. This larger column has a lifetime of about 24 h.

The most common eluant used for the determination of anions in ion chromatography contains 0.003 M $NaHCO_3$ and

0003-2700/81/0353-1488$01.25/0 © 1981 American Chemical Society

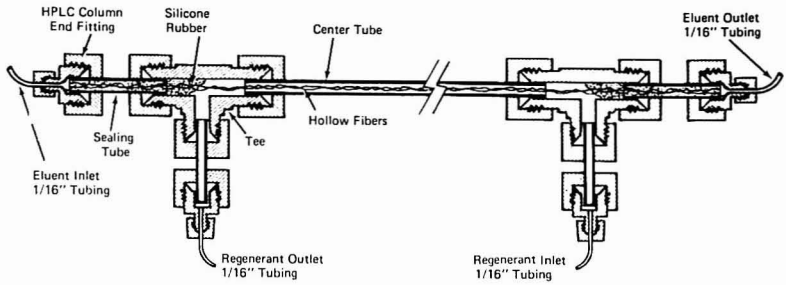


Figure 1. Schematic drawing of a hollow fiber suppressor.

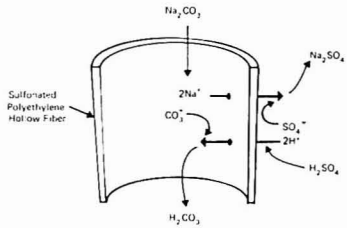


Figure 2. Theory of operation of the hollow fiber suppressor.

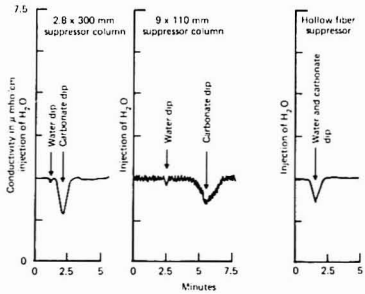


Figure 3. Chromatographic response to an injection of water with the use of suppressor columns and the hollow fiber suppressor.

0.0024 M Na_2CO_3 in deionized water. The suppressor converts these eluant electrolytes to carbonic acid which has little conductivity because of its weak acid character. When an injection of deionized water containing no anions is made, two negative peaks are seen in the chromatogram. The first, called the water dip, is related to the plug of injected water moving through the system with eluant of slightly higher conductivity on either side of it. The second, called the carbonate dip, is larger and is the vacancy chromatogram for the carbonate not in the injected sample but present in the eluant. In other words, carbonic acid elutes through the unexhausted portion of the suppressor column at a reduced rate because of ion-exclusion effects. Figure 3 shows the water dip and the carbonate dip for the two freshly regenerated suppressor columns and the hollow fiber device.

The base line for the 9 × 110 mm suppressor was unsteady because it had not "aged". Large suppressor columns require many hours of rinsing after regeneration, depending on the batch of resin used, to wash out leachables, and this one gave a steady base line the following day. Note that the larger suppressor's water dip came later due to increased void volume

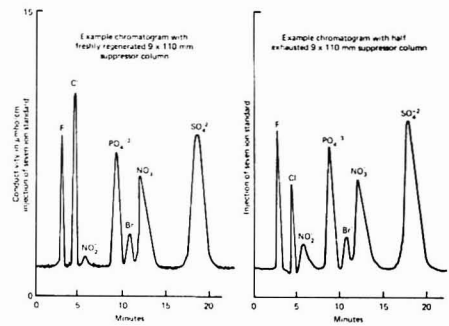


Figure 4. Response variations observed with suppressor column exhaustion.

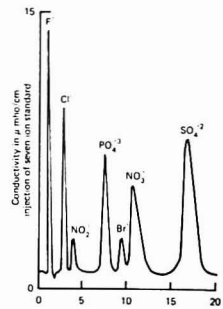


Figure 5. Chromatogram of the seven ion standard using the small suppressor column.

and that the separation between the water dip and the carbonate dip was much greater for the larger suppressor because of increased ion-exclusion effects. Finally, both dips were combined in the hollow fiber suppressor because of the absence of ion-exclusion effects.

The carbonate dip elution time approaches the water dip elution time with the use of a suppressor column as the resin bed exhausts. This can affect the response factor of ions coeluting with the variable carbonate dip. Figure 4 shows this effect on an injection of a mixture of seven anions with a freshly regenerated 9 × 110 mm stripper and when this column was about half exhausted. In the first chromatogram, the carbonate dip eluted at about 6 min, coeluting with NO_2^-. In the second chromatogram, the carbonate dip eluted at about

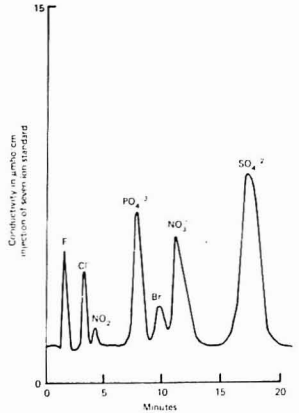


Figure 6. Chromatogram of the seven ion standard using the hollow fiber suppressor.

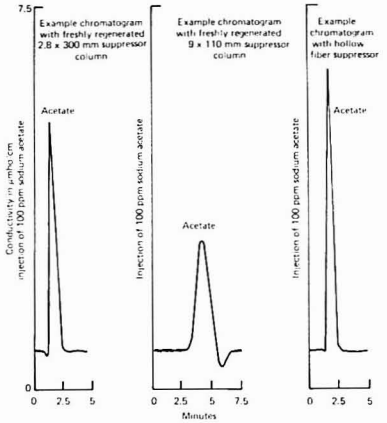


Figure 7. Chromatographic response to an injection of acetate with the use of suppressor columns and the hollow fiber suppressor.

4 min, coeluting with Cl^-, resulting in a larger response for NO^{2-} and a smaller response for Cl^-.

Figure 5 shows the chromatogram of the same seven ions using a freshly regenerated 2.8 × 300 mm suppressor column. Here the carbonate dip eluted between F^- and Cl^- and would migrate under F^- as the suppressor exhausted. Figure 6 shows the chromatogram of the same seven ions using the hollow-fiber suppressor. The carbonate dip coeluted with F^- but its effect is easier to cope with because it is constant since the hollow fiber suppressor does not exhaust with use. When the chromatograms in Figures 4–6 were compared, the band spreading with the hollow fiber device as most apparent in the peak width and height for F^- was greater than with the suppressor columns. The band spreading of each suppressor was quantitated by removing the analytical column from the system, changing the eluent to deionized water, and injecting a sample. The resultng peak was then triangulated and the peak width at base line measured and converted to microliters. The injection volume was then subtracted from this value and the result used as an indication of the band spreading of the system without the effect of the analytical column. The band spreading of each suppressor was 130 μL, 300 μL and 525 μL, respectively, for the 2.8 × 300 mm suppressor, the 9 × 110 mm suppressor, and the hollow fiber suppressor. The increased band spreading with the use of the hollow fiber suppressor has a deleterious effect on ions eluting early in the chromatogram. The effect is not noticed for the broader peaks of later eluting ions.

The determination of weak acid anions, such as acetate, using a suppressor column is complicated by ion-exclusion effects in the unexhausted portion of the column. Figure 7 shows chromatograms for the injection of a NaAc standard using the 2.8 × 300 mm suppressor, the 9 × 110 mm suppressor, and the hollow fiber device. Both suppressor columns, and especially the 9 × 110 mm one, broaden and retard the acetate peak due to ion exclusion effects. As the columns exhaust, these ion-exclusion effects decrease, resulting in sharper and taller peaks that elute sooner. The use of the hollow fiber device theoretically could have resulted in the loss of the acetate response (and there may indeed be some loss) since potonated acetate is not rejected from passage through the fiber wall. However, Figure 7 clearly demonstrates the applicability of acetate determination using a hollow fiber suppressor.

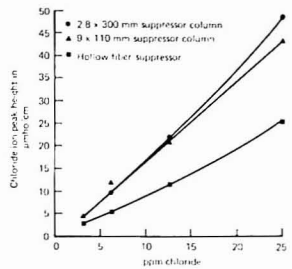


Figure 8. Calibration curves for chloride.

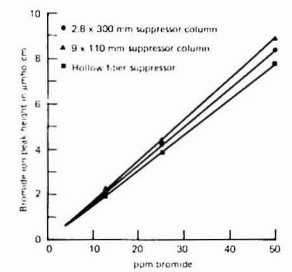


Figure 9. Calibration curves for bromide.

Comparisons were made between the use of the suppressor columns and the hollow fiber device to determine response linearity for chloride, bromide, and acetate (see Figure 8–10). The data in Figure 8 indicated that the use of both the 2.8 × 300 mm and hollow fiber suppressors resulted in increased response factors with increasing concentration of chloride. The linearity with the 9 × 110 mm suppressor was good. The lower response with the hollow fiber device was caused by the broader chloride peak as a result of band spreading in the hollow fiber device. Although the linearity of the 9 × 110 mm suppressor was good, the data in Figure 4 indicate that as the 9 × 110 mm column exhausts and the carbonate dip begins

Table I. Response Variations Observed during the Lifetime of the 2.8 mm × 300 mm Suppressor Column

ambient temp, °C	elapsed time since regeneration, h	peak height in chart units for F^-	Cl^-	NO_2^-	PO_4^{3-}	Br^-	NO_3^-	SO_4^{2-}	Ac^-
22.0	0.3	77.0	28.7	10.5	34.0	9.5	26.0	42.2	
22.0	0.7								29.8
22.0	0.8	75.0	29.0	10.0	33.5	9.2	25.0	42.0	
22.0	1.5	76.2	31.0	12.0	34.5	9.5	26.5	43.0	
22.0	2.5								34.0
22.0	3.2	77.0	32.5	17.0	35.5	10.2	27.5	42.8	
22.0	4.1	78.8	32.0	18.8	35.5	10.2	27.2	43.2	
22.0	5.1	79.0	31.0	22.2	35.7	10.0	27.2	43.0	
22.0	5.5								51.0
22.5	6.2	79.0	32.0	27.2	36.5	11.2	29.6	44.3	
22.5	6.8	79.0	32.0	30.5	36.8	11.2	29.8	44.0	
22.0	7.3								76.0
22.5	7.7	81.5	32.0	33.8	36.5	11.6	30.5	45.0	
22.5	8.1	83.5	31.8	35.5	36.2	11.2	30.0	44.7	
				Regenerated Suppressor					
22.5	0.2	72.0	31.8	10.8	37.5	11.4	30.5	44.5	
22.5	0.5	73.0	31.8	11.5	37.0	11.0	30.0	44.2	
22.5	0.8								31.0

Table II. Response Variations Observed during the Use of the Hollow Fiber Suppressor

ambient temp, °C	elapsed time, h	peak height in chart units for F^-	Cl^-	NO_2^-	PO_4^{3-}	Br^-	NO_3^-	SO_4^{2-}	Ac^-
20.5	0.3	29.0	24.3	12.0	33.8	11.2	28.8	45.2	
21.0	1.0	28.8	22.0	11.6	34.2	11.0	29.0	45.0	
21.0	1.5								42.8
21.0	2.0	28.8	22.2	10.5	35.6	11.5	30.5	45.5	
21.5	2.5	29.2	22.6	10.8	36.0	11.0	30.0	47.0	
21.5	3.0	29.8	22.8	10.6	36.0	11.6	31.2	46.0	
21.5	4.2								43.8
22.0	4.5	29.6	23.0	10.2	35.5	11.1	30.0	46.5	
22.0	5.5	30.5	23.5	9.5	36.5	11.8	32.0	47.2	
22.0	6.0								44.2
22.0	6.6	30.6	23.8	10.0	36.5	11.0	30.0	46.0	
22.0	7.1								43.5

to coelute with chloride, the responsiveness of chloride would change significantly.

The data in Figure 9 indicate that the use of any of the suppressors tested would result in linear response to bromide.

The data in Figure 10 indicate that the responsiveness of acetate falls off at higher concentration with the use of the 2.8 × 300 mm suppressor. This is expected because of the weak acid nature of acetic acid. the linear responsiveness with the use of the hollow fiber suppressor at the higher concentrations of acetate was fortunate but cannot be readily explained. The hollow fiber suppressor calibration curve for acetate did not pass through the origin of the plot because acetate coeluted with the carbonate dip.

The final comparison made was to inject the seven-anion standard and the acetate standard periodically during the lifetime of the 2.8 × 300 mm "small" suppressor column and for a comparable length of time using the hollow fiber suppressor to observe response variations with time (see Tables I and II). The data in Table I indicate a general instrumental upward drift in the response of Cl^-, PO_4^{3-}, Br^-, NO^{3-}, and SO_4^{2-} not related to exhaustion of the suppressor column as evidenced by the response continuity for these ions when the column was regenerated. Acetate and F^- response, measured by peak height, increased with suppressor column exhaustion. However, the acetate and F^- responses remained constant when response was measured by peak area using a planimeter. In contrast, both the peak height and peak area response of NO_2^- varied by a factor of about 3 with exhaustion of the suppressor column. Nitrite forms nitrous acid in the unexhausted portion of the suppressor column and nitrous acid reacts with the resin affecting response depending on suppressor column exhaustion. The data in Table II indicate that the use of the hollow fiber device results in stable response from all of the ions tested. Thus, the significant advantage of the hollow fiber suppressor with regard to calibration is that

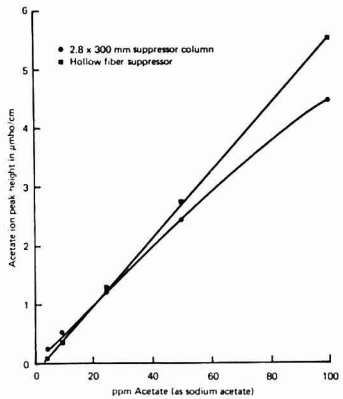


Figure 10. Calibration curves for acetate.

responsiveness is not a function of suppressor exhaustion but remains reasonably constant with use.

CONCLUSION

The replacement of the conventional ion-exchange resin bed suppressor column with the hollow fiber suppressor allows continuous operation of an ion chromatograph without varying interference from base line dips, ion-exclusion effects, or chemical reactions. Future work needs to be directed at reducing the band spreading of hollow fiber suppressors, at the development of aminated membrane suppressors for cation determination using ion chromatography and at easier means of fabricating hollow fiber suppressors.

LITERATURE CITED

(1) Maugh II, T. H. *Science* **1980** *208*, 164.
(2) Small, H.; Stevens, T. S.; Bauman, W. C. *Anal. Chem.* **1975**, *47* 1801.
(3) Wheaton, R. M.; Bauman, W. C. *Ind. Eng. Chem.* **1953**, *45*, 229.
(4) Koch, W. F. *Anal. Chem.* **1979**, *51*, 1571.
(5) Wetzel, R. A.; Anderson, C. L.; Schleicher, H.; Crook, G. D. *Anal. Chem.*, **1979**, *51*, 1571.
(6) Heftman, E. "Chromatography", 2nd ed.; Reinhold: New York, 1976; p 296.

RECEIVED for review March 2, 1981. Accepted May 8, 1981. A United States Patent application has been filed on behalf of the authors covering the subject of this contribution.

Laser Ionization Mass Spectrometry of Nonvolatile Samples

E. D. Hardin[1] and M. L. Vestal*

Department of Chemistry, University of Houston, Houston, Texas 77004

A new laser ionization mass spectrometer has been developed which employs a moving stainless steel belt onto which the sample is electrosprayed for continuous sample introduction. Ionization is produced by focusing the output of a tunable dye laser onto the moving belt. The mass spectrometer system is a conventional quadrupole system, with the exception of a gated boxcar integrator to process the pulsed ion beam. Mass spectra have been recorded for a number of nonvolatile biomolecules including saccharides, amino acids, peptides, nucleosides, and nucleotides. Generally these spectra show intense cationized molecular ions, often including multiple alkali addition, and little fragmentation. The major limitation on the technique at present is the rather poor reproducibility of the spectra. Ion time-of-flight distributions have been measured which show that ions produced by laser desorption/ionization have broad kinetic energy distributions with most probable kinetic energies of about 6 eV and with high-energy tails extending beyond 25 eV. The time-of-flight distributions also show that most of the high mass ions observed result from metastable decomposition of larger clusters formed initially at the surface.

In a number of areas of organic and biochemical research there is a growing need for high mass, high sensitivity mass spectrometry applicable to thermally labile molecules of low volatility (*1*). In particular, it is often very important to obtain easily identifiable ions characteristic of the intact molecule so that the molecular weight can be determined. In response to this need, several new techniques have been developed (*2*). These include field desorption (*3*), chemical ionization (*4*), plasma desorption (*5*), laser desorption (*6*), organic SIMS (*7*, *8*), and very rapid sample heating with "in-beam" chemical (*9–11*) or electron ionization (*12–14*). In our own laboratory we have recently discovered a new soft ionization technique which employs thermal production of a charged macroscopic particle beam containing the sample. This technique employs very rapid heating of a liquid solution to form a particle beam and impact of this particle beam on a mildly heated surface (*15*).

Several of these techniques, such as field desorption and chemical ionization, both conventional and "in-beam", have been relatively well characterized, and the apparatus is commercially available; however, with the exception of gas-phase chemical ionization, it appears that none are satisfactorily understood. Recent work employing these new ionization techniques has demonstrated that gas-phase ions characteristic of the intact molecule can be produced for previously intractable molecules. Despite the enormous advances of recent years many problems are not yet solved, and none of these new techniques has, as yet, achieved wide-spread acceptance.

The present research was undertaken to explore the feasibility and practicality of laser desorption and ionization for mass spectrometric analyses of nonvolatile organic molecules adsorbed on, or contained in, solid surfaces. In our view, a practical technique should provide both molecular weight and structural information on a wide range of nonvolatile and/or thermally labile compounds; it should be compatible with conventional rapid scanning mass analyzers, both magnetic and quadrupole; and it should be suitable for combination with the techniques commonly used for separating and purifying mixtures of involatile compounds such as liquid (LC) amd thin-layer chromatography (TLC).

Most of the earlier laser desorption studies have used some form of simultaneous ion detection, employing either time-of-flight analysis (*16*), electrooptical ion detection, or photoplate (*17*). Recently, the use of fast electrical scanning with laser desorption from a direct exposure probe in a chemical ionization source has been reported by Cotter (*18*). The use of repetitive pulsed laser desorption with magnetic scanning over a limited region of the spectrum has been reported by Heresch, Schmid, and Huber (*19*). The use of laser desorption using a moving belt inlet system with a tightly enclosed chemical ionization (CI) source and a quadrupole mass spectrometer has been reported by Hunt, Bone, and Shabanowitz (*20*).

In the present work we have developed a new laser desorption mass spectrometer which uses a moving belt system to continuously supply fresh sample to a fully open laser vaporization/ionization region. The mass spectrometer is a

[1]R. A. Welch Foundation Predoctoral Fellow.

0003-2700/81/0353-1492$01.25/0 © 1981 American Chemical Society

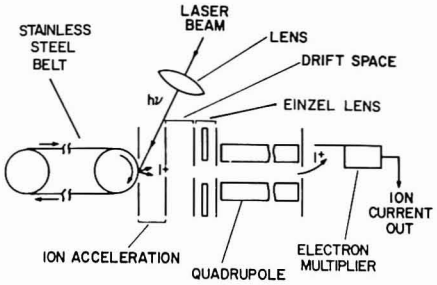


Figure 1. Schematic diagram of the laser ionization mass spectrometer.

conventional system, with the exception of a boxcar integrator to process the pulsed ion signal generated by pulsed laser ionization. With the addition of differential pumping on the moving belt inlet system, the laser ionization mass spectrometer could provide a viable alternative approach to a combined LC-MS system.

EXPERIMENTAL SECTION

The laser desorption mass spectrometer developed in this work is shown schematically in Figure 1. The apparatus consists of a continuous stainless steel belt, ion accelerating and focusing lenses, a quadrupole mass filter, and an off-axis electron multiplier. This apparatus is housed in a vacuum bell jar pumped by a 4000 L/s diffusion pump backed by a 300 L/min mechanical pump. The beam from a tunable dye laser passes through a Pyrex lens of 10 cm focal length and then through a Pyrex window and impinges on the moving belt as indicated in Figure 1. The angle between the laser beam and the quadrupole axis is approximately 45° and the extended quadrupole axis is normal to the surface of the belt at the point of incidence of the laser beam. The dye laser is pumped by a 400-kW nitrogen laser, and for the experiments reported here, the dye laser was operated at 483 nm using a 0.01 M solution of 7,7-diethyl-4-(trifluoromethyl)coumarin in *p*-dioxane in the dye cell. The laser pulses are typically 5–7 ns wide full width at half-maximum and typical pulse energies are 400 μJ when the laser is operated at a repetition rate of 25 Hz.

The ion optical system consists of a nearly uniform field accelerating region (0.34 cm) followed by a field free region (0.68 cm) and a thin einzel lens (0.68 cm). The einzel lens is normally operated in the accelerating mode with the central element negative (for positive ions) in the range 100–200 V. The back plate of the accelerating region and the moving belt are connected to the accelerating potential which is typically in the range 5–30 V off ground. The additional plates in the ion path are grounded as is the central axis of the quadrupole.

The stainless steel belt (150 cm in circumference, 0.1 cm wide and 0.005 cm thick) is driven by a small dc motor and gear train external to the vacuum system using a shaft coupled through a rotatable "O"-ring sealed vacuum feedthrough. Belt speeds used in the present work are in the range 10–30 cm/min. This range of speeds corresponds to 50–150 pulses/cm for a laser frequency of 25 Hz which generally removes most of the sample after one rotation of the belt. Spectra were taken with scan times allowing for approximately 5 pulses/amu. For measurement the output of the electron multiplier is coupled to a fast current amplifier which is sampled by a boxcar integrator gated to measure the ion current during the appropriate time interval following each laser pulse. Spectra may be recorded by scanning the quadrupole in the conventional manner and connecting the output of the boxcar to a recorder. For most of our recent work the instrument was interfaced to a Finnigan/Incos Model 2300 data system for data acquisition and reduction.

For the time-of-flight measurements the current amplifier was replaced by a fast pulse amplifier/discriminator, and the time between laser pulse and ion arrival was determined by using a time-to-pulse height converter, and the results were stored in a multichannel pulse height analyzer. For these measurements the quadrupole was set manually to the mass of interest and the time-of-flight spectrum was accumulated until the desired statistical precision was achieved. For these measurements the signal levels were intentionally reduced by increasing the resolution of the quadrupole so that not more than one ion was detected per laser pulse.

At present the moving belt and the quadrupole are housed in the same vacuum system. For application of sample the apparatus shown in Figure 1 is vented to atmosphere with the vacuum pumps valved off. Several methods of applying sample to the belt have been tried, but the most reproducible results have been obtained by using the electrospray technique as described by McNeal, Macfarlane, and Thurston (*21*). Typically, about 15 min is required to fully coat the belt with sample and an additional 15 min is required to evacuate the system to normal operating pressure of 10^{-6} torr or below.

Table I. Relative Intensity of Molecular Ions

sample	MH^+	$(M + alkali)^+$ [a]	$(M - H)(alkali)_2^+$ [a]
arginine	75	90	100
histidine	100	45	35
phenyl-alanine	0	0	100
serine	0	15	100
leucine	0	25	100
aspartic acid	0	35	100
glutamine	0	10	100
glutamic acid	0	100	75
gly-tryptophan	0	20	100
arg-glutamine	70	100	25
gly-gly-gly-glycine	0	100	100
guanosine	10	100	100
cytidine	0	100	0
adenosine	80	100	0

[a] Relative ion intensities were calculated for $(M + alkali)^+$ as the sum of MNa^+ and MK^+. For $(M - H)(alkali)_2^+$ the sum of $(M - H)Na_2^+$, $(M - H)NaK^+$, and $(M - H)K_2^+$. No salts were added to any of these samples.

RESULTS AND DISCUSSION

Laser ionization mass spectra have been recorded for a number of nonvolatile biomolecules including amino acids, peptides, nucleosides, and saccharides. Some examples of these results are presented in Table I. The most intense peaks in the spectra are generally those produced by alkali addition. In most cases this is true even when no alkali salts are intentionally added. Notable exceptions are the basic amino acids, e.g., arginine and histidine, for which intense protonated molecular ions, MH^+, are observed even when excess amounts of alkali salts are added to the samples. With other amino acids, such as phenylalanine, serine, leucine, glutamine, and aspartic acid, the most intense ions correspond to double alkali addition to the deprotonated molecular anion, $(M - H)K_2^+$, $(M - H)NaK^+$, etc., and the cationized molecular ions, MNa^+ and MK^+, are weak or absent completely. With the nucleosides the cationized molecular ion is generally the most intense, but protonation and multiple alkali addition are also observed. Of the molecules studied, only the nucleosides yield significant fragment intensities with the protonated and cationized base fragments being observed in all cases studied.

The background spectra consist mainly of K^+ and Na^+ and small clusters of salt adducts such as $KCl{\cdot}K^+$, $NaCl{\cdot}K^+$, etc.; at higher power densities ions characteristic of the stainless steel belt, such as Cr^+, Fe^+, and Ni^+, are observed. No doubly charged metal atoms have been observed. At higher masses several small peaks are observed which are apparently due

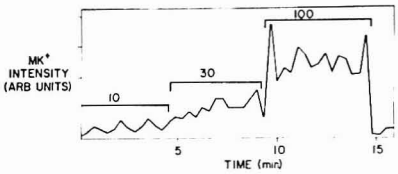


Figure 2. Intensity of cytidine MK^+ as a function of time. The parameter indicates the sample coverage on the belt over the indicated measuring times. Data were obtained by using 20-s scans over a 20 amu range including MNa^+ (m/e = 266) and MK (m/e = 282).

Table II. Summary of Quantitative Measurements on Cytidine

sample conen, ng/cm²	rel response[a]	rel std dev[b]
10	18	13
30	24	12
50	24	14
100	22	4
150	25	10
980	21	5

[a] Average response in arbitrary units divided by sample concentration. [b] Standard deviation of 14 measurements divided by sample concentration.

to alkali addition to residual pump oil or other background contaminants of the vacuum system.

We have generally experienced little difficulty in obtaining spectra of nonvolatile compounds with samples in the 0.1–1 $\mu g/cm^2$ range, and in most cases the detection limits are at about the 1 ng/cm^2 level or below. In essentially all cases studied, the most intense ions observed contain the intact molecule with a proton or one or more alkali atoms or ions added. The major difficulty has been the lack of reproducibility, both in the relative intensities of the major ions and in their absolute intensities. A major source of these variations appears to be due to the local variations in surface coverage by sample and by impurities and background contaminants. In general, deposition of samples by direct application of a liquid solution followed by evaporation of the solvent has given very poor results. The use of the electrospray technique described by McNeal et al. (*21*) has given considerably better results, but significant variations persist in most cases. An example of the quantitative response of the laser desorption system for one of the more favorable cases studied, the nucleoside cytidine, is shown in Figure 2. In this experiment one-third of the belt was coated with 10 ng/cm^2 of cytidine, one-third with 30 ng/cm^2, and one-third with 100 ng/cm^2. In each case an equimolar solution of cytidine and KI was used in the electrospray apparatus, and we assume that essentially all of the solution sprayed is deposited on the belt. The mass spectrum was scanned repetitively over a 20 amu range encompassing both the $M + Na^+$ (m/e = 266) and the $M + K^+$ (m/e = 282 amu) peaks; under the conditions of this experiment the $M + K^+$ is the most intense peak in the laser desorption mass spectrum of cytidine. The reconstructed mass chromatogram for this ion is shown in Figure 2 with the corresponding surface concentrations of cytidine indicated. As can be seen from the figure, the $M + K^+$ is approximately proportional to surface concentration of sample in this range of surface coverage, but the spectrum to spectrum fluctuations are quite large. The average response and the standard deviation of the results from this experiment and another covering a wider range of sample concentrations are summarized in Table II. It appears that, with careful use of the electrospray technique, linear response can be obtained over at least the range from 10 ng/cm^2 to 1 $\mu g/cm^2$.

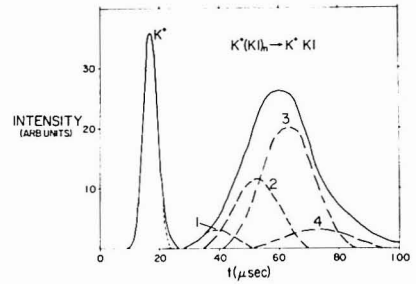


Figure 3. Measured time-of-flight distributions for K^+ and K^+-KI (solid lines). The dashed line under the K^+ indicates the calculated time-of-flight distribution corresponding to the initial kinetic energy distributions given by eq 4. For flight times shorter than 21 μs the experimental and calculated distributions are essentially identical. The dashed lines under the K^+-KI distribution correspond to calculated distributions for ions accelerated as $K^+\cdot(KI)_n$ with the value of n indicated on the figure which dissociate to $K^+\cdot KI$ in the field free region. The relative contribution of each which give the best fit to the experimental data is (in percent): n = 1, 8; n = 2, 29; n = 3, 51; n = 4, 8; n = 5, 4 (not shown on the figure).

TIME-OF-FLIGHT ANALYSIS

In these initial studies we have experienced considerable difficulty in obtaining reproducible results from the laser desorption mass spectrometer. In an effort to achieve a better understanding of the sources of these difficulties, we have initiated some more fundamental studies of the laser desorption process. The most fruitful of these investigations has been measurements of the time-of-flight distributions of mass-selected product ion beams produced by pulsed laser desorption.

The total time for an ion produced at the surface of the stainless steel belt to reach the detector is given approximately by

$$t = \frac{2d_1}{v_1 + v_0} + \frac{d_2}{v_1} \tag{1}$$

where

$$v_1 = \sqrt{(2e/M)(V_1 + T_0)} \tag{2}$$

$$v_0 = \sqrt{(2e/M)T_0} \tag{3}$$

and T_0 is the initial kinetic energy, M the mass of the ion, e the charge, V_1 the applied accelerating potential difference, d_1 the length of the accelerating field, and d_2 the total effective length of the drift region, including the einzel lens, the quadrupole, and the accelerating field in front of the multiplier. In the present appartus, d_1 = 0.34 cm and d_2 = 15.7 cm; the error in approximating the TOF through the lens, the quadrupole, the multiplier accelerating field is estimated to be less than 1%, which is insignificant for the present work. If an ion dissociates in the field free region (0.68 cm long) between the accelerating field and the einzel lens, it will be observed with the quadrupole set to transmit the product ion, but its velocity distribution, and hence its time-of-flight distribution, will correspond to that of the precursor ion. Kinetic energy release in the fragmentation process may broaden the distribution somewhat, but this contribution to the time-of-flight distribution is relatively small compared to its effect on the laboratory kinetic energy distribution.

The measured flight time distribution for K^+ from laser desorption of KI is shown in Figure 3. The results are in good agreement with the calculated time-of-flight distribution if

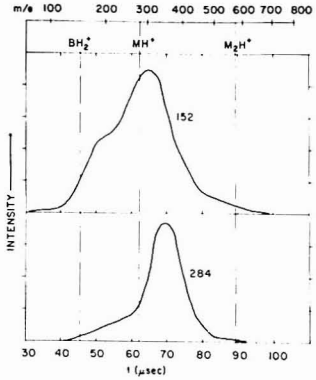


Figure 4. Measured time-of-flight distribution for MH^+ from guanosine (m/e = 284) and BH_2^+ (m/e = 190). The dashed lines indicate the maximum calculated flight time (corresponding to zero initial kinetic energy) for the base fragment, BH_2^+, the protonated monomer, MH^+, and the protonated dimer, MH_2^+, respectively.

we assume that the initial ion kinetic energy distributor is given by

$$f(E) = CE^n e^{-E/E_0} \quad (4)$$

with n = 2 and E_0 = 6 eV. The calculated time-of-flight distribution is shown by the dashed line in Figure 3. Except for a small discrepancy at longer times, the calculated distribution is in excellent agreement with the experimental results. The energy distributions produced by laser desorption appear qualitatively similar to those observed in SIMS (22); however, our results give rather lower energies than some of the earlier work at higher laser intensities (23).

The time-of-flight distribution found for K_2I^+, shown in Figure 3, is not compatible with the ions being formed primarily at the surface. Rather, it appears that most of the observed K_2I^+ results from unimolecular decomposition of larger clusters $K^+\cdot(KI)_n$, n = 2–5, in the field free region. If we assume that each of these ions is formed with the same energy distribution as was determined above for K^+, then the dashed curves shown in Figure 3 correspond to the expected flight time distributions for these ions. Adjusting the relative contributions of the individual clusters to achieve the best fit to the experimental curve, we obtain the results summarized in Figure 3. With the inclusion of the cluster corresponding to n = 5 (not shown in Figure 3) the sum of the individual time-of-flight distributions agrees with the experimental result over the entire time range with a maximum deviation of about 5%, which is well within the experimental uncertainty. In the mass spectrum a very weak intensity is observed at mass 371, corresponding to the cluster with n = 2, but the larger ions are not detected. These larger clusters have been detected, however, in SIMS experiments on alkali halide crystals (22). It appears quite clear that these larger clusters are being formed under the conditions of our laser desorption experiments but that they are metastable and are dissociating before reaching the detector. It is quite likely that a significant fraction of the total ionization may be lost by decomposition in the quadrupole.

Similar experiments have been conducted on the major ions in the laser desorption mass spectrum of guanosine; the results are summarized in Figures 4–6. It appears from the results that the protonated product ions arise from a completely different set of precursor ions than do the cationized species. Time-of-flight distributions for the MH^+ ion (m/e = 284) and the BH_2^+ ion (m/e = 152) from guanosine are shown in Figure 4. It appears that both of these ions are formed by metastable decomposition of a larger precursor; qualitative deconvolution of the results indicates that the major precursor is probably the protonated dimer of guanosine corresponding to m/e = 569. At most, about 10% of the MH^+ is formed at or near the surface. About 70% of the BH_2^+ is formed by metastable decomposition of the protonated dimer and about 30% by metastable decomposition of the protonated monomer. Direct formation of the BH_2^+ fragment at the surface appears negligible.

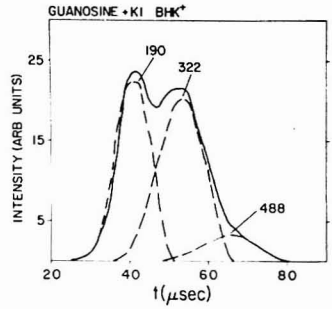


Figure 5. Measured time-of-flight distribution for the cationized base fragment BHK^+ of guanosine (m/e = 190). The dashed lines show the distributions calculated for ions initially formed and accelerated as the BHK^+ ion itself (190) and as MK^+ (322) and $MK^+\cdot KI$ (488).

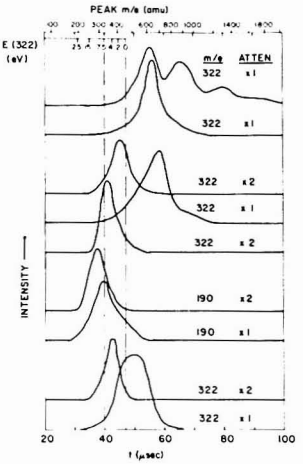


Figure 6. A series of consecutive measurements of the time-of-flight distributions for the MK^+ (322) and BHK^+ (190) ions in the laser desorption spectrum of guanosine with added KI. The scale at the top shows calculated position of the peak in the distribution as a function of mass assuming the energy distribution is that given in Figure 3. The inset scale shows calculated time-of-flight corresponding to m/e = 322 with the indicated initial kinetic energies. The accelerating potential for these measurements was 20 V.

A time-of-flight distribution for the cationized base fragment of guanosine, BHK^+ (m/e = 190), is shown in Figure 5. The resolution of this distribution into the distributions corresponding to the precursor masses is shown in the dashed lines on the figure. In this case it appears that about 40%

of the BHK^+ fragment is formed directly on the surface; about 50% is formed by metastable decomposition of the cationized parent ion MK^+ (m/e = 322), and the remainder is formed by metastable decomposition of the cluster of KI with MK^+ at m/e = 488.

In these initial studies it was found that the observed time-of-flight distributions were quite dependent on the laser power density and the relative concentration of the sample and alkali salt on the surface. The kinds of variations which are observed are illustrated in Figure 6. In these series of experiments the belt was coated with a relatively heavy coating of guanosine, about 1 $\mu g/cm^2$, along with an equimolar amount of KI. The time-of-flight distributions shown in Figure 6 were taken consecutively, starting from the top, following this single application of sample. The accelerating potential, V_1, was 20 V for this series of experiments. Each of these distributions corresponds approximately to one revolution of the belt. For runs 1–5 and 8 and 9, the quadrupole was set to transmit m/e = 322 (MK^+), and for runs 6 and 7 m/e = 190 (BHK^+) was monitored. For those experiments indicating an attenuation of ×1, the laser was operated at the usual nominal operating conditions corresponding to a peak power density of about 10^7 W/cm^2. In runs 3, 5, 6, and 8 the power density was reduced by a factor of 2 by interposing a ×2 neutral density filter in the path of the laser beam.

In the first run at "normal" laser power and with "freshly applied" sample, essentially no direct formation of MK^+ is observed; the time-of-flight distribution corresponds to clusters in the range 600–1800 amu. The peaks in the distribution indicate that the major precursors are probably M_2K^+ (605), M_3K^+ (888), $M_4K^+{\cdot}2(KI)$ (1337), and $M_5K^+{\cdot}(KI)_2$ (1786). Peaks corresponding to the first two of these precursors are quite clearly resolved, but the identity of the higher mass clusters is less certain. In the second experiment the thickness of the sample layer has presumably been reduced and the higher mass precursors are no longer observed. In this case the dominant peak corresponds to the M_2K^+ ion and there appears to be a small contribution from M_3K^+.

The dramatic effect of decreasing the laser power density by a factor of 2 is shown in the third run. In this case, most of the MK^+ is produced directly at or near the surface. The tail to longer times is probably due to M_2K^+ decomposition either in the accelerating field or in the drift region. Returning to full laser power by removing the ×2 attenuator in run 4 causes the peak in the time-of-flight distribution to return to that expected for M_2K^+ as in the first two runs; however, in the latter case the peak is more tailed to shorter times. This may indicate that as the sample is depleted from the surface, a new precursor, such as $MK^+{\cdot}KI$, begins to contribute to the observed product. In run 5 the laser power density is again reduced by a factor of 2 and now almost all of the MK^+ appears to be formed at the surface with only a very small fraction of the total intensity formed by metastable decomposition of large clusters. In runs 6 and 7 the quadrupole was set to transmit m/e = 190 corresponding to the BHK^+ fragment from MK^+. At low laser power, run 6, essentially all of the observed BHK^+ appears to be produced by metastable decompositon of MK^+ while at the higher power there is a significant contribution from a larger cluster, probably $MK^+{\cdot}KI$. Neither experiment appears to show any significant amount of direct formation of BHK^+ at the surface. The fact that the peak in run 6 occurs at shorter times than in the other runs implies either a significant fraction of the decomposition occurs in the accelerating field or the most probable kinetic energy of the precursor is shifted to a higher value. Since it appears, in general that the most probable kinetic energy decreases as the laser power is decreased, the former explanation seems more likely.

In run number 8 the quadrupole was again set to transmit mass 322 and the laser beam attenuator was in place, repeating run 5. Again, it appears at low laser power density that the MK^+ ions are primarily formed directly on the surface. Also, this run clearly shows that the most probable kinetic energy of the ions is significantly lower as the sample coverage is depleted. In the final run, the attenuator is removed and at the higher laser power most of the MK^+ ions are formed by metastable decomposition of larger clusters. In this final run, it appears that the precursors correspond to about equal amounts of $MK^+{\cdot}KI$ and M_2K^+.

It should be noted in connection with these experiments that the absolute ion intensity is a very steep function of the laser power density. Under the conditions of the experiments summarized in Figure 6 reducing the laser power by a factor of 2 may reduce the absolute ion intensity by as much as an order of magnitude. Furthermore, the absolute ion intensity in the final run of Figure 6 is about an order of magnitude less than the first run.

It should be noted that the results presented here were all obtained at laser power densities of about 10^7 W/cm^2 or less. With the laser and lens system used in this work it is quite straightforward to focus the beam spot on the surface so that the power density is 1–2 orders of magnitude larger. Some experiments were conducted early in this work at power densities up to 10^8 W/cm^2 but the results were quite disappointing. The pseudomolecular ions were smaller in intensity at these high-power levels and a rather large mass independent background signal was observed. Time-of-flight measurements with the quadrupole set to reject ions of all masses indicate that this background signal is mainly due to neutrals with very high kinetic energy, perhaps (depending on their mass which is presently unknown) with energies of several hundred electronvolts.

In the present apparatus the ions spend approximately the first 4% of their flight time in the accelerating field and the next 4% in the field free region from which metastable decompositions are observed. Most of the remainder (about 90%) of the total flight time is spent in the quadrupole mass filter. Ions dissociating in the quadrupole are not detected at any mass. As discussed above, it appears that most of the high mass sample ions observed in the laser ionization instrument are the result of metasable decomposition in the field-free region. This statement appears to be particularly true for experiments at high laser power density and high surface concentration of sample. Furthermore, since the drift region is quite short (0.68 cm) compared to the quadrupole (14 cm), it seems quite likely that a large fraction of the total ions produced may be lost due to unimolecular decomposition during transit through the quadrupole. If this is true, substantial improvements in performance may be achieved by providing an extended drift space between the desorbing surface and the quadrupole mass filter. Incorporation of an rf excited strong focusing quadrupole lens might provide a practical solution.

The major difficulty presently limiting the utility of the technique is the poor reproducibility. The ion time-of-flight measurements have provided some new insight into the ion formation mechanism. Work presently in progress is aimed at achieving a better understanding of the sources of the observed variability of the spectra; if this work is successful, the laser ionization technique may provide a practical method for routine mass spectral analysis of nonvolatile samples.

ACKNOWLEDGMENT

The authors are grateful to J. W. Rabalais for lending the time-to-pulse height converter and multichannel analyzer used in the time-of-flight measurements. We also acknowledge C. R. Hsieh for assisting with the calculations, L. M. Marks for

preparing the figures, and C. R. Blakley for many helpful discussions during the course of this work.

LITERATURE CITED

(1) Burlingame, A. L.; Baillie, T. A.; Derrick, P. J.; Chizov, O. S. *Anal. Chem.* **1980**, *52*, 214R.
(2) Daves, G. D., Jr. *Acc. Chem. Res.* **1979**, *12*, 359.
(3) Beckey, H. D. *Int. J. Mass Spectrom. Ion Phys.* **1969**, *2*, 500.
(4) Field, F. H. *Acc. Chem. Res.* **1968**, *1*, 42.
(5) Macfarlane, R. D.; Torgerson, D. F. *Science* **1976**, *191*, 920.
(6) Mumma, R. O.; Vastola, F. J. *Org. Mass Spectrom.* **1972**, *6*, 1373.
(7) Benninghoven, A.; Sichterman, W. K. *Anal. Chem.* **1978**, *50*, 1180.
(8) Day, R. J.; Unger, S. E.; Cooks, R. F. *Anal. Chem.* **1980**, *52*, 557A.
(9) Baldwin, M. A.; McLafferty, F. W. *Org. Mass Spectrom.* **1973**, *7*, 1141, 1353.
(10) Hunt, D. F.; Shabanowitz, J.; Botz, F. K.; Brent, D. A. *Anal. Chem.* **1977**, *49*, 1160.
(11) Hansen, G.; Munson, B. *Anal. Chem.* **1980**, *52*, 245.
(12) Dell, A.; Williams, D. H.; Morris, H. R.; Smith, G. A.; Feeney, J.; Roberts, G. C. K. *J. Am. Chem. Soc.* **1975**, *97*, 2497.
(13) Ohashi, M.; Tsujimoto, K.; Yasuda, A. *Chem. Lett.* **1976**, 439.
(14) Anderson, W. R., Jr.; Frick, W.; Daves, G. D., Jr. *J. Am. Chem. Soc.* **1978**, *100* 1974.
(15) Blakely, C. R.; Carmody, J. J.; Vestal, M. L. *J. Am. Chem. Soc.* **1980**, *102*, 5931.
(16) Kaufmann, R.; Hillenkamp, F.; Nitsche, R.; Schurmann, M.; Wechsung, R. *Microsc. Acta* **1978**, *2*, 297.
(17) Posthumus, M. A.; Kistemaker, P. G.; Meuzelaar, H. L. C.; Ten Noever de Brauw, M. C. *Anal. Chem.* **1978**, *50*, 985.
(18) Cotter, R. J. *Anal. Chem.* **1980**, *52*, 1767.
(19) Heresch, F.; Schmid, E. R.; Huber, J. F. K. *Anal. Chem.* **1980**, *52*, 1803.
(20) Hunt, D. F.; Bone, W. M.; Shabanowitz, J. Paper RPMP18, 28th Annual Conference on Mass Spectrometry and Allied Topics, May 25–30; ASMS: New York, 1980.
(21) McNeal, C. J.; Macfarlane, R. D.; Thurston, E. L. *Anal. Chem.* **1979**, *51*, 2036.
(22) Honda, F.; Fukuda, Y.; Rabalais, J. W. *J. Chem. Phys.* **1979**, *70*, 4834.
(23) Conzemius, R. J.; Capellen, J. M. *Int. J. Mass Spectrom. Ion Phys.* **1980**, *34*, 197.

RECEIVED for review February 13, 1981. Accepted May 12, 1981. This work was supported by the NIGMS under Grant GM24031 and by the Robert A. Welch Foundation.

Peak Resolution by Semiderivative Voltammetry

Jeffrey J. Toman and Steven D. Brown*[1]

Department of Chemistry, University of California, Berkeley, California 94720, and Materials and Molecular Research Division, Lawrence Berkeley Laboratory, 1 Cyclotron Road, Berkeley, California 94720

A technique based on semidifferential voltammetry has been developed for rapid electrochemical peak resolution. The approach was tested by resolution of synthetic fused peak systems. Subsequently, the approach was applied to semidifferentiated linear scan voltammograms of Cd^{2+}, Pb^{2+}, and In^{3+} and to semidifferentiated linear scan anodic stripping voltammograms of Cd^{2+}, In^{3+}, and Tl^{+}. Resolutions were directly characterized by peak height, potential, and half-width, as well as by the coefficient of determination between experimental and fit peaks. Studies of individual peak systems and of multiple peak systems showed that the method achieved excellent resolution accuracy, failing only as charge transfers became irreversible. Synthetic data were totally resolved with peak separations as small as 25 mV, while real systems were deconvoluted with separations as small as 40 mV. Peak parameters obtained from these resolutions allow observations of electrode processes, even in systems containing overlapped peaks.

A principal difficulty in the use of dynamic electrochemistry as a quantitative analytical technique is the problem of resolution of overlapping waves. This is of particular importance in linear sweep voltammetry (lsv) and anodic stripping voltammetry (asv) at a stationary mercury electrode because of the very broad, asymmetric nature of the peaks. Another difficulty is that the current-potential relationship is not describable by an analytic function. These problems are particularly unfortunate since lsv instrumentation is easy to use and is relatively inexpensive.

There have been two general approaches to electrochemical peak resolution, a "hardware" approach and a "software" approach. The hardware approach is typified by the methods of Martin and Shain (*1*) and Bond and Grabaric (*2*). In both methods a sample is run along with a blank solution containing a suitable background electrolyte and one of the overlapped components. The concentration of this component is varied in the blank until, upon subtraction of the blank voltammogram from the sample voltammogram (whether by analog or digital means), no trace of the overlapped component is left. Besides being very time intensive, the making of a suitable blank may not even be feasible for cases in which the supporting electrolyte is complex.

The software approach, that of resolution after data taking, is perhaps more promising. Amino (*3*) divides software resolution techniques into two types: frequency domain and time domain (curve fitting). Peak resolution in the frequency domain can be accomplished by the method of Kirmse and Westerburg (*4*). In this method the Fourier transform of an overlapped spectrum is divided by the transform of a single component, resulting in a sharpened spectrum. In electrochemistry Binkley and Dessey (*5*) have recently done work on the least-squares fitting of FT transformed square-wave voltammograms. In this procedure the transform of the overlapped peak is fit with the transforms of single peak data in a least-squares manner by varying what would be the peak height in the time domain. This procedure is advantageous in two ways. The fit is reduced in complexity by the reduction of points in going to the frequency domain, and fits may be done on both real and imaginary parts of the transform in order to obtain an averaged, improved fit. The procedure does rely on utilization of empirical single-peak parameters, however.

Curve fitting of electrochemical data has been hampered by the lack of analytic current–potential functions. Some work has been done in this area, principally by Perone and Coworkers (*6–8*). Boudreau and Perone (*8*) describe the application of an empirical peak shape function (the sum of skewed Gaussian and Cauchy functions) in the use of curve fitting for the resolution of square-wave voltammetric peaks.

[1] Present address: Department of Chemistry, Washington State University, Pullman, WA 99164.

0003-2700/81/0353-1497$01.25/0 © 1981 American Chemical Society

This function requires five parameters per peak and in addition requires that three "shape" parameters be found from single peak data. The other two parameters are determined from a least-squares minimization procedure. Overlapped peaks with separations as small as 30 mV are resolved.

This paper describes a curve fitting peak resolution technique for a stationary hanging mercury drop electrode in which lsv or asv data, after transformation, are fit with a wave shape function that is derived wholly from theory. Reversible lsv voltammograms are tranformed via a technique called semidifferential analysis into a form that is exactly equivalent to a sech^2 waveform. No empirical single peak parameters are assumed in the curve fitting algorithms, and all fit parameters have a direct physical significance.

THEORY

The detailed theory of convolution voltammetry has been described elsewhere (*9–13*). For the application of a linear potential ramp the semiintegral $m(E)$ is defined as (*9*)

$$m(E) = \int_{Ei}^{E} \frac{i(\gamma)\, d\gamma}{(E - \gamma)^{1/2}} \tag{1}$$

and the semiderivative $e(E)$

$$e(E) = \frac{\partial m(E)}{\partial E} \tag{2}$$

For a reversible charge transfer

$$\text{Ox} + ne^- = \text{Red} \tag{3}$$

assuming the appropriate boundary conditions, the shape of a semiintegral wave is given by (*10*)

$$E = E^{\tau}_{1/2} + \frac{Rt}{nF} \ln \left[\frac{m^* - m(E)}{m(E)} \right] \tag{4}$$

where

$$m^* = (D_o \nu)^{1/2} nFAC^*_{ox} \tag{5}$$

and where D_o is the diffusion constant of the oxidized species in solution, ν is the scan rate, n is the number of electrons transferred, F is the Faraday constant, A is the surface area of the electrode, and C^*_{ox} is the bulk concentration of the oxidized species. From application of eq 2 to eq 4, the semiderivative is (*11*)

$$e(E) = \frac{nFm^*}{4RT} \text{sech}^2 \left[\frac{nE}{2RT}(E - E^{\tau}_{1/2}) \right] \tag{6}$$

The semiderivative is seen to be a symmetric peak with a flat base line. The height of the peak is linearly proportional to the bulk concentration of oxidized species. At 25 °C the peak width at half the peak maximum (subsequently referred to as the half-width) is (*11*)

$$W_p = \frac{90.7}{n} \text{ mV} \tag{7}$$

For the case of a free metal in equilibrium with N labile metal complexes the semiderivative wave is (*9*)

$$e(E) = \frac{nFm^*}{4RT} \left[\frac{nF}{2RT}(E - E^{\tau}_{1/2}) + 1/2 \ln \sum_{1}^{N} \beta_i [X_i] \right] \tag{8}$$

Formation of labile complexes is seen not to affect the shape of either the semiintegral or semiderivative wave but rather moves both to more negative potentials. The treatment of several electroactive species is also straightforward, resulting in the linear superposition of semiintegral or semiderivative waves (*12*).

The above equations for lsv also apply asv under certain conditions (*9*). The only difference is that the diffusion constant and bulk concentration of oxidized species now are taken as equal to those of the reduced species in the mercury drop. For short plating time, large volume of solution, and reproducible stirring, metal amalgam concentration is proportional to the bulk oxidized species concentration for constant plating time (*14*). Under these conditions both semiderivative and semiintegral waves are proportional to oxidized species bulk concentration.

Overlapped electrochemical peaks in lsv and in asv were fitted by using the function

$$e(E) = A \text{ sech}^2 [B(E - C)] \tag{9}$$

A comparison of eq 7 with eq 9 shows that fit parameter A is related to the peak height (or bulk concentration of oxidized species), B is related to the peak half-width, and C is related to the peak potential.

EXPERIMENTAL SECTION

Reagents. For the lsv runs stock solutions of Pb^{2+}, Cd^{2+}, and In^{3+} were made approximately 1.0×10^{-2} M. Metallic AR Cd and Pb were dissolved in AR HNO_3; it was necessary to dissolve 99.95% In_2O_3 in a minimum amout of hot 72% $HClO_4$. The solutions were titrated with standard EDTA solution and stock concentrations of $[Pb^{2+}] = 1.96 \times 10^{-2}$ M, $[Cd^{2+}] = 2.09 \times 10^{-2}$ M and $[In^{3+}] = 2.02 \times 10^{-2}$ M were determined. The supporting electrolyte for these solutions was AR HCl diluted to 0.58 M. For studies of kinetic effects a backgroud electrolyte of 0.23 M HCl and 0.69 M $HClO_4$ was used.

For the asv runs Cd^{2+} and In^{3+} stock solutions were diluted to 2.09×10^{-4} and 2.02×10^{-4} M, respectively, from the stock solutions used in the lsv runs. In addition a Tl^+ stock solution was prepared from AR $TlNO_3$, standardized at a concentration of 8.84×10^{-3} M. An asv stock solution was then prepared by dilution to 8.84×10^{-5} M. The asv supporting electrolyte consisted of purified HCl diluted to 0.58 M with water collected from a preleached all-vitreous silica still. The HCl was purified according to the method of Mattison (*15*) by subboiling distillation. Preleached Teflon bottles were used to contain the purified HCl. All electrochemical cells were carefully cleaned between asv runs by rinsing with Transistar grade HNO_3.

Cell, Electrodes, and Equipment. The cell and electrodes used in this investigation were the same as those described earlier (*9*) with the cell thermostated to 24.9 ± 0.1 °C for the lsv experiments and to 23 ± 1 °C for the asv experiments. Equipment used was also described before (*9*), with the exception of a solid-state relay interfaced with a digital to analog converter to control stirring. A Digital Equipment Corp. MINC-11/2B microcomputer was used to control experiments and take data. Another computer with an LSI-11/23 CPU was used for data analysis. Scan rates were calibrated by monitoring the potential ramp with the computer and then fitting the ramp with a line, using a linear least-squares approach.

Procedures. For the lsv single peak studies 25 mL of 0.58 M HCl was pipetted into the cell and deaerated with Ar for 5–10 min to remove dissolved oxygen. After deaeration, a Hg drop was extruded and a voltammogram taken of the supporting electrolyte from −0.200 V to −0.900 V (vs. the Ag/AgCl electrode) at a scan rate of 1.0 V/s. The voltammogram was then written to disk. Scans were taken of Cd^{2+}, In^{3+}, and Pb^{2+} in different concentrations by adding standard additions of 1.0×10^{-2} M stock solutions with an Eppendorf pipet. See Table I for a summary of solutions studied in this paper.

After all data were taken the voltammograms were digitally filtered, semidifferentiated, and written to disk. It was found that the order of filtering and semidifferentiation had no affect on peak potentials, half-widths, or heights.

The curve fitting program described below was then applied to the semiderivative voltammograms. For a semidifferentiated voltammogram with two peaks, the program required about 4 min of running time on the LSI-11/23.

The asv studies were done in the same manner by adding

Table I. Composition of Solutions Used in This Work

LSV Systems

All solutions include 25 mL of 0.58 M HCl background electrolyte with:

Series

A: 5-20-μL additions of Pb^{2+} stock solution
B: 5-20-μL additions of Cd^{2+} stock solution
C: 5-20-μL additions of In^{3+} stock solution
D: 100 μL of In^{3+} stock solution and 5-20-μL additions of Cd^{2+} stock solution
E: 100 μL of Cd^{2+} stock solution and 5-20-μL additions of In^{3+} stock solution
F: 100 μL of Pb^{2+} stock solution and 5-20-μL additions of Cd^{2+} stock solution
G: 100 μL of both Pb^{2+} and In^{3+} stock solution and 5-20-μL additions of Cd^{2+} stock solution

LSV Stock Solution Concentrations

$[Pb^{2+}] = 1.96 \times 10^{-2}$ M $[Co^{2+}] = 2.09 \times 10^{-2}$ M $[In^{3+}] = 2.02 \times 10^{-2}$ M

ASV Systems

All solutions include 25 mL of 0.58 M purified HCl background electrolyte with:

Series

H: 5-20-μL additions of Tl^{+} stock solution
I: 6-20-μL additions of In^{2+} stock solution
J: 50 μL of Cd^{2+} stock solution and 5-20-μL additions of Tl^{+} stock solution
K: 50 μL of In^{3+} stock solution and 5-20-μL additions of Tl^{+} stock solution
L: 50 μL of both In^{3+} and Cd^{2+} stock solution and 5-20-μL additions of Tl^{+} stock solution

ASV Stock Solution Concentrations

$[Tl^{+}] = 8.84 \times 10^{-5}$ M $[In^{3+}] = 2.02 \times 10^{-4}$ M $[Cd^{2+}] = 2.09 \times 10^{-4}$ M

Table II. Fit Peak Parameter Dependence on Peak Separation for Synthetic sech^2 Fused Peak Systems[a]

series	potl	height	width	potl	height	width	R^2
1	−0.35	1.0	40.0	−0.5	1.0	40.0	
	−0.3500	1.0026	40.36	−0.5002	1.0001	39.87	0.9999
2	−0.4	1.0	40.0	−0.5	1.0	40.0	
	−0.3999	0.9999	40.01	−0.4999	0.9994	40.00	0.9999
3	0.42	1.0	40.0	−0.5	1.0	40.0	
	0.4199	1.0012	39.91	−0.4999	0.9993	40.05	0.9999
4	−0.435	1.0	40.0	−0.5	1.0	40.0	
	−0.4349	0.9999	40.01	−0.4999	1.0000	39.99	0.9999
5	−0.45	1.0	40.0	−0.5	1.0	40.0	
	−0.4500	0.9997	40.35	−0.4999	0.9960	39.92	0.9999
6	−0.46	1.0	40.0	−0.5	1.0	40.0	
	−0.4597	0.9928	39.93	−0.4995	1.0099	39.96	0.9999
7	−0.47	1.0	40.0	−0.5	1.0	40.0	
	−0.4686	0.9590	38.59	−0.4988	1.0592	40.38	0.9999
8	−0.48	1.0	40.0	−0.5	1.0	40.0	
	−0.4690	0.2352	25.63	−0.4919	1.6459	45.34	0.9996

[a] Units for potentials are in V; those for width are in mV; height units are arbitrary.

standard additions of freshly made 1.0×10^{-4} M stock solutions to 25 mL of deaerated supporting electrolyte. After deaeration the potential of the hanging mercury drop electrode was changed to −0.235 V vs. the Ag/AgCl electrode and stirring was instituted to ensure constant flux to the electrode during plating; after 10 s the potential was changed to −1.0 V and plating took place for 600 s. Six seconds before the end of the plating period, stirring was discontinued and the potential changed to −0.900 V. This potential was held for 15 s to ensure a homogeneous concentration of reduced species within the drop. Stripping then took place at a scan rate of 1.0 V/s to a final potential of −0.200 V.

For each asv series a scan was first taken of the supporting electrolyte alone to provide a background scan. After all data were taken and digitally filtered, the asv background scans were subtracted point by point from the stripping scans to remove the effects of capacitive current and other background currents (*16*). The resultant background subtracted voltammograms have the same shape as lsv voltammograms. Subsequently, semidifferentiation and curve fitting techniques were used on these voltammograms exactly as in the lsv runs.

Computer Programs. The program used to resolve overlapping peaks is based on the principle of sequential simplex optimization. The algorithm used was that of Nelder and Mead (*17*) as implemented by the FORTRAN subroutine NELMIN written by O'Neill (*18*). Corrections given by Chambers and Ertel (*19*), Benyon (*20*), and Hill (*21*) were included in NELMIN. The subroutine takes as input parameters the number of peaks, the limiting number of iterations, and initial guesses of the peak potential, height, and half-widths for each peak. A subroutine based on iterative peak stripping (*22*) was used to supply the simplex routine with the initial guesses for each peak. The iterative stripping subroutine fits a sech^2 function to the tallest peak in a voltammogram and subtracts this fitted peak from the voltammogram. A sech^2 function is then fit to the tallest peak in the subtracted voltammogram, and the process is continued until the specified number of peaks have been fit. Beginning with these initial parameters, NELMIN varies all peak parameters simultaneously to minimize the squares of the residuals between the experimental semidifferentiated voltammogram and the sum of the sech^2 functions. The program stops when the limiting number of iterations has been completed or when a specified tolerance has been achieved.

Control of the lsv and asv experiments was performed by MACRO-11 assembly language subroutines linked to a FORTRAN driver and other FORTRAN subroutines used for data storage and graphics. Data were stored on disk for later processing.

Table III. Fit Peak Parameters Dependence on Peak Height Ratios for Synthetic sech² Fused Peak Systems[a]

series	potl	height	width	potl	height	width	R^2
9	−0.45	0.1	40.0	−0.5	1.0	40.0	
	−0.4496	0.0995	39.76	−0.4999	0.9999	40.15	0.9999
10	−0.46	0.1	40.0	−0.5	1.0	40.0	
	−0.4593	0.0981	39.64	−0.4998	1.0025	40.09	0.9999
11	−0.47	0.1	40.0	−0.5	1.0	40.0	
	−0.4762	0.1378	46.21	−0.5005	0.9576	39.31	0.9999
12	−0.475	0.1	40.0	−0.5	1.0	40.0	
	−0.4870	0.2405	46.51	−0.5012	0.8436	38.91	0.9999
13	−0.48	0.1	40.0	−0.5	1.0	40.0	
	−0.4882	0.3470	40.13	−0.5026	0.7911	37.80	0.9999

[a] Units for potentials are in V; those for width are in mV; height units are arbitrary.

Table IV. Fit Peak Parameters Dependence on Peak Widths sech² Fused Peak Systems[a]

series	potl	height	width	potl	height	width	R^2
14	−0.45	1.0	10.0	−0.5	1.0	40.0	
	−0.4500	0.9961	10.08	−0.5000	0.9993	39.70	0.9999
15	−0.45	1.0	20.0	−0.5	1.0	40.0	
	−0.4500	1.0013	19.77	−0.4998	1.0024	40.06	0.9999
16	−0.45	1.0	30.0	−0.5	1.0	40.0	
	−0.4500	1.0001	30.00	−0.5000	1.0000	39.98	0.9999
17	−0.45	1.0	50.0	−0.5	1.0	40.0	
	−0.4500	1.0001	49.97	−0.5000	1.0003	40.00	0.9999
18	−0.45	1.0	60.0	−0.5	1.0	40.0	
	−0.4500	1.0002	59.99	−0.5000	1.0003	49.99	0.9999
19	−0.45	1.0	80.0	−0.5	1.0	40.0	
	−0.4499	0.9994	79.89	−0.5000	1.0027	40.05	0.9999
20	−0.45	1.0	90.0	−0.5	1.0	40.0	
	−0.4499	1.0028	89.29	−0.5001	0.9985	40.29	0.9999
21	−0.45	1.0	100.0	−0.5	1.0	40.0	
	−0.4495	0.9941	99.44	−0.5000	1.0075	40.77	0.9999

[a] Units for potentials are in V; those for width are in mV; height units are arbitrary.

Table V. Fit Peak Parameters for LSV Single Peak Data[a-c]

	Pb				Cd				
series	concn	potl	height	width	concn	potl	height	width	R^2
A1	1.57	−0.4784	0.577	50.7					0.8070
A2	3.14	−0.4783	1.105	47.8					0.9487
A3	4.72	−0.4777	1.616	46.3					0.9719
A4	6.29	−0.4781	2.189	44.6					0.9860
A5	7.86	−0.4778	2.684	46.1					0.9900
A6	9.42	−0.4776	3.175	45.0					0.9925
B1					1.67	−0.6875	0.426	34.3	0.6464
B2					3.34	−0.6875	0.843	41.4	0.9152
B3					5.01	−0.6878	1.354	41.5	0.9718
B4					6.68	−0.6871	1.900	42.5	0.9864
B5					8.36	−0.6872	2.281	44.3	0.9911

[a] Units for concentration are 1.0×10^{-5} M, for potential are V vs. the Ag/AgCl electrode, for peak height are $\mu A/V^{1/2}$, and for width are mV. [b] Units for slope and intercept are $\mu A/[V^{1/2} \cdot 1.0 \times 10^{-5}]$ and $\mu A/V^{1/2}$, respectively. [c] Units for potential are V vs. the Ag/AgCl electrode, for height are $\mu A/V^{1/2}$, for width are mV.

Processing included blank subtraction (*16*), digital filtering based on fast Fourier transform techniques (*23*), and semidifferentiation by a FORTRAN program employing the method of Grünwald as given by Oldham and Spanier (*24*).

RESULTS AND DISCUSSION

Synthetic Fused Peak Systems. The accuracy of resolution of overlapped lsv peaks was tested with data generated by using sech² functions with known height, half-width, and potential placed with varying amounts of overlap. In Table II, the effects of peak overlap are considered for two peaks of equal height and half-width. The 40 mV peak half-width used for both peaks is about that expected (45 mV) for a reversible two-electron charge transfer. In the table, R^2 is the coefficient of determination (*25*) for the fit and is defined as

$$R^2 = 1 - \left(\frac{\sum_{i=1}^{N} [Y_i - Y(X_i)]^2}{\sum Y_i^2} \right) \quad (10)$$

where Y_i is the experimental curve, $Y(X_i)$ the fitted curve, and N the number of data points. In all cases $N = 512$ for this study. Table II demonstrates that even though R^2 values remain greater than 0.999, the accuracy of resolution degrades substantially as the peaks are brought close together. The best measure of the accuracy of resolution is the peak height. Peak half-width and potential are also affected, but less severely than peak height. An error of 10% or greater in returned peak height was taken arbitrarily to constitute failure

Table VI. Average Peak Parameters and Results of Straight Line Fits of Concentration to Peak Height for ASV Data[a-c]

series	Cd			In			Tl				
	potl	height	width	potl	height	width	potl	width	slope	intercept	R^2
H				−0.6490 ± 0.0002			−0.5436 ± 0.0001	93.1 ± 1.5	0.0706	0.0249	0.989
I						29.1 ± 0.4			0.4546	−0.2065	0.999
J	−0.6936 ± 0.0002	1.1300 ± 0.0167	46.5 ± 0.3	−0.6511 ± 0.0006	0.7292 ± 0.0406	28.4 ± 0.2	−0.5445 ± 0.0023	100.0 ± 1.7	0.0273	0.0130	0.995
K							−0.5415 ± 0.0008	92.8 ± 0.9	0.0925	−0.0036	0.998
L	−0.6924 ± 0.0006	0.6139 ± 0.0104	48.0 ± 1.2	−0.6497 ± 0.0005	0.8008 ± 0.0232	27.5 ± 1.1	−0.5418 ± 0.0026	88.7 ± 6.2	0.0980	0.0395	0.996

[a] Slope, intercept, and R^2 refer to the least-squares straight line fit of the concentration of added species in each series to peak height. [b] Units for slope and intercept are $\mu A/[V^{1/2}1.0 \times 10^{-5}]$ and $\mu A/V^{1/2}$, respectively. [c] Units for potential are V vs. the Ag/AgCl electrode, for height are $\mu A/V^{1/2}$, for width are mV.

Figure 1. Fourier transform filtered lsv scan of lead at 9.42×10^{-5} M with the corresponding semiderivative.

Figure 2. Real semidifferentiated peak with corresponding fit components.

of resolution. Table II indicates that resolution fails at peak separations near 20 mV when peak half-widths are 40 mV and peak heights are equal.

Table III illustrates the effects of differing peak heights on the resolution of peaks. A peak ratio of 10:1 for overlapped peaks causes failure in the resolution when two peaks of 40 mV half-width are separated by 30 mV and when the height of the smaller peak is desired. Errors greater than 10% in the height of the larger peak occur at peak separations of 25 mV. When severe overlap occurs, errors in the peak potentials also occur. Coefficients of determination remain near 0.999, a reflection of the fact that coefficients of determination may remain close to 1 while returned peak parameters are very inaccurate.

Table IV shows the effect of changing peak half-widths on the resolution of two peaks of equal height separated by 50 mV. Even when one peak has a half-width of 100 mV, the accuracy of resolution remains better than 99% when the second peak has a half-width of 40 mV.

Single Peak Sysems. For background data on the resolution of overlapped systems, the fitting of single, semidifferentiated peaks was undertaken. Both lsv and asv peaks were used. Figure 1 shows a linear scan voltammogram and the resulting semidifferentiated voltammogram. Table V contains results for Pb and Cd lsv standard additions. The return of peak potentials with reproducibility better than 1.0 mV and peak half-widths close to the theoretical 45.3 mV for a two-electron charge transfer are indicative of close agreement between the theoretical sech^2 wave shape and the experimental semiderivative wave shape for the peaks. The accuracy of resolution degrades at low metal concentration as noise structure becomes significant. Peak half-widths become unreliable and R^2 decreases.

Results for asv single peak systems are summarized in the top half of Table VI. Results for Tl and In show very re-

Table VII. Dependence of Fit Peak Parameters on Scan Rate for LSV Single Peak Data

		scan rate, V/s							
	series	0.1017	0.2031	0.5077	0.9895	1.983	4.950	10.03	20.09
peak potential, in mV	B	−0.6764	−0.6761	−0.6756	−0.6754	−0.6755	−0.6752	−0.6780	−0.6750
	C	−0.6396	−0.6400	−0.6410	−0.6413	−0.6431	−0.6417	−0.6448	−0.6444
peak height, in $\mu A/V^{1/2}$	B	5.67	8.10	13.17	17.55	24.10	40.0	55.5	78.0
	C	17.3	22.1	29.2	33.8	27.2	20.9	16.0	11.8
peak width, in mV	B	44.7	46.1	44.0	45.4	44.3	44.0	41.3	46.0
	C	37.6	39.4	42.8	47.6	54.4	60.7	69.5	70.6
$H/\nu^{1/2}$, in $\mu A \cdot s^{1/2}/V$	B	17.78	17.97	17.48	17.64	17.11	17.98	17.53	17.40
	C	54.2	49.0	41.0	34.0	27.2	20.9	16.0	11.8
R^2	B	0.9942	0.9965	0.9849	0.9934	0.9826	0.9871	0.9715	0.9929
	C	0.9691	0.9739	0.9720	0.9709	0.9596	0.9522	0.9507	0.9088
$E_p - E_{p/2}$, in mV	B	28.7	28.7	28.0	28.9	27.9	28.7	28.4	29.4
	C	23.7	23.3	26.2	27.3	33.1	34.1	43.2	43.3

Table VIII. Average Peak Parameters and Results of Straight Line Fits of Concentration to Peak Height for LSV Data[a-c]

	Cd			In			Pb					
series	potl[c]	height[c]	width[c]	potl	height	width	potl	height	width	slope	intercept	R^2
A							−0.4779 ± 0.0003		45.9 ± 1.2	0.333	0.060	0.999
B	−0.6874 ± 0.0003		42.4 ± 1.3							0.285	−0.068	0.997
C				−0.6511 ± 0.0004		35.2 ± 1.2				0.413	−0.032	0.998
D	−0.6903 ± 0.0011		45.7 ± 1.2	−0.6530 ± 0.0011	2.426 ± 0.054	33.4 ± 0.9				0.286	0.115	0.998
E	−0.6915 ± 0.0012	2.496 ± 0.122	44.8 ± 1.4	−0.6520 ± 0.0012		33.1 ± 0.8				0.389	0.170	0.999
F	−0.6896 ± 0.0005		42.6 ± 1.6				−0.4819 ± 0.0023	2.584 ± 0.054	45.6 ± 0.6	0.297	−0.098	0.996
G	−0.6886 ± 0.0028		45.0 ± 1.2	−0.6499 ± 0.0018	3.317 ± 0.088	34.5 ± 0.7	−0.4799 ± 0.0014	2.697 ± 0.055	45.7 ± 1.1	0.279	0.263	0.995

[a] Units for concentration are 1.0×10^{-5} M, those for slope are $\mu A/[V^{1/2} \cdot 1.0 \times 10^{-5}$ M]. [b] Units for slope and intercept are $\mu A/[V^{1/2} \cdot 1.0 \times 10^{-5}]$ and $\mu A/V^{1/2}$, respectively. [c] Units for potential are V vs. the Ag/AgCl electrode, for height are $\mu A/V^{1/2}$, for width are mV.

Table IX. Dependence of Peak Potentials and Peak Widths on Scan Rate for Overlapped LSV Peaks[a]

		scan rate, V/s							
	metal	0.1017	0.2031	0.5077	0.9895	1.983	4.950	10.03	20.09
av peak potential, in V	Cd	−0.6744 ± 0.0014	−0.6743 ± 0.0019	−0.6725 ± 0.0019	−0.6732 ± 0.0012	−0.6724 ± 0.0019	−0.6724 ± 0.0036	−0.6730 ± 0.0014	−0.6746 ± 0.0028
	In	−0.6385 ± 0.0011	−0.6386 ± 0.0020	−0.6355 ± 0.0012	−0.6362 ± 0.0007	−0.6342 ± 0.0014	−0.6324 ± 0.0041	−0.6319 ± 0.0017	−0.6285 ± 0.0050
av peak width, in mV	Cd	43.4 ± 5.9	44.4 ± 5.2	49.4 ± 4.5	49.9 ± 4.0	50.9 ± 5.6	56.2 ± 4.9	50.3 ± 4.8	54.6 ± 6.2
	In	34.6 ± 1.0	34.4 ± 1.6	32.7 ± 2.6	35.6 ± 2.9	31.8 ± 3.3	30.9 ± 1.4	33.8 ± 1.0	31.9 ± 3.2
slope		3.35	4.27	5.67	5.74	5.58	5.57	6.97	4.41
intercept		−0.053	0.056	−0.154	0.186	1.11	−0.113	2.12	8.47
R^2		0.997	0.989	0.990	0.998	0.986	0.995	0.981	0.982

[a] Slope, intercept, and regression coefficient for standard additions of 20 μL of 2.09×10^{-2} M In^{3+} to 4.18×10^{-5} M Cd^{2+}. Units for slope and intercept are the same as in Table VI.

Table X. Dependence of Cd^{2+} Peak Height on Scan Rate for Overlapped Cd and In LSV Peaks[a]

$10^{-5}[In^{3+}]$, M	scan rate, V/s							
	0.1017	0.2031	0.5077	0.9895	1.983	4.950	10.03	20.09
1.62	5.73 (0.9395)	8.11 (0.9545)	13.9 (0.9653)	19.7 (0.9769)	27.4 (0.9740)	42.4 (0.9848)	59.7 (0.9620	89.2 (0.9840)
3.24	6.07 (0.9604)	8.88 (0.9656)	15.2 (0.9714)	20.0 (0.9815)	30.5 (0.9743)	47.6 (0.9745)	64.4 (0.9646)	89.8 (0.9640)
4.85	6.70 (0.9967)	10.27 (0.9984)	16.1 (0.9946)	21.8 (0.9968)	33.3 (0.9954)	50.5 (0.9943)	70.4 (0.9897)	90.8 (0.9963)
6.47	6.89 (0.9905)	9.86 (0.9938)	17.0 (0.9917)	24.9 (0.9936)	35.8 (0.9902)	62.0 (0.9936)	73.3 (0.9815)	97.0 (0.9926)
8.09	7.43 (0.9923)	11.71 (0.9913)	20.4 (0.9961)	24.6 (0.9968)	37.2 (0.9958)	54.5 (0.9963)	81.4 (0.9914)	102.7 (0.9908)

[a] Cd^{2+} concentration was 4.18×10^{-5} M. Units of peak height are $\mu A/V^{1/2}$. Value in parentheses is the coefficient of determination for the resolution.

producible peak potentials, and peak half-widths near those expected from theory (90.7 and 30.2 mV, respectively). As with the lsv results, the accuracy of resolution degrades when the asv peak height becomes small relative to noise.

Because the theory assumes a reversible charge transfer, fitting of peaks due to quasi-reversible or irreversible charge transfers is expected to be less satisfactory than for a reversible process. A study of the fitting of the In reduction peak in mixed chloride–perchlorate medium was made at different scan rates to investigate the effects of electron transfer reaction kinetics on the accuracy of resolution. Table VII summarizes results for Cd and In. Scan rates ranging from 0.1019 to 20.09 V/s produced only slight changes in peak potentials but dramatically changed peaks heights. From eq 5 and 6 the quantity (peak height/$\nu^{1/2}$) should be constant for a reversible peak. As seen in Table VII, Cd shows a value near 17.8 for all scan rates, while that for In steadily decreases, an indication of increasing irreversibility of the indium peak. For lsv peaks the accepted measure of reversibility is the value of $E_p - E_{p/2}$ (26). For a two-electron reaction the value expected is 28.3 mV, while for a three-electron process the value should be 18.8 mV. Table VII shows values close to 28.3 mV for the Cd, but significantly larger than 18.8 mV for In, and shows increasing values at faster scan rates, indicating an increasing irreversibility in the In charge transfer. As the peak becomes more irreversible, the accuracy of fit degrades slowly, as expected. The results in Table VII imply that the $sech^2$ wave shape is a reasonable approximation for even moderately irreversible peaks.

Multiple Peak Systems. Studies were made of overlapped peaks in lsv and asv. An example of an experimental semidifferentiated voltammogram is shown in Figure 2. Results for lsv are reported in Table VIII, while asv results are reported in the bottom half of Table VI. Systems were constructed by holding the concentration of one (or more) of the overlapped components constant while adding standard additions of another (electrochemically) overlapped component. The resolving process was performed for each standard addition. A successful resolution gave nearly constant peak heights for components not added and linearly increasing heights for the added component. Peak potentials and half-widths remained constant for all components. Slopes, intercepts, and regression coefficients were calculated for straight line fits of peak height vs. concentration of added component. Small intercepts (near zero) and regression coefficients close to 1 were taken as measures of the accuracy of the resolution.

An example of the method used to evaluate resolution is given by series D in Table VIII. In this series standard additions of Cd^{2+} were added in In^{3+}. Standard deviations in peak potentials (1.1 mV) and peak half-widths (about 1 mV) were small, and the height of the In peak stayed relatively constant. The straight line fit gave a slope very near that for the single peak Cd system (series B), a small intercept, and a regression coefficient near 1. In view of these results the resolution of these two peaks can be termed successful. Notice that the In peak, with a half-width of 33.7 mV, is not strictly reversible.

Series F reports for the resolution of Cd and Pb. These peaks are completely resolved as semiderivatives, so that this series provides a check on the semiderivative process itself without possible errors due to the curve fitting of overlapped semiderivative waves. Results agree well with those reported for individual Pb and Cd peaks in series A and B, respectively, indicating the success of the semiderivative method. The data in Table VI show that resolution appears to be successful in asv also. There are some differences between results reported in Table VI and VIII. In the asv study the half-width for the In peak is significantly less than that expected by theory; this is especially true in the series where both In and Tl occur. Since the chloride concentration and the scan rate were held constant for these two series, another factor must be responsible, possibly that of the different chemical environment in the mercury drop.

In addition to changes in peak half-width there appears to be an enhancement in the height of the Tl peak in systems also containing indium, as indicated by the difference in slopes for Tl standard additions in series K and L as compared to series H and J. These differences cannot be attributed to simple errors in the resolution nor can they be attributed to changes in the reversibility of one of the overlapped peaks. This can be demonstrated by a study of the effect of reversibility on the resolution of overlapped peaks. Tables IX and X present results of a study of the resolution of Cd and In as a function of scan rate. Standard additions of In were made to a solution of 4.18×10^{-5} M Cd and the same background electrolyte used for the systems reported in Table VII. Table IX shows that resolution fails as the In peak becomes increasingly irreversible. The Cd half-width increases dramatically while the In peak half-width remains fairly constant, in contrast to results from Table VII. There is also a steady increase in the intercept of the standard additions plot for In, another indication of the failure of resolution. Table X shows that the Cd peak heights increase as In is added or as the In peak becomes more irreversible. None of these effects occur in series K and L of Table VI. The enhancement of the Tl slope is then most likely due to an interaction between Tl and In in the mercury drop. Although Tl and In are known (27) to form an intermetallic compound, no reports have appeared on this interaction in electroanalytical chemistry, possibly because of the difficulty in getting physically significant results from resolution of the overlapped peaks.

LITERATURE CITED

(1) Martin, K. J.; Shain, I. *Anal. Chem.* **1958**, *30*, 1808.
(2) Bond, A. M.; Grabaric, B. S. *Anal. Chem.* **1976**, *48*, 1624.
(3) Annino, R. *Adv. Chromatogr.* **1977**, *15*, 33.
(4) Kirmse, D. W.; Westerburg, A. W. *Anal. Chem.* **1971**, *43*, 1035.
(5) Binkley, D. P.; Dessey, R. E. *Anal. Chem.* **1980**, *52*, 1335.
(6) Perone, S. P.; Gutknecht, W. F. *Anal. Chem.* **1970**, *42*, 906.
(7) Perone, S. P.; Sybrandt, L. B. *Anal. Chem.* **1971**, *43*, 382.
(8) Boudreau, P. A.; Perone, S. P. *Anal. Chem.* **1979**, *51*, 811.
(9) Toman, J. J.; Corn, R. M.; Brown, S. D. *Anal. Chim. Acta* **1981**, *123*, 187.
(10) Imbeaux, J. C.; Saveant, J. M. *J. Electroanal. Chem.* **1973**, *44*, 169.
(11) Dalrymple-Alford, P.; Goto, M.; Oldham, K. B. *J. Electroanal. Chem.* **1977**, *85*, 1.
(12) Ammar, F.; Saveant, J. M. *J. Electroanal. Chem.* **1973**, *47*, 215.
(13) Grenness, M.; Oldham, K. B. *Anal. Chem.* **1972**, *44*, 1121.
(14) Barendrecht, E. *Electroanal. Chem.* **1967**, *2*.
(15) Mattison, J. M. *Anal. Chem.* **1972**, *44*, 1715.
(16) Brown, S. D.; Kowalski, B. R. *Anal. Chim. Acta.* **1979**, *107*, 13.
(17) Nelder, J. A.; Mead, R. *Comput. J.* **1965**, *7*, 308.
(18) O'Neill, R. *Appl. Statistics* **1971**, *13*, 338.
(19) Chambers, J. M.; Ertel, J. E. *Appl. Statistics* **1974**, *23*, 250.
(20) Benyon, P. R. *Appl. Statistics*, **1976**, *25*, 97.
(21) Hill, I. D. *Appl. Statistics* **1978**, *27*, 380.
(22) Statham, P. J. *X-Ray* Spectrom. **1976**, *5*, 16.
(23) Hayes, J. W.; Glover, D. E.; Smith, D. E.; Overton, M. W. *Anal. Chem.* **1973**, *45*, 277.
(24) Oldham, K. B.; Spanier, J. "Fractional Calculus" (Vol. 111 in Math in Science and Engineering Series); Academic Press: New York, 1974.
(25) Mosteller, F.; Tukey, J. W. "Data Analysis and Regression"; Addison-Wesley: Reading, MA, 1977; Appendix A.
(26) Nicholson, R. S.; Shain, I. *Anal. Chem.* **1964**, *36*, 706.
(27) Sauerwald, F. Z. *Metallkunde* **1950**, *41*, 97.

RECEIVED for review December 1, 1980. Accepted April 1, 1981. This work was supported by the Director, Office of Energy Research, Office of Basic Energy Sciences, Chemical Sciences Division of the U.S. Department of Energy under Contract No. W-7405-ENG-48 and by Contract No. DE AC06-76R101830-ONWI between Battelle Memorial Institute and the U.S. Department of Energy.

Effect of Graphite Furnace Substrate Materials on Analyses by Furnace Atomic Absorption Spectrometry

W. Slavin,* D. C. Manning, and G. R. Carnrick

The Perkin-Elmer Corporation, Main Avenue, Norwalk, Connecticut 06856

Recent improvements in the graphite furnace have greatly reduced analytical interferences. Problems remain that appear to be related to the porosity of graphite and to the fragility of pyrolytic graphite protective coatings. We compare graphite tubes from several sources which have been coated in several different ways for their differences in analytical sensitivity for Cu, Al, Sr, Ti, and Mo. A separate set of experiments using the determination of Al in a chloride matrix shows even greater variation between graphite materials prepared differently. Experiments using the graphite furnace at steady-state temperature, in the platform and probe variations, showed less than 10% signal suppression from 50 μg of $CaCl_2$ or $CuCl_2$ on 2 ng of Al.

Our recent papers (*1–6*) have attempted to improve the analytical conditions for trace metal determination with the graphite furnace and atomic absorption spectroscopy. When the furnace is operated at a steady-state temperature (*2, 3, 5–9*) during the time the analyte is vaporized and the absorbance signal is integrated, many of the interferences previously reported for graphite furnace analyses have been reduced or eliminated. Larger amounts of sample can be analyzed if Zeeman background correction is used (*4*). However it is necessary that the furnace be designed in a way to take advantage of Zeeman background correction or the advantages of Zeeman correction will be more than offset by furnace deficiencies. Signal handling must be very rapid (*10*) to avoid errors, as recently emphasized by Siemer and Baldwin (*11*).

When all of these factors are controlled correctly, most of the interferences reported in the literature are very small or nonexistent and standardization may not require a close match to the sample matrix. The method of additions, with its poor precision and discomforting extrapolation, may not be required.

In this paper we show that the quality of the graphite used for the furnace tubes is an important factor still not adequately controlled. Graphite is a porous material, easily penetrated by liquids and gases. Atomic vapor passes quite freely through a 1 mm thick wall of hot graphite. Coating the graphite tubes with a thin layer of pyrolytic graphite was recommended (*12*) more than a decade ago to reduce the effects of the porosity of the graphite.

L'vov et al. (*13*) have recently explained quantitatively the retention properties of graphite for the analyte that has penetrated the graphite structure. The analyte can penetrate as a liquid or as a vapor and it can penetrate during the charring step as well as during the atomization step. This applies to the matrix as well as to the analyte and must be taken into account for those matrices, like halides, which interfere in the vapor phase (*2, 7*).

In the past, the model for the conversion of a sample into an atomic vapor assumed that, at some temperature depending upon the analyte and its matrix, the analyte became an elemental vapor and survived in the vapor phase until it exited the optical system through the tube ends or the filling hole (*12, 14, 15*). It is more likely that the analyte is constantly volatilized and adsorbed, some of it within the structure of the graphite near where the sample is applied and some at considerable distances along the tube. The process resembles gas chromatography. Analytical problems associated with earlier furnace designs arose because the temperature rise was slow and the graphite was very porous. Fast heating and a strong impervious barrier separating the sample vapor from the graphite have greatly improved performance. Manning and Ediger (*16*) found that a pyrolytic graphite coating increased the signals for several important metals by factors as

0003-2700/81/0353-1504$01.25/0 © 1981 American Chemical Society

much as 4-fold. Fernandez and Iannarone (*17*) found similar improvements when the tube was heated very rapidly, especially for the more refractory metals.

Szydlowski et al. (*18*) studied the surface of pyrolytically coated tubes with a scanning electron microscope using tubes from the Perkin-Elmer HGA-2100. They found that the temperature of deposition had to be greater than 2300 °C to achieve a pyrolytic coating. Smith and Leeds (*19*) reported that the substrate temperature must be between 1750 and 2250 °C to achieve a pyrolytic coating, with the pyrolytic properties improving rapidly at higher temperatures. They point out that "pyrolytic graphite is not a single invariant material but has a structure and related properties that are completely dependent upon the manufacturing process".

This being true, pyrolytic coatings deposited in the laboratory by the procedure of Manning and Ediger (*16*) must produce a good pyrolytic coating, at best, only in the center of the tube since the ends of the tube are too cool to form a satisfactory coating (*20*). The commercial procedure for depositing a pyrolytic coating utilizes an oven at approximately constant temperature through which flows a mixture of a hydrocarbon in an inert gas.

Many workers have observed differences in analytical sensitivity or the extent of interferences when ordinary and pyrolytic graphite are compared. Volland et al. (*21*) observed differences in the extent of halide interferences on Fe, Ni, Mn, and Mo. Montgomery and Peterson (*22*) showed that pyrolytically coated graphite tubes deteriorated rapidly when NH_4NO_3 was used for the determination of Cu in seawater. Different batches of tubes were very different. Uncoated tubes had lower peak height sensitivities than the initial results from coated tubes, but the sensitivities did not decrease with time. The variability of graphite in porosity and density has not been understood and the difficulty in quality control from batch to batch has been underestimated. Probably the graphite under the pyrolytic coating in the Montgomery and Peterson experiments was entirely different from those tubes which were uncoated.

Some compounds are particularly destructive of the pyrolytic graphite coating by procedures that are not well understood. Montgomery and Peterson (*22*) claim that $NaNO_3$ is destructive and Julshamn (*23*) found $HClO_4$ particularly destructive. This acid has been recommended to digest graphite and pyrolytic carbon prior to chemical analysis of these materials (*24*). Chromic acid is reported to exfoliate pyrolytic graphite (*19*), and aluminum chloride, sulfuric acid, and heat are the commercial process for exfoliating pyrolytic graphite. When any of these materials or processes cause small defects to appear in the pyrolytic coating, the adsorptive properties of the underlying graphite become important.

More than 15 papers have reported that a refractory carbide coating on graphite improved the analytical environment for some particular analyte elements. Probably these carbides perform the same function as the pyrolytic coating in providing a dense barrier between the sample and the porous graphite. These carbide coatings on top of pyrolytic graphite may seal defects in the pyrolytic graphite layer.

Graphite tubes were carbide-coated by Norval et al. (*25*) by sputtering W or Ta and carbidizing the coatings in a separate furnace at high temperature. In one tungsten-coated tube described by them, the peak absorbance for a Cu solution did not change during the 3000 firings of its life. In our experience, even with the best pyrolytically coated tubes that we have seen, the peak absorbance does change with time although the integrated absorbance using the L'vov platform often does not (*6*).

Several papers in the literature (*22*, *26*, *27*) and our own experience indicated that changes in analytical sensitivity with usage of the graphite tube might be related to the quality of the graphite. Differences in analytical sensitivity between tubes made in different ways should also be a distinguishing characteristic. Therefore we have chosen five test elements, Cu, Al, Sr, Ti, and Mo and we have run these on many different tubes. Our experience indicated that the most refractory metals were the most variable, so four of the metals that we chose required a relatively high temperature for atomization. We used Cu as an experimental control, an intermediate metal that usually has no problems.

Table I. Instrument Parameters

element	wavelength, nm	slit, nm	char temp, °C	atomization temp, °C	
				P-E pyro	others
Cu	324.7	0.7	900	2000	2250
Al	309.3	0.7	1500	2400	2600
Sr	460.7	1.4	1200	2500	2700
Ti	365.3	0.2	1400	2700	2700
Mo	313.3	0.7	1800	2700	2700

The second set of experiments relates to the study of the interferences associated with the determination of Al. This experimental protocol has revealed very wide discrepancies between furnace analyses that would have been expected to be very similar. In this paper, the effect of varying concentrations of $CaCl_2$ upon the determination of Al is reported. The extent of the interference is shown to vary greatly with the life of the tube. Therefore the experimental protocol consisted of adding a constant amount of Al and increasing concentrations of $CaCl_2$, up to about 1%. Different experimental environments were subjected to this protocol. These environments included sampling from the wall of a standard furnace tube, various platforms in various furnace tubes, and a variation of the wire probe technique (*3*, *5*).

EXPERIMENTAL SECTION

Equipment. All tests were performed on a Model 5000 equipped with an HGA-500, AS-40 autosampler and an 056 recorder. Instrument parameters were set according to specifications in the manufacturer's literature (*28*), as indicated in Table I. Some of the data were taken, recorded, and plotted by using a Perkin-Elmer Data System 10 and a Hewlett-Packard 7225A Graphics Plotter 17603A. The Ircon automatic recording optical pyrometer and the Leeds and Northrup optical pyrometer were used to measure the true temperature inside the graphite furnace tube. The indicated controller readings were calibrated against these devices, as described previously (*1*).

The Sensitivity Experiment. We incorporated into the test protocol five different standard Perkin-Elmer pyrolytically coated tubes (part no. 290-1766) and we got very homogeneous results from these even when the experimental protocol was repeated several months later. We compared these results with measurements reported several years ago on different (but similar) equipment by Fernandez and Iannarone (*17*).

Maximum power was used for atomization. Atomization temperatures were set by manually adjusting the HGA-500 controller until the pyrometer indicated the desired temperature on the inner wall of the tube. Argon was used as a support gas and flow was stopped during atomization.

All elements were fired 10 times in each tube and the last five results were used for the statistical analyses. When the elements were changed, the tube was fired twice with no sample to reduce carry-over contamination.

Several different tubes were tested in addition to the standard Perkin-Elmer pyrolytically coated tubes which were used as a reference. Two ordinary graphite tubes were Ta-coated in our lab by the process of Zatka (*29*) and these are identified as "Ta-soaked" in the tables. Two tubes were given to us by H. Human, CSIR, Pretoria, that had been made in his lab by the process described in their paper, Norval et al. (*25*). These are identified as "Ta-CSIR". One tube was made by our colleagues

Table II. Precision[c]

element	precision, % std P-E graphite[a]	std P-E pyro[a]	Ta-soaked	W-BSW	Ta-CSIR[b]
Cu	1.2	2.4	0.7	1.1	
Al	2.8	4.9	8.2		4.2
Sr	1.3	3.9		1.1	2.4
Ti	2.6	5.1		2.5	3.2
Mo	4.1	1.6		1.1	5.0

[a] Average of coefficients of variation for three tubes. [b] Average coefficients of variation for two tubes. [c] Values are coefficients of variation of the peak area data for each tube.

Table III. HGA-500 Graphite Furnace Conditions

Sampling from the Wall

	dry	char	atomize	clean out
temp, °C	140	1500	2200	2900
ramp, s	1	1	0	1
hold, s	20	40	5	1

Sampling from the Platform

	dry	char	atomize	clean out	cool
temp, °C	280	1600	2400	2900	20
ramp, s	1	1	0	1	1
hold, s	20	25	8	1	10

Sampling from the Tungsten Wire

	dry	char	cool	atomize	clean out	cool
temp, °C	450	2100	20	2200	2900	20
ramp, s	1	1	1	1	1	1
hold, s	20	30	10	15	1	10

at Perkin-Elmer, Bodenseewerk, Germany, by a process similar to that described by Norval. This tube was tungsten-coated and identified as "W-BSW". Two new pyrolytically coated tubes were tested and they are identified as "new-pyro" and are available as Perkin-Elmer part no. B009-1504.

In this work, sensitivity was defined as the amount of metal (picograms) that produced a 1% absorption signal (0.0044 absorbance). Thus the data in Tables IV and V are in pg/0.0044 abs. The concentrations of the test solutions were adjusted to be within the linear range for each test and typically produced absorbance signals between 0.15 and 0.7 abs. Peak height data were used for this work because changes in peak shape were among the results we wished to expose. Differences less than 2-fold are not significant using sensitivity as a criterion.

Although the protocol of this experiment was not designed to look specifically at precision, Table II shows the coefficients of variation obtained for each type of tube.

Aluminum in Chloride Experiments. For the Al in $CaCl_2$ experiments, the furnace conditions for sampling from the tube wall, from the platform, and from the wire are given in Table III. The internal argon purge gas flow was stopped during the atomization step. For the platform studies, a solid pyrolytic graphite L'vov platform (2) was used. In the experiment with $CuCl_2$ matrix, we replaced the graphite platform with a plate of tantalum. The Ta plate was 10-mm long, 3-mm wide, and 0.5-mm thick, which was smaller than the standard graphite platform.

For the wire probe studies, the tee-tube extension was made of isotropic (uncoated) graphite which was pressed into a tube of pyrolytically coated graphite. The indicated char temperatures in the probe work were not the actual temperature of the probe containing the sample but rather the temperature measured on the wall at the inside center of the sample tube. The probe was considerably cooler than this. Since we are not able to measure the probe temperature, we investigated the Al loss vs. char temperature for each series of experiments to ensure that Al was not being lost in the char step.

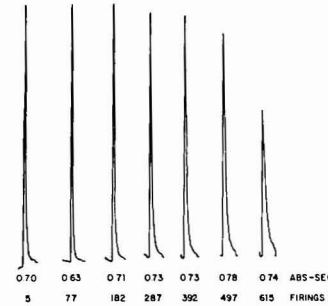


Figure 1. The changes in peak shape with increased number of firings. The sample is 2 ng of Al from a platform in a pyrolytically coated tube.

Table IV. Sensitivity (pg/0.0044 abs) for Standard Perkin-Elmer Pyro Tubes

	Fern. & Iann.	new no. 1	new no. 2	old no. 2	new no. 3	old no. 3	new no. 4	new no. 5
Cu	4	3	2	2	3	8	2	2
Al	21	15	16	20	15	26	11	9
Sr		2	2	2	3	10	1.3	1.3
Ti	91	94	116	195	111	850	60	93
Mo	11	11	12	27	12	90	13	9

In all these experiments the amount of Al introduced in each firing was 2 ng. The sample volume for wall and platform sampling was 20 μL and for wire sampling was 5 μL. Each datum represented the average of three firings in sequence. Thus each series of about 10 different concentrations of $CaCl_2$ represented about 30 firings. The data are reported in absorbance-seconds. The peaks at the end of the run were much broader, and, therefore, not so tall since the area remained nearly constant (Figure 1). This is a good example of the advantage of using area integration.

RESULTS AND DISCUSSION

The Sensitivity Experiment. The sensitivities that were obtained for standard Perkin-Elmer pyrolytically coated tubes are shown in Table IV. Also included for comparison are the sensitivities reported by Fernandez and Iannarone (*17*). The three tubes marked new no. 1, 2, and 3 were run in the first series. They are very similar and agree adequately with the data of Fernandez and Iannarone. Fernandez and Iannarone did not run Sr. When the test protocol was repeated several months later, tubes 2 and 3, now old and well-used, were retested and new similar tubes, no. 4 and 5 were added. Note that the new tubes agreed very well with the earlier sets of data but that the old tubes had lost sensitivity, particularly for Mo and Ti. By contrast, Al and Cu were not very sensitive to aging. The consistency of these data on new tubes has given us confidence in the test.

The data in Table V utilized the test protocol in the different tubes. The second "new pyro" tube and the second "Ta-CSIR" tube produced data which were indistinguishable from that shown in Table IV. The two "Ta-soaked" Zatka tubes produced no useful signal for the three refractory metals although the tubes worked well for Cu.

The typical standard pyro tube, the Ta-CSIR tube, and the new pyro tube all agreed with the reference data and were indistinguishable by this test. The W-BSW tube did not perform satisfactorily for the refractory metals. In addition the tube appeared to be contaminated with Al.

Table V. Sensitivity (pg/0.0044 abs) for Several Tubes

	Fern. & Iann.	std P-E pyro	new pyro	Ta-CSIR	W-BSW	Ta-soaked	std P-E ordinary graphite
Cu	4	3	2	1	3	7	10
Al	21	15	7	11	*a*	89	11
Sr		2	2	2	3	*a*	4
Ti	91	94	113	130	190	*b*	370
Mo	11	11	15	16	40	*b*	34

[a] Large spurious peak. [b] No peak at 10× expansion.

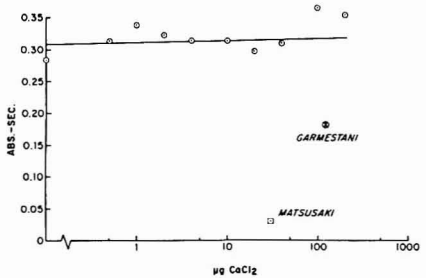


Figure 2. Sampling from the wall, the signal for 2 ng of Al in different amounts of $CaCl_2$. Rapid heating was used in a pyrolytically coated tube. Points are included from Matsusaki et al. (*30*) and Garmestani et al. (*31*).

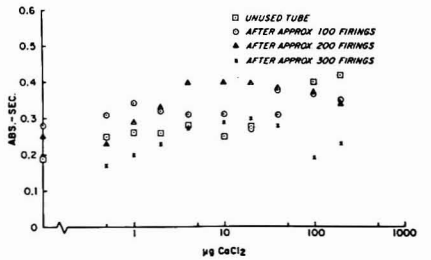


Figure 3. Sampling from the wall, showing change with the number of firings. Rapid heating was used in a pyrolytically coated graphite tube.

It is interesting to note the last column, marked "std PE ordinary graphite". Three of these tubes were run with essentially identical results. They were made from a high-quality graphite and were not pyrolytically coated. They performed particularly poorly for the refractory metals and for Cu but were fine for Al. The reference data by Fernandez and Iannarone (*17*) included sensitivity for the ordinary graphite tube which is in good agreement with our results. The only significant difference was for Ti where we found the tubes to be about 3-fold more sensitive than the earlier study.

Aluminum in Chloride Experiment. When the series of $CaCl_2$ solutions was atomized from the wall of a standard furnace, there was no large suppression of the analytical signal, although the data did not follow a very regular trend, as shown in Figure 2. For contrast, we have plotted points from the work of Matsusaki et al. (*30*) and Garmestami et al. (*31*), who have studied the same system. We have not seen the great suppression of signal they reported. The points were plotted by normalizing their signal for Al with no $CaCl_2$ to our point on the chart.

If the same tube was sampled repeatedly, the signal gradually declined as shown in Figure 3, but the trend remained erratic. When the analytical protocol was repeated with the standard platform and tube, Figure 4 shows (1) that the trend was much more regular, (2) the signal was larger, and (3) unfortunately, at large concentrations of $CaCl_2$, the suppression was much greater. As the tube wore on, the suppression started at lower concentrations of $CaCl_2$.

Other experiments with other similar platforms and tubes showed similar results. The change with time evident in the data varied from tube to tube. With several tubes the rate of increase in interference was greater than shown, while for several other tubes it was significantly less, although the experimental conditions were kept constant. These variations may be caused by differences in the pyrolytic coating.

When the protocol was repeated on a platform in a standard graphite tube that was not pyrolytically coated, the results were much better (Figure 5). The graphite used for the

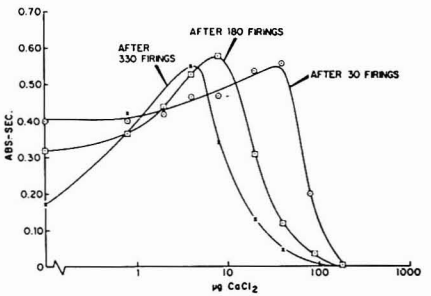


Figure 4. Sampling from a pyrolytic platform in a pyrolytically coated graphite tube.

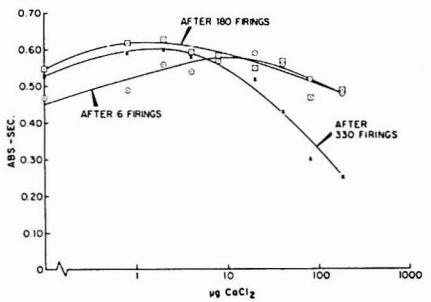


Figure 5. Sampling from a pyrolytic platform in an uncoated graphite tube.

pyrolytically coated tube is a different material from that used for the uncoated tube of Figure 5 and is believed to be more porous. We believe that when the coating begins to erode after a few firings, a larger proportion of the $CaCl_2$ matrix is retained

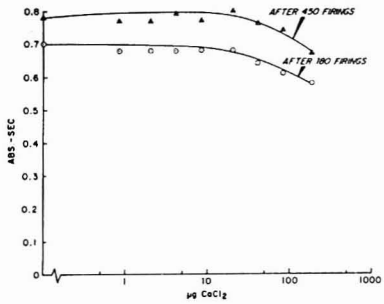


Figure 6. Sampling from a pyrolytic platform in new pyrolytically coated graphite tube.

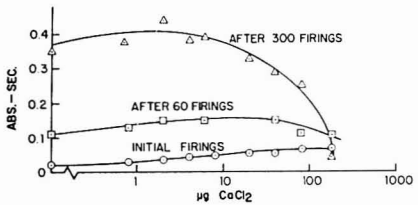


Figure 7. Sampling from a pyrolytic platform in a graphite tube treated by the Zatka process (*29*).

through the ashing cycle, increasing the typical vapor-phase interference between Al and chloride during the atomization step.

We therefore used a similar pyrolytic platform in the new graphite tube mentioned earlier, made of a more dense graphite coated with pyrolytic graphite. The results in Figure 6 show excellent performance.

In an effort to see if a carbide-coated graphite would provide useful results, we repeated the protocol in a standard graphite tube which had been Ta-carbide coated by the procedure of Zatka (*29*). The results in Figure 7 showed inadequate performance, although the performance improved with the age of the tube.

A similar set of experiments were conducted on Al in a $CuCl_2$ matrix with results shown in Figure 8. Since the interference is the effect of chloride on Al, there should not be a major difference from the previous set of results. In fact, the improvement of sensitivity from the platform and the tungsten wire over the wall was seen. We additionally performed this experiment using a Ta plate as a platform.

Discussion of Al in Chloride Experiments. In the context of this paper, we have demonstrated that the chloride interference on Al varied greatly with the properties of the sampling environment and with the age of the graphite tubes, which is probably the same thing. We believe that in all cases the differences in the performance of the various furnace arrangements at steady-state temperature reflected the amount of chloride available for the vapor-phase reaction.

As expected, the probe technique with tungsten wire worked well since the products of the char step were largely excluded from the furnace. The Ta platform provided a slightly better environment than the graphite platform, in similar tubes, at least for this particular analysis. The similarity of the good results from the metal probe and platform reflected the fact that some portion of the matrix survived the char step and interacted with the graphite tube, thus making the chloride available during atomization.

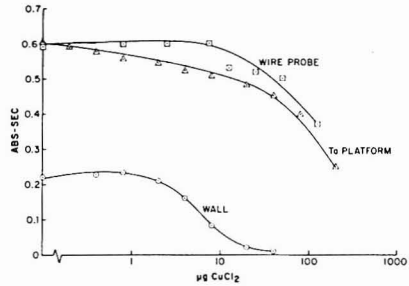


Figure 8. Sampling from various surfaces using 2 ng of Al in various concentrations of $CuCl_2$.

The data showed that the different physical environments produced different results and that the changes in the graphite with aging produced similar differences. The closer we came to an impervious surface on which to deposit the sample and an equally impervious tube to confine the atomic vapor, the smaller were the interferences.

A special problem has become clear during the progress of this work. The performance of the tubes coated by the Zatka process had been puzzling. Figure 7 shows that the performance improved with the number of firings. The data in Table V showed reasonable performance for Cu but no signal for solutions of Ti or Mo. In the Zatka process, the Ta carbide is formed by using a solution containing HF. The observations are well explained by the continued volatilization of F from the body of the tube. L'vov (*7*) has shown that gaseous metal fluorides are even more stable than equivalent chlorides. As the tube is fired, the F is gradually depleted and the Al sensitivity increases. The fluorides of Ti and Mo are very much more stable than that of Cu. The fact that Ta has nothing to do with the poor performance of the Zatka tubes is confirmed by the superior performance of the tubes made by the Ta-CSIR process (*25*) in Table V.

This has led us to an explanation of another effect we have frequently observed. Sometimes a particular batch of graphite tubes will require a short "break-in" procedure. The first few firings provide low sensitivity. In the final step of the manufacturing process for graphite, a fluorinated compound (often freon) is added to the machined tubes, followed by firing at high temperature. The fluorine that is evolved scavenges residual metal impurities. Those batches of graphite tubes which require breaking in have presumably not been heated long enough to drive off the fluorine.

While not fully proven, this study and other recent work in our laboratory have shown that pyrolytic coatings and metal carbide coatings produce similar, probably equivalent results. If the coatings are periodically renewed (*32*), the analytical performance does not degrade during the life of the tube. While the quality of the commercial graphite is variable, analytical results using these materials can often be improved in the laboratory by the procedures in the literature for pyrolyzing or carbide coating the graphite tubes.

ACKNOWLEDGMENT

We thank our colleagues, Sabina Slavin, W. B. Barnett, F. J. Fernandez, B. Welz, and Z. Grobenski for many useful discussions. W. Ulsamer, H. Kirch, and B. Hutsch of Ringsdorff-Werke have been most helpful.

LITERATURE CITED

(1) Manning, D. C.; Slavin, W. *Anal. Chem.* **1978**, *50*, 1234–1238.
(2) Slavin, W.; Manning, D. C. *Anal. Chem.* **1979**, *51*, 261–265.
(3) Manning, D. C.; Slavin, W.; Myers, S. *Anal. Chem.* **1979**, *51*, 2375–2378.

(4) Fernandez, F. J.; Myers, S. A.; Slavin, W. Anal. Chem. 1980, 52, 741-746.
(5) Manning D. C.; Slavin, W. Anal. Chim. Acta 1980, 118, 301-306.
(6) Slavin, W.; Manning, D. C. Spectrochim. Acta, Part B 1980, 35B, 701-714.
(7) L'vov, B. V. Spectrochim. Acta, Part B 1978, 33B, 153-193.
(8) Hageman, L. R.; Nichols, J. A.; Viswanedham, P.; Woodriff, R. Anal. Chem. 1979, 51, 1406-1412.
(9) Chakrabarti, C. L.; Wan, C. C.; Hamed, H. A.; Bartels, P. C. Anal. Chem. 1981, 53, 444-450.
(10) Barnard, T. Anal. Chem. 1979, 51, 1172A-1178A.
(11) Siemer, D. D.; Baldwin, J. M. Anal. Chem. 1980, 52, 295-300.
(12) L'vov, B. V. "Atomic Absorption Spectrochemical Analysis"; Hilger: London, 1970.
(13) L'vov, B. V.; Bayunov, P. A.; Ryabchuk, G. N. Spectrochim. Acta, in press.
(14) Fuller, C. W. "Electrothermal Atomization for Atomic Absorption Spectroscopy"; Chemical Society: London, 1977.
(15) van den Broek, W. M. G. T.; de Galan, L. Anal. Chem. 1977, 49, 2176-2186.
(16) Manning, D. C.; Ediger, R. D. At. Abs. Newsl. 1976, 15, 42-44.
(17) Fernandez, F. J.; Iannarone, J. At. Abs. Newsl. 1978, 17, 117-120.
(18) Szydlowski, F. J.; Peck, E.; Bax, B. Appl. Spectrosc. 1978, 32, 402-404.
(19) Smith, W. H.; Leeds, D. H. Mod. Mater. 1970, 7, 139-218.
(20) Slavin, W.; Myers, S. A.; Manning, D. C. Anal. Chim. Acta 1980, 117, 267-273.
(21) Volland, G.; Kölblin, G.; Tschöpel, P.; Tölg, G. Z. Anal. Chem. 1977, 284, 1-12.
(22) Montgomery, J. R.; Peterson, G. N. Anal. Chim. Acta 1980, 117, 397-401.
(23) Julshamn, K. At. Abs. Newsl. 1977, 16, 149-151.
(24) Buzzelli, G.; Mosen, A. W. Talanta 1977, 24, 383-385.
(25) Norval, E.; Human, H. G. C.; Butler, L. R. P. Anal. Chem. 1979, 51, 2045-2048.
(26) Eames, J. C.; Matousek, J. P. Anal. Chem. 1980, 52, 1248-1251.
(27) Carrondo, M. J. T.; Lester, J. N.; Perry, R. Anal. Chim. Acta 1979, 111, 291-295.
(28) Manual for the Graphite Furnace, Analytical Procedures, 1979, Bodenseewerk, Perkin-Elmer.
(29) Zatka, V. J. Anal. Chem. 1978, 50, 538-541.
(30) Matsusaki, K.; Yoshimo, T.; Yamamoto, Y. Talanta 1979, 26, 377-380.
(31) Garmestani, K.; Blotcky, A. J.; Rack, E. P. Anal. Chem. 1978, 50, 144-147.
(32) Clyburn, S. A.; Bartschmidt, B. R.; Veillon, C. Anal. Chem. 1974, 46, 2201-2204.

RECEIVED for review February 2, 1981. Accepted May 20, 1981.

Determination of Insulin in Serum by Enzyme Immunoassay with Fluorimetric Detection

William D. Hinsberg, III, Kristin H. Milby, and Richard N. Zare*

Department of Chemistry, Stanford University, Stanford, California 94305

An enzyme immunoassay for the determination of insulin in human serum is described, based on fluorimetric detection of enzyme activity. A sandwich method using horseradish peroxidase as the label is employed; the enzyme activity is measured by fluorescence using the substrate, *p*-hydroxyphenylacetic acid. The fluorescence measurements can be carried out by liquid chromatography–laser fluorimetry or by conventional cuvette spectrofluorimetry. The procedure allows the rapid and sensitive quantitation of insulin with a 45-min total incubation period and a 7.9 pM or 46 pg/mL detection limit. There is high correlation between the insulin concentrations in serum samples determined by this method and by radioimmunoassay (correlation coefficient $r = 0.97$).

The technique of enzyme immunoassay (EIA) has undergone rapid development during the past decade (*1*). EIA has attracted considerable attention as a replacement for radioimmunoassay (RIA), since it avoids difficulties associated with the radioisotopic method (such as special handling and disposal procedures, and limited reagent shelf life). Moreover, EIA is potentially the more sensitive approach because the enzyme label may in principle be detected at the single-molecule level (*2*).

The aim of the present study is to assess the extent to which an EIA method may be improved through utilization of a more sensitive system for the measurement of enzyme activity. Earlier work in our laboratory has shown that application of laser fluorimetric techniques to the quantitation of enzyme reaction products allows more sensitive determinations than are possible with conventional methods (*3*, *4*). Recently we demonstrated that laser fluorimetry may be successfully incorporated into a practical EIA procedure (*5*) for the analysis of insulin in human serum. In this paper, we describe an extension and improvement of this approach. We also discuss the potential advantages of EIA-laser fluorimetry and its limitations in the current state of development.

Figure 1 shows a schematic representation of the "sandwich" EIA method used in this work. During step 1, the antigen, Ag (insulin), is allowed to complex with solid-phase-bound antibody (Ab). In step 2, Ab labeled with the enzyme horseradish peroxidase (HRP) is added to the sample. The labeled antibody complexes the Ag that is bound to the solid phase. The amount of solid-phase-bound enzyme is thus directly related to the amount of insulin in the original sample. After a washing step, bound enzyme activity is measured. In our case this is accomplished by using the nonfluorescent substrate, *p*-hydroxyphenylacetic acid (HPA), which is converted upon enzyme catalysis to a fluorescent product identified (*6*, *7*) as 6,6′-dihydroxy-[1,1′-biphenyl]-3,3′-diacetic acid (DBDA), as shown in Figure 2. For quantitation of DBDA, a high-pressure liquid chromatography (HPLC)–laser fluorimeter is employed (*5*).

EXPERIMENTAL SECTION

Apparatus. The equipment and chromatography conditions used in this work have been described in detail (*5*) and included a reversed-phase high-pressure liquid chromatography system. For enhancement of DBDA fluorescence, the effluent pH was adjusted by postcolumn mixing with 0.075 M NaOH in 70% CH_3OH/30% H_2O (v/v). Both this NaOH solution and the column eluent were pumped at flow rates of 1.3 mL/min. The 325-nm line of a helium–cadmium ion laser (Liconix Model 4050 UV) was focused into a 4-μL volume of the effluent in a flowing droplet detector. The fluorescence signal was isolated by liquid filters (*3*) and focused onto a photomultiplier tube. Its signal was displayed directly on a strip-chart recorder.

In those analyses carried out with conventional spectrofluorimetry, a Perkin-Elmer MPF-2A instrument was employed, using

0003-2700/81/0353-1509$01.25/0 © 1981 American Chemical Society



Figure 1. Experimental protocol: Ag = antigen; Ab = antibody; E = enzyme; S = substrate; P = fluorescent product.

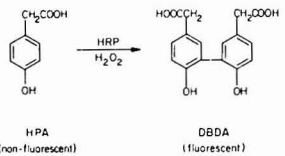


Figure 2. Enzymatic conversion of nonfluorescent substrate (HPA) to fluorescent product (DBDA).

standard 10 mm pathlength cuvettes. The excitation and emission wavelengths were 317 and 414 nm, respectively.

Reagents. The immunoassay reagents were purchased as the "Insolutec Kit" from Mochida Pharmaceutical (Tokyo) and have been described in detail elsewhere (*8*). These included plastic disks (1 cm diameter, 0.5 cm thick) coated with antiinsulin antibody, assay buffers (pH 7.4, containing animal protein), Tween 20 surfactant, 2% (w/v) sodium azide, and standard solutions of insulin. HPA was purchased from Aldrich and purified by sublimation and liquid chromatography (*5*). Human control sera were purchased as lyophilized samples from Nuclear Medical Systems (Newport Beach, CA; Lot no. R06L, R07M, R08H) and used to establish precision.

Procedures. Fresh human serum was prepared from blood samples obtained from the Stanford University Medical Center. After aliquots were taken for analysis by this method, the serum samples were frozen until RIA analysis was carried out using a modification of the method of Desbuquois and Aurbach (*9*).

In order to minimize nonspecific binding, we pretreated the antibody-coated disks by soaking at 4 °C for 24–72 h in 0.01 M phosphate buffer, pH 7.0, containing 0.01 M NaCl and bovine serum albumin (1 mg/mL). Just prior to use, the disks were rinsed with albumin-free buffer.

All incubations were carried out at room temperature (21 °C). Incubation times were controlled to within 3 s. To initiate the first reaction, disks were added to test tubes containing known (0.4 mL standards) or unknown (0.1 mL serum plus 0.3 mL assay buffer) amounts of insulin. After 15 min, 0.1 mL of HRP-labeled antibody solution was added to each tube. After an additional 15 min this second reaction was halted by adding 5 mL of a Tween 20 solution in saline. Fluid was withdrawn by aspiration. After this wash procedure was repeated three more times, the disks were transferred to clean test tubes. For the third reaction, 0.2 mL each of 0.53 mM H_2O_2 and 12 mM HPA in 0.01 M phosphate buffer, pH 7, were added to each tube. After a third 15-min interval, this reaction was halted by adding 20 μL of a 2% (w/v) sodium azide solution. A 0.2-mL aliquot of each sample was mixed with 0.2 mL of distilled methanol. Ten microliters of each resulting solution was injected onto the HPLC column. Peak heights

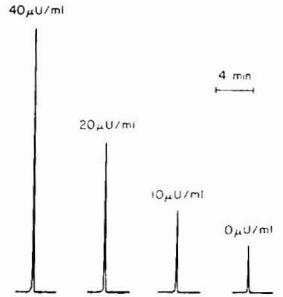


Figure 3. Chromatograms showing the DBDA peak as a function of initial insulin concentration (1 μU/mL = 42 pg/mL).

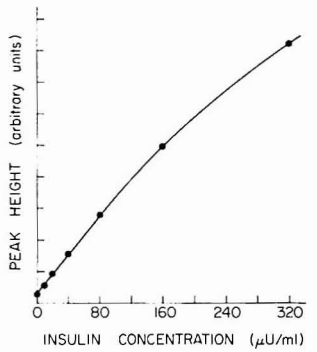


Figure 4. Standard curve showing DBDA peak height vs. insulin concentration. The solid circles are the averages of duplicate measurements.

were used to construct a standard curve and to determine insulin concentrations in the serum samples. Serum samples were analyzed in duplicate and the determinations averaged.

In some cases, 50 μL was taken from each tube after the final reaction was halted and mixed with 1.0 mL 0.075 M NaOH. The fluorescence of these samples was analyzed by using cuvettes and a conventional spectrofluorimeter.

RESULTS

Figure 3 shows typical chromatograms from four insulin standards analyzed by the above procedure. A single peak is observed to elute 2.5 min after injection. It corresponds to the fluorescent enzyme reaction product DBDA. The amount of DBDA formed is proportional to the amount of insulin in the original sample, consistent with the scheme outlined in Figure 1. It is traditional to express the concentration of insulin by its biological activity, where 1 μU/mL = 42 pg/mL = 7.2 pM. The peak for the sample containing no insulin (0 μU/mL) represents enzyme activity from nonspecifically bound HRP-labeled antibody.

Analysis of insulin standards during each run allows construction of standard curves. A typical curve is shown in Figure 4. The detection limit in this case is 1.1 μU/mL insulin (7.9 pM). This value fulfills the condition $h - h_b = 2\sigma_b$ where h and h_b are the mean peak heights for multiple samples of the lowest detectable level and the blank, respectively, and σ_b is the standard deviation in peak height measurements for multiple samples of the blank.

The precision of the present method was examined (see Table I). The intraassay (within-run) precision was estimated

Table I. Precision of the Fluorescence-EIA Method

	no. of samples	insulin concn, μU/mL	std dev	coeff of variation, %
within-run	7	17.9	1.3	7
between-run	6	13.5	2.8	21
	6	44.3	5.5	12

Table II. Comparison of Control Serum Insulin Levels[a]

	insulin concn in control serum[b]		
immunoassay method	low	medium	high
Becton-Dickinson RIA	8.7 ± 2	27 ± 5	42 ± 9
Biomed. Ref. Lab RIA	18.8 ± 4	21 ± 5	
Corning RIA	16.3 ± 4	34 ± 8	47 ± 9
Eiken RIA	6.7 ± 2	15 ± 5	33 ± 9
Immunonuclear RIA	7.0 ± 2	16 ± 4	39 ± 8
Pharmacia RIA	12.6 ± 2	24 ± 5	46 ± 9
Serono RIA	9.0 ± 2	20 ± 5	30 ± 10
present work[c]	13.5 ± 4	18 ± 2	44 ± 8

[a] RIA values from Nuclear Medical Systems RIA Control Sera Data Sheet. [b] Mean ± range in μU/mL. [c] Low and high values determined between-run; medium value determined within-run (see text).

from results of seven parallel analyses of a sample of control serum. Interassay (between-run) precisions were estimated by comparing insulin levels measured on six different days in aliquots of two control sera.

The use of control sera in this study allows a comparison of the accuracy of the present method with that of a number of RIA analyses for insulin. In Table II are listed the insulin concentrations obtained when a number of commercial RIA methods were used to analyze the control sera employed in this work. Also listed are the insulin levels obtained with the present method, which compare favorably with those from the RIA procedures.

To demonstrate the clinical applicability of our method, we made a double blind comparison to RIA using 43 samples of human serum. Figure 5 shows that our values correlate highly with RIA. The least-squares line is $y = 1.07x + 8.43$ with a correlation coefficient of 0.97.

To investigate the relationship of extended analysis time to lowered detection limit, we analyzed standard insulin samples by the above method except that the first reaction was increased from 15 to 60 min. In this case the detection limit, as defined above, was 0.5 μU/mL (3.6 pM). To assess the importance of temperature control, we carried out a series of EIA analyses, employing a water bath at 25.0 ± 0.3 °C to maintain the assay tubes at a constant temperature during incubation. No improvement in sensitivity or precision was observed.

Because our chromatographic analysis gave no indication of interfering components (only one peak was observed), we tested the possibility of using conventional cuvette spectrofluorimetry with this EIA system. Comparing peak heights from the laser fluorimetric method with the fluorescence signal using a standard instrument gave excellent correlations for both standards and serum samples (correlation coefficient $r > 0.997$). Thus at the concentrations studied, there is no need to employ the more powerful technique of HPLC laser fluorimetry.

DISCUSSION

This work demonstrates that incorporation of a sufficiently sensitive means of measuring enzyme activity into an EIA procedure can make possible substantial gains in both rapidity

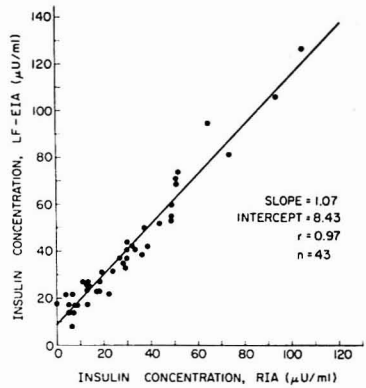


Figure 5. Correlation between insulin concentrations in serum determined by laser fluorescence enzyme immunoassay (this method) and radioimmunoassay (1 μU/mL = 42 pg/mL).

of analysis and assay sensitivity. Moreover, in the present method, measurement of enzyme activity is not a limiting factor, suggesting that further improvements are feasible, if desired.

Fluorimetric methods have been applied in both competitive binding EIA (*10*) and sandwich EIA (*11*) measurements of insulin levels in human serum. In the former, an overnight incubation was specified, and 2.5 μU/mL (18 pM) of insulin was detectable (*10*). In the latter, a total incubation period of over 5 h was called for, and the detection limit for insulin was ~2 μU/mL (14 pM) (*11*). EIA procedures for insulin in serum incorporating colorimetric enzyme determinations have been described which are similar in sensitivity and comparable or superior in rapidity to these fluorimetric EIA methods (*8, 12, 13*).

In the present work, we employ a modification of the most rapid of these colorimetric EIA methods (*5, 8, 13*). It permits application of laser fluorimetric procedures in the determination of enzyme activity. In the colorimetric EIA the reported limit of detection was 5 μU/mL (36 pM) of insulin and the total incubation period was, at a minimum, 3 h (*8, 13*). In our method, the limit of detection is almost 5 times lower, and the total incubation period is shorter by a factor of 4 than the colorimetric EIA procedure. Our detection limit may be improved an additional factor of 2 by extending the length of the first incubation.

The precision reported here is somewhat less than observed in the related colorimetric EIA (*13*), where much longer incubation periods were used. However the precision of the method is comparable to that reported for another EIA for insulin in serum (*12*) and is sufficient to allow its practical application as evidenced by the results of our double blind study (Figure 5).

Two factors prevent further optimization of the assay at this time. Improvements in sensitivity are restricted by the degree of nonspecific binding and our inability to distinguish antigen-bound label (signal) from that bound nonspecifically (blank). Further reductions in incubation period are constrained by our ability to manually process a reasonable number of samples in a rapid manner.

Detection of the fluorescent DBDA product is not a limiting element. Consequently a conventional fluorimeter can be utilized by suitable modification of the measurement protocol. Therefore, the advantages of speed and sensitivity demonstrated for this method can be realized by detecting DBDA

fluorescence in cuvettes, in flow injection analyzers, or following liquid chromatography.

The present work does indicate the potential of laser fluorescence enzyme immunoassay methods. If conventional fluorimetry is used, any further improvement in this assay will be limited by the ability to detect DBDA. However, the laser fluorimeter employed here is roughly 30 times more sensitive for detection of DBDA than is a standard spectrofluorimeter under the conditions used in this work. As a result, the following refinements of the assay should prove possible without requiring further improvement in DBDA detection: (1) the original sample size and the volumes used in the immunoassay steps may be scaled down, with an accompanying improvement in absolute sensitivity for insulin; (2) automation of the assay may allow further gains in rapidity; and (3) the limit of detection of insulin concentration in serum may be further improved by reduction of nonspecific binding.

Nevertheless, the present study based on fluorescence EIA demonstrates the most rapid and sensitive detection of insulin in human serum; moreover it is not dependent on the use of radioisotopes and it can be carried out by using conventional fluorescence equipment.

ACKNOWLEDGMENT

We thank Steven Lidofsky for assistance during the initial stages of this work and Jo Moore of the Palo Alto Veterans Administration Hospital for performing RIA analyses.

LITERATURE CITED

(1) Wisdom, G. B. *Clin. Chem (Winston-Salem, N.C.)* **1976**, *22*, 1243–1255.
(2) Rotman, B. *Proc. Natl. Acad. Sci. U.S.A.* **1961**, *47*, 1981–1991.
(3) Imasaka, T.; Zare, R. N. *Anal. Chem.* **1979**, *51*, 2082–2085.
(4) Lidofsky, S. D., Dissertation, Columbia University, New York, 1980.
(5) Lidofsky, S. D.; Hinsberg, W. D., III; Zare, R. N. *Proc. Natl. Acad. Sci. U.S.A.* **1981**, *78*, 1901–1905.
(6) Guilbault, G. G.; Brignac, P. J.; Juneau, M. *Anal. Chem.* **1968**, *40*, 1256–1263.
(7) Guilbault, G. G.; Sadar, M. H.; Peres, K. *Anal. Biochem.* **1969**, *31*, 91–101.
(8) Shinkai, H.; Sohma, M.; Takahashi, Y.; Kojima, R.; Hashimoto, M.; Ogawa, N. *Mol. Immunol.* **1980**, *17*, 377–381.
(9) Desbuquois, B.; Aurbach, G. *J. Clin. Endocrinol.* **1971**, *33*, 732–738.
(10) Matsuoka, K.; Maea, M.; Tsuji, A. *Chem. Pharm. Bull.* **1979**, *27*, 2345–2350.
(11) Kato, K.; Umeda, Y.; Suzuki, F.; Hayashi, D.; Kosaka, K. *Clin. Chem. (Winston-Salem, N.C.)* **1979**, *25*, 1306–1308.
(12) Albert, W. H. W.; Kleinhammer, G.; Linke, R.; Staehler, F. "Enzyme Labelled Immunoassay of Hormones and Drugs;" Pal, S. B., Ed.; de Gruyter: New York, 1978; pp 327–339.
(13) Yoshioka, M.; Tanaguchi, H.; Kawaguchi, A.; Kobayashi, T.; Murakami, K.; Seki, M.; Tsutou, A.; Tamagawa, M.; Minoda, H.; Baba, S. *Clin Chem. (Winston-Salem, N.C.)* **1979**, *25*, 35–38.

RECEIVED for review March 27, 1981. Accepted May 26, 1981. This work was supported by the National Cancer Institute of the National Institutes of Health under Grant NIH 5 R01 CA23156-04.

Inductively Coupled Plasma–BASIC Programmable Computer-Controlled Double Monochromator for Sequential Multielement Analysis

James P. McCarthy, Michael E. Jackson, Thomas H. Ridgway, and Joseph A. Caruso*

Department of Chemistry, University of Cincinnati, Cincinnati, Ohio 45221

An instrument is presented for the sequential determination of trace element constituents. An inductively coupled plasma source (ICP) is interfaced to a computer-controlled monochromator and is directly programmable in BASIC. The interface is simple and inexpensive to construct and utilizes a stepper motor controller chip (slave microprocessor). The reproducibility and linearity of response of the system are characterized. Accuracy and overall system performance are demonstrated for the analysis of EPA water quality control references and drinking water samples for the determination of eight elements.

The concurrent determination of both major and trace constituents in numerous applications creates the need for an analytical system capable of determinations over extended concentration ranges. The inductively coupled plasma has become increasingly popular in many diverse applications (*1–5, 7–9*). Major constituent analysis is necessary with soils (*1*) and alloys (*2*), while trace analysis is needed with food (*3*), environmental (*4*), and biological samples (*5*), as the toxicity or nutritional value of many elements is at the part-per-billion level (*6*).

Multielement detection instruments are widely utilized in ICP analysis. While the ICP polychromator system is typically capable of the analysis of 20–30 elements in 2–3 min, it is expensive and wavelength selection is inflexible, as the analytical wavelengths are fixed upon initial system alignment and are not conveniently modified by the user. Several commercially available polychromator systems employ auxiliary monochromators to add versatility in wavelength selection of at least one channel. The major advantage of these polychromator systems is that they provide simultaneous analysis and high sample throughput.

Recently, sequential slew scanning monochromator systems that provide rapid wavelength change between analytical lines and acquire data only at preselected wavelengths have become available with computer controlled/stepper motor operated gratings. Several commercial ICP sequential slew scanning spectrometer systems (ICP-SSS) are available with programmable monochromators (*11–16*). Floyd et al. (*11*) discuss ICP-SSS and suggest development criteria for a sequential system. Many of these design features, including a double monochromator for high stray light rejection, have been incorporated in the system described here.

Drawbacks of many of the sequential systems (*11–16*) and indeed of any computer-controlled hardware, include the

0003-2700/81/0353-1512$01.25/0 © 1981 American Chemical Society

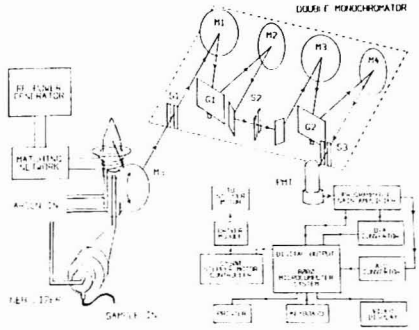


Figure 1. Block diagram of the ICP-SSS system described. Stepper motor positions gratings G1 and G2 by means of a sine drive mechanism. M5 is a rotatable first surface concave mirror; mirrors M1 and M3 are collimating optics, and M2 and M4 are focusing mirrors.

Table I. Operating Parameters

parameter	SSS	parameter	SSS
incident power	1000 W	obs ht	17 mm
reflected power	5 W	integration time	12 s
solution uptake	1.1 mL/min	load coil	3 turn
cooling Ar flow	13 L/min	nebulizer	fixed cross flow
carrier gas flow	1 L/min	photomultiplier	RCA-4837

construction of complex interfaces and/or the use of machine language or compiler-based language programming to achieve execution speed. Hardware and software modifications of these systems are difficult, limiting the versatility of instrument application. The ICP-SSS system described here is operated with a stepper-motor controller circuit directly programmable from BASIC. Parameters governing the operation of the stepper motor controlling the grating movement, such as acceleration/deceleration rate, slew speed, and step advance, are entered into the controller directly with BASIC commands. Description and characterization of this ICP–computer-controlled double monochromator are presented. Results of analyses of EPA water quality control reference standards and drinking water also are presented.

EXPERIMENTAL SECTION

Instrumentation and Hardware. A block diagram of the BASIC programmable system is depicted in Figure 1. The radio frequency generator, matching network, and torch enclosure are commercially available (Plasma-Therm Model HFP-2500D, Kresson, NJ). A conical spray chamber with fixed cross flow nebulizer was employed, and the load coil was 3 turns of $^1/_8$ in. copper tubing. Operating conditions of the plasma were adjusted to provide a satisfactory compromise of detection limits for the elements analyzed and are presented in Table I. The external optics used consist of a 3 in. diameter 8.2 cm focal length concave front surface mirror mounted on a rotatable mount similar to that described by Savage and Hieftje (*17*). Change of only the vertical observation height in the plasma is possible.

The spectrometer utilized was a 0.85-m Spex Model 1402 double monochromator equipped with an eight-phase stepper motor and wiring harness (Spex Industries, Metuchen, NJ). Gratings were blazed at 300 nm and ruled at 1200 grooves/mm. The gratings are mounted on a stepper motor controlled sine drive mechanism with a stepping resolution of 0.002 nm/step. The double monochromator configuration is as shown in Figure 1. Adjustable exit and entrance slits were each set at 30 μm, and the intermediate slit was set at 250 μm to preserve throughput yet allow sufficient stray light rejection. The full width half-maximum obtained was 0.03 nm. The spectrometer was used at $f/7.4$ to obtain necessary resolution at the expense of some throughput.

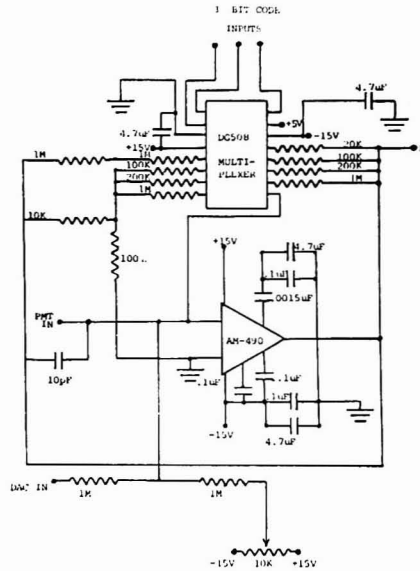


Figure 2. Eight gain programmable amplifier. Multiplexer allows any of eight resistances to be placed in the feedback loop (AM-490, DATEL Systems, Inc., Canton, MA; DG508, Siliconix, Santa Clara, CA).

The microcomputer system utilized is a variant of an 8080 system originally constructed by Woodward and subsequently implemented by Ridgway (*18*). Sixty-four K-bytes of memory provide sufficient storage for the data of 50 peaks. Hardcopy of data and other printouts was obtained on an Axiom Model EX-801 microprinter (Glendale, CA).

Photomultiplier current to voltage conversion was provided by a laboratory constructed 8 gain programmable amplifier. The circuit diagram of this amplifier is shown in Figure 2. An external offset voltage to null high background continuum signal also is provided. Signal averaging of the ADC values for summing and averaging of points at a rate of 115 μs/point and application of a Savitzky–Golay (*19*) filter for data presented on video display were programmed in assembly language. A 9-point filter is employed as noise components are significantly reduced with a minimal distortion of signal. Both of these subroutines are accessible from BASIC, and parameters may be entered into and results obtained from them in BASIC.

The Cybernetics CY500 BASIC programmable stepper motor controller integrated circuit (Cybernetics Micro Systems, Los Altos, CA) is directly programmable using BASIC. The ASCII equivalent of various characters which serve as commands are presented to the CY500. This integrated circuit can be programmed to output the appropriate number of pulses with ramped acceleration to and deceleration from a preselected rate. (Details of interfacing may be obtained from the authors or manufacturer's literature.) As the CY500 is virtually a microprocessor, once programmed, it operates independently of the host microcomputer and allows numerical calculations and display of data concurrent with spectrometer slewing between wavelengths.

The stepper pulses output from the controller chip drive an eight-phase stepper motor driver card (Airpax, Division of North American Phillips Corp.) which provides the proper applications of voltage to each of the motor phases. The maximum slew rate obtainable is 28 Å/s, the limiting factor being the exponential shape of the acceleration ramp of the stepper motor controller. This rate could be increased by hardware modification; however, the rate obtained was satisfactory.

Sample Preparation. Multielement standards were prepared by appropriate dilution of 1000 ppm stock solutions (Spex Industries, Metuchen, NJ) and acidified to 2% HNO_3 with redistilled HNO_3 (G. F. Smith Co., Columbus, OH). The concentrations of all analytes in a given standard were equivalent. The EPA Quality Control Reference for Water Quality Testing was diluted per instructions and acidified to 2% HNO_3 also. Drinking water samples were acidified to 2% HNO_3 and aspirated directly.

SOFTWARE DESCRIPTION

The controlling software can be divided into four subdivisions: (1) initialization and wavelength calibration, (2) determination of background and/or blank signal and detection limits, (3) determination of calibration curves for each element, (4) determination of the desired elements. Any of the desired subroutines are called by depressing the appropriate key on the keyboard.

Initialization and Wavelength Calibration. Upon initiating the operating program, the user enters the wavelength counter reading of the spectrometer and the number of analytical wavelengths to be analyzed. The wavelengths and corresponding elements are then entered and subsequently arranged in decreasing order in software. One of a series of potential argon reference lines is selected that is nearest to and of greater wavelength than the analytical line of highest wavelength. This is to provide time efficiency when the argon reference wavelength is located during analysis. A solution containing all of the elements of interest at a concentration of approximately 4 μg/mL is nebulized into the plasma and the wavelength calibration procedure initiated. The spectrometer slews to 10 nm higher than the argon reference and approaches it from the high wavelength side. Deceleration before reaching any wavelength is automatically provided by the controller chip. One-hundred-fifty data points are taken in a 0.3 nm region around the argon reference. The peak maximum wavelength is determined as the wavelength halfway between two points of 60% intensity on the high and low wavelength sides of the peak. As with the reference line, 0.3 nm of data are taken about the analytical line. A Savitzky–Golay smooth is applied, and wavelength of maximum intensity is determined. The data are displayed on a video screen for operator inspection. Selection of background correction wavelengths is accomplished by means of a movable cursor. While the operator works with the video display, the spectrometer slews to the next analytical line where the procedure is repeated until all of the chosen wavelengths have been located.

Analysis. The first stage of the subroutine for sample analysis is the initialization on an argon reference line. Only a 0.1-nm scan over the argon wavelength is required as the instrument is now calibrated in wavelength. At each analytical line, as the sample is nebulized, the spectrometer slews to the high wavelength background point and the computer produces an offset voltage from the digital to analog converter to null any continuum signal. Data are taken at this point for $^1/_{12}$th of the preselected integration time. Ten data points are taken across a peak at 0.04 Å separation (2 motor steps). Data are collected at each point for $^1/_{12}$th of the total integration time. The low wavelength background point is then measured. Background correction is implemented by subtracting the average of the two background values from each of the values across the peak. If the maximum value of these 10 points minus the blank signal is greater than 10 times the detection limit (determination of the detection limit and blank signal are described in a subsequent section), a Gaussian fit is applied to the eight of the ten points which lie over the peak maximum. The maximum of the Gaussian is the reported intensity. From our experiments utilizing parabolic, Lorentzian, and Gaussian fits, it has been shown that the parabolic and Gaussian functions for obtaining peak maxima provide greater

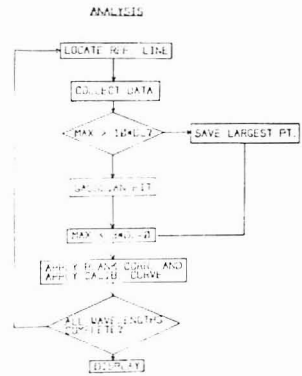


Figure 3. Flow chart for sample analysis routine.

Table II. Calibration and Scan Reproducibility (10 runs)

elem and line (nm)	error range, nm	std dev, nm
Cu 324.754	−0.004 to + 0.004	0.003
Al 308.215	0.001 to + 0.001	0.002
Mg 285.213	0.003 to + 0.004	0.002
Mo 281.615	−0.001 to + 0.003	0.001
Mg 279.553	−0.001 to + 0.003	0.001
Fe 259.940	0.002 to + 0.004	0.001
Mn 257.610	0.003 to + 0.005	0.001
Al 236.705	−0.004 to + 0.004	0.002
Cd 228.802	−0.004 to + 0.002	0.001
Zn 213.856	−0.003 to + 0.005	0.002

reproducibility than the Lorentzian fit or simply using the maximum value obtained from the raw data. This agrees with the findings of Kawaguchi et al. (*20*) and Floyd et al. (*11*) who also have utilized this approach. If the maximum value is less than 10 times the detection limit, then the maximum raw data value is used. A maximum intensity of less than three times the detection limit results in a reported value of zero for the signal. The resultant intensity is converted to concentration by means of calibration curves which have been previously determined in another subroutine. Display of data on the video screen and hardcopy are obtained while the spectrometer returns to the initialization wavelength. A flow chart for this routine is shown in Figure 3.

Blank Signal and Detection Limits. A subroutine is provided to determine any signal produced from a reagent blank and the detection limit of the signal. The reagent blank signal is determined by the procedure in the preceding section and is stored as a separate variable to be subtracted from the analyte signal providing blank correction. During the acquisition of the blank signal, the fifth point in the peak profile is measured for a number of times determined by the operator. Assuming no loss of steps from the motor, the fifth point should be at the analytical wavelength. Twice the standard deviation of these measurements at the fifth point is taken as the detection limit of the signal.

Characterization of Performance. The ability to reproduce signals and obtain preselected wavelengths accurately is critical. The precision of the stepper motor drive and calibration routine was characterized initially. A solution containing eight elements was aspirated into the plasma, and the spectrometer was calibrated for wavelength at ten analytical lines. Ten replicate calibrations were carried out and error ranges and standard deviations from the average instrumental wavelengths were obtained. The results are re-

Table III. HCl Reproducibility

wavelength, nm	RSD, %	wavelength, nm	RSD, %
Sn 286.333	0.58	Sn 242.949	0.53
Sn 283.999	0.52	Sn 235.484	1.47
Sn 270.651	0.54		

Table IV. ICP Reproducibility (10 runs)

Ar wavelengths, nm	% RSD (intensity)	Ar wavelengths, nm	% RSD (intensity)
416.418	0.64	360.652	0.46
383.468	1.09	346.108	0.98

Table V. EPA Quality Control Sample (mg/L in 2% HNO_3)

element	wavelength, nm	ICP-SSS	ref value
Cu	324.754	0.389 ± 0.08	0.374
Al	308.215	0.81 ± 0.04	0.852
Mo	281.615		
Mg	279.553		
Fe	259.940	0.79 ± 0.01	0.796
Mn	257.610	0.48 ± 0.02	0.478
Al	236.705	0.86 ± 0.05	0.852
Cd	228.802	0.052 ± 0.001	0.059
Zn	213.856	0.485 ± 0.008	0.478

ported in Table II. In the worst case observed, the instrumental wavelength for Mn at the 257.610-nm line varied from 0.003 nm on the low wavelength side of the line to 0.005 nm on the high wavelength side of the instrumental wavelength, a total error range corresponding to 4 motor steps. This error in scan reproducibility may be partially attributed to thermal drift as the instrument is not thermostated. As data are taken over 0.04 nm at the analytical wavelength, the precision of the instrument and calibration routine using the argon reference line location method is adequate. Potential error in wavelength location necessitates the 0.04-nm scan across the wavelength of interest to accurately determine intensity.

The performance of the monochromator and data acquisition instrumentation was evaluated for signal reproducibility. The ICP was replaced with a Sn hollow cathode lamp as the source and analysis carried out using the Sn emission lines. Since no argon was present to provide a reference wavelength, the 317.505-nm Sn wavelength was used. The results of ten replicate runs are reported in Table III. As can be seen from the data, reproducibility is excellent (0.5%) except for the 235.484-nm line, which may be attributed to its somewhat lower intensity.

Reproducibility of the plasma was studied. Four argon wavelengths were treated as analytical lines. The RSDs reported in Table IV are typically 1%. log plots of calibration data obtained with the ICP are shown in Figure 4. The slopes

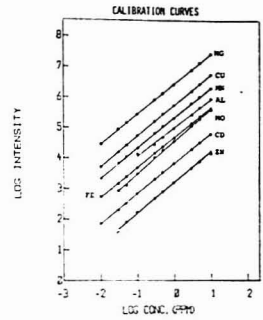


Figure 4. Multielement calibration curves for the elements determined.

of the calibration curves for the eight elements, excepting Mo and Al, are approximately unity with a maximum deviation of about 2%.

The accuracy of analysis was determined by comparison of results with certified reference values supplied with an EPA quality control water reference. Calibration solutions were acid matched to the 2% HNO_3 of the EPA sample. The results are shown in Table V. Correlation with the certified values is good. However, the relative standard deviation of the triplicates is higher than expected. This lower precision was due undoubtedly to the sample introduction system, since the nebulizer and spray chamber employed were not well characterized. In fact, the nebulizer obtained with the plasma source led to such high RSDs, it had to be replaced with the fixed cross-flow nebulizer. Determination of the nine wavelengths studied here were finished in slightly less than 7 min.

The same elements were determined in drinking water samples obtained from the EPA. The results of these analyses are reported in Table VI. The results are compared to values obtained at the EPA using atomic absorption analysis. Some deviation from the atomic absorption values is observed, especially for Fe data. The EPA analyses were performed some months prior to those by the ICP method and some leaching into the vessel walls may have occurred. RSDs are on the order of those obtained on the water quality reference as would be expected.

The detection limits shown in Table VII are at the part-per-billion level as would be expected. It is likely that improvements on these values could be obtained with further work on the sample introduction system.

CONCLUSIONS

The ICP–sequential system described has proven to be a viable alternative for multielement trace analysis. An advantage is the use of a BASIC programmable interface from the microcomputer to the grating drive stepper motor. This interface, while simple and inexpensive, provides flexibility

Table VI. AA and ICP-Sequential Analysis of Drinking Water (mg/L)

	sample 05		sample 06		sample 07	
elem and line (nm)	AA	ICP-SSS	AA	ICP-SSS	AA	ICP-SSS
Cu 324.754	ND[a]	0.023 ± 0.001	ND[a]	0.049 ± 0.003	ND[a]	0.153 ± 0.002
Al 308.215	ND[a]	0.102 ± 0.007	ND[a]	0.35 ± 0.03	ND[a]	0.084 ± 0.009
Mg 279.553	1.08	1.09 ± 0.04	1.89	1.91 ± 0.04	1.08	1.16 ± 0.04
Fe 259.940	0.140	0.09 ± 0.01	5.011	5.3 ± 0.2	0.43	0.40 ± 0.01
Mn 257 610	<0.03	0.0042 ± 0.0009	<0.03	0.0414 ± 0.0005	<0.03	0.0047 ± 0.0006
Al 236.705	ND[a]	. . .[b]	ND[a]	0.46 ± 0.05	ND[a]	. . .[b]
Zn 213.856	0.04	0.07 ± 0.02	0.10	0.111 ± 0.004	0.04	0.053 ± 0.004

[a] ND, not determined. [b] . . ., below detection limit.

Table VII. Detection Limits (mg/L)

elem and line (nm)	detect limit	elem and line (nm)	detect limit
Cu 324.754	0.001	Mn 257.610	0.0008
Mo 281.615	0.006	Al 236.705	0.083
Mg 279.553	0.0002	Cd 228.802	0.003
Fe 259.940	0.004	Zn 213.856	0.009

for multielement analysis and simplifies instrument development. Although slewing time is increased relative to other systems of this type owing to the use of the BASIC programmable interface, overall analysis time of 7 min is satisfactory for the determination of approximately nine elements. The instrumentation and software developed have proven quite adequate for the trace analysis of drinking water. Applications to other sample types are complete and will be given in an upcoming report.

ACKNOWLEDGMENT

We acknowledge EPA for providing water quality control references and drinking water samples analyzed. We express our appreciation to Kevin Mulligan for his help in the preparation of this manuscript.

LITERATURE CITED

(1) Dahlquist, R. L.; Knoll, J. W. *Appl. Spectrosc.* **1978**, *32*, 1–29.
(2) Butler, C. C.; Kniseley, R. N.; Fassel, V. A. *Anal. Chem.* **1975**, *47*, 825–829.
(3) Ward, A. F.; Marciello, L. F. *Anal. Chem.* **1979**, *51*, 2264–2272.
(4) Wolnik, K. A.; Kuennen, R. W.; Fricke, F. L. In "Developments in Atomic Plasma Spectrochemical Analysis"; Barnes, R., Ed.; Heyden & Son: London, in press.
(5) McQuaker, N. R.; Kluckner, P. D.; Chang, G. N. *Anal. Chem.* **1979**, *51*, 888–895.
(6) Barnes, R. M.; Genna, J. S. *Anal. Chem.* **1979**, *51*, 1065–1070.
(7) Dulka, J. J.; Risby, T. H. *Anal. Chem.* **1976**, *48*, 640A–653A.
(8) Greenfield, S.; Jones, I. L.; Berry, C. T. *Analyst (London)* **1964**, *89*, 713–720.
(9) Wendt, R. H.; Fassel, V. A. *Anal. Chem.* **1965**, *37*, 920–922.
(10) Abercrombie, F. N.; Silvester, M. D.; Cruz, R. B. In "Ultratrace Analysis in Biological Sciences and Environment"; Risby, T. H., Ed. American Chemical Society: Washington, DC, 1979; Chapter 2.
(11) Floyd, M. A.; Fassel, V. A.; Winge, R. K.; Katzenberger, J. M.; D'Silva, A. P. *Anal. Chem.* **1980**, *50*, 431–438.
(12) Kawaguchi, H.; Masushi, O.; Ito, T.; Mizuike, A. O. *Anal. Chim. Acta* **1977**, *95*, 145–152.
(13) Johnson, D. J.; Plankey, F. W.; Winefordner, J. D. *Anal. Chem.* **1975**, *47*, 1739–1743.
(14) Spillman, R. W.; Malmstadt, H. V. *Anal. Chem.* **1976**, *48*, 303–311.
(15) Bournans, P. W. J. M.; Van Gool, G. H.; Jansen, J. A. J. *Analyst (London)* **1976**, *101*, 585–587.
(16) Ediger, R. D.; Wilson, D. L. *At. Abs. Newsl.* **1979**, *18*, 41–45.
(17) Savage, R. N.; Hieftje, G. M. *Anal. Chem.* **1979**, *51*, 408.
(18) Woodward, W. S.; Reilley, C. N. *Pure Appl. Chem.* **1978**, *50*, 785.
(19) Savitzky, A.; Golay, M. J. E. *Anal. Chem.* **1964**, *36*, 1627–1639.
(20) Kawaguchi, H.; Ito, T.; Ito, A.; Mizuike, A. *Anal. Chim. Acta* **1980**, *122*, 75–79.

RECEIVED for review January 7, 1981. Accepted May 18, 1981. We wish to acknowledge the National Institute of Occupational Safety and Health without whose support through Grant R01-OH-00739 this project would not have been possible.

Two-Phase Mixed Indicator Titration Method for the Determination of Anionic Surfactants

Zhi-ping Li[1] and Milton J. Rosen*

Department of Chemistry, Brooklyn College, City University of New York, Brooklyn, New York 11210

The two-phase, mixed indicator titration method for anionic surfactants has been reexamined. The method is not quantitative for surfactants with alkyl chains containing less than 12 carbon atoms but may be extended to them by using 2:3 (v/v) chloroform:1-nitropropane as the organic phase and a multiple extraction–titration technique. A screening test is proposed for determining the suitability of the standard method for determining an anionic surfactant of unspecified chain length. Cl^- at concentrations in excess of 5×10^{-3} M in the aqueous phase interferes with both the standard and the extended methods. Na^+, Mg^{2+}, and SO_4^{2-} at concentrations of up to 4×10^{-1} M do not interfere with the determination of sodium dodecanesulfonate.

The two-phase mixed indicator titration method for the analysis of anionic surfactants, developed by Reid and coworkers (*1*, *2*) for the Commission Internationale d'Analyses of the Comité International des Dérivés Tensioactifs (70 Champs Elysees, Paris, France) is an excellent and well-established method. However, it has been apparent for some time now that the method is not quantitative for all anionic surfactants, particularly when the hydrophobic group is short. In an attempt to overcome this deficiency, the method was reexamined and its limitations explored.

A number of different types of surfactants, of approximately 99% purity, were analyzed by the method, under controlled conditions. In addition, the effect of the partitioning of the surfactant–indicator complex between aqueous and organic phases, the presence of various electrolytes, and the nature of the organic phase were explored. Finally, various modifications were made in the procedure to extend the range of application of the method.

EXPERIMENTAL SECTION

Materials. *Anionic Surfactants.* Sodium decanesulfonate (Anal. Found: C, 49.40; H, 8.71; S, 13.28. Calcd: C, 49.16; H, 8.66; S, 13.12), sodium dodecanesulfonate (Anal. Found: C, 52.99; H, 9.29; S, 11.74. Found: C, 52.92; H, 9.25; S, 11.77), and sodium tetradecanesulfonate (Anal. Found: C, 56.0; H, 9.76; S, 10.48. Calcd: C, 56.0; H, 9.67; S, 10.66) were purchased from Research Plus, Bayonne, NJ. *p*-$(C_8H_{13}OC_2H_4O)C_6H_4SO_3Na$ was synthesized in this laboratory (*3*) (Anal. Found: C, 51.14; H, 6.45; S, 10.19. Calcd.: C, 51.84; H, 6.53; S, 9.88). Aerosol AY (sodium diamyl sulfosuccinate), Aerosol MA (sodium dihexyl sulfonsuccinate), and Aerosol OT [sodium di(2-ethylhexyl) sulfosuccinate] were obtained from American Cyanamide Co. These materials were

[1] Visiting Scholar from Xinjiang Chemical Institute, Scientific Academy of the People's Republic of China.

0003-2700/81/0353-1516$01.25/0 © 1981 American Chemical Society

Table I. Assay[a] and Solubility[b] of Surfactants with Different Alkyl Groups

surfactant structure	assay, %	% of surfactant in $CHCl_3$ phase
$C_{16}H_{21}SO_3Na$	89.2	5.62
$C_6H_{13}OC_2H_4OC_6H_4SO_3Na$	89.8	6.18
$C_5H_{11}OOCCH_2CH(SO_3Na)COOC_5H_{11}$	95.9	16.43
$C_6H_{13}OOCCH_2CH(SO_3Na)COOC_6H_{13}$	96.8	17.61
$C_8H_{17}OOCCH_2CH(SO_3Na)COOC_8H_{17}$	98.2	*c*
$C_{12}H_{25}SO_3Na$	99.1	19.2
$C_{14}H_{29}SO_3Na$	99.0	*c*

[a] Procedure A; $CHCl_3$ organic phase; surfactant concentration $\approx 1 \times 10^{-3}$ M. [b] After the addition of 10 mL of acid mixed indicator solution. [c] Not determinable; stable emulsion formed.

all dried to constant weight in vacuo before use. The Aerosols are stated to have a purity of 99% or better.

Cationic Surfactant. Hyamine 1622 (Rohm and Haas Co.). The purity of this compound was first detemined by titration against sodium dodecyl sulfate (BDH Chemicals, Ltd.) whose assay had been determined by acid hydrolysis (*4*). On the basis of this, the molar absorptivity of the sample of Hyamine 1622 used throughout this investigation was determined to be 1266 at 269.5 nm and the concentrations of all subsequent Hyamine solutions were checked by ultraviolet absorbance.

Acid Mixed Indicator Solution. This was prepared from Dimidium bromide, Erioglaucine, and sulfuric acid in the usual fashion (*1*, *4*).

Analytical Method. *Procedure A:* To 10 mL of surfactant solution of (1–4) $\times 10^{-3}$ M concentration in a 250-mL, glass-stoppered, Erlenmeyer flask were added 10 mL of the acid mixed indicator solution and 15 mL of chloroform (or chloroform:1-nitropropane mixture). The mixture was titrated with a solution of Hyamine 1622 of concentration approximately that of the surfactant solution with vigorous shaking after each addition, until the pink color was just discharged from the chloroform layer.

Procedure B: The procedure was identical with that described in A, above, except that the containing vessel was a 150-mL separatory funnel. (Emulsions, which sometimes form, are readily broken by warming the mixture.) When the titration end point had been reached, the lower (chloroform or chloroform:1-nitropropane) layer was drained out through the stopcock at the bottom of the funnel and 15 mL of fresh chloroform was added. The mixture was vigorously shaken and then titrated with the Hyamine solution to a new end point. The lower layer was again removed. Titration and removal of the lower layer were repeated until no significant further addition of Hyamine solution was needed to reach the end point. The final assay of the surfactant was determined from the total volume of Hyamine added.

Partitioning of Surfactant between Aqueous and Organic Phases in the Presence of Acid Mixed Indicator. For determination of the percentage of surfactant that is soluble in the organic (chloroform or chloroform:1-nitropropane) phase, 10 mL of the surfactant solution, of approximately 1×10^{-3} M concentration, 10 mL of the acid mixed indicator solution, and 15 mL of the organic phase were shaken together vigorously in a 150-mL separatory funnel for 10 min. The mixture was allowed to stand in a constant temperature bath at 25 °C until the two separated phases were clear (2–3 h). The lower organic phase was drained into a 250-mL Erlenmeyer flask, 10 mL of acid mixed indicator solution was added to it, and the anionic surfactant content was determined by titration with approximately 1×10^{-3} Hyamine 1622 in the usual fashion.

RESULTS AND DISCUSSION

Results obtained by using the standard two-phase mixed indicator titration method (procedure A, with chloroform as the organic phase) are shown in Table I. The assay percentage is based upon an assumed 100% purity for the vacuum-dried surfactant. It is apparent that the standard procedure is not adequate for surfactants with alkyl chains containing less that 12 carbon atoms.

Table II. Effect of $CHCl_3$:1-Nitropropane Ratio and Surfactant Concentration on Sodium Decanesulfonate Assay (Procedure A)

$CHCl_3$/NP ratio (v/v)	surfactant concn, M	% of surfactant in organic phase[a]	assay, %
100% $CHCl_3$	1.017×10^{-3}	5.62	89.2
100% $CHCl_3$	2.035×10^{-3}		92.9
100% $CHCl_3$	4.109×10^{-3} [b]		93.7
4:1	1.013×10^{-3}		90.4
3:2	1.013×10^{-3}		90.9
1:1	1.013×10^{-3}		92.6
2:3	1.017×10^{-3}	15.45	93.9
2:3	2.035×10^{-3}		95.2
2:3	4.109×10^{-3}		95.4
1:4	1.013×10^{-3}		93.7

[a] After addition of 10 mL of acid mixed indicator solution. [b] 20 mL of surfactant solution used.

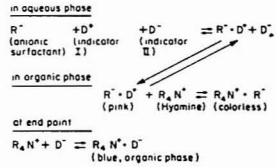


Figure 1. Equilibria involved in the two-phase, mixed indicator titration method for anionic surfactants.

The last column shows the percentage of the anionic surfactant present in the chloroform phase after the addition of the acid mixed indicator solution. It is noteworthy that, in the absence of acid indicator solution, almost all of the surfactants in Table I show no significant solubility in the $CHCl_3$ layer. There is an almost linear increase in the assay percentage with increase in the percentage of anionic surfactant soluble in the chloroform layer in the presence of acid mixed indicator solution. For the titration to be quantitative, it appears that about 19% of the surfactant must be in the chloroform phase prior to the addition of the Hyamine solution. The procedure for determining the percentage of surfactant soluble in the chloroform layer in the presence of acid mixed indicator can, therefore, be used as a screening test for determining the suitability of the two-phase mixed indicator titration for analyzing an anionic surfactant of unspecified chain length.

In view of these results, it was felt that the substitution of some of the chloroform by water-immiscible organic solvent of greater polarity might permit the extension of the method to surfactants of shorter chain length. Several solvents were tried and 1-nitropropane (NP) was chosen for further investigation. Table II shows some results obtained with different chloroform:nitropropane ratios, using sodium decanesulfonate. Since very low chloroform:nitropropane ratios tended to produce emulsions when shaken with the surfactant solution, the 2:3 chloroform:nitropropane ratio was used in subsequent work. Table II also shows the effect of change in the concentration of the surfactant solution. Similar experiments on sodium dodecane and tetradecanesulfonate showed no significant change in the assay with change in the concentration of the surfactant solution in the (1–4) $\times 10^{-3}$ M range when either $CHCl_3$ or 2:3 $CHCl_3$:NP was used as the organic phase.

The reactions which form the basis for this analytical method can be formulated as shown in Figure 1.

It is clear, from the results obtained, that the reason for the low assays in the case of the surfactants with short alkyl

Table III. Results Obtained by Procedure B (Surfactant Concentration ≈ 1×10^{-3} M)

surfactant structure	organic phase	assay, % 1st end point	2nd end point	3rd end point
$C_{10}H_{21}SO_3Na$	$CHCl_3$	89.2	93.8	
$C_{10}H_{21}SO_3Na$	$CHCl_3$	92.9	96.1	
$C_{10}H_{21}SO_3Na$[b]	$CHCl_3$	93.7	96.4	97.5
$C_{10}H_{21}SO_3Na$	2:3 $CHCl_3$:NP[c]	93.9	98.5	99.4
$C_{10}H_{21}SO_3Na$[a]	2:3 $CHCl_3$:NP[c]	95.2	99.4	99.4
$C_{10}H_{21}SO_3Na$[b]	2:3 $CHCl_3$:NP[c]	95.4	99.4	99.4
$C_6H_{13}OC_2H_4OC_2H_4SO_3Na$	2:3 $CHCl_3$:NP[c]	94.8	99.1	99.1
$C_6H_{11}OOCCH_2CH(SO_3Na)COOC_6H_{11}$	2:3 $CHCl_3$:NP[c]	97.8	99.2	99.2
$C_4H_{13}OOCCH_2CH(SO_3Na)COOC_4H_{13}$	2:3 $CHCl_3$:NP[c]	98.2	99.2	99.2
$C_4H_{17}OOCCH_2CH(SO_3Na)COOC_8H_{17}$	2:3 $CHCl_3$:NP[c]	99.5	99.5	
$C_{12}H_{25}SO_3Na$	2:3 $CHCl_3$:NP[c]	99.3	99.3	
$C_{14}H_{29}SO_3Na$	2:3 $CHCl_3$:NP[c]	99.2	99.2	

[a] Concentration of surfactant solution is approximately 2×10^{-3} M. [b] Concentration of surfactant solution is approximately 4×10^{-3} M. [c] 1-Nitropropane.

Table IV. Effect of Electrolyte on Assay of Sodium Dodecanesulfonate[a]

electrolyte	% at concn of electrolyte in aqueous phase (molar) 0	1×10^{-3}	5×10^{-3}	2×10^{-2}	5×10^{-2}	1×10^{-1}	2×10^{-1}	3×10^{-1}	4×10^{-1}
NaCl	99.1	99.1	99.1	99.3	99.4	99.6	100.4	101.1	101.9
Na_2SO_4	99.1	99.1	99.1	99.1	99.1	99.1	99.1	99.1	99.1
NaH_2PO_4	99.1	99.1	99.2	99.1	99.1	98.9	98.6	98.3	
$CaCl_2$	99.1	99.1	99.1	99.3	99.6	100.6	102.2	103.1	
$MgCl_2$	99.1	99.1	99.1	99.3	99.6	100.4	101.4	102.4	
$MgSO_4$	99.1	99.1	99.1	99.1	99.1	99.1	99.1	99.1	99.1

[a] Procedure A; $CHCl_3$ organic phase; surfactant concentration ≈ 1×10^{-3} M.

Table V. Effect of Electrolyte on Assay of Sodium Dodecanesulfonate[a]

electrolyte	% at concn of electrolyte in aqueous phase (molar) 0	1×10^{-3}	5×10^{-3}	2×10^{-2}	5×10^{-2}	1×10^{-2}	2×10^{-1}	3×10^{-1}	4×10^{-1}
NaCl	99.3	99.3	99.3	99.6	99.8	102.0	105.2	109.1	111.4
Na_2SO_4	99.3	99.3	99.3	99.3	99.0	99.3	99.3	99.3	99.3
NaH_2PO_4	99.3	99.3	99.4	99.2	99.2	98.8	98.5	98.2	
$CaCl_2$	99.3	99.5	100.0	100.9	102.6	105.3	110.6		
$MgCl_2$	99.3	99.3	99.5	100.6	102.4	105.3	111.0		
$MgSO_4$	99.3	99.1	99.1	99.1	99.1	99.1	99.1	99.1	99.1

[a] Procedure A; 2:3 $CHCl_3$:1-nitropropane organic phase; surfactant concentration ≈ 1×10^{-3} M.

chains is the low solubility of their comlex with indicator I in the organic phase. The anionic–indicator I complex remaining in the aqueous phase remains untitrated by the Hyamine 1622. (Measurements of the partition of Hyamine 1622 between the aqueous and organic phases used in these experiments in the presence of the acid mixed indicator in the absence of anionic surfactant showed that 85–95% of the Hyamine 1622 is in the organic phase.)

In order to titrate this remaining anionic surfactant, the initial titration with Hyamine was conducted in a separatory funnel (procedure B, Experimental Section), rather than in an Erlenmeyer flask and, when the end point of the titration had been reached, the organic (lower) phase was withdrawn and replaced by fresh organic phase. After being shaken vigorously, the mixture showed a pink color in the organic phase indicating that additional anionic surfactant–indicator I complex had been extracted from the aqueous phase into the organic phase. The titration with Hyamine 1622 was continued to a second end point. This extraction–titration procedure was repeated until no significant additional quantity of Hyamine was required to reach an end point. Table III shows some results obtained by use of this procedure. From the data, it appears that procedure B with a 2:3 (v/v) mixture of chloroform:1-nitropropane as the organic phase is suitable for analyzing all of the surfactants tested. Only two titrations are required to analyze most of the surfactants at a concentration of 1×10^{-3} M; in the case of sodium decanesulfonate, two titrations are required for concentrations of 2×10^{-3} M or higher, three for concentrations of 1×10^{-3} M.

The last factor investigated was the effect of electrolyte on the end point of the titration, both with chloroform as the organic phase and with 2:3 chloroform:1-nitropropane mixture. For these experiments, sodium dodecanesulfonate, which gives satisfactory and comparable results with both these organic phases, was used. Results are given in Tables IV and V.

The data indicate that Cl^- is the only ion tested that has an effect on the titration result, both in $CHCl_3$ and in $CHCl_3$–NP. (The effect of $H_2PO_4^-$ at high concentrations is most probably due to its effect on the pH of the aqueous phase.) Cl^- at concentrations in excess of 5×10^{-3} M in the aqueous phase causes overtitration when either chloroform or 2:3 chloroform:1-nitropropane is used as the organic phase. Na^+, Mg^{2+}, and SO_4^{2-} at concentrations of up to 4×10^{-1} M in the aqueous phase do not interfere with the analysis of sodium dodecanesulfonate. The Cl^- effect is probably due to its depression of the ionization of Hyamine 1622 which is a quaternary aminium chloride, thereby making the quaternary aminium ion less available for reaction with the anionic surfactant–indicator I complex. This common-ion effect of Cl^- has been noted previously by Longman (5) when methy-

lene blue is used as the indicator in the two-phase titration of anionic with quaternary aminium chloride but is in contradiction to his statement that this effect of Cl^- is not observed with other indicators.

LITERATURE CITED

(1) Reid, V. W.; Alston, T.; Heinerth, E. *Tenside* **1967**, *4*, 292–304.
(2) Reid, V. W.; Alston, T.; Heinerth, E. *Tenside* **1968**, *5*, 90–96.
(3) Chiang, Y. C. Master's Thesis, Brooklyn College, City University of New York, Brooklyn, NY, July, 1978.
(4) Rosen, M.; Goldsmith, H. A. "Systematic Analysis of Surface-Active Agents", 2nd ed.; Wiley-Interscience: New York, 1972; pp 427–428.
(5) Longman, G. F. "The Analysis of Detergents and Detergent Products"; Wiley-Interscience: New York, 1975; p 227.

RECEIVED for review March 9, 1981. Accepted May 18, 1981.

Atmospheric Pressure Active Nitrogen Afterglow as a Detector for Gas Chromatography

G. W. Rice, J. J. Richard, A. P. D'Silva, and V. A. Fassel*

Ames Laboratory[1] and Department of Chemistry, Iowa State University, Ames, Iowa 50011

An atmospheric pressure active nitrogen (APAN) afterglow has been evaluated as a selective detector for gas chromatography (GC). Selective detection for organo Hg, Pb, and Sn species at trace levels has been achieved. The GC-APAN system has also been observed to be a nonselective detector for organic molecules at nanogram levels through the detection of CN ($B^2\Sigma^+$) emission at 388.3 nm. The merits of the APAN detector in comparison to other emission-selective detectors is discussed.

Gas chromatography coupled with element-selective detectors is widely utilized in speciation studies of environmental pollutants, a subject of substantial current interest. In such studies an extended list of detection systems have been investigated to enhance the limits of detection.

A class of such detectors is the microwave-induced plasma (MIP) operated at low or atmospheric pressure with He or Ar as the plasma gas (*1–4*). Of the MIP detectors, the atmospheric pressure MIP in He, operated in a Beenakker type TM_{010} cylindrical resonant cavity is potentially the most versatile element-selective detector (*5*). Unfortunately, the MIP detectors have several operational limitations. The injection of relatively small amounts (microliters) of species into the plasma gas, such as a solvent plug from a GC or excessive hydrogen from dissociated hydrocarbons, can decouple the resonant cavity, resulting in total quenching of the discharge. Such a limitation has been circumvented by adopting one or more experimental manipulations. They are: (a) initiation of the discharge after the solvent peak elutes out of the resonant cavity, (b) selection of a solvent that elutes at the tail of the sample elution sequence, (c) utilization of elaborate gas switching instrumentation and routines to control the flow of GC effluents into the MIP, or (d) the use of fused silica capillary columns for reduced sample volumes. A limitation of MIP sources operated at reduced pressure is the buildup of carbonaceous deposits on the walls of the discharge with effluents containing carbon. Such deposits have to be periodically burnt off in situ, by operating the discharge in a mixture of He with O_2 or N_2 (*3*). To minimize the above limitations, alternate element-specific detectors such as the direct current atmospheric pressure argon plasma (*6, 7*) and inductively coupled plasma (*8, 9*) have also been evaluated.

A chemiluminescence detector, based on the reaction of organic compounds with active nitrogen (AN) sustained at low pressure (20–30 torr) to form excited CN ($B^2\Sigma^+$) molecules, has been recently reported (*10, 11*). The low-pressure AN source, however, is susceptible to a build up of polymeric deposits containing CN and thus requires periodic cleaning similar in nature to the MIP. The addition of HCl gas is also required to enhance the sensitivity for simple saturated hydrocarbon compounds. Finally, the fact that the "chemiluminescent" detector operates at low pressure whereas the GC operates at atmospheric pressure may also introduce some inconvenience in sample introduction.

The reactions of a variety of organic and organometallic compounds with metastable atoms and molecules of nitrogen present in low-pressure active nitrogen sources have been extensively investivated over several decades (*12*). In such reactions, the fragmentation and excitation of species, which lead to characteristic atomic and/or molecular emission, has been predicted to be the result of energy transfer from metastable atomic and molecular nitrogen present in the discharge source.

In a recent communication we described the operation and performance of an atmospheric pressure active nitrogen (APAN) afterglow as an efficient source for the excitation of atomic emission (*13*). In the present paper we report on the performance of the APAN afterglow as an element-selective GC detector.

EXPERIMENTAL PROCEDURES

Apparatus. The electrodeless ozonizer type discharge tube utilized in these investigations was slightly modified from the design previously described (*13*). The outer tube diameter was reduced from 28 mm to 18 mm and cooling of the inner tube eliminated. A 2 mm i.d. sample inlet was used for connection to the GC interface.

A conventional GC (Hewlett-Packard, Model 5700A) was modified by cutting a 3 cm diameter hole through the side of the oven wall to accommodate the transfer line from the GC column to the APAN discharge tube. The interface constructed for the transfer line is shown in Figure 1. The glass capillary transfer line minimized peak broadening from dead volume between the GC column and the discharge tube. Copper tubing wrapped with nichrome wire was used to produce uniform heating around the transfer line. A variable temperature control (Omega Engineering,

[1]Operated for the U.S. Department of Energy by Iowa State University under Contract No. W-7405-Eng-82. This research was supported by the Division of Chemical Sciences, Budget Code KC-03-02-03, Office of Energy Research.

0003-2700/81/0353-1519$01.25/0 © 1981 American Chemical Society

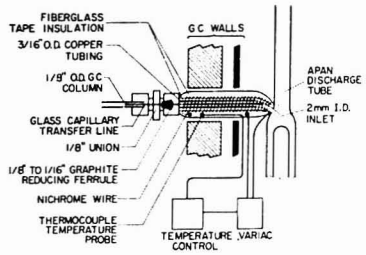


Figure 1. Schematic diagram of the interface between the GC and the APAN afterglow tube.

Table I. Operating Conditions of the GC-APAN System

(A) APAN Discharge	
N_2 flow rate	30 L/min (obtained from boiloff of 200 L liquid N_2 tank)
voltage	20 kV (Model EGV 20-6 transformer, Del Electronics, Inc., Mount Vernon, NY)
frequency	1800 Hz (Invertron 500 VA ac power supply, Aiken Industries, San Diego, CA)
input power to discharge	~400 W
(B) Spectrometric System	
monochromator	H20 UV/VIS (Instruments SA, Inc., Metuchen, NJ)
band-pass (fwhm)	2 nm
photomultiplier	Type R955 (Hamamatsu Corp., Middlesex, NJ)
PMT voltage	800 V
amplifier	Model 110 (Pacific Precision Instruments, Concord, CA)
recorder	Superscribe Series 4910 (Houston Instruments, Austin, TX)
(C) Analytical Wavelengths	
organolead compds	368.3 nm (Pb I)
organotin compds	326.2 nm (Sn I)
organomercury compds	253.7 nm (Hg I)
organic compds	388.3 nm (CN; $B^2\Sigma^+ \rightarrow X^2\Sigma^+$)
(D) GC System	
GC:	Model 5700 A (Hewlett-Packard, Avondale, PA)
carrier gas/ flow rate	N_2 at 80 mL/min
interface temp	230 °C
sample volumes	2.0 μL
(E) GC Columns	
organometallic compds	4% SE-30/6% SP2401 on 100/120 Supelcoport (Supelco, Inc., Bellefonte, PA) packed in 4 ft × 1/8 in. o.d. glass column
organic compds	5% SE-30 and 3% OV-17 on 100/120 Supelcoport (Supelco, Inc.) for hydrocarbon and aromatic compounds, respectively. Packed in 6 ft × 1/8 in. o.d. stainless steel columns

Inc., Stamford, CT) was used to maintain the desired interface temperature.

Details of the operational characteristics of the APAN discharge, spectrometric system used, analytical wavelengths observed, and GC parameters and columns chosen for the present investigations are summarized in Table I.

Organometallic and Organic Reference Samples. Stock solutions were prepared in anhydrous diethyl ether for the organic Hg, Pb, and Sn compounds (Alfa Products, Danvers, MA) at a concentration of 1.0 mg/mL. Serial dilutions were also prepared containing from 100 to 0.01 μg/mL. Hydrocarbon and aromatic

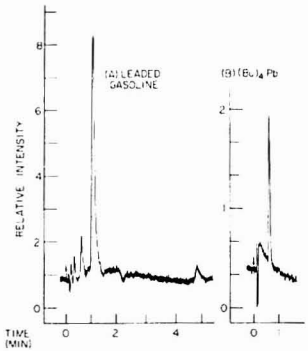


Figure 2. Chromatograms obtained from (a) leaded gasoline (temperature program: initial 40 °C, rate 8 °C/min; final 80 °C with 2 min hold) and (b) 20 ng of tetrabutyllead (isothermal at 175 °C).

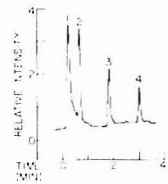


Figure 3. Chromatogram obtained from tetraalkyltin compounds: (1) solvent, (2) $(C_2H_5)_4Sn$, (3) $(C_3H_7)_4Sn$, and (4) $(C_4H_9)_4Sn$ (temperature program: initial 70 °C, rate 32 °C/min; final 170 °C). Each tin compound was present at a 10-ng level.

mixtures were prepared in pentane by the same manner from selected GC reference compounds (Chem Service, Inc., West Chester, PA).

RESULTS AND DISCUSSION

Organometallic Compounds. The specificity of the GC-APAN system for the detection of organometallic compounds is best exemplified by the chromatogram shown in Figure 2 obtained from a neat 2-μL injection of leaded gasoline.

The Pb-specific chromatogram was obtained by monitoring the Pb I emission at 368.3 nm. The species detected were attributed to a mixture of methyl- and ethyllead alkyl compounds normally present in leaded gasoline. No interferences from coeluting hydrocarbon compounds in the gasoline were observed. The relative sensitivity for organolead compounds can be approximated by the signal that was obtained from a reference sample containing 20 ng of tetrabutyllead, which is also shown in Figure 2.

A chromatogram of several tetraalkyltin compounds, obtained by monitoring Sn I emission at 326.2 nm, is shown in Figure 3. The signal from the diethyl ether solvent was due to stray light from CN emission. The signal from the solvent, considering that a 2-μL injection would contain 1.4 mg of diethyl ether, is negligible when compared to the signals obtained from the organotin compounds which were present at a 10-ng level.

A chromatogram for several diorganomercury compounds, obtained by monitoring Hg I emission at 253.7 nm, is shown in Figure 4. Each compound was present at a 2–5-ng level. The excellent resolution obtained with the GC-APAN system for the mercury compounds is exemplified by the near total separation of the di-*n*-propyl- and diisopropylmercury isomers.

Hydrocarbon and Aromatic Compounds. The production and excitation of the characteristic chemiluminescence

Table II. Limits of Detection, Linear Dynamic Ranges, and Selectivities Obtained for Various Organometallic and Organic Compounds by GC-APAN

species	compound	analytical wavelength, nm	limit of detection, ng	dynamic linear range	selectivity
Pb	tetrabutyllead	368.3	3	1×10^3	100
Sn	tetraethyltin	326.2	2	1×10^3	>1000
Hg	dimethylmercury	253.7	0.002	5×10^4	>10000
hydrocarbons	hexadecane	388.3	0.8	1×10^2	
aromatics	naphthalene	388.3	0.2	5×10^2	

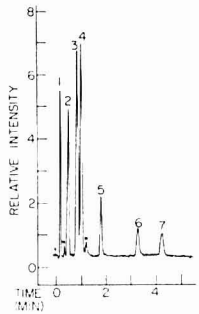


Figure 4. Chromatograms obtained from dioganomercury compounds: (1) $(CH_3)_2Hg$, (2) $(C_2H_5)_2Hg$, (3) $(i\text{-}C_3H_7)_2Hg$, (4) $(C_3H_7)_2Hg$, (5) $(C_4H_9)_2Hg$, (6) $(C_6H_{13})_2Hg$, (7) $(C_8H_{13})_2Hg$, and (*) impurities (temperature program: initial 50 °C, rate 32 °C/min; final 200 °C). Each mercury compound was present at a 2–5-ng level.

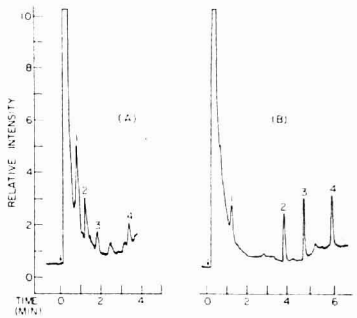


Figure 5. Chromatograms obtained from (a) hydrocarbon mixture in pentane containing (1) octane, (2) decane, (3) dodecane, and (4) hexadecane (temperature program: initial 50 °C, rate 32 °C/min; final 200 °C with 2 min hold) and (b) aromatic mixture in pentane containing (1) toluene, (2) napthalene, (3) biphenyl, and (4) *trans*-stilbene (temperature program: initial 80 °C with 2 min hold, rate 32 °C/min, final 190 °C with 2 min hold). Each compound present at a 10-ng level.

emission of CN ($B^2\Sigma^+ \rightarrow X^2\Sigma^+$) when hydrocarbon compounds are introduced into low-pressure active nitrogen sources is well documented (*12*). To the best of our knowledge, the observation of CN emission in an APAN afterglow has not been reported in prior investigations on active nitrogen.

The chromatograms obtained from a selected mixture of saturated hydrocarbon compounds and of aromatic compounds using the APAN detector are shown in Figure 5. Emission was monitored from the CN ($B^2\Sigma^+ \rightarrow X^2\Sigma^+$) $0 \rightarrow 0$ transition at 388.3 nm. Each compound was present at a 10-ng level. Irregularities in the base line were found to be the result of solvent impurities or column bleed at high GC oven temperatures.

The normally green APAN afterglow, caused by the emission from metastable atomic oxygen ($^1S \rightarrow {}^1D$), can visually be observed to transform into a long-lived and intense violet-blue emission from the formation of excited CN ($B^2\Sigma^+$) species. This transformation can be readily observed for organic effluents from the GC in quantities as low as 100 ng.

Analytical Potentials. The current limits of detection, linear dynamic ranges, and selectivity ratios for the various organometallic and organic compounds observed in the GC-APAN system are given in Table II. The limits of detection were obtained from peak heights that gave a signal to background scatter of three. The representative compound on which the limits of detection are based is also given. These limits will vary by factors dependent on the chromatographic conditions used and the mole fraction of the metal present in the organometallic compounds.

It is not surprising that the limits of detection for aromatic compounds are, in general, significantly better than those obtained for the saturated hydrocarbons. Kinetic studies have in the past revealed that unsaturated organic molecules (i.e., alkenes, aromatics) tend to form CN molecules at a much faster rate than saturated hydrocarbon compounds (*14*). Thus a more rapid reaction will undoubtedly be observed more

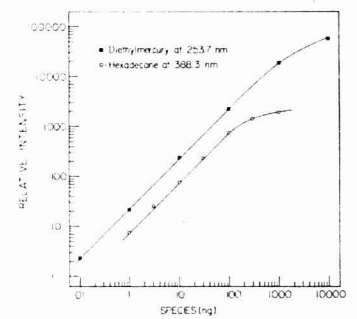


Figure 6. Analytical calibration curves obtained from diethylmercury and hexadecane.

readily for the short reaction time available in the APAN afterglow region due to the high flow rates utilized.

Typical analytical calibration curves obtained for organometallic and organic compounds are shown in Figure 6. The calibration curves for the organometallic compounds, when monitored at an emission wavelength specific for the metal, are generally linear over 3 to 4 orders of magnitude in concentration, as shown for diethylmercury. Calibration curves for organic compounds were observed to be linear over 2 orders of magnitude in absolute amounts up to a maximum of approximately 100 ng, after which a pronounced departure from linearity occurred. This observation may be due to depletion of the active species in the afterglow responsible for the formation of CN molecules.

Selectivity ratios were based on the ratio of the limits of detection for napthalene to the limits of detection for each representative organometallic compound at the analytical wavelengths used for each organometallic compound. Excellent selectivity was observed for the organomercury and organotin compounds; however, the selectivity for organolead compounds was observed to be significantly lower. This decrease in selectivity resulted from CN ($B^2\Sigma^+ \rightarrow X^2\Sigma^+$) emission, which occurs over the 310–460-nm region, being within the spectral band-pass of the monochroator at the 368.3 nm analytical wavelength used for the Pb compounds. Selectivity can be improved by observing emission from other emission lines not within the CN emission region (i.e., Pb I at 283.3 nm); however, a decrease in sensitivity is observed. Thus, a compromise must be made in choosing the optimum analytical wavelength as opposed to desired selectivity.

Comparison to Other GC Emission Detectors. The versatility of the GC-APAN system is highlighted by its capabilities as an element-specific detector for organometallic compounds, as well as a nonspecific detector for organic compounds.

There are several advantages in utilizing APAN as a detector for organic compounds as opposed to the recent use of low-pressure active nitrogen detectors. The formation of the excited CN molecules in low-pressure afterglows is significantly hampered by the formation of polymeric materials containing CN (*10*). A constant flow of dilute HCl gas into the afterglow is required to catalyze a significant enhancement in the emissions from saturated hydrocarbon compounds. The use of HCl has not been effective when used in the APAN afterglow. The formation of the excited CN ($B^2\Sigma^+$) state, being a collision-dependent phenomenon, is more favorably produced in the APAN afterglow. Deposits on the windows of the low-pressure cells from polymeric materials also give rise to increasing background signals from CN emissions; thus periodic cleaning of the cell is required. No such deposits have been observed on the APAN afterglow tube.

Finally, the interfacing of the GC column, maintained at atmospheric pressure, to low-pressure afterglows is much more difficult to manipulate and maintain than the simple interface design used with APAN. The chromatography developed with the APAN detector has thus far been characterized by well-defined, Gaussian shaped peaks. The interface to the APAN detector appears to have negligible effects on the chromatographic capabilities of the GC when compared to chromatograms obtained from the standard flame ionization detector on the GC unit used.

In contrast to the observations with MIP detectors, the APAN afterglow is not extinguished from the introduction of relatively large amounts of organic species. Thus, instrumental modifications and manipulations to vent the solvent effluent prior to the detection of the trace organic constituents are not necessary. The afterglow, being continually generated from the main discharge region of the ozonizer-type tube, is at most only temporarily quenched by the introduction of excessive amounts of organic effluents. As can be seen in Figure 2, the spectral background from the afterglow is temporarily quenched by the excessive amounts of organics, resulting in the negative deflection in the chromatograms. The characteristic green afterglow is immediately regenerated after the excess solvent effluent has been swept through the afterglow tube, with no apparent detrimental effects on the performance of the afterglow. Carbonaceous deposits, which can severely effect the performance of MIP sources maintained at reduced pressures, are not formed in the APAN afterglow tube, a factor which is probably the result of the high flow rates and pressure used.

The limits of detection, using GC-MIP systems for the species evaluated in this communication, appear to be better than for those obtained using GC-APAN. The one exception is for organomercury compounds, in which either detector appears about equivalent (*15*). Unfortunately, a vast majority of publications to date in which MIP detectors are used have reported limits of detection from integrated peak areas, typically in terms of nanograms per second detected. Thus, a true comparison of the limits of detection for the MIP and APAN detectors was not possible since the limits of detection for the GC-APAN system were based on peak heights.

LITERATURE CITED

(1) McCormack, A. J.; Tong, S. S. C.; Cooke, W. D. *Anal. Chem.* **1965**, **37**, 1470–1476.
(2) McLean, W. R.; Stanton, D. L.; Penketh, G. E. *Analyst (London)* **1973**, **98**, 432–442.
(3) Van Dalen, J. P. J.; deLezenne Coulander, P. A.; de Galen, L. *Anal. Chim. Acta* **1977**, **94**, 1–19.
(4) Quimby, B. D.; Uden, P. C.; Barnes, R. M. *Anal. Chem.* **1978**, **50**, 2112–2118.
(5) Beenakker, C. I. M. *Spectrochim. Acta, Part B* **1977**, **32B**, 173–187.
(6) Lloyd, R. J.; Barnes, R. M.; Uden, P. C.; Elliot, W. G. *Anal. Chem.* **1978**, **50**, 2025–2029.
(7) Treybig, D. S.; Ellebracht, S. R. *Anal. Chem.* **1980**, **52**, 1633–1636.
(8) Windsor, D. L.; Denton, M. B. *Appl. Spectrosc.* **1978**, **32**, 366–371.
(9) Windsor, D. L.; Denton, M. B. *J. Chromatogr. Sci.* **1979**, **17**, 492–496.
(10) Sutton, D. G.; Westburg, K. R.; Melzer, J. E. *Anal. Chem.* **1979**, **51**, 1399–1401.
(11) Melzer, J. E.; Sutton, D. G. *Appl. Spectrosc.* **1980**, **34**, 434–437.
(12) Wright, A. N.; Winkler, C. A. "Active Nitrogen"; Academic Press: New York, 1968; Chapter 5.
(13) D'Silva, A. P.; Rice, G. W.; Fassel, V. A. *Appl. Spectrosc.* **1980**, **34**, 578–584.
(14) Safrany, D. R. "Progress in Reaction Kinetics"; Pergamon Press: New York, 1972; Vol. 6, Chapter 1.
(15) Talmi, Y. *Anal. Chim. Acta* **1975**, **74**, 107–117.

RECEIVED for review January 21, 1981. Accepted May 14, 1981.

Adsorption of Sodium Mercaptoacetate on a Mercury Electrode

Robert S. Lawton and Alexander M. Yacynych*

Department of Chemistry, Rutgers, The State University of New Jersey, New Brunswick, New Jersey 08903

The adsorption of electroactive species at a mercury drop electrode has been investigated for the sodium salt of mercaptoacetic acid. Electrocapillary curves, linear sweep voltammetry, and cyclic voltammetry were employed in order to study the extent of adsorption and the surface coverage of the electrode. It has been found that both mercury(II) and mercury(I) mercaptide are weakly adsorbed, while the mercaptoacetic anion is not adsorbed at all.

Mercaptoacetic acid (thioglycollic acid) is an important industrial material with applications in electroplating, plasticizing, and the preparation of thioglycollate of ammonia, a compound used in the permanent waving of hair. A study of electrode adsorption for the sodium salt of mercaptoacetic acid is discussed in this paper. Previous work with mercaptoacetic acid has dealt with its polarography (*1–3*) and quantitative analysis utilizing cathodic stripping voltammetry (*4, 5*).

The cyclic voltammetry of sodium mercaptoacetate exhibits complex behavior due to the adsorption of electrochemical products at the mercury electrode. To date, there have been no studies which deal with this particular case. In the present paper, an investigation of the adsorption of both mercury(I) mercaptoacetate and mercury(II) mercaptoacetate has been carried out by using cyclic voltammetry, linear sweep voltammetry, and electrocapillary data.

EXPERIMENTAL SECTION

Apparatus. All voltammetric experiments that were carried out at slow scan rates (less than 180 mV/s) were performed with a three-electrode potentiostat constructed in-house and were recorded on a Houston-Instruments X-Y recorder. All voltammetric experiments that were carried out at 4 V/s were performed with a Wenking potentiostat, Model 61RS, and were recorded with a Hewlett-Packard oscilloscope, Model 120B. The Wenking potentiostat was driven with a triangular wave generator constructed in-house.

Plots of drop time vs. potential were obtained with a Heath dropping mercury electrode (DME), Model EUA-19-6. The drop times were measured from a trace of current vs. time, recorded on a Houston-Instruments strip-chart recorder, Series 5000. The hanging mercury drop electrode (HMDE) employed for all voltammetric experiments was a Metrohm E410. Both the DME and the HMDE were filled with triply distilled Bethlehem Instrument mercury. The size of the mercury drop (one-tenth revolution of micrometer head) which was used for each voltammetric experiment had an approximate area of 1.9×10^{-2} cm^2. The SCE reference electrode and the Ag-wire counterelectrode were isolated from the cell by porous frits.

Materials. The sodium salt of mercaptoacetic acid was obtained from both the Aldrich Chemical Co. and the Fisher Scientific Co. In each case, the reagent was used without further purification.

It was discovered that the mercaptoacetate had a finite "shelf life". This conclusion is based on the observation that a cathodic peak eventually appears at −0.55 V (vs. SCE) in the cyclic voltammograms (pH 5.7). A comparison with a cyclic voltammogram of dithioglycollic acid revealed that the cathodic peak at −0.55 V was due to the reduction of the disulfide, indicating that a small portion of the original mercaptoacetate had been oxidized by the atmosphere. Whenever this occurred, a fresh lot of sodium mercaptoacetate was purchased and the old lot was discarded.

Mercury(I) nitrate, reagent grade, was obtained from the G. Frederick Smith Co., and mercury(II) nitrate, reagent grade, was obtained from the J.T. Baker Chemical Co. Dithioglycollic acid was obtained from the Aldrich Chemical Co. All of these reagents were used without further purification. All other chemicals used were reagent grade. Also, all experiments were run in a potassium hydrogen phthalate (KHP) buffer of pH 5.7, and all solutions were prepared with triply distilled water.

Procedures. The cyclic voltammograms were recorded in the following manner: Steady-state experiments were done with switching potentials of +0.2 V. and −0.75 V. The scan rate employed was either 75 mV/s or 4 V/s. The only exception is the data in Figure 8, which was collected from steady-state voltammograms with various scan rates and with switching potentials of 0.0 V and −0.75 V. A 1-min, open-circuit, equilibration period was used before the start of all steady-state and linear sweep voltammograms. The first 40 s were done with stirring, the last 20 s were quiescent. The experiments with linear sweep voltammetry were performed with various scan rates and start potentials.

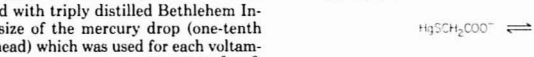
Data for Figures 5, 7, 9, and 10 were obtained in the following manner: Standard solutions of various concentrations were prepared in volumetric flasks with deaerated buffer. These solutions were prepared fresh for each calibration curve. This was done in order to minimize evaporation of electroactive species, which would result in undetermined changes in concentration. The electrochemical cell contained 100 mL of deaerated buffer at the start of each set of experiments. Aliquots from the standard solutions were pipetted into the cell, and the new concentration was calculated based on dilution considerations. This particular procedure was employed because it was less time-consuming than preparing a 100-mL solution of known concentration for each point on the calibration curve.

RESULTS AND DISCUSSION

Assignment of the Voltammetric Peaks. The voltammograms were characterized by four peaks: a set of anodic and cathodic peaks at approximately +0.1 V and a second set of peaks at approximately −0.35 V. The assignment of individual reactions to each of the waves has been done polarographically by several groups (*1–3*). On the basis of our own results, we agree with the conclusions of Kolthoff and his co-workers.

The following sets of reactions have been postulated for the voltammetric peaks observed:

At +0.1 V



(1)

At −0.35 V

$$Hg + HSCH_2COO^- \rightleftharpoons HgSCH_2COO^- + H^+ + e^- \quad (2)$$

In order to confirm the above postulated mechanisms, we performed several sets of experiments. In the first experiment, cyclic voltammograms were taken with a solution which was 0.12 mM in sodium mercaptoacetate and 0.12 mM in mercury(II) nitrate. A slight cloudiness was observed upon addition of the mercury(II) nitrate solution to the solution of sodium mercaptoacetate. This cloudiness is attributed to the formation of slightly soluble mercury(II) mercaptide. A 1-min equilibration, with open-circuit, was employed prior to the start of the first scan.

0003-2700/81/0353-1523$01.25/0 © 1981 American Chemical Society

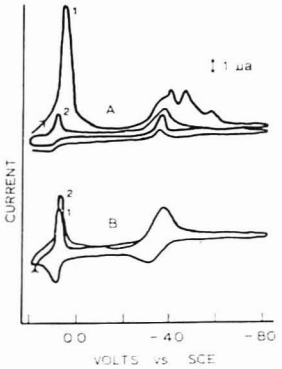


Figure 1. Cyclic voltammograms of (A) a solution which is 0.12 mM in both mercury(II) nitrate and sodium mercaptoacetate and (B) a solution which is 0.12 mM in sodium mercaptoacetate alone. Scan rate = 75 mV/s.

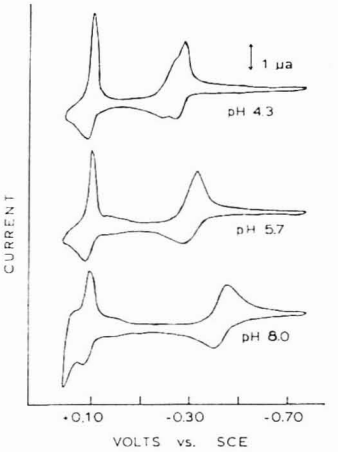


Figure 2. Steady-state cyclic voltammograms of three solutions at different pH values. Concentration of sodium mercaptoacetate was 87 ppm for each solution. Scan rate = 75 mV/s.

The data in Figure 1A demonstrate a significant difference between the first and second scans for the cathodic peak at +0.1 V. The tremendous enhancement of the first scan is attributed to the adsorption of mercury(II) mercaptide during the equilibration period, and its subsequent reduction at +0.1 V. Referring to Figure 1B, this notion is confirmed by the cyclic voltammograms on a solution of sodium mercaptoacetate alone. With only the sodium mercaptoacetate in solution, there is no significant difference between the first and second scans.

Cyclic voltammograms taken at different pH values also yielded confirmation of the postulated electrode reactions. Referring to Figure 2, the set of peaks at −0.35 V were observed to shift an average value of 63 mV per change in pH unit, indicating that one proton is reacting per molecule of mercaptide. This is consistent with eq 2. Also, the peaks at +0.1 V were found to be invariant with hydrogen ion concentration, indicating that eq 1 is also correct. The pH dependence of mercaptoacetic acid has been previously described by Liberti (*6*), who observed that both cathodic peaks are dependent on proton concentration below pH 4 and both peaks are independent of proton concentration above pH 10, while only the peak at −0.35 V has any pH dependence between these two values. An inspection of the dissociation constants obtained by Kolthoff for mercaptoacetic acid (*1*) reveals that the observed change in pH dependence stems from the fact that the mercaptoacetic acid is largely undissociated at high proton concentration, while it exists as a monovalent anion above pH 4 and as a divalent anion above pH 10.

Weak Adsorption vs. Strong Adsorption. There are nine different possible cases of adsorption or nonadsorption which could characterize a voltammetric peak. These different cases are outlined below: R = reactant, P = product, NA = not adsorbed, WA = weakly adsorbed, SA = strongly adsorbed; (1) RNA / PNA, (2) RWA / PNA, (3) RNA / PWA, (4) RSA / PNA, (5) RSA / PWA, (6) RNA / PSA, (7) RWA / PSA, (8) RSA / PSA, (9) RWA / PWA.

There exist certain criteria to differentiate between strong and weak adsorption. In the case of strong adsorption of a product, the voltammogram will reveal a prepeak on the cathodic scan and a postpeak on tha anodic scan. The opposite will be true if a reactant is adsorbed. This phenomenon is caused by the difference in free energy between a molecule which is strongly adsorbed and a molecule which is not. A weakly adsorbed molecule undergoes electron transfer at nearly the same potential as the diffusing molecule, so that there are no prepeaks or postpeaks. However, the weakly adsorbed molecule will still cause enhancement of the peak current, as compared to strictly diffusion-controlled conditions (*7*).

The exception to the above statements is the case of equally strong adsorption of both product and reactant, where the voltammogram will reveal neither a postpeak nor a prepeak. This is because both species will have the same free energy of adsorption. The prepeaks and postpeaks are eliminated because the stabilization due to adsorption is equivalent for each species, and the product molecules, once formed, can displace the adsorbed reactant molecules from the electrode surface (*8*). Therefore, the electrode is covered at all times and the ratio of the surface concentrations of reduced and oxidized species is Nernstian (*7*). The net effect of this is that cases 8 and 9 can become difficult to distinguish.

In the particular case of the mercaptoacetate system, at a pH of 5.7, no prepeaks or postpeaks were observed for either of the redox couples. Therefore, either of the redox couples could be described by any of the cases 1–3 or 9. The instance of equally strong adsorption of both product and reactant, case 8, would be possible only if all three electroactive species had the same free energy of adsorption. Otherwise, one of the two redox couples would have had a postpeak and a prepeak.

Qualitative Inspection of Cyclic Voltammograms. A qualitative examination of cyclic voltammograms, performed at various concentrations and scan rates, has proved informative with the mercaptoacetate system. Referring to Figure 3A,B, it was observed that the cathodic peaks at +0.1 V and −0.35 V have the symmetrical appearance which is indicative of an adsorption-controlled process (*7*). It was also observed that these cathodic peaks exhibit peculiar behavior at sufficiently high concentrations of sodium mercaptoacetate. Referring to Figure 3C, in the voltammogram performed at 313 ppm, it was observed that the cathodic peak current at +0.1 V had actually decreased. In addition, a cathodic current spike has appeared at −0.40 V. This current spike does not appear on the first reduction scan so that it can only be studied with steady-state cyclic voltammograms. This spike rapidly achieves a constant peak current which does not change with further increases in concentration. In contrast, the cathodic

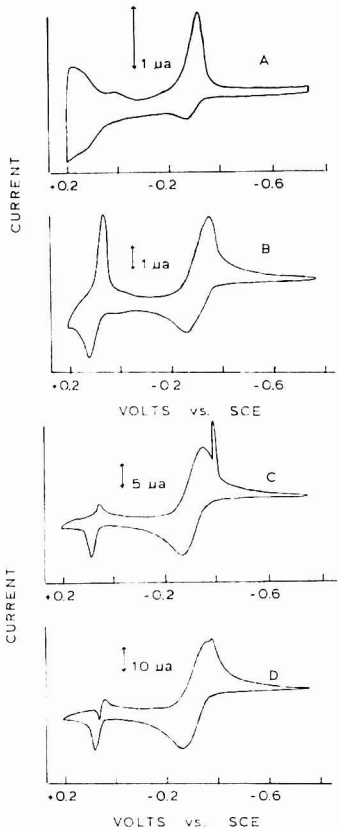


Figure 3. Steady-state cyclic voltammograms at various concentrations of sodium mercaptoacetate: (A) 7 ppm, (B) 99 ppm, (C) 313 ppm, (D) 588 ppm. Scan rate = 75 mV/s.

peak current at −0.35 V continues to grow with further increases in concentration. At 588 ppm (Figure 3D), the current spike has been engulfed by the peak at −0.35 V. In addition, the voltammogram at 588 ppm reveals that the cathodic peak at +0.1 V has actually become inverted (anodic current on a cathodic scan).

It was also observed that slower scan rates favor the inverted peak at +0.1 V. Referring to Figure 4, it can be seen that the peak in question is inverted at a scan rate of 9 mV/s, while it becomes positive at a scan rate of 75 mV/s.

All of the above data indicate that adsorbed species have a profound effect on the electrochemistry of sodium mercaptoacetate at a mercury electrode. A more complete discussion of these qualitative observations will be presented later in this paper, after the elucidation of the electrode mechanisms.

Dependence of Peak Height on Concentration and Scan Rate. A diffusion-controlled process will demonstrate a linear dependence both on bulk concentration, C_0^*, and on the square root of the scan rate, $V^{1/2}$. On the other hand, an adsorption-controlled process will demonstrate a nonlinear dependence on the bulk concentration and a linear dependence on the scan rate, V (7). Plots of the peak current dependence on concentration and scan rate were prepared for the mercaptoacetate system.

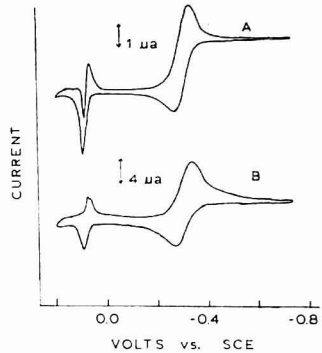


Figure 4. Steady-state cyclic voltammograms of a 220 ppm solution of sodium mercaptoacetate: (A) 9 mV/s, (B) 75 mV/s.

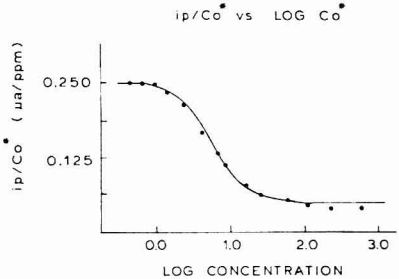


Figure 5. Ratio of peak current to log bulk concentration as a function of the bulk concentration for the cathodic peak at −0.35 V. All points were determined from steady-state experiments. Scan rate was 75 mV/s.

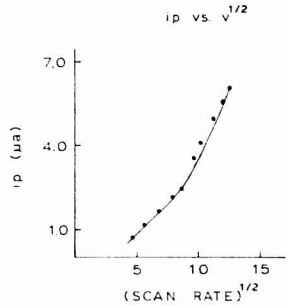


Figure 6. Peak current as a function of the square root of the scan rate (mV/s) for the cathodic peak at −0.35 V. Concentration of sodium mercaptoacetate was 550 ppb.

A plot of i_p/C_0^* (peak current/bulk concentration) vs. log C_0^* was prepared for the cathodic peak at −0.35 V (Figure 5). The above data yielded a reverse S-shaped curve, corresponding to the transition from Henry's law behavior to a diffusion-controlled dominated situation.

Plots of peak current vs. $V^{1/2}$ were prepared for the cathodic peak at −0.35 V, using linear sweep voltammetry with a start

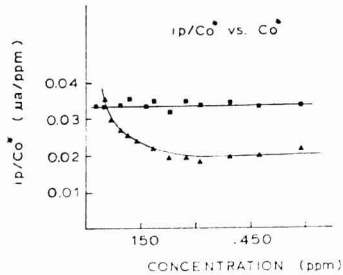


Figure 7. Ratio of peak current to bulk concentration as a function of bulk concentration for the anodic peak at +0.1 V (▲) and the anodic peak at −0.35 V (■). Scan rate = 75 mV/s. Data points measured from steady-state cyclic voltammograms.

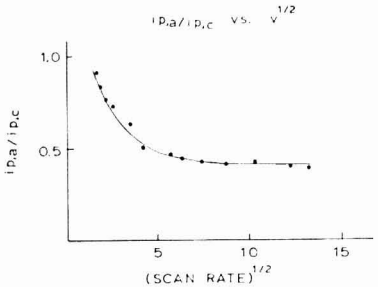


Figure 8. Ratio of anodic peak current to cathodic peak current as a function of the square root of the scan rate (mV/s) for the redox couple at −0.35 V. Concentration of sodium mercaptoacetate was 7 ppm. Switching potentials were 0.00 V and −0.75 V.

potential of 0.00 V. Referring to Figure 6, the nonlinear behavior at 550 ppb is indicative of an adsorption-controlled process. The same type of plot at 220 ppm is linear, demonstrating that the cathodic process at −0.35 V has become diffusion controlled. These data correlate nicely with the graph in Figure 5, further substantiating the postulated adsorption of mercury(I) mercaptide.

In the case of the anodic peaks at +0.1 V and −0.35 V, plots of i_p/C_0^* vs. C_0^* were prepared. The data for both peaks are graphed on the same axis in Figure 7. The nonlinear behavior of the peak current at +0.1 V is expected, since this peak corresponds to the oxidation of adsorbed mercury(II) mercaptide. The linear behavior of the anodic peak at −0.35 V indicates that the mercaptoacetic anion is not adsorbed. Scan rate experiments were performed at 7 ppm in order to confirm this conclusion. Figure 8 is a plot of the ratio of the anodic peak current to the cathodic peak current vs. the square root of the scan rate, for the redox couple at −0.35 V. The shape of the graph clearly demonstrates the weak adsorption of mercury(I) mercaptide and the lack of adsorption of the mercaptoacetic anion (7).

In the case of the cathodic peak at +0.1 V, a plot of peak current vs. scan rate yielded a linear relationship at 100 ppm, indicating that the mercury(II) mercaptide is adsorbed. This type of behavior is consistent with the symmetrical appearance of the cathodic peak at +0.1 V.

Calculation of Surface Coverage. Once having demonstrated that the mercury(I) and mercury(II) mercaptides were adsorbed, a surface coverage of the electrode was calculated for the mercury(II) mercaptide. A calibration curve was constructed at a scan rate of 4 V/s with steady-state cyclic

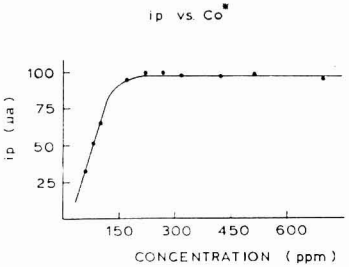


Figure 9. Peak current as a function of bulk concentration for the cathodic peak at +0.1 V. Scan rate = 4 V/s. Steady-state experiment.

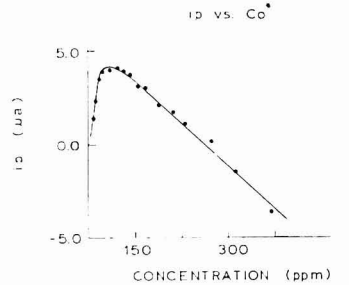


Figure 10. Peak current as a function of bulk concentration for the cathodic peak at +0.1 V. Scan rate = 75 mV/s. Steady-state cyclic voltammograms.

voltammograms, using the oscilloscope as a recorder. The data are plotted in Figure 9. The constant peak current attained at high concentrations corresponds to monolayer coverage of the mercury electrode (9). At all concentrations investigated, the cathodic peak at +0.1 V retains its symmetrical appearance, indicating that diffusion contributes only a minor portion of the total current. The negligible contribution of diffusing species is responsible for the plateau exhibited by the calibration curve at high concentrations. Integration of the peak area for the reduction at +0.1 V, using a 220 ppm solution, yields a surface coverage of approximately 18–22 Å^2 per molecule. This is in good agreement with an end-on orientation of the mercury(II) mercaptide in which the plane of the ring is perpendicular to the surface of the electrode.

In the case of the cathodic peak at −0.35 V, the calibration curve does not exhibit a flat plateau. Also, unlike the symmetrical peak at +0.1 V, the cathodic peak at −0.35 V exhibits tailing at a scan rate of 4 V/s. These observations indicate that diffusion is still making a considerable contribution to the reduction current at −0.35 V, even though the scan rate is 4 V/s. Therefore, a surface coverage was not calculated for the mercury(I) mercaptide.

In the case of the cathodic peak at +0.1 V, the calibration curve was quite different when constructed at a scan rate of 75 mV/s (Figure 1) as compared to the curve constructed at 4 V/s (Figure 9). Referring to Figure 10, it was observed that the peak current achieves a maximum value at approximately 80 ppm, before falling off with further increases in concentration. Integration of the peak with the greatest height in Figure 10 yields the same amount of charge per unit area as was obtained for monolayer coverage of the electrode. This indicates that the anomalous behavior at +0.1 V (i.e., decreasing peak current with increasing concentration) requires

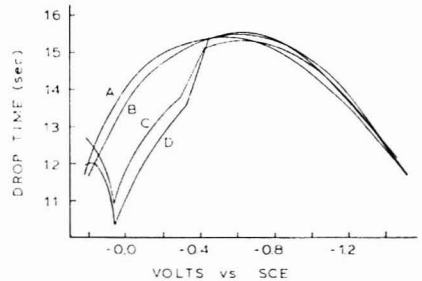


Figure 11. Drop time as a function of potential, recorded at several concentrations of sodium mercaptoacetate: (A) supporting electrolyte, (B) 10 ppm, (C) 1050 ppm, (D) 2350 ppm.

the prior formation of monolayer coverage of the electrode with mercury(II) mercaptide.

A comparison of Figure 9 with Figure 10 reveals that the inverted peak is favored by high bulk concentrations of sodium mercaptoacetate and slow scan rates. This is entirely consistent with the observations that were made from Figures 3 and 4.

At this point, it should be noted that chronocoulometry was considered by the authors as an alternative method for calculating surface coverage of the electrode. In the sodium mercaptoacetate system, however, the adsorbed species exist only within those potential windows that correspond to electrochemical reactions. This violates the boundary conditions of the chronocoulometric technique. Accordingly, the authors did not employ this technique.

Drop Time vs. Potential. Plots of drop time vs. potential were made for the sodium mercaptoacetate system. Referring to Figure 11, the most significant features of these plots are the discontinuities at approximately +0.1 V and −0.35 V, reflecting sudden changes in the interfacial tension of the mercury drop. Similar behavior has also been observed for adsorbed cadmium complexes (*10*). Referring to the discontinuity at +0.1 V, it was observed that this phenomenon is not apparent at 10 ppm, while it has become very prominent at 1050 ppm. It is interesting to note that this discontinuity appears at the same potential and within the same range of concentration as the inverted peak in the cyclic voltammograms that were performed at 75 mV/s. The significance of this will be discussed in the next section.

Discussion of Qualitative Observations. The results now allow a much more complete explanation of the data presented in Figures 3 and 4. Referring to the cathodic current spike observed at −0.40 V in Figure 3, we have attributed this phenomenon to a film rearrangement of adsorbed mercury(I) mercaptide. Bard (*11*) has observed a similar phenomenon for cysteine, which he attributes to the formation of a "compact" film of adsorbed species, caused by the attractive interactions between the adsorbed molecules. In view of the above explanation, it is not surprising that the current spike rapidly attains a maximum peak height that does not change with further increases in concentration. This would be expected since the "compact" film should eventually achieve maximum electrode coverage.

We have also been able to explain the inverted peak observed in Figure 4. To begin with, the inverted peak represents an oxidation current on a cathodic scan. It has been demonstrated that this oxidation current is favored by slow scan rates and high bulk concentrations (Figures 3 and 4). These data indicate that there is competition between the reduction of one adsorbed species and the oxidation of a second, diffusing species. Therefore, the peak at +0.1 on the cathodic sweep is actually the sum of two different processes. This interpretation of the data is consistent with the graph in Figure 10. The downward sloping portion of the plot is due to the increasing contribution of the diffusion-controlled oxidation current at higher bulk concentrtions of sodium mercaptoacetate.

In order to explain the oxidation of diffusion-supplied mercury(I) mercaptide on a cathodic sweep, it is necessary to refer to the electrocapillary curves. In Figure 11, the data demonstrate that the dissolution of the film of mercury(II) mercaptide, and the subsequent formation of a layer of mercury(I) mercaptide, is accompanied by a dramatic change in the surface tension of the mercury drop. More importantly, a comparison of the cyclic voltammograms (75 mV/s) and Figure 11 demonstrates that the inverted peak occurs at the same potential and concentration as the discontinuity in the electrocapillary curves. In other words, the oxidation of mercury(I) mercaptide on the cathodic sweep does not begin until the dissolution of the layer of mercury(II) mercaptide.

The combination of all of the above data leads to a possible explanation of the inverted peak. The most logical conclusion is that the adsorbed layer of mercury(II) mercaptide, when it attains monolayer converage, hinders the electron transfer of nearby, mercury(I) mercaptide molecules. This results in a localized excess of mercury(I) mercaptide, as well as a scarcity of mercury(II) mercaptide, in the proximity of the electrode. The electrode itself is covered with an adsorbed layer of mercury(II) mercaptide. When the integrity of the mercury(II) mercaptide layer is destroyed by reduction on the return cathodic sweep, the nearby mercury(I) species begins to transfer electrons as the adsorbed mercury(II) species is being reduced. The resulting current is then a sum of the two processes.

The above postulated mechanism also explains another aspect of the inverted peak. At approximately +0.06 V, immediately following the inverted peak, there is a small, positive peak. With regard to the above postulated mechanism, this small amount of reduction current can be attributed to the reduction of "extra" mercury(II) mercaptide that was formed by the oxidation of mercury(I) mercaptide on the cathodic sweep.

SUMMARY

Referring to our earlier discussion of the different possible cases of adsorption which might characterize a voltammetric peak, the data indicate that the redox couple at −0.35 V is described by case 2 (RWA/PNA), while the redox couple at +0.1 V is described by case 9 (RWA/PWA). This work also demonstrates that the mercury(II) mercaptide is adsorbed onto the electrode surface with an end-on orientation. The various mechanisms which have been elucidated are as follows:

$$E = +0.1\ \text{V};\ \text{Hg}^{\text{I}}\text{SR (adsorbed)} \rightleftharpoons \text{Hg}^{\text{II}}\text{SR (adsorbed)} + 1e^-$$

$$E = -0.35\ \text{V};\ \text{RSH (solution)} \rightleftharpoons \text{Hg}^{\text{I}}\text{SR (adsorbed)} + 1e^- + 1\text{H}^+$$

LITERATURE CITED

(1) Leussing, D. L.; Kolthoff, I. M. *J. Electrochem. Soc.* **1953**, *100*, 334–338.
(2) Liberti, A.; Cervone, E. *Ann. Chim. (Rome)* **1951**, *41*, 95–104; *Chem. Abstr.* **1951**, *45*, 10100e.
(3) Gorokhovskaya, V. I.; Klimova, L. I. *Zh. Obshch. Khim.* **1965**, *35* (11), 1913–1916; *Chem. Abstr.* **1966**, 6092 g.
(4) Florence, T. M. *J. Electroanal. Chem.* **1979**, *97*, 219–236.
(5) Moore, W. Michael; Gaylor, V. Frances *Anal. Chem.* **1977**, *49* (9), 1386–1390.
(6) Sartori, G.; Liberti, A.; Colazolari, C. *Com. Int. Thermodyn. Cinet. Electrochim., C. R. Reun. 2nd* 301–304; *Chem. Abstr.* **1952**, *46*, 10011g.
(7) Wopschall, R. H.; Shain, I. *Anal. Chem.* **1967**, *39*, 1514–1527.
(8) Heyrovsky, J.; Kuta, J. "Principles of Polarography", Academic Press: New York, 1966; p 293.
(9) Schmidt, C. L.; Swofford, H. S. *Anal. Chem.* **1979**, *51*, 2028–2033.

(10) Kalvoda, R.; Anstine, W.; Heyrovsky, M. *Anal. Chim. Acta* **1970**, *50*, 93–102.
(11) Stankovich, Marian T.; Bard, Allen J. *J. Electroanal. Chem.* **1977**, *75*, 487–505.

RECEIVED for review June 9, 1980. Resubmitted January 23, 1981. Accepted April 17, 1981. A.M.Y. thanks Rutgers Research Council, Biomedical Research Support Grants, and the National Institutes of Health (Grant No. GM 28125-01) for research support. R.S.L. thanks Rutgers University for the award of a University Fellowship.

Stopped-Rotation Voltammetry

Joseph Wang

Department of Chemistry, New Mexico State University, Las Cruces, New Mexico 88003

The technique of stopped-rotation voltammetry at a rotated disk electrode, which measures the current difference with the rotation speed switched on and off, is described. Sensitivity, precision, mass-transport properties, and linearity of response are reported. Well-defined current–potential curves are obtainable and compared with those obtained by differential pulse voltammetry. An asymmetric hydrodynamic modulation waveform and a relatively rapid stopped-rotation procedure (without the achievement of steady states) are employed to shorten the analytical cycle. Due to its inherent sensitivity and simplicity, the technique seems well suited for the measurement of low concentrations of electroactive materials.

In recent years, the use of solid electrodes for electroanalytical purposes has gained popularity, one of the primary reasons being their applicability to anodic oxidations. However, practical difficulties have hampered the attainment of precise quantitative data employing classical or potential pulse voltammetry at solid electrodes. Hydrodynamic modulation at solid electrodes has been shown to be a feasible technique for obtaining reproducible current–voltage data at low concentrations of electroactive species. Such modulation involves measurement of the current difference between two rates of convective transport, resulting with efficient discrimination against the nonconvective background current. Miller, Bruckenstein, and co-workers have done a great deal of work in developing the sinusoidal modulation of a disk electrode's rotation speed about a center value (*1*, *2*). The analytical usefulness of this approach has been exploited for obtaining voltammograms at submicromolar concentrations. The sinusoidal component of the current, which follows directly from the Levich equation is given by

$$\Delta i = 0.62nFAD^{2/3}\nu^{-1/6}C_b\frac{\Delta\omega^{1/2}}{\omega_0^{1/2}} \qquad (1)$$

where n is the number of electrons transferred per molecule, F is the Faraday, A is the disk area, D is diffusion coefficient, ν is kinematic viscosity, C_b is the bulk concentration of the electroactive species, $\Delta\omega$ is the peak to peak amplitude of the change in the rotation speed, and ω_0 is the center value of the rotation speed. $\Delta\omega$ is always much smaller than ω_0 (usually about 1–10% of ω_0), resulting with exploitation of only a very small portion of the steady-state analytical current of interest. In order to decrease the attenuation of the steady-state analytical response (i.e., increased current difference), Blaedel and Engstrom have suggested the pulsed-rotation voltammetry (PRV) in which the rotation speed of a rotated disk electrode is switched between two values (*3*)

$$\Delta i = 0.62nFAD^{2/3}\nu^{-1/6}C_b(\omega_H^{1/2} - \omega_L^{1/2}) \qquad (2)$$

The subscripts H and L designate the high and the low rotation speeds, respectively. Since low and high rotation speeds of 500 and 1500 rpm, respectively, are usually selected as the two current states, more than half the steady-state analytical current is not exploited for the quantitation (eq 2). Further increased current difference has been achieved by incorporating the PRV approach with the high surface area of a rotated porous disk electrode (*4*). Analogous procedures have been developed for electrochemical flow detectors, with the solution flow rate being pulsed to the surface of a stationary electrode (*5*, *6*), or with hydrodynamically modulated rotating disk electrode in a flow cell (*7*).

The purpose of the following work is to demonstrate the characteristics of stopped-rotation voltammetry (SRV), in which differential current measurements are made between zero and high rotation speeds. The main advantages of this procedure are its inherent sensitivity (i.e., exploitation of all the rotation-dependent analytical signal of interest for the quantitation (100% modulation)) and the simplicity of operation (turning on and off the rotational speed). Since the lower current (at $\omega = 0$) is not zero but a very small value, due to diffusion (linear and radial) and natural convection (*8*), an expression for the on–off current is not obtained simply by substituting $\omega_L = 0$ into eq 2; instead, and because of the theoretical limitations to evaluate the zero rotation speed current (*8*), Δi may be described by the following relationship:

$$\Delta i = 0.62nFAD^{2/3}\nu^{-1/6}C_b\omega^{1/2} - i_{\omega=0} \qquad (3)$$

Compared to previously reported hydrodynamic modulated rotating disk electrode approaches (discussed above) the SRV does not require any programming circuitry for changing the rotation speed, and thus it can be incorporated with every rotating disk assembly. These advantages and the various characteristics of the SRV are elucidated by application to the measurement of micro- and submicromolar concentrations of ascorbic acid and ferrocyanide.

EXPERIMENTAL SECTION

Apparatus. The rotating electrode assembly (Model PIR, Pine Instruments Co., Grove City, PA) with a 0.75-cm diameter glassy carbon disk electrode (Model DDI 15, Pine Instruments Co.) was used in conjuction with a cell of 200-mL capacity made from Pyrex glass. The salt bridges of the reference electrode (Ag/AgCl, Model RE-1, Bioanalytical Systems Inc., West Lafayette, IN) and of the counterelectrode (a Pt coil immersed in 0.1 M phosphate buffer) join the cell through two holes in its Plexiglas cover. The working

0003-2700/81/0353-1528$01.25/0 © 1981 American Chemical Society

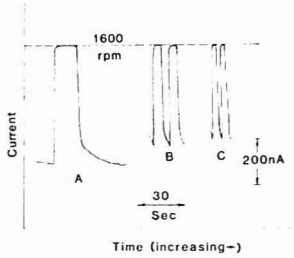


Figure 1. Stopped-rotation response for the oxidation of 3 μM $K_4Fe(CN)_6$: rotation speeds, 1600 (on) and 0 (off) rpm; cycling times (A) 15 (on) and 30 (off) s; (B) 5 (on) and 5 (off) s; (C) 3 (on) and 3 (off) s; applied potential, +0.7 V; supporting electrolyte, 0.1 M phosphate buffer (pH 7.4).

electrode was initially polished with a 0.1-μm alumina slurry, until a mirrorlike finish was obtained. Current–voltage data were recorded with a Princeton Applied Research Model 364 polarographic analyzer and a Houston Omniscribe strip-chart recorder.

Reagents. All solutions were prepared from deionized water and analytical grade chemicals. The supporting electrolyte was 0.1 M phosphate buffer (pH 7.4), prepared from a 1:4 mixture of KH_2PO_4 and K_2HPO_4. Millimolar stock solutions of $K_4Fe(CN)_6 \cdot 3H_2O$ and ascorbic acid were made up fresh each day. Aliquots of the stock solutions were added to the supporting electrolyte to give the desired concentration.

Procedure. A 200-mL aliquot of the buffer was pipetted into the cell and pretreatment of the electrode begun. This consisted of cycling the applied potential between +1.0 V and −1.0 V for 10 min, allowing 2 min at each potential. Following pretreatment, the desired working potential in the mass-transport limited (plateau) region was applied. Stopped-rotation measurements were performed only a short time (15 s to 2 min) after the working potential was applied. These were achieved by switching manually the rotational speed on and off, employing different cycling periods (as described later in this paper). SRV measurements of the analyte solution followed those of the background solution. All data presented were corrected for background.

The stopped-rotation voltammograms were developed pointwise by making 100-mV changes in applied potential and waiting about 30 s before applying the rotation pulse. Between analyses, the working electrode was stored in the empty cell.

RESULTS AND DISCUSSION

The Characteristics of the Stopped-Rotation Current Amplitude. Stopped-rotation current–time responses for 3 μM ferrocyanide, employing different cycling times, are shown in Figure 1. The stopped-rotation response times are around 3 s (on) and 25 s (off) (Figure 1A). For this reason, and in order to shorten the analytical cycle while still achieving the two steady-states, asymmetrical modulation waveforms (with the rotation "on" times shorter than the "off" times) have been employed throughout this study. Previously reported hydrodynamic modulation procedures, which based on pulsing the rotation speed or the flow rate (e.g., *3*, *5*) have used symmetrical square-wave hydrodynamic pulsings, with equal times for the high and low convection rates (i.e., without trying to reduce the length of the analytical cycle). Another way to shorten the analytical cycle is not to wait for the zero current steady state (Figure 1B,C). As the frequency is increased the decay to the zero current state is cut off, and the stopped-rotation current amplitude decreases. It is noteworthy that the 4.5- and 7.5-fold reductions in the cycling period results in current diminutions of only 16% and 20%, respectively. The change in current amplitude as a function of the cycling period reflects the time-dependent fall-off in the concentration gradient at the electrode surface (i.e., Cottrell current transient—$i \sim t^{-1/2}$) as the rotation is stopped. Mathematical

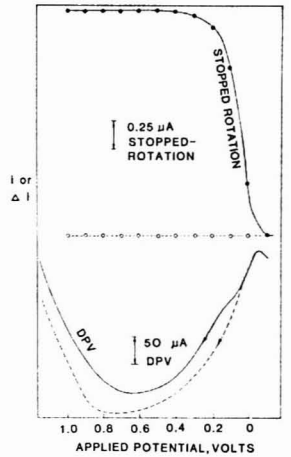


Figure 2. Stopped-rotation and differential pulse voltammograms of 6.25 μM ascorbic acid in 0.1 M phosphate buffer: SRV conditions, 1600 rpm for 15 s, 0 rpm for 30 s; differential pulse conditions, scan rate, 5 mV/s; amplitude, 50 mV; rotation speed, 1600 rpm. The dotted lines represent the blank solution.

analysis of the current decay as a function of time results with $it^{1/2}$ values of $0.346\Delta i_0$ and $0.357\Delta i_0$ for the 3 and 5 s non-steady-state operations, respectively (Δi_0 refers to the steady-state current amplitude (Figure 1A)). The dependence of the stopped-rotation current amplitude upon ferrocyanide concentration has been studied for the two cycling periods, shown in Figure 1A,B. Linear correlations between the current amplitude and the concentration are obtained. With the steady-state stopped-rotation operation the sensitivity is 167.2 nA/μM, while for the non-steady-state operation (5 s (on) and 5 s (off)) it is 140 nA/μM. When these data are normalized to the electrode surface area, values of 379 and 317 nA/(μM cm^2) are obtained, respectively. A lower sensitivity value of 222 nA/(μM cm^2) was calculated from data reported for PRV between 500 and 1500 rpm (*3*). The linear correlation between the steady-state current amplitude and the concentration indicates that $i_{\omega=0}$ (see eq 3) is a concentration-dependent component (as expected for diffusion and convective processes; a flow rate independent component was found to be linearly dependent on the analyte concentration in the case of a flow-through tubular electrode (*5*)).

The dependence of the steady-state stopped rotation current amplitude upon the difference in rotation speeds was evaluated by using 5.0 μM ascorbic acid, over $\Delta\omega$ range of Δ400–Δ2500 rpm (conditions: applied potential, +0.65 V; 15 (on) and 35 (off) s). A plot of Δi vs. $\Delta\omega^{1/2}$ (not shown) was linear, with zero intercept and a slope of 39.5 nA/$rpm^{1/2}$. When replotted on a log–log scale these data gave a straight line, with a slope of 0.51. This indicates, that under the experimental conditions of this work, the effect of the analyte flux at zero rotation speed is very small, and thus the current amplitude (eq 3) is approaching the Levich equation.

Analytical Applications. Stopped-rotation and differential-pulse voltammograms, obtained for the oxidation of 6.25 μM ascorbic acid under identical experimental conditions are compared in Figure 2. Such an experimental comparison between an hydrodynamic modulation procedure and a potential pulse technique has not been described yet. The differential pulse analytical response at this concentration level is almost completely obscured by the large (and irreproducible)

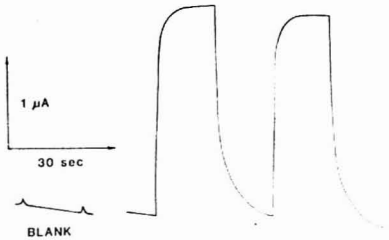


Figure 3. Current–time trace for 7 μM ascorbic acid: applied potential, +1.2 V; cycling times, 15 (on) and 15 (off) s; rotation speeds and supporting electrolyte, as in Figure 1.

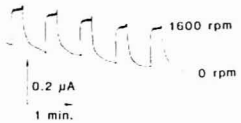


Figure 4. Stopped-rotation response for 0.6 μM ascorbic acid: applied potential, +0.85 V; conditions as in Figure 1A.

background transient currents, associated with the abrupt potential excitations. In contrast, the stopped-rotation voltammogram is characterized by its well-defined (and reproducible) wave and plateau regions. The SRV background (dotted line) is very low, indicating good correction for nonconvective currents and the absence of electroactive contaminants. The stopped-rotation half-wave potential is +0.05 V. Overall, the data of Figure 2 indicate the advantages of the hydrodynamic modulation procedure over the potential pulse technique for quantitative trace analysis using solid electrodes. It should be noted that the SRV data were taken in about 18 min, compared to 4 min for the differential-pulse voltammogram. The incorporation of the non-steady-state SRV (Figure 1B,C) with linear potential scan and its automated control would permit the achievement of rapid current–potential data; this possibility is now under investigation.

The nonconvective nature of solvent decomposition permits measurements to be made over a wider voltage range than for conventional scanning voltammetry. Figure 3 demonstrates the feasiblity of performing micromolar measurements at relatively extreme anodic potentials, well into oxygen generation; it shows the SRV response for 7 μM ascorbic acid obtained at applied potential of +1.2 V. The blank stopped-rotation current (shown on the left) is too low to be measured at this current scale, indicating minimized modulation response to oxygen generation. (The current spikes on both sides of the blank current amplitude are electrical noises due to rotation stepping.)

Figure 4 illustrates the sensitivity and precision obtained employing the SRV technique. The five current amplitudes shown are part of a series of 12 successive measurements of 0.6 μM ascorbic acid in 0.1 M phosphate buffer for which a relative standard deviation of 2.71% has been calculated. Different noise levels, of 12 and 4 nA, are observed for the rotation "on" and "off" current states, respectively. This is due to the carbon brush electrical contact of the Pine rotating electrode which is electrically noisier than the direct mercury contact used in various PRV studies (*3*, *4*). If the limit of detection is taken to be equal to the noise level at the rotation "on" operation, a value around 4×10^{-8} M is obtained. The use of a rotated electrode with a mercury contact (for which the noise level is around 1 nA (*3*, *4*)) would result with further lowering the detection limit. Overall, due to its significantly increased current amplitude (i.e., analytical signal) and using the same electrode assembly (i.e., same noise level), the SRV would have much lower detection limits than those of the sinusoidally modulated or the pulsed-rotated disk electrodes. The improved sensitivity and the simple instrumentation and procedure indicate considerable promise for SRV as a method of measuring low concentrations of electroactive materials.

LITERATURE CITED

(1) Miller, B.; Bellavance, M. I.; Bruckenstein, S. *Anal. Chem.* **1972**, *44*, 1983–1992.
(2) Miller, B.; Bruckenstein, S. *Anal. Chem.* **1974**, *46*, 2026–2033.
(3) Blaedel, W. J.; Engstrom, R. C. *Anal. Chem.* **1978**, *50*, 476–479.
(4) Blaedel, W. J.; Wang, J. *Anal. Chem.* **1980**, *52*, 76–80.
(5) Blaedel, W. J.; Iverson, D. *Anal. Chem.* **1979**, *49*, 1563–1566.
(6) Blaedel, W. J.; Wang, J. *Anal. Chem.* **1981**, *53*, 78–80.
(7) Blaedel, W. J.; Wang, J. *Anal. Chim. Acta* **1980**, *116*, 315–322.
(8) Adams, R. N. "Electrochemistry at Solid Electrodes"; Marcel Dekker: New York, 1969; p 90.

RECEIVED for review January 26, 1981. Accepted May 20, 1981.

Reversed-Phase Liquid Chromatographic Determination of Phenols in Auto Exhaust and Tobacco Smoke as *p*-Nitrobenzeneazophenol Derivatives

Kazuhiro Kuwata,* Michiko Uebori, and Yoshiaki Yamazaki

Environmental Pollution Control Center, 62-3, 1 Chome, Nakamichi, Higashinari-ku, Osaka City 537, Japan

Traces of phenols in auto exhaust and tobacco smoke were collected by using a fritted bubbler with 10 mL of 0.12% sodium hydroxide solution and determined by reversed-phase high-performance liquid chromatography via derivatization with *p*-nitrobenzenediazonium tetrafluoroborate in aqueous medium at pH 11.5. The analytical columns used (20 cm × 4.6 mm i.d.) were packed with LiChrosorb RP-18 (5 μm) and with Polygosil 60-5C_{18}, and the mobile phase was 85% methanol/15% water. Excellent separation of a number of the *p*-nitrobenzeneazo derivatives of water-soluble phenols was obtained. The detection limits of the phenols were 0.05–2.0 ng. Phenol vapors in synthetic air samples, except for *p*-chlorophenol, could be determined in the low parts-per-million or parts-per-billion levels with less than 6.5% of relative standard deviations.

Phenols have received much attention as photochemical products, and as odorous substances or metabolites in environmental, food, and biological studies. The previous article (*1*) discusses numerous methods of determining traces of phenolic compounds in such studies and describes a new method of determining traces of phenol in polluted air by reversed-phase high-performance liquid chromatography (LC) via derivatization with *p*-nitrobenzenediazonium tetrafluoroborate (NBDATFB) in a weak alkaline aqueous medium. In the method, various phenols are well separated as *p*-nitrobenzeneazo (NBA) derivatives by LC. However, quantitative determination is limited to phenol. Phenolic compounds other than phenol give complex peaks that are difficult to identify. Recently, published are several articles for determination of traces of phenols in polluted water by gas chromatography (*2–4*) and for determination of phenols in biological sample by LC via derivatization with diazotized *p*-phenylaniline or 3-methyl-2-benzothiazolinone (*5*) or without derivatization (*6, 7*). Separations of traces of numerous alkylphenols are achieved by LC without derivatization (*8, 9*). These methods, however, seem to give poor separation for phenol isomers, and effects on the analyses of other organics in complex samples are not discussed in detail.

So far, there are few published methods for separately determining trace levels of phenols in polluted gas sample by LC. This article describes an improved method to simultaneously determine a number of water-soluble phenols in low nanogram levels by LC via the derivatization with NBDATFB. Successful applications of the technique for determination of phenols at the low parts-per-million (v/v) or parts-per-billion (v/v) levels in synthetic air samples, auto exhaust, and tobacco smoke are presented.

EXPERIMENTAL SECTION

Reagents and Materials. Phenols used as standards were special grade from Wako Pure Chemical Industries (Osaka, Japan) and Tokyo Kasei Kogyo (Tokyo, Japan). The other chemicals, the solvents, the 0.1% NBDATFB solution and the buffer solution (0.51% sodium bicarbonate/0.21% sodium carbonate) for pH 11.5 used are previously described (*1*). The 200-mL stock solutions containing 1000 μg/mL of the phenols were made by dissolving the compounds in 0.5 mL of methanol and adding distilled water. Standards of lower concentrations were made by appropriately diluting the solutions with distilled water. The sampling solution of the phenol vapors was 0.12% sodium hydroxide aqueous solution. The analytical columns used were 20 cm × 4.6 mm i.d. seamless stainless steel tubes slurry-packed with LiChrosorb RP-18 (5 μm) (E. Merk, Darmstadt, West Germany) and with Polygosil 60-5C_{18} (Machery-Nagel, Dueren, West Germany).

Apparatus. A Water Associates (Milford, MA) ALC/GPC 244 liquid chromatograph equipped with a U6K injector and an ultraviolet (UV) absorbance detector adjusted to 365 nm was employed. The mobile phase was 85% methanol/15% water, and the flow rate was 1.0–1.3 mL/min.

Analytical Procedure. Five to one hundred fifty liters of a gas sample was bubbled at 1–2 L/min through a 30-mL fritted bubbler with 10 mL of the sampling solution. In the case of tobacco smoke, 140 mL of smoke from four puffs were filtered with a Toyo Roshi (Tokyo, Japan) No. 5A paper filter to cut particulate and tar substances off, and bubbled with a carrier of 1 L/min of clean air (*1, 10*). The solution was brought up to 20 mL with distilled water. Five milliliters of the solution was taken in a 15-mL tube, and 1 mL of the buffer solution and 3 mL of the NBDATFB solution were added. After 30 min of standing at room temperature, 1 mL of 1% sodium hydroxide solution was added. One milliliter of carbon tetrachloride was added to the sample, and the mixture was shaken and centrifuged. Then 2–40 μL of the aqueous layer was analyzed by LC for the para-unsubstituted phenols, while 2–10 μL of the organic layer was analyzed for the para-substituted phenols. Identification of the phenols was made by retention time on the LiChrosorb RP-18 and the Polygosil 60-5C_{18} columns, and the quantitation was performed by peak height on either of the columns.

RESULTS AND DISCUSSION

Eighteen water-soluble phenolic compounds were derived with NBDATFB in weak alkaline aqueous solutions and the derived products determined by LC. The derivatization conditions for LC analysis were examined as previously described (*1*).

Adjustment of pH for reaction was made by adding the sodium bicarbonate/sodium carbonate buffer to a sample solution containing 0.06% sodium hydroxide. Optimum pH range for reaction was determined as pH range where maximum UV absorbance for a phenol member of interest was achieved within 15 min after the reaction began. Table I indicates optimum pH ranges of the reaction medium prior to addition of the NBDATFB solution. All of the compounds reacted rapidly with NBDATFB around pH 11.5 in the aqueous medium although the suitable pH ranges for the derivatization were somewhat different for different phenols. The quantitative derivatization was performed with the mole ratio of NBDATFB to phenols being higher than 6:1 for all of the compounds. The reaction of *p*-chlorophenol with NBDATFB was rapid and quantitative but was extremely delayed in the presence of other phenols. The reaction seemed

0003-2700/81/0353-1531$01.25/0 © 1981 American Chemical Society

Table I. Optimum pH Ranges of the Reaction Media for Quantitative Derivatization

phenol	pH range[a]	phenol	pH range[a]
o-chlorophenol	10.5–11.6	2,5-xylenol	11.3–12.5
phenol	10.5–11.6	2,6-xylenol	11.3–12.5
m-cresol	10.5–12.0	2,3-xylenol	11.3–12.5
m-chlorophenol	10.5–11.6	*p*-chlorophenol	10.5–11.6
α-naphthol	10.5–11.6	*p*-cresol	10.5–12.0
o-cresol	10.5–12.0	*p*-ethylphenol	10.5–11.6
m-ethylphenol	10.5–12.5	3,4-xylenol	11.5–12.0
3,5-xylenol	11.3–12.5	2,4-xylenol	11.5–12.0
o-ethylphenol	10.5–12.5		

[a] pH of the reaction medium prior to addition of the NBDATFB solution.

Table II. Stability of the NBA Derivatives of the Phenols

phenol	concn as phenol,[a] μg/mL	absorbance,[b] × 10² 0 day[c]	4 days[c]	7 days[c]
o-chlorophenol	11.7	0.402	0.461	0.464
phenol	2.54	0.880	0.880	0.887
m-cresol	11.3	0.732	0.710	0.731
m-chlorophenol	10.2	0.507	0.500	0.524
α-naphthol	11.9	0.398	0.373	0.314
o-cresol	13.3	0.732	0.710	0.731
m-ethylphenol	4.75	0.518	0.496	0.500
3,5-xylenol	9.60	0.597	0.579	0.552
o-ethylphenol	6.75	0.536	0.515	0.523
2,5-xylenol	8.99	0.392	0.374	0.354
2,6-xylenol	4.18	0.300	0.310	0.274
2,3-xylenol	9.28	0.333	0.321	0.299
p-chlorophenol[d]	17.8	0.223	0.203	0.227
p-cresol[d]	3.83	0.253	0.237	0.246
p-ethylphenol[d]	5.12	0.282	0.262	0.287
3,4-xylenol[d]	4.86	0.349	0.302	0.330
2,4-xylenol[d]	7.46	0.232	0.214	0.227

[a] Concentration of phenol in an aqueous sample prior to derivatization. [b] Calculated from peak height for 2 μL of a final sample injected. [c] Storage time (at 25 °C). [d] Absorbance was determined by using the organic layer.

to occur after the other phenols reacted. An excessive amount of NBDATFB was required to accelerate the reaction. β-Naphthol reacted with NBDATFB but could not be accurately determined for the derivatization products.

Addition of 0.1% of sodium hydroxide to the aqueous medium was useful to stabilize the NBA derivatives of the phenols while still ensuring protection of the analytical columns. Table II shows that the UV absorbance of the derivatives remained constant at least for 4–7 days although the absorbance for *o*-chlorophenol and *m*-chlorophenol tended to increase with time.

The analytical columns packed with LiChrosorb RP-18 (5 μm) and with Polygosil 60-5C_{18} offered 11600 and 12500 theoretical plates (17.2 and 16.2 μm of HETP), respectively, for phenol. Table III indicates retention times of the NBA derivatives of the phenols on the columns. The relative standard deviations of the retention times on the columns were less than 0.6% more than on a day when the analytical conditions were not changed. Good separations of a number of the NBA derivatives were obtained on the columns. Figure 1 shows typical liquid chromatograms of the NBA derivatives of the phenols on the LiChrosorb RP-18 column. Separation aspects on the two columns were similar. The LiChrosorb column offered overlapped elutions for 2,3-xylenol and 2,6-xylenol and a separate peak for 2,5-xylenol, while the Polygosil column gave overlapped peaks of 2,5-xylenol and 2,6-xylenol and a separate peak for 2,3-xylenol from the two compounds.

Table III. Retention Times of the NBA Derivatives of the Phenols on the Analytical Columns

phenol	retention time, min: LiChrosorb RP-18[a]	Polygosil 60-5C_{18}[b]
o-chlorophenol	3.46	3.60
phenol	3.89	4.44
m-cresol	4.60	5.20
m-chlorophenol	4.72	5.00
α-naphthol	4.94	5.94
o-cresol	4.97	5.54
m-ethylphenol	5.09	6.00
3,5-xylenol	5.58	6.24
o-ethylphenol	5.70	6.42
2,5-xylenol	5.89	6.60
2,6-xylenol	6.16	6.42
2,3-xylenol	6.18	6.70
p-chlorophenol	6.66	7.20
p-cresol	7.34	7.66
p-ethylphenol	8.79	9.08
β-naphthol	9.59	9.90
3,4-xylenol	10.81	10.82
2,4-xylenol	12.68	12.16

[a] Column pressure, 2000 psi; flow rate of the mobile phase, 1.3 mL/min. [b] Column pressure, 1500 psi; flow rate of the mobile phase, 1.1 mL/min.

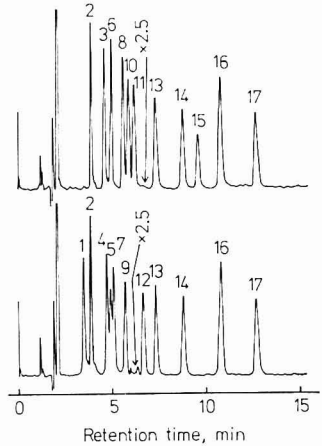


Figure 1. Liquid chromatograms of the NBA derivatives of the phenols. Conditions: column, LiChrosorb RP-18 (20 cm × 4.6 mm i.d.); mobile phase, 85% methanol/15% water; flow rate, 1.3 mL/min; pressure, 2000 psi; phenols injected, 10–40 ng. Peak identity: (1) *o*-chlorophenol, (2) phenol, (3) *m*-cresol, (4) *m*-chlorophenol, (5) α-naphthol, (6) *o*-cresol, (7) *m*-ethylphenol, (8) 3,5-xylenol, (9) *o*-ethylphenol, (10) 2,5-xylenol, (11) 2,6-, 2,3-xylenol, (12) *p*-chlorophenol, (13) *p*-cresol, (14) *p*-ethylphenol, (15) β-naphthol, (16) 3,4-xylenol, (17) 2,4-xylenol.

On the other hand, the Polygosil column offered a complete separation between *o*-cresol and *m*-ethylphenol that the LiChrosorb column could not produce. The two columns offered a very similar performance for quantitative determination of the phenols.

The analysis of the phenols via the derivatization offered two advantages over LC analysis without the derivatization. One was the increased sensitivities by 10–30 times and another was the reduced effects of other organic compounds. Table IV indicates the detection limits (a response to twice the noise level) and the linear calibration ranges for the phenols. Because the NBA derivatives of para-substituted phenols, such

Table IV. Determination Ranges of the Phenols

phenol	detection limit, ng	linear range,[a] μg/mL min	max
o-chlorophenol	0.5	1.00	200
phenol	0.05	0.50	160
m-cresol	0.1	0.50	80
m-chlorophenol	0.5	1.00	200
α-naphthol	0.5	0.50	140
o-cresol	0.1	0.50	80
m-ethylphenol	0.2	0.50	160
3,5-xylenol	0.2	0.50	120
o-ethylphenol	0.3	0.50	160
2,5-xylenol	0.2	0.50	120
2,6-xylenol	0.2	0.50	160
2,3-xylenol	0.2	0.50	120
p-chlorophenol[b]	2.0	4.00	160[c] (40[d])
p-cresol	0.5	0.50	160[c] (20[d])
p-ethylphenol	1.0	2.00	160[c] (40[d])
3,4-xylenol	0.5	1.00	160[c] (10[d])
2,4-xylenol	0.5	1.00	160[c] (10[d])

[a] Concentration of phenol in an aqueous sample prior to derivatization; 2 μL of a final sample were analyzed on the LiChrosorb RP-18 column. [b] Examined for samples containing *p*-chlorophenol only. [c] Calibrated by using the organic layer. [d] Calibrated by using the aqueous medium.

as *p*-chlorophenol, *p*-cresol, *p*-ethylphenol, 3,4-xylenol, and 2,4-xylenol, had poor water solubility, determination of the phenols by using the aqueous medium was limited to low concentration levels. However, when the aqueous medium was shaken with carbon tetrachloride after addition of 0.1% of sodium hydroxide, the NBA derivatives of the para-substituted phenols were completely extracted into the organic layer while the NBA derivatives of the para-unsubstituted phenols remained in the alkaline aqueous layer and were not

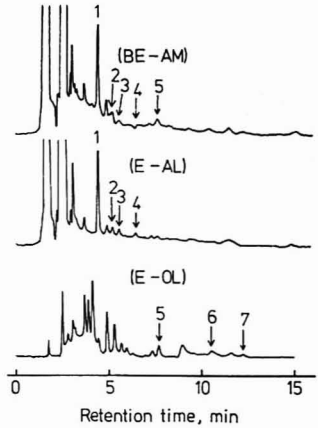


Figure 2. Effects of organic substances on determination of phenols in tobacco smoke (Peace). Conditions: column, Polygosil 60-5C_{18} (20 cm × 4.6 mm i.d.); mobile phase, 85% methanol/15% water; flow rate, 1.1 mL/min; pressure, 1500 psi. Aqueous medium before extraction (BE-AM), (1) phenol, (2) *m*-cresol, (3) *o*-cresol, (4) *o*-ethylphenol, 2,6-xylenol, (5) *p*-cresol; extraction–aqueous layer (E-AL), (1) phenol (2.40 ng), (2) *m*-cresol (0.29 ng), (3) *o*-cresol (0.25 ng), (4) *o*-ethylphenol, 2,6-xylenol; extraction - organic layer (E-OL), (5) *p*-cresol (1.47 ng), (6) 3,4-xylenol, (7) 2,4-xylenol.

detected in the organic layer. Thus, calibrations of the para-substituted phenols could be made by using the organic layer, and their linear calibration ranges were in the same levels as those of the para-unsubstituted phenols obtained by using the aqueous layer. The relative standard deviations of

Table V. Determination of the Phenols in Synthetic Air Samples

phenol	concn of phenol[a] ± std dev,[b] ppm (v/v) (RSD,[c] %) sample 1	sample 2	sample 3	sample 4	sample 5
o-chlorophenol				5.74 ± 0.284 (4.9)	
phenol	0.451 ± 0.0120 (2.7)		3.01 ± 0.152 (5.0)		27.3 ± 0.96 (3.5)
m-cresol	0.881 ± 0.0469 (5.3)		2.57 ± 0.080 (3.1)		16.0 ± 0.54 (3.4)
m-chlorophenol		0.501 ± 0.0185 (3.7)		3.78 ± 0.243 (6.4)	
o-cresol	1.01 ± 0.034 (3.4)		2.53 ± 0.095 (3.8)		18.8 ± 0.43 (2.3)
m-ethylphenol	0.612 ± 0.0215 (3.5)		1.74 ± 0.089 (5.1)		8.49 ± 0.382 (4.5)
3,5-xylenol		0.524 ± 0.0183 (3.5)		2.59 ± 0.097 (3.7)	
o-ethylphenol	0.905 ± 0.0305 (3.4)		2.11 ± 0.047 (2.2)		14.1 ± 0.29 (2.1)
2,5-xylenol		0.768 ± 0.0227 (3.0)		2.71 ± 0.121 (4.5)	
2,3-xylenol		0.794 ± 0.0179 (2.3)		2.24 ± 0.130 (5.8)	
p-chlorophenol			6.87 ± 1.157 (16.8)		1.20 ± 0.172 (14.3)
p-cresol	2.59 ± 0.089 (3.4)		3.11 ± 0.112 (3.6)		5.08 ± 0.213 (4.2)
p-ethylphenol	1.91 ± 0.101 (5.3)		1.86 ± 0.121 (6.5)		1.69 ± 0.061 (3.6)
3,4-xylenol	1.07 ± 0.019 (1.8)		1.42 ± 0.068 (4.8)		1.21 ± 0.067 (5.5)
2,4-xylenol	2.87 ± 0.081 (2.8)		0.636 ± 0.0401 (6.3)		3.03 ± 0.167 (5.5)

[a] Average concentration of phenol in 6 runs. [b] Std dev, standard deviation. [c] RSD, relative standard deviation.

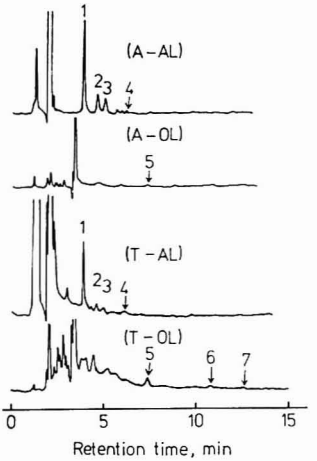


Figure 3. Analysis of phenols from polluted gases. Conditions, see Figure 1. Aqueous layer of an auto exhaust sample (A-AL): (1) phenol (9.17 ng), 1.46 ppm; (2) *m*-cresol (2.32 ng), 0.322 ppm; (3) *o*-cresol (1.76 ng), 0.231 ppm; (4) 2,6-, 2,3-xylenol (less than 0.2 ng). Organic layer of the auto exhaust sample (A-OL): (5) *p*-cresol (less than 0.5 ng). Aqueous layer of a tobacco smoke sample (T-AL) (Cherry): (1) phenol (2.45 ng), 490 μg/cigarette; (2) *m*-cresol (0.22 ng), 44.4 μg/cigarette; (3) *o*-cresol (0.16 ng), 32.3 μg/cigarette; (4) 2,6-, 2,3-xylenol (less than 0.2 ng). Organic layer of the tobacco smoke sample (T-OL) (Cherry): (5) *p*-cresol (1.12 ng), 60.8 μg/cigarette; (6) 3,4-xylenol (less than 0.5 ng); (7) 2,4-xylenol (less than 0.5 ng).

determined values of *p*-chlorophenol and the other phenols for standard samples were 4.0–6.9% and 1.2–5.6%, respectively, in the linear ranges. The relative standard deviations near the detection limits were 12–15%. Effects on the analysis of background peaks caused by organics in polluted gas were much reduced compared to ones previously reported (*1*). Even in the case of an extremely polluted gas such as tobacco smoke, background effects were minimized by the extraction technique. Figure 2 shows that unknown organics which appeared around the phenol, *m*-cresol and *o*-cresol peaks were transferred into the organic layer while little background peaks were observed at the *p*-cresol peak in the organic layer.

For investigation on the collection efficiency in the sampling system and on the accuracy of analysis of gas samples, 50 L of air samples containing 0.4–28 ppm of the phenol vapors were prepared in polyester bags by vaporizing the phenols dissolved in 0.3 mL of methanol at 80 °C for 1 h. Five liters of the synthetic samples were sampled at 25 °C three times at 1 L/min and three times at 2 L/min through two fritted bubblers with 10 mL of the sampling solution (six runs in total), and analyzed by the method presented. Stable vapor of α-naphthol was not obtained because of its low vapor pressure. The phenols of interest were completely trapped in the first bubbler and not detected in the second bubbler.

Table VI. Phenols in Auto Exhaust and Tobacco Smoke

sample	phenol found: phenol	*m*-cresol	*o*-cresol	*p*-cresol
Auto Exhaust,[a] ppm (v/v)				
Toyota Engine Model HMS87V (1977)				
no. 1	1.46	0.332	0.231	ND[b]
no. 2	1.24	0.310	0.210	ND
no. 3	1.28	0.263	0.168	ND
Tobacco Smoke,[c] μg/cigarette				
Hi-lite (Japan)	520	47.5	36.1	49.4
Seven-star (Japan)	314	51.7	34.5	37.4
Cherry (Japan)	503	42.4	35.2	60.8
Peace (Japan)	481	58.1	49.7	59.1

[a] Sample volume was 20 L. [b] ND, not detectable. [c] Average value in three runs.

Table V reports that the phenol vapors, except for *p*-chlorophenol, can be determined in the low parts-per-million or parts-per-billion levels with less than 6.5% of relative standard deviations.

Phenols in auto exhaust and tobacco smoke were determined. For auto exhaust, 20 L of gas was directly sampled from the exhaust vent of the engine operated at 2000 rpm. Identification of the phenols was performed by using the two columns and by changing methanol percentages in the mobile phase from 80 to 90%. Table VI reports analytical data of the polluted gases, and Figure 3 shows typical liquid chromatograms of the NBA derivatives of phenols from the sources. Cresols, other than phenol, were determined in the gases. Other phenolic compounds were difficult to identify or to quantitate because of the limited analytical sensitivities.

In closing, it is suggested that the technique by using LC might be applicable to determination of phenols in various samples other than polluted airs.

ACKNOWLEDGMENT

Authors cordially thank K. Negoro, Faculty of Engineering, Hiroshima University, for his continuous encouragement and advice in the study.

LITERATURE CITED

(1) Kuwata, K.; Uebori, M.; Yamazaki, Y. *Anal. Chem.* **1980**, *52*, 857–860.
(2) Prater, W. A.; Simmons, M. S.; Mancy, K. H. *Anal. Lett.* **1980**, *13*, 205–212.
(3) Voznakova, Z.; Popl, M. *J. Chromatogr. Sci.* **1979**, *17*, 682–686.
(4) Coutts, R. T.; Hargesheimer, E. E.; Pasutto, F. M. *J. Chromatogr.* **1979**, *179*, 291–299.
(5) Walter, W. M., Jr.; Purcell, A. E. *J. Agric. Food Chem.* **1979**, *27*, 942–946.
(6) Walter, W. M., Jr.; Purcell, A. E.; McCollum, G. K. *J. Agric. Food Chem.* **1979**, *27*, 938–941.
(7) Needham, L. L.; Hill, R. H., Jr.; Sirmans, S. L. *Analyst (London)* **1980**, *105*, 811–813.
(8) Shabron, J. F.; Hutubise, R. J.; Silver, H. F. *Anal. Chem.* **1979**, *51*, 1426–1433.
(9) Organ, K.; Katz, E. *Anal. Chem.* **1981**, *53*, 160–163.
(10) Kuwata, K.; Uebori, M.; Yamazaki, Y. *J. Chromatogr. Sci.* **1979**, *17*, 264–268.

RECEIVED for review March 2, 1981. Accepted May 6, 1981.

CORRESPONDENCE

Anion Peak Migration in Ion Chromatography

Sir: The use of ion chromatography, first described in 1975 (*1*) for the characterization of a variety of solutions with respect to their anionic and cationic composition is well documented (2–6). Mixed eluents containing various ratios of the carbonate–bicarbonate species are routinely used for the elution and separation of common anions in the standard methodology. As with all chromatographic techniques, the most effective use of the ion chromatographic process requires accurate characterization of the retention times of individual species and identification of analysis parameters which effect the retention characteristics of these species. In this correspondence, the behavior of the species of primary interest in ion chromatography (chloride, sulfate, and nitrate) is summarized and an explanation for the observed phenomenon proposed.

EXPERIMENTAL SECTION

Instrumentation. All chromatograms were obtained with a commercial Dionex Model 14 ion chromatograph equipped with a standard 3 × 500 mm anion separator column and a 6 × 250 mm suppressor column. Sample loop volume was 0.1 mL, conductivity detector response was maintained at 10 $\mu\Omega^{-1}$/cm full scale deflection and laboratory temperature was maintained at 22 ± 2 °C.

Reagents. Eluents used throughout the course of this study were prepared by dissolution of the appropriate amount of reagent grade Na_2CO_3 and $NaHCO_3$ in type II deionized water. Eluents are allowed to stabilize for a period of not less than 3 h before utilization; the pH of these eluents is recorded just prior to utilization. All samples analyzed are prepared by dilution of standard solutions; the concentrations of Na_2CO_3 and $NaHCO_3$ in the sample and the eluent used are rigidly matched. Standard solutions for chloride and nitrate are prepared by dissolution of their sodium salt while the sulfate standard is a 0.02 N H_2SO_4 solution manufactured by the Hach Chemical Co.; the normality of this solution was confirmed by titration with a standard base.

RESULTS AND DISCUSSION

Effect of Eluent Flow Rate. The effect of eluent flow rate on anion retention time is summarized in Table I. Increasing the flow rate causes a proportional decrease in retention time; this decrease in retention time is not dependent on the identity of the anion of interest as is illustrated by the constant ratio of retention time noted. These data illustrate that the ion chromatographic mechanism is significantly different than that predicted from the linear, nonideal rate theory of chromatography; the data agree poorly with respect to the von Deemter relationship which expresses the theoretical effect of flow rate of the mobile phase on the retention time of the soluble species for this treatment.

Effect of Solute Concentration. Table II summarizes the effect of changing concentrations of sulfate on the retention of itself and nitrate in the chromatographic system; a 300-fold increase in sulfate concentration has no effect on the elution characteristics of these species. As is illustrated in Table III, however, the concentration of nitrate in a sample clearly effects its elution characteristics; changes of retention times of up to 1.5 min as the concentration changes from 10 to 70 ppm are noted. Above this threshold concentration, the nitrate migration is less profound. The data indicate that the nitrate experiences an interaction with the exchange resin governed by nonlinear isotherms at concentrations less than 70 ppm and further suggest that the nonlinear behavior involves the desorption of the nitrate from the resin by the eluent ions.

Table I. Effect of Flow Rate on Anion Retention Time

flow rate		retention time, min		retention ratio
%	mL/min	NO_3^-	SO_4^{2-}	
10	0.76	15.9	11.8	1.347
15	1.26	9.6	7.2	1.333
20	1.74	7.1	5.3	1.340
30	2.36	4.6	3.4	1.353
40	2.59	3.4	2.6	1.308
50	3.54	2.8	2.1	1.308
60	5.33	2.2	1.6	1.341

Table II. Effect of Sulfate Concentration on Anion Retention Time

sulfate concn, ppm	retention time, min	
	NO_3^-	SO_4^{2-}
0	9.8	
50	9.7	7.2
100	9.8	7.2
200	9.8	7.2
300	9.7	7.2

Table III. Effect of Nitrate Concentration on Its Own Elution

concn, ppm	retention time, min	
	a	*b*
5		17.4
10	13.8	17.0
20	13.5	16.9
25		16.8
30	13.3	16.3
40	12.9	16.2
50	12.6	16.1
60	12.3	15.9
70	12.0	15.8
100	11.7	15.7

[a] In 0.003 M $NaHCO_3$/0.002 M Na_2CO_3 eluent, 25% flow rate. [b] In 0.003 M $NaHCO_3$/0.006 M Na_2CO_3 eluent, 10% flow rate.

Effect of Eluent Composition. The effect of eluent composition on the relative retention characteristics of the sulfate, nitrate, and chloride peaks is quite profound. Table IV illustrates the effect of eluent pH, ionic strength, and absolute bicarbonate and carbonate concentration on the elution characteristics. Trends noted include (1) that the behavior of the sulfate species is more profoundly effected by eluent composition, (2) that changing the concentration of carbonate has a larger net effect than changing the bicarbonate concentration, and (3) that in cases where the ionic strength was maintained, pH had no effect on the elution characteristics of the three species. The trends noted in the

0003-2700/81/0353-1535$01.25/0 © 1981 American Chemical Society

Table IV. Effect of Eluent Composition on Anion Retention

composition[a]	eluent properties: pH	ionic strength,[b] M	Cl^-	SO_4^{2-}	NO_3^-
0.001/0.001	10.10	0.0050	6.4		22.0
0.003/0.001	9.87	0.0063	6.0		20.4
0.003/0.002	10.11	0.0099	5.2	26.8	16.0
0.003/0.005	10.38	0.0171	4.5	14.7	12.4
0.006/0.005	10.22	0.0198	4.4	13.8	11.8
0.009/0.005	10.03	0.0025	4.3	12.7	11.1
0.003/0.007	10.56	0.0237	4.4	10.8	10.8
0.012/0.005	9.89	0.0252	4.3	12.2	10.7
0.009/0.007	10.17	0.0292	4.2	10.0	10.2
0.003/0.009	10.74	0.0315	4.1	8.8	9.9
0.012/0.009	10.17	0.0396	3.9	7.8	8.8
0.23/0.019	10.25	0.0792	3.5	5.2	7.4

[a] (mol/L of $NaHCO_3$)/(mol/L of Na_2CO_3). [b] Calculated assuming no significant ion pair formation.

Table V. Ion Size Parameters for Selected Anions

anion	ion size, Å	anion	ion size, Å
Cl^-	1.81[a]	SO_4^{2-}	2.30[b]
NO_3^-	1.89[b]	CO_3^{2-}	1.85[b]
		HCO_3^-	1.63[b]

[a] Pauling crystal radii (7). [b] Yatsimirskii thermochemical radii (8).

first two instances above are tentatively explained as illustrating ionic size/charge effects. The sequence of ionic size ($SO_4^{2-} > NO_3^- > Cl^-$) from Table V accurately mirrors the relative effect that increased carbonate and bicarbonate concentration in the eluent has on the species retention characteristics. This ionic size phenomenon has been attributed to the buildup of steric stress in the resin structure (9). The observation that increased carbonate ion concentration effects elution more than bicarbonate concentration reflects the electrostatic difference between the two species. Observation 3 allows us to conclude that the pH per se has no significance in determining the retention time of the species studied. It is proposed that pH effects the elution characteristics only by effecting the overall ionic strength of the eluent; in the systems studied in this paper, the effect of the OH^- ion on the total ionic strength was minimal and therefore no pH dependent behavior was observed.

LITERATURE CITED

(1) Small, H.; Stevens, T.; Bauman, W. *Anal. Chem.* **1975**, *47*, 1801.
(2) Wetzel, R. *Environ. Sci. Technol.* **1979**, *13*, 1214.
(3) Wetzel, R.; Anderson, C.; Schleicher, H.; Crook, D. *Anal. Chem.* **1979**, *51*, 1532.
(4) Hansen, L.; Richter, B.; Rollins, D.; Lamb, J.; Eutough, D. *Anal. Chem.* **1979**, *51*, 633.
(5) Lathouse, J.; Coutant, R. In "Ion Chromatographic Analysis of Environmental Pollutants"; Ann Arbor Science Publishers: Ann Arbor, MI, 1978.
(6) Gjerde, D.; Schmuckler G.; Fritz, J. *J. Chromatogr.* **1980**, 187, 35.
(7) Pauling, L. "The Nature of the Chemical Bond"; Cornell University Press: Ithaca, NY, 1960; p 514.
(8) Waddington, T. *Adv. Inorg. Chem.* **1959**, *1*, 180.
(9) Peters, D.; Hayes J.; Hefţje, G. "Chemical Separations and Measurements"; W. B. Saunders: Philadelphia, PA, 1974; p 583.

Dennis Jenke
Montana Energy and MHD Research and Development Institute
P.O. Box 3809
Butte, Montana 59702

RECEIVED for review March 23, 1981. Accepted May 7, 1981.

Comparative Precision of Silver Inquartation Techniques

Sir: Local assayers have recently noted a decrease in the precision of results obtained by using manufactured solid inquarts and have switched to solution inquartation, claiming vastly superior precision. The manufacturer contended that the solid inquarts gave results as good as can be obtained by fire assaying (*1*). It had been our observation that the precision of inquartation was limited by the fire assay process and that precision equal to the precision of pipetting could not be obtained, as some assayers were claiming. The precision is of interest, since the average weight of inquarts assayed as blanks is subtracted from the bead weight to obtain the weight of silver in the assayed sample of ore. The precision thus determines the detection limit for gravimetric determination of silver. We undertook comparative inquartation studies to resolve the conflicting statements.

EXPERIMENTAL SECTION

To study the precision of solution inquartation, we added 5-mL aliquots of a freshly prepared solution of 400 ppm silver (as silver nitrate) in 1% (v/v) nitric acid to a series of crucibles containing weighed portions (85 g) of a sample–flux–reducing agent mixture prepared in large batches (3000 g of silver-free litharge, 150 g of borax glass, 900 g of sodium carbonate, 900 g of silica, and 150 g of flour). The portion of the mixture taken corresponded to a sample of 15 g of silica, using a flux very close to that recommended by Bugbee for a bisilicate slag after production of the recommended size button (*2*). The solution inquarted crucibles were dried in a 95 °C oven for several hours and at 105 °C overnight.

To study the precision of the solid inquarts, we obtained new vials of inquarts from the manufacturer, older vials from local assayers, and very old boxes (in some cases more than 10 years past manufacture) obtained from forgotten storeroom supplies. Studies were performed on unbiased splits of 10 inquarts obtained by reduction of sample size by repeated employment of a Soiltest 10-in. splitter starting with the original box or vial of 1000 pieces. These inquarts were weighed and subjected to either of two studies, fusion and cupellation or dissolution and atomic absorption. The fusions and cupellations were performed at 1800 °F by using a large Denver Fireclay Co. electric assay furnace. Beads were weighed on a Cahn Model 26 electronic microbalance. The atomic absorption used was a Perkin-Elmer Model 303 at 10× scale expansion, equipped with recorder readout, an active 0.5-Hz filter, using large zero offset, and air-Mapp gas (*3*). The solutions for atomic absorption were prepared in 125 mL of 20% (v/v) nitric acid. The acid was dispensed with a measured precision of ±0.035% relative standard deviation, equivalent to ±0.0007 mg silver.

A final phase of the study used 1000-μL spikes of silver nitrate solutions of appropriate concentration in addition to either solid

0003-2700/81/0353-1536$01.25/0 © 1981 American Chemical Society

Table I. Results of Atomic Absorption Analyses of Sets of Ten Inquarts (Mean ± Standard Deviation)

manufacturer lot no.	our bottle no.	inquart wt, mg	silver wt, mg	silver concn, %
M	JF	101.77 ± 1.10	2.061 ± 0.028	2.021 ± 0.069
M351	R	103.50 ± 1.07	2.206 ± 0.023	2.132 ± 0.018
M351	S	103.47 ± 01.78	2.192 ± 0.067	2.120 ± 0.067
M2151	M	99.60 ± 2.31	2.221 ± 0.057	2.230 ± 0.027
M5666	RM	100.70 ± 1.16	2.141 ± 0.037	2.126 ± 0.035
M5666	A	99.51 ± 5.16	2.215 ± 0.132	2.159 ± 0.024
C0688	K	93.13 ± 2.53	1.429 ± 0.489	1.455 ± 0.682
		91.16 ± 4.50	1.382 ± 0.444	1.525 ± 0.511
C0688	X	95.81 ± 1.94	1.951 ± 0.052	2.036 ± 0.030
C0688	Y	97.19 ± 1.78	1.976 ± 0.043	2.034 ± 0.035
O40316	1	100.04 ± 0.41	2.050 ± 0.016	2.049 ± 0.016
	2	100.64 ± 0.26	2.052 ± 0.014	2.042 ± 0.014
	3	100.31 ± 0.73	2.052 ± 0.016	2.046 ± 0.020
	4	100.90 ± 0.37	2.052 ± 0.015	2.034 ± 0.019
	5	100.38 ± 0.27	2.053 ± 0.012	2.045 ± 0.011
	6	100.01 ± 0.29	2.049 ± 0.008	2.048 ± 0.012
	7	100.42 ± 0.27	2.046 ± 0.010	2.037 ± 0.010
	8	100.21 ± 0.52	2.045 ± 0.016	2.041 ± 0.015
	9	100.32 ± 0.44	2.049 ± 0.013	2.042 ± 0.011
	10	100.47 ± 0.15	2.049 ± 0.018	2.039 ± 0.018
solution		d.n.a.	1.990 ± 0.007	d.n.a.
solution		d.n.a.	2.211 ± 0.004	d.n.a.

Table II. Results of Fire Assay of Sets of Ten Inquarts (Mean ± Standard Deviation)

manufacturer lot no.	our bottle no.	inquart wt, mg	silver wt, mg	silver concn, %
C0688	K	92.85 ± 5.83	1.419 ± 0.429	1.429 ± 0.620
		90.63 ± 6.06	1.431 ± 0.397	1.596 ± 0.478
C0688	X	94.71 ± 1.60	1.822 ± 0.031	1.929 ± 0.034
		96.75 ± 1.89	1.909 ± 0.031	1.964 ± 0.061

or solution inquarts. All spiked samples were dried as described above for the solution inquarts.

RESULTS

The results of the atomic absorption study are shown in Table I in approximately the order manufactured. Sporadic evidence of historical problems with control of inquarts weights is evident from comparison of the newest lot (no. 040316, which showed a relative standard deviation of weight of the inquart itself of ±0.1% to ±0.7%) with the earlier manufactured lots. The earliest lots were found to have typical weight variations of approximately ±1% or 2% rsd. However, one vial of each of two more recent lots showed relative standard deviations of as much as ±5%. In one case, the concentration of silver in the inquart (obtained by dividing individual silver bead weight by the individual inquart weight before calculation of the mean and standard deviation) showed a relative standard deviation as small as expected, based on the experience with earlier lots. In another case, however, the relative standard deviation of silver concentration was approximately ±40%. This was ascribed to a second problem with manufacture, errors in control of the homogeneity of the nominally 2% silver–lead alloy. These results were confirmed by our preliminary fire assay study, the results of which are shown in Table II. That the error is not limited by the atomic absorption can be ascertained by comparison with the results for the solutions at the bottom of Table I.

In Table III are results of fire assays of sets of both solution in quarts and the newest manufactured lot of solid inquarts. The small sample size experiments ($n = 3$ and $n = 5$) were undertaken to illustrate the apparent precision which would be measured if common assay practice (a large number of samples and a small number of blank inquarts) were followed. The five sets of 10 were taken to allow more detailed statistical analysis. None of these experiments were paired. The results

Table III. Comparison of Fire Assay of Solid Inquarts and Solution Inquarts (Mean ± Standard Deviation)

	silver bead weight, mg	
n	solid[a]	solution
10	1.899 ± 0.017	1.901 ± 0.017
	1.910 ± 0.028	1.908 ± 0.031
	1.895 ± 0.023	1.914 ± 0.037
	1.904 ± 0.019	1.927 ± 0.022
	1.905 ± 0.027	1.916 ± 0.019
5	1.883 ± 0.023	1.889 ± 0.034
	1.890 ± 0.024	1.888 ± 0.020
	1.913 ± 0.030	1.873 ± 0.029
3	1.898 ± 0.003	1.908 ± 0.016
	1.888 ± 0.016	1.905 ± 0.006
	1.882 ± 0.015	1.917 ± 0.049
	1.887 ± 0.017	1.898 ± 0.043
	1.902 ± 0.030	1.893 ± 0.031

[a] Lot 040316 bottle 1.

of assays of five sets of 10 inquarts were found to have homogeneous variances and means at the 95% level of confidence when examined by using Bartletts χ^2 and the F test, respectively (4, 5). The grand standard deviation for these five sets of 10 each (45 degrees of freedom) was found to be ±0.022 mg for the solid inquarts and ±0.027 for the solution inquarted samples. Overall, the standard deviations (67 degrees of freedom) for the data in Table III were found to be ±0.022 for solid inquarts and ±0.028 mg for solution inquartation after χ^2 and F testing revealed homogeneity throughout. These values are indistinguishable from one another at the 95% level.

In Table IV are results of spiking both solution and solid inquarted sample–flux–reducing agent mixtures. The experiments with the lower level spikes were repeated. All four experiments were separate and unpaired. The data were

Table IV. Experimental Verification of Detection Limits, Using Spiked Samples

amt of silver added, mg	no. assayed	solid inquarts				solution inquarts			
		mean, mg	range, mg	blank	detected	mean, mg	range, mg	blank	detected
blank	5	1.883	0.056	a	d.n.a.	1.878	0.076	c	d.n.a.
	5	1.879	0.039	b	d.n.a.	1.888	0.080	d	d.n.a.
0.000	2	1.908	0.002	a	N	1.875	0.031	c	N
	2	1.868	0.047	b	N	1.908	0.033	d	N
0.010	2	1.928	0.071	a	N	1.916	0.055	c	N
	2	1.939	0.011	b	N	1.912	0.050	d	N
0.025	2	1.924	0.009	a	N	1.925	0.004	c	N
	2	1.918	0.032	b	N	1.934	0.059	d	N
0.050	2	1.915	0.016	a	N	1.987	0.021	c	N
	2	1.947	0.028	b	N	1.950	0.025	d	N
0.075	2	1.860	0.093	a	N	1.980	0.009	c	N
	2	2.001	0.041	b	Y	1.988	0.021	d	N
0.100	2	1.981	0.021	a	Y	1.998	0.019	c	Y
	2	2.025	0.013	b	Y	2.020	0.002	d	Y
0.250	2	2.155	0.042	a	Y	2.162	0.087	c	Y
0.500	2	2.371	0.031	a	Y	2.346	0.003	c	Y
0.750	2	2.586	0.036	a	Y	2.586	0.024	c	Y
1.000	2	2.848	0.026	a	Y	2.838	0.041	c	Y

tested by using the substitute t test employing ranges and means (6). The appropriate mean from the applicable set of five blanks (e.g., blank a) was compared to that from the pair of spiked samples run with the blanks (e.g., those means labeled a in each case), to see if they were the same (the null hypothesis) or whether there was a significant difference between them (the silver was detected). The columns headed "detected" summarize the results of these substitute t tests at the 0.05 level of significance.

DISCUSSION

The historical evidence of problems with control of both the weights and homogeneity of composition of solid inquarts shows that examination of each new vial and lot is warranted, before assuming that the inquarts can be used as received, as has been common assay practice.

The results of the work support our observation that the standard deviation of solution inquartation was substantially larger at ±0.028 mg than the error of ±0.0009 mg which the pipetting error (±0.043% relative) would predict for the 2-mg beads, suggesting control by factors inherent in the fusion and cupellation steps.

The comparison of solid and solution inquarts supports the contention of the manufacturer that solid inquarts give results as good as can be obtained by fire assaying. The use of inquarts of current manufacture (which we found to give ±0.022 mg standard deviation) and solution inquartation (±0.028 mg) gave statistically indistinguishable results.

Experiments with spiked samples showed that estimates of detection limits in routine assay (duplicate samples and five blanks) are such that results are best reported positive only when above 0.1 mg. Below this level, direct instrumental determination of silver by atomic absorption, perhaps incorporating fire assay preconcentration with arrested cupellation or using other precious metals (such as gold, platinum, or palladium (7) as the inquart material. (See, for example, ref 8.)

ACKNOWLEDGMENT

We are indebted to Don Book of the College of Agriculture, University of Nevada, Reno, for advice on statistics, to Robert De Palma of Bico-Braun International for supplying inquarts from the new lot and for candid conversations, and to Mary Kilby, of Rocky Mountain Geochemical Corp., and to Dan Kappes, Registered Professional Engineer, both of whom supplied some of the older inquarts used.

LITERATURE CITED

(1) de Palma, R., Bico-Braun International, Burbank, CA, private communication.
(2) Bugbee, E. "A Textbook of Fire Assaying"; Wiley: New York, 1922; p 163.
(3) Mansell, R. *At. Absorpt. Newsl.* **1967**, *6*, 6–8.
(4) Ostle, H. "Statistics in Research", 2nd ed.; The Iowa State University Press: Ames, IA, 1963; p 136.
(5) Crow, E.; Davis, F.; Maxfield, M. "Statistics Manual"; Dover Publications: New York, 1960; p 124.
(6) Bauer, E. "A Statistical Manual for Chemists", 2nd ed.; Academic Press: New York, 1971; p 69.
(7) Beaulieu, P. L. "Palladium Inquarts in the Classical Gravimetric Fire Assay and Fire Assay Collection-Atomic Absorption"; in progress.
(8) Haffty, J.; Riley, L.; Goss, W. *Geol. Surv. Bull. (U.S.)* **1977**, *No. 1445*.

[1] Current address: Amoco Research Center, P.O. Box 400, Naperville, IL 60540.

Patrick L. Beaulieu*[1]
Brenda A. Keller
Tamela R. Wortman

Nevada Mining Analytical Laboratory
Mackay School of Mines
University of Nevada, Reno
Reno, Nevada 89557

RECEIVED for review January 16, 1981. Resubmitted March 20, 1981. Accepted March 20, 1981.

AIDS FOR ANALYTICAL CHEMISTS

Thin-Layer Spectroelectrochemical Cell for Nonaqueous Solvent Systems

Rathbun K. Rhodes[1] and Karl M. Kadish*

Department of Chemistry, University of Houston, Houston, Texas 77004

Many advancements have been made in OTTLE (optically transparent thin-layer electrode) cell design since the initial report of the glass slide-gold minigrid assembly (*1*) for spectroelectrochemistry. These include the capability for monitoring in the ultraviolet (*2*) and infrared (*3*) spectral regions, the ability to perform precise (*4*) and cryogenic (*5*) temperature studies, and the flexibility of several working electrode materials (*6–8*). In addition, cells have been specifically designed to allow for ease of solution deoxygenation (*9*), for reduction of uncompensated solution resistance (*10*), and for characterization of eluent compounds in a flowing chromatographic system (*11*). However, little has been reported concerning the applicability of cells to a diversity of solvent systems.

Historically, most thin-layer studies have been restricted to aqueous solutions (*12–14*) and to nonaqueous solvents like dimethylformamide and acetonitrile (*2, 3, 15–19*). While these solvents are extremely useful, they are not universal from either solubility or mechanistic points of view. It would be highly desirable to have a design which is both easy to construct and inert to solvents of a wide range of dielectric constant and binding properties. It is the purpose of this paper to report several modifications to the basic OTTLE design (*1*) which make this possible.

In past cell designs, the inability to use particular solvents usually resulted from dissolution of one of the cell components. This dissolution process either contaminated the solution of interest or caused severe leakage problems at one of the sealant junctions (*20*). Replacement of these more interactive components (Plexiglas, glue, silicon rubber, or epoxides) by inert components such as glass and Teflon removed these problems. Described herein is a design which has proved useful in a wide diversity of nonaqueous solvents.

EXPERIMENTAL SECTION

Cell Construction. The complete thin-layer spectroelectrochemical cell used in these studies is shown in Figure 1. The platinum auxiliary (1) and saturated calomel electrode (SCE) reference (7) are of conventional design. The gold minigrid working electrode (3) is formed by clamping a 1000 lines/in. gold minigrid (Buckbee-Mears Co., St. Paul, MN) that is 15 × 5 mm and a 0.25-mm Teflon spacer (Dupont Tefzel, Wilmington, DE) between two glass slides (25 × 9.5 × 1 mm). This assembly is then heated at 300 °C in a muffel furnace for 4–7 min, thus sealing the Tefzel to glass. The resultant heat thinning gives an optical path length of from 0.05 to 0.10 mm. The Teflon lid (4) is 0.625 in. in diameter and 0.20 in. in height. A center cut (0.370 in. × 0.085 in. × 0.200 in.) is made to allow for insertion of the minigrid-slide assembly into the lid. In addition, a circular groove (0.515 in. o.d., 0.410 in. i.d., 0.080 in. deep) is cut into the lid bottom to give a tight fit with the solution reservoir, and a recessed cut (0.340 in. diameter × 0.080 in. deep) is made for easy removal of trapped air bubbles. The solution reservoir (2)–salt bridge assembly (6), separated by a cracked-glass frit (5), can be glass-blown in less than an hour and a half. The dimensions of this unit can be varied to accommodate the requirements of the spectrometer cell compartment. To maintain the integrity of the seals between the reservoir and lid and the lid and minigrid assembly, we applied several strpis of Teflon gasket tape. Devcon 5-min epoxy is then applied to the outer portions of the cell to stabilize the final positioning.

Reagents. Iron tetraphenylporphinato chloride (TPPFeCl) was prepared by acid hydrolysis of the μ-oxo-iron tetraphenylporphyrin dimer $(TPPFe)_2O$ (Strem Chemical Co.) as per the method of Summerville and Cohen (*21*). Ethylene chloride ($EtCl_2$), dimethylformamide (DMF), dimethyl sulfoxide (Me_2SO), and pyridine (Py) (Aldrich Chemicals and Fisher Scientific) were purified by literature methods (*22*) and stored over 4-Å molecular sieves prior to use. The supporting electrolyte tetrabutylammonium perchlorate (TBAP) was obtained from Eastman Chemical, recrystallized twice from an ethyl acetate–pentane mixture and dried in vacuo.

Apparatus. The potential of the working electrode is controlled by a Princeton Applied Research 364 polarographic analyzer (Princeton, NJ) in conjunction with a Hewlett-Packard 3310B triangle wave generator (Palo Alto, CA). Spectra are obtained by externally focusing a 75-W quartz tungsten–halogen lamp (Oriel 6329 source, Stamford, CT) through the thin-layer cell to an optical spectrometer, silicon diode-array detector (Tracor Northern 1223/1150/1710, Middleton, WI). Spectra result from the signal averaging of 100 sequential 5-ms acquisitions. Each acquisition represents a single spectrum from 325 to 950 nm at a resolution of 1.22 nm/channel. For spectrometers with a less intense spectral source, a more transmissive minigrid (100 lines/in.) can be used to obtain comparable spectra.

Procedure. Solutions were made up to be 1.0×10^{-3} M in porphyrin and either 2 or $5 \times 10^{-}$ M in TBAP. Dissolution of porphyrin was aided by an ultrasonic cleaner (Cole-Parmer, Chicago, IL). Since the TN-1710 is a single beam transmission spectrometer, a thin-layer solvent-supporting electrolyte spectral reference was acquired and stored for future absorbance calculations. The reservoir was then emptied and rinsed twice with fresh solvent, the salt bridge filled, and the SCE inserted. Porphyrin solutions were deoxygenated in a 10-mL volumetric flask using dried nitrogen passed through heated copper turnings to remove residual oxygen. Solutions were pushed by a positive nitrogen puressure into the thin-layer reservoir (also under nitrogen), the auxiliary electrode was inserted, and solution was aspirated into the slide assembly. Spectra were then taken during the course of the thin-layer cyclic experiments.

RESULTS AND DISCUSSION

Synthetic iron porphyrin electrochemistry has been studied in this laboratory because of the relevance to biologically significant model compounds. The electrochemical mechanism for TPPFeCl is known to be highly solvent dependent (*23*) and thus provides a good test for cell performance as a function of solvent. That it is also highly oxygen and impurity sensitive (*24*) provides a stringent test for the provision of a clean, oxygen-free environment.

A typical thin-layer cyclic for TPPFeCl reduction in Me_2SO is demonstrated in Figure 2. In theory, there should be no peak spearation between the oxidation and reduction waves. In practice, however, the observed peak separation in the cyclic voltammogram is due to uncompensated solution resistance,

[1] Present address: Ohio Medical Products, Madison, WI 53707.

0003-2700/81/0353-1539$01.25/0 © 1981 American Chemical Society

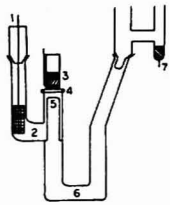


Figure 1. Diagram of the thin-layer spectroelectrochemical cell; (1) Pt auxiliary electrode, (2) solution reservoir, (3) Au minigrid working electrode, (4) connecting Teflon lid, (5) Pyrex/soft glass cracked frit, (6) solvent-supporting electrolyte salt bridge, (7) SCE reference electrode.

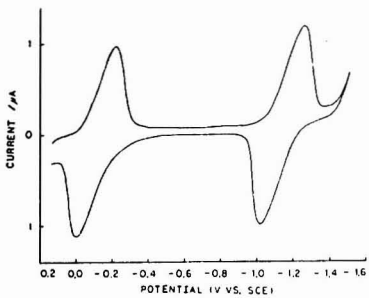


Figure 2. Thin-layer cyclic voltammogram of 1.0×10^{-3} M TPPFeCl and 2×10^{-1} M TBAP in Me_2SO. Scan rate is 2 mV/s.

a problem inherent to all thin-layer designs (*1*, *10*, *15*). TBAP concentrations of 0.2 M in high dielectric constant solvents and 0.5 M in low dielectric constant solvents are sufficient to keep the peak spearations to 250 mV or less (at a scan rate of 2 mV/s). Superimposable cyclics and spectra are found with multiple sweeps. These spectra show well-defined isosbestic points as expected for complete conversion of one species to another and are demonstrated elsewhere (*25*). Comparable results are found in the other solvents tested ($EtCl_2$, DMF and Py).

In discussion of the utility of any thin-layer design, questions must be answered about its ease of construction, ease of cleaning, permeability to atmospheric oxygen, solution residence time, and cell lifetime. In this case, the three principal components of the cell (slide–minigrid, Teflon lid, and reservoir–salt bridge) can each be constructed in less than 2 h. The assembly into a complete unit requires about 30 min with an additional 30 min for the final drying of the epoxy. The largest part of the 30 min assembly time deals with the proper cutting and seating of the Teflon tape gaskets which prevent solution leakage. A minimal amount of high-vacuum silicon stopcock can also be used with the gaskets to further minimize leakage. This has never been observed to change the electrochemistry of any system tested in this laboratory and has beneficial effects on cell lifetime.

After completion of the experiment, the cell can be easily broken down into its components. The reservoir is cleaned by conventional means, the lid rinsed with solvent, the minigrid–slide flushed several times with solvent, and the gaskets discarded. This quick breakdown allows for easy interchange of minigrid–slide assemblies to avoid cross contamination from different compounds and solvents.

This cell also proves to be easy to protect from oxygen. After the solution is initially deoxygenated, experiments can be run in the open for an hour and a half before appreciable oxygen (2×10^{-4}) diffuses back into the minigrid region from the surrounding atmosphere. When necessary, a nitrogen purge box can be used to lower this level of residual oxygen.

In theory, the solution being spectrally monitored remains in the minigrid region indefinitely. In practice, however, a finite solution residence time occurs due to evaporative convection in the slide assembly. The time for this effect to occur can be quantitated by multiple cyclic superimposition and/or open circuit spectral monitoring of a stable electrochemically generated species. With this cell, residence times of over an hour are found for nonvolatile solvents like DMF, Me_2SO, and Py. A more volatile solvent like $EtCl_2$ requires shielding of the electrode from the spectral source (except during the short spectral acquisition times) to maintain a residence time of over an hour. From other studies with this same cell (*26*) we know that extremely volatile solvents like methylene chloride are difficult to work with for more than 10 min, even with light shielding and a solvent saturated atmosphere. Thus, these most volatile solvents can only be used with great care.

The useful lifetime for this cell is ultimately limited by solution leakage around one of the Teflon gaskets (usually the slide-lid gasket). However, even with no applied silicon grease, the cell remains solution tight for at least 2 h in all solvents tested. This is easily enough time to complete most series of thin-layer experiments. When a little silicon grease is used on the slide lid gasket, cell lifetimes of over 20 h are not uncommon, and the electrochemistry remains unchanged.

Thus, the spectroelectrochemical cell described herein is suitable for work in a wide variety of nonaqueous solvents. These include: $EtCl_2$, DMF, Me_2SO, and Py (this work) and methylene chloride, acetone, acetonitrile, and methanol (*26*) and will undoubtedly be extended to further solvents in future studies. The electrochemical response for the cell is comparable to other minigrid designs; and this design allows for ease in construction and cleaning, a high degree of anerobicity, reasonable solution residence times, and long cell lifetime.

ACKNOWLEDGMENT

The authors wish to thank L. A. Bottomley, P. C. Minor, and R. Wilkins for helpful suggestions during the evolution of this cell design.

LITERATURE CITED

(1) Murray, R. W.; Heineman, W. R.; O'Dom, G. W. *Anal. Chem.* **1967**, *39*, 1966.
(2) Heineman, W. R.; Burnett, J. N.; Murray, R. W. *Anal. Chem.* **1968**, *40*, 1970.
(3) Heineman, W. R.; Burnett, J. N.; Murray, R. W. *Anal. Chem.* **1968**, *40*, 1974.
(4) Kreishman, G. P.; Anderson, C. W.; Su, C. H.; Halsall, H. B.; Heineman, W. R. *Bioelectrochem. Bioenerg.* **1978**, *5*, 196.
(5) Hawkridge, F. M.; Ke, B. *Anal. Biochem.* **1977**, *78*, 76.
(6) Meyer, M. L.; DeAngelis, T. P.; Heineman, W. R. *Anal. Chem.* **1977**, *49*, 602.
(7) Yildiz, A.; Kissinger, P. T.; Reilley, C. N. *Anal. Chem.* **1968**, *40*, 1018.
(8) Norvell, V. E.; Mamantov, G. *Anal. Chem.* **1977**, *49*, 1970.
(9) Norris, B. J.; Meckstroth, M. L.; Heineman, W. R. *Anal. Chem.* **1976**, *48*, 630.
(10) Tom, G. M.; Hubbard, A. T. *Anal. Chem.* **1971**, *43*, 671.
(11) Pinkerton, T. C.; Hajizadeh, H.; Deutsch, E.; Heineman, W. R. *Anal. Chem.* **1980**, *52*, 1542.
(12) Petek, M.; Neal, T. E.; Murray, R. W. *Anal. Chem.* **1971**, *43*, 1069.
(13) Kenyhercz, T. M.; DeAngelis, T. P.; Norris, B. J.; Heineman, W. R.; Mark, H. B. *J. Am. Chem. Soc.* **1976**, *98*, 2469.
(14) Stargardt, J. F.; Hawkridge, F. M.; Landrum, H. L. *Anal. Chem.* **1978**, *50*, 930.
(15) Rohrbach, D. F.; Heineman, W. R.; Deutsch, E. *Inorg. Chem.* **1979**, *18*, 2536.
(16) Pezchal-Heiling, G.; Wilson. G. S. *Anal. Chem.* **1971**, *43*, 550.
(17) Neal, T. E.; Murray, R. W. *Anal. Chem.* **1970**, *42*, 1654.
(18) Piljac, I.; Tkalcec, M.; Grabaric, B. *Anal. Chem.* **1975**, *47*, 1369.
(19) Piljac, I.; Murray, R. W. *J. Electrochem. Soc.* **1971**, *118*, 1758.
(20) Rhodes, R. K.; Kadish, K. M., unpublished work, University of Houston, 1979–1980.
(21) Summerville, D. A.; Cohen I. A. *J. Am. Chem. Soc.* **1976**, *98*, 1747.
(22) Perrin, D. D.; Armarego, W. L. F.; Perrin, D. R. "Purification of Laboratory Chemicals", 2nd ed.; Permagon Press: Oxford, 1980, pp 204, 224, 229, 402.
(23) Bottomley, L. A.; Kadish, K. M. *Inorg. Chem.* **1981**, *20*, 1348.
(24) Brault, D.; Rougee, M. *Biochemistry 1974*, *13*, 4591.

(25) Kadish, K. M. "The Chemical Physics of Biologically Important Inorganic Chromophores"; Vol. 1, Lever, A. B. P., Gray, H. B., Eds., in press.
(26) Kadish, K. M.; Rhodes, R. K. *Inorg. Chem.*, in press.

RECEIVED for review February 27, 1981. Accepted April 17, 1981. The authors wish to gratefully acknowledge the support of this research in part by the National Science Foundation (Grant CHE-7921536), the National Institutes of Health (Grant GM 2517-02), and the Robert A. Welch Foundation (Grant E-680).

Analysis of Fish and Sediment for Volatile Priority Pollutants

Michael H. Hiatt

U.S. Environmental Protection Agency, Environmental Monitoring Systems Laboratory, P.O. Box 15027, Las Vegas, Nevada 89114

The U.S. Environmental Protection Agency's (EPA's) water quality monitoring and hazardous waste monitoring programs require analysis of a variety of samples for volatile organic compounds. The samples analyzed are primarily sediments, soils, water, and fish. Determination of the volatile priority pollutants in water samples is routinely accomplished with acceptable results in accordance with the EPA-recommended Method 624 (*1*). However, the EPA-recommended procedures for the determination of volatile priority pollutants in sediment and fish (*2–4*) produce unacceptable results, as evidenced in other studies (*5, 6*) by low spike recoveries and high detection limits. An improved method was required for the Agency's monitoring programs.

The vaporization of volatile organic compounds from a sample under vacuum and subsequent condensation in a super-cooled trap seemed an ideal approach when compared to other methods available (*5–7*). Cryogenic concentration has been used successfully for the determination of tritiated methane and the radioisotopes of krypton and xenon (*8*) and appeared to be applicable to the determination of volatile organic compounds in solid matrices. Another advantage of vacuum extraction was that it did not require elevated temperatures or the addition of reagents which could produce unwanted byproducts due to sample degradation.

In this method volatile organic compounds are vaporized from the fish or sediment matrix under vacuum and are condensed in a purging trap cooled by liquid nitrogen. The purging trap is transferred to a conventional purge and trap device where the concentrate is treated as a water sample and is analyzed as described in Method 624 (*1*). With this method, the average recovery of volatile organic compounds from samples spiked at the 25 μg/kg level was found to be 94% for sediments and 74% for fish tissue.

EXPERIMENTAL SECTION

Samples. Sediments and fish samples previously found to contain less than detectable levels of volatile priority pollutants were used as matrices for this study. Spiked samples were prepared by placing 10 g of sediment or ground fish into a 125-mL septum vial and adding the compounds to be studied (Tables I–III). Two separate additions were necessary to add the organic compounds. The first addition was 10 μL of a water solution that contained acrolein and acrylonitrile (1 μg/μL), which are more stable in water than methanol. The second injection was 5 μL of a methanol solution that contained 250 ng (50 ng/μL) of the remaining volatile organic compounds. The spiked samples were sealed with a Teflon-lined septum cap and sonicated for 5 min. The sample vials were then sealed in cans containing activated charcoal and stored overnight in a freezer.

Apparatus. A diagram of the apparatus for vacuum extraction and cryogenic concentration is shown in Figure 1. The vacuum extractor can be assembled from materials normally available in the laboratory. The low pressure necessary for extraction is supplied by a vacuum pump capable of producing a 10^{-3} torr vacuum and a flow rate of 25 L/min. The concentrator traps (25 mL Tekmar purging tubes or equivalent) are used for condensing the volatile vapors and transferring the extract to the purge and trap device. The concentrator trap is connected to the transfer lines of the vacuum extractor with $^1/_8$ in. compression fittings and graphite ferrules. The transfer lines are made of glass-lined $^1/_4$ in o.d. stainless steel tubing. Gastight valves (V1–V4), Nupro B-4BKT, are connected with compression fittings and graphite ferrules. The 125-mL septum vial containing the sample aliquot is connected to the system with a one-hole rubber stopper pierced with the $^1/_4$ in o.d. tubing. A liquid nitrogen cold trap is placed between the vacuum pump and concentrator trap in order to prevent condensation of pump oil vapors in the concentrator trap. The helium line and pressure gauge are connected at a junction in the transfer line between the sample and V2 and are used primarily to test the apparatus for leaks. The helium used is 99.999% pure, and normally because of the small quantities used, it is not necessary to purify further. If it is desired, however, a gas filter trap can be added to the helium line to ensure purity. An ultrasonic cleaner, Branisonic 12, is used to agitate the sample during extraction.

Procedure. The vacuum extractor must be airtight and free of moisture before an extraction can be started. A clean 125-mL septum vial is connected, the vacuum pump started, and V2 to V4 are opened to evacuate the apparatus. The elimination of line condensation is accomplished by warming the transfer lines while evacuating the system. Heating tape is effective in creating even transfer line temperatures and can be used continuously during extraction. The vacuum extractor is pressurized with helium by closing V3 and opening V1. The apparatus is then leak-tested by applying soapy water on all connections and making the appropriate adjustments when leaks are located. When the apparatus is airtight, close V1 and open V3. Heat the transfer lines and concentrator trap for 5 min to eliminate any contamination from previous extraction at parts-per-billion concentration. The system is now ready for sample extraction.

To begin the extraction process close V2 (V3 and V4 remain open), cool the concentrator trap with a liquid nitrogen bath, and replace the empty 125-mL vial with the sample vial. Disconnect the vacuum source by closing V3. Open V2 to permit vapors from the sample vial to reach the concentrator trap. The sample vial is then immersed in the ultrasonic water bath. The equilibrium temperature generated in the ultrasonic bath is 50 °C. Therefore the bath is initially filled with 50 °C water and that temperature maintained by continuous ultrasonic operation.

After 5 min of ultrasonic agitation the vacuum source is connected by opening V3. The lower pressure hastens the transfer of volatile compounds from the sample to the super-cooled concentrator trap. After 15 min of vacuum close V3 and open V1 to fill the system with helium until atmospheric pressure is obtained. Close V1 and V2 to isolate the concentrate. The sample extraction is now complete and the concentrate is ready for transfer to a purge and trap device. The concentrate can be held in the liquid nitrogen bath for up to an hour prior to analysis.

Disconnect the sample concentrator trap from the vacuum extractor and connect it to the purge and trap device. Some outgassing is observed when the sample extract is melted;

This article not subject to U.S. Copyright. Published 1981 by the American Chemical Society

Table I. Percent Spike Recoveries for Volatile Priority Pollutants from Sediment Matrices with Three Analytical Methods

	vacuum extraction[a]	direct purge and trap of diluted sample[c,d]	modified purge and trap with thermal desorption[f,g]
chloromethane	98 ± 22	97 ± 16	91 ± 13
bromomethane	86 ± 24	69 ± 15	77 ± 15
vinyl chloride	108 ± 35	114 ± 27	87 ± 24
chloroethane	106 ± 27	101 ± 19	76 ± 20
methylene chloride	LC[b]	98 ± 18	77 ± 17
trichlorofluoromethane	80 ± 8	ND[e]	103 ± 37
1,1-dichloroethene	82 ± 9	87 ± 21	84 ± 20
1,1-dichloroethane	101 ± 7	87 ± 17	84 ± 29
trans-1,2-dichloroethene	92 ± 10	88 ± 24	78 ± 32
chloroform	102 ± 11	88 ± 19	77 ± 35
1,2-dichloroethane	96 ± 17	90 ± 34	81 ± 31
1,1,1-trichloroethane	106 ± 11	78 ± 21	93 ± 13
carbon tetrachloride	100 ± 13	94 ± 28	100 ± 33
acrylonitrile	89 ± 8	ND	ND
bromodichloromethane	96 ± 8	88 ± 37	93 ± 24
1,2-dichloropropane	96 ± 4	ND	88 ± 18
trans-1,3-dichloropropene	91 ± 6	ND	71 ± 21
trichloroethene	98 ± 6	73 ± 23	99 ± 12
benzene	94 ± 4	59 ± 24	83 ± 10
dibromochloromethane	98 ± 10	70 ± 29	87 ± 33
1,1,2-trichloroethane	98 ± 5	86 ± 34	77 ± 35
cis-1,3-dichloropropene	92 ± 7	ND	71 ± 21
bromoform	90 ± 9	70 ± 29	79 ± 41
tetrachloroethene	104 ± 13	57 ± 21	38 ± 76
1,1,2,2-tetrachloroethane	98 ± 8	90 ± 27	60 ± 33
toluene	102 ± 4	35 ± 24	77 ± 88
chlorobenzene	101 ± 5	ND	81 ± 13
ethylbenzene	97 ± 5	ND	80 ± 8
av compd recovery	96 ± 7	82 ± 18	83 ± 10

[a] 25 ppb spikes. [b] Laboratory contamination of fish prevented generation of valid data. [c] 20 ppb spikes. [d] Reference 5. [e] Not determined. [f] Reference 7. [g] 27 ppb spikes.

Table II. Percent Spike Recoveries for Volatile Priority Pollutants from Fish Matrices with Three Analytical Methods

	vacuum extraction[a]	direct purge and trap of diluted sample[c,d]	direct purge or trap of diluted sample[f,g]
chloromethane	85 ± 22	ND[e]	78[h]
bromomethane	126 ± 75	ND	71[h]
vinyl chloride	64 ± 11	25 ± 9	65[h]
chloroethane	69 ± 22	21 ± 5	70[h]
methylene chloride	LC[b]	ND	22
trichlorofluoromethane	99 ± 2	ND	54
1,1-dichloroethene	74 ± 8	59 ± 19	62
1,1-dichloroethane	90 ± 6	33 ± 9	69
trans-1,2-dichloroethene	86 ± 9	33 ± 11	49
chloroform	107 ± 31	38 ± 13	81
1,2-dichloroethane	92 ± 5	ND	79
1,1,1-trichloroethane	92 ± 8	60 ± 18	58
carbon tetrachloride	91 ± 9	95 ± 40	50
bromodichloromethane	64 ± 11	44 ± 13	67
1,2-dichloropropane	54 ± 7	36 ± 11	73
trans-1,3-dichloropropene	52 ± 9	ND	65
trichloroethene	65 ± 11	41 ± 8	59
benzene	57 ± 10	37 ± 25	68
dibromochloromethane	56 ± 9	42 ± 8	65
1,1,2-trichloroethane	66 ± 7	42 ± 7	77
cis-1,3-dichloropropene	54 ± 9	ND	74
bromoform	ND[e]	51 ± 8	62
tetrachloroethene	ND	55 ± 12	48
1,1,2,2-tetrachloroethane	61 ± 10	48 ± 15	71
toluene	ND	53 ± 14	66
chlorobenzene	64 ± 15	32 ± 8	68
ethylbenzene	ND	35 ± 12	60
av compd recovery	76 ± 20	44 ± 16	64 ± 12

[a] 25 ppb spikes. [b] Laboratory contamination of fish prevented generation of valid data. [c] 20 ppb spikes. [d] Reference 5. [e] Not determined. [f] 200 ppb spikes. Reference 6, precision data were not available. [h] 800 ppb spikes.

therefore, the extract should be kept frozen until the concentrator trap is attached to the purge and trap device. Warm the concentrator trap walls to loosen the extract and allow the ring of ice formed during condensation to drop to the bottom of the trap. To this partially melted extract add 5 mL of distilled deionized water containing the internal standards recommended in Method

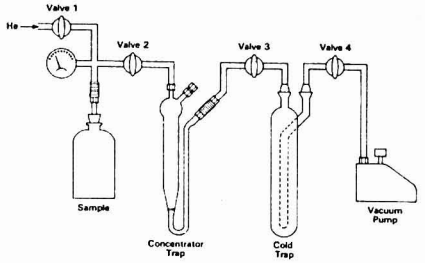


Figure 1. Vacuum extractor.

Table III. Percent Spike Recoveries for Volatile Priority Pollutants from Water Using Vacuum Extraction

	concn,[a] ppb	% recovery[b]
chloromethane	25	105 ± 22
bromomethane		110 ± 23
vinyl chloride		83 ± 12
chloroethane		103 ± 16
methylene chloride		126 ± 22
trichlorofluoromethane		99 ± 18
1,1-dichloroethene		98 ± 5
1,1-dichloroethane		96 ± 5
trans-1,2-dichloroethene		98 ± 5
chloroform		93 ± 8
1,2-dichloroethane		98 ± 10
1,1,1-trichloroethane		104 ± 9
carbon tetrachloride		102 ± 10
acrylonitrile	100	85 ± 13
bromodichloromethane	25	108 ± 10
1,2-dichloropropane		104 ± 7
trans-1,3-dichloropropene		109 ± 9
trichloroethene		105 ± 9
benzene		106 ± 7
dibromochloromethane		102 ± 11
1,1,2-trichloroethane		95 ± 8
cis-1,3-dichloropropene		109 ± 9
bromoform		104 ± 14
tetrachloroethene		105 ± 9
1,1,2,2-tetrachloroethane		90 ± 9
toluene		106 ± 7
chlorobenzene		101 ± 7
ethylbenzene		103 ± 5
2-chloroethyl vinyl ether		94 ± 50[c]
acrolein	100	113 ± 76[c]
av compd recovery		102 ± 8

[a] The organic compounds were added to 2 mL of water which represents the water content of 10 g of sediment. [b] Recoveries of spikes were calculated by comparing vacuum extracted determination to determinations where spikes were added directly to the purge and trap device. These recoveries are results for three separate analyses on four different days. [c] Average of three analyses on the same day.

624 (*1*). The purge and trap procedure is then performed in accordance with a modified Method 624 (*1*). In the modified procedure the extract solution is purged with the concentrator trap immersed in an ice water bath for 5 min followed by immersion in a 55 °C water bath for an additional 7 min. This modification provides reproducible conditions for melting the frozen extracts which should yield reproducible purging efficiencies.

RESULTS AND DISCUSSION

Preliminary data, obtained with the method described, have shown excellent spike recoveries for sediment samples and a general improvement of spike recoveries for fish samples compared to results reported for other methods (Tables I and II).

Recovery studies were performed by using freshly boiled, distilled, deionized water to which 250 ng of each of the volatile priority pollutants were added. A study using 2-mL water aliquots and extraction times that varied from 5 min to 1 h indicated that extractions from water were essentially complete after 5 min. Varying the volume of water from 1 to 8 mL had no detected effect on spike recoveries.

Acrolein and acrylonitrile were added only to the sediments studied. No acrolein was recovered from the spiked sediments which suggests that there is either a strong acrolein–sediment interaction or degration of the acrolein added. This finding appears to be consistent with other studies (*5*, *7*) which also did not report any acrolein recovered. Acrolein, however, was extracted from water solutions added to the sample vial with a good recovery (Table III). This suggests that the spiking procedure with overnight storing allowed ample time for sediment–volatile organic compound interactions to occur prior to testing the method.

This vacuum extraction method is an improvement over existing procedures and has immediate application to environmental analysis. It gives uniformly high recoveries for the individual volatile organic compounds (Tables I and II) and appears to be free of interferences due to sediment matrices and moisture content. The method should be reliable for the variety of sediment matrices encountered in environmental monitoring.

We are presently conducting a more thorough study to gain additional information on the effects of sample matrix, sample concentration, and spiking techniques. The detailed results of this study will be reported at a later date.

LITERATURE CITED

(1) *Fed. Regist.* **1979**, *44* (No. 233), 69532–69539.
(2) United States Environmental Protection Agency. Sampling and Analysis for Screening of Fish for Priority Pollutants. "Analysis of Fish for Volatile Organics by Head Space Analysis"; U.S. Environmental Monitoring and Support Laboratory—Cincinnati: Cincinnati, OH, Aug 23, 1977; p 14.
(3) United States Environmental Protection Agency. Interim Methods for the Sampling and Analysis of Priority Pollutants in Sediments and Fish Tissue. "The Analysis of Sediments for Volatile Organics by Head Space Analysis"; U.S. Environmental Monitoring and Support Laboratory—Cincinnati: Cincinnati, OH, Aug 23, 1977; p 18.
(4) "The Analysis of Fish for Volatile Organics by Head Space Analysis"; U.S. Environmental Monitoring and Support Laboratory—Cincinnati: Cincinnati, OH, undated; p 21.
(5) Blazevich, J. U.S. Environmental Protection Agency, Region X, Manchester, WA, personal communication, 1980.
(6) Easly, D. M.; Kleopfer, R.D.; Carasea, A. W. "The Analysis of Volatile Organic Compounds in Fish"; U.S. Environmental Protection Agency Region VII Laboratory: Kansas City, KS.
(7) Spies, David N. "Determination of Purgeables Organics in Sediment Using a Modified Purge and Trap Technique"; U.S. Environmental Protection Agency Region II: Edision, NJ, Oct 10, 1980.
(8) United States Environmental Protection Agency. Handbook of Radiochemical Analytical Methods; Environmental Monitoring Systems Laboratory—Las Vegas: Las Vegas, NV, Feb 1975; pp 55–69.

RECEIVED for review December 22, 1980. Accepted May 19, 1981.

Standardization of Helium Carrier Gas for Helium Detector Applications

Fikry F. Andrawes*

American Cyanamid Company, Stamford Research Laboratory, 1937 West Main Street, Stamford, Connecticut 06904

Terry B. Byers

Lockheed, 1830 NASA Road 1, Houston, Texas 77058

Everett K. Gibson

SN7/Geochemistry Branch, NASA-Johnson Space Center, Houston, Texas 77058

Carrier gas purity is a significant problem in all sensitive detectors, but for the helium ionization detector (HID) the purity of the helium carrier gas is essential for the operation of the detector. The presence of impurities in the carrier gas will influence the detector's background current, noise level, signal polarity, magnitude of response, and overall detector stability. The introduction of the helium ionization detector led to an efficient method to achieve an ultra-high-purity grade of helium (minimum purity of 99.9995%). In such grades of helium, impurities are in the range of a few parts per billion (*1*, *2*). Using this grade of helium in a leak-free chromatographic system, the detector will characteristically respond negatively to a small concentration of selected gases (Ne, H_2, Ar, O_2, and N_2) and positively to other gases (*3–5*). Addition of a small concentration of gaseous additive will provide a positive response to all gases and compounds tested (*3–5*). Recently the HID was operated in the saturation region of the detector field intensity to provide a sensitive and reliable response (*6*, *7*). In this work the detector was operated with a high-purity grade of helium (minimum purity of 99.995%) and the detector response was positive for all gases and compounds tested except neon. The use of the high-purity grade of helium, however, does not imply that the purity of the helium carrier gas used is not a significant factor. We have noticed that the detector response will vary with the carrier gas cylinder used due to a slight difference in purity level from one cylinder to another. In this work we evaluated the detector response when high-purity and ultra-high-purity grades of helium were used as carrier gases. A method to achieve a high-precision analysis using different cylinders of helium as a carrier gas was also investigated.

EXPERIMENTAL SECTION

A Varian 1700 gas chromatograph (Varian Aerograph, CA) was used in this work. The detector was operated at an applied potential of 150 V (1500 V/cm of electrodes) and maintained at 150 °C. A Valco eight-port gas sampling injection valve (Valco Instrument, Houston, TX) was adapted to the chromatograph with 100-μL sample loops. A Spectra-Physics SP-4000 was used to integrate peak areas.

The column used in this work was stainless steel tubing (2 m × 1.1 mm i.d. × 1.6 mm o.d.), packed with molecular sieve 13 × (60–80 mesh), and conditioned overnight at 150 °C with a helium flow of 14 mL/min.

A standard gas sample mixture was used during the course of this work; it consisted of 11 ppm H_2, 24 ppm argon, 5 ppm neon, 9 ppm O_2, 29 ppm N_2, 22 ppm CH_4, and 23 ppm CO (Scientific Gas Products, Houston, TX). Carrier gas used in this work was ultra-high-purity and high-purity grades of helium (Scientific Gas Products).

During the course of this work, a number of helium cylinders were used as carrier gas. Normally, opening the system to the atmosphere to exchange a cylinder will allow air and moisture into the system and purging this air and moisture completely requires several hours. In order to avoid this problem, we used a four-way valve (Whity, Cleveland, OH). This allows helium cylinders to be exchanged without opening the system to atmosphere.

Table I. Table of Responses to Various Gases[a]

gas tested	response for ultra-high-purity helium						response for high-purity helium					
	1	2	3	4	5	6	7	8	9	10	11	12
Ne	–	–	–	–	–	–	+	+	–	–	–	–
H_2	–	–	–	–	–	–	+	·	+	–	·	–
Ar + O_2	–	–	–	·	·	–	17	12	20	13	9	4
N_2	–	·	–	–	·	–	20	8	14	10	9	4
CH_4	61	65	61	69	51	49	20	35	34	37	40	34
CO	91	102	91	106	78	72	36	55	57	57	62	53

[a] Peak area in counts $\times 10^{-3}$. Signs indicate signal polarity.

RESULTS AND DISCUSSIONS

To evaluate the detector response when different grades and different cylinders of helium are used, we analyzed the sample mixture using six different cylinders each of ultra-high-purity and high-purity grades. The results obtained from these analyses are summarized in Table I. The detector response to Ne, H_2, Ar + O_2, and N_2 was negative when the ultra-high-purity helium was used as a carrier gas but the response to Ar + O_2 and N_2 became positive when high-purity helium was used. The response to Ne and H_2 was either positive or negative depending on the cylinder used. A positive response to Ne is due to a higher concentration of Ne in the carrier gas than in the sample analyzed. The negative response to H_2 in four cylinders of high-purity helium indicates that these cylinders have purity levels that are higher than that which produces the minimum background current, because at the minimum background current the detector response to H_2 is positive (*8*). The magnitude of the detector response to CH_4 and CO was higher when using the ultra-high-purity grade than when using the high-purity grade of helium as a carrier gas. It appears from Table I that the high-purity helium would be adequate for most chromatographic applications. The ultra-high-purity grade will improve the detector response, but this grade of helium is also more expensive. Table I also shows variation in the detector response within the two groups of helium grades. This variation may not be significant for some applications, but if high precision is required, the carrier gas purity should be standardized to a point in which this variation between cylinders is minimized.

We investigated the possibility of standardizing different cylinders of helium. A practical way to achieve this is to use helium carrier gas at the minimum background current. The addition of small concentrations of gaseous additives to the ultra-high-purity helium carrier gas will decrease the background current to a minimum point. After this point is reached, further increase in the concentration of the gaseous additives will increase the background positively (*8*). At the minimum background current all cylinders will contain a constant total impurity level, and consequently they should provide a constant response. This minimum background current can easily be achieved by adding a gaseous additive

0003-2700/81/0353-1544$01.25/0 © 1981 American Chemical Society

Table II. Detector Response at the Minimum Background Current[a]

gas tested	response for ultra-high-purity helium						response for high-purity-helium					
	1	2	3	4	5	6	7	8	9	10	11	12
$Ar + O_2$	21	19	20	19	18	16	18	12	17	21	20	18
N_2	18	17	14	16	14	12	12	13	13	19	16	14
CH_4	32	31	33	31	31	28	29	26	31	34	31	30
CO	53	50	53	50	50	46	47	47	52	56	52	49

[a] Peak area in counts $\times 10^{-3}$.

to the ultra-high-purity helium. However, the high-purity helium grade may contain a concentration of impurities greater than that at minimum background current. A typical analysis for impurities in high-purity grade helium as provided by the producers is 1 ppm of each of CH_4, O_2, Ar, and CO_2 and 10 ppm H_2, 14 ppm N_2, 14 ppm Ne, and 12 ppm H_2O. To purify the helium carrier gas, we used a hydrox purifier (Matheson, LaPort, TX) which contains a zirconium, titanium, and nickel alloy. This alloy when heated is effective in retaining some of these impurities, but others such as H_2, Ne, Ar, and N_2 just pass through. The H_2O content in helium is reduced to H_2 increasing the content of H_2 to twice that of H_2O. To further purify this helium grade, we inserted a well-conditioned molecular sieve trap upstream from the hydrox purifier. The molecular sieve trap will effectively retain most of the H_2O and CO_2. With this arrangement all the high-purity helium cylinders produced a partial negative response to H_2, Ar + O_2, and N_2. After a partial negative response to H_2, Ar + O_2, and N_2 was achieved, gaseous additive was added to the helium to achieve the minimum background current. The addition of gaseous additives was carried out via the permeation tube technique (*9*). H_2, Ar, O_2, or N_2 could be used as gaseous additives (*3–5*); however, we used H_2 in the work described here. Table II shows the magnitude of the detector response at the minimum background current using the two grades of helium. The variation in the detector response, when different cylinders of helium are used, is now minimized.

It appears from Table I that for most applications the high-purity grade of helium is adequate and provides a positive response for almost all gases and compounds tested. Ultra-high-purity helium shows an improved response, but it provides a negative response to some selected gases. The variation in the detector response with different cylinders of helium could be minimized by adjusting the total impurities to that which produces the minimum background current.

LITERATURE CITED

(1) Bourke, P. J.; Dawson, R. W.; Denton, W. H. *J. Chromatogr.* **1964**, *14*, 1387.
(2) Bourke, P. J.; Gray, M. D.; Denton, W. H. *J. Chromatogr.* **1965**, *19*, 189.
(3) Bros, E.; Lasa, J. *J. Chromatogr.* **1979**, *174*, 258.
(4) Andrawes, F.; Gibson, E. *Anal. Chem.* **1978**, *50*, 1146.
(5) Andrawes, F.; Gibson, E. *Anal. Chem.* **1980**, *52*, 1846.
(6) Andrawes, F.; Brazell, R. S.; Gibson, E. *Anal. Chem.* **1980**, *52*, 89.
(7) Andrawes, F.; Gibson, E.; Bafus, D. *Anal. Chem.* **1980**, *52*, 1377.
(8) Andrawes, F.; Byers, T. B.; Gibson, E. K. *J. Chromatogr.* **1981**, *205*, 419.
(9) O'Keeffe, A. E.; Ortman, G. C. *Anal. Chem.* **1966**, *38*, 760.

RECEIVED for review April 17, 1980. Resubmitted January 5, 1981. Accepted March 17, 1981. This work was performed, in part, under the auspices of the National Aeronautics and Space Administration, Contract NAS9-15800 to Lockheed.

Cooling System for High-Power Ion Lasers

S. W. Edwards and J. F. Schetzina*

Department of Physics, North Carolina State University, Raleigh, North Carolina 27650

Most commercial ion lasers are equipped with water cooling systems which require flow rates of 3–8 gal/min. In principle, ordinary tap water can be used in these systems. However, the use of poor quality water can lead to several detrimental effects. Particulate matter in the water can block water passages in the laser power supply and plasma tube and thus increase the system's flow impedance. This problem can be reduced but not eliminated by using filtered tap water. Water having an appreciable ion content is also undesirable as a cooling medium. Magnesium and calcium ions, for example, can precipitate out to form scale on the walls of the laser water passages thereby decreasing the efficiency of the cooling system.

The Spectra-Physics line of ion lasers, in particular, should be cooled with water which is sufficiently purified so that water in a 10 ft length of 0.5 in. diameter hose has at least 100 kΩ resistance when measured under flowing conditions (*1*). This requirement follows from the plasma tube design employed by Spectra-Physics in which the plasma tube anode passes through the water cooling jacket. Thus, the cooling water is in direct contact with the anode and can be considered to be at that potential. High conductivity water in the cooling system, therefore, provides an alternate path to ground. In extreme cases, this could lead to unstable laser output power or premature plasma tube failure.

This paper describes a simple recirculating loop cooling system designed to eliminate the above potential problems. The system employs off-the-shelf plumbing components where possible to minimize cost without sacrificing performance. The system is most appropriate for small industrial or university laboratories where the cost of commercial cooling systems of similar design may be prohibitive.

DESCRIPTION OF COOLING SYSTEM

The major components of the cooling system are shown schematically in Figure 1. The pump, laser, heat exchanger, and reservoir form a recirculating cooling loop which employs deionized water. The water purity is maintained by a deionizer located in a parallel line between the pump and the reservoir inlet.

The pump is a Burkes Model 3CT6M close coupled turbine pump (Burkes Pumps, Decatur, IL) of all bronze construction which provides a water flow rate of 4.3 gal/min at a pressure of 70 psi.

The water from the laser is cooled with an American-Standard Model BCF-06-036-001 shell and tube type heat exchanger (American Standard, Buffalo, NY). This particular model is a single pass unit having a diameter of 6 in. and a length of 36 in. The heat exchanger is used in a counterflow configuration as shown in Figure 1 in which water in the

0003-2700/81/0353-1545$01.25/0 © 1981 American Chemical Society

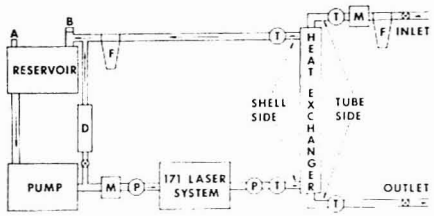


Figure 1. Schematic of cooling system: (A) reservoir vent; (B) reservoir fill cap; (D) deionizer; (F) water filter; (M) water flow meter; (P) water pressure gauge; (T) water temperature gauge.

recirculating loop passes through the shell side of the unit. Filtered tap water flowing through the tube side of the heat exchanger removes the heat generated by the laser.

The reservoir is constructed entirely of schedule 40 poly(vinyl chloride) (PVC) material which is readily obtainable from local plumbing supply houses. It consists of a 4 ft length of 6 in. diameter PVC tubing, two 6 × 6 × 1 in PVC tees, and two 6 in. PVC end caps which are bonded together with heavy duty industrial grade PVC solvent cement. The reservoir has a capacity of about 35 L and is normally filled with 25 L of deionized water during use. The water lines from the heat exchanger to the reservoir and from the reservoir to the turbine pump, which carry cool water, are made from 1 in. diameter PVC tubing. Hard copper tubing ($^3/_4$ in. diameter) is used between the laser and the heat exchanger.

The cooling system contains two water filters, two water flow meters, two pressure gauges, and four temperature gauges arranged as shown in Figure 1. Ameteck Plymouth Supreme Model PS-S1 water filters (Ameteck, Plymouth Products Div., Sheboygan, WI) with type S1 replaceable cartridges are used to remove particulate matter from the water in the recirculating loop and from the tap water flowing through the heat exchanger. Flow rates are measured with Hershey-American Model 430 water meters. These flow meters are of bronze construction and are obtainable from local plumbing suppliers. The differential water pressure across the 171 laser system is measured with two Ashcroft 0–100 psi dial type pressure gauges. Water temperatures at the inlets and outlets of the heat exchanger are monitored with Ashcroft 10–149 °C bimetal thermometers.

The deionizer consists of a series arrangement of two Barnstead type HN series 8900 mixed bed ion removal cartridges. When the cooling system is in use, the valve preceding the deionizer is adjusted to obtain the desired water pressure at the laser inlet (approximately 65 psi). This allows a fraction of the recirculating water to continuously pass through the deionizer thereby maintaining its purity.

COOLING SYSTEM PERFORMANCE

The above cooling system has been used for the past 3 years to cool a Spectra-Physics 171-18 argon ion laser with excellent results. In operation, a flow rate of 4.2 gal/min is maintained in the recirculating loop, as is recommended by Spectra-Physics. To adequately cool the laser system when it is operating under full output power, a minimum tap water flow rate of 6 gal/min at 23 °C is required. In the summer months, when the tap water reaches a maximum of 30 °C, a flow rate of 8 gal/min is employed. These are modest requirements which are ordinarily satisfied by standard laboratory plumbing facilities. With the laser operating at full output power (~50 A tube current) the cooling system extracts approximately 34 kW of heat from the system with an efficiency (2) greater than 0.5.

No problems with the cooling system have been encountered during the 3-year period it has been employed. The laser plasma tube has remained in a near virgin state with no visible evidence of scale buildup or other water contaminants. The Burkes turbine pump has performed flawlessly while providing a very stable water flow rate through the recirculating loop.

Although complete cooling systems of similar design are available from commercial vendors, the present system can be assembled in a matter of hours and at a substantial savings. The total cost of the cooling system described here is less than two percent of the cost of the Model 171-18 ion laser and its performance to date suggests that it is well worth the time and effort needed to construct it.

LITERATURE CITED

(1) Spectra-Physics Model 171 Ion Laser Instruction Manual (C/171 9/77); Spectra-Physics, Sunnyvale, CA; p 4-3.
(2) Simonson, John R. "An Introduction to Engineering Heat Transfer"; McGraw-Hill: New York, 1969; Chapter 2.

RECEIVED for review February 9, 1981. Accepted April 27, 1981. Work supported in part by NSF Grants DMR77-08443 and DMR79-11336.

Silanized Carbon Microneedle Emitters for Chemical/Field Ionization

David F. Fraley and Maurice M. Bursey*

William Rand Kenan, Jr., Laboratories of Chemistry, The University of North Carolina, Chapel Hill, North Carolina 27514

It is now possible to attach surface functional groups covalently to metal emitters used in some laboratories for field desorption (FD) mass spectrometry (*1*, *2*). These groups are not removed by the combined field, vacuum, and emitter heating used in FD. Further, the influence of the field on the acidity of attached carboxylic acid groups is profound: the carboxylic acid, in the strong electric field used in FD and field ionization (FI), is strong enough to protonate representative olefins, alcohols, and even alkyl halides. Because in FD untreated emitters may produce either $M^{+\cdot}$ or $(M + 1)^+$, this protonating ability of the modified acid surface emitter is particularly useful. In the field the heated carboxylic acid emitter cleanly ionizes all molecules with functional groups as $(M + 1)^+$. Further, although other methods for forming $(M + 1)^+$ ions exclusively have been found, they involve the use of acids which are strong even in the absence of an electric field: coating a surface with polyphosphoric acid (*3*) or mixing the sample with *p*-toluenesulfonic acid (*4*) runs the risk of acid-catalyzed decomposition of an especially fragile molecule to be analyzed before the ions can be obtained. In the absence

0003-2700/81/0353-1546$01.25/0 © 1981 American Chemical Society

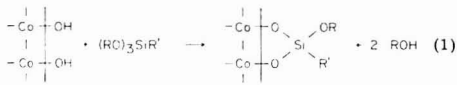
Table I. FI/FD Spectra at Untreated and Acid-Surface Carbon Emitters

compound	heating current, mA	untreated			acid surface		
		$(M-1)^+$	$M^{+\cdot}$	$(M+1)^+$	$(M-1)^+$	$M^{+\cdot}$	$(M+1)^+$
pyridine	0		100	70		100	70
	16 (365 K)[a]		100	70		30	100
benzonitrile	0		100	15		100	45
	17 (373 K)		100	15		30	100
carbon disulfide	0		100	30		100	25
	17 (373 K)		100	25		50	100
cyclohexane	0	20	100	20	20	100	10
	20 (390 K)	15	100	15	100	60	15
anthracene	0		100	30		100	40
	13 (343 K)		100	30		80	100

[a] Temperature at emitter tips at the midpoint between the support posts (*12*).

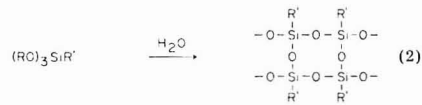
of a field, the carboxylic acid group, being weaker, is much less likely to destroy the sample before analysis than these others.

The usual description of attachment of a silane to an oxidized metal surface is illustrated in eq 1. We have adopted



(1)

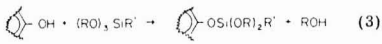
this model, with the understanding that polymerization of the silane with adsorbed surface water (eq 2) may also occur. Both



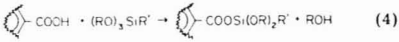
(2)

processes develop a surface containing R′ groups which cannot be removed by heat, vacuum, or electric fields. Since no special precautions beyond activation are taken to remove surface water and the emitters are then exposed to laboratory air prior to reaction with the silane, the possibility that eq 2 plays a significant role in fixing surface functional groups is great. This fixing is independent of the strength of any occasional bond to the underlying surface.

The strength of this kind of covalent bond to the carbon surface would be weak. The structure of high-temperature microneedles deposited from benzonitrile vapor has been found to be less regular than graphite (*5*) and probably consists of very small domains of graphite, irregularly juxtaposed. Such a material would resemble to some extent the material from which glassy carbon electrodes are made. The surface modification of these electrodes has been examined; the functional groups at the edge of the basal plane of graphite are formed by exposure to oxygen and include the common oxygenated functions: phenolic, quinone, carboxylic acid, and aldehydic groups (*6*). Silanization of the surface would occur by reaction with phenolic and carboxylic acid groups (eq 3 and 4). Silyl



(3)



(4)

ethers (eq 3) and esters (eq 4) are well-known derivatives in gas chromatography (*7*). They are rapidly formed but notoriously unstable to hydrolysis, and the derivatives are used promptly. Hence the durability of a carbon surface modified by treatment with a silane would be questionable if the only mechanism for modification to provide involatile functional groups was attachment of R′ chains singly to surface functionalities. As we have seen, however, this will not necessarily be the case. The application of previously developed silanization techniques for emitters to carbon, rather than the development of totally new chemistry, was therefore pursued as a first step.

EXPERIMENTAL SECTION

Carbon Emitters. Carbon emitters were grown in a VG Micromass (Altrincham, Cheshire) emitter activating unit following standard procedures (*8*). The average dendrite length was 20 μm.

Mass Spectrometer. A DuPont 21-492B instrument was used for field desorption. Since VG Micromass emitters have shorter support rods than DuPont emitters, they were mounted in the DuPont instrument by fabricating two 10.5-mm extenders from electronic connectors. Because of ion-source design, the distance from emitter to counterelectrode was 6 mm rather than the usual 3 mm in order to prevent arcs between the repeller plates and the emitter. The voltage between the emitter and the counterelectrode was established by settings of +3500 V and −7000 V, respectively.

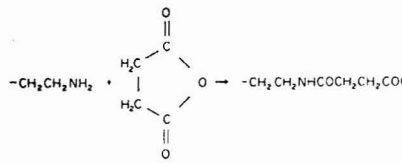
Surface Modification of the Carbon Emitter. Newly prepared emitters were heated to 190 °C for 15–60 min. A 5% (by volume) solution was prepared by the addition of 0.25 mL of 3-(2-aminoethylamino)propyltrimethoxysilane (PCR Research Chemicals, Inc., Gainesville, FL) to 5.0 mL of dry (Na) toluene. The emitter was suspended in this stirred solution for 3 min at ambient temperature. The silanized emitter was briefly washed in dry toluene and then suspended in a saturated solution of succinic anhydride in toluene at about 50 °C for 5 min. It was finally rinsed in toluene to remove excess succinic anhydride, examined under a microscope, and mounted in the mass spectrometer. Two precautions are noteworthy: the syringe used to transfer the silane must be flushed with acetone to avoid problems from the rapidly polymerizing silane, and the silane should be distilled and stored in an airtight vial before use.

The surface silane may be removed by dipping in concentrated hydrofluoric acid for 10 s. This procedure does not significantly degrade the carbon emitter performance.

RESULTS AND DISCUSSION

The reactions chosen to provide a protonating surface on carbon emitters are analogous to those recommended for cobalt emitters (*2*). In the context of involatilization through polymer formation, the chemistry may be formalized by reference to eq 2, in which the R group is $-CH_2CH_2CH_2NHCH_2CH_2NH_2$. Most likely the terminal amino group then reacts with succinic anhydride. Following convention (*6*, *9*, *10*) eq 5 is offered as a paradigm of the acylation, ignoring the likely zwitterionic nature of the product or its further reactions.

The attachment of the original silane did not significantly alter the sensitivity of the emitters. However, reaction with succinic anhydride is known (*2*) to alter the field ionization and field desorption spectra produced. Compounds chosen to represent a wide range of proton affinities (PA) and to



compare behavior on modified cobalt emitters were pyridine (PA 218 kcal/mol) (*11*), benzonitrile (PA 195 kcal/mol) (*11*), carbon disulfide (PA 168 kcal/mol) (*11*), and cyclohexane (PA unlisted in ref 11 but probably <168 kcal/mol). All these compounds were analyzed by field ionization. For field desorption, the compound whose behavior on modified cobalt emitters was known was anthracene. Results for the behavior of these compounds at untreated and acid-surface carbon emitters are summarized in Table I.

In Table I the results from the silanized and untreated emitters at no heating current are seen to be usually the same; it is only on heating that a difference appears. The second heating current value listed for each compound is the threshold value for protonation by the acid-surface emitter. At this value the base peak in the spectra of compounds with an easily discerned site of protonation becomes the $(M + 1)^+$ ion, and in the spectra of the cycloalkane becomes the $(M - 1)^+$ ion, in accordance with the behavior of alkanes in ordinary chemical ionization (eq 6) (*13*). At the protonation threshold

$$CH_5^+ + C_nH_{2n+2} \rightarrow CH_4 + [C_nH_{2n+3}^+]^* \rightarrow [C_nH_{2n+1}^+] + H_2 \quad (6)$$

current for the acid-surface emitter, or even slightly above it, the untreated emitter is seen to yield the same spectrum as with no heating current. These results are in accord with those obtained with metal emitters. The greatly increased acidity of the carboxylic acid group in the intense electric field at the emitter tip is accommodated by theory, because of the effect of an electric field on ionization of weak electrolytes (*14*). The pK of an acid in an electric field ought to decrease by a term proportional to the square of the electric field (*2*). Emitters of all types have tip radii of disperse dimension, which obscures the dependence of signal on field strength, and variation of field was not studied; controversy surrounding field effects has arisen from variations in the degree of importance attached to this point (*15–18*).

Protonation is not complete here, in contrast to the protonation at the acid-surface metal emitter. We believe this is the result of incomplete surface coverage, and indeed, after an arc has struck a working acid-surface emitter of any type, the usual effect is to decrease the intensity of the $(M + 1)^+$ peak. This would be expected if part of the acid polymer is destroyed by the arc, so that some ionization occurs by the classical mechanism at the now untreated surface. We have not found conditions for coating carbon emitters so that only $(M + 1)^+$ ions are formed. Excessive periods of time in the silanizing solution can produce emitters whose ionization efficiency is greatly reduced.

The existence of a threshold for protonation is concordant with the endothermicity of the protonation reaction at zero field. It also has been universally observed with acid-surface metal emitters (*1*, *2*) and although the onset of protonation varies with the geometry of each emitter to some extent, the threshold is lower for carbon than for cobalt emitters. This is a manifestation of the lower temperature of a cobalt emitter than a carbon emitter when the same heating current is passed through two otherwise identical emitters (*19*).

In summary, polymerization of silanes by surface-bound water allows the extension of results found for metal emitters to the much more common carbon emitters. While protonation is incomplete because of incomplete surface coverage by the polymer, a peak resulting from protonation becomes the base peak, and this observation clearly establishes the identity of the $(M + 1)^+$ peak in a functionalized unknown, a problem which has required much attention (*20*) in field desorption studies because of the problem of distinguishing whether the FD peak of highest mass is $M^{+\cdot}$ or $(M + 1)^+$ in an unknown. Extensions to other silanes, and the development of other methods for modifying functional groups at graphite surface, have begun.

ACKNOWLEDGMENT

We are grateful to J. R. Hass for access to a VG Micromass emitter activating unit.

LITERATURE CITED

(1) Youngless, T. L.; Bursey, M. M.; Pedersen, L. G. *J. Am. Chem. Soc.* **1980**, *102*, 6881.
(2) Youngless, T. L.; Bursey, M. M.; Pedersen, L. G. *Int. J. Mass Spectrom. Ion Phys.* **1981**, *38*, 223.
(3) Ligon, W. V., *Jr. Science* **1979**, *204*, 198.
(4) Keough, T.; DeStefano, A. J. *Anal. Chem.* **1981**, *53*, 25.
(5) Neumann, G. M.; Rogers, D. E.; Derrick, P. J.; Paterson, P. J. K. *J. Phys. D* **1980**, *13*, 485.
(6) Murray, R. W. *Acc. Chem. Res.* **1980**, *13*, 135.
(7) Poole, C. F. "Handbook of Derivatives for Chromatography"; Blau, K., King, G. S., Eds.; Heyden: London, 1978; p 152.
(8) Beckey, H. D.; Hilt, E.; Schulten, H.-R. *J. Phys. E* **1973**, *6*, 1043.
(9) Moses, P. R.; Wier, L. M.; Lennox, J. C.; Finklea, H. O.; Lenhard, J. R.; Murray, R. W. *Anal. Chem.* **1978**, *50*, 576.
(10) Willman, K. W.; Greer, E.; Murray, R. W. *Nouv. J. Chim.* **1979**, *3*, 455.
(11) Hartman, K. N.; Lias, S.; Ausloos, P.; Rosenstock, H. M.; Schroyer, S. S.; Schmidt, C.; Martinson, D.; Milne, G. W. A. "A Compendium of Gas Phase Basicity and Proton Affinity Measurements, NBSIR 79-1777; U.S. Department of Commerce: Washington, DC, 1979.
(12) Fraley, D. F. Ph.D. Dissertation, University of North Carolina at Chapel Hill, Chapel Hill, NC, 1981, Chapter 6.
(13) Munson, M. S. B. *Anal. Chem.* **1971**, *43*, 28A.
(14) Onsager, L. *J. Chem. Phys.* **1934**, *2*, 599.
(15) Holland, J. F.; Soltmann, B.; Sweeley, C. C. *Biomed. Mass Spectrom.* **1976**, *3*, 340.
(16) Beckey, H. D.; Röllgen, F. W. *Org. Mass Spectrom.* **1979**, *14*, 188.
(17) Holland, J. F. *Org. Mass Spectrom.* **1979**, *14*, 291.
(18) Beckey, H. D. *Org. Mass Spectrom.* **1979**, *14*, 292.
(19) Fraley, D. F.; Woodward, W. S.; Bursey, M. M. *Anal. Chem.* **1980**, *52*, 2290.
(20) Schulten, H.-R.; Beckey, H. D. *Org. Mass Spectrom.* **1974**, *9*, 1154.

RECEIVED for review March 2, 1981. Accepted April 27, 1981.

Elution of Adsorbed Organics from Graphitized Carbon Black

Robert L. Petty

Marine Science Institute, University of California, Santa Barbara, Santa Barbara, California 93106

In a recent article by Bacaloni et al. (*1*), the properties of graphitized carbon black (GCB) relating to adsorption of trace organics from water, and desorption with organic solvents, were examined. Several general classes of compounds were studied. Most of the substances tested, although subject to eventual breakthrough, were shown to be completely retained by the GCB. For desorption of the compounds, several solvent systems were examined. A 1:1 mixture of ether and hexane

0003-2700/81/0353-1548$01.25/0 © 1981 American Chemical Society

was judged to be optimal, and their standard method specified a 50-mL elution volume for desorption from a 100-mg GCB trap.

GCB has been used for some time in this laboratory for trace enrichment of hydrocarbons from seawater (2). The present paper reports a method which we have developed for desorption of trapped organics from GCB which requires only 2–4 mL of solvent and which provides partial fractionation of the adsorbates as they are desorbed.

EXPERIMENTAL SECTION

Reagents and Equipment. Chlorinated pesticides were obtained as a mixture from Applied Science. Aroclor 1254 was obtained from Monsanto, and individual PCBs were obtained from Supelco. Other compounds used as test substances were obtained from standard chemical suppliers and used without further purification. Methanol, methylene chloride, and hexane are "distilled in glass" grade, obtained from Burdick and Jackson. Ether is anhydrous "analytical reagent" grade from Mallinkrodt. Graphitized carbon black was obtained from Supelco (Carbopack B, 60/80 mesh) and cleaned by overnight Soxhlet extraction with methylene chloride. Gas chromatography was performed on a Hewlett-Packard 5840A chromatograph equipped with flame ionization and electron capture (^{63}Ni) detectors and capillary injector system. GC columns used were Hewlett-Packard fused silica capillaries, either 12 m (column A) or 50 m long (column B) by 0.21 mm i.d.

Procedures. Adsorption traps are prepared from dry GCB and 6 mm o.d. by 4 mm i.d. Pyrex tubing. The tubes are dry packed, with tapping, using glass wool plugs to hold the GCB in place. Approximate packing lengths of 2 cm and 4 cm are used, requiring about 100 and 200 mg of GCB, respectively. Traps are conditioned before their initial use, and regenerated after each subsequent use, by rinsing with 5–10 mL of either methylene chloride or ether, followed by 5–10 mL of methanol and approximately 5 mL of water. Solvents are added to the traps by means of a stainless steel reservoir (constructed from a length of $^1/_4$ in. tubing) having a volume of about 5 mL, which is attached via a Swagelok union.

Samples are applied to a trap by syringe injection of 1–8 μL solutions of the test compounds into the upper glass wool plug, followed by a 2-mL water rinse of the trap. Samples are eluted by adding a measured volume of methanol to the reservoir and allowing the methanol to pass through the trap by gravity flow while collecting the effluent in 1-mL fractions. After the methanol stops dripping from the trap outlet the next solvent (usually ether) is added to the reservoir and more fractions are collected. For a 2-cm trap, 1.0 mL of methanol and 3.0 mL of ether are usually used. For a 4-cm trap, a 2- or 3-mL volume of methanol is followed by 4–6 mL of ether. Void volumes of the traps are approximately 0.4 and 0.8 mL, respectively, so the first fraction of a new solvent always contains some of the previous solvent.

Sample recoveries are determined by GC analysis of 1–3 μL portions of the unconcentrated fractions. In the case of the Aroclor mixture, quantitation was by comparison of eluent fractions to a standard sample (external standard method), and in the case of the pesticide and miscellaneous compound mixtures, it was by the internal standard method. The internal standard is added to the container in which the eluent fractions are to be collected. A mixture of three PCBs (2,3,6-trichloro-, 2,3,5,6-tetrachloro-, and 2,2',4,5,5'-pentachlorobiphenyl) is used as the internal standard for the pesticide mixture, while a series of even carbon straight chain esters (C_8–C_{20} methyl esters) are used with the miscellaneous mixture.

Chromatographic conditions are as follows: column A (12 m), initial temperature 75 °C held for 4 min, program rate 6 °C/min, final temp 240 °C, column inlet pressure 10 psig; column B (50 m), 90 °C for 1 min and then to 180 °C at 10 °C/min and then to 250 °C at 3 °C/min, column inlet pressure 20 psig. For either column, the injector temperature is 240 °C, FID is 260 °C, and ECD is 300 °C. The splitless mode is used for sample injection, with a 0.6-min injection period.

RESULTS AND DISCUSSION

Three samples, each containing a mixture of compounds, were tested in the GCB desorption procedure. They included chlorinated pesticides, polychlorinated biphenyls (PCBs), and a miscellaneous mixture made up of several types of compounds.

Table I. Chlorinated Pesticide Mixture,[a] 2-cm Trap

compound	% in fraction[b] I	II	% recovery
α-BHC	100	0	100
lindane	20	80	65
heptachlor	100	0	75
aldrin	100	0	85
heptachlor epoxide	100	0	100
endrin	90	10	100
p,p-DDD	90	10	95
o,p-DDT	90	10	70
p,p-DDT	90	10	80

[a] Mixture of 65 μg of each component dissolved in 8 μL of hexane. [b] Percent of total recovered amount in first (methanol) or second (ether) 1.0-mL fraction.

Table II. Aroclor 1254,[a] 4-cm Trap

peak no.	% of recovered amount in fraction II[b]	III[c]	IV[c]	V[c]	VI[c]	% recovery
1	0	70	25	5	0	95
2	0	0	90	10	0	80
3	0	80	15	5	0	90
4	0	85	15	0	0	100
5	0	90	10	0	0	100
6	0	15	75	10	0	95
7	0	100	0	0	0	100
8	0	0	70	30	0	
9	5	70	10	10	5	90
10	0	70	25	5	0	115
11	0	95	5	0	0	100
12	0	0	70	30	0	100
13	0	30	15	50	5	85
14	0	60	40	0	0	110

[a] 2 μg in 2 μL of hexane applied to 4-cm GCB trap. [b] Methanol eluent (1 mL). [c] Ether eluent (1 mL fraction).

The components of the chlorinated pesticide mixture are listed, along with their elution and recovery data for a typical run, in Table I. In this run, an 8-μL portion of a solution containing 8 μg/μL of each component was applied to a 2-cm GCB trap. The trap was then eluted with water, methanol, and ether. Apparent absolute recoveries averaged about 85%, but precision on replicate runs was only about ±15%, and all component recoveries were seen to fluctuate within the 60–100% range on replicate runs. The poor precision was due to problems with the capillary GC analysis procedure, rather than to a variability in actual elution recoveries.

The major portion of all pesticide components, except lindane, was consistently eluted in the methanol fraction, with the major portion of the lindane always appearing in the first ether fraction. When this mixture was eluted from a 4-cm trap, using 3 mL of methanol, most of the components were split between fractions II and III (second and third milliliter of methanol). A portion of the α-BHC came off in fraction I, while lindane was again eluted mainly in the first ether fraction.

The results of elution of a sample of Aroclor 1254 from a 4-cm GCB trap, using 2 mL of methanol, are presented in Table II. Chromatograms of the eluted fractions are shown in Figure 1. Certain peaks in this complex mixture were selected and monitored through the elution sequence. It became clear upon analysis of the fractions that at least one,



Figure 1. Capillary gas chromatogram of Aroclor 1254 standard (STD) and eluent fractions (III, IV, V) from 4-cm GCB trap. Chromatographed on column B (see Experimental Section for details). See text for explanation of peak numbers.

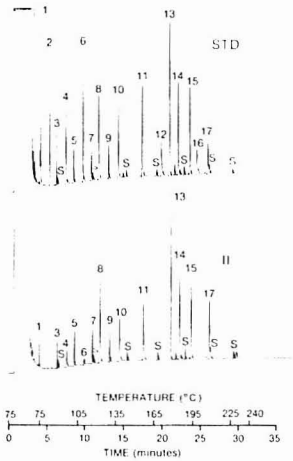


Figure 2. Capillary gas chromatogram of "Miscellaneous Mixture" standard (STD) and eluent fraction II from 2-cm GCB trap. See Table III for identification of numbered peaks. Peaks labeled S are internal standards (see Table III). Chromatographed on column A (see Experimental Section for details).

and probably several, of the peaks present in the chromatogram of the whole mixture (STD in Figure 1) was composed of more than one component. For example, fraction III exhibited a peak with retention time slightly shorter than that of peak 7/8 in the standard, while fraction IV had a peak with a slightly longer retention time. Also, peak 13 has a recovery pattern which exhibits two maxima, and peak 9, although eluting in an apparently smooth pattern, extends over five fractions. All of the other selected peaks are spread over only two or three fractions. In contrast to the pesticide mixture components, the PCBs are eluted almost entirely in the ether fractions.

A "miscellaneous mixture" was made up from several "off the shelf" chemicals, including aliphatic and aromatic hydrocarbons, alcohols, ketones, an aromatic chloride, and an ether. A range of molecular weights, structural types, and

Table III. Miscellaneous Mixture,[a] 2-cm Trap

peak no.[b]		amt[c]	% in fraction I[d]	II[e]	III[e]	% recovery
1	*p*-xylene	50	70	30	0	100
2	mesitylene	50	100	0	0	115
3	undecane	12		100		55
S	methyl octanoate					
4	naphthalene	25	0	100	0	15
5	dodecane	12	0	100	0	70
6	6-undecanone	95	95	5	0	100
7	tridecane	12	0	100	0	70
S	methyl decanoate					
8	1-chloronaphthalene	50	0	100	0	85
9	tetradecane	12	0	100	0	75
10	1-dodecanol	50	45	55	0	100
S	methyl dodecanoate					
11	dibenzyl ether	50	40	60	0	95
S	methyl tetradecanoate					
12	anthracene	25	0	0	0	0[f]
13	octadecane	50	0	95	5	80
14	1-hexadecanol	50	0	100	0	95
S	methyl hexadecanoate					
15	undecanophenone	50	0	75	25	95
16	fluoranthene	25	0	0	0	0[f]
17	phytol	50	0	100	0	90
S	methyl octadecanoate					
S	methyl eicosanoate					

[a] Mixtures of five multicomponent solutions applied in a total of 13 μL of hexane. [b] Numbers corresponding to chromatographic peaks in Figure 2. [c] Amount applied to trap, μg. [d] Methanol eluent. [e] Ether eluent. [f] Components were later eluted with toluene.

Table IV. Miscellaneous Mixture, 4-cm Trap

peak no.[a]	% in fraction 1[b]	2[b]	3[b]	4[c]	5[c]	6[c]	7[c]	8[d]
1	20	75	5	0	0	0	0	0
2	30	70	0	0	0	0	0	0
3	0	60	40	0	0	0	0	0
4	0	0	65	35	0	0	0	0
5	0	0	70	30	0	0	0	0
6	0	100	0	0	0	0	0	0
7	0	0	0	100	0	0	0	0
8	0	0	0	25	75	0	0	0
9	0	0	0	100	0	0	0	0
10	0	20	70	10	0	0	0	0
11	0	0	15	85	0	0	0	0
12	0	0	0	0	0	0	0	0
13	0	0	0	65	35	0	0	0
14	0	0	0	80	20	0	0	0
15	0	0	0	0	0	20	25	55
16	0	0	0	0	0	0	0	0
17	0	0	0	100	0	0	0	0

[a] See Table III for components. [b] Methanol eluent. [c] Ether eluent. [d] Ethylene dichloride eluent.

polarities was thus obtained. This mixture (see Table III for components) was applied to a 2-cm trap and eluted. The major portion of most of the compounds eluted in the first ether fraction (fraction II; see Figure 2). The smaller molecules, along with some of the more polar compounds, had significant portions in the methanol fraction. The polycylic aromatics (anthracene and fluoroanthene) were not eluted at all with ether (even with up to 10 mL), although it was later discovered that they can be eluted with a small volume (less than 2 mL) of toluene. A single experiment in which this mixture was eluted from a 4-cm trap with 3 mL of methanol followed by 5 mL of ether (see Table IV) resulted in most of the components again appearing in the first ether fraction, but with all compounds exhibiting a significantly greater degree of fractionation. All but two of the components were eluted in 2 mL or less.

The present GCB elution procedure offers distinct advantages over the previously described method (*1*). By using methanol as the initial eluent, residual water on the trap is removed in the first 1-mL fraction. This allows the organic solvent which follows to act much more efficiently in desorbing the components from the GCB. An immediate concentration factor of 25- to 50-fold is thus realized over the previous method by allowing adsorbates to be removed in 1–2 mL of solvent instead of 50 mL. As might be expected from previous HPLC applications of GCB (*3*, *4*), rudimentary fractionation of components is now possible with traps only 2 cm long, while a significant degree of fractionation is possible using longer (4 cm) traps. Employing a gradual solvent gradient for trap elution can improve the process even further.

Results obtained in this study may differ slightly from those obtained when samples are actually adsorbed from water, since components would tend to migrate into and through the trap during the adsorption procedure. This could affect the resolution of the fractionation process and would probably be most noticeable in the early eluting components.

LITERATURE CITED

(1) Bacaloni, Allessandro; Goretti, Giancarlo; Lagana, Aldo; Petronio, Bianca Maria; Rotatori, Mauro *Anal. Chem.* **1980**, *52*, 2033.
(2) Petty, Robert L. Pacific Conference on Chemistry and Spectroscopy, San Francisco, CA, 1978; Paper No. 84. Abstracts published by California Section, ACS, Berkeley, CA.
(3) Colin, H.; Eon, C.; Guiochon, G. *J. Chromatogr.* **1976**, *119*, 41.
(4) Colin, H.; Eon, C.; Guiochon, G. *J. Chromatogr.* **1976**, *122*, 223.

RECEIVED for review January 12, 1981. Accepted May 18, 1981.

Sample Introduction and Pressure Measuring System for Chemical Ionization Mass Spectrometers

A. J. Illies and M. T. Bowers*

Department of Chemistry, University of California, Santa Barbara, California 93106

G. G. Meisels

Department of Chemistry, University of Nebraska—Lincoln, Lincoln, Nebraska 68588

Chemical ionization mass spectrometry (CIMS) is now well established as a valuable research tool in both analytical and fundamental applications (*1–5*). One of the difficulties with using CIMS in magnetic sector instruments has been that of electrical discharges through the gaseous sample between the ion source, which may be at potentials up to 10 kV, and ground. The discharges occur when the electric field causes electrical breakdown of the sample gas resulting in a flow of electrons toward the anode (ion source) and of positive ions toward the cathode (ground) (*6*). The discharge is sustained by emission of secondary electrons at the cathode caused by impact of the fast moving positive ions. The breakdown voltage, which is a function of the parameter E/N, where E is the electric field strength (V/cm) and N the gas density (molecules/cm^3), varies considerably with gas sample. These differences depend upon the energy loss pathways available to the free electrons as they travel through the sample gas toward the anode.

A more poorly understood characteristic of electrical discharges is the quenching of the discharge at higher pressures (above ca. 50 torr) (*4*, *6*). This quenching of the discharge has been extensively used in most CIMS inlet systems where a large pressure drop is created through a nonconducting capillary leak. Disadvantages of using a capillary leak are (a) large sample backing pressures are required presenting a problem when small sample sizes or compounds with low vapor pressure are used and (b) the inability to measure the ion source pressure through a capillary leak. Futrell and Wojcik (*7*) solved this problem by using a chain of vacuum resistors between the ion source and ground with stainless steel turnings at each potential to create a uniform, controlled potential gradient.

We would like to present an alternate method. It was first used at the University of Nebraska—Lincoln on a modified Atlas CH-4 mass spectrometer operated at ion source potentials up to 3 kV and pressures up to 3 torr. The same technique has been extended at the University of California, Santa Barbara (UCSB), for use with a VG-Micromass ZAB-2F mass spectrometer operated at source potentials as high as 10 kV and pressures up to 1 torr. The basic features of the design are shown in Figure 1. The sample leak valve which is at ground potential feeds into a glass tube which has been packed with approximately 4 in. of glass wool. The end of this glass tube is in contact with the ion source potential. We believe that the glass wool may prevent discharging by reducing the positive ion velocities below that required for the emission of secondary electrons and/or providing a very large surface area which may act as the third body in the ion–electron recombination reaction

$$I^+ + e^- + M \rightarrow I + M \qquad (1)$$

In our experiment the glass tube is passed through a Cajon ultra torr fitting (Cajon Vacuum Products, Macedona, OH) which has an O-ring seal separating the vacuum system and atmosphere and is bakeable to ~250 °C. Connections to the ion source are made with VCR vacuum couplings and flexible stainless steel tubing (Cajon Vacuum Products, Macedona, OH).

0003-2700/81/0353-1551$01.25/0 © 1981 American Chemical Society

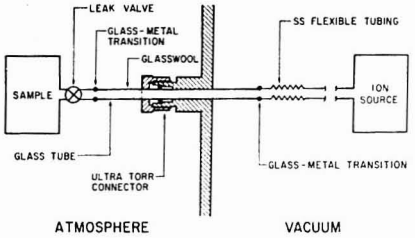


Figure 1. Schematic of sample introduction system.

We use the same method to measure the ion source pressure with a MKS-Baratron capacitance manometer. At UCSB an additional glass ring is included in the line leading to the capacitance manometer. This results in an intermediate ground. Thus, if discharging should occur it would be to the intermediate ground and not to the capacitance manometer. One must, however, recognize that when glass wool is placed in the gas line leading to the pressure transducer thermal transpiration will occur (*8*). The ion source pressure is then given by

$$P_{IS} = P_T(T_{IS}/T_T)^{1/2} \quad (2)$$

where P_{IS} and T_{IS} are the ion source pressure and temperature and P_T and T_T are the pressure and temperature at the Baratron head.

At UCSB this sample introduction system is used for all gaseous and volatile liquid samples in both EI and CI modes. The only disadvantage with the sample introduction system involves the removal of very polar samples from the glass wool. However, overnight pumping has removed all samples we have used to date.

LITERATURE CITED

(1) Illies, A. J.; Meisels, G. G. *Anal. Chem.* **1980**, *52*, 325.
(2) Polley, C. W.; Illies, A. J.; Meisels, G. G. *Anal. Chem.* **1980**, *52*, 1797.
(3) Meot-Ner, M.; Field, F. H. *J. Am. Chem. Soc.* **1975**, *97*, 5339.
(4) Mather, R. E.; Todd, J. F. J. *Int. J. Mass Spectrom. Ion Phys.* **1979**, *30*, 1.
(5) Munson, B. *Anal. Chem.* **1977**, *49*, 772A.
(6) Gould, R. F., Ed *Adv. Chem. Ser.* **1969**, No. 80.
(7) Futrell, J. H.; Wojcik, L. H. *Rev. Sci. Instrum.* **1971**, *42*, 244.
(8) Patterson, G. N. "Molecular Flow of Gases"; Wiley: 1956.

RECEIVED for review February 17, 1981. Accepted May 7, 1981. The work done at UCSB was supported by the National Science Foundation under Grant CHE77-15449 and at the Univerisity of Nebraska by the Department of Energy under Contract DEAS02-76-ERO-2567. We gratefully acknowledge this support.

CORRECTIONS

Smoothing of Digital X-ray Photoelectron Spectra by an Extended Sliding Least-Squares Approach

Andrew Proctor and Peter M. A. Sherwood (*Anal. Chem.* **1980**, *52*, 2315–2321).

There is an unfortunate typographical error in eq 8. The correct form is shown below:

$\underline{n = 2}$ (fit to a parabola, $y = au^2 + bu + c$).

$$y(u)_{n=2} = y(u)_{n=1} + a_2P_2(u,2m) =$$
$$\sum_{t=-m}^{m} (\{5[3t^2 - m(m+1)]u^2 + (2m-1)(2m+3)tu + m(m+1)[3m(m+1) - 1 - 5t^2]\}/\mathrm{NORM1})f(t) \quad (8)$$

Determination of Atmospheric Sulfur Dioxide without Tetrachloromercurate(II) and the Mechanism of the Schiff Reaction

Purnendu K. Dasgupta, Kymron DeCesare, and James C. Ullrey (*Anal. Chem.* **1980**, *52*, 1912–1922).

On page 1912, under Experimental Section, the preparation of the pararosaniline working reagent should read 133.3 mL of the 0.2% commercially purified stock reagent (Harleco) and 113.9 mL of concentrated HCl were diluted to 1 L, rather than 113.9 mL of 0.3% dye and 133.3 mL of HCl being diluted to 1 L.

AUTHOR INDEX

Andersen, N. H., 1357
Anderson, J. E., 1394
Andrawes, F. F., 1544
Årén, K., 1406

Baetjer, K., 1469
Balciunas, R., 1484
Bancroft, E. E., 1390
Barber, W. E., 1373
Barnes, R. M., 1336
Barnhart, S. G., 1432
Beaulieu, P. L., 1536
Blount, H. N., 1390
Bond, A. M., 1394
Bos, P., 1362
Bowers, M. T., 1551
Broderius, S. J., 1472
Brown, S. D., 1410, 1497
Brown, T. F., 1410
Bryden, C. C., 1418
Buda, M. J., 1386
Bursey, M. M., 1546
Bush, B., 1351
Byers, T. B., 1544

Cahen, D., 1426
Caldwell, K. D., 1314
Callis, J. B., 1357
Cameron, D. G., 1454
Carnrick, G. R., 1504
Carr, P. W., 1373
Caruso, J. A., 1512
Cetinkaya, M., 1469
Chiba, K., 1450
Choudhury, D. R., 1351
Christian, G. D., 1357
Cianetti, C., 1477
Clark, C. R., 1341
Crouch, S. R., 1484
Currie, L. A., 1463

Dasgupta, P. K., 1552
Davis, J. C., 1488
DeCesare, K., 1552
Delaney, M. F., 1460
Desreux, J. F., 1418
D'Silva, A. P., 1519
Dueszeln, J., 1469
Durfee, S. L., 1463

Edwards, S. W., 1545
Estes, S. A., 1336

Fabiani, C., 1477
Farnsworth, P. B., 1432
Fassel, V. A., 1519
Feder, A. L., 1383
Fleischmann, M., 1457
Fombarlet, C. M., 1386
Fraley, D. F., 1546
Frech, W., 1437
Frei, R. W., 1362
Funazo, K., 1377
Fuwa, K., 1450

Gabel, B., 1469
Gale, R. J., 1457
Gianelli, M. L., 1357
Gibson, E. K., 1544
Giddings, J. C., 1314
Gonon, F. G., 1386
Groh, R., 1325
Guiochon, G., 1318

Haartz, J. C., 1479
Halász, I., 1325
Hanekamp, H. B., 1362
Hara, S., 1365
Haraguchi, H., 1450
Hardin, E. D., 1492
Hiatt, M. H., 1541
Hinsberg, W. D., III, 1509
Holler, F. J., 1484
Hornung, R. W., 1479
Hulanicki, A., 1401

Illies, A. J., 1551

Jackson, M. E., 1512
Jagner, D., 1406
Jenke, D., 1535
Johnson, E. R., 1484
Jørstad, K., 1398
Josefson, M., 1406
Jurgensen, A., 1442
Juvet, R. S., Jr., 1369

Kadish, K. M., 1539
Karaiskakis, G., 1314
Kasahara, Y., 1380
Kauppinen, J. K., 1454
Keller, B. A., 1536
Kinoshita, T., 1380
Klouda, G. A., 1463
Kozicki, R., 1469
Kunen, S. M., 1463
Kuwata, K., 1531

Lahl, U., 1469
Lange, B. A., 1479
Lawton, R. S., 1523
Lewenstam, A., 1401
Li, Z.-p., 1516
Lierse, K., 1469
Lundberg, E., 1437
Lundeen, J. T., 1369

Malkin, S., 1426
Manning, D. C., 1504
Mantsch, H. H., 1454
Mascherpa, A., 1466
McCarthy, J. P., 1512
McDowell, L. M., 1373
Meisels, G. G., 1551
Milby, K. H., 1509
Miyamoto, S., 1365
Moffatt, D. J., 1454
Myers, M. N., 1314

Nimura, N., 1380
Notz, P. K., 1484

O'Dea, J. J., 1383
Osteryoung, J., 1383

Pappas, A. C., 1398
Petty, R. L., 1548
Podbielski, A., 1469
Procter, A., 1552
Pujol, J. F., 1386

Reilley, C. N., 1418
Rhodes, R. K., 1539
Rice, G. W., 1519
Richard, J. J., 1519
Ridgway, T. H., 1512
Rosen, M. J., 1516
Rothman, L. D., 1484

Salbu, B., 1398
Schetzina, J. F., 1545
Sefaja, J., 1457
Sherwood, P. M. A., 1552
Shono, T., 1377
Sidwell, J. S., 1390
Slavin, W., 1504
Small, H., 1488
Stachel, B., 1469
Stevens, T. S., 1488
Suzuki, T., 1380

Tanabe, K., 1450
Tanaka, M., 1377
Thiemann, W., 1469
Thomson, J. S., 1345
Tittarelli, P., 1466
Toman, J. J., 1497

Uden, P. C., 1336
Uebori, M., 1531
Ullrey, J. C., 1552

Vestal, M. L., 1492
Vijan, P. N., 1447
Vogh, J. W., 1345
Voigtman, E., 1442
Voogt, W. H., 1362
Voorhees, K. J., 1463

Walters, J. P., 1432
Wang, J., 1528
Warren, F. V., Jr., 1460
Wells, M. J. M., 1341
Westerlund, S., 1406
Winefordner, J., 1442
Wood, G. R., 1447
Wortman, T. R., 1536

Yacynych, A. M., 1523
Yamazaki, Y., 1531
Yarnitzky, C., 1383

Zare, R. N., 1509

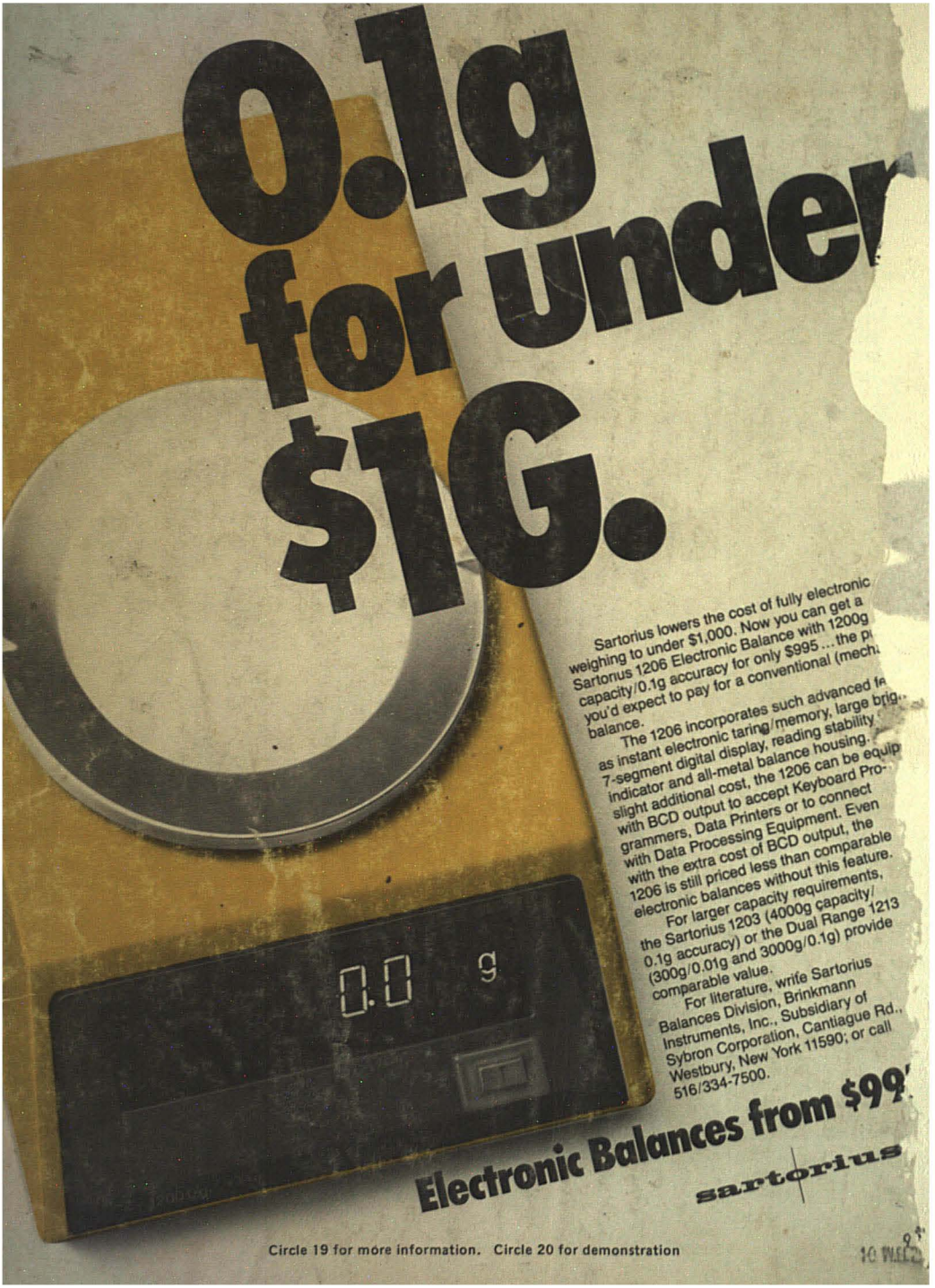
Future Articles

Kel-F–Graphite Composite Electrode as an Electrochemical Detector for Liquid Chromatography and Application to Phenolic Compounds
Duane E. Weisshaar, Dennis E. Tallman, and James L. Anderson

Single-Column Ion Chromatography for the Determination of Chloride and Sulfate in Steam Condensate and Boiler Feed Water
K. M. Roberts, D. T. Gjerde, and J. S. Fritz

Determination of Tetraallyllead Compounds in Gasoline by Liquid Chromatography–Atomic Absorption Spectrometry
J. D. Messman and T. C. Rains

Liquid Chromatography–Mass Spectrometry and Electron Impact and Secondary Ion Mass Spectrometry with Ribbon Storage Interface
Richard D. Smith, James E. Burger, and Allen L. Johnson



Circle 19 for more information. Circle 20 for demonstration